

*NASW-4435*

NASA/USRA  
UNIVERSITY ADVANCED DESIGN PROGRAM

PROCEEDINGS OF THE  
8TH ANNUAL SUMMER CONFERENCE

June 15-19, 1992

Washington, D.C.

(NASA-CR-195118) PROCEEDINGS OF  
THE 8TH ANNUAL SUMMER CONFERENCE:  
NASA/USRA ADVANCED DESIGN PROGRAM  
(USRA) 493 p

N94-25665  
--THRU--  
N94-25719  
Unclass

G3/80 0204290

**NASA/USRA UNIVERSITY ADVANCED DESIGN PROGRAM  
8TH ANNUAL SUMMER CONFERENCE**

**The NASA/USRA University Advanced Design Program is operated by the Universities Space Research Association (USRA) under a contract with NASA Headquarters (NASW-4435). Inquiries regarding the program may be directed to:**

**USRA Advanced Design Program Office  
3600 Bay Area Boulevard  
Houston, Texas 77058  
(713)244-2000  
FAX (713)244-2006**

## FOREWORD

The NASA/USRA University Advanced Design Program was established in 1984 as an attempt to add more and better design education to primarily undergraduate engineering programs. The original focus of the pilot program encompassing nine universities and five NASA centers was on space design. Two years later, the program was expanded to include aeronautics design with six universities and three NASA centers participating. This year marks the last of a three-year cycle of participation by forty-one universities, eight NASA centers, and one industry participant.

The Advanced Space Design Program offers universities an opportunity to plan and design missions and hardware that would be of use to NASA in the post-Space Station Freedom era of the early 2000's, while the Advanced Aeronautics Design Program generally offers opportunities for study of design problems closer to the present time, ranging from small, slow-speed vehicles to large, supersonic and hypersonic passenger transports. The systems approach to the design problem is emphasized in both the space and aeronautics projects. The student teams pursue the chosen problem during their senior year in a one- or two-semester capstone design course and submit a comprehensive written report at the conclusion of the project. Finally, student representatives from each of the universities summarize their work in oral presentations at the Annual Summer Conference, sponsored by one of the NASA centers and attended by the university faculty, NASA and USRA personnel, and aerospace industry representatives.

As the Advanced Design Program has grown in size, it has also matured in terms of the quality of the student projects. The comprehensive final reports are distributed through the National Technical Information Service. However, the results of the studies reach only a small audience, principally those who attend the Summer Conference. In order to broaden the distribution, a Proceedings volume, which summarizes the project results and roughly parallels the Conference presentations, is published. The present volume represents the student work accomplished during the 1991-1992 academic year reported at the Eighth Annual Summer Conference co-hosted by NASA Headquarters and NASA Goddard Space Flight Center, June 15-19, 1992.

## ACKNOWLEDGMENTS

We are most grateful to the students, the university faculty, and their teaching assistants for the excellent technical work contained in this volume. We are also indebted to those individuals from NASA Headquarters and from the NASA centers who conceived the program in the beginning, have provided valuable guidance to both USRA and the universities throughout, and through their keen interest in the student projects, are in large part responsible for the boundless enthusiasm of the students.

—USRA Advanced Design Program Office





## TABLE OF CONTENTS

|                |     |
|----------------|-----|
| Foreword ..... | iii |
|----------------|-----|

### SPACE PROJECTS

|  |   |
|--|---|
| UNIVERSITY OF ALABAMA, HUNTSVILLE<br>Systematic Propulsion Optimization Tools (SPOT) ..... | 3 |
|--|---|

|   |   |
|---|---|
| UNIVERSITY OF ARIZONA<br>Autonomous Space Processor for Orbital Debris Advanced Design Project in Support of Solar System Exploration ..... | 6 |
|---|---|

|  |    |
|--|----|
| UNIVERSITY OF CALIFORNIA, LOS ANGELES<br>Summary of 1991-1992 Projects ..... | 18 |
|--|----|

|  |    |
|--|----|
| and ECOLE POLYTECHNIQUE FEMININE<br>Manned Mission to Mars with Periodic Refueling from Electrically Propelled Tankers ..... | 22 |
|--|----|

|   |    |
|---|----|
| UNIVERSITY OF CENTRAL FLORIDA<br>Assured Crew Return Vehicle Post Landing Configuration Design and Test ..... | 31 |
|---|----|

|  |    |
|--|----|
| UNIVERSITY OF COLORADO<br>Autonomous Support for Microorganism Research in Space ..... | 40 |
|--|----|

|   |    |
|---|----|
| UNIVERSITY OF FLORIDA<br>Bioregenerative System Components for Microgravity ..... | 53 |
|---|----|

|   |    |
|---|----|
| FLORIDA A&M UNIVERSITY/FLORIDA STATE UNIVERSITY<br>The Extended Mission Rover (EMR) ..... | 67 |
|---|----|

|   |    |
|---|----|
| GEORGIA INSTITUTE OF TECHNOLOGY - MECHANICAL<br>The Enabler: A Concept for a Lunar Work Vehicle ..... | 74 |
|---|----|

|   |    |
|---|----|
| GEORGIA INSTITUTE OF TECHNOLOGY - TEXTILE AND FIBER<br>Designs for Lunar Projects ..... | 80 |
|---|----|

|  |     |
|--|-----|
| UNIVERSITY OF HOUSTON<br>1991-1992 Project Summaries ..... | 108 |
|--|-----|

|   |     |
|---|-----|
| UNIVERSITY OF IDAHO<br>Planetary Surface Exploration MESUR/Autonomous Lunar Rover ..... | 124 |
|---|-----|

|  |     |
|--|-----|
| KANSAS STATE UNIVERSITY<br>Automation of Closed Environments in Space for Human Comfort and Safety ..... | 137 |
|--|-----|

|  |     |
|--|-----|
| UNIVERSITY OF MARYLAND, COLLEGE PARK - AEROSPACE<br>MINOTAUR: Maryland's Innovative Orbital Technologically Advanced University Rocket ..... | 146 |
|--|-----|

|  |     |
|--|-----|
| UNIVERSITY OF MARYLAND, COLLEGE PARK - ELECTRICAL AND MECHANICAL                     |     |
| 1991-1992 Walking Robot Design .....   | 159 |
| MASSACHUSETTS INSTITUTE OF TECHNOLOGY  |     |
| Project Columbiad: Reestablishment of Human Presence on the Moon .....               | 170 |
| UNIVERSITY OF MICHIGAN   |     |
| Project APEX: Advanced Manned Exploration of the Martian Moon Phobos.....            | 178 |
| UNIVERSITY OF MINNESOTA  |     |
| Mars Transportation System.....  | 188 |
| OHIO STATE UNIVERSITY  |     |
| Project WISH: The Emerald City .....   | 196 |
| OLD DOMINION UNIVERSITY  |     |
| Extraterrestrial Surface Propulsion Systems.....                                     | 209 |
| PENNSYLVANIA STATE UNIVERSITY  |     |
| Comet Nucleus and Asteroid Sample Return Missions .....                              | 216 |
| PRAIRIE VIEW A&M UNIVERSITY  |     |
| Design and Development of the Second Generation Mars Habitat.....                    | 228 |
| UNIVERSITY OF PUERTO RICO  |     |
| First Lunar Outpost.....   | 237 |
| RENSSELAER POLYTECHNIC INSTITUTE   |     |
| The Lightcraft Project: Flight Technology for a Hypersonic Mass Transit System ..... | 250 |
| UNIVERSITY OF TEXAS, AUSTIN - AEROSPACE AND ENGINEERING MECHANICS                    |     |
| LEO, Lunar, Mars, and Asteroid Projects.....   | 251 |
| UNIVERSITY OF TEXAS, AUSTIN - MECHANICAL   |     |
| 1991-1992 Project Summaries.....   | 267 |
| UNITED STATES NAVAL ACADEMY  |     |
| Low-Cost Unmanned Lunar Lander .....   | 271 |
| UNITED STATES NAVAL POSTGRADUATE SCHOOL  |     |
| Summary of 1991-1992 Projects.....   | 274 |
| UTAH STATE UNIVERSITY  |     |
| Copernicus - Lunar Surface Mapper .....  | 298 |
| VIRGINIA POLYTECHNIC INSTITUTE AND STATE UNIVERSITY                                  |     |
| 1991-1992 Project Summaries.....   | 309 |

**UNIVERSITY OF WASHINGTON**

Project Minerva: A Low-Cost Manned Mars Mission Based on Indigenous Propellant Production .....325

**UNIVERSITY OF WISCONSIN, MILWAUKEE**

Pax: A Permanent Base for Human Habitation of Mars .....343

**WORCESTER POLYTECHNIC INSTITUTE**

Microgravity Ignition Experiment .....358

**AERONAUTICS PROJECTS****AUBURN UNIVERSITY**

Summary of the 1991-1992 Aeronautics Design Project .....367

**CALIFORNIA POLYTECHNIC STATE UNIVERSITY, SAN LUIS OBISPO**

Preliminary Design of Nine High Speed Civil Transports .....379

**CALIFORNIA STATE POLYTECHNIC UNIVERSITY, POMONA**

Supercruiser Arrow HS-8 .....391

**CALIFORNIA STATE UNIVERSITY, NORTHRIDGE**

Project Ares III .....406

**CASE WESTERN RESERVE UNIVERSITY**

Tesseract Supersonic Business Transport .....413

**UNIVERSITY OF KANSAS**

A Revolutionary Approach to Composite Construction and Flight Management Systems  
for Small, General Aviation Airplanes .....425

**UNIVERSITY OF NOTRE DAME**

Design Study to Simulate the Development of a Commercial Freight Transportation System.....437

**OHIO STATE UNIVERSITY**

The Design of Four Hypersonic Reconnaissance Aircraft .....453

**and ECOLE POLYTECHNIQUE FEMININE**

Design of a Refueling Tanker Delivering Liquid Hydrogen.....463

**PURDUE UNIVERSITY**

The Design of a Long-Range Megatransport Aircraft .....467

**WORCESTER POLYTECHNIC INSTITUTE**

Solar Powered Multipurpose Remotely Powered Aircraft .....477



---

## Space Projects



**SYSTEMATIC PROPULSION OPTIMIZATION TOOLS (SPOT)**

University of Alabama in Huntsville  
Department of Mechanical Engineering  
Huntsville, Alabama

Dr. Mark Bower  
John Celestian, Teaching Assistant

**Abstract**

This paper describes a computer program written by senior-level Mechanical Engineering students at the University of Alabama in Huntsville which is capable of optimizing user-defined delivery systems for carrying payloads into orbit. The custom propulsion system is designed by the user through the input of configuration, payload, and orbital parameters. The primary advantages of the software, called Systematic Propulsion Optimization Tools (SPOT), are a user-friendly interface and a modular Fortran 77 code designed for ease of modification.

The optimization of variables in an orbital delivery system is of critical concern in the propulsion environment. The mass of the overall system must be minimized within the maximum stress, force, and pressure constraints. SPOT utilizes the Design Optimization Tools (DOT) program for the optimization techniques.

The SPOT program is divided into a main program and five modules: aerodynamic losses, orbital parameters, liquid engines, solid engines, and nozzles. The program is designed to be upgraded easily and expanded to meet specific user needs. A user's manual and a programmer's manual are currently being developed to facilitate implementation and modification.

**Introduction**

Improved propulsion system designs and problems and problem solutions are vital to the future of the aerospace industry. To this end, propulsion optimization software can be a valuable tool to the design engineer. However, the software packages currently available are poorly organized and difficult to modify, thus placing the user in an unenviable position. Clearly the problem at hand is to develop a software package which delivers accurate results without sacrificing the user-friendly work environment.

This paper describes the Systematic Propulsion Optimization Tools (SPOT) program written by senior level engineering students at the University of Alabama in Huntsville. Its purpose is to develop the optimum system for delivering a payload into orbit. This is accomplished by optimizing the launch vehicle configuration based on the payload weight, engine types, and orbital parameters entered by the user. The code is written in FORTRAN with a QuickBasic user interface and employs a commercially available optimization routine, Design Optimization Tools (DOT), for all optimization calculations. This allows SPOT to be accurate, user-friendly, and easy to modify.

**Scope**

SPOT is designed to allow for quick analysis of either the effectiveness of a desired launch hardware combination, or to provide an optimized system to achieve a given orbit. The code allows the user to input any combination of elements within its parameters and to quickly obtain a "useful" answer.

In terms of hardware, SPOT can handle relatively large hardware combinations. The input vehicle can have anywhere from one to four stages. Each stage can be either liquid or solid-fueled and can have up to five engines. Between two and eight solid fuel strap-on engines can be used on the first stage to provide additional thrust. A propulsion system can be designed for payload weights of up to 100,000 pounds.

Some orbital mechanics constraints were also placed on the program in order to help make coding easier. Orbits are circular rather than elliptical. Any desired orbital radius within the feasible limits of the launch vehicle can be used. If the launch vehicle cannot reach the orbit input by the user, the program will relay this information to DOT which will modify the launch systems accordingly.

### SPOT Code

The user interface was written in QuickBasic instead of FORTRAN to provide a friendly work environment by offering a system of menus that can be easily navigated by the user. The menu-driven interface offers the option of optimizing any of three parameters: the size of liquid engines per stage, the number of solid engines per stage, or the number of strap-on engines on the first stage. Those variables not targeted for optimization are assigned values by the operator. After the optimization parameters are set, values for the desired orbital altitude, angle of inclination, launch site, and payload weight must be entered. SPOT then exits the user interface and begins executing the code within the main program.

### Main Program

The main program serves as the heart of the SPOT project by acting as the driver for the DOT, liquid, solid, and orbital modules. The data returned by these modules is combined with the input values from the data files created by the user interface. This combination is then developed into the objective and constraint functions for the optimization routine. In this case the objective function describes the total vehicle weight. This function is evaluated subject to the system constraints within the DOT routine.

The DOT routine iterates the objective function in search of an optimum value by adjusting the system design variables. The design variables are the number of solid engines, the liquid fuel mass, and the number of liquid engines. When DOT arrives at the optimum configuration, it returns an array to the main program. This array contains the values of the optimized variables. The main program then interprets the DOT array into the optimum mass values for the specified launch sequence.

### Liquid Module

The first module called by the main program is the liquid module, which determines the total initial mass of the liquid stages. In order to accomplish this task it must first receive information pertaining to the engine type of each stage, the number of engines used in each stage, and the propellant mass. The routine begins by determining which of the four possible stages were assigned liquid engines. After the liquid stages have been identified, the type of engine on each stage must be known. This allows a set of standard design variables characteristic to each

engine type to be initialized. These variables include miscellaneous mass, fuel flow rate, and tank length-to-width ratio among others. The module is now ready to begin its calculations.

The first computation determines the stage burnout time in terms of the fuel flow rate and propellant mass. After the burnout time is found, the volumes of oxidizer and fuel are found. These values allow the respective storage tanks to be sized and their weight computed.

In computing the mass of the fuel and oxidizer tanks the routine takes into account the stresses under a worst-case scenario of 12 G's. This, coupled with a design safety factor of 1.5, is used to design the tank thickness using the equation for hoop stress given below.

$$t = pr/\sigma$$

where  $t$  = tank thickness  
 $p$  = tank pressure  
 $r$  = tank radius  
 $\sigma$  = hoop stress

The total mass of each liquid stage is determined by adding the propellant mass (which is time-variant), the fuel and oxidizer tank masses, and the miscellaneous mass characteristic to the type of engines used. The total mass of the liquid stages is then determined by summation of the individual stage masses. This value is then returned to the main program.

### Solid Module

After the initial mass of the liquid stages is calculated, the main program calls the solid module to perform a similar task. The determination of the initial mass of the solid stages is less complicated than that of the liquid engines because the mass of the solid propellant is not a design variable. The routine begins by identifying which stages were assigned solid engines and the type of motors they were designated. Since the propellant mass is a constant dependent on engine type, it is necessary only to multiply the number of engines present by the mass of each engine to determine the initial stage mass. The total initial mass of the solid stages is then simply the summation of the individual initial stage masses. This value can then be returned to the main program for use in the objective function.



In addition to calculating the initial solid engine mass, this module must also determine the time to burnout of each solid stage. This value is simply read from the data file for the corresponding solid engine type.

### Orbital Module

The orbital module is concerned with two phases in the rocket's flight, the first being from launch until final stage burnout, and the second being from burnout to orbit (coast). During the first phase the specifics of the flight path are evaluated using the trajectory subroutine. It begins by gathering the values for drag force, thrust, and the system mass at an instantaneous moment during the powered flight of the vehicle. The radial and angular thrust are then determined using the relations below.

$$F_{\mu} = 1 (m)(g/r)^2 - F_d(\cos \beta) + \tau(\cos \beta)$$

$$F_{\theta} = -1(F_d) (\sin \beta) + \tau(\sin \beta)$$

where  $m$  = total mass of vehicle  
 $g$  = gravity  
 $r$  = distance of vehicle from center of Earth  
 $F_d$  = drag force  
 $\tau$  = rocket thrust  
 $\beta$  = angle of inclination

The next step in the solution process is to determine the radial and angular position, velocity, and acceleration. A Runge-Kutta subroutine is used to determine the velocities and position that are, in turn, used to calculate the acceleration values. This is done for time increments until the final stage burnout occurs. At this point the responsibility for the analysis of the vehicle's flight is transferred to the coast subroutine. This routine also used the general Runge-Kutta routine with the one exception of a thrust value of zero. The velocity and position of the vehicle are continually calculated until either the desired orbit is reached, or the vehicle comes to rest. If the rocket fails to reach the desired orbit, a warning message is returned to the main program.

The orbital module employs the services of three additional subroutines in its computational process. First, an aerodynamics routine is used to evaluate the instantaneous drag force experienced by the vehicle. Next, the orbital module calls the liqminor routine to determine the thrust delivered if a liquid engine is burning. In addition, it calculates the instantaneous mass of the liquid stages. Finally, subroutine solminor is called

to find the thrust delivered as the solid engine is burning, as well as the instantaneous solid stage mass.

### Conclusion

The driving concept behind SPOT is to provide the aerospace industry with a useful tool with which to evaluate launch and hardware configurations. While the actual program still contains some rough spots, the concept is very solid. With some additional work and modification, we will have achieved our objective and developed a useful design tool.

# **AUTONOMOUS SPACE PROCESSOR FOR ORBITAL DEBRIS ADVANCED DESIGN PROJECT IN SUPPORT OF SOLAR SYSTEM EXPLORATION**

**University of Arizona  
Aerospace and Mechanical Engineering Department  
Tucson, Arizona**

**Professor Kumar Ramohalli  
Dominique Mitchell, Teaching Assistant  
Brett Taft, Paul Chinnock, Bjoern Kutz**

## **Abstract**

This paper is regarding a project in the Advanced Design Program at the University of Arizona. The project is named the Autonomous Space Processor for Orbital Debris (ASPOD) and is a NASA/Universities Space Research Association (USRA) sponsored design project. The development of ASPOD and the students' abilities in designing and building a prototype spacecraft are the ultimate goals of this project. This year's focus entailed the development of a secondary robotic arm and end-effector to work in tandem with an existent arm in the removal of orbital debris. The new arm features the introduction of composite materials and a linear drive system, thus producing a light-weight and more accurate prototype. The main characteristic of the end-effector design is that it incorporates all of the motors and gearing internally, thus not subjecting them to the harsh space environment. Furthermore, the arm and the end-effector are automated by a control system with positional feedback. This system is composed of magnetic and optical encoders connected to a 486 PC via two servo-motor controller cards. Programming a series of basic routines and sub-routines has allowed the ASPOD prototype to become more autonomous. The new system is expected to perform specified tasks with a positional accuracy of 0.5 cm.

## **Introduction**

The subject of orbital debris has been reaching the spotlight since SkyLab's degenerating orbit put the world on alert as to where the debris that survived reentry would touch down on Earth. These problems have not gone away and are currently affecting today's space missions, as was demonstrated when Discovery's crew in September of 1991 and Atlantis's crew in November of 1991 had to alter their orbits in order to avoid a piece of space junk. The actual debris had a trajectory that would intersect NASA's four-mile safety envelope for shuttle missions. These events are a good indication of the growing trouble caused by orbital debris. Table 1 is a short outline of the types of problems caused by orbital debris.<sup>1</sup>

Table 1 Several problems with orbital debris

1. Loss or damage to satellites and spacecraft by collision with debris
2. Interference with astronomical observations on Earth and in orbit
3. Accidental reentry of satellites and other space hardware
4. Interference with scientific and military experiments
5. Spread of nuclear materials in orbit and on Earth
6. Potential explosions of unused fuel

Presently there are over 7500 pieces of orbiting debris of sufficient size to cause a disaster similar to that of the Challenger. Furthermore, there are countless numbers of untraceable pieces of smaller debris that are capable of causing enough damage to a satellite to make it inoperable. The kinetic energy related to orbital debris is the significant problem. Table 2 is a representation of the possible effects from orbital debris collisions at a velocity of 10 km/s (22,369 mph, i.e., kinetic energy).<sup>2</sup>

Table 2: Comparisons of kinetic energy of debris and collision effects

| Particle Size<br>(Diameter)          | Effects                             |
|--------------------------------------|-------------------------------------|
| < 0.01 cm                            | Surface erosion                     |
| < 0.1 cm                             | Serious damage                      |
| 0.3 cm at 10 km/s<br>(32,630 ft/s)   | Bowling ball at<br>60 mph (88 ft/s) |
| 1.0 cm aluminum<br>sphere at 10 km/s | 400 lb safe at<br>60 mph            |

These small pieces of debris have also been responsible for small craters in the space shuttle's windows on several missions, thus requiring the windows to be replaced after each mission at a cost of approximately \$50,000. Most recently, the new shuttle Endeavour received a small crater in one of its windows which was determined to be caused by a small piece of debris. This is a direct result of placing satellites into orbit without considering what to do with them or their rocket boosters after their useful life has expired. Figure 1 is an illustration of the artificial orbital population.<sup>3</sup>

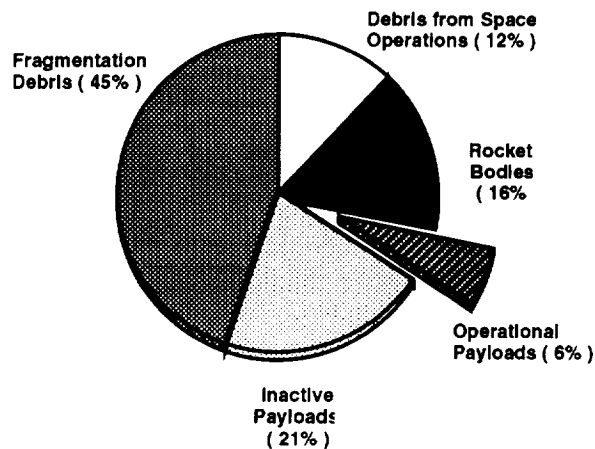


Fig. 1 Orbital population (Dec. 1989)

This figure shows that only 6% of all the artificial objects in orbit are functioning satellites. The rest of the objects are considered orbital debris. The table below shows the major elements of orbital debris.<sup>1</sup>

Table 3: Elements of orbital debris

- Deactivated spacecraft or satellites
- Spent rocket stages
- Paint flakes
- Fragments of rockets and spacecraft
- Engine exhaust particles
- Spacecraft rocket separation devices
- Spent Soviet reactors
- Intentional break-up of orbiting payloads

There are many myths regarding the seriousness of the debris problem previously mentioned. Some such myths include:

1) The major problem posed by orbital debris is the inability to track accurately the trajectory of the smaller pieces. [This is in part true; the smaller pieces are the reason for concern. However, it must be realized that the larger pieces through orbital collisions and explosions of excess propellant are the cause of the smaller pieces of debris.]

2) The problem of space debris will not be significant until the year 2000. [Why wait until the problem becomes serious in order to search for viable solutions? Furthermore, it can take about 10 years to develop a space craft from conception to production; thus there is no better time to start than the present.]

3) The body of knowledge about orbital debris is not well defined; thus more studies are needed to learn more about the problem. [This is an unfounded rumor. In fact, the majority of the larger pieces of debris are currently being tracked by the Space Surveillance Network (SSN) which is operated by Department of Defense. Also there are databases that have information about the large debris (i.e., trajectories, velocities, mass, geometry, etc.).]

Fortunately, students at the University of Arizona under the guidance of Dr. Kumar Ramohalli have been able to see through these myths and are now concerning themselves with a means to solve this problem. The concept of an Autonomous Space Processor for Orbital Debris is the answer to sweep up the problem of orbital debris. The two major goals of the ASPOD spacecraft are to deal with the orbital debris problem (by processing the trackable large pieces of debris before they have a chance of becoming small, untraceable projectiles that potentially could cause a lot of damage) and to utilize the resource (i.e. the debris) that is already in orbit (by using the materials from the debris to produce or build new device that will serve a purpose). The goal of ASPOD is to process large pieces of debris. The approximate number of objects and their total mass are shown in Table 4.<sup>2</sup>

Table 4 Approximate number and size of artificially-made orbital debris

| Object Size | Number of Objects | Percentage of Objects, % | Total Mass  | Percentage by Mass, % |
|-------------|-------------------|--------------------------|-------------|-----------------------|
| > 10 cm     | 7,000             | 0.2                      | 3,000,00 kg | 99.97                 |
| 1 - 10 cm   | 17,500            | 0.5                      | 1,000 kg    | 0.03                  |
| < 1 cm      | 3,500,000         | 99.3                     |             |                       |

Although objects over 10 cm in size constitute less than 1% of the number of objects in orbit, they contribute to over 99% of the total mass of orbiting objects.

Another misconception is that in the vastness of space, it is virtually impossible to rendezvous with orbital debris and that the propellant requirements to do so are too great. This is not true. In fact, a study conducted by the University of Arizona in 1989 identified several specific inclinations in which a majority of the large debris exist (see Figure 2).<sup>3</sup>

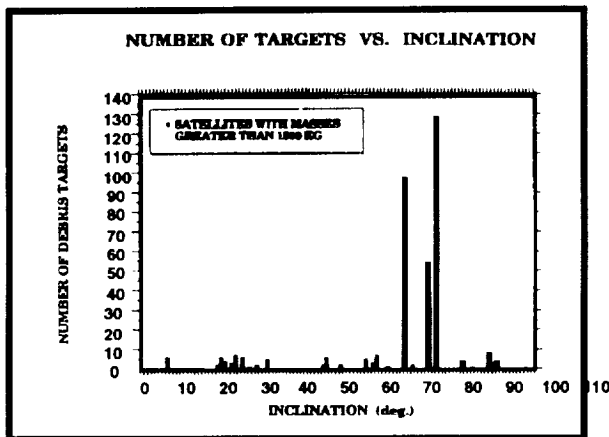


Figure 2: Distribution of orbital inclinations

Mission feasibility studies have shown that one of the envisioned spacecraft could process at least five of the large pieces of debris with reasonable propellant requirements. This is accomplished by taking advantage of nodal regression differences and the use of classic Hohmann transfer.<sup>3</sup>

#### ASPOD's Basic Mission Profile

The following is the overall mission scenario:

1. Launch from booster or Space Shuttle.
2. Use propulsion and programming to enter orbit and rendezvous with target debris.

3. Rendezvous with debris and use programming and one of two computer-controlled robotic arms to retrieve debris.
4. Programming selects the proper placement of second robotic arm to grip the piece to be cut off.
5. Both arms then move debris into the focal point of solar cutting device (solar cutter is an array of mirrors and Fresnel lenses).
6. After the piece has been cut, the second arm places the piece in storage bin. The process (from 4 to 6) is repeated until whole debris is placed in storage bin.
7. Programming instructs ASPOD to rendezvous with next target debris (steps 3 to 7 are repeated until all target debris has been processed).
8. ASPOD has then three options depending on retrieved payload i.e., orbital debris:

- a) rendezvous with Space Shuttle where debris will be downloaded and returned to earth. ASPOD will then be refueled and given new instructions and new target debris.
- b) rendezvous with future Space Station where debris will be downloaded and remanufactured for other uses.
- c) burn up on reentry into atmosphere.

This project was initiated in 1987 and has become an integral part of the Advanced Design Program at the University of Arizona over the past several years due in part to an increased interest in the problem of orbital debris and the continued funding of NASA/USRA. Moreover, the ASPOD project has met with great support over the years from both the University of Arizona and the surrounding community, resulting in numerous appearances in both local and national newspapers and news broadcasts.

#### Progress

Since 1987, the ASPOD project has maintained a steady level of progress, each year enhancing the former year's design along with incorporating necessary additional systems into the satellite to ensure that it will be truly be autonomous when completed. In this respect, the prototype

(test-bed) has excelled from the basic concept of a debris retriever to that of an integrated machine capable of maneuvering a piece of debris with a robotic arm through a focal point of a solar array that has utilized a solar tracker to align itself with the sun in order to maximize its cutting potential.

Consistent with the USRA philosophy, a new group of undergraduates was involved with the ASPOD project this year. This year's team consisted of 14 undergraduates and two graduate students with varying majors and interests. A complete list of these and past students can be found in the Appendix.

### Arm

The ASPOD design group was tasked with designing a second robotic arm for the ASPOD satellite. Improvements that were required included a greater increase in reliability, a lighter structure, higher stiffness, drive system simplification, and a high degree of controllability. The arm's improvements must be accomplished while maintaining the original arm's degrees of freedom and rough link lengths.

The design group that undertook this project included Paul Chinnock, George Williams, Peter Wegner, and Curt Bradley. Paul Chinnock was responsible for the design of a light, rigid structure of high reliability and easy to manufacture. George Williams was charged with drive system design. The drive system was required to be light, consume low energy, be very reliable, and fulfill motivation needs for the loading conditions specified. Peter Wegner needed to engineer the control system with a closed loop feed-back control using encoders. In addition the system needed to be light, to be very accurate, and to work in close conjunction with a remote computer for precise position control. Curt Bradley needed to design a support frame on which to mount the arm and straddle the mirror frame. Within the support frame design area, the arm's base needed to be positioned to maximize its usefulness.

The first semester consisted of brainstorming and iterative paper-based design. The design (see Figure 3) was finalized, and parts were ordered for manufacturing and assembling in the Spring semester. Throughout the manufacturing process, further simplifications were made to the individual pieces to shorten machining time. The entire two-semester project was packed with educationally rewarding experiences.

The arm is designed with linear ball-screw-to-ball-nut drives for high efficiency, reduced stresses at the axles, simplicity, and lightness. The arm's structure is built of

composite links and aluminum joints. The base is designed to travel a full 360 degrees of rotation and therefore uses a gear and chain assembly. Links are preloaded to increase stiffness. The arm's end has been designed to accept the arm end-effector.

The linear drives have preloaded ball nuts that eliminate play induced by wear and tear on the arm. The ball-screw-ball-nut linear actuator exceeds the first arm's drive system in reliability, reduced play, simplification, lightness, and reduced stresses. The arm's drive motors are DC brushless and offer torque for acceleration and deceleration for placement speed of 90 degrees per minute. The arm has been demonstrated at much higher speeds. Lagrangian dynamics was used to determine the torques required for all conditions. All three motors are the same and have 195 oz. of continuous torque.

The control system uses optical encoders to position the arm to an accuracy of 1 centimeter when loaded and unloaded with a 1-pound load. A 486 computer with two three-channel control boards is used for control. The controller boards convert the computer's digital signals to analog signals for the motors. The boards' output signals are amplified to the DC motor's requirements for input by two amplifiers. The controller cards, in addition to translating signals, have built-in stability programming for set bandwidths. The channels on the boards each have position, velocity, and acceleration registers. The optical encoders offer 270,000 pulses for a joint's entire range of motion exceeding accuracy requirements.

The Base Support Frame has carbon-graphite composite links preloaded with centered bolts and joints made of aluminum. The structure exceeds strength requirements and stiffness specifications. The deflection under double the load requirement (2.2 lbs) and worst torque position is 6.35 mm including arm and base structure linked.

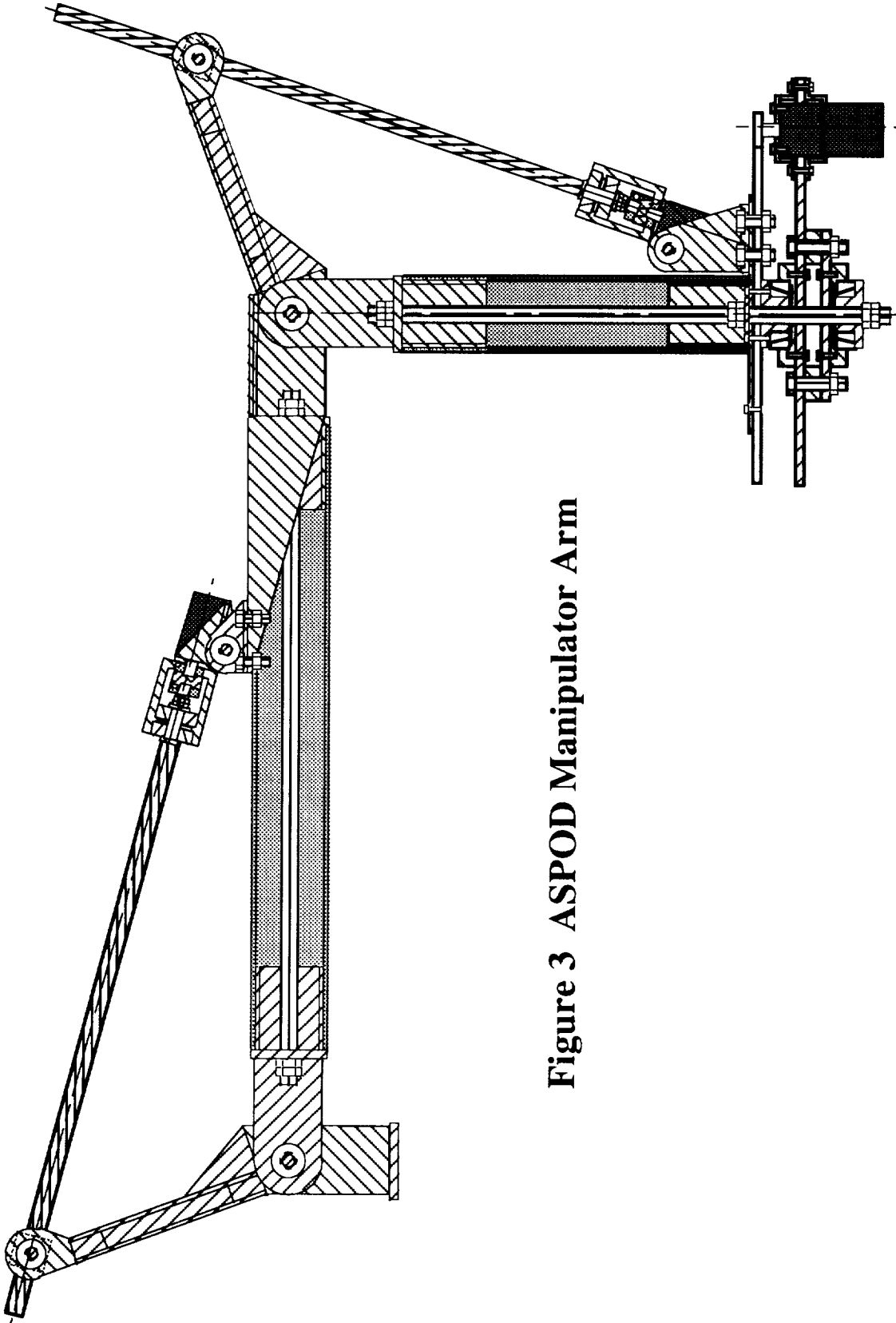


**Figure 3 ASPOD Manipulator Arm**

## End-Effector

Operating in conjunction with the ASPOD arm is the end-effector. The end-effector was designed as part of the ground-based working prototype for one of the twenty-first century's advanced space systems. The following were the original specifications to be met by the Autonomous Space Processor for Orbital Debris end-effector system.

**GRIPPING ABILITY:** The end-effector must be able to grip various sizes and shapes. It is proposed that it be able to pick up an object with a maximum weight of 1 lb. and that the jaws open 5 inches.

**DEGREES OF FREEDOM:** The design will have three degrees of freedom. The gripper will open and close. The "wrist" joint will rotate and the "elbow" joint will be a pinned hinge joint.

**MASS:** A maximum total weight of 10 lbs has been set for the end-effector and its components. This will lower the torques it must overcome while being tested on Earth and decrease the weight that will need to be lifted to orbit.

**SPEED:** A suitable range for the operation of the effector will be from 1/16 to 3/16 inches per second (in/s). The wrist will rotate in the range of 2 to 8 revolutions per minute. The elbow joint will move as slowly as necessary to keep acceleration at a minimum.

**SENSORS:** Encoders in joints will be used to relay rotation positions.

**MOTORS:** The end-effector and arm will be powered by 12-24V DC motors. Individual motor sizes will be determined by the torques they are required to produce.

**COMPATIBILITY:** The end-effector will be mounted on the robotic arm which is also under development. Cooperation with the robotic arm group will insure that the designs are compatible.

**DRIVE SYSTEMS:** A system of gears, drive screws, and chains will be used to relay torques from motors to joints.

**TOLERANCES:** Because of the high degree of accuracy required, machining tolerances of 0.002 inches must be adhered to on all load-bearing members.

## Achieved Design Specifications

The exact specifications for the ASPOD end-effector system are shown below.

**GRIPPING ABILITY:** The end-effector is able to grip objects of various sizes and shapes. It produces a

gripping force of approximately 8 pounds with a maximum opening range of 5 inches.

**DEGREES OF FREEDOM:** The end-effector design incorporates three degrees of freedom. The gripper opens and closes along a linear track. The "wrist" joint rotates more than 360 degrees in either direction. The "elbow" joint is a pinned hinge joint that moves through an angle of 220 degrees.

**MASS:** The end-effector weighs a total of 9.2 pounds. This meets the 10-pound limit set in the original design specifications.

**SPEED:** A suitable range for the operation of the hand will be from 1/16 to 3/16 (in/s). The wrist and elbow joints rotate between 6 and 8 revolutions per minute. This minimizes the inertial acceleration.

**SENSORS:** Magnetic encoders attached to the end of the motors are used to relay rotation positions.

**MOTORS:** The end-effector is powered by three motors. A 360 oz-in 12-V DC motor powers the elbow joint. The rotational joint is run by a 670 oz-in 12-V DC motor. And a 200 oz-in 24-V DC motor powers the gripper.

**COMPATIBILITY:** The end-effector is attachable to the parent robotic arm, which in turn works with the rest of the systems on the ASPOD vehicle.

**DRIVE SYSTEMS:** For all three degrees of freedom, power is transferred from the gear motor through shaft couplers and drive shafts. For the gripper and bending joints, a series of gears is used to relay power. But the rotational motor transfers torque by direct drive.

Beyond the basic quantitative constraints, the design team also followed a set of qualitative constraints or goals. The main concepts addressed by the design are efficiency, reliability and flexibility. To make the design "efficient" the prototype is representative of an uncluttered "common sense" assembly. The reliability of the end-effector components implies protection from failure and accidents, but also easy repair if an accident should occur. Finally, since the ASPOD system is still in the optimization stage of development, the end-effector is designed to be flexible with respect to changing performance needs. The result of careful design and analysis is shown in Figure 4. In this figure several general design features can be seen as examples of efficiency, reliability, and flexibility.

Notice the efficient layout of the components of the design. The twisting joint is situated before the bending joint. This arrangement better utilizes the capabilities of the bending joint. If the position of the joints were reversed,

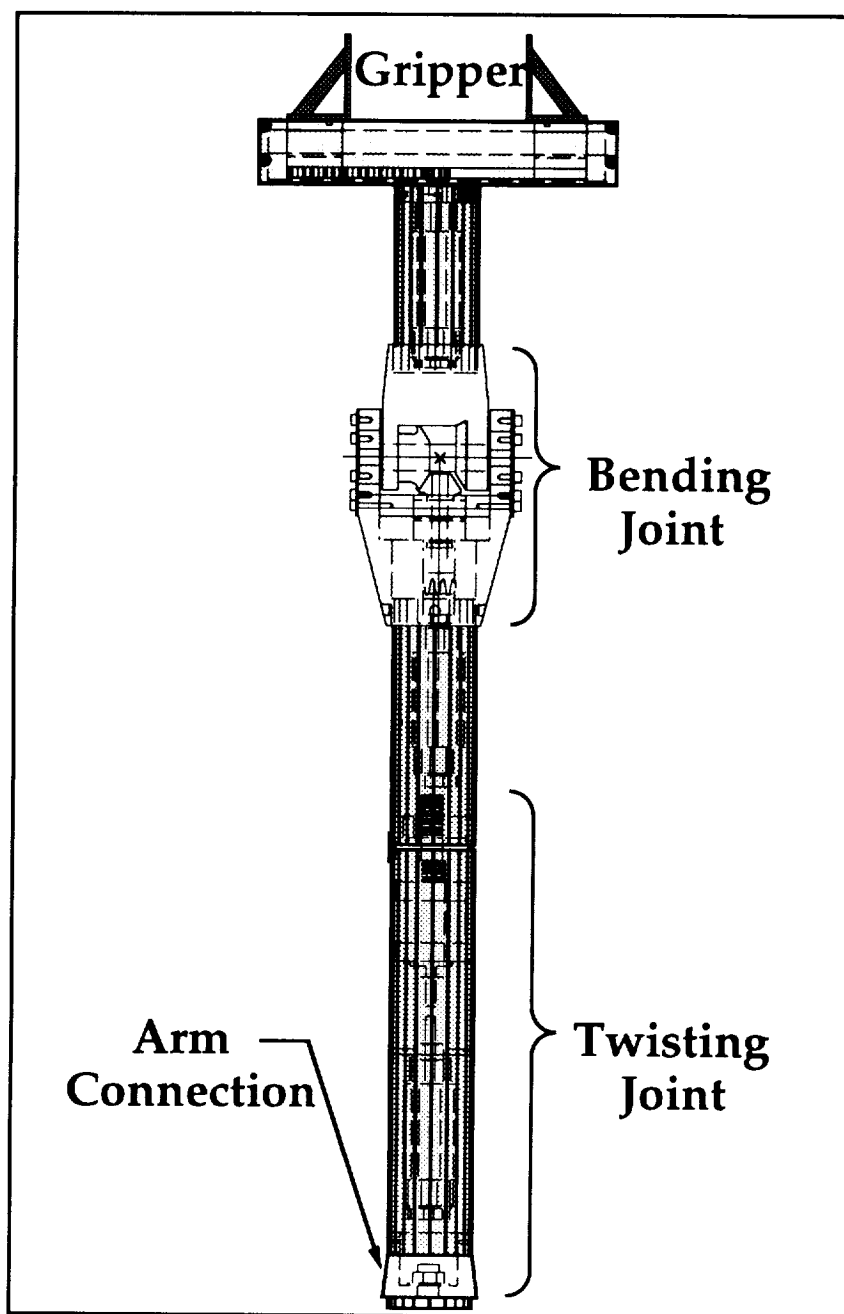


Fig. 4 ASPOD End-Effector



the bending joint would be redundant with the rest of the arm joints. Also, the selection of compact, high torque gear motors manufactured by "Micro Mo" allowed the designers to place the motors at each joint inside the aluminum support tubing. The internal motors are protected from the environment, while the short distance to the applied joint eliminated the need for complex drive systems. Along with the motors, all of the gearing and most of the wiring are enclosed for protection. The result is an efficient, uncluttered design.

The design layout also contributes to high reliability. High precision fits and internal mountings reduce gear wear while protecting parts. Since the motors are mounted to the joints in assemblies of simple parts, the joints and parts are easily disassembled and repaired in case of a problem.

The design of the assemblies also allows for easy redesign or configuration changes. This flexibility reduces the need for major redesign iterations. The linear gripper utilizes removable fingers on the jaws. This allows jaw redesign and implementation in a matter of minutes rather than longer, more costly periods of time. In addition, since the motors are in single assemblies with their driven joints, switching from the twisting joint first, bending joint second configuration to the opposite arrangement is accomplished in half an hour.

One of the most dramatic aspects of the flexible design is the control system. The control system allows the operator to program a desired output into the terminal. The computer-based control system then calculates the specific system requirements, provides the system commands, and moves the system to the desired state while checking for errors. This process starts at the computer terminal. The user specifies a move using one of the programming methods available. The controller card inside the computer converts the logical command to a voltage command and sends the command to the appropriate axis via the connection card. The power amplifier converts the output signal to an appropriate motor input command signal. While the motor is in a control mode, the controller card reads the encoder output, comparing the output to the desired position. The controller card will move the motor to the desired position and keep it there until another command is given. The major components used in the control system are the actuators, the feedback sensors, the interface hardware, the controller card, and the computer-based instructions.

The actuators used for the arm and end-effector are Pittman and Micro Mo high torque gear motors. The motors used for the bending and the twisting joint require a twelve volt

power output, while the gripper and arm motors require twenty-four volts. The controller card offers a convenient method for adjusting the output signal. Gain and offset potentiometers are supplied for each axis and can be adjusted for a desired output.

In the ASPOD Arm-Effector design, the actuators are all DC motors requiring an analog output from the controller card. Attached to the motors are the feedback sensors. In the case of the three Micro Mo motors, the feedback sensors are magnetic encoders. Magnetic encoders were chosen because they were cheaper and more readily available as an integral package from the manufacturer. The Pittman motors utilize BEI optical encoders reading off the output shaft. The encoders provide two square wave signals 180 degrees out of phase which are decoded into a number of counts per motor revolution. The position of each joint is then determined from a reference. This information is then used to command the motor.

In the control system the encoders and the motors do not interface directly to the controller card. First, the controller connects to a wiring interface card which in turn connects to the power amplifiers and the encoders. The interface card was supplied by Servo Systems with the controller card. The power amplifier circuits were constructed by the design team.

The power amplifier circuits were designed around a National Semiconductor LM12C operational amplifier. The circuit involves two power supplies powering a common bus. Each power amplifier circuit draws power off the bus to distribute to the appropriate motor. Each power amplifier circuit is interfaced between a motor and a control axis on the controller card.

The controller card is the main processor of the control system. The Omnitech Robotics MC-3000 card is a 3-axis controller card designed around three Hewlett Packard HCTL-1000 motion controller IC chips. Two MC-3000's are sufficient for the six axes of control required for the arm and end-effector. Although several control modes are available, the trapezoidal profile mode is being used. Trapezoidal mode is ideal for robotic applications because it offers reasonable velocity and acceleration control with positioning control. An acceleration/deceleration and a maximum velocity are specified by the user. When the card receives a position command, it accelerates the motor until maximum velocity is reached or until the motor is halfway to the desired position. Then the motor is decelerated at the programmed deceleration. After the motor is decelerated, the card checks for position, and adjusts to the programmed value.

Although a decoding program was provided by Servo Systems, a better user interface was desired. The goal was to have a program that fulfilled three objectives. The program should be easy to use, powerful, and, of course, should be able to run the robot arm through fixed routines. Originally the "C++" programming language was chosen for the program. However, it was later decided to use "Turbo Pascal 6.0." Turbo Pascal is easier to learn and compiles more quickly, significantly lessening development time. Turbo Pascal also came equipped with extra libraries for windows and mouse interface programming. These libraries were not included with C++.

To make the control program easier to learn and use, the program was designed to be menu-, windows-, and mouse-driven. A windows-based menu-driven program arranges methods and commands in a logical system. This interface allows new users with little or no computer experience to learn program basics in less than an hour. In the case of the menu commands, pressing the "Alt" key and the highlighted letter will open that sub-menu. Once the sub-menu is open, a command in that sub-menu may be executed by pressing the key corresponding to the highlighted letter. An alternate, easier method for choosing commands is by using the mouse. With this method, the mouse is used to move the cursor to the desired sub-menu, the right mouse button is "clicked" ( depressed and released ) opening the sub-menu. Then the right mouse button is clicked while the cursor is over the desired menu item. This procedure will execute the desired menu command. Some commands offer yet an additional method for their use. When each sub-menu is open, some of the commands have key sequences adjacent to them against the right hand side of the box. These key sequences are known as "Hot-Keys". By executing the Hot-Key sequence on the keyboard, the desired command can be effected without having to use the menus. Within this structure, three general control methods are available to adapt to the varying needs of the operator. These methods are a menu-executed trapezoidal command, a programmed set of routines, and direct keyboard or "hand " control.

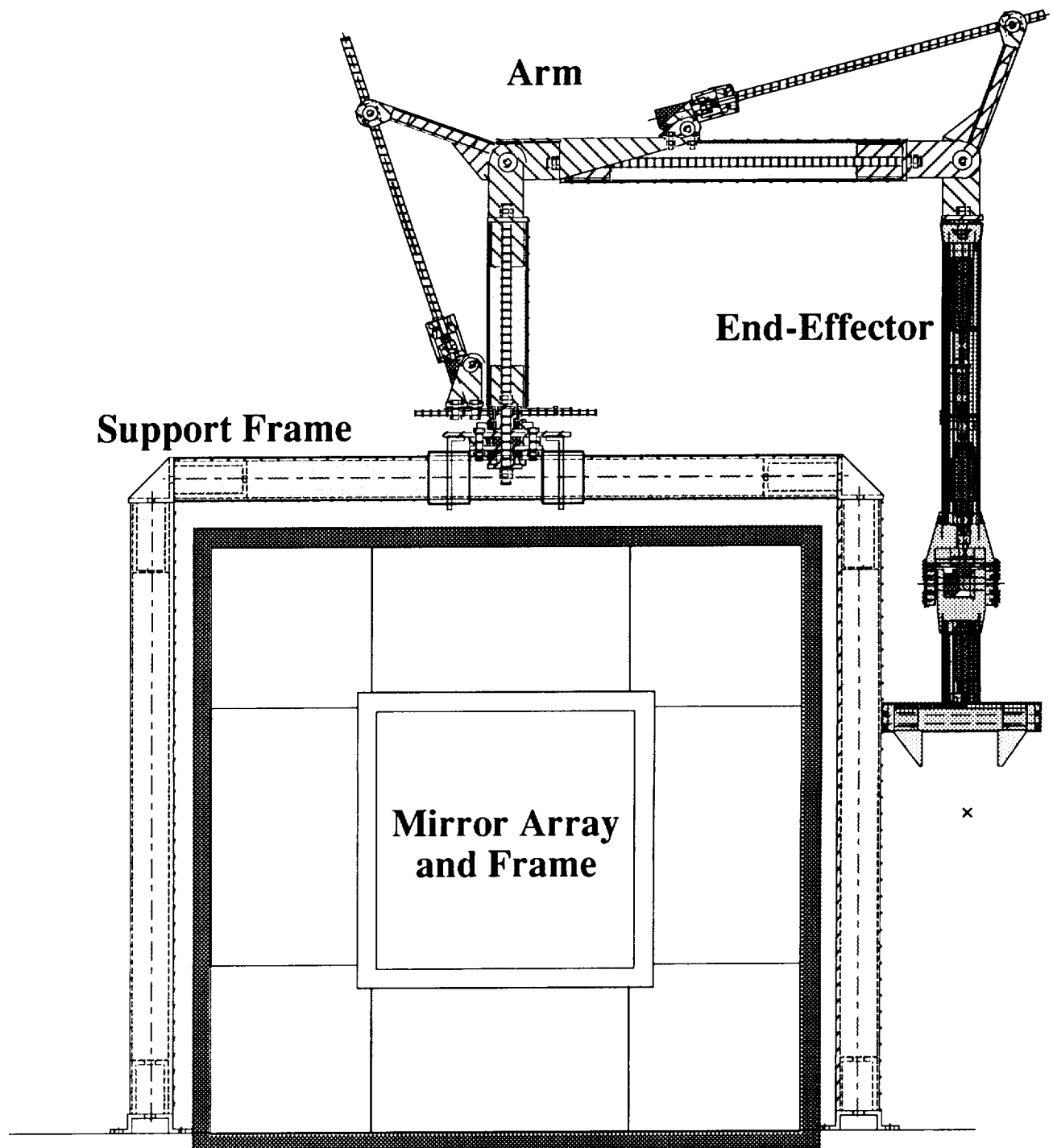
By using the mouse or keyboard commands to go through the menus the operator can execute a trapezoidal command. A trapezoidal command implies that the maximum velocity and the acceleration/deceleration are specified by the user. When this method is used the position versus time profile is in the shape of a trapezoid. The menu-executed trapezoidal command is advantageous when testing moves in order to build a routine. To see what will happen when a command is executed, enter the test values and execute. If the effect is not desired, return the arm to the original position and try again. By testing commands like this the user can come up with a programmed routine.

Once the user compiles enough commands, the full featured file editor can be used to construct a command file. A command file is constructed by placing the necessary commands (one per line) in a list with any needed values on the line following. To show how these commands might be used, an example routine is shown below.

```
set_base
776
reset
clr_act_pos
set_gain
10
set_zero
240
set_pole
40
set_timer
40
set_max_vel
127
set_accel
70
set_final_pos
10000
trap_mode
delay
2000
set_base
778
dac
255
delay
2000
dac
127
reset
set_base
776
reset
quit
```

The routine shown above operates the twisting joint of the end-effector and the gripper. After setting the zero, pole, gain, and other parameters, the twisting joint will turn 10,000 encoder counts at max velocity while the program delays for 2000 units ( about 400 units per second ). Then the gripper will close at full voltage for another 2000 units of delay. Finally the gripper voltage will be set back to zero, and both axes will receive a hard reset. Routines like this are easy to design and test using the file editor inside the controller program.

**Figure 5: Robotic Arm, Support Frame, and End-Effector Configuration**



Another alternative to trapezoidal commands and command routines is straight keyboard commands. Occasionally, the trapezoidal command mode is not the most convenient method for moving the arm. For this reason a set of "Hot-Keys" has been assigned to positive, negative, and zero voltage out commands for each axis. A list of these commands is located under the Commands menu. To move an axis, the user hits the "Escape" key until the "All axes have been reset" message is displayed. Then the Hot-Key sequence corresponding to the desired motion is hit. The joint should move. Once the axis has moved to the desired point, the user hits the home key to stop the motion. The home key will only stop the last axis to be activated by a voltage out command.

### **Conclusion**

The progress of ASPOD is highly encouraging with several large steps made in both the integrated system and the overall design approach. One major advancement in the development is an additional robotic arm which is capable of working with the existing arm in order to accomplish the tasks that are needed in the removal of orbital debris. This arm is built with a more stable linear drive system and the use of composites as an effort to decrease the weight of the arm itself. The main characteristic of the end-effector design was that it incorporated all of the motors and gearing internally, thus not subjecting them to the harsh space environment. Furthermore, a control system was developed in order to control the arm and end-effector. The total configuration of the arm, support frame, and end-effector is shown in Figure 5.

The future plans are to control both arms in tandem from a computer in order to move the debris into the focal point of the solar cutter. In this respect, a computer code is being written to tell the arms to perform certain functions with a single command from the comm-linked operator.

### **References**

1. Orbiting Debris, A Space Environmental Problem, Office of Technology Assessment, September 1990.
2. Space Debris a Potential Threat to Space Station and Shuttle, General Accounting Office Report, April 1990.
3. Ramohalli, Kumar, et al., Advanced Design For Orbital Debris Removal in Support of Solar System Exploration, USRA Summer Conference, June 1991.

From Sept. 1987 to June 1992, more than 60 students, ranging from high school to graduate students, have participated in the ASPOD program at the University of Arizona.

### **Student Participation:**

#### **1987 - 1988**

Graduate Students: David Campbell, Scott Reid

Undergraduate Students: Donald Barnett, Bryan Cindrich, Steve DiVarco, Catherine Dodd, Velda Dykehouse, Robert Flori, Reid Greenberg, Joseph Manning, Jim Matison, Ruzila Mohkhirhadi, James Poon, and Zenophen Xenophontos.

#### **1988 - 1989**

Graduate Student: David Campbell

Undergraduate Students: Jeff Brockman, Bruce Carter, Leslie Donelson, Lawrence John, Micky Marine, Dan Rodina.

#### **1989 - 1990**

Graduate Student: David Campbell

Undergraduate Students: Dan Bertles, Micky Marine, Ramon Gutierrez, Joseph Huppenthal, David Nichols, Mohamed Saad, Carlos Valenzuela.

#### **1990 - 1991**

Graduate Student: Micky Marine

Undergraduate Students: James Bartos, James Colvin, Richard Crockett, Kirby Hnat, David Ngo, Jennifer Putz, James Shattuck, Lee Sword, Sheri Woelfe.

Pre-University Students:

Angela Mcfadden, Jennifer Hamilton, Brenda Lundt.

#### **1991 - 1992**

Graduate Students: Dominique Mitchell, Brett Taft

Undergraduate Students: Curt Bardley, Sheila Caoile, Paul Chinnock, Greg Hart, Todd Jacobson, Bjoern Kutz, Dave Lye, Matt McCutchen, Angela Mcfadden, Ted Parvu, Mohamed Saad, Glen Sonnenberg, Peter Weginer, George Williams.

Pre-University Students:

William Dalby.

**SUMMARY OF 1991-1992 PROJECTS**

**University of California, Los Angeles  
Mechanical, Aerospace and Nuclear Engineering Department  
Los Angeles, California**

**Professor Rudolf X. Meyer  
Myles Baker, Teaching Assistant**

**HARDWARE DESIGN OF A GRAPPLING/DOCKING  
DEVICE ACCOMMODATING LARGE LATERAL AND  
ANGULAR MISALIGNMENTS**

**Myles Baker**

**Abstract**

In this hardware project, continued from last year, the students developed ideas for a new grappling and docking mechanism that would be able to accommodate a very large initial misalignment (up to one half of the spacecraft radius) and simultaneously a large angular misalignment (up to 20 degrees) between space tug and space vehicle. The students were made familiar with the project by visiting TRW, where they could study the prototype of the NASA Orbiting Maneuvering Vehicle (OMV, since canceled). The students' objective was to design a model, built in the University machine shop, that would demonstrate the potential for much larger misalignments than was possible with the OMV.

**Introduction**

In modern space operations, it is often necessary for two spacecraft to provide services to one another, such as orbital corrections, propellant replenishment, or repairs. These operations nearly always require that the spacecraft are rigidly linked to one another, requiring a grappling or docking procedure. Several such methods have been used or proposed in the past: Examples are the docking of Apollo capsules to Skylab and the Lunar Descent Modules, TRW's Orbital Maneuvering Vehicle, and the Space Shuttle fleet's mechanical arm for grappling satellites.

As was evidenced by NASA's recent difficulties in capturing an errant satellite for repair, the methods of spacecraft docking currently in use are still difficult to apply. Due to intolerance to even slight misalignments, very accurate (and therefore expensive) control of the spacecraft's relative positions is required, and even then a successful maneuver cannot always be assured. This motivated our design and construction of a spacecraft docking mechanism that would be extremely tolerant of both angular and translational misalignments.

**Mechanical and Electrical Design**

The device consists of two mechanisms, one on each vehicle (Figure 1). One spacecraft has a long, flexible docking probe which would be deployed before the docking procedure. The other vehicle (the tug) is equipped with a funnel-shaped capture cone, which is also deployed in flight. As the two vehicles come together, the tip of the probe slides toward the apex of the capture cone, where it is latched. The probe is then retracted, pulling the vehicles together and, at the same time, collapsing the capture cone. All motions are carried out electro-mechanically. At the end of the maneuver, the vehicles are rigidly linked, which would then allow the transfer of propellant, the application of thrust, or whatever else is required.

The dynamics of the capture is, at least in principle, very complicated, since it involves twelve degrees of freedom (six for each vehicle). To simplify the analysis, the probe was considered to be telescoping, with specified spring and damping characteristics. The forces and moments on the two spacecraft were computed as functions of the relative displacements and velocities. To further simplify the analysis, one of the vehicles was

assumed to be much heavier than the other and having much larger moments of inertia. The resulting simplified equations of motion were integrated numerically for several cases, obtaining their force and moment histories.

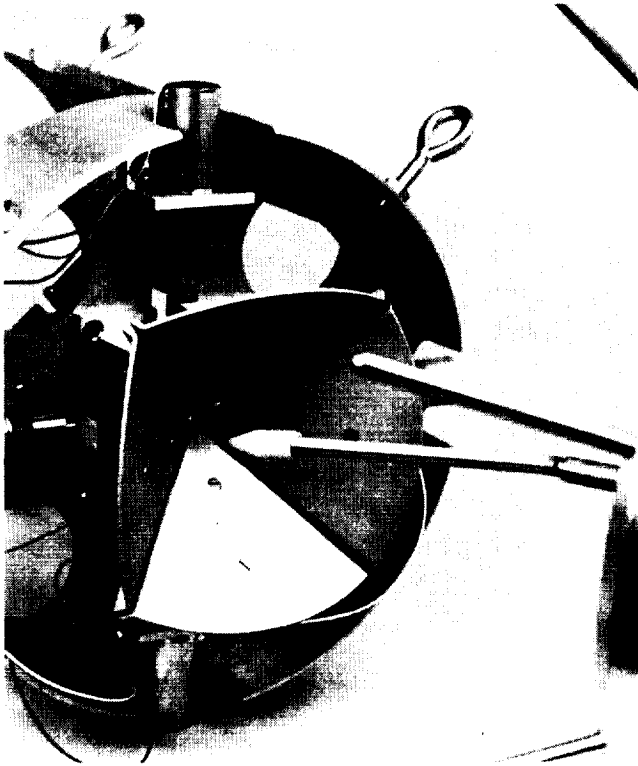


Fig. 1 Student-designed grappling/docking mechanism. Deployable capture cone (left), flexible probe (right).

Models were constructed to demonstrate feasibility. Through testing it was shown that a reliable docking could be accomplished with lateral misalignments of up to one half of the spacecraft radius, and angular misalignments of up to twenty degrees. While there is a significant amount of hardware involved in the grappling mechanism, it is simple, and only a small part of it would have to be on the spacecraft. The larger, heavier, and more complex capture cone would be on the servicing vehicle, under the assumption that one such spacecraft could service several spacecraft. The weight penalty to a spacecraft incorporating such a system would not be insignificant, but would be well justified for missions requiring periodic maintenance, and possibly for other missions as well.

## HARDWARE DESIGN OF A SPHERICAL MINI-ROVER

John Tarlton

### Abstract

In this hardware project the students designed the prototype of a novel mini-rover for the exploration of a planetary surface. In an actual application, a large number of such miniature roving devices would be released from a landing craft. Each rover would be equipped with a Cd 109 radio-isotope source (a gamma ray emitter) irradiating the planetary surface below the rover, and an x-ray fluorescence detector for a quantitative assay of high atomic weight elements in the planet's surface. (Similar, miniaturized, hand-held devices have recently been developed for use in gold mines). The device developed by the students was limited to demonstrating the mechanical and electrical drive. The geometric external shape is a sphere; hence there is no danger of the rover being turned on its back and stopped. Propulsion is by means of an interior mass, eccentric to the sphere and driven by an electric motor. In an inter-disciplinary effort in mechanical and electrical engineering, the students designed the mechanical parts, built the transistorized circuit board, and tested the device.

### Introduction

Robotic planetary exploration vehicles have been designed at a number of research centers. An example is Rocky III, designed and built at the NASA Jet Propulsion Laboratory. It has already demonstrated its ability to go over rough terrain and to pick up rock or soil samples with its manipulator arm. Another well-known example is the Russian Mars rover Marsokhod.

While most planetary rovers use some form of wheels for locomotion, we decided to develop an extremely simple miniature vehicle having the shape of a sphere. Propulsion is by means of a mass, interior to the sphere. The torque from an electric motor lifts the eccentric mass against gravity, thereby inducing a rotation of the sphere. A prototype, designed by the students and built by the University machine shop, is shown in Figure 2.

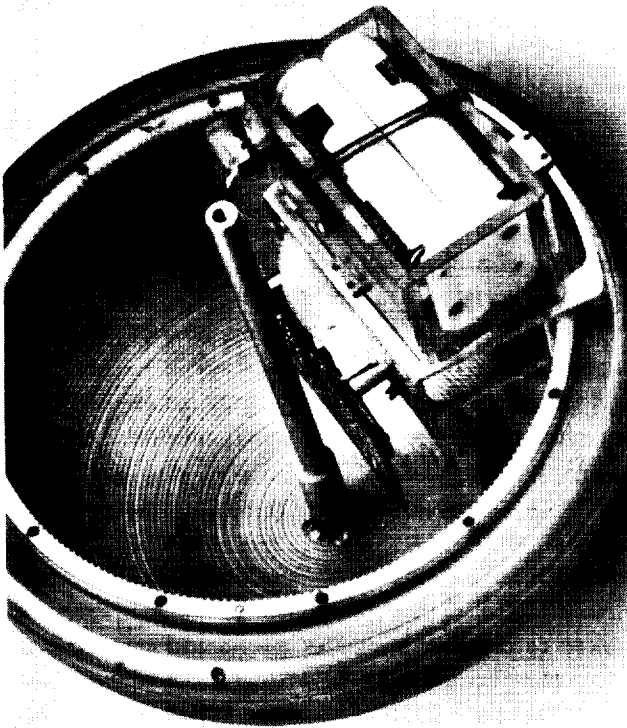


Fig. 2 Student-designed prototype of a spherical mini-rover for planetary exploration

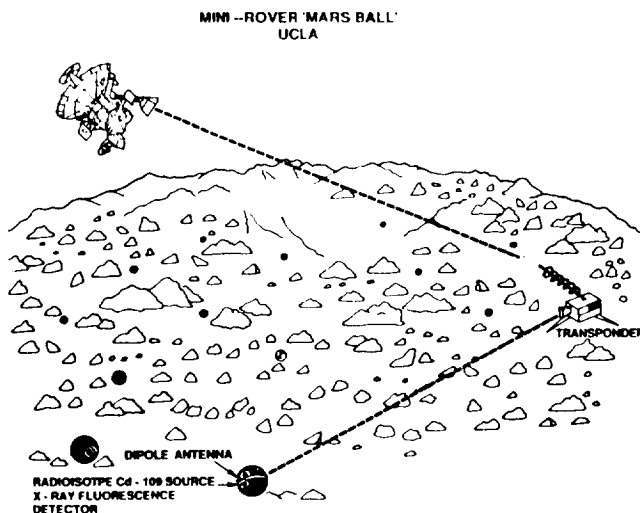


Fig. 3 Random motion, spherical mini-rovers released from a landing craft on Mars

In an actual application to planetary exploration, a large number of these spheres, each one perhaps no larger than five inches in diameter, would be released from a planetary lander. Their paths on a rough surface would be essentially random (Figure 3). In contrast to wheeled vehicles that can tip over, the eccentric mass and its drive mechanism can be designed such that no matter the orientation of the sphere, it can always recover the orientation needed for forward motion.

### Mechanical and Electrical Design

The model designed by the students is limited to demonstrating the mechanical and electrical drive of such a rover. In an actual application, the spheres would be equipped with a cadmium 109 radio-isotope source (a gamma ray emitter), irradiating the planetary surface below. A germanium crystal detector then would receive the x-ray fluorescence resulting from the gamma rays, and would allow one to determine the composition by elements, even if present only in trace amounts. A miniaturized, hand-held device of this type has recently been developed by the South African Bureau of Mines for use in gold mines.

The mini-rover designed by the students has the following features: (1) An eccentric, rotating mass consisting primarily of the source of electric power (dry cells); (2) a DC permanent magnet electric motor driving a pinion and ring-gear; (3) a circuit board for the control of the motor; (4) two hemispherical shells, electrically insulated from each other, which - in an actual application - would be used as a dipole antenna for data transmission (Figure 4). The similarities and differences between the student-designed rover and an actual mini-rover of this type are listed in Table 1.

An additional feature of the student-designed device is the rover's capability to back-off and reverse course when stopped by an obstacle such as a rock. Circuitry is provided to determine when the motor current exceeds a set threshold, an indication that the motor has stalled. If so, after a two-second time interval, the motor current is reversed. The rover then backs off and starts on a new path. In an interdisciplinary effort, the students designed not only the mechanical parts, but also designed and built the circuit board (Figure 5).





# MANNED MISSION TO MARS WITH PERIODIC REFUELING FROM ELECTRICALLY PROPELLED TANKERS

Laura Gogan, Joseph Melko, Fritz Wang

and

Ecole Polytechnique F  minine  
Sceaux, France

Professor Daniel Lourme

Sophie Ben Moha, Christ  le Lardon, Muriel Richard

## Abstract

In a joint study by students from the Ecole Polytechnique F  minine, France, and the University of California, Los Angeles, a mission concept that had the objective of evaluating the feasibility of a non-nuclear, yet fast, manned mission to Mars was considered. Ion-engine propelled tankers are postulated that would provide mid-course refueling of LOX and LH<sub>2</sub> to the manned ship. The scenario is therefore one of a "split mission", yet with the added feature that the cargo ships include tankers for mid-course refueling. The present study is a continuation of one first conducted last year. Emphasis this year was on the design of the tanker fleet.

## Introduction

Ion engine and other electric thrusters can have a very high specific impulse, but, for realistic levels of electric power on a space vehicle, have low thrust, resulting in very long travel times. In this mission study, it is proposed to combine the advantage of ion engines (high Isp) with the advantage of chemical propulsion (high thrust), by mid-course refueling the chemically propelled, fast, manned ship by means of electrically propelled tankers that would be launched several years ahead of the manned mission (Figures 6 and 7).

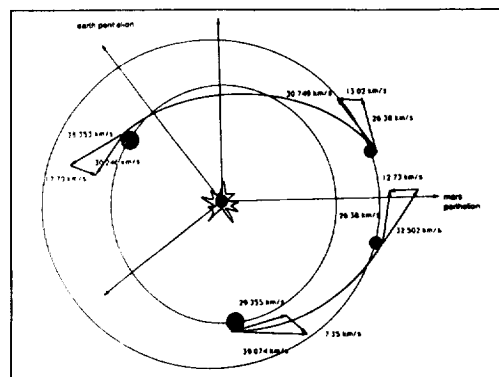


Fig. 6 Manned ship velocities in the Earth, Sun, Mars frames of reference

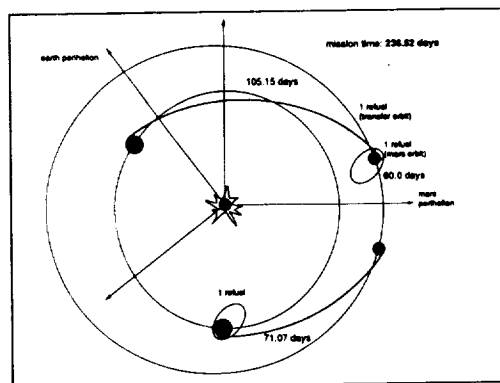


Fig. 7 Refueling points and elapsed days for the manned ship

Refueling a ship  $n$  times is equivalent to an  $(n + 1)$ -fold increase of its Isp. Because of the very high Isp of the electrically propelled tankers, the total mass that must be assembled in LEO is decreased in comparison with more conventional mission scenarios.

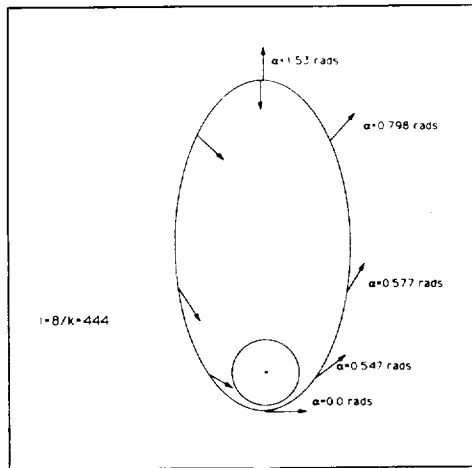


Fig. 8 Computed direction of the ion engine thrust needed for a sequence of orbits with constant periapsis radius

To allow rendezvous with a manned ship on a fast, hyperbolic trajectory leaving Earth or Mars, it is necessary for the tankers to follow trajectories which are characterized by a constant periapsis radius. This requires thrusting at an angle to the instantaneous direction of travel (Figure 8). Numerical studies of such trajectories have been carried out in sufficient detail to allow sizing of the ion engines and determining the propellant (argon) mass and the electric power requirement. A nuclear reactor of an upgraded SNAP-100 type was assumed, and the designs of power conversion equipment and radiators considered.

The difficult problem of long term storage in space of cryogenic propellants was considered, including the need for the re-condensation of the boil-off. The study also addressed the overall design of the tanker fleet, including their assembly in low earth-orbit.

Table 2 Mission events

- |    |   |
|----|---|
| A. | Manned ship is fueled, leaves LEO, escapes Earth, begins Earth-Mars Transfer (EMT). |
| B. | Manned ship rendezvous with Tanker #2, boosts                                       |

for EMT.

- |      |  |
|------|--|
| B/C. | Rendezvous with Tanker #3 during EMT.  |
| D.   | Manned ship aerobrakes and circularizes into Mars parking orbit.                       |
| E.   | Manned ship descends to Martian surface; surface exploration.                          |
| F.   | Manned ship rendezvous with Tanker #4, escapes Mars, begins Mars-Earth Transfer (MET). |
| G.   | Manned ship rendezvous with Tanker #5, completes boost for MET.                        |
| H.   | Manned ship retrofires with remaining fuel at Earth vicinity.                          |
| J.   | Manned ship aerobrakes to capture at Earth and return to LEO.                          |

This project was divided into five areas of specialization:

**Trajectories:** Determine the most efficient paths to get the tankers to the proper place at the correct velocity, at the proper time. Start times, start positions, thrust directions, and coast times. **Power Systems:** Narrow down possible power system scenarios. Select equipment for the chosen scheme. Determine shielding needs if nuclear power is used. Optimize the design by minimizing mass. **Aerobraking:** Determine the feasibility of, and requirements for, aerobraking at Mars to position tankers 4 and 5. Find configuration design constraints. Find the aerobraking trajectories and the aeroshield temperature distribution. Analyze possible alternatives to aerobraking. **Thermal Control:** Consider energy management and thermal environment control. Cryogenic recondensation of boil-off. Analysis of heat transfer during different mission stages or events. **Mechanical Design:** Develop the general physical configuration of the spacecraft. Integration of subsystems.

### **Design Specifications**

Certain initial assumptions and estimates were made to allow concurrent trajectory and tanker design. Mass was estimated at 330 metric tons. A thrust level of 40 newtons was chosen. Ion engines capable of a specific impulse of 16,000 seconds were chosen for the main propulsion system. The mass of the manned ship is assumed to be 35 metric tons without fuel.

Since safety is a primary concern, the scenario proposes sending out more tankers than the minimum of five required for a first mission. The more tankers that are available en route to Mars, the greater the safety. A network of tankers would allow for aborting the mission at any time and would allow for possible mechanical malfunctions of a specific tanker during the refueling process. The scenario is modeled on the assumption that there will be subsequent missions using the same fuel and refueling process. The extra tankers would then be utilized in later missions.

The project focuses on the design of the tankers and their mission profiles.

The tankers are required to place 189 metric tons of LOX and 27 metric tons of  $\text{LH}_2$  at the correct point in space, at the proper velocity, and at a specific time. In addition, the tankers must have the extra thrust capability to allow for a launch window of six days and a 6-day fueling opportunity for the manned ship. Auxiliary propulsion systems which allow for quick course changes must be provided for. The tanker must also bear the burden of maneuvering for docking.

Choosing the best source for the propellants is very important for this mission. These propellants will make up about 71% of the total tanker mass. The LOX alone will be 62% of the total tanker mass. The sources investigated were Earth, the moon, Mars, and Phobos. Sources were compared on the basis of the amount of mass which must be placed in LEO, development cost, initial equipment/mass investment, propellant transportation, and the probability of mission success.

Phobos may be the best source due to its location and extremely low gravity. The low gravity allows the tankers to take propellants directly from the surface rather than by rendezvous with chemically propelled surface-to-orbit

transport vehicles. This method would be very time efficient for tankers 4 and 5 as only 30% of the total tanker mass must be transported to Mars vicinity. It may be possible to have tanker 5 bring the production and storage equipment to Phobos and first fill tanker 5 and then fill its own tanks. The Phobos facility would replace the fourth tanker, fuel tanker 5, and refuel the tankers heading back to earth.

Although Phobos appears to be the most efficient propellant source, in our baseline design oxygen produced on the moon and ground-produced hydrogen will be used. Later missions may exploit Phobos, but the added complications pose too great a risk to the initial missions and too much of an investment. In addition, LOX production on the moon is assumed to have already begun as part of a moon base project. The acquisition of LOX on the moon greatly reduces tanker mission time and surface-to-orbit transfer costs when compared with LOX brought up from the earth to LEO.

Tanker 1 will collect LOX at the moon and return to LEO. (The manned ship will be in LEO and will receive the  $\text{LH}_2$  directly from earth.) Tankers 2, 3, 4, and 5 will receive  $\text{LH}_2$  in LEO and then move out to the moon to receive the LOX. They will continue on their missions without returning to LEO.

### **Power Systems**

The propulsion estimates translate into an electrical power requirement of approximately 4 megawatts.

Nuclear electric and solar electric means of producing the electrical power for the tankers were studied. Estimates of solar array size showed the required area to be larger than 40,000 square meters or roughly eight football fields. Initial weight estimates for the nuclear electric power system gave 24 metric tons. Therefore, the solar array, support structure, and servicing systems had to weigh less than 24 metric tons to be competitive. Achieving the required structural stiffness for such a sizable array appeared to be very difficult. In addition, the array orientation requirements and size severely restricted the tanker configuration. Aerobraking would be impossible, as a structure this large and fragile could not be folded behind the aerobrake and would be subjected to the g-loads required. The solar array would

not produce the public concern associated with nuclear systems, and would require much less development time. Nuclear electric power was chosen for the tanker ships.

**Reactor.** An extension of the SP-100 program would offer the most suitable nuclear power system based on power-to-weight ratios. The reactor would be a lithium-cooled "pin-type" reactor with advanced "PWC-11" cladding and structure configurations. Heat pipes transport the thermal energy to the power conversion equipment.

**Radiation Shield.** Shield size, weight and shape are determined by the size of the nuclear reactor and the vehicle configuration. The shield does not have to be man-rated, which greatly reduces its weight. It is only needed for the protection of the electronic equipment during the tanker's lifetime. Efficient shielding is accomplished by placing a circular shield on one end of the reactor and placing the rest of the tanker in the conical safe zone. Increasing the distance of electrical systems from the reactor reduces the required shield thickness.

**Power Conversion System.** A potassium Rankine cycle and a free piston Stirling engine were studied as possible candidates. The potassium Rankine system is more developed and is lighter than the Stirling engine for the required power levels. However, the Stirling engine is believed to have potentially greater efficiency. This translates into a lower thermal power requirement which reduces the reactor size, and therefore the shield mass. In addition, less waste heat must be radiated which greatly reduces the radiator size and mass. The free piston is the only moving part and there are no sliding seals. The piston works with a linear alternator. Research into Stirling engines at high power levels is currently underway and is expected to be mature by the mission time. An axial opposing cylinder configuration will further reduce vibrations.

**Radiator.** Heat is transported to the radiator and distributed by a series of heat pipes. The radiator is conical in shape to stay just within the reactor radiation safe zone. A reflector plate may be added at the end of a cylindrical or flat sided radiator to create the conical safe zone, without affecting the radiator heat transfer rate.

## Aerobraking

The given constraints on our design were that the tankers should withstand a maximum of 5 g deceleration. The change in velocity can be a maximum of 8.5 km/s when entering the Martian atmosphere. Aerobraking was considered as an option for slowing when approaching Mars. This operation performs the necessary aero-assisted capture and orbit transfer by utilizing its aerodynamic surface to produce drag and some lift. Important factors in an aerobrake capture system are the flight path angle, the ballistic coefficient, the closure angle, which is found to be 22° from various trade-off studies, and the lift-to-drag ratio.

For successful aerocapture, planetary features of the Martian atmosphere are an important consideration. Density and temperature can change dramatically due to seasonal and weather changes such as the very frequent dust storms on Mars. Estimates of the Martian atmospheric density are presently uncertain. Early missions will be necessary to develop confidence in analyzing and predicting the planetary characteristics. The surface terrain such as mountain ranges are an important factor as well.

The initial research into aerobraking focused on necessary size, shape, thermal, and flight characteristics. High L/D aerobrakes were initially considered but were rejected due to their large masses. Biconics seem to have extremely high point heating that pushes material limits. Raked spherical cones have reasonable mass and heating characteristics, but the low L/D ratio complicates control. Ballutes are much lighter than other aerobrakes, but they require a coolant load that negates any overall mass savings as compared to the raked spherical cone. The raked-spherical cone was therefore chosen as the best option.

Material selection and construction of the aerobrake become very significant, especially considering possible fatigue and thermal expansion. Stagnation point temperatures over 2400° Kelvin were found for some entries. Mass of the aerobrake and heat transfer to the cryogenics raise serious questions about aerobraking.

Nuclear thermal propulsion retro-firing was analyzed as a possible alternative to aerobraking. This system would need a very large amount of propellant that would make it

much heavier than the aerobrake configuration.

Another possibility uses the ion propulsion system for deceleration as well as acceleration. This increases the mission and operating time but the tanker mass savings would be approximately 10% when compared with the aerobrake configuration. A combination of ion propulsion and low energy trajectory to Mars moves a 308 metric ton tanker in approximately 580 days. For the tankers, ion engine retro-thrust is a very favorable alternative to aerobraking.

### Thermal Analysis

Thermal analysis is crucial to the successful design of the tankers. It encompasses every aspect of the tankers' main functions and requirements. The most important considerations are those that deal with the fuel tanks for the liquid propellants. The liquid hydrogen and oxygen have very low vaporization temperatures, approximately 20° Kelvin for LH<sub>2</sub> and 90° Kelvin for the LOX. Any heat added to the tanks may cause the propellants to warm and vaporize, which could be catastrophic to the mission. The first objective was to design a successful thermal blanket configuration for the LOX tank, first with radiation effects taken into account only, then including conduction. It was necessary to examine different materials in order to select the best possible configuration for a multi-layer insulation blanket. An available option was to use very optimistic values for the radiative properties of the materials. For example, absorptivity values were used in the range of 0.04 for the top layer of the blankets in order to greatly decrease the heat flux.

The next main problem for the thermal analysis was to see if refrigeration cycles were needed to keep the propellants from vaporizing, and if so, to design a successful configuration. An idea proposed was to use concentric cylindrical tanks for the LH<sub>2</sub> and LOX. This concept was not used, however, because it brought up many complications including fuel transfer, and extra weight. If two separate tanks were being designed, a refrigeration system for at least the liquid hydrogen tank becomes necessary. Possible suggestions included the use of Stirling engines and sorption pumps. One system that was studied was the Molecular Absorption Cryogenic Cooler proposed by a design team from the Jet Propulsion Laboratory, using the Joule-Thompson

process and using waste heat from the power conversion cycle (Figure 9).

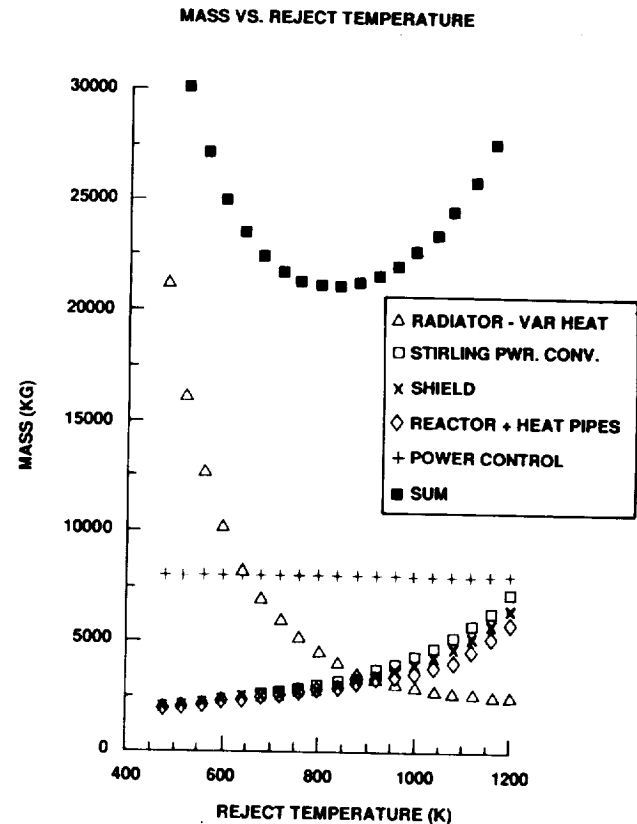


Fig. 9 Mass of refrigeration system vs. radiator temperature, for Stirling engine power conversion

Other thermal problems studied were the effects from excessive heating from the aerobrake, and the exchange of fuel. Thermal problems also could arise from the proximity of the tanks to the aeroshell.

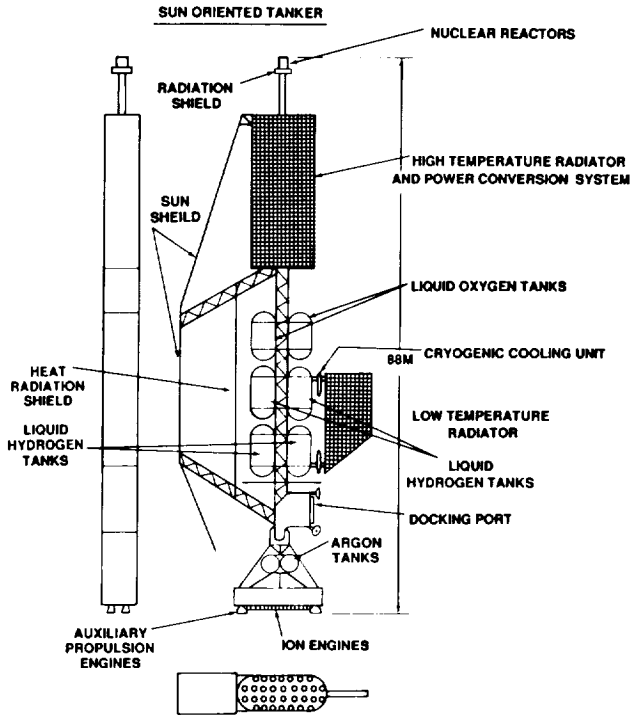


Fig 10 Sun-oriented tanker ship

### Mechanical Design

Emphasis was placed on the required mass in LEO as a rough indication of project cost. Other considerations included: (1) Maximize reliability, lifetime and reusability; (2) Minimize complexity; (3) Minimize the number of moving parts; (4) Minimize sliding seals; *no exterior sliding seals in gas storage systems*; (5) Minimize the use of flexible fluid lines; (6) Provide redundancy; (7) Connect independent systems in parallel; (8) Provide resistance for meteoroid damage; (9) Minimize on-orbit assembly; (10) Provide capability for emergency propulsion of the manned ship; (11) Provide docking clearance for ion and auxiliary engine exhaust cones; (12) Allow access for auxiliary engines to the main LOX and LH<sub>2</sub> tanks; (13) Place center of gravity of the docked configuration on a possible thrust vector; (14) Locate habited section of the manned ship in the radiation safe zone.

### Sun-oriented vs. axisymmetric slowly spinning ("Rotisserie Mode")

A sun-oriented tanker (Figure 10) has the mass benefits of less tank insulation and of a smaller cryogenic cooling system. Thermal fatigue is minimal.

An axisymmetric tanker is more conventional and has more mission flexibility. The tanker's spin sets up forces that make the separation of liquid and vapor easier. The refrigeration system is larger than in the previous configuration and requires extra equipment to cool to ultra low temperatures. More tank insulation is also needed.

### Baseline design

The baseline design (Figures 11 and 12) does not use aero-braking, is axisymmetric and thermally rolled about its axis of largest moment of inertia. The configuration is very stable and may rotate while docked. No configuration movements or adjustments are needed to accomplish all design objectives. Simplicity of control and a reduced LH<sub>2</sub> loss possibility were deemed more important than cooling system mass savings. The extra fuel and systems for the sun-oriented tanker tend to minimize possible mass savings. Microgravity vapor/fluid separation will make the refueling and refrigeration process more efficient.

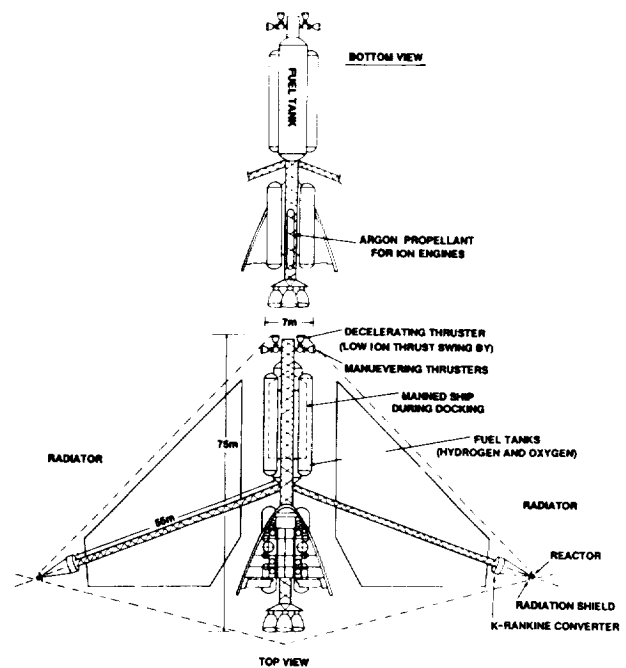


Fig. 11 Electrically propelled tanker, Alternative I

## **Optimization**

Once the general configuration was set, each subsystem was optimized for minimal mass. Figure 9 shows the optimization to find the best combinations. The individual curves were found by interpolating between estimates given in the literature and making certain assumptions. As an example, radiator mass was assumed proportional to area. The cryogenic storage system optimization followed the same procedure. Variables were tank wall thickness, LH<sub>2</sub> storage temperature (affects pressure), insulation thickness, low temperature radiator masses and sorbent pump mass. The power for the sorbent pump is reactor waste heat so the total power requirement is not affected.



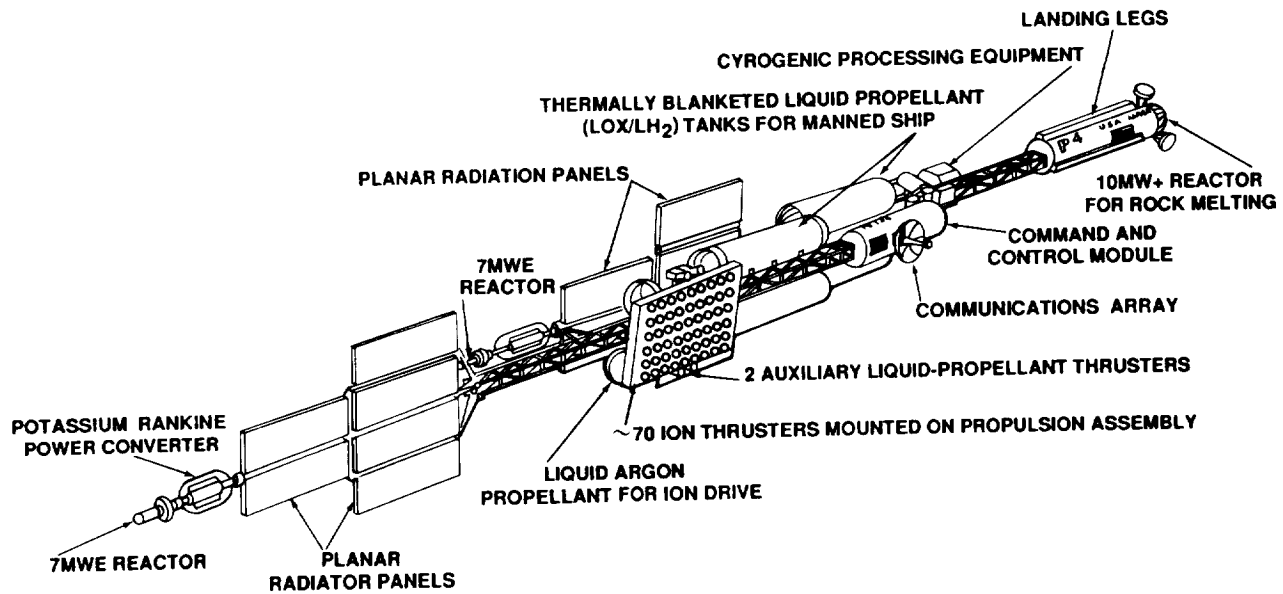


Fig 12 Electrically propelled tanker, Alternative II.

Table 3 Mass summary

|   |            |
|---|------------|
| Power System  | 27,000 kg  |
| Propulsion<br>Includes auxiliary engines and control thrusters. | 12,000 kg  |
| Cryogenic Storage System  | 5,700 kg   |
| Guidance, Navigation and Communications                         | 300 kg     |
| Structure   | 2,500 kg   |
| Docking Unit/Miscellaneous                                      | 3,000 kg   |
| Argon   | 35,000 kg  |
| LOX (auxiliary propulsion fuel included)                        | 204,120 kg |
| LH <sub>2</sub> (auxiliary propulsion fuel included)            | 29,160 kg  |
| Fully loaded tanker   | 318,780 kg |
| Mass in LEO (tanker)  | 114,660 kg |
| Mass in LEO (mission)   | 580,300 kg |

Table 4 Design summary

|   |  |
|---|--|
| Main propulsion   | 60 electron bombardment ion engines. Specific impulse: 16,000 seconds                    |
| Power system  | 4 MW .SP-100 type nuclear reactors (4). 1.4 MW free piston Stirling power converters (4) |
| Cooling system  | Molecular absorption cryogenic coolers with precool systems                              |
| Truss structures  | Ultra high modulus carbon fiber/epoxy tubes with aluminum end fittings                   |
| Tanker positioning is done mostly with the ion engines. <i>Aerobraking is not used.</i> |  |
| LOX is acquired from the moon. LH <sub>2</sub> is brought from earth.                   |  |

ASSURED CREW RETURN VEHICLE  
POST LANDING CONFIGURATION  
DESIGN AND TEST

University of Central Florida  
Mechanical and Aerospace Engineering  
Orlando, Florida

Professor Loren A. Anderson  
Pamela Kay Armitage, Teaching Assistant

### Abstract

The 1991-1992 senior Mechanical and Aerospace Engineering Design class continued work on the post landing configurations for the Assured Crew Return Vehicle (ACRV) and the Emergency Egress Couch (EEC). The ACRV will be permanently docked to Space Station *Freedom*, fulfilling NASA's commitment of Assured Crew Return Capability in the event of an accident or illness aboard Space Station *Freedom*. The EEC provides medical support and a transportation surface for an incapacitated crew member. The objective of the projects was to give the ACRV Project Office data to feed into their feasibility studies. Four design teams were given the task of developing models with dynamically and geometrically scaled characteristics. Groups one and two combined efforts to design a one-fifth scale model of the Apollo Command Module derivative, an on-board flotation system, and a lift attachment point system. This model was designed to test the feasibility of a rigid flotation and stabilization system and to determine the dynamics associated with lifting the vehicle during retrieval. However, due to priorities, it was not built. Group three designed a one-fifth scale model of the Johnson Space Center (JSC) benchmark configuration, the Station Crew Return Alternative Module (SCRAM) with a lift attachment point system. This model helped to determine the flotation and lifting characteristics of the SCRAM configuration. Group four designed a full scale EEC with changeable geometric and dynamic characteristics. This model provided data on the geometric characteristics of the EEC and on the placement of the CG and moment of inertia. It also gave the helicopter rescue personnel direct input to the feasibility study.

### Introduction

For years, America's journey into space has demonstrated the benefits associated with working in the unique environment of microgravity. Continuing in this tradition,

an ambitious and far-reaching program to further the advancement of space technology has been launched. With Space Station *Freedom* the United States enters an era marked by a permanent presence in space. The space station allows continuous rather than intermittent operations to be conducted in orbit. The space station opens doors to many new methods of research and experimentation. Included are better opportunities to observe the Earth and forecast future trends from a vantage point only partially exploited by previous shuttle missions.

Space Station *Freedom* is planned to initially have a crew of four, expandable to a permanent crew of eight. The crew will be rotated and resupplied by flights of the Orbiter on an interval currently planned for three months. Because of the isolation and potentially hazardous conditions involved in space operations, NASA is committed to the policy of Assured Crew Return Capability for Space Station crews in the event (1) a medical emergency occurs and an ill, injured, or deconditioned crewmember must be rapidly transported from the Space Station to a definitive health care facility on Earth; (2) a space station catastrophe forces a rapid evacuation of the crew from the station; and/or (3) the Space Shuttle Program (SSP) system becomes unavailable, and an orderly evacuation of the crew from the space station becomes necessary.

These events, or Design Reference Missions (DRMs), can be met by a concept known as the Assured Crew Return Vehicle (ACRV). Currently, NASA is considering three classes of ACRVs: water landers, runway landers, and open land or nonrunway landers.

The project objectives detailed in this report were developed in conjunction with the Kennedy Space Center ACRV Project Manager and are focused on requirements for a water landing ACRV and post landing operations. The craft configurations include an Apollo Command Module derivative (ACMD) and a Station Crew Return Alternative Module (SCRAM). The designs presented are: a one-fifth

scale model of the ACMD with a lift attachment point system; a one-fifth scale model of an on-board Apollo Flotation and Stabilization system; a one-fifth scale model of the SCRAM with a lift attachment point system; and a full scale model of an Emergency Egress Couch.

### **Previous UCF ACRV Projects**

The UCF senior-level Mechanical and Aerospace Engineering Design class has been working with the ACRV Project Office at KSC since 1989. During the 1989-1990 academic year four design considerations and solutions were investigated.

The first consideration was providing crew egress and rescue personnel support subsystems to ensure the safe and rapid removal of an ill or injured crewmember from the ACRV by recovery forces. An Emergency Egress Couch was designed to medically support a sick or injured crewmember during the ACRV mission. To move the couch from the floor to the hatch, a Four Link Injured Personnel Egress Mechanism (FLIPEM) was developed.

The second consideration was the proper orientation, attitude control, and stabilization systems required for the ACRV in the marine environment. Post landing orientation of the ACRV is achieved through the use of three CO<sub>2</sub> charged balloons similar to those used during the Apollo program. Attitude control systems were designed that deploy three multichambered ring segments and an appurtenance to act as a platform for the rescue personnel. Multiple underwater parachute assemblies were designed to provide motion reduction.

The third consideration dealt with providing full medical support to an ill, injured, or deconditioned crewmember aboard the ACRV from the time of separation from the space station to rescue by recovery forces. Extensive research was performed to select suitable medical support equipment and monitors as required by NASA. Equipment was integrated into unified packages and power requirements were addressed.

The fourth consideration was to provide for the comfort and safety of the entire crew from splashdown to the time of rescue. Design solutions were presented for food, water, waste management, atmosphere, contaminant/odor control, and environmental control systems.<sup>1</sup>

The format for the senior-level design class changed in the 1990-1991 academic year. The design requirement was increased from one semester to two semesters. The students

now design during the fall semester and build and test during the spring semester. The work continued on post landing operations for the water landing ACRV. The design objectives for this class were to determine the feasibility of the previously developed egress and stabilization systems for deployment on the ACRV. Four design teams were formed.

The first team designed, built, and tested a one-fifth scale model of the ACMD to be used as a test platform for the egress and stabilization systems. Test results indicated small deviations from the size and weight specifications provided by Rockwell International. Hardpoint accommodations and seal integrity were maintained throughout the water testing.

The second team worked during the fall semester investigating water test facility locations, as well as establishing designs for a permanent facility at the University of Central Florida. As a result of this investigation, stabilization testing with the ACRV model was performed at the O. H. Hinsdale Wave Research Laboratory (WRL) at Oregon State University in Corvallis, Oregon.

The third team designed, built, and tested a one-fifth scale working model of the Four Link Injured Personnel Egress Mechanism (FLIPEM) optimized in the previous academic year as well as a Two Slider Support Mechanism (TSSM) for egressing the couch out the hatch. Testing was conducted in the areas of lifting force with nominal and off-nominal loads, vertical and horizontal travel distances, redundancy characteristics of the FLIPEM and extension force, travel distance and redundancy characteristics of the TSSM. Test results indicate the design specifications for both systems were met or exceeded without interference to other systems.

The fourth team's objective was to determine, through modeling, the feasibility of reducing heave, surge, and pitch motions of the ACRV model on water using an underwater parachute system. Therefore, one-fifth scale models of the attitude ring and underwater parachute stabilization system, optimized during the previous year, were designed, built, and tested. Wave testing, in simulated sea states 2 to 4, at the O. H. Hinsdale WRL yielded results that indicate that the six-attitude sphere configuration produced minimal stabilizing effects on the ACRV model. The spheres, however, did have the effect of enhancing the flotation characteristics of the model. Numerous parachute arrangements, including single and multiple chutes per cable; an increase in the weight attached; the use of stiff and elastic cables; and devices to partially and totally open the chutes were tested. Results indicate that the parachutes did affect the motions induced on the model, but did not reduce or increase the frequencies out of the range that cause seasickness.<sup>2</sup>

A concept employing a Rocker Stoppers unit was built and tested at the water test facility to determine the effect a rigid system would have on reducing the oscillations. Two Rocker Stoppers were connected, nose-to-nose, at one end of a long threaded rod. The other end of the rod was connected to a metal plate attached to the model above the break line. Four of these arrangements were connected to the model. Since the Rocker Stoppers are made of rigid plastic, they perform the same work on the upstroke as on the downstroke. This configuration was tested in a simulated sea state 4 (1.2 ft wave height, 0.45 Hz) and the response compared with that from the clean model in the same sea state. The results indicate that a rigid system in this configuration reduces the heave amplitude the model experiences.<sup>3</sup>

### 1991-1992 ACRV Design Projects

The results of the testing from the 1990-1991 academic year revealed areas where further data was needed. The ACRV Project Office suggested that the senior-level design class develop designs applicable to the full scale ACRV for water landing and post landing operations. Four areas of interest were identified: craft retrieval or lifting characteristics, the geometric and dynamic characteristics of the EEC, the flotation characteristics of the SCRAM configuration, and the stabilization characteristics of a rigidly mounted flotation system for the ACMD. Four design teams were formed and tasked as follows:

#### Team #1-ACMD Configuration Model

The ACMD Configuration Model Team was to use geometric and dynamic constraints to design a one-fifth scale working model of the Apollo Command Module Derivative (ACMD) configuration with a Lift Attachment Point (LAP) system. This model was required to incorporate a rigidly mounted flotation system and the egress system designed the previous academic year. The LAP system was to be used to determine the dynamic effects of locating the lifting points at different locations. The team was then to build and test the model; however, due to higher priorities, this did not occur.

#### Team #2-ACMD Flotation Model

The ACMD Flotation Model team was to design, build, and test a one-fifth scale model of a flotation system. The flotation system had to move rigidly with the craft and provide a rigid work surface for the rescue personnel. The team was to address location, storage, deployment, and release or deflation. The model was not built and tested

because of higher priorities.

#### Team #3-SCRAM Configuration Model

The objective of the SCRAM Configuration Model Team was to design, build, and test a one-fifth scale model of the Johnson Space Center benchmark configuration, Station Crew Return Alternative Module (SCRAM), with a LAP system. They were to address the water retention by the inverted cone shaped heat shield and consider that the area might need to be drained prior to vehicle retrieval.

#### Team #4-EEC Configuration Model

The EEC Configuration Model Team was to design, build, and test a full-scale representation of the Emergency Egress Couch, complete with simulated human weight and medical equipment weight. This model was to include a helicopter recovery system and have changeable geometric and dynamic characteristics.

A one-fifth scale was used both geometrically and dynamically for all ACMD and SCRAM models. To accomplish this a Buckingham Pi dimensional analysis was performed and the Froude scaling factors were determined. These factors allow the model to accurately simulate the characteristics of the full scale craft. While the geometric dimensions of the craft scaled directly by one-fifth, other parameters, including volume, weight, and mass moment of inertia scaled by powers of one-fifth.

### 1991-1992 ACRV Design, Building and Testing Results

#### ACMD Configuration Model

The ACMD Configuration Model team designed a one-fifth scale model based on the Apollo Command Module derivative (ACMD). Current data for the weight and geometric dimensions of the ACMD were supplied by Rockwell International. To better simulate the ACMD after a water landing, the nose cone section was removed and the deck area exposed. The areas researched during the design process were: construction, center of gravity and moment of inertia, and lift attachment points.

Fiberglass was the material chosen for model fabrication. To allow access to the interior of the finished model, the model construction was planned in three pieces: a lower section, an upper section, and a hatch. Planned fabrication of the model consisted of plug, mold, and shell construction. The upper and lower sections of the model attach using

eight aluminum chest latches and a gasket seal. The hatch attaches to the model using a two-inch strap hinge, sealed with a gasket, and locked into place with 1 3/4-in turn buttons.

To incorporate the egress and flotation systems, the model was designed with the necessary space, hardpoints, and attachments. Hardpoints at the connection area of the flotation system distribute the load. These hardpoints consist of 1/8-in pieces of balsa core cut into 3-in squares. These pieces of wood are incorporated into the shell interior with layers of resin. Holes drilled into the floor serve as hardpoints for the egress mechanism.

The center of gravity (CG) and mass moment of inertia (MI) were modeled using a radial system. The radial system consists of two vertical 1/4-in threaded rods. One rod is placed in the top access hatch area and one in the bottom of the model, under the floor. Radial arms are made of hardwood dowels with a hole drilled through their centers. One or more of these arms are positioned along each vertical threaded rod by means of lock nuts. Weights consisting of groups of large metal washers are fastened along the radial arms and held in place with hose clamps on either side of the washer group. These weights are repositioned along the radial arms, as needed. The radial arm positions are varied along the vertical rods. By varying the weight amounts and positions and rotating the radial arms to any angle required, the center of gravity and moment of inertia are changed for accurate simulation (Figure 1). Pendulum tests performed on the empty shell determine the size and weight of the washers required.

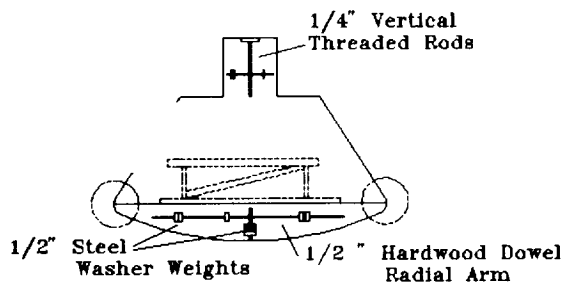


Fig. 1 Radial system, egress system, and flotation system

The Lift Attachment Point (LAP) system used to model retrieval of the craft was a dual attachment system with an angled lift. The dual attachment points offer redundancy. There are two attachment points each with its own sling; however, both are attached to a single lifting cable. The sling angle that offers the least force on the attachment points and the least tension on the cables is 60 degrees. The LAPs are placed on the upper deck area. This location

takes advantage of the parachute reinforcement area and a high location relative to the CG (Figure 2).

### ACMD Flotation Model

The ACMD Flotation Model team designed a one-fifth scale flotation and attitude system for the ACMD. The system forms a rigid body with the ACMD after deployment. Four areas incorporated into the design of this model were: (1) flotation, (2) attitude, (3) materials, and (4) inflation.

The flotation system was designed with a segmented ring constructed out of woven nylon fabric coated with butyl

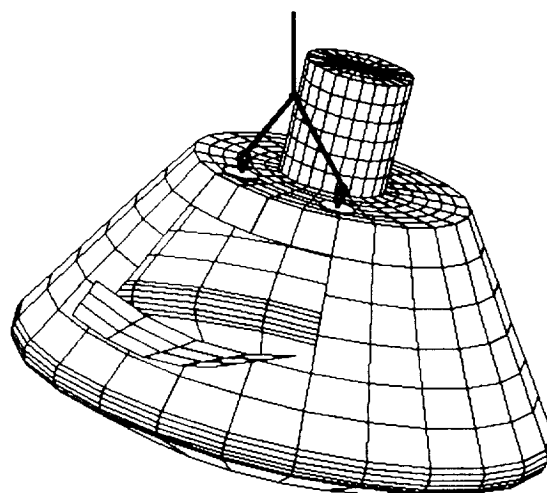


Fig. 2 Deck-mounted dual attachment with angled lift

rubber. This ring is composed of three or more sections, each extending around a portion of the ACMD along the water line. Each segment is stored in compartments along the water line. The storage space required is approximately 1/50 of the inflated volume. The segmented ring allows for the placement of the Reaction Control System jets. A rigid system is obtained by attaching the segmented ring to the ACMD inside the storage compartment and pressurizing the segments to rigidity. The volume of air needed to keep the ACMD model afloat provided it does not float was calculated from Archimedes' principle as 2.05 ft<sup>3</sup>. To achieve this volume, each segment has a radius of 4.6 inches, and the combined length of all segments is 46.3 inches.

The attitude system provides support to the Emergency Egress Couch (EEC) and counters the moment the EEC places on the craft. A telescoping beam configuration

provides the necessary support and attitude control for the EEC. This system consists of aluminum box beams that rotate ninety degrees from their storage position inside the ACMD, then telescope out to a specified length. A rigid surface is rolled out on top of the beams and an inflatable cylinder is attached at the end of the beams to provide the attitude control. The inflatable cylinder is constructed of woven nylon covered with butyl rubber (Figure 3).

The inflation method for the model is a threaded valve similar to that used for automobile tires. These valves are attached to the segmented ring sections and to the inflatable cylinder at the end of the attitude system. The segments are then inflated using a hand or foot pump. Inflation for the full scale ACMD needs further investigation.

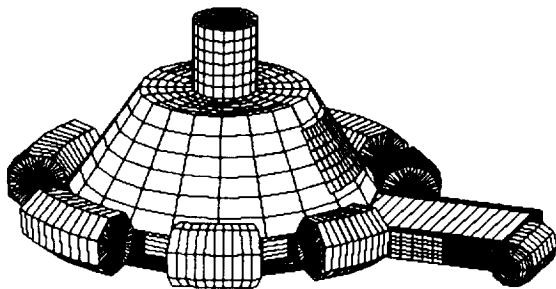


Fig. 3 Complete flotation and attitude systems

### SCRAM Configuration Model

The SCRAM Configuration Model team designed, built, and tested a one-fifth scale model of the Johnson Space Center benchmark configuration, the Station Crew Return Alternative Module (SCRAM). Current data for the geometric and dynamic constraints of the SCRAM were supplied by the ACRV Project Office at Johnson Space Center. Four areas were researched during the design process. These areas were: (1) construction, (2) center of gravity and mass moment systems, (3) heat shield shroud, and (4) lift attachment points.

The construction of the model was contracted to Guard-Lee, Inc. and completed in four sections. The crew compartment, lid, and heat shield were constructed of fiberglass, and the heat shield shroud of sheet aluminum. The lid was attached to the crew compartment by eight bolts and sealed with a weather stripping material. The heat shield was fastened to the crew compartment bottom with four symmetrically placed joints. The heat shield shroud

attached to the lip of the heat shield and the lip at the bottom of the crew compartment cylindrical section with bolts. This assembly was sealed with a silicone-based seal. Locking washers were used on all bolt assemblies to avoid crack propagation from the bolt holes.

The weight, mass moment of inertia, and CG were adjusted with the Adjustable Rotating Weight System (ARWS). The ARWS consists of a length of aluminum flat stock (arm) that is bent on each side 2 in from the center to 18.43 degrees upward and 10.7 in from the center 18.43 degrees downward. Slots are machined in the arm and a hole drilled through the center of the arm. Four wedge-shaped compression blocks mount on risers (threaded rod) that are placed in the arm slots. The compression blocks hold the risers in place. Weights are placed on the risers at the necessary locations and held in place by washers and bolts. A threaded spindle is mounted to a spindle retention plate that is affixed to a wood block fiberglassed to the bottom of the crew compartment. The whole system is placed over the spindle and bolted to the bottom of the crew compartment (Figure 4). This system was machined by F & E Machine, Orlando, Florida.

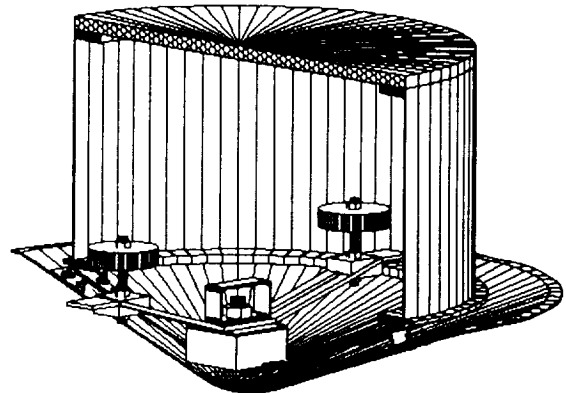


Fig. 4 Adjustable rotating weight system

Attached to the crew compartment lid is the Lift Attachment Point (LAP) system. The system is constructed of 3 pieces of angle iron bolted 90 degrees apart radiating from the center. Multiple holes drilled in the upper portion of the angle iron allow for different angles in the lifting lines. The attachment is accomplished with three D-rings attached to the holes in the angle iron. Three cables are connected to the D-rings and are clamped together at one central cable. The central cable is then attached to the lifting apparatus (Figure 5).

A three-phase test plan was developed to evaluate the

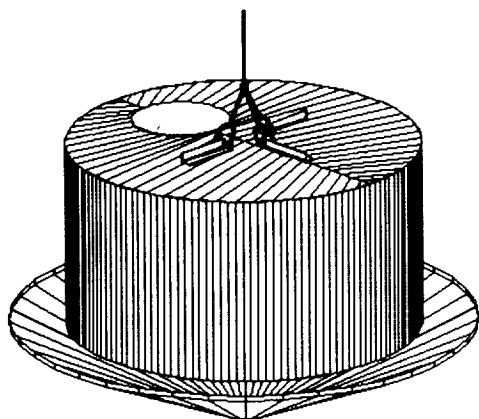


Fig. 5 Lift attachment point system

model. Phase I took place at UCF in the Senior Design Lab and consisted of a series of pre-tests to confirm the SCRAM model met its specifications. The tests included geometric similitude, ease of transportation, CG and mass moment of inertia adjustability, and the rapid and accurate positioning of the ARWS. Test results indicate that the model meets its geometric constraints. Model assembly and disassembly times were 12 and 15 minutes respectively. The required CG offsets are accomplished by accurate placement of the ARWS. Mass moment of inertia data was not specified; therefore, it was not configured to a specific value.

Phase II took place at UCF in the Fluids Lab and consisted of tests to determine the static draft and watertightness of the model, as well as the durability of the LAP system. Test results show the static draft of the craft at 120 lbs without the heat shield shroud is seven in, and with the heat shield shroud is 6 1/4 in. The model did not take on water in either configuration. The LAP system and model showed no signs of failure after a 208-lb static hang test and a 120-lb jerk test.

Phase III took place at Offshore Technology Research Center at Texas A & M University in College Station, Texas. Tests were completed to determine the SCRAM's flotation characteristics as well as various methods of vehicle recovery. This testing involved a number of changes to the model configuration and to the wave environment. Configuration parameters were established and sea state conditions set during the development of the model. All possible combinations of critical parameters could not be evaluated; therefore, a bracketed method of

evaluation was employed. The parameters evaluated were: weight, CG, open/closed heat shield, and sea state. A 76-lb and a 120-lb weight configuration were evaluated. The CG locations that were evaluated were 1.2 in above and 1.2 in below the empty craft CG, and 1.2 in from the vertical axis toward the hatch and away from the hatch. Three wave states were evaluated. The first was an intermediate regular wave state with a .52-ft wave height and a 1.252-second period. The second was a scaled sea state 4 regular wave, with a 1.2-ft wave height and a 2.22-second period. The third wave state was a random wave with a .334-ft average wave height and a 1.118-second average significant period. The test results provide the flotation and lifting characteristics of the SCRAM configuration. Additional design/operational suggestions, which were derived from the test results, were also provided to the ACRV Program. These suggestions were: (1) crew member extraction should not be attempted from a top hatch because of the pitch and heave motions of the craft; (2) the side hatch should be relocated to a higher vertical position to prevent vehicle flooding during crew extraction; (3) attenuators and stabilization loops should be integrated into the lifting crane cables, and the crane lifting capacity should have a safety factor of 5.0; and (4) in the open heat shield configuration, the lift attachment points should allow for lifting the vehicle at an angle to allow for water drainage and a smoother lift in rough seas.

### EEC Configuration Model

The EEC Configuration Model team designed, built, and tested a full scale model of the Emergency Egress Couch (EEC). The dynamic and geometric characteristics of the EEC that best suit the ACRV mission are currently to be determined. The maximum weight and geometric data is known. The EEC can weigh no more than 400 lbs and must not exceed the geometric constraints of  $7 \times 2 \times 1$  ft. The EEC consists of two basic litters, one human weight system, one medical weight system, three layers with flotation, two sets of lift attachment points (LAP), and a cover.

The basic litter was constructed in the UCF Engineering R & D Shop. The material chosen for the basic litter was Chrome-Moly steel tubing with a 1-in outer diameter and a 0.095-in wall thickness.

The basic litter consists of two frames  $7 \times 2$  ft that are joined together by ten 2-in spacers welded between the two frames. The bottom of each frame has three 2-ft runs spaced 1 ft 9 in apart for support. To avoid having any sharp objects on the EEC the corners have a 4-in radius.



The human weight system was a weighted dummy with the same dynamic and geometric characteristics as a human. The dummy weighed 102 lbs with the CG corresponding to the CG of a crewmember. The dummy was secured by strapping it to the upper litter.

The medical weight system is housed in the bottom litter and consists of two movable weight platforms mounted on two support strips along either side of the bottom litter. Weights can be added to vary the total weight of the EEC. The CG and mass moment of inertia can be varied by moving the weight platforms to the desired location.

Layers are used to change the height of the EEC and add flotation. There are three layers, one with a 2-in height and two with a 1-in height. The frames of the layers are  $7 \times 2$  ft and are constructed from pressure-treated wood that has been planed to the proper height. The corners have a 4-in radius for proper interface with the other EEC components. Two attachment holes are located in each 7-ft side of the layer frame. A polystyrene sheet fills the center of each frame for flotation.

Bolts are used to attach all the EEC components together. Both basic litters have two L-brackets welded on each 7-ft side of the litter. The L-brackets have holes drilled in the center. These holes line up with the holes in the layers. To attach the components of the EEC, the bolt passes through the angle iron from the bottom litter, through the layers to the top litter, and is secured by nuts and washers.

The EEC is equipped with two sets of LAPs and allows the harness to be attached in different configurations. The first set of LAPs emulates the LAPs on the Stokes litter. The second set of LAPs is for stability tests. The first set of LAPs are small metal plates that are welded close to the spacers on the top litter. The lift harness carabinier fits securely between the spacer and the metal plate. The second set of LAPs is designated by iron plates welded between the upper and lower tubular frames on the top litter. The lift harness carabinier is put through a semicircular opening cut in the iron plates and secured around the tubular frame (Figure 6).

A three-phase test plan was developed to evaluate the model. Phase I was performed in the UCF Senior Design Lab and consisted of a series of pre-tests to confirm that the EEC model met its specifications. The tests included verifying geometric constraints, weight, CG and mass moment of inertia variability, and safety. Test results indicate that the model meets its geometric constraints. There are no sharp edges and all components fasten securely. The weight, CG and mass moment of inertia are adjustable.

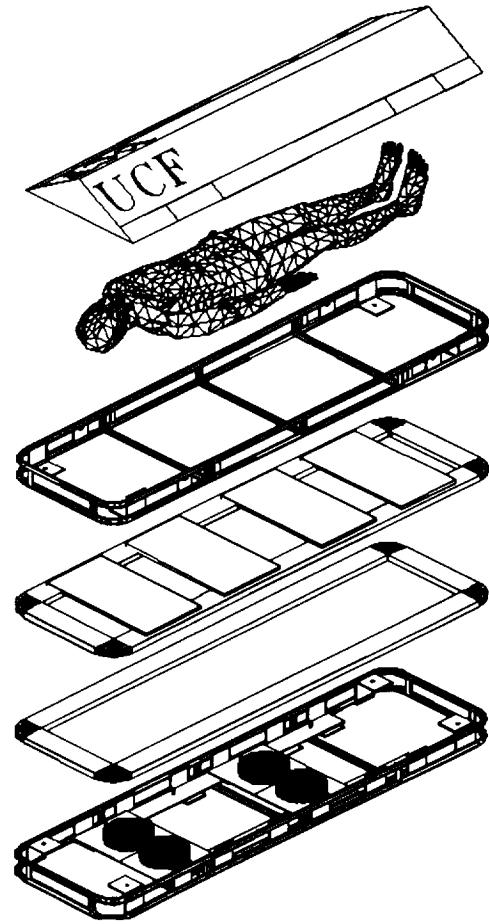


Fig. 6 EEC model

Phase II testing was performed at Patrick Air Force Base (PAFB) with the Department of Defense Manager Space Transportation System Contingency Support Office (DDMS), and the 41st Air Rescue Squadron (ARS). This testing phase consisted of compatibility tests, a spin test, a low hover test, a high hover test, and a slow forward flight test. These tests were performed for six configurations of the EEC. Test results and input from the 41st Air Rescue Squadron indicate that the EEC should be no longer than 6 feet 5 inches and have a tapered width. To use volume efficiently the medical equipment should be placed around the body in the top litter. The CG should be forward (toward the head), and weight should be kept to a minimum (Figure 7).

Phase III testing was performed at the UCF pool. This

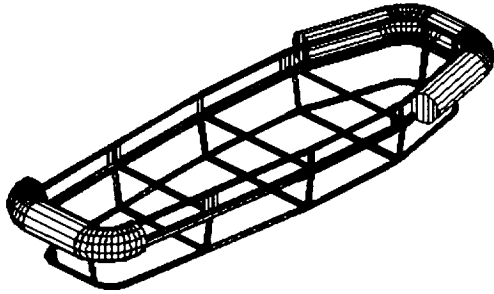


Fig. 7 Recommended configuration

testing phase consisted of flotation tests. These tests revealed that the EEC is buoyant when all layers containing polystyrene are attached. For additional buoyancy and stability, solid side floats that deploy only when necessary and flotation elements placed around the body in the top litter could be used.

### Summary

The 1991-1992 senior Mechanical and Aerospace Engineering Design class completed the design, building, and testing of the Assured Crew Return Vehicle Post Landing Configuration. The objective was to develop designs applicable to the full scale ACRV for water landing and post landing operation and provide data to NASA for feasibility studies. Work was conducted in the following areas: Craft retrieval or lifting characteristics, the geometric and dynamic characteristics of the EEC, the flotation characteristics of the SCRAM configuration, and the stabilization characteristics of a rigidly mounted flotation system for the ACMD.

A one-fifth scale model of the Apollo Command Module Derivative (ACMD) with a Lift Attachment Point (LAP) system was designed by the ACMD Configuration Team. This model incorporates a rigidly mounted flotation and stabilization system and the egress system designed the previous academic year. The LAP system was designed to determine the dynamic effects of locating the lifting points at different locations. This model was not built and tested, because of higher priorities.

The ACMD Flotation Model team designed a one-fifth

scale model of a flotation and stabilization system. The two systems were designed to move rigidly with the craft and provide a rigid work surface for the rescue personnel. This model was to be built and incorporated into the ACMD Configuration Model for testing. However, due to higher priorities this did not occur.

A one-fifth scale model of the Johnson Space Center benchmark configuration, the Station Crew Return Alternative Module (SCRAM) with a LAP system was designed, built and tested by the SCRAM Configuration Model Team. Testing took place in three phases. The fidelity of the model was established from geometric and dynamic characteristic tests performed on the model in Phase I and II. Results indicate that the model meets its geometric constraints, and CG offsets are accomplished by accurate placement of the ARWS. The model did not leak, and the model and LAP system withstood a 120 pound jerk test. Phase III testing took place at Offshore Technology Research Center at Texas A & M University. The facility accommodated all testing configurations and the staff provided excellent support. Tests were completed to determine the SCRAM's flotation characteristics as well as various methods of vehicle recovery. The parameters evaluated were: weight, CG, open/closed heat shield, and sea state. Two weight configurations, four CG locations and three wave states were evaluated. Test results provide the flotation and lifting characteristics of the SCRAM configuration. Additional design/operational suggestions were also provided to the ACRV Program, which were derived from the test results. These suggestions were: (1) Crew Member extraction should not be attempted from a top hatch, (2) The side hatch should be relocated to a higher vertical position, (3) Attenuators and stabilization loops should be integrated into the lifting crane cables, and the crane lifting capacity should have a safety factor of 5.0, (4) In the open heat shield configuration, the lift attachment points should allow for lifting the vehicle at an angle.

The EEC Configuration Model Team completed the design, building and testing of a full scale representation of the Emergency Egress Couch, complete with simulated human weight and medical equipment weight. This model includes a helicopter recovery system and has changeable geometric and dynamic characteristics. Testing occurred in three phases. Phase I results confirm the model meets its geometric constraints, the weight, CG and mass moment of inertia are adjustable, and the model components fasten securely and have no sharp edges. Phase II testing was performed at Patrick Air Force Base (PAFB) with the Department of Defense Manager Space Transportation System Contingency Support Office (DDMS) and the 41st Air Rescue Squadron (ARS). The 41st ARS provided excellent support and accommodated all testing

configurations. Tests were completed on six configurations to determine geometric and dynamic constraints for the EEC. Test results and input from the 41st ARS indicate that the EEC should be no longer than 6 ft 5 in and have a tapered width. To use volume efficiently the medical equipment should be forward and weight should be kept to a minimum. Phase III testing consisted of flotation tests. The tests revealed that the EEC is buoyant when all layers containing polystyrene are attached.

Several recommendations are suggested for future design projects in the area of post landing operations associated with the ACRV. The flotation and wave motion characteristics of the ACRV HL-20 configuration could be examined. The EEC could be redesigned to the recommended configuration and tested for compatibility with the ACRV and the SAR forces. The possibility exists that the Soyuz will be used as the ACRV. Therefore, a need exists to design and test the Soyuz configuration in post landing operations.

### References

- 1 Hosterman, K., and Anderson, L.A., NASA/USRA Final Report 1990, "Post Landing Designs for the Assured Crew Return Vehicle," Department of Mechanical and Aerospace Engineering, University of Central Florida, Orlando, FL, 1990.
- 2 Hosterman, K., and Anderson, L.A., NASA/USRA Final Report 1991, "Design, Building, and Testing of the Post Landing Systems for the Assured Crew Return Vehicle," Department of Mechanical and Aerospace Engineering, University of Central Florida, Orlando, FL, 1991.
- 3 Hosterman, K., Thesis Report and Presentation, "Analysis of a Deployable Heat Shield Stabilization System for a Space Station-based Assured Crew Return Vehicle," Mechanical and Aerospace Engineering, University of Central Florida, Orlando, FL. Spring, 1992.

### Acknowledgments

Appreciation is expressed to the senior design students in Mechanical and Aerospace Engineering who contributed to this work. A special note of appreciation is due to NASA, USRA, DDMS, and the 41st ARS whose sponsorship made this work possible. Additional thanks go to Rockwell International, Lockheed Space Operations, Boeing Aerospace Operations, and McDonnell Douglas Astronautics for their technical support.

**AUTONOMOUS SUPPORT FOR MICROORGANISM RESEARCH IN SPACE**

**University of Colorado  
Aerospace Engineering Sciences  
Boulder, Colorado**

**Professor M. W. Luttgies  
D. M. Klaus, Teaching Assistant  
M. L. Fleet, M. S. Miller, D. E. Shipley, and J. D. Smith**

**Abstract**

A preliminary design for performing on-orbit, autonomous research on microorganisms and cultured cells/tissues is presented. An understanding of gravity and its effects on cells is crucial for space exploration as well as for terrestrial applications. The payload is designed to be compatible with the COMercial Experiment Transported (COMET) launch vehicle, an orbiter middeck locker interface, and with Space Station Freedom. Uplink/downlink capabilities and sample return through controlled reentry are available for all carriers. Autonomous testing activities are preprogrammed with inflight reprogrammability. Sensors for monitoring temperature, pH, light, gravity levels, vibration, and radiation are provided for environmental regulation and experimental data collection. Additional experimental data acquisition includes optical density measurement, microscopy, video, and file photography. Onboard full data storage capabilities are provided. A fluid transfer mechanism is utilized for inoculation, sampling, and nutrient replenishment of experiment cultures. In addition to payload design, representative experiments were developed to ensure scientific objectives remained compatible with hardware capabilities. The project is defined to provide biological data pertinent to extended duration crewed space flight including crew health issues and development of a Controlled Ecological Life Support System (CELSS). In addition, opportunities are opened for investigations leading to commercial applications of space, such as pharmaceutical development, modeling of terrestrial diseases, and material processing.

**Introduction**

Gravity is easily taken for granted, but its constant inertial acceleration affects every aspect of our lives. In fact, gravity affects all Earth's life forms and has done so throughout evolution. The fight against gravity has led to the formation of extremely strong biological support structures such as cellulose, chitin, and bone. Animal movement must first counteract the force of gravity, therefore, muscle and other methods of movement (flagella, cilia, and contractile filaments) must reflect this in their structure and function. Gravity is also responsible for processes such as convection and sedimentation that cells and organisms have evolved to use. Life on Earth today is highly diverse and constantly changing, but no matter what the organism or its habitat, gravity has surely played an important role in its development and life cycle.

Many biological experiments have been performed in the microgravity environment of space to determine what influence gravity has on life. The results: gravity does play an important role in the development and maintenance of life, but the specific mechanisms of gravity perception, adaptation, and use are not well understood. For example, the bodies of astronauts are dramatically altered in microgravity. Bone and muscles decrease, the immune system is weakened, and cardiovascular and neurovestibular systems that control circulation and balance change. Major adaptations adjust the body to the new reduced gravity environment. But how is the presence or absence of gravity sensed by a bone or muscle cell? Why do cells and organisms respond to gravity the way they do? How can these gravitational responses be inhibited to insure astronaut health or enhanced to produce new plants or microorganisms with special desirable traits? The answers to these and many similar questions are unclear, and they will remain unclear until

biology and microbiology can be studied easily and extensively in microgravity.

Space Habitation, a NASA/USRA (National Aeronautics and Space Administration/Universities Space Research Association)-sponsored advanced design class at the University of Colorado, is devoted to addressing issues concerning space life sciences and the commercialization of outer space. In an effort to make the microgravity environment of space more easily accessible for biological research and commercial application, the Spring 1992 class has developed a design for a small, versatile, biological research tool called the Cell Module for Autonomous Space Support (C-MASS). C-MASS meets many current needs for biological research in space and is responsive to the changing directives of today's U.S. space program which emphasize reliable, faster, better, and less expensive missions.

### Background

Since 1958, the U.S. space program has brought the mysteries, challenges, and achievements of space exploration home to America. Recently, millions of viewers witnessed three space-walking astronauts from the Space Shuttle Endeavour working together to capture a stranded communications satellite by hand when hardware built for the job failed to work. The excitement and intrigue generated by space activities such as this provide an incentive propelling the nation forward in science and technology. However, even more important gains have come from scientific information and the many spin-off products and technologies derived throughout the space program. Space exploration, transportation, and life support challenge the limits of today's technology. Advancements in automation, computer technology, miniaturization, and remote sensing have followed. Spin-offs from those advancements include insulative and fire retardant materials, recycling technology, computer software, imaging systems, and medical techniques. Spin-offs mean better products, an increased standard of living, and consumer savings. For example, biotelemetry (the remote sensing of blood pressure, heart rate and rhythm, and temperature using very small, durable, light-weight sensors) was originally developed as a ground-based method to monitor astronauts. Now, biotelemetry packages are used to safely monitor heart attack patients in their own homes. This allows them to return to their

normal activities and eliminates the need for prolonged hospitalization and related medical costs.<sup>1</sup> Excitement in the space program is generated by human achievements like the satellite capture and the economic/technical importance of the space program arises from spin-offs that touch the lives of millions of people each and every day.

An area of great potential is space life sciences; this discipline addresses the issues, among others, of Controlled Ecological Life Support Systems (CELSS), astronaut health, and basic gravitational biology. The bioregenerative aspects of CELSS will greatly reduce the costs and Earth-dependency of life support systems, providing a means to fulfill long-term NASA goals such as a permanent return to the moon. Due to the lack of gravity in orbit, astronauts suffer from accelerated forms of many common ailments found on earth including osteoporosis (mineral loss in bones), muscle atrophy, space sickness, and cardiovascular alterations. For example, on Earth osteoporosis affects over 24 million elderly American today and is the cause of 1.3 million fractured bones each year (at an annual consumer cost of \$7-10 billion).<sup>2</sup> Developing treatment for the health problems astronauts face will lead to cures for diseases people suffer on Earth, saving lives, productivity, and money.

Basic gravitational biology focuses on the basic effects of gravity and mechanisms of gravity sensing in cells. With an understanding of the effects and perceptions of gravity at the level of the single cell, scientists may find ways to use the unique microgravity environment of space to perform biological manipulations or processes not possible on Earth. The value of these biological experiments could be well worth the high investment required for development and flight time. For instance, a single cell genetically altered in space to produce a beneficial byproduct could be brought back to Earth to reproduce, creating entire populations of cells or organisms with the same beneficial trait. In addition, the combination of gravitational biology and the unique environment of space may open the door to future commercial development of space.

The goals of space life sciences and the returns it will provide cannot be achieved instantly. A phased mission approach is required which employs many small missions, each contributing new technology, information, protocols,

and even spin-offs to bring the space program closer to its long-term goals in a step-by-step process. The phased mission approach is consistent with the Space Exploration Initiative (SEI), the new directive for the U.S. space program. SEI has a twofold strategy: "First, to develop and conduct small scale robotic/automated precursor missions designed to fill gaps in the nation's scientific and technological knowledge," and second to establish a "management culture" that can be relied upon to get the job done on time and for less money.<sup>3</sup> This new emphasis on smaller, low-cost payloads will allow industries and research organizations to get involved, transforming the space program into a search for commercial applications and developments as well as a mission of science and exploration.

Space life sciences is one of the gaps in scientific and technological knowledge to which SEI refers. As an empirical science, it depends on multiple tests done in the space environment. Early missions placed little emphasis on life sciences beyond the minimum necessary to sustain humans for a voyage to the moon and back. Today, principal investigators like biologists and physicians who are not directly involved with NASA need greater access to space.

Unfortunately, there is no way to learn how gravity is sensed or what the extent of its effects on life are without performing experiments in the microgravity environment of space. The costs of sending even small packages into orbit are extremely high, and stringent NASA requirements make flight-qualified hardware complex and time consuming to develop. Machines on Earth such as the clinostat (which slowly rotates specimens to produce a constantly reorienting gravity vector that averages over time to zero) and the centrifuge can only be used to alter how gravity is perceived by organisms. Short-term microgravity environments achieved on KC-135 aircraft or sounding rockets are only somewhat helpful because they do not produce long enough periods of microgravity for many biological experiments.

To fill the gap in scientific and technological knowledge for space life sciences, an effective infrastructure for biological experimental hardware must be in place. This will make more frequent and longer duration experiments possible using new generic hardware with variable capabilities to cut through integration costs and NASA paperwork difficulties.

## **Rationale/Overview**

The role of space habitation has been to address space life science issues and support the further exploration and commercialization of space through design work. In the past the class has focused on missions that would generate interest and excitement for the U. S. Space Program.

These projects concentrated on developing a CELSS and achieving the NASA long-term goal of returning to the moon. However, to accommodate the Space Exploration Initiative and immediate problems facing space life scientists, Space Habitation has recently turned its focus toward smaller missions emphasizing basic biological science and potential commercial applications. The design response developed by the Spring 1992 semester class is called the Cell Module for Autonomous Space Support (C-MASS).

C-MASS is a small autonomous payload designed to support on-orbit testing for a variety of microorganisms and cultured cells/tissues for periods of up to 30 days. It uses only existing or modified off-the-shelf hardware and currently available technology, thereby minimizing cost and maximizing reliability. C-MASS is designed for many types of experiments. It brings together an extensive variety of data acquisition capabilities not integrated in any existing space hardware of its size. The large commitment to data acquisition provides a means to obtain detailed information inflight instead of having to rely solely on the analysis of returned samples that cannot reveal time-dependent gravitational effects. C-MASS is also designed for compatibility with the Shuttle middeck locker, SpaceHab, Spacelab, COMercial Experiment Transporter (COMET), and Space Station Freedom (SSF). Carrier Versatility enables C-MASS to take advantage of benefits offered by each: access to frequent Shuttle missions, 30-day missions, and very low gravity levels on COMET, and even longer missions as well as extremely low gravity levels on the initial crew-tended stages of SSF. To perform onboard control experiments, a 1-g centrifuge is also incorporated into the design. The combination of autonomy, extensive data acquisition, and design for long duration missions makes C-MASS a unique and valuable research tool. Table 1 compares C-MASS with other current related hardware.

advantage of the quiescent environment offered by microgravity for performing highly sensitive experiments not possible on Earth. In another way, the long-term exposure to reduced gravity offered by C-MASS will allow for experiments designed to reveal adaptations that organisms may undergo over long periods and many generations in a microgravity environment. The experiments C-MASS can support will help answer questions concerning how cells are affected by gravity, and they will provide a means to explore future commercial opportunities.

Gravitational cell biology research focuses on the response of a variety of physical phenomena to changes in gravity and the effect those changes have on life. The role of these physical phenomena in extracellular, intercellular, and intracellular processes determines the effect gravity has on cellular functions. Among these physical phenomena are sedimentation and convection. In the absence of gravity these processes do not occur. Other weak physical forces such as hydrostatic pressure and surface tension, normally dwarfed in the presence of gravity, become much more pronounced in the microgravity of space. The absence of sedimentation and convection combined with the enhancement of hydrostatic pressure and surface tension cause both internal (intracellular) and cell-to-cell (intercellular) changes in cell activities.

Gravity causes dense materials to settle or sediment at the bottom of a medium. Plant cells called statocytes use sedimentation to sense the orientation of the gravity vector. Starch granules in the statocyte fall to the cell bottom and react with the cell wall providing a directional reference for plant growth. Cells must also create cytoskeletal structures to inhibit the sedimentation of other organelles such as nuclei. Intercellular sedimentation affects the distribution of cells and materials. In the presence of gravity, prolonged contact between cells of different densities, or between cells and dense materials is impossible. For these reasons, in microgravity, cell differentiation unlike any observed in a terrestrial environment should occur.

Convection currents are caused when gravity acts on thermal and/or density gradients within a fluid. Intracellular convection is responsible for cytoplasmic streaming which transports signals and materials within a cell. Intercellular convection creates shear forces that

disturb cells and affect the way they develop and communicate with one another. These effects require better characterization, a job impossible to do in nominal gravity, to understand the mechanisms by which they act.

Hydrostatic pressure is responsible for the rise of fluid in a capillary tube, and surface tension is a measure of fluid adhesion forces. Hydrostatic pressure is important in examining the work done by a system ( $W = P dV + V dP$ ). In the absence of gravity, the influence of these processes is much more pronounced, altering the fluidic environment both inside and outside cells. Therefore, as the pressure approaches zero, cellular events which involve a volume change, such as secretion or fission, are expected to be affected. Surface tension exists between a cell and its environment and between cells. Research in microgravity, where fluid can be easily manipulated, has provided insight into this behavior and should reveal the importance of fluid interactions in cellular functions.

The capabilities of C-MASS make it a valuable tool for supporting research that will identify and exploit the gravitational effects acting at the cellular level. The versatile fluid transfer system and variable experimental vials give C-MASS the ability to supply many types of organisms with different physical needs. The autonomous nature of C-MASS allows payloads on flights without the perturbations caused by crew presence that can ruin the quiescent microgravity environment.

The imaging systems and in-flight reprogrammability of C-MASS give investigators control over experiments from Earth to effect adjustments as needed during the flight. Onboard data acquisition from the sensors and spectroscopy will also provide a dynamic profile of experiments for postflight analysis which may help pinpoint key steps in cellular developmental processes. The environmental sensors will provide a time-dependent record of experimental conditions. This is crucial since cells and microbes are sensitive to variations in their surroundings. The data-intensive experiments made possible by C-MASS can be used to reveal how convection, sedimentation, hydrostatic pressure, and surface tension affect cellular processes.

### Quiescent Environment Experiments

The absence of disturbing processes such as convection and sedimentation in microgravity make it an ideal

environment for performing delicate experiments on cells and biomolecules, the modification of cell lines, the growth of synthetic tissue cultures, and the polymerization of macromolecules may all benefit from experiments that take advantage of the quiescent environment of space. Genetically engineered cell lines have numerous commercial benefits which range from methods of drug delivery to the production of pharmaceuticals. Liposomes (lipid shells of vesicles) are presently used in the analysis of membrane proteins, therapeutic drug delivery, and in generating immunogenicity. Liposomes are extremely delicate structures. At 1 g, gravity-induced convection currents cause excessive fracturing of the bilayer resulting in small liposomes.<sup>4</sup> A similar problem is encountered in cultured lymphocytes modified to destroy tumor cells in their host organism. Several billion cultured cells are needed per treatment and repeated treatments are necessary. However, only a few million viable cells are usually generated using processes on Earth. Lymphocyte cells grown *in vitro* suffer from fluid shear forces and poor nutrient and waste exchange causing low proliferation and misshapen cells.<sup>5</sup> Both the liposome and lymphocyte experiments have shown increased growth size and an increase in lymphocyte production when performed in a microgravity or simulated microgravity environment. Therefore, further study is warranted in these areas, as well as a variety of other cellular studies which have only been carried out in 1 g.

Other experiments that may benefit from the quiescence of space are DNA recombination and molecular cloning. These processes are widely used by the pharmaceutical industry. The final product is material which can be used for the replacement or increased reproduction of any protein in the human body.<sup>6</sup> It is possible that a microgravity environment would allow greater control over the production of human proteins in a host cell since it is known to affect both bacteria and liposome production. As in the two previous examples, a quiescent environment would minimize shear flow patterns caused by convection, guiding the cellular growth in a manner contrary to that found *in vivo*. It would also be possible to impose a small controlled force upon the cells as they grow. This may be especially useful in experiments such as the assembly of collagen, which has a well organized structure *in vivo*, but lacks this structure when growth is stimulated *in vitro*.<sup>7</sup> Artificial development of well organized collagen has potential uses for surgical implants to replace damaged tissue.

Communication between cells is necessary for processes like differentiation where a cell uses the genetic material common to all cells to express its genes in a particular manner. For instance, one cell forms skin while another forms an eye, although both cells began with the same information. Complex intercellular communications and specific cytoplasmic elements appear to be the key factors governing differentiation. Data suggest that mammalian cells undergoing differentiation are more sensitive to gravitational effects than nondifferentiating cells and that changes in gene expression can be induced.<sup>8</sup> One hypothesis presented by D. K. Kondepudi states that in microgravity a system evolving irreversibly toward an end status may proceed with equal probability to another end status, but a system that has evolved for generations at 1 g will give a single and well-known end.<sup>8</sup> Cells communicate through chemical signals carried in a fluid intercellular space. A gravitational change in the fluid due to a reduction in particle streaming or convection will alter the cell's ability to transmit or receive signals from its surroundings. An understanding of these mechanisms could allow the control over the differentiation of one cell into a desired tissue type enabling transplantable organs to be grown when needed. The quiescent environment of space offers a laboratory where intercellular communication is altered and may be controlled more carefully than on Earth.

Electrofusion of plant cells to form hybrids is also enhanced in a microgravity environment due to the lack of sedimentation and convection.<sup>9</sup> Plants are of interest for terrestrial uses such as pharmaceuticals and as food and oxygen sources for life supporting systems in space. The ability to hybridize a variety of plant cells permits scientists to breed plants with superior qualities such as greater biomass production with an increased resistance to disease. Ultimately, plants may be produced to support microgravity uses, lunar uses, and even Martian uses.

### Multigenerational Experiments

In addition to a quiescent environment, COMET provides the opportunity to conduct experiments over a 30-day period which allows for the production of multiple generations of rapidly reproducing organisms such as bacteria. Bacteria are extremely well-studied and provide excellent building blocks for gravitational biology research. They are of interest not only for comparison to



of the vial allows for imaging of the experiments, and the flexible portion permits the internal volume to fluctuate with the introduction and removal of fluids, thereby maintaining a "hard-filled" fluid environment. Depending upon the type of experimental vial, a semi-permeable membrane is placed in either the rigid or the collapsible portion, or it may be eliminated entirely. In the aerobic microorganism configuration, the membrane effectively separates the vial into two regions: an upper section that contains organisms in a nutrient solution and a lower section containing gases. In the cell tissue configuration, the membrane allows nutrient replenishment in the upper compartment while keeping cells isolated in the remaining portion. Membrane porosity is matched to these different requirements. In addition, the elimination of the membrane provides a single environment for the study of anaerobic organisms.

For aerobic bacteria and other microorganism experiments, the organisms are contained within the rigid upper region of a vial. This allows for an aliquot (a small sample) to be taken by the fluid transfer system and used to inoculate a new nutrient-filled vial once the population has reached its saturation point. This process can be repeated many times, allowing the researcher to study changes in behavior and structure over multiple organism generations. In contrast, for cell tissue experiments, the cells are placed on the other side of the semi-permeable membrane. This allows for fluid removal and nutrient replenishment without damage to the fragile tissues.

The non-rotating inner portion of the experimental volume can hold up to 42 sample vials. These are similar to the anaerobic experiment vial, but with a shorter rigid section, and may contain nutrients, fixative, or other experiment support fluids. This area may also be used for additional experiments not requiring any inflight assay capability.

The final element of the experimental volume is the DC stepper motor which positions the outer experiments for the various assay techniques. The motor is connected to the experimental volume via sprockets and a nylon chain. The volume will only be moved slowly a few times a day. These short durations and low accelerations were deemed to have minimal effect upon the microgravity experiments.

## 1-G Centrifuge

C-MASS's launch, orbital, and landing environments introduce many variables that are difficult to simulate in ground-based control experiments. Temperature profiles, vibrational levels, and the extreme launch and reentry loads can all play significant roles in organism development. This problem is compounded by the inherent variability of living organisms. The best results would be obtained by comparing organisms from the same origin that have been exposed to identical conditions with the exception of gravitational accelerations. Therefore a small 1-g centrifuge is provided onboard C-MASS. The inclusion of the centrifuge ensures that any observed alterations in organism structure, function, or behavior are due solely to spaceflight changes in gravity.

The centrifuge design presents some of the most difficult hardware challenges for C-MASS. All commercial centrifuges are designed for much higher rotational rates than required for producing accelerations of 1 g. Also, all other centrifuges designed for use in microgravity are either too large or unmodifiable to this particular configuration. Therefore, the C-MASS centrifuge is a unique instrument, but one that utilizes commercially available or readily producible components. In this way, it remains consistent with the drive to use only off-the-shelf hardware.

To maximize the commonality of the experiments in the experimental volume, the centrifuge utilizes an identical circular arrangement using the same types of sample vials. Like the experimental volume, only the outer ring will be capable of motion, while the center portion is fixed to minimize rotating mass. The 7.6-cm radial distance to the center of the outer ring experiments requires that the centrifuge rotate at 108.5 RPM. Motor control is achieved using a small DC gear motor that utilizes a feedback loop to control motor output to within 2 RPM. The gravity gradient across any single experiment is  $\pm 0.11$  g. Therefore, all rotating experiments will see accelerations between 0.89 g and 1.11 g during centrifuge operation.

Several options for fluid transfer within the centrifuge were examined. The simplest, most reliable, and least mass intensive of these is to simply stop the centrifuge for brief periods. Fluid transfer can then be accomplished

with the same device and in an identical manner to that used with the experimental volume. Although stoppage of the centrifuge for fluid transfer could affect experiments, it was determined that any changes would remain insignificant if the stoppage were for only a few minutes a day.

The identification of specific vial locations within the centrifuge is accomplished through the use of small photoelectric sensor and a machined groove of continuously varying depth in the vase of the centrifuge platter. By measuring the depth of this groove when the centrifuge comes to rest, the sensor and accompanying software can determine the relative position of any vial in the centrifuge. Based upon this information, the fluid transfer device can move to the appropriate vial. The accuracy of this system is well established in electronic micrometers.

### Fluid Transfer System

The fluid transfer system provides C-MASS with the capability of supporting a wide variety of experiments. This versatile system has the ability to remove or add fluids, such as fixative and nutrient media, to each of the experimental vials. Fluid transfer is necessary to sustain the experiments for the entire mission duration. For instance, the system can remove wastes and replenish nutrients, or it can inoculate a few cells in a new nutrient solution. These tasks are accomplished without contamination of the individual experimental vials.

In order to successfully transfer fluid, the experimental vials must be accessed without loss of closure. To accomplish this, a transfer tip, which is similar to a syringe, punctures the resealable membrane at the top of the experimental vial. Once the transfer tip has been inserted into the experimental vial, a combination of two valves and a pumping mechanism are used to force a maximum of 1 ml of fluid either into or out of the transfer tip. This fluid transfer scheme, known to be extremely reliable, is derived from an automatic, battery-powered pipettor typically found in laboratories.

The transfer tip design not only facilitates fluid transfer, it also prevents contamination of the experiments and reduces possible cell damage as well. A flexible plastic bag has been attached to the transfer tip needle on the inside of the transfer tip. This bag fills with fluid as it is

pumped from the experimental vial, blocking the liquid from entering the pumping mechanism, thus inhibiting the contamination of the pump. Also, 110 transfer tips are located inside C-MASS allowing for transfer tip exchange, avoiding cross contamination between experiments. To reduce cell damage, the fluid inlet into the transfer tip is located on the side of the needle tip instead of on the end. The fluid inlet can then be larger, reducing the shear forces experienced by the delicate cells.

The experimental vials in both the centrifuge and experimental volume are accessed using a robotic arm. An end effector on the robot arm holds the fluid transfer pumping mechanism and a transfer tip. To accomplish the fluid transfer system requirements, the robotics arm is capable of movement in three dimensions. Three stepper motors are used in conjunction with three orthogonal leadscrews. A diagram of the robotic arm can be seen in Figure 5. The robotic control mechanism uses the positioning system, discussed in the 1-g centrifuge section, to locate the different vials.

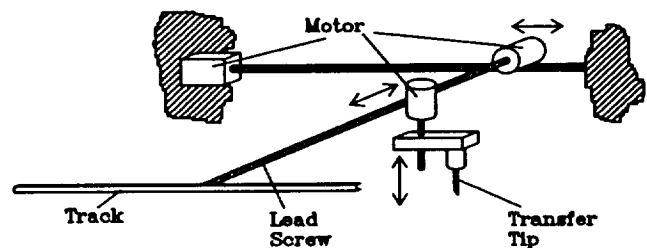


Fig. 5 Isometric view of the robotic fluid transfer arm

### Imaging System

Organism growth and development is a dynamic, non-linear process. It is simply not possible to completely understand changes due to microgravity and their underlying mechanisms through the analysis of only an end result. Fixing experiments to preserve them for later ground-based analysis is often done, but it alters cell

Table 1 A comparison of C-MASS to related hardware for supporting microbiological experiments in space

|           | Autonomous | Visual imaging | 1-g centrifuge | Variable fluid transfer | Carrier                 |
|-----------|------------|----------------|----------------|-------------------------|-------------------------|
| CGBA      |            | √              |                |                         | Shuttle                 |
| Biomodule | √          | √              |                |                         | Shuttle, ELVs           |
| Biorack   |            | √              | √              |                         | Shuttle                 |
| Biosample | √          | √              | √              | √                       | Eureca                  |
| C-MASS    | √          | √              | √              | √                       | COMET, Shuttle, Freedom |

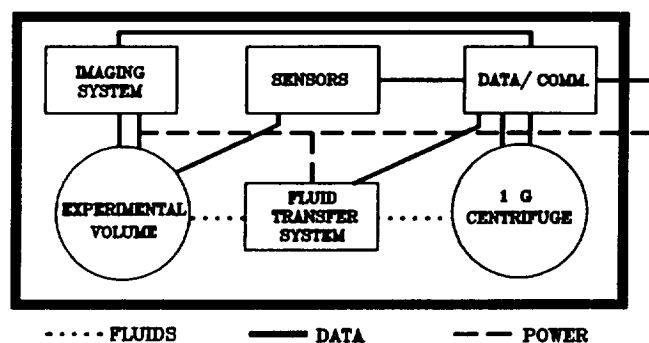


Fig. 1 A functional diagram of the C-MASS design

A functional diagram for C-MASS is shown in Figure 1. The diagram shows the six major subsystems and power, data, and fluid interfaces. Biological experiments are housed in the experimental volume and 1-g control centrifuge. The fluid transfer system is responsible for sample taking, nutrient delivery, waste removal, and organism transfer within the biological experiment vials. Data acquisition occurs through imaging systems and sensors. Imaging systems include photography, microscopy, and video for observing visible cellular changes in the microgravity of space. Sensors include spectroscopy and Enzyme-Linked ImmunoSorbent Assay (ELISA) for specific analytical techniques and environmental sensors such as vibration, radiation, temperature, pH, and light levels to record environmental conditions within the payload. The C-MASS communications system allows for data and video downlink as well as uplink, including in-flight

reprogrammability for adapting experiments while in progress. C-MASS is a small, low-cost, reliable payload designed to help fill the gap in space life science knowledge and technology.

#### C-MASS Subsystem Designs

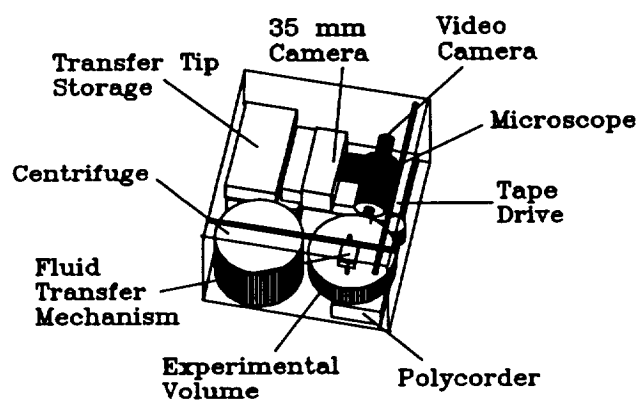


Fig. 2 Isometric view of C-MASS

An overall view of the C-MASS payload and its various subsystems is shown in Figure 2. C-MASS has outer dimensions of 11" x 14.5" x 15.75" for the limiting volume case of COMET. The design of the subsystems utilized an iterative process in which system requirements and objectives were identified. Next, design options using

current technology and off-the-shelf hardware, modified where necessary, were conceived for each system. Finally, trade studies were performed to determine the preferred method. The use of current technology and readily available hardware maximizes performance and reliability, while keeping costs and payload development time to a minimum. The subsystem descriptions that follow are reflective of this design philosophy.

### Experimental Volume

All microgravity experiments will take place in the experimental volume; therefore, it must be capable of supporting various microorganism and cell culture experiments for up to 30 days. This entails allowing fluid transfers between individual experiment containers; providing lighting for photosynthetic organism growth, spectroscopy, and visual imaging; and facilitating data acquisition. The experimental volume is designed to maximize the total volume available for experimentation and data acquisition.

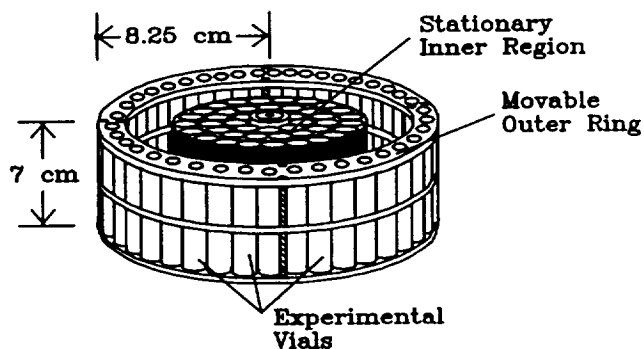


Fig. 3 Isometric view of the C-MASS experimental volume

The experimental volume consists of two separate regions: an outer positionable ring that permits visual data acquisition from experiments through the imaging system and an inner non-moving region. As shown in Figure 3, the entire volume is 8.25 cm in radius and 7.0 cm in height. The outer ring contains 40 individual experiment vials, each 1.2 cm in outer diameter and 5.0

cm high, for an internal fluid volume of approximately 3.0 ml per vial. These containers are placed with their centers at a radius of 7.6 cm from the center of the experimental volume with their long axis parallel to each other. The vial size and arrangement maximizes the number of experiments that may be conducted and exposed to the onboard data acquisition systems, while minimizing volume usage.

The space between the two regions of the experimental volume houses the various lighting sources used in C-MASS. An electroluminescent sheet provides ambient lighting for the outer experiment ring. A stationary light source is required for photography and microscopy, and several LEDs of varying wavelengths permit spectrophotometry as well as the use of fluorescent dyes and markers. The actual LED wavelengths can vary depending upon experimental requirements.

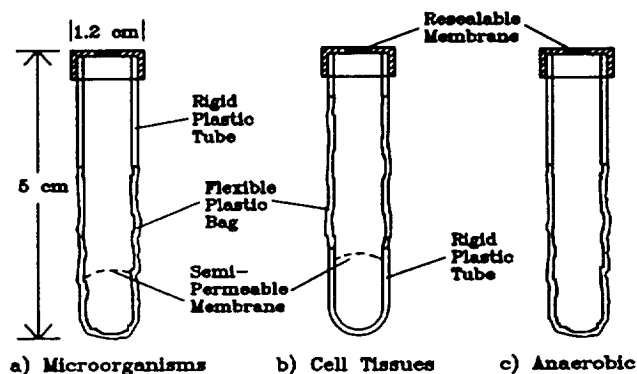


Fig. 4 Experimental vial options: a) microorganisms  
b) cell tissues c) anaerobic bacteria

In order to maximize the experimental capabilities of C-MASS, a flexible experimental vial design was chosen. Three basic vial designs were conceived: the aerobic microorganism vial, the cell tissue vial, and the anaerobic vial. Figure 4 shows the containers all have the same basic components, simply organized differently. The four basic components are a rubber cap containing a reusable membrane; a clear, rigid, optically clear, plastic cylinder; a flexible plastic bag; and a semi-permeable membrane. The resealable membrane may be pierced by a fluid transfer needle, allowing fluid addition or removal, while maintaining system closure. The rigid cylindrical portion

structure and prevents their use for beginning new cell lines for terrestrial use. The loads experienced during landing can also alter or even destroy experiments. Therefore, the ongoing visual record provided by the imaging system is essential for establishing a time line of organism development. The imaging system is responsible for producing high quality visual data of the outer ring experiments in the experimental volume. The centrifuge experiments will not be imaged due to volume limitations. The imaging system is comprised of three major components: a microscope, a video camera, and a photographic camera. Also, samples saved for return can be compared to those studied *in situ* in the space environment.

Due to the size of the biological organisms under study within C-MASS, a microscope is required for all imaging applications. Basic light microscopy of unstained cells provides very poor resolution of cellular features, and provides only a two-dimensional view. This poor resolution may be greatly enhanced using techniques known as differential phase contrast and the Nomarski method (differential interference contrast). The C-MASS imaging system will utilize these techniques to view cellular features and organism surface texture. Objective lenses range in power from 10x to 1000x, providing proper magnification for a variety of imaging applications.

A video camera is included in the C-MASS design for its capability of recording organism motion and the ability to provide real time images for downlinking. The output from the microscope can be directed to the small charge coupled device (CCD) camera head. The camera has a resolution of approximately 400,000 pixels with a 12 bit color capability. The video output is stored for later retrieval on Earth. Video images can also be downlinked to a groundstation, permitting researchers a small real time glimpse of the activity within an experimental vial.

Photography has a far greater resolution than video imagery due to the much smaller size of light sensitive crystals in film as compared to a video pixel element. Therefore, a photographic camera is also provided within C-MASS to yield high resolution pictures of the experiments within the experimental volume. As with the video camera, imaging is through the microscope. The camera utilized is a commercially available 35 mm electronically controllable, auto focus, auto aperture, auto timing, auto film advance camera with a film back capable

of holding a 250-exposure roll of 35 mm film. Several options exist for increasing the number of possible exposures with simple modifications to various camera components. Modifications to the shutter and film advance mechanism would permit the use of multiple rolls of 110 film rather than a single 35 mm roll. The ability to section the film into smaller exposure sizes is also possible. The optimal method for maximizing photography capabilities may require combination of both modifications.

### Sensors

The in-flight sensor measurements taken by C-MASS are extremely important since these will allow researchers to determine the dynamic effects of microgravity on experiments. Sensor selection was difficult because sensors placed in contact with organisms may form biofilms and condensate around them decreasing the accuracy of the sensor readings. Most of the sensors discussed in this section measure the environmental conditions in which the experiments take place. The sensors that fall into this category include temperature, illumination, gravity level, vibration, and radiation. C-MASS also incorporates a spectrophotometer, for obtaining experimental data concerning optical density, and ELISA for detecting the presence of specific biomolecules, such as proteins or peptides.

The wide variety of environmental conditions recorded are measured by the following sensors. The variations of temperature within C-MASS are measured using thermistors, small semiconductors that change their electrical resistance in response to temperature. These thermistors are strategically located throughout the facility and measure both air and surface temperatures between -30 and 100 degrees Celsius. Experiment pH is measured using one of the cameras in conjunction with an indicator chemical added to the solution. The pH indicator used is phenol red, or phenolsulfonphthalein, which changes from yellow to red between pH 6.4 and pH 8.2. Either the video camera or 35 mm camera can be used to photograph the vials containing the pH indicator. Video images can be downlinked for immediate quantification, or stored onboard until a later time. The illumination sensors are photoelectric diodes located in several different areas within the centrifuge and experimental volume. Accelerometers are used to measure both the gravity levels and vibrations between 40

micro-g and 10 g. Three orthogonal accelerometers are required to measure accelerations in three dimensions. Cumulative radiation is measured by three orthogonal film dosimeters, which are commonly used to detect radiation levels in laboratories.

The other sensors included in C-MASS provide analytical assay techniques. Spectrophotometry readings are obtained using several light sources and light detectors. The light sources are emitting diodes and the light detectors are photo diodes. There are six different light sources spanning the 200 nm to 1500 nm range, each aligned with a corresponding detector. Since the spectrophotometry sensors remain stationary, only the experiments located in the rotating part of the experimental volume have this assay capability. The other assay method is ELISA, a plastic sheet with specific antigens attached. These antigens are proteins that can chemically recognize other very specific reagent proteins. When the proteins come in contact with one another, the bound antigen produces a color change in proportion to the amount of reagent protein present. Using this method, very small amounts (as little as 10 picograms) of specific reagents can be detected and their concentrations determined. Currently, several hundred specific assays are possible using this technique.

#### **Data/Communications**

The valuable measurements taken by the sensors and imaging systems require a means of data storage and return. Communications are also necessary between Earth and C-MASS and between its various internal subsystems. The C-MASS is not only capable of downlinking data, but also of receiving uplink commands allowing for in-flight changes to be made. A standard XMODEM protocol is used for carrier-payload communications.

C-MASS provides the researcher with modular options in data storage. Depending on the amount of specified data to be taken, two different configurations can be used. In the event that large amounts of data are to be taken, an 8-mm magnetic tape drive will be placed onboard. Utilizing a modified tape changing mechanism, two 25-gigabyte tapes could be included for up to 50 gigabytes of storage for both sensor and video data. The second option is to store all sensor data in the 448K data acquisition scanner. This method would require that all

the sensor data be downlinked periodically instead of permanently recorded aboard C-MASS and that the video images be recorded on videotape. The advantage of the second option is that less volume is used which could allow, for instance, more fluid transfer tips to be available.

The data acquisition computer is the internal and external communications center for the payload. It controls the onboard operations of the subsystems such as sensors, fluid transfer, and environmental control. It also acts as the communications link with the ground receiving uplinked commands and downlinking requested data.

#### **Cost Analysis**

The total cost of construction and testing for C-MASS to produce a flight-qualified version of the payload was estimated at \$525,000. The actual hardware, modifications, and any raw materials made up only a small portion of that total, \$25,000, due to the predominant use of off-the-shelf components and commercially available products. Personnel costs for integration and testing made up the bulk of the estimate at \$500,000. This value covers the full-time salaries of an electrician, shop technician, project manager, and two other technicians for one year including overhead. It was presumed that this combination working in a small business setting could easily move C-MASS from its current preliminary design phase to ready-to use flight-qualified hardware within that time frame. The cost of C-MASS is competitive with other commercially developed space hardware of similar size and function, and it is much less than that of similar NASA-sponsored projects which take longer to complete.

#### **C-MASS Science Experiments**

Cells are the basic building blocks of life; therefore, an understanding of gravitational effects at the cellular level is absolutely necessary before large CELSS are created, astronaut health issues are treated, or the microgravity environment is used for commercial benefit. The specific physical processes altered in microgravity have both direct and indirect effects on cells which are still not completely understood. C-MASS, with its entourage of data acquisition hardware, can be used to document gravitational changes and alterations in ways not currently possible. C-MASS may also be used to take

Earth-based studies, but in anticipation for future space habitation. Microgravity experiments on the resistance of the bacteria *E. coli* to antibiotics<sup>10</sup> and their metabolic adaptation<sup>11</sup> were performed previously on short duration flights. For reasons not yet known, some bacteria grow faster in microgravity and show an increased resistance to antibiotics. Other microorganisms such as the motile *Paramecium* are strongly affected by the gravity vector on Earth since they must expend energy swimming against it. In microgravity the proliferation rate of *Paramecium* increases, possibly because the energy previously used to move can be transferred to reproductive activities.<sup>10</sup> However, to date no observed changes were maintained in subsequent generations on return to Earth. Multigenerational exposure to a reduced gravity environment may result in organisms genetically adapted to microgravity. Organisms which are unable to adapt will expire, and only those best suited for survival in microgravity will reproduce. Genetically adapted organisms returned to Earth may have specific traits that could be used in pharmaceutical production or for other scientific benefit.

The gravity-sensing properties of plants are currently under investigation, but a 30-day mission will allow observations of the development of some plants and photosynthetic cell colonies to maturity. One-celled algae, for instance, normally grow into an entire kelp plant on Earth. With its variable lighting capabilities, fluid transfer, and the ability to contain a variety of sample vial sizes, C-MASS could be used to observe the growth of a kelp colony under microgravity conditions. The results could provide valuable insights into gravity responses and cellular differentiation in space.

The multigenerational aspect of gravitational research is currently of interest as flights such as COMET become available and in anticipation for future long-term microgravity exposure on structures such as Space Station Freedom.

### Experimental Protocol

Although the protocol for each experiment may differ, they all have similarities and can be adapted to the capabilities and constraints of C-MASS. The following is an example of a bacteria experimental protocol that is compatible with C-MASS.

One of a number of sample vials containing growth medium will be inoculated with organisms prior to launch. After microgravity is achieved, the next sample vial will be inoculated by the transfer of an aliquot from the first. Every subsequent 48 to 72 hours, when these samples have saturated the medium, an aliquot will be extracted and transferred to another vial containing fresh nutrients. The initial sample will then be fixed with gluteraldehyde for postflight analysis. The process will be repeated until the end of the mission, providing multiple generations of bacteria grown in space. Temperature, pH, radiation, and optical density will be measured, and visual imaging will be performed on each active sample during the flight. Specific products and metabolic markers will be visualized with ELISA strips throughout the mission. The experiment will provide a dynamic profile of long-term gravitational adaptations and changes in the bacteria studied.

Since C-MASS is already designed, built and tested, it is imagined that a team of National Institutes of Health (NIH) scientists and industrial scientists would simply deliver their respective samples to the launch site a few days prior to launch. These personnel would then monitor their experiments daily with data transmitted from the ground stations. And finally, they would receive postflight samples for more thorough analysis.

### Conclusions

A preliminary design for C-MASS, a small payload capable of supporting a variety of microbiological experiments in space, has been presented. The important design characteristics have been described and examples of its capabilities and applications have been discussed. C-MASS adds a unique combination of autonomy, mission duration, and experimental capabilities not available with current space hardware. Furthermore, this design supports the low budget, high quality, and commercial application emphasis of SEI. It will provide researchers with generic hardware adding a needed component to the space infrastructure for biological research. Operationally, the researchers will use the C-MASS capabilities almost like another piece of laboratory equipment.

C-MASS may be used to satisfy scientific curiosity by offering a means to answer many of the basic questions concerning the effects of gravity on life. It may also be used to study cultured cells/tissues which are important in addressing astronaut health issues and the treatment of related diseases on Earth. In the future, C-MASS may be used to pave the way toward space commercialization by providing a facility that can utilize the space environment to produce novel biological products such as genetically altered species or specially modified cells. The important needs fulfilled by C-MASS and its commitment to SEI mandates make sit the next logical step in space life sciences development.

### References

1. Borer, J. S. Personal testimony to the Subcommittee of Science, Space and Technology of the U. S. House of Representatives, 1991.
2. Healy, B. National Institutes of Health, Dept. of Health and Human Services, Testimony to the subcommittee of Science, Space and Technology of the U.S. House of Representatives, 1991.
3. David, L., "SEI plans unfold," Aerospace America, April 15-17, 1992.
4. Claassen, D. E. and B. S. Spooner, "Effects of microgravity on liposome formation," ASGSB Bulletin, No. 4, 1990, p. 69.
5. Ingram, M. Treatment of brain tumors using immune cells grown in microgravity of NASA's rotating wall bioreactor. Testimony to the Subcommittee of Science, Space and Technology of the U. S. House of Representatives, 1991.
6. Swetly, P, "The Importance of biotechnology for the discovery of better and safer drugs," Medicinal Research Series (Modern Drug Research) Vol. 12, 1989.
7. Bergren, T. and M. W. Luttges, "Collagen self assembly in microgravity," ASGSB Bulletin, No. 4, 1990, p. 68.
8. Cogoli, A. "Changes observed in lymphocyte behavior during gravitational unloading," ASGSB Bulletin, No. 4, 1991, pp. 107-115.
9. Mehrle, W. et al, "Effects of microgravitation on electrofusion of plant cell protoplasts," Plant Physiology, 1989, pp. 1172-1177.
10. Gmunder, F. K. and A. Cogoli, "Cultivation of single cells in space," Appl. Microgravity Tech. Vol. 1, No. 3, 1988, pp. 115-122.
11. Klaus, D. and M. W. Luttges, "Metabolic adaptation of E. Coli in microgravity," ASGSB Bulletin, No. 5, 1991, p. 58.
12. Todd, P., "Gravity-dependent phenomena at the scale of the single cell," ASGSB Bulletin, No. 2, 1989, pp. 95-113.



**BIOREGENERATIVE SYSTEM COMPONENTS FOR MICROGRAVITY**

University of Florida  
Aerospace Engineering, Mechanics and Engineering Sciences  
Gainesville, Florida

Dr. Gale E. Nevill, Jr.  
Michael I. Hessel, Jr., Teaching Assistant

**Abstract**

The goal of the class was to design, fabricate, and test prototype designs that were independent, yet applicable to a Closed Loop Life Support System. The three prototypes chosen were in the areas of agar plant growth, regenerative filtration, and microgravity food preparation. The plant growth group designed a prototype agar medium growth system that incorporates nutrient solution replenishment and post-harvest refurbishment. In addition, the unit emphasizes material containment and minimization of open interfaces. The second project was a filter used in microgravity that has the capability to clean itself. The filters are perforated plates which slide through a duct and are cleaned outside of the flow with a vacuum system. The air in the duct is prevented from flowing outside of the duct by a network of sliding seals. The food preparation group developed a device which dispenses and mixes ingredients and then cooks the mixture in microgravity. The dry ingredients are dispensed from a canister by a ratchet-operated piston. The wet ingredients are dispensed from plastic bags through tubing attached to a syringe. Once inside the mixing chamber, the ingredients are mixed using a collapsible whisk and then pushed into the cooking device.

**Introduction**

During the 1991-92 academic year, the students of the EGM 4000/4001 Engineering Design class at the University of Florida have cooperated with personnel from the National Aeronautics and Space Administration, Kennedy Space Center. The class divided into three groups focusing on alternative growth media, air filtration, and food preparation. Prototype systems were designed, fabricated, and tested. An agar-based growth system, a regenerative filter, and a microgravity batter-based food preparation unit are all examined separately in the following report.

**AGAR PLANT GROWTH SYSTEM**

Past research on methods of plant growth in microgravity have focused on hydroponic and aeroponic systems of nutrient

delivery. Each of these methods of nutrient delivery has distinct advantages as well as unique problems associated with the plant growth process. It was the goal of the Plant Growth Group to design an Agar-Based Plant Growth Unit (ABPGU) that takes advantage of the desirable properties of the gelatinous matrix in addition to minimizing its associated problems.

A major problem facing agar-based growth media is the depletion of nutrients and water over time. Several different types of agar replenishment were tested in order to determine the most effective. These models included the use of a ceramic porous tube to deliver nutrients to the agar matrix, a wick used to draw nutrients from a reservoir, and a nutrient bath which allowed for surface contact between the matrix and the solution. The nutrient bath model proved to be the most effective and the final design of the ABPGU was dictated by this method of nutrient replenishment.

The Plant Growth Group took into account the planting, harvesting, and refurbishing processes, as well as how they apply in an integrated system. Planting and harvesting as individual activities received little focus because of the extent to which they have been studied. However, the activity of holding a seed in place after planting is of crucial importance. The use of agar offers a unique solution to the problem of seed containment. Seeds are contained within the agar matrix and remain stationary via two principles. First, the agar has a tendency to reseal small ruptures made in its surface, such as those ruptures that occur when a seed is imbedded in the agar surface. Secondly, the electrostatic interaction between the water within the agar matrix and the seed coat help to hold the seed within the matrix.

Much attention was focused on a refurbishing process that would be operable in microgravity. Refurbishing the ABPGU presents many challenges. First, plant material above the root line must be detached from the plant growth unit. Then the roots and agar must be cleared from the inside of the growth unit. This necessitates using two complimentary systems.

In order to remove plant material above the root line, the SPGU (Sectored Plant Growth Unit) hydro-refurbishing system, developed in 1991, will be employed (Figure 1). The SPGU involves the use of a refurbishing block that passes along the tracks of a plant growth surface. The refurbishing block has two jets, one of which will act as a water knife to cut the stems of the plants. The other jet is used to remove material from the plant orifices on the surface (Figure 2).

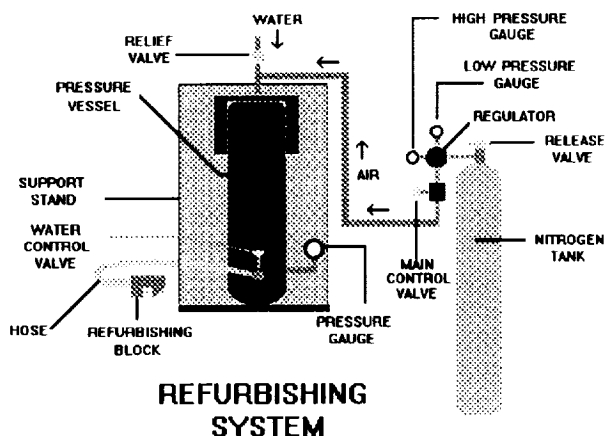


Fig. 1 SPGU Refurbishing System

Another system must exist to break up the mass of agar and plant material under the surface of a plant growth unit. The used agar must then be removed from the growth unit and transported to the resource recovery station. The growth unit is then prepared for a new cycle of implementation.

#### Testing of agar refurbishment concepts

Several tests were conducted in order to obtain the most effective agar refurbishment method. Preliminary tests were conducted using a combination of the refurbishing block along with a lateral jet. The water jet's effects were tested on an 8.25 X 13.5 X 3-inch block of agar underneath the SPGU Plexiglas surface. All activities were documented and the following conclusions were made:

1. To break up the agar sufficiently, it is necessary to rotate the jet.

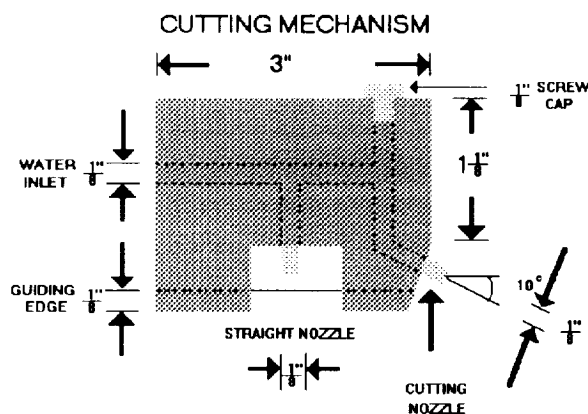


Fig. 2 Refurbishing block and nozzles

2. A water pressure of 60 psi is adequate for lateral refurbishment.

3. In order to vacuum out the agar, it is necessary for the agar to be near the vacuum nozzle.

#### Description

The ABPGU consists of a cylindrical Plexiglas container (12" diameter, 12" height) divided into three levels. The levels -- plant growth level, agar matrix level, and nutrient solution level -- are shown in Figure 3.

**Plant growth level** The plant growth level (PGL) was constructed from a 1/2-inch plate of Plexiglas. A line of holes (seed orifices), 3/8-inch in diameter, was drilled to allow placement of seeds in the agar matrix. Tracks were made on each side of the line of holes to accommodate the refurbishing block (Figure 4).

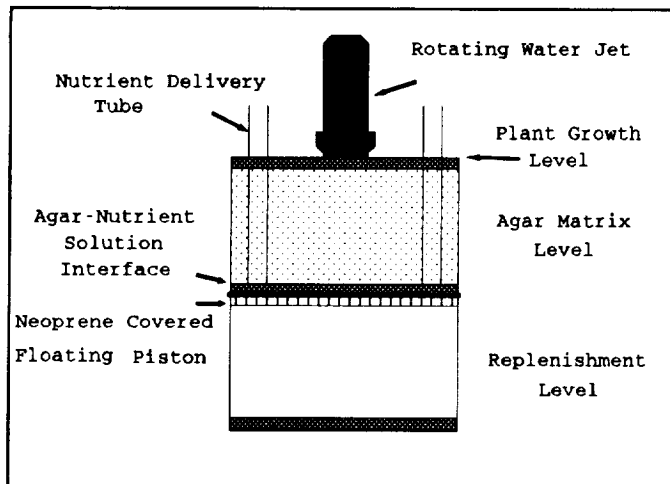


Fig. 3 Side view of plant growth unit

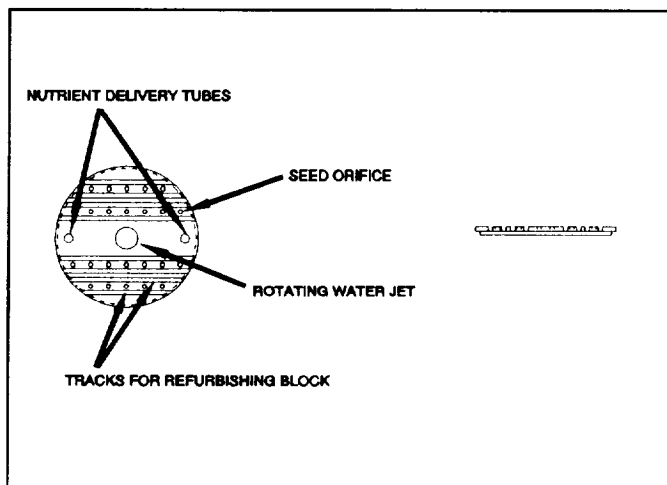


Fig. 4 Top and side view of plant growth level

In order to operate in microgravity, it is necessary to provide a seal at the seed orifices to prevent the agar-slush from escaping from the ABPGU. Several concepts that were considered include:

1. **Velcro** -- This concept involves a roll of velcro attached to the refurbishing block. As the block runs along tracks on the PGL, the velcro is unrolled and attached. Problems that were considered included the effectiveness of velcro when it gets wet, in addition to the refurbishment of

the velcro.

2. **Sliding door** -- This concept involves a track attached to the refurbishing block. As the block moves across the PGL track, the sliding door is pulled over the plant growth holes. It will be held in place by indentations in the PGL track.

3. **Refurbishing hood** -- This approach involve using as hood to capture any plant material, agar, or liquids that would be released during refurbishment. A filter could then be used to separate materials either to be reused or transported to the bioreactor. In addition, it is necessary to provide a seal at the plant growth surface during casting. A proposal is to use an additional neoprene-covered piston that would be placed over the PGL during the casting process. It would later be removed to allow for planting.

It may also be possible to incorporate the casting jets into this piston in such a way that the piston would seal the PGL and insert jets through the seed orifices to cast the agar. After the agar had sufficiently hardened, the piston would be removed to allow for the planting process.

**Agar matrix level** The agar matrix level (AML) contains a six-inch block of agar. The agar matrix is the medium through which the nutrient solution diffuses, providing plant roots with necessary nutrients and aeration. In addition, the matrix is solid, anchoring the plants to the ABPGU.

**Nutrient solution level** The nutrient solution level (NSL) contains approximately 1.5 liters of nutrient solution that is separated by the agar-nutrient solution interface, a 1/2-inch plate of Plexiglas with holes to allow diffusion of the nutrient solution through the agar matrix.

## Testing

### Locker-size test module

The locker-size test module (3" diameter, 4" height) was used to test a double-piston concept. Because of its size, it was primarily used in the testing of casting and containment methods.

### Casting of the agar

In space, the agar will be injected into the ABPGU in liquid form. During the hardening of the agar, it is

important to prevent any leakage through the plant growth surface orifices and the agar-nutrient solution interface. Methods must be considered that will seal these surfaces during agar casting; in addition, other problems include injecting the agar in microgravity, i.e., where will the air displaced by the injected agar go? Because of time and material constraints, the locker-size test module was manufactured to address these problems as described below.

The locker-size test module uses a two-piston concept which is controlled by water pressure (Figure 5). The agar-nutrient interface piston and the floating piston are moved toward the plant growth level (PGL), pressing out any excess air. The agar is then injected, and mechanical pressure is utilized to lower the two pistons evenly (Figure 6).

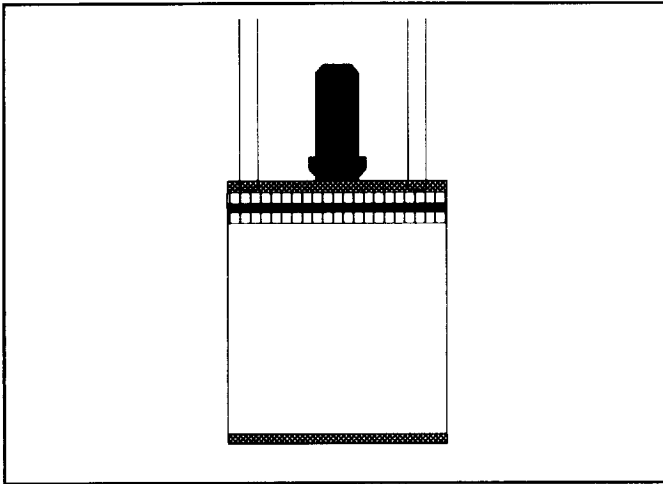


Fig. 5 Unit with both pistons at plant growth level

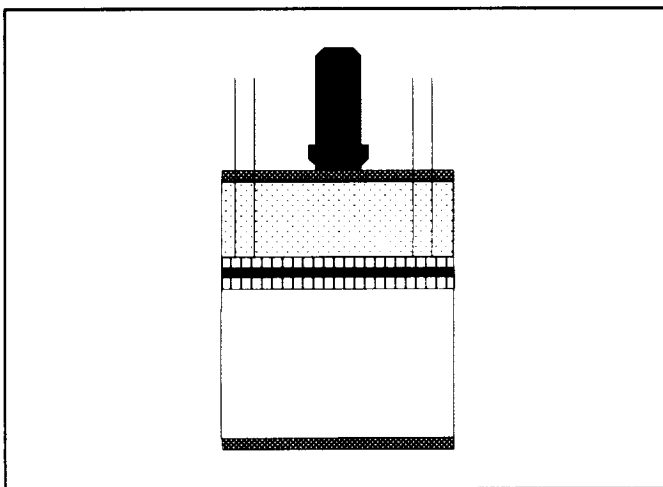


Fig. 6 Unit while agar is being injected

After 100-ml of agar has been injected, the interface piston

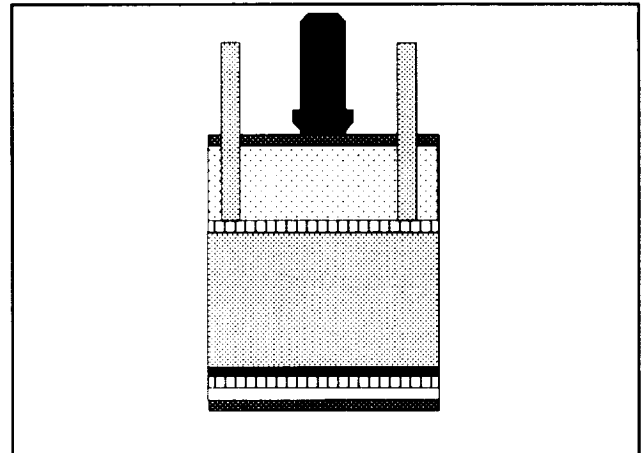


Fig. 7 Pistons separating due to entry of nutrient solution

is immobilized, while the floating piston forms a seal at the interface. Once a seal is formed, the pressure is maintained to hold the floating piston in place until the agar has hardened. The nutrient solution is then pumped in through the nutrient replenishment tubes to return the floating piston back to the base of the NSL (Figure 7).

Testing showed that this method is an effective means of eliminating possible air pockets in the agar matrix. Further testing in microgravity is needed to insure the effectiveness of this method.

**Containment** A major consideration for the use of the ABPGU in microgravity is the proper sealing of all components and surfaces. The seals provide the mechanism for containment of liquids as well as solids. Testing of the containment of the agar, nutrient solution, and water was done in several steps.

Blue-dyed water was used to examine the effectiveness of the floating piston to seal the agar/nutrient interface. This colored solution was used to provide the pressure necessary to maintain the seal between the neoprene (on the piston's surface) and the agar/nutrient interface. Tests revealed that the piston provided a more than adequate seal. The piston did not allow the mixing of the liquids in the nutrient solution level and the agar matrix level. To demonstrate this fact, liquid was cast into the agar level while the piston sealed the interface. The agar solidified

with no leakage into the nutrient solution level and no contamination from the blue-dyed water.

The test for containment of the nutrient solution during the growing process was done once the agar solidified. The test was designed to examine the hindrance of creepage. In the test, capillary tubes were inserted into the agar matrix to simulate the hydrophilic interaction between the water and the plant stem. The results showed that no liquid escaped from the agar, thereby demonstrating the effectiveness of the agar as a seal.

Tests were conducted to explore the concept of using agar as a means of holding the seed until proper root development occurred. In these tests, the seeds were manually inserted into the agar matrix and the orientation of the ABPGU was changed. The tests showed that the agar matrix provides an effective mechanism for seed containment. Tests were run using several different orientations to simulate changes in gravity.

**Refurbishment** Due to the small volume of the locker-size test module, testing of refurbishment concepts was conducted on the large-scale prototype as described below.

### Large-scale Prototype

The large-scale prototype was used to test the refurbishing processes. Containment and casting were hindered by the difficulty of machining a piston with adequately low tolerances for a container of large size.

**Containment** Water pressure was used to seal the floating piston against the agar/nutrient solution interface. Approximately 2 liters of agar was then poured through the PGL and allowed to harden overnight. However, due to inadequate tolerances of the floating piston, a tight seal was never formed at the interface resulting in a drop in water pressure. This resulted in a small amount of agar flow into the nutrient solution level.

**Refurbishment** The use of the refurbishing block to cut plant stems and clean the plant growth orifices was tested, and the results were published. Therefore, testing focused on the refurbishment of the agar-matrix level.

As a result of the malfunction of the containment system, testing of refurbishment was conducted using primarily the agar matrix level and plant growth surface. The floating piston was permanently positioned to form a seal at the interface, and the agar was recast and allowed to harden overnight. Then refurbishment was conducted using the 360°

rotating water jet to break up the agar and a wet-dry vacuum to extract the agar-water mixture.

Problems occurred because the wet-dry vacuum did not extract the water at a fast enough rate; hence, the agar matrix level overflowed with water. In addition, the agar used in testing was of a higher concentration than would normally be used, resulting in difficulty for the rotating water to break it up. To compensate, the flow rate of the rotating jet was reduced and the power of the vacuum was increased. These adjustments corrected the problems and demonstrated adequate refurbishment of the agar matrix.

### Conclusion

At the outset of the project it was decided to focus primarily on the aspects of replenishment, containment, and refurbishment. It was decided that the actual growth of plants in agar would not be studied in detail due to the abundance of studies already conducted.

The first generation large-scale prototype demonstrated that the agar matrix could be replenished. In addition, containment of liquid and solid materials was shown. The agar proved to be an effective mechanism for seed containment and inhibition of creepage. Problems with the casting process were envisioned with the first generation prototype. Also, problems with achieving adequately low tolerances occurred as a result of the machining process and due to the increasing size of the materials used.

The second generation small-scale prototype was designed and fabricated to deal with the problem of uneven agar casting in microgravity. Testing of this prototype, when subjected to changing gravitational vectors, proved the concept to be an adequate means of even agar casting.

### REGENERATIVE PARTICLE REMOVAL SYSTEM

A closed loop life support system requires many interfaces between mechanical and biological systems. The air-handling system in a plant growth chamber requires cleaning interfaces to remove solid contaminants from the air stream. This cleansing allows efficient circulation. The removal of particles from the atmospheric loop is also a necessary process for dehumidifying equipment to operate properly. This project focuses on a regenerative air cleaning system that

will remove solid particles from an airstream.

A regenerative particle removal system is one which is able to stay near its optimum efficiency at all times. Whenever the efficiency drops below some threshold, a cleaning operation will return it to its original condition. This type of system will not use replacement filters.

The concept of a regenerative air cleaner satisfies a need for long-term space applications. This concept could be implemented in the design of extra-terrestrial bases and in extended duration space travel, or in any system where extra space or replacement materials are in short supply. Over an extended period of time, a regenerative cleaner can justify its initial cost and weight through its reusability. By reducing maintenance needs, it may also provide greater long-term reliability.

A regenerative air cleaner can eliminate the use of replaceable mesh filters and save on maintenance and storage space. The use of replaceable or throw-away filters on a long-term space mission requires an abundant quantity of substitutes and storage space. The time and energy costs of the replacement and disposal activities would probably be quite high. Storage space for used filters must also be provided. A regenerative system negates these replacement factors and fits a closed system.

In the fall of 1991, this group determined the criteria for an air cleaning process and apparatus. An overall design consisting of removable filter plates was suggested. Along with this conceptual design, alternative concepts and methods were evaluated. These included organic filters, rotary filtration, electromagnetic field, and a sensor that determines when the filter needs cleaning.

### Prototype Design Description

Through matrix evaluation and objective decision-making, a final system design was selected. The design utilizes a rectangular duct with rectangular filter plates that fit together to form a matrix. The plates are perforated sheets of steel which are oriented perpendicular to the airflow direction. These plates will be able to slide through the duct and be cleaned outside of the airflow (Figure 8). This method will allow cleaning without interrupting the air circulation.

Each plate slides through apertures on two opposing sides of the duct. As the plate moves through the duct, a brush and scraper blade free the particles from the plate surface. The brush-scraper combination is attached to the nozzle of a vacuum hose. Loosened particles are drawn into the vacuum

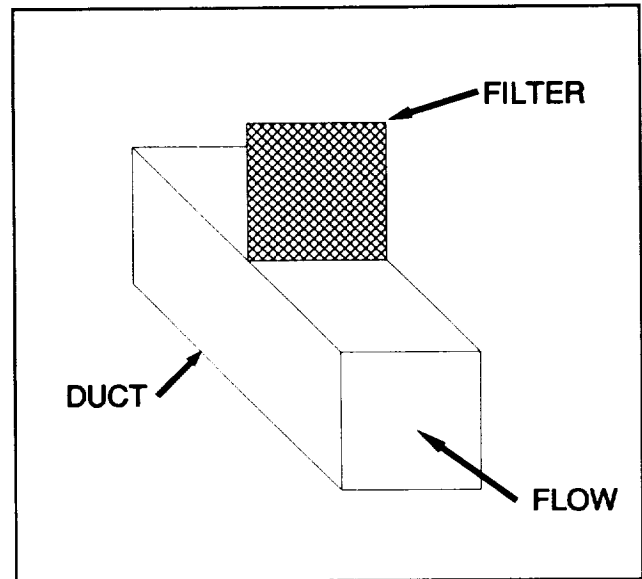


Fig. 8 Design concept schematic

system and collected in a nylon bag. This cleaning procedure is performed outside of the duct.

The apertures in the duct walls are governed by sliding seals. These seals prevent leakage during flow operation and provide clearance for plate movement when necessary.

### Prototype Construction

#### Perforated plates

Perforated screens were available from a variety of retail sources. Twenty-five square feet of perforated steel was purchased from the Harrington and King Perforating Company. The sheets are 0.6 mm in thickness, have circular holes which are 1.0 mm in diameter, and have 45% open area. These specifications were chosen to maximize the filtering efficiency while retaining an adequate flow rate.

The raw sheeting was cut into rectangles which measure 20 x 6 inches. A rectangular mild steel frame has been welded to each end of each plate. This provides an attachment point for the strings which will move the

plates.

### Duct

The unassembled steel duct was manufactured by Thompson Sheet Metal. The duct has a 6 inch x 8 inch cross-section, a length of 3 ft, and six pieces to allow for plate apertures (Figure 9). The fabrication of the duct allows the six side pieces to be snapped together. This has enabled the sides to be worked on separately for fastening seals, channels, and other mechanisms. In addition to the six sides, L-shaped channels were machined and attached to the inside of the duct to guide the movement of the filter plates.

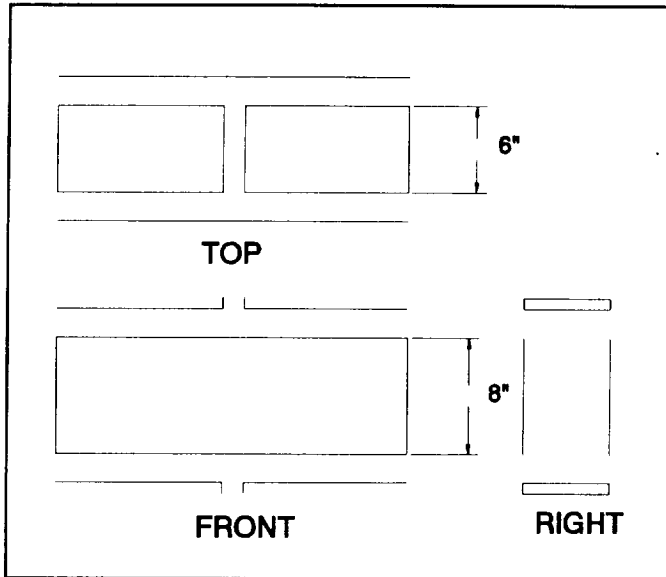


Fig. 9 Unassembled duct

### Plate movement

The plates are moved through two openings in the duct cross-section and guided by channels mounted on the duct walls. Two electric motors pull the filter plates back and forth by a cord and pulley system (Figure 10). The figure shows a schematic configuration for one plate.

The system uses two 500 mA motors turning at 40 revolutions per minute. Driving the plates with these motors causes the plates to move at a rate of 1 in per second. The motors are connected to the plates with multi-stranded Kevlar fiber. Kevlar's material characteristics assure high test strength and small stretch allowance. The small diameter and flexibility of the fibers have allowed adequate interfaces with the pulleys and spindles.

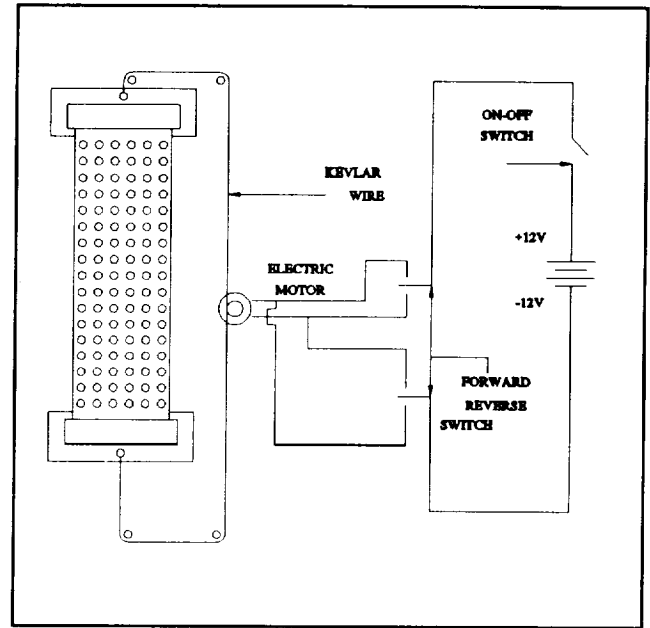


Fig. 10 Moving plate schematic

### Inter-plate Seals

Six seals prevent escaping airflow between the plates and the duct wall. In an implementation with a larger number of plates, the number of seals required is  $2(n + 1)$ , where  $n$  is the number of plates. Each seal is a strip of aluminum covered with a plastic coating. These strips run across the filter plates from one edge of the duct opening to the other. In the closed position, each strip fills the gap between two plates. The strips are able to rotate around their long axes. A  $90^\circ$  rotation, where the seals become parallel to the plates, opens the aperture and allows the plates to move (Figure 11). In addition to rotation, the seals translate along the duct edge. By moving the vertical seal up against the non-moving filter plate, space is generated for debris to pass out of the duct.

In this prototype, the seals are manually activated. A short wire on each end of each seal is used to force the rotation and translation. This is a process which could be easily automated, but this automation was not feasible within the time constraints of this project.

### Cleaning system

A filter plate cleaning system has been developed to integrate with the duct. It consists of a vacuum nozzle

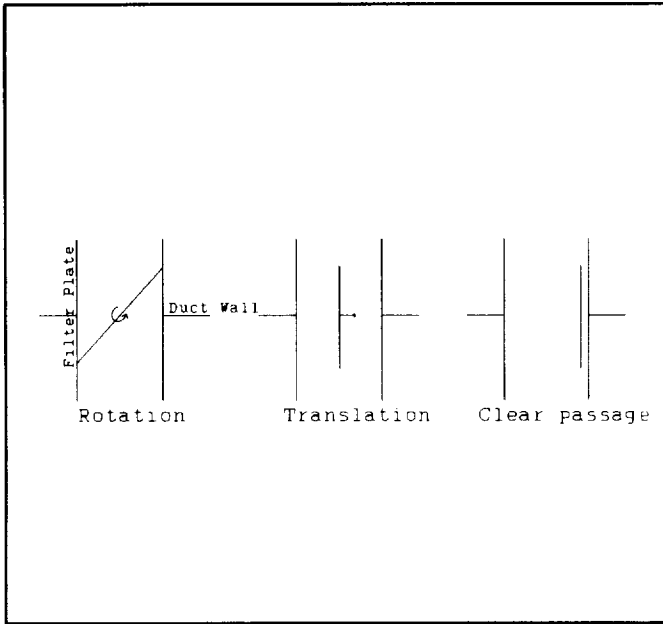


Fig. 11 Cross-section of seal placement

equipped with a brush and scraper combination (Figure 12). As a dirty plate moves through the duct aperture, the brush and scraper loosen debris. The debris is then gathered and removed by the operating vacuum.

The vacuum nozzle is a hollow wedge made of mild steel. The entry area is 0.875 x 6.0 inches. The exit area is 2.5 x 2.5 inches. In order to make the cleaning system more effective, the flow velocity across the plates has been maximized. Moreover, the distance between the nozzle and the plates has to be very small. Two vanes inside the nozzle help to regularize the flow and ensure that the flow is the same at all points across the nozzle entrance. A flow meter was used to measure the flow velocity at the nozzle exit. It is worth noting that the velocity decreases rapidly away from the nozzle. It decreased by almost one-half at 0.25" from the nozzle.

### Prototype Testing

#### Filtration testing apparatus

Efficiency of the system prototype was determined with the use of the following procedures. A blower (115 watts, 4 x 5.25-inch exit) was attached to the beginning of the duct to

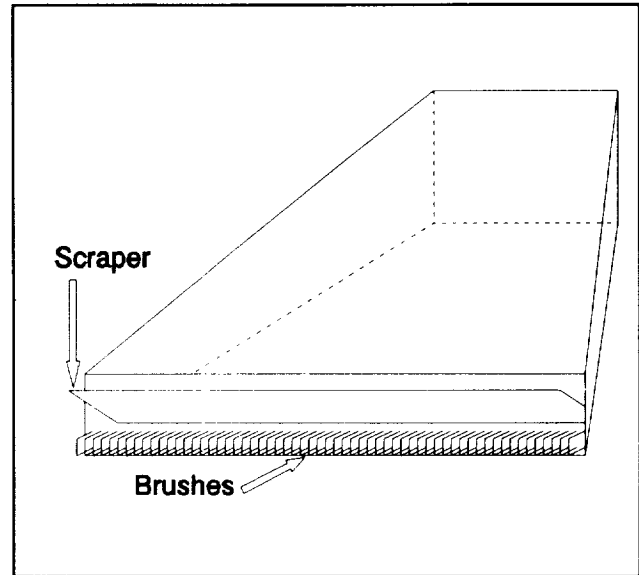


Fig. 12 Vacuum nozzle

produce airflow. The interface between the duct and blower was sealed to prevent backwards flow. Test particles (sawdust) were inserted directly into the blower intake. At the far end of the duct, a fine mesh of nylon was attached to catch unfiltered particles. The same nylon material was used to recover vacuumed particles from the cleaning system. The vacuum was driven by a 1.5 hp wet-dry vacuum apparatus. Mass readings of dust entered, dust cleaned, and dust exited were recorded.

Pressure and flow rate data were also taken during operation. Static pressure readings were taken from holes in the duct at 9 inches before and after the plates. A manometer accompanied by a pitot tube yielded the measurements. The flow rates were taken at the same position as pressure readings with a hot wire anemometer. The prototype was also tested for microgravity effects by altering the gravitational position vector and observing any changes in data. This was achieved by operating the system 90° from its original position on the longitudinal axis. An orientation of 180° rotation was not necessary due to the symmetry of the design.

#### System efficiency

Particle removal effectiveness was determined by evaluating the efficiency of the filter. Efficiency discussions require the following definitions.



E = Filter efficiency

TP = Total amount of particulate matter which flows through the duct in a given time interval, by mass.

FP = Amount of matter which is removed from the flow by the filter, by mass.

UP = Amount of uncaught matter which passes through the filter, by mass.

TP = FP + UP

E = FP / TP

= FP / ( FP + UP )

= 1 - ( UP / TP )

The filter efficiency was calculated by measuring the mass of particles which was able to pass through the filter. The mass of the nylon collection bag and its contents was determined before and after each filter test. The difference in the two masses is the value UP, the uncaught particle mass.

### Test results

Flow rates and pressures of the system were taken periodically during flow operation and averaged. At a flow rate of 500 fpm exiting the blower, the pressure drop across the plates was .02 in H<sub>2</sub>O. A higher flow rate of 600 fpm was achieved by combining the existing blower with a 1.5 hp wet-dry vacuum. This increased flow rate yielded a pressure drop of .053 in H<sub>2</sub>O. The measured flow rate of the vacuum system was 3400 fpm at the nozzle entrance.

The system was checked for efficiency with two data runs in the upright position and one in the rotated position. Table 1 summarizes these three tests with values of dust entered, dust exited, and efficiency percentage. The efficiency presented here is in respect to the total dust mass entering the system. Tests one and two are in the upright position and test three is the rotated orientation.

Table 1 Efficiency testing

|                           | 1   | 2    | 3    |
|---------------------------|-----|------|------|
| Dust entered (grams)      | 5.9 | 18.2 | 16.6 |
| Dust exited (grams)       | 2.2 | 2.3  | 2.7  |
| Filtration efficiency (%) | 63  | 88   | 84   |

The prototype was also tested for cleaning success. Three data runs were taken in similar conditions as the efficiency recordings. Table 2 displays the three tests and the values of dust entered, dust recovered, and percentage amount of dust recovered from total mass. Tests one, two, and three correspond to the same orientation as in Table 1.

Table 2 Cleaning system testing

|                        | 1   | 2    | 3   |
|------------------------|-----|------|-----|
| Dust entered (grams)   | 8.1 | 23.4 | 8.0 |
| Dust recovered (grams) | 0.9 | 4.8  | 2.8 |
| Percent recovered (%)  | 11  | 21   | 35  |

### Leakage

Flow leakage during system operation was minimal when the seals were in the closed position. However, when the seals opened to allow plate movement, flow and particles leaked out of the duct. Extensive particle leakage was observed through the lower seals when the system was in its upright position. The loss of recorded dust mass is attributed to this leakage. Another cause of particle leakage is the multiple sizes of the dust particles. Pieces smaller than 1 mm are expected to leak through the perforated plates. This fact shows that the mass readings may not be fully representative of the system's potential because some of the escaping mass was too small for the filter. The use of mixed particle sizes may have attributed to the low cleaning percentages and filter efficiency.

## A FOOD PREPARATION DEVICE FOR MICROGRAVITY

On extended space missions, it will be necessary to produce foods to satisfy the crew physically and psychologically. The production of these foods will be limited to those ingredients produced by the plant growth units on board or from supplies brought from earth.

The objective of this project is to design and manufacture a device for food preparation in microgravity. The project focuses on producing a variety of cooked foods containing similar ingredients. After researching the different foods that could be produced, the project team decided to focus on the preparation of pancakes, waffles, and other flour-based foods.

The food preparation device for microgravity was completed in three phases. Phase I consisted of the design and testing of a mechanism which dispenses wet and dry ingredients in measured quantities. This led to Phase II of the project which entailed mixing the ingredients into a batter substance. Phase III completed the hardware portion of the project by yielding a mechanism which, when integrated with the first two phases, cooked the batter.

## Developed Ideas

### Dispensing

Several types of dispensing mechanisms were investigated for both the wet and dry ingredients. The main considerations for a dispensing design include prevention of leakage, accurate measurement of ingredients, and control of ingredient flow. A matrix of the various concepts considered and a discussion of the results accompanies this section. Illustrations of the dispensing mechanisms considered are shown in Figure 13.

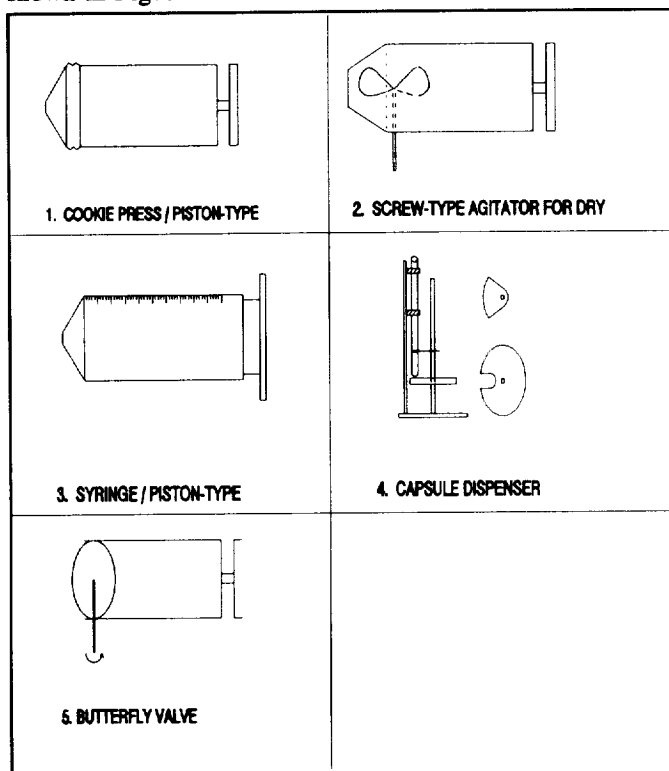


Fig. 13 Ingredient dispensers considered

**Experiments Performed** The first experiment involved the use of a cookie press to simulate a piston moving dry and wet ingredients. Dry ingredients will not move unless the exit diameter is the same as that of the container. The flour (the primary constituent of the dry ingredient mixture) became packed as it was displaced toward a smaller area. The wet ingredients flowed easily with piston displacement, but accurate measurements were hampered since the flow did not immediately cease when the displacement force was removed.

The next experiment involved the use of a screw-type mechanism. This was used to agitate dry ingredients at the dispenser exit and to eliminate packing tendencies. Although the dry ingredients moved well, this mechanism requires the implementation of an accurate measuring device. In addition, the agitating mechanism adds mechanical and automation complications.

The possibility of eliminating dry ingredients was considered by preparing a mixture of flour and milk in the piston-type device. This reduced the bulk of dry ingredients dispensed, but additional dry ingredient mixing (i.e., sugar and baking powder) is still required. Another drawback is that the amounts of some ingredients vary according to the desired recipe.

Another piston-type experiment was performed using a syringe and a check valve to dispense and accurately measure wet ingredients. The results were favorable since the flow of liquid ingredients ceased immediately, and no leakage was detected.

In addition to the mechanisms mentioned above, dissolvable capsules were considered for the dispensing of baking powder. The capsules held one-half teaspoon each and dissolved almost immediately when immersed in hot liquids. They did not, however, readily dissolve in cold liquids. Mechanisms for dispensing the capsules were investigated. A model was assembled, and it performed favorably, but further modification would be required for use in microgravity.

Another option for dry ingredient dispensing is the use of containers filled with pre-mixed portions of the dry ingredients (i.e., flour, sugar, and baking powder). These individual containers would hold a mix for pancakes, waffles, and other dry mixes. The preparation of these containers would take place in the food processing area. Each container would contain enough dry ingredients for one or two recipes. For example, one recipe of pancakes is equivalent to three eight-inch pancakes.

### Mixing

Six mixing mechanisms were examined. They included a blade-type mixer, a kneading-type sealed-bag mixer, a magnetic stirrer, a high-speed rotation apparatus, a shaker, and a collapsible whisk. Initially, the ingredients were mixed by conventional rotary mixer, and the resulting batter was used as a control mixture. The resulting batters and control mixture were then cooked on a conventional skillet to compare their texture and flavor. Illustrations of the mixing mechanisms considered are shown in Figure 14.

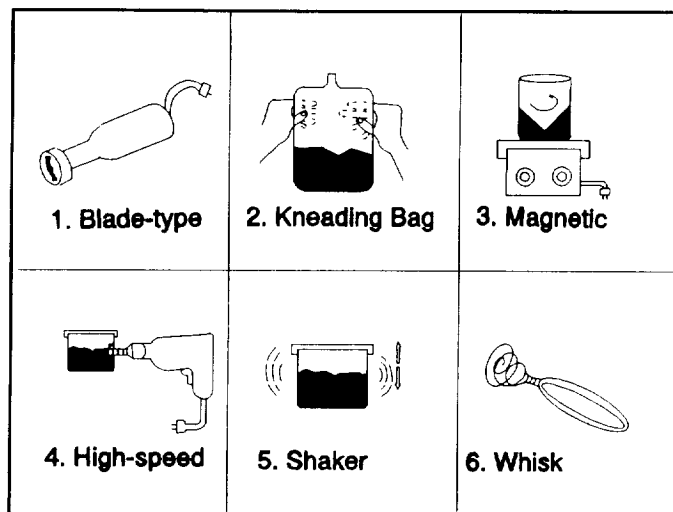


Fig. 14 Mixing mechanisms considered

**Experiments performed** The blade-type mixer quickly produced a smooth batter and a cooked product comparable to the cooked control mixture. The mixing time required was approximately 30 seconds. This time is shorter than that using conventional means which had a mixing time of approximately one minute. In microgravity, an additional mechanism would be required to oscillate the blade through the batter for thorough mixing.

The mixing of ingredients using the kneading-type sealed-bag method produced a lumpy batter in three minutes mixing time. However, the taste of the cooked product was comparable to the cooked control mixture.

A magnetic stirrer failed to mix the ingredients thoroughly because it could not overcome the viscous force of the batter as dry ingredients were added. For this reason the magnetic stirrer was discarded as a mixing option.

The high-speed rotation device consisted of a container adapted to rotate with a shaft connected to a power drill. The device yielded a lumpy batter unusable for cooking.

The shaking of ingredients in a container produced a batter comparable to that of the kneading method. However, this method would require complex mechanical manipulations.

A collapsible coil whisk was modified to fit a shaft and was used for mixing. The whisk reduces the number of

mechanisms required because the coil extends the length of the mixing chamber, thereby eliminating the need for an oscillating mechanism. In contrast, the blade-type mixer required an oscillating mechanism to mix the ingredients into a batter comparable to the control mixture.

## Final Design

### Overview

A constant area container with pre-mixed ingredients is used for dispensing the dry ingredients (flour, sugar, and baking powder). The dry ingredients are moved into a mixing chamber using a ratchet system. The wet ingredients (milk, eggs, and oil) are contained in individual bags. A syringe/check valve assembly is used for dispensing the wet ingredients from the bags. Once in the chamber, the ingredients are mixed with a collapsible coil whisk. A piston mechanism is used to move the batter out of the mixing chamber and into a cooking unit. The cooking unit has removable hot plates so that foods of different shapes can be cooked. A setup of the final design is illustrated in Figure 15.

### Setup

The dry ingredient ratchet container, the batter exit port, and the liquid ingredient insertion port are located at one end of the mixing chamber. The whisk-mixing apparatus and piston assembly are attached at the other end as depicted in Figure 15.

The mixing chamber is a Plexiglas cylinder machined to 4.75 inches in length and 3.765 inches inside diameter. The piston mechanism, also of Plexiglas, has an outside diameter of 3.760 inches. An AC motor for the mixing mechanism was modified from a common hand-held mixer.

### Operation

Initially, the piston and whisk are at one end of the chamber. As ingredients are inserted, the piston moves back, the whisk extends, and the ingredients are mixed into a batter. The piston and collapsible whisk allow the chamber to stay airtight, thus eliminating excessive air in the batter.

### Seals and Close-off Mechanisms

Since one of the primary design specifications is to

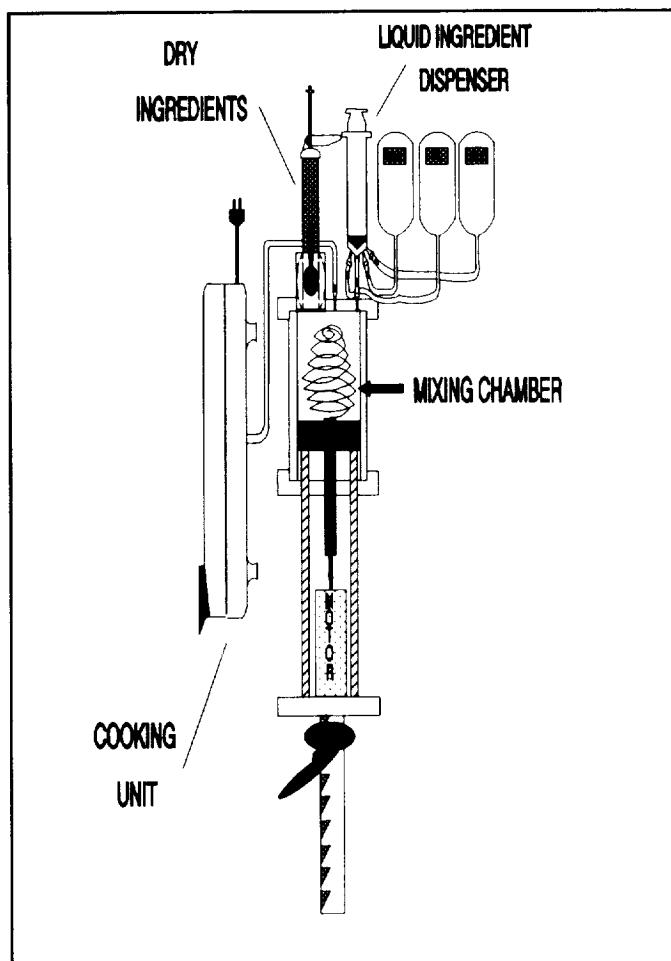


Fig. 15 Final design

prevent leakage, a variety of seals and close-off mechanisms were considered. Close-off mechanisms were investigated for the dry ingredient dispenser. Several concepts for leak prevention between the piston and mixing chamber were examined. A means to prevent backflow of wet ingredients in the dispensing tubes was explored. These seals and close-offs are depicted in Figure 16.

**Dry Ingredient Close-off** The close-off mechanism between the dry ingredient dispenser and the mixing chamber is necessary so that the dry ingredients can be restocked. A stopcock and an aperture system (such as a camera lens shutter) were investigated.

A canister of flour was attached to the stopcock. The

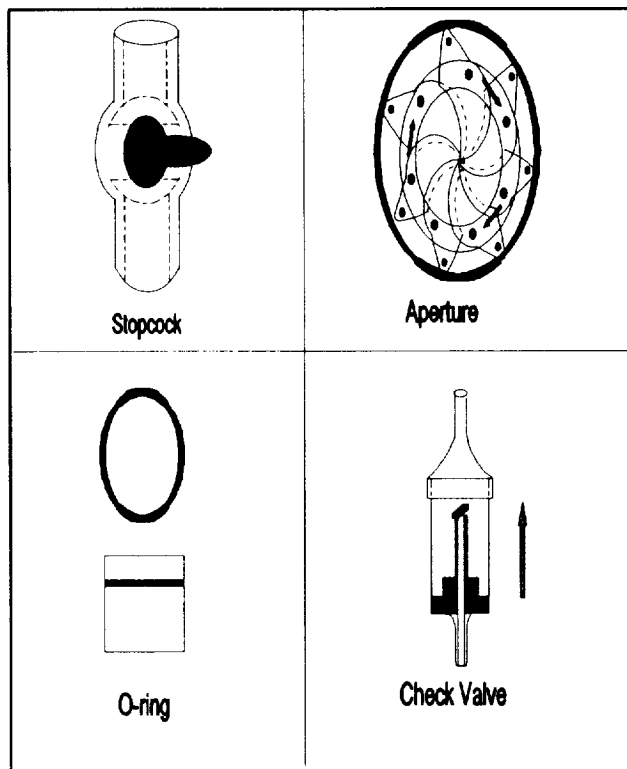


Fig. 16 Seals and close-off mechanisms considered

stopcock was opened, the flour was displaced, and the stopcock was closed. The flour did not hinder the closing of the stopcock, and the entire procedure was leak-proof.

For the purpose of preliminary experimentation, a canister of flour was attached to an aperture system. Not only did dry ingredient particles imbed themselves between the intricate petals of the device, but the slightest amount of moisture also caused the plates to remain open. Even though the sticking of the plates could be corrected, problems with leakage would still be present.

**Piston Seals** Another area of potential leakage is in the clearance between the walls of the mixing chamber and the piston. To prevent leakage, incorporating an O-ring, supplying oil as a hydrophobic repellent, and using a low tolerance with no seal in the design were considered.

A piston with an O-ring was manufactured from a

polyvinylchloride (PVC) pipe. This was done to study the manufacturing processes involved in machining pistons with O-rings. From these experiments, it was concluded that the manufacturing of a piston-seal assembly requires very exact machining of the piston and chamber. This exact machining was not feasible because of time constraints and lack of experience.

In another experiment, a film of oil was applied between the piston and chamber to repel liquid ingredients and lubricate the piston. However, this method did not provide the close wall tolerance necessary to expel most of the batter.

Finally, the elimination of a seal in the chamber assembly was considered, and a round piston and matching chamber were manufactured. Since the tolerance was maintained to within 0.005 inches, no leakage occurred while the piston was kept stationary. Further experiments were performed, and it was determined that the level of leakage was negligible.

**Pinch Valves** Tubing from the wet ingredient dispenser was mailed to Bio-Chem Corporation to determine the gap size required for the pinch valves. Since each pinch valve costs \$50 and three pinch valves are required, it was determined that the cost was not justified when the tubes could be closed-off manually. For this project, roll-off pinch valves are used to close off the tubes when not dispensing ingredients at a given time.

Experiments were performed with one electronic pinch valve and three roll-off pinch valves. Although the electronic pinch valve provided positive results especially in the area of automation, the cost restricted the use of these devices. Manually operated roll-off pinch valves provide positive results and are incorporated in the final design.

**Seals** A stopcock is used in the final design to close off the dry ingredients. The tolerance between the piston and mixing chamber is 0.005 inches. This tolerance is small enough to prevent leakage and yet allow the piston to move adequately within the chamber. A cap at the end of the mixing chamber acts as an additional barrier should leakage occur.

## Cooking

Two main considerations were made in the purchase of a cooking unit. These considerations are as follows:

1. The unit must be adaptable to cook pancakes, waffles, and other flour-based foods so that the foods physically resemble those food items.

2. The cooking surfaces of the unit must adapt so that foods of variable heights (such as muffins) can be cooked.

A cooking unit with removable plates and a variable height between the plates was purchased. The cooking unit is depicted in Figure 17.

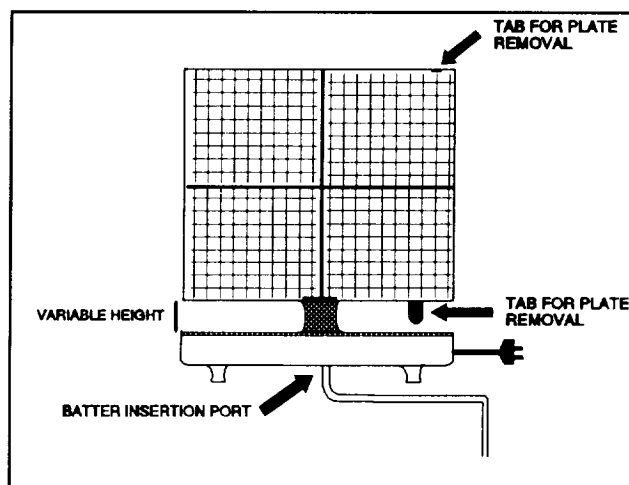


Fig. 17 The cooking unit

A port for batter extraction was connected at the end of the chamber (the same end as the ingredient insertion ports). A tube extends from the port, through the bottom center of the cooking unit, and into the space between the two plates. Because of time and cost limitations, it was decided that the tube would be removed upon injection of the batter. The complications associated with keeping the tube (and the batter within the tube) cool are eliminated by removing the tube from the cooking unit before cooking begins.

## Conclusion

Final testing took place in all orientations. Each separate component of the device worked well as an independent unit. However, when all of the components were put together to assemble the final design, problems with leakage occurred. The ingredients leaked in two areas: (1) between the piston and mixing chamber walls and (2) at the connection for the dry ingredient container.

Dispensing wet ingredients into the mixing chamber did not present difficulties. The roll-off pinch valves acted to close off ingredients not being dispensed so that sequential

ingredient insertion could take place. The check valves limited the flow of ingredients to one direction. Additionally, leakage did not occur at the entrance port to the chamber.

Favorable results were obtained from dry ingredient dispensing. However, the wet ingredients in the chamber leaked out around the connection of the dry ingredient container. This connection is sealed only by force applied at the opposing end of the container. Some modifications were made at the connection, and less leakage occurred.

As ingredients are inserted into the mixing chamber, the piston is intended to move back, keeping the system entirely air-proof. In the prototype, there was some difficulty in pushing back the piston. Also, there was some minor leakage around the piston.

The whisk mixed the ingredients into a smooth batter. It collapsed and extended during the proper stages of device operation.

The batter moved through the tube to the cooking unit with some difficulty. However, upon insertion of the batter into the unit, the batter spread evenly between the cooking plates.

### References

1. Chamberlain, Dennis. Personal interview. January 1992.
2. Hessel, Long, Richert, and Tullo. A Sectored Plant Growth Unit With Support Systems. Prepared for National Aeronautics and Space Administration, Kennedy Space Center, Florida and Universities Space Research Association, 1991.
3. Hessel, Michael. Personal interview. January 1992.
4. Maturo, Dr. Frank. Personal interview. January 1992.
5. Wheeler, Dr. Ray. Personal interview. January 1992.
6. Finger, Barry. Personal interview. November 1991.
7. Haggerty, J. J. Spinoff 1985, NASA, 1985.
8. Harrington and King Perforating Company. Cat. 105.
9. Heppner, D.B., Sudar, and Lee. Advancements in Oxygen Generation and Humidity Control by Water Vapor Electrolysis, Life Systems, Inc.: Cleveland, 1988.
10. Matteson, M.J. and Orr. Filtration: Principles and Practices, Marcel Dekker, Inc.: New York, 1987.
11. Mohler, Bill. Johnson Wire, St. Paul, MN. Personal interview. December 1991.
12. Raber, Robert R., ed. Fluid Filtration: Gas, American Society for Testing and Materials: Baltimore, 1986.
13. Thompson, Don. Thompson Sheet Metal. Personal interview. February 1992.
14. Tromble, Jon D., Dishwasher for Earth or Outer Space, Whirlpool Corp. Johnson Space Center, 1991.
15. Betty Crocker's Cookbook, (New and revised edition). Golden Press/New York. Western Publishing Company: Racine, Wisconsin. Eighth printing, 1983.
16. Pugh, Stuart. Total Design-Integrated Methods for Successful Product Engineering, Addison-Wesley Publishing Company. 1991.
17. All Electronics Corporation. Winter 91/92. Catalog #591. Van Nuys, California.
18. Electronic Engineers Master Catalog. Vol B and C, 1988-1989. 31st Edition. Hearst Business Communications.

## THE EXTENDED MISSION ROVER (EMR)

Florida A&M University/Florida State University College of Engineering  
Departments of Mechanical and Electrical Engineering  
Tallahassee, Florida

Professor W. Shields  
Anthony Halecki, Teaching Assistant

Manh Chung, Ken Clarke, Kevin Frankle, Fariba Kassemkhani, John Kuhlhoff, Josh Lenzini, David Lobdell, Sam Morgan, Robert Nock, Sabash Panigsahi, Cynthia Robbins, Mark Russell, Rowi Shah, Gail Wallace, Russell Willis

### Abstract

A key component in ensuring America's status as a leader in the global community is its active pursuit of space exploration. On the twentieth anniversary of Apollo 11, President George Bush challenged the nation to place a man on the moon permanently and to conduct human exploration of Mars in the 21st century. The students of the FAMU/FSU College of Engineering hope to make a significant contribution to this challenge, America's Space Exploration Initiative (SEI), with their participation in the NASA/USRA Advanced Design Program. The project selected by the 1991/1992 Aerospace Design group is the design of an Extended Mission Rover (EMR) for use on the lunar surface. This vehicle will serve as a mobile base to provide future astronauts with a "shirt-sleeve" living and working environment. Some of the proposed missions are planetary surface exploration, construction and maintenance, hardware setup, and *in situ* resource experimentation. This vehicle will be put into use in the 2010-2030 time frame.

### Project Management and Organization

The 1991/1992 Senior Aerospace Design class was organized in a matrix management fashion with all students involved in the project assigned to a design group and a management group. This provided the students with a true feeling for how projects are organized in the industrial sector. The class consisted of seven mechanical engineering students and nine electrical engineering students. Due to the diverse makeup of the class, students were often involved in interdisciplinary tasks.

### Mission Statement and Requirements

The purpose of an EMR is to provide transportation, shelter, and working quarters for a crew of four on long

duration lunar surface missions. The preliminary mission requirements as defined by the Mission Requirements Working Group which researched existing technologies and forecasts of available future technologies include:

- Mission Distance: 1000 km round-trip
- Mission Duration: 28 Earth days (1 lunar day)
- Maximum Crew Size: 4
- Maintain self-sufficient environment to support crew and cargo (oxygen, food, water, climate)
- Maintain interior environment during egress
- Provide shielding from environmental elements
- Collect/analyze/store data
- Possess robotic data sample/data collection capability
- Transport various experimental apparatus
- Travel over rough terrain (45° head-on, 20° traverse)
- Possess path-clearing abilities
- Provide internal navigation support
- Possess communication capability with base and Earth
- Possess unmanned capability
- Provide redundant systems
- Be easy to maintain

By keeping the expected traverse distance under 3000 km for a time period of approximately one month, the size of the fuel cell tankage was small enough to keep from interfering with the accomplishment of the mission objectives.

The multi-purpose nature of the vehicle design makes it flexible enough for use in many applications such as firsthand observation and assessment of the terrain within a 500-km radius of the base. Lengthy analysis and assessment of mineral deposits could be conducted from the vehicle, as well as setup of sensitive hardware such as space radio telescopes at a great enough distance from the permanent lander base to prevent interference from vibrations caused by the lander's engines.

The multi-purpose nature of the vehicle design makes it flexible enough for use in many applications such as firsthand observation and assessment of the terrain within a 500-km radius of the base. Lengthy analysis and assessment of mineral deposits could be conducted from the vehicle, as well as setup of sensitive hardware such as space radio telescopes at a great enough distance from the permanent lander base to prevent interference from vibrations caused by the lander's engines.

### System Design and Integration

The design of the EMR was based upon the forecast of future technologies consistent with those included within available references. Rather than trying to carry out detailed calculations on the transportation system, the approach was to ensure that the mass and size of the EMR did not exceed the limitations predicted by the available references. Figure 1 shows a side view of the vehicle.

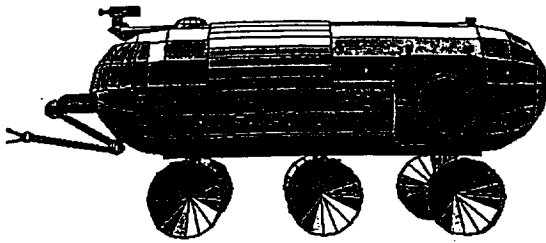


Fig. 1 Side view of vehicle

From the report released by Boeing Defense and Space Group, Advanced Civil Space Systems, in Huntsville, Alabama, a launch vehicle and lander system was found that would easily accommodate the EMR. The estimated payload delivered to the lunar surface was 45 mt based on the concept of delivering a fully integrated habitat to the lunar surface. This would fit into Boeing's LTV tandem stage expendable mode using the Direct, Lunar Orbit Rendezvous (LOR) high-thrust profile. The launch vehicle proposed by Boeing was in the range of 100-400 mt with a payload shroud of 10 m x 30 m. The preferred method of carrying the cargo is to hang it on the underside of the lander to make it easy to unload on the lunar surface. If the payload is to be underslung on the

lander, some deployment or assembly of the EMR may be needed on orbit if the launch vehicle is less than 10 m in diameter.

### Suspension

The rough terrain of the lunar surface represents great difficulties for the locomotion system of a ground-based vehicle. Mobility requirements for a lunar-based vehicle are very diverse. Mission requirements vary greatly, and the environment of locomotion may be literally anywhere on the moon. To meet these diverse needs, all practical mobility concepts, including tracked vehicles, walkers, and wheels, were examined.

Wheels will be the preferred mobility option for many missions. Wheels are mechanically efficient, can be designed into lightweight systems, and can be built with excellent reliability. A disadvantage in terrestrial all-terrain applications is their small footprint, but the reduced gravity field of the moon does not require a large ground contact area.

The EMR will use six cone-shaped carbon graphite wheels, each with a diameter of 72 inches and a thickness of 0.5 inches. Tread width is 20 inches for maximum traction to help prevent slippage on the lunar surface. Minimum ground clearance for the wheel is estimated to be 36 inches. Overall weight for six cone wheels is approximately 624 kg.

To accomplish the vehicle mission, the suspension system must meet the following requirements:

1. Ensure height mobility under lunar surface conditions of rough terrain, loosely cohesive soil with low bearing strengths, and a coefficient of resistance of motion ( $f$ ) of 0.6.
2. Overcome elevations of up to 25°.
3. Ensure reliable motion on the lunar surface despite obstacles such as groups of rocks, scarps, and counterscarps, fissures and craters.
4. Ensure a highly reliable operation of all systems without need for repair within the required service life.



5. Be within a definite geometric size with a minimum weight in keeping with the requirements of the space rocket capacity.

The final design for the primary and secondary suspension system is shown in Figure 2.

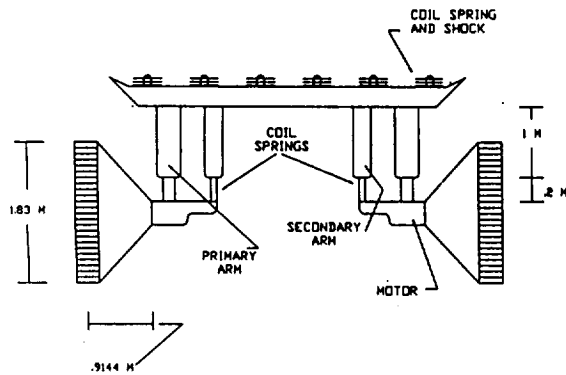


Fig. 2 Primary and secondary suspension

### Radiation Shielding

The problem of providing sufficient radiation shielding for the crew of the EMR was approached from a very conservative point of view. It has been suggested that a spacecraft with shielding equivalent to  $5 \text{ gm/cm}^2$  of aluminum would suffice for a manned Mars mission. This would seemingly be a sufficient amount of shielding for a lunar mission. However, this amount was deemed low and through an interactive research and mass trade-off process, a figure of  $10 \text{ gm/cm}^2$  shielding was agreed upon for normal radiation protection.

Since a high intensity radiation storm could prove lethal to crewmembers in the EMR, it is assumed that by the time this vehicle is deployed on the moon, an early warning system to detect radiation storms and solar flares will have been developed.

### Airlock

An airlock that allows the crew and equipment to enter or exit the vehicle without depressurizing the whole craft is necessary in order to satisfy mission requirements. A conventional airlock design will be used.

### Vehicle Shell

The internal shell will be made of 2219 aluminum alloy. Aluminum is a proven material for lining pressurized vessels because of its weight-to-strength ratio (0.5) and its manufacturing capability. It is easily maintained, and is suited for welding and forming. The internal framing will be welded together.

### Avionics

The primary purpose of the avionics system is to integrate successfully a comprehensive set of general aviation electrical and electronic functions into a complex system architecture. It should meet the users' needs by improving the safety and dependability of the vehicle system operations without increasing the requirements for astronaut training/experience by overexploiting advanced technology in computers, displays, and overall system design. The overall purpose will be to design a system at an affordable price. The system will be comprised of Avionics Vehicle Control, Robotic Arms/Video, Navigation, Communications, and Data Transfer/Acquisition to provide critical information, improved functional capability, and shared electronic displays without losing important considerations about overall system cost, reliability, producibility, and overall maintainability of the entire avionics system. The mass of the total avionics system is about  $100 \text{ kg} \pm 5 \text{ kg}$ ; the volume of the avionics system is  $4.5 \text{ m}^3$ , including the avionics display of  $0.5 \text{ m}^3$ , communication system of  $1 \text{ m}^3$ , and workstation of  $3 \text{ m}^3$ . The total power requirement of the avionics system is approximately 600 watts.

### Workstation

The concept of a modular, reconfigurable, expandable, general purpose, human-engineered workstation is envisioned for use by scientists, technologists, design and system engineers, and space and ground operators. The workstation encompasses concepts of machine independence, modularity, standardized interfaces, expert system technology, and human machine interaction techniques.

## Input and Output Devices

The primary input device of the workstation is the keyboard, which will either be attached or remote so that astronauts can enter data directly in memory without coming near the workstation. Other devices such as a touch-sensitive screen, optical character reader, and a light pen will also be available for input. There will also be a digital mouse or track ball to enhance the workstation's capabilities.

## Communication

Since communication between the base and the EMR is a top priority and the vehicle has a range of about 1000 km, a system of lunar orbiting satellites and a tower antenna at the base or on the vehicle are suggested. Figure 3 illustrates the case when the rover is on the far side of the moon and two satellites are required for communication with the base.

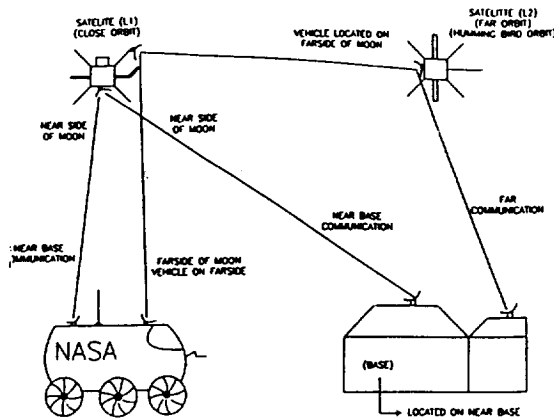


Fig. 3 Communication network

## Link Performances and Antenna Types

Link performance analysis deals with sizing communication system power and antennas so that the received signals are strong enough that the data can be extracted from the signal. Of the many types of antennas available, the dish reflector possesses a major advantage because it concentrates signal energy on the receiver, thus improving the signal-to-noise ratio.

## Navigation

Navigation on the moon is difficult because there is no coordinate system equivalent to the Earth's North and South poles. The navigation system is divided into the following main displays:

- **Attitude Indicator** -- provides indications of vehicle's pitch and roll. This instrument indicates pitch upslope (u) and downslope (d) within a range of  $\pm 25^\circ$ . The damper on the side of the indicator can be used to damp out oscillations.
- **Heading Indicator** - displays the vehicle heading with respect to lunar north.
- **Bearing Indicator** - shows the bearing to the base.
- **Distance Indicator** -- reports distance traveled by the vehicle in increments of 1 km.
- **Sun Shadow Device** - determines the vehicle's position with respect to the sun. This heading can be compared with the gyro heading at regular intervals as a check against gyro drift.
- **Speed Indicator** - shows the vehicle velocity from 0 to 20 km/hr, and is driven by odometer pulses from the right rear wheels.
- **Gyro Torquing Switch** - adjusts the navigation gyro to correct the heading indication during navigation update.

## Heads-Up Display

A helmet-mounted visual display system will provide an astronaut with a broad range of visual information for experiments and critical information about human aspects, the robotic arm, and the pathfinder. In addition, the display offers a nearly unlimited field of vision.

## Robotic Arm

The design of the robotic arm will incorporate key issues of compactness, versatility, reliability, accuracy, and weight. The arm can be used on both the lunar vehicle and lunar base for a variety of functions. The lunar

vehicle will have connections for the robotic arm on the lower center front and on the rear of the vehicle.

### Electronically-Scanned Laser Pathfinder

The electronic laser scanner will use a laser diode array(s) and charge-coupled cameras (CCD) to sweep across its field of view to measure the distance of objects from 0.5 to 20 m away. No mechanical moving parts will be necessary. The scanner device will guide the EMR around large to medium-scale obstacles.

### Moving Map Display Processor for Finding LC Path

A VLSI (Very Large Scale Integrated) circuit design will implement a processor to find the lowest-cost map path by associating a traversal cost at each pixel node and calculating at each node the total cost of a path from a unique originator node to that node. This design concept will be very important due to the mission requirement of capability for a 1000-km round-trip.

## Thermal/Fluid

### Environmental Requirements

The environment that will be experienced on the lunar surface poses many problems to the engineer. Because of the closed nature of the life support system on the EMR, the ability to revitalize the atmosphere becomes a major factor in maintaining the health of the astronauts. Several important conditions are temperature, pressure, humidity, composition, and purity. The biological needs of the astronauts must be quantified and the effects of certain conditions evaluated to ascertain their hazard levels.

### Waste Removal and Storage

Storage will consist of a cylindrical tank of thin stainless steel sheet with an insulation jacket to reduce heat dissipation. The waste will be treated chemically with active enzymes which break down the bacteria growth and reduce odors. The urinal system will be sealed when not in use to reduce accumulation of odors in the latrine. A forced air system will complement the toilet to ensure proper flow direction of waste material. The chemical treatment system will be controlled by a flow meter which can sense additions to the tank. The chemical treatment

will consist of sulfuric acid 10 (a triple salt monopersulfate compound) which will disinfect, control pH to between 2.0 and 2.5, and fix free ammonia and ammoniated compounds.

### Water Supply

The water will be stored in cylindrical tanks to minimize space requirements. Storage will be external to allow for modularity and maintenance. A pump will provide usable pressure for tasks such as showering, waste removal, and galley feedwater. The estimated power consumption is 391 W at a flow of  $0.456 \text{ m}^3/\text{hr}$ . See Figure 4 for details.

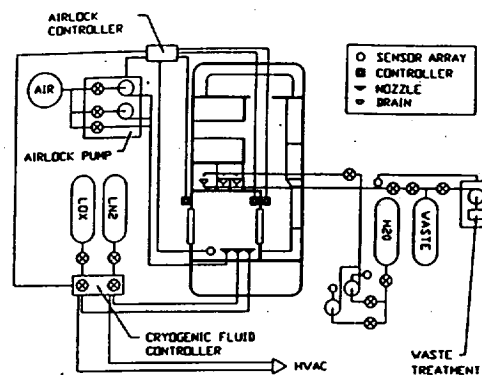


Fig. 4 Water supply and waste removal schematic

### Cryogenic Storage

The atmosphere in the vehicle will be composed of a mixture of 80% nitrogen and 20% oxygen, which is very close to the 78.084% nitrogen, 20.9476% oxygen plus traces of other gases for normal atmospheric breathable air. Nitrogen and oxygen will be stored in two separate cryogenic cylindrical tanks located outside the vehicle and mixed accordingly. Concerns for safety in the cryogenic fluid storage vessels are addressed in the design of: 1) the inner vessel pressure relief valve, 2) the inner shell burst-disk assembly, and 3) the annular space burst-disk assembly.

## Leak Containment

Because of the high vacuum that characterizes the lunar environment, maintenance of a suitable atmosphere in the vehicle is imperative. A pressure of approximately 12 psi, close to the sea level pressure of 14.7 psi on Earth, has been chosen for optimum crew health and performance. The inside living quarters cabin shell will be surrounded by another shell to provide a deterrent to leak propagation.

## Airlock Management

The airlock is the only outlet from the vehicle. It is also the last protection the astronauts have from any physiological problems that could result from the pressure decrease that occurs during EVA. A compressor will be used to depressurize the airlock. A second compressor will be carried in the vehicle for redundancy. The compressors will require no more than 15 kW of power during airlock pumpdown. The first stage of depressurization will require 7.2 kW, and the second stage requires 14.9 kW of power.

## Fire Suppression

The hazard of fire aboard the vehicle is compounded by the closed loop system and the restrictions it places on the emergency equipment. Though there are many ways to combat a fire, all use basically the same principle, which is the removal of oxygen from the flame. On the EMR, fire suppression will consist of removing all the air and replacing all available oxygen with inert materials ( $\text{CO}_2$ , Halon, dry chemical). This will be complemented through the use of  $\text{CO}_2$  in the cabin areas and Halon 1301 in the electrical compartments.

## Power Generation

### Radioisotope Generators

To meet critical power requirements, a dynamic isotope power system (DIPS) has been selected. The isotope used in the system is  $\text{Pu}^{238}$ , one of a group of reactor-produced fuels including  $\text{Cm}^{242}$  and  $\text{Cm}^{244}$ . Reactor-produced fuels can be divided into two classes: those that absorb one neutron and those that absorb more than one neutron. In the first class, a stable isotope captures one

neutron and thus becomes radioactive. In the second class, a stable isotope (one with a long half-life) absorbs more than one neutron until it ends up as the desired radioisotope.  $\text{Pu}^{238}$  is characteristic of the second class of fuels.

### Fuel Capsules

Metallic fuel capsules that hold long-lived alpha emitters must contain a vent for the helium gas generated by the radioactive decay of the nuclear fuel unless adequate space is provided within the system for the venting to occur. These vents can be either selective or nonselective. Selective vents pass helium, but retain any larger gas molecules and solid particulates from the fuel. Nonselective vents also retain solid particulates from the fuel, but pass helium and other gaseous effluents, including uncondensed fuel, impurity vapors, and possibly other fuel decay products such as radon.

### Overall Design

The overall design of the DIPS power system consists of five major components: (1) an isotope heat source, (2) a compressor, (3) a thermal radiator, (4) a turbine, and (5) a generator. The components have been integrated so that the complete system follows a closed Brayton cycle configuration. Based on this configuration, heat addition and rejection occur at constant pressure, while expansion and compression are assumed to occur at constant entropy. To simplify the design of the power system, it was organized so that both the compressor and the turbine make use of the same shaft.

### Radiator Design

The design of the radiator for the lunar rover will follow a configuration of a series of tubes through which the coolant will flow. The mass flow rate of the coolant (helium) was found to be 0.0904 kg/s and the specific heat,  $C_p$ , was determined to be a constant value of 5.193 KJ/Kmol·K.

### Future Considerations

If increased power requirements are necessary, dynamic power conversion units can be coupled with radioisotope heat sources. That results in the extension of the power generation range beyond that practically obtainable with

other systems such as telluride TE converter systems. Lower unit costs are obtained through higher power conversion efficiencies. A bar chart of the power requirements can be seen in Figure 5.

### Backup Power

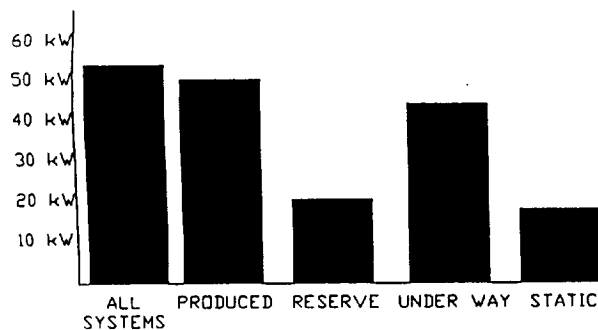


Fig. 5 Power requirements for lunar rover

The maximum power required for the EMR while traversing a 20° slope is 43.4 kW<sub>e</sub>. The maximum power requirement for static operation, which includes experimentation, is 18.6 kW<sub>e</sub>. The maximum power required if all systems are working simultaneously and at maximum operating conditions is 53.9 kW<sub>e</sub>.

### Propulsion System

The propulsion system for the EMR consists of electric motors designed to meet the following requirements: variable torque, variable speed, light in weight, high efficiency, and high torque for obstacle clearance combined with optimum speed to maximize the vehicle's exploration range.

### Motor

The brushless DC motor contains the following main components: (1) motor, (2) sensing system, (3) electronic commutator, and (4) control. The brushless motor consists of a rotor on which permanent magnets are mounted. These magnets are always arranged in pole pairs. The winding is placed in an external, slotted stator.

### Power Control Methods

A varying supply voltage to the commutation system will provide power control. The six switching transistors will control commutation at the proper angular intervals, and the series-connected power transistors will handle velocity and current control of the brushless motor. This can be accomplished by pulse-width or pulse-frequency modulation.

### Tachometers

Tachometers are often necessary in high-performance servo applications in which they provide velocity feedback for speed control purposes or servo system stability. For this system an Electro-Carft brushless DC tachometer will be used. The tachometer is based on a permanent magnet motor and a multi-coil stator structure, which is commutated by an MSI circuit.

### Summary

An Extended Mission Rover to provide transportation, shelter, and working quarters for a crew of four on long-duration lunar surface missions has been designed by students from the Departments of Mechanical and Electrical Engineering at the FAMU/FSU College of Engineering. The vehicle will serve as a mobile base to provide future astronauts with a "shirt-sleeve" living and working environment. The multi-purpose nature of the vehicle design makes it flexible enough for use in many applications on the lunar surface.

## THE ENABLER: A CONCEPT FOR A LUNAR WORK VEHICLE

Georgia Institute of Technology  
School of Mechanical Engineering  
Atlanta, Georgia

Professor James W. Brazell  
Craig Campbell and Ken Kaser, Teaching Assistants

### Abstract

The Enabler is an earthbound prototype designed to model an actual lunar work vehicle and is able to perform many of the tasks that might be expected of a lunar work vehicle. The vehicle will be constructed entirely from parts made by students and from standard stock parts. The design utilizes only four distinct chassis pieces and sixteen moving parts. The Enabler has non-orthogonal articulating joints that give the vehicle a wide range of mobility and reduce the total number of parts. Composite wheels provide the primary suspension system for the vehicle.

### Introduction

In the future, NASA will place a manned space station on the moon. The inhabitants of the base will need a lunar work vehicle to aid in the construction of the space station. The vehicle must be capable of maneuvering over the rough lunar terrain and of lifting and moving payloads. The vehicle must also be able to operate tools such as drills and winches.

The Enabler was designed to show how an actual work vehicle might be designed. The design is simple and utilizes only four distinct chassis pieces and sixteen moving parts. The entire vehicle is made of stock parts or parts that can be made by undergraduate mechanical engineering students. Undergraduate students at Georgia Tech will begin construction of the full-scale prototype vehicle during Fall Quarter, 1993.

Unique non-orthogonal articulating joints provide steering and pitch control for the Enabler. The joints make it possible for the Enabler to maneuver over rough terrain similar to that found on the moon. Each joint is composed of only two moving pieces, not counting

motors and assembly hardware. This design eliminates the need for complex steering assemblies.

The Enabler has a boom structure that can lift and move a payload inside a large work envelope. A combination of non-orthogonal and rotating joints on the boom makes it possible to approach any point on the work envelope from more than one direction. A mechanical tool interface attached to the boom makes it possible for the Enabler to operate a wide range of tools.

Although the Enabler performs many of the functions that an actual lunar work vehicle would perform, it is designed for use under earthbound conditions.

### General Parameters

The proposed work vehicle has an overall length of 6 m and an overall height of 2 m (see Figure 1). It is driven by six wheels, each of which is powered by a 1/2 hp motor. The vehicle can attain a top speed of 12 km/hr and can climb an effective grade of 20% from a standing start. Each wheel and its corresponding drive assembly, motor, reducer, and battery, is completely detachable from the chassis. In the event that one wheel drive unit is damaged, the entire unit can be removed and quickly replaced.

The main chassis of the vehicle has two T-Sections, a center section, four chassis joint pieces, and mounting hardware. The T-Sections and center section provide the interface between the chassis of the vehicle and the wheels. The chassis joint pieces are the main structure of the vehicle. Two pieces are mounted between two of the T-Sections. A 15° angle at the joint where the two pieces meet allows for articulation and steering of the vehicle.

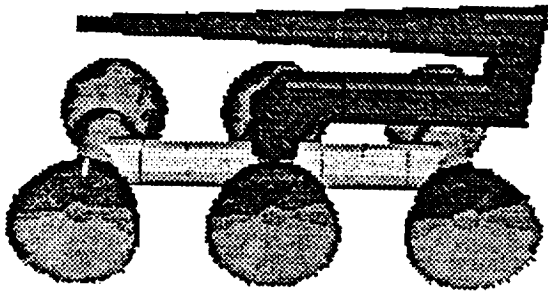


Fig. 1 Enabler overview

The vehicle has a six-piece boom structure with a tool interface mounted at the end of the boom. The boom and tool interface can lift a 50 N payload.

The vehicle can be operated through a Macintosh IIfx either onboard or remotely.

### Wheels

The wheels are made of a resilient composite material and are conical in shape. The wheel design is based on a similar design used for a candidate lunar rover vehicle.<sup>1</sup> The design is also outlined in several patents by Ed Markow.<sup>3,4</sup>

The diameter of each wheel at the rim is 1.2 m and the wheels are 0.5 m wide, as shown in Figure 2. The wheel thickness varies from 3.4 mm at the rim to 2 mm in the section adjacent to the hub, and the hub section is reinforced to prevent deflection. The hub thickness is 7.6 mm. Each wheel will weigh roughly 89 N.

The wheel is made of structural fiberglass. The fiberglass has an inherent spring rate and damping coefficient that provides part of the suspension for the vehicle. The wheels work together with the articulation joints to provide the entire suspension system. As the wheel is loaded, it deflects and moves outward; the scuffing between the wheel and the surface provides an additional damping effect.

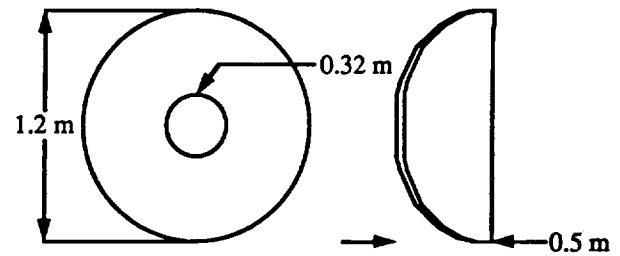


Fig. 2 Wheel

The spring rate for the wheel design was estimated by dividing the static load by the estimated static deflection. It was assumed that all the weight of the vehicle would be on two wheels in worst-case loading conditions. When all six wheels are in operation, the static deflection is estimated to be 5 cm.

The formula for the spring rate is

$$k = \frac{\text{force}}{\text{deflection}} \quad (1)$$

where the static force is 3340 N and the static deflection is 15 cm.

The spring rate for the wheel is intended to be 219 N/cm. This rate is varied during development by adding layers of fiberglass or slotting the wheel in low stress regions.

The angle that the centerline of the wheel makes with the ground (flat surface) affects the wheel's performance. For optimum power train efficiency the wheel should be angled down 15°. However, as the angle increases from 0°, the ratio of track width to vehicle width decreases and stability decreases. The angle was set at zero because it results in only a 3% power train inefficiency.

The fiberglass material of the wheel is not expected to provide enough traction by itself. Either metal cleats or a rubber tread will be added to improve the traction capabilities.

### Wheel Drives

Each wheel is driven by a DC motor, which is powered by one battery. The DC motor is coupled to a speed reducer, which in turn is coupled to a flexible coupling. The coupling mounts to the wheel and negates the effect of any bearing eccentricities.

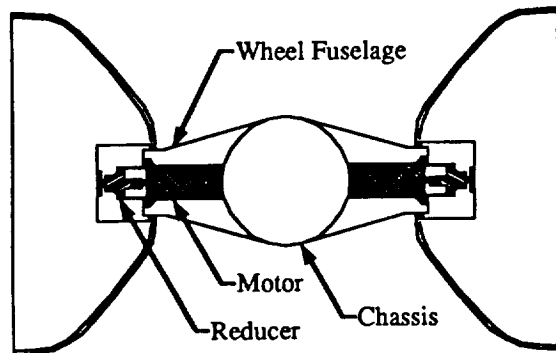


Fig. 3 Wheel drive assembly

All of the components of the wheel/wheel drive assembly—with the exception of the battery—attach to a wheel fuselage. The wheel mounts to the outside of the fuselage via a large ring bearing, while the other components mount to the inside of the wheel fuselage, as shown in Figure 3.

Each wheel fuselage is attached to the chassis of the vehicle by a band clamp. The clamp holds two flanges together, one at the end of the wheel fuselage and the other at the end of the T-Section of the chassis. The entire wheel/wheel drive assembly can be removed from the Enabler by simply removing the band clamp. This makes quick removal of a malfunctioning unit possible. Once a malfunctioning unit is removed, the Enabler can either operate without the unit, or the malfunctioning unit can readily be replaced if a properly functioning one is available.

### Chassis/Articulation

The two non-orthogonal chassis articulation joints provide steering and pitch control for the vehicle. These two identical joints are located between the T-sections and the center piece. The two main pieces that comprise each articulation joint have a  $15^\circ$  angle at the ends where

the two pieces connect. With a total of four pieces in the two joint assemblies, the chassis can rotate through a total angle of  $60^\circ$  for steering or pitching.

The non-orthogonal joints enable the vehicle to operate on rough terrain like that found on the moon. The ability to pitch the front and rear axles of the vehicle enables the vehicle to climb over objects through a series of joint rotations. Freewheeling the articulation joints makes it possible for each of the three axles to operate in different planes and still have all six wheels in contact with the ground.

Simple angular relationships exist between the rotation of each joint component for steering and pitching. To achieve the desired turn angle, the joint components must rotate at an angle of three times the turn angle relative to each other. For example, the maximum turn of  $30^\circ$  in one direction is attained by rotating the component of the joint closest to the end of the vehicle by an angle of six times the climb angle while keeping the other component stationary. A pitch angle of  $30^\circ$  is accomplished by rotating the end joint component  $180^\circ$  without moving the inner joint component. Pitch and turn orientations are illustrated in Figures 4 and 5, respectively.

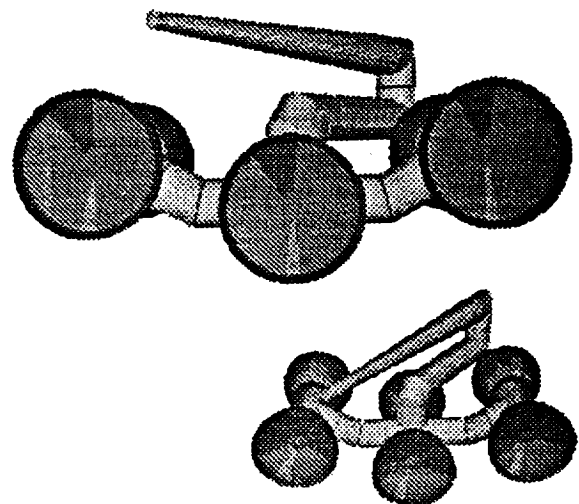


Fig. 4 Pitch orientations



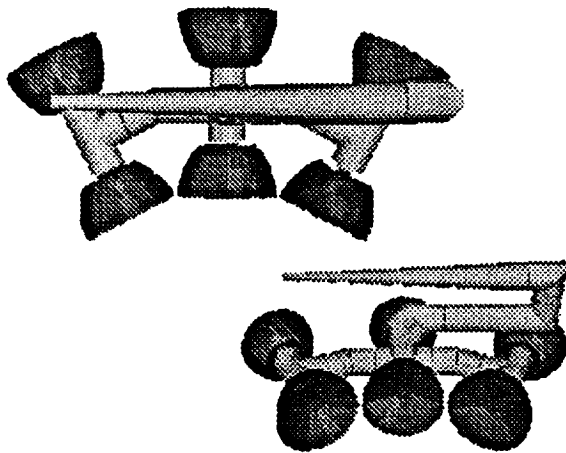


Fig. 5 Steering orientations

A 0.56 kilowatt, 24-volt permanent magnet DC motor with an output speed of 1750 RPM drives each joint. The use of a gearless speed reducer and pinion-gear assembly lowers the final rotational speed of each joint to a maximum of 27 RPM, so each joint can complete one rotation in 2.2 seconds. Since the top speed of the vehicle is only 12 kilometers per hour, this rotational speed is adequate for control of the vehicle. A fail-safe electronically controlled brake stops and holds the joint at the desired angle. It is not always necessary to power each joint; each drive system allows its joint to freewheel when power is not required.

### Boom

The boom gives the Enabler the ability to carry out several functions. It allows the Enabler to lift objects, push them, or pull them throughout a large range of motion; it also lets the operator manipulate the vehicle's tools.

The boom is mounted between the Enabler's central wheels and can extend 9 m from its base. It is capable of reaching any point within a hemisphere above the Enabler, and it can reach below the plane of the vehicle's wheels. The boom is not limited to one approach configuration; it can approach a point within its sphere of

operation from many angles. This freedom of approach configuration allows it to reach around obstacles. The boom derives its versatility by utilizing four joints. One joint, at the boom's base, allows the whole assembly to rotate 360° (Plane 1). Another joint, at an angle of 45° to Plane 1 allows the upper boom to rotate in a new plane (Plane 2). The next joint allows the boom tip to move in a plane 45° to Plane 2 (Plane 3). The final joint allows movement perpendicular to Plane 3. Therefore, the boom can place its tip at any point in any plane within its operational envelope (see Figure 6).

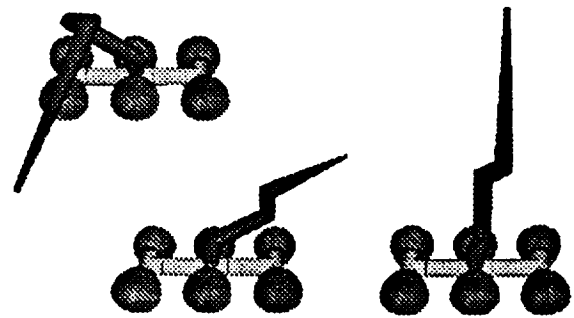


Fig. 6 Various boom orientations

The Enabler uses the boom to manipulate objects up to 50 N. A 24-volt motor moves each joint using a reduction gear box. Each joint rotates at 6° per second, thus completing one revolution in one minute.

The boom has a fail-safe tool interface that releases a tool only when inserted into the tool rack. The inventory of possible tools includes drills, winches, clamps, and shovels. The boom's ability to attain many approach angles enables it to drill holes at any desired angle.

### Controls

The Enabler is equipped with a comprehensive system through which the operator may manipulate and monitor the vehicle. The operator can manipulate the vehicle's speed, direction, approach configuration, and boom orientation with minimal input. The operator can also monitor the status of the vehicle as each command is carried out.

A Macintosh IIci-based console acts as the interface between man and machine; it also serves as the CPU for the vehicle. The operator enters commands and the IIci translates them into a digital signal. This signal is then sent through a fiber optic network to the various motor control devices. The fiber optic network eliminates signal disturbances caused by EMI and RF interference.

Smart cards are located in the motor control devices (see Figure 7). Each smart card intercepts the signal designated for its specific motor and translates the signal into an analog format. The analog signal drives the motor. The smart cards share some of the computational responsibilities with the CPU in that they monitor the motor's conditions through feedback sensors located in the drive units of each motor and compute the necessary adjustments.

Monitoring devices located throughout the vehicle send global feedback to the CPU. The feedback includes vehicle orientation from gyroscopes, chassis loading, use of strategically placed strain gauges, and boom and articulation joint orientations, using the speed and position sensors within the drive units.

The CPU interprets the global feedback and adjusts all outputs accordingly. For example, the CPU alters the orientation of the joints if the gyroscope indicates that the vehicle is unstable. The CPU signals the operator if there is a system problem such as a joint not being able to attain its indicated position or a wheel operating at an incorrect speed.

The CPU's ultimate function is to determine a position and speed for each motor individually in order to fulfill the operator's desires. For example, the CPU determines the appropriate articulation joint position as well as individual wheel speeds when the operator designates a turning angle.

The control system is reliable due to the simplicity of its design. It is easy to use because the CPU automatically executes the controller's commands. The system does not respond to unsafe commands and it automatically protects the Enabler from any dangerous situations that may arise. The system is fast because it divides control responsibilities.

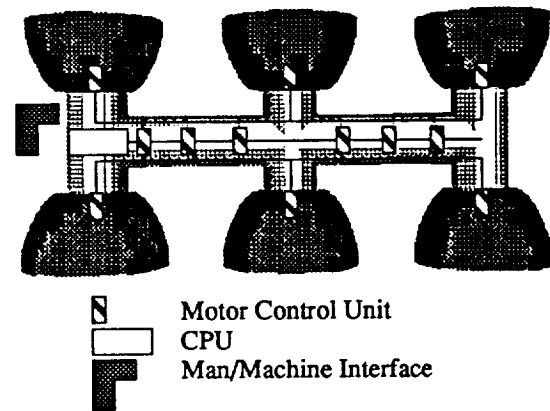


Fig. 7 Chassis controls schematic

### Conclusion

The Enabler has many of the features that an actual lunar work vehicle would have. The simple design cuts down on the total number of parts and the number of dissimilar parts. Ease of construction and good serviceability are desirable qualities for any mechanical design; they are essential qualities for a machine operating in a lunar environment where resources for construction and repair are limited. The Enabler can maneuver over rough terrain similar to that found on the moon. A highly maneuverable boom structure can lift and move a payload around a large work envelope. The unique joint design on the boom structure allows the boom to approach any point on the work envelope from many different directions. A mechanical tool interface enables the vehicle to use a wide variety of tools.

The Enabler serves as a proof-of-concept vehicle; it is not capable of actual lunar use. There are several problems with the operation of a lunar vehicle that are not addressed by the Enabler. The atmospheric conditions on the moon introduce heat transfer problems for several of the vehicle's systems. If the actual lunar vehicle uses electric motors like the Enabler, it will have to have a heat sink to provide a cooling system for the electric motors. Cooling the electronic components, especially the CPU, is another problem not addressed by the Enabler.

These are just a few of the many problems that still need to be addressed in designing an actual lunar vehicle.

However, the Enabler provides a solution to many of the questions that need to be answered in designing an actual lunar vehicle.

The Enabler was designed by senior Mechanical Engineering students at the Georgia Institute of Technology. The project was divided into six groups, each of whom was responsible for one section of the vehicle. The design decisions of the class are presented in this paper. The vehicle is under further development, and construction of the full-scale prototype will begin in the Fall of 1992. The completed vehicle will be exhibited at several professional exhibitions including the NASA/USRA Summer Conference in June, 1993.

### **Acknowledgments**

Co-authors are James A. Austin, Clark Beard, Glenn Ceniza, Thomas Hamby, Anne Robinson, and Dana Wooters. We would also like to acknowledge the assistance of Jim Brazell, instructor for the Senior Mechanical Engineering Design project; Lewis Dorrity, instructor for Textile and Fiber Engineering Design; Jeff Donnel, Writing Coordinator for the School of Mechanical Engineering; and Craig Campbell and Ken Kaser, Teaching Assistants, for their assistance in putting together this paper. We would also like to acknowledge the School of Mechanical Engineering at Georgia Tech, NASA, and Universities Space Research Association for sponsoring this design program. The initial design of the Enabler was proposed by 40 senior Mechanical Engineering students at Georgia Tech in the Fall of 1991. The design and construction of Enabler is an ongoing process that will be finalized by Mechanical and Textile Engineering students during the 1992-1993 academic year.

### **References**

1. "Design and Fabrication of Wheel for a Lunar Surface Vehicle." Detailed technical report. Grumman Aerospace Corporation, June, 1970. N70-31989 (NASA-CR-102755).
2. "Grumman Proposal for Lunar Roving Vehicle in Response to Request for Proposal IL-LRV-1."

Grumman Aerospace Corporation, 69-78 NAS, Aug., 1969.

3. Markow, Edward G, "Convolutd Cone Wheel," United States Patent Department, Patent Number 4705087, Nov., 1987.
4. Markow, Edward G. "Elastic Conoid Shaped Wheel," United States Patent Department, Patent Number 3698461, Oct., 1972.
5. Markow, Edward G. Phone conversation on Dec. 9, 1991.

## DESIGNS FOR LUNAR PROJECTS

Georgia Institute of Technology  
School of Textile & Fiber Engineering  
Atlanta, Georgia

Dr. J. L. Dorrity  
Suneer Patel, Teaching Assistant

# DESIGN FOR PRODUCING FIBERGLASS FABRIC IN A LUNAR ENVIRONMENT

Rafer M. Benson, Dana R. Causby,  
Michael C. Johnson, Mark A. Storey, Dal T. Tran,  
and Thomas A. Zahr

## Abstract

The purpose of this project was to design a method of producing a fabric material on the lunar surface from readily available glass fibers. Various methods for forming fabrics were analyzed to determine which methods were appropriate for the lunar conditions. A nonwoven process was determined to be the most suitable process for making a fabric material out of fiberglass under these conditions. Various resins were considered for adhering the fibers. A single thermoplastic resin (AURUM) was found to be the only applicable resin. The end product of the process was determined to be suitable for use as a roadway surfacing material, canopy material, reflective material, or packaging material. A cost analysis of the lunar process versus shipping the end-product from the Earth suggests that the lunar formation is highly feasible. A design for a lunar, nonwoven process was determined and included in the following document.

## Problem Statement

The purpose of this research project was to create a method of producing a fabric on the lunar surface. The fabric had to have a minimum width of half a meter, be composed of readily available fiberglass fibers, and be useful in a number of applications on the lunar surface.

The process to make the fabric was to be operational while fully exposed to the lunar environment. Any

beneficial effects of the lunar environment (such as microgravity) were to be incorporated into the design.

Because of the limited amount of power available on the moon, a power constraint was established. The maximum power available for the total process had to be no more than five kilowatts.

To make the process economically feasible, a constraint was placed on the use of non-lunar materials. Any Earth materials necessary had to be kept to a minimal weight.

The final requirement of the process was that the cost of producing a required mass of the end product (in a given amount of time) be less than the cost of shipping the same mass of product from the Earth.

## Resin

The resin used for this project is a super heat-resistant thermoplastic polyimide, Aurum, developed by Mitsui Toatsu Chemicals, Inc. Aurum was chosen because of its thermoplastic properties in addition to outstanding heat resistance, cold resistance, and mechanical/electrical properties, which are suitable for use in a variety of applications in the aerospace industry. The resin melt temperature is approximately 390-415° C. The glass fibers are assumed to have the resin in powder form already applied to them during the sizing process. This powdered resin acts both as a lubricant and a binder for the glass fibers. Because Aurum is a thermoplastic resin, it does not need to be cured but simply melted. As soon as the resin melts, it will bond to the fibers uniformly throughout the fiber mat to produce a fabric with a strength of 1156 kPa. The resin itself has a strength of approximately 136 kPa. One advantage of this type of polyimide resin is that it does not boil or foam when melted in a vacuum. The

final product is 15% resin by weight. After melting, the binder is allowed to cool by radiation and conduction.

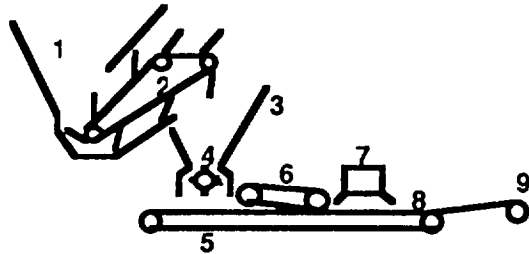


Fig. 1 Schematic of process

1. Main bin
2. Paddle conveyor
3. Secondary bin
4. Feed roller
5. Main conveyor
6. Compression conveyor
7. Infrared heating
8. Cooling area of main conveyor
9. Take-up roll

### Machine Components

#### Main Bin

Fiber that is to be used in this process is going to be in staple form and thus must be stored in large batches. A large storage container is needed to hold these fibers. This main bin will act as the storage container and provide surge protection for the rest of the system. The fiber will enter the bin from the production process through the large 3 m x 3 m opening in the top and be funneled to a smaller opening of 1.5 m x 0.75 m which leads to the paddle conveyor. The fiber will then leave the main bin via the paddle conveyor from the bottom portion of the bin.

The main bin will be made of aluminum due to the metal's low density but relatively high strength. Since the gravitational force on the moon is roughly 1/6 that of the Earth, the bin will not be subjected to high

forces. Therefore, the walls of the bin do not have to be very thick and will need little support.

#### Paddle Conveyor

The paddle conveyor consists of an aluminum frame, aluminum rollers, bearings, and a belt made of a thin sheet of an aluminum-copper alloy with a composition of 96% Al and 4% Cu. The belt is 17 m long, 1.5 m wide and 0.001 m thick and has a series of 5-cm-high paddles that are 0.3 m apart which will be used to carry the fibers from the main bin to the secondary bin. This conveyor will have one drive pulley, two non-drive pulleys, and three idlers which will keep the belt at proper operating tensions. The speed of the conveyor was determined to be 3.09 m/hr.

#### Secondary Bin

The purpose of the secondary bin is to supply the main conveyor belt with the fiberglass via the feed roller. The feed roller is located at the bottom of the secondary bin. The secondary bin is 1.5 meters high, 2 meters wide, and 0.005 meters thick. The bin walls are sloped 28 degrees from the vertical. The mass of the bin is approximately 120 kg.

#### Feed Roller

The feed roller is the mechanism that insures an even laydown of the fiberglass on the conveyor. Fibers from the secondary bin fall through a 2 m by 0.1 m opening to the feed roller which deposits onto the conveyor 70.7 kilograms of sized fiber per hour of operation. In order to achieve this laydown rate, the roller requires a speed of 7.06 revolutions per hour. Small "hooks" are located at certain intervals along the roller and are spaced in such a way as to allow random fiber orientation laydown on the conveyor. This will insure that the fiberglass mat has dimensional stability. The hooks are also slightly bent at the tip in order to grab fibers from the secondary bin if a clog occurs where the fibers enter the roller. There is clearance of approximately 1 mm between the tip of the hook and the secondary bin which provides a space so that fibers caught on the top of the hook will not be crushed between the hook and the bin. The hook spacing and the low gravity will combine to give an even laydown of fibers onto the web.

### **Main Conveyor**

The fabric process chosen requires a main conveyor to transport the fiberglass effectively from the feed roller to the mat formation process. This conveyor picks up the fibers from the feed roll and moves the fibers to the infrared heater positioned down the conveyor. The conveyor is 4.75 m long on one side from the center of the end roller to the center of the drive roller. The conveyor material will be 1.05 m wide and 10 mm thick. The speed of the conveyor will be 8.63 m/hr. Using formulas, values, and assumptions from conveyor literature, it was calculated that a 152.4-mm roller was necessary to uphold the tension in the belts and required revolutions per minute. A 42.75-mm shaft was found to be the size that would provide the necessary strength in the system. In fact, the shaft is over-designed for its purposes but was needed because of the large face width that is present in the system. A 1/4-hp motor was found to be needed to fulfill the desired speed of the conveyor. In order to achieve the 8.63 m/hr conveyor speed the pulley must rotate at 18 revolutions per hour. In addition to the drive pulleys, idlers must be employed to prevent sag in the conveyor belt. By calculation, the idlers should be placed 2.0 m apart. In order to fit the design, idlers will be placed 1.6 m apart, which will provide better tension restoration. The conveyor will be made of hot butyl material with a coating of silver. The hot butyl stands up well under high temperatures but has problems degrading in a vacuum. To take care of problems in the vacuum, silver is used to coat the butyl material. Experts on material processing have confirmed that this material design should be adequate. Skirt boards will be placed 78 mm from the edge of the conveyor belt. The skirts are used to keep any materials on the belt from falling off. The skirts will only be 50 mm high because of the small width of the product before and after compression.

### **Compression Conveyor**

The compression conveyor is used to compress the fibers into a web of the desired thickness (5 mm). This conveyor moves at the same speed as the main conveyor and is made of the same materials as well. The compression conveyor is 500.6 mm long, 1.05 m wide, and moves at a speed of 18 revolutions per hour.

The belt is 10 mm thick and is made of hot butyl coated with silver.

### **Infrared Heating Lamps**

Many of the heating processes used on Earth use convection as the primary way of transporting the heat. Large ovens need a medium to carry heat from the heating source to the material being heated. In a vacuum, heating is a much more difficult process than heating on Earth because heating by convection is no longer a possibility. Therefore, conduction and radiation are the only means of heating on the moon. Radiation doesn't require a medium to transport the heat, making it a good heating source on the lunar surface. The main considerations for heating by radiation are the emissivity of the material that is to absorb the radiation and the intensity of the radiation. Glass has a high emissivity and therefore a good absorptivity; it will be heated very easily by radiation. Given this, the resin will be melted by infrared lamps that will be housed in a mega reflector box 1 m long by 0.25 m wide by 0.33 m high. The housing of the lamp should reflect most of the radiation down to the mat, improving the efficiency. As the radiation is absorbed by the glass and resin, the temperature will rise up to the melting point of the resin. The entire fabric formation process will be operational during the time the equipment is exposed to the sun, influencing the amount of power required to heat the fabric. During this time of fabric formation, the temperature range on the moon is approximately 50 to 120° C. Therefore, the amount of power needed for the curing process will also change as the temperature varies between 50° and 120° C. Given these two numbers, the final curing temperature of the process (400° C), the mass rate and the specific heat of the glass, the power required to heat the fabric will range from 4.38 kW to 5.49 kW. When the power of the motors is added to these numbers, the total power ranges between 5.31 kW and 6.42 kW.

### **Take-Up**

The take-up roll, a device used in textile manufacturing today to take up fabric, was chosen because it is simple and easily implemented. There are problems with this method, however. A week's worth of fiberglass mat production produces a roll that has a mass approaching 12,000 kilograms and a diameter of

just over three meters. On the earth 1,200 kg would weigh nearly 26,200 pounds. Thanks to lunar gravity, that same mass on the moon weighs only 4,400 pounds, which is still heavy, but more manageable. The diameter of the roll could be greatly reduced if the width of the fabric were increased. However, power considerations prohibit this. Guide bars attached to the sides of the take-up roll keep the mat from spilling over the side. Based on these calculations, the rollers would only have to be changed 26 times per year.

### Mechanical Elements

Parts considered here include pulleys, idlers, shafts, bearings, and motors. On the main conveyor, two pulleys, one driving and the other non-driving, need to be installed to move the conveyor belt. Since the loads are so small compared to Earth uses, a 152.4-mm pulley with a 42.75-mm shaft will be able to support the necessary force requirements for all moving parts (rollers, pulleys). Again, the small shaft can be used because of low forces and speeds. In fact, the shafts will be over-designed for the process, which will allow for an increase in production rate if desired. Idlers are necessary to keep the belt from sagging in between the pulleys. For the main conveyor, idlers should be placed 1.6 m apart on both the upper and lower parts of the conveyor. 50.8 mm idlers will be sufficient to keep the conveyor at its proper tension. Bearings will be deep groove, single row ball bearings 43 mm in diameter, from the FAG Corporation. Since forces will be so small, the smallest and cheapest bearing that meets the need was chosen. The motor chosen to drive the moving elements was a 1/4 hp-Leeson Electric variable speed motor. This motor will be able to handle the roller, conveyors, and take-up. Five of these motors will be necessary. Gear reductions for each case will be necessary. The motors are still a little oversized, which means that the motors could perform at increased rates, if necessary. This is why the motors were chosen to be a little larger than needed. All parts will be made of aluminum.

### Lubricant

In the design of the fabric process, various pieces of equipment are needed. Many parts rotate and require the use of bearings. In order to keep these parts in

good working condition, a suitable lubricant is necessary. Considerations for a proper lubricant were difficult because of the performance environment. First of all, the lubricant needed to work in a vacuum, which ruled out many possible oils and greases. Secondly, the material needed to withstand the high temperature of the moon without losing its viscosity. Oils and greases, solid lubricants, laminar solids, ceramics, and polymers were explored. After looking at many possibilities, a mix between a grease and solid lubricant was chosen. Shell Apeizon High Vacuum grease and molybdenum disulfide were decided upon. Since most solid lubricants are applied with either a grease or oil, the best characteristics of each material were mixed to form an excellent lubricant. The grease works very well in vacuum situations, but has limited temperature effectiveness. The MoS<sub>2</sub> on the other hand has excellent temperature properties, but lacks the vacuum ability of the high vacuum grease. It should be noted that both the grease and the MoS<sub>2</sub> have been tested in vacuums at temperature extremes and have performed well. In mixing the two, the properties of the lubricant should become even better. By mixing the two together, the lubrication of the moving parts is fulfilled. From looking at experiments done in a vacuum at high temperatures, the estimated life of the lubricant is six months. This is very good, meaning that the lubricant will have to be changed only twice a year. A sufficient amount should be applied in order to achieve full-film lubrication, which will reduce friction forces and provide better efficiency.

### Control Scheme

In any process design, some control strategy must be formulated, though specifics are not given here for equipment since it was not required for this particular part of the design.

At the beginning of the process, weigh cells are necessary on the main bin to keep the fiberglass from filling too high. The control of these weigh cells will return to production of the fiberglass itself, where the regulation will be made. Secondly, a velocity control is necessary on the paddle conveyor to keep the flow into the secondary bin at the proper rate. Readouts will be taken from the weigh cells on the secondary bin and mass monitor on the web laydown conveyor. The

readings are put into the paddle velocity control and the paddle speed is regulated.

As previously mentioned, a weigh cell monitor will be employed to keep track of fiber buildup in the secondary bin. Next, a velocity control will be employed on the feed roller to keep the mat at a constant mass. Readouts from the mass monitors at the web laydown position and final take-up will be fed back to the feed roller velocity control. If mass readings are too high, the roller will slow down, and if too low, the feed roller speeds up.

A mass monitor will be employed on the conveyor to keep the mat at the correct mass. Values will be fed back to the velocity control of the feed roller and conveyor. A velocity monitor will also be supplied on the compression conveyor and connected to the velocity control of the conveyor. This will help to insure that the fiberglass fabric will not be torn or damaged through the processing points.

Next, a temperature monitor will be used to check the temperature of the formed fabric to insure that the resin is being cured and will obtain the necessary strength. A velocity control will also be employed on the take-up roll. Values from the mass monitor and velocity monitor will also be fed back to the velocity control of the feed roller to maintain the uniform feed that is necessary.

In general, two controls have been employed on the equipment in order to maintain operations even though one of the monitors may fail. This faulty piece of equipment could then be replaced without having to shut down the process. This is done to alleviate downtime and keep production going.

### Conclusions

A fiberglass fabric that is both useful and cost efficient can be produced on the lunar surface. Nonwoven fabric, while not as strong as a woven fabric, is easier to manufacture and has adequate strength for the intended uses described. The nonwoven process moves slowly and contains a minimum amount of moving parts; thus the design should be extremely reliable. Cost savings over a three-year lifespan of the

process are in the tens of billions of dollars, compared with shipping the fabric from the Earth. Research into more efficient heating methods and resins with lower melting temperatures could drive these cost savings even higher. Overall, production of a fiberglass fabric on the lunar surface is a highly feasible process that merits more research and development.

### Acknowledgments

Mr. Leon Bates, Dexter Aerospace Materials Division, The Dexter Corporation.

Mr. Hugh Berges, Plant Manager, Clark-Schwebel Fiber Glass Corporation.

Mr. J. W. Brazell, Department of Mechanical Engineering, Georgia Institute of Technology.

Dr. John Buckley, NASA Langley Research Center.

Mr. Paul Cavano, NASA Lewis Research Center.

Dr. Prashant Desai, Department of Textile and Fiber Engineering, Georgia Institute of Technology.

Dr. Lewis Dorrity, Department of Textile and Fiber Engineering, Georgia Institute of Technology.

Dr. James Hartley, Department of Mechanical Engineering, Georgia Institute of Technology.

Mr. Lee Hyde, Mitsui Toatsu Chemical, Inc.

Ms. Carol Jaster, Dow Chemical USA.

Dr. Lieng-Huang Lee, Xerox Webster Research Center.

Dr. Greg Olson, Department of Textile and Fiber Engineering, Georgia Institute of Technology.

Mr. Suneer Patel, Department of Textile and Fiber Engineering, Georgia Institute of Technology.

Dr. Roy Peck, Clark-Schwebel Fiber Glass Corporation.



Dr. Terry Sinclair, NASA Langley Research Center.

Dr. Wayne Tincher, Department of Textile and Fiber Engineering, Georgia Institute of Technology.

Dr. Steve Warner, Department of Textile and Fiber Engineering, Georgia Institute of Technology.

### References

1. Association for Finishing Process of SME. Radcore 1984 Conference Proceedings, Dearborn, Michigan, 1984.
2. Barnwell, F.T. Lubrication of Bearings, Butterworths Scientific Publications: London, 1956.
3. Corbman, Bernard P. Textile Fiber to Fabric, McGraw-Hill Book Company: Atlanta, 1983.
4. Doremus, Robert H., ed. Materials Processing in the Reduced Gravity of Space, Materials Research Society: Pittsburgh, 1987.
5. Engineering Conference of the Conveyor Equipment Association. Belt Conveyor for Bulk Materials, Cahners Publishing Company, Inc.: Boston, 1966.
6. Goetzel, Claus G., ed. Space Material Handbook, Addison-Wesley Publishing Company, Inc.: Atlanta, 1965.
7. Incropera, Frank A. and DeWitt, David P. Fundamentals of Heat and Mass Transfer, John Wiley and Sons: Chichester, England, 1985.
8. Krema, Radko. Nonwoven Textiles, Textile Trade Press: Manchester, England, 1962.
9. Lunenschloss, J. and Albrecht, W. Nonwoven Bonded Fabrics, John Wiley and Sons: Chichester, England, 1985.
10. "Moon." Encyclopedia Americana, Volume 15, 1985.
11. Nichols, Todd and Dover, William. Lunar Fiberglass: Properties and Process Design, Clemson University, 1986.
12. Rodriguez, Ferdinand. Principles of Polymer Systems, 3rd edition. Hemisphere Publishing Corporation, 1989.
13. Shand, M. Glass Engineering Handbook, McGraw-Hill Book Company: New York, 1984.
14. Shigley and Mishke, Mechanical Engineering Design, McGraw-Hill Book Company: New York, 1989.
15. Skeist, Irving, Ph.D. Handbook of Adhesives, 3rd edition. Van Nostrand Reinhold: New York, 1990.

## LUNAR PREFORM MANUFACTURING

Gregory N. Leong, Sandra Nease, Vicky Lager, Raffy Yaghjian, and Chris Waller

## Abstract

A design for a machine to produce hollow, continuous fiber-reinforced composite rods of lunar glass and a liquid crystalline matrix using the pultrusion process will be presented. The glass fiber will be produced from the lunar surface, with the machine and matrix being transported to the moon. The process is adaptable to the low gravity and near-vacuum environment of the moon through the use of a thermoplastic matrix in fiber form as it enters the pultrusion process.

With a power consumption of 5kW, the proposed machine will run unmanned continuously in fourteen-day cycles, matching the length of lunar days. A number of dies could be included that would allow the machine to produce rods of varying diameter, I-beams, angles, and other structural members. These members could then be used for construction on the lunar surface or transported for use in orbit.

The benefits of this proposal are in the savings in weight of the cargo each lunar mission would carry. The supply of glass on the moon is effectively endless, so enough rods would have to be produced to justify its transportation, operation, and capital cost. This should not be difficult as weight on lunar mission is at a premium.

## Introduction

## Purpose

The purpose of this project was to design a process to form long lengths of hollow glass filament-reinforced composite rods on the moon. It is believed that glass can be produced from compounds present in lunar regolith. By producing the glass in a vacuum, it is possible to achieve high tensile strength and a better fatigue life due to a lack of flaws in the fiber and to less crystallization of fibers after creation. Production of

the materials on the lunar surface will also present transportation savings.

## Possible Uses for Rod

These rods would be used as reinforcing beams in platforms, antennas, tethers, and solar reflectors. Another possibility for the use of the rods is to transport them from the lunar surface to future Space Stations to be used as construction materials.

## Constraints

The project was limited as follows: all processing will be done on the moon; all materials, other than glass fiber, would be transported to the moon; weight must be kept to a minimum; five kilowatts of power will be available for the entire process; and the process must be able to produce rods that vary in inner diameter from 1 cm to 10 cm.

## Process

## Manufacturing Methods

Many different methods for manufacturing fiberglass composite rods were considered for use on the moon. Because of the limiting factors of the lunar environment, machine simplicity took precedence over optimal rod properties. Through the use of a design matrix, it became clear that the pultrusion option was the best for optimizing rod properties while simplifying design. Figure 2 is a representation of the lunar pultrusion process as we envision it.

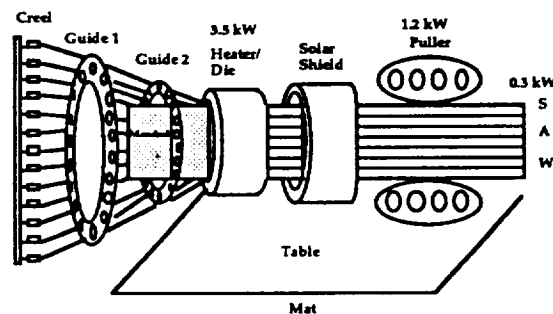


Fig. 2 Conceptualization of lunar pultrusion machine

## Pultrusion Machine

### Machine Components

**Creel.** To hold the packages for a 336-hour run, a V-creel of aluminum 6061-T6 would be required with the two halves being 10 m long and 2 m wide.

**Guides.** Two guides, one 92 cm in diameter and one 84 cm in diameter, are used to guide the 100 strings of glass fiber and matrix from the creel to the heater/die. Each are cast out of 6061-T6 aluminum. The guides are then welded to a stand which enables them to be moved as needed for the various sizes of rods being manufactured.

**Mandrel.** The mandrel is a 3.5 m hollow tube that will impart both shape and support to the pultruded rod. Both it and the mandrel stand will be cast of 6061-T6 aluminum. It will be necessary to have a set of mandrels of varying diameters in order to produce rods between 1 and 10 cm inner diameter.

**Heat Die.** Through the use of a thermoplastic matrix, the rate control of the process is simply the melting of the matrix. After extensive research of materials, it was decided that the heat die would be made of silver with a nichrome element and a plated black chrome insulation coating. From this design the power consumption of the die for a composite tube with an inside diameter of 10 cm, a thickness of 1 cm, a die length of 75 cm with a puller velocity of 0.001875 m/s, is 3386.1 Watts.

**Solar Shield.** Once the composite tube leaves the heat die, it enters a very thin cylindrical tube. In this tube of anodized aluminum with a white zinc oxide paint, the rod is cooled to hardening. For the case of a 10-cm inside diameter and 1-cm thickness composite tube traveling at .001875 m/s the length of the shield is calculated to be 2.25 m.

**Puller.** Friction calculations prove that 1.2 kW is more than enough to power a motor to pull the required load. To solve the problem of lubrication, molybdenum disulfide-based lubricants would be used, primarily Vac Kote. Also, the bearing chosen was ceramic, silicon nitride. These components, along with a variable gearbox with a vitron fluorestomer pulley system, would combine to form a very reliable system.

**Cutoff Saw.** The cutoff saw is the last stage of the pultrusion process. The purpose is to saw the rods periodically into 10 m lengths. A timer/controller such as a mercury switch will be used to turn the saw on and off and to load the saw down to the rod. The saw will be allowed a maximum 300 W.

**Scray.** Constructed of 6061-T6 aluminum, the scray is designed to hold half of the 720 rods of 12-cm outer diameter the machine could produce in one lunar day. Therefore, replacement of the full scray with an empty one would be required. The scray was designed with a folded lip on each side to allow for this.

**Rails and Tables.** The 6061-T6 aluminum tables will allow the components mobility for adjustments for different size rods.

**Dust Protection.** Because of the rough terrain of the lunar surface and the potential for dust, a 15 m x 15 m area should be cleared. A mat constructed of a thin aluminum sheet with a neoprene foam on the underside will be laid out under the machine prior to the installation of the pultrusion unit.

**Operating Cycle.** The pultrusion machine is set up to run for the 14 days of daylight during the lunar day and then to be shut down for the 14 days of darkness of the lunar night.

### Composite Rod

#### Glass Fibers

The glass used for the composite rods will be produced using the process designed by researchers at Clemson University. In short, the lunar surface (containing an abundance of silicon dioxide) will be used as the source of the glass. Since the production will be in the vacuum of space, the glass will be of a quality not attainable here on Earth.

#### Matrix

The selection of the matrix for this process and composite was extremely complex. The extreme environment of the lunar surface made processing and end-use characteristics of the resin chosen very

important. With all of the processing problems in mind, the liquid crystalline polymer Vectra was selected. Having a high radiation resistance and a high strength made it the perfect choice. In addition, Vectra is also available in fibrous form under the name Vectran. This would allow the pultrusion process to be done with both matrix and reinforcement in fibrous form.

### Composite Properties

The actual end uses of the pultruded rods were quite vague, so in determining the rod properties, spreadsheets were set up to allow the designer to vary volume fraction, inner diameter, outer diameter, and length of the rods and to be able to calculate the critical tensile and compressive loads of the chosen rod.

### Tension Analysis

Tensile calculations allow creation of a graph of composite area versus fiber volume fraction for given loads as shown in Figure 3.

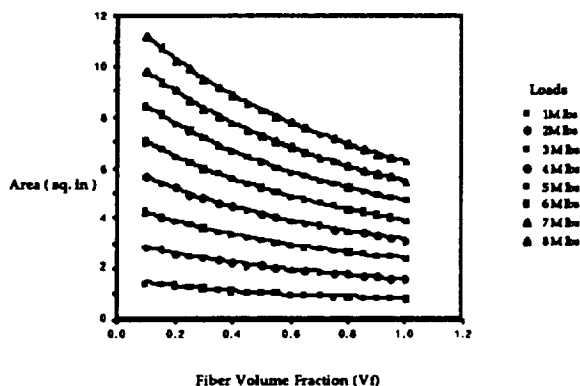


Fig. 3 Area vs. fiber volume fraction for tensile loads

### Compression analysis

Considering first mode buckling as the limiting factor for critical load, a similar graph can be generated for the ultimate compressive loads of various rod designs. This has been done in Figure 4 for our composite rod of length = 10 ft and inner radius = 2 in (5cm).

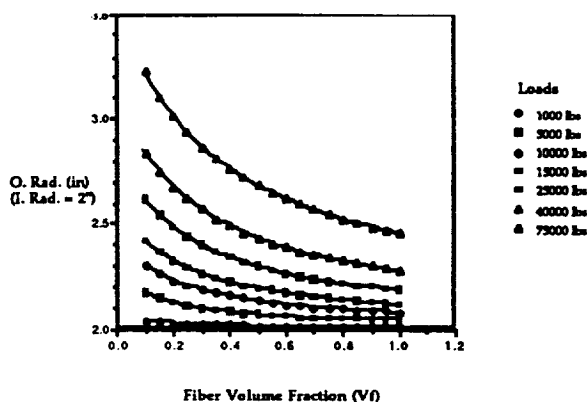


Fig. 4 Outer diameter vs. fiber volume fraction for compressive loads

From the previous graphs and the probable difficulty in pultuding a part with a fibrous matrix, we believe that 60% fiber volume fraction would be the optimum setting for the machine. Based on this assumption, the 3-m rod with an inner diameter of 10 cm and an outer diameter of 12 cm would have the capacity to carry approximately 5 Msi in tension and 35 ksi in compression.

### Cost Analysis

Based on the calculations for the 3 m rods with a 10 cm inner diameter and 12 cm outer diameter, the relative weight savings is 3,799.1 kg. This calculation shows that to take identical rods to the moon would require a cargo 3799.1 kg larger than that of the materials necessary to make the rods on the lunar surface. Based on the figure of \$100,000/lb of cargo, this translates to a savings of \$835.8M. With a cycle start-up labor cost of \$500,000, it seems obvious that even with a lengthy initial start-up, this design is easily justifiable for one cycle, and the savings will only increase as more rods are produced.

### References

1. Agarwal, Bhagwan and Lawrence Broutman. Analysis and Performance of Fiber Composites, New York: John Wiley & Sons, 1990.

2. Beers, Dr. David. Personal Interview. Hoechst Celanese. 19 Feb. 1992.
3. Brinegar, Willard. "Liquid Crystal Polymers." Modern Plastics Encyclopedia, 1989 ed.
4. Colton, Dr. Jonathan, et al. "On-Orbit Fabrication of Space Station Structures." SAMPE Quarterly, Atlanta, GA: Georgia Institute of Technology, July 1989.
5. Creative Pultrusion Inc. Design Guide Standard and Custom Fiberglass-Reinforced Structural Shapes, Alum Bank, PA.
6. Dole, John R. "Try Liquid Crystal Polymer." Chemtec April 1987: 242-245.
7. El-Shiekh, Dr. Aly. Personal Interview. North California State University. 17 Jan. 1992.
8. Ewald, Glenn W. "Pultrusion and Pulforming." Modern Plastics Encyclopedia, 1989 ed.
9. Heatrex. Electric Heat for Industry, Meadville, PA.
10. Herzl, George G. Aerospace Mechanisms, Lockheed Missiles & Space Company, Vol. 1. 1970; A-B.
11. Incropera, Frank P. and David P. DeWitt. Fundamentals of Heat and Mass Transfer, New York: John Wiley & Sons, 1990.
12. Lide, David R. Handbook of Chemistry and Physics 72 Edition, Chemical Rubber Publishing Company, 1991.
13. Loomis, William R. New Directions in Lubrication, Materials, Wear, and Surface Interactions: Tribology in the 80's, NASA Lewis Research Center, New Jersey: Noye Publications, 1985.
14. Mahaiko, Emil S. Low Damping Torque Brushless D.C. Motor, U.S. Patent 4,733,118, 1988 March 22.
15. Makhlis, F.A. Radiation Physics and Chemistry of Polymers, New York: John Wiley & Sons, 1972.
16. Miller, Edward, ed. Plastics Products Design Handbook Part B, New York: Marcel Dekker Inc., 1983.
17. Perrin, B.J. and R.W. Mayer. "Lubrication of DC Motors, Slip Rings, Bearings, and Gears for Long-Life Space Applications." Proceedings of the 3rd Aerospace Mechanisms Symposium, Pasadena, CA: Jet Propulsion Laboratory, 1968.
18. Pope, Larry E., Larry L. Fehrenbacher, and Ward O. Winer. New Materials Approach to Tribology: Theory and Application, Pittsburgh: Materials Research Society, 1989.
19. Popov, Egor P. Introduction to Mechanics of Solids, New Jersey: Prentice-Hall, 1968.
20. Rutledge, P. et al. "Oxidation and Protection of Fiberglass-epoxy Composite Masts for Photovoltaic Arrays in the Low Earth Orbital Environment." Materials Stability and Environmental Degradation, Pittsburgh: Materials Research Society, 1988.
21. Schnable, W. Polymer Degradation, New York: Hanser International, 1981.
22. Singletary, John B. Space Materials Handbook 2nd Edition, Ed. John B. Rittenhouse and Claus G. Goetzel. Wright Patterson Air Force Base, OH: Air Force Systems Command, January 1965.
23. Singletary, John B. Space Materials Handbook 2nd Edition Supplement I, Wright Patterson Air Force Base, OH: Air Force Systems Command, 1966.
24. Strong, Brent. Fundamentals of Composites Manufacturing: Materials, Methods, and Applications, Michigan: Society of Manufacturing Engineers, 1989.

25. Tortolano, F.W., ed. "Rising Star in the Plastics Lineup." Design News, 20 Nov. 1989: 54-662.
26. Wang, Dr. Youjaing. Personal Interview. Georgia Institute of Technology. 4 March, 1992.
27. Wilson, Marywood L. and Robert Miserentino. Pultrusion Process Development for Long Space Boom Model, NASA Technical Memorandum, January 1988.
28. "Advancing Technology in Materials and Processes." 30th National SAMPE Symposium and Exhibition, 1985 March 11-25; Anaheim, CA, Vol. 30.

## VARIABLE SPEED CONTROLLER

Christa Estes, Charles Spiggle, Shannon Swift,  
Stephen Van Geffen, and Frank Younger

### Abstract

This report details a new design for a variable speed controller which can be used to operate lunar machinery without the astronaut using his or her upper body. In order to demonstrate the design, a treadle for an industrial sewing machine was redesigned to be used by a standing operator. Since the invention of an electrically powered sewing machine, the operator has been seated. Today, companies are switching from sit down to stand up operation involving modular stations. The old treadle worked well with a sitting operator, but problems have been found when trying to use the same treadle with a standing operator. Emphasis is placed on the ease of use by the operator along with the ergonomics involved. Included with the design analysis are suggestions for possible uses for the speed controller in other applications.

### Problem Statement

The development of a variable speed controller that will enable a standing operator to control the rate per minute on an industrial sewing machine is needed.

The controller must:

- be hands free
- be no longer than 3 feet wide
- be no longer than 2 feet deep
- be no higher than 2 inches high
- be mobile so that it can be placed in the best possible position for each operator

The controller will have:

- a potentiometer
- 110 volts AC input
- 4-20 milliamperes output
- an automatic shutoff
- a pad surrounding the device
- no more than 15 pounds weight
- a pad with a nonslip contact area
- a compression-type spring for pedal return

## Variable Speed Controller

### Ergonomics

Ergonomics is one of the major forces necessitating the need for a new variable speed controller. According to the Georgia Tech Research Institute (GTRI) Economic Development Laboratory report, approximately 30% of the seated apparel workers surveyed reported discomfort in the upper leg, the knee, and the lower leg. Of the standing apparel workers, greater than 45% of the people reported discomfort in the left foot and 36% - 45% reported discomfort in the right foot. According to Mike Kelly of GTRI, this can be attributed to the operators placing all of their weight on one foot and then using the other foot to operate the treadle.

Other ergonomic factors that had to be considered were the length of a person's foot, the angle at which the foot is turned out normal to the body, the pressure exerted by the foot, and the force that could be used to turn an object.

It was found that the average length of a woman's foot is 228 mm with a standard deviation of 11 mm. The 95% female right foot is 258 mm. The 5% right foot length is 223 mm. The area that the foot covers is 89 cm<sup>2</sup> with a standard deviation of 10 cm<sup>2</sup>. There is not a statistical difference between the left and right foot. A man's foot was approximately 32 mm longer and it covers 19 cm<sup>2</sup> more. The 95% male right foot is 288 mm. The 5% male right foot is 240 mm.

The average angle at which the right foot is turned out, a position normal to the body, is 6.80° with a standard deviation of 5.10. A man's foot is turned out 2.30° more than a woman's. It was also found that one can turn his left foot out farther than the right foot. A typical person can rotate his right foot clockwise 50° and counterclockwise 45°.

The pressure exerted by the female foot averages .33 kg/cm<sup>2</sup>, with a standard deviation of 0.052. The least pressure exerted was 0.27 kg/cm<sup>2</sup>. S. Konz and V. Subramanian determined the pressure data by dividing the body weight in half and then dividing by the contact area. The pressure in lbs/cm<sup>2</sup> is 0.727. For a woman,

this translates into an average force of 64.748 lbs exerted by each foot.

According to Woodson and Conover, the upper-force limit for hip movement only is 40 pounds. It is possible to develop a CTD (cumulative trauma disorder) in the hip if the force of the motion involved is greater than 40 pounds. According to Mike Kelly of GTRI, there is no hard evidence to back up the possibility of CTD's occurring yet, but logical thought processes would lead one to this conclusion.

### Occupational Safety and Health Administration Requirements

The foot controller must follow Occupational Safety and Health Administration (OSHA) Regulations. These regulations are stated in the Code of Federal Regulations published by the executive departments and agencies of the federal government. The following regulation is located in the labor Code of Federal Regulations.

Labor 1910.217 (4) Foot pedals (treadle). (i) The pedal mechanism shall be protected to prevent unintended operation from falling or moving objects or by accidental stepping onto the pedal. (ii) A pad with a nonslip contact area shall be firmly attached to the pedal. (iii) The pedal return spring(s) shall be of the compression type, operating on a rod or guided within a hole or tube, or designed to prevent interleaving of spring coils in event of breakage.

Presently there are no OSHA standards concerning ergonomics. However, the federal government is in the process of making ergonomic standards in order to improve working conditions for employees.

### Design Process

After the initial problem was discussed, a brainstorming session took place. Information on ergonomics was gathered from GTRI. A consultant in the apparel industry was contacted to discuss modular apparel manufacturing. The Georgia Tech data bases were used to find books on different types of controls. From this information gathered, the alternatives were narrowed down to five. The five remaining were

1) lasers, 2) vacuum or air flow, 3) roller bar, 4) push bar, and 5) pressure sensors in the floor.

The laser could control the change in needle speed by determining the number of beams broken by the operator's leg. The operator could move his leg forward into the path of the beams. Ergonomically, this design had its advantages. Weight could be distributed on both feet. The operator's motion would be forward as he/she started to place the fabric into the sewing machine. There would be little trouble with operator safety. The major disadvantages to this design were the space necessary for its use and the trip hazards developed by the receptors for the lasers.

The vacuum or air flow idea was very similar to the laser idea. As the air receptacles were covered, the speed of the needle would increase. The operator would step into the air flow. Ergonomically, there was little problem with this design. The operator would be able to maintain weight on both feet. The operator's motion would be in the forward direction as he/she started the needle and pushed the fabric into the sewing machine with a forward motion. There would be little trouble with operator safety. The major disadvantages were the same as those for the lasers.

The idea of using a push bar with the thighs is similar to the knee press that is already on the market. As the bar is pushed in, the needle speed would increase. Ergonomically, this design had few disadvantages. Weight could be distributed on both feet. The operator would be able to use either leg or both legs to operate the machine. The operator's motion would be in the forward direction as he/she started the needle and pushed the fabric forward into the sewing machine. The major disadvantages with this design were the possible hazards from having a bar sticking out and the construction of a fail-safe switch.

The idea of the roller bar is similar to a computer mouse. As the mouse is moved in a normal forward direction, the needle speed would increase. A spring mechanism would be installed so that weight could be distributed to the foot operating the control. Ergonomically, this had some disadvantages. The constant rolling of the pedal, if directed from the hip, could cause hip problems. The operator's motion would be in the forward direction as he/she started the

needle and pushed the fabric forward into the sewing machine. The major disadvantage to this design is the possibility of the operator tripping due to the rolling motion of the bar.

The pressure rug alternative would increase or decrease the speed of the machine depending on where the operator is standing on the rug. Ergonomically, there were no disadvantages to this idea. There would be an anti-stress mat or carpeting for the operator to stand on. The operator would be able to maintain even weight on both feet. The sensors could be placed so that the operator's motion would be in a forward direction as he/she started the needle and pushed the fabric forward into the sewing machine. The major disadvantage of this design was the precision needed to reach the desired speed.

A trip to Southern Tech to visit the apparel laboratory resulted in the observation of several types of controllers. The design group discussed the controllers presently on the market and the controller alternatives with Carol Ring. The design group used her expertise in re-evaluating the design alternatives. Lasers and the vacuum or air flow seemed to be over-engineered. The roller bar would be too great a safety hazard, and the push bar would get in the way of the fabrics being processed. This left the pressure rug.

The pressure rug needed to be more precise, so the design group went back to the decision matrix to discover ideas that could be combined with the pressure rug to get precision. The idea of a disk that could be turned by the foot seemed to work, but pressure sensors did not apply. Carol Ring was asked to evaluate the design. After a discussion with her and with Dr. Dorrity and Mr. Brazell, it was decided to proceed with the design of a disk placed in an anti-stress mat.

### **Design Analysis**

The final design is based on a disk that will rotate no more than 15°. This rotation will activate a potentiometer, which will change the voltage; this in turn will change the speed of the needle. The disk will be placed in an anti-stress mat to help alleviate strain on the body. The actual design is described in detail in



the Foot Controller Design section. A working model was built to simulate the designed model. Details of the working model are in the Model section.

### The Controller Design

The general design consists of three parts: the base, the pedal, and the potentiometer.

The base is a polyisoprene rubber that provides excellent resiliency, durability, and chemical resistance. The resistance includes the ability to resist moisture and dirt as well as more dangerous chemicals. This type of rubber also provides an easy surface in which to cut and to mount the other pieces. The mat is 35 inches wide and 24 inches long. The base height is 2 inches. The corners of the base are rounded to prevent a trip hazard. The size of the base should allow it to be placed anywhere in front of the machine that the operator wishes. This alleviates the problem associated with the treadle used now. The treadle used currently can not be adjusted due to its height and its need for mounting.

The pedal is made of aluminum and is mounted with bearings to support the load as well as to provide easier turning of the pedal. The pedal is shaped like a human foot for easy placement of the operator's foot. There is a guard attached to the right side of the disk that will aid the operator in the movement of the pedal and the placement of the foot. This guard provides a greater area for the rotational force to be directed. The guard is made of aluminum. A rotational spring provides the force to rotate the disk back to the neutral position. The rotational spring is made out of music wire ASTM-A228. The bearings turn on a track of stainless steel to reduce the friction and abrasion wear between the rollers and the rubber of the base. This track is known as the roller guide. The pedal is placed on the mat so that the operator has room to place his/her left foot on the mat also. The pedal has a radius of 13 inches. The outer edge of the pedal has a turn of 350. The pedal rotates under the edge of the mat. There are dust sweeps on the edge of the mat to prevent dust particles and thread from getting inside the controller.

The potentiometer is connected to the disk by an aluminum rod. The rod is attached to the disk and as the disk turns, the rod turns the potentiometer. The

disk can not turn unless 15 pounds of force is placed on the heel area. There is a spring placed under the heel that is rated for 15 pounds force. The spring is 7/8 of an inch in diameter. When the 15 pounds force is met, the shaft can engage and the pedal can rotate. The shaft is 1.75 inches deep. Underneath the shaft is a disk which prevents the shaft from digging into the rubber. The potentiometer is turned by the motion of the foot pedal. The potentiometer provides a voltage that varies from 0 to 20 volts. This in turn feeds the circuit connected to the servo motor. The circuit on the sewing machine allows certain settings to add resistance to the circuit. This limits the current going to the motor. The variable resistance within the circuit of the microprocessor allows for speed control separate from that of the foot pedal. It allows the ability to sew many types of items with a smaller risk of mistakes.

### Materials List:

|              |                          |
|--------------|--------------------------|
| Mat          | Rubber                   |
| Pedal        | Aluminum                 |
| Guard        | Aluminum                 |
| Shaft        | Aluminum                 |
| Disk         | Stainless Steel AISI 304 |
| Roller Guide | Stainless Steel AISI 304 |
| Rollers      | Stainless Steel AISI 304 |
| Shaft Spring | Music Wire ASTM-a228     |

### Model

The model consists of three basic parts, the base, the pedal, and the potentiometer controller. The base is made of plywood with one-inch dowels attached as stops and as the axis of rotation for the foot pedal. The foot pedal is a fourteen-inch radius, 25° arc piece made of plywood. An aluminum rod is attached to both the potentiometer and the pedal. This rod changes the potentiometer and it also allows the needle-up action and automatic thread cut to take place. The controller is a standard part obtained from the JUKI research facility in Duluth, Georgia. The part is a series of four potentiometers linked together to add and subtract their voltages to obtain the desired ranges. The voltages are processed by the microprocessor of the sewing machine. This process changes the current being received by the servo motor, thus changing the speed of the sewing machine.

The pedal can lay flat against the base or be mounted on rollers. The stop for the left side would be moved back to provide the necessary range for these functions to take place. The rod could also be the spring for the device if a different potentiometer from the standard JUKI part was used.

### **Hazards**

Several hazardous conditions had to be considered in the design of the foot controller. The following hazards were addressed: tripping on the mat, tripping on the actual controller or disc, electric shock, spills, and the sewing needle.

One requirement of the design is that it must be fail-safe. This requirement was attained by using a tension spring to place the disc back in the neutral position. The shaft under the heel has a cutaway area that allows the disc to move when at least 15 pounds of force is applied. A 15-pound rated spring will be located under the heel.

Another hazardous condition that needed to be addressed was the mat in which the foot controller is embedded. This is raised off the floor enough to be considered a tripping hazard by OSHA regulations. This hazard can be alleviated by painting the area surrounding the anti-stress mat a bright yellow color. This is required by OSHA Regulation 1910.144(a)(3). Sloping the edges of the mat to the floor and rounding the corners will also help.

Tripping over the actual foot controller in the mat can also be a hazard. Therefore, the controller is flush with the floor when inactive, and at least 15 pounds force is necessary for the disc to move.

In order to prevent electric shock, the disc is made of an insulating material. The material of choice is aluminum.

The needle on an industrial sewing machine is a potential hazard. A tension spring is used to return the disc to the neutral position so that the needle does not remain in the up position. Therefore, the needle will not be active when the foot is not on the disc. Also,

sewing machines presently have a thumb guard to prevent fingers from getting under the needle.

Possible oil spills and other liquid spills had to be addressed. The rubber mat would need channels in it to allow the liquid to drain to a level lower than the foot until cleanup can take place. The aluminum disc would have a nonslip contact area attached to it. This is required by OSHA Regulations 1910.217 (4) (ii).

### **Possible Applications**

Throughout the design process, other applications besides an industrial sewing machine were considered. Some other possibilities are to use the variable speed controller on any turning operation such as a lathe or a pottery wheel. It could also be used on any motorized vehicle. The gas pedal on a car or truck could be replaced. This had definite possibilities with the upcoming production of electric cars. However, a larger potentiometer would be needed because the required voltage variation would be much larger. The controller could also be used on vehicles such as power boats, lift trucks, and the lunar rover.

### **Conclusion**

A variable speed controller was needed which would allow an operator to control the speed of a needle when the operator was in a standing position. An attempt was made to make the controller more ergonomically sound than the foot treadle normally used in a sit-down sewing operation. Whether or not the new controller was ergonomically more sound could be proven only after a testing period.

The final design consists of a disc that rotates clockwise and counterclockwise placed in an anti-stress mat. When the disc is rotated, a potentiometer is turned by a rod connected to both the potentiometer and the disc. The change in the turns on the potentiometer changes the speed of the needle. The controller can not operate unless 15 pounds of force is placed on the spring under the disc. The compression spring also acts as the return mechanism for the disc. Two bearings are placed under the disc approximately where the ball of the foot would rest.

Cleaning the controller after each shift is recommended. A thorough blowing off of lint, thread, and dust will help to prevent mechanical downtime. It is also recommended that oil dropped on the mat be wiped off as soon as possible.

One design recommendation is to change the shape of the disc to optimize the operator's comfort and to reduce the open area on the mat. Another recommendation is to find a rubber that is either porous or one that has better resistance to oil. This would eliminate the problem with the isoprene rubber's poor resistance to oil. The design could also be amended to include two potentiometers and a switch that would allow the operator to use either the right or left foot. Our final recommendation is to place the mat and controller in the floor to prevent a tripping hazard if a new facility is being constructed or if a facility is being remodeled.

#### References

1. Behan, R.A. Some NASA Contributions to Human Factors Engineering: A Survey. Washington, DC; NASA. Code of Federal Regulations, Labor, Title 29, Parts 1900 TO 1910 (&&1901.1 TO && 1910.441), 1973.
2. Canover, Donald W. and Wesley E. Woodson. Human Engineering Guide for Equipment Designers, Los Angeles: University of California Press, 1964.
3. Dieter, George E. Engineering Design - A Materials and Processing Approach. New Jersey: McGraw-Hill, Inc., 1991.
4. Gilbert, Charles. Management Consultant. Gilbert and Associates. Marietta, GA.
5. Grader, Jerome E. Technical Data, Basic Process Control. Rochester, New York; Taylor Instrument Companies.
6. Kelly, Michael J. Principal Research Scientist, Georgia Tech Research Institute, Atlanta, GA.
7. Konz S. and V. Subramanian. Engineering Anthropometry, Advances in Industrial Ergonomics and Safety 1. Philadelphia: Taylor & Francis, Inc., 1989.
8. Ortiz, D.J., M. J. Kelly, T. K. Courtney, and D. J. Folds. Phase 1 Report: Ergonomic Considerations in Conventional Trouser Manufacturing, Design and Development of A Self Study Course for Apparel Supervisors in the Practical Application of Ergonomic Principles. Atlanta, GA: Economic Development Laboratory, Georgia Tech Research Institute, Georgia Institute of Technology, 1989.
9. Ortiz, D. J., M. J. Kelly, T. K. Courtney, and D. J. Folds. Phase 2 Report: The Impact of a Chair as an Ergonomic Intervention in Conventional Trouser Manufacturing, Design and Development of A Self Study Course for Apparel Supervisors in the Practical Application of Ergonomic Principles. Atlanta, GA: Economic Development Laboratory, Georgia Tech Research Institute, Georgia Institute of Technology, 1989.
10. Popov, Egor P. Engineering Mechanics of Solids. New Jersey: Prentice-Hall, Inc., 1990.
11. Ring, Carol. Technician, Southern College of Technology.
12. Rodriguez, Ferdinand. Principles of Polymer Systems, New York: Hemisphere Publishing Corporation, 1989.
13. Roebuck, J. A., K. H. E. Kroemer, and W. G. Thomson. Engineering Anthropometry Methods, New York: John Wiley & Sons, 1975.
14. Sesek, Richard. Economic Development Laboratory, Georgia Tech Research Institute.

**ENABLER OPERATOR STATION**

**Andrea Bailey, John Kietzman, Shirlyn King, Rae  
Stover, and Torsten Wegner**

**Abstract**

The objective of this project was to design an onboard operator station for the conceptual Lunar Work Vehicle (LWV). The LWV would be used in the colonization of a lunar outpost. The details that follow, however, are for an Earth-bound model. The operator station is designed to be dimensionally correct for an astronaut wearing the current space shuttle EVA suit (which includes life support).

The proposed operator station will support and restrain an astronaut as well as to provide protection from the hazards of vehicle rollover. The threat of suit puncture is eliminated by rounding all corners and edges. A step-plate, located at the front of the vehicle, provides excellent ease of entry and exit. The operator station weight requirements are met by making efficient use of rigid members, semi-rigid members, and woven fabrics.

**Problem Statement**

The design of the lunar work vehicle's operator station must meet the following requirements both on the Earth-bound model and the conceptual lunar design:

- support the combined weight of astronaut and current space shuttle EVA suit
- provide operator restraint system
- provide rollover protection based on static load of half vehicle weight with appropriate safety factor (4) to account for dynamic loading
- provide easy access to vehicle controls
- maintain ease of ingress/egress to operator station
- remain within maximum chassis mounting width on the forward T-section of vehicle
- meet within maximum weight requirements through selection of materials

The dimensions for this operator station design are based upon the current shuttle suit dimensions due to lack of concrete information on either the Mark III or AX-5 suit:

- |  |         |
|--|---------|
| • helmet height                          | 381 mm  |
| • shoulder width:                        | 726 mm  |
| • seat height-foot<br>to buttock:        | 508 mm  |
| • primary life support<br>system height: | 813 mm  |
| • shoulder height-seated:                | 940 mm  |
| • seated height to top<br>of helmet:     | 1016 mm |
| • arm reach:                             | 813 mm  |

**Design Descriptions**

The seat design is divided into three categories: structure, fabric, and restraint. The actual design for each of these categories is discussed in detail in sections that follow.

**Structure**

The actual seat structure consists of the roll cage and the step-plate support mounted to the front of the T-section. Also considered were the material selection and the chassis mounting mechanism.

**Roll Cage: Design.** The primary consideration for the main structure of the operator station was to protect the operator in the event of a vehicle rollover. In order to provide such protection, the structure to the operator station was designed to be similar to a roll cage used in automobile racing. The general design consists of a slanted U-shaped main hoop with two vertical support bars (Figure 5). The front T-section of the vehicle is about 1067 mm wide, which allows the hoop to be designed with a wide radius, thus producing only simple curves.

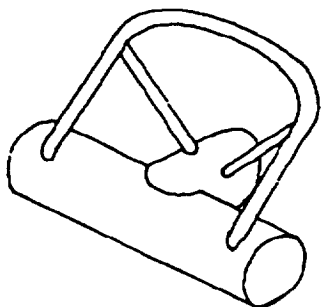


Fig. 5 U-shaped roll cage design

While this configuration would be preferred, integrating this design with the basic model of the Enabler forced a redesign. In redesigning the roll cage, the width given for mounting on the forward T-section was kept in mind. On the forward T-section, the wheel drives and their hubs are designed to detach easily from the central chassis section. This arrangement requires that the roll cage attach only to the central section of the chassis. The width at this point is approximately 510 mm. After allowing for welding, attachment hardware, and tool clearances, the usable width of the front T-section is roughly 460 mm. This is a limiting factor which forced design modifications, as seen in Figure 6.

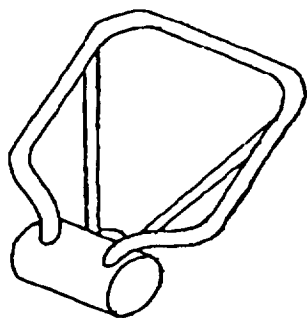


Fig. 6 Roll cage designed to meet mounting limitations

**Roll Cage: Material Selection.** Preliminary materials selection was based on the standards specified by

automobile racing sanctioning bodies, NHRA and NASCAR. Roll cage standards were consulted and found to specify either mild steel (AISI 1020 or 1018) or stainless steel (AISI 4140). Since steel is in widespread use and is cheaper and easier to work than composites involving carbon, it was selected for this design.

After the tubing sizes specified for racing roll cages were examined, a tubing manufacturer was consulted for information about available materials, diameters, and wall thicknesses. Reasonable tubing sizes, which are commercially produced, are those with outside diameters from 31.75 to 76.20 mm (1.25" - 3"). Available wall thicknesses for such tubing range from 2.11 to 3.96 mm (0.083" - 0.156"). The minimum bend radius specified for the design is five times the nominal diameter of the tubing. This factor of five results in a minimum bend radius which can easily be accomplished in most standard metal working facilities.<sup>14</sup>

ASTM data on the 1020 steel rated a yield strength of 262 MPa and a strength of 620 MPa on the 4140 steel. Because of its higher yield strength, 4140 stainless steel was specified for the design. In this application, the safety and space requirements were judged more important than the increased cost and difficulty created by using stainless steel.

In order to determine material strength requirements and final dimensions, a finite element analysis of the structure was performed. ALGOR software was used to prepare a model and analyze its performance. Due to constraints of the software used, each curved member was approximated as two separate straight tubular segments. Several design refinements based upon information from the models were incorporated into the final design chosen.

The forces used in this analysis were based on the assumption that static loads of half the vehicle weight, approximately 5300 N or 1200 lb., were acting upon the roll cage. The actual dynamic loads on the roll cage were considered by designing for a safety factor of four. A 5300 N force was placed at six locations oriented along the roll cage. The highest resultant stresses occurred in the case of a horizontal force, acting sideways, located at the top of the roll bar.

The finite element analysis was performed for various tubing sizes. The results indicated 76.2 mm outer diameter tubing with a 3.05 mm wall thickness as the most appropriate choice. Using 4140 steel results in a maximum stress in the structure of 143 MPa, with a safety factor of approximately 4.3. While smaller diameter tubing may be lighter in weight and more normal in appearance, any tube sizes below 50.8 mm with a 3.96-mm wall thickness cannot withstand the forces which act upon the structure. A choice of 50.8-mm tubing with 3.96-mm wall thickness material results in a safety factor of only 1.8. This was regarded as too small a margin for a human safety application where the true forces are not known.

The force analysis also showed that the highest stresses in the tubing occur near where the roll cage connects to the chassis. Thus, the design of the structure above the attachment points was not critical from a stress standpoint. The structure at the top of the roll cage was therefore designed for astronaut clearance in ingress/egress and minimal tubing use for minimal weight of the structure. Other structural configuration attempts yielded negligible improvements in reducing the critical stress near the chassis attachment points.

**Seat Frame.** The actual seat and backrest for the operator station are supported by 6.35-mm diameter steel cable held by cycles which are welded to the roll cage. The steel cable has a load limit of 6228 N (1200 lbs), which easily supports the estimated operator weight of 890 N (200 lbs). For the seat and backrest, cable was chosen for all structural members in tension because it weighs less than steel tubing. The cable passes through an eyelet and is fastened to itself with standard cable ties. The seat and backrest also include a cotton twill fabric, which is discussed in the section on fabric.

**Step Structure Design.** Because of the height of the vehicle and the mobility restrictions upon a suited astronaut, a step is required for ease of ingress/egress to the operator station. This step was integrated into the operator station design by placing it immediately forward of the front T-section. The size of the plate was based upon the competing requirement ease of ingress/egress and minimum weight. Operator ingress is accomplished by stepping onto the plate, turning

around the plate, and then sitting in the seat. The roll cage main hoop is used for position and orientation references during this action.

The step-plate is supported by steel tubes which connect it to the front T-section. The loads produced when an astronaut steps upon the plate are quite severe because of the long moment arm attached to the chassis. A finite element analysis of the step-plate and its supports was performed in order to specify the tubing size. The same ranges of tubing diameters (31.75 - 76.20 mm) and wall thicknesses (2.11 - 3.96 mm) considered for the roll cage were investigated for the step-plate.

A final design of a 31.75-mm outside diameter tubing with a 3.96-mm wall thickness was chosen for the supports of the step-plate. When a 1000 N (225 lbs) load is applied at the corner of the step-plate, a maximum stress of 358 MPa develops in the supports. Because of this high stress value, AISI 4140 steel was chosen for the support tubes. This material results in a safety factor of 1.7 for this load. While this safety factor is lower than that of the roll cage, the step-plate is not critical to the safety of the operator. An additional consideration is that the use of larger diameter tubing would have resulted in insufficient leg space for a suited astronaut.

The step-plate itself was designed of 6061-T6 aluminum for its superior strength-to-weight ratio compared to that of steel. It is bolted to the support arms using standard grade 5 bolts and washers.

**Attachment to Chassis.** The nature of rollover loads greatly complicates the attachment of the roll cage to the chassis. While dynamic loads are difficult to produce, the obvious static load in the event of a rollover is the weight of the front half of the vehicle. Therefore, the weight of the chassis must be transferred to the roll cage so that the operator will not be crushed. As a result, the connections between the roll cage and the chassis must support not only the weight of the roll cage but also the weight of the front of the vehicle.

The roll cage and step structure are welded to thin steel pads that distribute the point loads over a greater area. The pads are then welded to the skin of the chassis structure. Since that skin is relatively thin and

would deflect under such distributed loads, a load-carrying bulkhead system was designed into the front chassis T-section.

The use of steel for the chassis T-section as well as for the roll cage and step structure allows the assembly to be welded together. Standard TIG welding procedures for joining steel to steel can be implemented using a standard fillet weld to join the pipes. A weld depth of 3 mm was specified based on the welding of pipe of 3-4 mm wall thickness.<sup>2</sup>

### Fabric

The operator station's seat will have fabric in two locations on the structure, the backrest and the seat. The fabric will be looped around each cable and double-stitched to itself with polyester/cotton thread.

In choosing the fabric, several factors were taken into consideration. First, the fabric must be strong enough to support the entire weight of the astronaut. It must also have low elongation so that it will not creep or deform. Finally, cost and availability play a major role in the fabric selection.

For this design, a cotton twilled fabric will be used. This decision is based on the availability and cost of this type of fabric.

The fabric dimensions and shapes for the seat are given in Figure 7.

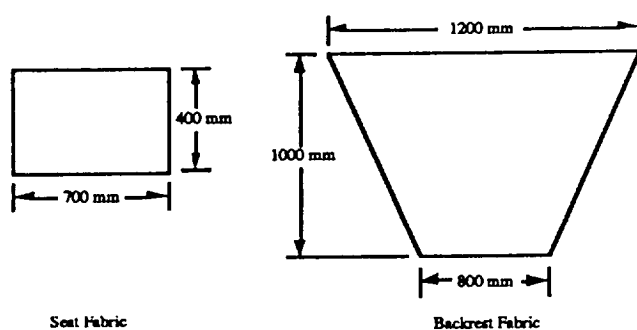


Fig. 7 Fabric dimensions and shapes

### Restraint

After considering a number of complicated seat belt designs, an aircraft-style lap belt was selected as a preliminary design. At low speeds, this type of lap belt, together with the contoured seat design should adequately restrain the astronaut. Also, the addition of an upper body restraint would hamper the astronaut's ingress/egress.

The restraint will be attached to the chassis by using the clip, already attached to the seat belt, and an eyelet that will be welded to the chassis near the seat attachments.

### Weight of Operator Station

The weight of the operator station, as described above, complete with mounting hardware is approximately 55 kg.

### Conclusions and Recommendations

The initial goal for this project was to design an operator station for the lunar work vehicle that would meet dimensional considerations of a suited astronaut and provide rollover protection. The design described in this report and supporting technical drawings list meets these requirements. While the design meets the constraints previously listed, further modifications could improve the existing design.

First, a re-analysis should be done on the roll cage of the operator station. The first recommendation would be to analyze the roll cage structure using materials other than steel. Other materials (aluminum, carbon fiber composites, etc.) would allow development of a lighter weight structure with potentially smaller tubing sizes. Also, the utilization of the Algor FEA system requires each member to be approximated as a straight tubular member. The number of members which approximate a curve could be increased to improve the accuracy of the FEA results.

Before some of the analysis can occur, the building of a full-scale model is necessary. The actual ingress/egress of the suited astronaut needs to be investigated. Along with this, the structural integrity of

the cable needs to be analyzed. The loaded shape of the fabric and cable must be studied experimentally. Depending on fabric thickness, the present design should be adequate; however, a mathematical analysis should be performed to determine the actual tensile loads present in the fabric and on the structure. In the analysis of the seat fabric, the actual pressure distribution caused by the astronaut should be investigated.

The restraint used in this design could also be improved. While this style of restraint (single lap belt with aircraft-style buckle) would work well, a larger size buckle would allow easier manipulation by the suited astronaut. Another style buckle to consider is similar to the handle-pull type used by tree climbers. Additionally, some type of spring or stiffer webbing should be used to hold the seat belt in an upright position to aid the astronaut in locating the belts.

#### References

1. Allied Fibers, Product Information, "Spectra®: High Performance Fibers," Allied-Signal, Inc., 1990.
2. Brazell, J.W. Private Communication: March 5, 1992.
3. Brown, Mariann F., Susan M. Schentrup. "Requirements for Extravehicular Activities on the Lunar and Martian Surfaces," Space Station and Advanced EVA Technologies, Society of Automotive Engineers, Inc., July 1990, pp. 71-79.
4. Cadagon, Dave. ICL Dover Inc., Frederica, Delaware, Private Communication, February 3, 1992.
5. Compton, William David. Where No Man Has Gone Before: A History of Apollo Lunar Exploration, National Aeronautics and Space Administration, 1989, pp. 227-240.
6. DuPont, Production Information. "Kevlar®: The Uncommon Material for Uncommon Solutions," Delaware 1991.
7. Fikes, John. AST, Navigation & Control Systems Branch, Preliminary Design Office, Marshall Space Flight Center, Huntsville, Alabama: Private Communication, February 12, 1992.
8. Finley, Roland L. "Piloted Rover Technology Study Task 9.4 Final Report NASA Contract NAS8-37857", c. 1990.
9. Gandhi, K.R., P.V. Cavallaro, J.J. Deluca, G.J. Piper, and D.W. Oplinger. "Light Weight Composite Rollbar for Army Towed Howitzer," 22nd International SAMOE Technical Conference, proceedings, November 6-8, 1990, pp. 868-882.
10. Hagle, James. Curator of Exhibits and Artifacts, U.S. Space and Rocket Center, Huntsville, Alabama, Private Communication: February 12, 1992.
11. Jones, Clyde S., Jr. and Frank J. Nola. Mobility System Activity for Lunar Rovers at MSFC, Marshall Space Flight Center, Huntsville, Alabama, September 9, 1971.
12. Morea, Saverio. Private Communication: February 4, 1992.
13. Moroso Technologies. Private Communication.
14. Oberg, E.; F.D. Jones, and H.L. Horton. Machinery's Handbook, 23 ed., New York Industrial Press, 1988.
15. Power, E.J. and G.A. Serad. "History and Development of Polybenzimidazole," Hoechst Celanese: PBI Products Division, Charlotte, N.C., 1986.
16. Press Release of Project: Apollo 16, National Aeronautics and Space Administration, Washington, D.C., April 6, 1972, p. 118.
17. Rodrigues, Ferdinand. Principles of Polymer Systems, 3rd ed., Hemisphere Publishing Corporation, New York, 1989.
18. Schieb, Eric. GT Motorsports: Private Communication.



19. Simmons, Gene. On the Moon With Apollo 16: A Guidebook to the Descartes Region, National Aeronautics and Space Administration, April 1972.
20. Swalley, Frank. Marshall Space Flight Center, Huntsville, Alabama, Private Communication: February 11, 1992.

## DUST CONTROL FOR ENABLER

Kevin Hilton, Chad Karl, Mark Litherland,  
David Ritchie, and Nancy Sun

### Abstract

The dust control group designed a system to restrict dust that is disturbed by the Enabler during its operation from interfering with astronaut or camera visibility. This design also considers the many different wheel positions made possible through the use of articulation joints that provide the steering and wheel pitching for the Enabler. The system uses a combination of brushes and fenders to restrict the dust when the vehicle is moving in either direction and in a turn. This design also allows for ease of maintenance as well as accessibility of the remainder of the vehicle.

### Introduction

The purpose of the Enabler project was to design a lunar work vehicle. The Dust Control group was responsible for the design of a device to restrict dust from interfering with astronaut and camera visibility.

In a previous Apollo mission, the astronauts noticed that lunar dust had a tendency to "rooster-tail" from the wheels of the lunar rover. The dust was electrostatically charged and thus stuck to almost everything, including the astronaut, the lunar rover, and the lenses of cameras. This presented a problem, especially for astronaut and camera visibility.

This report presents a possible solution to this problem.

### Problem Statement

The objective of the Dust Control group was to devise a system to keep dust down, so it would not interfere with visibility of the astronaut and the cameras. The device needs to satisfy the following criteria:

1. The device should not weigh more than 200 kg.

2. In the event of damage to the system, the astronaut must be able to repair or replace all damaged parts easily.
3. All main parts of the device should last 10 years. Replaceable parts should last a minimum of 2 months of continuous use.
4. The astronaut should have easy access to the sides of the vehicle at all times. Any dust control device should allow for this access.
5. The device should keep at least 80% of the dust down.
6. The device should be independent of vehicle power systems.
7. Parts of the device that may come in contact with rocks should be extremely durable. Attachments should be high-strength.
8. The device should be manufacturable on the moon at a later date.

### Materials Selection

Materials for the dust control device are a quintessential component for the design of the device. The materials must be able to withstand the harsh environment of the moon.

High doses of radiation cause most man-made polymers to degrade, and they would therefore not be the optimum choice. Radiation tends to cleave the carbon-carbon, carbon-nitrogen, and carbon-oxygen bonds. Radiation also has ill effects on some metals such as steel, causing embrittlement and loss of characteristics necessary for the metals' intended purposes.

The vacuum pressure also has detrimental effects on some materials. Some metals such as cadmium, zinc or

magnesium at greater than 125<sup>0</sup> C sublimate, and some polymers degrade under vacuum.

Strength is a very important characteristic, because the dust control parts must withstand the impact of the lunar soil and small rocks. However, a low coefficient of thermal expansion for the fender, a smaller Young's Modulus for the brushes and sheet and weight are factors to be considered in addition to strength. Since bolts hold the fender in place, the thermal coefficient should be as low as possible, and the material should also have the highest strength and lowest weight possible. Young's Modulus should be low enough for the material to flex but large enough to remain horizontal and strong enough to withstand the forces of the lunar soil coming off of the wheel.

Aluminum 356 was chosen for the support structure of the brushes, the hinges, and the attachment bracket because it is one of the lighter weight aluminums (2.68 g/cm<sup>3</sup>). It also has a respectable coefficient of thermal expansion of  $21.5 \times 10^{-6}/^{\circ}\text{C}$  which is not the least ( $19.0 \times 10^{-6}/^{\circ}\text{C}$  for A132) nor the most ( $25.0 \times 10^{-6}$  for A1220) toward the lower end of coefficients of aluminum alloys. It is 82.7% Al, 0.3% Mg, and 7.0% Si and has a tensile strength of 230 MPa, a yield strength of 165 MPa and the ductility of 4% EL in 5.08 cm. Radiation and vacuum pressure have little effect upon this aluminum.

S glass is the material of the brushes and knit inner sheet because it is stiff enough to remain horizontal when five fibers are braided together. High performance glass fibers could be used but they would be too stiff and would break more easily than the S glass, which will bend under the same stress. The glass bristles are to be Teflon coated. This will increase the abrasion resistance of the bristles. The Teflon coating will also allow the bristles to last longer, because it will reduce the abrasion and therefore reduce flaws created by the lunar soil. Flaws in the glass are the places where failure is most likely to occur. The S glass contains 65 (wt. %) of SiO<sub>2</sub>, 25 (wt. %) of AlO<sub>3</sub> and 10 (wt. %) of MgO and has the tensile strength of 4,500 MPa, Young's Modulus of 85,000 MPa, density of 2.48 g/cm<sup>3</sup>, and a coefficient of thermal expansion of  $3.0 \times 10^{-6}/^{\circ}\text{C}$ . The lower Young's Modulus is necessary because the bending allows the force to be dissipated over a greater distance. Since the distance is greater,

the stress is less than a stiffer fiber that does not bend as much. Radiation and vacuum pressure have little effect on S glass.

A molded woven graphite-fiber-reinforced borosilicate matrix is the material of choice for the fender. It has a density of approximately  $2.25 \text{ g/cm}^3$  with an elastic coefficient (E) of 380 GPa, an ultimate tensile strength of 2.2 GPa and a coefficient of thermal expansion of  $-6 \times 10^{-6}/^\circ\text{C}$ . The carbon fibers prevent micro cracks in the structure from propagating, and when the graphite is exposed it acts more like a lubricant. Complex shapes can be made by injection or compression molding into shaped dies at high temperatures. The low coefficient of thermal expansion, high strength, and fairly low density make this material the optimum one for the fender. Radiation and vacuum pressure have little effect on this material.

### Detailed Description of Parts

#### Hinge

The purpose of the hinge in the dust control device is to attach and remove the brushes with great ease. It also will make it easy to access the vehicle by raising the brushes up out of the way. Here the hinge will be made from steel, but on the moon it will be made from Aluminum 356.

There are four different parts to this hinge:

1. The brush bar will be attached to the upper part of the hinge by bolts and will use the three bolt holes at the bottom in the triangular shape. There is also a circular rod to attach the hinge to the chassis (Figure 8).

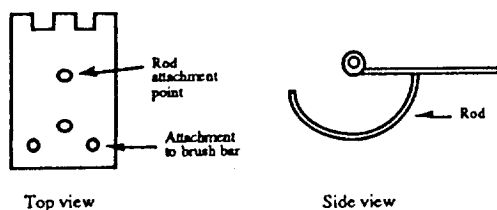


Fig. 8 Brush bar attachment

2. The lower part of the hinge will fit into the slotted part on the chassis. It has a hole in the center so that the rod from the upper half of the hinge can penetrate the lower half and keep the entire hinge in place (Figure 9).

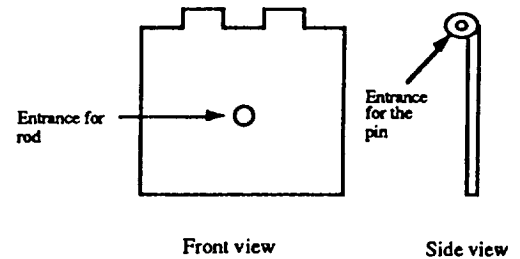


Fig. 9 Hinge and rod placement

3. The spring will wrap around the pin of the hinge in a effort to keep the hinge in the closed position (Figure 10).

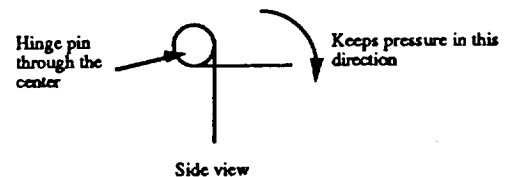


Fig. 10 Spring

4. The last part of the hinge is the pin that holds the two halves of the hinge together (Figure 11).

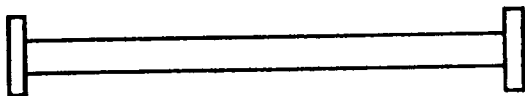


Fig. 11 Hinge pin

### Center Brush Assembly

The center brush assembly is the mechanism to control dust between the front and center wheels and center and rear wheels. Because of the large range of motion in these areas, the interference of the assembly is very critical. The center brush assembly consists of two major parts and some minor attachment parts.

### Brushes

The brushes are the key to the mechanism. They are able to accommodate a dual task. First, they are able to deflect the dust downward and away from the chassis. More importantly, the brushes do not interfere much in a full near side turn and allow the vehicle to perform unhindered movement.

The brushes are angled so that they are parallel to the opposite side brushes when in a full 30° near side turn. They are at an angle of 14° to the chassis. This allows the brushes to move back and forth with the least amount of angle between them when the maximum amount of interaction of the brushes occurs. The maximum forces between the brushes will be lessened by this setup.

The brushes are connected to a brush bar to form something like a comb. The brush bar slides into the groove from the edge of the solid piece framework. The straight brush bar slides in at the outer edge of the vehicle, while the angled brush bar slides in at the

inside. The brush bars are held in place by a pre-threaded wing nut. The angled brush bar is harder to replace, but should not have to be replaced very often because it has shorter brushes and is not the recipient of a large amount of dust.

### Solid Piece

The solid piece is much sturdier than the brushes. The solid piece is positioned so that it does not interfere with the solid piece on the opposite side, and it interferes with the brushes on the other side only in a limited capacity. The solid piece conforms very closely to the fender to minimize the dust that escapes between them and also serves as an attachment point for the brushes. The thin sheet allows the assembly to stay light while still providing complete dust protection.

The entire assembly is bolted to and supported by a hinge. The hinge provides several useful functions. The hinge allows the assembly to be lifted so that access to the vehicle's chassis is not impaired. Also, the hinge will allow the assembly to move if it is hit underneath by a large rock that the vehicle might be trying to climb. The hinge also can make it easier to attach the brush bars, especially the angled bar.

### Attachment Brackets

#### Purpose

The purpose of the attachment bracket is to provide hard attachment points for the fender and brush arm assembly, while allowing easy removal of the brush arm assemblies. It also must avoid the bolts that attach the main wheel bearings to the chassis, while providing for easy removal of the wheel bearing bolts. This must be accomplished inside a distance of no greater than five (5) inches axially on the lateral portion of the chassis (Figure 12).

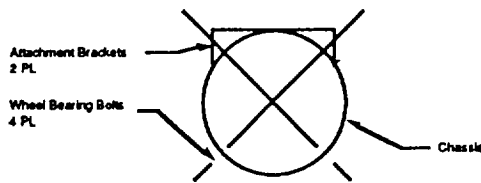


Fig. 12 Attachment bracket

### Design Elements

The attachment clamp consists of two steel "boxes" measuring approximately 300 x 120 x 80 mm (Figure 13). These boxes are welded to the chassis at approximately the location shown in Figures 12 and 13. In this position, they allow the brush arm assemblies to be mounted above the center of the chassis and to avoid the wheel bearing mounting bolts.

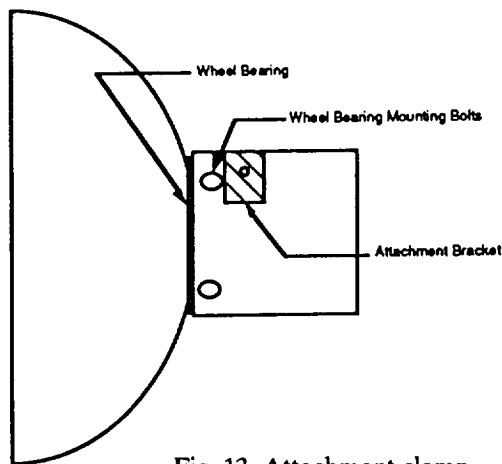


Fig. 13 Attachment clamp

### Materials

To facilitate mounting the attachment brackets, the material chosen is steel. This choice was dictated by the fact that steel has already been chosen for the chassis material. By choosing the same material, it is now possible to install the brackets by welding them directly to the chassis. This gives a very strong, solid attachment point for the brush arm assemblies. A firm attachment point was necessary because the brush arms will be undergoing violent displacements and should be

able to return to the exact point of rest that was intended by the designer.

### Fender

The fender's purpose is to prevent the dust from covering the vehicle when it leaves the wheel from  $0^\circ$  to  $90^\circ$  relative to the horizontal plane. The dust goes around the fender and then back down to the ground. The fender has 12.7 cm of clearance to keep the wheel from touching it when it is deformed from various obstacles. The fender leaves the chassis at a  $60^\circ$  angle to keep space between it and the conical wheel. The fender comes 5.08 cm below the outside of the wheel, which is also at a  $60^\circ$  angle to prevent dust from escaping and covering the vehicle with a thin dust layer. Polyethylene is the material used on the Earth vehicle, but we recommend using a molded woven graphite-fiber-reinforced borosilicate matrix for the lunar vehicle. The fender is 0.4 cm thick because it would be thick enough to withstand the stresses of impact of the lunar soil and small rocks. Each fender would weight 24.5 pounds, and all six fenders would weight 147 pounds.

### Front and Rear Dust Brush Assembly

To aid in keeping dust below the chassis in front of and behind the vehicle, a special dust brush assembly is required. The front and rear dust brush assembly differ from the center brush assembly used between the wheels for the following reasons:

1. The center brush assembly is too low to be used in front of and behind the vehicle. If the center brush assembly is used in front of and behind the vehicle, it would be subjected to impact from large rocks being climbed by the vehicle.
2. If used in the front of the vehicle, the center brush assembly would interfere with the seat.

The dust brush assembly consists of four main parts:

1. **The Base Support.** This aids in supporting the dust brushes. It is welded at the base to the hinge. On the other end, it is welded to the

arm support. The base support is hollow and the walls have a thickness of 4 mm along the entire length of the piece. The base support is made of steel in the Earth model, but aluminum is recommended for use on the moon.

2. The Arm Support. This also aids in supporting the dust brushes. This piece is angled at 30° to the horizontal, and is welded on both ends. At the lower end, it is welded to the base support. At the upper end, it is welded to the brush holder. This piece is also made of steel and is hollow with a wall thickness of 4 mm along the entire length.

3. Brush Holder. This holds the removable brushes. The brush holder is 60 mm x 60 mm x 410 mm. The housing is made of the same type rectangular steel tubing as used for the support arm, but one "long" face is cut open for brush attachment.

4. Brushes. These easily replaceable brushes are each composed of 6000 staggered bristles, held together by a steel "clamp," which can easily be slid into the brush housing. Staggered bristles are used to reduce the total number of bristles needed to function properly. These nylon bristles are 1 mm in diameter and 808 mm long. Teflon-coated fiberglass bristles are recommended for use on the moon.

The total weight of four assemblies needed for the vehicle, using the materials chosen for the moon, is 115 lbs. All materials chosen and reasons for their specification are discussed in the materials section of this report.

### Conclusions

The objective of this project was to design a 6-wheeled lunar work vehicle. The Dust Control group was to design a device to restrict lunar dust from interfering with astronaut and camera visibility. Astronauts noticed in previous missions that lunar dust kicked up by the wheels of the lunar rover would hover for long periods of time, thus interfering with visibility.

Also, the electrostatically-charged dust stuck to almost everything, including the camera lenses, which hindered filming.

In order to maintain astronaut and camera visibility, a device was designed to reduce the amount of dust thrown up by the vehicle's wheels. The total weight of the dust control system does not exceed 200 kg, while still providing the strength necessary to stand up to impact from rocks when the vehicle is traveling at speed. The design allows for occasional replacement of parts that will see a great deal of wear and tear. This replacement can be easily accomplished by astronauts wearing pressure suits. In the event that access to the vehicle is required, the brush assemblies rotate upward, allowing the astronauts to reach the interior of the vehicle with a minimum of effort. The dust control system will keep approximately 80% of the dust below the chassis while not interfering with the line of sight of the astronaut and the cameras. It does not require power from the vehicle drive motors and is extremely durable. All parts of the design will be manufacturable on the moon.

### Acknowledgments

We wish to acknowledge Dr. Stephen Liang, who helped us with our decision matrix and Dr. Desai, who helped with material selection.

### References

1. American Society of Metals. Metals Handbook Properties and Selections of Metals 8th Edition. American Society of Metals - Ohio, 1960.
2. Apollo 14 Preliminary Science Report. NASA Manned Spacecraft Center, Washington, D.C., 1971.
3. Apollo 15 Preliminary Science Report. NASA Manned Spacecraft Center, Washington, D.C., 1972.
4. Apollo 16 Preliminary Science Report. NASA Manned Spacecraft Center, Washington, D.C., 1972.

5. Barteneu, G.M. The Structure and Mechanical Properties of Inorganic Glasses. Wolters - Noordhoff Publishing, Groningen, The Netherlands, 1970.
6. Boyd, David C. and John F. Macdowell, eds. Commercial Glasses, Advances in Ceramics, Volume 18. Fall Meeting of the American Ceramic Society, October 17-19, 1984, Grossinger, New York. Columbus, Ohio: The American Ceramic Society, Inc., 1984.
7. Dunn, Barrie D. Metallurgical Assessment of Spacecraft Parts and Materials, Chichester: Ellis Horwood Limited, 1989.
8. The Effects of the Space Environment on Materials, Volume II, Society of Aerospace Material and Process Engineers, St. Louis, 1967.
9. Environmental Effects on Materials for Space Applications, AGARD Structures and Materials Panel, Canada, 1983.
10. Everhart, John L. Engineering Properties of Nickel and Nickel Alloys. New York: Plenum Press, 1971.
11. Jain, J., A. R. Cooper, K.J. Rao, and Chakravorty, eds. Current Trends in The Science and Technology of Glass, India - U.S. Workshop on Current Trends. The Science and Technology of Glass, Bangalore, India. November 13-20, 1988. Singapore: World Scientific Publishing Co., 1989.
12. Jenkins, A.D. Polymer Science, A Materials Science Handbook. New York: American Elsevier Publishing Co., Inc., 1972.
13. Johnson, Stewart W. and John P. Wetzel. Engineering, Construction, and Operation In Space II: Volume 1. New York: American Society of Civil Engineering, 1990.
14. Kurkjian, Charles R. ed. Strength of Inorganic Glass, NATO Advanced Research Workshop Entitled Strength of Glass, March 21-25, 1983, Algarve Portugal. New York: Plenum Press, 1985.
15. Lewis, M.H. Glasses and Glass-Ceramics, New York: Chapman and Hall, 1989.
16. Peterson, N.L. and S. D. Harkness, eds. Radiation Damage in Metals, Seminar of the American Society for Metals. November 9-10, 1975. Metals Park, Ohio: American Society for Metals, 1976.
17. Purser, Paul E., Maxime A. Faget, and Norman F. Smith. Manned Spacecraft: Engineering Design and Operation, New York: Fairchild Publications, Inc., 1964.
18. Rittenhouse, John B. and John B. Singletary. Space Materials Handbook, Third Edition, National Aeronautics and Space Administration, Washington, D.C., 1969.
19. Scholze, Horst. Glass, Nature, Structure and Properties, Third Edition. New York: Springer-Verlag, Inc., 1991.

## 1991-1992 PROJECT SUMMARIES

University of Houston  
Sasakawa International Center for Space Architecture  
College of Architecture  
Houston, Texas

Professor Larry Bell  
Michael Mortensen, Teaching Assistant

### PORTABLE HABITAT FOR ANTARCTIC SCIENTIFIC RESEARCH (PHASR)

Samantha S. Griswold

#### Abstract

The Portable Habitat for Antarctic Scientific Research, PHASR, is designed as a versatile, general purpose habitat system that addresses the problem of functional space and environmental soundness in a partially fabric-covered shelter. PHASR is used for remote field site applications that call for an easily transportable, compact habitat that can be quickly deployed. PHASR will also provide four scientists with a comfortable and efficient use of interior space.

PHASR is a NASA/USRA Advanced Design Program project conducted at the University of Houston College of Architecture, Sasakawa International Center for Space Architecture (SICSA). This report is prepared for NASA/USRA.

#### Introduction

The need for an environmentally safe portable field habitat for use in the Antarctic was realized after research for an Antarctic Planetary Testbed (APT) as well as a South Pole Station was undertaken by SICSA. Currently, the United States uses 2-man tents and huts for field research in the dry valleys and on the ice. The 2-man tents are 6 ft by 6 ft double-walled canvas with a 15 cm airspace. When using these tents, researchers place cold weather sleeping bags on the ground or ice. Cooking is done on a portable diesel stove. Huts of canvas and wood are constructed if the project is expected to last more than one season. The size is dependent upon the number of crew members. As

research efforts in the Antarctic increase, better habitation must be considered. The range of research performed in the Antarctic includes biomedicine, geology, geophysics, meteorology, etc. A habitat that is flexible enough to meet the requirements of a variety of scientists and to provide an atmosphere conducive to that research is greatly needed. With importance being placed on preserving and protecting the Antarctic environment, it is imperative that a habitat be designed that supports these efforts as well.

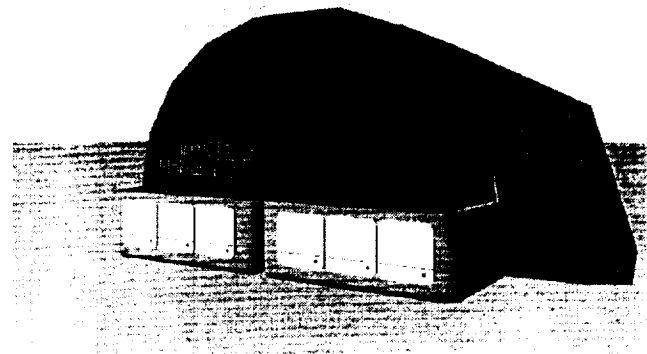


Fig. 1 3-D computer model of a deployed PHASR

#### Requirements

To meet habitat objectives, it was determined that PHASR should meet the following design requirements:

1. Ergonomically responsive
2. Easily transported by a broad range of transport methods



3. Easily deployed/assembled
4. Easily recovered and reusable
5. Environmentally safe

### Design

An investigation of the different geometric shapes feasible to form the exterior of the habitat was undertaken. To accomplish this, a volumetric trade-off study was used to determine which shapes performed best. Design studies were evaluated on the basis of wind and snow load, solar capability, volume, deployment, and rib structure. This study helped to justify many of the beginning design decisions that were made. The shape chosen for PHASR met minimum space requirements for a crew of four and also gave them maximum standing space.

Issues deemed necessary for the design include an ergonomic interior and the need for self-containment. By providing modules that break apart and reassemble to form an actual "interior," an ergonomic situation is achieved. Modules also contain fresh water and gray water storage so that the Antarctic environment remains unscathed. The system proposed in PHASR will provide better crew comfort, flexibility, and variability in the interior elements. PHASR contains the following four zones:

- Zone 1 - Workstation
- Zone 2 - Galley Area
- Zone 3 - Hygiene Area
- Zone 4 - Crew Quarters

Also, dividing PHASR in half separates the public and private areas that will assist in noise control and ease of circulation. A general configuration was established from information produced in the volumetric design studies. Then crew tasks and operations were considered.

The determination of characteristics of crew tasks and operations required to perform functions included frequency, duration, sequence, and volume. Also considered were special environmental requirements, privacy, and personal space requirements.

With the incorporation of the information above, the layout of PHASR maximizes the amount of horizontal and vertical space, accommodates the expected levels of activity at each station, provides the ability to isolate the work environment from the more private rest/relaxation areas, and provides a safe, efficient, comfortable work and living environment.

### Zone 1 - Workstation

The workstation area is located in the front of PHASR. It provides general scientific and technical support functions such as communications and lap-top computer systems.

It is within the workstation area, aside from "extravehicular" activity, that the majority of stress-related duties will occur. The workstation area can accommodate a crew of four.

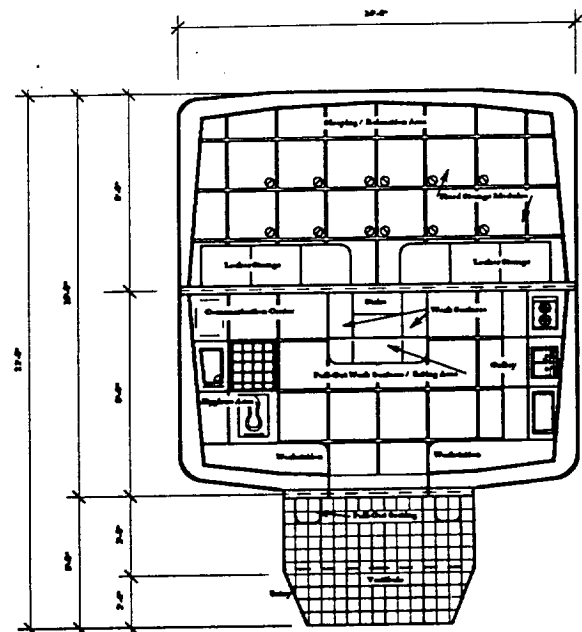


Fig. 2 Plan of PHASR

Preliminary concepts for the workstation area focused on creating a workspace geared toward individual tasks and team task configurations. Because space was limited, foldout and pullout work surfaces were used for additional desk space. The work surfaces near the stairs may be used if a group discussion area is desired. These

are some examples of PHASR's flexible working and living spaces that can be easily adapted to specific needs of different scientists. In addition, the geometry of the stacking interior elements were used to create unity between the interior and exterior.

Workstation requirements include:

- Ergonomic support of work activities
- Efficient use of volume
- Separation between work and sleeping/recreation
- Areas of privacy
- Vertical storage
- Capability for small repairs
- Capability for data processing

The workstation components include:

- Communication center
- Audio transmission
- Intercommunication system
- Computer
- Maintenance center
- Equipment stowage

The four workstations provide computer capability for documenting and processing research. The communication center provides audio communication and intercommunication. The seating system for the workstation consists of roll-up stools for easy storage. The sleeping area may be separated from the work area by a flap of fabric to ensure crew members of privacy when they are on different schedules.

### Zone 2 - Galley Area

Food preparation is performed on a surface that covers the sink. Additional food preparation surface is located to the side of the galley area near one of the main workstations. Fresh water and gray water are stored under the sink area. Utensil storage and the trash compactor are located under the counter-high modules. The dining area is formed by the foldout work surfaces that are attached to the main work surfaces by the stairs.

PHASR's galley must function as the primary source for preparation, storage, and disposal of food and waste. A small amount of food can be stored here, but larger amounts of food are stored in modules located in the sleeping side of the habitat.

The main requirements for the galley follow:

- Cooking
- Cleaning
- Hand washing
- Food preparation
- Water stowage

The components for the galley include:

- Ambient storage
- Refrigeration/freezer storage
- Food and beverage storage
- Toaster oven
- Electric coil burner
- Food preparation area
- Trash compactor/disposal
- Sink
- Water stowage modules

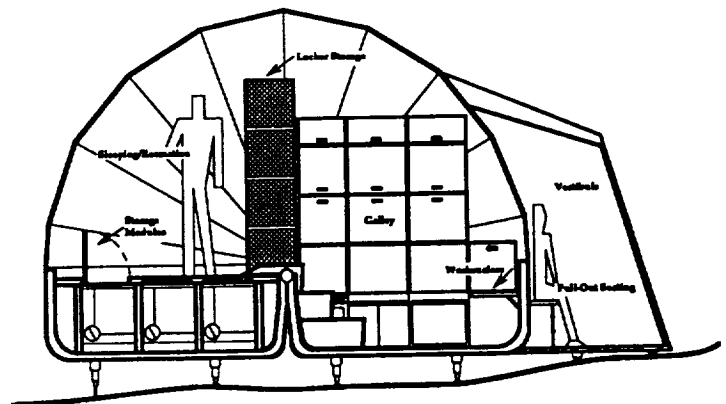


Fig. 3 Section toward galley

### Zone 3 - Hygiene Area

The hygiene area in PHASR contains some stationary elements and numerous stacking modules. It contains a toilet, cleansing area/shower, and sink.

Requirements for the hygiene area include:

- Full-body cleansing
- Hand/face cleansing
- Oral hygiene
- Personal hygiene
- Urination/defecation

- Sufficient ventilation
- Waste stowage

The components of the hygiene area are the:

- Shower
- Sink
- Personal hygiene stowage
- Toilet

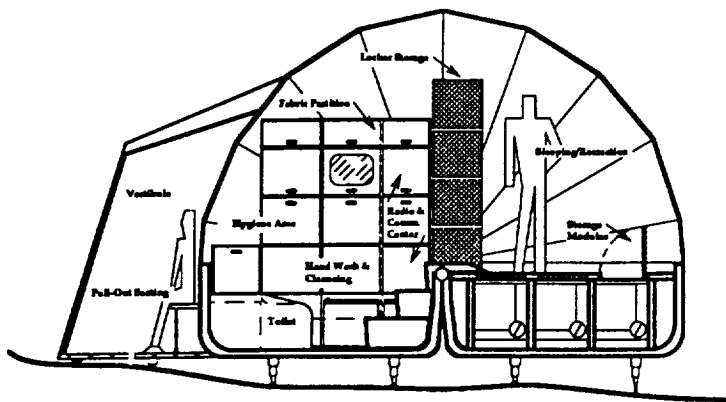


Fig. 4 Section toward hygiene area

PHASR's restricted volume of 931 cubic feet will mandate strict personal hygiene standards for biomedical and psychological reasons. Personal hygiene conditions in PHASR will significantly affect the compatibility achieved between crew members.

The hygiene facility is an important part of a crew's daily schedule. Foremost, this system should be simple, easily maintained, and easily repaired. A variety of waste management systems have been considered. The advantages and disadvantages of storing waste as compared to an incinerator toilet were investigated.

#### Zone 4 - Crew Quarters

The crew quarters are designed to be closed off from the rest of the module if different schedules are desired by the crew members. The sleeping compartment will have a TV, VCR, stereo, and personal storage. The sleeping area also provides vertical lockers from stacking components and storage modules under the floor.

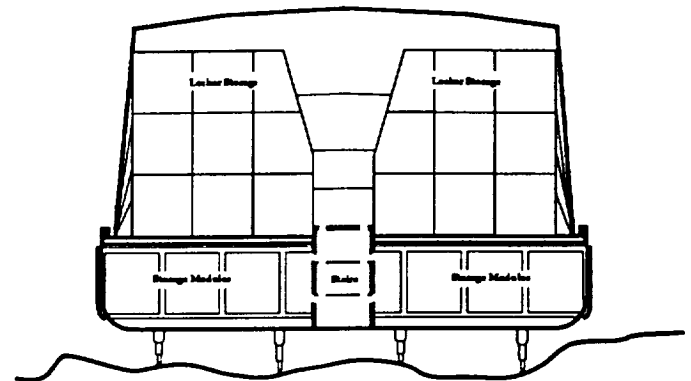


Fig. 5 Section toward crew quarters showing lockers

The requirements for the crew quarters include:

- Sleeping area for four people
- Accommodation for different physical sizes
- Community storage
- Private storage
- Recreation and leisure space
- Dressing/undressing area

The components of the crew quarters area are:

- Storage modules in floor
- Lockers from stacking components
- Cold weather sleeping bags
- Storage for portable TV, VCR, and stereo

#### Transportation

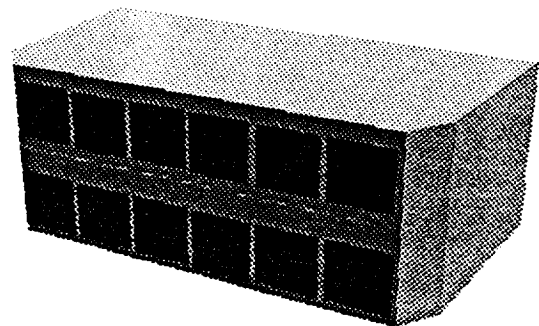


Fig. 6 Packaged PHASR

PHASR folds up into a packing size of 8' X 16' X 6'. It fits onto 1/6 of a standard pallet for the C-130 or C-141 aircraft and weighs under 2500 pounds fully packed.

### Assembly

Under normal conditions, it is estimated that PHASR can be fully deployed from the bare ground, leveled, and its furnishings assembled in 2-3 hours. Furniture modules contain simple slip-fit or drop-in type connectors. Some components are hinged. PHASR is leveled to adapt to a variety of terrain with a system of jacks and shocks. Although PHASR is designed primarily for use in cold weather, a double-layered, light-colored fabric could be used for hot climates. Also, a thick Styrofoam shell that is assembled on-site might be used in conjunction with the proper air conditioning system.

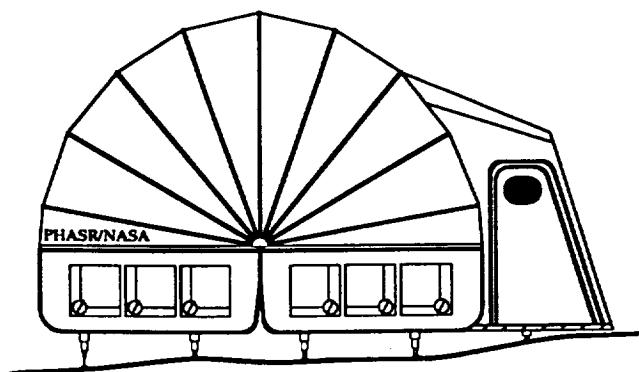


Fig. 7 Elevation of PHASR

### Recovery

PHASR's furniture modules are designed to be disassembled and packed so that PHASR can be closed — much like a suitcase — and airlifted to another location. This allows PHASR to be a reusable habitat, unlike some of the more semi-permanent structures used in the Antarctic today.

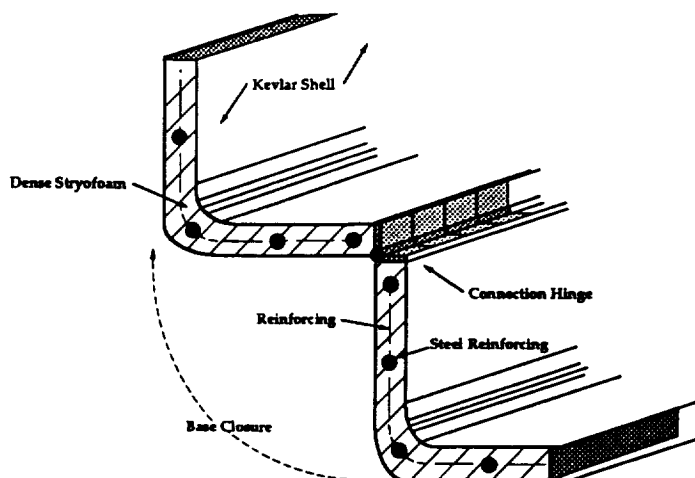


Fig. 8 Cross-section of PHASR structure showing connection hinges

### Environmental Safety

#### Solar Gain

Since PHASR is primarily passively solar heated, it is designed with a minimal use of seams and openings to prevent air infiltration. The dark fabric covering is automatically stretched rigid over the structural supports when PHASR is deployed. This combination, fabric and support ribs, is the tensioning system which forms PHASR's interior volume. The covering system and insulated shell have been designed to give PHASR a solar savings of 80 to 85% using direct gain from the 24-hour Antarctic summer sun. This translates into approximately 4,200 BTU's per day to heat PHASR.

Heat-gain calculations were approximated by using the LCR method. Calculations were made by using a 0.6 factor for infiltration at 20° for tight construction in a 15 mph wind. An absorption rate of 0.82 was used for the dark blue fabric of PHASR. The habitat fabric was calculated as solar glazing with a 4-inch airspace for an insulating property. This yields an R-value of 1.23. The base of the habitat was calculated with the R-value of 45. This is the minimum specified for the dense Styrofoam fill of PHASR's shell. Calculations were done for three

months with an average of 27° (the average temperature in January at US research base McMurdo).

### Power Systems

Power is supplied by a hybrid system of solar photovoltaics and wind generation. The combination of wind and solar power meets our needs of at least 1500 watts in an average 12-15 mph wind at 0° C. Currently specified is a wind system that provides a rated power of 1000 watts with a generated wind speed of 5-7 mph. This particular wind system has a shipping volume of four cubic ft and a weight of 70 lbs. Supplemental power will be provided by photovoltaic arrays. PHASR's solar arrays are 47.25 in X 21.00 in X 1.50 in and provide 70 watts of power.

### Material Specifications

Materials considered for PHASR include Kevlar for the shell of the base with a dense Styrofoam fill. The Styrofoam would be reinforced with a steel alloy.

Initially sought for PHASR was a clear fabric for the outer layer of the tent and a black fabric for the inner layer. This would give the maximum passive heat gain for the interior. However, heat-gain calculations showed that two layers of dark blue fabric would trap enough heat to be sufficient. It is imperative that the fabric specified for PHASR be able to withstand intense ultraviolet light, excessive bending, and extreme cold. Although we have looked extensively at a nylon because of its weight, it would need to be coated to withstand Antarctica's high ultraviolet light. PHASR's structural support system (ribs) are aluminum alloy or graphite. Both are ideal materials because of their weights.

Materials considered for the hard surfaces in the interior need to be nonporous, nonvaporous, lightweight, and easy to maintain. Nylon mesh can be used for many of the shelving units, while a graphite substance would be best for the harder surfaces.

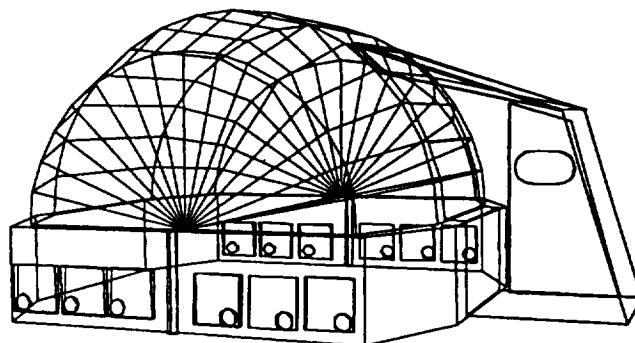


Fig. 10 Wire frame computer model of PHASR

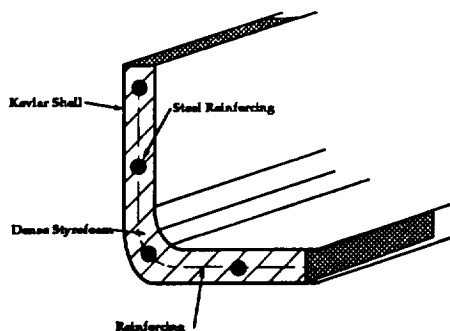


Fig. 9 Cross-section of Kevlar shell

## **LOWEST COST, NEAREST TERM OPTIONS FOR A MANNED MARS MISSION**

**Bob Sauls, Michael Mortensen, Renee Myers, Giovanni  
Guacci, Fred Montes**

### **Abstract**

This study is part of a NASA/USRA Advanced Design Program project executed for the purpose of examining the requirements of a first manned Mars mission. The mission, classified as a split/sprint mission, has been designed for a crew of six with a total manned trip time of one year.

### **Acronyms**

|                 |  |
|-----------------|--|
| ACRV            | Assured Crew Return Vehicle                    |
| ECLSS           | Environmental Control and Life Support Systems |
| EPV             | Emergency Pressure Vessel                      |
| EVA             | Extravehicular Activity                        |
| HLLV            | Heavy Lift Launch Vehicle                      |
| HMF             | Health Maintenance Facility                    |
| LEO             | Low Earth Orbit                                |
| LH <sub>2</sub> | Liquid hydrogen                                |
| LOX             | Liquid oxygen                                  |
| MTV             | Mars Transfer Vehicle                          |
| PV              | Photovoltaic                                   |
| SSME            | Space Shuttle Main Engine                      |
| TEI             | Trans Earth Injection                          |
| TMI             | Trans Mars Injection                           |

### **Program Objectives**

This study is part of a NASA/USRA Advanced Design Program project executed for the purpose of examining the requirements of a first manned Mars mission. The primary requirement is to assure that crew exposure to radiation and zero gravity are minimized. As a study of a first manned mission to Mars, no consideration has been given to in-situ resource utilization.

### **Mission Baseline**

This mission is classified as a split/sprint mission. Cargo and return fuel are sent prior to the launch of the Mars Transfer Vehicle (MTV). The cargo phase of the mission is sent on a low energy conjunction transfer orbit. All systems for the return mission will be verified after its arrival at Mars orbit and prior to the launch of the MTV. Once all systems have been checked out, the MTV will be launched on a high energy one-year flyby trajectory to Mars. On arrival at Mars, the MTV will be inserted into Martian orbit where the transfer vehicle fuel pallet will be exchanged with the cargo vehicle fuel pallet, which will coincide with a twenty-day surface mission. On completion of the surface mission, the lander will rendezvous with the MTV and the two will be sent on a return trajectory to the Earth. On arrival at Earth the MTV will be inserted into Low Earth Orbit (LEO) where the crew will descend to the surface directly via an Apollo-style return vehicle.

### **Requirements**

This mission has been designed for a crew of six with a total manned trip time of one year. Assembly of the return fuel pallet as well as the MTV will be accomplished in LEO. The Energia "B" with a payload capacity of 200 tons per launch and a shroud diameter of 8 m is the HLLV that will be used. Assembly will be conducted at a rate of six launches per year.

### **Assumptions**

It has been assumed for the purpose of this mission that precursor robotic missions have been carried out to determine the specific characteristics of the location on Mars to be explored. Another assumption is the availability of the Energia "B" launch vehicle along with the cooperation of the Russians. It is also assumed that the assembly of the mission elements such as the TEI and TMI fuel pallets as well as the final configuration of the transfer vehicle will take place in LEO. Due to the scale of a project such as this, an assumption has been made that funding would take place from many national and international sources and that NASA participation could be kept to a minimum.

## Vehicle Descriptions

### TMI Fuel Pallet

The TMI fuel pallet is a highly integrated structure consisting of a space frame truss system, eight liquid hydrogen tanks, four liquid oxygen tanks, and a rocket pack with two SSME's. The space frame connects the fuel pallet to the transfer vehicle as well as the SSME rocket pack. Modular LOX and LH<sub>2</sub> tanks, which are 7.62 m in diameter by 10.93 m long, allow for redundant components.

### TEI Fuel Pallet

The TEI fuel pallet is identical in every respect to the TMI fuel pallet with the exception that booster rockets would be incorporated in order to place the fuel pallet on a Mars trajectory and then into a Mars orbit in order to avoid firing the SSME's prior to the TEI burn.

### Transfer Vehicle

The transfer vehicle is comprised of a habitat, cupola, two emergency airlocks, an EPV, and an ACRV. The transfer vehicle is connected to the fuel pallet by a space frame structure.

The habitat is 13.45 m X 4.26 m X 7.62 m and contains two pressure vessels for safety and redundancy. The outer vessel contains all secondary functions, while the inner vessel contains living, sleeping, hygiene, galley, emergency communications, and the HMF. In case of emergency, the mission can be carried out from the inner vessel. Along the top of the habitat are modular logistics packs used to store all perishable items. There are four packs oriented linearly within a framing magazine. The packs are docked one at a time to the top hull of the habitat via a central airlock. As materials are used from within the pack, waste is collected and returned to the pack in order to keep the interior of the habitat clear. When a pack has been completely spent, it is undocked from the hull and moved down one position in the magazine, while the next pack is moved into position and docked. PV arrays are located along the bottom of the habitat and supply power throughout the mission. A radiator, for thermal control, is located on the back of the PV array. A communications dish is also located along the bottom of the habitat.

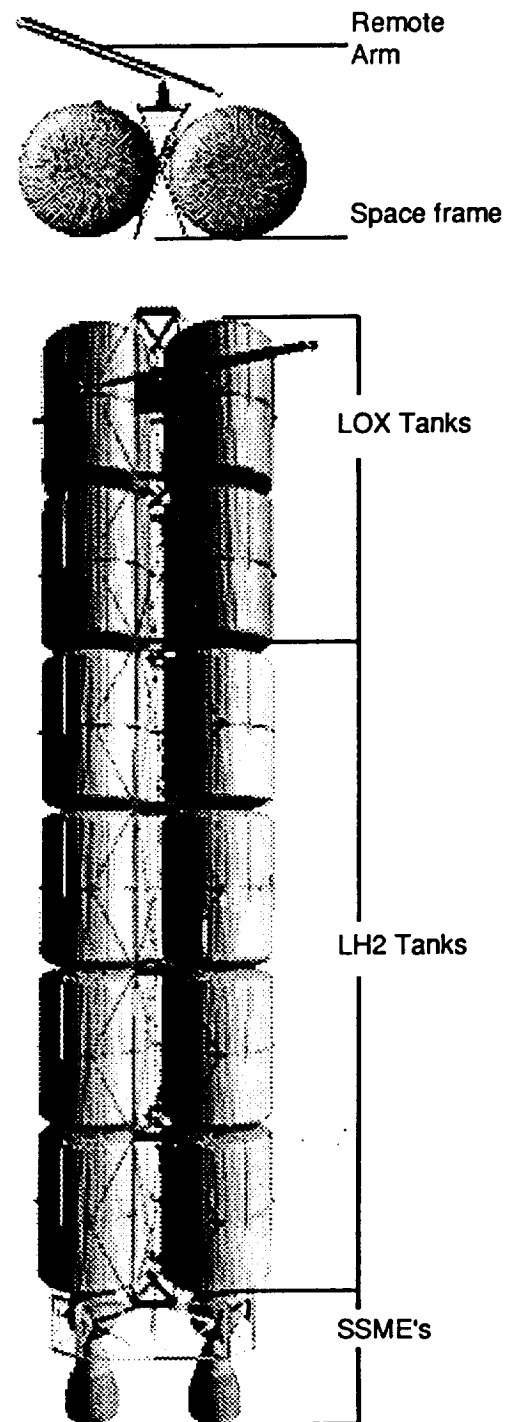


Fig. 11 Typical fuel pallet

A cupola, located centrally between the fuel pallet and the habitat, is used for remote operations as well as for visual inspection of the top half of habitat and logistics packs. The cupola will also be used as a viewing port since it is the only part of the vehicle with windows. The cupola is connected to the habitat by an inflatable tunnel which is connected to an emergency pressure vessel.

An ACRV is located below the EPV opposite the cupola. The ACRV will return the crew directly to Earth at the end of the mission. This vehicle can also be used in the event of an emergency to bring the crew to safety while in LEO.

The EPV is located at the back of the habitat and serves several functions. First, the EPV serves as a storage area for pressure suits and a changing area for donning and doffing the suits. The EPV is also used as an airlock for EVA activity. Finally, the EPV serves to separate the cupola, ACRV, EPV, and habitat into four independent pressure areas. Figures 12 and 13 show the configuration of the transfer vehicle.



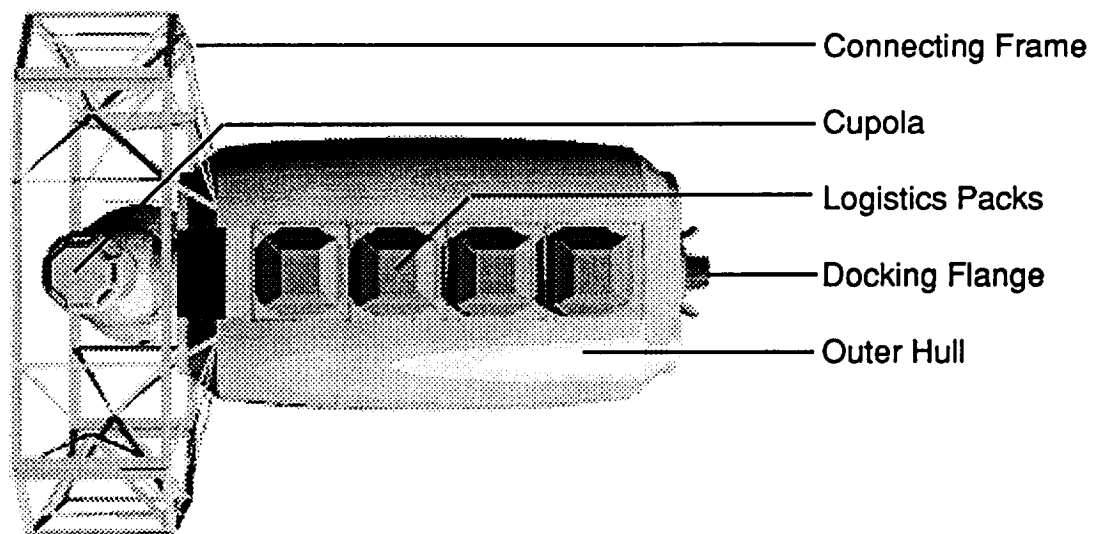


Fig. 12 Transfer vehicle top view

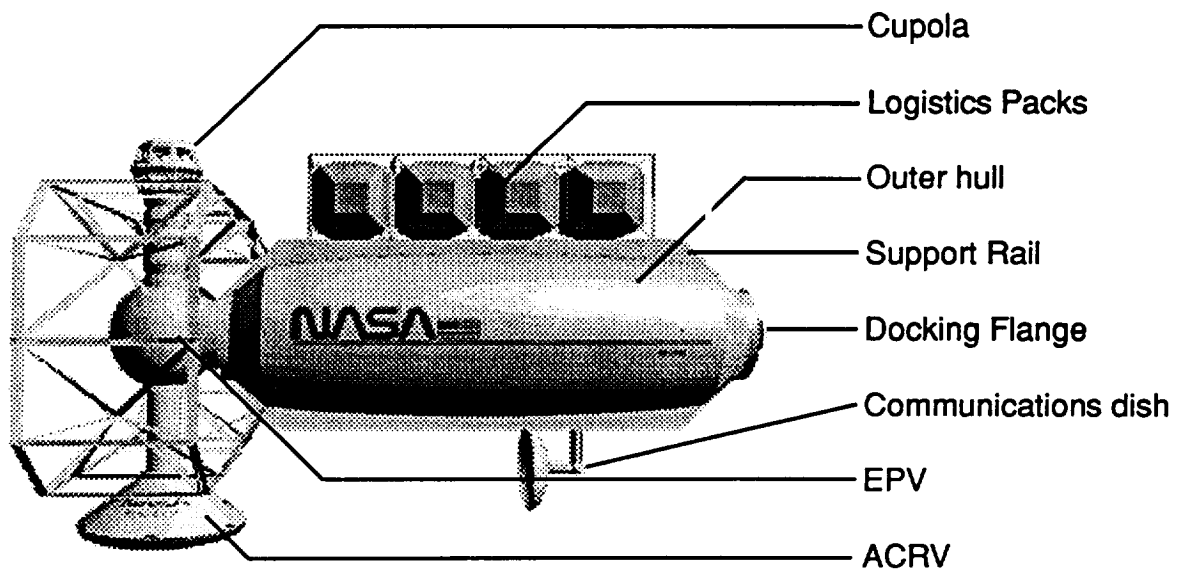


Fig. 13 Transfer vehicle side view

## Mars Lander

The Mars lander is used during the crew's 20-day surface stay. The lander consists of three main sections: a habitat, utility core, and support structure.

The habitat, 3.67 m at the base and 5.2 m in height, contains a command control center, two work stations, hygiene area, galley, and two emergency racks.

The utility core provides storage for the EVA suits as well as a common shaft for all electrical and plumbing between the ECLSS and the lander habitat. There are two means of egress from the utility. The primary means of egress is an inflatable airlock, which is used to increase usable volume during EVA activities. A second airlock is located opposite the inflatable in the utility core. This airlock will be used in emergencies only and requires that the utility core be depressurized, whereas the inflatable airlock does not. Logistics packs are located around the utility core on the exterior and contain supplies for the surface mission as well as storage for collected materials.

The space frame support structure is located below the utility core. This structure houses the ascent tanks for the lander as well as three RL-10 rocket engines. On ascent, the framing members and landing legs are left on the surface. Figures 14 and 15 show the front and side views of the Mars lander.

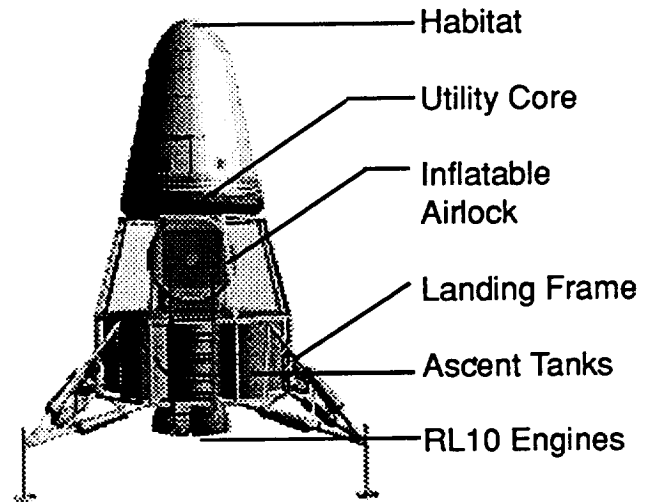


Fig. 14 Lander front view

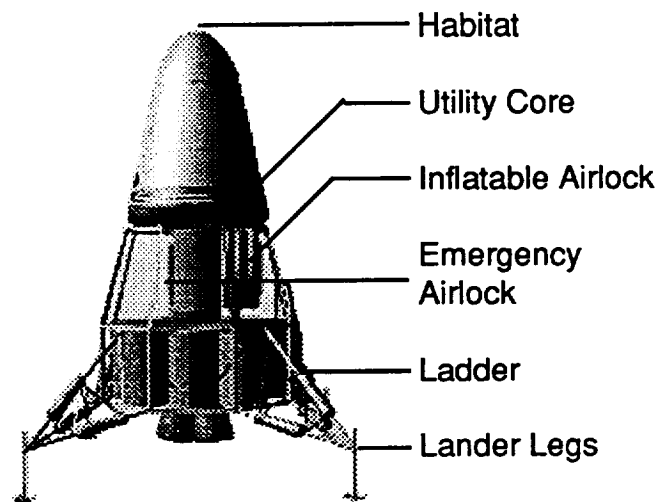


Fig. 15 Lander side view

## Modularity

LOX and LH<sub>2</sub> tanks, logistics packs, and space frame members have been designed with a high degree of modularity. This allows for easy replacement in the event of a malfunction or resupply from mission to mission.

## Cargo Accommodations

All logistics, supplies, and other cargo are located on the exterior of the transfer vehicle and Mars lander. This serves to reduce the chance of contamination between unrelated materials and contamination of sample materials collected on the surface. This will also help to keep unwanted materials from collecting in the vehicles over the one-year mission.

## Propulsion Systems

Cryogenic LOX and LH<sub>2</sub> were chosen because of the high, 475 sec Isp (O<sub>2</sub>/H<sub>2</sub>), practical maximum for cryogenic fuels, and for its reliability as a proven system. Fuel tanks have been sized (roughly) according to the required delta V's for two SSME's for the TMI and TEI stages. For the purpose of this investigation, it has been assumed that the boiloff is "low" and that a method of recycling the boiloff is available.

## Power Systems

Photovoltaics were chosen as the main power supply for the Mars mission. This decision was made due to their availability, high reliability, efficiency, and low level of risk. Unfortunately, the arrays require large amounts of surface area/mass, and are subject to degradation over time. They are also vulnerable to the surrounding solar/environmental conditions. Since the solar intensity on Mars is only about 40% that of LEO, the arrays have to be upscaled accordingly. We hope, however, to minimize these drawbacks by using state-of-the-art photovoltaic technology.

The transfer vehicle will derive most of its power from photovoltaic cells and use fuel cells during occultation while in Mars orbit. The transfer vehicle will require 20 kW: 1.5 kW for the life support systems for each of the six crew members and the balance for other systems and

equipment. Cell degradation is estimated at 5% within the first two years. Tandem photovoltaic cells (manufactured by Boeing and presently undergoing testing) will be used. The solar panels are made up of stacked gallium arsenide (Ga As) and gallium antimonide (Ga Sb) cells, which provide a combined efficiency of 23.5%. The arrays would need to be 150 m<sup>2</sup> in order to supply the MTV with 20 kW at Mars (50 kW at LEO). The array itself would weigh 366 kg, and the weight of the supporting structure would add approximately the same amount of weight. The array would also be laminated with a layer of microglass to prevent damage from radiation and micrometeorites.

The Mars lander will be powered solely by fuel cells. The vehicle will require an estimated 10 kW of power for its 20-day separation: 1.5 kW to cover the life support systems of each of the three crew members and the rest to cover other systems and equipment.

## Thermal Systems

Thermal control for the transfer vehicle is accomplished by a passive system located on the back of the PV array. The back surface of the array is coated with alumina for high emissivity and use as a radiator.

## Environmental Control and Life Support Systems

Life support for this mission is a partially closed loop system in which physical/chemical regeneration occurs and oxygen and water are recycled. Food, however, is not recycled, and waste is collected and stored. This system was chosen for its weight advantages over a purely open system and its compatibility with long-duration missions.

## Mission Sequence

### Trajectories

The TEI (Figure 16) is sent on a low energy conjunction trajectory prior to the launch of the transfer vehicle. The modified one year flyby trajectory of the transfer vehicle during the TMI and the TEI stage after the exchange of the fuel pallets is illustrated in Figure 17.

### Mission Stages

Assembly of the TEI fuel pallet begins with the insertion of the transfer vehicle into LEO. All components of the transfer vehicle are delivered with the first launch. Six additional launches are required to deliver the twelve fuel tanks of the TEI fuel pallet. These tanks are put into orbit and assembled over the course of approximately one year. On completion of the TEI fuel pallet, all systems are confirmed and the fuel pallet is sent on a low energy conjunction trajectory, which will take 270 days to reach Mars.

Next, seven additional launches are required to deliver the twelve fuel tanks of the TMI fuel pallet and the Mars lander. This assembly also requires approximately one year.

After the arrival of the TEI fuel pallet at Mars and the confirmation that "all systems are go," the transfer vehicle with the lander will be launched on a high energy 80-day trajectory to Mars. Near Mars the remaining fuel in the TMI fuel pallet will be used in order to establish an elliptical orbit around Mars.

Once in orbit around Mars, the lander will undock from the transfer vehicle and descend to the surface where its three crew members will conduct a 20-day mission on the surface. While the lander is on the surface, the three remaining crew aboard the transfer vehicle will maneuver the transfer vehicle in order to exchange the TMI fuel pallet with the TEI fuel pallet.

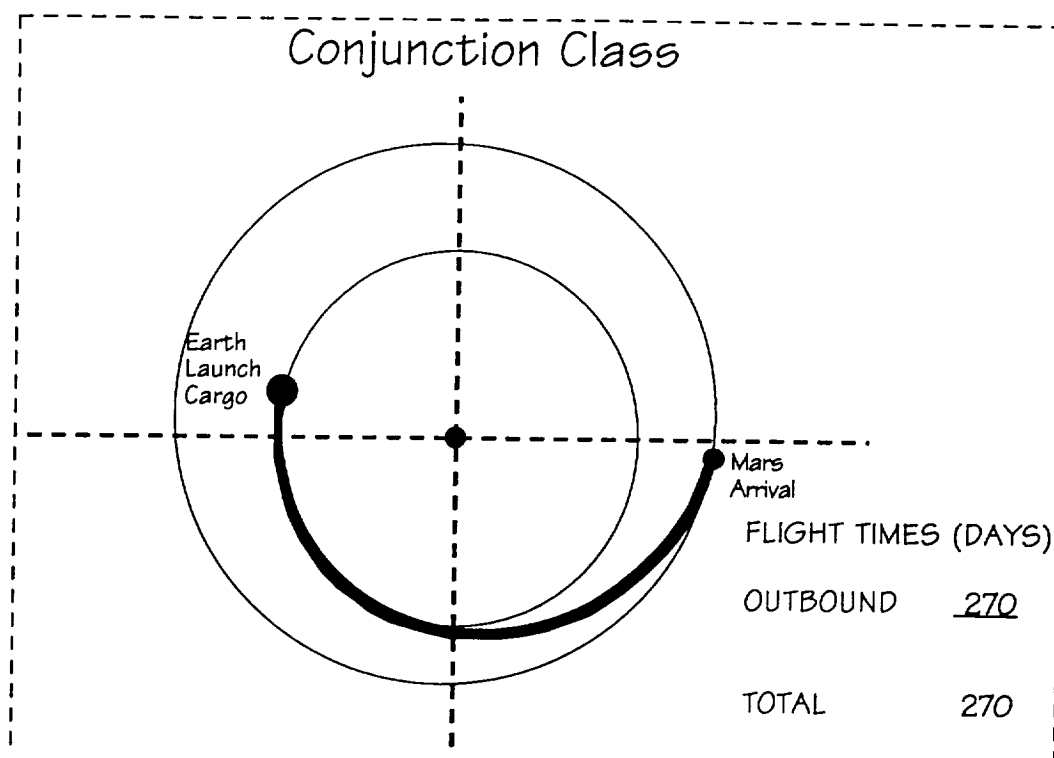


Fig. 16 Cargo trajectory

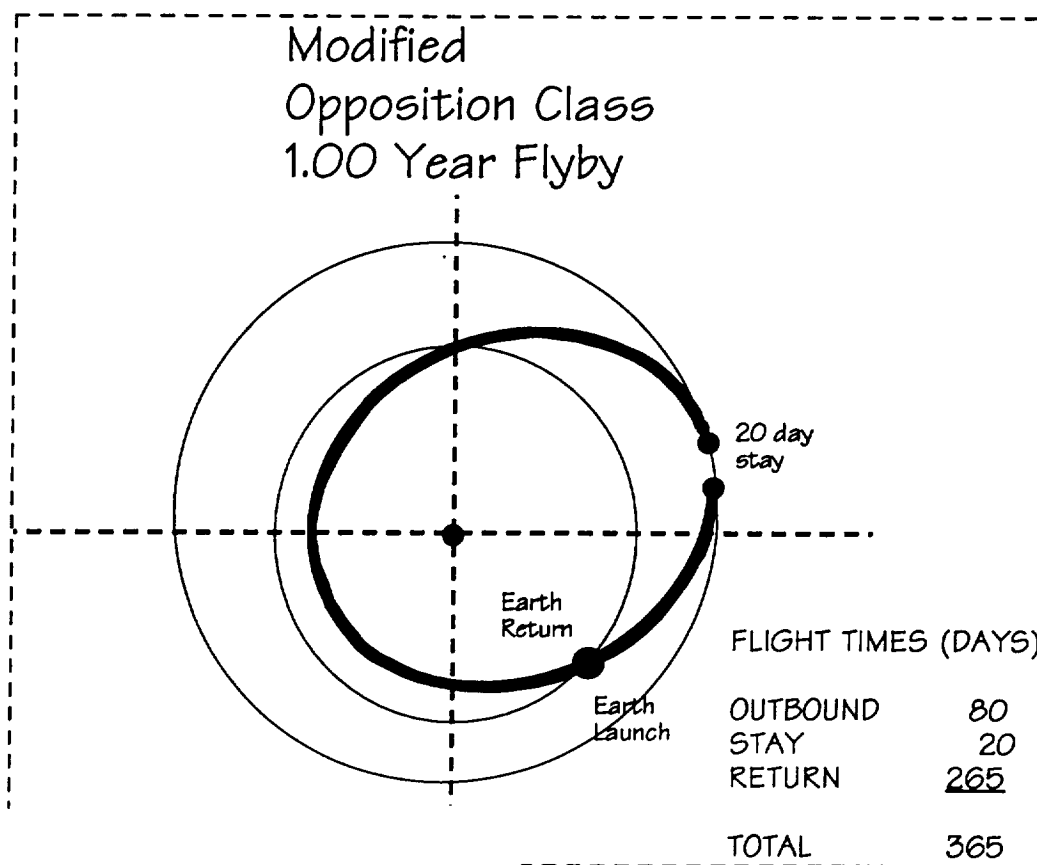


Fig. 17 Transfer vehicle trajectory

With the conclusion of the surface mission and the successful exchange of the fuel pallets, the lander ascends to Mars orbit and docks with the transfer vehicle.

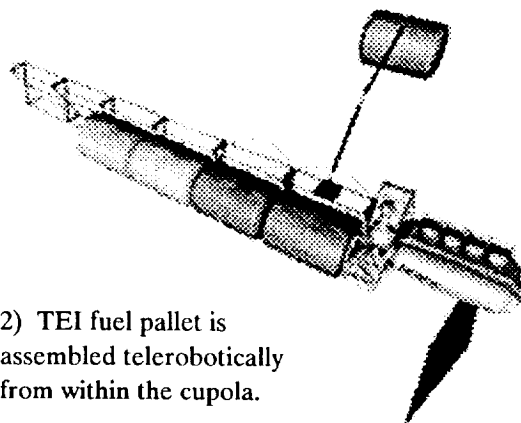
Next, the transfer vehicle with the lander attached makes the TEI burn and begins the 265-day trip back to the Earth where it will reestablish LEO. With the mission complete, the crew will descend to the surface in the ACRV.

A subsequent shuttle mission will be required in order to retrieve the lander and any other items needed for examination. Figure 18 shows the mission sequence in storyboard format.

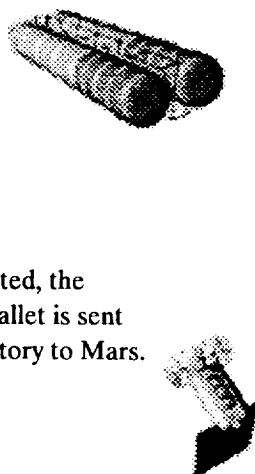
1) Components are delivered to LEO.



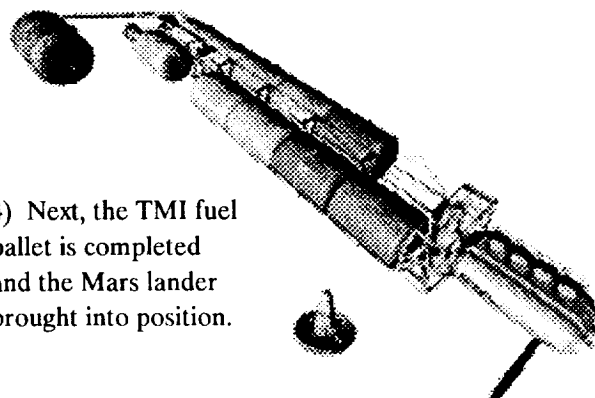
2) TEI fuel pallet is assembled telerobotically from within the cupola.



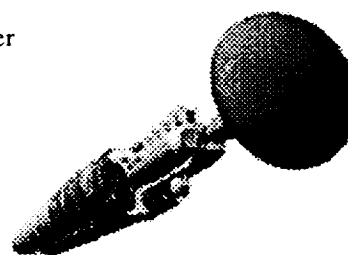
3) Completed, the TEI fuel pallet is sent on a trajectory to Mars.



4) Next, the TMI fuel pallet is completed and the Mars lander brought into position.



6) The transfer vehicle with lander is sent on a high energy trajectory to Mars.



5) The Mars lander is docked.

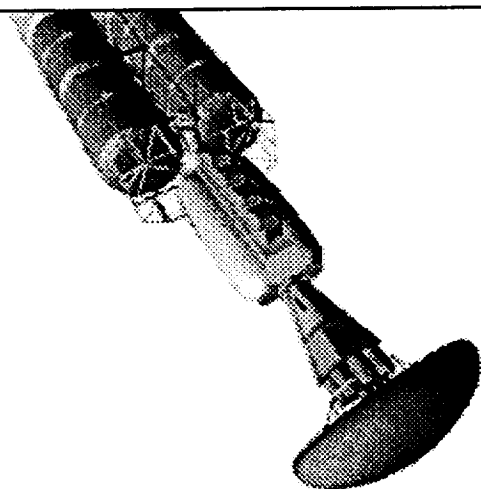
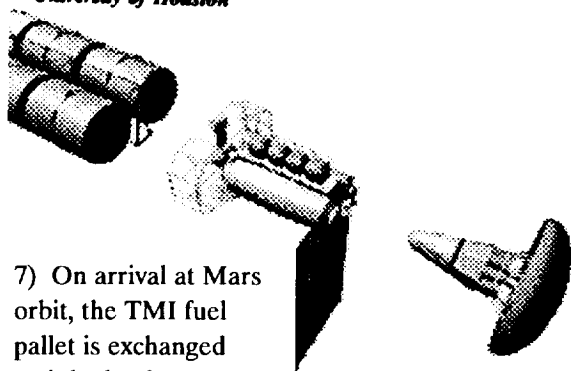
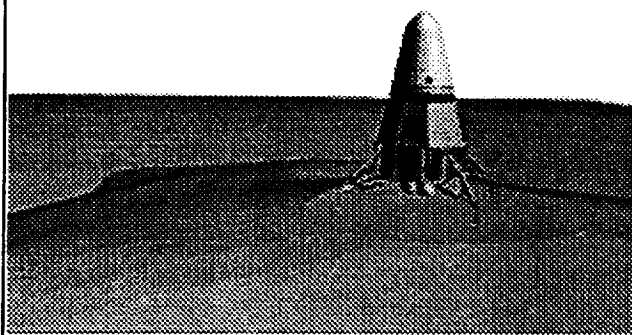


Fig. 18 Mission storyboard

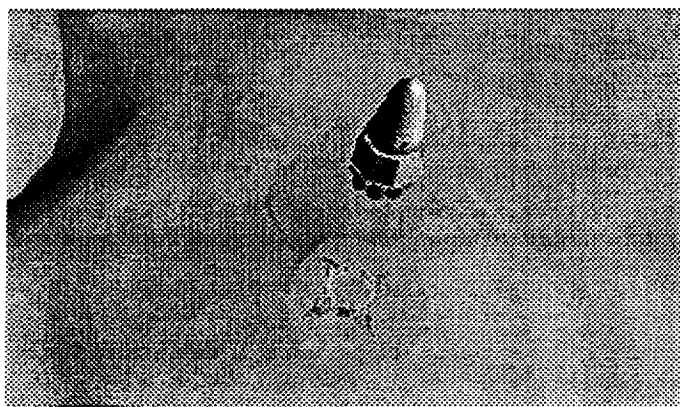
7) On arrival at Mars orbit, the TMI fuel pallet is exchanged and the lander descends to the surface.



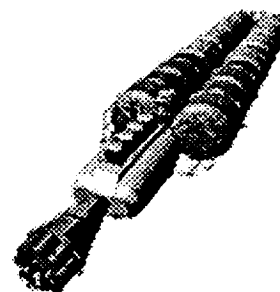
8) On the surface, the crew conducts a 20-day surface stay.



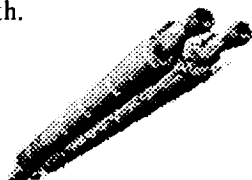
9) The lander returns to the transfer vehicle, leaving its landing frame behind.



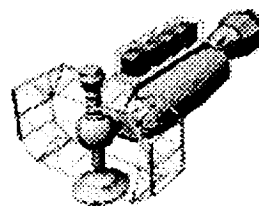
10) The lander docks with completed transfer vehicle.



11) The transfer vehicle with lander begins the 265-day journey back to Earth.



12) At Earth the transfer vehicle and lander are injected into LEO.



13) The crew returns to Earth in the ACRV.

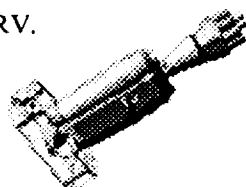


Fig. 18 Mission storyboard (continued)

## PLANETARY SURFACE EXPLORATION MESUR/AUTONOMOUS LUNAR ROVER

University of Idaho  
Department of Mechanical Engineering  
Moscow, Idaho

Associate Professor Larry Stauffer  
Matt DiLorenzo, Teaching Assistant

Dave Austin, Raymond Ayers, David Burton, Joe Gaylord, Jim Kennedy, Richard Laux,  
Dale Lentz, Preston Nance, Pete Peterson, Bob Picker, Sean Stack, Kurt Vanausdela

### Abstract

Planetary surface exploration micro-rovers for collecting data about the Moon and Mars have been designed by the Department of Mechanical Engineering at the University of Idaho. The goal of both projects was to design a rover concept that best satisfied the project objectives for NASA/Ames. A second goal was to facilitate student learning about the process of design. The first micro-rover is a deployment mechanism for the Mars Environmental SURvey (MESUR) Alpha Particle/Proton/X-ray instrument (APX). The system is to be launched with the 16 MESUR landers around the turn of the century. A Tubular Deployment System and a spiked-legged walker have been developed to deploy the APX from the lander to the Martian Surface. While on Mars, the walker is designed to take the APX to rocks to obtain elemental composition data of the surface. The second micro-rover is an autonomous, roving vehicle to transport a sensor package over the surface of the moon. The vehicle must negotiate the lunar terrain for a minimum of one year by surviving impacts and withstanding the environmental extremes. The rover is a reliable track-driven unit that operates regardless of orientation that NASA can use for future lunar exploratory missions. This report includes a detailed description of the designs and the methods and procedures which the University of Idaho design teams followed to arrive at the final designs.

### Introduction

For the 1991-92 school year, the NASA groups of the University of Idaho (U of I) capstone senior design

course were assigned to work on the development of micro-rovers for planetary surface exploration. The work for both semesters was done for the Universities Space Research Association (USRA) and the Intelligent Mechanisms Group at NASA/Ames Research Center (ARC), Moffet Field, CA. There was a different project with different customer requirements each semester, which led to two different types of micro-rovers accomplishing their particular tasks. Fall semester students worked on a rover for deployment of an instrument to collect data about the surface of Mars, while the Spring semester students developed a rover for exploration of the moon's surface. This paper gives a complete description of both projects including the development of prototypes for each.

## MESUR

### Project Description/Background

The U of I Fall Mechanical Engineering senior design team was requested on August 27, 1991 to design a deployment system for the instrumentation devices for NASA's MESUR (Mars Environmental SURvey) project. The purpose of the MESUR mission is to emplace a globally-distributed set of 16 landers on the Martian surface to make both short- and long-term observations of the atmosphere and surface. The MESUR concept was developed as a relatively low-cost, near-term approach to a Mars Network mission which would serve some of the objectives of the Mars science and Mission from Planet Earth. A mission of this sort will enable achievement of two general classes of scientific objectives that can not be met by any other means.<sup>1</sup> The first class



is a group of objectives that require the simultaneous operation of a number of globally-distributed surface stations. The primary examples are a global seismic network and a global network of meteorological stations. The second class is a group of objectives that require sampling of a large number of globally-distributed sites. Examples include geochemical sampling, high-resolution surface imaging, and measurement of the atmospheric structure along entry profiles. Particular emphasis would be placed on hard-to-reach sites (polar deposits, rugged volcano flanks, etc.) that would be difficult or impossible to investigate by other means.

To meet these objectives Ames Research Center has developed a system of landers that will contain the following instrumentation:<sup>1</sup>

- Atmospheric Structure Experiment
  - Accelerometers + pressure/temperature measurements
- Descent and Surface Imagers, e.g. CCD Array
  - Descent: black and white imaging
  - Surface: multi-band imaging
- Meteorology Package
  - Atmospheric pressure
  - Atmospheric opacity
  - Temperature, winds
  - Humidity (if possible)
- Elemental Composition Instrument
  - Alpha particle/proton/X-ray spectrometer
- 3-Axis Seismometer
- Thermal-Analyzer/Evolved Gas Analyzer

After discussing the MESUR project with Chris Leidic, our NASA representative for this project, the design team decided to focus its efforts on the elemental composition instrument - the Alpha Particle/Proton/X-ray Spectrometer (APX). Therefore, the design objective was to develop a system to deploy and transport the APX from the MESUR lander and obtain chemical analysis of rock samples on the Martian surface.

### Customer Requirements

To develop this system, the U of I design team considered several different designs for accomplishing the required functions of the APX deployment system.

The design parameters extracted from the MESUR documentation and NASA contacts for the APX deployment system are listed below.<sup>1,2</sup>

- Minimal mass
 

To make space travel economical, all payloads should be as light as possible. The MESUR project focuses on mass savings to justify its economical feasibility.
- Minimal size
 

Each of the lander ports is the approximate size of a cylinder 0.25 M high and 0.20 M in diameter. The entire APX deployment system needs to be designed to accommodate this port size.
- Simple design
 

The communication time delay from Earth to Mars is 40 minutes. For this reason, the APX deployment system should be simple to operate. Movements should be easy to initiate and control.
- Reliable design
 

The MESUR project will be ongoing for 10 years, and it is essential that all instrumentation perform during this period.
- Interior rock samples
 

The rocks on the Martian surface are believed to have a thin outer crust. This crust is simply atmospheric dust that has accumulated over time. Therefore, the outer crust needs to be removed before the APX can be placed on the surface.
- Multiple samples (if possible)
 

The main purpose of the MESUR project is to gather as much data on Mars as cheaply as possible. Taking multiple samples of rock specimens in the immediate vicinity of each lander with the same APX deployment system would definitely enable a much larger spectrum of data to be obtained without the need for additional equipment and costs.
- Low power usage
 

Each lander will be equipped with a Radioisotope Thermoelectric Generator (RTG) supplying 15 Watts (W) of power. The RTG supplies power to all equipment on the lander. The APX deployment system must operate on the least amount of power possible in order to ensure the power supplied by the RTG is adequate.
- Resistance to the Martian atmosphere and space travel
 

The Martian atmosphere has temperature extremes from -160° C to 35° C. Many fine dust particles are

also believed to be dispersed in the Martian atmosphere. The APX deployment system must withstand not only the temperature extremes, but also the wear and failure problems that result from the introduction of dust particles.

- **Impact resistance characteristics**

Upon landing on the Martian surface, the lander will hit with an impact that is equivalent to 40 times the static load. Impact stresses may also be introduced when the APX deployment system actually exits the lander and is placed (or possibly dropped) onto the Martian surface.

- **Orientation independent**

The landers do not experience precise and controlled landings. Rather, the landers are expected to land in any position (horizontal, vertical, upside down, etc.). The APX deployment system must then be able to perform regardless of how the lander is oriented.

### **Concept Development**

#### **Functional Decomposition**

The APX deployment system was designed using Quality Functional Deployment (QFD) methods of design. Using the above requirements from the customer, the functions that needed to be accomplished were developed. The three major functions of the design are as follows:

- Delivery of the system inside the lander from Earth to the Martian surface.
- Deployment of the system from the MESUR lander to the Martian surface.
- Location and obtainment of multiple rock samples on the Martian Surface.

Each of these functions was broken down into smaller detailed subfunctions whose requirements could be considered individually.

#### **Morphology/Concepts/Evaluation**

A morphology study was performed to establish a means of accomplishing these functions. In combining the components, four concepts were developed: a ribbon arm (remains attached to the lander and unrolls itself like a tape measurer), a folding arm, a spike-legged

walker, and a tank-style rover. These were then compared using weighted characteristics and a plus, minus, and zero scale to determine the best concept, using the tank as an arbitrary datum. It was determined that the spiked-legged walker concept fit the requirements best.

### **Detailed Design**

From this analysis, the final design concept is the APX Deployment System, which has two major components: the Tubular Deployment System (TDS), to hold the instrument in transit and remove it from the lander, and the APX Walker, to move the instrument to a sample, prepare the sample, and collect the data. These two components will interface with the existing landers which are currently being designed by Ames Research Center.

#### **Tubular Deployment System**

This system is designed to secure the APX Walker inside the MESUR lander during transit from Earth to the Martian surface. It interfaces directly with the existing lander design by fitting into one of the allocated instrumentation ports that are located around the lander's circumference. The major requirement of the design is the ability of the system to deploy the APX Walker from either side of the lander since the lander is expected to tumble upon contact with the surface of Mars.

The final design solution is the Tubular Deployment System (TDS) as shown with the APX Walker in Figure 1. The TDS consists of three concentric tubes that enclose the APX Walker and extend out of the lander in a telescoping fashion. The innermost tube holds the APX Walker during travel to Mars and has 140° of material cut out to allow the walker to escape onto the surface. The middle tube is cut out 130° for the same reason. The inner and middle tubes are guided by runners to allow them to move up and down in a straight path. The tubes and runners are constructed of rigid PVC and are connected together with a solvent adhesive compatible with PVC. The inner tube is capped at both ends with thin (0.5 mm) aluminum disks. These disks are attached to the tube with rivets through tabs and epoxy on the mating surfaces. There is also a similar cap

on the bottom of the middle tube, connected in the same manner as the inner tube caps.

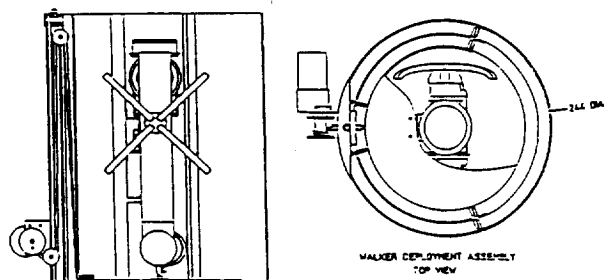


Fig. 1 Tubular Deployment System with APX Walker

The outer and middle tubes are connected together at the top (top being the end at which the APX Walker head is located) using a flange and pyrotechnic fastener system. The inner and middle tubes are connected together with a pyrotechnic fastener located in a hole drilled in the lower inner tube cap and the middle tube cap. In both cases, a spacer made of silicon rubber separates the connected components and provides vibration damping.

Vertical motion is provided through the use of an electric motor, nylon cable, and pulley system. The cable is connected to the bottom cap of the inner tube using a compression clamp mounted to the inside surface. The cable is then threaded through the pulley located at the top of the middle tube, through the pulley on the outer tube, and finally through the hole on the take-up spool. The take-up spool is press-fit and then held by a set-screw on the shaft of a 1-RPM reversible DC motor that supplies the motion. The advantage of using a motor, cable and pulley system is that once the APX Walker is on the surface, the motor can be reversed, lowering the TDS back into the port, therefore eliminating the chance of blocking the surface imaging camera's view.

Once the lander reaches the Martian surface, the operators of the MESUR lander determine which side of the lander is not in contact with the surface. They will then put a current to the appropriate pyrotechnic fastener that, upon releasing, will allow either the inner

tube or the inner and middle tubes to raise out of the lander, thus deploying the APX Walker to the correct side. The actual release of the APX Walker is accomplished through the use of another pyrotechnic fastener connected to an internal support assembly. The internal support assembly consists of a section of rectangular aluminum tubing, locating pin, and mounting flange connected between the caps of the inner tube.

### APX Walker System

This system consist of three separate subassemblies: the Body Structure Assembly, APX/Grinder Assembly, and the Tether Assembly. These subassemblies together perform the following functions: adjust orientation, move to the sample, prepare the sample surface, position the APX onto the sample surface, and transmit data collected to the lander. The APX Walker was designed symmetrically to allow the walker to function right side up or upside down. The overall mass of the walker is 1.01 kg and the center of gravity is located 86 mm from the rear of the walker.

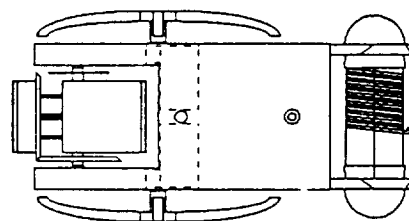


Fig. 2 Top view of APX Walker Assembly

As shown in the figure, the APX/Grinder Assembly is positioned in the front of the walker, and the electric drive motors (phantom lines in Figure 2) are positioned behind the APX/Grinder Assembly. The Tether Assembly is located in the rear of the Walker. The side and front views of the APX Walker are shown with the TDS Assembly in Figure 1.

The walking motion of the APX Walker is provided by two rotating spindles. Each spindle has four elliptical legs which are press-fit into the spindle. The spindles

are connected to the electric motor's drive shafts using a small set screw. The legs are produced from 7-mm square rod which is bent into an elliptical shape to allow the Walker to flip over more easily if it topples onto its side.

The overall physical characteristics of the APX Walker are listed in the table below.

Table 1 Physical characteristics of APX Walker

|  |  |
|--|--|
| Height<br>(with legs)<br>(without legs)              | 160 mm<br>60 mm                              |
| Length   | 255 mm                                       |
| Width<br>(with legs)<br>(without legs)               | 144 mm<br>100 mm                             |
| Approximate mass                                     | 1.01 kg                                      |
| Center of gravity<br>(measured from the rear)        | 86 mm  |
| Volume displacement<br>(with legs)<br>(without legs) | 5875 cm <sup>3</sup><br>1530 cm <sup>3</sup> |

The APX Walker has the following operational characteristics:

Table 2 Operational characteristics of APX Walker

|  |                      |
|--|----------------------|
| Power requirements<br>(including grinder and drive motors) | 2.5 Watts            |
| Maximum speed  | 0.3 m/min            |
| Turning radius   | 80 mm                |
| Operating range  | approx. 4 m diameter |
| Vertical clearance   | 58 mm                |

The values listed above are obtained from combining the three subassemblies of the APX Walker. A physical and operational description of each subassembly is provided in the following sections.

### Body Structure Assembly

The backbone of the APX Walker is the Body Structure Assembly which is shown in Figure 3. This assembly consists of eight separate parts that are joined together with aluminum braze.

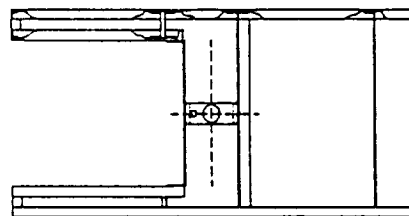


Fig 3 Body Assembly

The function of the Body Assembly is to provide interfaces for the three APX components: the APX/Grinder Assembly, the Tether Assembly, and the electric drive motors for the walker. Besides providing the interfaces to each of these components, the Body Assembly has the function of interfacing with the Tubular Deployment System (TDS).

The body assembly is simple in construction with all the parts made from 2024 T4 Aluminum alloy. This lightweight alloy gives the APX Walker the strength required to hold the three components in the walker and to absorb the impacts it will experience. This material also has reasonable machining characteristics that are needed in forming these parts.

### APX/Grinder Assembly

The functions that the APX/Grinder Assembly must be able to perform are detailed and listed below:

- Prepare surface

The brine/crust on the outer surface of the samples needs to be removed so accurate sampling can be achieved.

- **Position APX**

After the surface is prepared, the APX must be positioned onto the prepared surface. This must be performed accurately to ensure precise sampling.

- **Hold APX against surface during sampling**

The APX must be held securely against the surface of the sample until the sampling is completed.

The design concepts of the APX/Grinder Assembly began to develop during the Function Morphology portion of the QFD design method. First, a method of preparing the surface was selected. A disk grinder was chosen for this task for several reasons. A grinder seemed to be the simplest tool for removing the brine (as compared to a belt-driven sander, pneumatic chisel, drill and catch tray, or circular saw). Secondly, the base of the APX is circular, and a disk grinder would remove the brine in a circular area; thus the APX could rest firmly on the surface of the prepared sample. Lastly, the power requirements could be kept low if grinding pressure were kept to a minimum. Therefore, a high RPM, low torque electric motor would be used to power the grinder.

The design team then decided that positioning could be done most feasibly by placing the APX and grinder faces 180° apart and rotating the whole subassembly to switch their positions. The rotation method would keep the width to minimum and could be readily accommodated in the APX Walker design.

Additional concepts were developed:

- To keep simple and minimize power requirements and mass, the APX/Grinder Assembly should be able to rotate without requiring another electric motor in addition to the grinder motor.
- The rotation should be controlled so that the assembly will not rotate the APX and the grinder while the grinder is in use.
- Grinding and sampling need to be accomplished from a variety of positions and angles.
- Slight, but constant, pressure should be kept while grinding the sample surface.
- The rotation mechanism should be bi-directional to resist twisting.
- The controls should be integrated with the walker control panel and the lander's imaging system.

The side and front views of the APX/Grinder design are shown in Figure 4 (the top view is in the APX Walker Assembly, Figure 2).

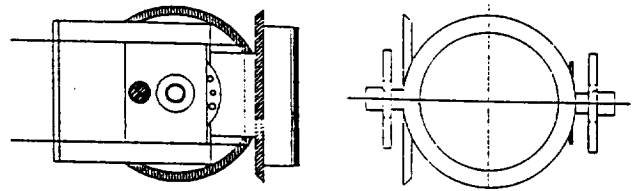


Fig 4 APX/Grinder Assembly

The APX/Grinder Assembly contains the following components: one grinder disk, two beveled gears, two solenoids, one APX/Motor cage, and one indexed positioning disk. The grinder disk is made of synthetic sapphire to ensure long-lasting capability to grind a very smooth surface. One beveled gear is coupled to the backside of the grinder, while the other is located on the axle (around which the entire assembly rotates). One solenoid engages the side-beveled gear when flipping the grinder and APX, and the other solenoid holds the entire assembly at the desired angle from horizontal. The APX and grinder motor are mounted inside a cage for protection. The positioning disk is located on the axle opposite the beveled gear and has indexed holes so the positioning solenoid can be used to hold the assembly at the desired angle from horizontal.

### **Tether Assembly**

Since the MESUR project encompasses seven to nine years, the Tether Assembly was chosen to supply power to the electrical motors because batteries aren't possible and a separate RTG would be too massive to place inside the walker. The power for the drive motors, grinder motor, and solenoids is supplied to the walker by a 4-meter tether connected to the lander's RTG. Inside the tether spool are the electrical brushes which distribute the power supply to the electrical components.

Since the tether is used only to supply power to the walker, the data from the APX is transmitted back to the lander using radio waves. To make the tether idea feasible for the walker, it had to perform the five following functions: supply power for the APX Walker drive motors, grinder motor, and solenoids; enable the tether to be unrolled or rolled from the spool without being wrapped up in the APX Walker's legs; allow the tether to operate when the walker is upside down or right side up while moving either forward or reverse; assist the walker in sliding side-to-side on the Martian surface during turns; and enable the APX Walker to have an operating range of two meters from the lander.

The tether assembly (shown in Figure 5) has four major parts that include the spool, wheels, worm gear mechanism, and the gears that connect the other three parts. Since it has only four major parts, the tether is simple and reliable. The assembly's mass is 0.34 kg. This amount of mass ensures the wheels and spool remain in contact with surface while the walker is moving.

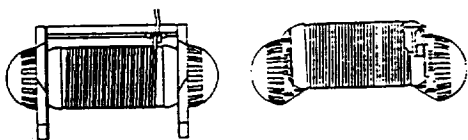


Fig. 5 Tether Assembly

When the Tether Assembly is connected to the APX Walker, it functions in the following manner:

- The spool is used as a wheel when the Walker is right side up. In this configuration, the tether simply rolls out as the APX Walker moves forward, and rolls up while it moves backwards.
- The wheels are used when the APX Walker is inverted. These wheels, directly coupled to the spool, cause the tether to roll in and out. Only two gears are

necessary to facilitate this action; one connected to the spool and the other connected to the wheels.

- As the spool or wheels rotate, a worm gear mechanism (like those found on fishing reels) guides the tether so that it will not bind up and get tangled on the spool or in the walker legs.
- The spool ends, wheels, and the back end of the APX Walker are rounded so the walker can turn around on the Martian surface.

### Discussion

While developing the APX Deployment System, the University of Idaho Design Team built and tested a walker prototype. This prototype was very similar in overall dimensions, mass, and operation to the final APX Walker design. Constructing and testing this prototype allowed the design group to make some observations concerning the operation and manufacturing of the APX Walker.

If the desired range of the APX Walker is increased greatly, changes will need to be made in the imaging system which locates samples. Currently, the camera positioned on the lander is expected to perform all required imaging functions. If its range is increased, the walker might be unable to use the lander's imaging system, requiring one of its own.

Since the parameters of the lander are not set, the APX Walker and TDS can be readily scaled up or down if modifications to the lander or port sizes deem it necessary. The dimensions of the APX/Grinder can also be scaled to account for any changes in the dimensions of the APX.

Due to its simplicity and precision, the control system can be readily integrated with a computer control center. This system could incorporate software that would enable the user to input a vector pattern, thereby automating the APX Walker movements. This would save operating time because the operator would no longer have to wait for the time delay between each input.

## Conclusions

The systems designed by the University of Idaho Design Team will satisfy the required functions and parameters that were essential to the MESUR project. The design team has made the following conclusions based on calculations concerning the final design, and by building and testing the prototype walker.

- The APX Walker mass is within the limits of the design criteria (1.01 kg). The aluminum construction of the walker provided sufficient rigidity and support for internal components; however further reduction in the walker mass could be accomplished by using less dense materials and alloys.
- The prototype was easily controlled using simple 12 V power sources. Upgrading the electrical components of the walker for use with the lander's RTG power source (15 V) would require little effort and provide the same simple operating characteristics.
- Costing approximately \$900, the APX Deployment System is an economically feasible alternative for the MESUR project.
- The prototype's maneuverability was impressive. Having a short turning radius and slow speed, the walker prototype maneuvered easily around and over obstacles.
- The prototype's APX/Grinder Assembly also displayed the ability to sample at various locations, heights, and sample surface angles.
- The Tether Assembly on the prototype performed well and the tether did not tangle with the walker legs; however, power was not supplied to the prototype using the brushes inside the spool.
- The walker legs on the prototype were 7-mm circular rod, and the walker experienced slipping during operation. Therefore, in the final design the legs are constructed of 7-mm square rod. This will help alleviate the traction problem by increasing the area in contact with the surface.
- Several samples can be obtained at each landing site increasing the value of the MESUR mission.

## AUTONOMOUS LUNAR ROVER

### Planet Surface Exploration

NASA is developing an automated planetary exploration system to search for minerals on distant planets. The system involves deploying many autonomous vehicles to search the surface of a planet randomly for extended periods of time. The small, simple vehicles will wander around transporting a sensor package, searching for specific substances such as water or minerals. Once the sensor package detects the substance, it marks the location and reports back to the command base.

For this project, these autonomous roving vehicles will move about the surface of the moon for over a year. During this time, many of the vehicles may become stranded, stuck, disabled, etc. But the idea is that, if the substance exists, at least one of the several rovers should encounter the substance during its period of operation.

This lunar exploration project will provide NASA two major benefits. The first benefit is the collection of data about the lunar surface. Each rover's sensor package can be programmed to search for a specific element or compound, allowing for a wide-range search. These data will help broaden our understanding of the formation of the planets and moons of our solar system. The second benefit is an operational test of the exploratory technology which can be applied on future planetary exploration missions.

### Project Description/Background

USRA, in conjunction with NASA, assigned the Spring senior design class NASA group the task of designing an autonomous roving sensor platform capable of transporting a payload across the lunar surface and constructing a working prototype. The payload, consisting of the sensor package and the power system, will be provided by another contractor. Since the payload has yet to be defined, its specifications will be assumed for design purposes.

The rover will require a rechargeable or regenerative power supply in order to cover as much terrain as possible during its one-year life span. The

communications requirements will be limited due to mass and power constraints, but the vehicle should relay its position to other vehicles and/or a base station to be relayed back to Earth. The vehicles should be capable of limited cooperative behavior so that they do not duplicate effort.

### Project Objectives

The project objectives include creating a vehicle that is autonomous in the sense that: (1) it does not require any contact with humans; (2) it does not require remote directional or intelligent control; (3) it can avoid obstacles; and (4) it can negotiate the lunar terrain for approximately one year. The vehicle must be durable enough to withstand a tumble down a crater and mobile enough to traverse rugged terrain. The navigation and obstacle avoidance mechanisms should be reliable and compact. It is understood that a certain percentage of the rovers may not find what they are searching for, may malfunction, or may be disabled before the mission is complete. In order to increase the chances of a successful mission, several of the units must be deployed at one time. The vehicles must be lightweight and inexpensive so that a large number of rovers can be transported and deployed in a single trip to the moon.

### Problem Statement

The customers need a reliable, autonomous vehicle to transport a NASA sensor package across the lunar surface for a minimum of one year as part of their space exploration program. The vehicle should be as small and lightweight as possible while still possessing the ability to transport its cargo and negotiate the lunar terrain. The vehicle must be capable of continuous operation in the lunar environment. After being placed on the surface of the moon, the vehicle must operate independent of human intervention. This type of vehicle is also needed to test the reliability of the design for possible application on other planets.

### Research on Tracks vs. Wheels

For the first half of the semester, two groups worked separately on the project. The groups then combined at midterm with two similar but different concepts. At this

point, our customer suggested that the newly formed group reevaluate both concepts with set criteria to determine the better design. This reevaluation of the designs centered around the fundamental difference between the two concepts, to have a wheeled rover or one with tracks.

The reevaluation of the concept started with a literary search. This search revealed Dr. M.G. Bekker's research, which was an intricate part of the lunar roving vehicle design team for the Apollo program; Bekker is considered an expert in his field. In his book Introduction To Terrain Vehicle Systems, Dr. Bekker states:

"A few years ago, I was engrossed with proving that in lunar surface locomotion, the wheel cannot be challenged by exotic solutions. It soon became clear, however, that conventional forms - particularly of small vehicles - may be unacceptable and this led me to a methodical search for new vehicular forms and elements."<sup>3</sup>

Though this statement does not include a proof of any sort, Bekker may have answered the entire reevaluation process with it.

Bekker<sup>3</sup> demonstrates a method to calculate the tractive force for both wheeled and track vehicles. The tractive force is the force the track or wheel exerts on the ground and is dependent on soil conditions,  $c$  and  $\phi$ , soil cohesion factor and shearing angle, respectively. This tractive force results in thrust for the vehicle; therefore, the larger the tractive force is, the larger the vehicle thrust will be. The equations to calculate the tractive force are as follows:<sup>3</sup>

$$T_n = 4A_{wc} + W \tan(\phi) \text{ (for the wheeled vehicle)}$$

$$H_n = 2A_{tc} + W \tan(\phi) \text{ (for the track vehicle)}$$

Where  $T_n$  is the tractive force for the wheeled unit and  $H_n$  is the tractive force for the track unit. For both equations  $W$  is the weight of the vehicle,  $c$  is the soil cohesion factor and  $\phi$  is the shearing angle of the soil.  $A_w$  is the contact area for a rigid wheel and  $A_t$  is the contact area for the track.



Figure 6 shows a comparison between two vehicles of equal weight (approximately equal to the engineering requirement for this project) on the same soil, one with rigid wheels and the other with tracks. It shows that a track system will create a larger tractive force in all soils except when the cohesion is zero ( $c = 0$ ). This larger tractive force is due to the greater contact area the track has over the wheel. When the cohesion is zero ( $c = 0$ ), the tractive effort for both systems is equal to  $(W \tan(\phi))$ . Note, both equations are soil dependent and exact soil cohesion factor for the moon is not on record; therefore, parametric studies for a range of cohesion factors and shearing angles were conducted to verify the conclusion that the track will create a larger tractive force and, consequently, a larger vehicle thrust. The track concept results in larger tractive force and vehicle thrust than the wheel concept. The reevaluation of the design concept and the results of these calculations resulted in the selection of the track over the wheel.

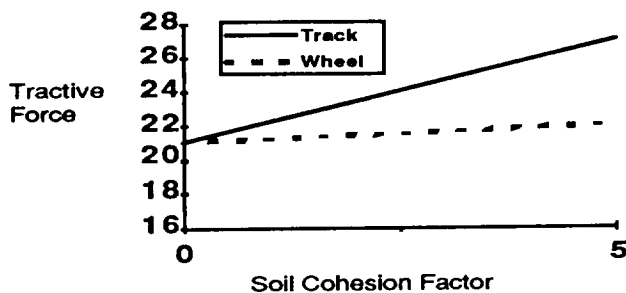


Fig. 6 Tractive force vs. soil cohesion factor<sup>3</sup>

### Design Specifications

Customer desires for the rover and their priority of importance include:

- Able to transport sensor package
- Durable
- One-year life span
- Lightweight
- Able to withstand lunar conditions
- Small
- No maintenance
- Ease of manufacture

- Inexpensive
- Few moving parts

### Engineering Requirements

- Mass less than 20 lb<sub>m</sub>
- Volume less than 1.0 ft<sup>3</sup>
- Withstand temperature range -157° C to +121° C
- Operate at gravity equal to 5.32 ft/s<sup>2</sup>
- Operate at pressure 10<sup>-13</sup> times that of Earth
- Withstand a 30-ft freefall onto an unyielding surface on the moon.

### Specifications

This list contains the "musts" and "wants" for the rover design project.

#### Must:

- transport sensor package/power supply
- have a mechanical lifetime of one year (minimum)
- survive a 30-ft fall onto a non-yielding surface on the moon
- negotiate terrain (avoid obstacles, climb, descend, etc.)
- successfully operate in the lunar environment
- require no maintenance or human interaction
- be capable of deployment by a single person

#### Want:

- smaller than 1.0 ft<sup>3</sup>, 20 lb<sub>m</sub> (w/o sensor package/power supply)
- minimum number of moving parts
- solar energy collection capability
- low cost

#### Not responsible for:

- the black box/sensor package (electronics with power supply)
- signal transmission (assumed to be with black box)
- packaging for transport
- deployment

### Concept Development

An important step in the lunar roving vehicle design process was the functional decomposition. The functions

of the rover can be broken into seven groups: locomotion, traction, sensor support, sensor protection, self-righting ability, obstacle sensing ability, and obstacle negotiation. Once the functions of the rover had been decomposed into smaller subfunctions, the next step was to determine methods for performing each individual function. This step, commonly referred to as the morphological study, involved some minor research and brainstorming for possible methods. In considering design concepts, the group determined and weighted characteristics that were significant in selecting options from the morphology to perform functions. These characteristics fell into four basic groups: physical characteristics, design simplicity, survivability, and mechanical reliability.

Once the characteristics were determined, they were weighted in the order of importance. The evaluation of the morphological study on these weighted characteristics led to four concepts: a legged vehicle, a tank vehicle, a four-wheel vehicle, and a two-wheel vehicle.

To evaluate the best concept, another set of characteristics was determined and weighted. A majority of the characteristics used in the concept building were used in the evaluation as well. The weighted characteristics formed the design matrix. This design matrix showed that the best designs are the tank and the four-wheel units. These two negotiate the terrain better and have a higher mechanical reliability than the other two. A comparison between these two led to the choice of the tank vehicle as the final concept for the Lunar rover.

### **Detailed Design**

#### **Overall Concept Description**

The lunar rover was designed to be lightweight, compact, and durable. The design incorporates a composite body aluminum/foam sandwich structure and an external chain and sprocket drive mechanism. The rover's overall weight without the sensor package is 16 lb<sub>m</sub>. The symmetric design allows the vehicle to operate on either side with a ground clearance of 1.50 in. Hemispheres, which are constructed of a carbon-reinforced epoxy composite material, are attached to the

outer surfaces of the sprockets to prevent the rover from balancing on its side.

The rover platform will be able to support and protect the sensor package which performs the search functions on the lunar surface. The design concept avoids obstacles by climbing over, going around, or reversing and turning away from them. A tank-track-style locomotion system was incorporated to decrease ground pressure, which improves ground clearance, and to increase traction surface area. The tracks consist of two roller cable chains that are joined by cross members. These cross members will be made of small aluminum channel stock and be attached to the chain so that the channel faces out for traction purposes. A tensioning system will be used to apply the proper tension to the tracks at manufacture, due to the construction of the tracks they should not stretch under most situations.

The outer surface is made of polished and anodized aluminum and will reflect more radiation than it absorbs. This will reduce the amount of heat transferred to the internal mechanisms and electronics of the rover.

Figure 7 shows the final design concept of the tank-track style autonomous lunar rover (without control system and sections of track cut away).

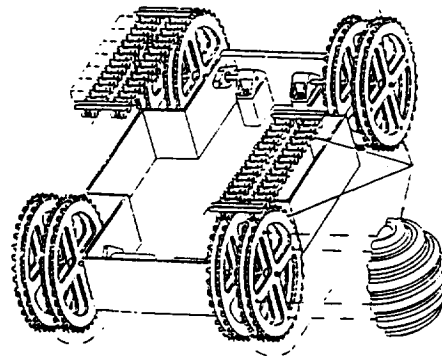


**Fig. 7** Tank-track-style autonomous lunar rover (without control system and sections of track cut away)

## Structural frame and body

The body of the rover acts as an external frame and all of the components are mounted directly onto it. The body is made of composite plates. The composite structural plates consist of a foam core sandwiched between two thin aluminum sheets. The aluminum sheets are bonded to the foam core with epoxy resin. The foam core that we have specified is Divinycell HT 110 with a density of  $7.0 \text{ lb/ft}^3$ . The system of plates also allows for easier construction of the rover. The joints between the plate pieces are sealed and bolted for strength and to protect the internal parts of the rover from the lunar environment. The body is built up from the bottom plate to the top. The internal components mount directly to the bottom plate and then the side plates are added. The top plate adds rigidity to the body package.

## Control System

The control system design serves two functions in controlling the rover. The first feature enables the rover to operate symmetrically, such that it has no top or bottom, only a front and a rear. The controller senses the orientation of the rover and switches the polarity of the drive motors to maintain a forward direction. For example, if the rover were initially traveling forward and somehow became inverted, the motors would reverse direction, and the rover would continue going forward.

The second feature allows the rover to avoid obstacles. The system senses when the rover encounters resistance traveling forward, then guides the rover back and away in another direction. The assumption here is that the rover went forward into an obstacle and backing away would remove the rover from the problem. Since the forward direction is no longer a safe or valid path, the controller turns the rover to the left by some set angle and proceeds forward again on a new path.

## Drive Train and Tracks

The rover is driven by an external track system consisting of two separate tracks. The two tracks run independently of one another, which allows the vehicle to turn when the tracks rotate at different velocities. Each track is driven and guided by sprocket sets in the front and rear of the vehicle. The sprocket sets rotate on

shafts which are in fixed positions coming out of the vehicle's body. Only the rear sprocket sets are driven by the vehicle's motors, while the front sprocket sets are idle and act as tensioning guides. The rear shafts are directly driven by the motors, eliminating gear trains where frictional losses could occur. The vehicle is designed so that, regardless of which side is up, the rear sprockets are always driving the tracks. This allows the part of the tracks in contact with the ground to be in tension which optimizes their performance.

The sprockets are made of aluminum and have 36 teeth with a pitch diameter of 5.73". Each sprocket has a hub with a set screw and a key for connecting it to the shaft. Because the track consists of two chains running parallel to one another, there are two of these sprockets on each shaft. These sprockets must be lined up so that corresponding teeth are in the same angular position in order for the track to run smoothly. Each track consists of two roller-cable chains which are connected by cross pieces acting as the traction. The advantage to this type of a chain is that the links are not in sliding contact with one another and require no lubrication. Each roller link consists of a stainless steel pin capped with molded Teflon rollers that are centered on the cable. The cable itself is made of braided stainless steel  $1/16$ " in diameter. Aluminum brackets are included on the roller links, and act as mounting plates for the cross members. The cross members are aluminum U-channel stock and are mounted on every other bracket with the open channel facing out from the track.

The front shafts specified in the design are made of ground 303 Stainless Steel and are  $0.375$ " in diameter. Calculations were made to find stresses in the shafts under static and impact loading situations. The two front shafts and the two motor shafts pass through wall-mounted bearing assemblies, which are positioned on the inner side walls of the body. These assemblies consist of exterior bearing mounting plates with internal bronze bushings. The front shafts are also internally supported by pillow block assemblies, in addition to the wall-mounted bearings. The two pillow block assemblies sit on top of supports which align them with the shaft centerline. These supports are mounted to the lower plates of the vehicle's body in the same fashion as the motor mounts. The pillow block assemblies consist of a support block, which also contains bronze bushings.

## Conclusions

### Prototype Performance

On the rover's initial run, it climbed a grass hill at a slope of about 40°. The mercury switch circuit successfully reversed both motors when the rover flipped over. The rover climbed up a steeper slope on a loose dirt surface, and later ran down some concrete steps. Basically, the prototype could climb steep inclines on various surfaces, withstand minor impacts, and continue functioning properly when flipped over.

### Recommendations

Our main recommendation is to have further consulting and more extensive testing performed on the control circuit. It may be better to use a mechanical rather than a mercury switch due to the extremes of the lunar environment. More extensive research should be performed in order to confirm that our specified materials will survive the environmental extremes. A material likely exists that could be used for a one-piece, continuous, flexible track similar to that used on the prototype. If this material is located, it would greatly simplify the current two-chain track design. Also, an active tensioning system should be designed for the tracks. This would allow the tracks to be automatically adjusted to a set tension whenever they expanded or contracted due to temperature changes or were stretched due to extended use. Further work should be done on the heat transfer problem to determine a way to cool the rover. If the internal temperatures experienced in the rover could be lowered, the reliability of the components would increase.

### Summation

Using the Quality Function Deployment method of design, the senior design class from each semester developed a small micro-rover based on separate customer requirements. The first semester's project for the MESUR mission provided a simple, lightweight, and reliable machine that accomplished the customer requirement of obtaining a rock sample from the Martian surface. It can also obtain multiple samples at each site. This feature adds a great value to the

MESUR mission with minimal costs. The second semester's Autonomous Lunar Rover is capable of reliably transporting a sensor across the surface of the moon to gather important information. The development of prototypes of these designs showed the successful achievement of these goals.

### References

1. Ames Research Center, MESUR Mars Environmental SURvey. Ames Research Center, Moffet Field, California: July 1991.
2. Leidic, C., Ames Research Center Phone Conference, October 1991.
3. Bekker, M. G. Introduction to Terrain-Vehicle Systems, University of Michigan Press, 1969.
4. Bekker, M. G. Theory of Land Locomotion: The Mechanics of Vehicle Mobility, University of Michigan Press, 1956.
5. Comer, David J. Digital Logic and State Machine Design, 2nd Ed., Saunders College Publishing, 1990.
6. Cooper, Henry Jr. Apollo on the Moon, Dial: New York, 1969.
7. Goetzl, Claus G., Rittenhouse, John B. Space Materials Handbook, Lockheed Missile and Space Company, Addison-Wesley, 1965.
8. Johnson, Curtis D. Process Control Instrumentation Technology, 3rd Ed., John Wiley and Sons, 1988.
9. Kopal, Zdenek. Physics and Astronomy of the Moon, 2nd Ed., Academic Press: New York and London, 1971.
10. Lynn, Douglas, "EE 344: Digital Circuit Lab," University of Idaho, 1991.
11. Moon, The. Encyclopedia Americana, International Edition, Vol. 19, Grolier Inc., Danbury, CT, 1991.

## **AUTOMATION OF CLOSED ENVIRONMENTS IN SPACE FOR HUMAN COMFORT AND SAFETY**

**Kansas State University  
Department of Mechanical Engineering  
Manhattan, Kansas**

**Professor Allen C. Cogley  
Nathan P. Tucker, Teaching Assistant**

### **Abstract**

For prolonged missions into space and colonization outside the Earth's atmosphere, development of Environmental Control and Life Support Systems (ECLSS) are essential to provide astronauts with habitable environments. The Kansas State University Advanced Design Team have researched and designed a control system for an ECLSS like that on Space Station Freedom. The following milestones have been accomplished:

- Completed computer simulation of the CO<sub>2</sub> Removal Assembly.
- Created a set of rules for the expert control system of the CO<sub>2</sub> Removal Assembly.
- Created a classical controls system for the CO<sub>2</sub> Removal Assembly.
- Established a means of communication between the mathematical model and the two controls systems.
- Analyzed the dynamic response of the simulation and compared the two methods of control.

### **Introduction**

#### **Design Team Description**

The Advanced Design Team at Kansas State University is composed of students from several academic disciplines. Currently participating

disciplines include Computer Science, Mechanical engineering, and Chemical Engineering. The team's graduate Teaching Assistant is an electrical engineer. Faculty support comes from the Mechanical, Electrical, Chemical, and Computer Engineering Departments as well as the Computer Science Department.

### **Physical System**

The Carbon Dioxide Removal Assembly, designed to remove carbon dioxide from the cabin air, involves removal of CO<sub>2</sub> by molecular sieves. The process is required to remove carbon dioxide generated by the respiratory processes of the astronauts and to maintain acceptable levels of carbon dioxide within the cabin.

Figure 1 is a block diagram representation of the CO<sub>2</sub> Removal Assembly. The system takes input air from the Temperature Humidity Control Subsystem (1), and valves (2,11) direct the air flow, allowing it to flow across one of the desiccant beds (3,10), which dehumidify the air using zeolite 13X and silica gel. The moisture must be removed to avoid poisoning the desiccant found in the adsorbing sorbent bed (8,14). Because the dry air is heated in the process, it is forced across a heat exchanger (6) by a blower (5), and the air is cooled before being sent through a sorbent bed. The sorbent beds remove the carbon dioxide by means of zeolite 5A, which acts as a molecular sieve adsorbing the carbon dioxide. The dry air returning from the molecular sieves through unidirectional control valves (13,9) is revitalized by the moist desiccant of the second desiccant

bed (10). After the air is rehydrated it is then returned to the Temperature and Humidity Control Subsystem (12) and redistributed throughout the cabin.

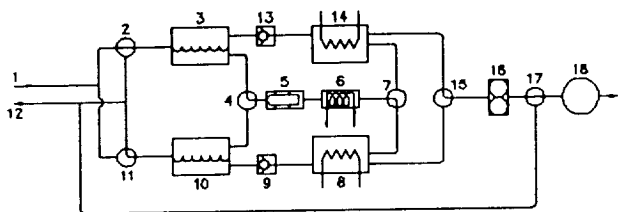


Fig. 1 CO<sub>2</sub> removal assembly

Concurrently, a second desorbing sorbent bed (14) is being heated, causing the separation of the carbon dioxide from the desiccant. The desorbed carbon dioxide is drawn from the bed by means of a pump (16) and is sent to an accumulator tank (18). After the adsorbing desiccants have become saturated, the desorbing beds are once again dry. The control valves (5,7,15) redirect air flow in the system. The previously adsorbing beds begin the desorbing process and the previously desorbing beds begin adsorbing. The system is presently configured to cycle every thirty minutes.

Mathematical models of the various components were created to allow analysis of the subassembly's performance. The role of the modeling is to duplicate the actual system's response to a given set of parameters. Knowing how an actual system should respond, it is possible to explore control systems for use in governing the subassembly. The control systems regulate the state variables throughout the subassembly.

### Controls

#### Description

The CO<sub>2</sub> removal subassembly is responsible for maintaining the partial pressure of CO<sub>2</sub>

within normal limits as the astronauts and other equipment and experiments produce it. NASA grades air quality by the partial pressure of CO<sub>2</sub>, with normal CO<sub>2</sub> pressure being 0.0667 kPa. When the CO<sub>2</sub> partial pressure is above 0.4 kPa, the air is classified as "degraded;" above 1.015 kPa the condition is classified as "emergency." The CO<sub>2</sub> removal subassembly removes CO<sub>2</sub> from the cabin environment and stores it as a gas in a CO<sub>2</sub> accumulator tank until a Bosch reactor breaks it down to solid carbon and water.

The CO<sub>2</sub> removal subassembly uses a variable speed fan to force air through the system's beds, ducts, and heat-exchangers. The desiccant beds and the CO<sub>2</sub> sorbent beds operate on 30-minute cycles, where one bed adsorbs mass for 30 minutes while the companion bed is desorbing. After 30 minutes the beds reverse roles and the full adsorbing bed desorbs its mass, while the empty desorbing bed adsorbs mass.

### Classical Controls

There are two inputs that control the operation of the CO<sub>2</sub> removal subassembly, the partial pressure of CO<sub>2</sub> in the cabin and the pressure of CO<sub>2</sub> in the CO<sub>2</sub> accumulator tank. The cabin CO<sub>2</sub> pressure input is used as input to a classical control to maintain the cabin CO<sub>2</sub> pressure. If the partial pressure of CO<sub>2</sub> in the cabin deviates from the desired 0.0667 kPa, the system would modify the air flow rate.

The input from the CO<sub>2</sub> accumulator tank was based on the gas pressure in the tank. The Bosch reactor is an important producer of fresh water and a shortage of CO<sub>2</sub> may mean a corresponding shortage of fresh water. The Bosch reactor shuts down if the pressure of the supply CO<sub>2</sub> (the CO<sub>2</sub> tank) dips below 101.125 kPa, so the system is turned on if the pressure in the CO<sub>2</sub> accumulator tank drops below 137 kPa. This safety buffer of 36 kPa assures that the tank pressure should not go below the lower limit of 101.125 kPa.

Internal to the CO<sub>2</sub> removal subassembly are controls that maintain the pressure of the CO<sub>2</sub>

accumulator tank and a valve that is positioned before the CO<sub>2</sub> accumulator tank and after the CO<sub>2</sub> pump that controls the purity of the CO<sub>2</sub> entering the tank.

The cabin air is driven through the system by a variable speed, zero-inertia fan that is controlled to maintain cabin pressure of 0.0667 kPa. Classical control of the fan speed is accomplished by using a proportional-integral-differential (PID) compensator in a negative feedback loop. The PID compensator uses an error function  $\delta$ , defined as the difference between the actual CO<sub>2</sub> cabin pressure and the desired cabin pressure. The magnitude of the change in the pump speed is given in the following equation.

$$\Delta \text{fanspeed} = \delta + \frac{d\delta}{dt} + \int \delta dt \quad (1)$$

The fan speed is then adjusted by this amount, increasing or decreasing the tank pressure.

### Expert Systems Control

The expert system uses triangular functions to control the simulation. A triangular function consists of three values: low, medium, and high, as shown in Figure 2.

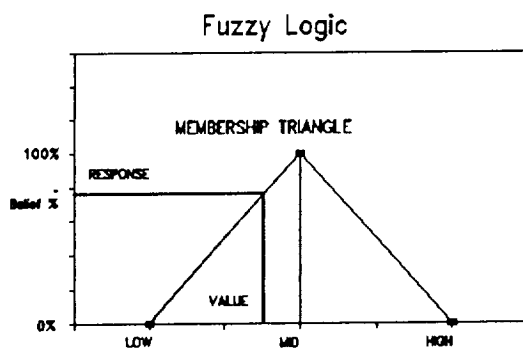


Fig. 2 Fuzzy logic membership triangle

A function is used to calculate a percentage belief when the value being considered is in the range low to high. When the value does not lie in

the range low to high, the percentage belief is zero.

The percentage belief is used to determine directly the amount of change that must be made. This expert system uses two triangles to control the simulation. The left triangle represents the low pressure function. The right triangle represents the high pressure function. There is also overlap between the high and low triangles. This is not uncommon in fuzzy logic. The intersection point of the two triangles is chosen to correspond to the target control value and to a 50% belief in both triangles. This is done so that when the system variable deviates from the target value, the belief is immediately greater than 50% in one of the triangles, prompting the system to try to correct it. The slope of both triangles is adjusted to control the rate at which the expert system changes the simulation. Pump speed, pump duration, and pressure deviation are factors used in determining the adjustments to the triangular functions. The pressure can be controlled more accurately when the pump speed is changed more often. However, this can cause wear on a pump and must be taken into consideration.

### Dynamic System Simulation

#### Introduction

The simulation with controls needed to be tested thoroughly. This would result in two benefits. First, it would be possible to determine if the physics of the CO<sub>2</sub> removal process were being correctly modelled. Second, it would allow an insight into the abilities of both the system and the controllers to handle various situations. The method used to evaluate the control systems was to determine which "weighting factor" provided the most desired response. The major characteristic sought in the solution was the ability of the controller to dampen out initial transients and settle upon a closely bound mass flow rate and, therefore, CO<sub>2</sub> rate. This resulted in the system being run at a nearly constant rate,

which greatly reduces wear on the fan due to cycling.

Although many tests were run, the test condition used for the evaluation of the controllers was a simple twin step function with an initial offset. It was desired to maintain cabin CO<sub>2</sub> at 0.0667 kPa throughout the test. The initial value in the cabin was set at 0.07 kPa. The CO<sub>2</sub> production rate was initially given as  $1.7 \times 10^{-5}$  kg/sec, indicative of resting astronauts. At four hours into the simulation, this value was increased to  $7.0 \times 10^{-5}$  kg/sec, a number representing a double-sized crew performing hard work. Finally, at eight hours the level was decreased to  $3.0 \times 10^{-5}$  kg/sec a level appropriate for the standard four-man crew performing typical functions.

### Classical Control Results

The classic, or PID, controller was designed around the corrective algorithm that follows.

$$\dot{m} = \dot{m} + \left( \frac{\delta}{k1} + \frac{d\delta}{k2} + \frac{\int \delta dt}{k3} \right) \quad (2)$$

where  $\dot{m}$  refers to the mass flow rate through the blower. In its initial form the values of  $k1$ ,  $k2$ , and  $k3$  were all equal to unity. This resulted in two major effects. First, the controller was able to vary the flow rate quickly resulting in the controller's exhibiting a very high frequency. Second, the influence of the derivative term was very small. Figure 3 shows this controller's response to the test conditions detailed in the preceding paragraph. The partial pressure of CO<sub>2</sub> in the cabin corresponds to the top curve and is scaled along the right-hand axis. The mass flow rate through the system is the bottom curve, and is scaled along the left-hand axis.

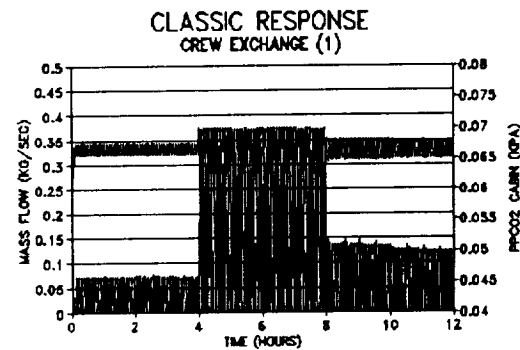


Fig. 3 System response with weighting (1,1,1)

This figure obviously has little if any dampening evident; therefore, this initial set of constants scored poorly on the scale of desirability. This led to the need to increase the impact of the derivative term and to lower the frequency of the controller as the original constants lead to value searching at unrealistic rates.

For a second try, the values of  $k1$  and  $k3$  were increased to 10. This would result in a slower frequency due to the controller changing the mass flow at a slower rate and a better dampened system as the relative impact of the derivative term would be increased. The results of this controller when subjected to a similar test are shown in Figure 4. This controller was able to achieve an appreciable amount of dampening during the four to eight hour interval corresponding to the highest CO<sub>2</sub> production rate. However, at other times it was unable to achieve dampening, and so this set of weighing factors did not represent a satisfactory solution.



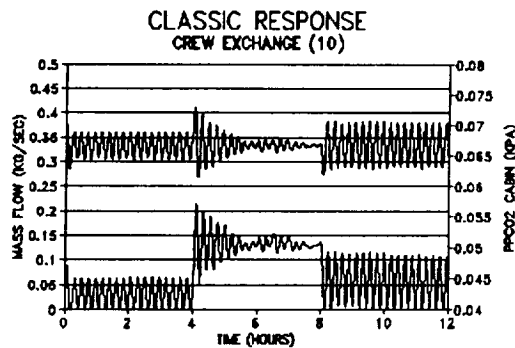


Fig. 4 System response with weighting (.1,1,1)

There is no reason that the values of  $k_1$  and  $k_3$  had to be left equal to each other. Since the system was well-behaved and smooth, it was not necessary to incorporate a large integral term. This fact allows us to assign a very large value to  $k_3$  and, in essence, to reduce the PID controller to a nearly PD controller. By reducing the input from the integral term, it was possible to increase the contribution of one of the remaining terms and maintain a similar controller. Since the value of  $k_2$  was already fairly small, it was decided to decrease the value of  $k_1$  back to 25 to increase the effectiveness of the proportional term.

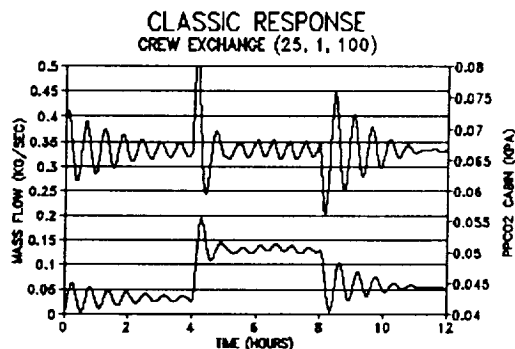


Fig. 5 System response with weighting (.04,1,.01)

The net result was a controller with the constants set at  $k_1 = 25$ ,  $k_2 = 1$ ,  $k_3 = 100$ . These constants do not represent a calculated attempt at optimizing the controller, but rather a logical qualitative approach to examine the effect of the different error terms on the overall responses to the test. The data for its response to the test case is shown in Figure 5.

This controller exhibits several characteristics. First it suffers from a large spike in partial pressure corresponding to the onset of the step functions. The maximum value attained was 0.084 kPa of  $\text{CO}_2$ . The duration of the spike was for only a few minutes, and is not a problem to the crew. On the positive side, this controller was able to quickly reduce the magnitude of the oscillations and rapidly achieve a steady mass flow rate. In comparison to our previously listed criteria, this set of constants was elected as best for use in the classical PID controller.

The PID controller was very successful in regulating the system and maintaining desirable cabin conditions. The effect of the constants on the response of the system was as expected, lending an air of credibility to the model and the controller. Again, the controllers tested were chosen for their capable and satisfactory performance, rather than as the result of a formal optimization study.

### Expert Control Results

The expert controller was subjected to testing using the same cabin conditions as described above. It was again necessary to attempt to modify the expert controller to provide some degree of dampening to lessen the wear on the fan and motor driving the air through the sorbent beds. The understood restraint on maximizing dampening is that the system must maintain the cabin  $\text{CO}_2$  levels at approximately the 0.0667 kPa set point.

The expert system algorithm first generates a belief, a percentage basis of its need to execute a change. This belief is multiplied by a weighting

factor to generate a new mass flow rate. The actual algorithm follows.

$$\dot{m} = \dot{m} \pm (k_1(2\% \text{ Belief} - 1)) \quad (3)$$

The most obvious characteristic of this equation is that the controller's frequency is proportional to  $k_1$  or the weighting factor; that is, a large factor will generate a high frequency controller. The inverse of this is that a small weighting factor will result in a lower frequency controller.

The original controller was designed with  $k_1$  equal to 0.05. The result of this controller when tested with the crew exchange scenario is shown in Figure 6. The upper curve corresponds to the right-hand axis and displays the partial pressure of  $\text{CO}_2$  in the cabin in kPa. The left-hand axis goes with the lower curve to show the mass flow rate in kg/sec.

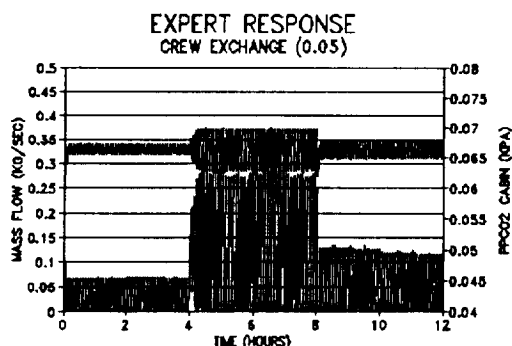


Fig. 6 Dynamic response with weighting (.05)

The controller exhibits no apparent dampening, and so does not appear very suitable for our application. The next course of action was to remember, as with our work on the PID controller, that a lower frequency controller provided smoother mass flow rates and an increase in dampening. Following that hunch, the value of  $K_1$  was lowered to 0.005 and the test was run again.

This served to slow the controller's time of response, and also to achieve a slight dampening

effect. The results for this run are shown in Figure 7. The quickest dampening however was limited to the region when  $\text{CO}_2$  was the highest. This trend was similarly observed in the PID controller when the frequency was slightly too high. This indicates that the weighting factor is close to the desired value and only needs fine tuning.

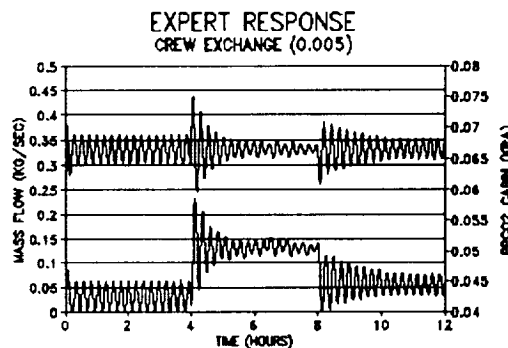


Fig. 7 Dynamic response with weighting (0.005)

The final variation on the expert system weighting factor was to set  $k_2 =$  to 0.002. The graph in Figure 8 represents the results of that test. It can be seen that the increase in controller frequency enabled the controller to decrease the amplitude of the transient spikes. That reduction, coupled with the fact that the dampening was even more successful, made the weighting factor of 0.002 appear to be the most capable option for the expert controller.

Again, it is important to stress that the expert controller, like the classic controller, is not optimized. Although the apparent best choice from among several options was taken, the values are not presented as optimums. No mathematical solution was undertaken as an attempt to find the best weighting factor; rather, the selected controller is merely a functional and capable controller for the system.

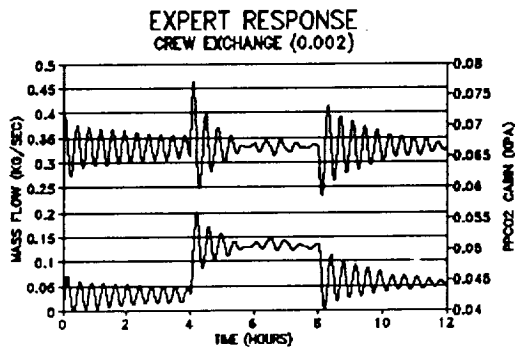


Fig. 8 Dynamic response with weighting (0.002)

### Dynamic Case Studies

In addition to the situation utilized in the examples above, the controllers and simulation were subjected to a series of other tests. First, the simulation was tested to determine its response to a sinusoidal  $\text{CO}_2$  production rate that always created a heavier load on the same sorbent bed. This would provide insight into the system's response at being excited at a given frequency. The results for this test can be found in Figures 9 and 10. Here, as before, the upper curve is the partial pressure on the right axis, and the mass flow rate is the bottom curve scaled along the left-hand axis.

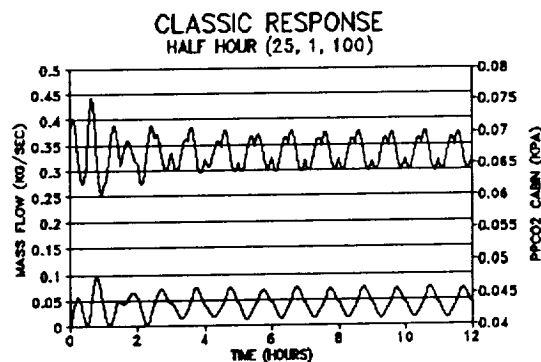


Fig. 9 Classical response to half hour cycle

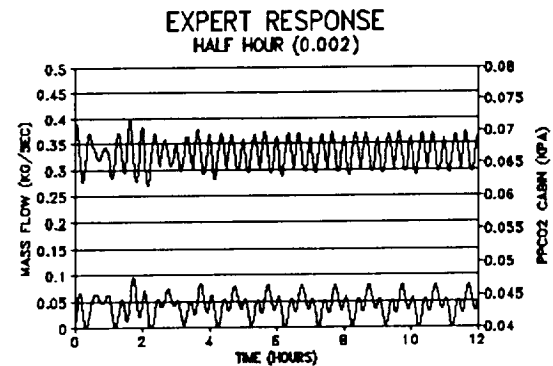


Fig. 10 Expert response to half hour loading

The next case was conducted to determine the natural frequency of the controllers. By imparting a single impulse, in this case a short-term high  $\text{CO}_2$  production spike, it is possible to observe the system's natural frequency. The results of this test can be seen in Figures 11 and 12. The expert controller has a higher frequency than the classical controller. That does not necessarily imply that the expert controller has the faster response capability, only that it cycles at a higher rate. Also in this scenario it is easy to observe the dampening abilities of the control systems as they reduce the oscillation's amplitudes. The final point of interest is the visibility of the half hour frequency imparted due to bed switching. It is responsible for the steady state oscillations visible in the graphs.

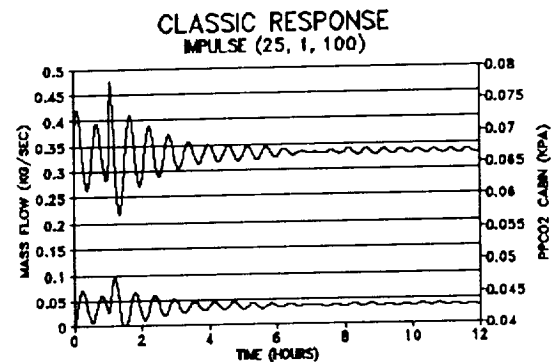


Fig. 11 Classical response to an impulse

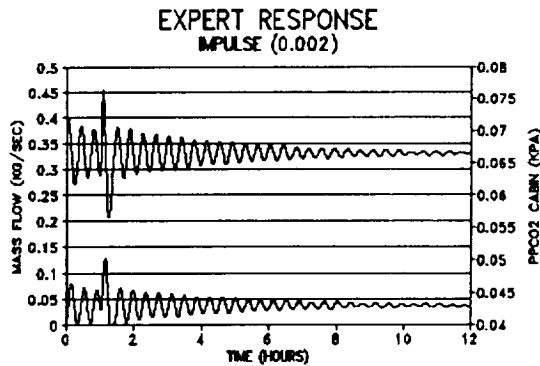


Fig. 12 Expert response to an impulse

The final scenario examined was the controllers' ability to handle a massive  $\text{CO}_2$  production rate. This would simulate a fire in a Space Station module, or possibly a leak in the  $\text{CO}_2$  accumulator tank. The results of this trial are given in Figures 13 and 14. The classical system was able to respond more quickly, as evidenced by its more rapid increase of the mass flow rate. The slower response of the expert system resulted in the  $\text{CO}_2$  partial pressure reaching a value of 14 kPa as opposed to the PID's peak value of 12 kPa. The major consideration, however, is how long before the  $\text{CO}_2$  level returns to acceptable limits. Here, both controllers show the situation under control by two hours later.

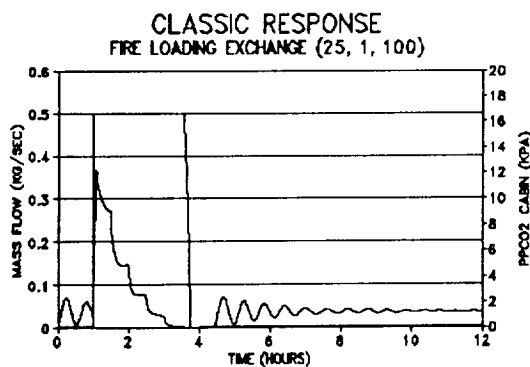


Fig. 13 Classical response to a fire

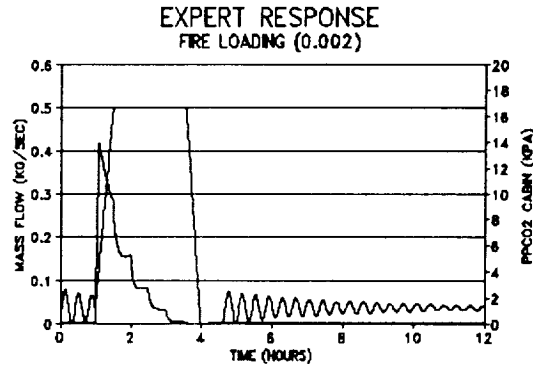


Fig. 14 Expert response to a fire

### Conclusions

The first conclusion that can be gathered from this report is that the simulation presented is a success. The physical phenomena modeled are accurate and respond correctly to parameter changes. This implies that the simulation is capable of being used as a test bed for evaluating almost any parameter's influence on the system's behavior. It is possible to determine the effects of possible disasters (such as a fire), or merely to examine how the system operates under normal conditions.

Both controllers were found to be capable of handling the tasks assigned. There is currently no way to determine if one controller is superior to the other. Neither was formally optimized, and so the limits of their abilities is still not known.

### Recommendations

It is recommended that a formal optimization of the controllers be done. Once optimization is completed, a rigid and weighted set of criteria should be drafted. After testing the controls with the simulation code, the control schemes could be scored against the criteria. Once this is completed, the better control system should be implemented as the control scheme of choice.

Note that a single type of control may not necessarily be the best choice. Rather, a control hierarchy where an expert system oversees a series of classical controls (or vice versa) might be the most effective choice.

**MINOTAUR**  
**MARYLAND'S INNOVATIVE ORBITAL TECHNOLOGICALLY ADVANCED UNIVERSITY**  
**ROCKET**

University of Maryland College Park  
 Department of Aerospace Engineering  
 College Park, Maryland

Professors Mark J. Lewis and Dave Akin  
 Charles Lind, Teaching Assistant

### Abstract

Over the past decade, there has been an increasing interest in designing small commercial launch vehicles. Some of these designs include OSC's Pegasus, and AMROC's Aquila. Even though these vehicles are very different in their overall design characteristics, they all share a common thread of being expensive to design and manufacture. Each of these vehicles has an estimated production and operations cost of over \$15K/kg of payload. In response to this high cost factor, the University of Maryland is developing a cost-effective alternative launch vehicle, Maryland's Innovative Orbital Technologically Advanced University Rocket (MINOTAUR). A preliminary cost analysis projects that MINOTAUR will cost under \$10K/kg of payload. MINOTAUR will also serve as an enriching project devoted to an entirely student-designed-and-developed launch vehicle.

This preliminary design of MINOTAUR was developed entirely by undergraduates in the University of Maryland's Space Vehicle Design class. At the start of the project, certain requirements and priorities were established as a basis from which to begin the design phase: (1) carry a 100 kg payload into a 200 km circular orbit; (2) provide maximum student involvement in the design, manufacturing, and launch phases of the project; and (3) use hybrid propulsion throughout. The following is the list of the project's design priorities (from highest to lowest): (1) safety, (2) cost, (3) minimum development time, (4) maximum use of off-the-shelf components, (5) performance, and (6) minimum use of pyrotechnics.

### MINOTAUR Overview

MINOTAUR is a four-stage custom/modular rocket (Figure 1). It stands 30 meters tall, has a gross lift off weight of 30,000 kg, and generates 750 kN of thrust at lift off. Stages 1-3 are composed of modules, each approximately eight meters tall and weighing 2250 kg, in a 7-5-1 configuration respectively. Each module is identical in size and mass except for its nozzle. The nozzle design for each stage module is different to achieve optimal performance from varying ambient pressures during ascent. Stage 4 is a scaled-down (52%) custom version of the modular design.

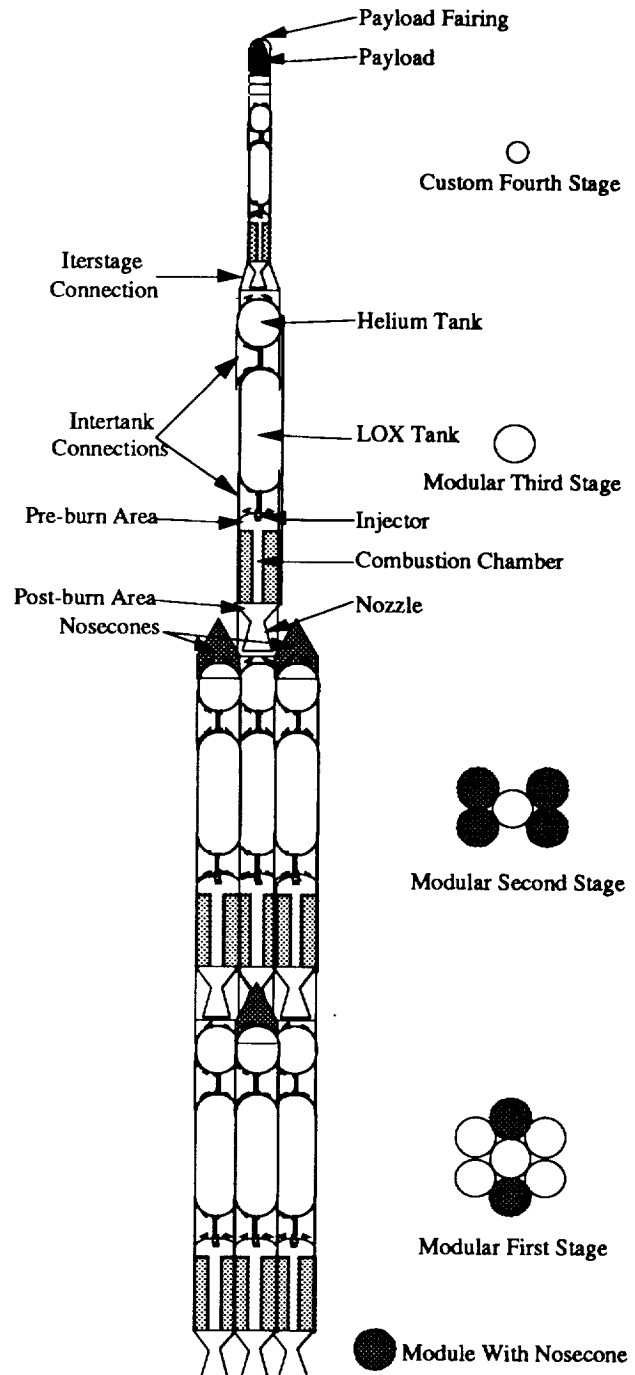


Fig. 1 MINOTAUR side and top view

MINOTAUR has also been developed to explore the possible use of hybrid technology in a viable orbital vehicle. MINOTAUR's propulsion system consists of a liquid oxidizer and a solid grain of fuel, each stored in separate chambers. The oxidizer is introduced to the grain and combined during firing in the holding chamber for the fuel grain. A pressurant is needed to keep the oxidizer at high pressure for blow down to the combustion chamber to occur. The hybrid is considered as the medium between the complexities of liquid systems and the simplistic mechanical operation of a pure solid.

### Mass Budget

The mass budget is a detailed component mass list assembled to identify the overall vehicle masses and margins. The current mass budget is divided into six parts: one for each modularized stage, the fourth custom-designed stage, a stage mass summary, and overall conclusive masses. Tables 1 and 2 show the system mass lists for the module and fourth stage. A complete component mass list can be found in the final report. The first, second, and third stage typical module masses do differ slightly even though they are basically the same module. The difference lies primarily in nozzle mass for reasons already explained.

Margins were added to the vehicle's inert mass to compensate for any mass increase during production. After production is completed, any remaining positive margins can be used to increase payload mass capability or to achieve a higher altitude.

Center of gravity calculations were done to help predict the dynamic stability of the vehicle. The center of gravity of each component was calculated, and then transformed into a module, fourth stage, and vehicle center of gravity. The reference station for all center of gravity calculations was the exit plane of the first stage nozzle. Figures 2 and 3 show mass and center of gravity vs. time of flight, respectively.

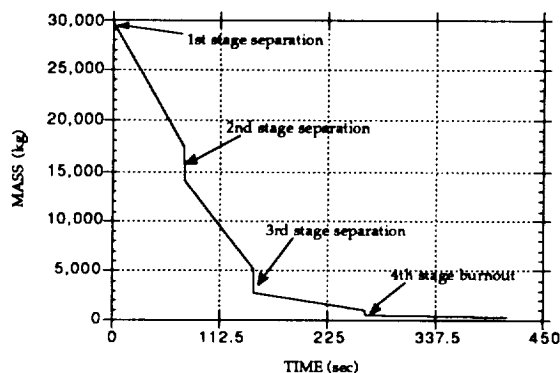


Fig. 2 Mass vs time graph

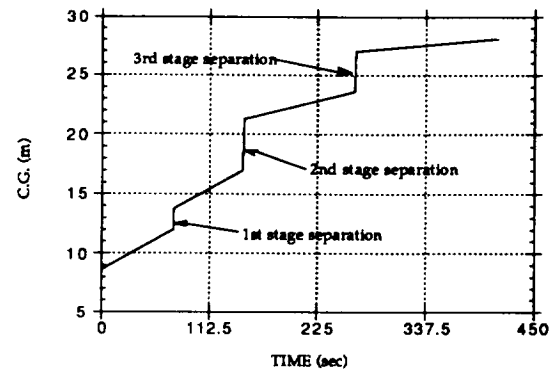


Fig. 3 Center of gravity vs time graph

Table 1 Module mass list

| System                   | Module Mass(kg) |
|--------------------------|-----------------|
| Combustion chamber       | 78              |
| Oxidizer tank            | 193             |
| Pressurization tank      | 59              |
| Ignition                 | 2               |
| Propulsion               | 61              |
| Destruct                 | 18              |
| Intertank                | 53              |
| Avionics/electronics     | 8               |
| Roll control (3rd stage) | 5               |
| Subtotal                 | 477             |
| Inert mass margin        | 7%              |
| LOX                      | 1215            |
| HTPB                     | 552             |
| Total mass               | 2244            |

Table 2 Stage 4 mass list

| System               | Stage 4 Mass(kg) |
|----------------------|------------------|
| Combustion chamber   | 22               |
| Oxidizer tank        | 30               |
| Pressurization tank  | 13               |
| Ignition             | 2                |
| Propulsion           | 11               |
| Destruct             | 14               |
| Intertank            | 27               |
| Avionics/electronics | 39               |
| Roll control         | 5                |
| Power                | 9                |
| Subtotal             | 163              |
| Inert mass margin    | 9%               |
| LOX                  | 180              |
| HTPB                 | 82               |
| Total mass           | 425              |

## Vehicle Costing

One of the most important requirements of the project is to produce a vehicle at low cost. Therefore, the production effort will have to keep cost in mind at all times. This will mean that elegance and high performance will sometimes have to be sacrificed in order to meet cost requirements.

Cost estimates of the vehicle components have been divided into major vehicle systems. The cost estimates are derived from the following major sources: supplier cost figures for appropriate or similar components, general cost formulas using component mass values (primarily applied for structural elements), and costing formulas from Space Mission Analysis and Design, by Wertz and Larson<sup>3</sup> (primarily applied for electronic components). Table 3 outlines MINOTAUR's systems cost.

Table 3 Vehicle costing

| System              | Cost(\$K) |
|---------------------|-----------|
| Combustion chamber  | 132.3     |
| Oxidizer tank       | 198.3     |
| Pressurization tank | 70.7      |
| Intertank           | 34.9      |
| Propulsion          | 64.8      |
| Destruct            | 16.8      |
| Interstage          | 14.9      |
| Separation          | 15.4      |
| Power               | 1.0       |
| Avionics            | 160       |
| Pad structures      | 10.8      |
| Flight insurance    | 50        |
| Margin              | 30        |
| Total cost          | 799.9     |

## Trajectory Model

A FORTRAN trajectory model, HYTRAJ (hybrid trajectory), was developed to verify MINOTAUR's capability of meeting the requirement of putting a 100 kg payload into a 200 km orbit. The end condition required for this is a circular orbit at 7784.3 m/sec. HYTRAJ models the kinematics of the rocket. No dynamics are used to compute the rocket's performance in flight. The trajectory is defined using a preset pitchover function. The rocket launches vertically, performs a pitchover maneuver from 3 to 8 seconds into the flight, then is modeled as flying at zero angle of attack, and therefore zero lift, through the region of high dynamic pressure, and finally flies to tangential velocity at 200 km. This program assumes a rotating Earth which is accounted for using a simple vector addition technique. The Earth has a varying gravity based on altitude. It models drag forces and can be used to predict angles of attack. Aerodynamic heating at the nose is computed as is the variation of thrust with altitude and an

ablating nozzle. The time step used in HYTRAJ is 0.1 seconds.

HYTRAJ results indicate that the current design can reach the required orbit as shown in Figure 4. The altitude reaches 200 km while the flight path angle goes to 1.57 rad (90 degrees) and the velocity is 7784 m/sec. The sudden increase in velocity around 130 secs is due to a coordinate transformation from Earth-fixed to space-fixed coordinates. This jump accounts for the velocity of the launch site (378 m/sec) due to the Earth's rotation.

## Payload Accommodations

To develop payload accommodations for a given payload, the following criteria must be identified early in the mission planning process.

1. structural, electrical and avionics interfaces
2. adapters for separation systems, etc.
3. communications architecture
4. launch system environment before and during launch.

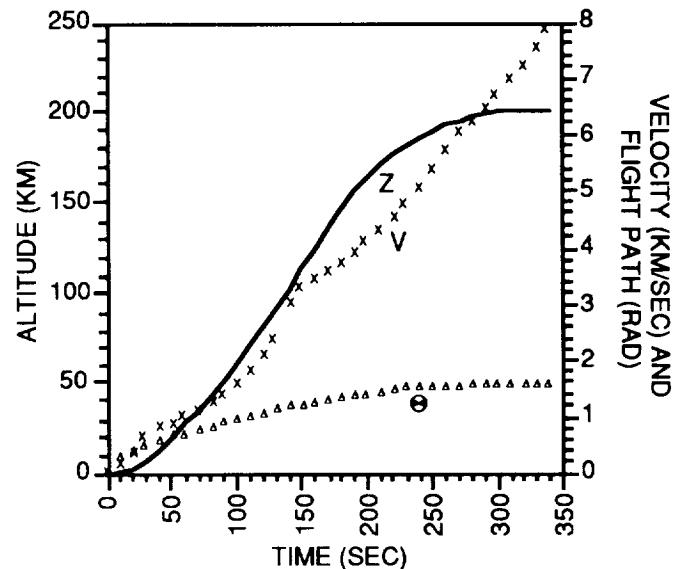


Fig. 4 Trajectory model

Items 1-3 are dependent upon the particular payload chosen for a launch. Once a payload is chosen, all details pertaining to the accommodation requirements need to be analyzed quickly so integration can become a smooth and efficient process. Item 4, however, is dependent upon the launch vehicle. Based on predicted launch characteristics, MINOTAUR's payload environment requirements are shown in Table 4.

As determined by MINOTAUR's trajectory code, payload separation will begin at 200 secs when dynamic pressure = 0.5 N/sq m. This time also corresponds to the approximate point where the heat transfer from the payload fairing to the payload is greater than the heat transfer from the rarefied atmosphere to the unprotected payload. Therefore, the



payload fairing is separated to eliminate unnecessary heat transfer to the payload. Another benefit from early fairing separation is that after separation less inert weight is being carried by the rocket. By ejecting the payload fairing before third stage separation, the vehicle's performance is increased.

Table 4. Payload Environment Requirements

| Payload Environment  | Pre-launch | Ascent      |
|----------------------|------------|-------------|
| Thermal              | Pending    | 1341 W/sq m |
| Electromagnetic      | Pending    | Pending     |
| Contamination        | Pending    | Pending     |
| Loads                |            |             |
| Venting              | NA         | 1 psi +/-   |
| Aerodynamic          | NA         | .5 N/sq m   |
| Axial acceleration   | NA         | 4.5 g       |
| Lateral acceleration | NA         | 1 g         |
| Axial dynamic        | NA         | 30 Hz       |
| Lateral dynamic      | NA         | 15 Hz       |
| Acoustic             | NA         | Pending     |

### Heating Analysis

Two heating models, one from NACA Rep. 1381<sup>1</sup>, the other from Anderson's Hypersonic and High Temperature Gas Dynamics<sup>2</sup>, were used to determine the stagnation point heating of MINOTAUR's payload fairing. These models were originally developed for aerodynamic heating analyses of reentry vehicles. Since it was uncertain if the models could be used for anything else but re-entry analysis, they were used as verifiers of each other's validity for fairing heat transfer. Both of these models were used for MINOTAUR's trajectory code to determine the maximum heat transfer to the fairing. Figure 5 shows how the two models compare for the 0.21-meter radius of MINOTAUR's payload fairing.

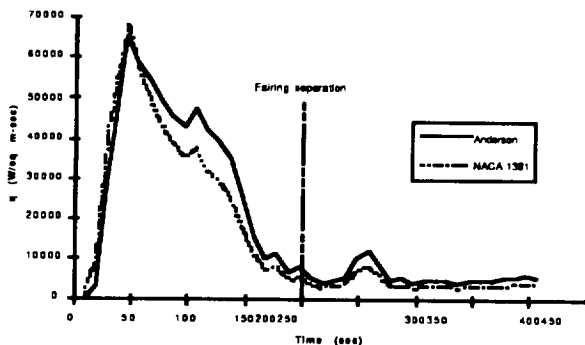


Fig. 5 Stagnation point heat transfer for a 0.21-m sphere

These models were relatively close in their prediction of nose heating, and were therefore considered valid. Anderson's model was chosen to be used for any future analyses because it yielded the highest heat transfer rates. Designing the

payload fairing to a lower heat transfer rate than might occur during launch increases the chance of thermal load failure. By integrating the resulting curve from Anderson's model as seen in Figure 5, the maximum stagnation point heat load was determined to be 7200 KJ/sq m.

### Separation Systems

The separation systems are divided into two basic types: payload fairing separation systems, and stage separation systems. Both systems require the design and fabrication of a Marmon clamp. A Marmon clamp is a continuous ring held together by an angular clamp. By releasing the clamp tension, the joint is separated and pulled away from the upper stage by means of a spring which is attached to both the lower stage and the Marmon clamp itself. As seen in Figure 6, the clamp is composed of a metal strap and many shoe segments. Marmon clamps were chosen over the shape charge or zipper for three basic reasons: both the shape charge and the zipper require an explosives engineer to design, are very dangerous to handle, and are very expensive. On the other hand, Marmon clamps are student-designed and manufactured, and therefore have a very low cost. Marmon clamps also have a built-in mechanical redundancy because they are releasing at more than one point.

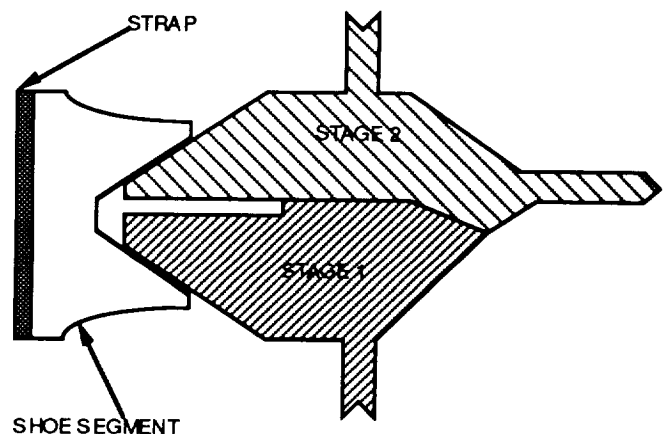


Fig. 6 Marmon clamp design

### Destruct System

The destruct system was designed to meet the first and foremost design priority, safety. For this reason the use of pyrotechnics was ruled out. The destruct system was designed to depressurize the rocket and bring it down in a controlled manner. The rocket will receive a signal from the ground which will be distributed to each module. The valves will then be actuated using 6-V Airtronics servos powered by 4 "D" cell batteries. These batteries will be located on top of the modules and will be accessible through the stage fairings. The LOX and helium tanks are depressurized by activating two electrically actuated butterfly valves per tank. The flow of LOX is cut off from the combustion chamber using a modified pressure relief valve. This allows the propellant to burn itself out. The advantage of this system is

that solenoid valves and constant pneumatic pressure are not needed. The butterfly valves are constructed from stainless steel because of its high strength to weight attributes, good low temperature material characteristics, and relative low cost.

### Propulsion System

The characteristics of MINOTAUR's propulsion system as described in the overview follow.

Hydroxyl-terminated polybutadiene with no additives (save the carbon black) is used for the solid grain. The oxidizer was chosen to be liquid oxygen. A helium pressurant will provide the pressure differential to blow down the oxygen into the combustion chamber. Thrust vectoring uses a liquid injection system of oxygen. Roll control for the upper stages feeds off the main blow down supply of helium.

The valves for release of the helium and oxygen are butterfly and ball valves, respectively. They are electrically actuated with the main oxygen valve being heated. The configuration of the grain is a 3-point rounded star. The ignition system consists of propane injection onto the grain, with ignition provided by a sparking electrical element.

The main LOX injector is a shower head injector. The conical, 15° half angle nozzle is coated with silica phenolic.

### Regression model

The requirement for accurately estimating the fuel's regression rate is an important aspect of the hybrid rocket system. In a hybrid, as in a solid, the regression rate of the fuel is the driving factor in the engine's performance and physical characteristics. The rate of regression gives the amount of fuel that is burned from the grain per second. The regression rate in turn determines the fuel's combustion characteristics, which in turn determine the rocket's performance. The regression model is needed to represent the coupling of the various chamber conditions (pressure, temperature, burn area, etc.).

Combustion takes place in the turbulent boundary layer above the solid fuel grain as shown in Figure 7.

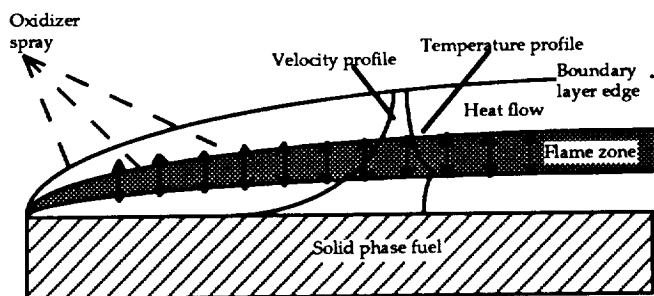


Fig. 7 Hybrid combustion model

The fuel is transported within the boundary layer (crossing the fuel), mixed with the oxidizer, and burned. Due to the fluid mechanics of the situation, regression rate is a function of the local mass flux (which depends upon the regression rate at all points upstream as well as the instantaneous port area) and the local burning perimeter. Pressure can also be a factor if enough radiation is involved. This coupling does not allow the use of a solid rocket regression rate (rate proportional to pressure raised to an empirical constant) for a hybrid system.

### Grain configuration

A 3-point rounded star grain configuration was chosen.

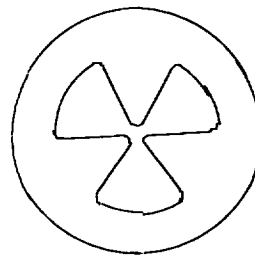


Fig. 8 Grain design

The grain design must provide the constant thrust profile that the trajectory model has established. The star provides a relatively neutral burn and covers the wall during the firing to help protect the chamber. The star configuration that was chosen was based on the assumption of a volumetric loading of 70%. This loading was chosen to allow a large flow of oxidizer through the system to aid in combustion.

### Oxidizer pressurizing system

MINOTAUR utilizes liquid oxygen as the oxidizer. To keep the liquid oxygen pressurized and provide the liquid oxygen to the combustion chamber at 300 psi, a pressurizing system is required. A pressure-fed system using helium stored at 3000 psi and 294° K will be used.

Helium has been chosen as the pressurant because of the mass savings over other possible pressurants. The storage conditions of 3000 psi and 294° K have been verified as the best workable design. Figure 9 is a plot of system mass vs. storage pressure which shows 4000 psi to be the optimal pressure. Below and above this pressure, system mass increases; however, there is a high availability of system components built for use at 3000 psi. Due to this high availability and since the mass increase between a 3000 psi and a 4000 psi system is less than 3 kg per module, the 3000 psi system was chosen.

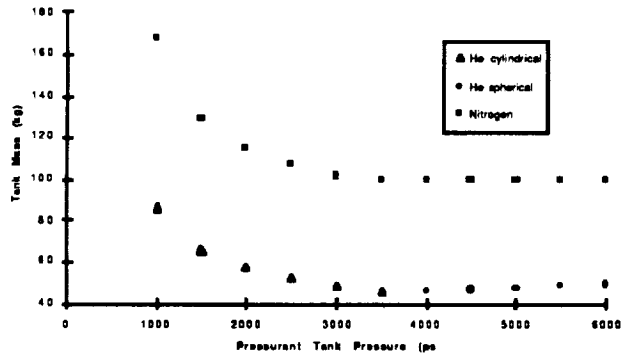


Fig. 9 Pressurant comparison

### Roll control system

The upper stage roll control system is a helium propellant cold gas propulsion system with two pairs of opposing thrusters arranged to provide a rolling moment without imparting a pitch/yaw moment. The entire system consists of the helium, piping and valves from the helium supply, four nozzles, and an aluminum circular mounting plate with mounting brackets to mount the system to the intertank structure (see Figure 10).

The amount of helium required is 1.46 kg at 3000 psi, stored in the fourth stage helium tank at 294° K. The helium supply for the roll control system will be regulated down to an operating pressure of 400 psi. Above this pressure, very little mass savings can be realized and the helium supply may not be able to provide the necessary pressure.

Standard 3/8" and 1/4" stainless steel pipe and fittings will be used to provide the necessary flow for the system. An ASCO 7985G2 two-way valve will be used to split the helium supply into two 400 psi flows which will provide the necessary mass flows for each pair of thrusters. Two ASCO 8223G3 two-way solenoid actuated valves will be used for pulsing the helium into the thrusters. The minimum duration thrust pulse for this configuration will be 35 ms. The nozzles will be 0.4 cm stainless steel and will have an area ratio ( $A_e/A^*$ ) of 8.31 with  $A_e = 0.679 \text{ cm}^2$ ,  $r_e = 0.4649 \text{ cm}$ ,  $A^* = 0.0817 \text{ cm}^2$  and  $r^* = 0.1613 \text{ cm}$ . The entire system will be fastened to a 0.063" Aluminum plate which will be mounted to the intertank structure between the helium and liquid oxygen tanks of the fourth stage. A small portion of the nozzles will protrude through the skin of the vehicle. Thermal and structural loads due to this have been accounted for in the design of the system.

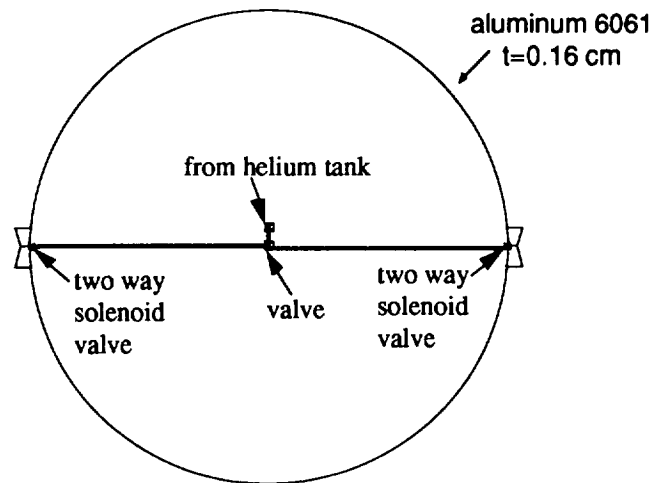


Fig. 10 Roll control system

### Nozzle design

In examining the choice of materials to be used for a nozzle, two designs were evaluated for cooling the throat, a heat sink nozzle, and an ablative nozzle. Transient 1D analysis was used to determine the required thickness of the heat sink nozzles. As seen in Table 5, they tended to be very thick and heavy.

Table 5 Nozzle insert comparison

| Material | Thickness (cm) | Throat insert weight (kg) |
|----------|----------------|---------------------------|
| Graphite | 18             | 130                       |
| Nickel   | 10             | 186                       |

Ablative nozzles were found to be lighter. The composite materials selected were pyrolytic graphite for the throat and silicon-phenolic for the remaining expansion skirt. The pyrolytic graphite has an erosion rate of 0.11 mm/sec and can withstand the high temperatures at the throat; however, the cost of graphite products is five times that of the silica phenolic. Since the heating drops off drastically after two radii down the nozzle, the more economical silica-phenolic of constant thickness will be used in the last half of the expansion/ straightening section of the nozzle. Graphite is brittle at cool temperatures. To add ruggedness and durability to the nozzle, it will be wrapped with two layers of graphite-epoxy as a high strength outer shell. This graphite-epoxy shell will also be wound over a steel flange which will mount to the thrust chamber.

The converging and diverging sections of the nozzle will be made as a single piece. The mold used to make the nozzle will be separable at the throat. Once the phenolic has hardened the mold may then be pulled out of the converging and diverging sections.

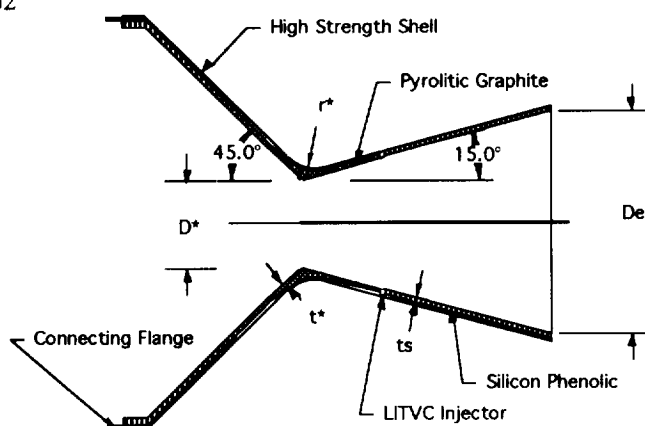


Fig. 11 Nozzle design

### Thrust vectoring design

Liquid injection thrust vectoring (LITVC) was chosen as the thrust vectoring system. LITVC allows for a fixed nozzle which eliminates the need for a flexible bearing. The plumbing involved could be performed in-house for increased student involvement and decreased cost. LITVC utilizes the pressure from shock waves acting against the side of the nozzle and the momentum of the fluid flow to generate a torque on the vehicle.

The thrust vectoring system will consist of eight liquid injectors surrounding each nozzle. Each injector will have 300 psi with which to spray liquid oxygen into the flow. The solenoids will be digitally pulsed to allow for differential thrust vectoring. Typical performance data for oxygen is 300 sec of side Isp. Side Isp is the side force exerted by the injection of the fluid on the nozzle divided by the mass flow of the fluid. The LITVC system was designed to provide a side force equal to 7% of the axial thrust, which is equivalent to 4° of gimbaling.

### Injector design

A flat plate injector was chosen to meter the LOX to the combustion chamber. The requirement on the injector is to administer the flow of oxygen to the grain in the smallest droplet size and at the slowest and most turbulent velocity possible to allow for complete combustion inside the chamber. Figure 12 shows the first stage injector.

It utilizes short tube orifices which have a drag coefficient,  $C_d = 0.88$ . Note that the ignition system is mounted internally to the injector, this is to save space in the combustion chamber. The injector is mounted flush against the top of the chamber to protect the wires of the ignition system. The thrust chambers insulation may be modified to also reduce vibration which cause chugging and loss of performance. Blocks of propellant may be placed in front of the injector which will also help to mix the flow. The plate design allows for in-house manufacturing.

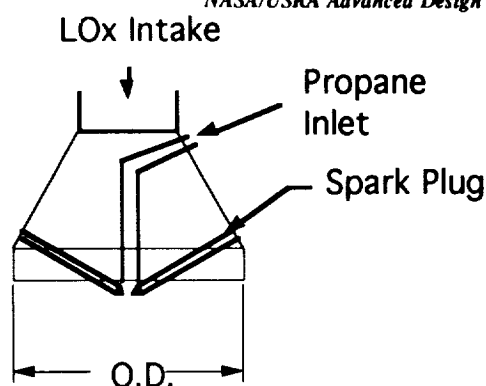


Fig. 12 Injector design

Table 6 Injector specifications

| Stage               | 1    | 2    | 3    | 4   |
|---------------------|------|------|------|-----|
| Mass flow (kg/s)    | 38.0 | 12.3 | 10.7 | 1.2 |
| Number of holes     | 513  | 139  | 139  | 27  |
| Outer diameter (cm) | 6.3  | 3.3  | 3.3  | 1.5 |
| Mass (kg)           | 5    | 3    | 3    | 2   |

### Ignition system

The final design of the ignition system is an augmented spark igniter with propane as the ignition fluid and spark plugs as the spark generator.

The propane tank will be situated in the intertank region, attached to the combustion chamber. A pipe 0.5 cm in diameter will lead from the tank into the LOX line and down through the center of the LOX injector, 1.0 cm into the combustion chamber. The exit area of the pipe will be 0.667 cm on the modules and 0.065 cm on the custom stage. Two spark plugs will be used for redundancy. The spark plugs will be located under the exit of the propane pipe. (Refer to Figure 12.)

### Off-nominal performance

The off-nominal performance of a rocket deals with the variations in total impulse that occur with either changes in altitude or throat area ratio. As altitude increases, total impulse increases (very rapidly at first, then slowly levels off at a maximum of about 100,000 meters above sea-level). This information was determined from the required thrust and a pressure-altitude table. Also, the total impulse decreases exponentially with a reduction in throat area ratio. This information was determined using a complete thrust calculation over various area ratios for each of the modules based on a varying internal pressure with area. Therefore it is important to maximize thrust near the surface of the Earth and to be aware that the ablation rate on the throat is very important. The effect of the ablation rate depends on the trajectory analysis, and the ablation cannot be greater than the .00011 m/s that was chosen or the rocket will not have enough total impulse to reach orbit. If there is an irregular

ablation rate, slow at the beginning but slowly increasing, it might be possible for a larger area to decrease.

### Structural Design

Many factors were considered in designing a structure that would not only meet the load requirements, but also be suitable for production and assembly in the University environment. The major aspects for designing a suitable structure for MINOTAUR are outlined in Table 7.

Table 7 Structural design requirements

| Structural design concern        | MINOTAUR characteristics |
|----------------------------------|--------------------------|
| <b>Loading criteria (HYTRAJ)</b> |                          |
| Axial acceleration               | 4.5 g's                  |
| Lateral acceleration             | 1 g                      |
| Axial natural frequency          | 30 Hz                    |
| Lateral natural frequency        | 15 Hz                    |
| Maximum dynamic pressure         | 125 kPa                  |
| Internal venting pressure        | 7 kPa                    |
| <b>Production and handling</b>   |                          |
| Safety                           |                          |
| Cost                             |                          |
| Maximum student involvement      |                          |
| <b>Factors of safety</b>         |                          |
| Sealed pressure vessels          | 3.0                      |
| Testing on all individual parts  | 1.25                     |
| Proof testing of one unit        | 1.5                      |
| No structural testing            | 2.0                      |

### Intertank structure

There were two main designs that were researched for the design of the intertank structures, monocoque and skin stringer. For this launch vehicle, the skin stringer design was chosen.

Monocoque designs are less capable of withstanding the same loads as the stringer and honeycomb design, but they have the advantage of being easier to manufacture and their load analysis is much simpler. However, a problem arises with monocoque structures when cutouts for access doors, plumbing, and wiring are made. The structure that is removed to allow for the above mentioned elements constitutes a portion of the load-carrying ability of the structure. In order to make up for this loss, the rest of the structure has to be made thicker and consequently heavier.

Skin stringer structures are harder to manufacture, but they utilize the weight of the structure in terms of load carrying capability more efficiently. In this configuration, the lengthwise members are the main axial load carrying members. The primary objective of this monocoque skin is to take the torsional loads incurred on the vehicle. In this

configuration, if cutouts were made in the skin, the load carrying capacity would not be appreciably affected as in the simple monocoque design since the majority of the axial loads are taken up by the stringers anyway and the stringers do not have any cutouts in them. Figure 13 shows the analysis between monocoque and skin-stringer for a given aluminum cylinder under loading as prescribed in Table 7.

### Material Choice

In choosing the material for the intertank design, there were two main categories from which to pick, metals and composites. Composites have the advantage of being able to supply "tailored" strength and rigidity in the direction needed. However, in order to use composites, all loads must be known with a great degree of precision. More than likely, failure would occur if unaccounted-for-loads were to appear in an undesigned-for direction. Metals, however are isotropic, possessing the same material characteristics in all directions.

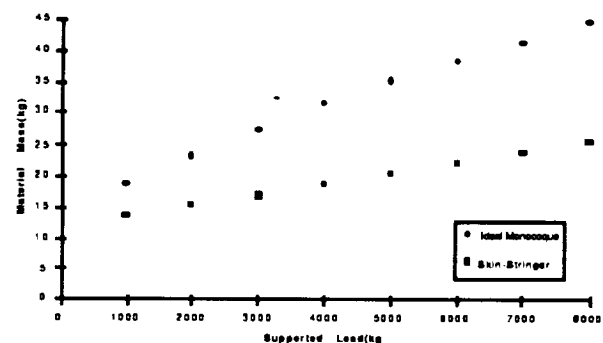


Fig. 13 Intertank structure comparison

Therefore, in designing for maximum loads in one direction, over-design in the other directions automatically occurs, thereby giving an extra degree of safety. Also, the structural analysis and the cost of manufacturing for metals are lower than those for composites. In view of these points, a metal structure was chosen. The candidate metals in these studies were Aluminum 6061(MIL-T-6), Titanium-8Al-1Mo-1V(MIL-T-9046) and Stainless Steel 17-7 PH (MIL-S-25043). The same stress levels are applied to identical structures made from these materials. The mass of structure is obtained by using the above-mentioned theories. Figure 14 shows the results from the material analysis. It is easily seen that Aluminum 6061 is the best choice, and therefore was chosen as the intertank and interstage material.

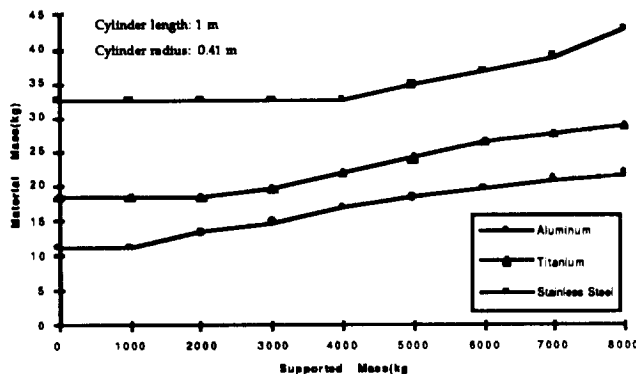


Fig. 14 Intertank material comparison

### Interstage connections

A skin stringer structure was used. The buckling stresses can not be predicted using the statistical method mentioned before. The loads analysis for interstage fairings is exactly the same as that for the reinforced section of the intertank structure. Both the first and second stages will be connected by 0.0127-m diameter (0.5 inch) bolts attaching through the intertank connection stringers. The second stage will also have struts connecting the outer modules. This will alleviate torques on the stringers caused from thrust vectoring. On the first stage, there are 10 bolts on each set of stringers connected. The second stage is the same except it uses only four bolts on each set of stringers.

### Structural dynamics

The response of the launch vehicle to dynamic loads during launch and pad operations are crucial factors in preparing for flight. Applied loads come from a variety of sources. Transportation, assembly, steady state acceleration from the engines, acoustic noise during transonic regime and liftoff, separation, launch pad wind, payload insertion, engine vibrations, and aerodynamic loads are possible sources of dynamic input into the launch vehicle. These loads will act over various frequency ranges at different periods of the flight.

The launch vehicle will have its own natural frequencies based on the stiffness of the structure. When the applied loads excite the natural frequencies of the vehicle, the loads on the vehicle and corresponding payload will approach extreme values. In order to avoid this resonance phenomena, the design of the vehicle should take the dynamic inputs into account.

In order to minimize the loads that a payload will experience, the payload must be designed to have natural frequencies decoupled from the launch vehicle's natural frequencies. A coupling of responses between the launch vehicle and payload will make the problem worse.

At this stage of the design, the only factors that can be determined are the launch vehicle's natural frequencies. The dynamic loads that will be put into the vehicle during flight are special to the vehicle and can not be determined until after the first flight. Since the payload is currently a 100 kilogram lump of mass at this point, the desired payload frequency characteristics will be designed into the payload after the launch vehicle frequencies are known. Mathematical representations of the launch vehicle were developed using MSC NASTRAN as the finite element software package. These models were used to estimate the natural frequencies of the launch vehicle and one of the modules. The results are as follows:

Table 8 Structural dynamics results

| FEM model                   | Natural frequency |
|-----------------------------|-------------------|
| Dry unpressurized module    | 16.54 Hz          |
| Fueled pressurized module   | 7.34 Hz           |
| Free-free vehicle in flight | 10.08 Hz          |
| Fixed vehicle on launch pad | 5.66 Hz           |

### Guidance, Navigation, and Control

The total guidance, navigation, and control system (GN&C) is made up of several elements that must work together to safely get the payload into orbit. The navigation system keeps track of the vehicle's position, attitude, and velocity to give feedback to guidance system. A strapdown inertial navigation system (INS) with an embedded global positioning system (GPS) receiver provides navigation information to the GN&C system (see Table 9). The guidance system uses the navigation information along with the vehicle's equations of motion to make steering commands that will keep the vehicle on its nominal trajectory. The guidance computer carries out all of the guidance functions. The control system carries out the steering commands from the guidance computer. The main control actuator for the vehicle is the liquid injection thrust vector control system (LITVC). Cold gas thrusters (CGT) control roll in the top two stages of the vehicle. Both LITV and CGT are controlled by series of on/off valves connected to controller boards. The controller boards open the proper valves as directed by the guidance computer.

The primary duty of MINOTAUR's GN&C system is to get the payload safely into the desired orbit. The low altitude orbit of 200 Km places very tight requirements on the final burnout conditions. The system must also limit the aerodynamic loadings on the vehicle's structure while the vehicle is flying through the atmosphere. Failure of GN&C in meeting the requirements will insure loss of the vehicle and failure of the program.

## Navigation Sensors

A strapdown INS was chosen as the navigation sensor because it can be used as an attitude sensor as well as a position and velocity sensor. The INS selected is the H764-C3 GPS/INS built by Honeywell Inc. Space Systems Group. The system uses a GPS receiver to lower the overall system position and velocity errors. The system is based around Honeywell's GG1320 ring laser gyros.

Table 9 Navigation System Specifications

| Integrated GPS/INS       | Performance                   |
|--------------------------|-------------------------------|
| Position                 | 16 m                          |
| Velocity                 | 0.03 m/s rms                  |
| Pitch & Roll             | 0.01 Degrees rms              |
| Yaw                      | 0.02 Degrees rms              |
| Thermal Operating Range: | -54°C to 55°C passive cooling |
| Power Requirements:      | 65 W at 28 Vdc                |
| Weight:                  | 9.1 kg                        |

## Communications

The communications system includes consideration for ground-based tracking, downlink of telemetry, and uplink of commands.

The first requirement of the communications system is that commands from the ground be accepted onboard. It should be noted that there are no requirements for the spacecraft to accept commands post-launch (except for the destruct system which is separate). The spacecraft will be autonomous after launch. A subordinate requirement is that it must be possible to identify what commands have been received onboard the spacecraft.

The second communications requirement is that telemetry is downlinked so that in the event that there is a catastrophic launch failure, it will be possible to identify the cause of the failure. The communications system must be capable of communicating with Wallops Island (WFF) or Bermuda (BDA) regardless of spacecraft attitude if it is within line-of-sight of the station.

The third requirement is that sufficient tracking must be collected such that the spacecraft can be reacquired on the second pass of WFF. Tracking data will be collected by WFF and BDA. Ranging data from BDA will be available for 115 to 144 seconds after fourth stage burnout, which is sufficient to generate acquisition data for WFF 80 minutes later.

The fourth requirement is that the system must be compatible with the equipment at WFF. (BDA equipment is equivalent so that compatibility with WFF implies compatibility with BDA).

Commands to the spacecraft will be via an umbilical that disconnects at launch. Details of commands depend on details of procedures required to launch; however, they include tank fill and tank drain and launch commands that cannot be executed while personnel are within the launch area. Critical commands require one command to load the command and one command to execute the command after personnel have verified the command. In the interest of safety (a high mission objective), most, if not all, commands should be denoted as critical.

The downlink from the spacecraft will be via a NASA standard S-Band transponder, using 3 dipole antennas, a solid state amplifier, a data rate of 10 kbps, and will be frequency shift key (FSK) modulated. The use of a NASA standard transponder gives compatibility with WFF. Space-ground link system (SGLS) and Tracking and Data Relay Satellite System (TDRSS) S-Band antennas are not compatible with WFF and so cannot be used in communicating with WFF. The use of an omni antenna is to meet the requirement of spacecraft-to-ground communication regardless of spacecraft attitude. Clearly, this link is at its most important when the attitude is not as expected. The dipole antennas mount to the skin of the fourth stage, under a skin blemish which is integral with the antenna. The use of a solid state amplifier over Travelling Wave Tube Amplifier (TWTAs) is recommended by Wertz and Larson<sup>3</sup> (and others) at S-Band frequencies for rf power outputs below 30W. As analysis below shows, MINOTAUR will operate at a fraction of that power level. A data rate of 10 kbps is the current estimate for data volume requirements; however, D. Loveless recommended doubling the data rate to allow for growth and data encoding. In the link margin calculations, data rates of 10 and 20 kbps are shown. The use of fsk modulation is based on its simplicity and the fact that it is not susceptible to phase disturbances. Its chief disadvantage relative to other encoding methods is its poor use of the spectrum, but that is unimportant due to the low data rate.

The Launch Trajectory Acquisition System (LTAS) is a form of C-Band tracking used during launch support. It uses several C-Band antennas to form a single stream of inertial positions (i.e., instead of being angles, ranges, or Doppler shifts, it is x, y, z in Greenwich Rotating (GROT) coordinates). It is available from WFF and BDA. Additionally, S-Band ranging would be possible from WFF and BDA, with the maximum usefulness coming after fourth stage burnout.

## System Architecture

The computer system will serve as the "central nervous system" during MINOTAUR's testing and launch. Mission critical activities will be performed and monitored at all system levels of the rocket. The success of MINOTAUR is contingent on the development of a computer system capable of meeting all design requirements.

The design and development of the computer system began by defining the system operating requirements:

- The monitoring of equipment for purposes of collecting telemetry and ensuring the proper functioning of the equipment
- The capability of ground communication to receive commands prior to launch and downlink telemetry
- Computing guidance corrections and "instructing" the liquid injection thrust vector controllers
- Designing the system to be autonomous, thus requiring minimum ground support
- Designing for the highest achievable reliability.

These requirements were used as a baseline as well as a guideline for the development of MINOTAUR's computer system.

### Computer configuration

The configuration of the system is detailed in Figure 15. At the heart of the system is the Main Flight Computer. All the time-related functions will be operated from this central unit. It will activate the stage separation systems and will update the other processors when the separation occurs. It will also update the Guidance Computer as the center of gravity shifts with time. The engine start/shut-off systems will also be controlled by the Main Flight Computer.

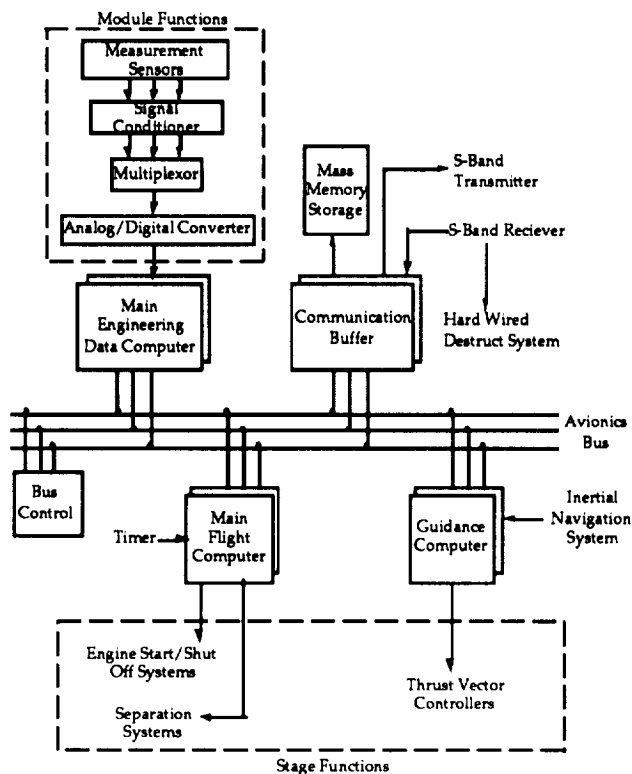


Fig. 15 Computer configuration

The Guidance Computer will receive data updates from the Inertial Navigation System (INS). It will use this data in conjunction with the updates from the Main Flight Computer to perform the guidance correction computations.

These corrections will be sent to the liquid injection thrust vector controllers for processing.

The Engineering Data Computer will collect the telemetry from each module and interstage connections. These values will be "validated" against predefined acceptable margins to ensure the proper functioning of the system being monitored. The sensors being utilized include thermocouples, strain gauges, pressure sensors, and flow meters.

### Hardware

Before the actual hardware items could be investigated, an estimate of the size and throughput of the computer system needed to be performed. The results are summarized in Table 10. This was based on the method outlined by James R. Wertz and Wiley J. Larson<sup>3</sup>. The analysis was based on a 10-Kbit telemetry data stream. The frequencies were selected based on the restrictions of the liquid injection valves. They could only operate at a rate of 10 Hz and this was used as the baseline for the estimate. This reveals an expected 340 Kwords of memory and a throughput rate of 930.4 thousand instructions per second (KIPS).

Table 10 Computer System Requirement

| Component               | Frequency (Hz) | Memory (K words) | Throughput (KIPS) |
|-------------------------|----------------|------------------|-------------------|
| Command Processing      | 10             | 5.0              | 7.0               |
| Telemetry Processing    | 1              | 3.5              | 0.3               |
| Kinematic Integration   | 10             | 2.2              | 15.0              |
| Error Determination     | 10             | 1.1              | 12.0              |
| Thrustor Control        | 10             | 1.0              | 6.0               |
| Orbit Propagation       | 1              | 17.0             | 20.0              |
| Complex Autonomy        | 10             | 25.0             | 20.0              |
| Fault Correction        | 10             | 12.0             | 10.0              |
| Application Total       |                | 66.8             | 90.3              |
| Executive               |                | 5.5              | 74.4              |
| Run Time Kernel         |                | 12.0             |                   |
| I/O Handlers            |                | 2.7              | 67.4              |
| BIT & Diagnostics       |                | 1.1              | 0.5               |
| Math Utilities          |                | 1.4              |                   |
| Subtotal: COTS          |                | 12.0             |                   |
| Subtotal: Non-COTS      |                | 10.7             | 142.3             |
| Operating System        |                | 22.7             | 142.3             |
| Ttl                     |                |                  |                   |
| Total                   |                | 90.8             | 232.6             |
| Uncertainty Requirement |                | 78.8             | 232.6             |
| On-Orbit Spare Computer |                | 169.6            | 465.2             |
| Requirement             |                | 239.2            | 930.4             |



## Electronic sensors

As one of the design requirements, the computer system is responsible for the monitoring of the equipment for purposes of collecting telemetry and ensuring the proper functioning of the systems. If a failure should occur, there must be adequate data to locate and identify the source of the failure. An important aspect of telemetry then is the placement of the sensors. Critical failure modes were identified and sensors were placed correspondingly. For improved reliability, sensors are dual redundant.

## Power budget

The first requirement of the system is to calculate power to the rocket for a total of 20 minutes, starting at T minus 6 minutes. This amount of time was chosen because it allowed for pre-launch separation of ground power and a test of on-board avionics system operation as well as extra time at the end of rocket burn for telemetry broadcasting and a safety margin. Table 11 shows MINOTAUR's power requirements.

## Batteries

The battery estimate was based on a power-time area integration which yielded estimates for the battery capacity required. The batteries were then rated at 70% efficiency for the purpose of providing a safety margin. Two batteries are

Table 11 Component power requirements

| Component                    | Power (W) | Voltage(V) |
|------------------------------|-----------|------------|
| INS                          | 68        | 28         |
| Communications               | 12        | 30         |
| CPU                          | 60        | 6          |
| Sensors                      | 20        | 9          |
| LITVC (96 @ 10W)             | 960       | 24         |
| Intertank valves (28 @ 30W)  | 840       | 6          |
| Roll Control (4 @ 10W)       | 40        | 24         |
| Igniter tanks (14 @ 10W)     | 140       | 24         |
| Igniter plugs (28 @ 25 W)    | 700       | 12         |
| Total                        | 2840      |            |
| Peak Power @ launch          |           |            |
| Avionics                     | 160       |            |
| LITVC(28 @ 10 W)             | 280       |            |
| Intertank valves (14 @ 30 W) | 420       |            |
| Igniter tanks (7 @ 10 W)     | 70        |            |
| Igniter plugs (14 @ 25 W)    | 350       |            |
| Total                        | 1280      |            |

required to avoid a possible power spike damaging the avionics. The required battery capacity was computed as 2.53 A\*hrs for the avionics battery and 2.63 A\*hrs for the propulsion system battery. The batteries were chosen to be sealed lead-acid batteries for three main reasons: (1) Nickel-Cadmium (Ni-Cd) batteries have hysteresis problems and

this limits the amount of discharge a battery can take – the lead acid batteries do not have the problem to this degree; (2) the Ni-Cd batteries as a rule cost about four to six times more than the lead acid batteries; and (3) excluding specially manufactured batteries, Ni-Cds use approximately eight times the number of cells, complicating the type and amount of electrical connections. The batteries finally chosen (from among the sealed lead-acid companies on the basis of cost) were PowerSonic batteries. The avionics battery consists of two 12-V and one 6-V cells rated at 3.0A\*hrs. The propulsion battery consists of two 12-V cells rated at 3.0A\*hrs.

## Testing

The primary launch requirements of this program are to have a suborbital launch in August 1993 followed by the integrated orbital launch in August 1995. To get to the orbital launch, a logical series of launches has been planned to test different aspects of MINOTAUR's design:

Late summer '93 Fourth Stage Sounding Rocket  
Rail-launched at 80 deg and 3.5 g's  
(Wallop's requirement)  
Fin stabilized  
\$20K

Winter '93-94 Module Sounding Rocket  
Rail-launched as above  
Thrust vector control (TVC)  
System technology demonstration  
\$200K

Summer '94 Top Stage & Module Sounding Rocket  
Vertical launch  
Separation system  
Flight termination system  
TVC  
System technology demonstration  
\$340K

Winter '94-95 Top Stage & 3 Module Sounding Rocket  
Ignition of multiple modules  
TVC on multiple modules  
300 kg payload capability  
Vertical launch  
Separation system  
System technology demonstration  
\$390K

Summer '95 Orbital vehicle  
\$1M

All of these launches will occur at the existing launch facilities at Wallops Island, Virginia. All production and testing are to be completed at existing and planned campus facilities. After further investigation of the testing requirements of this program, it was concluded that some aspects of testing could not be performed on campus (i.e. static test firings) due to the lack of campus facilities.

### University Facilities

Part of the problem of designing a launch vehicle to be constructed at a university location is the lack of available space. This is particularly true at the University of Maryland. Space is limited, but the design requirement to provide maximum student involvement dictates the need for producing a good portion of the launch vehicle on the campus.

Table 12 Production Facilities

| Facility                                    | Work to be done                 |
|---|---------------------------------|
| Space Systems Lab Neutral Buoyancy Facility | electronics and milling         |
| Aerospace Laboratory                        | system testing and construction |
| Glenn L. Martin Wind Tunnel                 | aerodynamics testing            |
| Vibrations Lab                              | vibration testing               |
| Composite Research Lab                      | fabrication of He tanks         |
| Manufacturing Building                      | system testing and checkout     |

Even with these buildings, the size of the modules restricts the available to a greater extent. During production, facilities management will become a crucial factor. The assumption made in this proposal for the use of campus space in the future is based on the notion that the MINOTAUR program will receive all the facility space that is requested.

The requirement to maximize student involvement in the design, production, and operations of the MINOTAUR launch vehicle is a key factor in the decision to use university facilities. Cost is probably even more important. A result of the diversity of the university is the wide range of assets at the design team's disposal. Items that are available include fabrication tools, assembly space, testing space, transportation, computer facilities, and the experience at hand in the professors of the university. Other items which are covered by using campus facilities include reliability, safety, and minimization of development time.

### Launch facilities

The primary requirement for the Wallops Island launch site is to provide a launch pad and use of existing service structure, tracking and data acquisition equipment, and safety and emergency equipment. The primary requirements for the University of Maryland at Wallops are to provide assembly and transportation equipment, all launch vehicle communications and control equipment, and all propellant fueling equipment. All necessary personnel for vehicle assembly and integration will be provided by the University of Maryland.

### Conclusion

As the complete report explains, with proper, though not excessive, funding, the University of Maryland's Aerospace Engineering Department has the capability to design and launch a low-cost launch vehicle. This launch vehicle will be completely designed and built by the university's students. Outside testing and manufacturing will be kept to a minimum to keep total costs low.

### Acknowledgments

The primary editor of this report was T. Rice. The co-editor was W. Vincent. MINOTAUR's preliminary design team consisted of the following nineteen people: P. Adams, L. Boyce, K. Dawson, P. Freeman, L. Gieseker, V. Gowda, A. Jarrah, P. Margoiles, M. Miller, S. Nassau, M. Priztlaff, D. Rabine, T. Rice, A. Shank, R. Snyder, W. Vincent, T. Willard, T. Wilson, and P. Wood. The design team would like to thank Dr. Dave Akin and Dr. Mark Lewis for their guidance and wisdom throughout the entire semester. Thanks are also sent to the USRA for its continued support of this program.

### References

1. Allen, Julian H. and Eggers, A.J., The Study of the Motion and Aerodynamic Heating of Ballistic Missiles Entering the Earth's Atmosphere at High Supersonic Speeds. NACA Report 1381, 1958.
2. Anderson, John D., Hypersonic and High Temperature Gas Dynamics. McGraw-Hill. New York, 1989.
3. Wertz, J. R. and Larson, W. J., Space Mission Analysis and Design, Kluwer Academic Publishers, Boston, MA, 1991.

## 1991-1992 WALKING ROBOT DESIGN

University of Maryland, College Park  
Departments of Electrical and Mechanical Engineering  
College Park, Maryland

Profesors Shapour Azarm, Wijesuriya Dayawansa, and Lung-Wen Tsai  
Jon Peritt, Teaching Assistant

### Abstract

The University of Maryland Walking Machine team designed and constructed a robot. This robot was completed in two phases with supervision and suggestions from three professors and one graduate teaching assistant. Bob was designed during the Fall Semester 1991, then machined, assembled, and debugged in the Spring Semester 1992. The project required a total of 4,300 student hours and cost under \$8,000. Mechanically, Bob was an exercise in optimization. The robot was designed to test several diverse aspects of robotic potential, including speed, agility, and stability, with simplicity and reliability holding equal importance. For speed and smooth walking motion, the footpath contained a long horizontal component; a vertical aspect was included to allow clearance of obstacles. These challenges were met with a leg design that utilized a unique multi-link mechanism which traveled a modified tear-drop footpath. The electrical requirements included motor, encoder, and voice control circuitry selection, manual controller manufacture, and creation of sensors for guidance. Further, there was also a need for selection of the computer, completion of a preliminary program, and testing of the robot.

### Introduction

The University of Maryland Walking Machine team designed, manufactured, assembled and analyzed a walking robot, "Bob Terpinator," as a prototype walking machine. Funding was mostly provided by a grant from USRA. Significant donations were also made by various other companies. Bob was designed to provide a means for land-based explorations without the limitations of "wheeled" transport vehicles. The long-term goal of the project was the production of a semi-autonomous walking machine able to navigate a broad range of terrain. The short-term goal was participation in the SAE Sixth Annual Robotic Walking Machine Decathlon which was designed to test many aspects of a walking machine's abilities. This provided the team with more specific design parameters to work from as well as a good test forum for Bob's capabilities.

For this competition, a walking machine was defined by its motion. It had to be "supported discontinuously and propelled by articulated mechanisms (legs)," and each leg was required to move with respect to the body and other

legs. The competition evaluates the viability of robot entries through ten events, hence the title "Decathlon." The events can be grouped in two categories and were chosen to test a diverse set of robotic abilities.

#### Manually Controlled

- Dash walking ability and speed
- U-Turn dimensions and confined space movement
- Slalom maneuverability
- Hockey precision of controls and ability to manipulate objects
- Obstacles agility over low obstacles
- Stairs agility over steep obstacles

#### Autonomous

- Dash tracking and "wheel alignment"
- Slalom accuracy under programmed control
- Sensors navigation using static external references
- Guidance response to dynamic, non-tethered control

In addition to these events, judges considered esthetics, structural integrity, safety, start-up procedure, and overall design.

The Walking Robot course was two semesters long with responsibilities divided to allow student participation in either one or both semesters. The seventeen students in the Fall Semester 1991 decided on a general design and then split into six groups (legs, body, controls, sensors, motors, and programming) to continue the evolution of specific aspects of the robot. Groups worked independently, and the entire class met for progress reports once a week. Many designs were considered and ruled out during this phase, and most calculations were completed. Groups from the first semester submitted final design recommendations, complete with assembly instructions, at the end of the term. Several students continued through Winter break, and thirteen students resumed organized work at the beginning of the Spring Semester 1992.

These students revised and completed earlier designs, manufactured parts, assembled Bob, evaluated performance, and solved problems. To accomplish this, the students divided into four groups with specific responsibilities. The Leg group handled leg design and drivetrain interface. The Body group's tasks included the chassis, drivetrain, bigfoot, and hockeystick assembly. The Electronics group interfaced the mechanical components with the programs and the user. This included motor, encoder, and voice control circuitry selection, manual controller manufacture, and creation of

sensors for the ninth event. The Programming group selected the computer, completed the preliminary program and devised ways to test it before the robot was completed. Once the robot was assembled, the entire team collaborated to solve the various problems that occurred.

### Evolution of Design

In designing the walking machine, "Bob Terpinator," the primary consideration was defining the leg mechanism. Once the method for propulsion had been determined, all other aspects of the robot were designed with leg parameters in mind. At the first meeting, the students decided the best approach was to evaluate successful University of Maryland entries from past competitions. After watching videos and discussing the positive and negative aspects of various machines, the group determined the following goals:

- i) the robot will participate in all ten events
- ii) the robot will not require significant reconfiguration for any event
- iii) the robot will utilize an independent turning mechanism
- iv) the robot will have a footpath that can be generated by a single motor

The first two goals expressed the spirit of the competition. In exploring new terrain or cleaning up hazardous waste, a machine would have to complete tasks similar to the events. Under such circumstances, complex reconfiguration would not be an option. The third and fourth goals define a general direction for a simple, practical design. It seemed that the most common mistake made in past years was to overestimate a program's ability to handle complex mechanical relationships. Simplicity was the watchword for the semester.

To participate in all events without reconfiguration, a versatile leg-path would be needed. For the events which tested walking motion and speed, the path required a long horizontal region to provide rapid forward motion. Events involving obstacles suggested a path with a substantial vertical component to allow clearance. Students considered many options and finally decided that a modified four-bar mechanism could be designed to meet these criteria. The final design produced a modified tear-drop walking path, similar to that of Maryland's 1991 entry. By adding a pantograph for amplification, a stride with an eleven-inch base and a maximum height of seven inches was achieved. After analyzing the torque curve for this path, the students decided to include springs to equalize torque. Designs for all other components revolved around these decisions. The following sections detail the student's progress throughout the design phase.

### Legs

The Leg group began designing Bob in the Fall of 1991. The final leg design was based on reliability and simplicity, two invaluable engineering concepts. Since the competition tested rather diverse robotic abilities, an additional practical constraint was the walking path, the curve that the legs would trace when going through one full revolution. Given these constraints, the leg group defined three objectives for a successful design:

- i) design two legs that could run 180 degrees out of phase
- ii) ensure separation of functions, including walking, turning, sensing, and manipulating
- iii) design mechanism with three degrees of freedom for propulsion, elevation and rotation

With these objectives in mind, the original leg design consisted of a set of "L" shaped or inverted "T" legs. This satisfied the original constraints and objectives; it was simple, reliable, and followed the desired walking path. It also allowed independent rotation control of each leg, which the group felt was important.

Although this design seemed useful, like all designs it had to be analyzed, reviewed and revised. First, the group considered whether the legs could support the robot during all points of the walking path. They discovered that the peak torque requirements with this design would be too high for the driving motor. At this point, the most important design decisions in the entire design process were made. They separated the legs into two sets of two, and chose to drive these sets independently with separate motors. This provided lateral stability while maintaining reduced support torques. The drawback, however, was the increased complexity. This was addressed by combining parts of the four-bar linkage and the pantograph. This design came after the strengths and weaknesses of many others were considered.

After these important decisions were made, the design had to be finalized, which included design of the four-bar hybrid with an amplifying pantograph, and evaluation of driving torque requirements. A detailed analysis with kinematic and stress calculations for each link ensured proper interface with the robot and no internal motion conflicts.

The walking path was the single largest consideration in determining the final leg configuration. The four-bar linkage provided the desired walking path without requiring any leg alterations during the competition (see Figure 1). However, to create the desired walking path, one that was flat on the bottom for walking and high enough to clear all the obstacles in the competition, the four-bar linkage would need to be enormous. This problem was solved with a pantograph which amplified the motion of the basic four-bar

mechanism and made it useful for a robot with Bob's dimensions (Figure 2). However, the number of links for the two systems led to very heavy leg systems and increased complexity. To reduce the weight and complexity, redundant links were removed producing the hybrid four-bar of Figure 3.

When the four-bar linkage and the pantograph were finalized, the torque profile of the walking path and the stresses in the links were calculated. The peak torques in the walking path occurred where the robot made the transition from the flat "walking" section of the path into the "lifting" section. This peak torque provided the information for sizing the motor. One option for reducing the peak torque requirement, discussed later, was the use of springs.

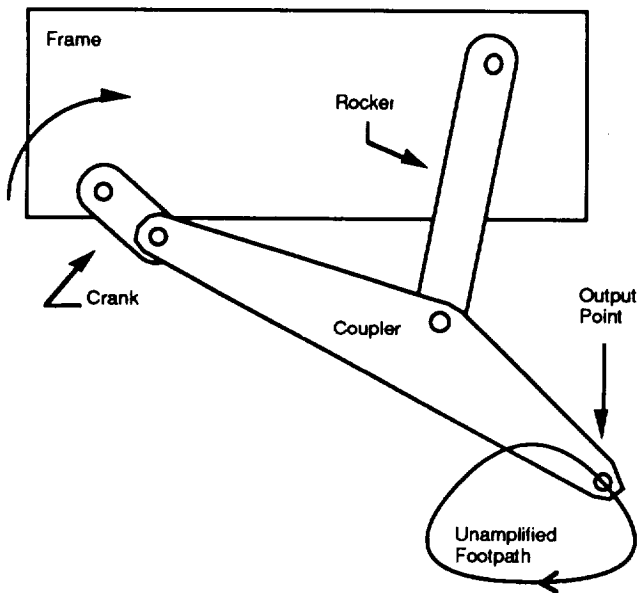


Fig. 1 Leg

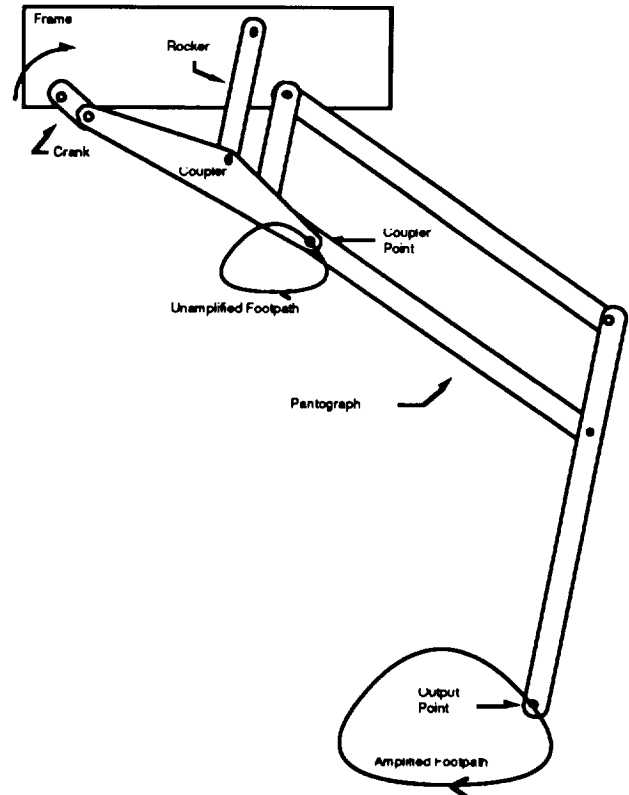


Fig. 2 Leg

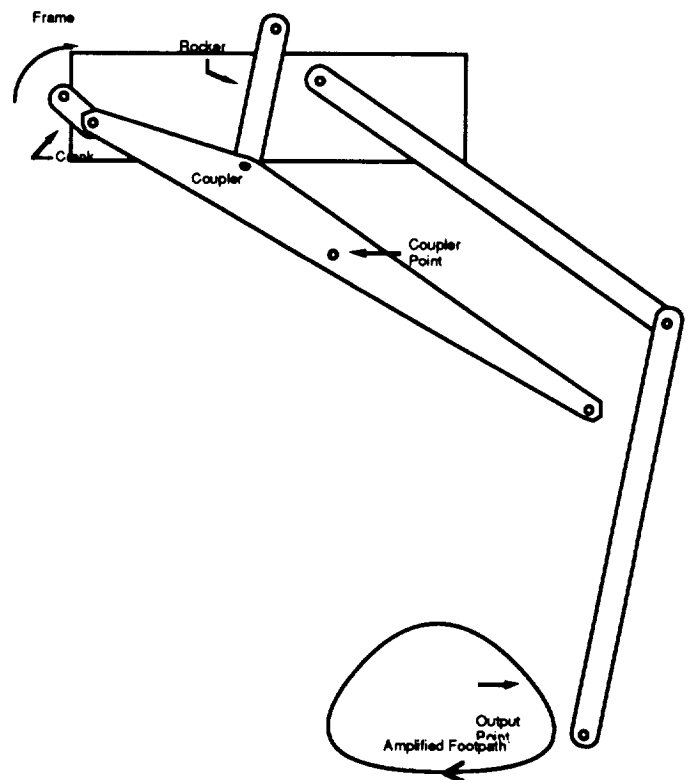


Fig. 3 Leg

Next, the shear and bending stresses in the parts were determined using the following equations:

$$s = Mc/I$$

$$t = VQ/(It)$$

where  $s$  is the normal stress due to bending and  $t$  is the shear stress.

After the stress analysis was performed, the group determined that the links with the lowest factors of safety were 2 and 5 (see Figure 2). This prompted investigation of possible buckling in the links due to the length/width ratio of the members. Buckling in the members was checked using the following equation:

$$C_c = [2(p)E/sy](1/2) = 75$$

where  $E$  is the modulus of elasticity, which happens to be ten million psi for 6061-T6 Aluminum,  $sy$  is the yield stress of the Aluminum, and  $C_c$  is the so-called "critical slenderness ratio."

In links 2 and 5 the slenderness ratio was found using the following equation:

$$C = KL/t$$

where  $K$  depends on the mode of buckling,  $L$  is the length of the link, and  $t$  is the thickness of the link.

Values of 108 and 144 were calculated for links 2 and 5, respectively. This implied that the links did, in fact, yield elastically. Since this was the case, the critical buckling stress was found using the following equation:

$$s_c = p2E/C2.$$

This revealed factors of safety in buckling of 4.4 for link 2 and 1.6 for link 5. At this point, the detailed analysis was complete, and although the factor of safety for link 5 was relatively low, the design was final.

## Body

The Body group was responsible for integrating the control circuitry, batteries, motors, legs, and accessories into a coherent design that would function under all the conditions of the competition. As such, the design depended heavily upon the specific parameters of the leg mechanisms and control hardware. It became a matter of balancing simplicity, performance, weight, esthetics, and cost.

The frame and bodypan design and construction were challenging problems. The torque generated by the footpath

meant strength was essential; however, weight was an important consideration. The group decided to use an external frame of two 32" side members, connected together by two 21" crossmembers at their ends. Each of the frame components was constructed from 2" x 2" x 1/8" tubular 6061-T6 aluminum beams. Plates of 1/4" aluminum were attached to the top and bottom of the frame. A 2" x 5/8" x 20" prismatic delrin shaft was sandwiched between the plates for added stability. This created an effective, lightweight I-beam. In order to control the outside leg set, one of the motors had to be at a higher level than the other. Each motor was attached to the I-beam, one on the top, the other on the bottom (see Figure 4).

Torsion of the motors was another problem. Two solutions were used for strengthening against the torsional effects at the motors. One was to use the motor itself as a lever arm, and then clamp it at a point away from the gear train. Another solution was to stiffen the I-beam with offset compression/tension bolts. These were simply constructed with 1/2" aluminum tubing and 1/4" bolts.

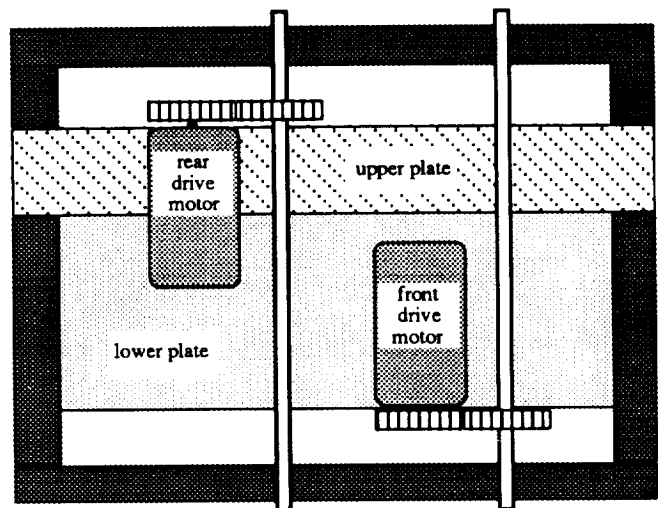


Fig. 4 Body

The transfer of power from the motors was accomplished through 1045 carbon steel rods. The 3/4" face width gears were keyed and held axially with set screws. The ratio of the gears from the motor to the shaft is 2 to 1. The end resulting torque is transferred to the four-bar mechanism through an aluminum link that is keyed and set with a screw. The encoders for the legs were set with a gear ratio of 1 to 1 with respect to the main drive motors.

The central turning mechanism, "bigfoot," was simple in design. There were two main components for the structure of bigfoot. The main structure is a PVC pipe held in compression with a 5/8" all-thread rod. The threaded rod is

centered in two thrust bearings. The foot components rotate about the shaft, motor, and body of the walking machine. When the body is supported by the bigfoot, the machine rotates. The second component of bigfoot was the foot: consisting of the foot shafts and the hockeystick. This integrated design reduced the total number of degrees of freedom required to control the machine.

Since the robot only turns when bigfoot is stationary with respect to the ground, attaching the hockeystick to bigfoot allowed the operator to turn the robot without concern for the motion of the puck. By positioning the hockeystick so that the puck remains at the center of bigfoot's turning radius, the robot can settle onto bigfoot, turn and stand, without moving the puck. The user can reposition the hockeystick behind the puck by turning bigfoot, also without moving the puck. The robot then moves forward and drags the puck with it. The hockeystick was designed with linear bearings and delrin rods to compensate for the vertical "bob" of the robot's forward motion. The rods move up and down freely as the robot navigates the course. The blade of the stick was made from transparent acrylic for visibility.

Electronic components were housed in a 30 x 12 x 7-inch box made from 1/16-inch aluminum and attached to the bottom of the lower plate. Rechargeable batteries are held in place with velcro. The computer components needed extra protection from jarring, so a container with cushioning was designed to the specific dimensions of the computer boards. This was bolted to the bottom of the components box. An external disk drive was also mounted directly to the side of the box. Extra room was provided for wiring, amps, and the power supply.

## Controls

All of Bob's motions are provided by three motors: one for each of two leg sets (walking) and one for bigfoot (turning). To control the motors, a closed-loop servo motor system consisting of a PID controller card, a motor drive amplifier with a power source, and three incremental encoders was needed. A closed-loop system (with encoders to report on motor position and velocity) has the advantage over an open-loop system (stepper motors) in that it can compensate for gear slippage and manual positioning of the legs. The controller card is a three-axis controller with an internal processor that is used to compute complex positioning and velocity profiles. It controls each of the three motors independently and simultaneously by sending analog signals to the amplifiers. The motors run at speeds proportional to the amplifier voltages and generate torques that are proportional to the currents. The encoders, which are attached to each motor shaft, convert the rotation of the motor into two square wave signals that are 90 degrees out of phase (quadrature output). These signals are then fed back

to the controller card to calculate the direction and speed of the motor. Decisions for each component of the system were made by evaluating efficiency, cost and reliability.

The first task of the fall semester Controller group was selection of the motors. They had to meet the following requirements which were specified by the Leg and Body groups:

|                                       |            |
|---------------------------------------|------------|
| Leg motor requirements (at load):     |            |
| Maximum Continuous Torque             | 200 lb-in  |
| Intermittent Peak Torque              | 400 lb-in  |
| Speed                                 | 30-50 RPM  |
| Direction                             | Reversible |
| Bigfoot motor requirements (at load): |            |
| Maximum Continuous Torque             | 40 oz-in   |
| Speed                                 | 1-10 RPM   |
| Direction                             | Reversible |

The controller must interface with the computer, amplifiers, and encoders. Model 5638 from Technology 80, Inc. is a closed-loop servo controller that uses an LM628 Precision Motor Controller IC from National Semiconductors. It was chosen because of its accuracy, reliability, and adaptability. Conveniently, the controller card is designed to plug directly into one of the expansion slots of an XT Compatible computer and sends commands via the I/O lines. Each axis on the controller card connects to the amplifiers through a 40-pin connector and uses a 34-pin connector to interface with the incremental encoders.

The mechanical position of the robot is controlled using indexed quadrature encoders for each leg. Model 755A by Encoder Products Company was chosen because of its size, high precision, low cost, and rugged structure. The quadrature encoder generates two square signals that are 90 degrees out of phase as well as an index that occurs once per revolution. The controller card decodes the signals to interpret the direction and speed.

An amplifier that closely matches leg set requirements is Model 6410-2 from Technology 80, Inc. It was chosen because it can be run from a single supply in the forward and backward directions. The amplifier for the bigfoot motor had to be able to handle 1-2 Amps of current. A Power Amplifier by National Semiconductors, the LM12, was chosen.

There are three methods for providing user control. The first is the computer interface. The method developed minimizes the number of commands and takes advantage of the 5 input pins of the parallel port of the XT 8088 computer. Commands are input to the computer through a 16-button keypad. The 16 keys are encoded into four bits by using a 74LS138 priority encoder; the fifth bit is used as an enable bit to check that a new key was pressed. The CPU constantly polls the parallel port looking for a key press, then starts the appropriate command.

A backup method to control the motors was implemented. As a safety precaution, a manual control was designed to override the computer if complications or failures arose. A switch on the main control box activates six relays that in turn bypass the CPU and place the op-amps into manual mode. In this mode, a joystick is used to control each leg, and a resistor network is used to control bigfoot. Each of these components produce  $\pm 10V$  outputs, which mimic the signals provided by the controller card.

To facilitate event ten, the robot responds to six commands given by voice. The design uses a VCP200 voice recognition chip from Voice Control Products, Inc. It receives a quasi-digital signal as an audio input from an LM324 op-amp and decodes the signal into digital logic levels which are then fed into another 74LS138 priority encoder like the one used by the keypad.

There was only one more item for the controls group to handle. Event nine called for sensors to read the external environment. Up to five beacons could be placed outside the contest area. The sensors could be either active (producing the signal which they then detect) or passive (simply reading signals produced by external sources). Passive sensors were chosen because they are slightly easier to build than active ones. It was decided that they would respond to light sources because light detectors were readily available and light sources are cheap.

The sensor design went through several stages. It called for two light detectors attached to arms which swept back and forth. As the arms swept through their motions, the detectors would produce logic level signals when light was seen. By measuring the angles of the arms at the points where light was detected and using geometry, the distance and angle to the light could be calculated. A three-bar mechanism would be used to produce the sweeping motion of the arms. Unfortunately, arms which sweep back and forth do not have a direct angular relationship with their drive motor. In order to measure the angle to the light source, an encoder would be mounted on the drive motor and a microprocessor would be used to keep track of the motor's angular velocity and the time to reach the measured angle. Alternatively, an encoder could be used at the pivot point of one of the arms.

The second method is preferred for its simplicity; however, since motors with built-in encoders were available from a previous year's walking robot, the first method was suggested. Unfortunately this method led to a complicated interface card and extra programming.

An alternative method, which uses a turntable with a light detector offset from the center (a top view of the new sensors is shown in Figure 5), was developed. The turning sensor has a direct relationship with its drive motor. As the sensor turns, the motor's encoder is used to clock a binary

counter. When a light source is detected, a logic level signal is produced which latches the count into buffers. The CPU can then poll the buffers and read the angle to the light. Again geometry is used to calculate distance and angle to the light; however, this time the calculations and results are slightly more straight forward. One problem with this method is getting power to — and receiving signals from — the detectors on a rotating turntable. A commutator could have been used (a circular trace with spring contacts), but commutators are very noisy and might have introduced errors in the signals. Instead, an onboard power supply and relay LEDs were used.

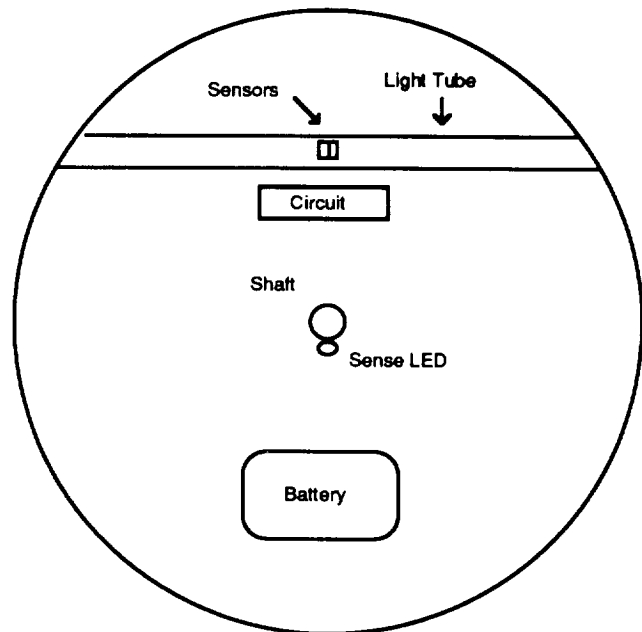


Fig. 5 Controls



## Programming

During the Fall semester, the class determined that Bob needed a computer for controlling the unique footpath. The essential components for Bob's brain were selected, ordered, and received. An uncomplicated motherboard, a disk drive, a disk drive controller card, and a video monitor card with a parallel port were necessary for efficient operation of the robot. For developmental purposes, a keyboard and monitor were borrowed from the University's facilities. The group used an IBM XT motherboard (8088 microprocessor), a 3.5", 1.44M high density floppy drive, a disk drive controller card, and a monochrome video driver card with printer port. These items were ordered and received at the end of the fall term 1991.

## Manufacture and Assembly

The Spring semester 1992 was devoted to finalizing designs, machining and ordering components, assembling the robot, and solving problems. Through most of the semester, students worked in four groups and reported progress at weekly meetings. Three weeks before competition, Bob was largely assembled, and students worked more closely together to evaluate Bob's performance and to solve problems.

## Legs

The leg group had one design which needed further optimization, the "sandwich" joints. As designed, the joints would not adequately transmit the driving torque necessary to power the robot. Optimizing the design required reviewing bearing selection to ensure the bearings could transmit the necessary torque and still provide the lateral support needed to stabilize the robot. Many possibilities were considered, including needle bearings, journal bearings, roller bearings, and ball bearings. The criteria for the final decision were: the bearings' ability to transmit torque under stress, their durability under shock and repeated loading, their size, and their cost. Having designed the links, finding the proper bearing became a much more challenging task than originally assumed. The final constraints listed, size and price, turned out to be the most difficult to deal with. This led the group to a close examination of several types of bearings including the needle and journal type. Needle type bearings were ruled out for several reasons. Needle bearings use the shaft that is rotating as their inner race, or inner rotating surface. The group was concerned about the bearings' ability to function under axial thrust and angular misalignment, particularly in conjunction with each other. Also, needle bearings would be difficult to mount, and replacement might be necessary. The journal bearings seemed to be a good selection due to their mechanical simplicity; however, eventually they were rejected because of their inability to transmit torque effectively under angular

misalignment. Ultimately, roller bearings suited our application most closely with their ability to transmit torque under axial misalignment and axial thrust, and the available sizes, but their cost was prohibitive. In this regard we were very fortunate to receive a contribution from the Torrington Company; they donated all the Fafnir bearings that we needed. This contribution allowed the group to move closer to completing the design.

The final concern in the design of the legs was the interface with the robot. The joint that connects two legs to the robot frame was critical. Originally, the proposal was to use artificially aged aluminum as in the rest of the robot. Based on calculations made by the group, aluminum would not withstand the bending stress inherent in the "shoulder plates." The group investigated other materials, including stainless steel and various types of hardened and unhardened carbon steel. Stainless steel did not have the requisite strength. Hardened steel had an overabundance of strength for the bending stresses, but it is difficult to machine. From a manufacturing perspective it was unacceptable. This led the group to the final decision, 1018 steel, which had the strength and manufacturing characteristics that the group desired. This decision completed the design from a manufacturing standpoint.

After finalizing the design, the group began manufacturing the pieces. The first plan was to machine the pieces manually. However, although the leg components seemed simple, time and tolerance requirements made this unfeasible. Since the legs included two sets of connected leg-pairs with a pantograph, the group decided that identical reproduction of parts was critical. If they were out of tolerance, the components of the connected leg-pairs would be subjected to a pre-stress from incompatibility with one another.

Moreover, the bearings required a very close tolerance in their mounting holes to function properly. The group was concerned about students' abilities to adhere consistently to these tolerances; therefore, the decision was made to have most of the leg components machined on a computer numerically controlled (cnc) milling machine. This provided a short machining time, identical reproduction of parts, and the ability to store the programming for modification if necessary. On campus at the University of Maryland there is a cnc machine shop run by one of the professors. The group contracted with this shop to manufacture all of the moving pieces in the leg. We provided the shop with all the necessary raw material and bearings for sizing the holes. They built a prototype leg set to insure proper function. The advantage of cnc machining became clear at this point. If the pieces were not properly designed, the programming could have been altered to suit the group's needs relatively simply; if there were no modifications, the remaining pieces could be made very quickly since the programming was already done.

The "foot" was the one piece of the leg manually machined by the group. It consisted of a one inch by one inch aluminum tube with holes drilled. These were for placement of rubber bumpers ("toes") which the robot rests upon and allowed adjustment for different positions.

After verifying that the mechanism did, in fact, function properly, including all joints and connections, the remaining pieces were ordered from the machine shop. After obtaining all the pieces from the machine shop, assembly began. Pins for the joints were pressed into the center links, and all the bearings were press-fit into the "sandwich" links. When the links were together, washers were included between them to guarantee proper spacing. The feet were then connected to the links, and finally the entire mechanism was attached to Bob's body. During final assembly, shims were added at each joint to reduce the robot's lateral movement as much as possible. These shims were placed between the bearing and stop ring on the connecting pin at each joint.

The connecting pins that ran through the joints were press-fit into the center piece and had grooves machined into them at the ends to hold the retaining ring. These pins were made of precision ground stainless steel—an expensive material, but one that ensured that the pins would interface optimally with the bearings. Any interference could cause growth of the inner race which would affect the bearings' rolling motion and ultimately lead to alignment problems.

The drive shaft, connected to the driving link (link 1), needed to be fastened securely. The group proposed keying the shaft and link and using a set screw. The Leg group worked closely with the Body group, who was in charge of the drive shafts, to make certain that these parts would match. Finally, the toe placement on the foot needed to be optimized. This task was addressed by the leg group by leaving many holes at various spacings to allow for a suitable combination for the competition.

## **Body**

The Body group decided to have students machine most parts. Based on designs from the first semester, materials were ordered, and the parts for the frame and body pan were machined. For ease of assembly, all nuts and bolts were 1/4 inch in diameter. As more weight was added to Bob, it became clear that extra support for the bodypan would be necessary, so an angle bar was added underneath the bottom plate. Aluminum adapter plates were attached to the face of the motors for encoder placement.

Because of time constraints, the group decided to use the bigfoot apparatus from the 1990 robot. Since the design for this semester had been based on that model of bigfoot, only minor modifications were necessary. It was attached to the lower plate of the body as described in the design. Brackets for the hockeystick were mounted to the feet, and the

hockeystick was added. Holes were drilled into the delrin rods and pins were inserted to keep the hockeystick up out of the way during events that did not involve it.

The drivetrain was machined and assembled without deviating from the design. Careful attention was given to dimensions to be sure leg placement would be within specified tolerances.

## **Controls**

As problems arose, it became apparent that a backup power supply might be necessary. Using an LM12 Power Amplifier, a system was built that can supply up to 15 Amps of current. The disadvantage of the design is the requirement of two supplies. Since the robot would run in reverse only for short periods of time, the Negative supply was reduced from -24V to -12V to minimize the weight of the batteries.

An amplifier using  $\pm 12V$  supplies was built using the design from last semester with minor modifications. This amplifier takes  $\pm 10V$  input from the controller and runs it through an LM12 power op-amp. The anticipated current was less than 3 Amps.

The voice controller design from the previous semester enabled the robot to recognize various commands given by voice. Modifications were made on the original design to minimize the sensitivity at the input of the VCP200 chip. From the updated design, resistor values were changed on the LM324 to allow the audio input to the VCP200 to accept only commands of sufficient strength. With these modifications, the robot would respond to six commands accurately in a relatively noisy environment. To ease connection of the voice control circuit to the computer, the output of the VCP200 was fed into an 8 x 3 encoder similar to that used by the Keypad unit. This provided a modular control input design: to switch from manual control to voice control, one simply has to unplug the hand unit and plug in the voice control unit.

During construction of the sensors many different techniques were used. The circular sensor disk was made out of double-sided copper-clad board with the light detection circuit etched directly on it. The technique known as "board scratching" was used instead of photo-plotting. Scratching is an alternative method to silk-screened boards drawn with CAD/CAM software and then etched in an acid bath. The circuit schematic was drawn using a schematic program. A file containing circuit point-to-point connections was produced. This file was then fed into a board layout program which was used to draw the traces and pads to be routed on the copper-clad board. At this point the circuit would normally be silk-screened to the copper board. Instead, the drawing was sent to a third program which controls a milling machine. The machine moved a milling bit over the copper-clad board, etching traces as it went. Scratching

the board was more convenient because results were immediate and changes could be made easily. This process produced a very professional looking board which was easy to work with. The second technique used was wire wrapping. The sensors interface circuit was built on a pc proto-board. Instead of soldering wires point-to-point, wire wrap sockets were soldered to the board, wires were wrapped between pins to be connected, and chips were placed. This allowed for easy correction of mistakes.

After the sensor board was populated and debugged, the shaft and driven gear were attached. The sensor motor mount was then machined; the bearings and the motor with drive gear were mounted. Next, this whole assembly was attached to the front of the robot. Even though the light tubes prevented any light from reaching the photo sensors from any direction but the ends, the sensor board was covered to ensure further no extraneous readings would be made. This produced a very clean, wafer-like disk. The disk was mounted in its bearings and a clip was attached to keep it from jostling as Bob walked. Finally, a light-blocking cover was built and mounted to control the sensor field of view.

## Programming

During the semester, the programming group faced the tasks of assembling and testing the computer parts ordered last semester and creating software capable of controlling the robot during all the events. The hardware and software development decisions were based on balancing the costs with the needs of the robot design. Most of the hardware decisions and purchases were completed in the Fall term 1991 and have previously been described. Additions to the original hardware design included a portable power supply for the computer, an audio speaker, and an LED power indicator. The software decisions made during the Spring term 1992 consisted of selecting a programming language, interfacing with the controller software, and developing the final version of the robot's software.

Hardware development began this semester with the assembly of the computer components. The following computer components were assembled and tested: an IBM XT motherboard (8088 microprocessor), a 3 1/2" disk drive, a disk drive controller board, a monochrome video card with printer port, and the 5638 Servo Motor Controller board. An LED power indicator was attached to the motherboard to indicate whether the power was activated. A speaker was also attached to the hardware so that music could be played to identify the different routines Bob entered during competition. The music was also added to improve the competitive nature of the robot.

The portable power supply was designed to provide power to the computer during competition. The supply was designed for four different voltage levels,  $\pm 5$  VDC and  $\pm 12$  VDC. Two 12-Volt batteries provided the voltage for the

power supply. This eliminated the need for any type of rectification and ripple filtration. The power supply consisted of four separate power conditioning units combined on a common PC board. In order to maintain the required voltage levels to within  $\pm 5.0\%$ , LM78xx and LM79xx series voltage regulators were used. Over-current protection is provided at the input of each of the four regulators by having a resistor in series with the input and a power transistor in parallel with the resistor. If the voltage across the resistor exceeds a predefined limit, the transistor is turned on, and current is shunted into the input of the voltage regulator. The regulator is then driven into thermal overload, effectively shutting down the entire circuit.

Once the 5638 Controller board was received and installed into the motherboard, post-installation testing was conducted to verify controller function. The test software that was received with the controller was run, and accurate operation was verified. Three small motors were attached to the controller board in order to simulate the three actual motors that would be used on the robot.

Various programming languages were explored for the software development. Several test routines were written in Microsoft C, Assembly, and Microsoft Quick Basic. Microsoft Quick Basic was determined to be the most capable, efficient, and uncomplicated language available. It possessed the necessary capabilities that were required such as:

- i) parallel port input/output ability
- ii) adequate running speed
- iii) compatibility with the available controller board routines

The necessary functions and motions of the robot were evaluated to determine what should be included within the software routines. The following are the functions that were selected for control over the robot from the hand-held control panel:

- 1) Stop
- 2) Home Position
- 3) All Legs Down
- 4) Bigfoot Right 45 degrees
- 5) Bigfoot Left 45 degrees
- 6) Bigfoot Right 10 degrees
- 7) Bigfoot Left 10 degrees
- 8) Bigfoot Down
- 9) Legs Forward 10 degrees
- 10) Legs Backward 10 degrees
- 11) Hop Forward
- 12) Hop Backward
- 13) Walk Forward—Slow, Med, Fast
- 14) Walk Backward—Slow, Med, Fast
- 15) Stairs
- 16) Autonomous Events – Slalom, Dash, Beacon

The Stop function immediately stops all motors on the robot. The Home function brings the robot into a standard position with one set of legs all the way at the top and one set of legs completely down. The All Legs Down function brings all four legs of the robot into their lower most point so that they are all resting on the ground.

The Bigfoot Right and Left functions turn bigfoot to the right or to the left by the number of degrees indicated. This allows bigfoot to be used for turning the robot and for rotating the hockey stick during the hockey stick event. Bigfoot Down lifts the walking legs of the robot in preparation for turning; this lowers the robot so that it rests on bigfoot.

The Legs Forward and Backward 10 degrees functions move the highest set of legs forward or backward by 10 degrees. This is useful during the obstacle course in order to tap the top of the obstacle. Hop Forward and Hop Backward are used for fine adjustments while setting up for the events. They move the robot a small amount forward or backward.

The Walk Forward and Walk Backward functions are used for any walking that the robot does. Three speeds of walking are available: slow, medium, and fast. The Stairs function is an automated stairs climbing routine to be used during the stairs climbing event. Autonomous Events are run completely without human interference and consist of the Slalom, Dash, and Beacon competitions.

The individual routines for all the above functions were written and debugged first with the small motors and then with the actual robot for fine tuning purposes.

### Performance Evaluation

Robot assembly was completed two weeks before the competition. Upon testing, various problems arose in the following: (1) high motor torque requirement, (2) overheating of electronics, (3) programming algorithms, and (4) misjudgment of time.

The high motor torque requirement was attributed to drivetrain friction. The weight of the robot was higher than expected which increased motor deflection, causing the gears to mesh poorly. This problem was diminished by rigidly securing the drive motors to the body.

The high torque requirement demanded more current to drive the motors, thereby overheating the amplifiers. A booster was added to increase the current output from  $\pm 10$  volts to  $\pm 14$  volts. In addition, a fan was added to cool the components. Even with these changes, the torque produced when the computer and batteries were placed on-board was

too much. The power op-amps were overloaded several times.

The leg motion consisted of a propelling phase (bottom of footpath) and a return phase (top of footpath). The return phase was faster than anticipated, while the propelling phase was slower. The result was a stomping walk. Compensation was made by adjusting the algorithm timing.

Most of the students overestimated their abilities and/or underestimated the time needed to complete a task. As a result, the robot was still being worked on through the competition. Needless to say, Bob did not perform in many events. He did, however, do a wonderful stomp/lurch walk for event one (the "dash").

A further result of the rush to make Bob work was the decision not to worry about specialized events. There was no pretesting of the hockey stick nor the sensors. The hockey stick was a flawless design and in all likely scenarios would have performed marvelously. At least the test models worked without a hitch. The sensors did respond to the beacons and it was clear that the angle counting was working. However, an integrated test was never performed, so the accuracy was never tested. Nor could an evaluation be made of their performance during the distinctive walking motion which earned Bob his name.

### Conclusion

The class was by no means a loss. Even though the competition did not go as planned, it was still a terrific learning experience for the students. They learned what it was like to work as an integrated team. They found out the group dynamics of a large volume of people that got twenty hours of sleep between them. And most importantly, they learned many new skills and techniques which they will be able to take to prospective employers. Some of the more valuable skills include:

- modern techniques of design and manufacture
- better estimates of abilities and requirements
- better social skills as they apply to the work place
- improved time management and organizational abilities

Even though Bob did not walk, he was not a failure. He utilized a clever walking motion which integrated vertical travel as well as horizontal clearance. This was accomplished using a very unique and innovative mechanism. The footpath was designed to accommodate rather tall obstacles while still providing a long stride. This meant further coverage during each step. Bob had the best hockey stick design at the competition. While his hockey stick was designed to work with his walking motion, other robots had hockey sticks which looked like afterthoughts. They were invariably attached to the front of

the machines and would lose contact with the pucks as the machines turned. This meant that the other robots would have to be backed up and repositioned behind the puck again.

While all of the other robots had been designed to compete in most events, Bob was the only one designed to compete in every event. The mechanical and programming designs accomplished this. Even the electrical designs would have sufficed had more leeway been given to errors in torque and current requirements for the motors.

But this is not the end for Bob. In all likelihood, next year's class will use the same leg mechanism. This will give them a definite advantage. The legs were the most time costly aspect of the robot. Having them already designed with only a need for refinement will leave more time for debugging and refining other aspects. This should produce a better robot which has already been put through its paces and give time for operator practice.

**PROJECT COLUMBIAD**  
*Reestablishment of Human Presence on the Moon*

**Massachusetts Institute of Technology**  
**Department of Aeronautics and Astronautics**  
**Cambridge, MA**

**Professor Joseph Shea**  
**Professor Stanley Weiss**  
**Professor Harold Alexander**  
**Professor Peter Belobaba**  
**Greg Loboda, Teaching Assistant**

**Maresi Berry**  
**Mark Bower**  
**Charles Bruen**  
**Patrick Cazeau**  
**Michael Clarke**  
**Scot Cook**  
**Johan Denecke**  
**Joseph E. Dennis**  
**Kathryn Fricks**  
**Henri Fuhrmann**

**Suzanne Garber**  
**Debabrata Ghosh**  
**John Goetz**  
**James Haughwout**  
**Beth Kader**  
**Lawrence Kaye**  
**Jonathan Kossuth**  
**Erik Larson**  
**Celia Liu**  
**Alou Macalou**

**Patrick Malone**  
**Jacqueline Moore**  
**George Nagy**  
**Aaron Newman**  
**Michael O'Connor**  
**Jose Ortiz**  
**Victor Owour**  
**Charles Roburn**  
**Paul Stach**  
**Jon Strizzi**

**Paul Tompkins**  
**Ralph Vixama**  
**Edward Walters**  
**Ben Weintraub**  
**John Woyak**  
**Jean Yoshii**  
**Jane Yu**

### **Abstract**

In response to the Report of the Advisory Committee on the future of the U.S. Space Program and a request from NASA's Exploration Office, the MIT Hunsaker Aerospace Corporation (HAC) conducted a feasibility study, known as Project Columbiad, on reestablishing human presence on the Moon before the year 2000. The mission criteria established were to transport a four person crew to the lunar surface at any latitude and back to Earth with a 14-28 day stay on the lunar surface. Safety followed by cost of the Columbiad Mission were the top level priorities of HAC. The resulting design has a precursor mission that emplaces the required surface payloads before the piloted mission arrives. Both the precursor and piloted missions require two National Launch System (NLS) launches. Both the precursor and piloted mission have an Earth orbit rendezvous (EOR) with a direct transit to the Moon post-EOR. The piloted mission returns to Earth via a direct transit. Included among the surface payloads preemplaced are a habitat, solar power plant (including fuel cells for the lunar night), lunar rover, and mechanisms used to cover the habitat with regolith (lunar soil) in order to protect the crew members from severe solar flare radiation.

### **Executive Summary**

In 1990, the Report of the Advisory Committee on the future of the U.S. Space Program proposed a plan known as Mission from Planet Earth which included the establishment of a lunar exploration base. Under the direction of NASA's

Exploration Office, the MIT Hunsaker Aerospace Corporation performed a feasibility study on the reestablishment of human presence on the Moon before the end of the decade. The project became known as Project Columbiad, named after the fictional cannon in Jules Verne's From the Earth to the Moon.

The primary objectives of Project Columbiad were to transport a four person crew to the lunar surface and back with a 28-day stay on the lunar surface. Project Columbiad was also designed to have the capacity to land at any latitude on the lunar surface and be able to abort at any time -- meaning within the next lunar launch window. Other goals of the mission were to provide the foundation for the aforementioned future lunar exploration base and in the meantime to provide an opportunity for preliminary lunar exploration and scientific research. Still other goals of a high profile mission such as this are to boost national confidence and at the same time to promote international cooperation.

Safety of the crew members was always the primary concern during the design of the mission. Redundancy standards for the mission were set at two levels for mission success and three levels for crew safety. High levels of subsystem reliability were achieved through the use of proven technologies. Results of the initial studies indicate an expected human survivability probability of 99.7%. It is expected that in the next design iteration of Project Columbiad, this probability will reach the targeted 99.9%. At this stage in the design the overall mission probability of

success reached the targeted 95% probability.

Beyond safety, cost was the primary driver of the mission design. The final estimate for the complete first mission cost, including research, development, testing, and evaluation (RDT&E), was \$12.8 billion -- a relatively low cost for a mission of this size. With the cost spread out over the remaining decade, the cost per year is within the scope of the NASA budget. The primary factor contributing to this low project cost is the use of already well-developed and tested technology.

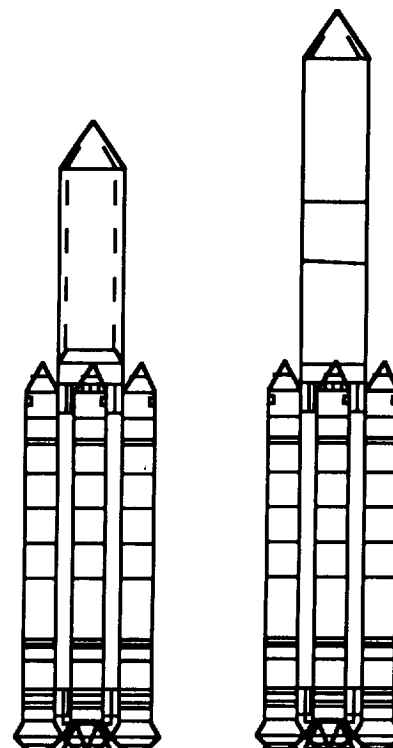
In order to make many of the design choices, a trade study regarding Columbiad's trajectory was made. In the Apollo missions of twenty years ago, a lunar orbit trajectory was used in order to reduce the initial weight and, hence, cost of the missions. Given the constraints for Columbiad to land at any latitude and to stay on the Moon for 14-28 days, the lunar orbit trajectory has several complications due to the mission goal for abort at any time. For this reason, a direct transit from the Earth is a better choice and was selected for the Columbiad missions.

The second critical trade study that was conducted was the choice of launch vehicle. The National Launch System (NLS) was chosen first for its high reliability and second for its launch capacity. The NLS has a high expected reliability due to the large number of flight tests that have already occurred for much of its hardware. Despite the fact that the NLS does not match the Saturn V's launch capabilities, it will be the largest reasonable launch vehicle available by the end of the decade. Another reason to use the NLS instead of reviving the Saturn V or designing an entirely new launch vehicle is that the NLS can be used for other types of missions and would not be a launch vehicle built and designed solely for these lunar missions as the Saturn V was. These other markets for the NLS aid in bringing down the cost of the NLS vehicle and raising the reliability.

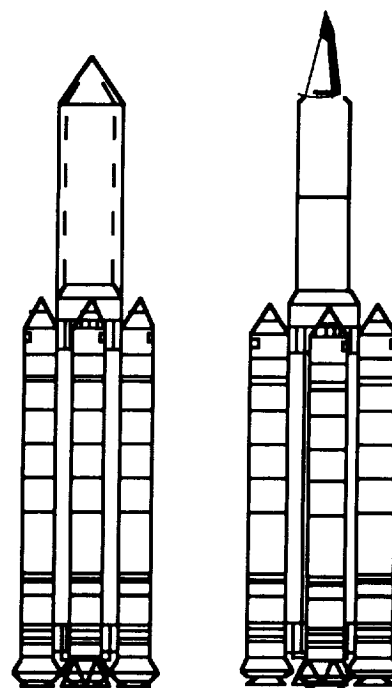
The current design for the NLS allows only a 72-metric ton payload to a 200 km circular orbit. Therefore two additional Redesigned Solid Rocket Motors (RSRM) were added on to the baseline NLS for a total of four RSRMs. This NLS configuration allows the insertion of a 100,000-kg payload (including a 10% margin) into a 200-km apogee launch trajectory. With this launch capacity, a minimum of two launches is required for a single piloted mission and an additional two launches are required for a precursor mission. Therefore an Earth orbit rendezvous is necessitated.

A total of four NLS launches is required for a complete Columbiad mission. Each precursor and piloted mission launch has a payload mass of approximately 95,600 kg. The packaging of the two missions is shown in Figure 1. The first two launches in quick succession are for the precursor while the third and fourth launches for the piloted mission are launched only after the success of the precursor mission has been confirmed. All launches are scheduled

from Kennedy Space Center, Launch Pads 39A and 39B.



Precursor Mission



Piloted Mission

Fig. 1 NLS Launches for Columbiad

The precursor mission was designed to be as modular as possible with the piloted mission for cost considerations. Therefore, each precursor mission vehicle is composed of three propulsive elements (two are identical with the piloted mission stages) in addition to the surface payloads: Primary Trans-Lunar Injection (PTLI), Lunar Braking Module (LBM), and Payload Landing Module (PLM). Again, the PTLI is by itself on the first launch for the precursor mission (Launch 1) while the LBM, PLM, and surface payloads are on the second launch for the precursor mission (Launch 2). The surface payloads include a habitat (BioCan) and a payload bay for other equipment.

The piloted mission is composed of three propulsive elements in addition to the Crew Module: Primary Trans-Lunar Injection (PTLI) stage, Lunar Braking Module (LBM), and Earth Return Module (ERM). The PTLI is the only component on the first launch for the piloted mission (Launch 3) while the LBM, ERM, and CM are grouped together on the second launch for the piloted mission (Launch 4).

Before translunar injection the vehicle must be established in a circular LEO for rendezvous. The NLS vehicle does not perform the circularization burn into a 200-km altitude for any of the four launches. In the precursor mission, the PTLI performs a circularization burn, and then raises its altitude to 275 km at the desired trajectory window where it will await rendezvous with the surface payload in the second launch. For the surface payloads launch, it is the LBM that performs both the circularization burn and the burn to higher orbit. Once again, for the piloted mission, the PTLI performs the circularization burn and, then, raises its altitude to 275 km at the desired trajectory window where it will await rendezvous with the piloted launch. For the piloted launch, it is the LBM that performs both the circularization burn and the burn to higher orbit.

**Table 1: Precursor Mission Profile**

| Event                       | Location       | $\Delta V$ (m/s) |
|-----------------------------|----------------|------------------|
| Circularization of Launch 1 | 200 km LEO     | 177              |
| Launch 1 burn to higher LEO | 200-275 km LEO | 43               |
| Circularization of Launch 2 | 200 km LEO     | 177              |
| Launch 2 burn to higher LEO | 200-275 km LEO | 43               |
| Earth Orbit Rendezvous      | 275 km LEO     | 60               |
| Trans-Lunar Injection       | LEO            | 2460             |
| Trans-Lunar Injection       | LEO            | 680              |
| Midcourse Corrections       | Midcourse      | 120              |
| Lunar Braking into LLO      | Prior to LLO   | 1060             |
| Lunar Braking to Moon       | LLO to Moon    | 1700             |
| Hover and Land              | Moon           | 500              |

Once the vehicles have completed rendezvous, the Trans-Lunar Injection is performed by two stages: the PTLI and the LBM. The PTLI separates from the remaining stages upon the completion of its burn. The LBM completes the

burn and then performs midcourse corrections that are required during the three-day transit. Upon lunar arrival, the LBM inserts the vehicle into LLO, and then performs the major portion of the descent burn before it is staged and crashed safely away from the landing site. For the precursor mission, the PLM then performs the final descent and hover burn before landing and deploying the habitat. A brief mission profile along with propulsive requirements for each stage is featured in Table 1.

On the piloted mission, the ERM performs the final descent and hover burn before landing. After the 28-day lunar stay, the ERM launches the CM into LLO and then into the Earth transfer orbit. The ERM also performs any midcourse corrections. The ERM separates from the Crew Module (CM) just before reentry into the Earth's atmosphere, and then the CM proceeds to reenter the atmosphere safely. The piloted mission is completed when the CM lands at Edwards Air Force Base. A brief mission profile along with propulsive requirements for each stage is featured in Table 2. An outline of the trajectory that Columbiad vehicles will follow is shown in Figure 2.

**Table 2 : Piloted Mission Profile**

| Event                       | Location           | $\Delta V$ (m/s) |
|-----------------------------|--------------------|------------------|
| Circularization of Launch 3 | 200 km LEO         | 177              |
| Launch 3 burn to higher LEO | 200-275 km LEO     | 43               |
| Circularization of Launch 4 | 200 km LEO         | 177              |
| Launch 4 burn to higher LEO | 200-275 km LEO     | 43               |
| Earth Orbit Rendezvous      | 275 km LEO         | 60               |
| Trans-Lunar Injection       | LEO                | 2460             |
| Trans-Lunar Injection       | LEO                | 680              |
| Midcourse Corrections       | Midcourse          | 120              |
| Lunar Braking into LLO      | Prior to LLO       | 1060             |
| Lunar Braking to Moon       | LLO to Moon        | 1700             |
| Hover                       | Moon               | 500              |
| Lunar Launch                | Moon to LLO        | 2200             |
| Earth Return Injection      | LLO                | 1060             |
| Midcourse Corrections       | Midcourse          | 120              |
| Reentry                     | Earth's Atmosphere | 100              |

In order to minimize the thermal stresses that the vehicle structures encounter during the mission, a decision was made to spin the transit vehicle at a rate of approximately once per hour. If a launch slippage occurs for either Launches 2 or 4, then the PTLI may initiate a spin while it waits in LEO. The PTLI would despin shortly before docking occurred with Launch 2 or Launch 4.

To equalize the payload weights of the launches, the TLI burn was split between two stages. The four launch weights were roughly equalized by allocating approximately 85% ( $\Delta V = 2460$  m/s) of the TLI burn to the Primary TLI stage. This left a  $\Delta V = 680$  m/s to be included in the next stage.



A separate stage was not designed for this small  $\Delta V$ . Instead, the propellant was included in the following stage, the LBM.

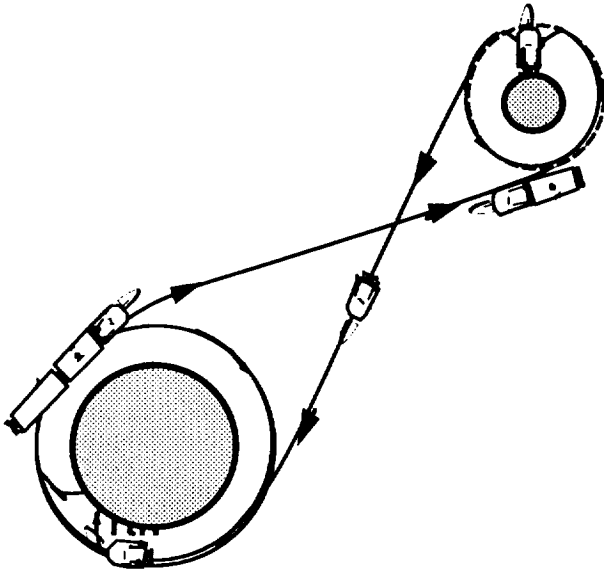


Fig. 2 Columbiad Mission Trajectory

To reduce the height of the vehicle landing on the surface of the Moon, a decision was made to stage just prior to the hover and landing phase of the lunar descent. Therefore, for both missions, the LBM is staged after completing the major portion of the descent. The ERM and PLM are both equipped with landing gear and propulsion systems to conduct the final descent phase. This is a significant aid as it reduces the height of the landing vehicle by 12-13 m.

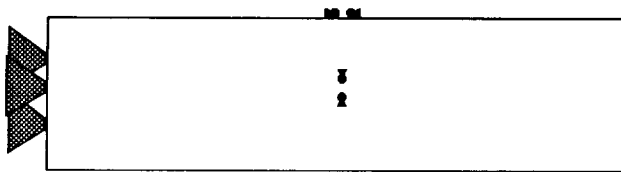


Fig. 3 Primary Trans-Lunar Injection Stage

The PTLI stage, shown in Figure 3, has five RL10 engines and performs four burns. The first PTLI burn circularizes the PTLI's Earth Orbit at 200 km. The second burn is the initial burn to transfer to a higher orbit, and the third burn completes the higher orbit transfer at 275 km. The fourth burn is the only burn occurring when the PTLI is attached to the other stages. When this burn is complete the PTLI has expended its fuel and is staged off.

The dry mass budget for this stage is 11,587 kg and the

wet mass budget is 94,825 kg. Since the PTLI must remain in orbit about the Earth for up to 40 days, independently of the rest of the vehicle, it has its own power; Guidance, Navigation, and Control (GNC); and Command, Communications, and Control (C<sup>3</sup>) systems on board. Included among its apparatus is a low gain antenna for communication with Earth and a Reaction Control System (RCS) for stationkeeping.

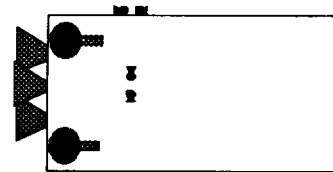


Fig. 4 Lunar Braking Module

The LBM, shown in Figure 4, has three RL10 engines and performs six burns plus midcourse corrections. The first LBM burn circularizes the vehicle's Earth Orbit at 200 km. The second burn is the initial burn to transfer to a higher orbit and the third burn completes the higher orbit transfer at 275 km, where docking with the PTLI occurs. The fourth burn is the Secondary Trans-Lunar Injection burn that occurs just after the PTLI stage is staged off. The fifth burn brakes the module into LLO, and the sixth and final burn completes most of the lunar descent burn before it is staged.

The dry mass budget for this stage is 6,731 kg and the wet mass budget is 62,285 kg. The LBM does not have its own power source. Either the ERM or the PLM provides the necessary power for it during its burns.

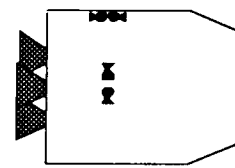


Fig. 5 Earth Return Module

The ERM, shown in Figure 5, utilizes three RL10 engines to perform three burns plus midcourse corrections. The first ERM burn is extremely critical because it prevents the CM from crashing into the lunar surface after the LBM has initiated the descent to the lunar surface. The second burn is the launch from the lunar surface into LLO and the third burn injects the vehicle into an Earth return trajectory.

The dry mass budget for the ERM is 5,553 kg, including 500 kg for landing legs that are jettisoned off after lunar launch. Within the stage, an additional payload weight of 3000 kg to the lunar surface can be stowed. This weight is

twice the minimum necessary to resupply the habitat for future piloted missions. Therefore the total wet weight budget is 26,210 kg. The ERM has an RCS for both rendezvous and midcourse correction burns. It also contains a high gain antenna so that the crew can communicate with Earth in the vicinity of the Moon. The ERM supplies power to both the LBM and the CM in addition to itself.



Fig. 6 Crew Module

The crew module, shown in Figure 6, is designed as a biconic reentry vehicle with a maximum lift to drag ratio of 1.1. The lift to drag ratio allows for reentry maneuvering and extends the downrange and cross range distances of the vehicle. The vehicle safely houses the four crew members for the transit to the Moon and back to Earth, including the reentry phase. The budgeted mass of the CM is 6330 kg which includes the 730 kg heat shield.

Table 3: Piloted Mission Mass Summary

| Stage                   | $\Delta V_{total}$<br>(m/s) | Wet Mass<br>(kg) | Length<br>(m) |
|-------------------------|-----------------------------|------------------|---------------|
| PTLI                    | 2680                        | 94,825           | 15.96         |
| LBM                     | 3780                        | 62,285           | 12.7          |
| ERM                     | 3880                        | 22,710           | 9.97          |
| Piloted Payload to Moon |                             | 3500             | (in ERM)      |
| Crew Module             |                             | 6330             | 7.69          |
| Nose Cone (Launch 3)    |                             | 820              | 5             |
| Total Mass              |                             | 190,470          |               |

Total Length  
Total Mass for Launch 3 (PTLI stage) - 94,825 kg  
20.96 m  
Total Mass for Launch 4 (Piloted launch)- 95,645 kg  
27.66 m (plus 2.7 m)

The total height allowance for an NLS payload is 35 m including a nose cone. The height of Launch 4 is less than the total height of the LBM, ERM, and CM because the LBM stage is recessed into the launch vehicle by 2.7 m. This height adjustment is not needed for Launch 4; however, it is needed for Launch 2, and in the interests of modularity, the height adjustment occurs on both Launches 2 and 4. There was no need to recess the PTLI stage for launches 1 and 3.

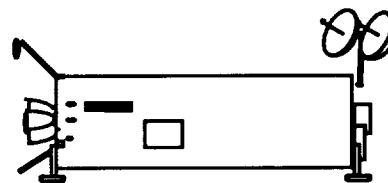


Fig. 7 Payload Landing Module and BioCan

The PLM, shown in Figure 7, has three RL10 engines and performs only one burn. The PLM burn is extremely critical in that it prevents the surface payloads from crashing into the lunar surface after the LBM has initiated the descent to the lunar surface. The PLM is also involved with the deployment of the surface payloads.

The dry mass budget for this stage is 2,743 kg. This dry mass budget does not include the weight of the landing legs. The landing legs are part of the surface payloads budget of 26,500 kg. The propellant mass is 3,582 kg although a greater amount of LOX and LH2 are stored in the propellant tanks because the tanks share the space with the lunar base fuel cell system. The total wet weight budget of the PLM is 6,325 kg. With the fixed propellant mass, the total wet weight budget of the combined PLM and surface payloads is 32,825 kg.

The PLM, also shown in Figure 7, has an RCS for both rendezvous and midcourse correction burns. It also has a high gain antenna in order that the crew can communicate with Earth while on the Moon. The PLM is responsible for providing power to itself and to the LBM during transit to the Moon in addition to its power duties on the surface. A self-deploying power system was designed for the power requirements of the habitat during the "hibernation state" (the period between the PLM touchdown and arrival of the crew). 2.5 kW of continuous usable power is supplied by two 10 m<sup>2</sup> arrays that partially track the sun and are deployed from an external surface of the PLM.

The surface payloads, shown in Figures 10 to 13, are either packed into the payload bay located just on top of the PLM, or they are packed into the habitat (BioCan) which is located above the payload bay. The payload bay has a large door on the side so that the crew members can access the packaged payloads. The payload bay is also connected to the habitat's emergency exit/entry airlock. The pathway for this airlock is only clear after the payload bay has been emptied out. The primary airlock is unobstructed on the opposite end of the BioCan.

One of the primary requirements for the lunar habitat is to provide protection against radiation from solar flares. For extended operations on the lunar surface, precautions are mandatory. In particular, Project Columbiad's 5-year campaign plan overlaps with the period 1999 to 2004 which is predicted to be a peak period in the solar flare cycle. Thus

solar flare protection of the habitat is given a high priority in the surface operation requirements of the piloted mission. For Project Columbiad applications, a 25 Radiation Exposure Man (REM) *maximum* was set for the entire mission duration (36 earth-days). For almost all of the solar flares that will occur, the radiation dosage is much lower than the 25 REM with the amount of protection that the BioCan provides.

Columbiad's strategy for solar flare protection is to cover the habitat with regolith, the lunar soil. A depth of 50 cm

is needed to provide the desired level of protection. This operation is performed by a regolith collecting machine that brushes the dirt from the lunar surface and dumps it into a dump-bucket attachment on the rover. The rover, in turn, pours the regolith onto a drivable conveyer, which dumps it to different heights on the side and top of the habitat. A regolith support structure is also designed to hold the regolith on a 45° incline along the sides of the habitat (see Figure 8).

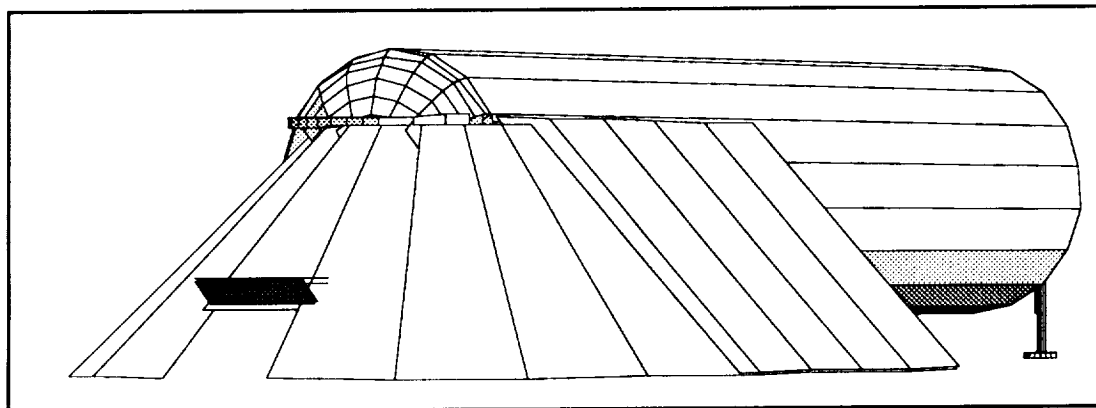


Fig. 8 Habitat with Regolith Support Structure

The habitat, shown in Figure 8, is the lunar home for four astronauts. It is a 10-m long and 6-m diameter double-walled cylinder. The external skin is integrated with the external structure of the PLM. The internal cylinder, made of composite material, is separated by a thin layer of sealed vacuum from the external cylinder and is pressurized with 5 psi of breathable atmosphere. The internal space is arranged to optimize the layout of all subsystems based on their predicted need and frequency of use. A 2-m by 1-m airlock door on one end of the habitat provides the primary access to the habitat. In case of an emergency, a secondary airlock that opens into the cargo bay from the crew quarters can be used. The total estimated mass of the habitat is less than 10,000 kg.

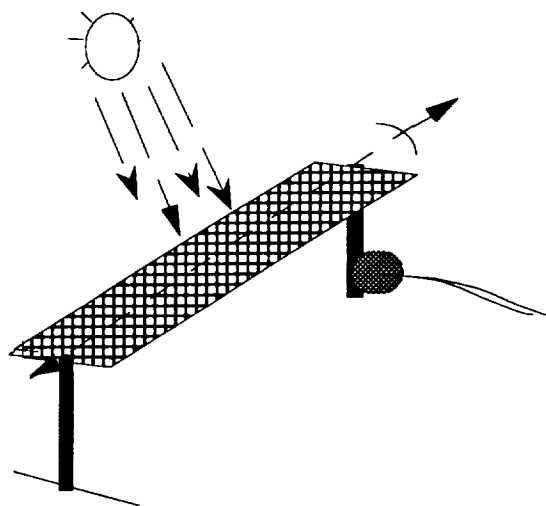


Fig. 9 Solar Lunar Power Plant

A solar power plant, shown in Figure 9, is designed to meet the power requirements of running all the base operations. A 250 m<sup>2</sup> photovoltaic array provides 35 kW of continuous daytime usable power during the lunar day. The rest of the power goes into charging up alkaline fuel cells system for 35 kW of night power. The fuel for the fuel cells is stored along with the propellant for the PLM. The total

mass of the power system hardware is approximately 1000 kg. All fuel cells and other power conditioning hardware are located inside the PLM and the cargo bay.

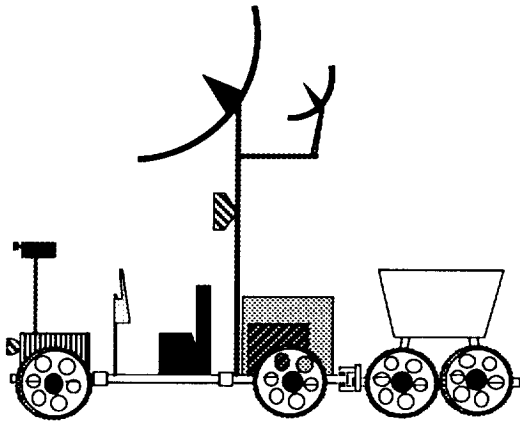


Fig. 10 Lunar Rover

The Rover, shown in Figure 10, is the surface transportation vehicle, capable of ferrying 1500 kg of payload. It is a six-wheel drive, four-wheel steered vehicle. The fully deployed rover is 5 m long and 2.5 m wide. The height of the vehicle is 2.5 m, including the height of its fully deployed high gain antenna. The vehicle is battery powered for a 120-km nominal mission range at an maximum velocity of 20 km/hour. To ensure the walk-back capability of the astronauts, all missions are limited to within a 50-km radius of the habitat. The maximum mission duration is 8 hours. The vehicle is unpressurized, but the astronauts can hook up their EVA suits to the Portable Life Support System (PLSS) packs onboard the rover. The astronauts' PLSS backpacks are held in reserve for off-the-vehicle activities and for emergency procedures. Essentially, the rover is the workhorse for all surface operations. The regolith collector and the conveyor both require the rover for their operation.

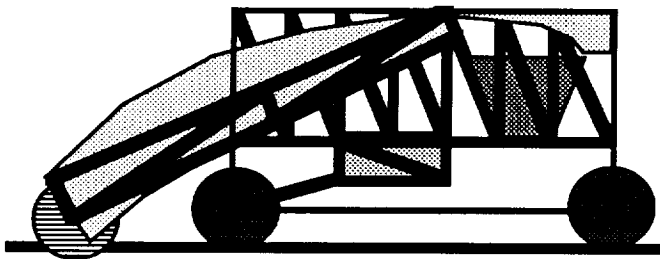


Fig. 11 Regolith Collector

The regolith collector is quite similar in operation to a street sweeper. Loose lunar soil is swept up by a brush at a nominal rate of  $0.05 \text{ m}^3$  per minute. The regolith particles

slide up a shroud and collect in a  $1 \text{ m}^3$  hopper. After every twenty minutes of soil collecting, the hopper dumps the collected regolith into a dump-bucket attached to the rover. The armature arm can be raised to lift the brush above 50-cm obstacles in the collector's way. The drive mechanism of the wheels can be preprogrammed and/or operated remotely within line of sight. The regolith collector runs on 7.5 kW of power, stored on board in Sodium-Sulfide cells. Maximum operating time of the machine, limited by the total stored power, is 8 hours. The cells require 12 hours to charge up to the maximum power levels.

The Lunar conveyor, shown in Figure 12, is a multipurpose conveyer system. The main use of the conveyor is to transport loose regolith to any height on the regolith support structure. The expandable design consists of four segments, each 4 m long for a total length of 16 m. The belt width is 1 m. The entire system sits on 16 wire-mesh wheels and can be driven around as an articulated, 4-wheel-drive vehicle. The power required to run the conveyor is 5 kW. This determines a maximum feed rate of  $0.28 \text{ m}^3$  of regolith over a 16.00 m distance in one minute. Each connection point is a pin which gives the conveyor the flexibility to deliver its payload up inclines and over obstacles. With torsional clamps, the joints can be made rigid to allow for transport over trenches.

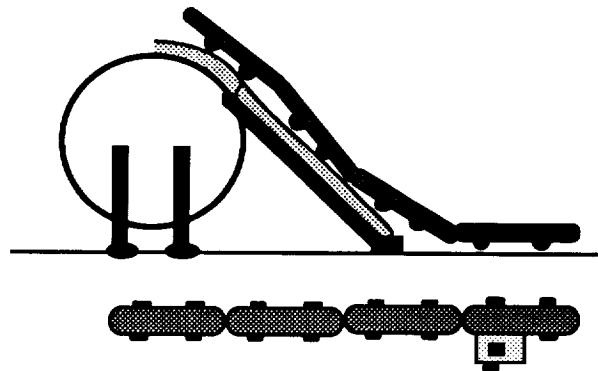


Fig. 12 Regolith Conveyor on top of Regolith Support Structure

**Table 3: Precursor Mass Summary**

| Stage                     | $\Delta V_{\text{total}}$<br>(m/s) | Wet Mass<br>(kg) | Length<br>(m) |
|---------------------------|------------------------------------|------------------|---------------|
| PTLI                      | 2680                               | 94,825           | 15.96         |
| LBM                       | 3780                               | 62,285           | 12.7          |
| PLM                       | 500                                | 6325             | 6.77          |
| Surface Payloads          |                                    | 26500            | 12.5          |
| Nose Cone (Launches 1, 2) |                                    | 820              | 5             |
| Total Mass                |                                    | 190,755          |               |

**Total Length**

Total Mass for Launch 1 (PTLI stage)      94,825 kg  
20.96 m

Total Mass for Launch 2 (Piloted launch)      95,930 kg  
34.27 m (plus 2.7 m)

The total height allowance for an NLS payload is 35 m including a nose cone. The height of Launch 2 is less than the total height of the LBM, PLM, and the surface payloads because the LBM stage is recessed into the launch vehicle by 2.7 m. This height adjustment brings the total height of the launch within the 35 m limit.

## PROJECT APEX: ADVANCED MANNED EXPLORATION OF THE MARTIAN MOON PHOBOS

University of Michigan  
Department of Aerospace Engineering  
Ann Arbor, Michigan

Professor Joe G. Easley  
Jim Akers, Teaching Assistant

### Abstract

A preliminary design has been developed for a manned mission to the Martian moon Phobos. The spacecraft carries a crew of five and is launched from Low Earth Orbit in the year 2010. The outbound trajectory to Mars uses a gravitational assisted swingby of Venus and takes eight months to complete. The stay at Phobos is 60 days at which time the crew is busily engaged in setting up a prototype fuel processing facility. The vehicle will then return to Earth orbit after a total mission duration of 656 days. The spacecraft is powered by three nuclear thermal rockets which also provide the primary electrical power via dual mode operation. The overall spacecraft length is 110 m, and the total mass departing from Low Earth Orbit is 900 metric tons.

### Introduction

Mars is the most like Earth of all the planets in the solar system. Understanding the evolution of the Martian climate will advance our understanding of the changes in the Earth's climate which will be of vital importance to the survival and enhancement of life here on Earth.

The manned exploration of Mars is a massive undertaking which requires careful consideration. A mission to the moon of Mars called Phobos as a prelude to manned landings on the Martian surface offers some advantages. One is that the energy requirement, in terms of delta V, is only slightly higher than going to the Moon's surface. Another is that Phobos is a potential source of water and carbon which could be extracted and processed for life support and chemical propellants for use in future missions; thus Phobos might serve as a base for extended Mars exploration or for exploration of the outer planets.

The design of a vehicle for such a mission is the subject of our Aerospace System Design course. The materials and equipment needed for the processing plant would be delivered to Phobos in a prior unmanned mission. This study focuses on what it would take to send a crew to Phobos, set up the processing plant for extraction and storage of water and hydrocarbons, conduct scientific experiments, and return safely to Earth. The size, configuration, and subsystems of the vehicle are described in some detail.

### Objectives

1. Send a crew from Earth to the Martian moon Phobos.
2. Set up a prototype processing facility to extract water and hydrocarbons.
3. Conduct scientific experiments including an augmented robotic mission on the Martian surface.
4. Bring crew and Phobos samples back to Earth safely.



Fig. 1 Composite Picture of Phobos

### Assumptions

1. Heavy lift launch vehicle with a minimum capability of 150 metric tons with designed growth to 250 metric tons is available to place the components of the spacecraft into Low Earth Orbit (LEO) for assembly.
2. Phobos is a carbonaceous chondrite asteroid containing water (20% by mass).

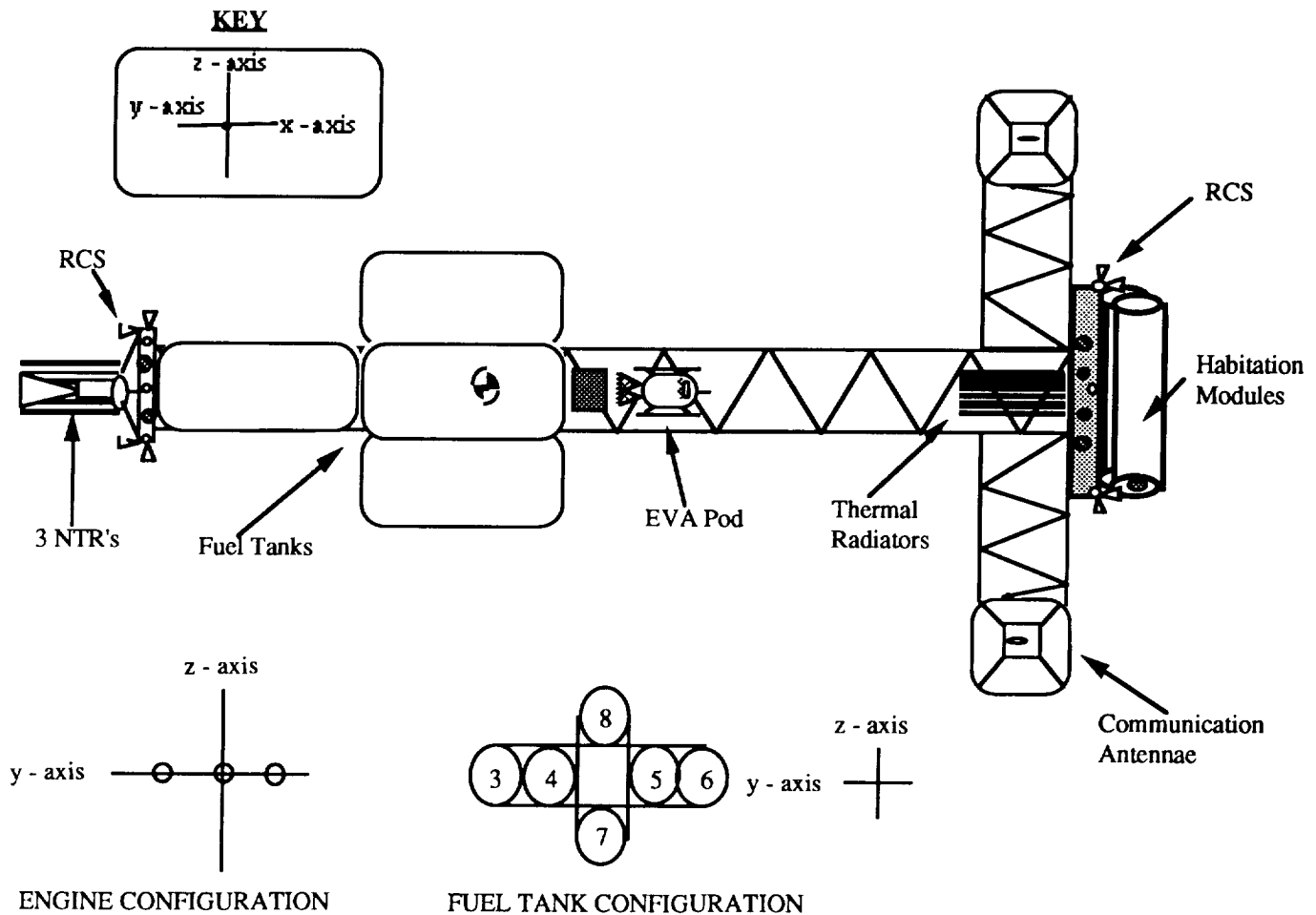


Fig. 2 Spacecraft Configuration - Top View

- Unmanned precursor missions have determined a preliminary landing site, Stickney Crater, and delivered materials and equipment for the processing plant.

### Phobos

Figure 1 shows Phobos, one of two moons of Mars (the other being Deimos). Phobos is 27 km long, 21.4 km wide, and 19.2 km high. Stickney Crater, which is on the end of Phobos facing Mars, is approximately 10 km in diameter. Phobos is in a low, almost circular orbit about Mars, with the semi-major axis equal to 9378 km and the eccentricity of the orbit only 0.015. Phobos orbits almost over the equator of Mars with an inclination of 1.02 degrees with a sidereal period of 7 hours 39 minutes 13.85 seconds.<sup>1</sup>

The gravity of Phobos is only .001g and the mass is estimated to be  $9.8 \times 10^{15}$  kg. Because of its low albedo of 0.05 and low density, Phobos is assumed to be an asteroid that was captured by Mars. Phobos' spectrum of reflectivity shows that it is similar in composition to a type 1 carbonaceous chondrite asteroid. Type 1 meteorites which

have been analyzed on Earth show abundance of  $\text{SiO}_2$  and  $\text{H}_2\text{O}$  in addition to other silicates ( $\text{MgO}$ ,  $\text{FeO}$ ) which are assumed to be present on Phobos.

### Spacecraft Integration

The primary objectives in the design of the spacecraft were (1) to promote the safety of the crew by designing a stable ship that utilizes artificial gravity and (2) to provide shielding to the crew and ship components against all forms of radiation.

The spacecraft, shown in Figure 2, has an overall length of 110 m. Two habitation modules are attached at the front of the ship by the truss structure. Located behind the modules, two communication trusses extend 25 m each with counter-rotating platforms for antennae and navigation equipment. Eight fuel tanks are stacked around the main truss; two of which are feeder tanks. Each tank is 19.5 m long and has a diameter of 9 m. Three nuclear thermal rockets are stacked perpendicular to the truss in the y-direction. The total mass departing from LEO is 900 metric tons.

## Artificial Gravity

Due to the long duration of this mission, the safety and comfort of the crew aboard the spacecraft were a high priority. After extended periods of time in a weightless environment, the human body begins to lose muscle mass due to minimal exertion of the muscles. Demineralization of bone tissue also begins, resulting in loss in strength and performance. To promote the health of the crew, artificial gravity was deemed necessary.

The optimal configuration for the mission was a tumbling scheme in which the spacecraft spins about the lateral body z-axis as shown in Figure 2. The spin rate was chosen to be in the range of 2.6-3.1 rpm, below the maximum allowable human rotation rate of 4 rpm. In addition, an artificial gravity in the range of 0.3g-0.5g was found to be the best compromise between maintaining crew health and minimizing system mass. A 0.01g lateral acceleration will be experienced by the crew during spin/despin operations.

The spacecraft will be tumbling during transit to Phobos and on return to Earth. No artificial gravity will be provided at Phobos, as the ship will be docked with the asteroid. The spacecraft will also need to despin for propulsive maneuvers and course corrections. In an emergency, despin can be achieved in five minutes.

## Radiation

One of the primary hazards to the crew during the Mission to Phobos is radiation exposure. The four types of radiation encountered are Solar Flares, Galactic Cosmic Radiation (GCR), Solar Wind, and radiation from the propulsion nuclear reactors. The maximum total radiation exposure limit was set at 65 REM/yr and 33 REM/month per person. These levels of radiation will increase the chance of dying from cancer (the major effect of radiation) from 16% (the level on earth) to just under 18%. From these values, a radiation shielding configuration was developed.

A layer of tungsten and lithium hydride is placed between the nuclear reactors and the propellant tanks. This layer provides a "cone of safety" for the fuel tanks, habitation modules, and the communication platforms. For solar flare protection, the sleeping quarters are sheltered. Lithium hydride will be placed in the ceiling and walls of the sleeping quarters with water under the floor. The total radiation exposure is estimated to be 95 REM.

## Propulsion and Power System

The APEX mission entails a duration significantly longer than any previous manned missions. The most important design trade-off is the choice of the primary propulsion system. This determines the overall characteristics of the design. Nuclear Thermal Rocket (NTR) engines were chosen to reduce the overall trip time, increase reliability, and increase efficiency.

## Nuclear Thermal Rockets

The reactor design chosen for the mission is based on an improved version of a Rocketdyne, NERVA derivative, Carbide reactor.<sup>2</sup> Reactor mass is estimated to be seven metric tons with a thrust of 334,00 N (75,000 lb). The maximum Isp available must be improved to 1040 seconds or higher to ensure an effective Isp of 1000 seconds at full throttle during normal operation. The use of three NTR's provides a total thrust of 1,020,000 N with a maximum acceleration of 0.19g. The nuclear core will operate for up to 12 hours during full power propulsive maneuvers with a lifetime of three years. Three NTR engines will be used to escape LEO while only two engines will be needed for the rest of the mission.

## Fuel and Tank Staging

Hydrogen has a significantly higher Isp than any other fuel which made it an attractive fuel choice. Since liquid hydrogen has a tendency to leak or boil away, the fuel tanks were designed with refrigeration. Refrigeration will reduce hydrogen boil off to zero.

A refrigerated fuel tank has a mass of 9100 kg. To reduce mass during the mission, the tanks will be dropped at various locations during the course of the mission. An intermediate tank staging scheme was selected to maintain ship symmetry, to reduce space clutter, and to provide reusability. One tank will be staged near Earth with six staged in orbit around Mars. The spacecraft will return with the final two feeder tanks.

## NTR Operation for Propulsion

The reactor core of the NTR can be brought to full power within 60 seconds. The normal source flow through the tie tubes is the main propellant. The flow originates either directly from the tanks or from flow which has been previously routed through coolant loops in the thrust nozzle. This flow then proceeds via the tie tubes in the core to an outlet in the reactor. This heated propellant is routed to the turbines which power the propellant feed pumps. The flow is again rerouted and sent back through the core. This time the propellant proceeds directly through the flow channels in the fuel elements and is exhausted to space.

After a main burn is completed, the cooling process continues for up to six hours to remove heat from the reactor core.

## Dual-Mode Operation for Power

For normal operation, the APEX spacecraft will require 175 kWe of electrical power. This power provides for life support, communications, experiments, and for cryogenic cooling of the fuel tanks. The power system must also be



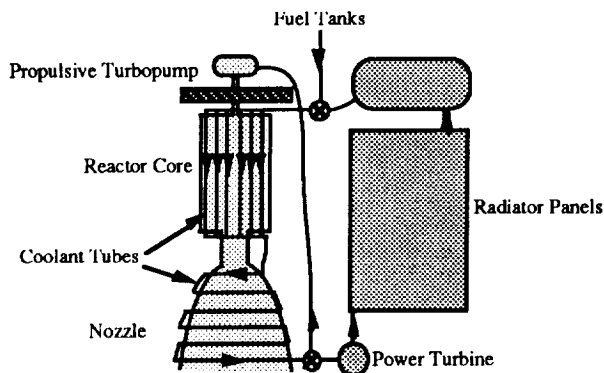


Fig. 3 Dual Mode Nuclear Thermal Rocket

capable of producing this power level for the duration of the two-year mission. For this purpose, a nuclear reactor is the best solution. To minimize shielding needs (and thus weight), the spacecraft will be using a Dual Mode Nuclear Thermal Rocket (DMNTR) which combines the power-producing nuclear reactor with the propulsion system.

An NTR must have a cooling system to keep the reactor and nozzle from melting. This is accomplished by running the propellant through cooling pipes in the reactor core and on the nozzle. The propellant is then fed through the reactor core again and is expelled out the nozzle. Power is produced by adding a turbo-brayton cycle to the coolant system. During electrical production, helium-xenon (He-Xe) is fed through the coolant system instead of the hydrogen used for the propulsive burns. The He-Xe passes through the reactor's cooling pipes and is routed to a turbine to produce power. From the turbine, the He-Xe passes through heat pipes to radiate the heat and traverses back into the reactor's coolant system. This differs from the propulsive burns in that the cycle is closed (see Figure 3).<sup>3</sup>

Project Apex will use three nuclear thermal rockets that

are designed for dual mode capability. Only one reactor will be necessary for power production, the other two reactors will be used as backups. Each reactor will have its own coolant system with turbomachinery, but will share a common radiator. Individual radiator systems would be too heavy.

### Back-up Power

The design of the DMNTR does not allow power production during a propulsive burn. The He-Xe working fluid to drive the power-producing turbines does not adequately remove the excess heat when the reactor is running at full power. This requires the use of a backup power source to provide electrical power during the propulsive burns. The maximum amount of time that power from the DMNTR would be unavailable for electrical power generation would be approximately 6 hours.<sup>3</sup> Power during these periods will be provided by a regenerative H-O fuel cell. The fuel cell will provide 20 kWe, enough for basic life support, communications, and computers for up to 24 hours.

### Power Transmission

To deliver the power to the user, two independent transmission and distribution systems will be employed (See Figure 4). The power will be transmitted at 270 volts DC. DC power was chosen because of its extensive use in space, reliability, and simplification. For reliability and redundancy, only one distribution and transmission system will be necessary for normal operation with the second used as a backup. Voltage conversion to the user will be handled by small, low-powered, standardized, modular converters.

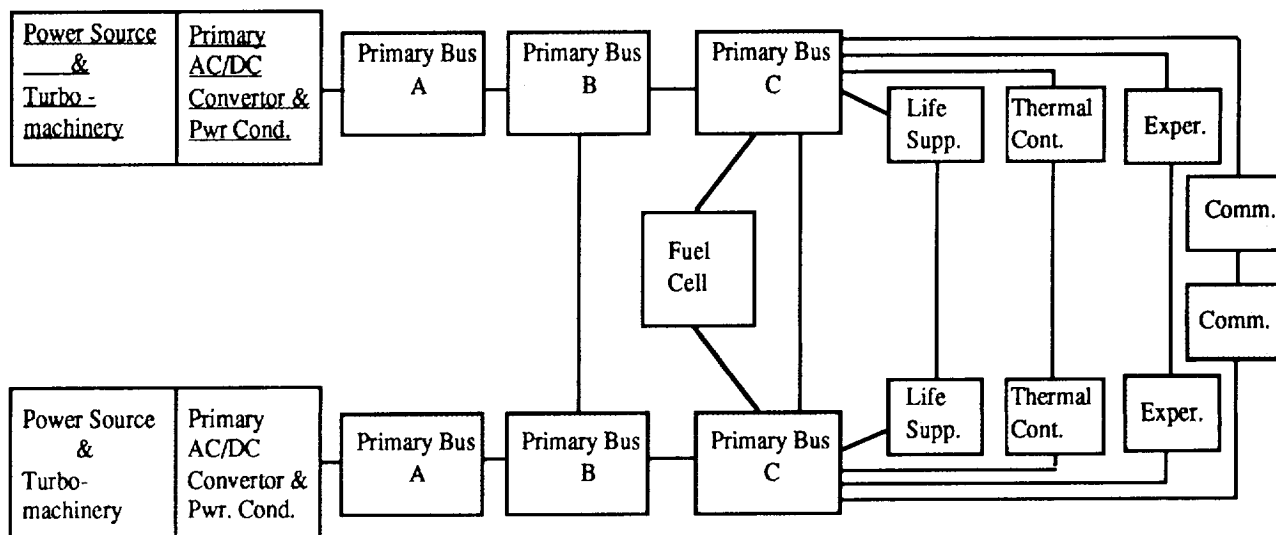


Fig. 4 Power Distribution Schematic

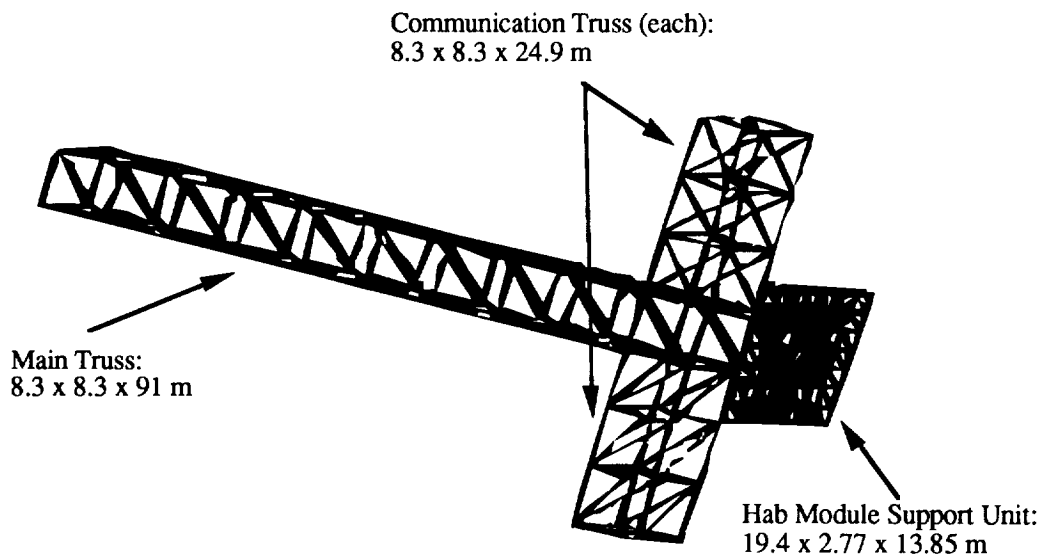


Fig. 5: Truss System

### Thermal Control

Electricity produced and provided to the user generates large amounts of heat that must be rejected for the spacecraft to be habitable. Advanced systems such as Liquid Droplet Radiators and Curie Point Radiators are attractive solutions but are not compatible with the ship's rotation. Because of this, a standard heat-pipe radiator will be used. There are two sources of heat that must be dissipated: the nuclear reactors and the habitation modules. The habitation module radiators will use an internal two-phase water loop to transport the heat and an external two-phase ammonia loop to reject heat. Heat rejection at the nuclear reactors will be handled by a He-Xe mixture used for power production.

### Structures

The structural components of the APEX spacecraft were designed to provide support for other subsystems. Emphasis was placed on strength, durability, and minimization of the total structural mass.

### Truss System

The truss system is composed of three parts (Figure 5). The main truss extends from the nuclear thermal rockets to the habitation modules. The communications truss extends outward from the main truss so that communication equipment can have an unobstructed path from which to receive and transmit. The habitation module support unit provides support for the habitation module and the air locks.

Each part of the truss system was designed to be collapsible and self-deploying. This reduces the payload volume required to launch the trusses to LEO and greatly reduces onorbit assembly time. A collapsible box truss with

precompressed joint springs was chosen. Graphite-epoxy was chosen as truss material for its high yield strength and low density.

A Finite Element (FE) analysis was performed on the proposed designs of the three trusses. The primary constraint for the main truss was a large enough moment of inertia to result in a minimum natural frequency of one hertz. The maximum acceleration experienced by the truss was 0.56g in compression. From the FE analysis, it was determined that the box truss was to have a cross-section of 8.3 m by 8.3 m with the dimensions of each member being .1575 m (outer diameter) and .1372 m (inner diameter). Each truss has a 1.4 factor of safety.

### Habitation Modules

The two habitation modules are based on a NASA Space Station module with modifications (see Figure 6). The first layer is a meteorite shell of aluminum. Multi-Layer Insulation (MLI) follows the meteorite shell for thermal control. Standoffs acting as spacers between the first two layers prevent shifting and crushing of the MLI. Stringers running the length of the module control bending. Bulkheads encircling the cross-section prevent expansion in the radial direction.

The structural components were designed to withstand an internal pressure of 11 psi. The dimensions of the outer module shell are 4.7 m x 16.9 m. In addition, two airlocks, one on each module at opposite ends, were designed with the same structural configuration as the habitation modules.

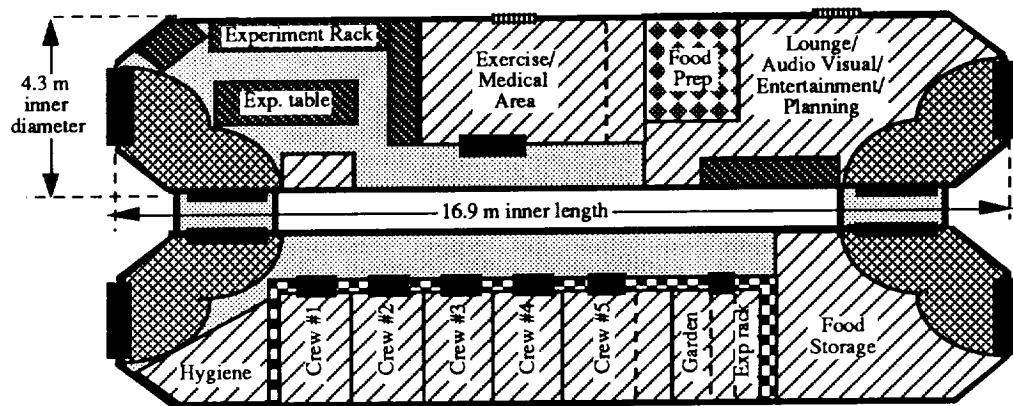


Fig. 7 Habitation Module Layout

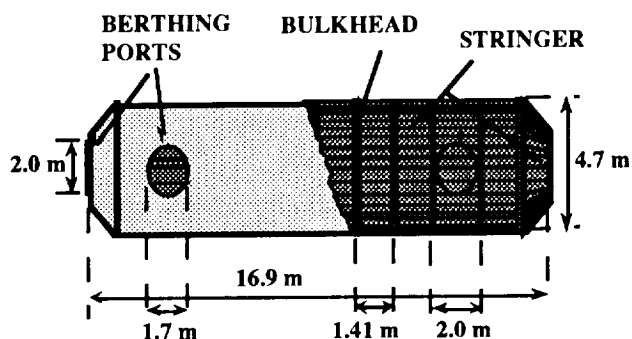


Fig. 6 Habitation Module Structural Support

### Human Factors

#### Habitation Module Layout

There will be two cylindrical modules in which the crew will live during transit to and while on Phobos. The modules are designed to compensate for both microgravity and artificial gravity environments. Both modules have one floor with access between modules. The five crew quarters, hygiene facilities, galley, wardroom, medical facility, and laboratory are shown in Fig. 7. A command center is located in the crew quarters as well as in the laboratory for radiation protection.

#### Life Support System

A partially-closed environmental life support system was chosen for the spacecraft. The life support system consists of temperature and humidity control, atmosphere control, fire detection and suppression, waste management, air revitalization, and water recovery and management. Figures 8 and 9 show the air and water recycling processes. A 90% efficiency for air recycling and a 95% efficiency for water recycling are assumed; 1000 kg of oxygen and 5550 kg of water will be carried during the mission. Both amounts include 15% contingency supplies. In addition, 4720 kg of

dried food will be provided for the crew. The Halon 1301 system was chosen for fire suppression as it leaves no corrosive or abrasive residues within the cabin and few ill effects for humans.

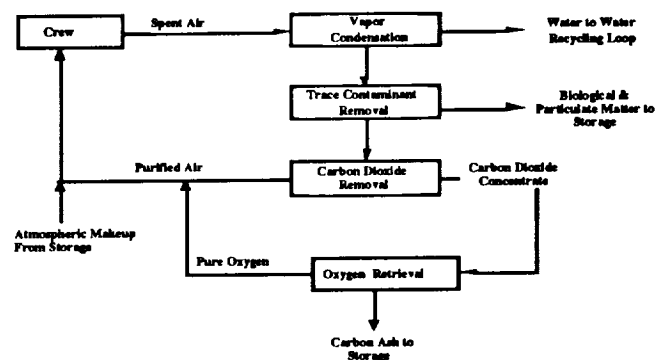


Fig. 8 Air Recycling Process

### Communications

The communications system of Project APEX maintains a 50 Megabit per second (Mbps) full duplex connection from

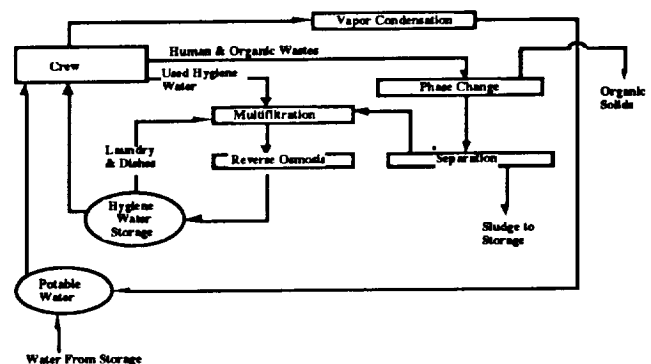


Fig. 9 Water Recycling Process

the spacecraft to Mission Control on Earth; this allows for the continuous transmittal of voice and video communications, experimental data and observations, and telemetry information. Seven major links are required in the design (see Figure 10):

1. Ground Terminal (GT): A 20-meter (diameter) antenna near Johnson Space Center (Mission Control), transmitting in the S-band to the Geosynchronous Relay Satellites (GRS).
2. Geosynchronous Relay Satellites (GRS): Three satellites in orbit about Earth with S-band downlinks to the GT and 24-meter antennas transmitting in the Ka-band to the Mars Piloted Vehicle (MPV), Mars Relay Satellites (MRS), and Phobos Relay Point (PRP).
3. Mars Piloted Vehicle (MPV), the spacecraft: Two 9-meter antennas mounted on both ends of the communications boom of the spacecraft, transmitting in the Ka-band to the GRS.
4. Transitional Relay Point (TRP): A 1-meter antenna mounted on top of the spacecraft, transmitting in the Ka-band to the MRS; the TRP will be used during the landing operations on Phobos.
5. Mars Relay Satellites (MRS): Two satellites in orbit about Mars with Ka-band downlinks to the PRP and 9-meter antennas transmitting in the Ka-band to the GRS.
6. Phobos Relay Point (PRP): A 2-meter antenna mounted on a 50-meter pole on the surface of Phobos, transmitting in the Ka-band to the MRS; the PRP will be used during the assembling operations on Phobos and will be left connected to the processing plant after the crew departs from Phobos.
7. Extra Vehicular Activity (EVA): Half-wave dipole antennas mounted in the astronauts' space suits, transmitting in the UHF-band to the MPV and PRP.

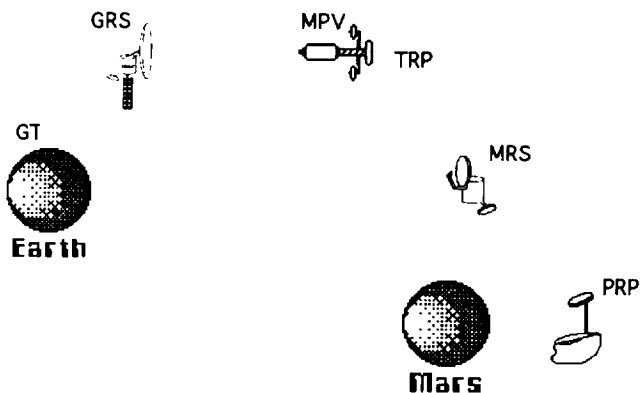


Fig. 10 Main Communication Links

## Guidance, Navigation and Control

Guidance, Navigation, and Control (GN&C) of the spacecraft is achieved by the computer-managed interaction of the navigation, telemetry, and propulsion systems. The computer system consists of nine radiation-hardened, space-ready General Purpose Computers (GPC), each providing 16 MIPS of computing power. All computers will be linked in a FDDI-2 network. The navigation system consists of four star trackers to determine the spacecraft's attitude and position, an Optical Alignment System to recalibrate the star trackers, nine Inertial Measurement Units to sense linear rates of acceleration, and nine Ring Laser Gyroscopes to measure angular rates of acceleration. This system will also monitor the spinning motion of the spacecraft. The telemetry system consists of a long range, high gain radar and a short range landing radar. These radars will guide the spacecraft into the proper Phobos rendezvous position.

## Mission Analysis

Several factors, including  $\Delta V$ 's, mission duration, stay time on Phobos, expected radiation dosage, and proposed launch date, went into the selection of an appropriate mission trajectory. To reduce radiation exposure, it was desirable to plan a mission around a solar minimum. An aggressive launch date was chosen allowing ten years for technological development.

## Opposition Class

Project APEX will use an opposition class mission with a total mission time of 656 days. The proposed departure date from Earth will be November 19, 2010. The outbound trajectory includes a Venus swingby to conserve fuel. Once the ship reaches Phobos on October 3, 2011, the stay time for setting up the processing plant and conducting experiments will be sixty days. The ship will then arrive

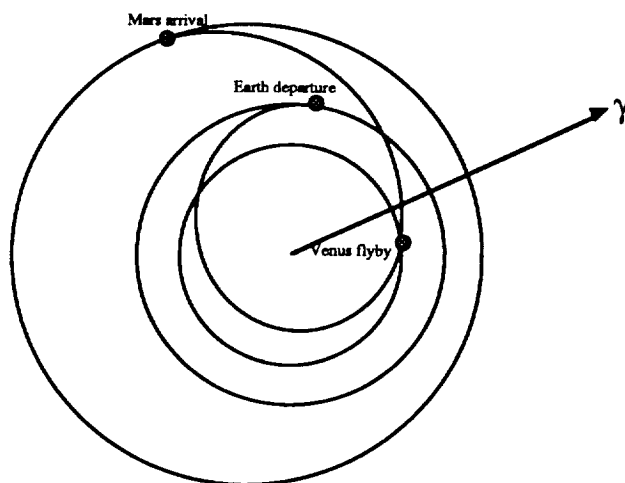


Fig. 11 Outbound Trajectory

back at Earth on September 5, 2012.

### Earth Departure

The spacecraft will leave from LEO (see Figure 11). A single perigee kick will be used to break up the escape burn. The perigee kick was necessary to increase the ship's orbital energy without taking large losses due to G-Loss.<sup>2</sup> The first will put the spacecraft on an elliptical orbit with a period of two days. The second will give the spacecraft the required escape velocity to travel to Mars.

The main concern when doing perigee kicks is the radiation received while passing through the Van Allen radiation belts. These are two belts of high radiation

surrounding the Earth. Using Apollo astronaut exposure levels, the astronauts will receive approximately 6 REM per passage. The total for the first 30 days of the mission will be approximately 28 REM, which is below the 33 REM per month limit.

### Rendezvous with Phobos

When it reaches the Martian system, the spacecraft will insert itself into an orbit of 9400 km, which is 22 km higher than Phobos' orbit. Once the ship's position relative to the moon has been determined, a phasing burn will be performed placing the ship at 6 km from Stickney Crater.

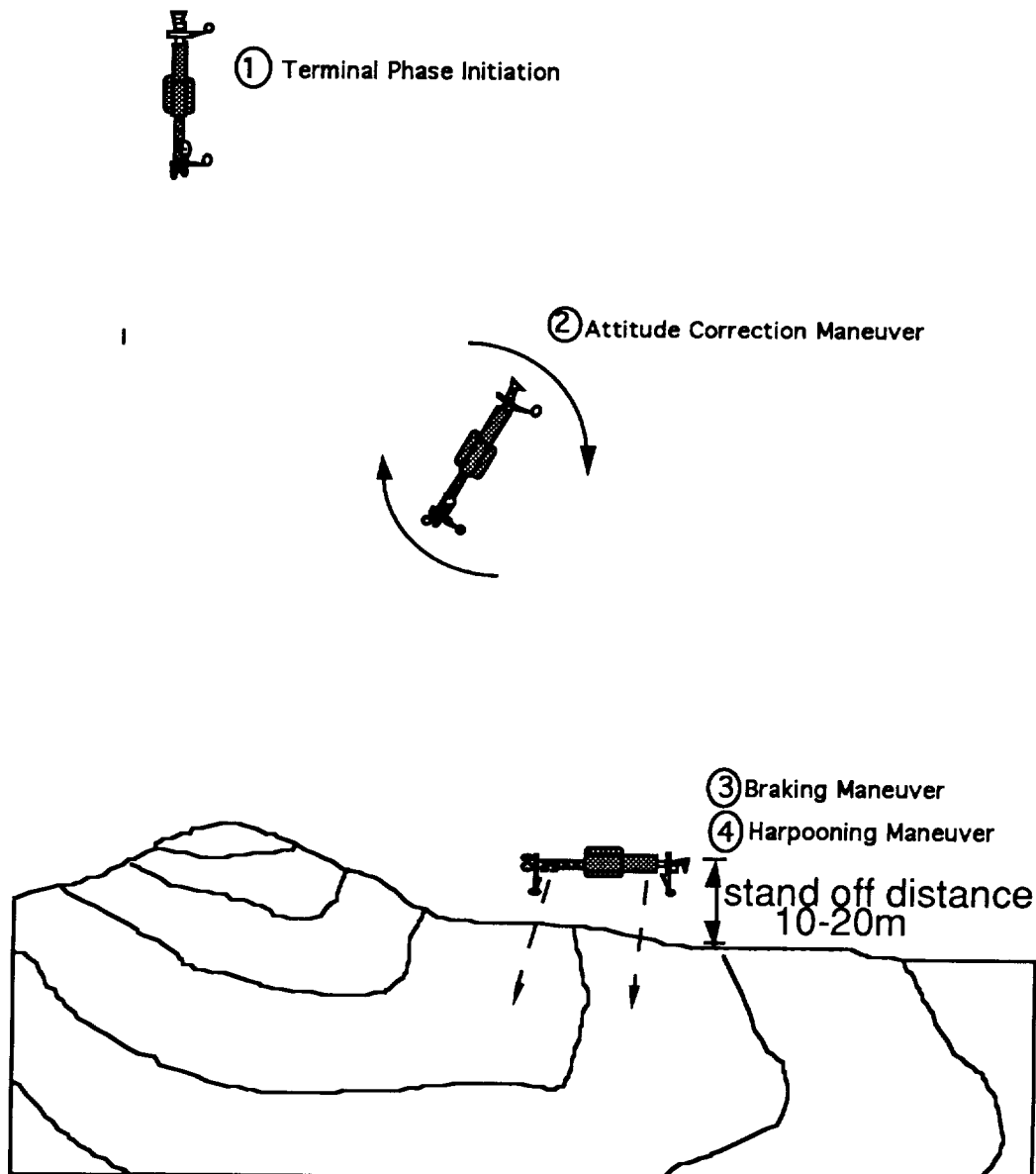


Fig. 12 Landing Maneuver

The spacecraft will land on Phobos near Stickney Crater. Since the gravity of Phobos is very low, the spacecraft will essentially "dock" with Phobos (see Figure 12). When the spacecraft is within twenty meters of Phobos, it will shoot harpoons into the surface and pull itself to the surface. After landing, the ship will remain tethered to the moon's surface because of the extremely low gravity.

### Return to Earth

Once the mission at Phobos is finished, the RCS thrusters will be used to push the spacecraft away from Phobos (see Figure 13). After a safe distance is achieved, the main engines will be used to send the craft towards Earth. At Earth, a propulsive burn will be used to insert the spacecraft into high elliptical orbit. From there, the crew will be quickly removed by orbital transfer vehicles and the craft then slowly brought back to LEO.

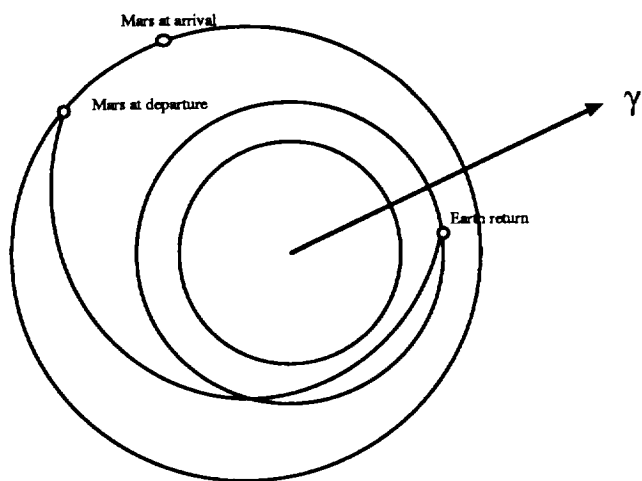


Fig. 13 Inbound Trajectory

### Scientific Research

The scientific objectives for the Mission to Phobos consist of the following:

1. Assessment of the effects of long-duration space travel on human and plant physiology.
2. Assessment of possibilities for extraterrestrial fuel and metals production.
3. Assessment of use of extraterrestrial resources for manufacturing of construction products.
4. Determination of origin of Phobos.

Investigative categories include human life science, plant life science, materials science, manufacturing, Phobean and

Mars soil analysis, and isolation/psychology. In addition, we propose to control a rover on the surface of Mars to acquire more information about Mars in order to facilitate a future manned Martian landing.

### Phobos and Beyond

The utilization of space resources makes for effective exploration of the planets of the solar system. We propose to use materials that already exist on Phobos in an innovative approach to reduce the need, and thus the expense, of bringing everything from Earth. The economy of utilizing space resources is obvious and, the presence of Phobos is the key. The advantages and future use of Project APEX are described below.

A processing plant could be constructed on the Martian surface to create methane. Many current plans have the hydrogen needed for this reaction being shipped from Earth.<sup>4</sup> Extracting the hydrogen from Phobos could be accomplished at a fraction of the cost.

The majority of the fuel in a trip to the Martian system is used in the initial burn at Earth. Launching Phobos-processed fuel to Earth High Elliptical Orbit (HEO) for future mission use provides great cost savings.

Ultimately, Phobos could be used as a refueling station for descending to the Martian surface and for both manned and unmanned missions to the outer solar system.

### Conclusions

The results presented in this report are the products of a preliminary design study of a Manned Exploration of the Mars moon, Phobos. We propose to use technology which may not exist at this time, but can be developed and tested within ten years. Additional areas of advanced research development are needed to support the overall mission success. These include the development of a heavy lift launch vehicle; automated rendezvous and docking capability; maneuverable extravehicular activity suits; telerobotic devices and telepresence robotics; and micro-gravity fuel transfer.

A preliminary estimation indicates that the development and production of the APEX spacecraft will cost \$11.4 billion with an overall mission cost of \$12.7 billion.

As this mission is concerned with making a mission to the Martian system economically feasible, it can be viewed as a precursory mission in a larger plan for much greater, permanent human involvement in space. The Space Exploration Initiative (SEI) is the present attempt by the United States to formulate this large scale plan; this mission can be considered as a small element of that overall, long-term mission.

### References

- <sup>1</sup> Cutts, James A., *Mariner Mars 1971 Television Picture Catalog*, Jet Propulsion Laboratory, Pasadena, CA., 1974, p. 395.
- <sup>2</sup> Borowski, S., *Nuclear Thermal Rocket Characteristics for Human Exploration Initiative Missions*, AIAA report 90-1949, AIAA/SAE/ASME/ASEE 26th Joint Propulsion Conference, Orlando, Florida, 16-18 July 1990.
- <sup>3</sup> Zubrin, R. M., *The Use of Low Power Dual Mode Nuclear Thermal Rocket Engines to Support Space Exploration Missions*, AIAA/NASA/OAI Conference on Advanced SEI Technologies, Sept. 1991.
- <sup>4</sup> Zubrin, R. M., Baker, D. A., *Mars Direct: A simple, Robust, and Cost Effective Architecture for the Space Exploration Initiative*, 29th Aerospace Sciences Meeting, Reno, NV, 7-10 January 1991.

Fifty-four students participated in the design of Project APEX as part of AE 483: Space System Design. The project was conducted during the 1992 winter term.

## MARS TRANSPORTATION SYSTEM

University of Minnesota  
Department of Aerospace Engineering and Mechanics  
Minneapolis, Minnesota

Professors William Garrard and Andrew Vano  
Dave Rutherford, Teaching Assistant

### Abstract

The University of Minnesota Advanced Space Design Program has developed a sample Mars exploration scenario. The purpose of the design project is to enhance NASA and university interaction, to provide fresh ideas to NASA, and to provide real world design problems to engineering students. The Mars Transportation System in this paper is designed to transport a crew of six astronauts to the Martian surface and return them to Low Earth Orbit (LEO) starting in the year 2016. The proposed vehicle features such advanced technologies as nuclear propulsion, nuclear power generation, and aerobraking. Three missions are planned. Orbital trajectories are of the conjunction class with an inbound Venus swingby providing a 60-day surface stay at Mars and an average total trip time of 520 days.

### Introduction

The vehicle and mission profile in this report are the result of a joint study by the University of Minnesota, the Universities Space Research Association (USRA) and the NASA/Marshall Space Flight Center (MSFC). The goal of the Advanced Space Design Program is to provide NASA with fresh ideas and to provide engineering students with real world design problems. Each year schools involved with the program take on a new project and work with a mentor NASA center. This report is a summary of the conceptual design of a Mars Transportation System developed as part of the senior design curricula at the University of Minnesota.

The following mission requirements and assumptions were given to the design class.

### Mission Requirements

- 1) Three missions to Mars will be planned starting in 2016.
- 2) The astronauts will remain on the surface for 30-100 days.
- 3) Landing sites will be selected for scientific interest and will include polar, volcanic, and canyon regions.
- 4) Artificial gravity will be provided for at least the outbound portion of the mission.
- 5) The above objectives will be accomplished in a cost effective manner with acceptable levels of safety.

### Mission Assumptions

- 1) The surface of Mars has been accurately mapped.
- 2) A satellite system for navigation and communication is in place around Mars.
- 3) Nuclear propulsion and aerobraking are mature technologies.
- 4) A Heavy Lift Launch Vehicle (HLLV) system is operational.
- 5) Space Station Freedom is operational.
- 6) A minimal lunar base is operational.

Students were organized into ten disciplines: Systems Layout, Mission Operations, Structures, Aerodynamic Analysis, Crew Systems, Thermal Analysis, Orbital Mechanics, Avionics/Power, and Earth-to-Orbit (ETO)/Orbital Assembly. An iterative design process was used to define detailed design requirements, conduct trade studies, select a baseline configuration, and optimize the conceptual design. A student systems integrator conducted all interdisciplinary meetings and assigned/tracked action items. A Configuration Control Board (CCB) consisting of discipline group leaders selected the vehicle(s) configuration.

### Mars Transportation System

The Mars Transportation System (MTS) is illustrated in Figure 1 and consists of eight major components: the Mars Transfer Vehicle Habitation Module (MTV HAB), the propulsion system and fuel tanks, the biconic lander, the Earth return aeroshell, the Mars ascent/descent vehicle, Mars aeroshell, a communication and navigation array, and a central truss which serves as a common mounting bus for all of the other sub-components. Masses of the major components are presented in Table 1.

| Component                    | Mass(mT)     |
|------------------------------|--------------|
| Truss                        | 15.7         |
| Biconic                      | 143.4        |
| Aeroshell(Earth)             | 12.5         |
| MTV HAB                      | 63.9         |
| Ascent/descent vehicle       | 26.9         |
| Engines, fuel tanks, and RCS | 57.0         |
| <u>Aeroshell(Mars)</u>       | <u>39.7</u>  |
| Total(dry)                   | 359.1        |
| <u>Propellant</u>            | <u>705.2</u> |
| Total (with 15% contingency) | 1118.2       |

Table 1 MTS Vehicle mass breakdown



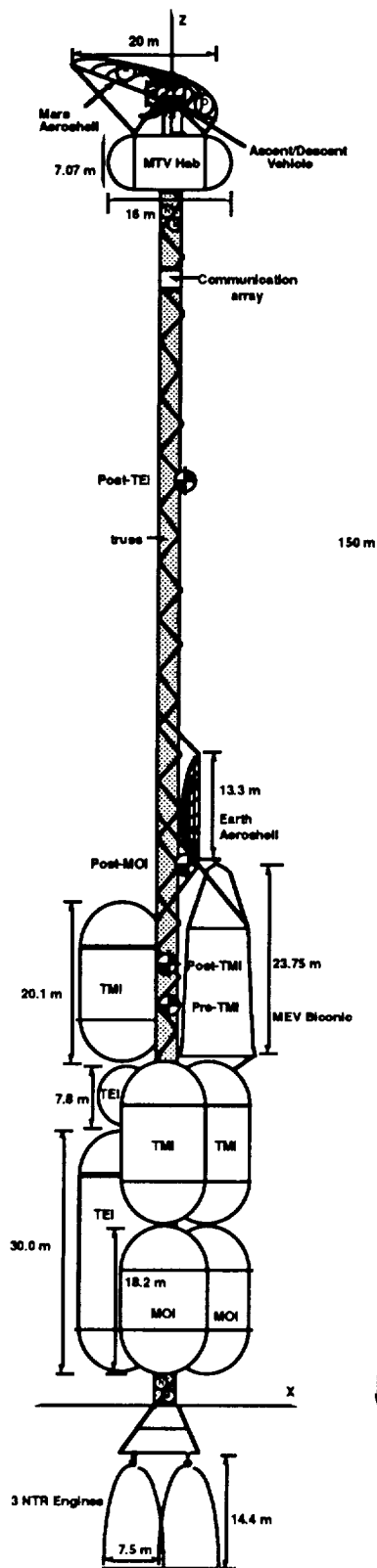


Fig. 1 Mars Transportation System

Each of these components will be discussed in detail in the following presentation.

### Truss

The spine of the MTS system is the common mounting bus provided by a central truss and thrust structure. The truss is 150 meters long with a 3-meter equilateral triangle cross section. The truss members are constructed of boron-aluminum metal-matrix composite (MMC) and typically have outside diameters of 13 cm and wall thicknesses of 2 mm.

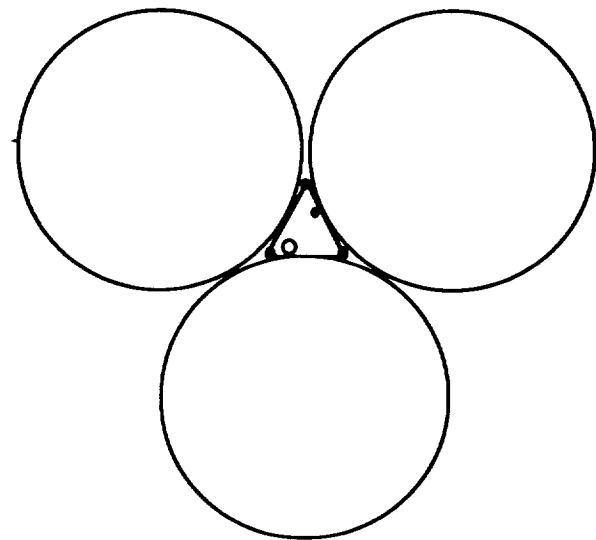


Fig. 2 Cross-section of truss with fuel tanks attached

The decision for selecting a central truss mounting structure was the result of the design requirement for artificial gravity. It was decided that the dynamics of tether systems are too unreliable, leaving the truss as the only practical option.

The truss also serves the secondary purpose of separating the habitation area from the radiation generated by the Nuclear Thermal Rockets (NTRs) and the Dynamic Isotope Power System (DIPS). In addition to the distance to reduce the radiation exposure, a blast shield is designed on the end of the truss to provide additional protection. A final line of defense to protect the crew from radiation generated by the NTR engines and DIPS power system is provided by positioning the fuel tanks along the truss between the radiation source and habitation module. Figure 2 is a cross-section of the MTV which shows how the fuel tanks are

attached to the truss and the location of power trunks, communication/control lines, and fuel lines within the truss.

Finite element modeling of the truss has shown that it has excellent static and dynamic performance criteria. Under full thrust the truss should compress only 7 cm and when rotating at a rate sufficient to generate 1 g of simulated gravity on the Trans Mars Injection (TMI) coast, it should only stretch 25 cm. The safety factors for this design are 1.3 for tension and 65.5 in compression. To prevent harmonic resonances from shaking the truss apart, a series of accelerometers and Reaction Control System (RCS) pods are used to identify and counteract these resonance frequencies before their amplitude grows to a dangerous level.

The truss is constructed in Low Earth Orbit (LEO) by assembling 5 prefabricated bays of 30 meters length each.

### MTV HAB

While in space the crew will reside in the MTV HAB. Dimensions of the module are presented in Figures 3 and 4. This single pressure vessel is designed to provide life support for a crew of six for 550 days. The habitat module consists of four main areas: living areas, science or work areas, a storm shelter, and an airlock. These areas are arranged so as to minimize the noise created by work, training, or exercise activities in the living areas.

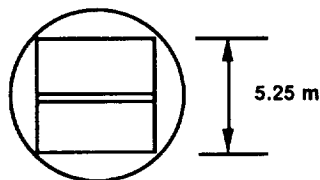


Fig. 3 Cross-section of MTV HAB

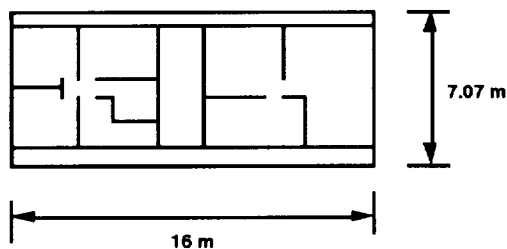


Fig. 4 Floorplan of top level in MTV HAB

After Mars Orbit Injection (MOI) the crew transfers from the MTV HAB into the descent module. Upon arrival on the Martian surface the crew lives in the habitat provided in the biconic lander. If at any time the surface habitat should become unable to support the crew members they will return to orbit and carry out studies from orbit within the MTV. Sufficient consumables and Environmental Control and Life

Support System (ECLSS) redundancy allow the crew to spend the entire 520 days in the MTV HAB if necessary.

The proposed ECLSS system for the MTV HAB is a partially closed loop which reuses only non-potable water. This greatly increases the safety factor of the mission as the crew will not rely on the reuse of its primary water supply for life. A complete backup system is provided in the HAB in case of partial or total failure of the primary ECLSS system.

### Biconic Mars Excursion Vehicle

Because the wake area behind the largest single element aeroshell is insufficient to contain all of the equipment that needs to go to the surface of Mars, an unmanned biconic lander is designed to carry the rovers, the Mars Habitation Module (MHM), and all other surface equipment. The external shape of the biconic lander is presented in Figure 5. The higher g-loadings and harder landing makes it an unacceptable vehicle for the crew transfer.

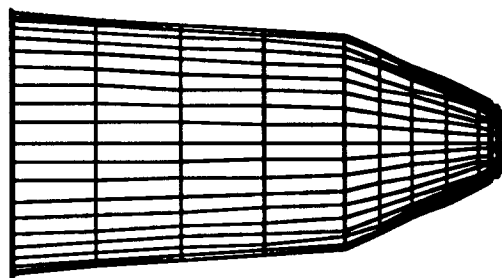


Fig. 5 45° Flared Biconic aerodynamic model

Once on the surface, the crew traverses across the Martian landscape to reach the biconic. A sophisticated navigation system should keep this distance very small, approximately 0.5 km.

On the surface, the crew resides in the MHM, significantly smaller than the MTV HAB, but able to provide all life support functions for a surface stay of 60 days. Figure 6 shows a vertical cross-section of the lander. Power is provided by a DIPS power system, which is deployed away from the MHM to reduce the crew's exposure to radiation, and which remains active after the crew departs to provide power for the rechargeable robotic rover and the transmitters onboard the biconic.

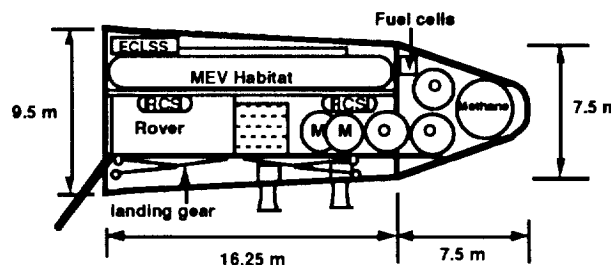


Fig. 6 Schematic of Biconic lander

The biconic lander features an advanced thermal protection system based on the one currently used by the space shuttle. A cross-section of the thermal protection system is shown in Figure 7. The most significant change is the addition of a  $\text{ZrB}_2$  coating to the outer skin of the tile to provide increased heat resistance.

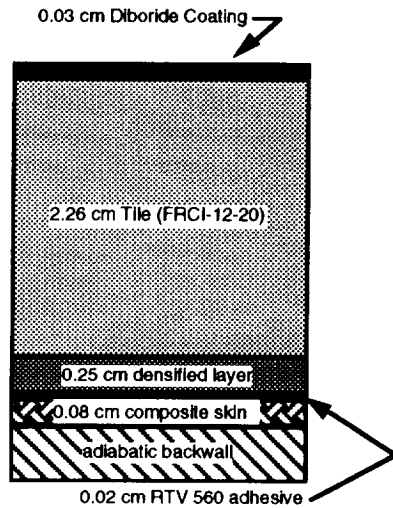


Fig. 7 Advance Thermal Protection System tile

#### Aeroshell-Assisted Mars Ascent/Descent Vehicle

The Aeroshell-Assisted Mars Ascent/Descent Vehicle is illustrated in Figures 8 and 9. This vehicle provides an accurate lander which transports the crew to and from the surface of Mars. The ascent vehicle is a secondary stage which is placed on top of the landing gear of the descent stage. Like the lunar excursion modules from the Apollo program, the descent stage remains on the surface to act as a launch platform for the ascent stage.

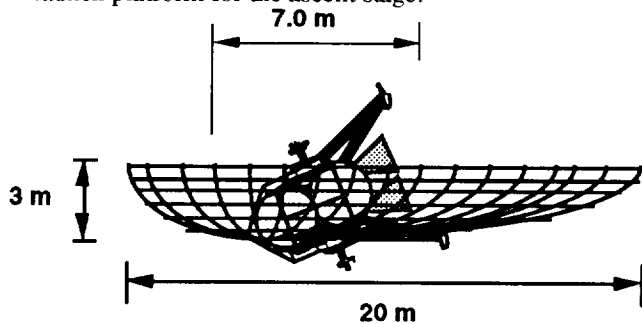


Fig. 8 Ascent /descent vehicle nested in Mars aeroshell

Once the ascent stage has returned the crew and the 2 mT of soil samples to low Martian orbit, it maneuvers the crew back to the MTV and docks with the airlock. This must be

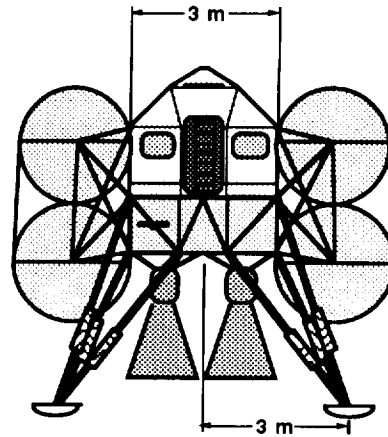


Fig. 9 a. Front view of ascent/descent vehicle

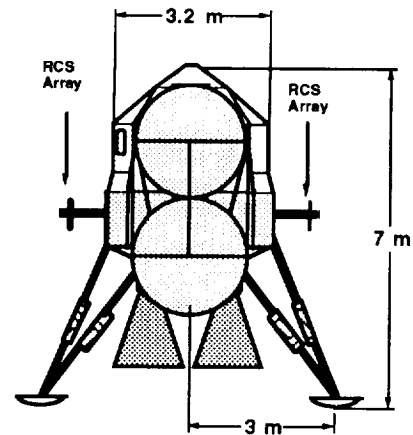


Fig. 9 b. Side view of ascent/descent vehicle

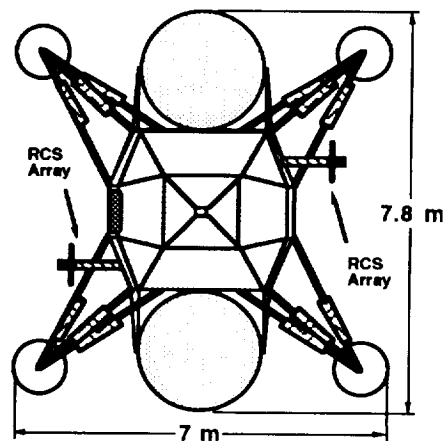


Fig. 9 c. Top view of ascent/descent vehicle

carried out within 8 hours because there is no life support system onboard the ascent stage. The astronauts will rely on the personal life support systems on each of their Extra Vehicular Activity (EVA) suits until back aboard the MTV. While this may seem like a short time, it allows several opportunities for the ascent stage to dock with the MTV.

### **Propulsion System and Tanks**

Perhaps the key technology which enables the mission scenario presented in this report is the Low Pressure Nuclear Thermal Rocket (LPNTR). This engine is a development from the standard solid core NTR but differs in that it does not need a complicated turbopump system since its combustion chamber pressure is very low (approximately 1 - 2 atmospheres). With such a low pressure in the combustion chamber, the pressure in the fuel tanks is enough to drive fuel into the engine. One drawback is that large nozzles are required to develop as much thrust as possible from the expanding exhaust gas. This is a small price to pay for the increased performance due to the LPNTR's higher operating temperature and reduced complexity of its design. The final engine system is a set of three independent engines mounted on gimbals that can swing  $\pm 7^\circ$  in any direction in order to compensate for single engine out situations and shifts in the center of gravity location.

The tanks for the Mars Transportation System (MTS) are designed so they may be easily manufactured and transported to LEO. All of the tanks have an outside diameter of 11.2 meters and hemispherical endcaps. The length of the tanks is all that needs to be changed for different tank volumes. The tanks are constructed of Kevlar 49 and E-glass and are covered with super-insulation to reduce the amount of liquid hydrogen which boils off.

### **Earth Capture Aeroshell**

To return to Earth, the crew climbs back into the Mars Ascent Vehicle (MAV), taking the samples of Martian soil and the memory subprocessor unit from the MTV main computer with all of the mission information stored on it. As the crew nears Earth they stop rotation of the MTS, enter the MAV, and maneuver to the Earth aeroshell near the center of the vehicle. This maneuver will be performed about one day before the MTS arrives at Earth. As the MTS nears Earth, the docked MAV/Earth capture aeroshell package breaks away from the truss and aerocaptures into Earth orbit while the truss coasts past Earth and enters into a heliocentric orbit. Sufficient ECLSS and consumables are aboard the MAV and Earth capture aeroshell to support the crew for 3 days, as well as enough fuel to achieve a propulsive  $\Delta v$  of 1 km/s.

### **Communication and Navigation Array**

Essential to the success of this mission is an accurate navigation system and communication system which allow continuous communication with the Earth. These goals are met by an advanced integrated avionics package which is based on the existing Airplane Information Management System (AIMS).

Accurate navigation while in space is accomplished using a star tracker and an Inertial Measurement Unit (IMU). While either of these systems can be used independently, they are cross-checked in order to attain an even higher degree of accuracy. Navigation on the surface of Mars is accomplished through the use of radio beacons placed on the surface, two orbiting satellites, and the MTV. The pressurized rover has an additional 'dead-reckoning' system which acts as a backup in case of a communication's failure.

The communication needs for the mission are met by an advanced phased array antennae system onboard the MTV. This system is far more flexible than the dish-based systems currently in use. Not only will it enable communication with the Earth while the vehicle is rotating, but it also features fewer moving parts and much higher redundancy than a dish system with similar performance characteristics. The frequency of the proposed system lies in the Ka band and has a data transmission rate of nearly 100 Mbps, sufficient for television quality video.

While on the surface the crew's transmissions are relayed to the MTV and the two orbiting communication/navigation satellites and the MTV. They are then be amplified and directed to the Earth.

### **Landing Sites**

Three different landing sites are chosen for the three missions to Mars. The sites are Olympus Mons, Valles Marineris, and Mangala Valles. These sites are chosen on the basis of geologic/scientific interest as well as ease of access.

Olympus Mons is located at  $13^\circ$  N latitude, and  $139^\circ$  W longitude. The Olympus Mons formation consists of large volcanoes and fissure vents. The mission to this area allows the crew to come close to a semi-active volcanic assemblage. The astronauts explore the surrounding territory to determine the age of these volcanoes, when they last erupted, and what types of ashen substances they have erupted in the past.

The second site, Valles Marineris, is located at  $6^\circ$  S latitude, and  $78^\circ$  W longitude. This site is composed of a sequence of thick plateau rocks, capped around their western

region by ridged plains. At this site the crew explores the effects of volcanic tectonics as well as wind and water erosion on the formation of the canyons. The astronauts determine when the water that carried the ashen sediments was present and if its presence was due to migrating glaciers from the ice caps or lakes and streams.

Mangala Valles, the third site, is located at  $7^{\circ}$  S latitude,  $147^{\circ}$  W longitude. This site possesses numerous channels and possible underground wells. The astronauts determine the effects that volcanic tectonics played in the formation of the channels. The possibility of glaciers in the equatorial regions, which may have caused major glacial slides, is also investigated.

### Crew Activities

On the surface of Mars, six astronauts explore the planet and perform experiments. The astronauts are divided into one group of four and one group of two.

The two-person crew spends half their mission time traveling in the pressurized rover and the other half of their time stopping to take samples and drill. Because the pressurized rover's oxygen capacity is twelve days the mission time is limited to ten days. In the event of treacherous terrain, or if the crew needs to spend more time at one site than another, extra time has been allotted for each trip.

The four-person crew uses the unpressurized rover along with the large coring drill on daily excursions. This crew obtains core samples at radial directions around the base camp and takes the samples back to the habitation module for testing. They set up and take down equipment at the beginning and end of each excursion. The four-person crew is also responsible for testing the samples brought back by the pressurized rover team. The crew works in shifts of two teams for ten hours on, ten hours off.

During the time in transit, all six astronauts will work in 8-hour shifts on interplanetary research and preparation for the excursion on Mars.

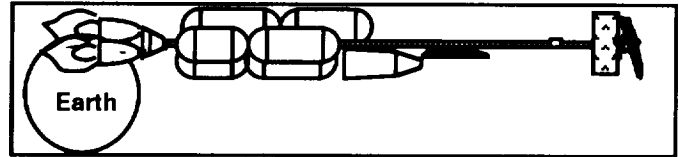
### Mission Profile

#### ETO and On-Orbit Construction

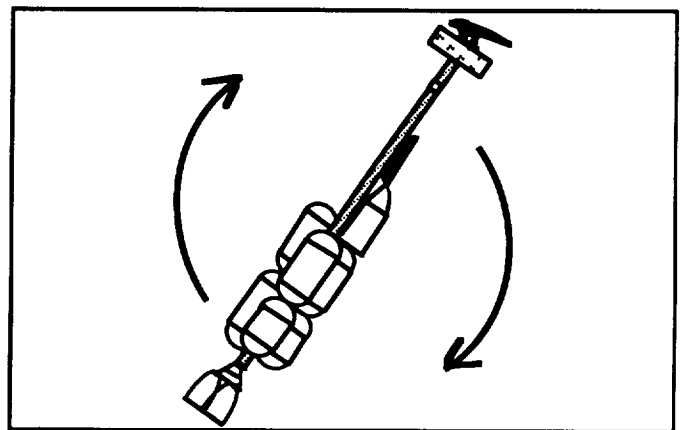
Two of the most important portions of the entire design project are the ETO and construction in LEO. Since launching a complete MTV directly from the Earth's surface is cost-prohibitive, all of the components are designed to be packaged and launched by projected launch vehicles. The vehicle chosen was the NLS-derived HLLV which features 4 LOX/RP boosters with a maximum payload of 224 metric tons. All components are designed to fit within the payload

shroud and mass to LEO restrictions of this vehicle while minimizing the amount of orbital construction required.

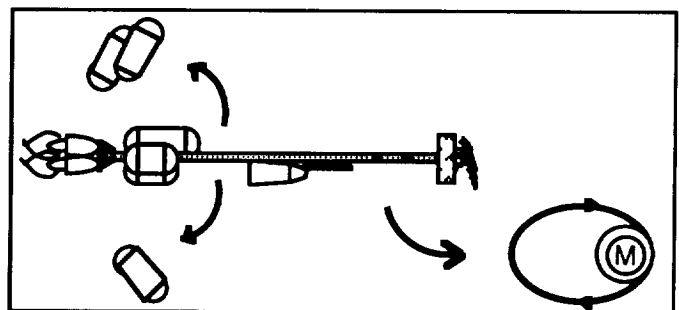
### Graphic Mission Profile



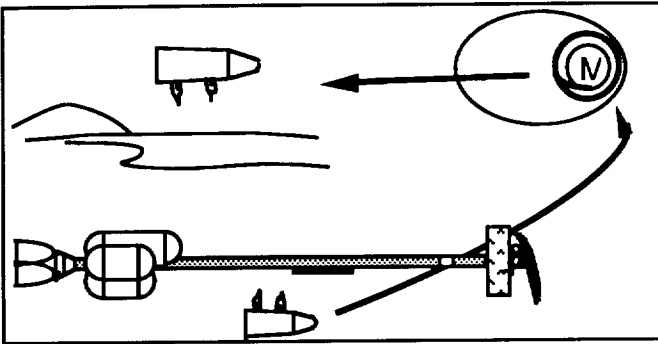
Phase 1. The NTR engines fire for the Trans-Mars Injection.



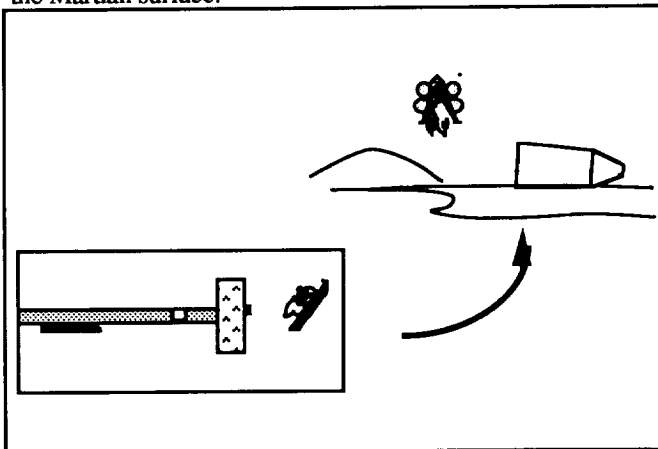
Phase 2. The rotation to generate artificial gravity is initiated and the MTS coasts to Mars. A mid-course correction and plane change requires stop and restart of rotation.



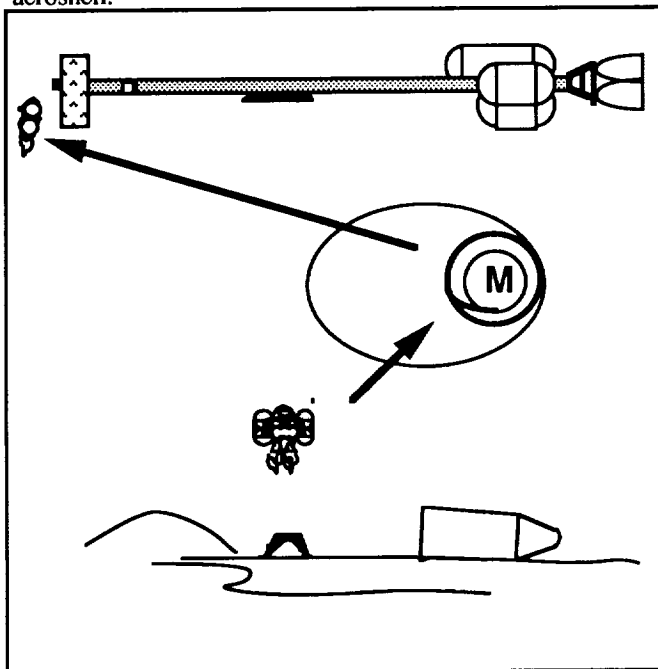
Phase 3. At Mars Orbit Injection the MTS stops rotating, jettisons empty fuel tanks, and propulsively brakes into an elliptical parking orbit around Mars.



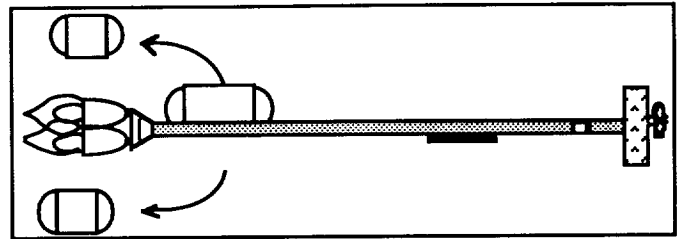
Phase 4. The biconic releases from the MTV, transfers to a circular parking orbit, performs a deorbit burn, and lands on the Martian surface.



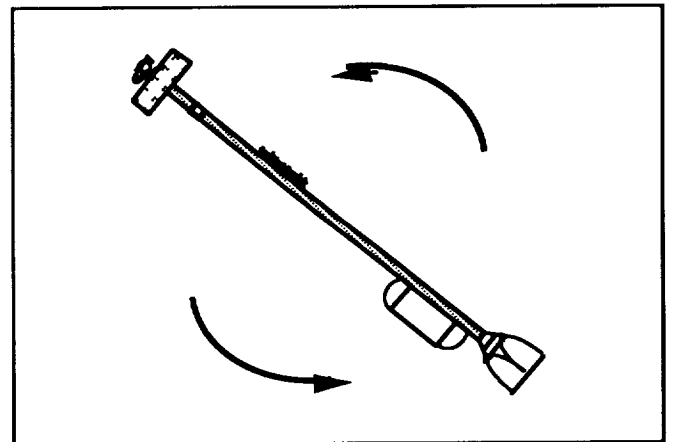
Phase 5. The crew lander separates from the MTV, changes orbits, and lands after aerobraking and jettisoning the aeroshell.



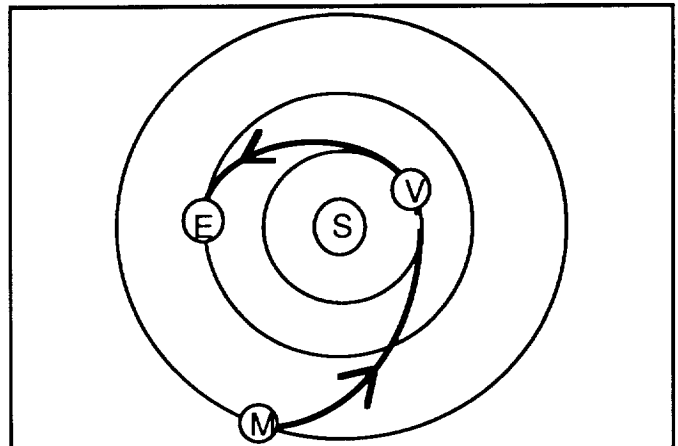
Phase 6. After completion of the stay on Mars, the crew returns to Martian orbit in the ascent module to rejoin the MTV.



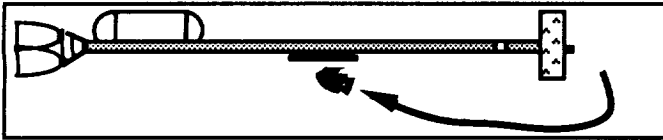
Phase 7. MTV jettisons the empty MOI tanks and performs Trans-Earth Injection burn.



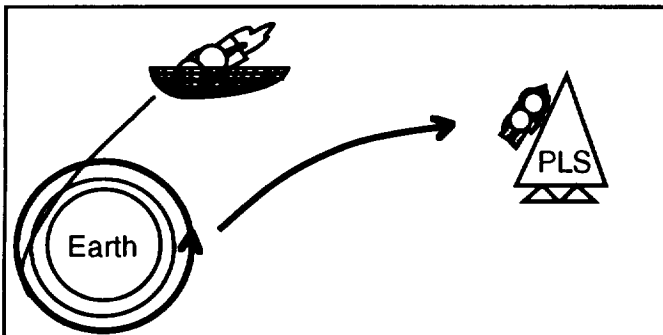
Phase 8. Artificial gravity is once again generated on the coast by rotating the ship. Due to reduced vehicle mass only 0.5 g is generated.



Phase 9. The MTS stops rotation for the Venus swingby maneuver. After the swingby, rotation is reinstated until one week before EOI.



Phase 10. The crew enters the Mars ascent vehicle, taking with them the soil samples and the memory units and maneuver to the MAV into the Earth Return Aeroshell.



Phase 11. Over a period of several days, the MAV and Earth Return Aeroshell aerobrake into a Low Earth Orbit. The crew rendezvous with the Space Station or Personnel Launch System vehicle. The MTV coasts past Earth and enters into a heliocentric orbit.

#### Outbound leg: Mission Phases 1-4

During this phase of the mission the crew completes its training and hones its skills to prepare for their arrival at Mars. Studies focus on research which cannot be conducted onboard a space station. These include effects of long-term exposure to simulated gravity on the human physiology, ECLSS demonstrations, and studies of micrometeoroid population and radiation fluxes in deep space.

#### Mars Surface Operations: Mission Phases 5-6

The 60 day surface stay does not offer much time for the extensive ground operations which are to be conducted. Five long-range pressurized rover trips and approximately 50 unpressurized trips are planned. Along with setting up the initial camp and surveying the area for interesting sites of

intense study, the crew will unload and assemble the rovers. Surface studies focus on the geologic history of Mars and the possibility of past or existing life forms on the planet.

#### Inbound Leg: Mission Phases 7-11

Once the crew has completed the surface operations, their next goal is to return to the MTV with the samples of Martian soil and initiate the TEI burn. On the return trip the artificial gravity will once again be initiated (Phase 8), and the crew continues scientific studies on the samples they collected.

#### Conclusion

Before this project becomes reality, several questions must be answered. First, the third launch window with the high chance of major solar flares raises the question whether the new technology of the year 2022 will be sufficient to ensure the safety of the crew. Second, a trip of this magnitude will have profound effects upon the crew's psychological makeup. The psychological and physiological effects on the crew are not well understood and therefore must be examined before a trip of this type is undertaken. Third, much of the technology used by the MTS remains in the conceptual stage. NTRs have not been developed much beyond laboratory designs and aerobraking remains a theoretical idea with very little hard data. This design relies heavily on these technologies.

Even with the assumptions made in it, this design represents a scenario which is very possible within the predicted timeframe. The two vehicle landers represent an optimal solution to the lander problem, which maximizes the payload to the surface while maximizing crew safety at the same time. The nuclear power sources for the surface operations are able to support robotic exploration long after the crew returns to Earth. The choice for three consecutive opposition class missions provides for a maximum amount of research without the prohibitive stay time associated with conjunction class missions. Finally, the rotating truss represents an excellent solution to the crew conditioning problem.

**PROJECT WISH:  
THE EMERALD CITY**

**The Ohio State University  
Department of Aeronautical and Astronautical Engineering  
Columbus, Ohio**

**Dr. Hayrani Oz  
Jim Dunne, Teaching Assistant  
Stan Butchar, Tommy George, Rob Hellstrom, Tricia Kringen,  
George Owens, Mike Perrea, Paul Semeraro, and Phil Thorndike**

**Abstract**

Phase III of Project WISH saw the evolution of the Emerald City (E-City) from a collection of specialized independent analyses and ideas to a working structural design integrated with major support systems and analyses. Emphasis was placed on comparing and contrasting the closed and open cycle gas core nuclear rocket engines to further determine the optimum propulsive system for the E-City. Power and thermal control requirements were then defined and the question of how to meet these requirements was addressed. Software was developed to automate the mission/system/configuration analysis so changes dictated by various subsystem constraints could be managed efficiently and analyzed interactively. In addition, the liquid hydrogen propellant tank was statically designed for minimum mass and shape optimization using a finite element modeling package called SDRC I-DEAS, while spoke and shaft cross-sectional areas were optimized on ASTROS (Automated Structural Optimization System) for mass minimization. A structural dynamic analysis of the optimal structure also conducted using ASTROS enabled a study of the modes, frequencies, displacements, and accelerations of the E-City. Finally, the attitude control system design began with an initial mass moment of inertia analysis and was then designed and optimized using linear quadratic regulator control theory.

**Introduction**

Project Wandering Interplanetary Space Harbor (WISH), a three-year advanced design project at the Ohio

State University, began as a possible follow-up to the current Space Exploration Initiative (SEI) program set forth by President Bush and NASA. The goal of Project WISH is to design conceptually a spacecraft to be used in the exploration of the solar system during the mid-21st century. This design entails a Permanently Manned Autonomous Space Oasis (PEMASO), designated the Emerald City (E-City), with a mission to support colonization and exploration efforts throughout the solar system. Home to 1000 colonists, the E-City must have the capability to re-station itself almost anywhere in the solar system within a transit time of three to five years. Envisioned to become operational in the year 2050, PEMASO must be self-sufficient, requiring no additional resources from Earth once deployed. Based on the SEI time line, by the middle of the 21st century, humans should be firmly established on the moon and Mars, and a great deal of experience in working and living in space will have been accumulated. At a nominal orbit of four Astronomical Units (AUs), the E-City will be in an ideal location to mine the asteroids for natural resources as well as to obtain hydrogen from Jupiter's atmosphere.

Phases I and II of Project WISH established the groundwork for Phase III and were conducted during the 1989-1990 and 1990-1991 academic years. Phase I encompassed a general level study of the major systems required for the E-City while Phase II completed a more in-depth study into the disciplines of orbital mechanics, propulsion, attitude control, and human factors. Guidelines were also established for the design of the ship and were used to carry out two particular missions of interest: a Saturn Envelope mission and an Earth-to-Mars mission.



Phase III Project WISH (Figure 1) saw the evolution of the E-City from a collection of specialized independent analyses and ideas to a working structural design integrated with major support systems and analyses. Optimization and system integration were key in establishing the final design parameters. Detailed analyses and studies were conducted in propulsion, power and thermal control systems, mission/ system/ configuration design, static and dynamic structures, and attitude control.

### Propulsion

The propulsion system is one of the most challenging design aspects of Project WISH in terms of the performance requirements it needed to achieve. Achieving total delta-V's ranging from 50-100 km/sec as a propulsion capacity is no easy task.

Throughout the three-year period of Project WISH, feasibility studies of several conceptual propulsion systems have been performed. The Phase I design team had analyzed chemical, nuclear, and anti-matter rocket engines before recommending anti-matter as the most probable system. The Phase II design team, reconsidering that the anti-matter engine was too conceptual in nature for the time frame of Project WISH, proposed to use a gas-core nuclear rocket engine, the space radiated gas core nuclear rocket (SRGCNR), or open-cycle engine. The Phase II team had hoped that the high specific impulse it generated and its projected technological feasibility engine would prove satisfactory to the needs of E-City. However, due to hazardous radiation emitted from the exhaust plume and high mass penalty associated with these engines, it was decided to reconsider once more the system used for main propulsion.

The open-cycle engine operates by using fissioning gaseous uranium to transmit thermal energy to a hydrogen propellant. The hydrogen is then exhausted out the nozzle at high speeds. The advantage of this engine is the high value of specific impulse that it can generate. Specific impulse is a measure of the amount of momentum transfer per unit weight of propellant. The higher the specific impulse, the less propellant that is needed to achieve a certain velocity. Since the open-cycle can produce specific impulse values within the range of

2000 - 6000 seconds, the Phase II team felt that this engine was sufficient for E-City.

The open-cycle engine has two serious drawbacks, both of which are related. Because the uranium is in contact with the hydrogen propellant, there is a loss of uranium out the nozzle. The Phase II team calculated that the amount of uranium loss would approach almost 2 metric tons per engine per day of operation. The second drawback is that the exhaust plume from this type of engine contains large amounts of harmful radiation. This results in excessive shielding required to protect the inhabitants of E-City.

Using the open-cycle propulsion system, the Phase II team had calculated that it would require at least 33 engines for a mission from Earth to Mars. A trip to Saturn would require 172! This also added to the mass of E-City. Still, because the specific impulse seemed to be the governing parameter for the propulsion system, these drawbacks were tolerated.

This year, in an effort to solve the plume radiation problem and reduce the mass of E-City, another type of nuclear rocket engine was studied. Known as the closed-cycle, or nuclear light bulb (NLB) engine, its nature of operation immediately solves problems associated with the open-cycle engine.

The NLB functions in much the same way as the open-cycle engine, except that the gaseous uranium is enclosed in internally cooled, transparent structures. Neon surrounds the gaseous core to separate it from the transparent enclosure and to attenuate the extreme temperature of the uranium. Thermal radiation from the uranium is transmitted through the neon and transparent structures to a seeded hydrogen propellant. The seeding is made up of microparticles of tungsten to help increase the amount of thermal energy transmitted to the propellant. Because the gaseous uranium does not come into contact with the propellant, the exhaust plume does not contain any harmful radiation.

The uranium and neon are part of an intricate closed-cycle system designed to keep the engine from overheating. Essentially, the hot gases are run through the turbopumps and heat exchangers to convert liquid hydrogen propellant into a gaseous state. The cooled uranium and neon are then recycled back into the system

## EMERALD CITY CONFIGURATION

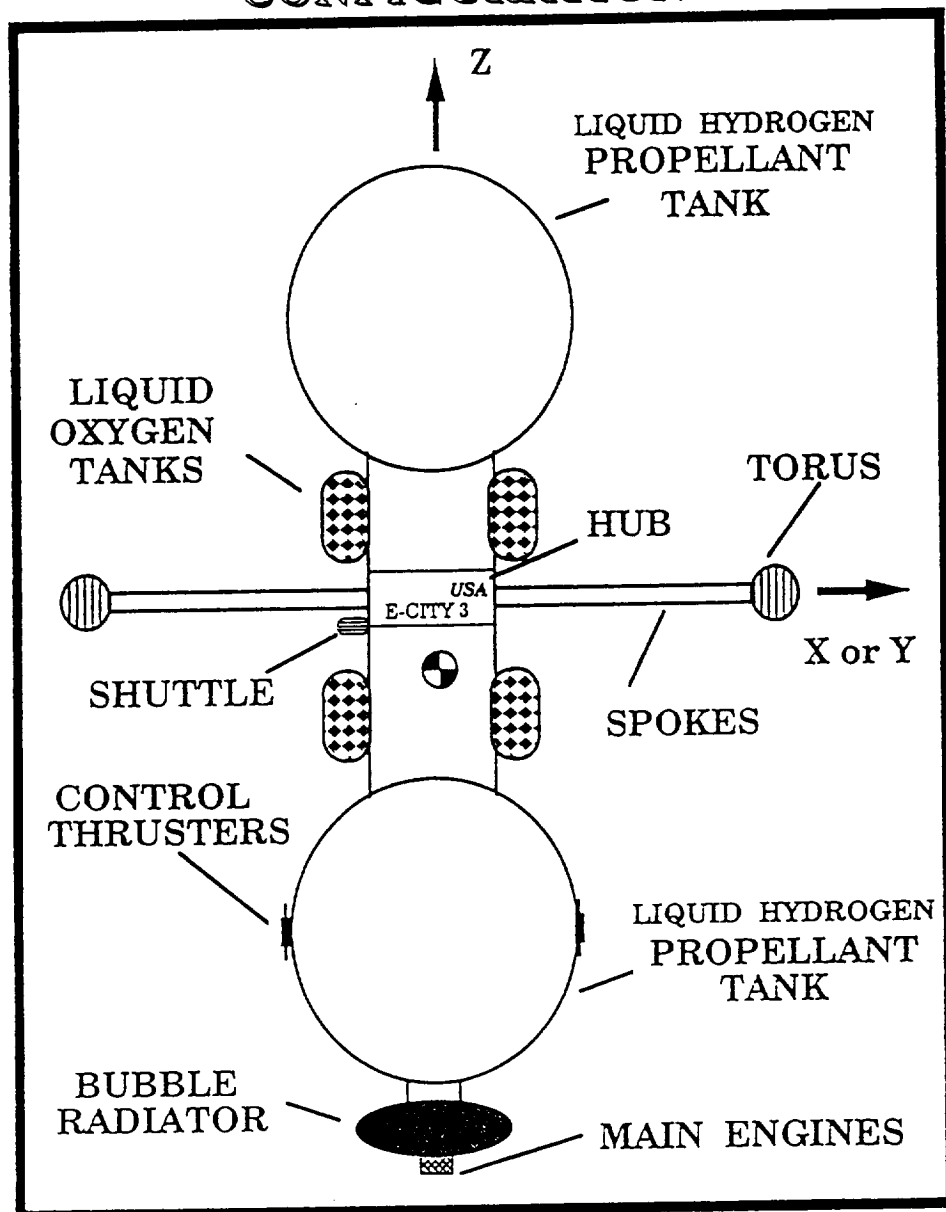


Fig. 1 Emerald City configuration

for further thermal control of the NLB. It is the closed-cycle process of the NLB that prevents uranium loss during operation.

The NLB does not generate as high a value of specific impulse as the open-cycle engine. However, the thrust it produces is ten times higher than that of the open-cycle. From this year's analysis, it was found that an increase in the thrust, and specifically the thrust-to-weight ratio, would dramatically reduce the number of engines required for a given mission.

With the radiation problem taken care of and the mass penalty reduced, it seemed that the use of the NLB engine as the main propulsive system was warranted. However, until an analysis was performed that directly compared the NLB to the open-cycle engine, a final decision on the best system for E-City could not be made.

Using the previous Project WISH reports and information provided by NASA Lewis Research Center, it was possible to achieve comparable results between the NLB and open-cycle engines. The information provided by Dr. Borowski contained performance parameters for seven experimental NLB engines. Some of these engine characteristics were engine thrust, uranium radiating temperature, specific impulse, and hydrogen propellant flow rate. By representing these parameters as a function of the radiating temperature, it was discovered that most of the NLB engine characteristics increased parabolically. The only exception was for specific impulse, on account of thermodynamic factors associated with NLB operation.

Through curve fit approximations of the data using a software package, it was possible to find any desired parameter as a function of the radiation temperature. Based on the functions generated by curvefitting, two FORTRAN programs were written expressly for the purposes of Project WISH.

The accuracy of the programs was checked with known data points supplied by Dr. Borowski. The average percent deviation was 0.59%, which proved that the curve fit functions were adequate for the purposes of Project WISH.

Performing the calculations necessary to determine the number of engines required for a given mission with a specific impulse of 3100 secs, thrust of 9.4 million

Newtons per engine, and a thrust to weight ratio of 9.6 per engine, it was found that only one engine was required for a mission to Mars and the envelope mission to Saturn would require 14 NLB engines.

As expected, the NLB engine far exceeded the open-cycle engine in terms of performance requirements and projected available technology for E-City. Use of the NLB means that the plume radiation problem is eliminated. The fact that the number of engines required for a given mission is more than ten times less than an open-cycle system points to a further reduction in total engine mass. Based on the results of the analysis, the NLB engine is the recommended propulsive system for E-City.

## Mission, System, and Configuration Design

### Mission Profile

The Saturn envelope mission profile was chosen as the baseline because it has the most demanding performance requirements of all the feasible missions.<sup>1</sup> It requires a delta-V of 50 km/sec for transfer from the nominal orbit of 4 AU.

The primary objective of the structural design was to minimize the dry mass while fulfilling essential performance parameters. The driving factor determining the overall mass is the amount of propellant required for the mission. Equation 1 shows the relation between the dry mass and the propellant mass,

$$m_p = m_{dry} \left[ \exp \left( \frac{\Delta V}{I_{sp} g} \right) - 1 \right] \quad (1)$$

The value of  $m_p/m_{dry}$  was 4.19 using a delta-V of 50,000 m/s and an  $I_{sp}$  of 3095 sec, which dramatically shows the impact of adding mass.

### System Parameters

The computation of system parameters (masses, dimensions, forces, etc.) was automated so that the effect of changes in the configuration could be analyzed interactively. The 30 design variables that were used are those that affect the dry mass of the E-City.

The configuration of the E-City is the result of integrating the requirements dictated by a low mass, structurally sound design, good controllability, and minimum stress on the inhabitants. The inhabited and rotating torus section was found to be the most efficient geometry for the living space. Its dimensions were determined by human factors considerations studied in reference 1 on the Phase II design.

The closed-cycle nuclear engine allows minimization of the radiation shield to that required to protect the inhabitants from cosmic and solar radiation, and it surrounds the torus. It consists of 14 meters of liquid hydrogen contained in a separated pressure vessel, with a vacuum between it and the inhabited torus for enhanced thermal insulation.

The hydrodynamic effort of tank rotation is a potentially more serious problem, and is caused by a radial acceleration (caused by rotation) that is up to 100 times greater than the longitudinal acceleration (from thrust). At some point the tank will effectively "run out of gas" because the propellant is forced away from the main feed orifice (drain) and against the wall. If there is no thrusting, the propellant will pile up along the walls with a tube of gas running down the centerline, and none of the  $\text{LH}_2$  will reach the drain, even with full tanks.

The number of tanks used in the final design will not depend on the total tank mass. Software<sup>2</sup> was developed to compare the total mass and total surface area for various aspect ratios and numbers of tanks. Studies show that the total mass decreased as the number of tanks was increased. On the other hand, the total surface area increased. This comparison also conclusively showed that a sphere was the most optimum shape for the tank configuration regardless of the number of tanks used.

The primary disadvantage of one tank is the potential loss of the entire propellant load due to tank failure, whether caused by collision or random failure. Redundancy was the primary consideration in dividing the propellant load into two tanks.

## Structural Design

### Static Structure

The static structural analysis played a pivotal role in the design of the E-City. It was used as the initial basis for the determination of cross-sectional areas and other dimensions, which were then analyzed as a whole for the dynamic behavior of the entire vehicle. Those areas that needed further modifications to meet structural dynamic criteria were then treated and allowances made for the required modifications. The majority of the static structural analysis was included in a parameters program,<sup>2</sup> since the overall mass was related to the component dimensions and their densities.

### Propellant Tanks

It was the intent of this design effort to optimize the tank configuration so that the total mass was minimized. Since the tank is the single largest component on the E-City, mass minimization was essential to gain the highest performance possible. Pressure vessel theory is fine for determining the overall stress characteristics of the propellant tank, but is inadequate for pinpointing stress concentrations due to the combined loads of thrusting, rotation, and pressure.

The models were created on I-DEAS utilizing the symmetry of the tank to reduce the size of the model and the number of elements in the finite element model. A benefit of this method of modeling was to reduce the computing time necessary to solve the finite memory required to execute the mesh solver.

Initially the tank structure was optimized, maintaining a constant volume and using only the pressure forces in an attempt to obtain a uniform stress pattern. Considering the magnitude of the thrusting forces, the best approach to obtain the optimum configuration was to initially design only for the pressure forces. Once this was completed, the thrusting force effects would be analyzed. Another advantage to this approach is that the I-DEAS results could be compared and verified with thin pressure vessel theory.

Once the structural configuration was finalized, optimization of the wall thickness was then performed to achieve a maximum principal stress equal to the working

stress of the aluminum, 165 MPa with a factor of safety of 1.5. Analyzing the effect of the thrusting forces and their effect on the design of the tank concluded the stress analysis.

Stress analyses were performed on several models covering various height to diameter aspect ratios (ARs) in order to achieve the optimum structural tank shape. The initial model consisted of a cylindrical tank with hemispherical end caps with an AR of 6, corresponding to a height of 1845 m and radius of 154 m.

Based on the results of this analysis, it was shown that the optimum configuration for the tank is, in fact, a sphere and not a cylinder. This agrees with thin pressure vessel theory.

In an effort to create a finite element model that would correctly represent the actual tank, a 3-D model was generated. Initial analyses were performed using internal pressure only to obtain the optimum tank wall thickness, as stated previously. Internal pressure was applied using the face pressure option on I-DEAS.

Comparing the mass of the original tank with an aspect ratio of six, 99.137 MKg, with the optimized spherical tank mass of 71.696 MKg showed a mass saving of 27.7%. This also produced a significant saving in propellant mass. Optimizing the cylindrical tank to a spherical tank also yielded a significant reduction in surface area of 31.4%, especially important from a heat transfer point of view.

In the next case the thrusting forces were applied to the previous tank configuration. As this was only a quarter of the tanks, only 25% of the total thrusting forces were applied to the bottom centerline nodes. The stress patterns were nearly identical to those observed for the same model under pressure forces only. The maximum principal stress increases to 516 MPa, which, again, is concentrated at the top and bottom nodes along the centerline. If only the stresses in the center portion of the tank are considered, they range from 200 to 275 MPa, which is significantly larger than the 165 MPa working stress. The maximum displacement profile for this case was 3.11 m. An actual tank could fail due to exceeding the 248 MPa maximum stress of aluminum.

The analysis of the spherical tank consisted of finite element modeling of the pressure vessel to determine the

locations of any stress concentrations using I-DEAS. The objective of the analysis was to determine the optimal placement of the supports to minimize the amount of reinforcement that would be needed. The initial assumption used for the thickness of the tank was based on thin pressure vessel theory:

$$\sigma = pr/2t \quad (2)$$

where  $\sigma$  is the stress,  $p$  the pressure inside the tank,  $r$  the radius of the tank, and  $t$  the thickness of the tank wall.

The thickness of the tank was .0141 meters using a working stress of 165 MPa for the aluminum alloy selected, with a pressure of 0.2 atm (20265 Pa) and a radius of 230 meters. The radius used was about 5% larger than necessary for the initial configuration to give conservative results.

The stresses and deflections reached acceptable values when the tank supports were moved out sideways. Even though the applied forces at burnout were twice as high as during the initial acceleration, the stress contours were nearly identical, which implied that the tank pressurization was the dominant force.

### Torus

A torus was determined to be the most efficient shape for the crew living quarters by the Phase II design team. It is designed as a totally enclosed ecological system, with energy as its only input after the Biosphere II Project.<sup>1</sup> Volume requirements were set at 19,000 cubic meters per person to allow extra space for manufacturing, food processing, and other as yet unconsidered needs. It will be constructed of aluminum alloy and sized so that rotation will provide one-g of artificial gravity. Current dimensions include a major radius of 894.6 meters and a minor radius (tube) of 322.8 meters. The pressure of the enclosed atmosphere was set to 1 atm and of the same composition as that of each to minimize the long-term impact on the inhabitants since little is known of such long-term effects.

The most efficient cosmic radiation shield was determined last year by the Phase II design team to be 14 meters of liquid hydrogen. It was determined that the shield must rotate with the torus. The spinning shield was required because there was no apparent failsafe method

to maintain separation between the torus and shield during maneuvering. The torus rotates with a linear velocity of 97.1 m/s and any mechanism to maintain separation induces potentially unacceptable vibrations in the torus and dissipates rotational energy. The difficulty in maintaining separation is exacerbated by the vibration mode shapes induced by thrusting. A failure of the mechanism separating the rotating torus and stationary shield could have catastrophic consequences, and no viable alternatives were discovered to alleviate this problem; therefore the shield must rotate with the torus.

The spokes are the only interface between the crew quarters and the mechanical subsystems of the E-City. They act as cantilever beams and transmit the thrusting forces to the torus and cosmic radiation shield. The shaft is the central connecting structure for the tanks, propulsion module, and torus coupling. The primary force on the shaft is due to the axial thrusting load. In this case the bending moment was assumed to be negligible compared to the axial pressure during thrusting and was used to develop the preliminary estimate of the cross-sectional area. The radius was determined by the optimal placement of thrusting loads on the tanks.

The majority of the static structural analysis was performed by a computer program developed to provide interactive parameter analysis. Using software also reduced the second design iteration to one day as the

program reached maturity. A spherical propellant tank provided the optimum configuration with the lowest mass and lowest surface area. Some optimization of the tank wall thickness was provided by calculating the thickness in sections. The minimum mass tank configuration was obtained by transmitting the thrusting loads through the tank walls without the addition of special supports or reinforcements. The mass of the spokes and shaft were computed using simplified formulas as starting values for optimization using ASTROS.

### Structural Dynamics

A dynamic analysis is necessary for a complete evaluation of the E-City. The modes, frequencies, displacements, and accelerations of the E-City are needed for the design of the subsystems. Humans inhabiting the torus should not be subjected to intense acceleration, and certain frequencies that are resonant to the various subsystems must be avoided. In addition, structural mass should be minimized, yet not fail when the E-City is under the influence of external loads.

The dynamic analysis was carried out using the Finite Element Method. To perform the finite element analysis on the E-City, the software package ASTROS was employed. ASTROS is similar to NASTRAN and also has the capability of optimizing a model for a minimum mass configuration, a feature used in later analysis.

Table 1 Results of static shaft and spoke optimization

|   | Shaft          |           | Spokes   |           |
|---|----------------|-----------|----------|-----------|
|   | Initial        | Optimized | Initial  | Optimized |
| Cross-sectional area (m <sup>2</sup> )            | 6.28625        | 1.13964   | 12.59779 | 0.12560   |
| Wall thickness (m)                                | 0.01000        | 0.00181   | 0.10000  | 0.00010   |
| Mass per element (*1000 kg)                       | 333.17         | 60.40     | 7469.70  | 74.47     |
| Initial structural mass<br>(torus, spokes, shaft) | 367 610 000 kg |           |          |           |
| Optimized structural mass                         | 187 397 000 kg |           |          |           |
| Percent reduction                                 | 49.0%          |           |          |           |

The finite element model utilizing bar elements with six degrees of freedom each has six spokes with four elements, each having a 20-m radius; a 24-element torus with a 35-m tube radius; and a 200-m-long shaft with ten elements, each having a 100-m radius. The total finite element model had 318 degrees of freedom. The optimization feature of ASTROS was used to minimize the total masses of the shaft and spokes subject to Von Mises's yield criterion under static axial thrust loading.

The initial wall thickness of the shaft was 10 mm and 100 mm for spokes. After optimization, these were reduced to 0.29 mm and 1.00 mm, respectively. The torus was not optimized due to some computational limitations encountered in the software. The designed structural mass of the shaft and spokes was reduced from 2.2794 billion kg to 0.00239 billion kg. Table 1 shows the results of the static optimization.

The statically optimized structure was dynamically analyzed by ASTROS under the modes discipline with the output being the natural frequencies and modes of vibration of the system. The modes were illustrated visually through the use of the graphics package PATRAN, and the significant modes were identified to study the axial vibrational dynamics due to thrust loads.

The out-of-plane motion of the torus is of significance for crew comfort since it will result in lateral swaying motion of the living quarters. It was decided to study this motion so that displacements and accelerations due to thrust loading on the statically optimized design could be defined. Therefore, only the symmetric torus modes with significant axial displacements were taken into account in the modal axial dynamics. Three such modes were chosen for a reduced-order model of the axial dynamics. Table 2 identifies these modes. The next step was to simulate the reduced modal dynamics due to thrust loading which requires a state-space formulation of the equations of motion. The problem was programmed via the PRO-MATLAB software, and the displacements and accelerations at each grid point in the axial direction were determined. It was found that maximum vibrational displacement of typical torus points for the optimized design, discussed in the previous sections, would be about 8 m at the beginning of the thrusting period and would reach six times this value at the end of the thrusting period when the fuel tanks are empty. Thus the analysis established the need for further design for active and/or passive control of structural vibrations.

Table 2 Modes selected for study of axial dynamics under thrust loading

| Mode # | Mode Description | Frequency |         | Period<br>(sec) |
|--------|------------------|-----------|---------|-----------------|
|        |                  | rad/s     | Hz      |                 |
| 16     | Rigid torus      | 0.030760  | 0.00490 | 204.29          |
| 19     | Rigid torus      | 0.101903  | 0.05081 | 19.68           |
| 22     | Ruffle torus     | 0.155079  | 0.06267 | 15.96           |

### Attitude Control System Design

Subject to altering disturbances which must be controlled, a Mass Moment of Inertia (MMI) analysis of the E-City is required to study the vehicle's stability and control characteristics. The MMI study is essential to Project WISH's attitude control system optimization. Modeling E-City as a rigid body consisting of lumped masses, Phase I established the basis for a MMI study. The work in the previous two years focused on obtaining an order of magnitude estimation of the MMIs, and the whole ship was modeled as spinning.

Phase II emphasizes a more rigorous approach to the ship's configuration, which includes a more accurate and complex MMI analysis. This year's work was devoted to a dual-spin configuration which requires that only the torus and spokes rotate about the spin axis. Developing a reliable and user-friendly FORTRAN program to calculate the MMIs of an evolvingly complex E-City structure is the motivation behind Phase III of the dual-spin MMI analysis. Accurately calculating the MMI ratios required by an ensuing attitude control study and defining the ship's structure were the goals.

To calculate two MMI ratios which are required for the attitude control analysis, the following ratios were used:

$$r1 = Iz_{spn}/I_x \quad (3)$$

$$r2 = I_{xspn}/I_x \quad (4)$$

in which  $Iz_{spn}$  is the sum of the torus and spokes MMI component about the spin axis,  $I_{xspn}$  is the sum of the torus and spokes MMI about the x or y axis, and  $I_x$  is the ship component about the x or y axis. Because of the axial symmetry about the z axis, the center of mass (CM) will lie on the z axis. Its location, denoted by  $Z_{cm}$ , is designed as the displacement of the mass center from the torus center.

Since this was a configuration consisting of many components, the Parallel Axis Theorem must be incorporated to transfer each component's MMI with respect to the CM location. This component is then added to each component's individual MMI to obtain a total contribution. Finally, the two ratios  $r1$  and  $r2$  were obtained, and the attitude control design was initiated.

The attitude dynamics of the E-City were studied in Phase I of Project WISH, during which the stable configurations of the spacecraft were determined. A study conducted during Phase II determined the state response due to initial disturbances and the attitude control design requirements needed to damp out these disturbances. In Phase I the entire E-City was assumed spinning.

Due to the dual-spin nature of the E-City and the configuration changes that took place in Phase III of Project WISH, the attitude control design needed to be reassessed. The objective in Phase III was to control effectively, and in a manner acceptable to the crew, the gyroscopic wobble of the station following a disturbance. This included optimizing the number of control clusters, the number of thrusters per cluster, the propellant mass requirements, and the control power required.

To begin the study, it was assumed that the control thrusters would be placed in clusters evenly distributed around the main propellant tank. Next the torque on the spacecraft was determined in matrix form using the selected configurations. This torque matrix was non-dimensionalized and substituted into the non-dimensional gyroscopic state equation of a dual-spin body, given by:

$$\dot{\hat{X}} = [A]\hat{X} + [B]\hat{T} \quad (5)$$

where  $X$  is the state of the system model,  $T$  is the torque matrix, and  $A$  and  $B$  are matrices defined in Ref 2. The  $A$  matrix is dependent upon the MMI ratios established in the MMI analysis. The linear quadratic regulator control theory was used to obtain the state response that minimized the control design performance index, given by:

$$CDPI = \frac{1}{2} \int_0^\infty (w_x \hat{X}^T \hat{X} + w_c \hat{T}^T \hat{T}) d\tau \quad (6)$$

where  $w_x$  is the state weighting and  $w_c$  is the control weighting parameters, respectively.

By using the control law obtained from the minimization of CDPI, designers used the following equation to determine the non-dimensional control power:



$$S^* = \int_0^\infty \hat{T}^T \hat{u}^{-T} \hat{u}^{-1} T d\tau \quad (7)$$

where  $\hat{u} = D_t^{-1}[D]$

The D matrix is a non-dimensional thruster distribution matrix related to the thruster configuration placement. The root-mean-squared power required to damp out an initial disturbance is then found from

$$P_{rms} = (v_{ex} I_x n^2 / 2D_t) * \text{sqrt}(S^* / \tau_c) \quad (8)$$

where  $n$  is the spin rate of the torus in rad/sec,  $I_x$  is the moment of inertia of the ship about the x-axis,  $v_{ex}$  is the exhaust velocity of the control thrusters, and  $\tau_c$  is the non-dimensional control time.

To reduce the amount of power required for control, the number of clusters was computed against  $P_{rms}$  for various weighting parameters,  $w_c$  and  $w_x$ , and several initial disturbances. The results were used to determine the optimal number of clusters.

After this was accomplished, the state response due to an asteroid impact was modeled to determine its effect on the E-City. Two cases were evaluated assuming perfectly plastic collisions: a head-to-head collision and a tail-to-tail collision. This analysis was done to quantify what the chosen initial disturbance would "feel like" to the ship and what this would represent in physical terms.

Determining the acceleration levels experienced by the crew due to gyroscopic attitude dynamics was the next step in the control optimization process. Through this analysis, the number of thrusters in each cluster, propellant mass per control effort, maximum thrust per cluster, settling time, the state weighting  $w_x$ , and the control weighting  $w_c$  were determined. The primary constraints based on human factors were the lateral swaying acceleration felt by the crew while moving onboard and the settling time. It was desired that this acceleration disturbance would immediately settle to zero after the initial disturbance without overshoot.

The acceleration levels were determined for a person running in the spin direction of the torus. This would be the direction for which the crew would experience the highest g levels. The weighting parameters  $w_c$  and  $w_x$

were then varied to determine the control settling time, propellant mass, maximum thrust, and acceleration level profiles. Various design parameters were then studied against values of  $w_c$  for a specific  $w_x$ . Several iterations were completed to determine the patterns for the various parameters in relation to increasing or decreasing weighting parameter values. Results of attitude control system optimization are listed in Table 3.

Table 3 Attitude control results

|                             |                   |
|-----------------------------|-------------------|
| Thrust available/engine     | 2.58 million (N)  |
| Isp/engine                  | 437 sec           |
| Control power required      | 722 billion Watts |
| Maximum thrust/cluster      | 289 million (N)   |
| Number of engines/cluster   | 112               |
| Control propellant          | 32.1 million (kg) |
| $w_c$ (control weighting)   | 640               |
| $w_x$ (state weighting)     | 375               |
| Number of thruster clusters | 50                |

## Power and Thermal Control System

### Power System

The E-City is composed of numerous subsystems that will require electrical and/or thermal energy to operate properly. The primary concern of the power system is to supply continuous energy to each of E-City's subsystems for as long as necessary to complete a given mission. The thermal control systems must be able to dissipate the waste heat generated by the various power devices on board.

A rotating particle bed reactor capable of generating a maximum of 5000 MWth is sufficient to supply power to E-City. A converter coupling network is required, which is essentially a switch that channels the thermal energy from the reactor to either the magnetohydrodynamic (MHD) or thermoelectric converter. During normal operation, the thermal energy is channeled completely through the highly efficient MHD converter. In an emergency situation, the thermal power can be redirected to the thermoelectric converter as a type of backup system. The usable electrical power generated by the converters is sent to the power coupling network. The remaining unconverted thermal energy, referred to as

waste heat, is dissipated by sending it to an external radiator.

The power coupling network is responsible for supplying power to the propulsion, attitude and control, heat transfer, and ship operations systems. Depending on the operating mode of the ship this network is responsible for supplying the appropriate amount of power to each system. It also serves the purpose of redirecting power to systems in emergency situations.

From the power coupling network, the usable power is distributed to the four major systems of E-City. The propulsion and attitude control systems need start-up power only. The heat transfer subsystems require power to either actively and/or passively dissipate the waste heat created by all the power generating devices of E-City. The systems required for navigation, life support, communications, shuttle and maintenance, and other miscellaneous tasks must receive power for all phases of E-City's operation.

Once the power system was established, the next step was to envision typical operating modes of the ship. These operating modes would be based on the startup, burn time, and shutdown of the engines and/or attitude and control thrusters.

The start-up procedure is essentially a type of chain reaction sequence. The rotating particle bed reactor can supply only 5000 MWth for starting up the engines. This is enough power to start only one NLB engine. It would be highly impractical to add 13 more particle bed reactors, simply to start the remaining engines.

Using the fact that an NLB engine is a power generating device in itself, it does not seem unlikely that one modified NLB engine could generate power to start the remaining engines. This modified engine, referred to as the start-up engine, would possess some type of moderator/thermal energy network. This network would be capable of using the energy output from the start-up engine to start the remaining engines.

There are two start-up phases. The first start-up phase refers to the rotating particle bed reactor generating 4800 MWth to start a fission reaction in one NLB engine. The second phase startup refers to the startup engine supplying power to start the rest of the engines.

Once the engines and thruster are operating, they no longer need any external power source. Minimal power for systems monitoring engine and thruster status are needed for propulsion and attitude control. The only systems requiring power are heat transfer and ship operations.

The shutdown of the main engines is a crucial operating mode for E-City. It entails powering down the main engines by terminating the fission reaction occurring within them.

The fifth and final operating mode of E-City takes place when the burn time for the mission has been reached, and the main engines are shut down. At this time, unless E-City is utilizing NLB engines as attitude control thrusters, the particle bed reactor needs only to supply power to ship operations.

### **Thermal Control**

Thermal control systems can be characterized broadly into two categories: active and passive. This study defines active systems as those required to dissipate internally generated heat and passive systems as those required to isolate the station from external heat sources. Basic heat exchange equations were used along with several simplifying assumptions to create the thermal model of the E-City.

The most critical portions of the E-City needing passive control of heat transfer are the hydrogen propellant storage tanks. The only external heat source considered was solar radiation. The intensity of solar radiation decreases exponentially with distance, so only the worst case of a 1-AU orbit was considered. This is the closest orbit with which the E-City will be tasked.

Most of the heat generated by the nuclear engines will be directed away from the station in the form of exhaust energy. In addition, the necessity for radiation shielding and use of active thermal control systems will help limit heat input from the engines into the tank. Waste heat generated in the torus section of the station will be controlled by radiators and by re-radiation from the sections facing away from the tank.

Calculations show that with a bare, uninsulated tank, all of the liquid hydrogen would boil off in approximately 1.4 hrs. However, merely by painting the tank white, the boiloff time can be nearly doubled. In order to arrive at a design point, maximum boiloff rate was selected as the sole design criterion. The first step was to determine the surface temperature. Using the assumptions made earlier, the only heat input will be solar radiation. It was then necessary to calculate the maximum heat flux corresponding to the chosen boiloff rate and finally to determine the amount of insulation needed to stay under this limit. The conduction equation was used to solve for the insulation thickness.

Many insulation options are available to the spacecraft designer. As noted earlier, simple external coatings can have a dramatic effect on skin temperatures and will be utilized on the current design. More critical in a cryogenic installation is the insulating material between the outer skin and the inner pressure vessel. Multi-Layer Insulations (MLI) can offer a performance increase of up to 600 times that of plain fiberglass based on thermal conductance. The principal behind the MLIs is that of multiple layers of radiation shields separated by low conductance spacers. The MLI chosen is made of 0.0005" aluminum foil radiation shields with fiberglass mat spacers. This additional mass of the insulation adds approximately 6.4% to the tank mass.

Because of the tremendous amount of heat generated internally by the E-City, some system must be used to actively dissipate this heat. Research done in the phase one report was utilized in the selection of the particular system, and work done in this year emphasized sizing the system.

Several criteria considered when choosing which radiator in use were: external environment, amount of waste heat to be rejected, radiator surface area, circulating fluid system, and micrometeoroid damage sensitivity. Ideally the radiator must not depend on surface area while minimizing the mass.

Two types of radiators that were considered for our application were the Liquid Droplet Radiator (LDR) and the Rotating Bubble Membrane Radiator (RBMR). Briefly, the LDR uses nozzles to spray molten metal onto a collector. As the metal droplets travel through space, between the spray nozzle and collector, they radiate their

heat to space. The mass of the LDR is low because the metal droplets are the actual radiator and the majority of the mass is concentrated in the supporting structure. No protective shielding is needed because any meteoroids simply pass right through the spray carrying some of the molten metal with it. The major disadvantage of the LDRs is this loss of metal, which also can occur if the spray nozzles are unable to maintain an accurate aim on the collector.

The system chosen was the RBMR. It uses a two-phase working fluid with an operating principle similar to the LDR. In this system the molten metal is sprayed onto an outer envelope or bubble. The droplets condense and radiate energy as they hit the bubble. By rotating the radiator, the metal droplets are collected in a trough around the circumference by centrifugal force and recirculated again for reuse. The advantages of using this type of radiator are its high heat capacity, relatively low mass, and resistance to critical meteoroid damage. A final consideration is that spray nozzle accuracy would not be a problem since the system is fully enclosed. Since it will be located on the despun portion of the space station, it will need some form of drive to spin it, but this should not entail a great mass penalty.

Once the radiator configuration was decided upon, it was then necessary to arrive at a size and placement for it. A computer program was written to determine the amount of heat generated by the various E-City modes of operation and then to calculate the needed radiating surface area and the dimensions of such a system. The heat sources that were taken into account were the propulsion units and the power generation system. The program requires inputs such as: configuration and operating mode; reactor powers of power plant, propulsion engines, and control thrusters (if used); power conversion efficiencies; power required by the ship; and number of engines or thrusters. The program then calculates the total amount of waste heat that must be dissipated and the necessary radiating surface area. In addition, the output gives the dimensions for three possible geometric configurations corresponding to that surface area. The results are shown in Table 4. These results assume that nuclear thrusters will not be utilized due to their slow startup time and that the engines and reactor operate at full power at all times.

**Table 4 Active thermal control system design parameters for Phase 2 start-up case**

|   |           |
|---|-----------|
| Power of main reactor (MWth)                                | 5,000     |
| Power conversion efficiency (%)                             | 40        |
| Power for ship ops (MWe)                                    | 22.85     |
| Number of engines   | 14        |
| Reactor power of start-up engine (MWth)                     | 160,000   |
| Reactor power of each engine (MWth)                         | 160,000   |
| Engine waste heat percentage                                | 0.0       |
| Waste heat from main reactor (MWth)                         | 4,977     |
| Waste heat from start-up engine (MWth)                      | 97,600    |
| Waste heat from main engines (MWth)                         | 0.0       |
| Total waste heat to dissipate (MWth)                        | 102,577   |
| Surface area needed for radiator (sq m)                     | 1,149,301 |
| Length of a cylindrical radiator of radius 100 m (m)        | 1,1830    |
| Radius of a spherical radiator (m)                          | 311       |
| Major axis of an ellipsoid radiator w/minor axis of 50 m(m) | 431       |

### Summary of Results

The summary of the masses of the E-City for the Saturn envelope mission is given in Table 5.

**Table 5 Masses of E-City components (millions of kgs)**

| Component       | First Guess | Modified Guess | Optimized |
|-----------------|-------------|----------------|-----------|
| Torus           | 84.9        | 84.9           | 185       |
| Shield          | 1416.3      | 1416.3         | 1416.3    |
| Tank            | 49.1        | 124.4          | 58.3      |
| Spoke and shaft | 0           | 2279           | 2.39      |
| Other           | 0           | 0              | 125.6     |
| Dry mass        | 1551.9      | 3909.1         | 1840.12   |
| Propellant      | 6503        | 16380.4        | 7710.6    |
| Total mass      | 8054.9      | 20289.5        | 9550.7    |

### References

1. "Project WISH: The Emerald City Phase II," The Ohio State University, NASA/USRA Advanced Space Design Class Final Report, July, 1991.
2. "Project WISH: The Emerald City Phase III," The Ohio State University, NASA/USRA Advanced Space Design Class Final Report, July, 1992.
3. "Project WISH: The Emerald City Phase I," The Ohio State University, NASA/USRA Advanced Space Design Class Final Report, July, 1990.

## EXTRATERRESTRIAL SURFACE PROPULSION SYSTEMS

Old Dominion University  
Mechanical Engineering and Mechanics Department  
Norfolk, Virginia

Professor Robert L. Ash  
Dexter L. Blackstock, Teaching Assistant  
K. Barnhouse, Z. Charalambous, J. Coats, J. Danagan, T. Davis,  
J. Dickens, P. Harris, G. Horner, T. James III, W. Johnston, R. Krueger,  
A. Lucero, J. McWithey, E. Morris Jr., A. Nelson, R. Rayno, J.  
Scheiderer, E. Schneider, G. Singer, C. Wallace

**Abstract**

Lunar traction systems, Mars oxygen production, and Mars methane engine operation were the three topics studied during 1992. An elastic loop track system for lunar construction operations was redesigned and is being tested. A great deal of work on simulating the lunar environment to facilitate traction testing has been reported. Operation of an oxygen processor under vacuum conditions has been the focus of another design team. They have redesigned the processor facility, including improved seals and heat shields. Assuming methane and oxygen can be produced from surface resources on Mars, a third design team has addressed the problem of using Mars atmospheric carbon dioxide to control combustion temperatures in an internal combustion engine. That team has identified appropriate tests and instrumentation. They have reported on the test rig that they designed and the computer-based system for acquiring data.

**Tracked Lunar Construction Vehicles**

Lunar regolith (soil) will be used as a construction material for future bases on the moon.<sup>1</sup> Hence, there will be a need for construction machinery that can excavate and/or move significant quantities of lunar soil. While current versions of lunar and Mars rover designs utilize six-wheeled vehicles, tracked vehicles have been the preferred configurations for terrestrial, earth-moving applications. The work reported here is a continuation of the study of tracked vehicle concepts for lunar construction operations.

Trautwein<sup>2</sup> reported on a Lockheed "loopwheel" design for a Mars rover. The loopwheel concept utilized a continuous elastic loop or track and looked very similar to a terrestrial tracked vehicle, except that the Lockheed elastic track supported the vehicle. The loopwheel design or Elastic Loop Mobility System (ELMS) thus produces a different footprint when it traverses soil than the footprint produced by a conventional linked track terrestrial vehicle. Since the loop section between the wheels (or drive drums) supports the vehicle, it exerts a larger downward pressure force than its linked track counterpart. As a consequence, ELMS can combine the tractive performance attributes of tracked vehicles with the suspension and load distribution characteristics of pressurized tires. However, performance data for these systems is lacking and no attempts to evaluate ELMS for lunar construction applications have been reported.

**Elastic Loop Mobility System**

It is assumed that the tracks are driven by electric motors located within the wheels (drive drums) used to drive the loops. In that way, the motors can be sealed hermetically in the drive drums, and the drive drums can be connected to the construction vehicle frame via a pivoted interface. The interface can carry electrical connections and coolant passages, which will be required to cool the motors, but do not transmit mechanical shaft power. Since construction operations will likely take place via either fully autonomous or teleoperated control, these vehicles must be very reliable and simple to repair. Hence, the elastic loop and drive drum units, along with the ancillary hardware, should be modular.

The elastic loop mobility system is shown schematically in Figure 1. The design is a 1/6 scale approximation of the lunar construction utility vehicle (LCUV), defined in an unpublished Advanced Program Office study at Johnson Space Center in 1988. That study determined that an LCUV with a 25,000 kg payload capability was required for robotic construction operations on the moon. Their vehicle mass allowance was 7500 kg (making a maximum total mass of 32,500 kg.), and they assumed a tracked vehicle with a total footprint area (two tracks) of  $6.8 \text{ m}^2$ . Hence, the maximum pressure that is anticipated for the full scale vehicle on the lunar surface ( $g = 1.622 \text{ m/s}^2$ ) was estimated to be 8000 Pa. For terrestrial tests, using the 1/6 scale model, the maximum design load is equivalent to a total vehicle mass of 225 kg. The minimum lunar vehicle load corresponds to an unloaded LCUV and yields a footprint pressure on the order of 2000 Pa, which is equivalent to a prototype mass of 56 kg (124 lb). Initial traction testing has been directed toward the lightly loaded configuration.

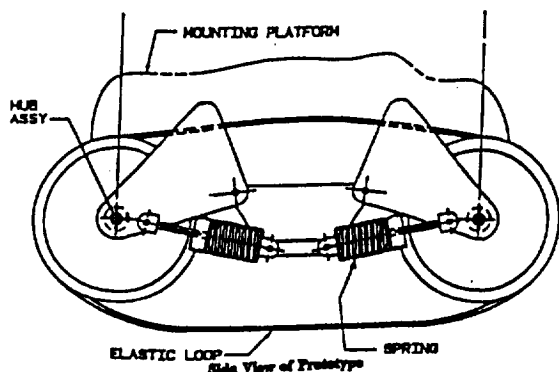


Fig. 1 Schematic view of ELMS prototype track

By preserving the track contact width to length ratio between the prototype and the full scale vehicle, track-side (above ground) interaction with the soil can be made insensitive to lunar gravity effects by loading the track with an appropriate force. Hence, a total track load of 124 lb on earth simulates the full scale, unloaded LCUV on the moon.

The 1992 design utilized new elastic loops (tracks), made of 1060 carbon steel, 1.3 mm (0.05 in.) thick, 203 mm (8 in.) wide, and 2311 mm (91 in.) in circumference.

The loops were joined by lapping the steel belts with a 32 mm overlap that utilized round head machine screws spanning the belt 25.4 mm apart. A continuous neoprene rubber gearbelt (Figure 2.), 50.8 mm wide with a tooth spacing of 22.2 mm (7/8 in.), was fastened to the inside of the steel loop using countersunk, flathead screws, spaced at every fifth rubber tooth.

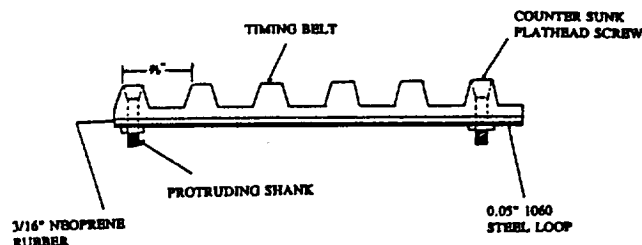


Fig. 2 Side view of gearbelt loop connection

The polyvinyl chloride (PVC) plastic drive drums were 305 mm (12 in.) in diameter and 203 mm wide. The drive drums had teeth machined into them with the same 22.2 mm or 7/8 in pitch as the gearbelt. The gearbelts were restrained by 76 mm (3 in.) wide, 4.8 mm (3/16 in.) thick rubber strips mounted on each side of the drive drum, as shown in Figure 3.

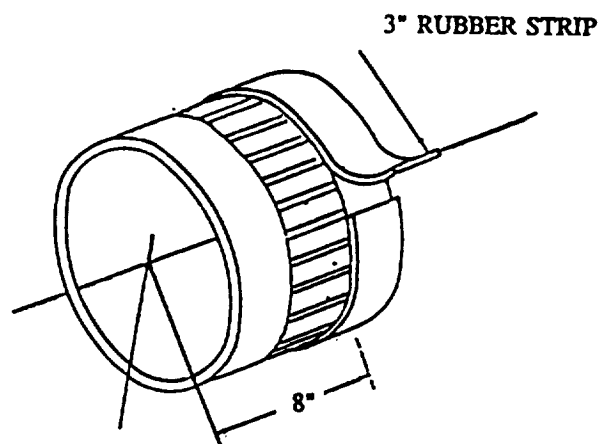


Fig. 3 Schematic of drive drum

The drive system was completely redesigned in order to enhance reliability and repairability. The new design utilized new motor mounts and sealed ball bearings to eliminate previous problems with assembly and wear. Details of the new design are contained in the final team report. Preliminary tests have confirmed the improved performance of the new design and validated the finite element analyses of the track.

### Simulated Lunar Traction Tests

Some literature is available on predicting the behavior of tracked vehicles under different soil conditions (see Bekker<sup>3,4</sup> and Garber and Wong,<sup>5</sup> in addition to Trautwein<sup>2</sup>). However, the behavior of this loopwheel, or ELMS, in a lunar environment has not been studied or reported.

Carrier<sup>6</sup> has reported on Soviet experiments with wheeled vehicles and soil characterization on the lunar surface, starting with their Lunokhod rover vehicle performance data in 1971. The Lunokhod vehicle had open wheels with grousers and carried a cone penetrometer experiment which was used to measure load-bearing properties of lunar soil. In addition, Perkins<sup>1</sup> has produced an extensive literature survey of lunar soil measurements and predictions. The influence of gravity, packing density, vacuum, soil composition, grain size, grain shape, and electrostatic forces on soil behavior must all be considered. However, Perkins' survey indicated that most researchers consider lunar soil to behave similarly to wet beach sand. Hence, some traction testing at Virginia Beach, Virginia, will be reported at a later date. However, the 1992 design team considered establishing the equivalence between terrestrial simulations and lunar behavior to be a critical requirement.

Tests were conducted to determine the minimum traction test soil volume dimensions (diameter and depth of contained soil simulant) required to minimize the influence of testbed containment on the measurements. The influence of footprint size on soil sinkage depth was studied using three track footprint models. The track footprints were made by wrapping galvanized sheet metal (air conditioning duct) around wooden contours cut in the shape of the envisaged track. Tested model track widths were 13 mm, 28.5 mm and 38 mm, with length-to-width

ratios of 4, 3.67 and 3.67, respectively. For these "track penetration" tests, the minimum soil volume was determined to be 300 mm (diameter) by 125 mm (depth). The test data were not controlled adequately, and subsequent tests will be reported more fully.

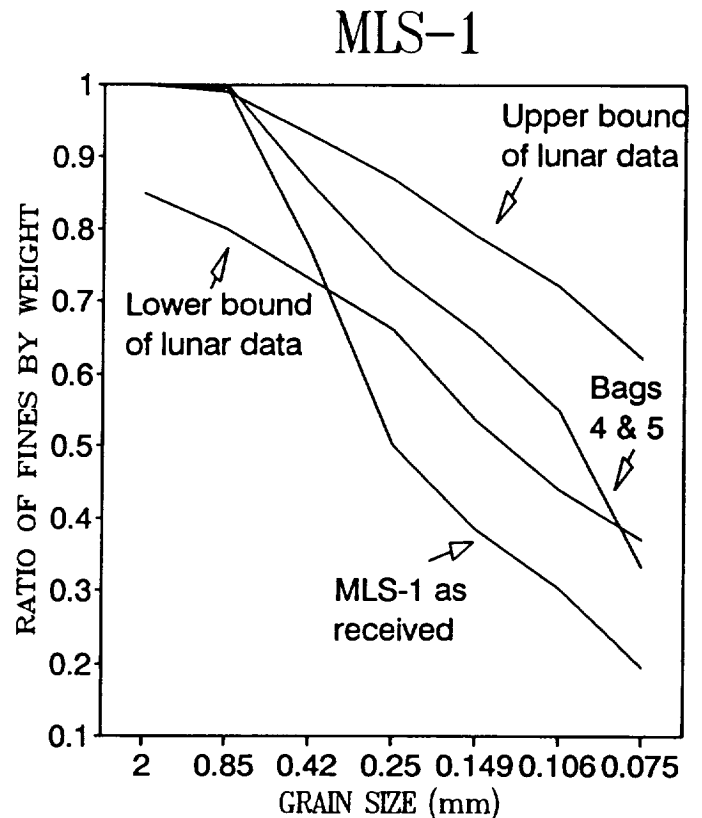


Fig. 4 Comparison of grain size distribution between MLS-1 lunar simulant and lunar soil distribution bonds

Wieblen and Gordon,<sup>7</sup> have studied lunar surface conditions and made recommendations on how lunar soil can be simulated. On the basis of their study, they determined that lunar soil can be approximated closely by material from an abandoned rock quarry in Duluth, Minnesota. By crushing, grinding, and then sieving the rock, they have been able to approximate lunar particle shape, angularity, and size. However, this mined basalt does not contain the glass fraction associated with lunar soil. They were able to produce the glass agglutinates using a plasma torch furnace. Weiblen, Murawa, and Reid<sup>8</sup> have reported on preparation and validation of Minnesota Lunar Simulant (MLS-1); nearly 50 kg of MLS-1 simulant was procured from Dr. Weiblen at the University of Minnesota. The soil particle distributions

from the MLS-1 shipment (different bags of material) are compared in Figure 4. Additional details concerning the lunar simulant properties and comparisons are in the full 1992 team report.

A comparison between the sinkage depth for sand and MLS-1 at various loadings (pressures) is shown in Figure 5.

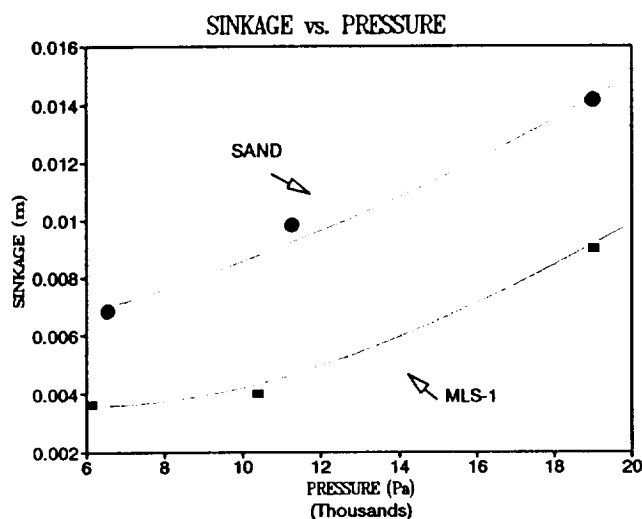


Fig. 5 Comparison of probe sinkage depth as a function of applied pressure, for sand and lunar simulant (MLS-1)

Shear tests for the track units, with and without grousers, were considered, both in air and in vacuum. The influence of gravity was also a concern. The only way gravity effects could be considered was to find soil grains that were the same shape and size as lunar soil but with much lower density (preferably 1/6); no such materials have been identified at this time. A vacuum facility has been built to study the influence of vacuum on shear and traction properties. However, the initial vacuum chamber lid design was found to exhibit excessive deflections during testing and a new design is required. That facility and its modifications will be reported by a future design team.

A "full scale" (for the 1/6 scale prototype) traction test bed was designed and built. The testbed was made of plywood and 2 x 4's and was hinged so that, when filled with sand, the testbed grade could be adjusted until the

ELMS started to slide. That testbed is shown schematically in Figure 6.

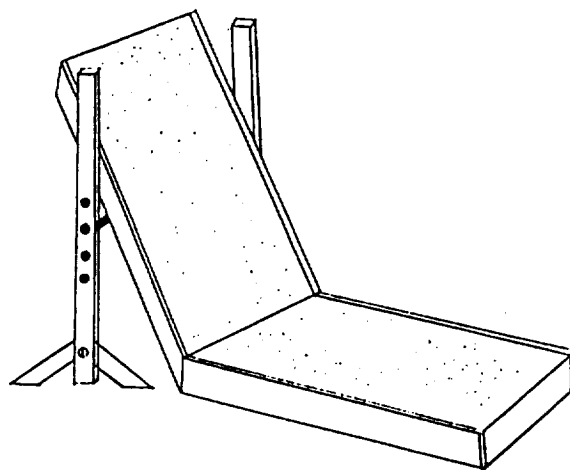


Fig. 6 Schematic of ELMS traction testbed

## Summary

The 1992 LCUV Design Team has made significant progress in developing a traction test program that can permit the evaluation of elastic loop track systems for lunar construction operations. While the tests performed this semester are preliminary, a variety of more detailed future design projects that can contribute to the evaluation of future lunar construction vehicles have been identified.

## Mars Methane Engine

Since carbon dioxide (from Mars' atmosphere) and water (from Mars' North pole or from permafrost) are likely to be the only feedstock ingredients utilized by early Martian surface outposts, it is likely that methane and oxygen will be the earliest *in situ*-produced fuel and oxidizer on Mars. Furthermore, because the feedstock molecules are water and carbon dioxide, it is very likely that methane and oxygen will be produced in their stoichiometric ratio. Unlike air-breathing propulsion systems on Earth, nitrogen is not available as a diluent to control the combustion temperature on Mars. Furthermore, it will not be desirable to shift the amount



of methane and oxygen consumed away from the stoichiometric mixture because of the hardware and energy costs associated with producing each propellant molecule. Consequently, it is desirable to consider using carbon dioxide from Mars' atmosphere as a diluent to control combustion temperatures. The 1992 Mars methane engine design team has progressed from operating an internal combustion engine with controlled ratios of methane, oxygen, and carbon dioxide to developing instrumentation and test plans for conducting a computer-based study of parametric design data for internal combustion engine operations on Mars.

A one-cylinder Megatech Mark III laboratory engine was used in the preliminary tests. Spark advance and compression ratio could be varied for that engine. Since most engine research programs are concerned with engine performance rather than the fuel and oxidizer behavior, considerable research was directed toward defining appropriate tests. Ferguson<sup>9</sup> has indicated that the variation of spark advance for maximum engine rpm with different fuel-oxidizer-diluent settings is useful in evaluating propellant performance. In addition, since the fuel, oxidizer and diluent are pressurized, accurate measurements of cylinder pressure as a function of cylinder volume were required to determine horsepower and fuel consumption data. Instrumentation and data acquisition requirements have been defined in terms of measuring these parameters.

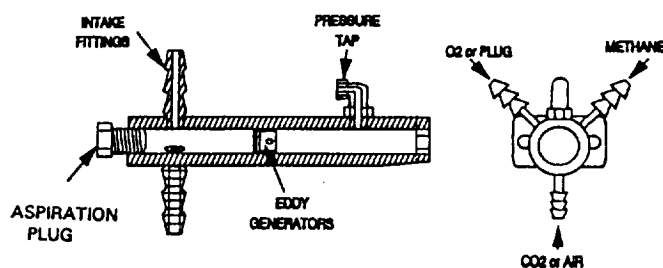


Fig. 7 Schematic view of the three-gas carburetor design

A carburetor had to be designed to permit mixing of gaseous methane with oxygen and carbon dioxide. That design is shown schematically in Figure 7. Cylindrical rod

vortex or eddy generators were incorporated in the design to facilitate mixing of the three gases.

Gas flows were measured using rotameters. Air flows (baseline tests) and carbon dioxide flows were measured with a Cole-Parmer (Model N064--63C) rotameter, while methane and oxygen flows were each measured with Cole-Parmer Model N064-63ST rotameters. Depending on the float configuration, flow rates could be measured between 100 and 60,000 standard cubic centimeters per minute (SCCM).

Instrumentation was not available for measuring instantaneous combustion chamber pressures. Dr. David L. Reuss of General Motors Research Laboratories in Warren, Michigan, assisted the design team in selecting an appropriate pressure transducer. An AVL North American piezoelectric pressure transducer (Model 8QP500c) and a Model 3057-A01 charge amplifier unit were selected. The cylinder head of the Megatech engine was modified to accommodate the pressure transducer and to incorporate its water cooling requirements.

An optical encoder was selected as the device to measure engine crank position. Since crank position can be related directly to instantaneous volume, accurate instantaneous crank position data were required. A Lucas Ledex optical encoder, Model K3DM-100-5 SE-4A-M, was selected. That encoder produces 100 pulses per revolution, providing adequate resolution of position for an engine crank with an appreciable moment of inertia and preventing significant high frequency fluctuations. Considerable design effort was devoted to protecting the encoder from both the mechanical energy and vibrations produced by the engine.

Exhaust temperatures were measured with a chromel-alumel (type-K) thermocouple probe. The probe was housed in a 1.6 mm diameter Inconel 600 sheath and could tolerate temperatures up to 1400° K. The thermocouple probe extended into the muffler and was in close proximity to the exhaust valve. Provisions were made in the muffler to facilitate exhaust gas sampling for a gas chromatograph analysis.

An IBM PC-based data acquisition system has been selected for recording pressure, crank position, and speed data. A Data Translation unit, Model LPC LAB-SP0159, has been used to acquire the encoder signal and record

chamber pressures. Each encoder pulse (every 3.6°) triggers a pressure measurement. A schematic view of the overall system layout is shown in Figure 8. It is expected that the data acquisition system will be modified to acquire exhaust temperature data in follow-on work. Experiments will be performed during the summer.

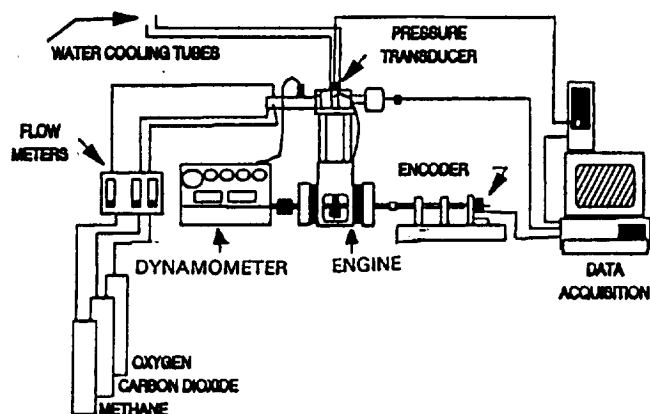


Fig. 8 Schematic layout of Mars methane engine test unit

### Low Pressure Mars Oxygen Production

Ash, Dowler and Varsi<sup>10</sup> reported on the feasibility of *in situ* propellant production on Mars in 1978. Through the support of The Planetary Society and USRA, the design team designed and built an electrochemical processor that demonstrated that oxygen could be produced directly from Mars' atmosphere.<sup>11</sup> Subsequently, Ramohalli and coworkers at the University of Arizona<sup>12</sup> have improved and refined the zirconia-based oxygen separation technology. However, virtually all of the performance data have been produced at cell operating pressures near 1 bar. Since the surface pressure on Mars is on the order of 7 mb, the need to impose a compression ratio in excess of 140:1 on the feedstock is questionable.

The current design group has focused on modifying the oxygen processor to enable repeatable measurements at operating pressures on the order of 100 mb. Due to the cell operating temperatures (on the order of 1000° K), start-up and shut-down cycles have created severe problems in maintaining vacuum integrity. The design team has been able to accomplish the tedious task of

isolating a number of leaks, including a problem with the ceramic (alumina) housing which encased the zirconia cell. It was discovered that the flange region at the top of the ceramic housing (Figure 9) leaked, even though it appeared to be a continuous part. Further investigation showed that the O-ring seal between the face plate and ceramic housing had also melted. Hence, a major effort was devoted to redesigning the upper part of the oven unit to reduce the temperatures in that zone. A 3M epoxy that could maintain the ceramic seal was found, and the aluminum heat shield, shown schematically in Figure 10, was found to be capable of lowering the flange-ceramic housing interface temperatures to acceptable levels to protect the O-ring seal.

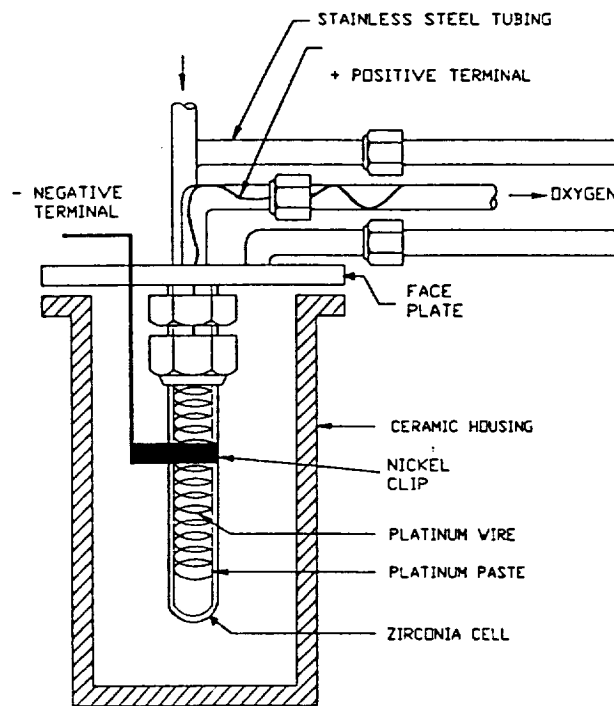


Fig. 9 Schematic of oven cell unit assembly

The other area of investigation was to characterize the electrical behavior of the zirconia cell at different operating temperatures. Problems were encountered there in isolating the cell electrically from the remainder of the system. The electrical connections have been modified as shown in Figure 9, to facilitate those

measurements. Tests will be conducted during the summer to validate the performance.

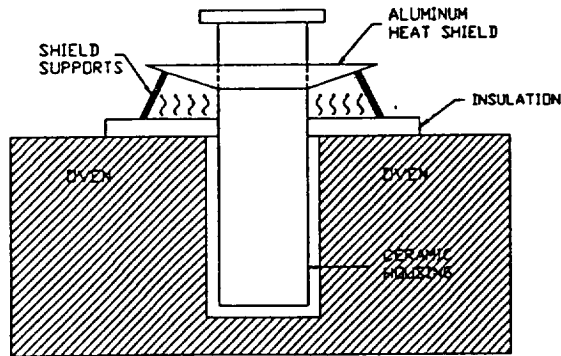


Fig. 10 Schematic view of conical heat shield used to protect the flange region

#### References

1. Perkins, S.W. "Modeling of Regolith Structure Interaction in Extraterrestrial Constructed Facilities," Ph.D. Dissertation, University of Colorado Center for Space Construction, 1991.
2. Trautwein, W. "Operational Loopwheel Suspension Systems for a Mars Rover Demonstration Model," Lockheed Missiles and Space Co. Report, LMSC-TRD 568800, July 1972.
3. Bekker, M.G. Off Road Locomotion, University of Michigan Press: Ann Arbor, MI, 1960.
4. Bekker, M.G. Introduction to Terrain-Vehicle Systems, University of Michigan Press: Ann Arbor, MI, 1969.
5. Garber, M. and Wong, J.Y., "Prediction of Ground Pressure Distribution Under Tracked Vehicles -- An Analytical Method for Predicting Ground Pressure Distribution," J. Terramechanics, Vol. 18, pp. 1-23, 1981.
6. Carrier, W.D. III. "Soviet Rover Systems," AIAA Space Programs and Technologies Conference, Huntsville, AL, Paper number 92-1487, 1992.
7. Weiblen, P.W. and Gordon, K.L. "Characteristics of a Simulant for Lunar Surface Materials," Symposium on Lunar Bases and Space Activities in the 21st Century, Paper No. LBS-88-213, Houston, 1988.
8. Weiblen, P.W., Murawa, M.J. and Reid, K.J. "Preparation of Simulant for Lunar Surface Materials," Proceedings of the Aerospace Division of the ASCE, Space 1990 Conference, Albuquerque, NM, April 1990.
9. Ferguson, C.R. International Combustion Engines, John Wiley and Sons: New York, 1986.
10. Ash, R.L., Dowler, W.L., and Varsi, G. "Feasibility of Rocket Propellant Production on Mars," Acta Astronautica, Vol. 5, pp. 705-724, 1978.
11. Ash, R.L., Werne, J.A., and Haywood, M.B. "Design of a Mars Oxygen Processor," The Case for Mars III, Edited by C. Stoker, AAS Science and Technology Series, Vol. 75, pp. 479-487, 1989.
12. Colvin, J., Schallhorn, P., and Ramohalli, K. "Full System Engineering Design and Operation of an Oxygen Plant", 27th AIAA/SAE/ASME/ASEE Joint Propulsion Conference, Sacramento, CA. Paper No. 91-2444, 1991.

## COMET NUCLEUS AND ASTEROID SAMPLE RETURN MISSIONS

The Pennsylvania State University  
Department of Aerospace Engineering  
University Park, Pennsylvania

Professors Robert G. Melton and Roger C. Thompson

Thomas F. Starchville, Jr., Teaching Assistant

C. Adams, A. Aldo, K. Dobson, C. Flotta, J. Gagliardino, M. Lear, C. McMillan, J. Ramos, T. Rayer, D. Smuck, G. Szydlowski, G. Traub, D. Wentzel, L. Williard, M. Wright, T. Zimmerman

### Abstract

During the 1991-92 academic year, the Pennsylvania State University has developed three sample return missions: one to the nucleus of comet Wild 2, one to the asteroid Eros, and one to three asteroids located in the Main Belt. The primary objective of the comet nucleus sample return mission is to rendezvous with a short period comet and acquire a 10 kg sample for return to Earth. Upon rendezvous with the comet, a tethered coring and sampler drill will contact the surface and extract a two-meter core sample from the target site. Before the spacecraft returns to Earth, a monitoring penetrator containing scientific instruments will be deployed for gathering long-term data about the comet. A single asteroid sample return mission to the asteroid 433 Eros (chosen for proximity and launch opportunities) will extract a sample from the asteroid surface for return to Earth. To limit overall mission cost, most of the mission design uses current technologies, except the sampler drill design. The multiple asteroid sample return mission could best be characterized through its use of future technology, including an optical communications system, a nuclear power reactor, and a low-thrust propulsion system. A low-thrust trajectory optimization code (QuickTop 2) obtained from the NASA Lewis Research Center helped in planning the size of major subsystem components, as well as the trajectory between targets.

### Introduction

Three Advanced Design Program projects have been completed this academic year at Penn State. At the beginning of the fall semester the students were organized

into eight groups and given their choice of either a comet nucleus or an asteroid sample return mission. Once a mission had been chosen, the students developed conceptual designs. These were evaluated at the end of the fall semester and combined into three separate mission plans, including a comet nucleus sample return (CNSR), a single asteroid sample return (SASR), and a multiple asteroid sample return (MASR). To facilitate the work required for each mission, the class was reorganized in the spring semester by combining groups to form three mission teams. An integration team consisting of two members from each group was formed for each mission so that communication and information exchange would be easier among the groups.

The types of projects designed by the students evolved from numerous discussions with Penn State faculty and mission planners at the Johnson Space Center Human/Robotic Spacecraft Office. Robotic sample return missions are widely considered valuable precursors to manned missions in that they can provide details about a site's environment and scientific value. For example, a sample return from an asteroid might reveal valuable resources that, once mined, could be utilized for propulsion.<sup>1,2</sup> These missions are also more adaptable when considering the risk to humans visiting unknown and potentially dangerous locations, such as a comet nucleus.

### Comet Nucleus Sample Return Mission (CNSR)

#### Background

Presently, much of the scientific community's understanding of the universe has come from remote

observation of the cosmos, but technological advances within the past thirty years have allowed for the study of retrieved cosmic materials on Earth. These Earth-returned samples have proved to be of immense scientific value, providing many answers and potential paths of inquiry.

Although comets have been observed for many centuries, a mystery still shrouds the composition of the comet nucleus. Comets are thought to have been formed simultaneously with the Sun and planets and therefore consist of the most chemically primitive solid matter known to have survived in the planetary system.<sup>3</sup> Thus, the examination of a sample from a comet nucleus would greatly add to knowledge of the solar system's origin.

### Mission Objectives

A CNSR mission is proposed to return a comet nucleus sample in its own environment to Earth for study. The primary mission objective consists of three phases: rendezvous with a short period comet, acquisition of a 10 kg sample from the nucleus, and maintenance of the sample composition and crystalline structure for return to Earth. The secondary objective for the CNSR mission is to monitor comet activity through perihelion by using a penetrator equipped with scientific instrumentation.

The comet Wild 2 was determined to be the most suitable target because of its low inclination to the ecliptic plane, its short orbital period, and its recent change in perihelion distance. An encounter with Jupiter changed Wild 2's perihelion distance from 6.2 astronomical units (AU) to 1.6 AU. Consequently, the now short-period comet has the crystalline structure of a long-period comet.<sup>4</sup> A tethered coring unit will reach the comet nucleus and extract a sample that will be housed in a protective environment so that it may be returned to Earth in an unaltered state. Upon rendezvous with the comet, a sampling probe will extract a two-meter core sample from a target site where undisturbed material maintains a temperature less than 130° K.<sup>3</sup> The comet must have a relatively low mean temperature to retain its volatile material—any material above that temperature is believed to have experienced too much heating to be of great scientific value.

The last phase of the primary objective is to maintain, as best as possible, the sample's undisturbed state during the transit to Earth. This involves monitoring and controlling the sample's pressure and temperature, as well as keeping it physically stable. A chemically or physically altered comet sample would lead to false conclusions and a distorted picture of the origins of the solar system.

The secondary objective of the CNSR mission is to obtain as much information as possible on the activity of Wild 2. This ensures that the sample is representative of the comet and allows it to be placed in the proper context with respect to other comets investigated only by remote sensing. Sufficient characterization of the sampled comet also eliminates the need for multiple samples. To fully characterize the comet, a penetrator will be left behind to monitor the comet through perihelion. Characterization of the comet includes the determination of size, shape, density, and surface temperature distribution. The penetrator will monitor temperature and gas production changes of the comet until perihelion.

### Mission Profile

The spacecraft will be launched on an Atlas IIA equipped with a Centaur IIA to inject the spacecraft into a low parking orbit and to provide the necessary Earth escape velocity (see Figure 1). The upper stage will then separate from the spacecraft, systems will be checked, and instrument booms and solar arrays deployed (see Figure 2 for spacecraft configuration). After Earth escape additional correction maneuvers during interplanetary cruise will insure accurate targeting for Wild 2.

At 100 to 200 km from Wild 2, the comet approach maneuvers reduce the relative velocity to 2 m/s. The comet's exact size and spin rate will then be determined and during the global characterization phase the surface will be mapped for candidate sampling sites. Candidate sites will be mapped in detail from an altitude of 50 km, and the coma gas and dust will be analyzed. While the spacecraft awaits final site selection it will return to an altitude of 100 km.

After a target site has been selected, the spacecraft will return to a low, *forced* synchronous orbit at 0.5 km above the selected site, reducing contamination of the surface by the thruster plumes. A sampling probe powered by liquid

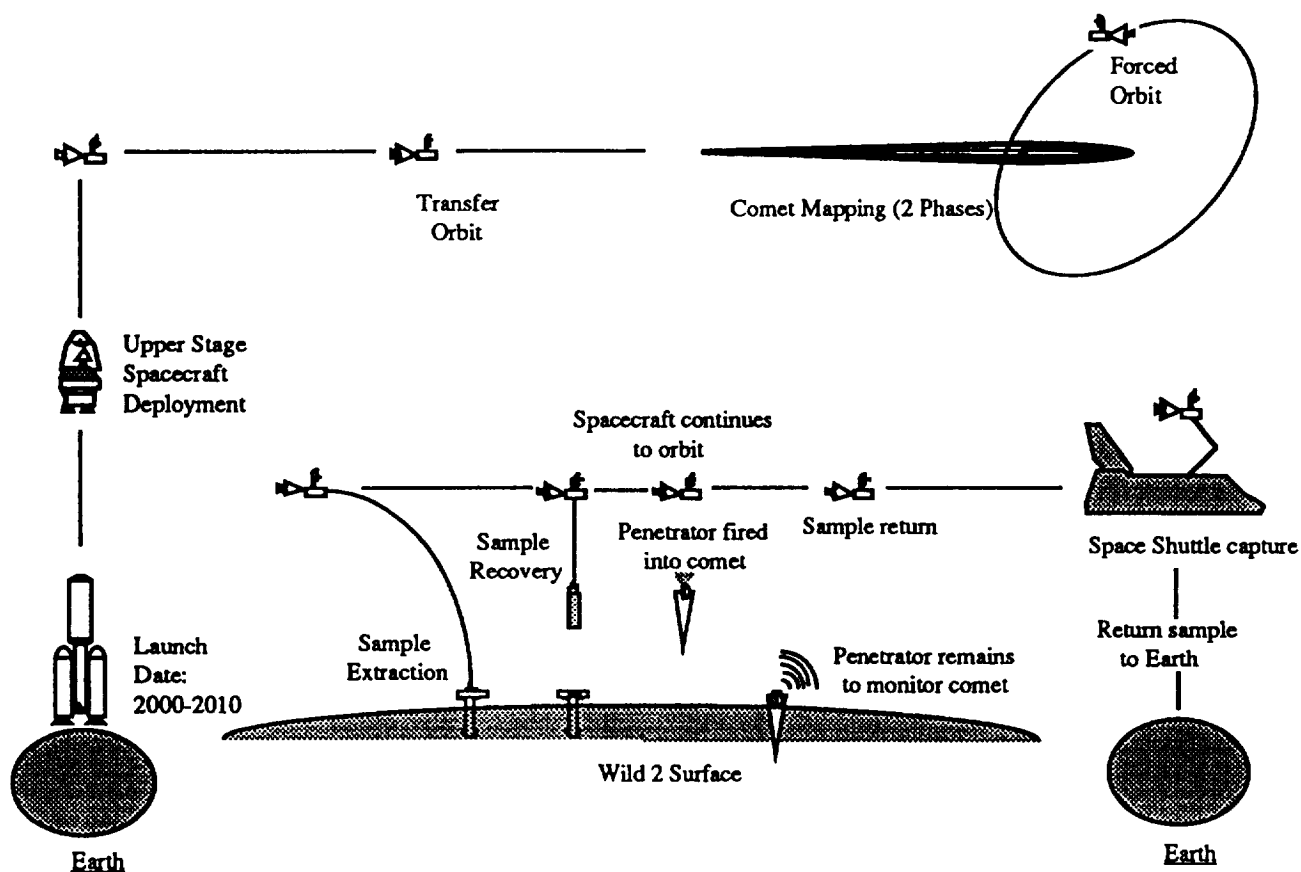


Fig. 1 CNSR mission profile

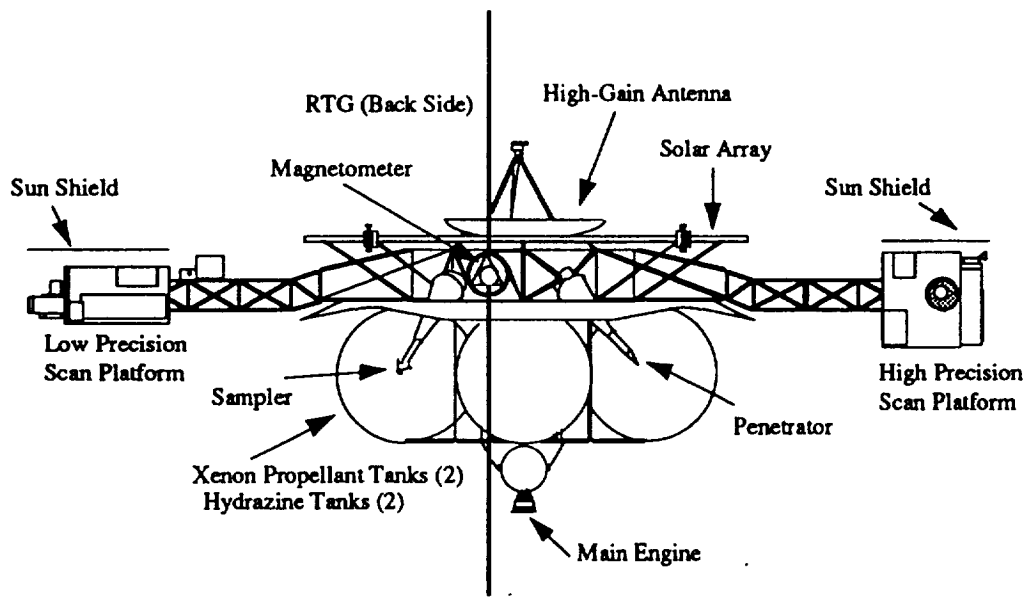


Fig. 2 CNSR spacecraft configuration

propellant rocket thrusters will then be jettisoned from the spacecraft to impact the target site. Because the spacecraft and the sampling penetrator are connected, a synchronous orbit must be maintained during extraction. Drilling commands will be sent from the spacecraft through cabling enclosed in the tether. After extraction, the tether will be used to retrieve the specimen from the sampling penetrator. Finally, a monitoring penetrator will be deployed and anchored into the comet to monitor Wild 2's activity. This penetrator will be equipped with scientific instrumentation to observe comet activity and return data. An optical communication system powered by a radioisotope thermoelectric generator (RTG) will relay the information to Earth. The RTG will also provide power for the scientific instrumentation.

After the sample has been safely retrieved, it will be returned to the spacecraft and hermetically sealed within multi-layer insulation. Once the sample has been secured in a thermally controlled environment, the spacecraft will depart from the comet leaving behind the monitoring probe. Heat pipes and phase change materials will be used to direct heat from the other spacecraft subsystems away from the sample.

The spacecraft will leave the comet and be placed on a direct Earth return trajectory. The Earth return trajectory will contain no additional maneuvers except those needed for navigational corrections. Upon arrival at Earth, the spacecraft's relative velocity will be reduced, and it will be placed in a circular Space Shuttle-accessible orbit and remain there no longer than approximately two weeks. The sample will then be retrieved by the Shuttle and returned to the surface in a thermally safe environment.

Table 1 Spacecraft mass budget

| Element                           | Mass (kg) |
|-----------------------------------|-----------|
| Spacecraft structure              | 1309      |
| Bus                               | 801       |
| Booms (truss structure)           | 102       |
| Fasteners & joints (10%)          | 90        |
| Deployment mech. (10%)            | 90        |
| Contingency (25%)                 | 225       |
| Sampler                           | 95        |
| Penetrator                        | 262       |
| Power                             | 93        |
| Solar array                       | 10        |
| RTG                               | 83        |
| GN&C                              | 83        |
| Scientific instruments            | 134       |
| Communication                     | 7         |
| Computer                          | 12        |
| Total                             | 1990      |
| 10% electric wiring               | 199       |
| 10% mass margin                   | 199       |
| Thermal (8% dry mass)             | 159       |
| Total dry mass                    | 2547      |
| Propulsion                        | 2602      |
| Propellant                        | 2312      |
| Tankage (10%)                     | 231       |
| Valves, tubing (25% of tank mass) | 57        |
| Total wet mass                    | 5149      |

#### Overall Mass, Power, and Cost Budgets

The spacecraft will have a total mass of 5149 kg (see Table 1) and require a total operating power of 528 watts (see Table 2). A cost model<sup>5</sup> was applied to the mission estimating a total cost of \$1.88 billion FY92 dollars (see Table 3).

Table 2 Power budget

| Spacecraft component | Power (w) |
|----------------------|-----------|
| GN&C                 | 20        |
| Mapping              | 150       |
| Communications       | 122       |
| Computer system      | 50        |
| Structure            | 50        |
| Thermal              | 40        |
| Sample extraction    | 27        |
| Avg. power           | 459       |
| Margin (15%)         | 69        |
| Total avg. power     | 528       |

Table 3 Cost estimation<sup>5</sup>

| Mission Component      | Cost (\$M) |
|------------------------|------------|
| Computer               | 47.97      |
| Communications         | 17.83      |
| Power                  | 135.31     |
| Sampler                | 240.13     |
| Penetrator             | 368.00     |
| Thermal                | 123.04     |
| Propulsion             | 0.51       |
| GN&C                   | 129.33     |
| Scientific instruments | 209.26     |
| Structure              | 524.38     |
| Launch system          | 85.00      |
| Total                  | 1880.76    |

### Single Asteroid Sample Return Mission (SASR)

#### Mission Objectives

The primary objective of this mission is to extract a core sample from a target asteroid and return this sample to Earth for detailed compositional analysis. Secondary mission objectives entail performing a wide variety of scientific observations that will enable humankind to better understand the physical nature of asteroids, their

possible origin, and their effect on the interplanetary environment.

#### Mission Profile

The mission designers selected 433 Eros as the target asteroid because of its accessibility, its relatively large size, and its well-known orbital parameters. In addition, at least three launch windows will exist for a mission to Eros between 1992 and 2010.<sup>6</sup>

Figure 3 illustrates the mission profile. The spacecraft will begin the mission with the landing struts, instrument booms, and high-gain antenna collapsed enabling them to fit in the launch vehicle shroud and withstand all launch forces. An Atlas IIA launch vehicle will propel the spacecraft into Low Earth Orbit (LEO). While in LEO, the spacecraft will perform checks of all systems. A Centaur will then inject the vehicle into the required transfer orbit after which the spacecraft will deploy the landing struts, booms, and high-gain antenna. Scientific measurements of the interplanetary environment will begin at this time. At a distance of one million km from Eros, the spacecraft will begin to photograph the asteroid and perform scientific observations. Once the spacecraft descends to an altitude of 2.5 km, it will maintain its position above a location on the surface. A passive/active sensing technique will utilize visual images and laser radar scans to identify a safe landing zone that is within the maneuvering range of the vehicle. The spacecraft will then land at this location and anchor into the surface with barbed spikes. Once secured on Eros, the scientific instruments will perform several observations and then cease operations to allow power to be concentrated on the drilling process. The drill will then proceed to extract a five-foot-long core sample. Once this sample is stored on the spacecraft, pyrotechnic charges will separate the vehicle's upper portion from the rest of the spacecraft and depart from the asteroid, leaving the drill and landing struts behind. If enough propellant remains, the spacecraft will perform the maneuvers required to complete a detailed map of Eros. Once the mapping is completed, or discovered to be beyond the capacity of the propulsion system, the spacecraft will begin the voyage back to Earth. On the return trip, the vehicle must again execute a mid-course correction. Upon arrival at Earth, the spacecraft will maneuver into LEO where it will remain until it can be retrieved by the Space Shuttle.



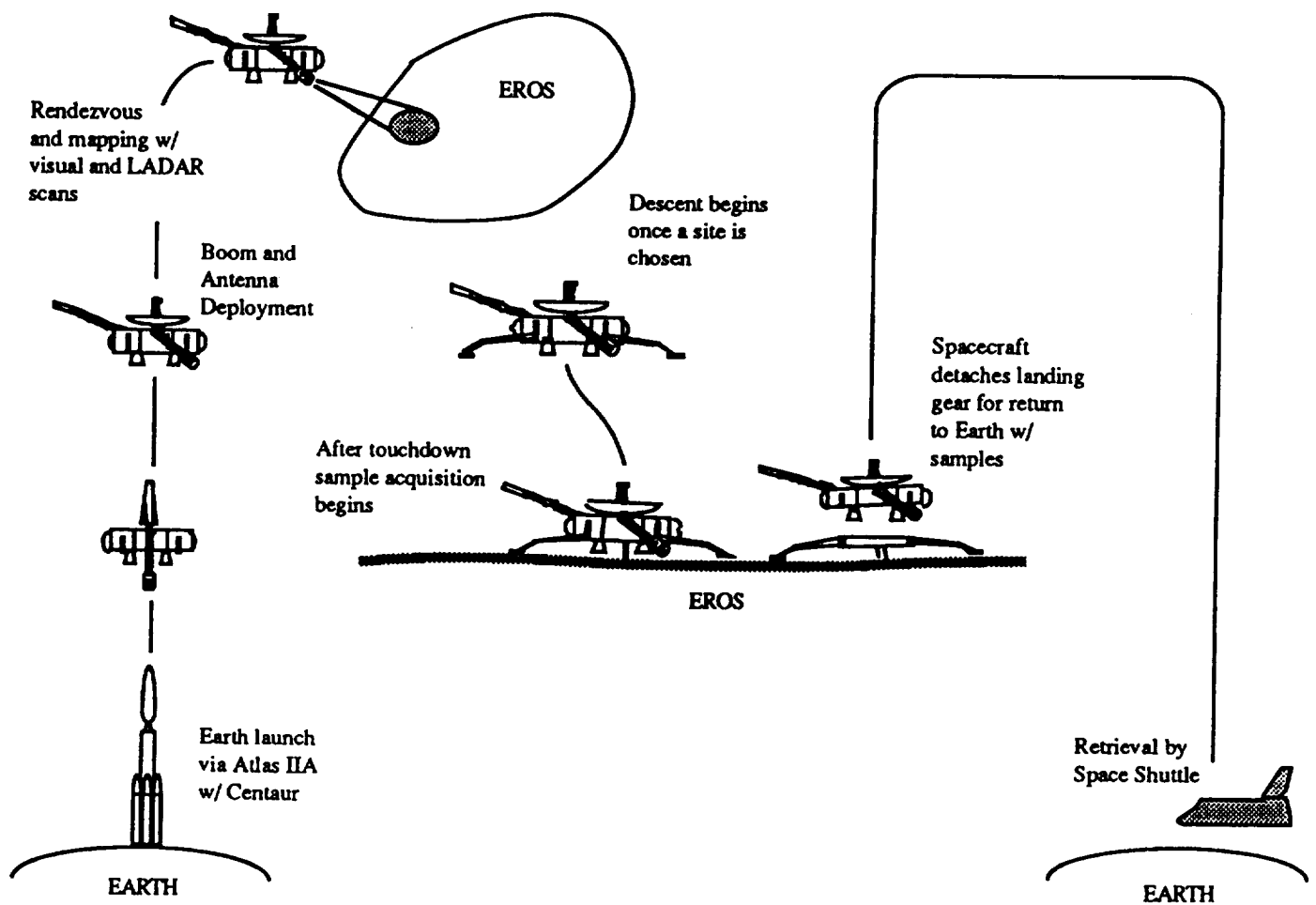


Fig. 3 SASR mission profile

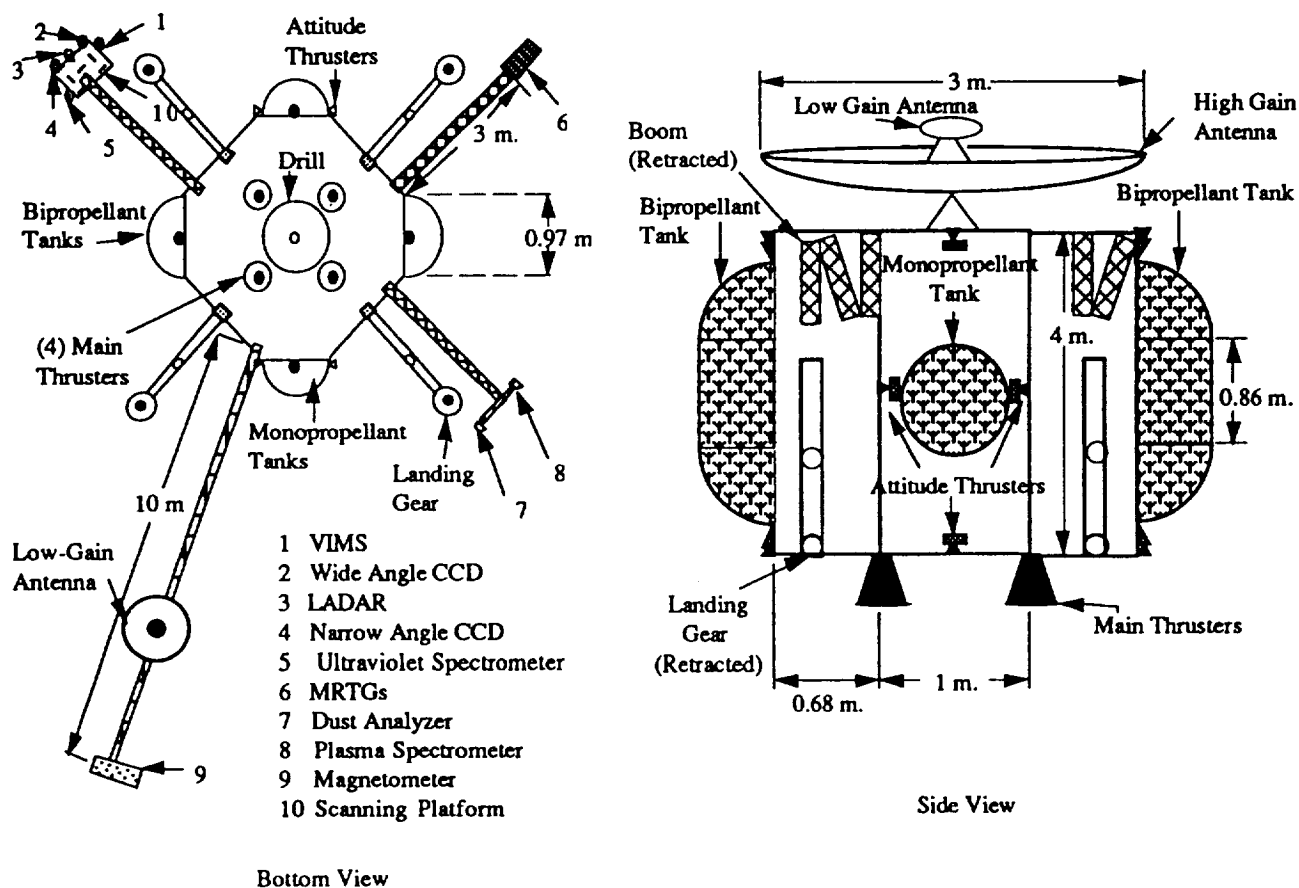


Fig. 4 SASR spacecraft views

### Spacecraft Description

Figure 4 illustrates the basic spacecraft configuration. The spacecraft structure will be a semimonocoque design constructed chiefly from beryllium. It will use three modular RTGs for general power consumption and will employ three batteries to provide the power required for drill operation. The vehicle will be propelled by four main thrusters that use a bipropellant consisting of monomethylhydrazine and nitrogen tetroxide. Twelve attitude thrusters will utilize hydrazine as a monopropellant. The control system will incorporate

three-axis stabilization with momentum wheels. Spacecraft communications will be accomplished by one high-gain antenna and two low-gain antennas that operate in the Ka-band. The scientific payload will include: a visual and infrared mapping spectrometer, an ultraviolet spectrometer, a plasma spectrometer, a magnetometer, a dust analyzer, a laser radar system, and two charge-coupled device cameras. The thermal subsystem design consists of thermal blankets and heaters for the majority of the spacecraft. Thermal requirements for the drill necessitate the additional use of heat pipes and second-surface mirrors. The electronics will be mounted on cold

rails from which heat will be transferred by heat pipes to the second-surface mirrors. In addition, the infrared-sensing instrument will require a radiative cryogenic coolant system. The command and data handling system must be highly autonomous, utilizing higher-order languages and hybrid architecture.

#### Overall Mass, Peak Power, and Cost Budgets

Table 4 shows the overall spacecraft mass budget and peak power budget. The peak power values are not totaled because all the subsystems will not be simultaneously operating at peak requirements during any particular time of the mission. Therefore, a total value for peak power would be of no significance. Table 5 summarizes the overall estimated cost budget for this mission in FY92\$M.<sup>5,7</sup>

Table 4 Spacecraft mass and peak power budgets

| Subsystem          | Mass (kg) | Peak Power (w) |
|--------------------|-----------|----------------|
| Propulsion         | 3633.11   | 150.0          |
| C&DH               | 121.35    | 451.1          |
| Drill              | 450.00    | 7500.0         |
| Attachment         | 150.00    | 181.0          |
| Structure          | 550.00    | N/A            |
| Scientific payload | 116.2     | 114.2          |
| Communications     | 32.00     | 80.0           |
| Power              | 550.00    |                |
| GN&C               | 200.00    | 550.0          |
| Thermal            | 50.00     | 60.0           |
| Total              | 5852.66   | N/A            |

Table 5 Overall mission cost budget<sup>5,7</sup>

| Segment Description | Cost (FY92\$M) |
|---------------------|----------------|
| R & D testing       | 1141.16        |
| First unit          | 57.09          |
| Ground segment      | 1530.65        |
| Launch segment      | 115.70         |
| Total               | 2844.60        |

#### Multiple Asteroid Sample Return Mission (MASR)

##### Mission Objective

The goal of this mission is to return sample material from three asteroids to Earth for scientific analysis. Asteroids Euterpe, Psyche, and Themis will be sampled, covering three major classes of asteroids, S (stony iron), M (metallic), and C (carbonaceous), respectively. The MASR mission utilizes numerous state-of-the-art technologies including a nuclear reactor for the power system, a low-thrust propulsion system, a deployable truss structure, and an optical communications system.

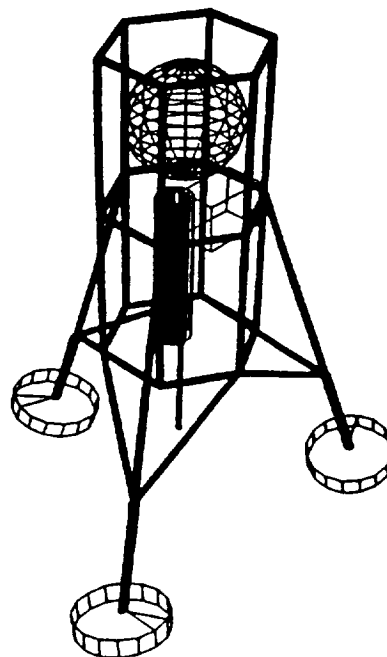


Fig. 5 Sampler/lander

### Spacecraft Configuration

The spacecraft configuration consists of a tethered lander and a main spacecraft (see Figures 5 and 6). The tethered lander is stored inside the main spacecraft body and consists primarily of a drill and a small GN&C system. The spacecraft employs a reactor with shielding and radiator panels separated from the main spacecraft

body by an expandable truss. This configuration keeps the harmful radiation from the reactor away from sensitive subsystems like the computer or scientific instruments. The main spacecraft body contains all required propellant, the lander, and all other subsystems.

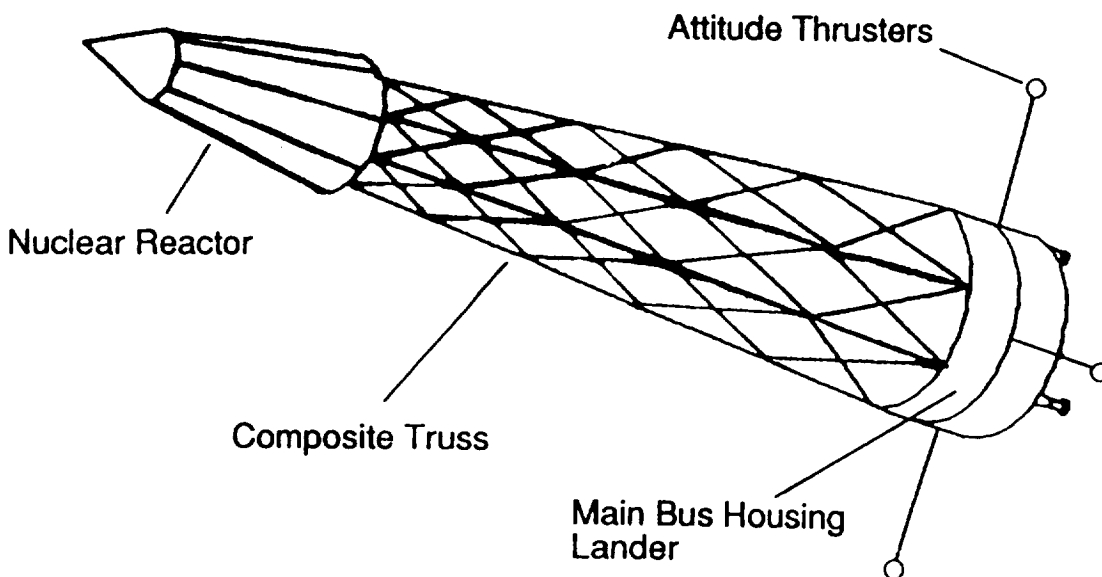


Fig. 6 MASR high technology spacecraft

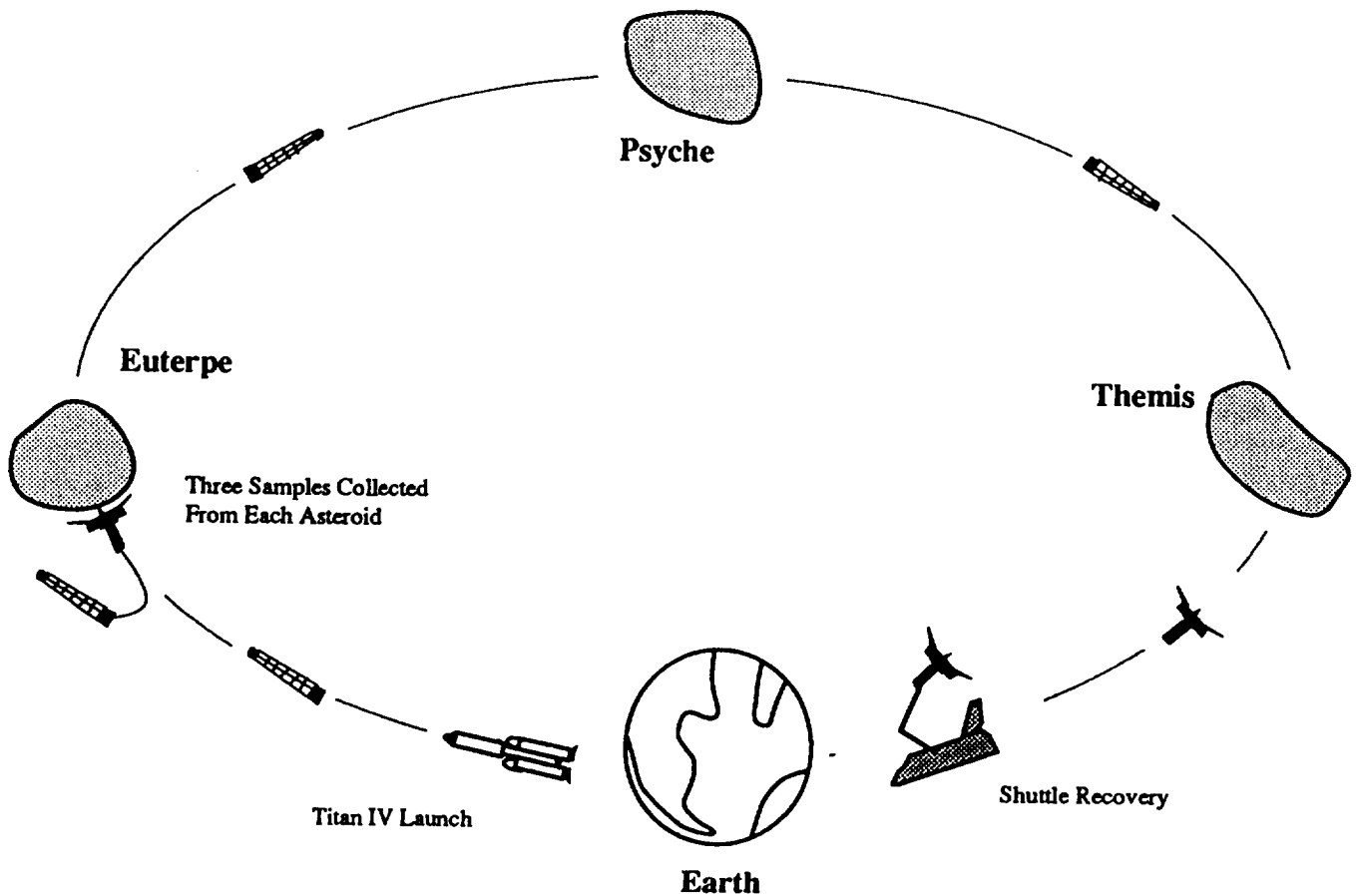


Fig. 7 MASR mission scenario

### Mission Profile

The following description of the mission plan is summarized in Figure 7. The mission scenario begins by launching the spacecraft into LEO with a Titan IV on March 1, 2002. The Titan IV will be used because it is the only current launch system that can accommodate the spacecraft's mass, 15,800 kg, and size, 16 m long by 4.5 m diameter. During the launch phase, communication with the spacecraft will be through an omnidirectional antenna. Before the nuclear reactor is activated, power

for the communication and housekeeping systems will be supplied by batteries. Once in LEO, the spacecraft will then deploy the partially collapsible truss structure and optical communications system, again by battery power. The omni antenna will then be switched off and the optical communication system used for the remainder of the mission. The reactor will be powered up and a functional check-out performed on all subsystems. The spacecraft will now rely on the nuclear reactor for power. A series of xenon thrusters will be activated, propelling the spacecraft toward the first target asteroid. The thrusters will cycle through thrust and coast stages to

achieve the most efficient trajectory. This thrust profile has been calculated by NASA's QuickTop 2 (QT2) computer program.

Once the main spacecraft detects the asteroid with sensors, the rendezvous and docking (RVD) processor will take control and implement the necessary orbital maneuvers to orient the main spacecraft in the proper attitude. While the main spacecraft is approaching the asteroid, several scientific instruments will be collecting data to determine the best possible landing sites. A mass spectrometer, laser altimeter, and a radiometer will provide a complete map of the asteroid's surface. The main computer system will analyze this data and select the four best sites, three to sample and one as a backup. These landing sites may require additional maneuvering of the main spacecraft. The lander, while still attached to the main spacecraft through a tether, descends toward the asteroid and one of the landing sites. The lander's propulsion system will consist of 12 xenon thrusters powered by the reactor through a cable in the tether. The RVD processor on the main spacecraft will also control the lander during its rendezvous with the asteroid.

The lander attaches itself to the asteroid by drills in the landing pads. Three core samples, from three different locations on the asteroid, will be extracted from the asteroid along with other scientific data. While the lander is maneuvering to the next sampling site, the main spacecraft, while orbiting above, will follow it to the next site. This is necessary due to the limited length of the tether. Each sample will be encased in its coring barrel to prevent contamination. All samples and scientific information will be stored on the main spacecraft. Power and communications for the lander will be provided by the main spacecraft through the tether.

After the three samples are taken from the asteroid, the lander will then rendezvous with the main spacecraft. The RVD processor will also control these maneuvers and will dock the lander in the center of the main spacecraft. Once the lander is secure, the main spacecraft will then proceed to the next asteroid. Because of the large amount of data needed to be stored for these RVD maneuvers, data will be transmitted to Earth between asteroid encounters. When the next asteroid is located by the long-range sensors, the rendezvous and sampling scenario will then be repeated.

After the last sample is obtained, the lander will return and dock in its station in the center of the base of the main spacecraft. The main spacecraft will then begin its journey back to Earth. The return leg of the mission is similar to the first leg in that it will consist of a series of thrust and coast periods as calculated by QT2. Along with the thrust and coast periods the program provides the appropriate orbital paths for returning to Earth.

The ship will approach Earth to enter an orbit where it may release the lander, or the sample container alone, if feasible. This orbit will be designed such that the Space Shuttle, or its replacement in 2026, will be able to retrieve the samples.

After the sample container or lander is released, the main spacecraft will have completed its duties. The reactor will then be shut down using systems that are designed to function independently of the spacecraft. Two proposals have been suggested for dealing with the spacecraft after the mission is complete. The main goal is to eliminate possible contamination to the environment after the reactor is shut down. One proposed method is to have the main spacecraft thrust into a high nuclear-safe orbit that will not decay for approximately 1000 years. Another solution is to send the spacecraft on an Earth escape trajectory. If reentry were to occur after spending a long time in space, a majority of the radioactivity would have decayed. However, as an added safety feature, the nuclear system will be designed to safely accommodate accidental reentry. The SP-100 has been designed to remain inoperable, to survive the intense heat and aerodynamic forces of reentry, and to bury itself on impact in water, soil, or pavement.<sup>8</sup>

#### **Overall Mass, Power, and Cost Budgets**

Mass, power, and cost budgets<sup>5</sup> are shown in Table 6. A substantial safety margin is included in each of these categories to ensure a reliable design.

Table 6 Mass, power, and cost budgets

| Subsystem        | Mass (kg) | Power (w) | Cost <sup>5</sup> (\$M) |
|------------------|-----------|-----------|-------------------------|
| Communication    | 52        | 57        | 158                     |
| Computer         | 45        | 89        | 20                      |
| Drill            | 160       | 1200      | 329                     |
| GN&C             | 260       | 394       | 34                      |
| Landing gear     | 15        | 300       | 69                      |
| Launch vehicle   | N/A       | N/A       | 150                     |
| Power            | 6000      | N/A       | 150                     |
| Propulsion       | 1800      | 86000     | 1423                    |
| Scientific inst. | 120       | 250       | 180                     |
| Structure        | 220       | N/A       | 373                     |
| Micromet. prot.  | 128       | N/A       | 7                       |
| Thermal          | 125       | N/A       | 16                      |
| Margin           | 400       | 1,000     | 50                      |
| Total            | 9325      | 89290     | 4227                    |

### Conclusion and Recommendations

Three design projects completed by the students have been discussed. There are still some unresolved issues in each of the missions which need to be addressed. First, a redesign of the monitor penetrator in the CNSR mission is required to place the RTG and optical communications package away from the rocket engine. Two members of the SASR team found that the hardness of the asteroid surface cannot be determined. A sampler drill to accommodate this variable should be examined. Using the QT2 trajectory code, the MASR mission length was calculated to be approximately 24 years. Missions of this length cause serious wear on systems. Reducing the length could be as simple as visiting the asteroids in a different order or visiting fewer asteroids.

Samples returned from the Moon by the Apollo astronauts have provided a wealth of information about its composition. Missions that return samples from comets and asteroids are important because they may reveal the intricate building blocks of the solar system. In addition, asteroids may contain mineral deposits that

could be refined for use as propellants. Perhaps one day humans will visit the asteroids and comets, but until then these robotic missions can provide information of considerable significance to cosmologists and planetary geologists.

### References

1. Barnes-Svarney, Patricia. "Grabbing a Piece of the Rock," *Ad Astra*, Vol. 2, October 1990, pp. 7-13.
2. International Asteroid Mission, International Space University 1990 Design Project Final Report, York University, Toronto, Canada, Summer Session, 1990.
3. Stetson, D.S., Lundy, S.A., and Yen, C.L. "The Mariner Mark II Comet Rendezvous/Asteroid Flyby Mission," AIAA Paper No. 84-2016, AIAA/AAS Astrodynamics Conference, Seattle, WA, August 20-22, 1984.
4. Feingold, H., Hoffman, S.J., and Soldner, J.K. "A Comet Nucleus Sample Return Mission," AIAA Paper No. 84-2027, AIAA/AAS Astrodynamics Conference, Seattle, WA, August 20-22, 1984.
5. Cyr, K. "Cost Estimating Methods for Advanced Space Systems," SAWE Paper No. 1856, Index Category No. 29, July 29, 1988.
6. Lau, C.O. and Hulkower, N.D. "On the Accessibility of Near-Earth Asteroids," AAS Paper No. 85-352, AAS/AIAA Astrodynamics Specialist Conference, Vail, CO, August 12-15, 1985.
7. Wertz, J.R. and Larson, W.J. *Space Mission Analysis and Design*, Kluwer Academic Publishers, Boston, MA, 1991.
8. General Electric Space Nuclear Power Tutorial, Conducted at NASA Lewis Research Center, May 29-31, 1991.

**DESIGN AND DEVELOPMENT OF THE SECOND GENERATION MARS HABITAT****Prairie View A&M University****Department of Architecture****Prairie View, Texas****Dr. Ikhlas Sabouni****Roy Smith, Teaching Assistant****Steven Taylor, Brock Harrell, Earnest Crawford****Abstract**

The second generation of Mars Habitat is to be utilized as an advanced permanent base for 20 crew members to live on Mars for a period of 6-12 months. It is designed to be a self-contained environment accommodating five main facilities: living, working, service, medical, and a greenhouse. The objective of the design is to create a comfortable, safe living environment. Hexamars-II and Lavapolis-II are two different concepts for the advanced Mars Habitat. The design team assumes there will be an initial habitat located near or on the site from earlier missions that satisfies the requirement for a short-term habitation for the crew to use while constructing Hexamars-II or Lavapolis-II. Prefabricated structures and materials will be shipped to the site before the long-term crew members arrival. Partial construction and preparation for the long-term habitat will be done by crew members or robotics from a previous mission. The construction of the long-term base will occur in phases. Hexamars-II consists of six sphere-shaped inflatable modules that will be partially buried below the Martian surface. The construction of each sphere will occur in ten steps. Shape charges will be used to create the crater in which the spherical structure will be placed. The interior core will be unloaded and put into place followed by the exterior structure. Foundation will be filled, interior bladder will be inflated, floor-to-floor joists connected, and sand pockets filled. Finally, the life support system and interior partitions are put in place. Each sphere consists of three levels of which the lower level will be safe haven. Particular attention is given to structural support, the dominance of internal pressure, the process of construction, and human factors.

**Introduction**

We are all currently living in space upon the Spaceship Earth, a self-sustaining ecosystem in orbit around the sun, which provides the energy for life.

Man has created miniature environments to support his life as he ventured into space away from the mother ship.

Skylab was America's first facility that housed astronauts for several months as they observed the dynamics of the sun. We have learned much about long-duration space flight from the experience of these missions. Skylab has since been destroyed, as its orbit decayed and it burned up in the atmosphere.

There are many reasons for the advocacy of the space movement. The exploration of the unknown, a quest for knowledge of our origin, and conquering the challenge of adventure are all inherent emotions of our species which have brought us, as a civilization, to where we are now.

Mars is the planet most similar to Earth compared to any other in the solar system. It has an atmosphere, there is an expectation of finding water at the poles, and its gravity is roughly half that of Earth's. If life existed or does exist anywhere else in the solar system, scientists argue that it would be on Mars. Mars offers the best possibility for terraforming; that is, modifying the environment to sustain life as we know it. However, there are many factors which must be addressed before we can live beyond the comforts of our planet.

During the last two years undergraduate students from the Department of Architecture at Prairie View University have been researching and designing a human settlement on Mars. The structural system and the process of construction were the main objectives of the



research for this year.

### Objectives

The second generation of Mars Habitat is to be utilized as an advanced permanent base for 20 crew members to live on Mars for a period of 6-12 months. It is designed to be a self-contained environment accommodating five main facilities: living, working, service, medical, and a greenhouse. The objective of the design is to create a comfortable, safe living environment. There will also be a need for the development of an oxygen plant, solar fields, Controlled Ecological Life Support System (CELSS) facilities, materials processing plant, and a nuclear power plant.

### Assumptions

Hexamars-II and Lavapolis-II are two different concepts of the advanced Mars habitat. The design team assumes there will be an initial habitat located near or on the site from earlier missions, which satisfies the requirements for a short-term habitation for the crew to use while constructing Hexamars-II and Lavapolis-II. Prefabricated structures and materials will be shipped to the site before the arrival of the long-term crew members. Partial construction and preparation for the long-term habitat will be done by crew members or robotics from a previous mission. The construction of the long-term base will occur in phases.

### Hexamars-II Site Location

The site location of Hexamars-II is three degrees north latitude and 99 degrees east longitude between Pavonis Mons and Ascreaus Mons. The site is congruous with the angle of space entry into Mars orbit. Another appealing factor about the site is the comfortable temperature conditions due to its location near the equator.

### Materials Used for Construction

The basic materials used for the construction of Hexamars-II will consist of aluminum arches, radial floor beams, secondary bracing, and central support columns. Other major materials needed would include Kevlar-29

for the inflatable bladder, rigidized foam for the walls, partitions, and flooring, and hardened rubber or cables for the connection of the inflatable bladder. The advantage of using inflatable structures over other types is their extremely low weight to volume ratio characteristics.

### Construction Considerations

For the construction of Hexamars-II, environment, time, and manpower need to be considered. The environmental factors include one-third Earth gravity, continuous solar and cosmic radiations, temperature extremes, solar wind, meteorites and dust. The use of basic construction methods, modular components, and minimal on-site fabrication will conserve precious time. With this in mind it will help to cut down on site equipment and manpower needs.

In the initial stages of construction the crew will stay in self-supporting modules from previous missions. There are two types of construction designs for Hexamars-II. The first concept uses only inflatable materials to form the sphere which consists of interior bladder and exterior rigidized foam (Figure 1). The second concept uses an inflatable sphere with aluminum I-beam arches for support (Figure 2). In the first concept, cables and a special connection device are used to connect the Kevlar-29 to the interior structures (Figures 3 and 4), while soft rubber at the ends of the floor beams is used for the same purpose in the second concept (Figure 5).

### Methods of Construction

The first step of construction will use detonation charges to create the craters needed for the placement of Hexamars-II. The design team chose to use shaped charges (specially designed explosives used by the military) as detonation devices (Figure 6). There are three major advantages to using this form of explosives: the use of minimal explosives, the confinement of destruction, and the ability to penetrate deep into the regolith.

In the next phase of construction, the telescopic interior core will be unloaded and set into place inside the crater. The core will then be extended and the inflatable bladder will be pressurized (Figure 7).

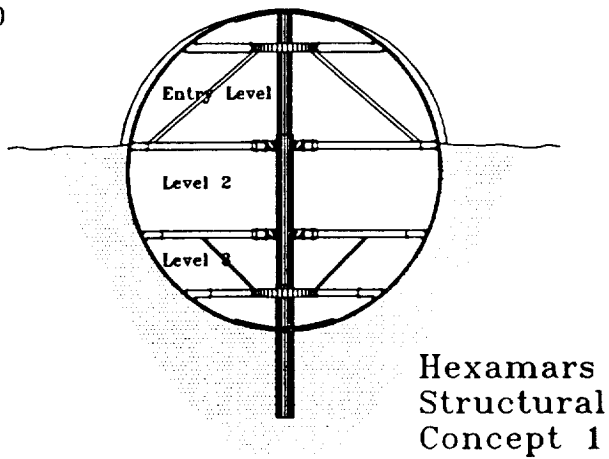


Fig. 1 Hexamars-II Structural concept 1

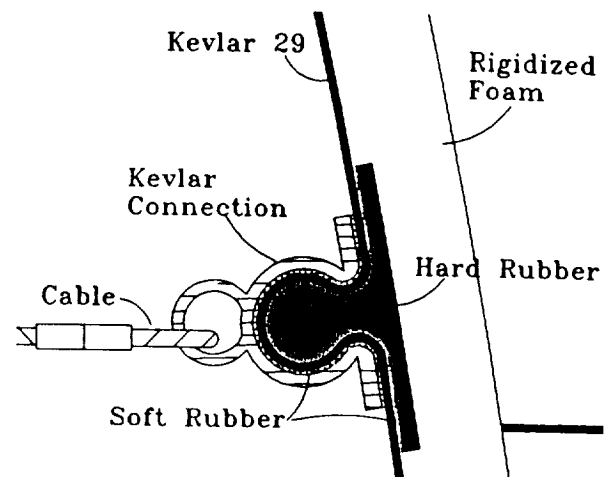


Fig. 4 Connecting device for concept 1

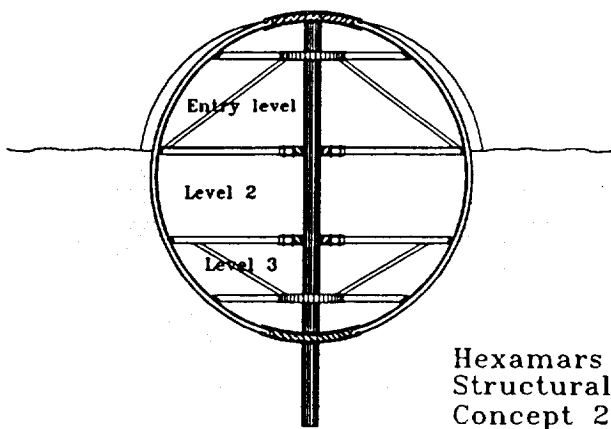


Fig. 2 Hexamars-II Structural concept 2

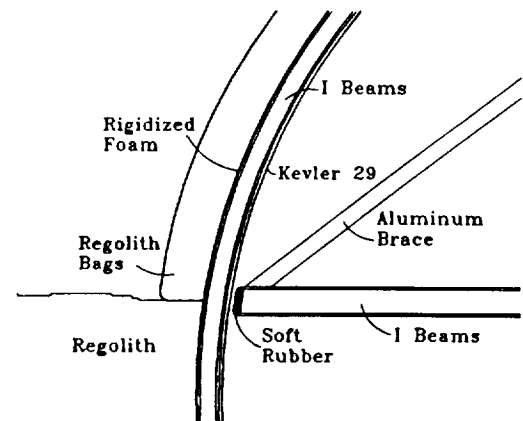


Fig. 5 Interior structure for concept 1

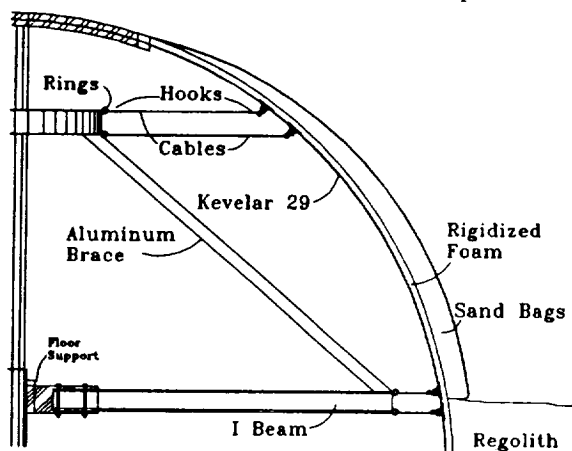


Fig. 3 Connection between Kevlar-29 and interior structures in concept 1

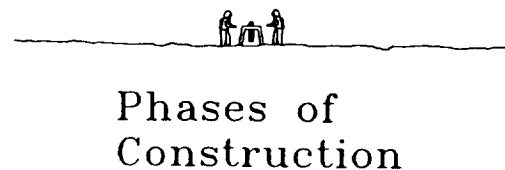


Fig. 6 Use of detonation charges

If the second concept is to be used, the exterior I-beams need to be unloaded and placed around the interior core before pressurization takes place.

Once the structure is in place and pressurized, the crater can then be filled with regolith. Then, regolith-filled bags are placed around the habitat to provide radiation protection to the interior portion of the sphere.

The last step of construction will be the placement of floor beams (Figure 8), connecting floor panels (Figure 9), interior partitions, and the installation of the life-support systems.

### General Functional Relationships

The basic design of Hexamars-II aims at providing a safe and comfortable environment for the crew members. In the layout of the facility the team investigated the effects of placement of different modules and the safety risk it posed on the crew and facilities. The facilities of Hexamars-II included the habitat itself, surface vehicles, utilities, and launch and landing area.

The Habitat was broken up into six different spheres: living quarters, storage, medical, science, greenhouse, and communications. For the safety of the crew the science lab sphere was located farther away from the rest of the habitat; emergency air locks and safe havens are also located in each of the spheres. To provide circulation convenience to the crew, the living quarters are located in the central portion of the base, and the remaining facilities branch off it. Surface vehicles, which include manned rovers, tele-operated rovers, and construction equipment vehicles, are located in a construction shack near the habitat main entrance. Utilities consist of oxygen plant, nuclear power plant, and solar panel fields. These facilities are located safely away from the main base. The launching and landing facilities are located the farthest distance away from the habitat for safety reasons.

### Lavapolis-II Site Location

The selection of an appropriate site is critical to the long-term success of the Mars base. An equatorial site is most economically accessed from low Mars orbit and simplifies rendezvous maneuvers. The most striking

geological features, Olympus Mons, the largest volcano in the solar system, and the Colossal Valles Marineres, the colossal canyon, are located there. The site chosen for Lavapolis-II is at the base of Ceraunius Tholus, a 115-km wide, 22-km high volcano in northeast Tharsis at 24 degrees north, 97 degrees west, at the area where an impact crater has pulverized a 2-km wide channel.

The advantage of the subsurface site of a lava tube is that it is naturally protected from the hazards of meteorite impact and solar radiation with constant, relatively benign temperatures of 20 degrees Celsius. Modest site preparation inside the lava tube will prepare the tube as a receptacle for more conventional self-enclosed habitats. Accessibility, spatial distribution, and proper raw materials are needed to fulfill the mission of the base.

Precursor survey missions will define an optimal location for penetrating the roof of the lava tube. Construction will begin soon after the turn of the century. The surface features of the selected site should include the ability to sustain roadways between the launch facilities, habitat, and surface operations.

### Construction Considerations

Lavapolis-II concept will provide a uniform approach to habitation on Mars inside a lava tube. The design uses a rotational hyperboloid as the primary form of the units. Aluminum framing molded into curvilinear trusses with a mechanized aluminum arch, wheeled support base truss (Figure 10), and floor supports are all contained in a structural circle (Figure 11). The inflatable portion of the structure is envisioned as an envelope made of multi-ply fabric such as Kevlar-29, a high strength aramid fiber. The inflatable portion is attached to the structural rings (Figure 12). Each cylindrical unit consists of two structural rings with an inflatable shell (Figure 13).

### Component Design and Arrangement

The compact modules consist of two rotational aluminum arches supported by two ground trusses (Figure 14). The rotational arch comes manufactured with the Kevlar attached to it (Figure 15). The actual amount of space occupied while stored for transportation

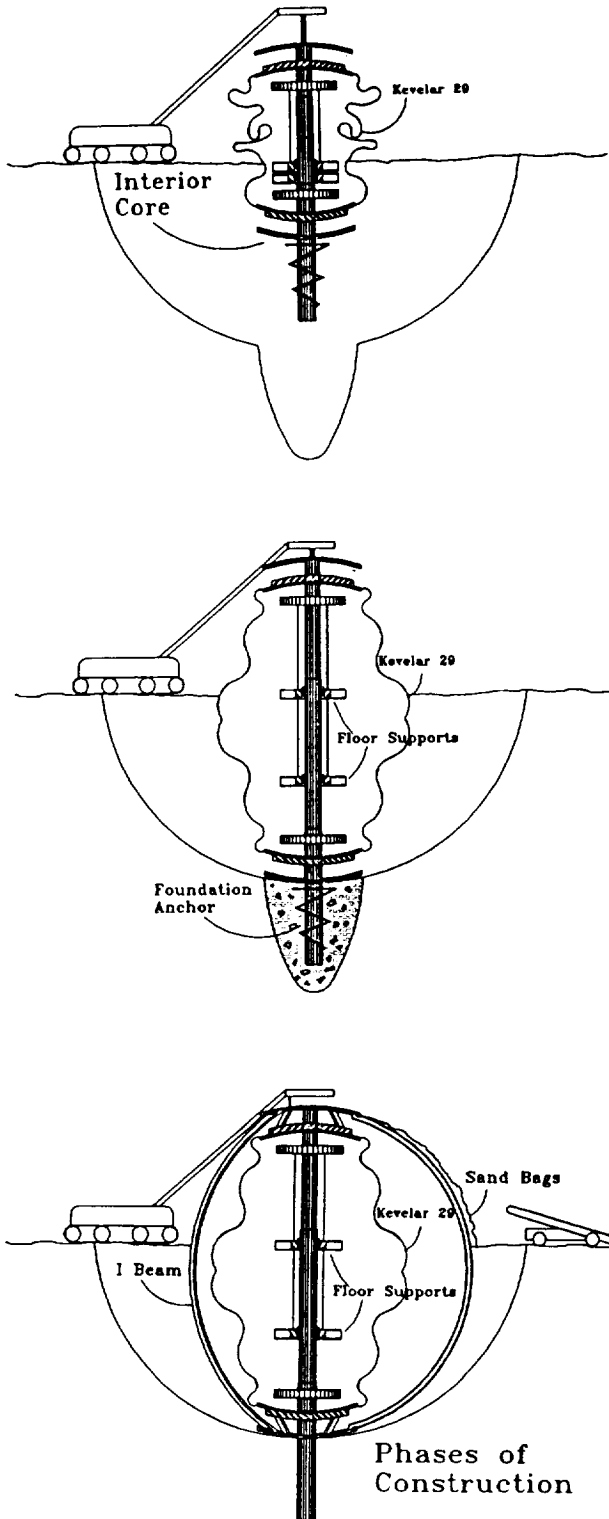


Fig. 7 Phases of construction for Hexamars-II

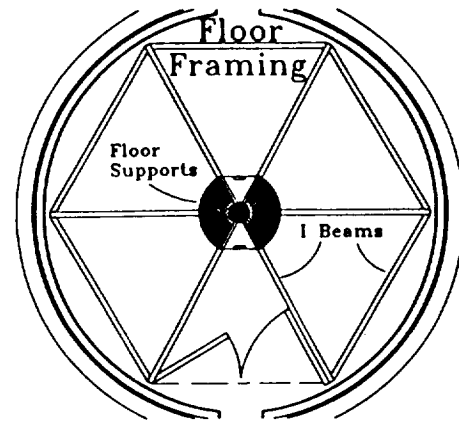


Fig. 8 Floor system

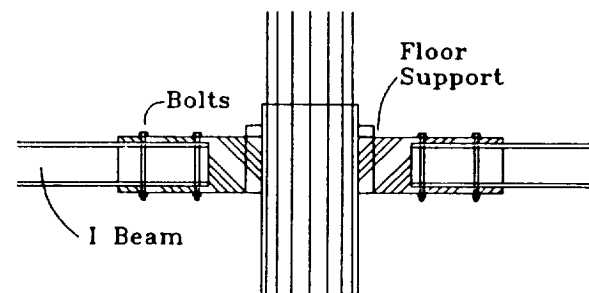


Fig. 9 Connection between floor beams and interior telescopic core

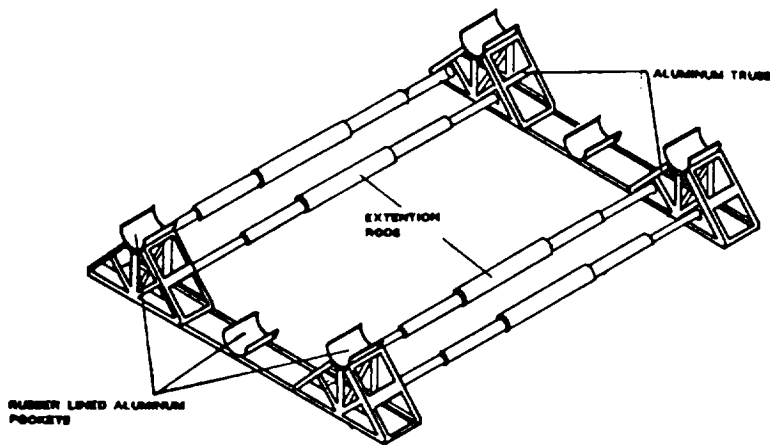


Fig. 10 Ground support components

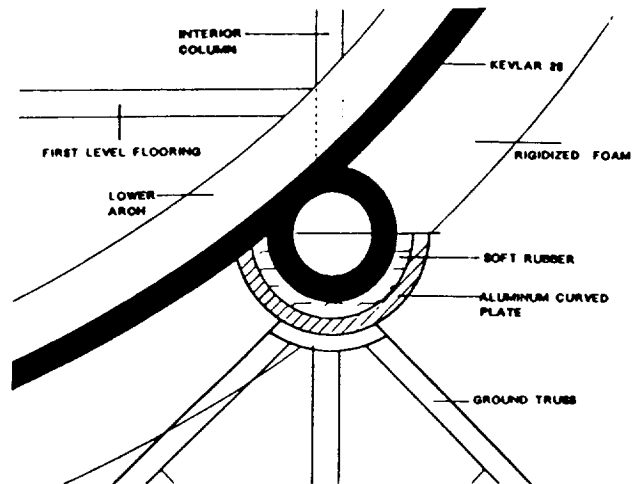


Fig. 12 Connection between inflatable cylinder and ground truss

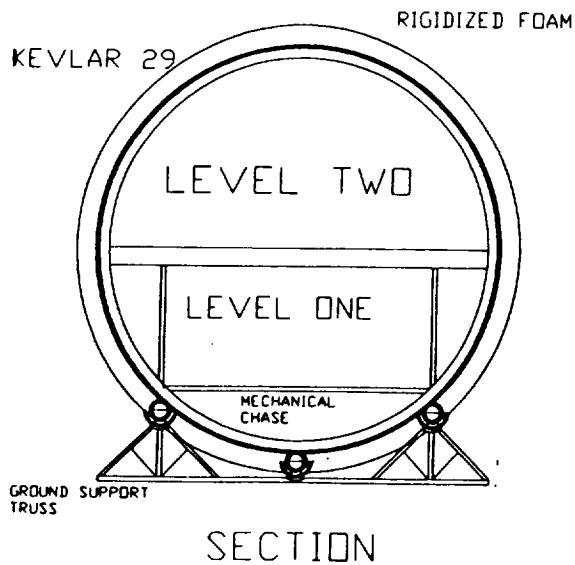


Fig. 11 Section in one of the cylindrical modules

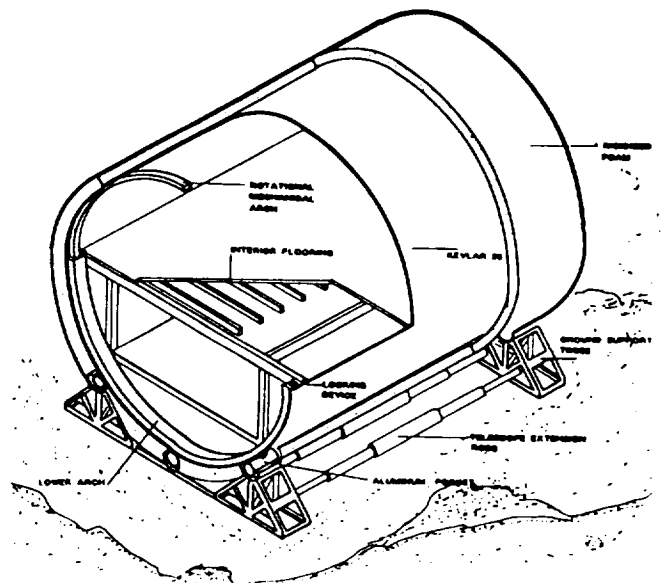


Fig. 13 One cylindrical unit

is minimum. Interior construction parts are modular and interchangeable. The components will be unloaded from the space carrier into the tube and assembled on the site.

The procedures for the first unit construction include minor excavation inside the lava tube to clear the path for construction. A crane will lower the semicircle with the attached Kevlar onto the ground truss. When the arch meets the base, the couple, which is lined with a soft durable rubber to eliminate the possible rupture of the Kevlar, is locked into place. The motorized crank is then activated to rotate the hidden arch into a locked position above the lower arch completing the two circular ends of the hyperboloid. The unit is then expanded to its maximum length.

The flexibility of the unit is achieved by alteration of components: shifting arches and a contractible brace truss. The units are adaptable to suit the requirements of up to three levels of habitat with living areas, exercise areas, health maintenance facility, crew quarters, communications, clinic labs, EVA support and maintenance, and mechanical systems.

### **Conclusion**

Early in the research, different habitat layout concepts and different materials and technology ranging from Earthlike to spaceframe to inflatable technology were investigated, presented, and discussed with professionals from Johnson Space Center, USRA, College of Architecture at the University of Houston, and the Departments of Aerospace and Mechanical Engineering at University of Texas at Austin. The advantages and limitations of each concept were discussed during these reviews. As a result of this discussion and the constraints of using the existing technology and the need to minimize volume, weight, and construction time, the design team chose to work with inflatable structures.

This study explored the feasibility of using inflatable spheres in the design of Hexamars-II and inflatable cylinders in the design of Lavapolis-II. A third concept was also studied (Martiana) in which inflatable spheres and cylinders were used together to create spatial variety within the habitat. The same construction methods and materials of Hexamars-II and Lavapolis-II were used in the design of Martiana.

In all three concepts, a number of spheres and cylinders with air locks in between were used to create different enclosures that can be contained in case of emergency. Dual egress in each module and safe havens were two additional safety measures that were used.

The use of a number of enclosed spherical and cylindrical modules with air locks was an important factor of the design to allow for future expansions by connecting additional modules to the existing habitat without having to depressurize the existing structure. Linear and radial spatial organizations were chosen to make the expansion of the base feasible.

The form of the habitat was related to the site, the physical environment, and the quality of space and construction. The Lavapolis-II linear pattern responded to the tubular nature of the lava tube and to the geometry of the cylinders. The radial shape of Hexamars-II provided circulation convenience to the crew by designating the central sphere for living quarters and by branching all other facilities from it (Figure 16).

The design team focused more on achieving safe and simple structural systems for the base and on developing easy methods of construction with minimal on-site fabrication and manpower.

As in every design developed by an architect, engineer, or scientist, there are strengths and limitations especially with the existing technology and the limited data about the extra-terrestrial environment of Mars; this study was not any different. The advantage of this research was not only in developing an optimum design for a Mars base, but also in introducing new ideas of space design in the Department of Architecture, increasing the awareness of space design among the students, and providing an opportunity and a challenge to explore different technologies representing a departure from the traditional conventional architecture of Mother Earth.

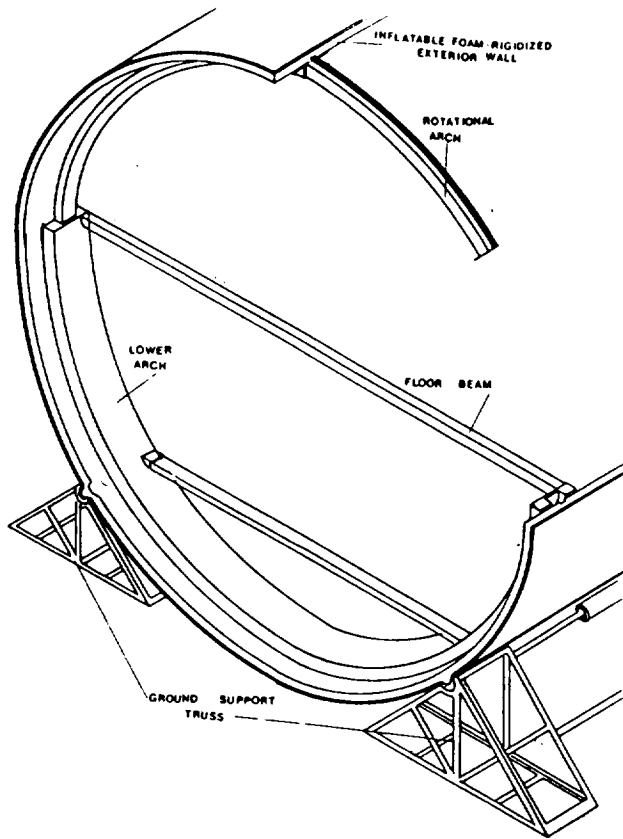


Fig. 14 Rotational and structural system

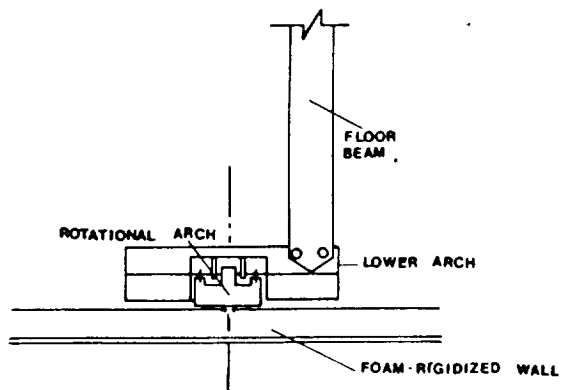
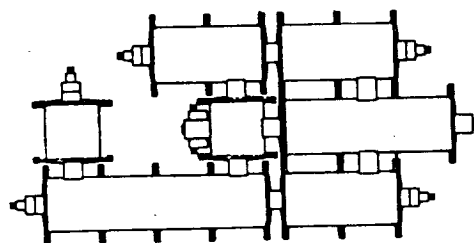
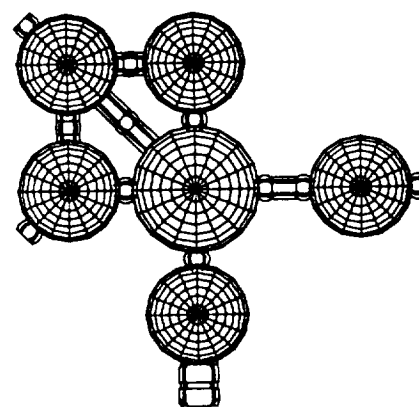


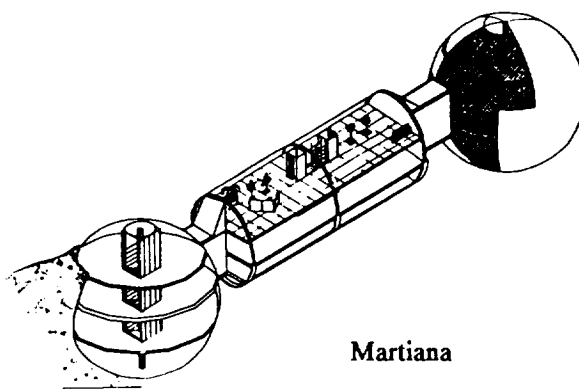
Fig. 15 Section in the structural aluminum arch



Lavapolis-II



Hexamars-II



Martiana

Fig. 16 Spatial organization of Hexamars-II, Lavapolis-II, and Martiana



**FIRST LUNAR OUTPOST**

**University of Puerto Rico  
School of Architecture  
Rio Piedras, Puerto Rico**

**Professor Aureo F. Andino, A.I.A.**

**Daniel Silva, Teaching Assistant**

**Nelson Ortiz, Model Consultant**

**Omar Alvarez, Julio A. Colón, Myrelle Colón, Alicia Diaz, Xochiquetzal Y. Escobar,**

**Alberto Garcia, Isabel C. González, Edwin Hill, Carlos Jiménez, Isaac Laboy,**

**Carlos G. Ramos, José A. Solis, Pablo R. Tirado, Frances Villarine**

**Abstract**

Design and research efforts at the University of Puerto Rico have focused on the evaluation and refinement of the Habitability Criteria for prolonged human permanence in space during the last four years. Living quarters for a Mars mission and a third generation lunar base concept were proposed. This academic year, 1991-92, work on further refinement of the habitability criteria and design of partial gravity furniture was carried on.

During the first semester, design alternatives for furniture necessary in a habitat design optimized for lunar and Martian environments were developed. Designs are based on recent research data from lunar and Mars gravity simulations, and current NASA standards. Artifacts will be submitted to NASA architects to be tested in KC-135 flights.<sup>1</sup> Test findings will be submitted for incorporation in future updates to NASA habitat design standards.

Second semester work was aimed at integrating these findings into the First Lunar Outpost (FLO), a mission scenario currently being considered by NASA. The mission consists of a manned return to the moon by crews of four astronauts for periods of 45 days. The major hardware components of the mission are: (1) a Crew Module for the delivery of the crew and their supplies and (2) the Habitat Module, which will arrive on the Moon unmanned. Our design efforts concentrated on this

Habitat Module and on application of habitability criteria. Different geometries for the pressure vessel and their impact on the interior architecture were studied. Upon the selection of a geometry, a more detailed analysis of the interior design was performed, taking into consideration the reduced gravity, and the protection against radiation, micrometeorites, and the extreme temperature variation.

A proposal for a FLO was submitted by the students, consisting essentially of a 24-foot (7.3 m.) by 35-foot (10.67 m) high vertical cylinder with work areas, crew quarters, galley, wardroom, leisure facilities, health maintenance, waste management, EVA operations facilities, and safe havens.

**Introduction**

The First Lunar Outpost (FLO) is a mission scenario currently being considered by NASA. The mission consists of a manned return to the moon by crews of four in periods of 45 days (lunar day, night, day). The major components of the mission are: (1) the Habitat Module and (2) the Crew Module. The two modules are to be delivered by common lander elements, with the exception that the Crew Module has an ascent stage. The Habitat Module will arrive on the Moon unmanned and will remain on the lander. The Crew Module will deliver crew and supplies, landing approximately 1 km from the habitat.

---

<sup>1</sup>The KC-135 is a specially modified jet transport that flies a parabolic arc to produce short periods of less than one g acceleration force.

Design efforts concentrated on the design of the Habitat Module and on the application of the habitability criteria. Three different geometries suitable for the

pressure vessel and their impact on the interior architecture were studied. These geometries were the cylinder, the sphere, and the cone. Precedents in the use of these geometries in manned space missions were studied before undertaking a preliminary habitat design for each one by different student groups. The vertical cylinder was chosen from these preliminary designs. Upon this selection, a more detailed analysis of the interior design was performed, taking into consideration the reduced gravity, and protection against radiation, micrometeorites, and the extreme temperature variation.

A proposal for an FLO was submitted by the students, consisting of 24-feet (7.3. m.) by 35-feet (10.67 m) high vertical cylinder with working areas, crew quarters, galley, wardroom, leisure facilities, health maintenance facility, waste management, EVA operation facilities, and safe havens.

### Habitability Concept Definition

Three previous habitability studies developed by the students arrived at a concept definition which could be summarized as follows:

*"Habitability is that state of equilibrium which results from the interaction between components of the Individual-Architecture-Mission Complex which allows a person to sustain psychological homeostasis, adequate performance, and acceptable social relationships."*<sup>2</sup>

A diagram that presents the concept visually was developed to communicate the interdependence of the three parts of the complex. The individual's stress due to isolation, interpersonal stress due to confinement, and impersonal stress induced by a totally artificial or alien environment may cause a person to suffer psychological problems, which may impair the fulfillment of the mission or even the individual's motivation for survival in such an environment. The mission, together with the individual's values can provide the proper motivation and driving force for striving to accomplish expected goals and objectives as understood by the individual. But since psychology is shaped by built environment, it is the architecture of the environment that holds the key to factors that lead to quality of life, beyond the level of mere survival in a hostile environment. Sights, motions, and sounds, as well as careful consideration of all sensory stimuli will have to be envisioned and provided for before

we can be fully capable of designing the appropriate environment for human inhabitants in extraterrestrial space.

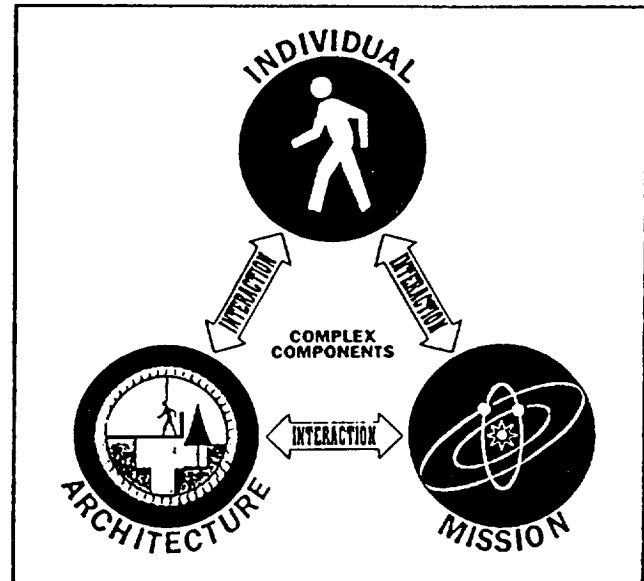


Fig. 1 Habitability concept diagram

### Sights

Photobiological systems are particularly adapted to wavelengths somewhere between the 400 and 70 nm, the portion of the spectrum called "visible." In extraterrestrial space, intensity of contrast between the lighted and the shaded are extreme, since there is no atmospheric diffusion, refraction, or optical filtering phenomena. Color and depth perception will be perceived as a new experience.

### Sounds

As we know, sounds travel in pressure waves and through a medium like air or water. These are called fluid-borne vibrations, which are medium composition and density dependent. Extraterrestrial atmospheres created for human habitation must, to some extent, reproduce Earth's atmosphere, to make sound transmission possible, and even be able to reproduce the quality of sounds, which are related to performing arts to be perceived.

## FLO (Habitation Module)

- 6.1 EVA support area
  - 6.1.1 Airlock/Hyperbaric chamber
  - 6.1.2 Donning/Doffing stand
  - 6.1.3 Suit storage
  - 6.1.4 Suit maintenance
- 6.2 Stowage
- 6.3 Wardroom
- 6.4 Galley
- 6.5 Crew quarters
- 6.6 Medical facility
- 6.7 Exercise
- 6.8 Personal hygiene
- 6.9 Body waste management
- 6.10 Laundry facility
- 6.11 Trash management facility
- 6.12 Operations area
  - 6.12.1 Workstations
- 6.13 ECLSS

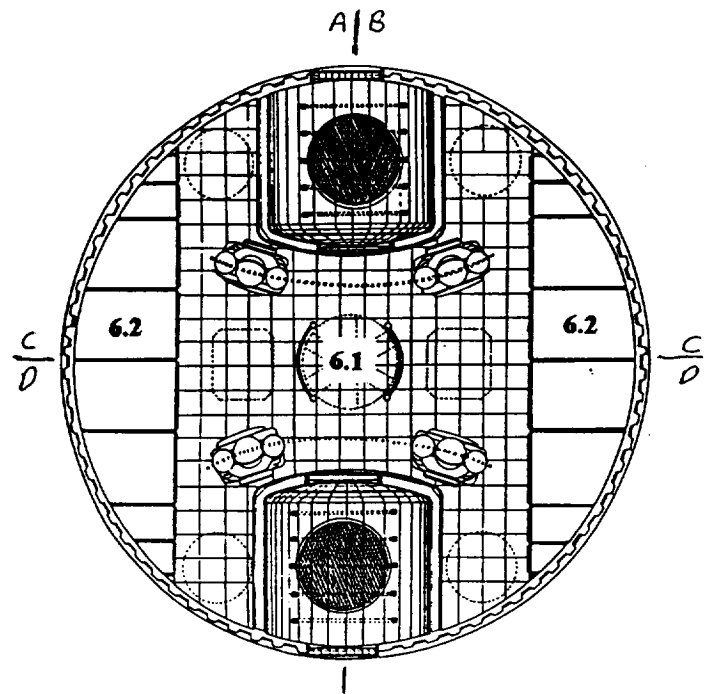


Fig. 6.1 First Level

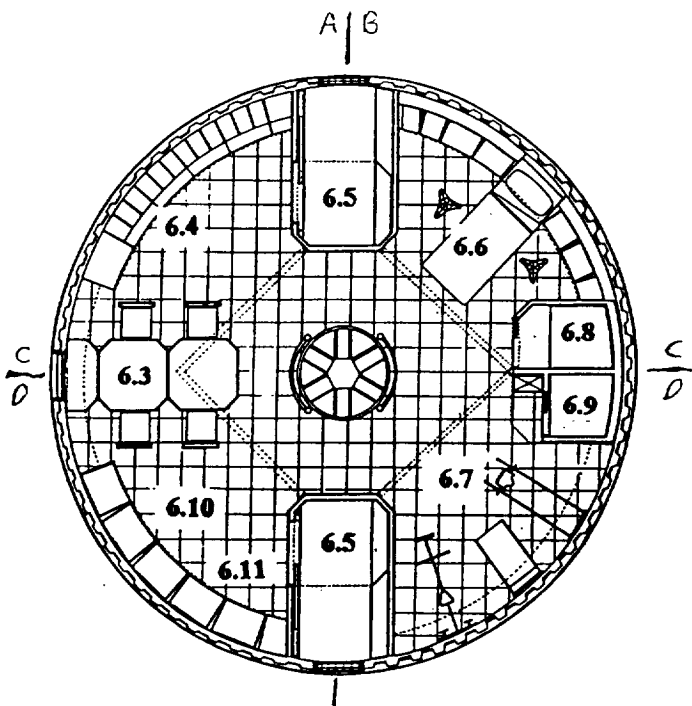


Fig. 6.2 Second Level

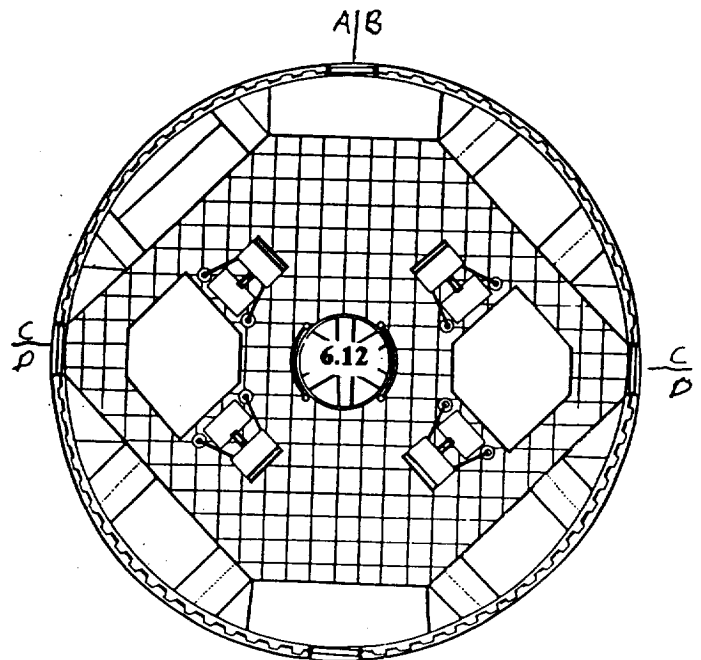


Fig. 6.3 Third Level

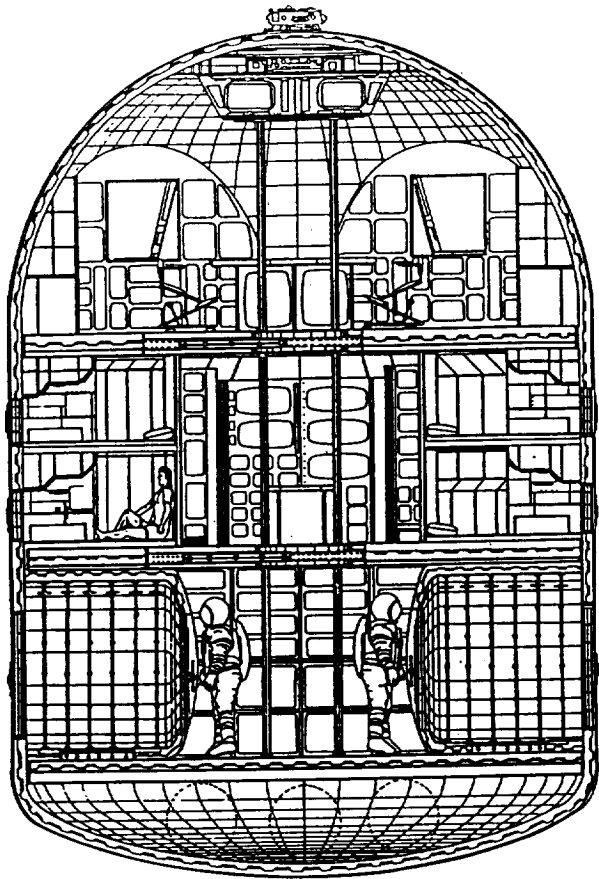


Fig. 6.4 Section A-A

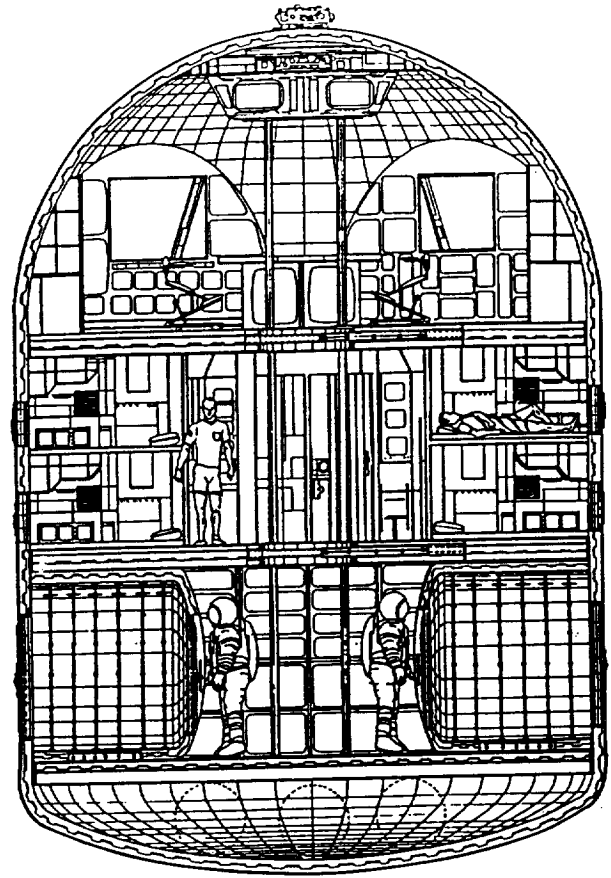


Fig. 6.5 Section B-B

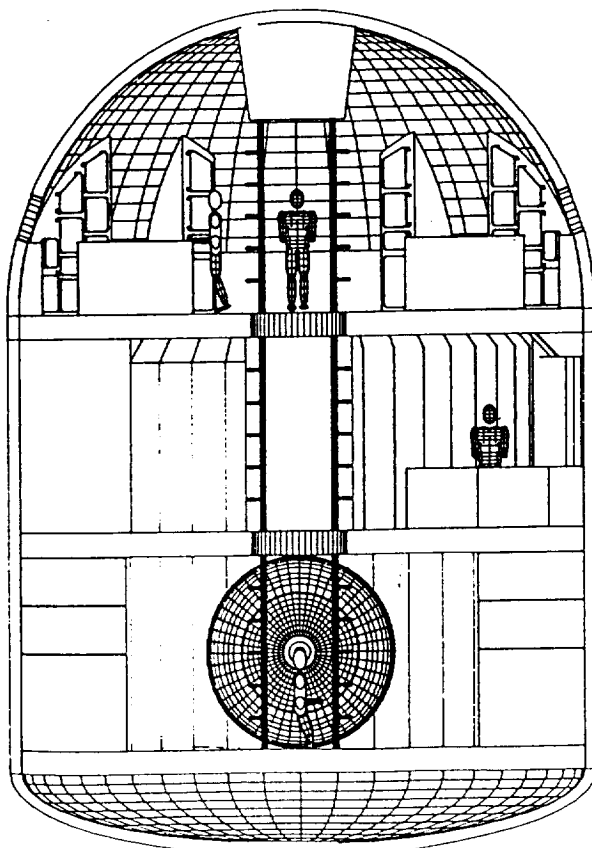


Fig. 6.6 Section C-C

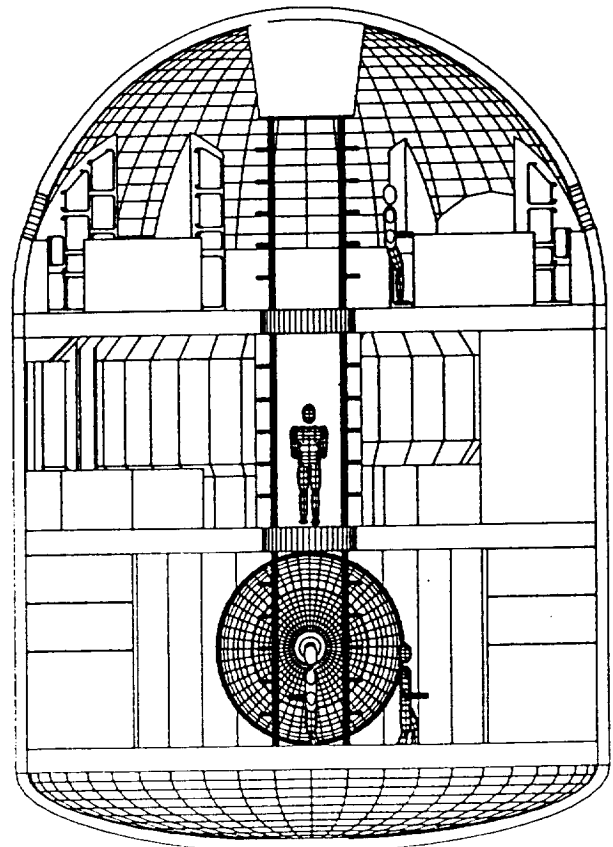


Fig. 6.7 Section D-D

## Smells

Sight, hearing, and touch have been well-studied, but the sense of smell is not as easy to study in a quantitative manner. Nevertheless, smells must be taken into account when designing areas like laboratories or waste management facilities to control the propagation of annoying smells.

## Motions

Vertigo and dizziness are a result of the malfunction of inner ear components like the vestibule and the semicircular canals. Reduced gravity environments will affect such sensors and will require upper body control, in addition to the usual bipedal erect balance which *Homo Sapiens* has evolved through millions of years. In a reduced gravity environment, a period of acclimatization to reduce muscular impulses, as well as to slower and softer movements, is required.

Even if these environmental factors are taken into account, we have identified seven problems which will arise from living in such alien conditions. These are:

**Upset equilibrium.** Reduced weight has a disturbing effect in the vestibular part of the inner ear, upsetting equilibrium. This can alter perception and accentuate psychological problems mentioned earlier. Its effects can be transitory or permanent, as was the case with early astronauts and cosmonauts.

**Diminished stimulation.** Reduced gravity may cause a reduction of the tone and threshold of the central nervous system. Brain activity may tend to diminish, possibly triggering apathy and fantasy.

**The solipsism syndrome.** Common sense holds that it is inherently ridiculous to think that the only reality is that which is perceived by the observer. But with the advent of access to extraterrestrial space, this academic oddity has become a real psychological danger. The absence of stimuli in the regular, ordered terrestrial environment can easily persuade a person that the real world begins and ends at the limit of the individual's sphere of perception.

**Loss of identity.** Increasingly long communication intervals reinforce the solipsism syndrome by straining more the link with reality. Even at a quite neighborly

distance, such as the Moon, communication will have time lags significant enough to disjoint a conversation, to lose the sense of connectedness, and to chop off interchange into a series of separate one-way messages.

**Fear.** Existence in a hostile environment kept at bay by a fragile life support system can induce anxiety and fear. This is especially critical during periods of low activity, which precede the short bursts of extreme activity under stress when major operations are to take place. Stress should be directed toward mission goal fulfillment to prevent phobias from getting out of control and causing critical conflicts to arise. Special procedures and therapy have to be provided in such cases.

**Claustrophobia.** The fear of enclosed places is a disqualifying tendency for anyone who is interested in pursuing life in extraterrestrial space. Testing will reveal such tendencies, but severe experiences in extraterrestrial space may induce it. Preventive and therapeutic measures have to be provided for inhabitants on conditions that would emulate artificially sensation of interior and exterior spaces.

**Sexual frustration.** The withdrawal of normal sexual outlets for prolonged periods naturally invites historical comparisons. The importance of the problem depends largely on the sexual drive of each individual, the key being the inevitable sublimation of directing such energy and drives toward a full programmed schedule of work to attain the goals and objectives of the mission.

Natural selection gave humans a specific body construction. Muscles and bones proved support to fragile organs. This creates problems when humans dwell beyond the frontiers of the terrestrial environment. In order to be productive, humans require a level of comfort as a required necessity for habitation beyond Earth.

## Lifestyle Analysis

One important aspect of FLO operation is the crew. Living conditions must not be limited to the level of mere survival, but there must also be quality and style, promoting personal fulfillment and adequate performance. Work, rest, and leisure must be balanced, so that maximum advantage could be taken for productive

work without sacrificing maintenance functions or time for recreation, which is necessary to maintain high morale.

There is the possibility that a new group of four astronauts will come to the FLO every forty-five days, depending on the availability of the lunar transportation system, to replace the previous group. They will land on a site approximately one kilometer away from it, and will transfer their supplies, using a rover type of transport during the first two days, alternating the moon-bound group with the Earth-bound group in their transfer ride on the rover. Consideration must be given to waste disposal so as not to contaminate the site. After the Earth-bound group has left, the new group in the FLO will begin installation of their experiments, organization of their research, and their work in general. For that they will spend days number three and four.

From then on, a routine for ordinary days (37) will be established in a way that allows circadian cycles of the crew to stagger sleep and wake hours, so that there is always someone on duty. The last two days of the crew period will be dedicated to preparations for return to Earth and collection of data to close or transfer experiments to the incoming crew.

A typical 24-hour period in the life of a crew member includes a sleep period of six hours, followed by one hour for personal hygiene, breakfast, and a health maintenance check-up. All of these take place in the second level. Then there will be a period of four hours for work (research, operation, reports, etc.) in the third level, or EVA, in some instances. That would be followed by two hours of exercise, a meal, and a rest period of one hour in the second level. After that, crew members will take two hours for programmed or extemporaneous recreational activities, which will be followed by another period of four hours for work at the third level. The day will conclude with two more hours of exercise and one hour for a meal and another medical check-up.

During weekends, or every seven days of twenty-four hours, the typical day's routine will be interrupted by meetings of all four crew member, exchanges, and celebrations. These must be made to coincide also with the times of crew transfer at the beginning and end of the 45-day cycle. Crew transfer time must also coincide with

the lunar sunrise/sunset to insure proper illumination of landing/take-off sites.

Most of the crew work will be done inside the FLO (IVA), but there will be occasions that work will require extravehicular activity (EVA). For those times, there will be four suits with life support systems for four hours. Since work among crew members is staggered, not all of them will engage in EVA at the same time. Egress and ingress is through two hyperbaric chambers at the first level, which also contain a "car-wash"-type system to remove regolith dust particles from incoming astronauts as they enter from EVA. One of the chambers will be maintained in vacuum, as long as there is a crew member in EVA, to permit rapid reentry, if needed, while the other will be kept pressurized to permit the exit of a crew member to help those in EVA, when required.

### **Installation Process**

The FLO habitat, a rounded-top vertical cylinder will be launched from Earth assembled with a lander folded underneath. As it descends on the moon, it will unfold hexapod supports that will be designed to accommodate to uneven terrains, and it will land unmanned on the surface of the moon in any of the sites being considered. It will deploy two arms (extended 100' by 10' wide) containing a solar energy collector array. The two arms will align themselves by rotating around the envelope body until they reach a position parallel to the North-South line, except at polar landing sites, and the flat surface of the arms will rotate following the sun for maximum exposure. This will recharge its batteries and will start ECLSS operation. Rotating around the oculus of the observatory in the apex will be segment-shaped panels for temperature control. Antennae, cameras, and other external attachments will be automatically deployed, and will signal to Earth the readiness of the habitat to receive a crew.

Then, a Crew Module transporting four astronauts will be launched to land at a distance of one kilometer from the habitat. It will be a conical vessel mounted over a similar lunar lander. The first crew will also have to carry a lunar surface rover, so that future crews will be able to transfer supplies from their landers to the FLO, and to deal with the problem of waste stowage. Every forty-five days a new crew will arrive, and the returning crew will

start its journey back to Earth in the same conical vehicle, which will be designed for reentry.

The FLO differs from the Apollo landings (a first generation of lunar bases) in that it will have an infrastructure of translunar vehicles capable of keeping a flow of astronauts for the 45-day mission cycles and capable of initiating rescue missions when necessary. Essentially it will be a permanently manned outpost for as long as it is resupplied from Earth. Thus, we can consider it to be the beginning of the second generation of lunar bases.

As technology for the development of recyclable biomes develop, the FLO will evolve by addition of plant growth and physicochemical modules, depending less upon Earth resupplies. The third generation of lunar bases will come into being when autosufficiency is attained.

### Reduced Gravity Furniture

#### Partial gravity sitting posture research

Humans have developed a sitting posture adequate to Earth's gravity that has been a result of thousands of years of evolution. With the advent of the Space Age, a neutral body posture for a reduced gravity that differs from the Earth's gravity sitting posture was assessed. Humans have been on the moon, but they spent most of their time standing or on a seat or a hammock while inside their extraterrestrial vehicle. Therefore, the appropriate sitting posture for Lunar gravity is not known exactly. The Mars gravity sitting posture is also not fully understood. They are between the familiar sitting posture of Earth's gravity and the neutral body posture experienced in microgravity.

The KC-135 aircraft, NASA's reduced gravity simulator, was chosen to conduct the necessary tests for this kind of research because it can create a complete body experience in reduced gravity. The major disadvantage of this method is the limited time, approximately 30 seconds, of reduced gravity available continuously. On June 1991, a KC-135 flight experiment determined the best walking gait and sitting posture for Mars gravity. A regular office chair and an ergonomic chair were tested to determine their feasibility for use in a reduced gravity environment. Both of these chairs were secured to the floor of the

aircraft; no translation was possible. Swiveling was only done with the office chair, but was found to be difficult. The ergonomic chair tested had no provision for swiveling. These issues need to be investigated in the future. It was found that there was not enough friction between the body and the office chair to hold the person in place. A seat belt was suggested to secure the person to the chair, but using a seat belt each time one sits is not the best design solution. The ergonomic chair was more effective in securing the person. Better reach was achieved using it. But it was found that a heel rest was needed in order to maximize forward reach. The angle of the seat and the knee rest needed to be optimized for the partial gravity condition. For this purpose, a second generation sitting posture experiment was conducted in August 1991. This time the research was conducted in both Mars and Lunar gravity. The results of these tests are still being analyzed.

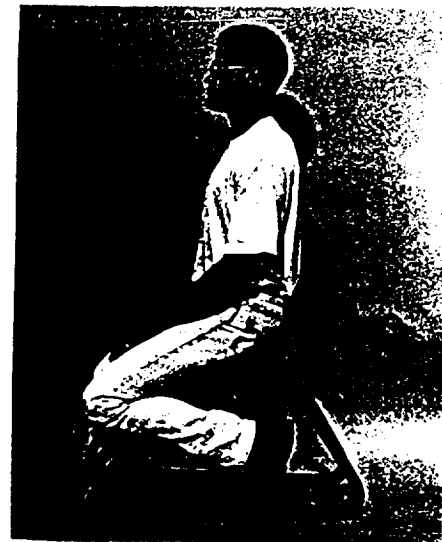


Fig. 2 Ergonomic chair

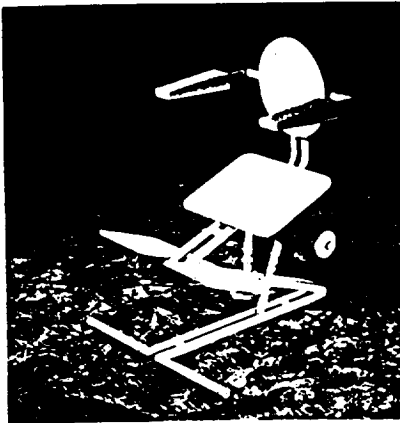


Fig. 3 A design alternative

### **Application of Habitability Criteria**

#### **Personal identification**

Many astronauts and cosmonauts have expressed a need to feel that they are not engulfed in a cold impersonal dwelling that does not respond to their personal preferences in any way during their ventures into extraterrestrial space. They felt their environment should not only provide adequate protection for their survival, but should also have quality of life enhancements to make their experiences more significant and to support homeostasis in a way to make them more able to fulfill mission objectives efficiently. They should be viewed as part of the human family venturing into a new frontier and setting the pace that others will follow. Personal objects, such as portraits of loved ones and other momentos, will impart a homey character to the crew quarters of the FLO, which each crew member is able to influence with his or her own decoration. Because of the limited space of the FLO, the crew quarters is the only personal space available and should be viewed as a protective womb since it also serves as a safe haven in case of solar flare emergencies. It will be protected by high shielding and will contain additional survival necessities. Rescue portholes at the external end will ensure astronaut egress in case of total FLO failure. The size (6.5' x 4' x 4') is quite small by terrestrial room standards, but it seems capable of solving the need for personal identification. We have departed from

precedents set by Japanese hotel rooms, which are currently being used.

#### **Social interaction**

In prolonged stay in extraterrestrial space it seems very important for humans to feel the presence of others. Besides company and security, it is necessary to promote positive interpersonal dynamics and good social interaction. Crew quarters open to the wardroom, thus providing for the option of being able to share and interact even as each person chooses to leave the door open during normal operating conditions. The workroom, located between the galley and personal storage, will be the meeting place for the entire crew. The four members can sit around the table for meals and meetings, can watch videos, or look out on the lunar landscape through an adjacent porthole window.

#### **Mental landscapes**

Acute places are tight and small enclosed spaces, such as we have in the FLO, and generally in all living quarters in extraterrestrial space. On Earth we have the precedents in elevators, bathrooms, and in some temporary dwellings. Human behavior is modified, not only by the apparent size of volume of a dwelling, but also by the image that it conveys. Therefore it is important that they contain symbolic elements that would evoke positive memories and sensations from previous experiences. Such elements can be called mental gardens, or even landscapes, which help people to transcend their immediate physical reality. In the FLO, it will be attained by making the wardroom side of the second level the "home" of the crew. Colors, photographs, and images created in the galley and storage doors will accomplish that effect. One side of the crew quarters, toilet and washroom will be completely covered by a mirror, to enhance the apparent size of the space. On the gymnasium wall, monitors coordinated with the exercise machines will literally create programmed landscapes, which will stimulate crew members. The third level, which contains the work area, lighting, furniture, and other features, will be set as a command bridge of a vessel, from which all operations will be controlled. There will be four porthole windows, permitting a view of the actual landscape around the FLO. The first level, with its two hyperbaric chambers, will be the "entrance lobby", and as such is designed as a reception space for



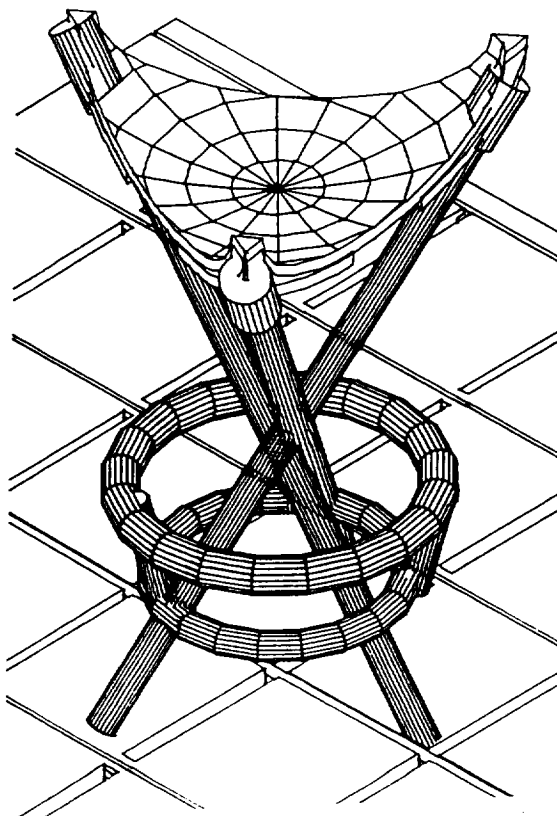
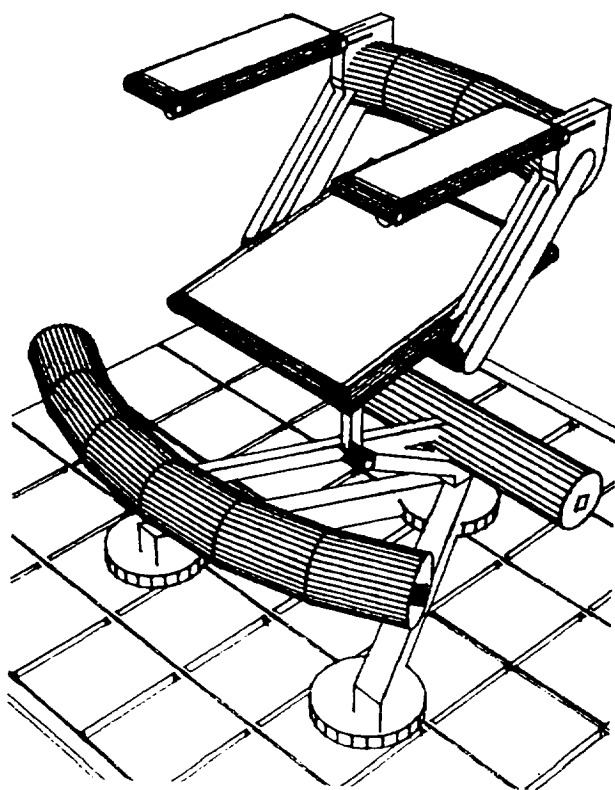
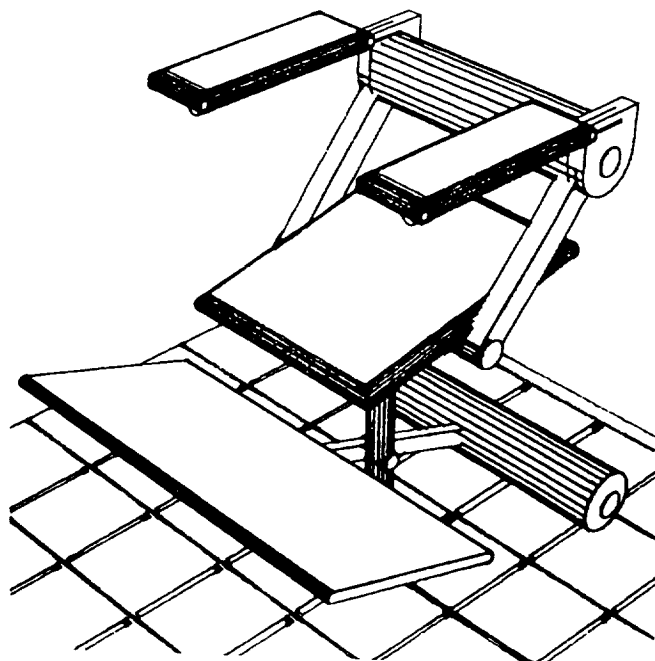
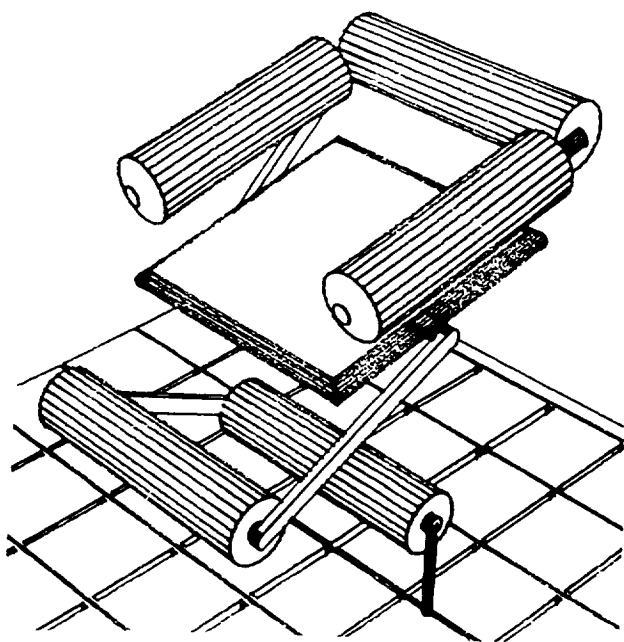


Fig. 4 Additional ergonomic chair design alternatives

incoming astronauts and the gateway for returning astronauts.

### **Privacy**

Even though interaction dynamics among crew members should be promoted, they should be balanced by allowing a certain degree of privacy and occasions of solitude, since they will be living in close quarters for periods of forty-five days, as the mission requires. Absence of privacy is an important factor for humans in restricted environments. In the FLO each crew member has his or her assigned individual private area with sliding door that can be closed tightly. Personal hygiene areas also have doors, and there are four privacy curtains, which can subdivide the intermediate level into the health maintenance area, the gym, the locker-dressing area, and the galley.

### **Contact with nature**

In previous studies this criterion was related to functioning biomes of closed environmental support systems (CELSS). The FLO, being a second generation lunar base, will not yet be self-sustaining, in that air, water, and food supplies will have to be shipped in every 45 days with each arriving group of astronauts. This way plant growth modules could be added to recycle protein for human consumption, oxygen, and water. But the biological growth in the FLO will be related to research, rather than to a CELSS. Nevertheless, we must be aware of the fact that individuals here will be exposed to prolonged immersion in a totally artificial environment. Absence of contact with natural or living things causes a destabilizing effect on humans. That could be offset by adding planters, fish bowls, and the like, which would not be directly or exclusively related to research in order to promote a healthy contact with nature. Soviet cosmonauts have expressed their enjoyment of flowering orchids in their space station.

### **Equalitarian conditions**

Equalitarian conditions among crew promote more relaxed interpersonal relationships, making them more productive and attuned to the mission. Functional or role differentiation promotes better interaction than arbitrary rank or hierarchical distinctions. In architectural terms,

such equalitarian conditions are reflected in the quality, location, and size of the crew quarters.

### **Variability**

Studies suggest that similar elements or very repetitive features in an acute place cause boredom and irritability, which are related to environmental stress. It is important that within the FLO there be a certain degree of variability. Architecturally this could be attained through changes in color and intensity of illumination. Circadian cycles could be maintained, if general illumination of the major interior spaces were programmed according to terrestrial day and night cycles. Decor in the three different levels corresponds also to their specific function; namely, access/egress, dwelling, and work correspond to gateway, home, and command bridge, respectively. Functional rotation of housekeeping duties among crew should also help to fulfill this criterion.

### **Aleatoric conditions**

Astronauts and cosmonauts who have stayed for prolonged periods in space have expressed their appreciation for pleasant surprises, which depart from daily routine, and promote their enjoyment of unexpected changes. Crews will experience the need for celebrating special events (e.g. birthdays, holidays, etc.) between their arrivals and departures, thus, enhancing the routine of ordinary days. The sights through porthole windows, as a lunar landscape passes through day-night-day cycle and the rotation of the stars around the hovering Earth over the lunar horizon will be sights that the crew will behold, in addition to other new and unforeseen experiences. A fractal screen could be made to vary continuously in areas, such as the second level, to maintain the environmental excitement that the fulfillment of this criterion entails.

### **Functionality**

A place to be habitable must also satisfy certain objective and measurable physical conditions. These are specified in the NASA STD-3000 Man-Systems Integration Standards, and include temperature, atmospheric pressure and composition, humidity level, and other life support parameters. It must include radiation, fire, and other hazard detection, warning, and protection. The possibility of sudden depressurization

due to envelope puncture or leakage must be considered. Ease of re-supply input and waste disposal through the airlocks in the first level, redundancy of systems hardware in the CELSS, airlocks, self-healing membranes, and a reasonable supply of spare parts and tools are also necessary to comply with this criterion.

### **Comfort**

This criterion is related directly to the interaction of the human body, its form and size, with the artifacts and furniture. The size of the areas of the FLO also must be taken into account. In lunar gravity ( $1/6$  G) human posture and movements are different from those which we find in the terrestrial environment. Before final design of the FLO, testing of the artifacts to be used on the moon through simulation must take place to gain a better understanding and insight regarding posture and motion in lunar gravity.

### **Stability and security**

Stability refers to that inertia which resists unbalancing forces. Human muscle tone and reflexes developed in a normal 1G environment will find  $1/6$  G alien. Starting and stopping locomotion will be different. Horizontal circulation will have to be insured in the FLO by using textured floors that will enhance friction. Grab bars will promote the use of upper body muscles when rapid movements are necessary. Vertical circulation is proposed through the use of ladders with one-foot step separation. Such an alternative is being studied in water tank reduced-gravity simulations at NASA/JSC, as well as the capacity of a crew member to carry a load while ascending the ladder.

### **Sensorial Stimulation**

FLO dwellers must not be deprived of sensorial stimulation, even in such a restricted environment. It is important that they have as close to normal, and as varied as possible, range of stimuli. Sensations are the primordial matter of experience. Surfaces in the FLO will be treated with colors to stimulate the eye and with textures that will stimulate the tactile sense, as well as to solve acoustical problems and the reduced friction problem mentioned earlier. Simulated landscapes and fractal artwork serve also as means of sensory stimulation. The olfactory gustatory senses must be accounted for in

the variety of smells and taste of the food supplied to the crew. Odor control in air handling units is a necessity in such confined a environment.

### **Music and environmental sound**

The problem of absolute silence in extraterrestrial space is offset by the sound generated by the ECLSS. Fans and other sound sources will have to be tuned to produce a harmonious, agreeable, and pleasant sound at a level that contributes positively to the environment. Electronic sound masking will also be necessary to permit some conversations to be made privately and noise to be kept within acceptable limits. Within crew quarters there will be a stereophonic sound system that each crew member can control within his or her own space.

### **Sense of orientation**

In reduced gravity this criterion is not as critical as it is in zero gravity, wherein an up and down direction orders the dwelling. However, color coding is still used to aid in orientation. Location of a color stimulus, be it on the ceiling, floor, or wall, can make a great difference in the character of the habitat, its perceived size, its sense of well-being, and psychological pleasantness. The FLO's interior walls will be mostly beige, which is a neutral color that can be modified easily by shining different colors of light on it according to circumstances, e.g., red blinking lights in an emergency. They could be varied randomly to improve the style and quality of life. Ceilings on public areas are peach to give a sense of warmth to the dwelling, and doors or interior airlocks, yellow. Crew quarters interiors may vary according to individual crew member preferences through changes in lighting, since it is mostly neutral, and blue doors. Machinery areas are gray, with safety orange doors on airlocks.

### **Conclusions**

This study sustains the following conclusions we have reached pointing towards the direction in which the design of the First Lunar Outpost should develop:

Because of the greater volume functionality and empathy with the human form, the vertical cylinder is the most appropriate geometry for the habitat envelope.

Twenty-four-foot diameter in a three-level cylinder is adequate to house functions and living quarters of a crew of four for 45-day missions.

Locomotion within the habitat module will require textured surfaces, bars for upper body control, and special furniture design, taking into account reduced gravity body posture.

Still, there are many questions that need to be dealt with before the FLO can get to a final design stage:

Testing of tools and furniture in reduced gravity simulations is necessary to refine the data regarding body posture, anthropometry, and biomechanics in lunar gravity.

The transportation of supplies and waste stowage from the crew lander and FLO habitat will require a rover capable of traveling the one-km distance that exists between the two. This, including the modular containers that will carry food, clothes, air, and water that have to be outfitted for every incoming crew, has yet to be designed.

Foresight to deal with catastrophic conditions and accidents could lead to design adjustments that will improve chances for survival for the crew. These should be studied and analyzed in more specific detail.

Environmental lighting used to vary the character of this acute place; the use of holograms to enrich the environment, evoking mental landscapes; the use of fractals to induce variations in wall patterns, or ceiling surfaces; and the use of photosensitive membranes to create a new sense of indoor-outdoor by transparency variation within the habitat are some of the quality of life enhancements that could also be included in further design development.

Lifestyle considerations will bring forth new kinds of activities, pastimes, and recreation to enhance the routine of ordinary days and develop new forms of social interaction to satisfy needs of FLO dwellers.

Habitability criteria must be refined as new research brings new insights to be considered for the habitat design, so that the FLO can be truly another step in the path towards colonization of the Moon.

This work collects research, insights, and efforts of a group of people interested in the architectural implications of the return of humans to the Moon. By sharing them through this medium, we aspire to raise consciousness regarding the contribution that architectural designers can make for the conquest of space and to call upon others in that field to participate in the endeavor.

## References

1. Angelo, J., The Extraterrestrial Encyclopedia, Facts on Life Publications, New York, 1985.
2. Allen, J., Biosphere 2, Penguin Books, New York, 1991.
3. Alred, J. et al., Lunar Outpost, Systems Definition Branch, Advanced Program Office, Johnson Space Center, Houston, 1989.
4. Andino, A., et al., Habitability: Camelot II, NASA/USRA Advanced Design Program, University of Puerto Rico, School of Architecture, June, 1989.
5. Andino, A., et al., Habitability: Camelot IV, NASA/USRA Advanced Design Program, University of Puerto Rico, School of Architecture, June, 1990.
6. Andino, A., et al., Selenia: A Habitability Study for the Development of a Third Generation Lunar Base, NASA/USRA Advanced Design Program, University of Puerto Rico, School of Architecture, June, 1991.
7. Gatland, K., Space Technology, Harmony Book, New York, 1981.
8. Heiken, G., Vaniman, D., French, B., Lunar Sourcebook: A User's Guide to the Moon, Cambridge University Press, Cambridge, 1990.
9. Johnson Engineering Corporation, Outfitting Concepts for Lunar Habitats, Houston, TX, 1989.
10. Johnson Engineering Corporation, New Initiatives Habitability Concepts, Houston, TX, 1989.

11. Kerrod, R., Living in Space, Crescent Books, New York, 1986.
12. Levedev, V., Diary of a Cosmonaut: 211 Days in Space, Phytoresource Research, Inc., Texas, 1988.
13. Mendell, W.W., Lunar Bases and Space Activities of the 21st Century, Lunar and Planetary Institute, Houston, Texas, 1985.
14. Moore, G.T., et al., Genesis Lunar Outpost, University of Wisconsin, Milwaukee, 1990.
15. National Aeronautics and Space Administration, Man-systems Integration Standards, NASA, STD-3000, Volumes I, Washington, D.C., 1989.
16. National Aeronautics and Space Administration, JSC Reduced Gravity Program: User's Guide, Houston, TX, 1987.
17. Prohansky, H., Environmental Psychology: Man and His Physical Setting, Holt, Reinhart, and Winston, Inc., New York, 1967.
18. Sasakawa International Center for Space Architecture (SICSA), Lunar Base Habitat Study, NASA/USRA Final Report, University of Houston's College of Architecture, Houston, TX, 1989.
19. Sasakawa International Center for Space Architecture (SICSA), The Manned Lunar Outpost, University of Houston's College of Architecture, Houston, TX, 1989.
20. Universities Space Research Association: Lunar and Planetary Information Bulletin, No. 58, Houston, February, 1991.

**THE LIGHTCRAFT PROJECT:  
FLIGHT TECHNOLOGY FOR A HYPERSONIC MASS TRANSIT SYSTEM**

**Rensselaer Polytechnic Institute  
Department of Mechanical Engineering,  
Aerospace Engineering, and Mechanics  
Troy, New York**

**Professor Leik Myrabo  
Kenneth Bouchard, Teaching Assistant**

**Abstract**

Rensselaer Polytechnic Institute has been developing transatmospheric "Lightcraft" technology aimed at creating an efficient, economically affordable, hypersonic mass transportation system. The system utilizes laser-energized airbreathing engines to accelerate minimum-volume passenger capsules, and gains a high level of reliability by using remote "centralized" space power sources, e.g., satellite solar power stations.

The most critical portion of the Lightcraft's acceleration trajectory involves flight propulsion at hypersonic velocities within the Earth's atmosphere, using a "Magneto-Hydro-Dynamic (MHD) Fanjet" mode. Of all the propulsion modes proposed for the Lightcraft's combined-cycle engine, the MHD-Fanjet mode has received the least critical inquiry, largely because of its complexity. During the 1991-1992 academic year, Rensselaer's ADP teams produced a detailed conceptual design for the MHD-Fanjet engine, including the specific details of its integration with the other three propulsive modes. To facilitate this process, students built a full-scale mockup of a 1/12th section of this annular engine, complete with a working model of the shroud translation system. The class also made preliminary design calculations for the double-dipole, "cusplike" superconducting magnets that provide the external magnetic field needed by the MHD air accelerator, as well for an onboard microwave power system to enhance the electrical conductivity of the air plasma working fluid. In addition, a large hypersonic model of

the MHD accelerator was designed for future tests in RPI's Hypersonic Shock Tunnel in order to validate present analytical performance models.

Another group continued design work on a full-sized prototype of a one-person "Mercury Lightcraft" (a transatmospheric flight simulator), with major emphasis on the detailed design of the major structure, robotic landing gear, and exterior aeroshell.

## LEO, LUNAR, MARS, AND ASTEROID PROJECTS

The University of Texas at Austin  
Aerospace Engineering and Engineering Mechanics Department  
Austin, Texas

Dr. George W. Botbyl  
Professor Wallace T. Fowler  
Anthony Economopoulos, Teaching Assistant

### SPACE HABITAT, ASSEMBLY AND REPAIR FACILITY

Todd A. Colangelo (Team Leader),  
Debora C. Hoetger, Addison C. Kuo, Michael C. Lo, Leland R. Marcus, Phillip P. Tran, Chris J. Tutt, Chad M. Wassmuth, Gregory M. Wildgrube

#### Abstract

Integrated Space Systems (ISS) has designed a Low Earth Orbit Assembly Facility for submission in the 1992 AIAA/LORAL Team Space Design Competition. This facility, the Space Habitat, Assembly and Repair Center (SHARC), will be used to construct, assemble, and service space vehicles. SHARC's primary mission will be the construction of interplanetary vehicles, but it will also be able to perform repair and refueling operations of craft which are in an Earth orbit. This facility has been designed using only present and near-present technology, with an emphasis on minimizing cost.

#### Introduction

Integrated Space Systems (ISS) designed a Space Habitat, Assembly and Repair Center (SHARC) in Low Earth Orbit to meet the future needs of the space program. The goal is to meet the general requirements given by the 1991/1992 AIAA/LORAL Team Space Design competition with an emphasis on minimizing the design costs. During the spring semester of 1992, a baseline structural configuration was created along with preliminary designs of the major subsystems.

#### Assumptions and Requirements

The initial mission requirements were set by AIAA; the facility must be able to:

- support simultaneous assembly of three major vehicles
- conduct assembly operations with minimal EVA
- provide storage locations with easy access to work areas
- maintain orbit indefinitely
- assemble components 30 ft long with a 10-ft diameter in a "shirt-sleeve" environment.

The design team made the following assumptions to further refine the mission parameters:

- "Three major vehicles" were defined as two lunar vehicles and one Mars vehicle. For relative sizes, see Table 1.
- SHARC must begin limited operations after eight launches.
- No Heavy Lift Launch Vehicle (HLLV) of Shuttle-C will be available.
- The maximum crew size is eight and the maximum work tour is 35 days.
- A garbage collection system will be available to deal with orbital debris.

SHARC's baseline configuration design was based on the above requirements and assumptions.

Table 1 Interplanetary vehicle sizes

| Vehicle | Total Mass (mt) | Fuel Mass (mt) | Maximum Diameter (m) | Length (m) |
|---------|-----------------|----------------|----------------------|------------|
| PhTV    | 1311.3          | 811.5          | 23.1                 | 58.4       |
| PhCV    | 467.0           | 262.8          | 18.8                 | 43.1       |
| MTV     | n/a             | n/a            | 27.4                 | 8.3        |
| LTV     | 94.1            | 80.9           | 13.7                 | 6.9        |
| LTS     | 191.7           | 159.2          | 15.2                 | 22.9       |

## Structural Configuration

Twelve different conceptual designs were reviewed; the chosen design is called the Hammerhead II.

The Hammerhead II configuration, shown in Figure 1, is composed of two 35-ft x 200-ft double deployable trusses separated by 4 35-ft erectable trusses. There are two smaller bays for lunar vehicles and one large bay for assembling the Phobos and Mars Transfer vehicles. A track system mounted by remote manipulator arms will encircle each bay allowing the arms to assist in vehicle assembly, hence minimizing EVA. There is a total of seven robotic arms to help in vehicle assembly: 1 30-ft arm for each lunar bay, 2 30-ft arms for the Mars bay, 1 30-ft arm for storage of parts, and 2 60-ft arms located on the sides of the main deployable trusses for berthing and transporting payloads.

A general storage area is located in the 21-ft x 50-ft x 35-ft area between the two double fold deployable trusses, making it easily accessible to all assembly bays. An alternate storage area is located on the double fold deployable truss leading out to the solar arrays, which is accessible by a robotic arm. The spring-loaded 31-ft x 14-ft-diameter Phobos fuel tanks will be located near the Mars bay ready to be jettisoned for safety.

The emergency escape pod is located in the center of the four habitation and control modules and is accessible from two pressurize corridors for quick use. The modules are arranged in a racetrack configuration to provide dual egress in case of emergencies. The two control modules will contain windows which will overlook the lunar bays to help in vehicle assembly and payload berthing.

The eight sets of solar arrays and the battery system are located at the end of the double fold deployable truss. The 40-ft x 20-ft pressurized sleeve, which is attached to the airlock, can contain a 30-ft x 10-ft component and is accessible to the robotic arms. Finally, the shuttle will dock upside down to the remaining airlock. This provides plenty of clearance for docking, and the Shuttle can be rigidly connected to the double fold deployable truss through attachment points in the Shuttle payload bay.

## Orbit

It was determined that the orbit of SHARC should be at an inclination of 28.5 deg. and an altitude of 380 km. This altitude is accessible to all current medium and heavy lift launch vehicles in use with only minor reductions in payload capacity. The inclination angle was chosen because it provides an ideal transportation node for future Mars and Lunar exploration missions. This inclination can also be

reached by rockets from both the Kennedy Space Center and Kourou. In addition, the ballistic coefficient of SHARC was determined by an accurate model. Included in the research was a scenario for utilization of the Space Station Freedom as a habitation depot for the workers on SHARC. However, calculations showed that the high synodic period of the two facilities imposed additional design requirements which would lead to an increase in cost and complexity.

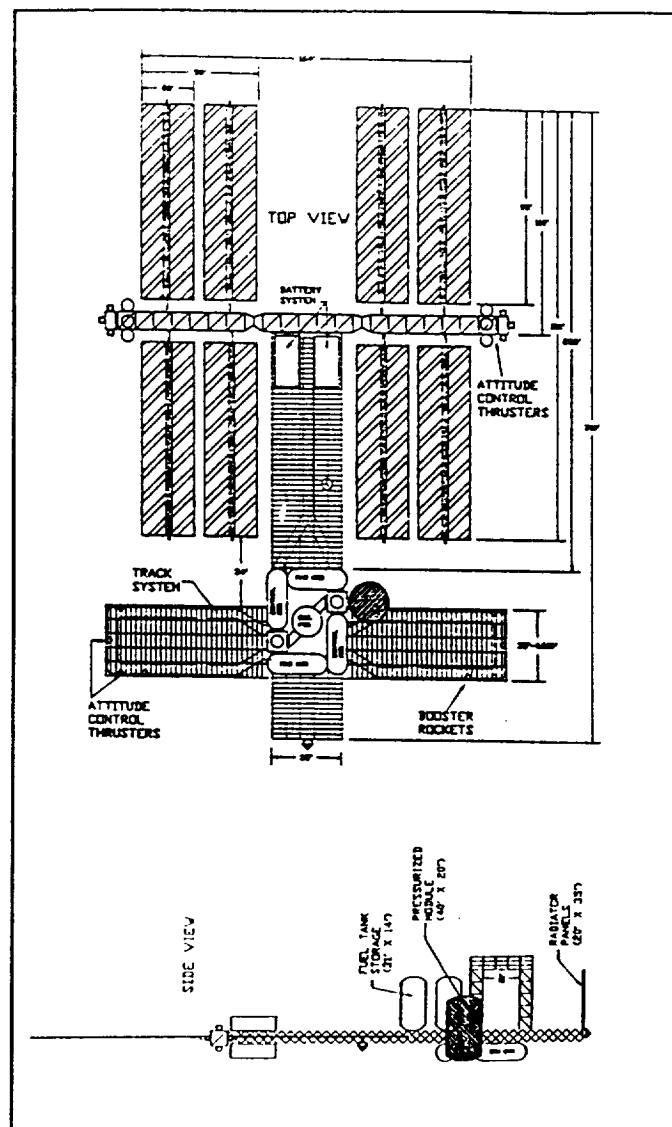


Fig. 1 The Hammerhead II configuration

## Crew and Life Support

A work tour on SHARC will consist of a maximum crew of eight over a period of 35 days. The shuttle will stay



docked at SHARC for the full duration of the mission. Each astronaut would work for 8 hours per day, 6 days a week. Life support supplies would be carried on the Shuttle. Any assembly materials will be sent to SHARC in an unmanned vehicle which would be launched 3 to 10 days after the Shuttle.

The Crew and Life Support group performed sizing estimates for a closed-loop life support system involving full air and water recycling. Further calculations were made involving specific supply requirements. Preliminary estimates revealed that 147 kg of nitrogen gas and 343 kg of food will be required for each work tour. 107 kg of methane and 183 kg of solid waste matter will be generated during the work tour and will have to be removed.

### Power

The amount of power required to run SHARC was determined by considering the power requirement of each subsystem, and estimating power consumption of exterior flood-lighting for bays, robotics, power tools and EVA. This calculations resulted in a power requirement of 62 kilowatts. Assuming 10% line losses, the total power required is 68 kW.

Photovoltaic silicon solar arrays were chosen as the primary power system. It was determined that a total area of 1854 m<sup>2</sup> is required to provide the 68 kW of power. The arrays are arranged as eight pairs of fold-out panels which deploy along an erectable mast or boom for stability. The total mass of the arrays is 2267 kg and have a calculated lifetime of 10 years after which they will have experienced approximately 25% degradation in efficiency.

The storage system chosen to power SHARC during eclipse periods is composed of 27 Nickel-Hydrogen (Ni-H<sub>2</sub>) individual pressure-vessel batteries connected in parallel for increased capacity and redundancy. The batteries are arranged together in groups and are placed in thermally controlled cases for optimum performance. The cases are placed between the two large sets of solar arrays. Each Ni-H<sub>2</sub> battery has a capacity of 100 amp-hours, an energy density of 25 W-hr/kg, and a mass of 112 kg. The total mass of the battery system (not including wiring) is approximately 3024 kg. For a worst case scenario, the batteries have a lifetime of 2 years if they are required to generate continuous peak power. Using a more probable average power of 48 kW, the lifetime will increase 5 to 6 years. After this time, the batteries will experience significant degrading and must be replaced.

### Robotics

The construction and operation of SHARC will require the extensive use of robotics. The need for robotics stems from the hazardous nature that long-term EVA operations would present to astronauts and the need to relieve crew work loads. In addition, SHARC's main purpose of servicing space vehicles necessitates the use of robotics.

Two principal robotic systems were selected for use on SHARC: a remote manipulator system (RMS) and flight telerobotic servicer (FTS). These two systems are advanced versions of the ones to be used on Space Station Freedom. The use of robotic systems like these would reduce the uncertainties and costs in building SHARC.

On SHARC, the primary function of the RMS will be to capture and move large cargo to the assembly area. The FTS can attach itself to the assembly, or it can be an extension of the RMS, and proceed to work on light, precession assembly tasks. In addition, the FTS will be used to examine the structural elements of SHARC for maintenance purposes.

### Guidance and Navigation Control/Reboost

The Guidance and Navigation Control (GNC)/ Reboost subsystem determined the propulsion requirements of SHARC during operation in space. Based on an accurate drag model, the propulsion system must be able to reboost SHARC from an altitude of 364 km to 380 km every two months. The total required  $\Delta V$  was found to be 9.107 m/s. In addition, SHARC will be rotated 90 degrees during reboost periods, and there will be enough propellant stored to allow one additional reboost without resupply. The location of the attitude thrusters and the reboost thrusters is shown in Figure 1.

Propellants were compared on the basis of specific impulse and storage requirements. Hydrazine (N<sub>2</sub>H<sub>4</sub>) was selected for standard attitude control, while the reboost thrusters will use an OME/UR bipropellant (N<sub>2</sub>O<sub>4</sub>/MMH) rocket produced by Aerojet.

### Communications

The communications subgroup used existing Space Station Freedom information as a basis for choosing the communication system for SHARC. Communications will be separated into a local system and a space to ground system. The local system will consist of an optical network because of its low power requirements and higher efficiency.

The maximum data rate for the local system is 10 Mega-bits per second (Mbps) with the option of using point to point fiber optics for a maximum data rate of 100 Mbps.

The space to ground system will consist of two virtual channels operating at a data rate of 150 Mbps. The frequency will be in the range of approximately two GHz to overcome any atmospheric or noise attenuation. The data will be transmitted to the Tracking and Data Relay Satellite System (TDRSS) and then to the Data Interface Facility which will allocate the data to the appropriate users. This link design will maintain continuous contact with the ground stations so that tracking and telemetry can be monitored.

### Thermal Control

The thermal control group identified the different station elements that have specific operating temperature ranges; various passive thermal measures were studied to determine if they would be adequate to maintain the operating temperature ranges. This proved true in the case of the cryogenic fuel tanks. For the rest of the station, it was estimated that a peak load of 60 kW of waste heat must be dissipated. Therefore, an active thermal control system was designed using Freon-12 as a working fluid. A radiator panel 35 ft x 20 ft was found to be adequate for the thermal needs.

## COMMON LUNAR LANDER

**James M. Ruhnke (Team Leader)**

**Daniel W. Driggers, Sean P. Hearrell, Kevin W. Key, Brian X. Le, Glenn J. Love, Robert W. McMullen, Scott A. Messec**

### Abstract

The Austin Cynthesis Corporation was formed to design a Common Lunar Lander (CLL) capable of carrying a lightweight (less than 500 kg), unspecified payload to the moon. The system could be utilized in further scientific study of the Moon by carrying payloads of scientific instruments custom-packaged for specific explorer missions. Additionally, it could establish and/or support a manned lunar base, through the transfer of small amounts of building materials, electronic equipment or other supplies. The Corporation has divided the task into three main parts: launch vehicle selection, lander design, and conceptual payload selection. Initial mass estimates led to consider a class of launch vehicles (including the Delta, Atlas, and Titan). The lander design itself has been divided into several subsystems: structures, power, thermal control, avionics, communications, and propulsion. Ideas for payloads include a common power system to satisfy various payload power requirements, a lunar experiment package, a materials utilization and testing platform, a surface rover, and a ground communications relay station.

### Introduction

The Austin Cynthesis Corporation (hereafter referred to as "the Corporation") was formed to respond to a Request for Proposal for the design of a Common Lunar Lander (CLL) capable of carrying a lightweight (less than 500 kg), unspecified payload to the Moon. The Corporation believes that such a system could make a large contribution towards the continued progress of the civil space program. The system could be utilized in further scientific study of the Moon by carrying payloads of scientific instruments, custom-packaged, for specific explorer missions. Additionally, it could help establish and/or support a manned lunar base, through the transfer of small amounts of building materials, communications equipment, a lunar rover vehicle, or other supplies. Due to its unique design philosophy, the potential missions the CLL could perform will truly be limited primarily by the payload designer.

The RFP received by the Corporation required the contractor to evaluate all mission phases: Earth launch,

lunar transfer, lunar capture, and descent to the lunar surface. Additionally, the contractor was required to design conceptually a variety of potential payloads which the lander might be required to carry. To fulfill these requirements, the Corporation has divided the problem into three main parts: launch vehicle selection, lander design, and conceptual payload selection.

### Launch Vehicle Selection

Initial mass estimates led to the selection of the Delta, Atlas, and Titan class of launch vehicles. As the design progressed, mass estimates eliminated the Delta and currently available Atlas/Centaur as possibilities. However, planned upgrades to the Atlas/Centaur vehicle, to be ready by 1993, should comfortably meet the total mass requirement.

### Lander Design

#### Structures

The lander design (Figure 2) has been broken into several subsystems: structures, power, thermal control, avionics, communications, and propulsion. The structures group has created a three-legged space frame design which provides for a two-meter diameter platform to which payloads will be affixed. This platform is hexagonal with diametric crossbeams. Small members may be connected between the main platform crossbeams to provide payload attachment points. The structure has been analyzed for particular static loads only; the short time available for the completion of the design precluded any attempt to perform dynamic modeling.

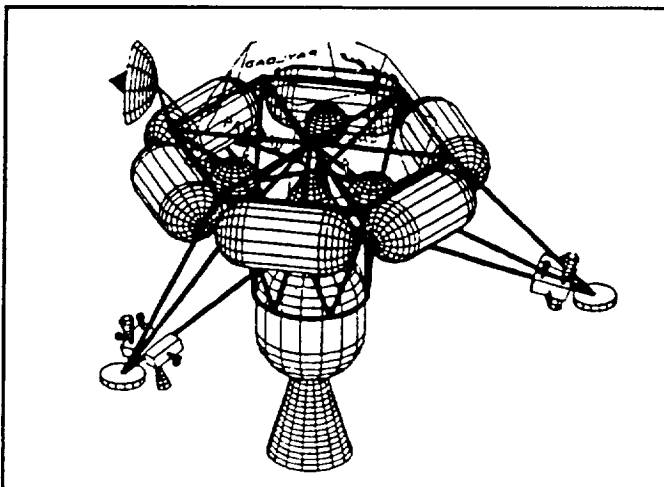


Fig. 2 Fully configured Common Lunar Lander

#### Power

Because of the short mission duration of the lander itself (its mission will end when it has reached the lunar surface), the power group has determined fuel cells to be the optimum power source. Other than offering a limited amount of startup power, the lander itself will not be responsible for powering the payloads. For payload power requirements, the possibility of carrying a "common" power supply module as additional payload has been investigated. It was determined that no system can exist which will use a standardized module to supply power to all possible payload configurations. However, it would be practical to develop a "family" of power supplies from which a "best fit" could be chosen for a particular mission.

#### Thermal Control

Thermal control of the lander will be accomplished using primarily passive systems to reduce weight and complexity. Spacecraft orientation, reflective paints, insulation, heat exchangers, and phase-change devices will be used to maintain the lander subsystems within their operational temperature ranges. Additionally, the structure of the lander itself can be used as a heat sink for the payloads, if required.

#### Avionics

The avionics subsystem will change significantly with payload mounting configurations. Therefore, the avionics must either be configured before each mission or else they must be adaptable for a range of lander and payload configurations. The pace of development of fully autonomous avionics systems indicates that an acceptable system would be available before the lander is scheduled to become operational.

#### Communications

The communications system is based on previous NASA explorer spacecraft. It is also shared between the lander and its payloads, as duplication of antennas, transmitters, and receivers is deemed unnecessary. It is expected that communications requirements for the payloads will be minimal during lunar transit, so that the lander will dominate communications use. After landing on the Moon, the lander itself will not require communications leaving the system to be used exclusively for payload needs.

C-4

## **Propulsion**

The propulsion system of the lander consists of fine (25 N) and coarse (450 N) reaction control jets for attitude control, a solid rocket motor for lunar capture, and one storable bipropellant engine for deorbit, lunar descent, and landing. The fine control jets will be used for precision attitude maneuvers during free flight; the coarse jets will be used to compensate for moments about the center of mass of the spacecraft generated by the main engine thrust vector.

## **Payload Design**

While the RFP has tasked the Corporation with the conceptual design of multiple payloads for the lander, the primary task is the design of the lander itself and most resources have been spent there. While several ideas for payloads have been advanced, time allowed for only a handful to be examined in any detail. These ideas include a common power system to satisfy various payload power requirements, a lunar experiment package, a materials utilization and testing platform, a surface rover, and a ground communications relay station. Other sample payloads which were proposed but not studied in this project included ground-based communications relay stations, families of transport containers (with options for power, pressurization, etc), modular building components, and a ballistic payload distribution system (to scatter small, shock-resistant items in an area around the lander).

## **Contents of Final Report**

The Final Design Report Document includes information on (1) the requirements for the design project, (2) the ideas proposed as solutions to the design problem, (3) the work which has been completed in support of the design effort, justifications, (4) validations and verifications of decisions made during the project. A project schedule, including current status of the items included on the schedule, as well as cost and management summaries are also included. Finally, suggestions for future work to be done in support of the project have been written.

## **FAR SIDE LUNAR ASTRONOMICAL RESEARCH EXPEDITION**

**Dawn M. Hannula (Team Leader)**

**David W. Bishop, Rudhmala P. Chakrabarty,  
William A. Hargus, Ambrose D. Melendrez,  
Christopher J. Niemann, Amy L.  
Neuenschwander, Brett D. Padgett, Sanjiv R.  
Patel, Leland J. Wiesehuegel**

## **Abstract**

Lone Star Aerospace, Inc., has completed the preliminary design of a lunar observatory on the far side of the Moon. An observatory located on the far side of the Moon has many advantages over an Earth based observatory such as: (1) lower instrument weight due to the Moon's weaker gravity, (2) non existent atmospheric signal attenuation and filtering due to near vacuum conditions on the Moon, (3) sighting of the entire sky due to the slow rotation of the Moon, and (4) stability of the lunar surface which optimizes the use of large baseline instruments. The technical aspects of this project include site selection and precursory mission details, scientific instruments, communication, power systems, habitation and transportation, spacecraft design, thermal systems analysis, robotic systems analysis, and trajectory analysis. The site selection group focused its efforts on finding a suitable location for the observatory. Hertzprung, a large equatorial crater on the eastern limb, was chosen as the base site. Two preliminary base designs have been developed. These two designs differ in the positioning of the larger instrument packages that will be placed on the lunar surface as well as in the type of habitat module that will be utilized.

## **Introduction**

Lone Star Aerospace, Inc. (L.S.A.) has completed the preliminary design of a lunar observatory on the far side of the Moon. Such a base would not only establish a long term human presence on the Moon, but would also allow more accurate astronomical data to be obtained.

A lunar observatory is more desirable than an Earth based observatory for the following reasons:

- Instrument weight is reduced due to the Moon's weaker gravity.
- Near vacuum conditions exist on the Moon.
- The Moon has slow rotation to reveal the entire sky.

- The lunar surface is stable for long baseline instruments.

All the conditions listed above are favorable for astronomical data recording.

The site selection group focused its efforts on finding a suitable location for the observatory. Hertzprung, a large equatorial crater on the eastern limb, was chosen as the base site.

### Primary and Secondary Base Designs

Two possible base designs were developed. After analyzing these two designs, a primary base design and a secondary base design were selected. These two designs differ in the positioning of the larger instrument packages that will be placed on the lunar surface as well as in the type of habitat module that will be utilized. The primary base design consists of a main base with a Space Station Common Module (SSCM) type habitat and three large independent instrumentation fields - one separate field for the Very Low Frequency Array (VLFA), one for the Optical Interferometer (OI), and one for the Submillimeter Interferometer (SI). The secondary base, on the other hand, consists of a main base with an inflatable habitat and one large instrument field in which the fields for the VLFA, OI, and SI overlap each other.

The advantages of the primary base were analyzed. The main advantages of this base were as follows:

- Less interference between elements of the VLFA, OI, and SI.
- Easier placement and maintenance of the habitat.
- Easier expansion of any of the large instrumentation fields.
- Easier maintenance of an instrument element (since maintenance would not cause dust build up on nearby instruments as it would in the secondary base's overlapping instrumentation field).

The advantages of the secondary base were as follows:

- Less range required by transportation and robotics elements.
- Larger habitat.
- Less power and communications cable required to reach the instruments.

After analyzing these advantages and considering the fact that the main purpose of constructing the base is to obtain the most accurate astronomical data possible, the base with the SSCM and three independent instrumentation fields was chosen as the primary base. A sketch of the primary base is shown in Figure 3.

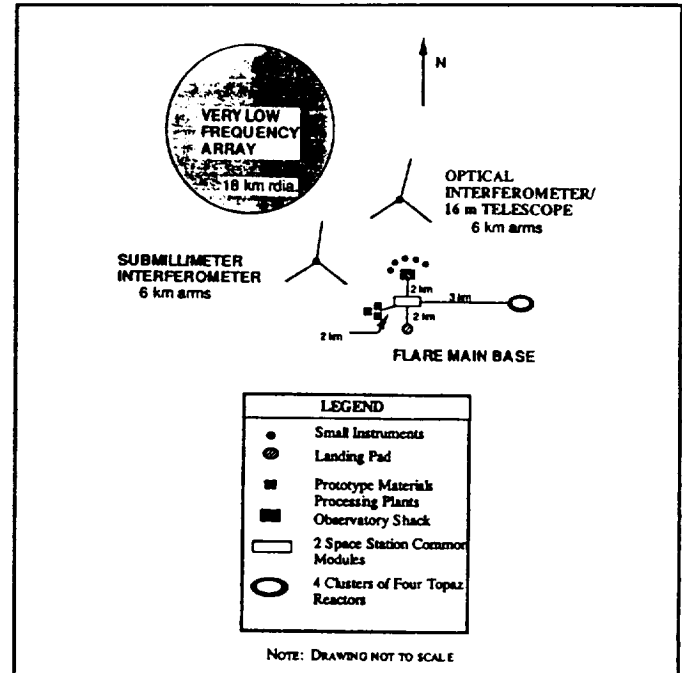


Fig. 3 Layout of the primary base

### Overview of Subsystems

The design of the far side lunar observatory involved investigation into seven subsystems. These subsystems included instrumentation, habitation and transportation, power and communications, robotics, thermal systems, cargo spacecraft design, and trajectory analysis. The following sections give a brief overview of each of these subsystems.

### Instrumentation

Astronomical, geological, and environmental instrumentation packages will be placed on the lunar surface. The following is a list of the major instruments to be utilized:

- Very Low Frequency Array,
- Submillimeter Interferometer,
- Optical Interferometer,
- Transit Telescope,
- 16 m Telescope,
- Moon-Earth Radio Interferometer.

The mass of the total instruments package has been estimated at 91 metric tons.

### **Habitation and Transportation**

Two SSCM modules connected end to end will provide for habitation on the lunar base. Two airlocks at either end of this arrangement will provide adequate ingress and egress. A partially-closed environmental control and life support system will be utilized. MOSAP and LOTRAN vehicles will provide lunar transportation.

### **Communication and Power**

During the construction phase, a satellite in an L2 halo orbit will relay data from the lunar surface to a geostationary satellite in Earth orbit to the Earth's surface. When the base becomes fully operational, however, a radio-free sky is desired to take accurate astronomical readings. Therefore, a fiber optic cable will be used as a communication link from the base to a transmitter/receiver station on the near side of the Moon. It will be laid out by a robotic rover from the base to the limb of the Moon. From there, the signal can be broadcasted directly to Earth without interfering with astronomical observations.

The base will be powered by four clusters of four Soviet manufactured Topaz reactors. These will supply the base with approximately 160 kWe of energy. Use of this cluster arrangement will prevent the total loss of power to the base in the event of a failure. If an emergency occurs and a cluster must be shut down, the other reactors can still produce 120 kWe for the base.

### **Robotics**

Four robotic elements will set up the far side lunar base. They include a crane, an excavator/digger, and two assembly robots. They will dig holes, bury the habitation modules and reactors, lay power and communications cable, and set up the instruments. These robotic elements will use a combination of artificial intelligence and telerobotics to successfully navigate and construct the base.

### **Thermal Systems**

The lunar base will be thermally controlled with the use of both radiators and heat exchangers. Radiators will be used to cool the reactors and heat exchangers will be used to cool the habitat and some of the smaller astronomical instrument packages. Manufactured shades will be used if passive cooling of the larger instrument packages is necessary.

### **Cargo Spacecraft Design**

A cargo spacecraft designed by Eagle Engineering will be used to carry the 180 metric tons of materials from Low Earth Orbit to Low Lunar Orbit. A Lunar Operations Vehicle will then transport these materials to the lunar surface.

### **Trajectory Analysis**

Cargo spacecraft trajectories will consist of spiral trajectory with a time of flight of approximately 130 days. Any manned missions to the base will use hybrid free-return trajectories.

### **Management and Cost**

Lone Star Aerospace was composed of a project leader, integration leader, chief technical engineer, administrative leader, and seven technical departments (each with its own department leader). This type of management structure has worked quite efficiently. No major problems have arisen in the design of the far side lunar observatory.

A cost analysis on the design of the lunar base has been performed based on the hardware costs incurred over the past fifteen weeks as well as the number of man-hours utilized. These figures were then compared to the estimated cost for the project as presented in the proposal. The total cost for the design of this base has been calculated to be \$51,853, well under the budget agreed upon in the proposal.

## SYSTEMS INTEGRATION FOR MARS PLANETARY SURFACE OPERATIONS NETWORKS

**Matthew F. Kaplan (Team Leader)**

**Kent B. Allen, Sherie L. Bradfute, Eric D. Carlson, Francois Duvergne, Bert J. Hernandez, David J. Le, Quan A. Nguyen, Brett T. Thornhill**

### Abstract

A permanently manned Mars base will require a robust surface infrastructure to operate successfully. Frontier Transportation Systems (FTS) is designing a set of vehicles to meet the needs of such a base. The Systems Integration for a Mars Planetary Surface Operations Network (SIMPSONS) Project will support the following base operations: (1) exploration, (2) base expansion, (3) mining, (4) cargo transport (including fuel and interplanetary payload), and (5) personnel transport. The vehicles which make up the network will be land rovers, lifters, fixed-route transports, rocket hoppers, and aircraft. Modularity and ease of integration into the network will be emphasized in vehicle designs. For each vehicle, several conceptual designs have been developed along with a decision process for selection. The technical aspects of the design for each vehicle will be handled by groups devoted to vehicle subsystems. The subsystem groups are structures, power/propulsion, guidance and control, safety/life support, robotics, and communications. An integration group oversees these subsystem groups, ensuring that the vehicles meet their requirements as expected.

### Introduction

Frontier Transportation Systems (FTS) has designed an integrated transportation network to support an advanced Martian base. The following paper represents the completion of the SIMPSONS project (Systems Integration for Mars Planetary Surface Operations Networks).

This project focuses solely on the surface-to-surface transportation at an advanced Martian base. Several elements, such as interplanetary transfer vehicles, orbiting nodes, and ascent/descent vehicles will be necessary for the sustenance of such a base. Any one of these components would be a significant project in itself; thus, they do not fall within the scope of the project.

### Assumptions and Goals

FTS defined the SIMPSONS project with the following assumptions:

- Advanced Martian base exists.
- Transportation node in low Mars orbit exists.
- Supply route between LEO and LMO is available.
- Water is present on Mars.

In order to precisely determine the exact goals of our transportation system, the supported base needed a clear definition. FTS researched the most likely arrangements and locations of an advanced Martian base and selected a specific configuration. The base after which we modeled our system will be located at Utopia Planitia (30°N, 240°W). Its favorable proximity to possible mining locations will facilitate the transport of raw materials to the base. Also, this latitude aids the ascent/descent vehicles by minimizing the plane change required to reach the orbiting transportation node which is at an inclination of 25°. Furthermore, this region is the largest flat area on Mars, which makes spacecraft landings, long distance travel, and communications easier. Finally, radiation shielding provided by the Martian atmosphere is increased at this location due to its low altitude (-1 km).

The following operations will be required of this type of advanced base:

- Mining of regolith for H<sub>2</sub>O and O<sub>2</sub> to provide life support and fuel.
- Conducting scientific exploration and research.
- Expanding the base.

The base will accommodate a crew of 12 to 18 persons with the possibility of expansion. The main components of the base, shown in Figure 4, include the centrally located habitat area, a manufacturing facility, two nuclear power plants, two landing pads, and a garage/maintenance facility.

Surface transportation is needed for travel between some of the more distant elements of the base, as well as for mobility of crew and payload from one area of the base to another. Scientific expeditions require the use of both manned and unmanned transportation systems to reach distant sites of interest. Likewise, outposts such as scientific stations or mining sites need maintenance and replenishment of supplies. This can be accomplished by surface rovers or rocket hoppers. Closer to the base, raw materials must be delivered to the manufacturing facility for the production of necessities, such as oxygen and fuel, for base sustenance and maintainability. All of this requires a

flexible transportation system, capable of transferring heavy cargo on a regular basis, and of transporting cargo over distances farther than the confines of the base.

Ultimately, the transportation system selected for the Mars base should be compatible with all payloads and should be adaptable to meet many tasks, including those unforeseen. Along with vehicles for the transfer of non-pressurized cargo, pressurized vehicles will also be needed for long range excursions. A transportation system composed of a set of modular vehicles which fulfills the needs of an advanced Martian base is presented in the final report. These vehicles include an aerial tram, a heavy lifter, a rocket hopper, Martian aircraft, and several different rover designs. This executive summary outlines the purpose and design of each vehicle, as well as recommendations for future analyses.

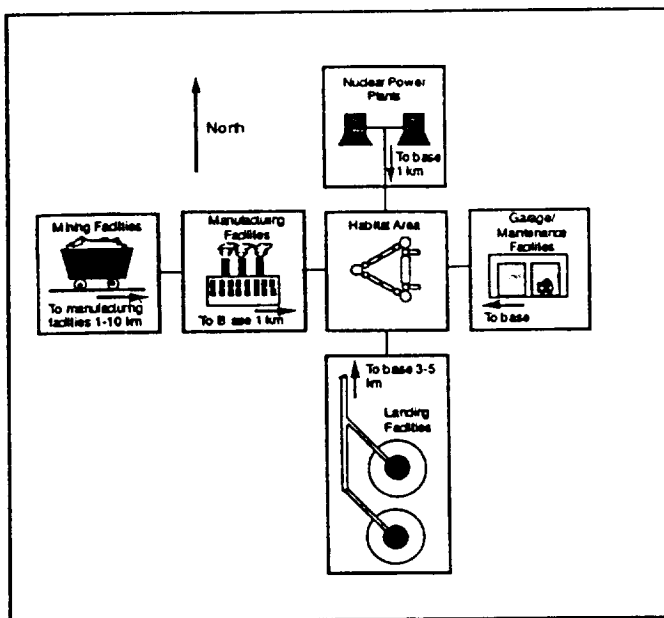


Fig. 4 General layout of the advanced Martian base

### Aerial Tram

To support the mining operations of this base, it will be necessary to refine 216 MT of regolith per day. Upon analyzing the important aspects of a fixed route transportation system, FTS selected an aerial tram as the most efficient and economical mode of cargo delivery. The aerial tram is easy to construct, as it merely involves the setting up of two stations and intermediate trestles for support. In addition, the tram is easily automated, inexpensive to build and operate, and it requires little maintenance. The other fixed route types of transportation

that were evaluated included trains, elevated rails, and magnetically levitated trains.

The aerial tram requires little mass to construct. The carriers are a simple automated design made of light-weight aluminum. The main mass to be concerned with, other than the payload chambers, is the weight of the hauling/carrying rope which will be made of a zinc-coated steel. The trestle mass should not be of concern, as the use of in-situ materials to form Martian concrete from which to construct these structures will eliminate the need to deliver the heaviest materials from Earth.

The tram we have designed will transport 36 MT per hour for the duration of only a quarter of a day. This will increase the lifetime of the system because it reduces the likelihood of fatigue and the opportunity for failure in general.

This system was a good choice from the perspectives of both the present and the future. From the present point of view, it can be constructed with the technology of today, and has proven to be a safe and reliable system on Earth. From a futuristic point of view, the aerial tram is an advantageous choice with regards to its ability to expand. First, the tram was designed to be strong enough to carry four times the amount it will actually be carrying. Thus it will be possible to increase its transport capacity in the future to support a larger crew. Secondly, the expansion of the base can be facilitated by first expanding the tram itself since it is possible to construct an additional route that is powered from the same driving station of an existing route. Finally, the tram may be used to efficiently transport humans in either pressurized or non-pressurized passenger cabins on future routes.

### Heavy Lifting Vehicle

The lifter is designed to perform the loading and unloading processes within the base vicinity. This vehicle has to operate off of many platforms, ranging from the descent vehicle and the rover flatbed to the Martian surface. FTS will require that there be at least three lifting vehicles. One would be located at the landing pad, one at the base, and one extra should be present at any given time in case of mechanical failure. A crane design was chosen after evaluating forklifts and other lifting vehicles.

The crane must meet the following requirements:

- Maximum lifting capacity of 30 MT
- Capacity for cargo up to 6 m wide and 10 m long
- Total range of 10 km



- Fully telerobotic
- Flexible
- Durable
- Low maintenance
- Simplicity of design.

In our evaluations, we looked for the least massive crane which still satisfied the original requirements. Therefore, FTS selected trusses as the main lifting component to reduce weight. The selected crane, shown in Figure 5 is a composite of many Earth lifting vehicles. As shown, the crane has a horizontal truss and a vertical truss structure similar to the tower configuration of lifting cranes. The horizontal truss moves along the vertical truss in a forklift type movement. In the back of the crane is a large container which is filled with indigenous material to act as a counterweight. The horizontal truss has a maximum extension of about 10 m which provides flexibility in reaching the payload, and the vertical truss has a height of about 13 m. The grasping mechanism which hooks onto the payload can vary in position along the horizontal truss.

The crane is supported by a tracked wheel, which enables the crane to carry the cargo from one place to another. The empty weight of the crane was computed to be no more than 30 MT. By adding regolith as a counterweight, the total weight could go up to as much as 100 MT. The trusses and the grasping mechanism will be made mainly of aluminum alloy materials, which provide lightweight and high strength characteristics.

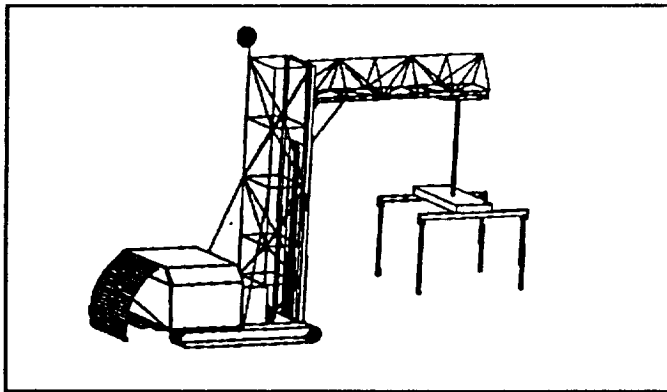


Fig. 5 3-D view of the Mars crane

The grasping mechanism has three degrees of freedom that can accommodate a maximum cargo width of 6 m. The lifter will get its power from a closed-cycle, internal combustion engine, using  $\text{CH}_4$  and  $\text{LOX}$  for fuel and oxidizer, respectively. The lifter needs about 422 kW of power to travel 2 km/hr with a mass of 100 MT. The

hoisting of the cargo using the grasping mechanism needs about 40 kW for a hoist rate of about 0.4 m/s. Also, the power required to translate the horizontal truss at a rate of 0.3 m/s along the vertical truss with 30 MT attached is about 50 kW. The crane will be controlled telerobotically by an operator from a command module located either in the habitation module or near the landing pad, where the majority of the loading and unloading processes will occur. To aide in telerobotics, the crane will need various sensors to accomplish the following tasks:

- Avoid obstacles
- Detect tilting of the vehicle due to uneven distribution of cargo mass
- Detect the range to the obstacle during loading and unloading processes
- Provide warnings of undue strains in support members.

### Ballistic Martian Hopper

A ballistic rocket hopper provides a shorter transit time and a greater operating range. With a given payload of 6.5 MT, this vehicle can complete two missions: 1) carrying one autonomous rover with various scientific payloads, or 2) carrying a rover and a crew of two, with supplies for seven days. Our hopper can transport either payload to a site up to 1000 km from the base, where the small rover would then enable exploration within a 10 km radius around the landing site. Due to the fuel selection for our overall system (methane/oxygen), on-site refueling away from the base would not be feasible; thus the hopper is limited to one hop from and one hop to the base.

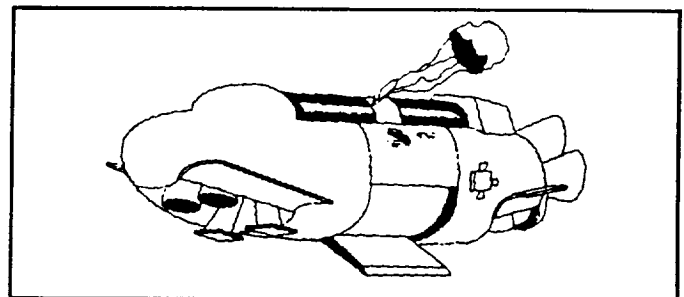


Fig. 6 Rocket hopper conceptual design

Figure 6 shows that the cargo bay was placed at the vehicle's center. The hover engines were then balanced around the bay in two equal, self-contained, and coordinated

sets. This arrangement provides stability in firing and reduces shifting of the center of mass as fuel is consumed.

The trajectory of our craft was modeled by three phases -- launch, ascent, and touchdown. The launch is basically a hovering maneuver until the reaction control system (RCS) jets are fired to attain the proper attitude for the ascent phase. The main engines located at the rear of the vehicle are then fired for the ascent phase, sending the vehicle into a ballistic trajectory. When the hopper descends to 100 m altitude, a parachute is deployed.

The end result of our analysis consists of a partial load-bearing, functionally gradient material (FGM) skin supported by a graphite/magnesium interior structure. The skin is limited in its ability to bear loads by two main considerations. First, the engines of the undercarriage are recessed, and the ascent and descent thrust cannot be carried by the exterior skin. Also, there are several panels in the skin (clamshell doors, payload door) which would have to be carefully supported so as not to provide weak points in the structure.

Since the hopper must be able to operate autonomously and possibly telerobotically, its command and data handling system will have to be provided with information such as attitude, altitude, velocity and position, and surface mapping. The hopper will require an IMU capable of measuring the changes in attitude and position in three axes to fully define the state of the vehicle.

### **Unmanned Martian Aircraft**

With the low martian gravity and despite the thin atmosphere, studies performed at the Jet Propulsion Laboratory in the late 1970's underlined that there were no technical difficulties involved in designing and operating a remotely piloted Mars airplane. It also appeared that such a vehicle could be most useful in increasing the capability of a Mars surface crew by providing for long range exploration and mapping.

The Mars airplane is well suited for long range scientific exploration, especially over rough terrain, and it can fulfill a wide range of missions such as surface imaging, atmospheric sounding, high altitude meteorology, and radio science. In addition, an unmanned Mars airplane can perform other useful functions such as deployment of remote observing stations, servicing of manned outposts, and search and rescue missions.

In order to enlarge the scope of operation, FTS evaluated both a large and a small aircraft. Because of the thin

atmosphere and the need to keep aircraft dimensions and power requirements reasonable, the payloads of the aircraft need to be restricted. The large and small aircraft are restricted to 300 and 100 kg, respectively. The large aircraft has a range of over 12,000 km, and the small one has a range of 8000 km.

For both aircraft, a classical configuration was adopted since this configuration allows high lift-to-drag ratios and high stability. Moreover, the high tail volume can tolerate large shifts in the center of gravity resulting from payload deployment. Other features include an inverted V-tail to reduce mass as well as drag, high aspect ratio wings (22) in order to minimize the induced drag and large propellers for efficient high altitude flight in the thin Martian atmosphere.

Because of the composition of the Martian atmosphere (95% CO<sub>2</sub>), only non air-breathing engines combined with propellers can be used. Because of its high power/mass ratio, a closed loop, internal combustion engine (CH<sub>4</sub>/O<sub>2</sub>) was chosen. In order to cut the total weight, an all composite structure was chosen, composed of high strength Thoronol 300 carbon-fiber and epoxy composites. This allows for a structural weight fraction between 15 and 20 %.

In order to minimize the take-off distance and thus the runway length, both aircraft are supposed to use a short-take-off device such as a catapult. The landing distance will also be shortened by using slow-down devices, such as nets. The landing gear for both aircraft will be a simple skid very similar to those used on gliders.

Like the rocket hopper, the small aircraft must have the capability to select a suitable site to land and to perform the landing autonomously. Nevertheless, the capacity to be remotely piloted should be available as an emergency back-up or for complex maneuvers. The computer will navigate mainly by a terrain-following procedure, using medium and high resolution images provided by previous or current remote-sensing satellites. The very high resolution images needed for high-precision procedures (vertical landings, for example) would have to be provided by previous aircraft missions. The command and data handling system could also rely on ground-based beacons for navigation. In addition, the avionics also need aircraft attitude, attitude rates, position, and position rates for navigation.

### **Rovers**

The seven rover configurations which were designed for the SIMPSONS Project are: (1) fuel transport vehicle (FTV), (2) manned, short-range vehicle (MSRV), (3) materials transport vehicle (MTV), (4) Mars autonomous

rover for ground exploration (MARGE), (5) human-operated Mars exploration rover (HOMER), (6) light cargo vehicle (LCV), and (7) heavy cargo vehicle (HCV). Table A shows the range and payloads for each vehicle.

Table 2 Ranges and payload masses for FTS Rovers

| Vehicle | Range (km) | Payload (MT) |
|---------|------------|--------------|
| FTV     | 10         | 7.0          |
| MSRV    | 30         | 2.2          |
| MTV     | 30         | 7.0          |
| MARGE   | 200        | 2.5          |
| HOMER   | 200        | 10.0         |
| LCV     | 200        | 2.5          |
| HCV     | 20         | 10.0         |

The FTV will refuel the lifters, aircraft, and rovers, and serve as a backup to the pipelines that provide fuel for the hopper at the launch pad. The MSRV can be used for transportation in the base area, or it can serve as a short range exploration vehicle when included as payload on the hopper. The MTV is designed as a backup system to the tram. Since the transport of mined materials to the refining facilities is essential to life support, it is very important that we do not allow this operation to have a single point failure. MARGE will conduct autonomous long range unmanned exploration. HOMER will serve as a mobile lab for long range manned missions. The light cargo vehicle is an autonomous/telerobotic rover whose main purpose is the transportation of light cargo around the base area. The HCV, which will be operated telerobotically, will transport payloads of up to 10 MT within 20 km of the base to aid in such operations as base expansion by moving habitation modules from the descent vehicle to the base.

All of the components of the rovers should be modular. The advantages of this concept are that the modular blocks can be used as spare parts on almost any vehicle, and that new configurations can be made in-situ to meet unforeseen needs of the base. The astronauts will be able to construct (with robotic aid) any new vehicle configurations within the maintenance facility. The modular components were designed to fit on both a large and a small basic chassis design.

FTS selected hemispherical wheels as the mobility system for both the large and small chassis. The chassis was designed to be constructed of two-celled monocoque aluminum alloy beams. We selected a cell thickness of 5.0 mm for Al 2014-T6 beams after performing a static analysis

of several different thicknesses and materials using NASTRAN.

For the purpose of commonality, the main power system for all vehicles with the exception of the rocket hopper and the tram were designed to run on a methane/oxygen internal combustion engines. This commonality in power source will facilitate maintenance of the vehicles and will also simplify the production of fuel since a common fuel is utilized. In addition, a modular concept (coined "legobility") designed for the rovers which employs the interfacing of various subsystem modules (black boxes) to configure a task-oriented rover (i.e. an unmanned autonomous rover or a manned mobile habitation module) is presented. This concept facilitates maintenance and also introduces redundancy into the system since spare parts are more readily available when needed. All these vehicles, when working together, will provide the support required for the sustenance of the advanced Martian base and indirectly, will lead the way to the settlement of Mars.

## Recommendations

Due to the time frame and scope for which this project was undertaken, further analyses of each vehicle and its subsystems should be performed. Although this project gives an overall design for each of the vehicles which will be included in the integrated Martian transportation system, future studies will be required to develop these vehicles beyond the preliminary design stage. For further design of the tram, we recommend an analysis for reliability, and we recommend further research into the feasibility of using indigenous materials for the construction of the trestles. For future studies of a Martian lifting vehicle, we recommend a more detailed structural analysis of the grasping mechanism and the analysis of truss stability. For the hopper, the following areas must be studied further in order to achieve a complete vehicle:

- Vehicle lift-to-drag ratios
- Materials research/analysis
- Aerobraking
- Thermostructures
- IMU calibration.

The Martian aircraft needs further analysis in its thermal system, state estimation, takeoff and landing and artificial intelligence for surface terrain following. A dynamic analysis is required for further studies of the rover, as well as a more in depth analysis of the engine performance characteristics.

## ASTEROID EXPLORATION AND UTILIZATION

**Brian M. Radovich (Team Leader)**

**Alan E. Carlson, Medha D. Date, Manny G. Duarte, Neil F. Erian, George K. Gafka, Peter H. Kappler, Scott J. Patano, Martin Perez, Edgar Ponce, Joseph D. Silverthorne**

### Abstract

The Earth is nearing depletion of its natural resources at a time when human beings are rapidly expanding the frontiers of space. The resources possessed by asteroids have enormous potential for aiding and enhancing human space exploration as well as life on Earth. Project STONER (Systematic Transfer of Near Earth Resources) is based on mining an asteroid and transporting raw materials back to Earth. The asteroid explorer/sample return mission is designed in the context of both scenarios and is the first phase of a long range plan for humans to utilize asteroid resources. Project STONER is divided into two parts: asteroid selection and explorer spacecraft design. The spacecraft design team is responsible for the selection and integration of the subsystems, consisting of GNC, communications, automation, propulsion, power, structures, thermal systems, scientific instruments, and mechanisms used on the surface to retrieve and store asteroid regolith. The sample return mission scenario consists of eight primary phases that are critical to the mission.

### Introduction

The Earth is nearing depletion of its natural resources at a time when human beings are rapidly expanding the frontiers of space. The resources which may exist on asteroids could have enormous potential for aiding and enhancing human space exploration as well as life on Earth. With the possibly limitless opportunities that exist, it is clear that asteroids are the next step for human existence in space.

The final report comprises the efforts of NEW WORLDS, Inc. to develop a comprehensive design for an asteroid exploration/sample return mission. This mission is a precursor to proof-of-concept missions that will investigate the validity of mining and material processing on an asteroid.

## Scenarios

Project STONER (Systematic Transfer of Near Earth Resources) is based on two utilization scenarios: 1) moving an asteroid to an advantageous location for use by Earth and 2) mining an asteroid and transporting raw materials back to Earth. The asteroid explorer/sample return mission is designed in the context of both scenarios and is the first phase of a long-range plan for humans to utilize asteroid resources.

The final report concentrates specifically on the selection of the most promising asteroids for exploration and the development of an exploration scenario. Future utilization as well as subsystem requirements of an asteroid sample return probe are also addressed.

Project STONER is divided into two primary areas: asteroid selection/mission design and explorer spacecraft design. The asteroid selection team has narrowed the possible 4800+ known asteroids to ten, considering physical attributes of each candidate asteroid as well as mission trajectory and  $\Delta V$  requirements. From that group of ten, a final asteroid was chosen for more in-depth study.

The mission design team formulated mission scenarios and -- working with the other teams -- investigated possible problem areas and contingency plans. In the design of the spacecraft, subsystems that have been studied are: GNC, communications, automation, propulsion, power, structures, thermal systems, scientific instruments, and mechanical retrieval devices.

## Spacecraft Overview

The Hawking spacecraft, designed to study an asteroid and return a sample to Earth, was named after Steven F. Hawking as a tribute to his continuing efforts to expand the limits of man's understanding of the universe. The Hawking is an adaptation of the Mariner Mk II series of spacecraft. Utilization of the Mariner Mk II design can accelerate development of the spacecraft and significantly reduce cost.

The Hawking spacecraft consists of three component vehicles: orbiter, lander, and the sample return craft (SRC); the spacecraft is shown in

Figure 7. Each of these vehicles has specific mission objectives and contributes directly to the fulfillment of the primary mission goal: return a sample of asteroidal material to the earth for analysis. Analysis of the samples is crucial in determining the composition of different taxonomic classes, and is a necessary step before utilization of asteroids can begin.

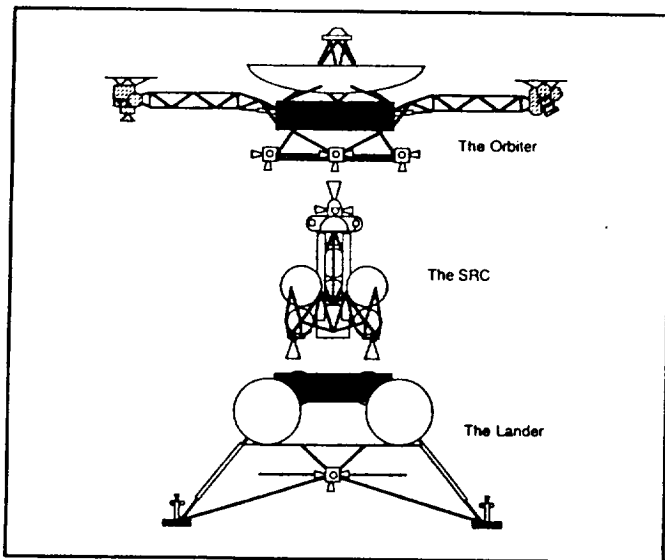


Fig. 7 The Hawking spacecraft

### Mission Phases

The sample return mission scenario consists of nine phases, the successful completion of each being critical to the overall mission.

**Phase 1:** Hawking is launched into LEO orbit aboard an existing launch vehicle.

**Phase 2:** Hawking is injected into the interplanetary transfer trajectory by its upper stage.

**Phase 3:** During the interplanetary cruise, the spacecraft performs radio science experiments and studies of the solar wind.

**Phase 4:** Hawking inserts itself into the asteroid's orbit, positioning itself several asteroid radii ahead of the body and slightly to the sun side. This position allows the spacecraft to map the asteroid, determine its rotational axis, and locate scientifically interesting features, all to help determine a desirable landing site.

**Phase 5:** Once a landing site is chosen, the lander/SRC separates from the orbiter. The orbiter remains several asteroid radii away to serve as a relay for the lander/SRC and to provide reconnaissance for the rovers. The lander/SRC approaches and docks with the asteroid using its attitude control thrusters.

**Phase 6:** Samples of scientific interest are identified and retrieved by either the robotic arm or the rovers, and placed in the SRC.

**Phase 7:** The SRC is launched from the lander in a non-destructive manner (i.e., springs, pneumatic pistons) so the lander can remain intact to perform more analysis of the asteroid. At an altitude of approximately 0.5 km above the lander, the SRC rotates and fires the booster's engines to inject itself into the transfer trajectory back to Earth.

**Phase 8:** After the injection burn, the booster stage is jettisoned (Figure 8) and the communication antenna and solar panels are deployed (Figure 9). During the interplanetary cruise of the SRC, the integrity of the sample is maintained by minimizing g-loads during maneuvers and keeping the sample at a low temperature.

**Phase 9:** Upon arrival at Earth, the SRC inserts itself into a highly elliptical orbit. After accurate ground-based orbit determination, the SRC circularizes into LEO where it waits for pick-up by either the Space Shuttle or Space Station Freedom.

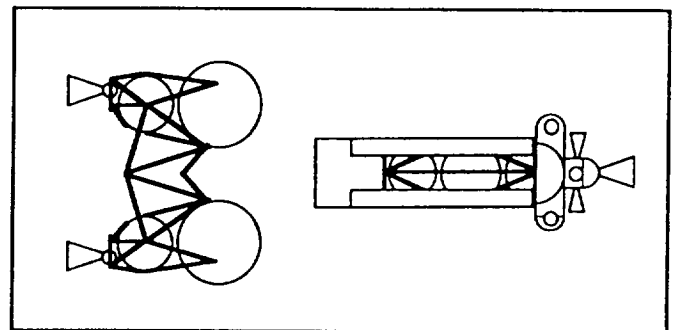


Fig. 8 The separation of the SRC from its booster

### Benefits

There are many benefits to be gained from studying asteroids. Presently these bodies have been almost totally neglected in the exploration of the solar system. It is believed that because of their primitive state they hold clues to the formation of the solar system. Also, utilization of

asteroids as a future space-based source of raw materials could reduce the total cost of future space missions.

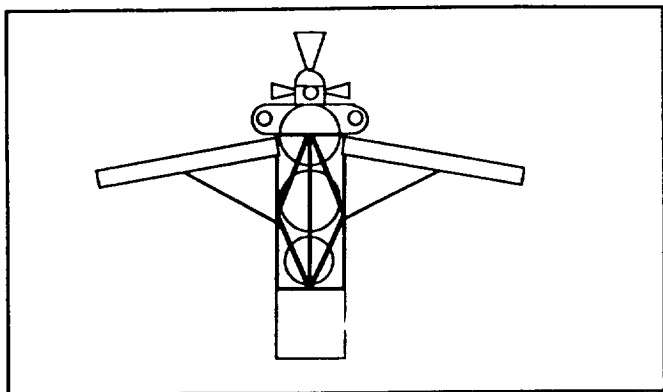


Fig. 9 Deployment of the communication antenna and solar panels of the SRC during the return trip

**1991-1992 PROJECT SUMMARIES**

**University of Texas at Austin  
Department of Mechanical Engineering  
Austin, Texas**

**Dr. Steven P. Nichols  
Hank Kleespies, Teaching Assistant**

**Abstract**

The Department of Mechanical Engineering at The University of Texas at Austin participated in seven cooperative design projects this year. Six of the projects were associated with the Johnson Space Center and include the design of a thermal control system for an inflatable lunar habitat module, a vibration isolation system for a Space Shuttle cycle ergometer, a radiator shading device for a lunar outpost, a reusable astronaut safety tether, a resistive exercise device for use on the Space Shuttle, and a fleet of autonomous regolith throwing devices for radiation shielding of lunar habitats. The seventh project is associated with the Jet Propulsion Lab and involves the design of a shock absorbing wheel for a small six-wheeled Martian Rover Vehicle.

**DESIGN OF A THERMAL CONTROL SYSTEM  
FOR AN INFLATABLE LUNAR HABITAT  
MODULE**

NASA is considering the establishment of a manned lunar base within the next few decades. To house and protect the crew from the harsh lunar environment, a habitat is required. A proposed habitat is a spherical, inflatable module. Heat generated in the module must be rejected to maintain a temperature suitable for human habitation. This study presents a conceptual design of a thermal control system for an inflatable lunar module. The design solution includes heat acquisition, heat transport, and heat rejection subsystems.

The study discusses alternative designs and design solutions for each of the three subsystems mentioned above. Alternative subsystems for heat acquisition include a single water-loop, a single air-loop, and a double water-loop. The vapor compression, vapor absorption, and metal hydride adsorption cycles are the three alternative transport subsystems. Alternative rejection subsystems include flat plate radiators, the liquid droplet radiator, and reflux boiler radiators. Feasibility studies on alternatives of each subsystem showed that the single water-loop, the vapor compression cycle, and the reflux boiler radiator were the most feasible alternatives. These three subsystems were combined to create a final design. The mass of the entire system is 4430 kg. The average power consumption is 17 kW.

The heat generated within the module is primarily due to science experiments, communication systems, the life support system, and the thermal control system. It was determined that for a crew of twelve, the maximum heat load generated within the module is 90 kW. To remove this heat, a single water-loop acquisition system was designed. The single water-loop system maintains the module at a temperature range of 18 to 24° C. The humidity is maintained at 50%. The system also meets ventilation requirements by providing five air changes per hour.

The vapor compression cycle used in this design was a two-stage cycle. To remove 90 kW of internal heat, 52 kW of electrical power is required. If a multiple stage operation is used, the system can be operated at lower power during lunar night or when the internal heat load decreases. Using a multiple stage operation, a 52% reduction in average power consumption is attained.

The reflux boiler radiator is an evaporation-condensation device used for transferring and rejecting heat. This radiator consists of a closed tube, with a fixed volume of working fluid. The working fluid is evaporated at the bottom of the tube, and condenses due to gravity along the sides of the tube. During condensation, the heat is transferred through the radiator walls and radiated to the lunar environment.

Due to redundancy requirements, 20 radiators were used. The radiators are rectangular and provide a total surface area of 345 m<sup>2</sup>. The radiators were initially designed to reject the maximum heat load at lunar noon. A control system was then designed to adapt the radiators for lower heat loads and lower sink temperatures. To control the rejection capability of the radiators, the radiator area must be varied. The area of the radiators was varied by both bypassing radiators as well as using the variable conductance concept. The variable conductance concept consists of using an inert gas at the top of a reflux boiler radiator. The inert gas responds to changes in heat loads by expanding or contracting, thus varying the area available for condensation. By using these two methods of control, the radiator rejection capability can be controlled such that the temperature inside the module is maintained within 18 to 24° C.

## VIBRATION ISOLATION SYSTEM FOR A SPACE SHUTTLE CYCLE ERGOMETER

Low frequency vibrations generated during exercise using the cycle ergometer onboard the Space Shuttle can disrupt sensitive microgravity experiments. The design team worked with engineers from the Manned Systems Division at the Johnson Space Center to generate alternatives for the design of a vibration isolation system for the cycle ergometer. It is the design team's objective to present alternative designs and a problem solution for a vibration isolation system for an exercise cycle ergometer to be used onboard the space shuttle.

In the development of alternative designs, the design team emphasized passive systems as opposed to active control systems. This decision was made because passive systems are less complex than active control systems, external energy sources are not required, and mass is reduced due to the lack of machinery such as servo motors or compressors typical of active control systems.

Eleven alternative designs were developed by the design team. From these alternatives, three active control systems were included to compare the benefits of active and passive systems. Also included in the alternatives was an isolation system designed by an independent engineer that was acquired late in the project. The eight alternatives using passive isolation systems were narrowed down by selection criteria to four considered to be the most promising by the design team. A feasibility analysis was performed on these four passive isolation systems. Based on the feasibility analysis, a final design solution was chosen and further developed.

The design solution uses spring and damper components attached at four corners of the ergometer base. The design team chose to lower the ergometer's natural frequency by lowering the spring constant of the system as opposed to increasing the overall mass. The design team discovered that the low-frequency ergometer vibrations require very low spring constants to begin attenuation. It was found that for operating frequencies above 4 Hz, acceptable attenuation is possible. For lower frequencies the spring constants become so low that ergometer deflections exceed acceptable limits. From the development of this design, the design team concluded that passive systems are not effective at isolating vibrations for the low frequencies and constraints considered for this project.

Recommendations are made for the design and application of passive isolation systems. These recommendations involve modeling the ergometer system and combining the spring isolation system with an active isolation system. The design team assumed a lumped mass for the cycle and rider with forces and moments acting at the center of mass. Additional research is recommended into the feasibility of a combined active and passive isolator system for the cycle

ergometer. This would allow the passive system to operate at high frequencies and the active system to act only at low frequencies. This would provide the required damping at all frequency ranges.

## JPL MARS ROVER WHEEL

The Jet Propulsion Laboratory (JPL) has identified the need for a shock absorbing wheel for a small six-wheeled Martian Rover Vehicle. This wheel must meet requirements of minimum mass, linear radial deflection, and reliability in cryogenic conditions over a five-year lifespan. The diameter of the wheel is 12.7 centimeters. Additionally, axial and tangential deflections must be no more than 10% of the radial value.

The team designed a wheel to meet these criteria by use of finite element and dimensionless parameter analysis. Dimensionless parameter techniques developed by the Waterways Experimental Station were used to choose a wheel width. Due to the complex geometry of the wheel, a finite element model describing its behavior was constructed. This model was then used to develop wheel geometry that gave the deflection ratios specified by JPL. Figure 1 illustrates the configuration of the finite element wheel model.

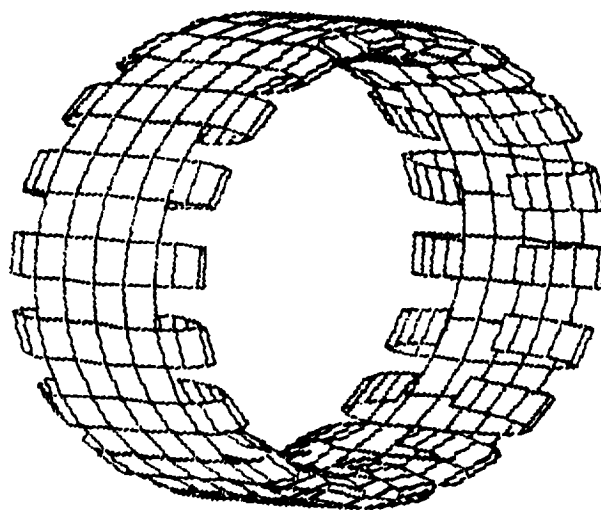


Fig. 1 Finite element model of the Mars rover wheel

A composite material was selected for its high strength, toughness, fatigue resistance, and damping characteristics in the cryogenic conditions. The team chose an aramid fiber-filled thermoplastic composite. Pellethane resin was found to be the most suitable material for this composite application.



## DESIGN OF A RADIATOR SHADING DEVICE FOR A LUNAR OUTPOST

The National Aeronautics and Space Administration is designing a thermal control system for an outpost to be placed permanently on the moon. One of the functions of the thermal control system is to reject waste heat, which can be accomplished through a radiator. At the lunar equator, a radiator may absorb more heat than it rejects during the lunar midday. This problem can be solved either by increasing the temperature of the radiator by means of a heat pump or by reducing the radiation incident on the radiator. The incoming radiation can be reduced by using a shading device that focuses incident solar radiation above the radiator while shading the radiator from other planetary radiation (Figure 2). Two design teams worked with engineers from the Johnson Space Center on design problems associated with this radiator concept.

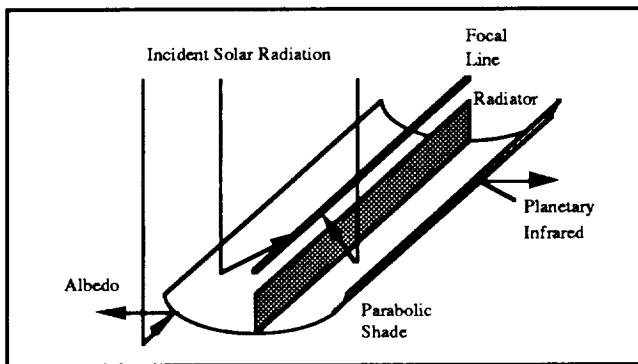


Fig. 2 Parabolic shade configuration

The first design team developed concepts of shading devices for the radiator and for deployment and retraction of the radiator and shade system. Preliminary design of the concepts included support structures, mechanical and thermal stress analyses, and thermal performance. A catenary shaped shade was selected as the most feasible design. In addition, the team developed ideas for removing lunar dust from the shading device.

The second design team designed and built an adjustable catenary shade for simulated lunar environment testing. The simulated lunar environment will be created inside a vacuum chamber at the Johnson Space Center. The shade is remotely adjustable to study the effects of varying focal lengths on the heat rejection problem. The catenary shape closely resembles a parabolic curve for the required aspect ratios. This allows parabolic focal lengths to be used as a basis for design. Figure 3 illustrates the configuration of the catenary shade test fixture.

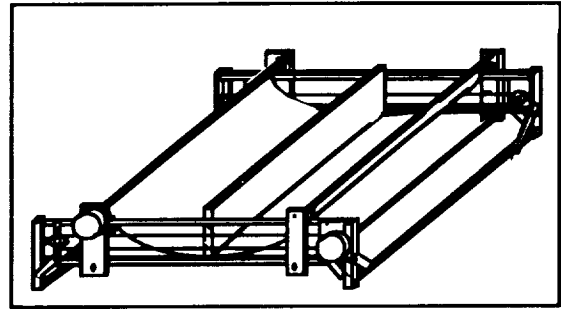


Fig. 3 Adjustable catenary shade test fixture

## REUSABLE ASTRONAUT SAFETY TETHER

The objective of this project was to design a reusable kinetic energy absorber for an astronaut safety tether to be used during extravehicular activities on the Space Station. Currently, the kinetic energy of an astronaut drifting away from the Space Shuttle is absorbed by a safety tether that cannot be reused after it has been deployed. Safety tethers limit the tension in the tether line to prevent damage to the astronaut's space suit or to the structure of the spacecraft. For use on the Space Station, NASA engineers desire a reusable safety device. The device must limit the tension in the tether line, absorb the kinetic energy of a drifting astronaut, signal the astronaut that the safety device has been deployed, and allow resetting after use.

A brainstorming session led to a large number of design concepts using hydraulic, pneumatic, magnetic, electrical, and mechanical methods. The design team selected a constant force spring alternative for further development. The design consists of a pair of constant force springs assembled to make the sum of their forces available at a single point. The springs limit the tension in the tether line and absorb the kinetic energy of the astronaut by uncoiling. A grip roller mechanism prevents recoil of the springs and allows resetting.

The team designed and constructed a prototype of the constant force spring energy absorber. Testing of the prototype confirmed that the device can absorb the kinetic energy and limit the force as required. Recommendations for design improvements were made after testing the prototype. The most critical shortcoming of the prototype is its excessive weight. The springs used in the prototype were made of stainless steel, but they could be made lighter using a composite material. In addition to using lighter composite materials, considerable weight can be reduced by eliminating all but the structurally necessary material from the device.

obtain a maximum launch velocity of 12 m/s, a spring with a maximum compression of 50 cm and a 6.75 kN/m spring constant is used. Each unit has a 200 Watt power requirement.

Three challenging problems were encountered in the design of the device. The first problem is that the scraping method requires a high cutting force. Because the device is lightweight, the traction generated by the device is low. This makes effective scraping difficult to achieve. The second problem with this configuration is that it has a tendency to tip. The tendency to tip is caused by a number of factors including the high acceleration used to launch the regolith, the low device mass, and the high launch position of the regolith with respect to the center of mass of the device. The third problem is the uncertainty of regolith dispersion as it is thrown in the lunar environment.

An impetus for furthering this design project is the versatility of this device. A manned lunar base will require a number of operations which could be performed by this device. An effort must be made throughout the design process to achieve modularity and versatility. A fleet of autonomous devices could perform tasks before the lunar base is established and continue to be of use after astronauts occupy the base.

Incorporated into the design of this device must be an attempt to make it modular so that it may be used for other tasks. One potential use for these devices is to gather regolith for mineral extraction. Regolith contains oxygen and hydrogen. NASA intends to extract the oxygen and hydrogen from the regolith for lunar base use. The regolith throwing devices could be easily modified to gather regolith and throw it into a bin for processing later. Although other methods have been proposed to gather and mine regolith for mineral extraction, modifying the regolith throwing device for this operation makes unnecessary the construction and transportation of another device to the moon.

These devices could also be used for remote surveying of the lunar surface. Because of the automatic operation of these devices, little human operation will be required for this function. This will be of special advantage as it reduces expensive and dangerous extravehicular activity. In addition to remote sensing, these devices could be used as transportation modules to carry small items around the lunar base.

Another possible use for these devices is the clearing of areas for lunar roadways. A previous study recommended that lunar roadways be constructed by clearing the top surface of the lunar regolith and compacting the remaining surface. These devices could be used to clear the roadway rather than transporting a specific device to the moon for this purpose.

The regolith throwing devices could also be modified to excavate craters. Craters will be dug on the lunar surface for the partial burial of lunar habitats and other lunar base buildings. These devices could be programmed to repeatedly clear a certain area of regolith, thus excavating a crater.

## LOW-COST UNMANNED LUNAR LANDER

United States Naval Academy  
Aerospace Engineering Department  
Annapolis, Maryland

Assistant Professor Walter K. Daniel

### Abstract

Two student groups designed unmanned landers to deliver 200 kilogram payloads to the lunar surface. Payloads could include astronomical telescopes, small lunar rovers, and experiments related to future human exploration. Requirements include the use of existing hardware where possible, use of a medium-class launch vehicle, an unobstructed view of the sky for the payload, and access to the lunar surface for the payload. The projects were modeled after Artemis, a project that the NASA Office of Exploration is pursuing with a planned first launch in 1996.

The Lunar Scout design (see Figures 1 and 2) uses a Delta II launch vehicle with a Star 48 motor for insertion into the trans-lunar trajectory. During the transfer, the solar panels will be folded inward and the spacecraft will be powered by rechargeable nickel-cadmium batteries. The lander will use a combination of a solid rocket motor and hydrazine thrusters for the descent to the lunar surface. The solar arrays will be deployed after landing. The lander will provide power for operations to the payload during the lunar day; batteries will provide "stay-alive" power during the lunar night. A horn antenna on the lander will provide communications between the payload and the Earth.

### Introduction

Project Artemis is NASA's program to put a lander on the lunar surface in 1996. The lander will carry payloads such as a lunar telescope, a possible robotic lunar rover or various other experiments. These payloads will be used ultimately to determine the feasibility of developing a lunar outpost for future manned missions and to demonstrate mining equipment to process hydrogen, nitrogen, and helium from the moon's soil. Thus, the lander project is named Lunar Scout since it will go up

and survey the lunar surface to provide information as to the possibility of future lunar missions.

### Requirements

The requirements for Lunar Scout are as follows:

- Use off-the-shelf hardware for economy.
- Provide a two-year spacecraft lifetime.
- Allow for systems shutdown during lunar night except for equipment to provide heat to critical components.
- Launch in 1996.
- Make a soft landing on the lunar surface between  $\pm 60$  degrees latitude.
- Deliver 200 kg payload to lunar surface.
- Provide 10 Watts power during two-week lunar night to heat the spacecraft.
- Use Delta II launch vehicle.

### Orbital Dynamics and Propulsion

A two-body problem with the Earth and moon was used to do a patch conic transfer. A Delta II launch vehicle carries the 3775 kg spacecraft to a 1366.7 km circular orbit where a Star 48A lunar insertion motor kicks the Scout into the elliptical transfer orbit which passes through the center of the moon. The three-dimensional view of the problem shows the launch point at Cape Canaveral at 28.5 degrees North latitude. The launch is slated for 1996 when the moon's orbital plane will also be at its maximum inclination of 28.5 degrees which will provide for a minimum energy transfer. At the patch point at an altitude of approximately 66,300 km above the lunar surface, the lander enters the moon's sphere of influence. At an altitude of 200 km the retrograde liquid rocket will fire for 135 sec to reduce the velocity to zero. The remaining 30 km to the lunar surface will be computer-controlled using the radar altimeter and

thrusters. Table 1 shows the breakdown of the mass budget.

Table 1 Mass Budget

| Component                   | Mass (kg) |
|-----------------------------|-----------|
| Payload                     | 200.0     |
| Structure                   | 45.0      |
| Electronics                 | 25.0      |
| Communications              | 18.84     |
| Batteries                   | 8.18      |
| Solar array                 | 33.0      |
| Attitude control sensors    | 20.06     |
| Solid rocket motor          | 2547.32   |
| Propellant                  | 675.36    |
| Propulsion support hardware | 108.74    |
| Main engine                 | 51.2      |
| Attitude control thrusters  | 32.24     |
| Total                       | 3775.0    |

There is a total mass of 3775 kg at takeoff; mass upon touchdown is approximately 530 kg. Attitude control sensors consist of a wide angle sun sensor and a star tracer. There are sixteen 2-Newton thrusters arranged in four four-engine clusters to provide for the variation of the center of mass due to the burning of the liquid propellant. There are also four 4.5-Newton vertical thrusters located around the lander body.

### Structure

The structure will be made of 1.25-in diameter 6061-T6 aluminum tubing with a 0.125-in wall thickness. The propulsion subsystem consists of bipropellant tanks and a thrust nozzle located at the bottom of the lander. The three lander legs will be stowed folded up in the payload fairing and will be springloaded to lock into place when the fairing splits away. The 0.30-m diameter landing pads will be made of aluminum flex-core to absorb the impact upon lunar touchdown. Upon landing, the spacecraft will deploy six 1.1-m<sup>2</sup> solar panels to provide power. The panels will rotate down to a 45 degree angle and be supported by the edges of the lander legs. The lander is equipped with a payload adaptor ring of 1.3-m diameter to allow for attachment of a variety of different 200 kg

payloads. The available payload envelope is a cylinder of 1.7 m diameter and 1.8 m height. The payloads, however, can be slightly taller if their diameter is small, e.g., a lunar telescope.

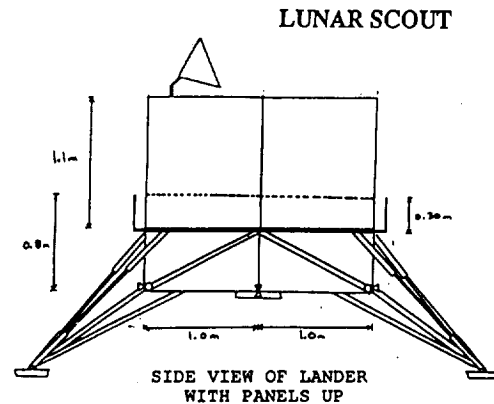


Fig. 1 Side view of Lunar Scout with panels up

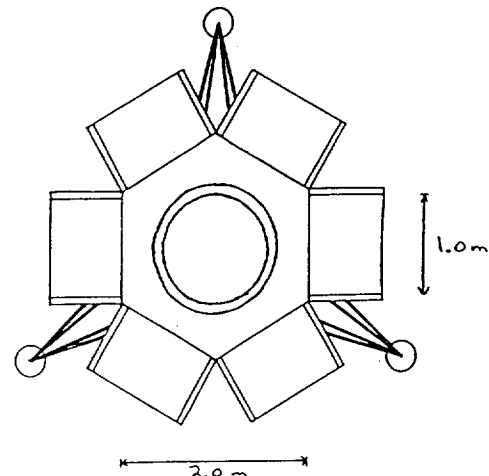


Fig. 2 Top view of Lunar Scout with solar panels folded out

### Power

The goals of the power system are to provide 500 Watts via solar panels during the daytime and 10 Watts via batteries during the lunar night. Prior to launch, the batteries will be fully charged to provide power to systems intermittently during the trajectory to the moon. After landing, the solar panels will deploy and begin providing power. During the daytime, the solar panels will provide between 240 W and 750 W of power to the payload depending on the position of the sun relative to the spacecraft. The solar cells used are 4 cm by 4 cm gallium arsenide on germanium to provide for lighter weight and smaller size arrays. In the nighttime, all systems will shut down and the batteries will provide 10 W to heat the vital systems and the payload. The battery consists of 22 seven-A\*hr cells and a 28 V bus. Degradation of the battery from charge and discharge was taken into account even though the battery will only undergo 28 cycles in its two-year lifetime.

### Communications

Communications will be made in the S band using a 2.3 gigahertz, 0.13 m wavelength signal on the Deep Space Network. The telemetry downlink will use two 0.30 m omni-directional antennas with a bit rate of 10 BPS and 5.79 W power requirement. The data downlink will use a 19.5 W feedhorn antenna with a bit rate of 1000 BPS. The feedhorn antenna will provide for a 23 degree horizontal by 21 degree vertical bandwidth. Since the Earth stays in the same position in the lunar sky relative to the lander, the angle of the feedhorn will be set prior to launch and will only need to be rotated once upon landing to be aimed at the Earth. The ground station uplink will use a 4-m dish to communicate with the lander and will require 4.5 W of power. The small 4-m dish uplink was chosen so as not to tie up one of the larger antennas for the two-year projected lifetime of the Lunar Scout.

## SUMMARY OF 1991-1992 PROJECTS

Naval Postgraduate School  
Space Systems Academic Group  
Monterey, California

Professor Brij N. Agrawal  
Daniel Sakoda, Teaching Assistant

### HIGH TEMPERATURE SUPERCONDUCTING INFRARED IMAGING SATELLITE

B. Angus, J. Covelli, N. Davinic, J. Hailey, E. Jones, V.  
Ortiz, J. Racine, D. Satterwhite,  
T. Spriesterbach, D. Sorensen, C. Sortun, R. Vaughan,  
and C. Yi

#### Abstract

A Low Earth Orbiting platform for an infrared (IR) sensor payload is examined based on the requirements of a Naval Research Laboratory statement-of-work. The experiment payload is a 1.5-meter square by 0.5-meter-high cubic structure equipped with the imaging system, radiators, and spacecraft mounting interface. The orbit is circular at 509 km (275 nmi) altitude and 70° inclination. The spacecraft is 3-axis stabilized with pointing accuracy of  $\pm 0.5^\circ$  in each axis. The experiment payload requires two 15-minute sensing periods over two contiguous orbit periods for 30 minutes of sensing time per day. The spacecraft design is presented for launch via a Delta II rocket. Subsystem designs include attitude control, propulsion, electric power, telemetry, tracking and command, thermal design, structure, and cost analysis.

#### Introduction

The high temperature superconducting infrared imaging satellite (HTSCIRIS) is designed to perform a space-based infrared imaging and surveillance mission. The design requirements originated from the Naval Research Laboratory through a statement-of-work. The spacecraft is designed for a 3-year life in low-Earth orbit at 509.3-km altitude and 70° inclination. The satellite operates in a sensing mode and a standby mode. The satellite is nadir

pointing during the sensing mode where the spacecraft body frame tracks the moving local vertical with a specified roll axis orientation. The system is designed for two 15-minute scans over two consecutive orbits for each 24 hours. During the sensing mode, 150 watts of power are required. The standby mode operates in a sun-tracking orientation where the solar arrays charge the batteries and the imaging payload faces away from the sun. The standby mode requires 100 watts.

#### Payload Description

The payload weighs 362.9 kg and has dimensions of 1.52 x 1.52 x 0.51 meters. The payload attaches to the spacecraft bus on one 1.52 x 1.52 meter square surface. The infrared (IR) telescope and associated radiators are mounted opposite the mating face. The IR telescope has a 4° x 4° field-of-view and is mounted at a 45° angle to the surface of the payload. The telescope has a hinged protective cover that opens approximately 50° after the satellite is deployed.

The entire cryogenic cooling system is contained within the payload, and is designed to maintain the infrared detector at 65° Kelvin during the sensing mode. The cryogenic refrigeration system is designed to replenish the cold reservoir of liquid nitrogen when not sensing. The mechanical portion of the cryogenic cooling system is not operated while in the sensing mode.

The orientation of the payload is continuously measured by an inertial measurement unit (IMU). The IMU is periodically updated through two star sensors which are mounted on the front (+x-axis) face of the payload. Finally, a data processor is included within the payload to format the infrared data for transmission.

## Mission Requirements

Mission specifications were outlined in a statement-of-work (SOW) generated at the Naval Research Laboratory (NRL). The following table shows the specifications for the orbit, attitude control system, electric power system, command, and telemetry.

Table 1 Requirements

|   |   |
|---|---|
| Design life                               | 3 years   |
| Orbit altitude                            | 509.3 km  |
| Orbit inclination                         | 70°   |
| Method of attitude control                | 3-axis stabilized   |
| Pointing accuracy                         | ±5° each axis   |
| Slew time                                 | 90° in 15 minutes   |
| Settling time                             | 1 minute  |
| Rate stability                            | 0.003° per second   |
| RF communication                          |   |
| Low data transfer rate                    | 16 kbits (minimum)  |
| High data transfer rate                   | 150 mbits   |
| Bit error rate                            | 10 <sup>-11</sup> (Encrypted)<br>10 <sup>-9</sup> (Unencrypted) |
| Minimum elevation angle                   | 10°   |
| Link availability due to rain attenuation | 99%   |
| Maximum ground antenna diameter           | 20 feet   |
| Electric power                            |   |
| Sensing mode                              | 150 watts   |
| Standby mode                              | 100 watts   |

## Spacecraft Configuration

The spacecraft bus is a box-like structure, 1.524 m square by 1.016 m tall. The bus is required to provide a stable platform to orient the sensor for imaging and standby modes. It is also required to provide electric power, command uplink, telemetry downlink, as well as real time transmission of the imaging data. The bus is constructed around a cylindrical aluminum monocoque thrust tube attached to an aluminum monocoque conical adapter cone. The cone protrudes through the face opposite the payload (the bottom face) and provides the

interface to the launch vehicle. The thrust tube and adapter carry the spacecraft launch loads. Four aluminum honeycomb panels are attached to the thrust tube and cone, constituting the sides of the spacecraft. These panels act as mounting surfaces for equipment and provide radiating surfaces for thermal control of the bus. An additional panel is located along the payload mounting face and provides a mounting surface for the payload.

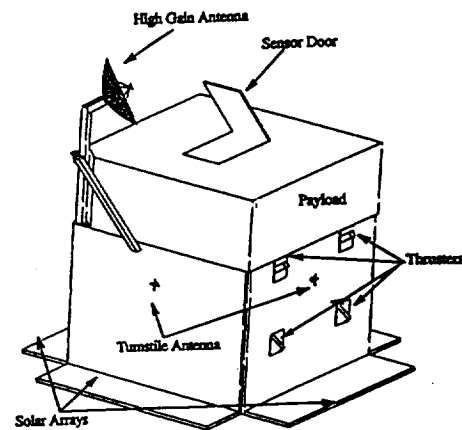


Fig. 1 Spacecraft configuration

## Solar Arrays

Fixed solar arrays are located parallel to the bottom face and are mounted on panels that extend outboard from the bus. The arrays are 0.38 m wide by 1.47 m long. The silicon solar cells are mounted parallel to the anti-Earth face and are designed to provide maximum power to recharge the nickel hydrogen batteries as well as supply house-keeping power in the standby mode. The entire spacecraft power is provided by four rechargeable nickel-hydrogen batteries during the imaging mode.

### Telemetry and Telecommand

Telemetry and communications are provided through one wide-band downlink antenna (WBDL), two omnidirectional transmit antennas, and two omnidirectional receive antennas. The omnidirectional transmit and receive antennas are paired on the pitch and anti-pitch faces to provide continuous telemetry and command capability. The WBDL antenna is gimbal-mounted to a boom that extends along one corner of the spacecraft, above the payload face, to allow horizon-to-horizon coverage during imaging revolutions. The support equipment, transmitters, receivers, and amplifiers are mounted interior to the bus. The high heat dissipating components are mounted to external panels. Two interior aluminum honeycomb panels provide mounting surfaces for the non-critical equipment. These equipment panels lie orthogonal to (and centered on) the axis of the conical adapter cone.

### Attitude Control

Attitude control for the spacecraft is provided by four reaction wheels. Eight magnetic torque rods provide momentum desaturation. The reaction wheels are mounted near the top of the bus. Three of the wheels are inside the adapter cone with the fourth, the yaw wheel, inside the bus on the top of the uppermost equipment panel. Three of the wheels are oriented on mutually orthogonal axes with the fourth at a 45° angle from the other three. The torque rods are mounted, two per axis, on opposite side panels of the bus toward the top surface. Initial orbit correction and emergency attitude control (despin) are provided by eight 1-lbf hydrazine thrusters, mounted in groups of four on the pitch and anti-pitch faces of the bus. The thrusters are utilized as a backup to the primary attitude control system in addition to station keeping. The fuel and pressurant tank are located at the center of the adapter cone with the surface of the tank aligned with the top face of the bus.

### Thermal Control

The thermal control system incorporates a passive design that maintains the bus and components at nominally low temperatures, and provides active heating to maintain temperatures within limits. The system is

composed of passive radiating and insulating material, applied to the surfaces of equipment and structures, and electric heaters attached to temperature sensitive components. Louvers are attached to the batteries as an additional measure to dissipate more heat energy.

### Mass Summary

The following table depicts the mass properties of the subsystems.

Table 2 Mass summary

| Subsystem              | Mass      |
|------------------------|-----------|
| Payload                | 362.0 kg  |
| T T & C                | 148.5 kg  |
| Electric power         | 97.0 kg   |
| Propulsion (dry)       | 8.3 kg    |
| Attitude control       | 42.4 kg   |
| Thermal control        | 24.8 kg   |
| Structure              | 164.9 kg  |
| Mechanical integration | 73.3 kg   |
| Subtotal               | 921.2 kg  |
| Mass margin (20%)      | 184.2 kg  |
| Propellant             | 12.9 kg   |
| Total                  | 1118.3 kg |

### Launch Vehicle

The launch vehicle is required to place the satellite in a circular orbit with a 509.3 km altitude and a 70° inclination. A Delta II (7320) launch vehicle was chosen for this mission. This launch vehicle is a two stage liquid-propelled rocket with three solid strap-on boosters. Typically a Delta II has nine solid strap-on boosters, but these are not required since this satellite has such a small mass.

### Payload Envelope

The Delta II standard shroud is 2.184 m in diameter and 1.448 m high. It then expands to 2.54 m by 2.032 m. The payload has dimensions of 1.524 m x 1.524 m x 0.508 m. The necessary internal shroud diameter, therefore, is



2.155 m. The two-stage Delta II (7320) vehicle normally uses the 6019 attachment fitting. It weighs 57 kg and has a 1.524-m outer diameter at the attachment point.

### Launch Sequence

The Delta II can be launched from either Cape Canaveral or Vandenberg AFB. Since the desired launch inclination is  $70^\circ$ , a West Coast launch is the best choice. The Delta II for this spacecraft will be launched from Vandenberg pad SLC-2W at a  $158^\circ$  launch azimuth.

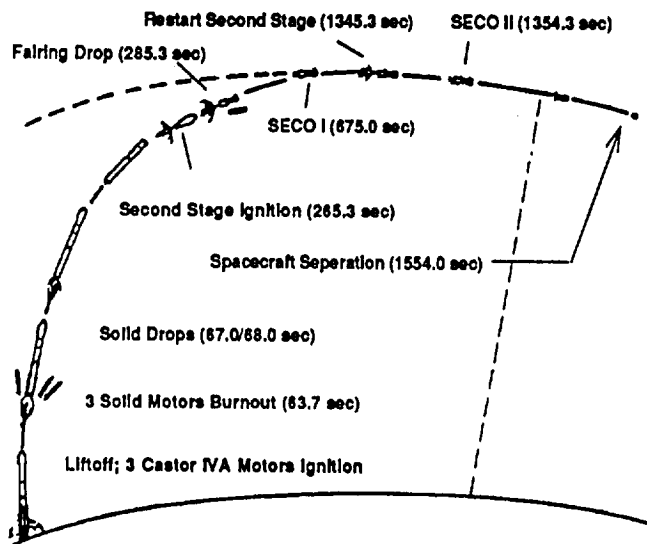


Fig. 2 Delta II launch sequence

The Delta II (7320) has two liquid stages as well as three solid strap-on boosters. The first stage RS-27 engine and the three solid rocket boosters are ignited on the ground at lift-off. Following burnout of the solids, the spent cases are jettisoned about one second later. The RS-27 engine continues to burn until main engine cutoff (MECO). This takes approximately 255 seconds.

After a short coast period, the first-to-second-stage separation bolts are blown, followed by second stage

ignition approximately five seconds later. The next major event is the payload fairing separation, which occurs early in the second stage flight.

The second stage burns for approximately 410 seconds, at which time stage two engine cutoff (SECO 1) occurs. The vehicle then follows a Hohmann transfer trajectory to the desired Low Earth Orbit altitude. After SECO 1 occurs, approximately 670 seconds later, the second stage is re-ignited and completes its burn to circularize the orbit. Satellite separation then begins approximately 200 seconds after stage two engine cutoff command (SECO 2).

### Spacecraft Separation

The launch vehicle and the spacecraft are attached by three attachment bolts and bolt catcher assemblies. The separation sequence is described as follows.

"Upon separation, the bolts and catcher assemblies are retained by the spacecraft. . . . Following release of the three explosive nuts, the spacecraft/launch vehicle is stabilized by the launch vehicle attitude control system. Subsequently, three retaining latches are released followed by retrofire of the launch vehicle yielding a minimal separation tip-off of the spacecraft."<sup>1</sup>

Fifteen seconds after the explosive bolts are fired, the latches are released. This delay allows the angular rates to dissipate. At this point the second stage retro-rocket fires providing the required relative separation velocity from the spacecraft. Expected angular velocities at separation are a little more than 0.2 degrees per second. This can be reduced by employing additional steps in the separation process. The angular velocity can be increased to 30 degrees per second (within a 5% accuracy) by using control jets.

### Orbit Analysis

The infrared imaging mission dictates the orbital parameters for this spacecraft. These parameters were defined within the statement of work by NRL. The orbit requires 509.3-km altitude and a  $70^\circ$  inclination as summarized in the following table. The ground path of

this high inclination orbit yields maximum time over land masses and passes over the majority of the habitable land on the Earth. The characteristics of this orbit make the choice ideal to carry out successfully the mission of imaging a wide variety of targets with both land and water backgrounds.

Table 3 Orbit parameters

| Parameter              | Value      |
|------------------------|------------|
| Apogee                 | 6887.43 km |
| Perigee                | 6887.43 km |
| Period                 | 1.58 hours |
| Inclination            | 70°        |
| Arg. of Perigee        | N/A        |
| Long. of the asc. node | TBD (1)    |
| Eccentricity           | 0.0        |
| Altitude               | 509.3 km   |

(1) Longitude of ascending node determined by launch date

### Orbital Perturbations

Orbital perturbations due to atmospheric drag, the Earth's oblateness, and effects from the Sun and moon were analyzed. The statement of work generated by NRL states that the allowable tolerance for altitude is 1.85 km (1 nmi) and 1° tolerance for inclination.

Altitude loss due to drag was calculated using the Artificial Satellite Analysis Program (ASAP) Version 2.0 developed by the Jet Propulsion Laboratory. The results indicate altitude loss at the rate of 4.50 km per year. This value was higher than the result from hand calculations and is used for propellant budget estimation.

Changes in inclination are attributed to the perturbations arising from the oblateness of the Earth and effects from the sun and moon. No cumulative effect on the inclination arises for this mission's circular orbit. The change in inclination due to the sun and moon were calculated and are presented in Figures 3 and 4. The maximum value for the effects due to the sun is 0.0084° per year. The maximum change in inclination due to the moon was found to be 0.023° per year.

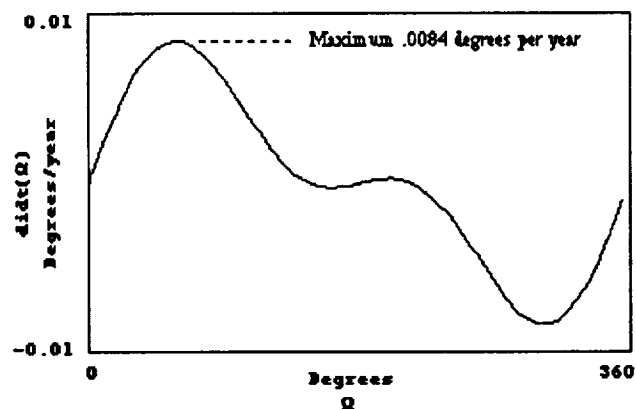


Fig. 3 Perturbation effects due to the sun

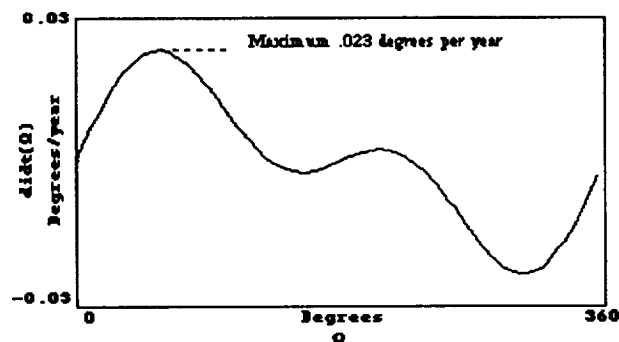


Fig. 4 Moon's influence on  $di/dt$  ( $i_1 = 28^\circ$ )

Effects in the longitude of the ascending node,  $\Omega$ , were determined because inclination changes are a function of  $\Omega$ . In addition, the longitude of the ascending node yields the daily ground track shift. The longitude of the ascending node shifts  $-2.6^\circ$  per sidereal day. Each sidereal day, 15.14 orbits are completed, resulting in the orbit ground track shifting  $0.84^\circ$  East per 15 orbits.

## Swath Width

The swath width of the spacecraft is required since transmission of the imaging data occurs simultaneously with imaging. This means that the receiving ground station must be in view while the spacecraft is scanning the target area. The footprint of the spacecraft's downlink is taken as  $10^\circ$  below the line-of-sight of the horizon. The result is a footprint whose angle is  $65.7^\circ$  subtended from nadir with respect to the spacecraft. The target object must be within a  $90^\circ$  scan of the spacecraft resulting in a  $\pm 45^\circ$  angle from nadir with respect to the spacecraft.

The spacecraft, during the scan mode, adjusts the rate of roll to allow the fixed imaging payload to scan the target area. Simultaneously, a directional antenna is controlled to maintain contact with the ground station in view. The 509.3-km circular orbit defines the swath widths of 3165 km and 911 km for the ground stations and observation targets, respectively.

## Subsystem Description

### Communication, Telemetry, Tracking, and Command

The radio frequency communication subsystem (RFCS) is the interface between the satellite and the ground station. The RFCS includes the Command and Telemetry Subsystem (CATS), which provides the interface between the payload, spacecraft bus, and the ground station. As described in the statement of work, the Radio Frequency Communication Subsystem (RFCS) is required to provide the following capabilities:

- Omnidirectional command receive
- Omnidirectional low data rate (16 Kbps minimum) transmission
- Directional high data rate (150 Mbps maximum) transmission

The high-data-rate downlink system (HDRDS) is required to provide optimal spectrum usage for 150 Mbps with bit-error-rate of  $10^{-11}$  encrypted and bit-error-rate of  $10^{-9}$  unencrypted. The HDRDS is permitted a downlink with 99% availability due to rain attenuation. A minimum  $10^\circ$  elevation angle is required for data

collecting ground terminals. The ground station is assumed to have a 6-m (20 ft) diameter receive antenna.

A front-fed (symmetric) parabolic antenna was chosen for the High Data Rate Wide Band Downlink antenna design. Parabolic reflector antennas offer narrow beams over a wide range of frequencies. They are also simple to design and construct and have a proven performance record. For an offset parabolic antenna, the reflected beam is not intercepted by the feed horn which reduces the side lobes. The reduction in side lobes increases antenna efficiency.

The antenna sits on a boom extended from the spacecraft allowing a larger field of view. The antenna is gimbaled to provide a wider range of pointing angles. The front-fed parabolic antenna will provide a 19- to 63-km diameter footprint with a 2.1 degree half-power beam width (HPBW). Antenna pointing control will consist of an open loop, onboard attitude and computer steer. This design provides  $\pm 0.2^\circ$  of pointing accuracy with about 1 dB loss, assuming the attitude and control system maintains pointing within design tolerances. Using a closed-loop system would require the use of an auto-track receiver and a more complicated three-dimensional uplink beacon which must be constantly tracked. The additional cost and complexity of this system was not deemed necessary for this mission.

The principal objectives for spacecraft tracking, telemetry, and command (TT&C) are to provide information of operational use, failure analysis, and prediction of spacecraft performance. In routine operations, the telemetry verifies commands and equipment status and also alerts personnel of any unusual occurrences. Telemetry can also be used to analyze any degradation that might affect performance and predict its effect on spacecraft lifetime. The TT&C consists of two sets of omnidirectional turnstile antennas, Command and Data Handling system (C&DH) and the Air Force Satellite Control Network (AFSCN).

The turnstile antenna consists of two half-wave dipole antennas intersecting in the middle and at a  $90^\circ$  angle from each other. This provides the necessary  $180^\circ$  arrangement for near omnidirectional coverage. They extend from the plane of the spacecraft a distance of  $\lambda/4$  (0.0375 m) for optimal gain out to  $\lambda/2$  (0.075 m) for

minimal gain, where  $\lambda$  is the wavelength. Tables 4 and 5 summarize the communication and TT&C subsystems.

Table 4 Communication subsystem summary

| Unit                  | Qty. | Length (cm) | Width (cm) | Height (cm) | Weight (kg) | Power (watts) |
|-----------------------|------|-------------|------------|-------------|-------------|---------------|
| Downlink transmitter  | 2    | 16.7        | 7.6        | 17.3        | 3           | 22            |
| Wide band transmitter | 2    | 22.8        | 22.8       | 11.4        | 19          | 75            |
| WBDL antenna          | 1    |             |            |             | 15          |               |
| Antenna actuator      | 1    |             |            |             | 4.5         | 5             |
| Omni xmit antenna     | 2    |             |            |             | 1.7         | 5             |
| Omni rcv antenna      | 2    |             |            |             | 1.6         | 5             |
| Hybrid divider        | 2    | 5           | 5          | 0.6         | 0.25        |               |
| Receiver/demod        | 2    | 17.8        | 17.2       | 17.8        | 6.8         | 2             |
| RFCS total:           |      |             |            |             | 51.85       | 114           |

Table 5 Command and telemetry subsystem summary

| Unit                   | Qty. | Length (cm) | Width (cm) | Height (cm) | Weight (kg) | Power (w) |
|------------------------|------|-------------|------------|-------------|-------------|-----------|
| Data interface (DIU)   | 2    | 35.5        | 21.6       | 24.1        | 19.9        | 25        |
| Remote interface (RIU) | 2    | 24.4        | 23.1       | 24.9        | 29.9        | 6         |
| Telem & command (TCU)  | 2    | 21.1        | 35.6       | 19          | 8.1         | 15        |
| Uplink processor       | 2    | 9.9         | 14.2       | 11.7        | 3.6         | 9.5       |
| Downlink processor     | 2    | 9.9         | 14.2       | 11.7        | 3.6         | 9.5       |
| CATS Total:            |      |             |            |             | 65.1        | 65        |
| Total Comm/TTC         |      |             |            |             | 116.95      | 179       |

### Electric Power Subsystem

The satellite electrical power subsystem consists of four solar arrays that nominally generate 34.2V at 4.3A at end-of-life (EOL), four 10Ah NiH<sub>2</sub> batteries, and power conditioning equipment for a fully regulated bus at 28 V ( $\pm 4$  V). Regulation is achieved by use of two partial shunt regulators on each solar panel and one series dissipative regulator at the battery discharge terminal. One of the partial shunt regulators on the panel regulates the voltage supplied to the housekeeping bus when that array is aligned as such. The other partial shunt regulator is used

to regulate the battery charging voltage, when the array is aligned for battery charging.

There are four arrays mounted in a stationary manner. Each array is capable of filling the role as either charge array or housekeeping array. Two arrays are normally required for battery charging and one for housekeeping. Each array is composed of seven parallel strings of 73 cells in series. The cells selected are 10 ohm, 0.02 cm thick, 2.5 cm x 6.2 cm silicon cells with back-surface reflector and TiO<sub>x</sub>Al<sub>2</sub>O<sub>3</sub> anti-reflective coating. The manipulation of the solar array's power distribution is done from ground control.

The batteries are designed to carry the electrical demand during eclipse and the additional load that arises during sensing and data transfer. Four 10Ah  $\text{NiH}_2$  batteries are used. The batteries are designed to operate to a 60% depth-of-discharge (DOD). The batteries will have approximately 21 hours to recharge fully after reaching the 60% DOD.

Radiation degradation of the solar cells was calculated for the duration of the mission. The results on the cell parameters are depicted in Table 6.

Table 6 Radiation degradation of solar cells

|              | EOL  | BOL  |
|--------------|------|------|
| $P_{MAX}(W)$ | 148  | 158  |
| $V_{OC}(V)$  | 42.8 | 44.4 |
| $I_{SC}(A)$  | 4.69 | 4.74 |
| $I_{MP}(A)$  | 4.34 | 4.36 |
| $V_{MP}(V)$  | 34.2 | 36.6 |

### Propulsion

The MR-111C 1-lbf thruster built by Rocket Research Company was chosen for this design. Table 7 gives the design and performance characteristics of the thruster.

Table 7 MR-111C Thruster characteristics

|                           |                                   |
|---------------------------|-----------------------------------|
| Propellant                | Hydrazine                         |
| Catalyst                  | Shell 405                         |
| Steady state thrust (N)   | 5.338 - 1.334                     |
| Feed pressure (MPa)       | 2.7579 - 0.5516                   |
| Chamber pressure (MPa)    | 1.2066 - 0.3447                   |
| Expansion ratio           | 74:1                              |
| Flow rate (g/sec)         | 2.404 - 0.635                     |
| Mass (kg)                 | 0.33113                           |
| Specific impulse (sec)    | 229 - 226                         |
| Minimum impulse bit (N-s) | 0.0845 @ 2.4132 MPa<br>& 20 ms On |

The propulsion subsystem is required to perform on a primary basis detumbling of the spacecraft, spin-down,

and delta V maneuvers for orbit maintenance. The secondary requirements of the propulsion subsystem are to provide redundancy for desaturation of the reaction wheels, perform slew maneuvers, and deorbit.

Eight thrusters, located on the positive and negative roll face, are used. The thrusters are canted  $35.8^\circ$  off the normal to the face and oriented to thrust in the x-z plane. The canting of the thrusters provides a moment arm with components in the x, y, and z planes. Figure 5 shows the placement of the thrusters on one face.

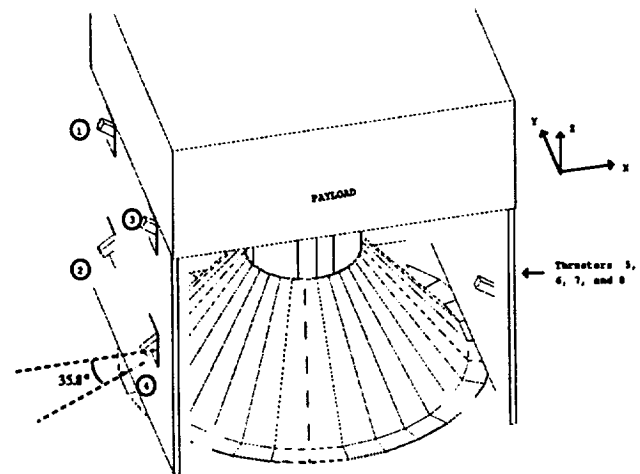


Figure 5 Thruster location and cant angle

The thruster numbers and locations are shown in Table 8, while the thruster operations are depicted in Table 9.

Table 8 Thruster placement

| Thruster Number    | Location <sup>1</sup> (meters) | Moment arm <sup>1</sup> (meters) | Moment created <sup>1</sup> (N*m) |
|--------------------|--------------------------------|----------------------------------|-----------------------------------|
| (1) anti-roll face | [-.762,-.427,-.241]            | [-.146,-.427,.203]               | [-1.11,1.11,1.54]                 |
| (2) anti-roll face | [-.762,-.427,.241]             | [-.146,-.427,-.203]              | [1.11,-1.11,1.54]                 |
| (3) anti-roll face | [-.762,.427,-.241]             | [-.146,.427,-.203]               | [1.11,1.11,-1.54]                 |
| (4) anti-roll face | [-.762,.427,.241]              | [-.146,.427,.203]                | [-1.11,-1.11,-1.54]               |
| (5) roll face      | [.762,-.427,-.241]             | [.146,-.427,.203]                | [-1.11,-1.11,-1.54]               |
| (6) roll face      | [.762,-.427,.241]              | [.146,-.427,-.203]               | [1.11,1.11,-1.54]                 |
| (7) roll face      | [.762,.427,-.241]              | [.146,.427,.203]                 | [1.11,-1.11,1.54]                 |
| (8) roll face      | [.762,.427,.241]               | [.146,.427,-.203]                | [-1.11,1.11,1.54]                 |

<sup>1</sup>Note: All distances are measured from the beginning-of-life center of mass for the spacecraft

Table 9 Thruster operations

| Operation           | Thruster number | Redundant      |
|---------------------|-----------------|----------------|
| Orbital insertion   | 1, 2, 3, and 4  | 5, 6, 7, and 8 |
| Atmospheric drag    | 1, 2, 3, and 4  | 5, 6, 7, and 8 |
| Positive roll (+X)  | 2 and 3         | 7 and 6        |
| Negative roll (-X)  | 1 and 4         | 8 and 5        |
| Positive pitch (+Y) | 2 and 4         | 7 and 5        |
| Negative pitch (-Y) | 1 and 3         | 8 and 6        |
| Positive yaw (+Z)   | 1 and 2         | 8 and 7        |
| Negative yaw (-Z)   | 3 and 4         | 6 and 5        |

The propellant budget is outlined in the following table.

Table 10 Propellant budget

|   |          |
|---|----------|
| Propellant for $\Delta v$ maneuvers and control                 | 11.03    |
| Allowance for off-nominal performance                           | 0.11     |
| Allowance for off-nominal operations                            | 0.11     |
| Mission margin (reserves)                                       | 1.10     |
| Contingency   | 1.10     |
| Total required propellant                                       | 13.45    |
| Residual propellant (trapped in motor case, tanks, lines, etc.) | 0.27     |
| Loading uncertainty   | 0.07     |
| Total propellant load   | 13.79 kg |

A survey was conducted of off-the-shelf positive expulsion tanks based on the above minimum fuel tank diameter and the diameter of the satellite cylinder ( $\approx 0.5$  meters). The TRW 80225-1 sphere used by the OTS-Marex program was selected since it was the closest match in propellant capacity. The required tank diameter was determined to be 0.322 meters.

#### Attitude Control Subsystem

The choice of configuration was driven mainly by the requirements to be able to slew about multiple axes in varying geometries and to maintain reasonably accurate 3-axis stability. Adequate redundancy is crucial because

the ACS must be able to orient for both payload operations and power collection. Three orthogonal Reaction Wheel Assemblies (RWAs), one along each body axis, allow somewhat independent control of rotation about each axis. A fourth RWA is skewed 45° out of plane with respect to the others to back up any single RWA failure. In the event of an RWA failure, the redundant rate will be commanded  $\sqrt{3}$  times the normal rate to achieve the desired effect while the undesired components are temporarily taken up by the other wheels.

Momentum dumping is accomplished by pairs of orthogonal magnetic torque rods. Normal operations call for the pairs to work simultaneously to rapidly desaturate the RWAs before slew maneuvers and to activate periodically to keep the RWA bias low. Specifically, automatic desaturation begins at 210 rpm. This minimizes dynamic coupling in the Euler equations. The rods can work singly in the event of a failure. Redundancy for momentum dumping is provided by the propulsion system, available in the event of complete torque rod failure. Both the magnetic dumping system and the propulsion system give limited three-axis stability in the event of multiple RWA failure.

Attitude errors are induced by solar, aerodynamic, gravity gradient, magnetic disturbance torques, and perturbations during desaturation and  $\Delta V$  maneuvers. The two Attitude Control Computers (ACC) receive data from the IMU, the Earth sensor, one of two sun sensors in view, and the backup gyro assembly to compute and

store two sets of these errors: (1) the Euler angles with respect to the standard nadir pointing sensing coordinates and (2) the Euler angles with respect to the sun-tracking coordinates, which track the incoming sun vector and can be considered "inertially" fixed. From these, each computer can calculate the direction cosine matrix used in its duty slew direction. In the event of a single computer failure, the other assumes the load for both. The first set of errors includes the orbital rate, while the second set is fixed with respect to the orbit normal coordinate system. Twelve independent transformations exist in each case (sign ambiguities are removed), and the computer defaults to the one which results in the minimum total correction path (or slew path), but any specific direction cosine matrix can be chosen. The duty ACC then commands the RWAs to perform the chosen sequence of single-axis slews to reach the target axes (i.e., to zero the Euler angles). From here, smaller slews can be commanded to accomplish offset nadir pointing, or to correct a thermal problem. Single-axis slew sequences are not the fastest method, but they simplify constraint checking, allow separate orthogonal error computation, and minimize dynamic coupling.

The design of two primary controllers covers the operation of all the modes and will be discussed here: (1) the sensing mode controller and (2) the slew controller. Only subtle changes separate the controllers between sun-tracking and sensing mode, sun-tracking and  $\Delta V$  mode, and slew and acquisition. The component selection summary is depicted in the Tables 11 and 12.

Table 11 ACS Sensors and electronics

| Component                             | Mass (kg) | Power (w) | Manufacturer               |
|---------------------------------------|-----------|-----------|----------------------------|
| Backup spring restraint gyro assembly | 1.3       | 19.5      | Heritage:DMSP              |
| Precision pointing Earth sensor       | 3.8       | 4.0       | Barnes                     |
| Attitude control computers (2)        | 2.5 ea    | 6.0 ea    | MIL-STD-1750 (GPS Version) |
| Sun sensor (sense mode)               | 0.04      | 1.0       | Adcole                     |
| Sun sensor (sun-track mode)           | 0.04      | 1.0       | Adcole                     |

Table 12 ACS Angular momentum devices

| Component       | Storage Capacity (Nms) | Peak Torque (Nm)             | Mass (kg) | Power (w)            | Manufacturer |
|-----------------|------------------------|------------------------------|-----------|----------------------|--------------|
| Roll RWA        | 19.9                   | 0.3                          | 9.09      | < 140 Peak < 10 Nom. | Honeywell    |
| Pitch RWA       | 19.9                   | 0.3                          | 9.09      | < 140 Peak < 10 Nom. | Honeywell    |
| Yaw RWA         | 19.9                   | 0.3                          | 9.09      | < 140 Peak < 10 Nom. | Honeywell    |
| Redundant RWA   | 19.9                   | 0.3                          | 9.09      | < 140 Peak < 10 Nom. | Honeywell    |
| Torque rods (6) | N/A                    | .003 max @ 10Am <sup>2</sup> | 1.76 ea   | 1.6 ea               | Ithaco       |

### Thermal Control Subsystem

Thermal control of the spacecraft bus is achieved using a near passive thermal control system. Passive control systems are simpler, more reliable, and more cost effective than active systems. The most attractive of these features are the simplicity and reliability. Passive components of the system include optical solar reflectors (OSR), multi-layer insulation (MLI), temperature sensors, fiberglass standoffs, and space-qualified coatings/paints. Temperature sensors are used to control strip heaters located on critical elements. A pair of temperature sensor-controlled louvers are used for thermal control of the batteries. All items are generally readily available hardware.

Critical components are kept above their low temperature limits by applying heater power. The bus is equipped with 15 heaters that range in size from 2.5 w to 20 w. Spacecraft heaters are electrical resistance elements that are mounted directly to the exterior surface of the critical component. The heaters are controlled by a closed loop system that includes local temperature sensors. Although the heaters function autonomously, the provision has been made for ground controlled operation with availability of adequate telemetry channels.

The nickel-hydrogen batteries require a very narrow temperature range of 0° C to 10° C. The batteries were placed on the  $\pm X$  panels with MLI on the interior of the spacecraft and louvers facing space. Additionally, the batteries are thermally decoupled from the rest of the spacecraft to eliminate spurious heat inputs from other components.

A thermal model was generated using the PC-ITAS® thermal analysis software by Analytix, Corp. The model used in the analyses consisted of 80 active nodes. Two orientations were studied: the Earth-sensing mode and the on-orbit standby mode. Results of the analysis are given in Table 13.

Table 13 Thermal analysis results

| Component             | Sensing min/max (°C) | Standby min/max (°C) |
|-----------------------|----------------------|----------------------|
| Payload/bus/interface | +3/+11               | 0/+30                |
| Batteries             | 0/+13                | 0/+18                |
| Fuel tank             | -11/+10              | -9/+29               |
| Solar arrays          | -57/+13              | -44/+66              |
| Antenna               | -14/-13              | -43/-27              |
| ADCS electronics      | -40/-10              | -39/-10              |
| TT&C electronics      | -49/+91              | -46/-14              |
| EPS electronics       | -37/+33              | -46/+4               |
| Reaction wheels       | -40/-10              | -39/-10              |

### Structure Design

The primary load-carrying members for axial compressive loads and bending moments are the central cylinder and conical adapter. These are monocoque shells of 6061-T6 Aluminum designed to withstand the ultimate quasi-static loads during launch. The design loads used a factor of safety of 1.5 for the axial and lateral



limit loads of 7.2 and 2.5 g's of the Delta II launch vehicle. Aluminum 6061-T6 was chosen for its ease of machining and large strength-to-weight ratio.

The spacecraft is made up of seven aluminum honeycomb panels in addition to the cylinder and conical adapter. The top panel supports the load of the payload and transmits it to the central cylinder and cone. The two equipment panels support the subsystem components. The remaining panels make up the body of the spacecraft bus. The panels are designed for stiffness to meet the design criteria for a minimum natural frequency of 50 Hz and stress due to dynamic loads. The adapter ring transfers the loads from the conical section to the 6019 adapter of the Delta II. The frame of the spacecraft bus is made of aluminum square tubing. It provides the mounting surfaces for the side panels and the parabolic antenna.

A finite element analysis of the structure was done using the CASA/GIFTS Finite Element Analysis software on a MicroVAX 2000 cluster. Static analysis of the spacecraft was performed using the loads for the Delta II launch vehicle. The maximum translational deflection occurs at the tip of the antenna support. This deflection is only 1.2 mm. The maximum rotational deflection of 2.2 mm also occurs at this point. The maximum stress in the spacecraft is 87.9% of the maximum yield stress using Von Mises' yield criterion. This results in a margin of safety of 13.8%.

The finite element model was also studied for dynamic analysis. The requirement that the fundamental modal frequency be above 50 Hz was never satisfied. Due to time constraints, modifications to the structure design were not possible. The fundamental modal frequency was found to be 22.76 Hz.

### Spacecraft Testing

The spacecraft test plan (Figure 6) promotes the use of "proto-flight" testing in accordance with the "USAF Military Standard Test Requirement for Space Vehicles (MIL-STD-1540B)." This is done in an effort to lower costs incurred in the testing phase. A test model is used for dynamic testing and thermal balance. A full vehicle is then built to flight standards and undergoes system level testing and is used as the flight unit.

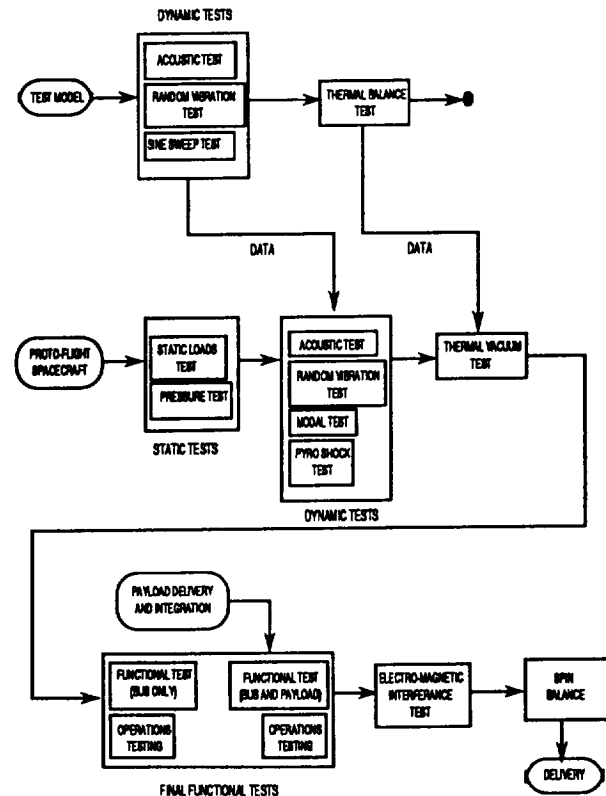


Fig. 6 Spacecraft testing flow diagram

Component level testing will be done for functionality and for random vibration. The components selected are all flight-qualified with validated quality. Once attached to the flight vehicle, the components will undergo all system level testing.

The test model will be fitted with mass and electrical simulation components. The test model is used for acoustic, random vibration, sine sweep, and thermal balance testing. The data gained is used in the component testing as well as the system level testing.

System level testing includes static load, pressure, acoustic, random vibration, modal, pyro shock, and thermal vacuum testing for environment compatibility.

Functional testing will be performed for mechanical devices, interface fittings, and operating limits. Functional testing will also be done for electrical performance.

### Cost Analysis

A cost analysis of the spacecraft development and launch was done using the "Unmanned Space Vehicle Cost Model," Revision 6 (USCM6). The USCM6 is a parametric estimating tool. Mathematical expressions are derived relating cost as the dependent variable of selected independent cost driver variables. These relationships are derived by statistically correlating the historical cost data of several related or similar systems to physical and/or performance characteristics of those same systems. This approach assumes that the driving forces that affected cost in the past will continue to affect cost in the future. Table 14 presents the cost analysis summary.

Table 14 Cost analysis summary (millions \$)

| Category                            | Most Likely | Low Est. | High Est. |
|-------------------------------------|-------------|----------|-----------|
| Satellite                           | 73.43       | 47.97    | 98.88     |
| Launch                              | 39.1        | 39.1     | 39.1      |
| Program level                       | 29.59       | 22.68    | 36.5      |
| Aerospace ground equipment          | 9.64        | 7.14     | 12.15     |
| Launch & Orbital Ops Support (LOOS) | 3.53        | 2.71     | 4.36      |
| Total                               | 155.29      | 119.6    | 190.99    |

### Conclusion

A spacecraft design is presented to provide mission support for the High Temperature Superconductor Infrared Imaging payload. The requirements were outlined in a statement-of-work generated by the Naval Research Laboratory. A preliminary design was done as part of the AE 4871 Advanced Spacecraft Design course during the Fall quarter. Due to time constraints,

deficiencies in the structure design could not be corrected. An additional deficiency arose due to neglect of the interaction between the antenna slew and the attitude control maneuver for spacecraft slew.

### Acknowledgments

The design team would like to thank Professor Brij Agrawal for his guidance and assistance throughout the quarter. We also wish to thank Professor Edward Euler and Mr. Dan Sakoda of NPS for their invaluable help. Dr. Alan Schaum, George Price, Woody Ewen, Nelson Hyman, and Porter Lyon of the Naval Research Laboratory provided valuable insight into all facets of the satellite design. Finally, we appreciate the continued interest and support of Dr. Kim Aaron, our NASA/USRA representative at the Jet Propulsion Laboratory.

### References

1. Angus, B. et al. Spacecraft Design Project, High Temperature Superconducting Infrared Imaging Satellite, Naval Postgraduate School, December 1992.
2. Commercial Delta II Payload Planners Guide, MDC H3224B, December 1989, pp. 3-5.
3. Agrawal, B.N. Design of Geosynchronous Spacecraft, Prentice-Hall: New York, 1986.
4. Solar Cell Array Design Handbook, JPL Publication SP43-38, Volumes 1, 2, and 3, October 1976.
5. Wertz and Larson. Space Mission Analysis and Design, Kluwer Academic Press, 1989.
6. Space Division Unmanned Space Vehicle Cost Model, 6th Edition, Space Division Report Number: SD TR-88-97, November 1988.

## LOW EARTH ORBIT COMMUNICATIONS SATELLITE

**D. Moroney, D. Lashbrook, B. McKibben,  
N. Gardener, T. Rivers, G. Nottingham, B. Golden,  
B. Barfield, J. Bruening, D. Wood, D. Pauls,  
W. Bell, D. Price, and C. Baldwin**

### Abstract

A current thrust in satellite communication systems considers low-Earth orbiting constellations of satellites for continuous global coverage. Conceptual design studies have been done at the time of this design project by LORAL Aerospace Corporation under the program name GLOBALSTAR and by Motorola under their IRIDIUM program. This design project concentrates on the spacecraft design of the GLOBALSTAR low-Earth orbiting communication system.<sup>1</sup> Overview information on the program was gained through the Federal Communications Commission licensing request.

The GLOBALSTAR system consists of 48 operational satellites positioned in a Walker Delta pattern providing global coverage and redundancy. The operational orbit is 1389 km (750 nmi) altitude with eight planes of six satellites each. The orbital planes are spaced 45°, and the spacecraft are separated by 60° within the plane. A Delta II launch vehicle is used to carry six spacecraft for orbit establishment. Once in orbit, the spacecraft will utilize code-division multiple access (spread spectrum modulation) for digital relay, voice, and radio determination satellite services (RDSS) yielding position determination with accuracy up to 200 meters.

### Introduction

GLOBALSTAR is a satellite system designed to provide global radio-determination satellite services (RDSS) for real-time position location and tracking, and voice and data services to mobile users. Rather than being a completely self sufficient system, GLOBALSTAR is intended to be integrated into the existing public switched telephone network (PSTN), personal communications networks, and private, specialized, and cellular networks. By complimenting existing carriers' networks, GLOBALSTAR is designed to make RDSS,

voice, data, fax, and freeze-frame video available to users anywhere in the world. The GLOBALSTAR program concept (which defined the design parameters for this preliminary design) is defined in the Federal Communications Commission (FCC) licensing request submitted by Loral Aerospace Corporation.<sup>2</sup>

### Specifications

The spacecraft is designed in accordance with the parameters set forth in the filing of the FCC license request. A constellation of 48 operational satellites, positioned in a Walker Delta pattern, provides global coverage and redundancy. There is no allocation for on-orbit spares, since a minimum of two satellites are in view at any time within the target area. Table 15 depicts the design and performance specifications of the spacecraft.

Table 15 Design and Performance Specifications

|                     |  |
|---------------------|--|
| Orbit               |  |
| Altitude            | 1389 km (750 nmi)  |
| Eccentricity        | 0° (circular)  |
| Coverage            | 75° N/S latitude   |
| Launch vehicle      | Delta and Ariane   |
| Mission life        | 5 years  |
| Initial launch date | 01 July 1996   |
| Station keeping     |  |
| Stabilization       | 3-axis stabilized  |
| Pointing accuracy   | ±1.0° all axes   |
| Electrical          |  |
| Bus                 | 28 Vdc   |
| Operation           | Continuous (100% during eclipse)   |
| Thermal control     | 600 watts for 33 minutes (max.)  |
| Payload             |  |
| Mission             | Direct voice and data relay network; voice and data link position location |
| Power requirements  | 800 watts for 20 minutes (peak); 50 watts (nominal)                        |
| Mass                | 60 kg  |

The spacecraft consists of the communication payload and the following subsystems: structure; telemetry, tracking, and command (TT&C); electrical power; thermal control; attitude control; and propulsion subsystems. In addition, launch vehicle integration and orbit dynamics were studied. The Delta II launch vehicle was selected for placing six spacecraft into orbit at a time. The spacecraft is deemed compatible with the Ariane launch vehicle also because of the stringent mass, volume, and environmental loads of the Delta II.

### Payload

The mission of the satellite constellation is to provide voice, data, messaging, and position location information to users via cellular telephone during those times when terrestrial cellular networks are not within range or are unavailable. Coverage extends from 75° South latitude to 75° North latitude. Both the user and a gateway must be in the field-of-view of at least one spacecraft to complete a communication link. Radio Determination Satellite Service (RDSS) can provide position accuracy of approximately one mile for single satellite operations and approximately 200 meters resolution when two satellites are in view.

The uplink and downlink between users and the spacecraft are at L-band (1610.0 to 1626.5 MHz). Gateway to spacecraft links are at C-band with uplink at 6525.0 to 6541.5 MHz and downlink 5199.5 to 5216.0 MHz. User channels provide voice and data at a variable 1.2 to 9.6 kbps with encoding/decoding. The spacecraft does not have onboard processing. Encoding and decoding is accomplished on the ground.

Six elliptical spot beams provide coverage over the spacecraft footprint. The elliptical beams are aligned with the major axes in the direction of the ground track path. Frequency reuse is provided by utilizing the same frequency range on two beams at a time but widely separated on the ground. The L-band is divided into 13 subbands of 1.25 MHz bandwidth for frequency-division-multiple-access (FDMA). Within each subband, spread spectrum techniques are used for code-division-multiple-access (CDMA). Two antenna beams of the total six are enabled at any one time over a 60 millisecond duty cycle yielding a system of beam hopping time-division-multiple-

access (TDMA). This combination of FDMA, CDMA, and TDMA provides a total of 2626 full-duplex channels per spacecraft.

The payload mass and power budgets are shown in Tables 16 and 17, respectively.

Table 16 Payload mass budget

| Component               | Quantity | Mass (kg) |
|-------------------------|----------|-----------|
| C-band antenna          | 2        | 1 each    |
| L-band antenna          | 6        | 10 total  |
| C-L band transponder    | 1        | 20        |
| L-C band transponder    | 1        | 20        |
| Timing and control unit | 1        | 8         |
| Total                   | 11       | 60        |

Table 17 Payload power budget

|                          |              |
|--------------------------|--------------|
| Peak load                | 827.6 watts  |
| Peak transmitted power   | 43.32 watts  |
| Peak thermal dissipation | 784.28 watts |

### Orbit Analysis

Orbit analysis for the constellation of satellites considered the ground coverage, phasing of satellites, number of planes, and number of satellites per plane for global coverage between 75° North and 75° South latitude. Additional consideration was given to the radiation environment, space debris, and atmospheric drag.

### Global Coverage

The payload requirements allowed no flexibility in orbit altitude or eccentricity. The goal of the analysis was to minimize the total number of satellites necessary to provide 100% coverage in the prescribed area. The total number of satellites is 48. They are distributed in eight orbit planes separated by 45° of the ascending node. Each orbit plane has an inclination of 52°. Six satellites

are placed in each orbit plane, evenly spaced. Overlap was determined to allow a minimum of two satellites in view at all times. Phasing of the satellites between adjacent orbit planes is  $7.5^\circ$  in true anomaly for collision avoidance. The constellation orbit planes are shown in Figure 7.

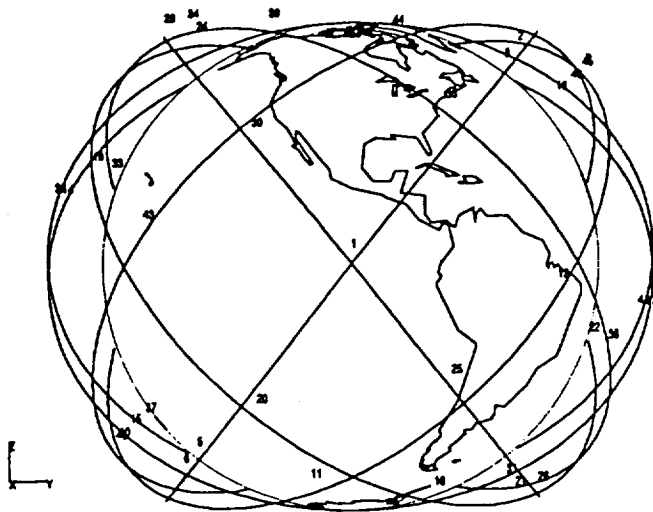


Fig. 7 Constellation orbit planes

### Orbit Environment

The altitude of the satellites equates to 1.22 Earth radii. The radiation level experienced due to Van Allen Radiation Belts exposure is lower than that normally experienced by a geosynchronous satellite. Minimal shielding of electronic components is necessary, and solar array degradation over the five-year life of the satellite does not adversely affect the design.

The scheduled launch for initial constellation establishment is at a time of minimum solar activity. However, solar activity may be near a maximum at end-of-life (EOL), which may interfere with satellite communication at that time. Solar activity directly affects the amount of atomic oxygen in the upper atmosphere. 100 particles per cubic centimeter of atomic oxygen are normally present at the constellation's operational altitude during low solar activity. During solar maximum,  $10^5$  particles per cubic centimeter are present. Atomic

oxygen may accelerate the degradation processes near end-of-life.

### Orbit Perturbations

Orbit perturbation analysis was performed using the Orbital Workbench® software by Cygnus Engineering. The Cowell propagation method was used with zonal harmonics J2 through J6, tesserals, lunar gravity, solar gravity, and solar pressure forces. Results identify that the only stationkeeping required is in-plane to maintain altitude. Additionally, total on-orbit atmospheric density is less than  $10^{-13}$  kg/m<sup>3</sup> during solar maximum and less than  $10^{-14}$  kg/m<sup>3</sup> nominally. Atmospheric drag at the operational altitude is considered negligible.

### Orbit Injection

The launch vehicle will place the satellites into an injection orbit that is slightly elliptic and coplanar with the operational orbit. The injection orbit was chosen to allow one satellite to be transferred into its operational orbit for every three orbit periods of the elliptical injection orbit once the initial satellite is injected. The injection orbit parameters are given in Table 18.

Table 18 Injection orbit parameters

|                        |         |
|------------------------|---------|
| Semi-major axis (km)   | 8052.22 |
| Eccentricity           | 0.035   |
| Inclination (deg)      | 52.0    |
| Radius at apogee (km)  | 8337.0  |
| Radius at perigee (km) | 7767.15 |
| Period (min)           | 119.85  |

### Launch Vehicle

#### Description

The spacecraft is designed to be compatible with both the Delta II and Ariane launch vehicles. The Delta II was chosen as the targeted launch vehicle for this study because of the stringent mass, volume, and environmental loads. The Delta II 7925 is capable of putting a payload

mass of 3300 kg into the required transfer orbit.<sup>3</sup> The Delta II 7925 launch vehicle configuration is shown in Figure 8. The first stage is a liquid propellant booster with strap-on solid rocket motors. The second stage is powered by a pressure-fed propulsion system. The third stage is a PAMSTAR 48 solid rocket motor.

spacecraft. The SLD is designed to withstand the launch loads for all six satellites. This eliminates the need for any single satellite to bear the weight of the other satellites in a stacked configuration. The spacecraft are attached to the SLD via two dispensing rails fixed with pyrotechnic bolt-latch fittings, which also serve to compress a spring-plunger mechanism at the end of each rail. The bolts are fired, releasing the springs and deploying the spacecraft. The dispensing rails provide their own bearing race that rigidly supports the spacecraft. The mating rails on the spacecraft are attached at the top of the spacecraft. The SLD is shown in Figure 9.

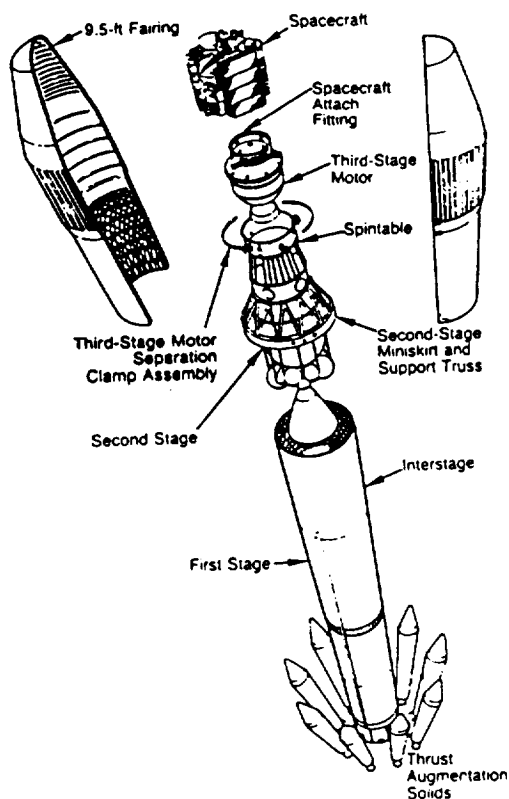


Fig. 8 Delta II 7925 launch vehicle

#### Satellite Launch Dispenser

Satellites are launched to establish a full orbit plane for a single Delta II launch. The spacecraft are stowed in a Satellite Launch Dispenser (SLD), which holds six

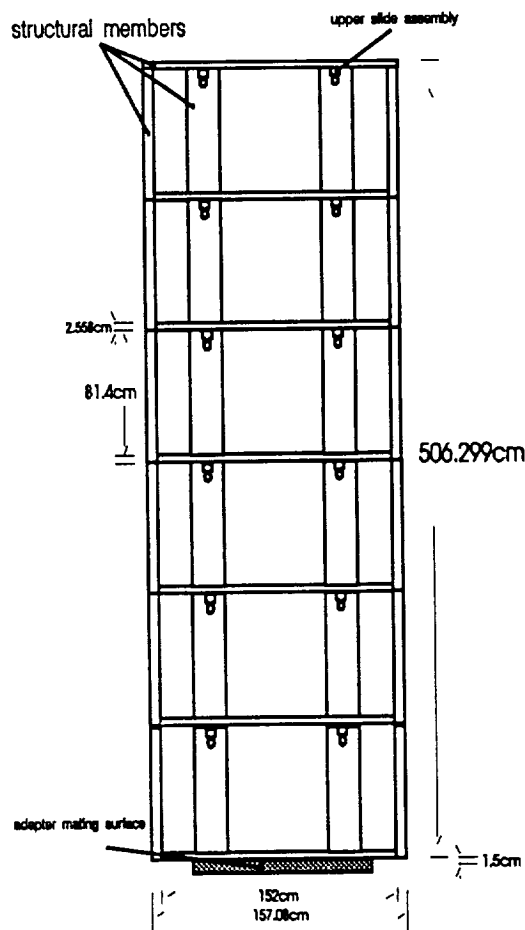


Fig. 9 Satellite Launch Dispenser (SLD)

## Subsystem Description

### Telemetry, Tracking, and Control (TT&C)

The TT&C system must be able to communicate both spacecraft commands and ephemeris data as well as to downlink subsystem health and performance data. The ground-based portion consists of two TT&C stations located in CONUS to perform tracking and relay functions. Data is then relayed to the Satellite Operational Control Center (SOCC) where telemetry is processed and attitude control and system commands are originated. The SOCC then relays the commands back to the TT&C ground stations and distributes ephemeris data to the gateway network.

The TT&C subsystem is independent of the payload and consists of the remote tracking unit (RTU) and the remote control unit (RCU). Full redundancy is employed. The RTU provides encoding, decoding, modulation, demodulation, and transmit/receive functions. The RCU interprets and performs commands, acts as the databus controller, and stores subsystem data for downlink.

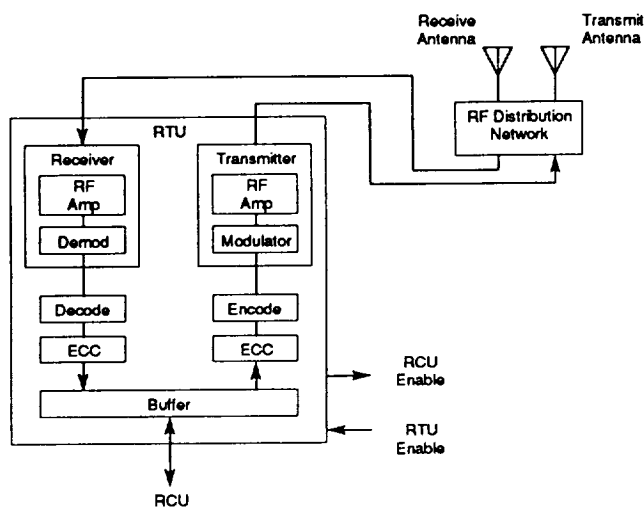


Fig. 10 Remote Tracking Unit (RTU)

The RTU is composed of a receiver, transmitter, coding section, and antennas. Pulse code modulation (PCM) is employed by the transmitter and receiver. Two antenna

pairs are connected and attached on the anti-Earth and Earth-facing sides. The anti-Earth antenna pair is used primarily for during spacecraft deployment. The Earth-facing pair is exposed once the payload antenna is deployed. Microstrip antennae arrays are used. Figure 10 shows the block diagram for the RTU.

The RCU consists of two independently addressable microprocessors along with associated memory and timing circuits. When command data is received via uplink, those commands not requiring immediate action are stored in a command buffer within each RCU. Each RCU has memory set aside for the storage of commands to be executed at a specified time. Commands are retrieved and executed by the active RCU from its command buffer until it either receives a command that requires immediate action, or it receives a new list of spacecraft commands. Health and performance data are collected by the RCUs by periodically polling the spacecraft systems. Data is then stored in RAM until it can be down-linked. Figure 11 shows the block diagram for the RCU.

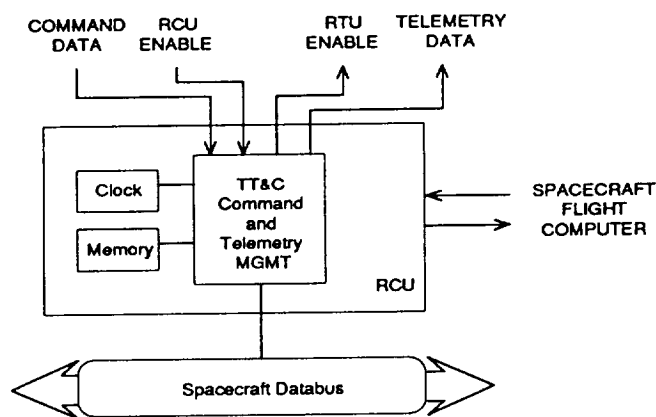


Fig. 11 Remote Control Unit (RCU)

### Electric Power Subsystem (EPS)

The power requirements for the spacecraft are driven by the potential use of the communication payload in the global environment. This equates to the global

distribution of potential users and the orbital coverage provided. The following factors were considered.

- 90% of the global population is in the Northern Hemisphere.
- China, India, and the former USSR have the largest populations, but are not expected to provide a significant market due to economic limitations.
- The United States, the fourth largest country, has a population of 250 million with a distribution of 42% in the Boston-New York-Washington, D.C. triangle; 10% on the West Coast; and 10% in the Midwest region.
- 80% of Canada's population (27 million) lives within 100 miles of the U.S. border.
- Western Europe is expected to provide the bulk of the European customer market for the remainder of this century due to economic failures in Eastern Europe; particularly large are France (pop. 58 million) and "West" Germany (pop. 61 million).
- Japan (pop. 122 million) is considered the most significant Asian customer region.

Payload power usage was divided over geographic market regions by primary power demand (U.S., Western Europe, and Japan); secondary power demand (S. Korea, Hong Kong, U.A.E., etc.); and tertiary power demand (no significant marketing potential). Peak payload power is expected over the Northeastern U.S. seaboard at 1800 local time. This loading will experience seasonal variation, but is not expected to exceed 800 watts for 16 minutes. Spacecraft housekeeping requirements are 200 watts, meaning that the EPS must provide 850 watts for 20 minutes. The EPS sizing is based on this 255 watt-hour requirement (illuminated or in eclipse). The orbital pattern repeats a similar ground track once every 72 hours.

The EPS design consists of two deployable solar arrays with solar array drive assemblies (SADAs), a single nickel-hydrogen ( $\text{NiH}_2$ ) battery, and the power control unit. The EPS provides a fully regulated dual power bus at 28V. The solar cells are 2 cm x 4 cm x 200 micron, 10  $\Omega$ -cm base resistivity, with back surface reflector and back surface field. Each wing has three panels with dimensions 120 cm x 80 cm and 1 panel with 120 cm x 140 cm. Each wing has 40 series strings of 95 cells each. The solar arrays, once deployed, provide two degrees of freedom. Each SADA allows rotation in the panel roll axis for orbit

longitude variation, and tilting of the deployment arm at the attachment base for inclination variation.

The  $\text{NiH}_2$  battery is composed of 23 cells. Each cell is an individual pressure vessel housed in an insulated aluminum sleeve. The five-year design life requires 24,000 charge/discharge cycles. Space-rated  $\text{NiH}_2$  cells are considered safe for this cycle life to a nominal 40% depth-of-discharge. A majority of the discharges are expected to be in the 30% range. This provides considerable power margin and avoids any memory effect from constant cycle levels.

The mass budget for the EPS is given in the following table.

Table 19 EPS Component Summary

| Component               | Mass (kg) |
|-------------------------|-----------|
| Battery module          | 30.0      |
| Solar array subassembly | 16.0/wing |
| Wiring harness          | 9.6       |
| Deployment mechanism    | 6.0/wing  |
| Array drive assembly    | 16.0      |
| Array drive electronics | 2.5       |
| Power control unit      | 5.6       |
| Shunt resistor bank     | 2.23      |

### Propulsion Subsystem

The propulsion subsystem provides for maneuvers required after dispensation from the SLD, including despin, orientation changes, deceleration, and orbit maintenance. Orbit accuracy is set at 1° from the intended position. The propulsion subsystem also provides for deorbit at the end-of-life of the spacecraft. The system consists of six 2.2-N hydrazine thrusters, a 49-cm diameter propellant tank, pressurant tank, and plumbing. The mass summary of the propulsion subsystem is given in Table 20.



Table 20 Propulsion mass summary

| Maneuver                           | $\Delta V$<br>(m/s) | Isp (sec) | Change<br>(kg) | Final<br>(kg) |
|------------------------------------|---------------------|-----------|----------------|---------------|
| Launch mass                        |                     |           |                | 374.00        |
| Attit.<br>orientation              | 1.00                | 224.00    | .17            | 373.00        |
| Orbit<br>injection                 | 149.39              | 223.96    | 24.57          | 349.26        |
| EOL deorbit                        | 146.00              | 218.23    | 22.93          | 324.84        |
| Propellant<br>holdup               |                     |           | 0.98           | 323.84        |
| Margin                             |                     |           | 57.17          |               |
| Component                          |                     |           | Mass<br>(kg)   |               |
| Tank,<br>pressurant,<br>propellant |                     |           | 70.0           |               |
| Thrusters<br>(ea)                  |                     |           | 0.344          |               |
| Piping                             |                     |           | 4.5            |               |

Figure 12 shows the location of the thrusters on the spacecraft. The operation of the thrusters for injection, station-keeping, and orientation maneuvers are given in Table 21.

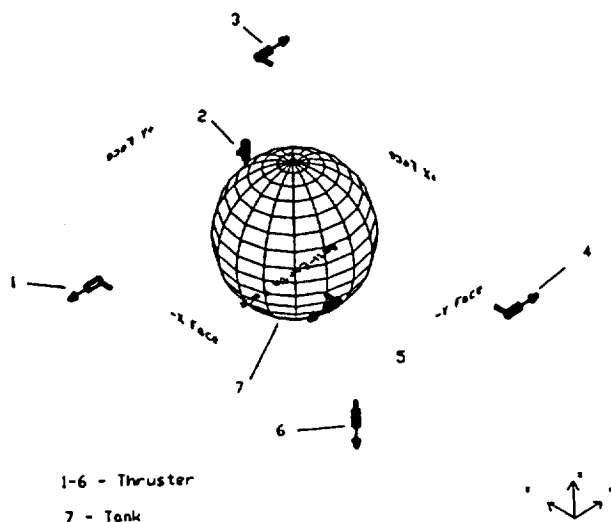


Fig. 12 Thruster locations

Table 21 Thruster operation

| Operation                       | Thruster(s)            |
|---------------------------------|------------------------|
| Injection                       | 5 & 6                  |
| Station-keeping                 | (1 & 2) or (5 & 6)     |
| Positive/negative roll (+x/-x)  | 5/6                    |
| Positive/negative pitch (+y/-y) | 1, 4, or 6/ 2, 3, or 5 |
| Positive/negative yaw (+z/-z)   | 1 or 3/ 2 or 4         |

### Attitude Control Subsystem (ACS)

The ACS provides autonomous attitude control through the use of a bias-momentum wheel to control pitch and damp disturbances in roll and yaw. Magnetic torque rods are used for roll control and momentum wheel desaturation. The magnetic torque rod used to control roll provides a 50 amp-m<sup>2</sup> magnetic dipole and is offset by an angle of 71°. A single torque rod can counter errors in both roll and yaw. The torque rod used to desaturate the momentum wheel also provides a 50 amp-m<sup>2</sup> magnetic dipole. Attitude sensors include a solar aspect sensor for initial orientation, two-axis scanning Earth horizon sensor (EHS) for nadir angle determination and a two-axis magnetometer to measure magnetic field strength. An attitude control computer provides onboard processing.

The ACS functions include initial orientation establishment, countering torques from spacecraft motors (i.e., solar array drive), and damping internal and external disturbance torques. Initial orientation establishment is done when the spacecraft is first released from the SLD where an initial angular velocity is imparted. Thrusters are fired for despin following solar array deployment. The momentum wheel then starts spinning to provide gyroscopic stability. The spacecraft slowly begins rotating about its major axis to acquire the sun. If after five revolutions it does not acquire the sun, it begins rotating about the roll axis. The spacecraft then rotates about its y-axis in order to locate the Earth. The satellite then maintains its attitude to within  $\pm 1^\circ$  accuracy.

The ACS design considered solar, gravity gradient, magnetic, and internal torques. The magnetic disturbance torque is the primary force acting on the

spacecraft. An analysis was done using the MATHCAD software application to find the time constants and gains of the ACS required to overcome the magnetic disturbance torque.

### Thermal Control

Thermal control of the spacecraft is intended to dissipate heat generated by the communication equipment and maintain temperatures of the components within operational limits. Thermal louvers, radiators, cold plates, and phase changers encompass the pseudo-active thermal control of the spacecraft. A stacked thermal package design is proposed as the solution. The stacked thermal package is shown in Figure 13. Four of these packages (two per side) comprise the backbone of the thermal control system.

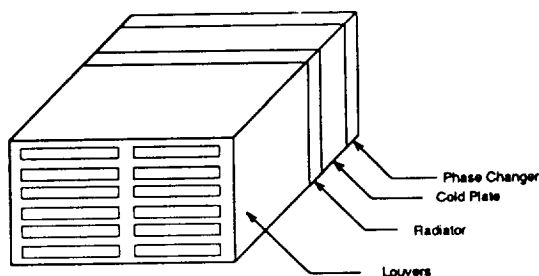


Fig. 13 Stacked thermal control package

Equipment to be cooled bolts to a cold plate through holes in the phase changer. The phase changers themselves are not strong enough to be weight-bearing. Heat dissipates mostly in the phase changer, melting the parafin inside. The cold plate spreads the heat evenly across its surface, where conduction to the optical surface radiators (OSRs) takes place. The heat is then free to radiate to space. The efficiency of the radiative transfer is determined by the opening and closing of the thermal louvers. Each blade of the thermal louver is controlled by a separate bimetallic actuator.

Heaters are required on the fuel tank, the six propellant lines, and the battery elements. Insulation surrounding the batteries, propellant tank, propellant lines and various other system equipment is necessary to reduce the power required to keep them within temperature limits. Thermal blankets and paint will provide a passive means of thermal control. Thermal blankets and thermal insulation are composed of multi-layered kapton separated by a thin nylon mesh.

A detailed thermal analysis of the spacecraft was performed using the PC-ITAS Version 7.3 software application by ANALYTIX Corp. All heat-generating pieces of equipment are included in the model. The results yield node temperatures for steady-state and transient cases. Figure 14 shows the thermal model developed using the PC-ITAS program.

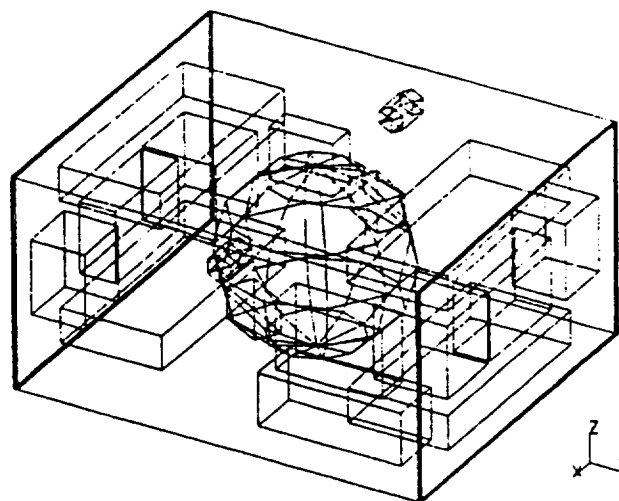


Fig. 14 Thermal analysis model

### Spacecraft Structure

The spacecraft structure consists of a frame of rectangular tubing with panels attached to all sides. The  $\pm$ pitch axis panels provide structural support for the majority of the equipment and thermal control system. The  $\pm$ roll axis panels support the minor heat generating equipment and the solar arrays. The Earth panels are

designed primarily to provide a mounting surface for the phased array antenna. The anti-Earth panel is used as an access panel for construction and integration and as an attachment face for the second TT&C antenna.

The rectangular frame consists of two sizes of rectangular cross-sectional tubing. The lateral tubing has 2.0 in x 1.5 in outside dimensions. The thickness is 1/8-in; the material, 6061-T6 aluminum. The longer dimension is aligned with the Z-axis to absorb loads, to maximize the area moment of inertia, and to minimize deflections. Axial frame members consist of 1/8-in rectangular cross-section 6061-T6 aluminum with 1.5 in x 1 in outside dimensions. The shorter dimension is aligned with the X-axis.

Equipment panels are made of 6061-T6 aluminum honeycomb with core thickness of 25.4 mm and face thickness of 0.2 mm. The honeycomb equipment panels are designed to support 54 kg of component mass under 36 g's of dynamic loading with a fundamental frequency above 30 Hz.

A finite element model was developed and analyzed for the Delta II launch loads in the X, Y, and Z directions. The launch loads and results are given in Table 22.

Table 22 Delta II launch loads and margins of safety

| S/C Dir.   | g's Accel. | Least M.S. |
|------------|------------|------------|
| Yaw axis   | 8.5        | 12.0       |
| Roll axis  | 15.0       | 1.1        |
| Pitch axis | 15.0       | 76.0       |

The finite element analysis results show positive margins of safety for all load conditions with a minimum of 1.1 for the load case corresponding to acceleration in the roll axis. The dynamic frequency of the model, however, shows lower mode frequencies than that required for the Delta II launch. The fundamental frequency of the structure from the finite element model is 19.18 Hz. Due to time constraints, this problem could not be fixed. Figure 15 shows the finite element model.

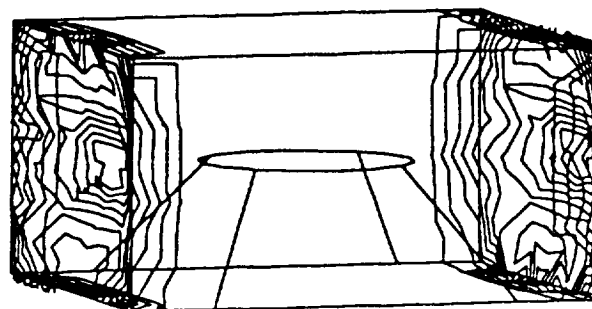


Fig. 15 Structural finite element model

### Spacecraft Testing

Testing of the spacecraft is involved in each phase of the program. Testing is done in the development, qualification, acceptance, prelaunch, and on-orbit phases of the spacecraft life. The test plan is designed to perform development testing of qualification and prototype hardware and computer program design concepts as early as possible to ensure early detection and resolution of design, fabrication, compatibility, performance, reliability, and life expectancy problems. The test plan outlines acceptance tests on all units before installation on the spacecraft and prelaunch validation tests to demonstrate that the space vehicle and the launch vehicle have been successfully integrated. Once in orbit, full operational capability is tested. The general test plan is shown in Figure 16. Descriptions of the various tests are given in the final report.

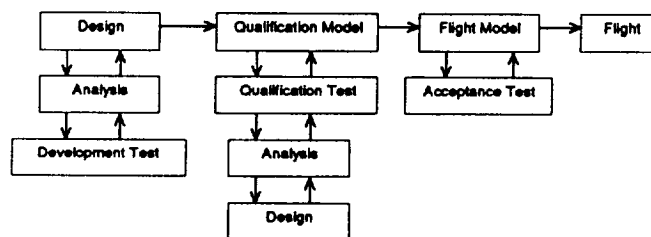


Fig. 16 General test plan

### Cost Analysis

Various methods of cost analysis were employed. Bottom-up costing was utilized where component costs were available. Some components were not individually priced and were grouped into categories based on their function. Costs for such components were formulated by use of Cost Equivalent Relationships (CERs).<sup>4,5</sup> CERs are parametric equations based on historical cost data and rationalized to cost versus mass of the subsystem. Therefore, even though components may have been identified, the parametric equations required that they be lumped together to form one total mass. Costs which were not currently available for space flight, such as the payload antenna, overall structure, and the SLD, reflect the additional cost of RDT&E amortized over the entire buy.

Costs for testing the satellites were formulated based on specific costs to test the entire satellite separately and as a stacked unit. Component level costs were not formulated since most components chosen were already flight-qualified. Costs of testing the payload antenna are included in the costs of system testing. These costs were formulated by use of CERs developed for testing. The total cost of testing was then amortized over the 48 satellites and applied to the first unit cost.

The theoretical first unit cost (TFUC), including the amortized system test costs, launch and orbit insurance (16% of the total cost of the program) is \$ 271.728 million. The total cost of the procurement of the 48 satellites is \$753.231 million. This reflects a learning curve of 95% applied over the entire buy.

Revenue generated from this program is broken down by year for RDSS service as shown in Table 23. This estimate is based on achieving a 40% share of the U.S. market by the year 2006. The incorporation of international markets is expected to increase this revenue base significantly. It is interesting to note, however, that viability of the system is achieved by accounting for only the U.S. market.

Table 23 Revenue from RDSS service

| Year | RDSS Customers<br>(x10 <sup>3</sup> ) | Total annual revenue<br>(\$x10 <sup>6</sup> ) |
|------|---------------------------------------|---|
| 1997 | 212                                   | 64.3  |
| 1998 | 271                                   | 76.3  |
| 1999 | 338                                   | 88.9  |
| 2000 | 412                                   | 102.1   |
| 2001 | 416                                   | 98.2  |
| 2002 | 419                                   | 94.3  |
| 2003 | 422                                   | 94.9  |
| 2004 | 424                                   | 95.5  |
| 2005 | 427                                   | 96.0  |
| 2006 | 441                                   | 99.2  |

### Conclusion

The preliminary design of a low Earth orbiting communication satellite is presented for global communication. Forty-eight satellites distributed over six orbital planes, evenly spaced within the plane, constitute the space segment. The ground segment consists of at least two control stations and multiple gateway stations for spacecraft control and connection to land-based communication systems, respectively. The spacecraft are launched six at a time via a Delta II launch vehicle. This preliminary design shows the viability of the system. The structure requires further study due to the low frequency of its fundamental mode.

### Acknowledgments

The design team would like to thank Prof. Brij Agrawal for his guidance. The team would also like to thank Dr. Edward Euler and Mr. Dan Sakoda of NPS. Mr. Tony Navarra and Mr. Bob Wiedeman of Loral Aerospace Corp. provided the FCC Licensing Request and were very helpful. The Lockheed FSAT Project Office is due our sincere appreciation; in particular, Mr. Larry Van Erdun, Mr. Bill Rust, Mr. Marty Gerbasi, Mr. Larry Tong, Mr. Jim Kim, Mr. Bruce Simpson, and Mr. Kevin Vogler deserve special recognition. Finally, we appreciate the comments and interest expressed by Dr. Kim Aaron of the Jet Propulsion Laboratory.

### References

1. Moroney, D. et al. Spacecraft Design Project: Low Earth Orbit Communication Satellite, Naval Postgraduate School, December 1991.
2. GLOBALSTAR SYSTEM APPLICATION before the Federal Communications Commission, Loral Cellular Systems Corporation, June 3 1991.
3. Delta II Commercial Spacecraft Users Manual, McDonnell Douglas Astronautics Company, Huntington Beach, CA, July 1987.
4. Werts, J.R. Space Mission Analysis and Design, Kluwer Academic Publishers, 1991.
5. Elbert, B.R. Introduction to Satellite Communication, Artech House, 1987.

## COPERNICUS - LUNAR SURFACE MAPPER

Utah State University  
Mechanical & Aerospace Engineering  
Logan, Utah

Professor Frank J. Redd  
Shaun D. Anderson, Teaching Assistant

### Abstract

The Utah State University (USU) 1991-92 Space Systems Design Team has designed a Lunar Surface Mapper (LSM) to parallel the development of the NASA Office of Exploration lunar initiatives. USU students named the LSM "Copernicus" after the 16th Century Polish astronomer, for whom the large lunar crater on the face of the moon was also named. The top level requirements for the Copernicus LSM are to produce a digital map of the lunar surface with an overall resolution of 12 meters (39.4 ft). It will also identify specified local surface features/areas to be mapped at higher resolutions by follow-on missions. The mapping operation will be conducted from a 300 km (186 mi) lunar-polar orbit. Although the entire surface should be mapped within six months, the spacecraft design lifetime will exceed one year with sufficient propellant planned for orbit maintenance in the anomalous lunar gravity field. The Copernicus LSM is a small satellite capable of reaching lunar orbit following launch on a Conestoga launch vehicle which is capable of placing 410 kg (900 lb) into translunar orbit. Upon orbital insertion, the spacecraft will weigh approximately 233 kg (513 lb). This rather severe mass constraint has insured attention to component/subsystem size and mass, and prevented "requirements creep." Transmission of data will be via line-of-sight to an earth-based receiving system.

### Systems

#### Introduction

The moon remains the only body in the solar system for which there has been actual sample return. In fact, some of the approximately 840 (381 kg) pounds of lunar material returned is still undergoing investigation at NASA's Johnson Space Center. But, while Apollo and its precursor missions have provided a wealth of information about our nearest neighbor, many fundamental questions remain unanswered. This fact was underscored in late 1990 with the Galileo spacecraft. Galileo, en route to Jupiter, made a flyby of the earth-moon system, and it imaged a region on the far side

of the moon that had never been seen before.

Before questions concerning the nature and origin of the moon can be properly addressed, high-resolution lunar data, such as that provided by Galileo, must be collected on a global scale. In the 61 lunar missions that have flown to date, none have provided a global survey, which leaves the current data set limited in two fundamental ways. First, the data is the product of technology that is 25-years-old and is, therefore, very low quality. Second, the data is confined to low latitudes because it was generated by spacecraft which flew in near-equatorial orbits. To complete global assessment of the lunar topography, geochemistry, and surface mineral distribution, the spacecraft must be in a near circular, polar orbit. Such an orbit is necessary because it allows the planet to turn underneath the orbit plane, permitting the spacecraft to pass over the entire surface. It also maintains a constant altitude and, therefore, constant data resolution. In the history of lunar exploration only two U.S. spacecraft have been in polar orbits. These spacecraft were among the five in the Lunar Orbital Program (LOP) from August 1966 to August 1967. However, the orbits of the LOP spacecraft were highly elliptical. Furthermore, the data was analog and had low signal to noise ratios. As a result, the data cannot be enhanced as can be done with the data from today's digital instrumentation.

Scientific interest in the moon can be separated into two broad categories: resources and mapping. Data returned concerning resources will describe the global surface mineral distribution. A high-resolution lunar map will provide the data necessary to answer questions of selenology (called geology on earth) or those processes which shape the surface of the moon. A lunar map is also critical to future surface robotic exploration and establishment of a manned lunar base.

Single spacecraft that address both of these categories, such as the Lunar Observer proposed by the Jet Propulsion Laboratory (JPL), have been studied extensively.<sup>1</sup> The Lunar Observer design, with its 13 separate instruments, became very difficult and costly to implement and, as a

result, never gained congressional support.

In November of 1991, NASA's Associate Administrator for Exploration, Dr. Michael Griffin, outlined a new approach to lunar missions in his paper "Exploration Program Plan."<sup>2</sup> This approach reflects a new design philosophy which has emerged in the space engineering community. By separating diverse, often conflicting, mission requirements, this new design philosophy yields smaller, more reliable spacecraft. In addition, the development of such a spacecraft more easily meets the constraints of budget and schedule, making them more acceptable to congress. Dr. Griffin proposed two separate lunar missions: one devoted exclusively to mapping and the other to resources. Griffin also pointed out that these missions should be within the \$100 million class, which is very inexpensive relative to other interplanetary missions.

This year's Space Systems Design Course at Utah State University designed a spacecraft to address the mapping interests in lunar science. A key element in the design was to generate a high-resolution, topographical map of the lunar surface emphasizing the low cost/fast turnaround approach outlined above.

Copernicus - Lunar Surface Mapper is named after a 16th century Polish astronomer for whom a large lunar impact crater is also named. The Copernicus project includes the design of each spacecraft subsystem with the goal of incorporating as much detail into the design as possible within the time limitations of the course. This report includes the design of each subsystem, an analysis of the mission operation requirements, and a realistic cost analysis.

### **The Copernicus Mission Requirements**

A list of top-level requirements for the Copernicus project was generated during fall quarter 1991. These requirements were the result of both science objectives in NASA's Office of Exploration and a great deal of research performed by the students of the Space Systems Design class. The Copernicus top-level requirements are as follows:

- Map the lunar surface to a global resolution of 12 meters (39.5 ft);
- Produce stereo images using digital mapping techniques;
- Operate in a circular, polar orbit maintained at an altitude of 300 kilometers (186 miles);
- Transmit the data to earth via line-of-sight communications;
- Complete the mission within one year; and
- Achieve lunar orbit following launch on a Conestoga launch vehicle.

One major modification in the top-level requirements occurred during the course of this project. The initial resolution requirement was to map the lunar surface globally to 5 meters (16.4 ft.) and maintain the capability to map specific sites to 1 meter (3.28 ft). After completing a preliminary design and showing the resulting spacecraft capabilities, this requirement was reexamined. A detailed discussion of the spacecraft capabilities under both resolution requirements is given in the next section. However, the reduction in resolution does not significantly effect the science return. As mentioned, the main interest in a high-resolution, topographical map is selenology. And selenological features such as cratering, faulting, and volcanism simply do not have much diversity below 12 meters (39.4 ft).

Launch on a Conestoga vehicle represents the most constraining requirements: weight and volume. The Conestoga launch vehicle, which can deliver 410 kg or 900 pounds (lb) to a translunar trajectory, is smaller than those typically considered for lunar missions. The Conestoga was chosen for the Copernicus project because it represents the smallest reasonable launch vehicle possible for a lunar mission. Smaller launch vehicles, such as the Pegasus, have been studied for lunar missions, but they rely on very constraining translunar trajectories.<sup>3</sup> These trajectories are designed to save weight by reducing the fuel required to achieve lunar orbit but take over 100 days to complete. With a one-year mission life, such trajectories were considered far too confining. The next step up in launch vehicle performance is the Delta II which can deliver approximately 1,300 lb (590 kg) to a translunar trajectory and has a substantially larger payload envelope. While the Conestoga is more limited in terms of both weight and volume and does not have the flight history of the Delta II, it will be a much less expensive launch. Furthermore, baselining the Copernicus spacecraft for a Conestoga launch leaves plenty of margin should other options become necessary.

### **The Copernicus Spacecraft**

Figure 1 shows an isometric view and specifications for the Copernicus spacecraft with the original resolution requirement. Important features to note in this preliminary design are the dual-gimballed, high-gain parabolic antenna and the deployable solar panels. A high-gain antenna was required to support the extremely high data rate of 31 megabits per second (Mbps). This data rate, resulting directly from the resolution requirement of 5 meters (16.4 ft), is actually a factor of greater than 100 higher than any previous planetary mission. While the hardware required to process this data rate does exist, it is not yet space qualified. As a result, high development costs would be expected.

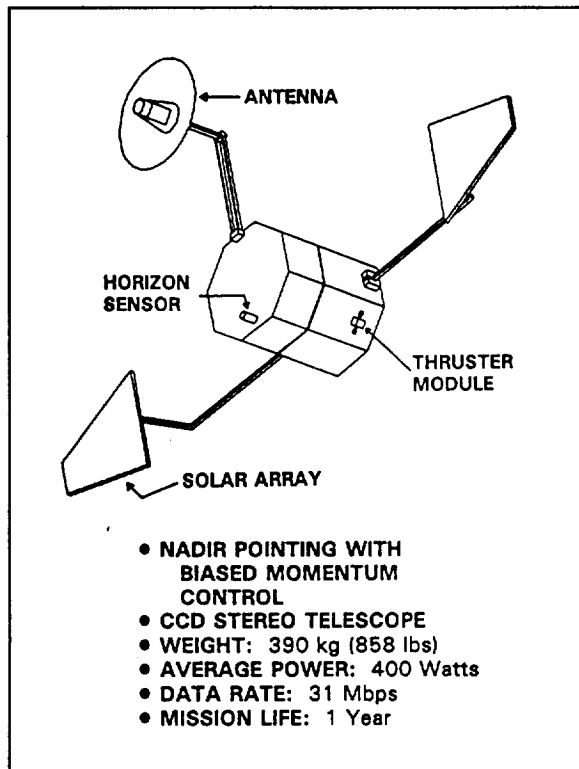


Fig. 1 Preliminary design of Copernicus

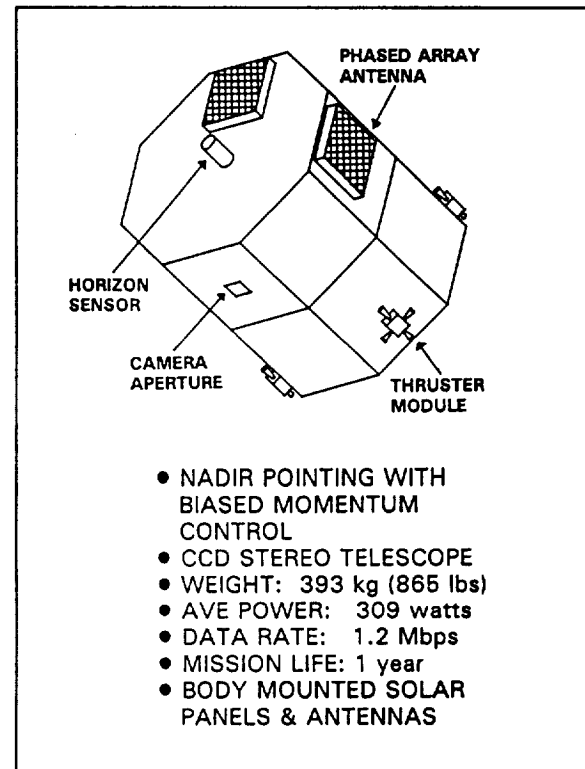


Fig. 2 Final design of Copernicus

Another result of the 5 meter (16.4 ft) resolution requirement was the need for deployable solar panels. These panels, in addition to the body-mounted cells, were required to meet the power needs that could not be met by the body-mounted solar cells alone.

Figure 2 shows an isometric view and specifications of the Copernicus spacecraft in its current configuration. Note that the antennas and solar cells are now completely body-mounted. All of the changes shown are a direct result of relaxing the resolution requirement. At a 12 meter (39.4 ft) resolution, the data rate was reduced to 1.2 Mbps, allowing the use of phased array antennas which use electronic steering and are, therefore, much more reliable. Also, the average power was reduced nearly 25%, eliminating the need for deployable panels. This final configuration of Copernicus is much more reliable and much less expensive than the preliminary design.

### Mission Operations

**Mapping Mechanics** Because large shadows in the image data are undesirable, mapping can only be performed at a beta angle of 10° to 40°. The beta angle is measured from an incoming light ray to nadir, or the line joining the

axis of the telescope to the center of the moon. Because the spacecraft will be in a polar orbit, the beta angle will change continuously. An optimum operational sequence where the spacecraft maps according to latitude and, therefore, according to beta angle, is highly desirable for data storage and transmission. However, the development of such a strategy requires a model that simultaneously predicts the position of the earth, moon, sun, and spacecraft. Such a model was beyond the scope of this project. Consequently, a scenario was assumed where the spacecraft takes data during an entire half orbit, mapping from the north pole to the south pole. While such a strategy would never be used during the real mission, this assumption results in a spacecraft that is more capable than necessary and ensures that the problem has been bounded. If a "pole-to-pole" strategy were possible, a map could be completed in roughly one month (27.3 days), the time it takes the lunar surface to rotate under the orbit plane. In reality, the time to complete the map is roughly six months. A conservative one year mission life was assumed for Copernicus, allowing for losses in data during transmission, etc.

**Swath Overlap** A swath overlap of 25% was assumed for the post-mission reconstruction of the map. After the



data has been collected on earth, scientists will begin the process of piecing together the global map. This process includes visually lining up consecutive image swaths, which is impossible without overlap. Previous planetary mapping missions have used swath overlaps in the range of 15 to 25%. The latter was chosen to be conservative.

**Data Transmission** During the preliminary design phase of Copernicus, an effort was made to avoid using NASA's Deep Space Network (DSN) for reception. The reason for this was the high demands that will be placed on the DSN during the time frame that Copernicus would fly. Other spacecraft that will require tracking during the Copernicus flight include Magellan, Galileo, Mars Observer, and Ulysses. In fact, it had been assumed that other large antennas around the world could be rented or that three 10-meter dishes would have to be built. This assumption was shown to be too confining, however, because the communications subsystem design is very dependent on a particular ground station. Because of this and a later commitment by the DSN to provide 10 hours of coverage per day using the 26-meter receiving antennas, the DSN was incorporated into the design.

## Payload

### Push-Broom Design

The camera is a push-broom type which means it has linear charged coupled device (CCD) arrays placed across track or perpendicular to the spacecraft's orbit path. Every time the satellite passes over 12 m (39.4 ft) on the ground, the arrays will be sampled, or in essence a picture will be taken. Each picture is 12 m (39.4 ft) by 48 km (29.8 mi). These pictures will then be placed side by side to create a map of the lunar surface. The satellite will use two arrays or cameras, one facing 10° forward and the other facing 10° aft. This will provide two views of the surface which will be used to create a topographical or three-dimensional map.

### Stereo Imaging

The Copernicus Lunar Surface Mapper is loosely based upon the French satellite SPOT.<sup>4,5</sup> The first satellite of this series was launched in 1986. SPOT's mission is to map the surface of the earth. It employs a unique approach to stereo imaging. Instead of looking straight down on the object to be mapped, it has two identical stereo telescopes, each built in at an angle. When the satellite is in position A as shown in Figure 3, it views the surface at a given angle. As it moves to position B, it sees the same point on the surface at a different angle. Therefore, every portion of the surface

is mapped from two different angles, creating a stereo image pair for each portion of the mapped surface.<sup>4,5</sup> These stereo image pairs can be sent back to earth and reconstructed, creating an exact three-dimensional representation of the object.<sup>6</sup>

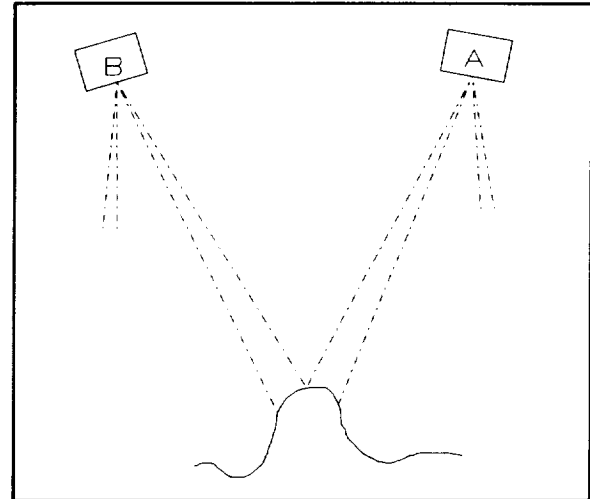


Fig. 3 Stereo image pairs

## Detector

A charge-coupled device (CCD) will be used to detect the incoming light from the moon. A CCD captures and converts light energy into an electrical signal.

A 12 m (39.4 ft) resolution equates to mapping 12 square meters (39.4 ft<sup>2</sup>) per 1 picture element (pixel) of the CCD array. Therefore, it was necessary that the CCD array be a minimum of 4,000 pixels long. Utilizing the push-broom technique, a linear CCD array with a high output rate was the best choice. The following factors influenced the selection of the Loral Fairchild CCD191 6,000 x 1 linear array.<sup>7</sup>

- **Detector Size:** The CCD191 exceeds the 4,000 pixel requirement.
- **Reliability:** The CCD191 is space-qualified.
- **Light sensitivity:** The CCD191 satisfies the need for a high dynamic range and responsivity necessary for lunar mapping.
- **Output rate:** Each CCD array has 2 parallel taps; each tap outputs 3,000 pixels in serial, yielding an approximate 4 MHz output rate.<sup>8</sup>

Since only 4,000 pixels are necessary to map a full 48 km (29.8 mi) swath, the data from 2,000 pixels (1,000 on each end of the array) will be discarded.

### Data Management and Storage

Data management requirements were to design a system that uses existing technology and components in order to accomplish the following:

- **Data Processing**
  - Upload data from payload
  - Process data
  - Download data to telemetry
- **Housekeeping**
  - Remote maintenance
  - Onboard upkeep
  - Status monitoring

In the event that a component did not exist to complete a functioning subsystem, a design study was performed. Special considerations were taken and consulting with professional engineers was done to assure that our design could be accomplished through research and development.

### Data Processing

For adequate scientific return, a 15 m (49.2 ft) resolution would be sufficient. However, due to the capability of image compression and accessible mass storage, a 12 m (39.4 ft) resolution was selected with a criteria of a 25% swath overlap. The data management subsystem was designed to meet the mission's top level requirements, including the 300 km (186 mi) orbit, 12 m (39.4 ft) resolution, and 25% swath overlap.

**Data Processing Requirements.** The design requirements for data processing are set by the mission's orbital altitude and resolution criteria.

|                        |                          |
|------------------------|--------------------------|
| Orbital Altitude:      | 300 km (186.5 mi)        |
| Orbital Period:        | 2.293 hrs (137.6 min)    |
| 1/2 Orbital Period:    | 1.146 hrs (68.8 min)     |
| Orbital Velocity:      | 1323 m/s (0.882 mi/s)    |
| Relative Ground Speed: | 110.25 m/s (0.0685 mi/s) |

**Resolution:**            **12 m (39.4 ft) with a 25% overlap**

|                       |                |
|-----------------------|----------------|
| Bytes/Pixel:          | 1 byte         |
| Pixels/Array:         | 4,000          |
| # of Arrays:          | 2              |
| CCD Camera Data Rate: | 882 Kbytes/sec |
| 1/2 Orbit Data In:    | 3.64 Gbytes    |
| Compression Ratio:    | 10:1           |
| Mapping Data:         | 364 Mbytes     |

|                           |                            |
|---------------------------|----------------------------|
| Map Encoding (20%):       | 72.8 Kbytes (5.824 Mbits)  |
| Telemetry Encoding (20%): | 72.8 Kbytes (5.824 Mbits)  |
| Stored Data:              | 509.6 Mbytes (4.077 Gbits) |
| Communications Data Rate: | 1.2 Mbps                   |
| Download Time:            | 3,397.5 sec (56.6 min)     |

A map encoding margin of 20 percent was suggested as a minimum amount of encoding used for digital mapping.<sup>9</sup> The telemetry encoding margin was a requirement given from the communications subsystem for transmitting data back to the earth via phased array antennas.

**Compression.** Data rate calculations were made assuming a statistically lossless 10:1 data compression. It is presumed that the V.Q. (Vector Quantization) Compression as developed at Utah State University will be used to attain such a compression ratio. Presently, it is proposed that each bit (pixel) x 8 bit (pixel) x 8 bit vector will be represented by an 8 to 12 bit mean with an approximate 20 bit codebook address. These figures are educated guesses that may well be altered to the scenario best suited for this mission which would be determined in a more detailed manner with development and research.<sup>10</sup> One possible concern which arises from the scientific community is how the homogenous nature of the lunar surface can be adequately represented when only 10% of the actual data is being received for reconstruction of the lunar map.<sup>9</sup> At this point, there is every reason to believe that it can be; the nature of V.Q. and its utilization of a codebook would appear very amenable to the processing of a moderately homogenous image.<sup>11</sup>

**Mass Storage.** The raw incoming data (without error correction or encoding) presented to the mass storage will be 3.64 Gbits per half orbit. The Solid State Recorder manufactured by Fairchild Space was chosen for this design using the parameters for a 4.5 Gbyte device. This includes a margin for encoding and error correction. The data rates required by this mission fit well within the device specifications. Equipped with its own power supply, chassis, I/O hardware, and error correction, the Solid State Recorder is approximately 30.0 cm x 33.5 cm x 20.0 cm and weighs approximately 23 kg (50.6 lb).<sup>12</sup>

### Command, Control, and Communications

#### Requirements

The design for the command, control, and communications subsystem is based on two main requirements: first, to downlink data from the satellite to

the earth at 1.2 Megabits per second (Mbps), and second, to uplink commands from the satellite to the earth at 2 Kilobits per second (Kbps). The data is the signal containing the mapping information collected from the payload. Commands consist of control, handshaking, and emergency communications. To maximize the quality of the mapping pictures, the downlink data must have a minimal amount of erroneous data; thus, minimization of the error probability is an important factor of the required downlink data rate.

The data rates of 1.2 Mbps and 2 Kbps were determined from the amount of data storage provided in the data management subsystem and the amount of time required for a ground station antenna on earth to receive the downloaded data. The Copernicus satellite, which will be using the Deep Space Network (DSN) for communications, is allowed to transmit data to an existing DSN receive antenna for 10 hours per day. This time limitation and the available data memory determined the downlink data rate to be at least 1.2 Mbps. For uplink, however, time for receiving the commands is not such a constraint, and 2 Kbps is a high enough data rate for the necessary uplink communications.

The design that most appropriately meets these requirements is composed of five phased array antennas, three omnidirectional antennas, and the electronics to control these antennas and data transmitting/receiving. Phased array antennas are relatively flat antennas that consist of multiple elements that electronically steer the transmitting signal. These antennas will be used, under normal conditions, for data downlink. To achieve full steering ability from any satellite position, five phased array antennas are placed on different sides of the satellite structure. The omnidirectional antennas, which are small biconical antennas, will receive commands and, in emergency situations such as when the steered signal loses track of the receive antenna, transmit data. Three of these antennas are placed on opposite sides of the satellite for full steering capability.

### Phased Array Antenna

The phased array antenna that will be used on the Copernicus satellite was chosen to fit design specifications and limitations and to perform effective communications. Each antenna is electrically steerable to an optimal  $\pm 45^\circ$  (a maximum of  $\pm 60^\circ$ ) from the perpendicular axis; therefore, five antennas are required so that at least one faces toward the earth at any particular time. To achieve the required data rate of 1.2 Mbps, each antenna has a transmitting gain of 16 dB. The size of each is 41 cm  $\times$  41 cm (16.14 in  $\times$  16.14 in.) and 7.62 cm (3 in.) thick.<sup>13</sup> Each antenna weighs approximately 2.25 to 4.5 kg (5 to 10 lbs) and is made of

copper-clad teflon fiberglass and copper-clad epoxy fiberglass.

## Spacecraft Structural Design

For ease in assembling and testing, a modular design was used. Two modules were utilized, an upper module which houses the electronic components of the satellite and a lower module containing the propulsion systems and momentum wheel.

### Upper Module

The configuration of the electronic components in the upper module is shown in Figure 4. To aid in the attitude control of the satellite, the components were placed as symmetrically as possible about the geometric center of the satellite. This module may be assembled and tested separately. This decreases the possibility of contamination or damage from the corrosive and carcinogenic hydrazine fuel.

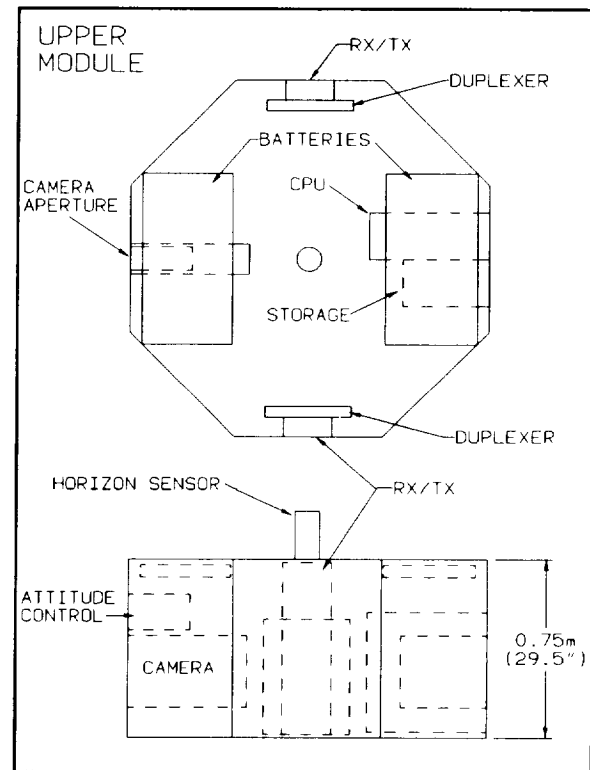


Fig. 4 Top and side view of upper module structure of satellite

Stringers running down each corner of the spacecraft will be used to connect the components to the satellite structure. The stringers will be 0.62 meters (24.4 in) apart and extend along the length of both modules. Several components will

require mounting arms to connect to the stringers. The other components will utilize arms of aluminum tubing to connect to the stringers.

The aperture of the camera must be protected during translunar flight. A square protective cover 12 cm (4.7 in) wide will be included on the upper module for this purpose. This cover will be secured with explosive bolts and removed after lunar orbital insertion.

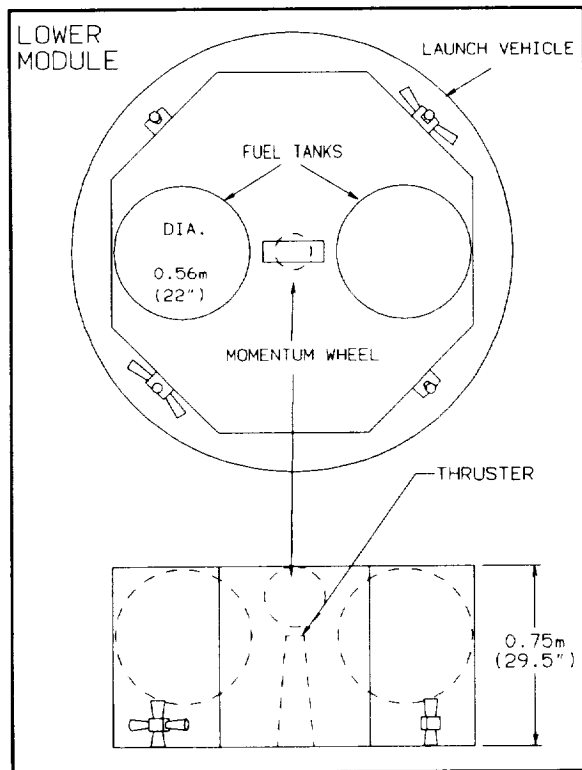


Fig. 5 Top and side view of lower satellite module

### Lower Module

The momentum wheel and all of the fuel elements are housed in the lower module. One phased array antenna will also be connected to the lower module. This will likely be used in testing the upper module and would not be installed on the lower module until final assembly. The lower antenna will be covered during lunar insertion to protect it from the 418 N (100 lb) insertion thruster. After insertion, explosive bolts will be used to separate the cover from the antenna. The lower module of the satellite is shown in Figure 5.

The use of body-mounted solar cells dictated a satellite structure that was somewhat larger than needed to house the components. This allowed for a design in which everything

could be connected to the structure independently. No two components had to be stacked or connected to each other.

### Attitude Determination and Control

The attitude control system will provide orientation data of the Lunar Surface Mapper (LSM) in three-dimensional space. It will point and maintain a nominal nadir orientation for mapping the lunar surface. The system will also provide guidance and navigation while the craft is en route to the moon.

### Sensors

The primary attitude sensor will be a Barnes Dual Cone Scanner with Sun Fans (DCS). The DCS is a combination horizon, sun, and moon sensor the also provides altitude information.<sup>14</sup> The DCS integrates all of the needed sensors into one unit reducing the error possibility encountered with coordinating multiple sensors.

The DCS with Sun Fans and MANS, designed to function as an autonomous earth sensor for the TAOS mission, flies in late 1992. Earth horizon sensors normally sense the IR signature of the CO<sub>2</sub> band in the atmosphere. This requires a slight modification for the DCS because of the different IR signature of the moon.

### Translunar Flight

The DCS provides translunar navigation data.<sup>2</sup> After translunar insertion, the LSM will be spun about the pitch axis at a rate of 17 rpm.<sup>3</sup> This allows the DCS to view the entire sky approximately once every minute. The craft will be spun up using the uncompensated angular momentum of the DCS assisted by the hydrazine thrusters.

### Actuators

The attitude control actuators must maintain the position of the LSM to within the pointing requirements as specified in Table 1.<sup>15</sup> They must also maintain the orbital altitude. A momentum bias system provides attitude control. A single momentum wheel mounted on a double-gimballed platform makes use of the unique gyroscopic properties of a momentum bias system.<sup>16</sup> The momentum bias system couples the roll and yaw axes while pitch control is independent. The combination of the momentum wheel on the platform provides three-axis stabilization.

The momentum wheel is a Type B T-Wheel manufactured by Ithaco.<sup>17</sup> Located near the center of gravity of the LSM, mounting is such that the spin axis is parallel with the pitch axis of the LSM. The wheel spins up after the LSM has achieved lunar orbit. The initial spin rate will be such that

|               |                    |
|---------------|--------------------|
| Pitch & Roll  | $\pm 0.07$ degrees |
| Yaw           | $\pm 0.02$ degrees |
| Altitude      | $\pm 500$ meters   |
| Sun Az & El   | $\pm 0.01$ degrees |
| Earth Az & El | $\pm 0.02$ degrees |

Table 1 Attitude pointing requirements

the camera is always nadir pointing. Variations in the spin rate will be necessary due to solar and gravitational torques on the LSM. Wheel saturation, if it occurs, will be countered through the use of hydrazine thrusters.

### Propulsion

#### Requirements

The functional requirements for the propulsion subsystem include the following:

- Correct for translunar injection errors;
- Insert the spacecraft into a circular, polar orbit around the moon with an altitude of 300 km (186 mi);
- Maintain the mapping orbit at 300 km  $\pm$  10 km (186 mi  $\pm$  6.2 mi) for one year; and
- Provide propulsion for attitude control purposes.

#### Mono-Propellant

A mono-propellant or hydrazine system was selected upon completion of a trade study including solid and bi-propellants. A mono-propellant system will be able to accomplish all aspects of the mission with one system. A single pipe delivery system is all that will be required because hydrazine does not need an oxidizer to burn.

#### Thrusters

Three different types of burns were needed to satisfy mission requirements. The first type will perform a lunar orbit insertion with a change in velocity of 854 m/s (2801 ft/s). A single 444.8 N (100 lbf) thruster will be used for the insertion burn. Two burns will be performed to insert the spacecraft into a 300 Km (186 mi) orbit. The second type will require the hardware to correct for orbital deterioration or loss of altitude. Four 4.45 N (1 lbf) thrusters will be used to accomplish orbital correction. The third type of burn will be for attitude control or pointing of the spacecraft and desaturation of the momentum wheel (see

Section 6.0). Eight 0.89 N (0.2 lbf) thruster plus the previous 4.45 N (1 lbf) thruster, will work together to accomplish this task.

#### Tanks

Storage and pressurization of the hydrazine will occur in two titanium tanks that will each be 56.1 cm (22.1 in) in diameter. The tanks will be divided into two parts by a bladder. One side of the bladder will have pressurant in the form of gaseous nitrogen, and the other side will contain hydrazine. The tank pressure will be 2.9 Mpa (420 psi) at launch and blow down to about 861 Kpa (125 psi) at the end of mission life. The titanium tanks were chosen because they are off-the-shelf components that are slightly oversized for mission parameters.

### Power

#### Functional Requirements

The power subsystem must provide and regulate the power levels of each subsystem. The orbit average power used by the satellite is 268 watts. This is the average power required if an orbital sustenance maneuver (OSM) is not required. If an OSM is required, the orbit power jumps to 378 watts (the orbit peak power). A twenty percent power availability margin is needed for safety reasons. This means that in addition to the 268 watts average power, an additional 54 watts need to be provided. The safety margin also requires 76 watts of power to be added to the orbit peak power requirement which happens during an OSM. Therefore, there must be 454 watts available for use during any orbit. The orbit average power, including reserves and battery charging, is 309 watts.

#### Solar Cells

The efficiency of gallium arsenide is approximately six percent greater than silicon, making it more suitable for use on the limited surface area of the Copernicus spacecraft.<sup>18</sup> Another advantage of gallium arsenide over silicon is the ability of gallium arsenide to operate with more efficiency at higher temperatures.<sup>19</sup> They are also more resistant to radiation. The initial design included solar panels on the skin of the craft as well as panels located on two deployable arms extending from the body. After further calculations, the deployable arms were eliminated and solar cells were placed on the ends of Copernicus. With this final configuration, there will still be enough power to meet mission requirements.

## Power Storage

Battery requirements need to meet the demand of 4,000 cycles (charging and discharging) during the life of the mission. For a single battery, this is a difficult requirement to meet. However, using two battery packs cuts the cycle requirement to 2,000 cycles per battery and is much more reasonable. Having two batteries increases the weight; however, it reduces cycling as discussed previously and adds reliability to the spacecraft. Initially, it was thought that nickel-cadmium batteries could not provide power for this many cycles, and nickel-hydrogen batteries seemed to be the answer. Nickel-hydrogen batteries can cycle up to 4,000 times with a 40% depth of discharge and can be custom made to deliver almost any voltage and current requirements.<sup>20</sup> Further investigation into nickel-cadmium batteries yielded different information than found initially; they were reimplemented into the design for reasons of reliability, cost, and weight.

The nickel-cadmium batteries used in the Copernicus are capable of 2,000 cycles at a 40% depth of discharge, 10 amperes of current, and 35 volts end of life voltage. The weight is approximately seventeen kilograms per battery, costing \$160,000 each.<sup>21</sup> Two battery packs consisting of 14 cells each will provide power storage for Copernicus.

## Thermal Management

Upon completion of a SINDA thermal analysis, it was determined that the batteries will be the only component that will get too hot. A radiator is the simplest means of cooling components. An aluminum rod was chosen for the radiator because of its low density and high thermal conductivity. The section of the rod that protrudes from the satellite will be coated with silvered teflon which has a low absorptivity to emissivity ratio.

Another critical area of concern was the hydrazine fuel. The fuel freezes at 271° K. Therefore, heaters will be needed to keep the hydrazine tanks warm. If the tanks are kept relatively warm, the route from the tanks to the thrusters, if adequately insulated, should not be a problem. Results indicated that a 9-watt immersion heater in each hydrazine tank should keep the tanks adequately warm. However, the heaters will not have the ability to heat an abundant amount of fuel in a short period of time. The heaters may even need to be on constantly to guarantee that the temperature of the hydrazine does not drop significantly.

## Conclusions

### Design Approach

The small satellite philosophy has been stressed throughout the design of Copernicus. A key element of this philosophy is the use of "off-the-shelf" components wherever possible. This approach has many advantages in terms of the cost and complexity of the design. However, one aspect of using off-the-shelf components that has not received attention in this design is component interfacing. Off-the-shelf components in various systems rarely "speak the same language" in terms of power, data rates, etc., and can have a significant impact on the development of any small satellite.

### Launch Vehicle Selection and Mass Reserves

Demonstrating that a lunar mapping mission is possible within the limitations of the Conestoga is a critical outcome of this design effort. As mentioned in the introduction, launch on the Conestoga will result in a substantial cost savings over flying on a Delta II. While it is difficult to accurately estimate launch costs, rough numbers suggest a \$15 million savings. Staying within the volume and mass limitations imposed by this choice of launch vehicle was a constant design challenge. At the conclusion of the preliminary design, a mass reserve of 20% was imposed on the design to ensure that, even with uncertainties in the mass estimation of each subsystem, the Conestoga would still be possible. This reduced the mass limit from 410 kg (900 lb) to 327 kg (720 lb). However, late in the design it became necessary to choose an off-the-shelf launch vehicle interface due to the lack of time for a custom design. A McDonnell Douglas PAF 6306 interface was selected. This interface, capable of holding a 2600 kg (5512 lb) spacecraft, is far beyond the needs of Copernicus. The PAF 6306 has a mass of 50 kg (110 lb), which eliminated a significant portion of the 20% mass reserve. With a final launch weight of 393 kg (865 lb) Copernicus retains a 4% margin for launch of the Conestoga. However this margin would increase substantially if a lighter, custom interface were designed.

### Power Reserves

As with mass, a 20% reserve was placed on the power design. However, after the resolution requirement was relaxed, the power reserve grew to 30%, even with the elimination of the deployable solar panels.

## Redundancy

The limited use of redundancy was consistent with the low-cost approach to the Copernicus design. In fact, the transponder and bolt cutters on the two deployable shields are the only redundant systems aboard the Copernicus spacecraft. These redundancies eliminate two single-point failures. They have a low mass and are relatively inexpensive and, therefore, do not significantly increase the cost or complexity of the design. The lack of redundancy dictates a meticulous fabrication and test program to insure against failure.

## Mission Costs

Two cost models were generated for the Copernicus design. One was a component level cost assessment performed by each subsystem. This hardware model did not include estimates for development, fabrication or assembly. It was based simply on cost estimates provided by the manufacturer of each component. In order to get a better estimate of the overall cost, including development, a test and evaluation version of the Satellite Cost Model developed by The Aerospace Corporation was employed<sup>22</sup>. This model uses empirical relationships derived from NASA and Department of Defense (DOD) spacecraft that were developed over a fifteen year period ranging from 1963 to 1978. This software allows the user to estimate the research, development, testing, and fabrication costs for all components on the spacecraft. A summary of the software output is shown in Table 2.

It should be noted that nonrecurring costs comprise \$62.1 million of the \$94.9 million spacecraft cost. These results agree well with estimates from NASA's Office of Exploration and with the hardware estimate that was performed. However, because this model was generated from data on larger spacecraft it is likely that the estimate is high.

|              |                |
|--------------|----------------|
| SPACECRAFT   | \$94.9         |
| LAUNCH       | \$30.0         |
| <b>TOTAL</b> | <b>\$124.9</b> |

Table 2 Mission cost in millions of 1992 dollars

## References

1. Ridenoure RW (editor). Lunar Observer: A Comprehensive Orbital Survey of the Moon. Mission and System Definition Summary, JPL D-8607. Jet Propulsion Laboratory, Pasadena, CA, 15 April 1991.
2. Griffin MD. Exploration program plan. NASA Office of Exploration, NASA Headquarters, Washington, D.C., 19 November 1991.
3. Belbruno EA, Ridenoure RW, Fernandez J. Robotic lunar exploration using the Pegasus winged rocket and ballistic lunar capture: An update. AIAA Paper 92-1562, AIAA Space Programs and Technologies Conference, Huntsville, AL, 24-27 March 1992.
4. Langeraux P. France puts Landsat on the SPOT. Aerospace America, May 1986, p.8.
5. Gavaghan H. France launches SPOT, a commercial spy in the sky. New Scientist, January 1986, p.25.
6. Phone conversation with Canadian firm McDonald Detwyler, February 1992.
7. Loral Fairchild: CCD191 6000 Element Linear Image Sensor. Loral Fairchild Imaging Sensors, Milpitas, CA, 1991.
8. Onishi, Steve. Telephone conversations, Loral Fairchild, February 1992.
9. Cook R. Jet Propulsion Laboratory: Responses to Copernicus Preliminary Design Review. March 1992.
10. Megill, Rex. Private communications, EER Systems, Globesat Division, November 1991 - March 1992.
11. Israelson, Paul. Utah State University: Lecture, Electrical Engineering Department. 25 April 1992.
12. Gerber, Andy. Telephone conversations, Fairchild Space, 23 April 1992.
13. Sanford, Gary. Telephone conversations, Ball Aerospace Corporation, April, 1992.
14. Barnes R. All Sky Scanner: Application Of Scanning Earth Sensor On Spin Stabilized Spacecraft. American Astronautical Society (AAS 92-020), 1992.

15. EDO Corporation. Promotional Literature, Fact Sheet, EDO Corporation, Barnes Engineering Division Dual Cone Scanner with Sun Fans Model 13-350 (9/91).
16. Kaplan MH. Modern Spacecraft Dynamics & Control. John Wiley & Sons, New York, 1976.
17. Ithaco Corporation. Promotional Literature, Fact Sheet, Ithaco Type B T-Wheel (IPS-16 1/92).
18. Applied Solar Energy Corporation: Gallium Arsenide on Germanium Space Solar Cells. City of Industry, CA.
19. Griffin MD, French JR. Space Vehicle Design. American Institute of Aeronautics and Astronautics, Washington, D.C., 1991.
20. Eagle Picher. Nickel Hydrogen Space Batteries. Joplin, MO.
21. Telephone conversation, Gates Aerospace Ni-Cad Batteries. (904) 462-3617 (Kathy).
22. Campbell H, Newton ML. SCM - Satellite Cost Model, Test and Evaluation Copy. Upgrade Date: 24 June 1991. The Aerospace Corporation, Engineering Group, El Segundo, CA.



**1991-1992 PROJECT SUMMARIES**

**Virginia Polytechnic Institute and State University  
Department of Aerospace Engineering  
Blacksburg, Virginia**

**Professor Antoni K. Jakubowski  
Davy A. Haynes, NASA Langley Research Center**

**PROJECT PARAS: PHASED ARRAY RADIO  
ASTRONOMY FROM SPACE**

**Kenneth Nuss, Christopher Hoffmann, Michael Dungan,  
Michael Madden, Monia Bendakhlia (Ecole  
Polytechnique Feminine, France)**

**Abstract**

An orbiting radio telescope is proposed which, when operated in a Very Long Baseline Interferometry (VLBI) scheme, would allow higher (than currently available) angular resolution and dynamic range in the maps and the ability to observe rapidly changing astronomical sources. Using passive phased array technology, the proposed design consists of 656 hexagonal modules forming a 150-m diameter antenna dish. Each observatory module is largely autonomous, having its own photovoltaic power supply and low-noise receiver and processor for phase shifting. The signals received by the modules are channeled via fiber optics to the central control computer in the central bus module. After processing and multiplexing, the data are transmitted to telemetry stations on the ground. The truss frame supporting each observatory panel is a novel hybrid structure consisting of a bottom graphite/epoxy tubular triangle and rigidized inflatable Kevlar tubes connecting the top observatory panel and the bottom triangle. Attitude control and station keeping functions will be performed by a system of momentum wheels in the bus and four propulsion modules located at the compass points on the periphery of the observatory dish. Each propulsion module has four monopropellant thrusters and four hydrazine arcjets, the latter supported by either a photovoltaic array or a radioisotope thermoelectric generator. The total mass of the spacecraft is about 20,500 kg.

**Introduction**

The objective of this project is to design a large orbiting radio telescope capable of resolving astronomical objects in greater detail than possible with ground-based facilities. The telescope would be placed in a geosynchronous orbit and operate in a Very Long Baseline Interferometry (VLBI) scheme observing wavelengths in the centimeters. A high-orbit-based VLBI system offers several obvious advantages over ground-based systems:

- (1) Effective aperture of the system can be significantly increased providing three to six-fold improvement in angular resolution or at least an order of magnitude increase in the areal resolution. The ultimate limit may be set by interstellar scintillation.
- (2) Due to the telescope's orbital motion, the u-v baseline plane is increased and well-filled, permitting a higher dynamic range in the maps.
- (3) The projected baselines change faster than those of ground-based arrays and, therefore, imaging of rapidly changing sources (that vary on time scales of less than a day) would be possible.
- (4) With an orbiting antenna, problems associated with atmospheric radiation and/or absorption, and radio noise caused by high-energy particles striking the outer layers of the ionosphere can be controlled or eliminated.
- (5) For certain large baselines located outside the Earth's atmosphere, a high degree of phase stability should be achievable.

The following are some of the assumptions and technical requirements established for the PARAS project:

1. The radio telescope will use a phased array antenna. This may greatly simplify structural and construction aspects of the antenna. Aiming the antenna at different radio sources will be done by electronic phasing without maneuvering in space. Also, phasing may possibly compensate for small deformations in the antenna surface.

2. The spacecraft will initially be placed in the geostationary orbit and the observatory surface will always face away from the Earth side with a  $0.1^\circ$  accuracy.

3. The antenna will have a large diameter, between 100 and 150 m, to achieve high sensitivity and a high degree of directivity.

4. The antenna will operate in the VLBI scheme in conjunction with the major ground-based radiotelescopes.

5. The antenna will observe in the centimeter range. Exact wavelengths and electronic design will be selected at a later time. Preliminary selections are 1.35 cm (22 GHz) and 18 cm (1.7 GHz).

6. While the antenna is not required to maintain exactly the same location over the Earth, the antenna position, velocity, and acceleration have to be determined and recorded with errors less than 10 m for position, 1 cm/sec for velocity, and  $10^{-5}$  cm/sec<sup>2</sup> for acceleration. From the radioastronomy data itself, it should be possible to determine the antenna's orbital parameters even more accurately.

7. The radiotelescope components will be launched into low Earth orbit (LEO) by the National Launch System (NLS) having a cargo bay 27-m long and 6.7-m in diameter. In LEO, the collapsed modules will be deployed and the radiotelescope will be robotically assembled. The complete facility will then be transferred to geosynchronous orbit by a low-thrust propulsion system, using either an orbital transfer vehicle or the radiotelescope's own propulsion system.

8. The observatory life will be 10 years.

9. A technology level projected for 2010 may be used in the design process.

## Design Overview

To meet objectives of this project we propose a large, 150-m diameter phased array antenna consisting of planar arrangement of 655 hexagonal modules (Fig. 1). Each module contains a 6.7-m hexagonal panel with printed circuitry as the observational dipole array and a fiber optics interconnection system. The correlation receiver located on the back of each panel preprocesses the signals from each panel before they are sent by fiber optics to the central computer in the bus module at the center of the entire antenna. Each module has its own power supply system consisting of gallium arsenide solar arrays on the front and back sides of the panel, a charge/discharge controller, and a sodium-sulphur battery. The truss frame supporting each panel is a hybrid structure consisting of a bottom triangle made of graphite-epoxy tubes and rigidized inflatable Kevlar tubes connecting the top panel and the bottom triangle. The modules are fastened together using connectors located on three corners of the triangular base structure.

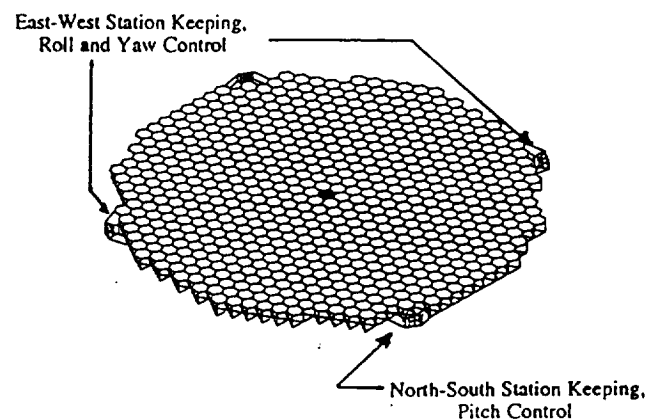


Fig. 1 PARAS configuration

The central bus houses its own power supply system and various subsystems including a central computer for spacecraft operations, data processing, communications, attitude control, and guidance systems. Attitude determination and control will be performed by a system of star trackers, sensors, gyroscopes, and momentum

wheels. Station keeping will be exercised by four clusters of chemical and arcjet thrusters located at compass points on the antenna dish.

### Structures

The structure of the spacecraft must be able to support the observatory panels and be stiff enough so as not to deflect more than 3 cm from a reference plane under operating conditions. Also, it should not plastically deform under accelerations caused by thrusters during orbital transfer or orbital corrections. Emphasis has been placed on strength, durability, reliability, self-deployability, and ease of assembly while also trying to minimize the total mass. The observatory is designed to be launched in a cylindrical container 27-m long and 6.7-m in diameter. The launch vehicle is assumed to have a launch capacity of at least 30 metric tons.

Five preliminary structural designs break down into three groups:

1. Self-deployable truss structures: box truss and tetrahedral truss.
2. Self-deployable non-truss structures: Inflatable raft and wrap rib design.
3. Non-self-deployable modular hexagonal truss design.

Both nontruss concepts, inflatable raft and wrap rib design, have been found to have the lowest structural mass, 3000 kg and 2500 kg, respectively; however, consideration of stiffness, reliability, ease of assembly, and launch packing efficiency lead to a conclusion that the modular truss can provide the best solution for the observatory. This is the only design that cannot deploy itself into a complete supporting structure for the observatory. All 656 sections of truss are unfolded out of the launch vehicle in LEO and then are robotically snapped together like building blocks to construct the 150-m diameter structure. The 6.7-m hexagonal observatory panels are used as part of the structure. At three corners of the hexagon are 5.8-m tubes which connect the panel to a triangular truss directly beneath it; the triangular truss is composed of similar tubes. Cross wires between the panel and the triangle add torsional stability to the module. To reduce mass of the modular

truss, the initially selected 5.8-m long vertical graphite epoxy tubes have been replaced with rigidized inflatable Kevlar tubes, resulting in a hybrid module design (Figure 2). These tubes will be folded under the observatory panels during launch. Upon removal from the cargo container and exposure to the sun, a chemical within the tube will sublime and inflate the tube to a desired pressure. After a few hours of curing, the Kevlar becomes rigid and the module can be attached to the truss. The complete configuration is assembled radially in a spiral-like fashion, starting from the central bus. When the modules are joined together to form a complete truss, there are three vertical members arranged in a cluster at each attachment point. This allows the use of the inflatables, since the vertical beams are redundant structural members. If one of the inflatables forms with a dimple or crease, which could make it more susceptible to failure, there are two other members to back it up. Using inflatable vertical members reduces the mass of the modular truss structure to less than the mass estimate for the wrap rib design.

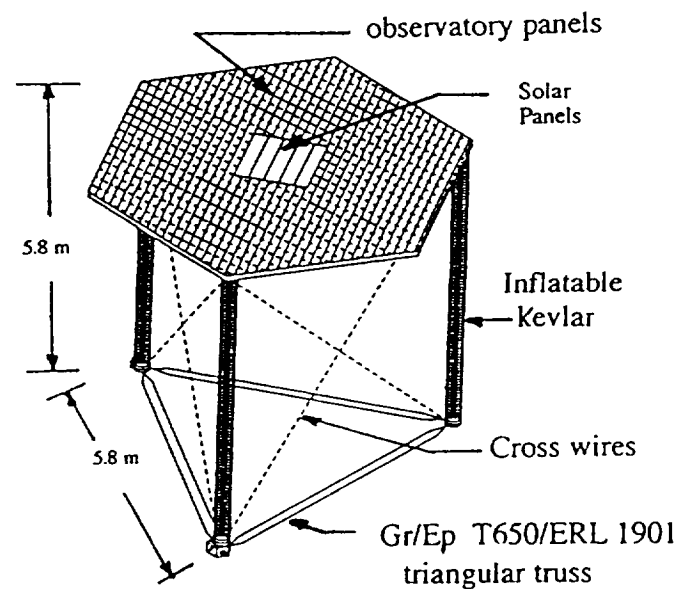


Fig. 2 Observatory module

The triangular base of each module is made of T650-35/ERL 1901 graphite epoxy tubes, 2.5-cm in diameter and 2-mm thick. Anodized aluminum foil coating plus an additional spray of 1 micron of  $\text{SiO}_2$  meets the absorptivity, emissivity, and radiation resistance

requirements (Figure 3). The inflatable tubes are 30-cm in diameter and composed of reinforced prepreg Kevlar matrix developed by CIBA-GEIGY for the European Space Agency. A Kapton foil can act as a gas barrier, and a metallic aluminum layer can serve as a thermal control coating for the tube (Figure 3). Cross wires can be made of graphite fibers impregnated with Teflon and coated with  $\text{SiO}_2$ . The bottom and top joints are made of titanium and serve as caps for the inflatables. Each joint has a male and a female part that can be used to snap the modules together into the truss (Figures 4 and 5). Each observatory panel is made of a structural component and a facesheet used as the base for the antenna circuitry. Several sandwich configurations have been investigated for the design of the observatory panels. They include structural foam core with a polyimide film facesheet, various Nomex honeycomb cores with graphite/epoxy faces, and Kevlar core with Kevlar faces. The final selection (based on mass, strength and thermal properties) resulted in the adoption of a honeycomb structural foam panel (made of Rohacell 311G or its future derivatives) as a structural component and a polyimide film (such as Upilex S) as a facesheet.

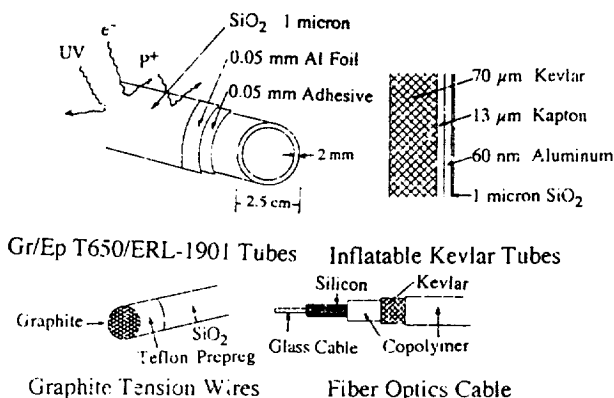


Fig. 3 Selected materials

Structural calculations of the whole configuration included finite element static and dynamic analyses. Because of the complex nature of the truss and the large number of members, a complete and exact model would have required very large computer calculation time. Therefore, to reduce calculation time, it was necessary to simplify the structure and reduce its size, while maintaining sufficient accuracy of the solution. Using

node restraints to simulate the presence of additional structure allowed modeling of only a quarter of the antenna dish. The actual elements of the modules were represented using beam, plate, and node fastener elements. Five load cases have been investigated: (1) solar pressure load, (2) thrusters firing in the east-west direction, (3) thrusters firing in the north-south direction, (4) thrusters firing in the vertical (z) direction, and (5) orbital transfer using a thrust of 500 Newtons applied at the bus location. All member loads have been found to be well within the maximum loads. For case one, a non-thrusting case pertaining to astronomical observations, maximum surface deflection at the perimeter was 6 mm, well within the allowable value. During an orbital transfer, the deflection is 1.38 m; however, all the member loads are very low.

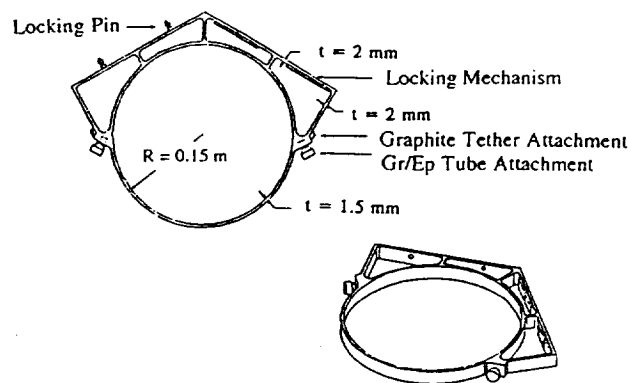


Fig. 4 Bottom connector joints and member attachments

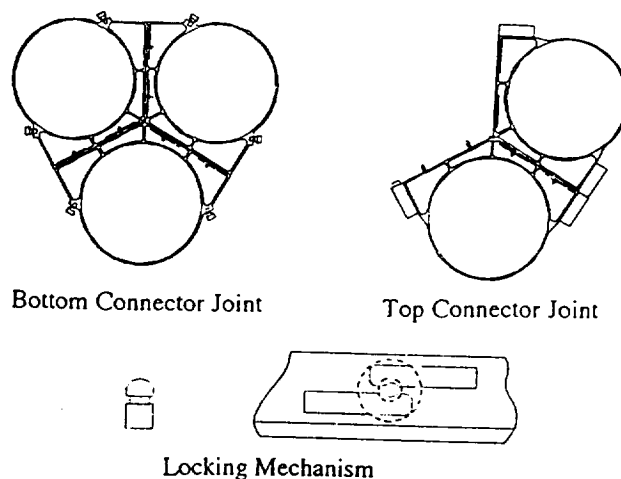


Fig. 5 Connector joints and locking mechanism

## Electronics

The phased array receiving antenna will use printed circuitry technology. A pattern of dipoles, patch elements, and circuitry will be etched onto the surface of the polyimide thin sheets. An additional 25  $\mu\text{m}$  of film will cover the circuitry to protect it from radiation damage. The size and pattern of the antenna elements will be determined by electronic and astronomical considerations.

An electronic assembly, including a low-noise receiver and processor unit for phase shifting, will be located on the back side of each observatory panel. The intermediate frequency (IF) data will be channeled via fiber optics to the central control unit in the bus and down-linked directly to telemetry stations on the ground. A clock reference for the PARAS antenna will be based on hydrogen maser oscillators (stable to within 20 femtosec) at the telemetry stations on the ground and will be relayed directly to the PARAS. The IF data will be recorded on magnetic tape on the ground-based telemetry stations and later correlated with the data recorded by the cooperating ground-based radio telescopes at a processing facility in the U.S. or elsewhere.

Each module will have its own autonomous electrical power supply of 80W consisting of photovoltaic solar arrays, a recharging sodium-sulphur battery, and a charge/discharge controller. Two fixed (non-steerable) arrays employing gallium arsenide on germanium (Ga As/Ge) substrate solar cells will be mounted on the front and back side of the panel. The front array, placed at the center of the panel, has an area of  $0.64\text{m}^2$ ; the array mounted on the back has an area of  $1.43\text{m}^2$ . An energy storage system using highly efficient sodium-sulphur batteries was selected to level loads and to provide power during eclipse periods and when the solar incidence angle is too high ( $>70^\circ$ ). Such batteries, currently under development, should have high energy density (around 200 W hr/kg) and allow for over 2500 cycles with an operational depth of discharge of 80%. Each module will be equipped with a battery having 500 W/hr capacity. The excess energy will be radiated directly to space.

## Spacecraft Bus

The central bus houses the central computer for spacecraft operations and data processing, the primary attitude control hardware, the communications system, thermal control subsystem, and bus power supply system. The central computer will act as the spacecraft's data and information relay/processor. The signals received from the observatory modules, coherently amplified and frequency translated, will be multiplexed for transmission to a ground station at a faster rate than the signal itself. By using information buffers, only a minimum data can be lost. Telemetry and timing signal information uplinked from the ground station will be fed to the control systems.

The communications system will use techniques similar to those developed for the Tracking and Data Relay Satellite System (TDRSS). Downlink and uplink frequencies will be around 14 GHz and 15 GHz, respectively, and a relatively high data rate, of perhaps 100 M bits/sec, array may be needed. The system will use two 1.8 m parabolic antennas and require about 200 W.

The average power required for the bus system's operation is estimated at 900 W with short peaks reaching 1250 W. This power will be supplied by a Ga As/Ge photovoltaic array/nickel hydrogen battery system. Eight solar arrays, each  $1.62 \times 1.06$  m, will be placed on top of the bus panel, and two solar arrays,  $1.9 \times 3.34$  m each, will be mounted on the back side, angled down  $46^\circ$  from the observing plane. The secondary power storage will contain two 90-cell  $\text{NiH}_2$  batteries having a capacity of 60 Ahr. Since the computer and communications system work efficiently at voltages such as 120 V, the solar arrays will be wired to produce a voltage of  $124.5 \pm 7$  volts.

The thermal control system will maintain the bus equipment at operable temperatures. A semi-passive system incorporating thermal control coatings and a multilayer insulation (MLI) blanket surrounding the hexagonal housing inside the bus module may provide 95% of the temperature control. Additional fixed conductance heat pipes and space radiators will provide more accurate temperature control for selected electronics.

The bus design is primarily dictated by placement of the components to be housed inside. A smaller hexagonal cylinder, 2.3-m in diameter and 2-m long, will contain

those components (Figure 6). This housing structure consists of aluminum panels attached to a longeron-stringer frame with three floor panels, one for the power control and batteries, one to mount the momentum wheels, inertial measurement units and related computers, and a bottom panel for the central control computer, data processor, and communications package. An important consideration in designing the bus internal layout is a desire to keep the center of the mass-to-optical-center distance as short as possible in order to minimize the solar radiation pressure torque.

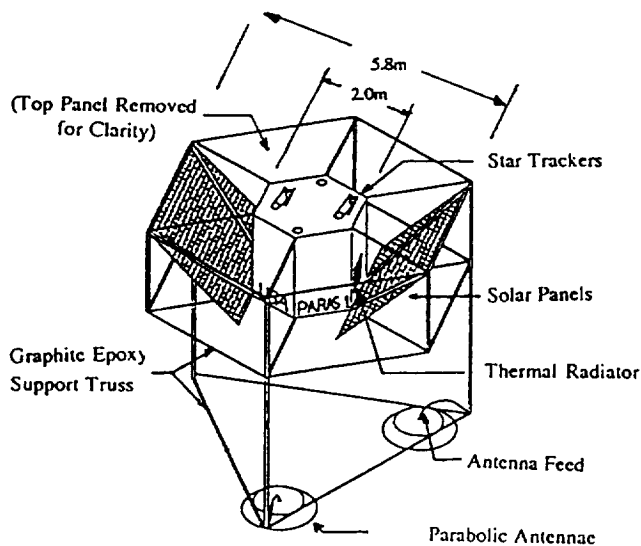


Fig. 6 Spacecraft bus

### Station Keeping and Attitude Control

The main sources of orbital perturbations will be solar radiation pressure, gravity gradient torques due to the Moon and Sun, gravitational effects due to varying Earth/Moon/Sun orientation, and the oblateness of the Earth. For a spacecraft such as PARAS that has a large surface area extended in one plane, the primary perturbing force is the solar radiation pressure; indeed, the solar pressure torques (pitch and roll) dominate the dynamic behavior of the spacecraft. For conventional geostationary satellites, the north-west station keeping (NWSK) requirements are significantly larger than those for the east-west station keeping (EWSK). However, for the PARAS, both the EWSK and NWSK maneuvers

require very similar  $\Delta V$ , because the Earth's oblateness and the solar radiation pressure cause the spacecraft to drift east or west of its designed Earth longitude. Numerical calculations have indicated that over the 10 year mission the required  $\Delta V$ 's are:

NSSK -- 483.8 m/s

EWSK -- 427.1 m/s

The  $\Delta V$ 's required for momentum dumping and maneuvering are:

Roll -- 0.126 m/s-year

Pitch -- 0.06 m/s-year

Yaw -- ~ 0.0 m/s-year

Attitude and orbital parameters (position, velocity, and acceleration) will be determined by a system composed of four sun sensors, two fixed-head horizon sensors, two fixed-head star mappers, and two inertial measurement units, as well as ground-based observations transmitted to PARAS over the 14-GHz uplink channel. Information coming from these sources can be combined in the PARAS central control computer, which computes PARAS position, controls momentum wheels, and activates, if necessary, the appropriate thrusters. The data on position and orbital parameters of PARAS are transmitted to the ground station via the 15-GHz downlink.

The primary attitude control will be exercised by four momentum wheels arranged tetrahedrally to offer control on all three axes with a safe degree of redundancy. The assembly can generate torque of 1 Nm and store 700 Nms of angular momentum. The system will maintain a  $0.1^\circ$  accuracy and restrict angular drift rate to  $0.01^\circ/\text{sec}$ . Momentum wheels controlling roll will typically need desaturation five or six times weekly. The wheels controlling yaw may need only two or three desaturations over the mission life. The wheels controlling pitch will randomly need desaturation, probably no more than 20 times per year. All momentum dumping operations will be performed by a monopropellant hydrazine thruster system composed of 16 engines in four clusters on the periphery of the spacecraft. The thrusters will act as backup attitude control devices should the momentum wheels fail or unexpectedly shut down because of overspeeding or overheating.

Station keeping maneuvers will be accomplished by hydrazine arcjet thruster system consisting of 16 engines in four clusters. The north-south corrective maneuver (NSSK) will take place every 405 days; over a 52-day period, thrusters will fire for six hours per day (three about apogee and three about perigee). The east-west (EWSK) maneuvers will be done every two weeks; over a 3-day period, thrusters will fire for three hours per day.

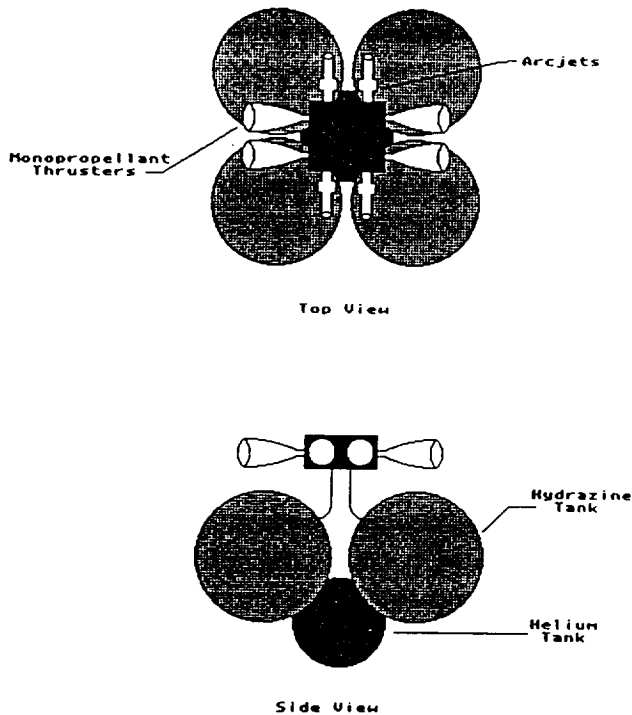


Fig. 7 Thruster cluster

The hybrid propulsion system consisting of 16 chemical monopropellant and 16 arcjet engines has been selected on the basis of detailed trade studies comparing chemical, ion, arcjet, and resistojet options. The main considerations were low total mass, reliability, and thruster firing times possibly not exceeding two or three hours per day. The 32 thrusters are divided into four equal size clusters, each including four chemical and four arcjet units (Figure 7). Each cluster rests at a compass point on the PARAS dish and is mounted to a special truss attached to either two or more joints of the adjacent observatory modules. The clusters on the east and west compass points perform the north-south functions and pitch control. The clusters on the north and south points

perform the east-west functions as well as roll and yaw control (Figure 8).

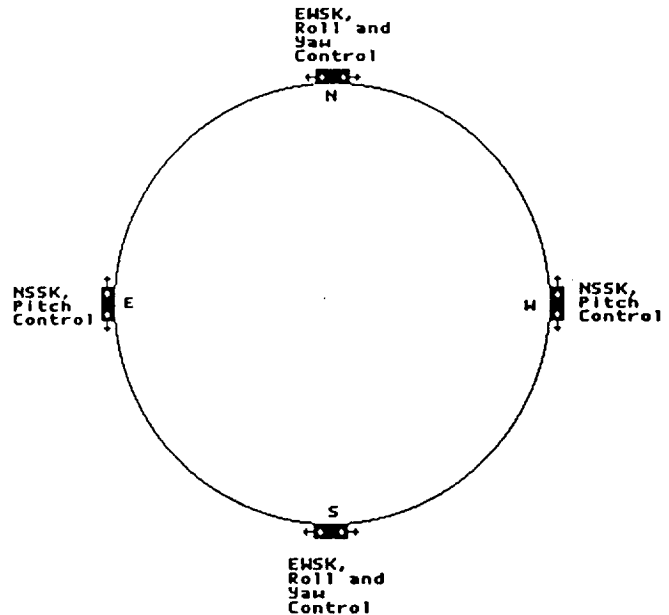


Fig. 8 Thruster assignments

The proposed electrical power station for the arcjet engines consists of the radioisotope thermoelectric generators (RTG) and sodium-sulfur battery storage. Each compass point propulsion cluster has its own power module: the east-west points have one 625-W MOD series generator and 16.4-kW-hr (13.1 kW-hr available) battery. The north-south points have two 625-W MOD RTG's and 28.1-kW-hr (22.5 kW-hr available) battery. The key characteristics of the thrusters are given in Table 1.

Table 1 Thruster characteristics

|                          |                                |
|--------------------------|--------------------------------|
| $N_2H_4$ thrusters       | Arcjet                         |
| Thrust 0.05 N            | Thrust 0.5 N                   |
| Isp 229 sec              | Isp 760 sec                    |
| Chamber pressure 6.8 atm | Thruster efficiency 40%        |
| Pressurizing gas He      | Input power 5 kW               |
|                          | Power processor efficiency 95% |

Table 2 PARAS mass summary

|                     |           |
|---------------------|-----------|
| Observatory Modules | 15,500 kg |
| Bus Module          | 710 kg    |
| Propulsion System   | 4,280 kg  |
| Total mass          | 20,490 kg |

Table 3 PARAS main characteristics

|   |  |
|---|--|
| Antenna type                                  | Phased array   |
| Nominal diameter                              | 150 m  |
| Observing wavelength<br>(tentative selection) | 1.35 cm, 18 cm   |
| Mapping time                                  | A few hrs to 48 hrs                                    |
| Orbit   | Geosynchronous   |
| Propulsion/station<br>keeping                 | 16 monopropellant<br>thrusters<br>16 hydrazine arcjets |
| Power systems:<br>Observatory                 | GaAs/Ge arrays and<br>NaS battery                      |
| Central bus                                   | GaAs/Ge arrays and<br>NiH <sub>2</sub> battery         |
| Arcjets                                       | RTG and NaS battery                                    |
| Operational lifetime                          | 10 years   |
| Total mass                                    | 20,500 kg  |

Table 4 Expected Astronomical Performance

|                    |  |
|--------------------|--|
| Linear resolution: |  |
| at 1.35 cm         | 30 microarcsec which<br>corresponds to 4 light<br>days at the galaxy M87       |
| at 18 cm           | 0.1 milliarcsec  |
| Sensitivity:       | if 24-hr observation, a<br>dynamic range map of<br>100 to 1 may be<br>achieved |
|                    | at 1.35 cm for 25-50 sec   |
|                    | at 18 cm for 5-10mJy<br>sources  |

## PRESSURIZED LUNAR ROVER (PLR)

**PLR I: Kenneth Creel, Jeffrey Frampton, David  
Honaker, Kerry McClure, Mazyar Zeinali**

**PLR II: Manoj Bhardwaj, Vatsal Bulsara, David  
Kokan, Shaun Shariff, Eric Svarverud, Richard Wirz**

### Abstract

The objective of this project was to design a manned pressurized lunar rover (PLR) for long-range transportation and for exploration of the lunar surface. The vehicle must be capable of operating on a 14-day mission, traveling within a radius of 500 km during a lunar day or within a 50-km radius during a lunar night. The vehicle must accommodate a nominal crew of four, support two 28-hour EVA's, and in case of emergency, support a crew of six when near the lunar base. A nominal speed of 10 km/hr and capability of towing a trailer with a mass of 2 mt are required. Two preliminary designs have been developed by two independent student teams.

The PLR I design proposes a 7-m-long cylindrical main vehicle and a trailer which houses the power and heat rejection systems. The main vehicle carries the astronauts, life support systems, navigation and communication systems, lighting, robotic arms, tools, and equipment for exploratory experiments. The rover uses a simple mobility system with six wheels on the main vehicle and two on the trailer. The nonpressurized trailer contains a modular radioisotope thermoelectric generator (RTG) supplying 6.5 kW continuous power. A secondary energy storage for short-term peak power needs is provided by a bank of lithium-sulfur dioxide batteries. The life support system is partly a regenerative system with air and hygiene water being recycled. A layer of water inside the composite shell surrounds the command center allowing the center to be used as a safe haven during solar flares. The PLR I has a total mass of 6197 kg. It has a top speed of 18 km/hr and is capable of towing 3 metric tons (in addition to the RTG trailer).

The PLR II configuration consists of 2 4-m-diameter, cylindrical hulls which are passively connected by a flexible passageway, resulting in the overall vehicle length of 11 m. The vehicle is driven by eight independently suspended wheels. The dual-cylinder concept allows



articulated as well as double Ackermann steering. The primary power of 8 kW is supplied by a dynamic isotope system using a closed Brayton cycle with a xenon-hydrogen mixture as the working fluid. A sodium-sulfur battery serves as the secondary power source. Excess heat produced by the primary power system and other rover systems is rejected by radiators located on the top of the rear cylinder. The total mass of the PLR II is 7015 kg.

### Pressurized Lunar Rover I

#### Configuration

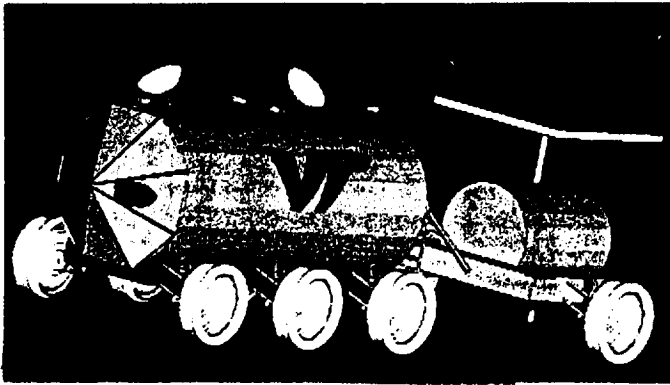


Fig. 9 View of PLR I

Simplicity and low total weight have been the driving principles behind the design of PLR I. The overall configuration consists of a 7-m-long, 3-m-diameter cylindrical main vehicle and a two-wheeled trailer (Figure 9). The cylinder of the main body is capped by eight-section, faceted, semi-hemispherical ends. The trailer contains the RTG power source and is not pressurized. The shell of the main body is constructed of a layered carbon fiber/foam/Kevlar sandwich structure. Included in the shell is a layer of water for radiation protection. The layer of water extends from the front of the rover over the crew compartment and creates a safe haven for the crew during a solar flare-up. The carbon fiber provides the majority of the strength and stiffness and the Kevlar provides protection from micrometeoroids. The Kevlar is covered with a gold foil and multi-layer insulation (MLI) to reduce radiation degradation and heat transfer through the wall. A thin thermoplastic layer seals the fiber and provides additional strength.

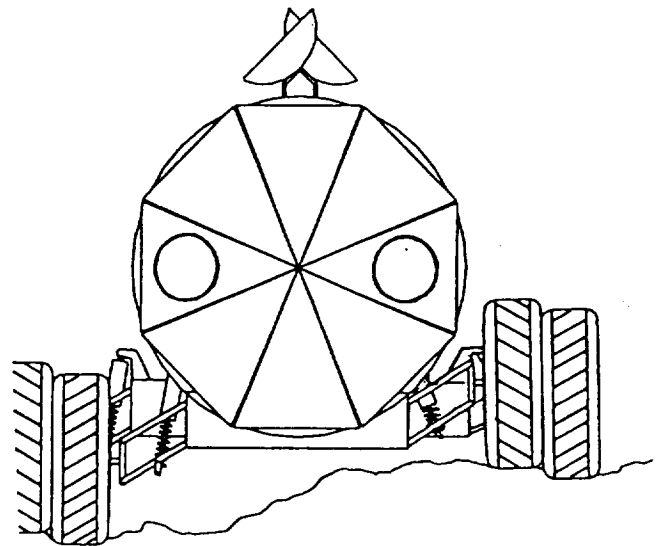
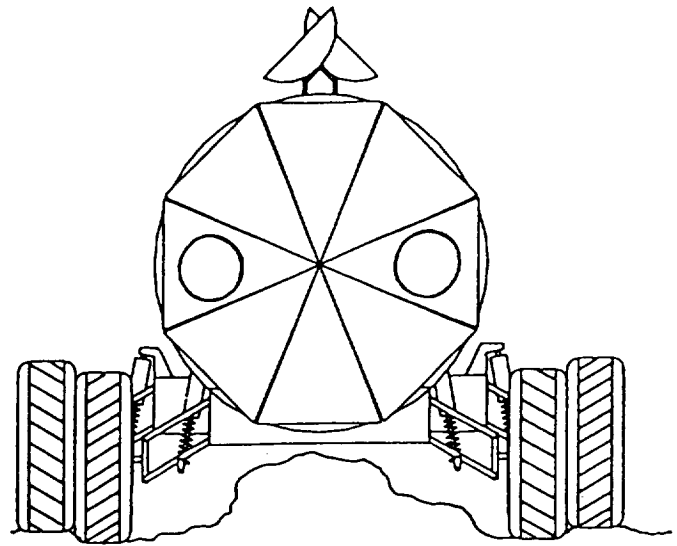


Fig. 10 Front view of main body

#### Mobility

A double A-arm suspension provides a ground clearance of more than 0.85 m, reliability, stability, and total independence of the wheels. The A-arms are connected to the main body with simple pivot joints that allow for up-and-down motion only (Figure 10). They are also connected to the kingpin by the same kind of joints. The A-arm shape allows for the placement of the shock

inside the arms. The chosen design provides effective performance with minimal mechanical complexity, thus minimizing the chance of suspension failure. Six wheels are chosen on the basis of load and mobility considerations. Tires made of a composite flexible plastic matrix are proposed. They have a 1.5-m-diameter and a width of 0.5 m and would experience a sinkage of approximately 5 cm in the soft lunar soil. The high performance/high torque brushless motors (Inland RBE-6202-B50) are mounted with harmonic drive units inside each of the wheels. The rover is steered by electrically varying the speeds of the wheels on either side of the rover. Each wheel supplies a torque of 521 Nm to turn the rover within its own length with zero forward velocity. The tire's rounded cross-sectional shape should minimize friction during a turn. To slow or stop the rover, the motors are used as generators charging the batteries.

### Interior Layout

A few interior layouts of the rover are shown in Figure 11. The command center is located in the front two meters. The command center is also used as a safe haven in case of a solar flare warning. The exterior shell is shielded with a layer of water and the interior is separated by an aluminum divider. When there is no danger, the aluminum divider is kept open to create more space. Immediately behind the command center is the lab area on the right and the first pair of bunks on the left. This area is also two meters in length. The next section contains the galley on the right and storage on the left. The bathroom is adjacent to the galley. An airlock and the remaining two bunks are located in the rearmost portion of the rover. When not in use, the two upper bunks can be folded down to create two couches for the crew to relax or eat on.

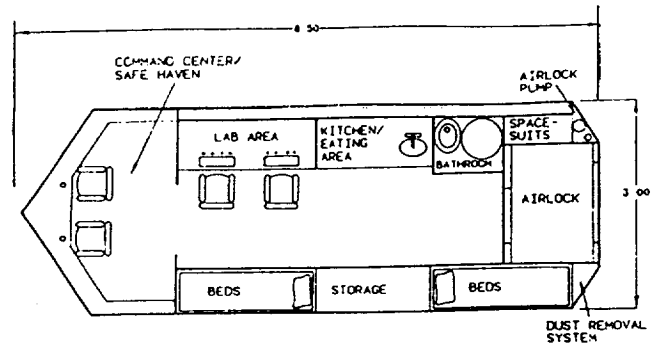
### Power System

The power system supplies power to four major areas:

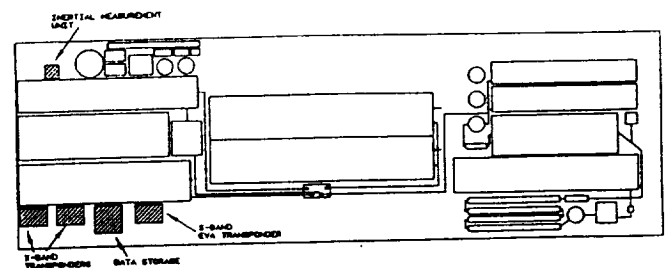
- Life Support 1.5 kW
- Drive System 4.5 kW ave./8 kW max
- Communications/ Controls/ Lights 1.0 kW
- Battery Charging 0.1 - 0.2 kW

Average and peak power requirements have been established at 6.5 kW and 9.5 kW, respectively. These values have been derived by examining power profiles for typical short duration missions (such as a 1-day soil

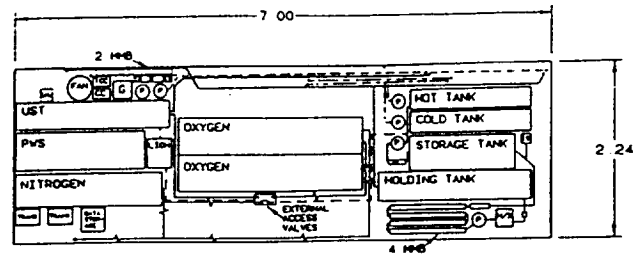
### Main interior layout



### Underfloor electronic layout



### Floor layout



### Ceiling computer layout

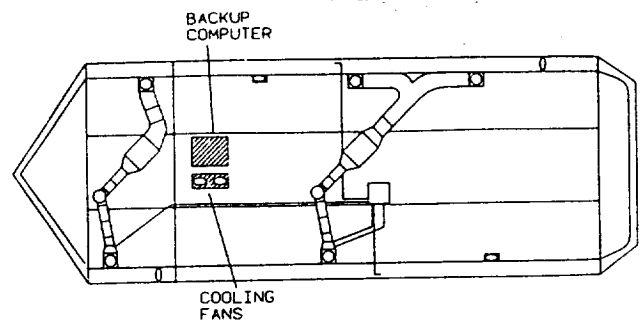


Fig. 11 Interior layouts

sample mission) and long duration missions (e.g., 12-day optical interferometer mission). A trade study of photovoltaic, dynamic isotope and radioisotope thermoelectric generator (RTG) power systems has resulted in selection of the modular silicon-germanium RTG as the superior candidate. The RTG provides the needed redundancy and survivability without a need for multiple space parts. With the modular RTG, the total power is supplied by several modules. If a single module fails, the rover continues to be operational and returns to the lunar base using the remaining power.

The RTG will be liquid cooled. A  $9 \text{ m}^2$  radiator is positioned on a boom on top of the RTG housing and is connected to the RTG via a thermal joint which allows the radiator to be steered. A critical design factor with the RTG is crew safety. This factor, in addition to versatility, led to the use of the RTG in tow. The trailer (Figure 12) houses the RTG and its required thermal controls. The RTG's external deployment requires less radiation shielding. The latter consists of multi-layer foil which, in combination with the main rover's foil shielding, provides adequate radiation protection for the crew members. The RTG's external positioning adds a significant versatility. For example, the RTG power can be used to charge lunar base batteries when the rover is not in operation. Also, docking to the lunar base will be facilitated with the trailer unhooked.

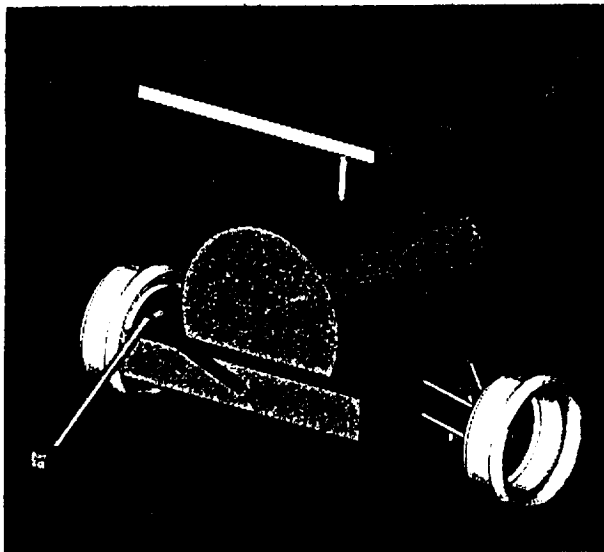


Fig. 12 View of the trailer

Secondary power and peak power are provided by a bank of batteries that are continuously charged by the RTG. A small array placed on the PLR thermal control radiator shield charges the batteries if the RTG is detached. The lithium-sulfur-dioxide-type battery is chosen because of its high energy density and degree of discharge. There are ten separate stacks, each containing 10 cells in series that supply 6 kW-hrs. The batteries are placed under the crew beds in the PLR's midsection.

### Life Support System

The Life Support System (LSS) breaks into five modules:

- Air Revitalization Module (ARM)
- Water Management Module (WMM)
- Food Provision Module (FPM)
- Waste Disposal Module (WDM)
- Crew Health Module (CHM)

The Air Revitalization Module (ARM) maintains the cabin atmosphere at a temperature of 295 K, relative humidity of 50%, pressure of 1 atm and composition of 79%  $\text{N}_2$ /21%  $\text{O}_2$ . To maintain temperature, the ARM removes excess heat due to crew metabolism, electronics, solar radiation, lunar radiation, and lunar-reflected solar radiation. Thirty layers of multi-layer insulation (MLI) reflect solar radiation and greatly reduce conductive heat transfer. The maximum excess heat load is 2540 W. Eleven fans circulate air throughout the PLR and provide a uniform temperature distribution. Two condensing heat exchangers extract excess heat and humidity. A  $3.272 \text{ m}^2$  radiator, which is augmented by a thermal heat pump that utilizes a Rankine-Rankine cycle, rejects the excess heat. The excess humidity is sent to the Water Management Module (WMM).

To maintain atmospheric pressure and composition, the ARM monitors cabin pressure and composition with pressure taps and a mass spectrometer. Control software in the LSS control computer uses the measurements to decide if, and how much, nitrogen and oxygen should be released into the cabin from storage tanks. The ARM also removes contaminants: lithium hydroxide sorption beds remove carbon dioxide; platinum catalysts remove carbon monoxide; charcoal and activated charcoal sorption beds remove odors and other contaminants.

The Food Provision Module (FPM) provides food and drink, which are supplied by the lunar base. It is assumed that the supplied food is dehydrated, canned, and/or storable at ambient conditions. An energy-efficient microwave prepares food.

The Water Management Module (WMM) provides potable water for drinking, cooking, EVA, cleaning, and hygiene purposes. The design calls for a recycling system consisting of a potable water supply and a water recycling system. The potable water supply consists of a storage tank containing 0.3 m<sup>3</sup> of water for drinking, food preparation, and EVA purposes. The water recycling system utilizes heat, a series of four multi-media sorption beds (1-in radius, 40-in long), an alcohol catalyst, and iodine to purify waste water. The flow rate through the beds is 79 cc/min, which gives a contact time of 26 minutes. Due to media usage rate, one multi-media bed exhausts its media every 140 hours of processing, roughly 10 days in operation.

The Waste Disposal Module (WDM) disposes of waste materials in a sanitary method that ensures crew health and stores wastes in such a manner that facilitates recycling at the lunar base. Dry wastes, such as trash, are disposed of by a hand cranked compactor. Human wastes are collected and stored by a design that combines the earth toilet's simplicity and the space station toilet's ease of recycling and water savings. A personalized cup collects urine and a water-iodine mixture carries the urine to the urine storage tanks. Collection bags collect feces and vomitus.

For crew morale and fitness, the design calls for, among others, an exercise bike that recharges some of the batteries during operation. For crew health, the design focus is on radiation shielding. The shielding protects the crew from RTG radiation, nominal solar radiation, micrometeors, and solar flare events.

Table 1 LSS mass and power summary

|       |                  |                    |
|-------|------------------|--------------------|
| Mass  | 765 kg (empty)   | 1,490 kg (stocked) |
| Power | 1378 W (average) | 2,330 W (peak)     |

The mass total does not include the shielding.

## Electronic Systems

The electronic systems include communication, navigation, and computer systems.

The communication system provides direct voice, video, and data communication with Earth, person-to-person communication, and EVA short-range communication. For Earth-Moon communication, the system takes advantage of lunar relay satellites assumed to be orbiting the Moon. The system uses X-band (8400-8500 MHz), which has low power requirements yet provides a high data transmission rate of 20 Mbps, low quality television images, and overall good performance with proven technology. In addition, the system has the capability to communicate directly to Earth should a satellite fail. The on-board transponders allow simultaneous transmission and reception through two 0.9 m antennas. To communicate with crew doing EVA work, the PLR uses S-band and an omnidirectional 0.1 m whip antenna.

The navigation system directs the PLR through the lunar terrain and accurately determines its location on the Moon. The system uses a strapdown inertial measurement unit, consisting of three laser gyroscopes and three accelerometers, to measure the rotation and acceleration in all three dimensions. In addition, two star mappers mounted on the PLR exterior periodically correct the position. Four cameras mounted on the rover provide information on the local terrain. The rover also uses a laser rangefinder assembly to determine the distance to objects and, with the computer, generates a rough topological map.

The PLR computer is crucial for monitoring and controlling vehicle systems. The primary computer is installed in the command center. The PLR has a secondary computer capable of maintaining the basic needs of the rover. A bank of display screens shows camera, computer, and navigation system outputs.

The main characteristics for PLR I are presented in Table 6.

Table 6 PLR I main characteristics

|                        |                 |
|------------------------|-----------------|
| Nominal speed          | 10 km/hr        |
| Maximum speed          | 18 km/hr        |
| Maximum incline        | 35 deg.         |
| Minimum turn radius    | 7 m             |
| Ground clearance       | 0.85 m          |
| Range:                 |                 |
| at 10 km/hr            | 1680 km radius  |
| at 18 km/hr            | 3192 km radius  |
| Towing Capacity        |                 |
| (6 km/hr, 30 deg. max) | 4.2 metric tons |
| Nominal power          | 6.5 kW          |
| Maximum power          | 9.5 kW          |
| Total mass             | 6,197 kg        |

### Pressurized Lunar Rover II

#### Configuration

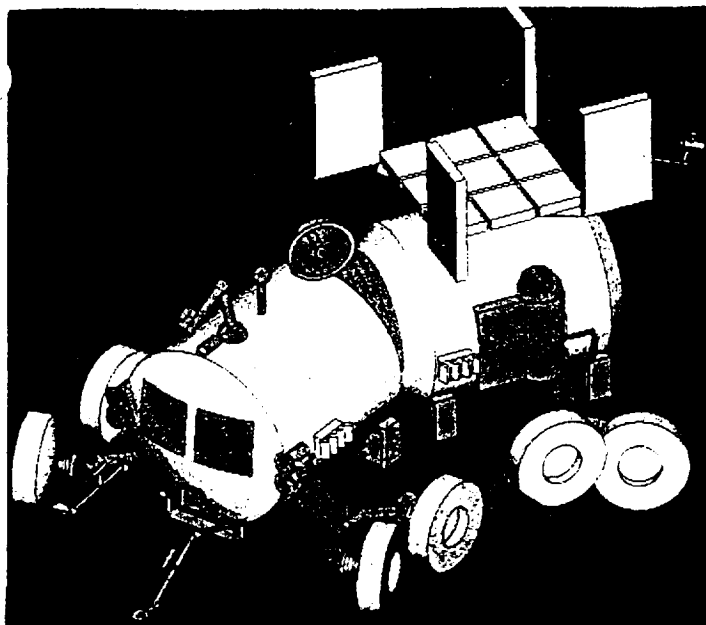


Fig. 13 View of PLR II

The PLR II configuration consists of 2 4 m-diameter, cylindrical hulls passively connected by a flexible pasageway, resulting in the overall vehicle length of 11 m (Figure 13). The rover's shell is made of two

graphite/epoxy laminates separated by a NOMEX honeycomb core. A multi-layer insulation and an aluminum bumper shield provide thermal barrier and micrometeoroid protection (Figure 14).

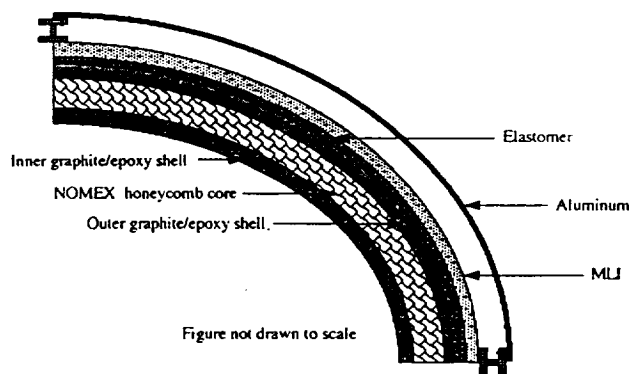


Fig. 14 Pressure hull cross section

#### Mobility

The cylindrical hulls are supported by aluminum saddles which are connected by an articulation joint (Figure 15). The joint controls yaw and allows for free pitch and roll between the two hulls. The articulated turning of the rover is controlled by a motor attached to the yaw axis. An unusual "pinned wheel" concept is chosen for improved mobility. Each side of each hull is supported by two wheels which are connected at their centers by a hollow cylindrical bar pinned at its midpoint (Figure 16). The bar is attached at the pin through a passive suspension system to the saddle. The bar ends are bent away from the hull making Ackermann steering possible. This configuration should allow a large degree of vertical motion by the wheels while still maintaining constant ground contact (Figure 17). The independent suspension consists of a double transverse wishbone suspension using two telescopic shock absorber-dampers balanced by springs.

A dual steering system, combining double Ackermann and articulated frame steering, has been chosen. As the steering wheel is turned, an electronic control system

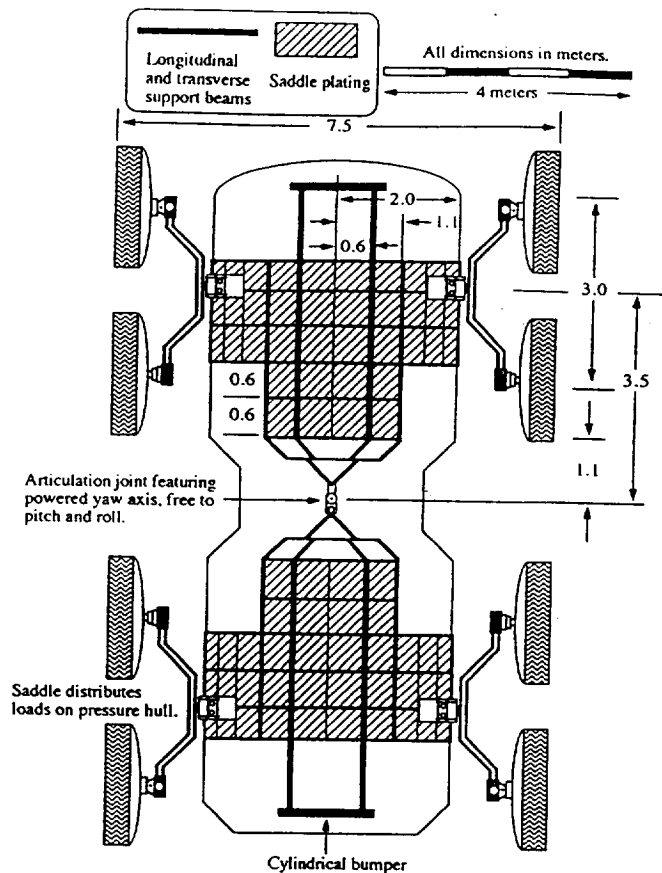


Fig. 15 Vehicle substructure

turns the front and rear wheel pairs (using motors mounted at the bar ends) and the articulation joint to produce the geometry for an ideal, neutral steer turn. This geometry produces a minimum turn radius of 9.4 m. However, after the articulated frame has been turned through its full angle, the ideal geometry may be sacrificed by turning the wheels further. This leads to a slight oversteer condition which will allow a tighter turn. In an emergency, the driver has the option of utilizing skid steering, since the wheels are already individually powered.

The wheel/tire assembly consists of the wheel well containing the drive motor as well as the wheel, tire, and required gearing and support (Figure 18). The drive motor rotates a 0.45 m radius rigid cylindrical frame that is rigidly connected to the back of the wheel. Slightly

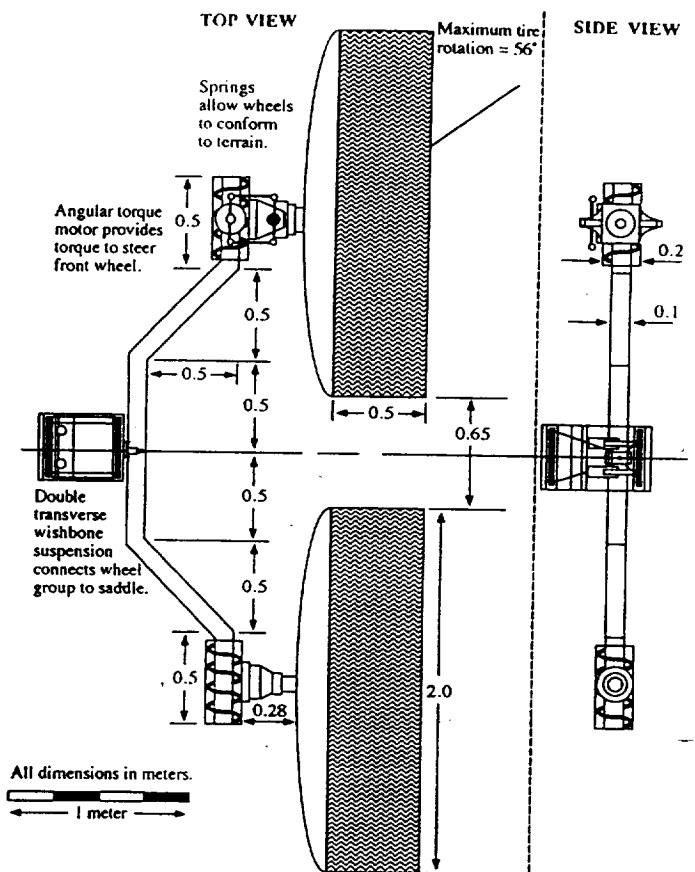


Fig. 16 Wheel group

elastic rings fill the area between the frame and the tire. These rings support the tire to enhance traction. The drive motors and articulation motor will have equal pull capabilities. High performance DC brushless motors with variable speed drive, rated at 600 Nm and 1.5 kW, will be mounted inside the hubs of the wheels. Smaller motors will be used for wheel turning.

### Power System

To determine power requirements, a few possible lunar missions were analyzed and their power profiles were estimated. These missions included a 14-day lunar survey, a four-day transport mission and a two-day search and rescue mission. It was established that a continuous power of 8 kW is needed; the peak power required if all

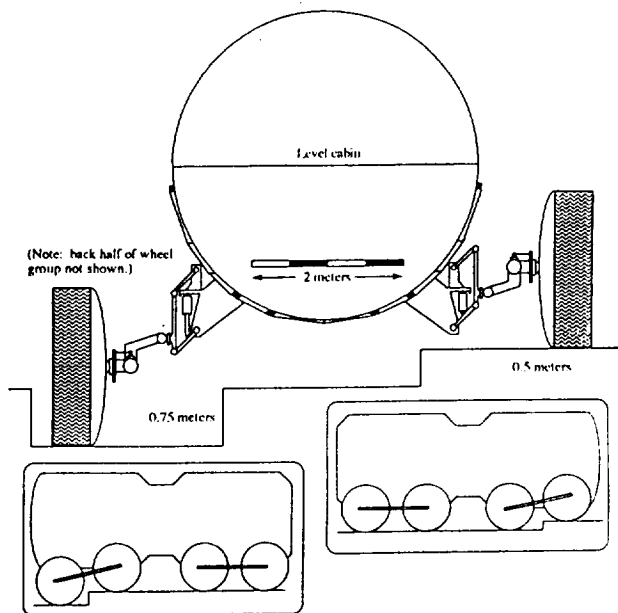


Fig. 17 Maximum suspension displacements

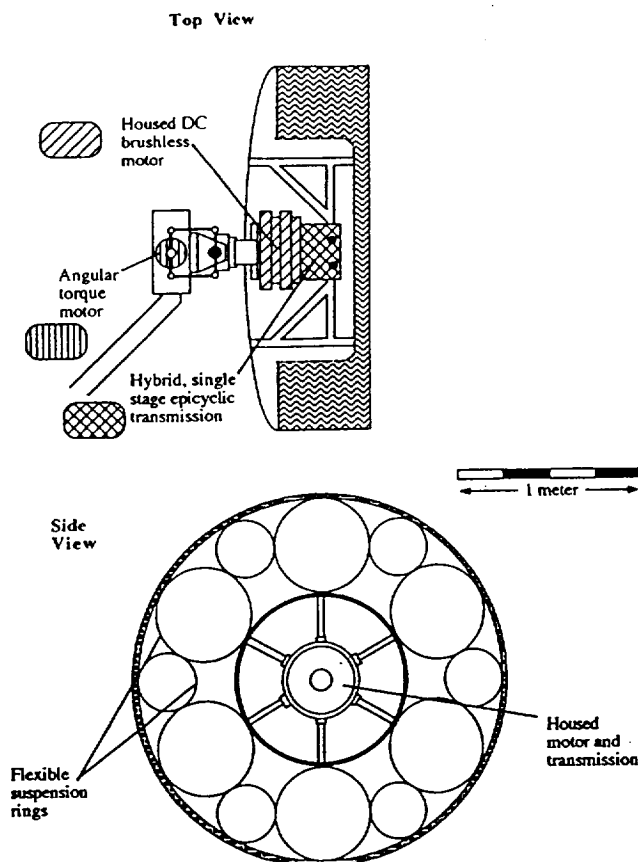


Fig. 18 Wheel assembly

eight wheels have to be driven at once would be 12 kW. The power system will consist of a 8 kW primary source and a 4kW storage capacity. A dynamic isotope power system (DIPS) using a closed Brayton cycle (CBC) has been chosen as the primary energy source. Eight plutonium 238 powered heat source units (HSU) will heat a xenon-hydrogen mixture used as a working fluid in the turboalternator compressor assembly generating electrical energy. The radiator of the CBC system has an area of  $15\text{m}^2$ . To protect the crew from the radiation given off by the HSU, a shield made of tantallum alloy will partially encase the HSU.

For secondary energy storage a sodium-sulfur battery, sized for 4 kWhr capacity has been selected.

### Thermal Control

Passive, semi-passive, and active thermal control techniques will be used to control the temperature inside the rover. The most critical part of the interior thermal design is the rejection of approximately 25 kW waste heat produced by the power system which is located in the rear module under the floor. The power system is carefully insulated with MLI, and 20 heat pipes serve to transport the heat to the  $15\text{m}^2$  space radiator on top of the rover. A climate control system will cool the interior during a lunar day and heat the interior (using waste heat from the power system) during a lunar night. The crew life support is provided by a partially closed environmental control system that reclaims air and water.

### Electronic Systems

The communications system allows for communication with the lunar base, with an option for direct communication with Earth via a lunar satellite link. The rover is fitted with a parabolic reflector dish for S-band transmission, and an omnidirectional antenna for local EVA communication.

The PLR II guidance, navigation and control subsystem consists of an inertial guidance system, an orbiting lunar satellite, and an obstacle avoidance system. In addition, the rover is equipped with a number of external fixtures including lights, telerobotic arms, cameras, manlocks, a docking fixture, and a scientific airlock.

Table 7 PLR II Main Characteristics

|                       |            |
|-----------------------|------------|
| Nominal velocity      | 10 km/hr   |
| Maximum velocity      | 14.7 km/hr |
| Maximum gradient      | 26.5 deg.  |
| Wheel diameter        | 2 m        |
| Climbable step height | 0.53 m     |
| Minimum turn radius   |            |
| Neutral steer         | 8.6 m      |
| Oversteer             | 6.6 m      |
| Range                 | 2000 km    |
| Continuous power      | 8 kW       |
| Maximum power         | 12 kW      |
| Total mass            | 7015 kg    |



**PROJECT MINERVA: A LOW-COST MANNED MARS MISSION  
BASED ON INDIGENOUS PROPELLANT PRODUCTION**

**University of Washington  
Department of Aeronautics and Astronautics  
Seattle, Washington**

**Professor Adam P. Bruckner**

**Hobie Anderson, Teaching Assistant**

**Kelly Caviezel, Todd Daggert, Mike Folkers, Mark Fornia,  
Steven Hamling, Bryan Johnson, Martin Kalberer, Mike Machula,  
Kevin Mahn, Leslie McCullough, Clint Schneider, Vincent Westmark**

**Abstract**

Project Minerva is a low-cost manned Mars mission designed to deliver a crew of four to the Martian surface, using only two sets of two launches. Key concepts which make this mission realizable are the use of near-term technologies and *in-situ* propellant production, following the scenario originally proposed by R. Zubrin of Martin Marietta. The first set of launches delivers two unmanned payloads into Low Earth Orbit (LEO): one consists of an Earth Return Vehicle (ERV), a propellant production plant, and a set of robotic vehicles, and the second consists of the upper stage/trans-Mars injection (TMI) booster. In LEO, the two payloads are joined and inserted into a Mars transfer orbit. The landing on Mars is performed with the aid of multiple aerobraking maneuvers. On the Martian surface, the propellant production plant uses a Sabatier/electrolysis-type process to combine six tons of hydrogen brought from Earth with carbon dioxide from the Martian atmosphere to produce 100 tons of liquid oxygen and methane, which are later used as the propellants for the rover expeditions and the manned return journey of the ERV. Once the *in-situ* propellant production is completed, approximately two years after the first set of launches, the manned portion of the mission leaves Earth. This set of two launches is similar to that of the unmanned vehicles; the two payloads are the Manned Transfer Vehicle (MTV) and the upper stage/TMI booster. The MTV contains the manned rover and the habitat which houses the astronauts *enroute* to Mars and on the Martian surface. During the 180-day trip to Mars, artificial gravity is created by tethering the MTV to the TMI booster and inducing rotation. Upon arrival the MTV performs aerobraking maneuvers to land near the fully-fueled

ERV, which will be used by the crew a year and a half later to return to Earth. The mission entails moderate travel times with relatively low-energy conjunction-class trajectories and allows ample time for scientific exploration. This set of missions can be repeated every two years in order to continue exploration at a variety of sites and gradually establish the infrastructure for a permanent base on Mars.

**Introduction**

For centuries humans have pondered the nature of Mars and developed many theories to support what was observed. Speculation on the presence and extent of life on Mars has long held the interest of both the scientific community and the general public. For the past 28 years Mars has been explored by unmanned space probes, beginning with the Mariner series in the late 1960's and followed in the mid-1970's by Viking I and Viking II. These missions have answered some of the questions surrounding Mars and have given rise to new ones. With the Mars Observer establishing the return to exploration of the red planet in 1993, Mars is currently receiving attention as a possible target for manned exploration in the early 21st century.

The National Space Council (NSC) has the responsibility of defining the future objectives of America's space program in what is known as the Space Exploration Initiative (SEI). NASA, the Department of Defense, and the Department of Energy are the primary participants that assist the NSC with forming the SEI, which includes a plan for the manned exploration of Mars. SEI's plans require in-orbit construction and multiple launches, and consequently would be extremely complex and costly. This is one reason

why SEI did not receive any funding from Congress for fiscal year 1991, and why it continues to have difficulty in drawing support.<sup>1</sup> Therefore, an opportunity exists to develop a simple, low-cost alternative to SEI's present concept of placing humans on Mars for the purpose of effective exploration.

Such a mission has been suggested by R. Zubrin of Martin Marietta.<sup>2,3</sup> His so-called Mars-Direct Mission Architecture is based on the premises of using near-term technologies, going to Mars directly from Earth's surface on a conjunction class trajectory (thus circumventing in-space construction and dependence on Space Station Freedom), and manufacturing the propellant for the return journey on Mars from indigenous materials, i.e., the Martian atmosphere.

This year's Advanced Design Program at the University of Washington designed the Minerva manned mission to Mars, based on the Zubrin scenario and incorporating a number of new ideas. These range from the selection of the heavy lift vehicle and the design of the trans-Mars injection booster to the design of the manned habitat, the Mars rovers, and the Earth return vehicle.

The mission is undertaken in two main segments; in the first an unmanned spacecraft delivers a propellant production plant and the Earth Return Vehicle (ERV) to the surface of Mars. During the year and a half following the arrival of the unmanned spacecraft, the propellant production plant manufactures methane and oxygen by combining hydrogen brought from Earth with carbon dioxide from the Martian atmosphere, using a Sabatier-type chemical process complemented by water electrolysis. This process is very effective, converting only 6 tons of H<sub>2</sub> into 78 tons of O<sub>2</sub> and 22 tons of CH<sub>4</sub>.

Once it has been confirmed that the necessary propellant for the return journey has been successfully produced and stored (about 2 years after the unmanned launch), the manned mission leaves Earth. To alleviate the problems of extended zero-gravity (~ 180 days) a 2.5 km tether is connected between the manned vehicle and its spent Trans Mars Injection (TMI) booster, and the two are spun at 1 RPM to produce artificial gravity. The capture of both the unmanned and manned vehicles at Mars is effected via aerobraking and a modest retro-rocket maneuver. Once on the surface, the crew

of four astronauts uses CH<sub>4</sub>-O<sub>2</sub> powered manned and unmanned rovers and a rocket propelled hopper to explore Mars.

One of the advantages of the Mars-direct scenario based on conjunction class trajectories is that the surface stay time on Mars is much longer than in the case of a high energy opposition class mission, i.e. ~ 1.5 years vs. ~35 days. Thus the astronauts will have ample time to carry out an in-depth exploration of a large area of the planet.

This summary report discusses the basic mission architecture and its major components, including the orbital analysis, the Unmanned Mars Transfer Vehicle (UMTV), the Manned Transfer Vehicle (MTV), Earth Return Vehicle (ERV), aerobrake design, life sciences, guidance, communications, power, propellant production, surface rovers, and Mars science. Also presented is an evaluation of the cost per mission over an assumed 8-year initiative. Although the scope of this report covers only the exploration of Mars, many of the same technologies and philosophies can apply to lunar and other planetary mission concepts.

### **Mission Scenario**

The Mars mission model described here is arbitrarily based on an 8-year Mars exploration initiative, as shown in Fig. 1. The program consists of an unmanned mission to Mars followed two years later by simultaneous manned and unmanned missions. This launch procedure is then repeated every two years for a total of 8 years, ending with a manned mission to Mars in the eighth year. This model results in four manned and four unmanned missions to Mars.

Our proposed program will benefit by using a relatively small number of large, low-cost heavy lift launch vehicles (HLLV's). Although any HLLV capable of lifting at least 70,000 kg into LEO can be used, the single-stage-to-orbit (SSTO) vehicle Antares VII, which was developed during our 1991 design study,<sup>4</sup> has been chosen for the Minerva mission. The Antares system is a partially reusable, modular system based on a single unit vehicle. This unit uses a Dual Mixture Ratio Engine (DMRE), a new type of rocket engine studied by Pratt and Whitney specifically for SSTO applications.<sup>5</sup> The single Antares units can be clustered together to provide variable payloads to LEO,

ranging from 10,000 kg to 70,000 kg, and beyond. Figure 2 shows the basic Antares I and the Antares VII vehicles with their standard payload fairings.

Project Minerva uses the Antares VII vehicle to place the Mars transfer vehicles (both manned and unmanned) and their TMI booster stages into orbit. No in-orbit assembly is required, other than the straightforward rendezvous, docking, and connection of the spacecraft and their TMI boosters.

All launches proceed from the Kennedy Space Center and insert their payloads into a 150 x 300 km elliptical orbit of 28.5° inclination. This orbit is then circularized to a 300 km parking orbit, where rendezvous and docking maneuvers occur. The program OPGUID, which was provided by NASA's Marshall Space Flight Center, was used to analyze all mission launches.

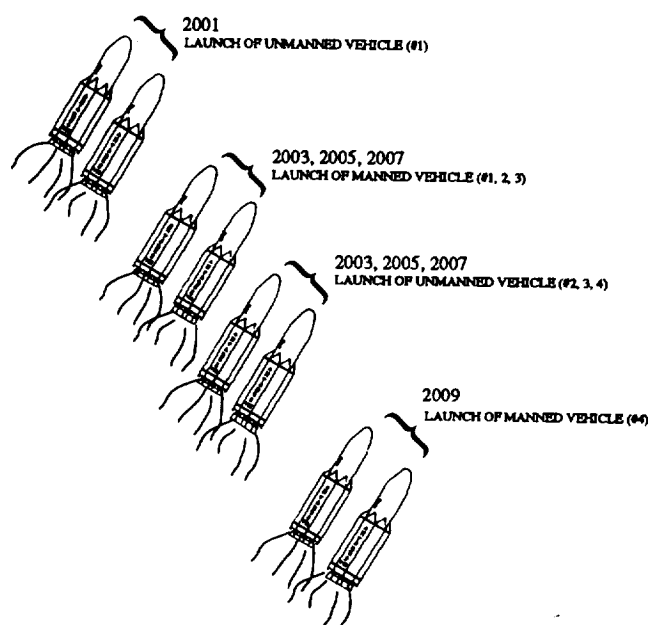


Fig. 1 Mission model

To boost each transfer vehicle to Mars, 105 metric tons\* of propellant are required. Since the Antares VII has a payload of 70 tons, an upper stage is required to deliver the necessary propellant to LEO. This upper stage also doubles as a TMI booster (see Fig. 5). For the manned segment the spent TMI booster stage is used as a counter mass for the rotating tether that supplies artificial gravity to the crew. The unmanned spacecraft simply discards the spent TMI booster once it is on its way to Mars.

\*Henceforth, "ton" will be understood to mean metric ton.

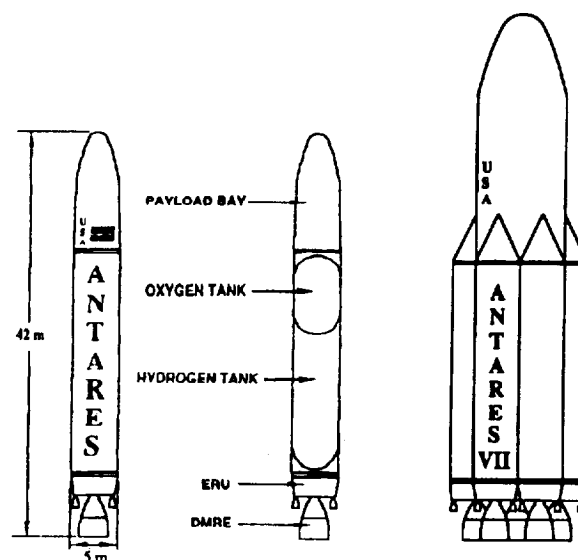


Fig. 2 Antares vehicle configurations

In both the unmanned and manned missions the TMI booster is placed into LEO first. The propellant tanks of the Antares VII vehicle are partially filled in order to allow it to lift off with its fully fueled 250 ton upper/TMI stage. At an altitude of 109 km the upper stage separates and delivers itself to a 300 km circular parking orbit with the 105 tons of propellant needed for the TMI burn. After the upper/TMI stage has been successfully delivered to LEO, the transfer vehicle is launched directly by an Antares VII operating as an SSTO vehicle. The two are joined using an Apollo-Soyuz type docking procedure and, after deployment of the aerobrake and a functionality test of all major systems, the journey to Mars is initiated.

The unmanned segment of the mission has the primary purpose of producing propellant for the manned return trip, and delivering the ERV. It also has the secondary purpose of deploying an unmanned rover to scout around for areas of interest, deploy scientific instruments for a variety of measurements, and collect Martian samples for later analysis.

After about 1.4 years, all of the propellant for the return trip will have been manufactured and stored on Mars in the ERV and the minimum energy window for the manned mission will be available. The manned mission is launched in the same manner as the unmanned mission. Since the

astronauts would be appreciably weakened by a six-month stay in zero-gravity, artificial gravity at 0.4 g is generated by tethering the MTV to its spent TMI booster and rotating the assembly at 1 RPM.

### Abort Capabilities

Abort capabilities are crucial for the manned mission. However, the direct to Mars mission architecture does not allow a return to Earth without the *in-situ* propellant manufactured using CO<sub>2</sub> from the Martian atmosphere.

If any system fails during or shortly after the TMI burn, the landing retro-rockets can be used to slow the MTV and place it in a highly elliptical, 300 km perigee orbit about Earth. Since the  $\Delta V$  capability of the retrorockets is small, the window of opportunity to abort after the TMI burn is only about two hours. A short burn at first apogee decreases the perigee altitude to within the Earth's atmosphere, where the already deployed aerobrake is used to lower the apogee to LEO. A further maneuver circularizes the orbit at 300 km, where the astronauts wait until the Space Shuttle can rendezvous for rescue at a later time.

### Astrodynamics

There are many factors that influence the type of transfer trajectory from LEO to low Mars orbit (LMO) and vice-versa. Some examples are the type of propulsion system used (chemical, nuclear, or electric), life support mass for the manned vehicle, sensitivity to radiation, tolerable solar flux, and desired stay time on the surface of Mars. Minimizing the required energy is an important factor in defining the capability of any mission. Energy savings ultimately result in a savings of propellant and an increase in payload capacity.

The first design consideration is opposition versus conjunction class missions. Although the quickest round-trip time to Mars would be an opposition class mission, there are many drawbacks to that type of trajectory. An opposition class mission is defined as a high energy trajectory in which the departure position of Earth and arrival position at Mars are on generally the same side of the sun. Because of the high energy involved, a very large mass of propellant is required. This class of mission would take

approximately 1.6 years, with only 0.1 year on the Martian surface. In addition, it would require an extended period of time closer to the sun than Earth's orbit on the return journey.<sup>2</sup> The increased particle radiation levels at this distance from the sun would be hazardous to the astronauts and would require additional shielding. The solar heat load to the vehicle would also be very high. This type of mission also requires a high-energy aerocapture at Mars, submitting the astronauts to between 8 and 10 g of acceleration. It is for these reasons that a conjunction class mission was selected for Project Minerva.

Conjunction class missions are close to minimum energy transfers, in which the departure position of Earth and the arrival position of Mars are approximately on opposite sides of the sun. The total mission time using a conjunction class trajectory is approximately 2.6 years.<sup>2</sup> The risks involved are longer radiation exposure and an extended period of zero gravity for the astronauts. Solar radiation exposure will be limited, since the mission will remain outside the Earth's orbit at all times. In addition, the vehicle will rotate about a tether to provide the astronauts with artificial gravity.

The following windows, excess velocities, and energy values for manned and unmanned segments have been specified utilizing Jet Propulsion Laboratory data.<sup>6</sup> Two types of missions will be flown, an unmanned flight followed by a manned flight. The first unmanned mission will depart from Earth in 2001 and the first manned mission will depart in 2003, as shown in Figs. 3 and 4. The launch windows have been identified by the minimum departure energy limits. The departure energy,  $C_3$ , is equal to the square of the hyperbolic excess velocity. The first manned and unmanned flight windows are assumed to be limited by a maximum  $C_3$  value of 10 km<sup>2</sup>/s<sup>2</sup>. For a near-minimum energy conjunction class mission, the launch window for the unmanned mission opens March 4, 2001 and closes April 2, 2001. For a minimum energy transfer, the unmanned departure date would occur March 19, 2001, with arrival at Mars on September 10, 2001. The arrival window at Mars is from August 18, 2001 to October 17, 2001. The maximum hyperbolic excess velocity for the given launch window is 6.3 km/s at Martian arrival and the corresponding maximum entrance velocity in the Martian atmosphere at 100 km altitude is 7.95 km/s.

The manned mission, as shown in Fig. 4, has a minimum departure  $C_3$  of  $8.81 \text{ km}^2/\text{s}^2$ . The launch window for Earth departure, limited by a maximum  $C_3$  value of  $10 \text{ km}^2/\text{s}^2$ , is from May 22, 2003 to June 22, 2003. The minimum  $C_3$  departure date from Earth is June 7, 2003 with a Mars arrival date of December 25, 2003. The Mars arrival window is from November 17, 2003 to January 27, 2004. The maximum arrival hyperbolic excess velocity for the given launch window is  $3.6 \text{ km/s}$ .

The mission dates and Earth to Mars trajectory have been selected by performing trade studies between the energy of the transfer orbit and the stay time on Mars.<sup>7</sup> If minimum energies for arrival at Mars and departure to Earth are used, the manned vehicle will arrive at Mars on December 25, 2003 and the return trip will begin on June 28, 2005. This results in a total surface time of 1.44 years (526 days), which should be ample to complete a considerable amount of scientific experimentation and exploration. (The low energy windows for the conjunction class missions discussed above allow a range of 1.35 to 1.55 years (493 to 566 days) of surface stay time).

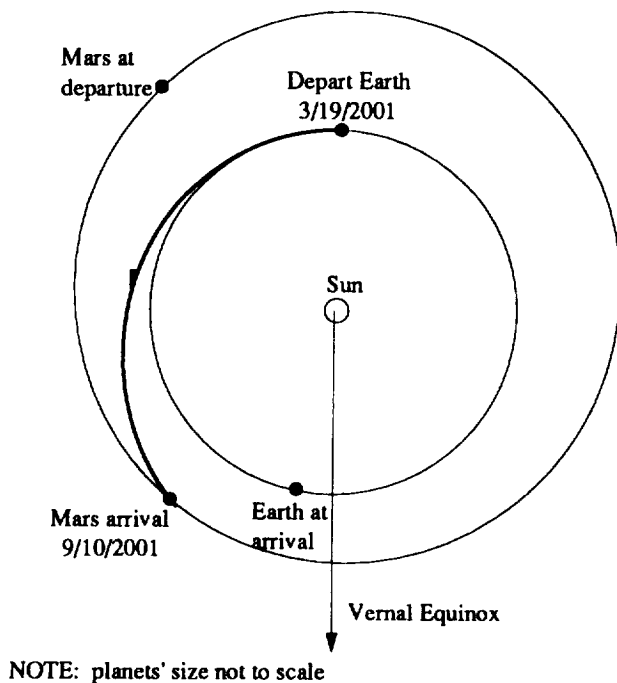


Fig. 3 Outbound unmanned transfer trajectory

The window for Mars departure with a maximum  $C_3$  of  $14 \text{ km}^2/\text{s}^2$  is June 17, 2005 to July 9, 2005. For the return vehicle, the departure date from Mars for a minimum departure energy is June 28, 2005, with an Earth arrival date of January 6, 2006. The Earth arrival window is from December 28, 2005 to January 15, 2006.<sup>8</sup> The maximum Earth arrival hyperbolic excess velocity for the given launch window is  $3.6 \text{ km/s}$ . The capture at Earth will be similar to that used in the Apollo program, i.e., a ballistic reentry. The entrance velocity will be  $11.6 \text{ km/s}$  at an altitude of  $100 \text{ km}$ .<sup>8</sup>

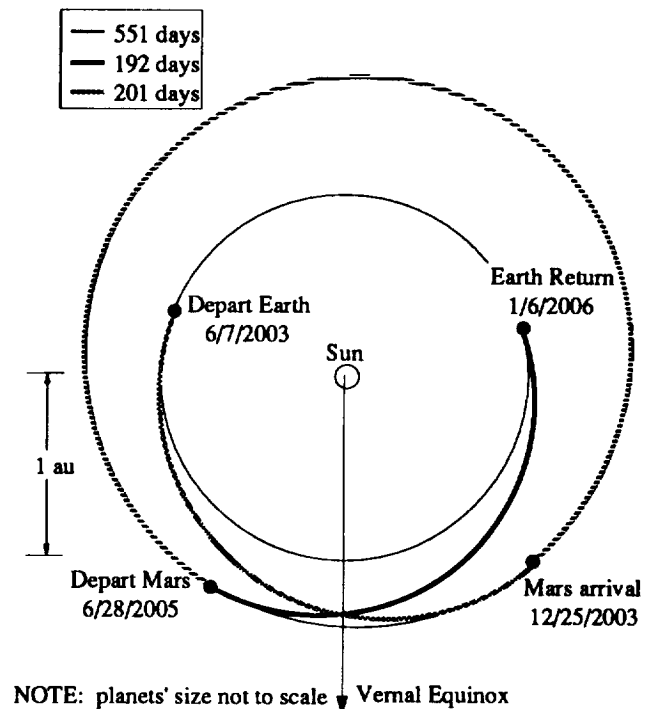


Fig. 4 Manned mission transfer trajectories

## Design Of Transfer Vehicles

### Upper Stage/TMI Booster Vehicle

In addition to performing the burn to LEO, the upper stage also has the role of performing as the TMI booster (see Fig. 5). It carries 105 tons of propellant for the TMI burn. The upper stage also requires a propulsive system with a high thrust and high specific impulse. To allow for redundancy and eliminate the possibility of a single point failure, at least two engines need to be used. Pratt and Whitney's RL10-A4 and the Space Shuttle Main Engine

(SSME) were considered, but Japan's Mitsubishi LE-7 engine<sup>9</sup> was found to have the characteristics most desirable for this mission.

This engine is similar to the SSME but smaller, and is used as a first stage engine in the Japanese H-2 launch vehicle. The LE-7 operates on a staged combustion cycle and has a vacuum thrust of 1180 kN and vacuum specific impulse of 449 sec.<sup>9</sup> It burns liquid oxygen and liquid hydrogen at a ratio of 6:1. The LE-7 has already been designed, built, and tested, and is scheduled for first flight in 1993, after which it will become available in the U.S.

The upper stage/TMI booster has a diameter of 8.2 m and a length of 29.4 m. The payload fairing length of the Antares VII is increased by 5 m to accommodate this configuration. A docking mechanism is attached to the top of the TMI stage via a stub adapter.

An orbital maneuvering system (OMS) is used for the orbital circularization and rendezvous maneuvers. The OMS and reaction control systems are similar to those used on the Space Shuttle.

### Unmanned Mars Transfer Vehicle

The mission requires that two types of vehicles be placed safely on the surface of Mars. The first vehicle sent is the unmanned Mars transfer vehicle (UMTV), shown in Fig. 6. The UMTV has a diameter of 9.1 m and a height of 32.0 m. At the base (in stowed position) the aerobrake is folded up against the vehicle with an effective diameter of 11.1 m. The vehicle consists of the ERV stage atop the UMTV descent stage. The ERV contains a habitat in which the astronauts live during the return trip to Earth. Centered in the middle of the ERV habitat is the Earth Re-entry Module (ERM). The astronauts and their payload re-enter the Earth's atmosphere in the ERM, while the ERV detaches and continues on its hyperbolic trajectory back out to deep space. Below the habitat are two hemispherical propellant tanks which will carry 96 tons of methane and oxygen that the propellant production unit will make on the Martian surface. The ERV sits atop the UMTV and has a height of 20 m, including its 5.5 m-long nose cone, and a diameter of 9.1 m. The ERV is attached to the UMTV by studs and pyrotechnic separation nuts so that the two vehicles can be separated just prior to launch of the ERV.

The payload bay comprises the main section of the UMTV, and houses the unmanned rover, science equipment, and propellant production unit. Shuttle-like tiles shield the latter from the ERV exhaust at the start of the return journey. Protecting the unit will enable it to be used in subsequent missions, should the need arise. The UMTV also carries eight tons of hydrogen, six for propellant production and two for descent maneuvers. The oxygen required for landing is contained in the ERV LOX tank and is piped to the two descent engines in the UMTV. Using this tank for both descent and take-off reduces the vehicle mass. Table 1 lists the mass breakdown of major unmanned system components.

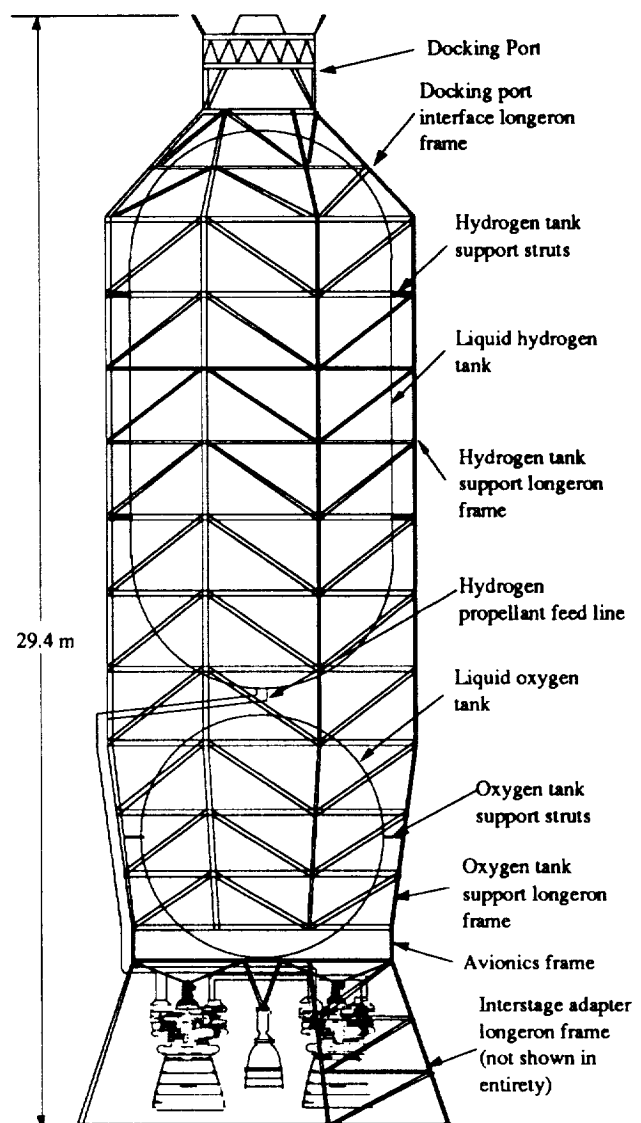


Fig. 5 Schematic of upper stage/TMI booster

### Earth Re-entry Module

Re-entering the entire ERV into the Earth's atmosphere at the end of the mission would incur unacceptable mass penalties. This consequence led to the concept of using a smaller Earth re-entry module (ERM) just large enough for the astronauts and any returning Martian samples. The ERM is similar to the command module of the Apollo lunar missions; however, it is based on a Boeing design capable of returning four astronauts.<sup>10</sup> Prior to re-entry at Earth it separates from the ERV. Two small solid rockets located on the ERV provide sufficient  $\Delta V$  to the ERV so that its trajectory does not overlap that of the ERM. After re-entering with the use of an ablator heat shield and deployable parachutes, the ERM splashes down for a water recovery. The ERV remains in a hyperbolic trajectory, continuing back out into deep space. (It is not desirable to have the ERV re-enter and break up in the atmosphere because of the danger of scattering plutonium from its dynamic isotope power system).

Table 1 Mass breakdown of unmanned transfer vehicle

| SYSTEM COMPONENT                             | Mass (ton)  |
|--|-------------|
| Earth Return Vehicle                         | 18.0        |
| Structure of Payload Bay and Engine Supports | 10.0        |
| Propellant for Landing ( $LH_2$ & $LOX$ )    | 10.0        |
| Hydrogen Feed Stock                          | 6.0         |
| Propellant Tanks                             | 3.0         |
| Aerobrake                                    | 9.0         |
| Power Supply                                 | 7.6         |
| Propellant Manufacturing Unit                | 2.0         |
| Retro-Rocket System for Martian Descent      | 0.7         |
| Piping and Wiring                            | 1.0         |
| Reaction Control System                      | 0.5         |
| Unmanned Rover                               | 1.0         |
| Science Equipment                            | 0.5         |
| <b>TOTAL</b>                                 | <b>69.3</b> |

The ERM re-entry velocity is 11.6 km/sec and is comparable to that of the Apollo missions. It has a ballistic coefficient of  $280 \text{ kg/m}^2$ ,  $L/D$  of 0.5, and an angle of attack of 25 degrees. This type of design was chosen due to its cross range capability, simple structure, and reliable recovery method (water landing). The shield is made of a brazed stainless steel honeycomb and filled with an ablative type carbon-carbon composite.

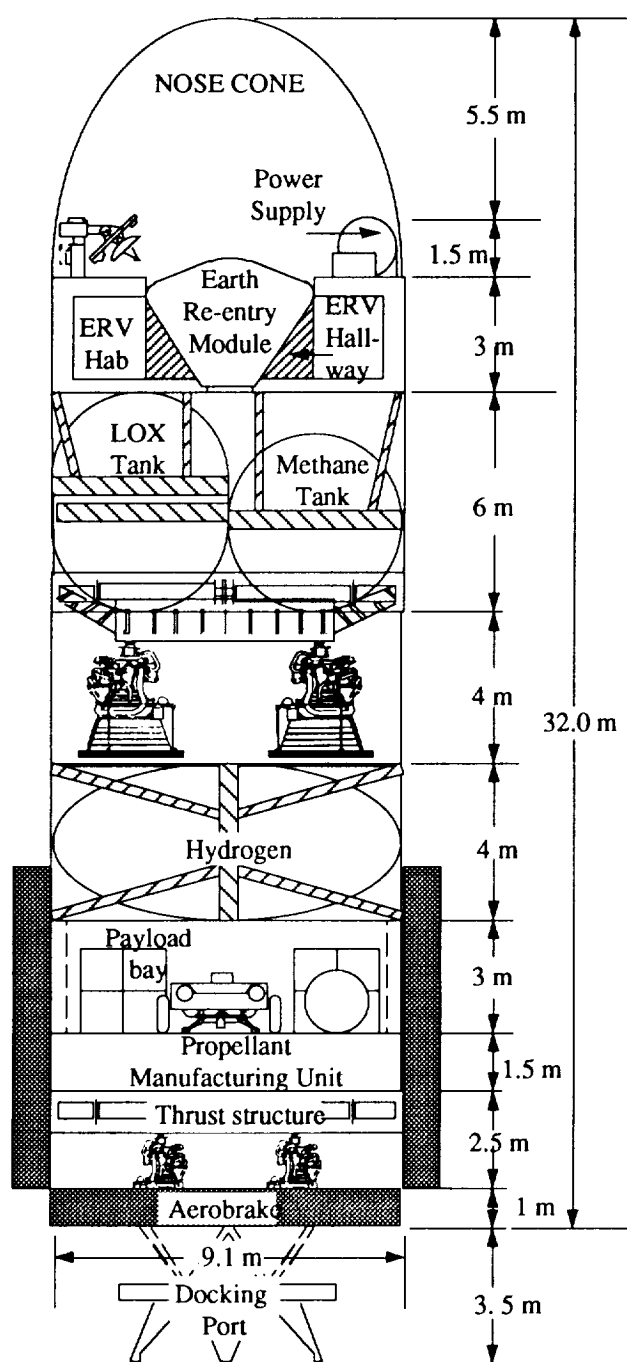


Fig. 6 Unmanned Mars transfer vehicle (UMTV)

### Mars Descent and Earth Return Engines

The UMTV, as well as the MTV, use retrorockets for final descent after atmospheric entry at Mars. The engines required to successfully complete this part of the mission must be highly reliable. This requirement is satisfied by the Pratt and Whitney RL10A-4 engine, due to its simple cycle and conservative design. As for the reliability of the engine, "the RL10 has accumulated over 20 hours of operation in space; 174 engines have produced 282 in-space firings without a single engine failure, and the engine has demonstrated the highest reliability of any operational liquid rocket engine."<sup>11</sup> The two RL10A-4 engines used for the descent stage use LOX/LH<sub>2</sub> as propellant. These engines have a specific impulse of 449 sec, a thrust of 185 kN, and a mass of 167.8 kg each. In addition, the ERV uses four RL10A-4's modified to burn LOX/LCH<sub>4</sub> propellant, which incurs a reduction in specific impulse to 376 sec and an increase in engine mass to 363 kg.<sup>11</sup>

### Manned Transfer Vehicle

The Manned Transfer Vehicle (Fig. 7) is similar to the UMTV, except that instead of an ERV there is the habitat which houses the astronauts enroute to Mars and on the Martian surface. In the MTV payload bay are carried the manned rover, more science equipment, and three more tons of hydrogen for additional propellant production on Mars. The manned vehicle has a height of 15.6 m and a diameter of 9.1 m (not including the aerobrake, which is similar to that of the UMTV). Table 2 shows the mass breakdown of the major system components.

Artificial gravity is provided during the manned voyage from Earth to Mars by tethering the MTV to the expended TMI booster in a "dumbbell" configuration, as shown in Fig. 8, using a 2.5 km tether made from Spectra 1000. The entire system is designed to rotate at one RPM which produces 0.4 g, approximately the same as the gravity on Mars. Without this artificial gravity, the crew would require significant recovery time upon arrival at Mars.

The habitat module and TMI booster are rigidly connected during the TMI burn. Immediately after this burn, the MTV separates from the spent TMI stage, rotates 180°, and attaches to the tether mechanism on the TMI stage. Subsequently, the tether is deployed using a tension control

device to prevent tether snap oscillations. The reorientation of the MTV before deployment keeps the apparent artificial gravity force vector in the same direction as during engine firing and aerobraking.

Table 2 Mass breakdown of manned transfer vehicle

| SYSTEM COMPONENT                             | Mass (ton)  |
|--|-------------|
| Habitat                                      | 28.0        |
| Structure of payload bay and engine supports | 5.0         |
| Propellant for landing                       | 10.0        |
| Propellant Tanks                             | 3.5         |
| Aerobrake                                    | 9.0         |
| Power on Mars                                | 2.0         |
| Manned Rover                                 | 3.0         |
| Science Equipment                            | 1.5         |
| Reaction Control System                      | 0.5         |
| Retro-Rocket System                          | 0.7         |
| Piping and Wiring                            | 1.0         |
| Tether                                       | 2.0         |
| Hydrogen                                     | 3.0         |
| <b>TOTAL</b>                                 | <b>69.2</b> |

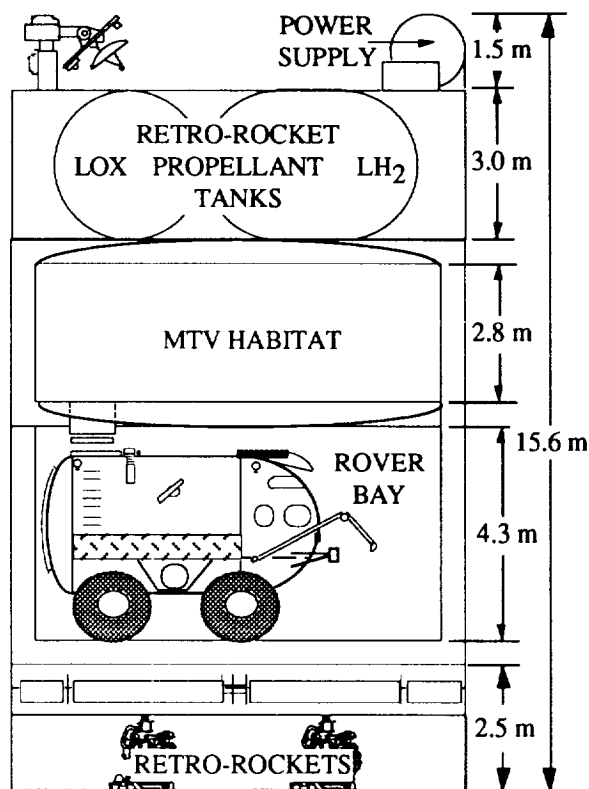


Fig. 7 Cutaway view of manned transfer vehicle



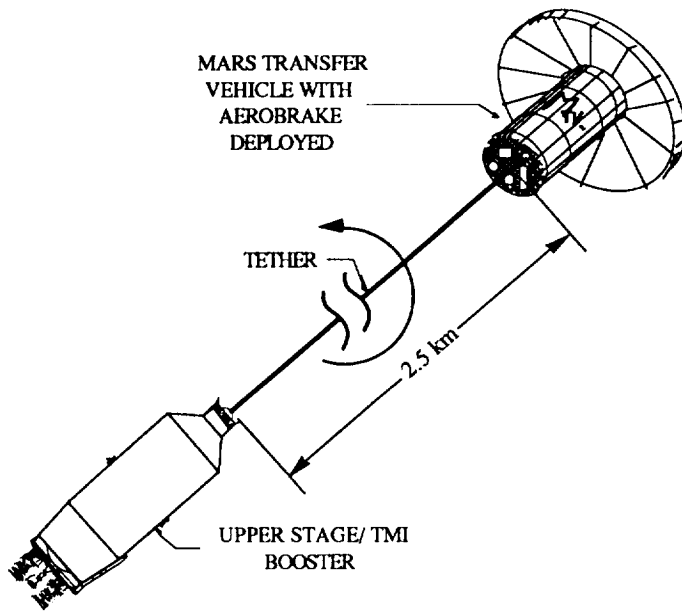


Fig. 8 Deployed tether

Prior to entry into Mars orbit, the tether and spent TMI booster are detached. A tether system is not used on the ERV for the return journey to Earth, since the crew will have plenty of time to recover from the effects of ~180 days of zero gravity once they are back on Earth.

### Habitat

The MTV habitat is designed to shelter four astronauts on the two-year mission. This crew size was selected to provide the minimum psychological stress to individual crew members, while keeping life support requirements manageable and realizable. The MTV habitat provides the four astronauts with a safe, "shirt-sleeve" environment in which to live and work. In addition, all systems are closed and self-supporting (see Fig. 9). To these ends, it uses chemical regeneration systems instead of biological systems. Chemical systems have been proven reliable in the past and are well understood, whereas biological systems, although very promising, are not yet scaled for such long term missions.<sup>12</sup>

To protect the crew from harmful radiation and space debris, the MTV has galactic cosmic radiation and meteor shielding. Solar flare and radiation belt protection comes from a special water jacket that surrounds the airlock and can be filled when needed. Another consideration which

influences the design of the MTV is the effect of zero gravity. Without artificial gravity the crew would require significant recovery time upon arrival at Mars. This concern led to the design of the tether system described earlier to provide artificial gravity at 0.4 g.

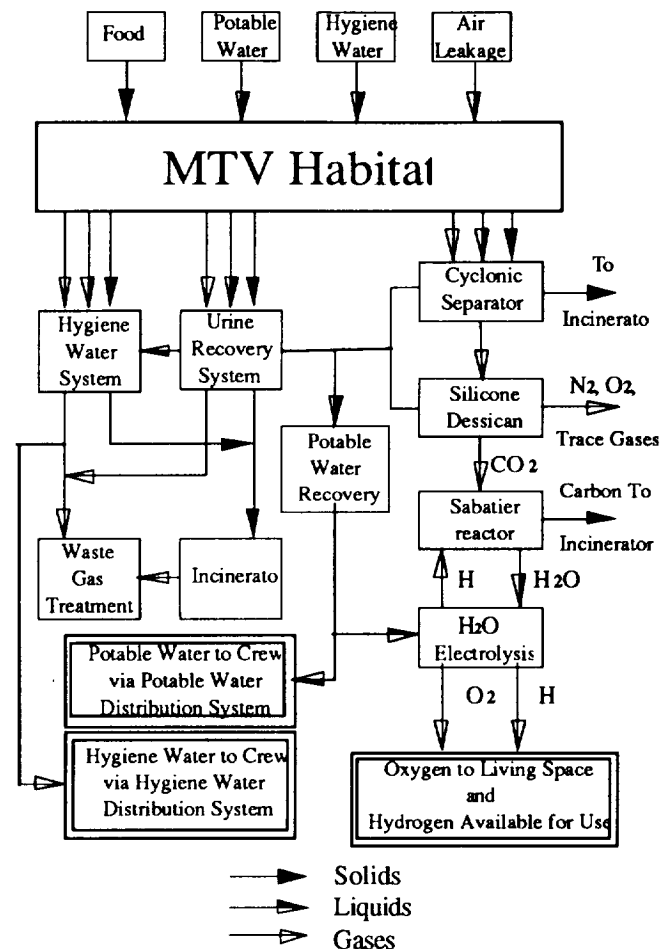


Fig. 9 Chemical regeneration system schematic

The habitat level on the MTV has a floor area of 51 m<sup>2</sup> and consists of eight rooms, as shown in Fig. 10. The MTV has one 3.51 m<sup>2</sup> stateroom for each member of the crew. The staterooms have a fold-out bed, desk and chair, storage space for personal items and clothing, and a small window. The bathroom is equal in size to a stateroom and houses the shower, toilet, and laundry equipment. The science room (11.4 m<sup>2</sup>) is the main control center for the MTV and contains the analysis lab used to perform experiments. The airlock is where the astronauts will seek safety during solar particle events (SPE), in which case a

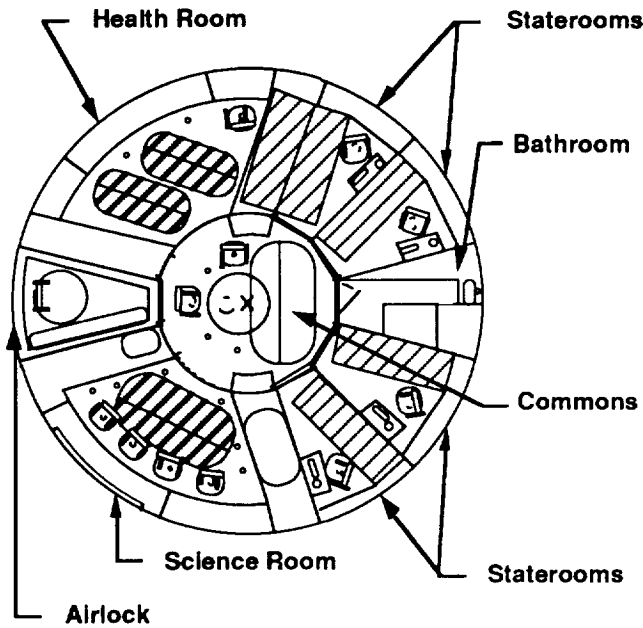


Fig. 10 Habitat floor plan

Once on Mars, the crew will use the airlock to enter the rover or payload bay (see Fig. 7). The airlock is the same size as a stateroom ( $3.51 \text{ m}^2$ ) and contains a three-day food supply for the crew during a SPE. The health room ( $11.4 \text{ m}^2$ ) will enable the astronauts to exercise, conduct biological and space-flight experiments, and use medical equipment and supplies. The commons area ( $7.68 \text{ m}^2$ ) is in the center of the MTV habitat level and contains the cooking facilities, the ship's library, and the table and chairs.

### Aerobrake

The aerobrake is an integral part of both the manned and unmanned missions. The aerobrake geometry selected is a blunt body with low lift to drag (L/D) ratio. It serves to slow the incoming craft at Mars and ensure capture, and to provide thermal protection of the craft within its wake zone. The aerobrake is folded up like an umbrella around the TMI stage during launch from Earth (see Fig. 11). It is opened and locked firmly into place in LEO, before the journey to Mars is initiated.

The deployed aerobrake (Fig. 12) has a symmetric modified conical shape with a cone half-angle of  $60^\circ$ . The middle section is a spherical shape with a radius of curvature of 9.1 m. This aerobrake has a coefficient of drag of about 1.8 and a lift to drag ratio of approximately 0.5.

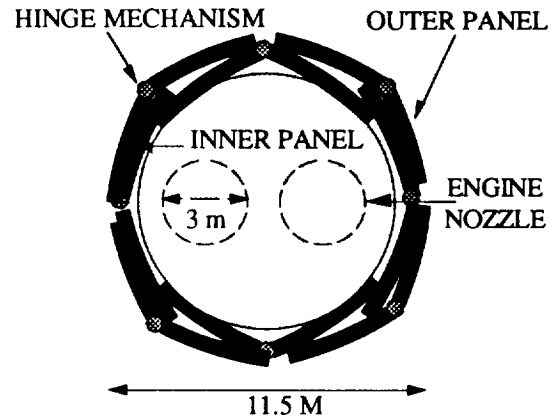


Fig. 11 Top view of aerobrake launch configuration

The cross-sectional diameter of the aerobrake is 22.5 m (with 6.7 m extended outward from the vehicle), providing a total cross-sectional area of  $398 \text{ m}^2$ . Protecting the entire vehicle by having it within the aerobrake's  $25^\circ$  wake angle would have required a much larger, extremely heavy aerobrake. Instead, protection outside the wake zone is provided by thermal tile shielding on the vehicle, as shown in Fig. 12.

### Heat Shielding

For the unmanned mission a heating rate of approximately  $35.2 \text{ W/cm}^2$  will exist at the stagnation point. The manned mission will have a heating rate of approximately  $15.7 \text{ W/cm}^2$ . To withstand these heating rates both missions will use AETB-8 (Alumina Enhanced Thermal Barrier)<sup>13</sup> which can withstand heat fluxes up to  $53.4 \text{ W/cm}^2$ . This material has a density of approximately  $128 \text{ kg/m}^3$  and will result in a heat shielding mass of 1800 kg. The upper part of the vehicle not shielded by the aerobrake is protected by Shuttle tiles, as noted earlier.

### Structure and Operation

The aerobrake is stored against the side of the spacecraft during Earth launch in a flower petal format. The aerobrake consists of eight identical "petals" that are folded around the transfer vehicle (see Fig. 11). Each petal has four main support struts, four radial ribs, and two sets of circumferential members to provide rigidity. In LEO the aerobrake is deployed by opening up the petals by means of the main support struts, fastening the petals together, and locking the support struts into place. The aerobrake doors

for the retro-rocket engines, located at the bottom of the spacecraft, are then tested to ensure all systems are operating properly. A manual override system for the aerobrake doors is provided on the manned spacecraft in the event of mechanical failure. The aerobrake petals are discarded when the retro-rockets are fired at Mars and fall away from the vehicle. The main support struts are then lowered to provide landing legs for the vehicle.

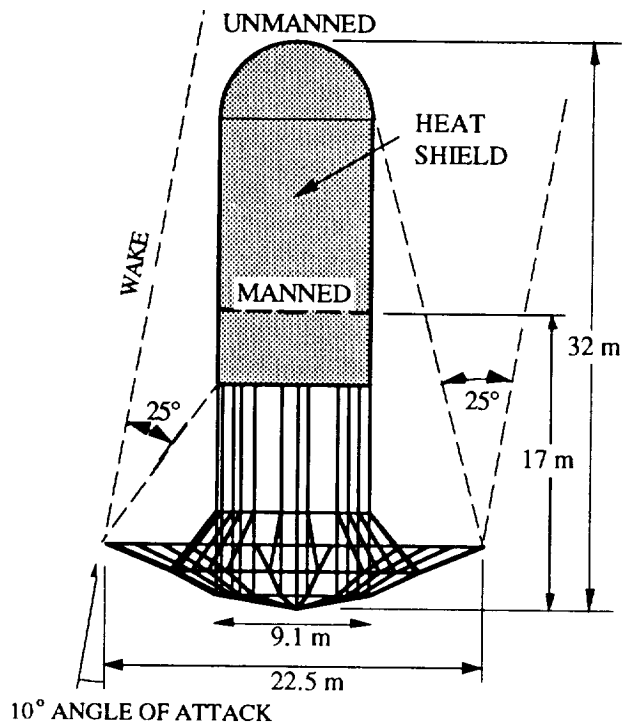


Fig. 12 Deployed aerobrake and transfer vehicle

The structural components of the aerobrake are made of Graphite/Epoxy (fiber volume of 55%) which has a density of  $1490 \text{ kg/m}^3$ . This composite has a very low coefficient of thermal expansion ( $-0.36 \times 10^{-6} \text{ K}^{-1}$ ) which is necessary because the aerobrake experiences high heating rates. The aerobrake structure was designed to withstand  $8.3 \text{ g}$  deceleration. For minimal displacements, diameters of  $20 \text{ cm}$  for the main tubular support struts and  $10 \text{ cm}$  for the other structural elements are needed to provide adequate rigidity. A thin graphite/epoxy sheet attached to an aluminum honeycomb core covers the structural members of the aerobrake; to this is attached the heat shielding material. The overall mass of the aerobrake, including structure, heat shielding, and thermal tiles on the vehicle body, is approximately  $9000 \text{ kg}$ .

## Aerocapture

Upon completing the transfer orbit to Mars, both the manned and unmanned missions will make a first close pass within the Martian atmosphere (at approximately  $50 \text{ km}$  and  $45 \text{ km}$ , respectively) to ensure aerocapture into a highly elliptical  $24.6$ -hour, one-Martian-day orbit (MDO). The altitude for this first pass is determined by the hyperbolic excess velocity. The manned mission, with a lower hyperbolic excess velocity, needs to pass through less atmosphere than the higher energy unmanned mission. The corridor height, which is similarly defined by hyperbolic excess velocity, defines the acceptable margin of error in periapsis altitude for a given mission pass. The manned mission has a corridor height of approximately  $55 \text{ km}$ , whereas the unmanned mission has a  $25 \text{ km}$  corridor.<sup>14</sup>

After this initial aerobrake at a close altitude a small adjustment burn is made at apoapsis to raise the periapsis to  $250 \text{ km}$ . This one MDO matches the rotation period of the planet and has an apoapsis radius of  $37,180 \text{ km}$  (see Fig. 13). The MDO is not a necessity, but a precautionary measure to ensure that all equipment is functioning properly prior to descent and that the landing site is confirmed to be clear of dust storms and large boulders. It is unlikely that the aerobrake would suffer any atmospheric dust-related damage, even during the close first pass. Dust storm effects are believed to occur only at altitudes below  $40 \text{ km}$ , which is below the first pass altitude for both missions.<sup>15</sup>

Descent for both missions is initiated by a small impulsive retro-burn at apoapsis to reduce the periapsis altitude from  $250 \text{ km}$  to an altitude within the atmosphere again. Although both the manned and unmanned spacecraft could then descend directly to the Martian surface, they are placed into a second elliptical orbit in order to launch a small communications satellite into a Mars synchronous circular orbit at  $20,406 \text{ km}$  radius. This orbit allows communication between the habitat and the rover while on Mars. Insertion of the satellite into this orbit is accomplished by a small booster. After the satellite is deployed the spacecraft makes a final periapsis pass and descends at an angle of attack of  $10^\circ$  below the local horizontal.

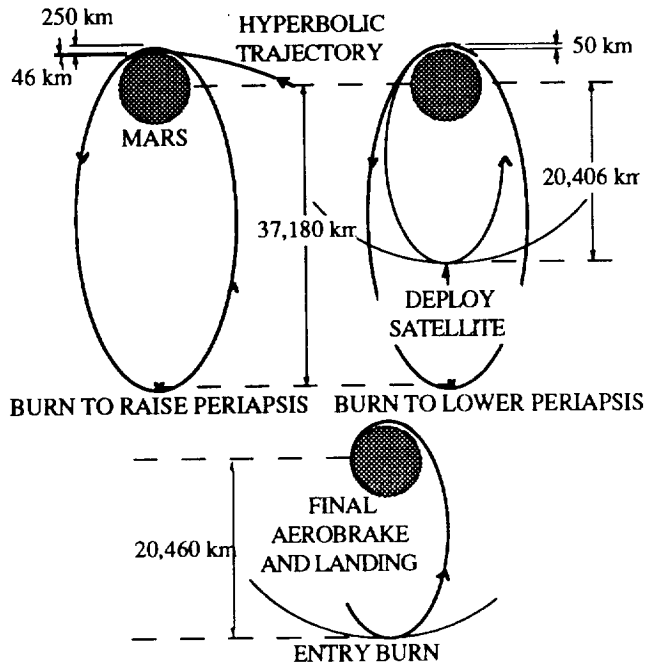


Fig. 13 Aerocapture and descent at Mars

### Guidance, Communications, And Controls

The tasks of communication, navigation, guidance and control of a mission such as this encompass a wide range of requirements, constraints, objectives, and solutions, some of which are unique to this mission. One such requirement is the need for artificial gravity during the outbound leg of the manned mission. The solution, as already stated, is to tether the manned Mars transfer vehicle (MTV) to the spent TMI booster, and slowly spin the vehicles about the center of mass. Although this poses some difficulties, especially for the onboard navigation and control, it requires no new technologies. In fact, most of our objectives are achieved with existing off-the-shelf systems.

### Landing Capabilities

The manned MTV must land relatively close to the previous unmanned landing site, where the fully fueled ERV is waiting. The MTV will be carrying a rover with a 500 km radius of operation or a one-way range of 1000 km that, if necessary, can transport the astronauts to the Earth return vehicle (ERV). A "homing" beacon at the unmanned site will help guide the MTV to the landing site. Control during entry is provided by attitude thrusters that adjust the angle of attack of the vehicle.

### Communication

Guidance and navigation of both the outbound and return trips will be made possible with the use of the Deep Space Network (DSN)<sup>16</sup> and onboard guidance control systems that will work in conjunction with the DSN. The onboard system includes navigation devices such as Sun and star sensors, rate-integrating gyros for attitude determination, and computer systems that continually check and compare the trajectory of the vehicle against the desired trajectory.

The DSN will also form the backbone of our communication scheme. A high gain antenna will be in constant contact with the DSN, allowing communication and data transmission to occur at all times.

The small communication satellite, deployed at Mars during the aerobraking maneuver, will allow the habitat to communicate with the manned and unmanned rovers during excursions. It will also be used as an emergency communication link between the habitat and Earth during the periodic 12.5-hour blackouts that occur when the habitat is not in a direct line of sight with Earth.

### Power Systems

The MTV and ERV power needs are supplied by Dynamic Isotope Power Systems (DIPS). Each DIPS system consists of a spherical plutonium dioxide ( $^{238}\text{PuO}_2$ ) heat source surrounded by a tungsten gamma ray shield. The gamma ray shield is, in turn, surrounded by a lithium hydride neutron shield. Two Stirling engines are connected to the spherical ( $4\pi$ ) heat source/radiation shield assembly by heat pipes. Waste heat is taken from the Stirling engines by a pumped loop heat exchange system which is connected to the spacecraft's heat pipe radiators, located on the outer cylindrical wall.

Heat is generated by the plutonium dioxide through radioactive decay. The harmful decay products are weak gamma rays and neutrons. The gamma rays are blocked by the thin layer of tungsten and the neutrons are blocked by the substantially thicker lithium hydride shield. Each DIPS is designed so that the crew will receive no more than 10 rems per year from the  $\text{PuO}_2$  decay.<sup>17</sup>

Each DIPS has two Stirling engines for redundancy. Normally, the two Stirlings will run at 50% power, but in the event that one fails, the remaining Stirling engine can run at 100% power and supply the vehicle with the power it needs. Table 3 shows the characteristics of the 15 and 20 kW<sub>e</sub> DIPS for the manned and unmanned spacecraft, respectively.

Table 3 DIPS characteristics

|                                | MTV                | UMTV                |
|--------------------------------|--------------------|---------------------|
| Number of DIPS                 | 1                  | 3                   |
| Output Power per DIPS          | 15 kW <sub>e</sub> | 20 kW <sub>e</sub>  |
| Thermal Power (BOL)            | 54 kW <sub>t</sub> | 108 kW <sub>t</sub> |
| Thermal Power (EOL)            | 50 kW <sub>t</sub> | 100 kW <sub>t</sub> |
| Total Output Power             | 15 kW <sub>e</sub> | 60 kW <sub>e</sub>  |
| Total Thermal Power (BOL)      | 54 kW <sub>t</sub> | 216 kW <sub>t</sub> |
| Total Thermal Power (EOL)      | 50 kW <sub>t</sub> | 200 kW <sub>t</sub> |
| Operating Lifetime             | 10 years           | 10 years            |
| Stirling Engines               | 2                  | 6                   |
| Stirling Engine Efficiency     | 30%                | 30%                 |
| Mass per DIPS(kg)              |                    |                     |
| Shield and Heat Source Mass    | 1250               | 1550                |
| Stirling Engines               | 240                | 320                 |
| Radiator Mass                  | 300                | 400                 |
| Structural Mass                | 210                | 280                 |
| <b>Total</b>                   | <b>2000</b>        | <b>2550</b>         |
| <b>Total Power System Mass</b> | <b>2000</b>        | <b>7650</b>         |

(BOL) - Beginning of Life

(EOL) - End Of Life

### In-Situ Propellant Production

In-situ propellant production is used to produce the propellant needed for the ERV because of its huge mass savings. Taking hydrogen to Mars on the unmanned spacecraft allows all propellant for the return trip to be produced before the astronauts leave Earth. The ERV uses methane/LOX engines because of the ease in producing methane by combining hydrogen with the Martian atmosphere, which is mostly carbon dioxide (CO<sub>2</sub>). The unmanned spacecraft carries the propellant production unit to make methane and oxygen at Mars. Table 4 shows the major characteristics of the propellant production system.

Methane and oxygen are produced by utilizing already proven technologies: an enhanced Sabatier type reaction and electrolysis (see Fig 14).<sup>18</sup> The Sabatier process produces methane by the reaction  $\text{CO}_2 + 4\text{H}_2 \Rightarrow \text{CH}_4 + 2\text{H}_2\text{O}$ . The electrolysis process produces oxygen by:  $2\text{H}_2\text{O} \Rightarrow 2\text{H}_2 + \text{O}_2$ . The methane and oxygen are produced and then liquefied and pumped into storage tanks on the ERV.

Table 4 Propellant production characteristics

|  |                    |
|--|--------------------|
| Total Propellant Produced                      | 100 tons           |
| Fuel (Methane)                                 | 22 tons            |
| Oxidizer (Oxygen)                              | 78 tons            |
| ERV Mixture Ratio (mass ratio)                 | 3.5:1              |
| Production Time                                | 550 days           |
| Power Required                                 | 60 kW <sub>e</sub> |
| Initial H <sub>2</sub> Feed stock (from Earth) | 6 tons             |
| Propellant Plant Mass                          | 1.5 tons           |

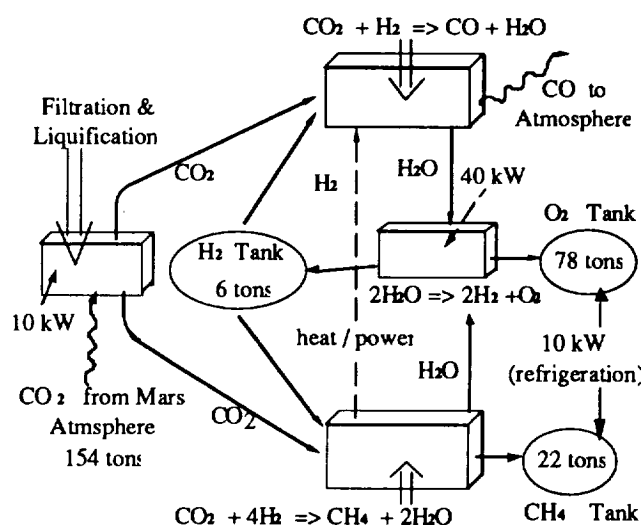


Fig. 14 Schematic of propellant production process

The propellant manufacturing unit is singly redundant. Two identical chemical plants will run at 50% capacity, but in the event that one fails, the remaining one will run at 100%, producing the propellant in the allotted time (before the manned mission leaves Earth).

All the propellant can be produced from a feed stock of 5.5 tons of H<sub>2</sub>. Six tons are taken from Earth to account for boil-off during the Mars transfer. The manned mission will take three more tons of hydrogen for the production of propellant for the manned rover, which also runs on methane and oxygen.

## Rovers And Robotics

On any mission aimed at the exploration of Mars, it is desirable to collect samples and conduct experiments at a wide variety of sites. To do this, Project Minerva has a group of four rovers designed to facilitate a detailed exploration of the Martian surface.

### Unmanned Rover

The unmanned rover (Fig. 15) has a mass of 1000 kg and is powered by a methane/oxygen internal combustion engine. Its dimensions are 3.5 m long, 2.5 m wide, and 1.5 m high, with a maximum ground clearance of 65 cm. The payload bed can be tilted fore and aft to facilitate loading and unloading of cargo. The rover has a maximum radius of exploration of 200 km. Before the manned spacecraft arrives, the rover will deploy seismic detectors and survey the Martian terrain. The unmanned rover will also have the task of transferring the extra hydrogen brought by the manned vehicle to the propellant manufacturing unit of the unmanned vehicle. This extra hydrogen is for manned and unmanned rover use during the 1.44 year stay time on Mars. Afterwards, the unmanned rover will primarily act as a "mother ship" for the hopper and minirover. It will be able to be teleoperated from both the manned rover and habitat.

### Hopper

The hopper travels to inaccessible regions of Mars via ballistic trajectories and soft landings. The hopper has a dry mass of 250 kg and is powered by an 8000 N methane/oxygen, pressure-fed rocket engine. It has a nominal round trip range of 15 km. The hopper can accommodate the mini rover or a single bucket seat on its payload bed. This will allow the minirover or an astronaut to journey where the manned rover cannot. The dimensions of the hopper are 2.1 m long, 1.6 m wide, and 1.25 m high.

### Manned Rover

The manned rover (Fig. 15) is the prime instrument used in the exploration of the Martian surface. This rover is capable of taking core samples to a depth of 10 m, delivering scientific experiments, collecting samples, and performing limited sample analysis. Powered by a 35 kW methane/oxygen internal combustion engine, the rover has the capability of traversing 1000 km with a maximum radius of exploration of 500 km. The manned rover has a ground clearance of 1 m.

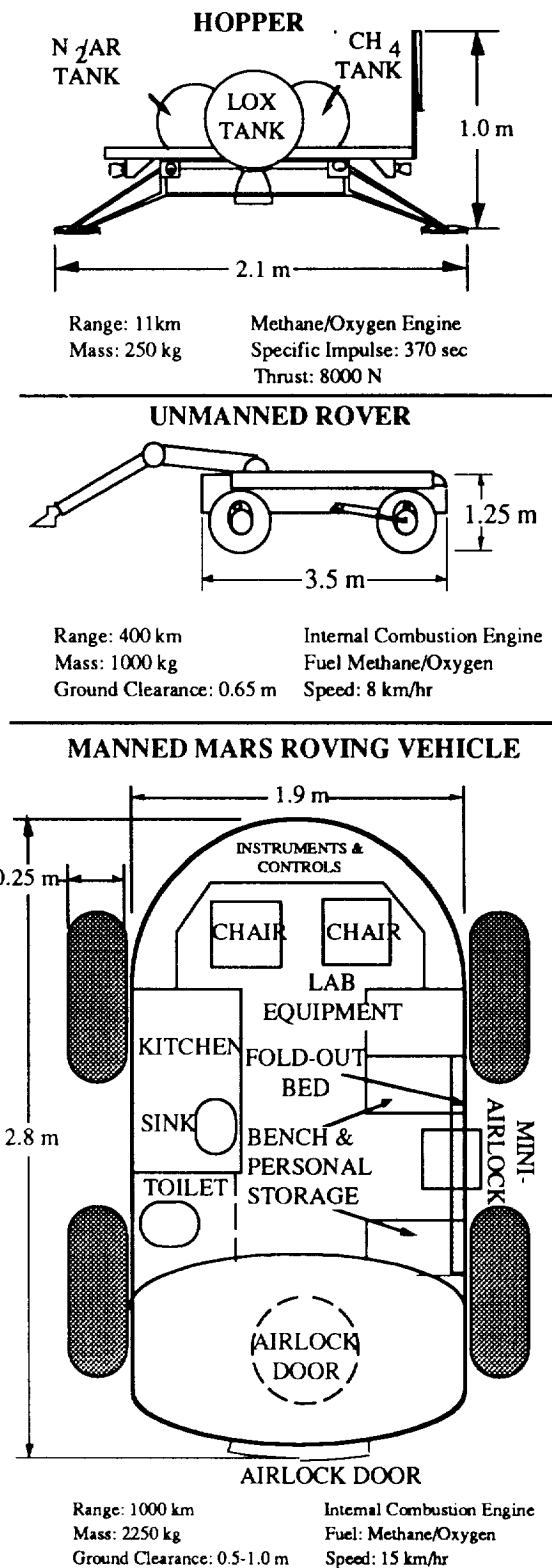


Fig. 15 Overview of rovers and hopper

With a dry mass of only 2250 kg, the manned rover provides a versatile tool for the exploration of Mars. The shirt-sleeve environment of the rover can accommodate two astronauts for up to two weeks and has an emergency back-up capability of supporting all four astronauts for up to a week. An airlock located at the rear of the rover allows easy access to the MTV habitat, through the ceiling airlock door, and to the surface of Mars through the back airlock door. The manned rover stores its life support end products for processing and distillation at the habitat.

### Mini Rover

The mini rover, which has a three-section articulated design,<sup>7</sup> has a mass of 50 kg, and is powered by rechargeable nickel hydride batteries, which give it a range of about 2 km, depending on the terrain. The dimensions are 1.5 m long, 1 m wide, and 0.8 m high. It has 6 conical shaped wheels, allowing a high level of mobility. It can be used to scout around the outside of the habitat, to piggyback aboard the unmanned rover for remote scouting, or as the primary payload of the hopper for reaching normally inaccessible areas of Mars.

### Mars Science

While the overall mission rationale is to explore Mars, potential landing sites had to be determined and a scientific payload package put together. In late 1992, Mars Observer will begin its mission to further explore Mars robotically. Minerva will seek to increase the knowledge of Mars, as well as to provide manned exploration of the "Red Planet."

The ideal landing site was determined by the number of scientific questions that could be answered, the safety of landing, and the establishment of a site near the equator to facilitate an easier orbital insertion. The four sites considered were the Lunae Planum, the Mangala Vallis, the Chryse Planitia, and the Argyre Planitia regions (see Fig. 16).

The primary site is located on the southern edge of the Lunae Planum, so that the rovers can reach the Juventae Chasma and the Ophir Chasma, which are within the Vallis Marineris. Figure 17 shows the Lunae Planum ideal landing site. The area also offers possible river basins and cratered areas.<sup>19</sup> Goals relating to site selection are the

determination of elemental composition, tectonic activity (past or present), geologic/morphologic studies, and exobiological analysis. The existence of carbonates would give evidence of past life and that liquid water once existed on Mars.



Fig. 16 Possible landing sites on Mars

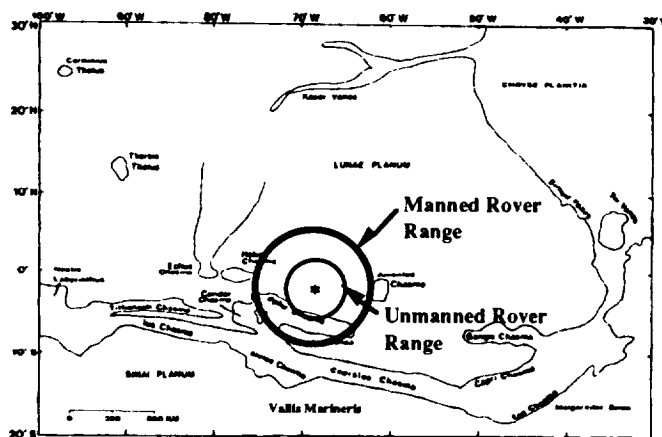


Fig. 17 Lunae Planum. Landing site is denoted by asterisk

The scientific package includes field equipment, exobiology and geoscience measuring instruments of various types, and sample collection containers for both field use and for possible Earth return.<sup>20</sup> Also included are astronomical instruments to be used during the space flight to Mars.

### Economics

The mission model for the Minerva project is based on an assumed eight-year Mars exploration initiative. The eight-year initiative begins with an unmanned mission to Mars in 2001, followed two years later by a manned and an additional unmanned mission. This launch procedure is then repeated every two years for eight years, resulting in a total of four unmanned and four manned missions to Mars (see Fig. 1). This model is assumed to end after eight years for cost analysis purposes but could continue as long as desired.

The vehicle costs have been broken down into three categories: Research and Development (R&D), Production Costs, and Operations and Support (O&S). The vehicle costs are the costs necessary to produce the number of launch vehicles required. A cost was estimated for each of these categories on a per year basis, based on previous missions. The R&D costs were assumed to last for 28 years and the O&S costs were assumed to last for 18 years, while the production costs were calculated on a per vehicle basis. The total for the vehicle costs amounts to \$12 billion (in 1992 dollars).

The unmanned mission costs were calculated by dividing the mission into different components and estimating the cost based on previous space systems. The unmanned mission also contains its own R&D and O&S costs. These costs are also assumed to last for 28 and 18 years respectively. A cost was then estimated for each of these categories and the amount was summed. The total for the unmanned mission vehicle costs amounts to \$23.5 billion.

The manned mission costs were estimated based on the same method as the unmanned mission, allowing for differences in components. These costs were also assumed to last for 28 and 18 years, respectively. The total for the manned mission amounts to \$20.5 billion.

By summing these costs we can come up with a total mission cost. The total cost for our eight year Mars Exploration Initiative is \$56 billion (see Table 5). This cost is considerably lower than other manned Mars missions suggested by NSC.<sup>21</sup>

Table 5 Total mission cost in billions of dollars

|              | Vehicle   | Unmanned    | Manned      | Total       |
|--------------|-----------|-------------|-------------|-------------|
| Mission1     | 3         | 7           | 5.5         | \$15.5      |
| Mission2     | 3         | 5.5         | 5           | \$13.5      |
| Mission3     | 3         | 5.5         | 5           | \$13.5      |
| Mission4     | 3         | 5.5         | 5           | \$13.5      |
| <b>Total</b> | <b>12</b> | <b>23.5</b> | <b>20.5</b> | <b>\$56</b> |

### Conclusion

Project Minerva is a viable and low-cost approach to the manned exploration of Mars. The mission architecture follows the proposal recently expounded by R. Zubrin of Martin Marietta for a class of Mars direct mission based on near term technologies and *in-situ* propellant production. The mission scenario that has been presented here involves an unmanned mission followed two years later by a manned mission. Both use the Antares VII heavy lift launch vehicle that was the subject of the 1991 University of Washington advanced design project.

The unmanned mission delivers a propellant production unit, six tons of liquid hydrogen feed stock, and an Earth return vehicle to Mars. The hydrogen is combined with carbon dioxide from the Martian atmosphere using a Sabatier and electrolysis process to produce a total of 100 tons of liquid methane and oxygen which are needed for the return journey to Earth and by the rovers. The manned mission carries with it a manned rover capable of exploring an area within a 500 km radius of the landing site. Both missions use low energy conjunction class trajectories to Mars. Artificial gravity at 0.4 g is provided for the manned spacecraft by connecting it to the spent trans-Mars injection booster with a 2.5 km long tether and rotating the system at 1 RPM. Both the unmanned and manned spacecraft make use of aerobraking maneuvers followed by retrorocket firing to effect a soft landing on Mars. The Lunae Planum area of Mars is proposed as an optimal landing site for maximum scientific return.



After a 1.44 year stay on the Martian surface, the crew returns to Earth aboard the fully fueled Earth Return Vehicle, again on a low energy trajectory, and re-enters the Earth's atmosphere six months later in an Apollo-like capsule. The total mission cost for an eight year program involving four unmanned and four manned flights is on the order of \$56 billion.

### Acknowledgments

The AA 420/421 class of 1992 completed this project with invaluable help from many sources. Most importantly, thanks go to Prof. Adam Bruckner and to Prof. Abraham Hertzberg for guidance and encouragement through the year, and to teaching assistant Hobie Anderson. We also wish to thank David Carlile, last year's teaching assistant, for his very helpful comments and suggestions. Project Minerva was put together by a class of 32 students over a six-month period. The entire class deserves recognition for the many hours and hard work that they put into this effort.

Robert Zubrin, of Martin Marietta, was very influential in the initial concept of this manned Mars mission. We also wish to thank him for his valuable time when he visited our class and listened to our ideas.

We are also grateful for the help we received from outside sources. From the Boeing Company alone, there are numerous people to thank. These include Dana Andrews, Tim Vinopal, John Anderson, and Gordon Woodcock. People from other companies are Charles Limerick at Pratt and Whitney, Ronald Greely at Arizona State University, and Michael Tauber and Demetrius Kourtides from NASA Ames Research Center.

Finally, thanks are due to NASA and USRA, and Frank Swalley of MSFC, our NASA center mentor, for giving us the opportunity to develop this project. In addition, we would like to acknowledge our Department of Aeronautics and Astronautics at the University of Washington for additional funding and other help.

### References

1. "NASA's Role in Moon and Mars Missions Narrows," Aerospace America, Vol. 30, April 1992, p. 1.
2. Zubrin, R., Baker, D., and Gwynne, O., "Mars Direct: A Simple, Robust, and Cost Effective Architecture for the Space Exploration Initiative," AIAA Paper No. 91-0326, 1991.
3. Zubrin, R., "In-Situ Propellant Production: The Key Technology Required for the Realization of a Coherent and Cost-Effective Space Exploration Initiative," Paper No. IAF 91-668, 42nd Congress of the International Astronautical Federation, Montreal, Canada, October 7-11, 1991.
4. Project Antares: A Low Cost Modular Launch Vehicle for the Future, Final Report, Space Systems Design, AA420/421 NASA/USRA Advanced Design Program, Department of Aeronautics and Astronautics University of Washington, Seattle, WA, June 1991.
5. Limerick, C.D., "Dual Mixture Ratio H<sub>2</sub>/O<sub>2</sub> Engine for Single Stage to Orbit Application," Journal of Propulsion and Power, Vol. 7, No. 1, 1991, pp. 65-67.
6. Sergeyevsky, A., Snyder, G., and Cunniff, R., Earth to Mars Ballistic Mission Opportunities, 1990-2005, Jet Propulsion Laboratory Publication 82-43, Pasadena, CA, 1983, pp. 109-111, 133-135.
7. Project Minerva: A Low Cost Manned Mars Mission Based on Indigenous Propellant Production, Final Report, AA420/421 Space Systems Design, NASA/USRA Advanced Design Program, Department of Aeronautics and Astronautics, University of Washington, Seattle, WA, June 1992.
8. Sergeyevsky, A., Snyder, G., and Cunniff, R., *Opus Cit.*, pp. 103-105.
9. Wilson, A., ed., Interavia Space Directory, 1990-1991, Jane's Information Group, United Kingdom, 1990.

10. Andrews, D., Boeing Space and Defense Group, Seattle, WA, Personal Communication, April, 1992.
11. Brown, J.R. and Limerick, C.D., Expander Cycle Engine Applicability to Advanced Space Missions, 1989 JANNAF Propulsion Meeting, May 23-25, Cleveland, Ohio.
12. Mendell, W., "A Personal History of the Human Exploration Initiative with Commentary on the Pivotal Role for Life Support Research," NASA N91-13855, p. 103.
13. Kourtides, D.A., Chiu, S.A., Iverson, D.J., and Lowe, D.M., "Thermal Response of Rigid and Flexible Insulations and Reflective Coatings in an Aeroconvective Heating Environment", NASA TM 103925, March 1992.
14. Woodcock, G.R., Space Transfer Concepts Analysis for Exploration Missions, Boeing Defense and Space Group, Advanced Civil Space Systems, Huntsville, Alabama, March 1991, p.193.
15. Sherwood, B., and Woodcock, G.R., "Engineering Aerobrakes for Exploration Missions," Acta Astronautica, Vol. 21, No. 6/7, 1990, p. 399.
16. Polocz, S., "Mars Observer Mission and Systems Overview," Journal of Spacecraft and Rockets, Vol. 28, No. 5, 1991, pp 491-497.
17. Eichholz, G.G., Radioisotope Engineering, Marcel Dekker Inc., New York, NY, 1972, pp 244, 387-389.
18. Chemical and Process Technology Encyclopedia, McGraw-Hill Book Company, New York, 1974, p. 603.
19. Nedell, S.S., Squyres, S.W., and Andersen, D.W., Origin and Evolution of the Layered Deposits in the Valles Marineris, Mars, Academic Press, Inc., 1987.
20. Budney, C.J., Snyder, G.C., Ionasescu, R., and Wallace, R.A., eds., "SEI Science Payloads: Description and Delivery Requirements," Report No. JPL D-7955, Rev. A, Jet Propulsion Laboratory, Pasadena, CA, May 17, 1992.
21. Asker, J. R., "NASA Offers Five Alternatives for Landing on Mars by 2018," Aviation Week and Space Technology, Vol. 131, November 27, 1989, pp. 30-31.

**PAX: A PERMANENT BASE FOR HUMAN HABITATION OF MARS<sup>1,2,3</sup>****University of Wisconsin-Milwaukee****Department of Architecture****Milwaukee, Wisconsin****Professor Gary T. Moore****Patrick J. Rebholz, Teaching Assistant****Joseph P. Fieber, Janis Huebner-Mothes, and Kerry L. Paruleski****Abstract**

The Advanced Design Program in Space Architecture at the University of Wisconsin-Milwaukee supported the Synthesis Report<sup>1</sup> and two of its scenarios--"Architecture 1" and "Architecture 4"--and the Weaver ExPO report on near-term extraterrestrial explorations<sup>2</sup> during the spring of 1992. The project investigated the implications of different mission scenarios, the Martian environment, supporting technologies, and especially human factors and environment-behavior considerations for the design of the first permanent Martian base. This paper presents the results of that investigation. The paper summarizes site selection, development of habitability design requirements based on environment-behavior research, construction sequencing, and a full concept design and design development for a first permanent Martian base and habitat. The proposed design is presented in terms of an integrative mission scenario and master plan phased through initial operational configuration, base site plan, and design development details of a complete Martian habitat for 18 crew members including all laboratory, mission control, and crew support spaces.

**Humans to Mars: Purpose and Objectives**

The purpose of this project was to support *America at the Threshold: Report of the Synthesis Group on America's Space Exploration Initiative* (called the "Synthesis Report"<sup>1</sup>) which recommended that NASA explore what it called four "architectures," i.e., four different scenarios for habitation on Mars.

The Advanced Design Program in Space Architecture at the University of Wisconsin-Milwaukee supported the Synthesis Report and the Weaver ExPO SEI reference mission report<sup>2</sup> by pursuing five objectives:

- explore the implications of different mission scenarios,
- understand the Martian environment,
- analyze supporting technologies, and
- investigate human factor and environment-behavior (EB) considerations for the design of a Martian base.

**Procedure**

The work was accomplished in an overlapping sequence of eight phases:

1. Mission scenario--analysis and integration.
2. Base design research and requirements--background research and development of design requirements for master plan and site plan.
3. Concept design exploration--schematic design studies to develop and explore different site planning and habitat concepts.
4. Habitat design research and requirements--literature review of the full range of human factors and EB considerations in habitat design, and development of research-based design requirements.
5. Habitat schematic design--schematic designs for each space (laboratories, crew quarters, etc.) in response to design requirements.
6. Interior design development--detailed design development of all interior spaces and refinement of design details.
7. Design integration--final design development and integration across the habitat as a whole, including preparation of various presentations of the project in

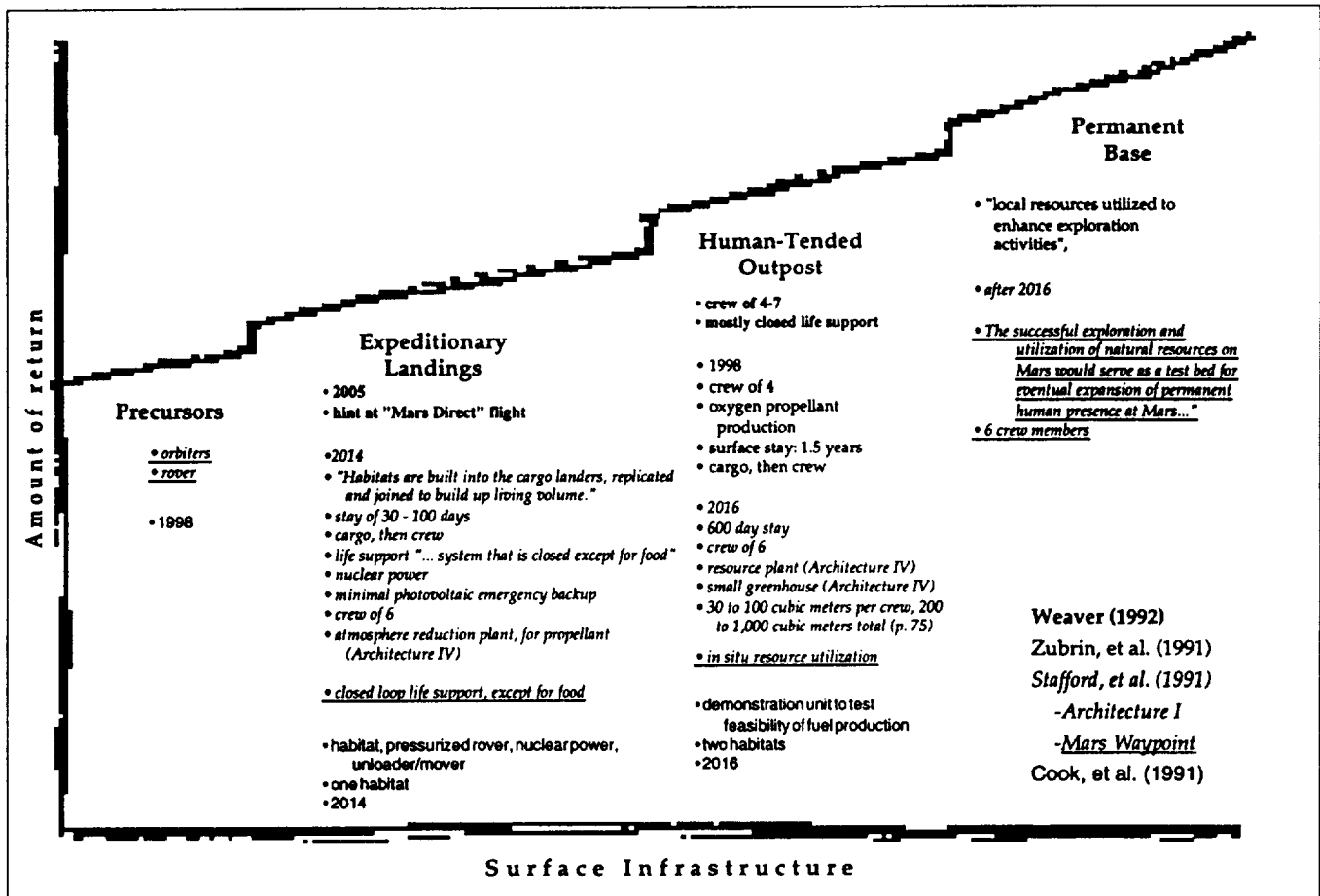


Fig. 1 Integration of previously published Mars mission scenarios.

mid-fidelity models of each module floor showing lighting, colors, and textures and of the habitat and regolith-containment space-frame structure, and drawings of site location, site plan, and construction sequence to initial operating configuration (IOC) and next operational configuration (NOC).

8. Presentations, slides of all models, drawings, and diagrams to explain the EB basis of habitat and base design, technical report, and papers at national and international meetings.

### Mars Mission Scenario

Our thinking, based on an integration of the Synthesis Report, the ExPO report, and Zubrin's "Mars direct"

scenario,<sup>1</sup> indicates the likelihood of the following four-phase Mars mission scenario:

1. Precursor telerobotic missions around 1998.
2. Expeditionary landings around 2005 to 2014 on the order of 500 days total trip time with a stay of 30 to 100 days.
3. Longer duration missions on the order of 1,000 days with a typical stay time of 500 to 600 days between 2007 and 2016 to establish *human-tended campsites or outposts*.
4. Long-duration missions to establish the initial operating configuration of the first permanent base (IOC) between 2009 and 2022.

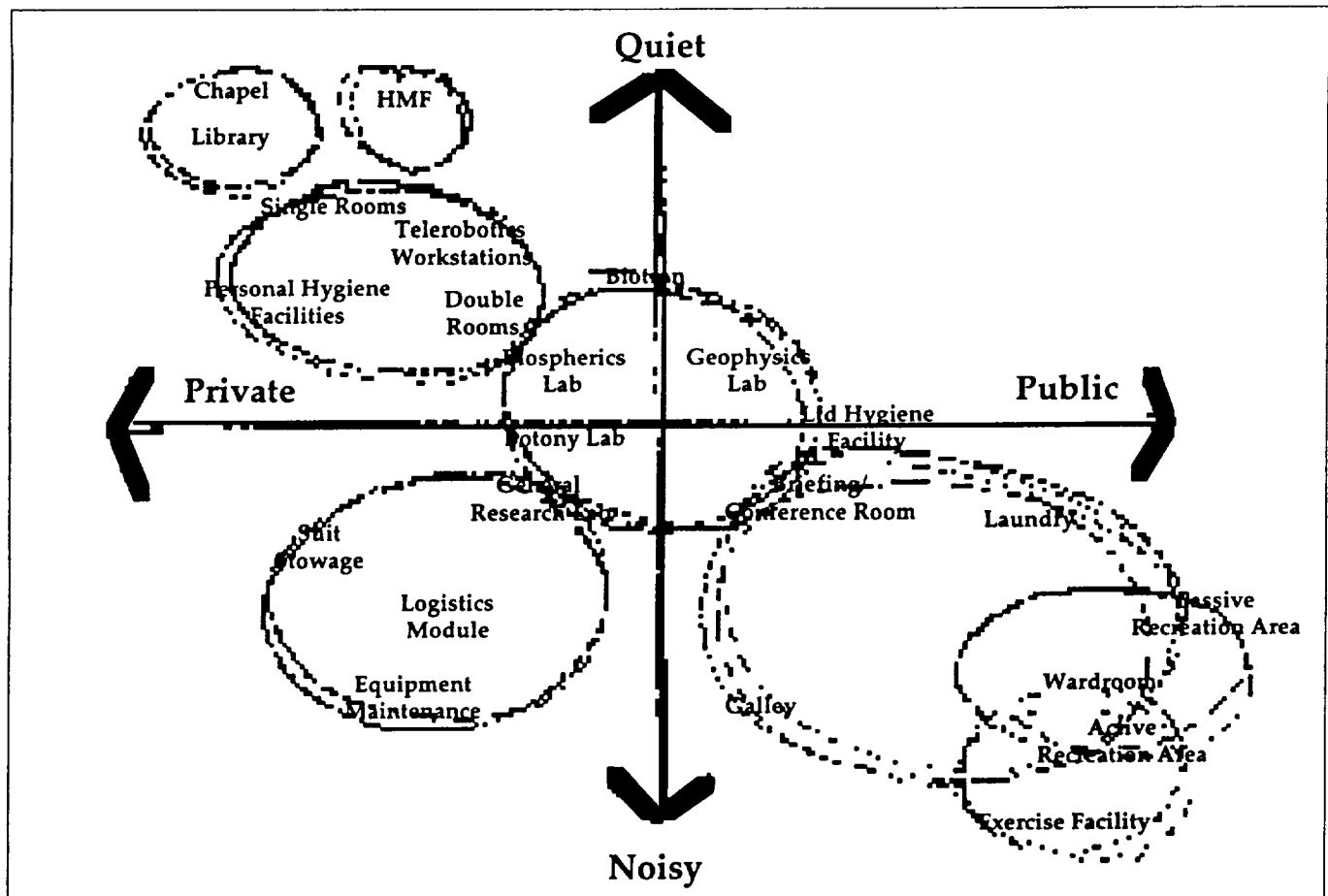


Fig. 2 An example of two EB issues considered in the design of Pax: needs for privacy and for social interaction, and for quiet and more active spaces. The beginnings of the layout of the habitat (a "bubble diagram") emerges from the overlap of these two gradients.

There are significant EB habitation issues to be explored and solved in a long-duration permanent Martian base. The focus, therefore, of our current research and design work has been on the EB determinants of a long-duration permanent base.

Our work built off what the Synthesis Report referred to as the Mars "Waypoint" (by which is meant Mars planetary activities for human exploration of Mars and the Solar System, i.e., as a waypoint to later exploration into the Solar System). We accepted the Synthesis Report recommendations of a crew size of 6 crew members for the initial human-tended outpost and the ExPO recommendation of a crew size of 18 for the permanent IOC base. The base is designed assuming a mostly closed-loop life support system (closed except for

food, which will be produced on an experimental basis in a pair of biotrons or Martian greenhouses) and remote automatic emplacement, checkout, and verification of the habitat and life support system.

The Mars waypoint assumes significant transfer of learning from orbital and lunar facilities including evaluation of lunar habitats. Our previous work in the USRA Advanced Design Program was instructive. An early phase of our Martian work was an analysis and critique of the five lunar habitats<sup>4</sup> designed by the Space Architecture Design Group since 1989--especially the two habitats taken into design development--for positive lessons to be transferred to the design of the first Martian habitat.

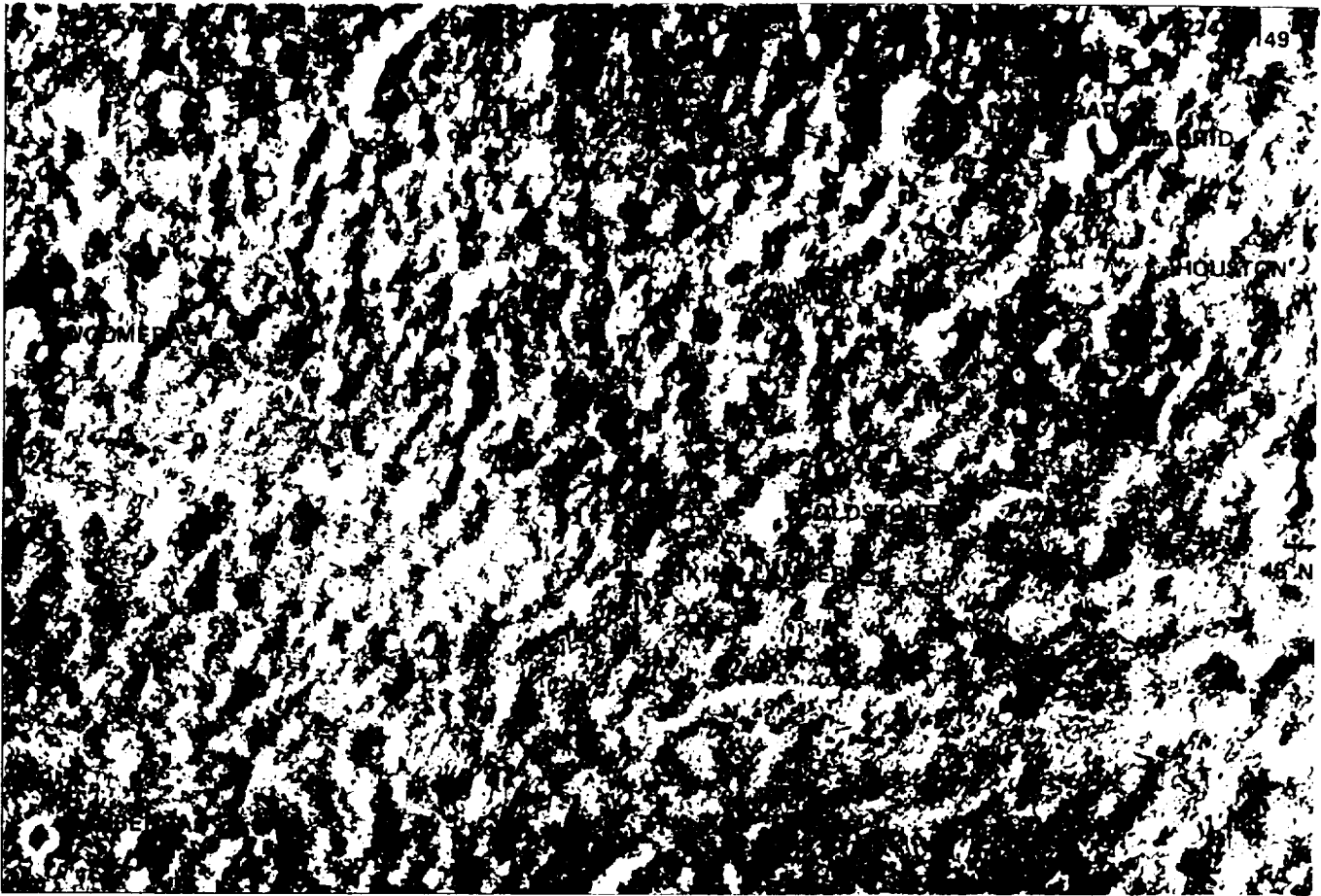


Fig. 3 Viking 2 mission location at 45° north latitude, 251° west longitude.

### **Human Factors and Environment-Behavior Considerations**

Until recently, human factors and EB considerations were not viewed as significantly important elements for successful extraterrestrial exploration. Instead, science and engineering were paramount in the eyes of the designers. "There is now an increased awareness on the part of planners that design does affect behavior."<sup>5</sup> By studying the effects of human behavior in isolated and confined environments and deriving design requirements, human factors considerations can have a profound impact on the success of extraterrestrial space exploration.

A permanent Martian base will provide for a multinational, multi-racial, mixed-gender crew for stay times as long as two years. The base will include mission-related

facilities such as research labs, mission operations workstations, airlock and dust-off chamber, storage for logistics, and life-support system. It will also contain crew-support facilities such as crew quarters, individual and group passive recreation areas, an active exercise facility, a wardroom for eating, teleconferencing, and meeting, hygiene facilities, and a health maintenance facility, as well as special places for privacy and psychological retreat.

The driving force behind the design of Pax, proposed as the first permanent Martian base and habitat (named for the international Peace Settlement, opposite of the Latin name of the planet, Mars, the God of War) is human factors and EB requirements that impact on habitability for long-duration habitation.

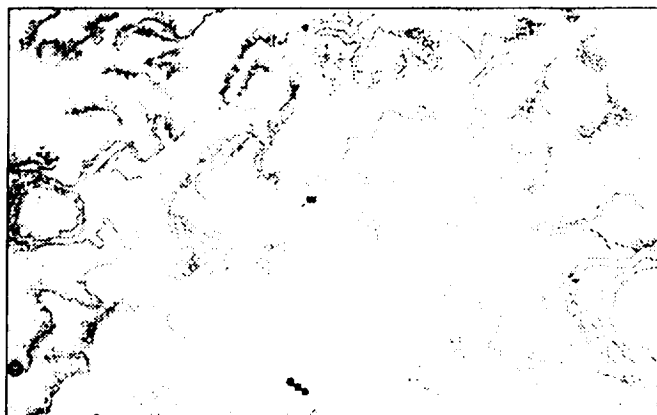


Fig. 4 Pax base site plan showing the central habitat with launch and landing facility each 2.5 km away from the habitat.

A full range of EB issues was investigated, from pragmatic issues of anthropometrics, productivity, and functionality to more abstract issues of community and privacy, imagery and symbolism. Considerations included but were not limited to anthropometric effects of one-third gravity, safety, astronaut satisfaction and productivity, minimization or relief of stress, social interaction and privacy, orientation and wayfinding, perceptual variety, efficiency, functional convenience, and place and identity--the quality of "home."

#### Site Selection

It is proposed that Pax be constructed at the Viking 2 landing site, 45 degrees N latitude, 251 degrees W longitude, known as Utopia Planitia. The site is near varied geologic surface features important for research. The site is located in the northern hemisphere, away from the origination of southern dust storms during the summer season. The terrain in the immediate area, generally level according to Viking 2 photos, is appropriate for a transportation system and launch and landing facility. The elevation of the site is relatively low with respect to the other features on the surface, thus providing some radiation protection from the accumulated, albeit thin atmosphere. Finally, current theory on water location<sup>6</sup> suggests the search be conducted near the north pole. The proposed site for Pax is on the south edge of the polar cap advance in the winter season.<sup>2</sup>

#### Base Layout: Site Plan

The base layout follows a north-south axis, with the habitat, solar array fields, and radiator fields being in the center, the auxiliary nuclear power plant 2.5 km to the south, and the launch and landing facility 2.5 km to the north. Winds are from the west and southwest; launch and landing patterns will not endanger the habitat, and any possible nuclear residue will be carried away from the base and habitat.

#### Habitat Design Concept

Concept or schematic design studies were conducted early in the research and design process of this project to explore different base layout master and site-planning concepts. The implications of four alternative concept designs were explored, analyzed, and then compared at a preliminary design review (PDR). They were:

- hard module habitat partially buried and partially set in the edge of a Martian crater;
- inflatable habitat partially buried and partially set in the edge of a Martian crater;
- Earth-like technology for Martian surface application; and
- space-frame construction spanning between crater edges.

The advantages and limitations of each concept design were analyzed. An attempt was made to combine the best of each concept. From the PDR, it was found that there are considerable advantages for surface construction with a combination of hard module and inflatable structures covered with a space-frame regolith containment system. This was the integrative concept that was adopted and developed throughout this project.

A modular space-frame construction system provides the protective shelter for the habitat itself. This framing system will combine open square and triangular geometries to produce a roof-and-column support system. The proposed system is a kit of components, redundant in size and shape, that will allow the astronauts relative ease of construction. The system will consist of a structural space frame, column support system, textile regolith containment and radiation shielding system, and Martian regolith.

The habitat, or central portion of Pax, will be constructed in several stages. Construction can commence when two rigid modules and six crew members are on-site, and their equipment, rovers, and logistics are emplaced. Additional modules and their crew will arrive, bringing the compliment of rigid modules to four, and the number of crew members to 12.

The habitat for a final crew size of 18 at IOC will be comprised of five operational modules, each two floors in height: a 9-m hard-module entry module for dust-off, suit stowage and maintenance, and full recreation and exercise center; two 12-m inflatable modules, one for laboratories and mission command, the other for crew quarters and the crew support facility; and two additional 9-m hard modules serving as two Martian greenhouses. The fourth hard module, part of the initial deployment, will be transferred elsewhere on the Martian surface to serve as a hazardous laboratory.

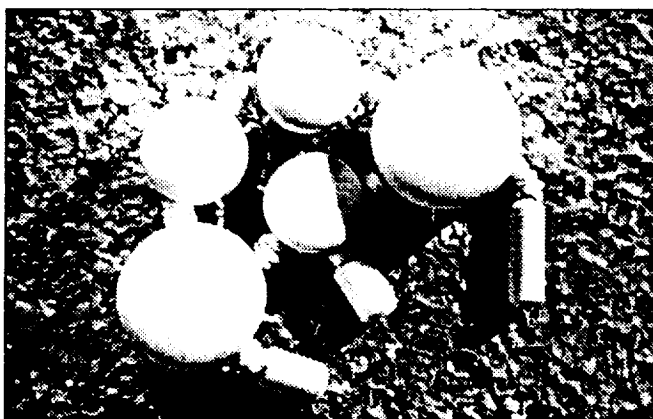


Fig. 5 Model representation of Pax showing the five modules—entry and active recreation flanked by laboratories on the left, crew quarters on the right, and two greenhouses in the background.

### Construction Sequence

The sequencing of a Mars mission from initial lift-off from Earth to IOC and NOC is a critical, and early, mission design decision to be made. Based on our analyses, the advantages of Zubrin's "Mars direct" mission scenario, or mission "architecture" as NASA calls it, became apparent. Adopting large segments of this scenario suggested a split-sprint mission, with cargo

transportation and initial robotic emplacement preceding the first landing of humans on Mars. Thus the construction sequencing we have recommended proceeds in eight phases:

1. Landing of two 9-m hard modules as the initial campsite or outpost, followed by six crew members who begin to prepare the site for further development.
2. Excavation of the footprint for the IOC Martian habitat.
3. Landing of two additional 9-m hard modules as the second phase outpost, followed by six additional crew members who begin assembly and raising of the space frame and regolith containment system.
4. Emplacement and inflation of the two 12-m inflatable crew support and laboratory facility modules.
5. Moving the rigid entry module from the campsite location and connecting it and a primary entrance airlock to the inflatables.
6. Transporting the fourth and fifth components, both rigid modules dedicated to greenhouse functions, underneath the space frame shelter utilizing a lift and trailer system, and attaching them with flexible connections to the laboratory and crew inflatables.
7. Docking two additional rigid modules, a logistics and emergency airlock module to the crew support inflatable, and a combination laboratory logistics and emergency airlock module to the laboratory inflatable. This completes IOC.
8. Expansion of the base as necessary to various NOCs, e.g., removal of the crew or laboratory logistics module/airlocks and excavation for the emplacement of additional 12-m or larger inflatable modules.

### Overall Design Organization of the Habitat

There were seven factors that went into creating the basic *parti* or conceptual framework governing the design process for Pax. They are:



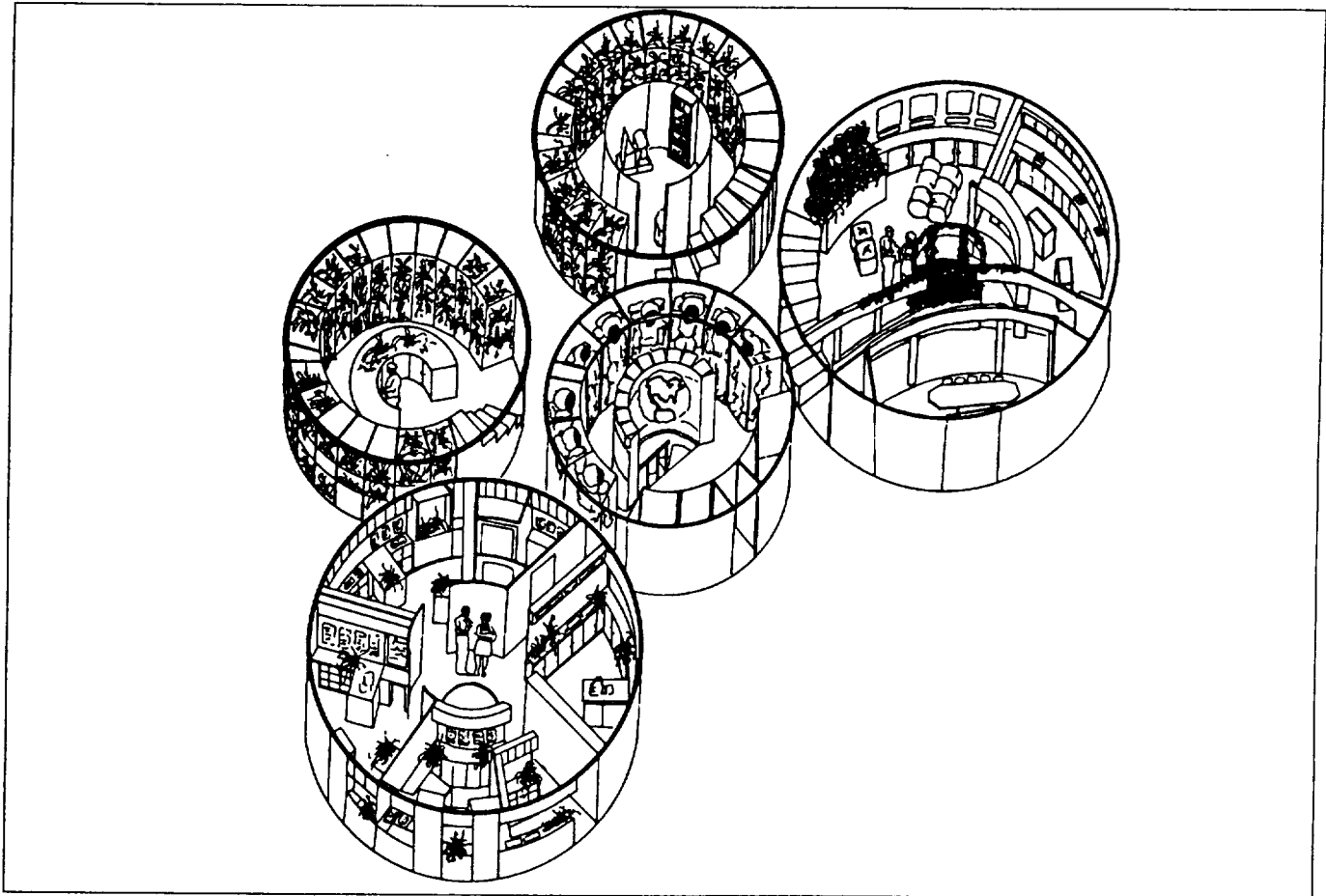


Fig. 6 Axonometric drawing of the main floor (entry level) of Pax, illustrating the embracing entry (center) and separation from crew support facility (lower left to upper right); greenhouse modules are on the upper left.

- embracing entry
- separation of work and play
- circulation efficiency
- dual egress
- creation of a central focus for each module
- homelike environment
- sense of place

Because Pax is to be the astronauts' "home" for two years or more, a designated entrance will mark the "front door" to home. By situating the modules in an embracing formation, slightly set back in the center, crew members will have a sense of "moving within." The indented area is intended to mark a focal point in the habitat. The embracing feature is evident in both the plan and

elevation of the habitat. From the surface of Mars, entry into the habitat is a sequential process. The crew will enter under the shelter system to the primary airlock. From this airlock, the crew will pass through a dust-off chamber before entering the primary circulation space.

Since the crew does not egress the habitat to conduct intravehicular activity (IVA), the concept of designing Pax through a separation of "work" and "play" may help the crew differentiate activities. By physically separating the laboratory and crew support spaces, the crew may feel as though they were going to work, similar to on Earth. Later they have the opportunity to "leave work" and go home for peace and recreation.

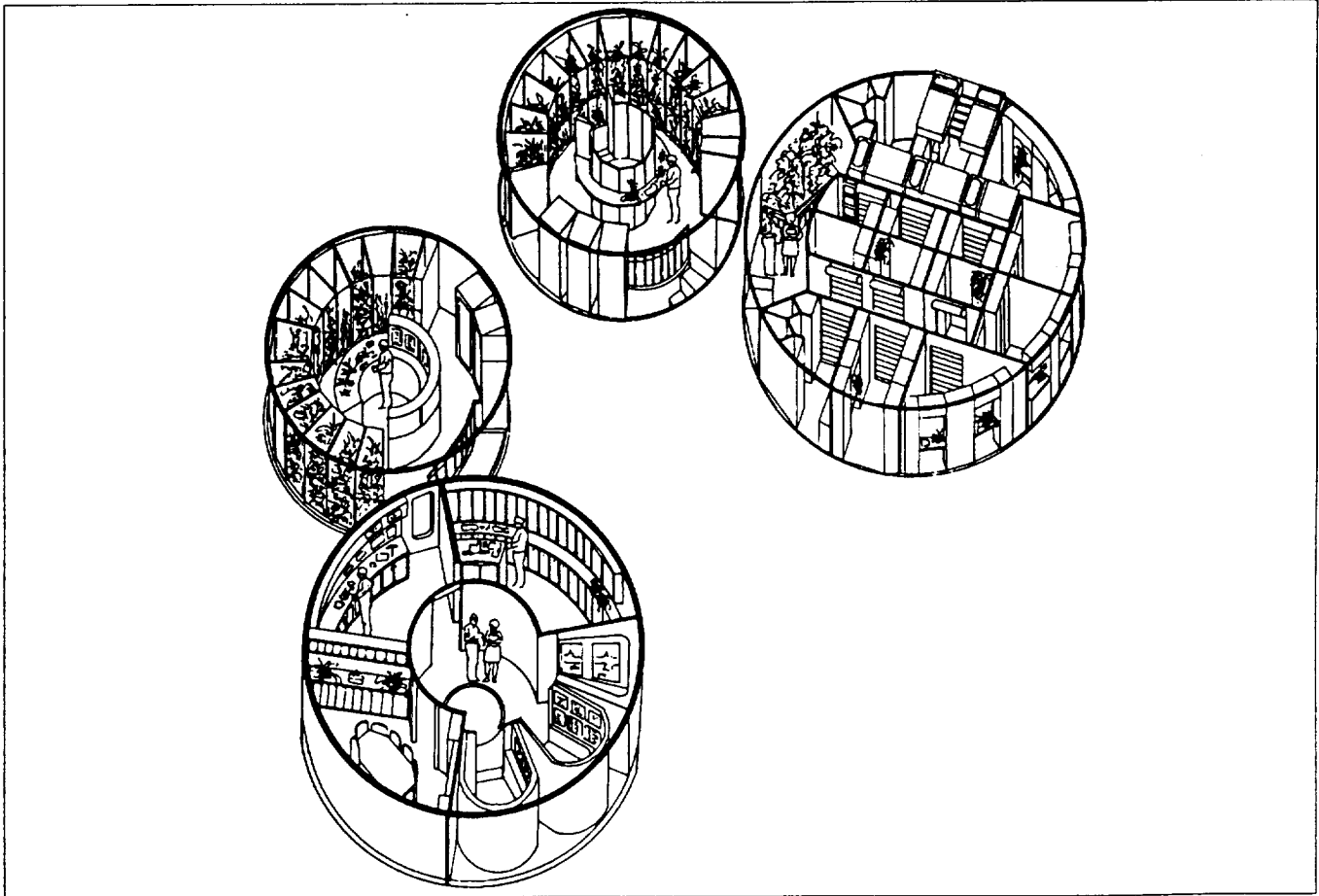


Fig. 7 Axonometric drawing of the upper floor of Pax, illustrating the central focus and group interaction space in each module and the creation of a sense of place and homelike environment in all spaces.

The habitat is organized in an efficient manner. From module to module there are clear, linear circulation paths. Time will not be wasted by excessive walking. Clear circulation and way finding are important in keeping stress levels down. Siting the individual habitat volumes in a straight line would be far too monotonous. Pax is formed in a continuous, looped path. This allows for a variety of circulation routes while still being efficient. As an example, vertical circulation is located either in the center of a module or along the perimeter and horizontal circulation is in the shape of an arc in the crew support module and vertical in the laboratory module.

Dual egress is a critical element in extraterrestrial living. In the event of an emergency, the crew must be able to emergency exit any of the habitat volumes in two opposite directions. Suits and EVA chambers are located in three areas to permit suited egress to the outside.

The entry module acts as the central focus for the habitat as a whole. Creating a central focus in each of the

modules and inflatable is also considered important in making Pax livable. It unifies the volume. Each of the five components also has designated focal points in which the crew can gather.

The ability for the crew to personalize the spaces may provide for a more productive mission. Allowing the crew the luxury of bringing pieces of "home" with them is important in keeping stress levels down. The Martian living environment will be different from that of Earth. Yet the crew should live in a comfortable and familiar way. The crew will be able to bring with them a sense of home. For example, the library can be filled with books that the crew has requested, and the crew quarters can each be decorated to suit individual tastes.

In designing individual spaces, the intent is to create a sense of place appropriate to the functions occurring. For example, the galley should give the impression that it is a galley and not mission operations. The private crew quarters should appear quite different in ambiance from a laboratory.

### Habitat Components

There are five primary components to the proposed habitat--referred to as the entry module (a 9-m hard module), the laboratory and crew modules (both 12-m inflatables), and two greenhouse modules (the other 9-m hard modules). Two logistics/EVA modules and the entry EVA/dust-off module (all Space Station-derived) make up the balance of the habitat. Each habitat space integrates design issues and requirements with the intention of making each space productive, habitable, and comfortable.



Fig. 8 The laboratories in Pax were designed with efficiency and human factors in mind.

The entry module will serve several purposes. Dedicated as a major entry point, the module combines utility with a sense of first impression. Safety, cleanliness, and a sense of arrival are incorporated. This area also serves as a decision point for translation to the laboratory and crew modules. The entire crew will utilize this space. Composed of two levels, entrance from the surface of the planet will be into the upper level of the entry module, while active group recreation resides on the lower level.

The entry module is flanked by the two larger inflatables. It is linked to these inflatables by flexible connectors.



Fig. 9 The greenhouse facilities allow for plant growth for experimentation, food production, or crew recreation.

One inflatable has been dedicated to mission control and laboratory functions of the base. This 12.5 m-module is composed of two levels. Mission control and the botany laboratories occupy the upper level, while additional laboratories and the health maintenance facility (HMF) are on the lower level.

The crew support inflatable accommodates the basic needs of the crew. This inflatable is located to the right of the entry module when approaching from the surface of Mars. This two-level, 12.5-m habitat is comprised of a galley, wardroom, group recreation space, and laundry facility on the lower level, and personal quarters for 18 crew members and two personal hygiene facilities (PHF) on the upper level. Access to this inflatable is through a flexible connection on the lower level from the entry

module. Additionally, a second access point is from another connector on the second level through to private contemplation spaces in the adjacent greenhouse modules.

The two greenhouse modules will decrease the dependency on fresh food supplies from Earth and will provide human factor benefits from access to nature. There are two distinct emphases for the greenhouse modules. One will concentrate on food production and the other will address research and, to a lesser degree, be a place for individual crew members to care for plants. Also included in one of the greenhouse modules are a library and a chapel as retreat areas for the crew.



Fig. 10 The crew quarters provide for single crew members as well as couples.

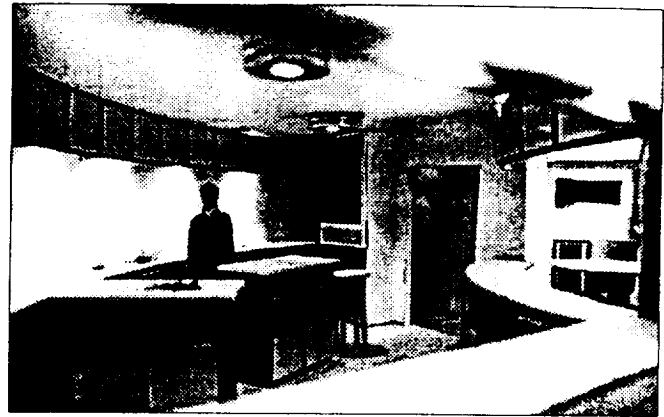


Fig. 11 The galley's design allows for a number of individuals or small groups to use the facility at once.



Fig. 12 A library space within one of the greenhouse modules provides a place for the crew to go to escape from the day-to-day activities of the habitat.

#### **Interior Design Including Considerations of Color, Lighting, and Materials**

Seldom have lunar and Martian designs been taken to a level of design development where the particulars of interior configuration and its impact on human productivity and satisfaction can be examined. An important part of our design work, especially in this project for a first Martian habitat, has been to investigate interior architecture and how it impacts on habitability.

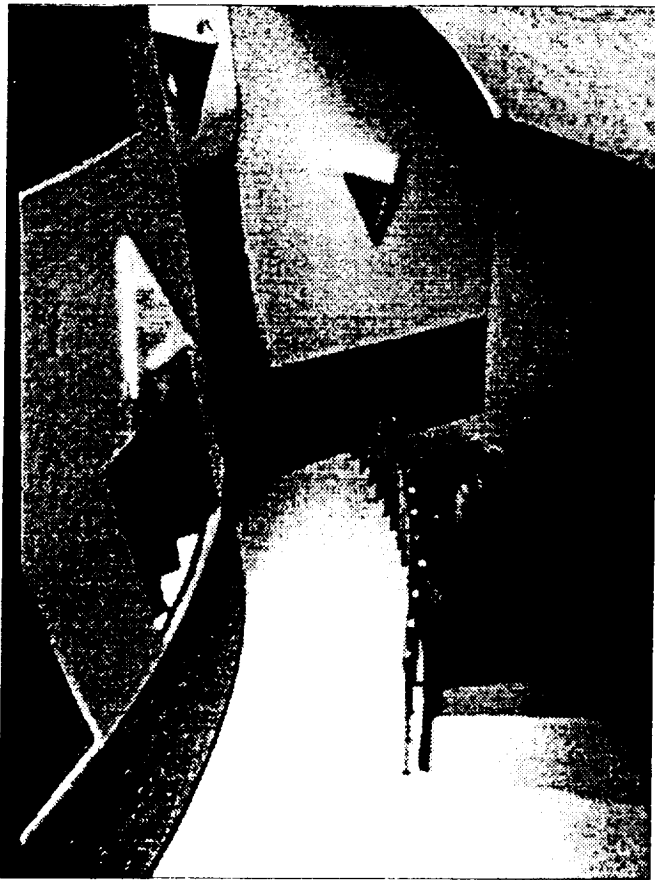


Fig. 13 Use of alternative shapes and sizes within the habitat help to relieve monotony and to create spaciousness.

Careful consideration has been given to technical details, color, lighting, and materials based upon color and material design recommendations from NASA-Ames Research Center and the NASA STD-3000 standards.

The color selection was based on three activity area definitions. High activity areas, e.g., social and recreation spaces, contain large wall spaces in light, lively, warm earth tones and warm pastels. Moderate activity areas, e.g., designated work areas, are finished in calm, low saturation colors. Low activity spaces, e.g., quiet, cozy environments, are finished in light blues and grays.

Pure colors are used rather than drab colors. Bold colors are limited. Shades and pastels are used on large surfaces. Contrasting colors are used to break monotony. Pax therefore makes liberal use of gray tones, pale blue-

grays, burgundies, taupes, off-whites, silvers, deep blues, and terra cottas. A basic color scheme was chosen for particular spaces. A continuity of color was provided from one area to another to relieve the habitat from appearing "chopped up" and discontinuous. Bright colors were used to highlight certain special features, either architecturally or visually. Color also augments the translation pathways throughout the habitat.

Similarly, Pax incorporates a number of lighting systems to increase visual stimulation, add variety, and augment the tasks to be performed. Lighting was used to highlight special architectural features in each area of the habitat.\*

Material recommendations were derived from NASA Man-Systems Integration Standards. Materials will go through sophisticated testing to determine whether outgassing from the product is detrimental to humans or the space environment. Materials were chosen to aid mission activities and tasks. For example, surface materials in the laboratories allow for ease of task and maintenance. While reflective properties, non-contamination and non-discoloring properties, durability, and deterioration were considered, a variety of materials with textural surfaces are included to vary the environment and to stimulate the confined astronauts visually and tactilely.

#### Summary:

##### Major Strengths and Limitations of the Design

Uncountably many decisions go into any design. All decisions that are made have the overall objectives of the design as their driver and, hopefully, empirical research as their justification. Sometimes these design decisions conflict with each other. This design, as all design, has strengths and limitations. Following are some of the most notable.

- One of the strong points of this proposed design for the first Martian base is economic in nature. The habitat uses rigid modules already on-site from an initial exploratory landing. The four pre-landed hard modules make up over half of the habitat. Taking advantage of these saves extra mass that would otherwise need to be delivered.

- Another of the large scale elements of the base that works well is the radiation shielding. Its design allows it to be in place before the modules of the base are put in place, providing shielding during base construction. A protected area is provided around the modules giving easy access for maintenance. The structure--being an encompassing space frame--also allows for easy expansion.
  - The zoning of the habitat works well. Work is separated from leisure, public from private, noisy from quiet, and active from passive. This can be seen in the functions of the individual modules and in the difference in the floor levels within each module.
  - Within the habitat, a number of spaces provide for privacy, a place for a crew member or small group to get away. The crew quarters are the primary location for crew "escape." Passive recreation also can allow privacy. The chapel and library are two more areas that allow for this important need for occasional isolation.
  - Spatial variety is another way this design excels. Supplementing the rigid modules with inflatable modules adds variety to the spaces. Although all of the habitat modules are generally the same shape, a number of different types of spaces are created within. While some shapes may be pie-shaped, others are rectilinear, and still others are curvilinear. A variation in ceiling height and floor levels helps further to create this variety of spaces throughout the habitat.
  - Active recreation is isolated from other functions within the base, preventing excess noise and vibration created in the space from becoming a problem.
  - Using 9-m and 12-m circular modules minimizes circulation space while maximizing net usable activity space and volume.
  - The entry EVA chamber is separated from other spaces, helping to keep dust from spreading throughout the habitat.
  - Dual egress is allowed throughout the habitat; there are always two ways of escaping any area.
  - The modular rack system allows easy changeout, replacement, and rearrangement throughout the habitat, not only at IOC, but also if the habitat is expanded to various NOCs.
  - Using a number of enclosures (modules) allows containment of trouble areas in the event of an emergency, yet allows large spaces and easy connection of associated functions.
  - The loft-type crew quarters make efficient use of vertical space.
  - The connection of the crew quarters to the greenhouse allows convenient access to quiet spaces for the crew during off-hours.
  - Situating the library and chapel within a greenhouse creates a restful environment.
  - Having two greenhouse modules, each with its own atmosphere, adds to the scientific benefit and productivity of the base.
- There are also limitations and other issues where the base and habitat could be improved:
- The site location needs further investigation, e.g., the choice of the Utopia site does not allow direct communication with Earth.
  - The habitat may be larger than necessary for 18 crew members, and might be optimized to a smaller volume.
  - Spaces exist with no function (e.g., the center of the first floor in the crew support module). While these are desirable aesthetically, they may be extraneous in terms of efficiency, mass at lift-off, and economics.
  - Even though the radiation shielding makes views possible, views out of the base are limited to one window in a mission command workstation. Smart windows could also be considered.
  - A drawback of the structure is its complexity. A large amount of mass, hundreds of pieces, will need to be delivered to the Martian surface. The structure will

likely involve extensive EVA time in assembling the truss-work.

- There is a redundancy of equipment and spaces within the labs; dual functioning could cut down on the amount of space and equipment needed.
- The vertical circulation throughout the habitat needs more thought (e.g., convenience, comfort, practicality, extent of use).
- The nature of the laundry facilities (closet-like) and location (on a major circulation intersection) makes it problematic.
- A more direct connection between the galley and wardroom would be desirable.
- The airlock attached to the labs may be used as much as if not more than the entry EVA. This airlock should therefore have suit storage and a preparation area outside of the equipment lock.
- Consideration could be given to growing plants throughout the habitat to minimize boredom of the dead Martian landscape.
- The means of transportability of the modules from the exploratory site to the IOC site needs consideration, e.g., while the 9-m module can easily be transported to Mars, it may not be able to be moved about the surface of Mars easily.
- The structural and construction systems for each of the modules need careful consideration.
- Mass at lift-off needs to be reduced where possible and quantified in order to be optimized.

### Issues for Future Research and Design Development

Four areas of primary research and design development need to be conducted as a result of the above project.\*\*

1. More attention needs to be given to the development of human factors and EB requirements for all scales of Martian campsites/outposts and permanent

habitats. Some work has been done on requirements for lunar and Martian bases in our center<sup>7</sup> as well as by Joyce Carpenter and Deborah Neubek at NASA-JSC, but as far as we can determine, no work has yet been done for Martian bases. The first missions will likely be 14- to 45-day missions to the Moon, which will more than likely be a testbed for future Martian exploration and habitation. A full range of habitability requirements for 14- to 45-day lunar missions needs to be developed. An interesting issue would be to investigate, first, the quantitative space demands and then the qualitative habitability requirements for short-duration missions, and how they would change for increasing numbers of crew members and for increasing mission durations. One part of this would be the definition of usable space (e.g., the tables in NASA-STD-3000 on usable volumes), and how it should vary with crew composition, mission profiles, and mission durations. It would similarly be very useful to conduct an analysis of usable space to gross space, and usable space to surface area (i.e., correlated to mass at lift-off).<sup>7</sup>

2. Minimally necessary activity spaces and their minimally necessary sizes (both in terms of  $m^2$  of floor plan and  $m^3$  of volume) need to be investigated. Our work to date has suggested a minimally necessary set of laboratory and crew support spaces, but considerably more work needs to be done to refine this list. Similarly, our work to date has begun to suggest possible spatial allocations for each of these spaces (for 12 and 18 crew members), but again, the work has only scratched the surface, indicating the importance of careful human factors analyses--and perhaps terrestrial simulations--of these quantitative requirements.
3. The design concepts expressed in this paper and companion technical report could be subjected to independent investigation and corroboration. Any design is made up of a variety of design concepts, not just one overarching *parti*. The concepts, sometimes called patterns, are generic, or, at least, the central idea is generic, though the particular form a pattern takes depends on contextual circumstances. These and other patterns<sup>8</sup> could be articulated, assessed qualitatively against existing research literature, and then subjected to empirical tests in simulated environments (using experimental or quasi-

experimental methods). This would result in a series of tested principles that could be applied to the design of any Martian (and perhaps) lunar base and habitat.

4. The implications of different images for the likely crew compositions need to be considered. For example, are high-tech or more homey, Earth-like environments more appropriate for NASA- and related space-agency highly trained, highly self-selected crews? There is an ideological assumption in our work to date, but it has not been tested, that bringing home to Mars is appropriate. The importance of this assumption needs to be questioned, Antarctica and other simulation research needs to be checked, and perhaps first-hand empirical research needs to be conducted with current and recent American, Russian, and other astronauts on the appropriateness or lack of appropriateness of this assumption. Similarly, research needs to be done profiling the personality characteristics of astronauts likely to go to Mars (e.g., possibly a variation of an environmental response inventory with characterization of environmental dispositions), with base design decisions based on these profiles and preferences.
5. Quantitative considerations of structure, construction, efficiency, and minimization of mass a lift-off need to be weighed carefully and balanced against qualitative EB habitability considerations.

A fundamental dilemma underlies all of this needed research and design investigation. First is the advisability of thoroughly investigating a narrow range of issues (e.g., human factors/environment-behavior issues) versus a more comprehensive analysis of the complete range of Martian base issues (e.g., habitability and construction technology, or simultaneous consideration of two or three different prototypes, the latter allowing the exploration of the possibility of major changes during the life of the base, and the possibility of taking concept designs into further design development before capitalizing on certain alternatives while abandoning others). Another way to put it is to ask is it more important at this stage of Martian design exploration to "design society" or to focus on the solution of knowable, manageable issues?

### Acknowledgments

The Space Architecture Design Group for 1991-92 is comprised of Dr. Gary T. Moore, project director and faculty advisor; Joseph P. Fieber, Janis Huebner-Moths, Kerry I. Paruleski, and Patrick J. Rebholz, NASA/USRA TAs and team leaders; and Adam Demler, Peter Froelich, Andrew Haynes, Renee Jankuski, Scott Maner, Cory Peterson, Amy Schwalbach, and Scott Starks of UW-Milwaukee who contributed to the design project reported in this paper. Our thanks to Kay Nute of USRA for editorial assistance, and to Paul Olson of UW-Milwaukee for photographic assistance. Address: Advanced Design Program in Space Architecture, Department of Architecture, University of Wisconsin-Milwaukee, Milwaukee, WI 53201-0413; Tel: 414/229-3818 or 229-5940; Fax: 414/229-6976; E-mail: gtmoore@csd4.csd.uwm.edu.

### References

1. Stafford, T.P. America at the Threshold: Report of the Synthesis Group on America's Space Exploration Initiative. U.S. Government Printing Office: Washington, D.C., 1991.
2. Weaver, D. SEI Reference Mission. Paper presented at the ExPO Technical Interchange Meeting, Exploration Programs Office, February 1992.
3. Zubrin, R.M., Baker, D.A., and Gwynne, O. Mars direct: A coherent architecture for the Space Exploration Initiative. Paper presented at the 27th Joint Propulsion Conference, Sacramento, California.
4. Moore, G.T., Huebner-Moths, J., Rebholtz, P.J., Fieber, J.P., and Paruleski, K.L.. Lunar base requirements for human habitability. In Sadeh, W.Z., Sture, S., and Miller, R.E. (eds.) Engineering, Construction, and Operations in Space III: Space 92, Proceedings of the Third International Conference, New York: American Society of civil Engineers, Vol. 1, pp. 224-239.
5. Fisher, J., Bell, P., and Baum, A. Environmental Psychology, 2nd ed., Holt, Rinehart, and Winston: New York, 1978.



6. Carr, M.H. Scientific objectives of human exploration of Mars. Paper presented at the Third Case for Mars Conference, Boulder, Colorado, July 1987.
7. Moore, G.T. and Rebholtz, P.J. Aerospace architecture: A comparative analysis of five lunar habitats. Paper presented at the American Institute of Aeronautics and Astronautics Aerospace Design Conference, Irvine, California, under review.
8. Moore, G.T. and Huebner-Mothes, J. Genesis II advanced lunar outpost: Human factors design response. In Bell, L. (ed.), Proceedings of the First International Design for Extreme Environments Assembly, University of Houston: Houston, in press.

## MICROGRAVITY IGNITION EXPERIMENT

**Worcester Polytechnic Institute  
Mechanical Engineering Department  
Worcester, Massachusetts**

**Professor Vahid Motevalli  
William Elliott, Teaching Assistant  
Keith Garrant, Ryan Marcotte**

### Abstract

The purpose of this project is to develop a flight-ready apparatus of the microgravity ignition experiment for the GASCAN II program. The microgravity ignition experiment is designed to study how a microgravity environment affects the time to ignition of a sample of  $\alpha$ -cellulose paper. A microgravity environment will result in a decrease in the heat transferred from the sample due to a lack of convection currents, which would decrease time to ignition. A lack of convection currents would also cause the oxygen supply at the sample not to be renewed, which could delay or even prevent ignition. When this experiment is conducted aboard GASCAN II, the dominant result of the lack of ignition will be determined. The experiment consists of four canisters containing four thermocouples and a sensor to detect ignition of the paper sample. This year the interior of the canister was redesigned and a mathematical model of the heat transfer around the sample was developed. This heat transfer model predicts an ignition time of approximately 5.5 seconds if the decrease of heat loss from the sample is the dominant factor of the lack of convection currents.

### Introduction

One of the most important issues for long-term space occupation, such as in a space station, is fire safety. The very low gravity condition in space can drastically affect the phenomena of combustion and fire. In order to maintain fire safety, the initiation of the combustion phenomenon, ignition, must be understood. While ignition has been studied, the effect of a microgravity environment on the ignition process is not completely understood. The purpose of this project is to determine how the microgravity environment affects ignition time.

A major factor in the ignition process is heat transfer. As a fuel source is heated, products are released due to molecular breakdown of the sample. This process is referred to as pyrolysis. These products mix with the surrounding air and, when a sufficient amount of heat has been transferred to the sample, make ignition possible.

There are three ways in which heat is transferred into or away from an object. These are radiation, conduction, and convection. Heat may be transmitted by the emission and absorption of radiation. In addition to heat transfer due to radiation, there is heat transfer due to the contact of two objects of different temperatures. This is referred to as conductive heat transfer. Finally, heat may be transferred by convection currents in the air.

Convection currents result from buoyancy forces caused by earth's gravity. When a substance is hotter than the surrounding air, the temperature of the air near the surface of the substance increases because of the transfer of heat. Convection currents force the less dense heated air to rise away from the hot substance and the cooler, more dense air to sink to the surface of the substance, as shown in Figure 1.

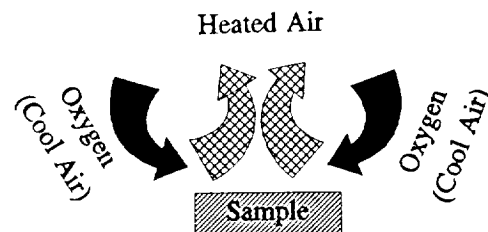


Fig. 1 Convection currents on Earth

Oxygen (Cool Air)

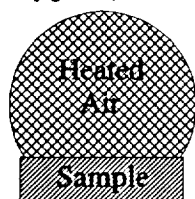


Fig. 2 Lack of convection in microgravity

Due to the lack of gravity in a microgravity environment, convection currents are not present. This lack of convection currents causes a cloud of heated air and pyrolysis products to form around the object, as shown in Figure 2. This will cause a reduction in the heat transferred away from the object, increasing the object's temperature, therefore decreasing the time to ignition. The absence of convection currents also prevents the cooler, oxygen rich air from sinking towards the object. It is possible that the lack of this oxygen may stop ignition from occurring at all. The purpose of this experiment is to determine how these conflicting processes affect the time to ignition by collecting and comparing data regarding ignition in microgravity and on Earth, and analyzing the results.<sup>1</sup>

### Previous Projects

The microgravity ignition experiment is a continuing project. The first Major Qualifying Project (MQP) on this project was completed in 1986. This project determined the purpose of the experiment and resulted in construction of a prototype. In addition, various types of sensors were investigated for the measurement of flux, temperature, and ignition.<sup>2</sup>

Later groups considered many different substances for the test sample. Eventually, National Bureau of Standards  $\alpha$ -cellulose (paper) was selected for its relative consistency. This was chosen because the properties of the paper are relatively constant, and the heat required to ignite the paper is not excessive.<sup>3</sup>

The initial combustion chamber was redesigned by the

1990 MQP group. The 1991 MQP group investigated the reliability of the equipment for the experiment. They discovered that the moisture content of the  $\alpha$ -cellulose paper affected the time to ignition. A procedure for drying the test sample was then developed. In addition to this and their development of the alignment apparatus and procedure, low temperature testing of the experimental components was conducted.<sup>3,4</sup> Modifications in the chamber have been made by this year's team.

Previous projects also considered many possible heat sources. An Argus type 44 infrared heat lamp with a gold-plated reflector was chosen for the heat source. The 1991 MQP group designed and fabricated a lamp alignment apparatus. Using this device they developed a procedure for aligning the bulb both horizontally and vertically. This focuses the lamp and allows the point of maximum heat flux to be concentrated on the test sample.<sup>4</sup>

Jeff Goldmeer's master's thesis developed a heat transfer model for a copper plate. This model had problems finding the convection coefficient because of the difficulty in modeling the heat transfer caused by the contact of the copper with the teflon backplate.<sup>5</sup> This model was used as a basis for the heat transfer model of  $\alpha$ -cellulose paper.

### Experimental Apparatus

#### Chamber

The experiment consists of four combustion chambers. The combustion chamber is an aluminum cylinder to which four aluminum plates are mounted. Plates one and two mount the infrared heat lamp on the cylinder. Plates three and four are used to position a teflon holder. This holder supports the paper sample and all sensors mounted within the ignition chamber. Plate four also contains ports for a pressure transducer and two purging valves. The chamber is designed to be airtight and contain dry air at slightly higher than atmospheric pressure. Figure 3 shows a diagram of the total configuration of the canister.

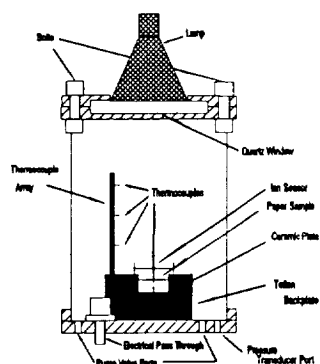


Fig. 3 Experimental canister

### Heat Lamp

The heat lamp is an Argus model 44 infrared heat lamp. It consists of a 250-watt bulb that requires 24 volts to operate. This bulb is mounted within a gold-plated parabolic reflector. The bulb and reflector are separated from the experimental chamber with a circular quartz window.

### Instrumentation

**Ion Sensor** There are currently four types of sensors that are used in the experiment. One of these is an ion sensor. Three of the canisters that contain a paper sample also contain the ion sensor. The ion sensor is used to determine when ignition occurs. It consists of two stainless steel wires that are mounted above the test sample forming an open circuit. When the sample burns, ions that allow a current to pass between the two wires are produced, completing the circuit. When the circuit is completed, a voltage is produced indicating that ignition has occurred.

**Thermocouples** Another type of sensor used is a thermocouple. The thermocouples are used to measure temperature. Three of the canisters contain four thermocouples in each chamber. One of the thermocouples is used to measure the backface temperature of the sample. The other three are set up in a thermocouple array to determine the temperature at

different distances from the test sample. This data can be used to approximate the temperature gradient within the canister.

**Pressure Transducer** The pressure in these three canisters is monitored throughout the experiment with a pressure transducer. The data provided by the pressure transducer can be used to determine the pressure rise caused by the lamp and/or pyrolysis at any point during the experiment. This is useful in more complete thermodynamic analyses. The data can also be used to determine if the seal of the canister was intact at the beginning of the experiment. This is necessary in order to establish that the environment inside the canister contained only the dry air with which it was purged.

**Flux Meter** One canister will not contain a sample of  $\alpha$ -cellulose paper. It will instead contain a gardon gage. This will be used to measure the flux output of a bulb in microgravity. This was done because the flux output of the lamp may be different due to the lack of convection currents within the bulb in microgravity. This canister will not contain an ion sensor, a sample backface thermocouple, a thermocouple array, a pressure transducer, or purge valves.

**Purging Apparatus** In order to produce repeatable results, it required that a dry environment be maintained within the canister. This is because the paper sample would absorb any moisture present in the air which would affect the time to ignition of that sample. It was decided to provide this dry environment by purging the sealed canister with dry air. This method consists of two valves, one inlet valve and one outlet valve, mounted directly to the bottom aluminum plate. The three canisters which contain the paper sample also contain these valves.

**Data Acquisition** The data acquisition system developed this year in Marcotte's MQP controls the experiment sequencing. In addition, it stores the results of the experiment in non-volatile EE PROMS. This allows the data to be maintained even when the GASCan batteries are drained. The data acquisition system also contains the preflight diagnostics. All of the electric systems of the experiment can be tested with a personal computer. The chips for the data acquisition system are rated to  $-25^{\circ}\text{C}$ .<sup>1</sup>

### Sequence of Experiment in Space

The three experiments contained within the GASCan II will be run in a sequence, with microgravity ignition being the first experiment in the progression. The sequence will be started by an astronaut at the beginning of the first sleep period. Running the experiments during the sleep period will provide an environment with the least activity and the lowest acceleration. The astronaut will flip a switch, signaling the power up of the GASCan. Figure 4 illustrates the sequence of the microgravity ignition experiment.

After the GASCan itself has been powered up, power will be provided to canister one of microgravity ignition. This is the canister that contains the gardon gage instead of the paper sample. The lamp will be turned on and run for 15 seconds. The software designed by the electrical engineering portion of the team will sample the data for the duration of the run. After 15 seconds the software will turn the lamp of canister one off and pause for 5 seconds before signaling canister two.

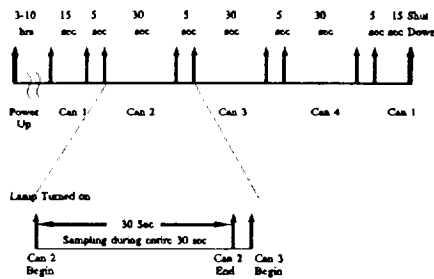


Fig. 4 Experimental sequence

When the software controlling canister two receives its signal, the lamp is turned on, sampling from all the sensors begins, and a timer is started. This continues until the ion sensor detects ignition of the paper sample. At this point, the lamp will be turned off. Sampling of the sensors will continue until the timer, which was started at the beginning of the run, reads 30 seconds. Canister two is then powered down. If ignition is not detected within

30 seconds, the lamp will be turned off and sampling will stop at the 30 second mark. Canisters three and four are run identically to canister two.

Canister one will be run again 5 seconds after the power down of canister four. It will be run following the same procedure that was used during its first run. The data from this run will be compared with the data from the first run to determine if drainage of the batteries has caused any changes in the flux output of the lamp.<sup>6</sup>

### Heat Transfer Model

A mathematical model of the heat transfer in the canister for a copper plate was developed in Jeff Goldmeer's master's thesis. This model was redone to take into account some changes in the chamber design and the use of  $\alpha$ -cellulose paper. First, the energy balance was considered.

$$E_{\text{stored}} = \alpha I - \dot{q}_{\text{cond}} - \dot{q}_{\text{conv}} - \dot{q}_{\text{rad}} \quad (1)$$

The energy stored by the paper is:

$$E_{\text{stored}} = \rho c d \frac{\delta T_s}{\delta t} \quad (2)$$

The heat transfer due to convection is:

$$\dot{q}_{\text{conv}} = \bar{h}(T_s - T_{\infty}) \quad (3)$$

The heat transfer due to radiation is:

$$\dot{q}_{\text{rad}} = \sigma \epsilon (T_s^4 - T_{\infty}^4) \quad (4)$$

The teflon backing was redesigned in order to eliminate conductive heat transfer with the sample, which was a major problem with the Goldmeer model. Because of this, conductive transfer can be ignored. Combining this fact with equations (1), (2), (3), and (4) yields:

$$\rho c d \frac{\delta T_s}{\delta t} = \alpha I - \bar{h}(T_s - T_{\infty}) - \sigma \epsilon (T_s^4 - T_{\infty}^4) \quad (5)$$

Finally, solving this equation for  $h$  results in:<sup>5</sup>

$$\bar{h} = \frac{\alpha I - \rho c d \frac{\delta T_s}{\delta t} - \sigma \epsilon (T_s^4 - T_\infty^4)}{T_s - T_\infty} \quad (6)$$

In addition the following equation was used for the heat flux from the lamp with  $I_0$  and  $\tau$  being constants:<sup>7</sup>

$$I = I_0 \left[ \left( 1 - e^{-\frac{\tau}{a}} \right) + e^{-\frac{\tau}{a} \left( \frac{t-t_0}{a} \right)} - e^{-\frac{\tau}{a}} \right] \quad (7)$$

In order to predict the temperature change of the sample in microgravity, the convection coefficient was set to zero and was solved using Lotus 123. A graph of the results for the sample temperature is shown in Figure 5. Figure 6 displays a graph of the flux output of the lamp and the reradiation loss of the paper.

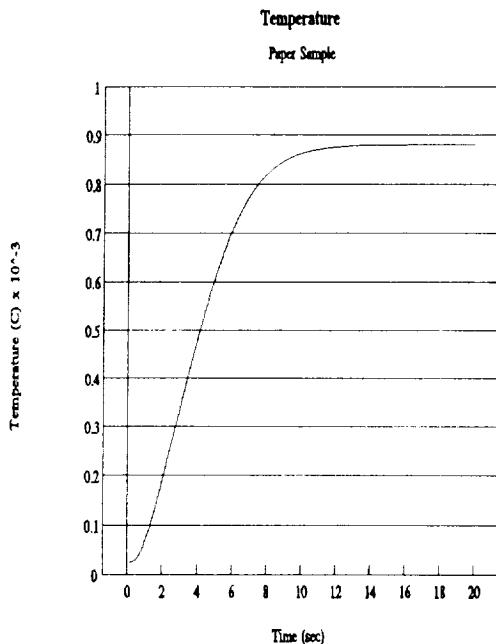


Fig. 5 Temperature of the paper sample

According to Figure 5, the sample will reach its

pyrolysis temperature of approximately 625 degrees C at approximately 5.5 seconds. The 1991 team determined that the average time to ignition on earth using the baseplate with conduction was 13 seconds. This predicted decrease in the ignition time is a result of the lack of convection currents and the assumption of zero conduction loss. If the lack of convective heat transfer overpowers the lack of oxygen supply, then this prediction will be accurate. However, this model is not valid if the sample does not ignite because of the oxygen deficiency.

Figure 6 shows Hagdoust's estimate of the warming curve of the lamp. In addition, if the lamp is continuously operated, it is predicted that a steady state condition will be reached at approximately 14 seconds. At this point, the heat flux from the lamp equals the reradiation loss from the sample. This results in the flattening of the curve seen in figure 6.<sup>1</sup>

## Results

A baseline experiment was run using the new teflon backplate. Due to problems with the new experiment controller, Labtech Notebook was used to acquire the data.

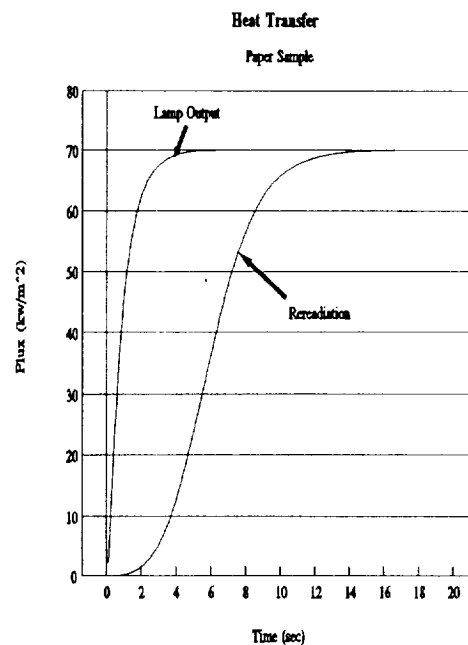


Fig. 6 Flux output of the lamp and reradiation loss of the paper

Figures 7 - 10 show the results of this experiment. These figures display the changes in temperature that occur within the canister and not the actual temperatures that are felt. The temperatures measured by the thermocouples are close to but slightly less than what was expected. It is possible that this is because the thermocouple junctions are large and that the backface thermocouple was not in contact with the paper. However, the results show the expected trends. Figures 7 - 10 display the results for the thermocouple array from one run. Figure 10 illustrates the results for the backface thermocouple from two separate tests. Both sets of results show the correct trend and show that the results obtained are very repeatable.<sup>1</sup>

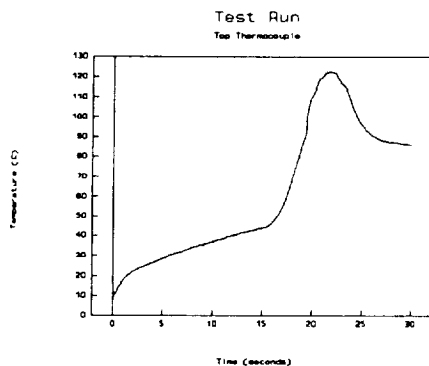


Fig. 7 Top thermocouple

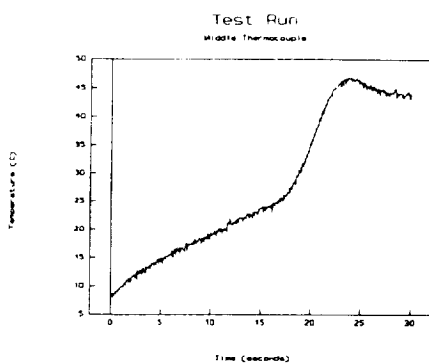


Fig. 8 Middle thermocouple

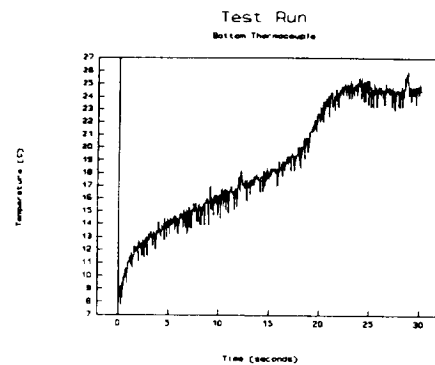


Fig. 9 Bottom thermocouple

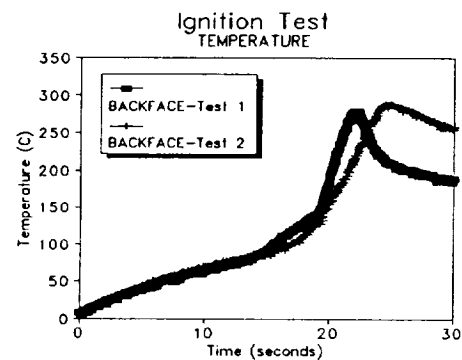


Fig. 10 Backface thermocouple

## References

1. Garrant, K.E., Lusk, A.L. Microgravity Ignition, Worcester Polytechnic Institute, Major Qualifying Project, 1992.
2. Blacker, P.L., Dilorenzo, J.E., Vlangas, C.P. Shuttle Project II-Microgravity Ignition, Worcester Polytechnic Institute, Major Qualifying Project, 1988.
3. Forget, P.L., Mattor, E.E., Siemasko, J.S. Microgravity Ignition Experiment, Worcester Polytechnic Institute, Major Qualifying Project, 1990.
4. Maranghides, A., Roy, P. Microgravity Ignition Report, Worcester Polytechnic Institute, Major Qualifying Project, 1991.

5. Goldmeer, J. Determination of Natural Convection Coefficient in Low-Gravity, Worcester Polytechnic Institute, Master's Thesis, 1991.
6. Marcotte, R. Microgravity Ignition Controller Design, Worcester Polytechnic Institute, Major Qualifying Project, 1992.
7. Hagdoust, M.H. Experimental Evaluation of Transient Natural Convection Coefficient, Worcester Polytechnic Institute, Master's Thesis, 1991.



---

**Aeronautics Projects**



## SUMMARY OF THE 1991-1992 AERONAUTICS DESIGN PROJECTS

Auburn University  
Department of Aerospace Engineering  
Auburn University, Alabama

Dr. J. O. Nichols  
Brent Foreman, Teaching Assistant

### Abstract

The Auburn University design groups have completed a study of regional transport aircraft culminating in two approaches for the design of a regional transport aircraft. Under the sponsorship of the NASA/USRA Advanced Design Program, the design project was suggested by S. J. Morris, center mentor at Langley Research Center, and implemented in the senior-level design courses at Auburn University. The first design (the DART-75) is based on a 75-passenger turbofan-powered regional aircraft, and the second design (the Eagle RTS) on a 66-passenger twin-turboprop powered regional aircraft design. The DART utilizes a three lifting surface configuration with aft-mounted turbofans and advanced aircraft components, and has a range of 1050 nautical miles. General descriptions of the structures, weight and balance, stability and control, performance, and engine design are included. The Eagle RTS has a similar layout to the DART, with aft-mounted pusher-props, and a range of 836 nautical miles. A study of the narrow-body aerodynamics, performance, stability and control, structures and materials, propulsion, and cost analysis is included. Both aircraft are designed for regional use and should breathe new life into the 50-100 passenger aircraft market.

**N94- 25708**

### DESIGN OF THE ADVANCED REGIONAL AIRCRAFT, THE DART-75

Steve Elliot, Jason Gislason, Mark Huffstetler,  
Jon Mann, Ashley Withers, Mark Zimmerman

### Introduction

The need for regional aircraft stems from the problem of hub airport congestion. Regional travel will allow a

passenger to commute from one spoke city to another spoke city without entering the congested hub airport. In addition, those people traveling longer routes may begin the flight at home instead of traveling to the hub airport.

At this time, there is no American aerospace company that produces a regional transport for under 100 passengers. The intention of the Developmental Advanced Regional Transport (DART-75) is to fill this void with a modern, efficient regional aircraft. This design achieves the efficiency through a number of advanced features including three lifting surfaces, partial composite construction, and an advanced engine design.

Efficiency is not the only consideration. Structural integrity, fatigue life, ease of maintenance, passenger comfort and convenience, and environmental aspects must all be considered. These factors force the design team to face many tradeoffs that are studied to find the best solution. The final consideration that cannot be overlooked is that of cost.

The DART-75 is a 75-passenger medium-range regional transport intended for spoke-to-spoke, spoke-to-hub, and some hub-to-hub operations. Included are the general descriptions of the structures, weight and balance, stability and control, performance, and engine design.

### General Design

The configuration, as seen in Figure 1, has three lifting surfaces, which enable the airplane to be trimmed without using negative lift. Three lifting surfaces also provide a more efficient takeoff and landing. The lifting surfaces include the canard, uniquely shaped wing, and a lifting horizontal tail. Table 1 gives some basic design and geometrical parameters of the aircraft.

**PRECEDING PAGE BLANK NOT FILMED**

The semi-diamond shaped wings are designed to provide efficient fuel placements. The large inner portion of the wing, where structural integrity is most easily maintained, is used to hold most of the fuel. Therefore the outer portion can be made lighter, thus decreasing overall weight of the aircraft. The inner portion of the diamond also provides for around half of the lift of the airplane, therefore maximizing efficiency though structural soundness. To eliminate the cost involved in the development of a new airfoil design, the NACA 2412 standard airfoil was adopted for the DART 75. This airfoil provides the lift and drag characteristics necessary for this design. By choosing an existing airfoil, more time was given to determine the actual flight characteristics of the uniquely designed wing.

Table 1 Basic design parameters

|                        |          |
|------------------------|----------|
| Number of Seats        | 75       |
| Number of Crew         | 5        |
| Range (n mi)           | 1050     |
| Cruise Mach            | 0.7      |
| Wing Area (sq ft)      | 615      |
| Wing Span (ft)         | 75       |
| Aspect Ratio           | 9.14     |
| M. A. C. (ft)          | 10       |
| Fuselage Diameter (ft) | 11       |
| Fuselage Length (ft)   | 95       |
| Tail Span (ft)         | 26       |
| Canard Span (ft)       | 26       |
| Takeoff Thrust (lb)    | 35,000   |
| Cost Range (millions)  | \$ 18-28 |

With a span of 75 feet, the semi-diamond shaped wing has an aspect ratio of 9.14. The canards and the tail both span 26 feet. The tail, while providing a marginal lift increase, is mainly used as a control surface and as a stability measure.

The canard is placed forward and low on the fuselage to decrease interference on the engine inlets at various angles of attack. The semi-diamond wing is placed higher than the canard, at mid-length of the body. The engines are located behind and slightly above the wing. This stacking effect will help eliminate the possibility of canard

vortices entering the engine.

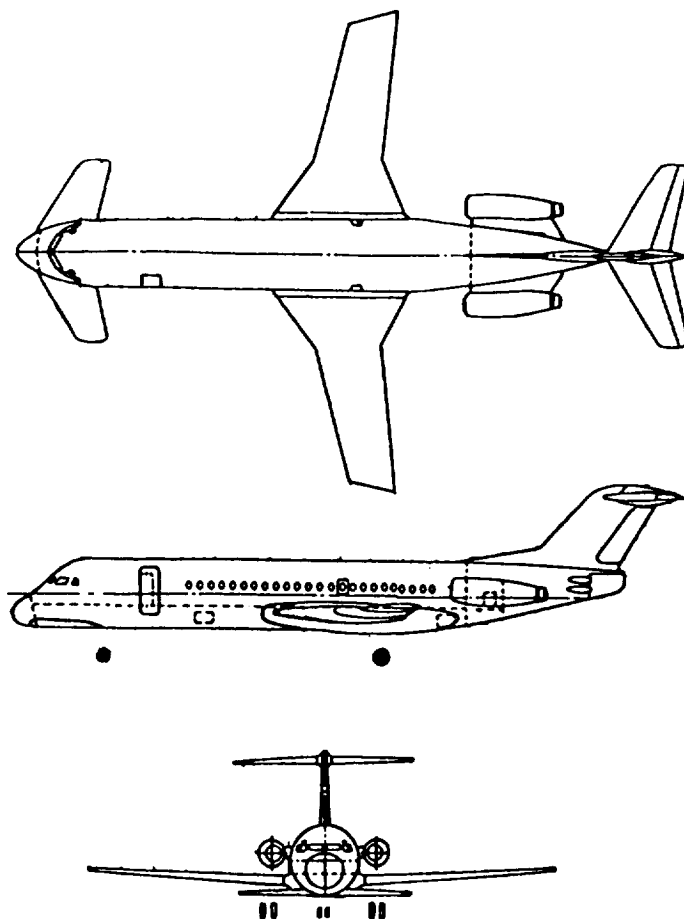


Fig 1 Three-view of the DART-75

The body of the DART has a diameter of 11 feet. The basic interior configuration consists of the flight deck, followed by the stewards' area, galley, and lavatory. Next is the passenger compartment containing five abreast coach seating with an overhead storage compartment on each side. The rear stewards' section consists of an additional lavatory and possible galley. There are three stewards to accommodate the 75 passengers.

The aircraft has a two-person flight crew assisted by an advanced technology glass cockpit. A digital fly-by-wire flight control system will be utilized for the aircraft.

The preliminary cost estimate of the DART-75 was slightly over 30 million dollars per plane. This cost seemed rather high to be competitive, but research into the cost of aircraft in this class resulted in a change of this impression. The new Canada Air Regional Jet costs about \$18 million per plane, and only carries 50 passengers. In light of these estimations, the cost of the DART was expensive, but not unreasonable.

The cost of the DART-75 was estimated using the DAPCA IV model of aircraft cost. In this method, a factor representing the amount of composite materials used has to be chosen. A slight reduction in this number results in a considerable decrease in cost. By using slightly fewer composite materials, the cost of the DART-75 can be reduced to about 28 million at 100 units. The overall weight of the aircraft will not be greatly affected since only slight modifications in the amount of composite materials were made. The final cost per aircraft will range from about 18 million to 28 million dollars, depending on the number of aircraft produced.

### Structures

One of the most important aspects of any aircraft design is the structural integrity of the craft. To determine the integrity of the plane, the loads must be identified and calculated. From the loads, the shear forces and moments can be determined, and then finally the levels of stress can be calculated. These steps must be taken for the wing, canard, tail, and fuselage.

The construction of the DART-75 will not vary much from conventional designs. The actual material make-up of the DART will consist mainly of an aluminum alloy. However, some composites will be used to construct the top of the wings, horizontal tail, canard, and parts of the fuselage. The determination of the type of composite used, whether graphite epoxy or fiberglass, will require time for further investigative analysis.

The structures will consist of a relatively thin skin along with stringers to handle most of the bending stress. This

construction is approximated by a stiffened beam of skin and stringers, where the skin does not handle any normal stress. The stringers that are used to calculate the stresses were assumed to be rectangular. The stiffened beam approximation and the rectangular stringers tend to make these estimates conservative.

Using these estimations, the stress levels in the stringers are calculated. The material used for the structural members was 6061-T6 wrought aluminum. This material is very widely used in the aircraft industry, and is known to have yield strength of 35,000 psi and an endurance limit of 13,500 psi. The endurance limit is the amount of stress that can be applied to the specimen an indefinite number of times without the specimen breaking. Some of the structural members are designed to have maximum stress levels under the endurance limit. Although this makes for a slightly heavier aircraft, it extends the life of the structural members to infinity, at least in theory. However, the members that are most important are those which endure the maximum levels of stress.

In the wing the maximum stress occurs where the large diamond-shaped portion ends. This stress was determined to be about 16,100 psi. This value gives the vital members a safety factor of 2.19. In both the canard and tail the maximum stress occurs at the root of the structure. The maximum stress in the canard is 11,400 psi and 13,300 psi in the tail. These values correspond to safety factors of 3.07 and 2.63, respectively. The maximum stress in the fuselage occurs near the center of gravity of the craft, and has a value of 7600 psi. This level of stress translates into a safety factor of 4.6. These values for stress are only approximations used in the calculations, but are acceptable values for this preliminary design project.

### Weight and Balance

In estimating weight, a combination of formulas was used from two sources, Torenbeek and Nicolai. The two sources allowed tailoring of the weight calculations to our specific design and gave a good approximation to the weight that is appropriate in this stage of the design.

The weight is divided into major structural groups and individual groups of components within the major groups (see Table 2). The balance analysis was done with reference to Torenbeek's book. The calculation was done

by breaking down the aircraft into major components and subcomponents with a simple center of mass technique. The forward tip of the fuselage was used for the reference datum line, while the center of gravity was calculated along the length of the aircraft.

Table 2 Weight and balance calculations

| Component                 | Weight (lb) | CG Loc. (ft) | Total CG<br>Loc. (ft) |
|---------------------------|-------------|--------------|-----------------------|
| Fuselage                  | 13325       | 38           |                       |
| Wing                      | 4590        | 55           |                       |
| Tail                      | 1054        | 94           |                       |
| Canard                    | 659         | 8            |                       |
| Engines                   | 4500        | 75           |                       |
| Main gear                 | 1624        | 53           |                       |
| Nose gear                 | 541         | 15           |                       |
| Avionics                  | 200         | 15           |                       |
| Fuel                      | 22100       | 45           |                       |
| Passengers                | 13825       | 43           |                       |
| Furnishings               | 4712        | 40           |                       |
| Baggage                   | 3750        | 35           |                       |
| Eng. acc.                 | 1972        | 72           |                       |
| Surface cont              | 1426        | 53           |                       |
| Reserve fuel              | 1625        | 40           |                       |
| Misc.                     | 7386        |              |                       |
| MZFW                      | 63000       |              |                       |
| MTOW                      | 80000       |              |                       |
| W empty                   | 40870       |              |                       |
| MTRW                      | 80545       |              |                       |
| Total no pass., full fuel |             |              | 46.03                 |
| Total reserve fuel, pass. |             |              | 44.06                 |
| Total no pass., res. fuel |             |              | 45.20                 |
| Total full fuel, pass.    |             |              | 45.00                 |

Different loading configurations were examined in order to represent all of the extremes encountered in flight. This gives a defined set of center of gravity positions, two of which are the most fore and aft center of gravity locations. The difference in the two positions gives the center of gravity travel that can occur in flight. The four payload-type configurations are: full load (all passengers and full fuel), full fuel and no passengers (and

no baggage), reserve fuel and all passengers, and reserve fuel only. Table 2 shows the figures calculated for each of the configurations. The centers of gravity for the fuel, baggage, avionics and other accessories were placed to satisfy stability requirements.

### Stability and Control

The subjects of stability and control deal with how well an aircraft flies and how easily it can be controlled. These factors are especially important for a commercial transport because of the passenger comfort requirements. A passenger aircraft must adjust quickly and smoothly to perturbations in the atmosphere and changes in flight conditions.

There are many criteria that must be satisfied before an aircraft is considered statically stable. Many stability parameters were determined by using one of the Army's Missile Aerodynamic Design Programs written by William David Washington in 1980 and modified by Dr. John E. Burkhalter of Auburn University in 1990. One criterion for the DART to be stable is that the moment curve slope must be negative. The moment curve slope for the DART is approximately -4.304 per radian. The numbers obtained from the program are approximate since modifications were made to the program for a cranked wing configuration.

A stable aircraft must also be able to be trimmed. The Y-axis intercept of the pitching moment curve must be positive and was determined to be 0.152 for the DART. Another important stability parameter is the stick-fixed static margin. The static margin must be positive for a stable aircraft, and the static margin for the DART at cruise was found to be 2.73 ft, or 34% of the mean aerodynamic chord. Acceptable values for the static margin for commercial transports range from 25 to 50% of the mean aerodynamic chord. This means that the center of pressure is 2.73 ft behind the center of gravity and that, therefore, the DART is statically stable.

The maneuver margin is another important stability parameter. The maneuver point should be behind the center of gravity. The maneuver margin was determined to be 10.2 ft. Therefore, the maneuver point at cruise for the DART is 10.2 ft behind the center of gravity.

The stability characteristics of the yaw and roll planes are closely coupled. The upward sweep of the wings generates a dihedral effect that produces restoring forces and moments in the yaw and roll directions. A dihedral angle of about  $8^\circ$  is necessary in order to reduce the body interference factor on the dihedral effect.

The DART-75 will use three control surfaces. Elevators will be used on the tail to control pitch and attitude changes. Due to the close coupling of the yaw and roll controls, the rudder mounted on the vertical tail plane and the ailerons on the wing are interdependent. These surfaces will give adequate response to perturbations and sideslip forces. These controls are conventional in design and should give the DART-75 handling qualities similar to other regional jets. Dynamic analysis of the aircraft was omitted due to time and resource constraints. However, when a model is produced, further analysis may be done.

### Performance

The DART's performance data was obtained through the use of two main sources, Shevell's book and USAir Operations Chief Engineer Mike Pulaski. The drag polar was calculated by using Roskam's methods.<sup>6</sup> This method shows the drag polar to be:

$$C_D = 0.02167 + 0.0301 C_L^2$$

for the clean configuration and

$$C_D = 0.065341 + 0.0309 C_L^2$$

for the dirty configuration.

The dirty drag polar was obtained from several figures and charts providing data for several different aircraft. The coefficient of lift is assumed to have a maximum value of 1.75 for the clean configuration and 2.2 for the dirty configuration. The coefficient of lift for maximum lift over drag, incorporating the calculated drag polar, is 0.75.

The next calculation involved the determination of the flight speed. The maximum cruise speed of the DART is Mach 0.7 at 30,000 feet with takeoff speed at 140 knots and landing at 120 knots. The DART has a range of 1050

nautical miles. Knowing the engine's specific fuel consumption and the weight of the fuel showed the endurance of the flight to be around five and a half hours. If operating at full power, the maximum aircraft endurance is calculated to be around five hours.

The DART will climb from sea level to around 75 % of cruise altitude in approximately 10 minutes. This will be at an initial climb angle of between  $8^\circ$  and  $14^\circ$  at a climb rate of between 3400 to 5500 ft per minute. After reaching the 22,500 ft level, the DART will begin to level off to a more relaxed climb angle ranging from  $2^\circ$  to  $5^\circ$ . The climb rate will then be 1000 to 3000 ft per minute. Another five minutes and the aircraft will be at a cruise altitude of 30,000 ft.

The DART's performance proves to fit well with the mission profile. Comparing the calculated values with those values that are known for today's aircraft achieved reasonable results. The landing and takeoff field lengths are respectable and compare well with any regional aircraft in existence today. The range and endurance meet the need for a medium range, very fast aircraft.

### Propulsion

Due to the multi-faceted role of the regional aircraft, a propulsion system designed for this aircraft must be able to handle many different flight conditions. The engines will not be the best design for any one situation, but they should be a good compromise for the situations in which the airplane is to be used.

To achieve this goal the turbofan engine has been selected for consideration primarily due to its proven technology. Each engine will produce 12,500 lbs of static thrust, be able to provide reverse thrust, and will comply with the latest aircraft noise regulations. Since there have been so many aircraft designed for turbofan engines, there is an abundance of research that has already been conducted in this field. Trends in turbofan engine design tend to increase the engines bypass ratio rather than improve the engines core design. The increase in bypass ratio allows the engine to produce the same thrust with a smaller TSFC and with less noise.

The engine used on the DART will be rated for a static thrust of 12,500 lbs and will produce 2500 lbs of thrust at

30,000 ft and a Mach of 0.7. The TSFC of the engine is approximately 0.6293 lbs of fuel per hour per lb of thrust, which was calculated using a computer program discussed later. To achieve such a low TSFC an engine needs a bypass ratio of between 7 and 10. The weight of the engine is about 1800 lbs with a length of 7.3 ft and a diameter of 5 ft.

Most engines that are put on higher performance aircraft are d-rated. In other words the engines can produce greater power when needed than the actual design power required for any flight situation. Hence, the actual engine on the DART-75 will be *capable* of producing from 1000 to 5000 lbs more static thrust than the rated power. This increase of power would allow for greater single engine takeoff and climb performance and would also allow the airplane to climb to a higher altitude in case it needed to avoid disturbances. The increase in thrust to 17,500 lbs would require an engine that weighs 2535 lbs, is 8.32 ft long, and is 6.36 ft in diameter. The added increase in weight would only change the total aircraft weight by 1570 lbs, which would be an increase of only 2.0%. However, the increase in static thrust would change the single engine thrust to weight ratio on takeoff from 0.156 to 0.22.

The calculation of this engine was done using the ONX engine analysis program. This program was derived from the book *Aircraft Engine Design* by J.D. Mattingly, W.H. Heiser, and D.H. Daley. The program allows the engineer to input Mach number, altitude, atmospheric conditions, bypass ratio, burner can temperatures, and component efficiencies. The program then calculates the engine's mass flow rate, thrust, and thrust specific fuel consumption (TSFC). The burner can temperature was estimated at 3000° R. The fan pressure ratio is 1.4 and the compressor pressure ratio is 39.0. These values were derived by iterations done with the ONX program. A total number of over 200 iterations using different bypass ratios and fan and compressor ratios was used in the program before an optimal engine based on the lowest TSFC was found. The engine is also based on the two nozzle non-mixing design.

A bypass ratio of 9.6 was chosen because it proves to be the highest bypass ratio that can be obtained using a standard fan and keeping the engine flow stable. A higher bypass ratio can be obtained; however, to keep the engine flow stable, a fan cascade with variable pitch fan

blades would be required. This design would require a significant increase in engine weight and would decrease the reliability of the engine. Therefore, it was determined that, the simpler design would satisfy the airplane operator's needs better than the variable pitch blade design.

The engine will reverse thrust using ballistic reversers. The failure of ballistic reversers is known to be very unlikely. In fact, there has never been a recorded failure of the clamshell type reverser. The only other option for thrust reversing is available through a variable pitch fan design of a turbofan engine. This option is to deflect the blades in such a way as to give them a negative angle of attack. Reversing thrust in this manner is more efficient than in the ballistic way but it would once again add unwanted weight and complexity to the engine design.

### Conclusions

The regional aircraft currently available are old and inefficient. A new regional transport could well take over the regional market. The DART-75 is the proposed new regional transport with single class accommodations for 75 passengers and a crew of five. This aircraft will achieve success through its efficiency, excellent multi-role capability, advanced general design, and competitive cost.

The DART-75 will be capable of point-to-point, hub-feeder, as well as shuttle-type services. The wing shape, decreased weight, and efficient engines combine to yield good short field performance, excellent range, and competitive cruise speed. These factors make the DART-75 a very versatile craft that will appeal to many airlines for different types of missions.

### References

1. Layton, D. Aircraft Performance. Matrix Publishers, Inc.: Chesterland, Ohio, 1988.
2. Miuvdi, BB and J.W. McNabb. Engineering Mechanics of Materials. Macmillan: New York, 1984.
3. Nicolai, L. Fundamentals of Aircraft Design. University of Dayton: Dayton, Ohio, 1975.



4. Pulaski, M, Chief Operation Engineer. Packet of Aircraft Characteristics, Flight Handbook, USAir, Pittsburgh, Pennsylvania.
5. Raymer, D.P. Aircraft Design: A Conceptual Approach. AIAA Education Series, 1991.
6. Roskam, J. Methods of Estimating Drag Polars of Subsonic Aircraft. J. Roskam, Lawrence, Kansas, 1971.
7. Shevell, R. Fundamentals of Flight. Prentice-Hall: Englewood Cliffs, New Jersey, 1989.
8. Torenbeek, E. Synthesis of Subsonic Airplane Design. Delft University Press, 1982.

## **Eagle RTS: A Design of A Regional Transport**

**Paul Bryer, Jon Buckles, Paul Lemke,  
Kirk Peake**

### **Introduction**

The Eagle RTS (Regional Transport System) is a 66-passenger aircraft designed to satisfy the need for accessible and economical regional travel. The first design objective for the Eagle RTS is safety. Safety results primarily from avoidance of the hub airport air traffic, implementation of anti-stall characteristics by tailoring the canard, and proper positioning of the engines for blade shedding. To provide the most economical aircraft, the Eagle RTS will use existing technology to lower production and maintenance costs by decreasing the amount of new training required.

In selecting the propulsion system, the effects on the environment were a main consideration. Two advantages of turbo-prop engines are the high fuel efficiency and low noise levels produced by this type of engine. This ensures the aircraft's usage during times of rising fuel costs and growing aircraft noise restrictions.

The design of the Eagle RTS is for spoke-to-spoke transportation. It must be capable of landing on shorter runways and have speeds comparable to that of the larger aircraft to make its service beneficial to the airlines. With the use of turbo-prop engines and high lift devices, the Eagle RTS is highly adaptable to regional airports. The design topics discussed include: aerodynamics, stability, structures and materials, propulsion, and cost.

### **Aerodynamics**

The fuselage of the Eagle RTS resembles an elongated "teardrop" shape with pusher-prop engines located behind the swept-back wings. This configuration will allow for minimum body drag while allowing for maximum flexibility in designing the interior arrangement. Figure 2 provides a three-view of the Eagle RTS.

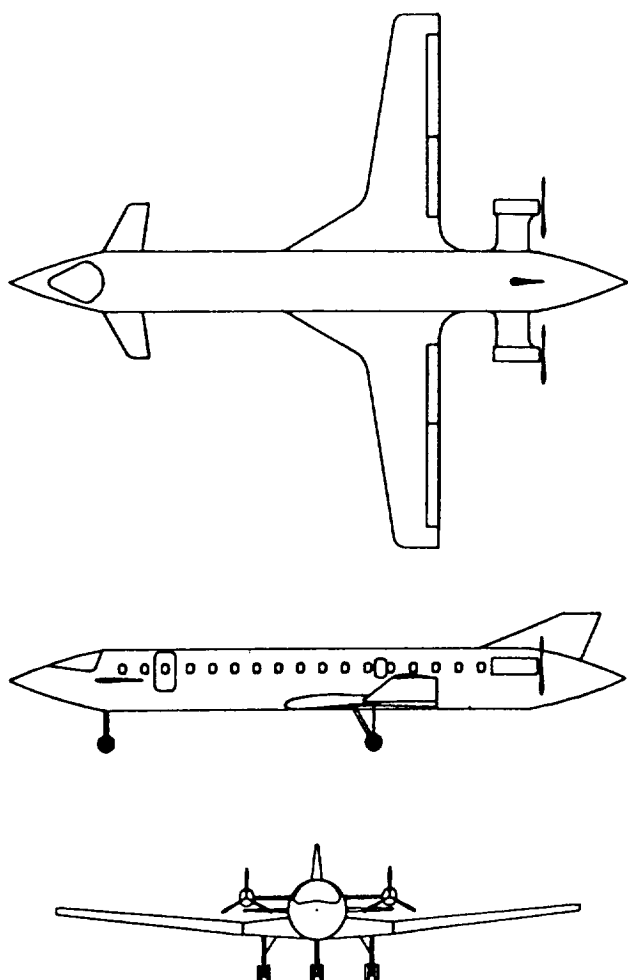


Fig. 2 Three-View of the Eagle RTS

The airfoil selected for the wing is the NACA 632-615 series airfoil. This airfoil was selected because it has the most efficient cruise characteristics and a high stall angle of attack.<sup>1</sup> The choice of airfoil was also influenced by Daniel P. Raymer's recommendation of a wing thickness ratio for twin turbo-prop aircraft of 0.14.<sup>2</sup>

The Eagle RTS uses a compound wing design with sweep angles of 9° and 60° and wing loading of 70 lb per sq ft. These angles were chosen to provide a wing area which produced a maximum lift coefficient and a minimum wing loading while providing for large fuel

tanks.

The drag polar was calculated using Roskam's Methods for Estimating Drag Polars of Subsonic Airplanes,<sup>3</sup> which shows the drag coefficient to be:

$$C_D = 0.0615 + 0.032 C_L^2.$$

The Eagle RTS will employ the use of a canard to prevent stall characteristics such as spins and uncontrolled rolls. The canard airfoil selected for the Eagle RTS is the NACA 0009 series. The canard will cruise at an angle of attack of 2° while stalling at an angle of attack of 9° ± 1°. Because the canard will stall at 9° the main wing will never reach its stall angle of attack of 12°. The canard was also employed to eliminate the negative lift normally generated by the tail.

One disadvantage of a canard is the effect of trailing vortices on the main wing aerodynamics and the engine efficiency. To minimize these effects, Raymer's approach was used, where both the main wing and engines are placed as far aft and above the canard as possible.

The aspect ratio for the Eagle RTS is important in determining the induced drag and efficiency of the aircraft. The aspect ratio for the Eagle RTS was found to be 6.5, corresponding to a induced drag of 0.032 and an efficiency factor of 0.775. According to Richard S. Shevell, an efficient aircraft operates between an Oswald's efficiency factor of 0.75 and 0.9.<sup>4</sup>

### Performance

Two important factors in aircraft performance are rate-of-climb and range. The rate-of-climb at cruise velocity and cruise altitude of 25,000 ft with full passenger and fuel load was found to be 928 ft/min. In the initial analysis it was estimated that the range would be 1000 nmi. To find the maximum range, we use a maximum lift to drag ratio. Using an efficiency of 0.8 and a TSFC of 0.547 lb/hr-HP the range was calculated to be 836 nmi. Although below what was specified at the beginning of the design process, the range of this airplane was deemed to be adequate.

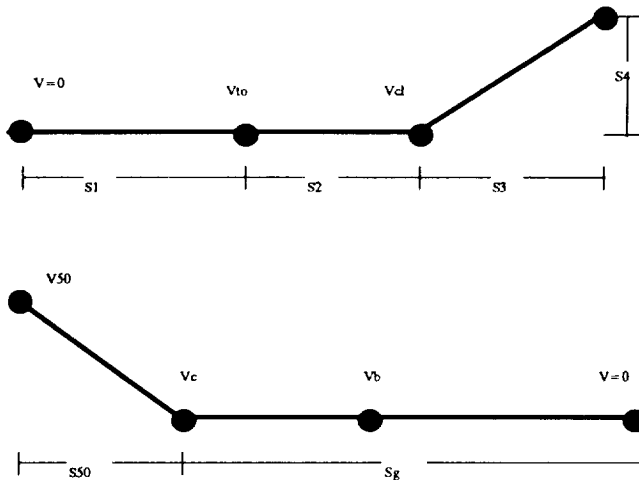


Fig. 3. Takeoff and landing breakdown

The total takeoff distance required is 4700 ft. Figure 3 gives a diagram of takeoff and landing roll distances, and Table 3 gives the takeoff and landing distances for the Eagle RTS.

Table 3 Takeoff and landing information

**Takeoff Parameters:**

$V_{TO} = 186.05$  ft/s       $V_{CL} = 202.96$   
 $S_1 = 3563.64$  ft       $S_2 = 762.82$  ft       $S_3 = 370.04$  ft  
 $STO = 4696.4952$  ft

**Landing Parameters:**

$V_{S0} = 219.87$  ft/s       $V_C = 194.5$  ft/s       $V_B = 155.6$  ft/s  
 $S_{S0} = 1964.44$  ft       $S_G = 1719.623$  ft  
 $STL = 3684.063$  ft       $STL_{commercial} = 6140.0$  ft

The total landing distance is 3700 ft, roughly two-thirds the takeoff distance. FAR requirements for a commercial aircraft show the landing distance to be 6100 ft. With the addition of ground spoilers this landing distance will decrease.

**Stability Analysis**

The stability analysis of the Eagle RTS includes a

comparison of pitching moment versus angle of attack, neutral point location, and the stability margin. This is normally described by the moment coefficient,  $C_m$ . In order to find this value of  $C_m$  and subsequently the variation of it with angle of attack, the neutral point or static margin must be found.

Table 4 C.G. locations for various loading conditions

| Configuration                              | C.G. Location (ft.)* | Static Margin (ft.) |
|--|----------------------|---------------------|
| Full passengers and bags, full fuel        | 50.7509              | 12.390              |
| 3/4 passengers and bags, 1/2 fuel          | 51.5363              | 11.604              |
| No pass., no bags, no fuel (empty landing) | 56.8650              | 6.280               |
| Avg. passenger weight                      | 170 lb               |                     |
| Avg. baggage weight                        | 3130 lb              |                     |
| Total passenger weight                     | 11,220 lb            |                     |
| Avg. fuel weight                           | 14,280 lb            |                     |

\* Measured from the nose of the aircraft

Table 4 shows the component weights and center of gravity locations for various loading conditions. Due to the changing configurations of passenger and baggage loadings, the neutral point of the aircraft should be found first. In this case, the neutral point was found to be 15.892 ft forward from the trailing edge of the wings, or 58.1 ft aft of the nose. The aerodynamic center was found to lie 63.14 ft from the nose, while the center of gravity is located 50.7509 ft aft from the nose. All are for the fully loaded aircraft configuration.

Finally, the variation of  $C_m$  with angle of attack for various deflections of the canard may be found. The significance of the canard surface in this design is its freedom from propulsive interference, which allows it to better trim the large moment produced by high lifting

devices. An unfavorable aspect of the canard is its destabilizing effect on the airplane. However, this can be counteracted by proper positioning of the center of gravity.

In the commercial aviation market, passenger ride comfort is a prime consideration in customer satisfaction. This gives rise to dynamic stability analysis, which plays a major role in aircraft handling and ease of flying. The phugoid or long period mode is characterized by changes in pitch, altitude and velocity. In this analysis, the period of the phugoid motion was found to be 6.91 minutes and the time to half amplitude of 103 minutes. The short-period was determined to be 0.147 minutes and a time to half amplitude of 2.42 minutes. Although this aircraft is balanced and stable, the automatic stabilization computer must be used to augment both the short and long period frequencies.<sup>5</sup>

### Structures and Materials

The exterior dimensions of any commercial aircraft are based primarily on the number of passengers the aircraft will carry. The number of passengers is of prime importance since it dictates the cabin dimensions, airline profit and feasibility, and future applications of the aircraft. Based on these factors and market influences, the Eagle RTS will accommodate 66 passengers with a four-abreast seating configuration.

The mission profile for the Eagle RTS included eight phases: start-up, taxi, takeoff, climb, cruise, loiter, descent, landing, and shutdown. A preliminary weight estimation of the Eagle RTS then determined the gross takeoff weight to be approximately 70,000 lbs. Using the fraction method of component weights by referencing similar aircraft, the weight of the major component groups is given in Table 5.

The next phase of the design is to determine construction materials for construct the Eagle RTS. Material selection is based on the maximum loads applied to the aircraft during flight. The wing loading was determined to be 100 lb/ft<sup>2</sup>, with a 1.5 safety factor for normal cruise conditions.

Table 5 Component weight breakdown

| Component                          | Weight (lbs)    |
|------------------------------------|-----------------|
| Fixed equipment                    | 11,014.0        |
| Fuselage                           | 8204.0          |
| Wing mass                          | 8540.0          |
| Landing gear mass                  | 3190.0          |
| Empennage mass<br>(including tail) | 1899.0          |
| Engine mass                        | 6304.0          |
| Nacelles mass                      | 1823.0          |
| <b>Total Component Weight</b>      | <b>40,974.0</b> |

The materials used for the construction of the Eagle RTS will be an integration of aluminum alloys and composites. The skin and stringers of the upper surface will be constructed of an aluminum alloy, 7075 (Al-Zn), which has high tensile stresses allowances. For the lower surface of the wing, the alloy 2024 (Al-Cu) will be used. Based on the values determined from the MSC/NASTRAN results, the materials used are sufficient to withstand the loads applied during flight.

As previously stated, aluminum alloys will be the dominant material used on the Eagle RTS. This is mainly because of their strength characteristics, high corrosion resistance, availability, low cost, and acceptability. Another alloy used on the Eagle RTS is aluminum-lithium, which demonstrates very high strength characteristics and low weight. However this material will be in limited use since the raw material cost is greater than that of standard alloys.

In order for the Eagle RTS to operate at its maximum efficiency, the weight of the aircraft must be minimized. Composite materials will be used in limited areas to maximize efficiency and minimize cost. Composites demonstrate a weight savings of approximately 25% over metals, can be tooled to any shape while maintaining their physical properties, and give a smoother surface than metals. These materials will adjust the empty weight of the Eagle RTS to 40,415 lbs. The composites will be used in the leading and trailing edges of the wing, the inboard and outboard flaps, rudders, elevators, and landing gear doors. A final estimate of the final gross take-off weight

is calculated to be 69,045 lbs.

### Propulsion

The propulsion system for the Eagle RTS was selected to allow cruise at 25,000 feet at a speed of 260 knots (Mach 0.4). Viable options at this speed were turboprop and turbofan type engines, but fuel savings of 25% for the turboprops resulted in their selection.

Once the engine type was selected for the Eagle RTS, the thrust required, engine size, and propeller specifications were determined. In level, unaccelerated flight the thrust required is equal to the drag on the aircraft. The thrust required at the cruise altitude of 25,000 feet was determined to be 6300 pounds. This is 3150 hp per engine for a twin turboprop configuration. The highest rated engine currently on the market is the PW 126 produced by Pratt & Whitney, Canada (P&WC). It is cruise-rated at 2192 effective horsepower (ehp) at 1200 rpm. However, P&WC is currently testing engines with effective horsepower in the range of 3000 ehp.<sup>4</sup>

The dimensions and weight of the engines for the Eagle RTS can be calculated using the scaling equations.<sup>2</sup> Using the PW 126 as a baseline engine, the Eagle RTS engine is calculated to have a length of 97.1 inches, a width of 31.2 inches, a height of 37.2 inches, and a weight of 1675.6 pounds.

When noise is a consideration, the helical tip speed of the propeller blades should be kept at or below 700 feet per second. At a rotational rate of 1200 rpm and a cruise velocity of 260 knots, the propeller disk diameter is calculated to be 104 inches.

Engine placement is crucial to aircraft safety. The propeller blades require a minimum clearance of 9 in. For that clearance and the instances of blade shedding, vortices shedding from the canard, and noise considerations, the engines have been placed on pylons on the aft section of the fuselage, mounted in a pusher configuration.

### Cost Analysis

The direct operating costs (DOC) of the Eagle RTS are divided into three sections: fuel, crew salaries, and

maintenance. The fuel cost was calculated by determining the amount of fuel burned per year. Assuming an average of 4000 flight hours per year, the fuel cost is \$1.5 million per 1000 flight hours. The crew salaries are estimated to be \$209,000 of the DOC. The maintenance costs per year can be estimated by determining the maintenance hours required per flight hour. The maintenance cost per year was calculated to be \$30,000. The majority of the maintenance costs are due to the type of engine selected for the Eagle RTS. The remaining cost of the DOC is the depreciation and insurance value. Therefore the direct operating cost of the aircraft per 1000 flight hours was determined to be \$1.04 million.

The calculation of the total cost of the Eagle RTS is based on calculations from Raymer.<sup>2</sup> The selling price (in 1992 constant dollars) for the Eagle RTS, including an investment factor, is set at \$10.2 million for 500 aircraft, with the total cost of the Eagle RTS project estimated to be \$5.1 billion. Also, each aircraft will have an expected operational life of 60,000 flight hours or approximately 15 years. At this price and operational life, the Eagle RTS will surely be competitive with the other aircraft in the regional commercial market.

### Summary And Conclusions

The Eagle RTS was developed to meet a specific gap in the commercial aircraft industry. It was designed to carry passengers between metropolitan areas while avoiding the congested hub airports. The aircraft is designed to maximize performance while minimizing operational costs.

Several interesting conclusions were reached during the final phases of the design. Only time and research will provide an answer to the problem of canard tip vortex shedding on the placement of the engines, engine performance, and the aerodynamic effects on lifting surfaces. In terms of the weight of the aircraft, the values represent preliminary design estimates only, since time limitations and constant adjustments in the configuration were required. On the performance side, the range came out significantly better than our initial assessment, and the endurance is competitive with the specified needs. Also, the aircraft computer system will calculate the optimal engine fuel flow to maintain peak engine efficiency. Since

the aircraft aerodynamics were developed assuming non-laminar flow, proper cleaning and maintenance will further minimize fuel consumption and further lower the operational costs of the aircraft. In the final analysis of the design, the Eagle RTS is well researched and will fill a void that exists in today's regional transport market.

#### References

1. Thirty-first Annual Report of the National Advisory Committee for Aeronautics, 1945. U.S. Government Printing office, Washington, D.C.
2. Raymer, D.P. Aircraft Design: A Conceptual Approach. AIAA Education Series, 1989.
3. Roskam, J. Methods for Estimating Drag Polars of Subsonic Airplanes. The University of Kansas, 1971.
4. Shevell, R.S. Fundamentals of Flight. Prentice Hall: Englewood Cliffs, New Jersey, 1989.
5. Nelson, R.C. Flight Stability and Automatic Control. McGraw-Hill: New York, 1989.

**PRELIMINARY DESIGN OF NINE HIGH SPEED CIVIL TRANSPORTS**

**California Polytechnic State University, San Luis Obispo  
Aeronautical Engineering Department  
San Luis Obispo, California**

**Dr. Doral Sandlin and Professor Robert van't Riet  
Dani Soban and Ty Hoang, Teaching Assistants**

**Abstract**

Sixty senior design students at Cal Poly, SLO have completed a year-long project to design the next generation of High Speed Civil Transports (HSCT).

The design process was divided up into three distinct phases. The first third of the project was devoted entirely to research into the special problems associated with an HSCT. These included economic viability, airport compatibility, high speed aerodynamics, sonic boom minimization, environmental impact, and structures and materials. The result of this research was the development of nine separate Requests for Proposal (RFP) that outlined reasonable yet challenging design criteria for the aircraft. All were designed to be technically feasible in the year 2015.

The next phase of the project divided the sixty students into nine design groups. Each group, with its own RFP, completed a Class I preliminary design of an HSCT. The nine configurations varied from conventional double deltas to variable geometry wings to a pivoting oblique wing design.

The final phase of the project included a more detailed Class II sizing as well as performance and stability and control analysis.

Cal Poly, San Luis Obispo presents nine unique solutions to the same problem: that of designing an economically viable, environmentally acceptable, safe and comfortable supersonic transport.

**Introduction**

Progress in aviation feeds on itself, with each new triumph a stepping stone for the next. For example, it is

the dawn of the commercial airline industry that has truly connected vast continents, and indeed, the world. From this, international tourism and business have flourished, and the demand on the air transport industry is growing.<sup>1</sup>

Global air traffic is estimated to continue to grow at an annual rate of 3.6% well into the next century. This would mean an increase from approximately 986 million passengers today, to about 2,086 million in 2010, generating approximately 2.5 billion revenue-passenger-mile per year. Even more encouraging is that all market areas are charted for healthy growth, especially the Pacific market. It is regions such as this where the need for a supersonic transport (SST) will be felt most acutely.<sup>2</sup>

This demand is driven largely by international business, an area where the time wasted on seemingly endless transcontinental flights is far more costly than airfare itself. Several contemporary studies have shown that whether on vacation or non-business trips, most people would certainly pay a premium to cut this time in half.<sup>2,3</sup> A supersonic commercial transport is ideally suited to this task.

The first and only currently operational supersonic commercial transport was a British and French collaborated aircraft named the Concorde. This Mach 2.2 aircraft entered service in 1974 to a storm of environmental protests. Sonic boom prevented overland supersonic flight, and the noise from the Rolls-Royce Olympus engines gained the Concorde the reputation of being a noisy airplane. For this reason, the Concorde was banned from most airports around the world.<sup>4</sup>

Although it was a revolutionary airplane for its time, only fourteen Concorde airplanes were built. For this reason, the cost per airplane skyrocketed, causing the airframer to lose money. Concorde was limited to first-class only, driving the cost up to \$0.76 per passenger mile

(1974 U.S.D), a 38% increase over current subsonic first class fare. In addition, unexpectedly high fuel costs coupled with the fact that the Concorde was not fuel-efficient drove the cost up further.<sup>5</sup>

Over the past twenty years, many designs for supersonic transports have been evaluated and discarded. Only in the past few years, with NASA sponsoring different programs,<sup>5</sup> has interest in the HSCT been rekindled. With many lessons learned from the Concorde's mistakes, it is believed that a next generation HSCT is imminent. Cal Poly, San Luis Obispo would like to present nine unique solutions to this challenge. Table 1 presents the range of Mach numbers, passenger capability, and ranges for the nine designs.

Table 1 Nine design solutions

|                  | Mach | #<br>Passengers | Range<br>(nm) |
|------------------|------|-----------------|---------------|
| OPUS 0-001       | 2.2  | 60              | 4,800         |
| Stingray         | 2.4  | 250             | 4,800         |
| Swift            | 2.5  | 250             | 5,700         |
| TBD <sup>3</sup> | 3.0  | 270             | 4,800         |
| Phoenix          | 2.5  | 152             | 5,150         |
| MM-122           | 2.2  | 250             | 5,200         |
| The Trojan       | 2.0  | 250             | 5,200         |
| RTJ-303          | 1.6  | 300             | 4,700         |
| The Edge         | 2.4  | 294             | 5,250         |

### Special Problems in HSCT Design

There are several areas that pose unique challenges for the designer of an HSCT. The first set of these challenges can be categorized as environmental challenges. These include noise from takeoff and landing, sonic boom considerations, and NOx emissions. Figure 1 shows the areas of concern for takeoff and landing noise. Currently, aircraft must meet stringent FAR 36 Stage 3 noise requirements, and there is indication that a more restrictive Stage 4 requirement is on the horizon. A successful HSCT must make every effort to minimize sideline and takeoff noise. While all nine Cal Poly designs selected engines that do meet Stage 3, it was

concluded by all teams that a supersonic transport could not meet Stage 4 requirements in the near future.

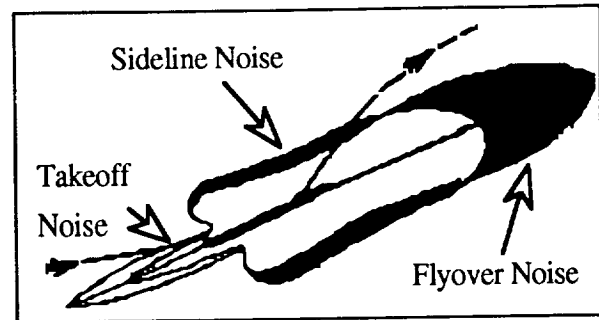


Fig. 1 Typical areas of sideline and takeoff noise

Sonic boom is an obvious concern when dealing with an aircraft that travels faster than the speed of sound. The sonic boom can be characterized by the N-wave shape shown in Figure 2. The effects of a sonic boom can be minimized in two ways: reduce the actual magnitude of the overpressure of the wave or delay the rise time of the shock. This is achieved by extensive aerodynamic tailoring of the aircraft. A long, slender aircraft minimizes sonic boom. Unfortunately, this introduces conflicts in internal volume, manufacturability, aerodynamic efficiency, and airport compatibility. In light of these compromises, it was concluded by all nine design teams that overland supersonic flight was not a feasible goal at this time.

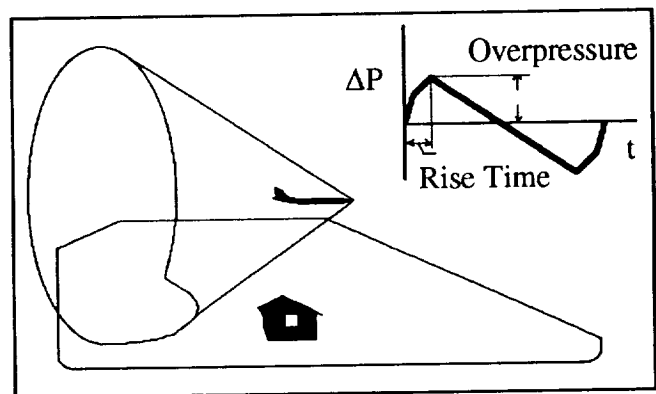


Fig. 2 Sonic boom and N-wave characterization



Aircraft exhaust contains emissions of nitrous oxide that destroy the earth's fragile ozone layer. This ozone layer is found at altitudes of 60,000 to 90,000 feet. Unfortunately, the ideal traveling altitude for a supersonic transport is 55,000 to 85,000 feet. Therefore, every effort was made to reduce engine emissions of nitrous oxide.

The next set of challenges are the technical issues. These include aerodynamics, engine analysis, and physical restraints necessary for airport compatibility. The first of the aerodynamic concerns is the dual flight regimes characteristic of supersonic transports. The aircraft must be optimized for both subsonic and supersonic flight. Often this requires contradictory solutions for optimum performance in each of the two regimes. For example, for subsonic flight, a high aspect ratio wing is ideal. For supersonic flight, however, a low aspect ratio wing provides the most efficient performance. The aircraft designer must make careful tradeoffs to end up with an aircraft that performs well in both regimes.

At supersonic speeds, wave drag becomes a primary concern. This drag, caused by pushing an object through the air at speeds greater than Mach 1, can be minimized by careful area ruling of the fuselage. This introduces restrictions on internal volume. The design challenge lies in optimizing passenger comfort in the form of internal volume, while obtaining maximum aerodynamic efficiency through area ruling.

As an aircraft transitions between subsonic and supersonic flight, the aerodynamic center shifts aft. This can cause severe weight and balance, as well as stability problems, and must also be a design concern.

Finally, aerodynamic heating is of considerable concern. Energy from air molecules slowed down to zero velocity at stagnation points along the aircraft are transferred to the surface of the aircraft in the form of heat. Figure 3 shows the typical temperature distribution along a Mach 2.5 aircraft. These extensive temperatures introduce challenges in terms of material selection. Figure 4 shows the relative decrease in the strength of various materials as their temperature increases. Tradeoffs must be conducted in materials between strength, temperature, manufacturability, and cost.

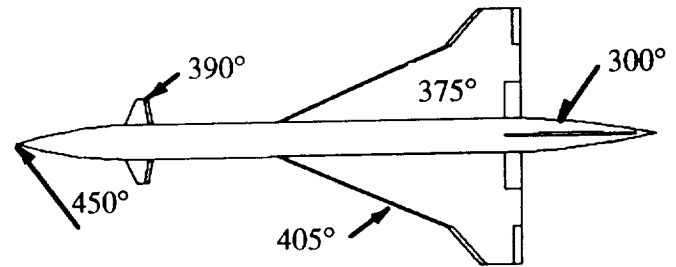


Fig. 3 Typical temperature (°F) distribution for a Mach 2.5 aircraft

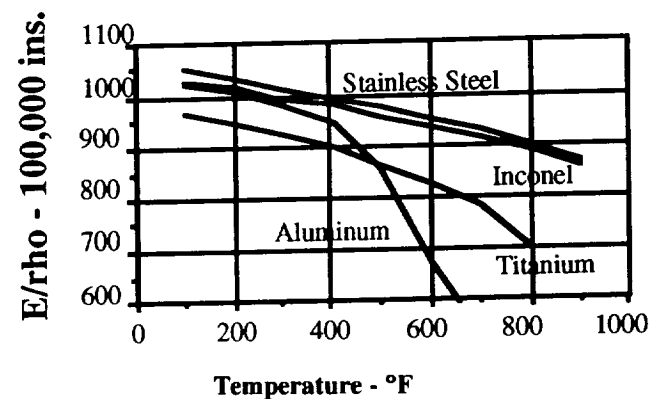


Figure 4- Effect of Temperature on Selected Materials

Propulsive improvements must be made in order for a next generation supersonic transport to be viable. Improvements must be made first and foremost in thrust specific fuel consumption (TSFC). In addition, the engines must be quieter, and produce less emissions, as discussed previously.

Finally, airport compatibility must be addressed. A supersonic transport that cannot operate out of existing airports and gates, or one that requires extensive special equipment, would not be a marketable product. Sheer size is the first concern. Figure 5 shows how an HSCT must fit into the box created by the largest aircraft operated today- the Boeing 747-400.

### The Designs

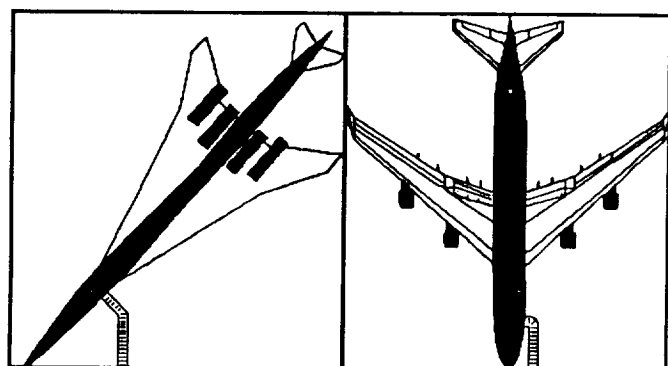


Figure 5- Comparison of size of HSCT to B-747 box

In addition to size, there are other airport compatibility requirements that must be met. It was assumed by all nine groups that extensive airport remodeling to permit an HSCT would not be acceptable. The airport compatibility requirements are found in Table 2. A landing speed of less than 200 knots is required so as to allow smaller aircraft to take off and land relatively quickly after an HSCT. The maximum field length of most major aircraft is 12,000 feet, so viable HSCT must reduce their takeoff and landing distances to this. Current gates can accommodate a sill height of only 17.6 feet, and finally, the pavement loading of the new aircraft must not be greater than that of a 747-400. Damaging the runway is not conducive to promoting an HSCT.

Table 2 Airport compatibility requirements

|                    |             |
|--------------------|-------------|
| Landing speed      | < 200 kts   |
| Field length       | < 12,000 ft |
| Gate height        | < 17.6 ft   |
| Pavement loading   | < = 747-400 |
| Fuels              | Existing    |
| Service equipments | Existing    |

With the above considerations in mind, brief summaries of the nine Cal Poly solutions are presented. While extensive Class I and II preliminary designs were performed, space limitations in this document prevent all but the briefest overview. For those interested in the more complete analysis, please feel free to contact the university for copies of individual reports.

#### Opus 0-001

Based on research into the technology and issues surrounding the design, development, and operation of a second generation High Speed Civil Transport, the Opus 0-001 ( Figure 6) team completed the preliminary design of a sixty passenger, three engine aircraft. The design of this aircraft was performed using a computer program which the team wrote. This program automatically computed the geometric, aerodynamic, and performance characteristics of an aircraft whose preliminary geometry was specified.

The Opus 0-001 aircraft was designed for a cruise Mach number of 2.2, a range of 4,700 nm and its design was based on current or very near term technology. Its small size was a consequence of an emphasis on a profitable, low cost program, capable of delivering tomorrow's passengers in style and comfort at prices that make it an attractive competitor to both current and future subsonic transport aircraft. Several hundred thousand cases of cruise Mach number, aircraft size and cost breakdown were investigated to obtain costs and revenues for which profit was calculated. The projected unit flyaway cost was \$92 million per aircraft.

#### Stingray

The Stingray (Figure 7) is the second-generation High Speed Civil designed for the 21st century. This aircraft is designed to be economically viable and environmentally sound transportation competitive in markets currently dominated by subsonic aircraft such as the Boeing 747 and upcoming McDonnell Douglas MD-12. With the Stingray coming into service in 2005, a ticket price of 21% over current subsonic airlines will cover operational costs with a 10% return on investment. The cost per aircraft

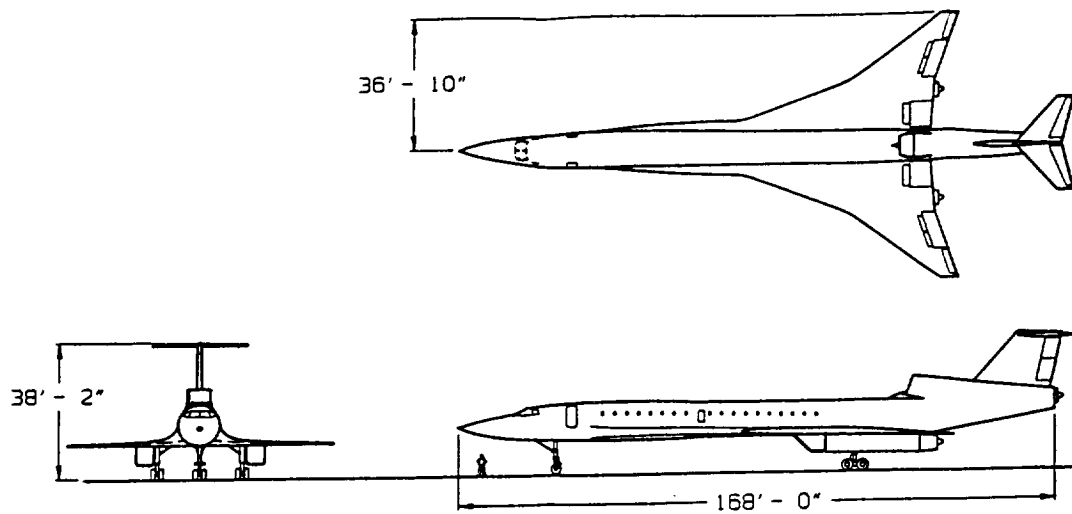


Fig. 6 Three-view of Opus 0-001

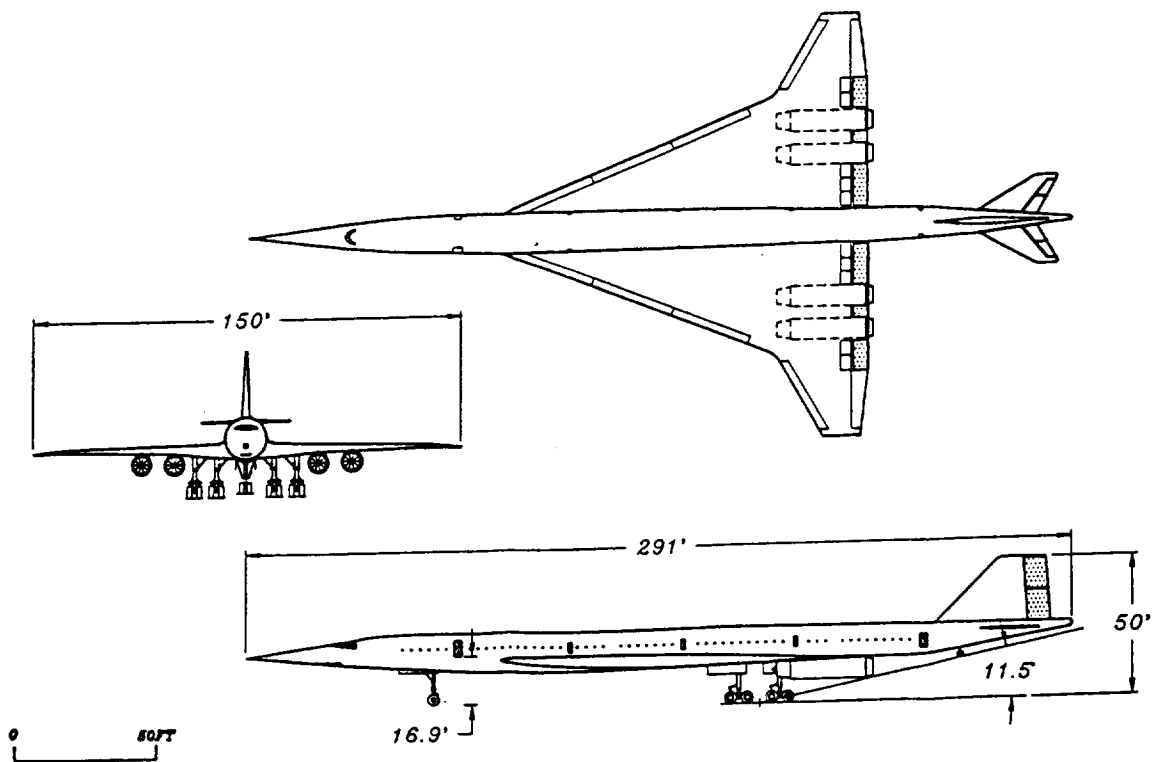


Fig. 7 Three-view of Stingray

will be \$202 million with the Direct Operating Cost equal to \$0.072 per mile per seat.

This aircraft has been designed to be a realistic aircraft that can be built within the next ten to fifteen years. There was only one main technological improvement factor used in this design, that being for the engine specific fuel consumption. The Stingray, therefore, does not rely on nonexistent technology.

The Stingray will be powered by four mixed flow turbofans that meet both nitrous oxide emissions and FAR 36 Stage III noise regulations. It will carry 250 passengers a distance of 5,200 nm at a speed of Mach 2.4. The shape of the Stingray, while optimized for supersonic flight, is compatible with all current airline facilities in airports around the world. As the demand for economical, high-speed flight increases, the Stingray will be ready and able to meet those demands

### **Swift**

Another solution to the HSCT problem is the Swift (Figure 8) aircraft design. This conventional double delta design is capable of a payload of 246 passengers in three classes. This size of aircraft requires a fleet size of 350 units with a 20% economy class fare increase based on a 50 % time savings, 80 % load factor and a 12 % Return on Investment (ROI). The class distribution is 5 % first, 34 % business, and 61 % coach. The aircraft is powered by four mixed flow turbofans that propel it at Mach 2.5.

The primary design goal of the Swift is simplicity. The aircraft was designed to be feasible using today's technology.

### **TBD<sup>3</sup>**

The TBD<sup>3</sup> (Figure 9), a 269-passenger, long-range civil transport, was designed to cruise at Mach 3.0 utilizing technology predicted to be available in 2005. Unlike other contemporary commercial airplane designs, the TBD<sup>3</sup> incorporates a variable geometry wing for optimum performance. This design characteristic enabled the TBD<sup>3</sup> to be efficient in both subsonic and supersonic flight. The TBD<sup>3</sup> was designed to be economically viable

for commercial airline purchase, be comfortable for passengers, and meet FAR Part 25 and the current FAR 36 Stage III noise requirements. The TBD<sup>3</sup> was designed to exhibit a long service life, maximize safety, be easy to maintain, as well as be fully compatible with all current high-traffic density airport facilities.

Several interior concerns were addressed in the design. The TBD<sup>3</sup> was equipped to accommodate the many needs of our passenger: first class, business, economy (coach). Specific market studies were analyzed so as to best fit our class breakdown to the projected market needs. In addition to interior concerns, external challenges were also addressed. The materials chosen for the TBD<sup>3</sup> allowed minimum weight penalties while maintaining the safety of high-speed flight. The most sensitive weight component was the swing wing mechanism and wing box which spans the fuselage. The structural design and materials were carefully analyzed to minimize the penalty for the swing wing option. With an aircraft this large, (considering specifically thrust power and weight) control surfaces would contribute heavily into the actual feasibility of the TBD<sup>3</sup>.

### **Phoenix**

The Phoenix is an aircraft that can succeed where the Concorde failed. It is a true second generation HSCT (Figure 10). The Phoenix can transport 152 people up to 5,150 miles at speeds of up to Mach 2.5 in luxurious comfort. Supersonic flight over land is still prohibited by the majority of countries around the world. The Phoenix will overcome this loss of flight paths by concentrating on the transoceanic routes. This will take full advantage of its supersonic speed. The Phoenix also has acceptable subsonic performance. This will enable it to successfully compete with subsonic aircraft on routes that are partially over land. Using its mixed flow turbofan engines, the Phoenix will meet the stringent FAR 36 Stage III noise requirements. This will allow it to land at airports the world over, further increasing its market share.

Two unique features of the Phoenix are its canard and its leading edge gates. The fully moveable canard helps to provide rotation at takeoff and trim in supersonic flight. The leading edge gates are deflected vertical to the leading edge, adding turbulence and thus strengthening the vortices over the wing, increasing lift. The Phoenix

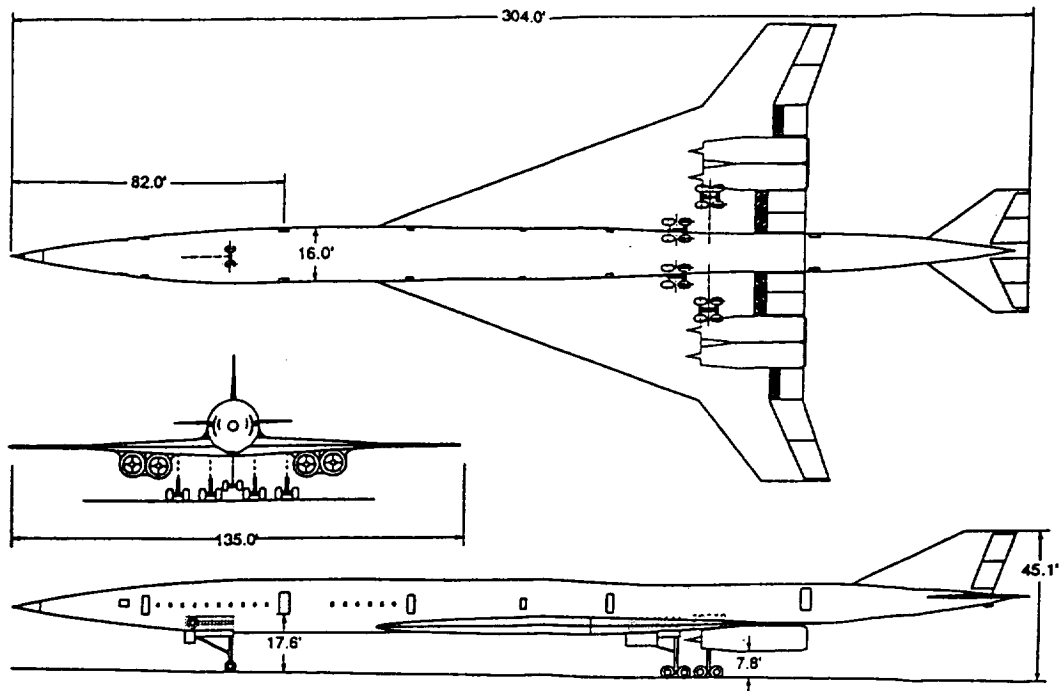


Fig. 8 Three-view of Swift

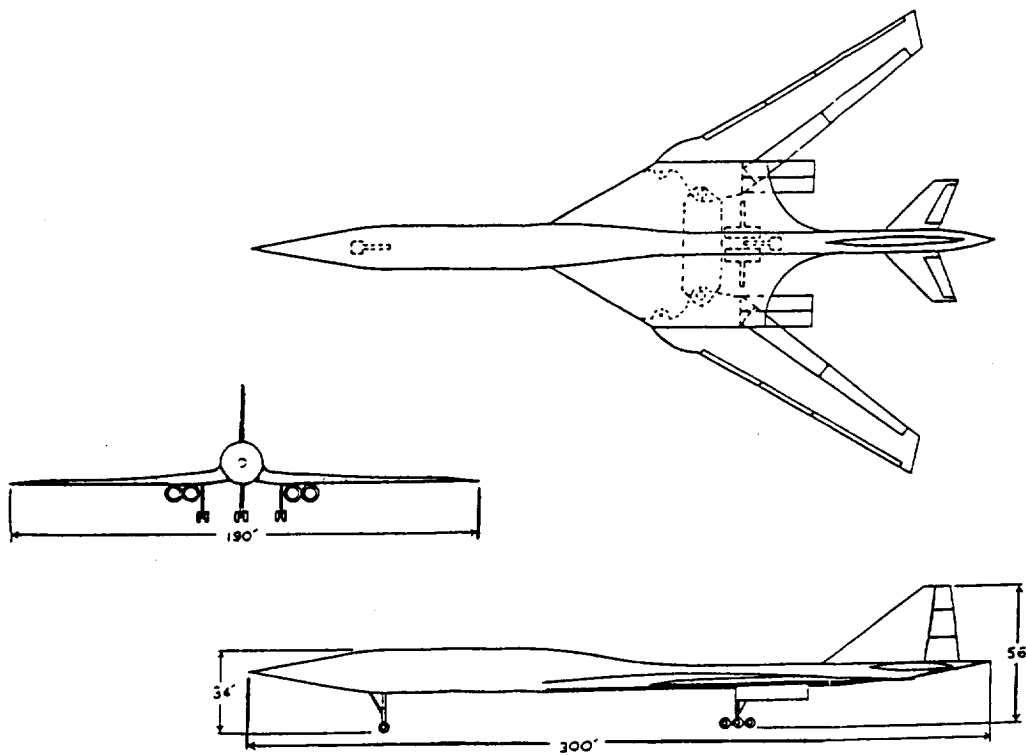


Fig. 9 Three-view of TBD³

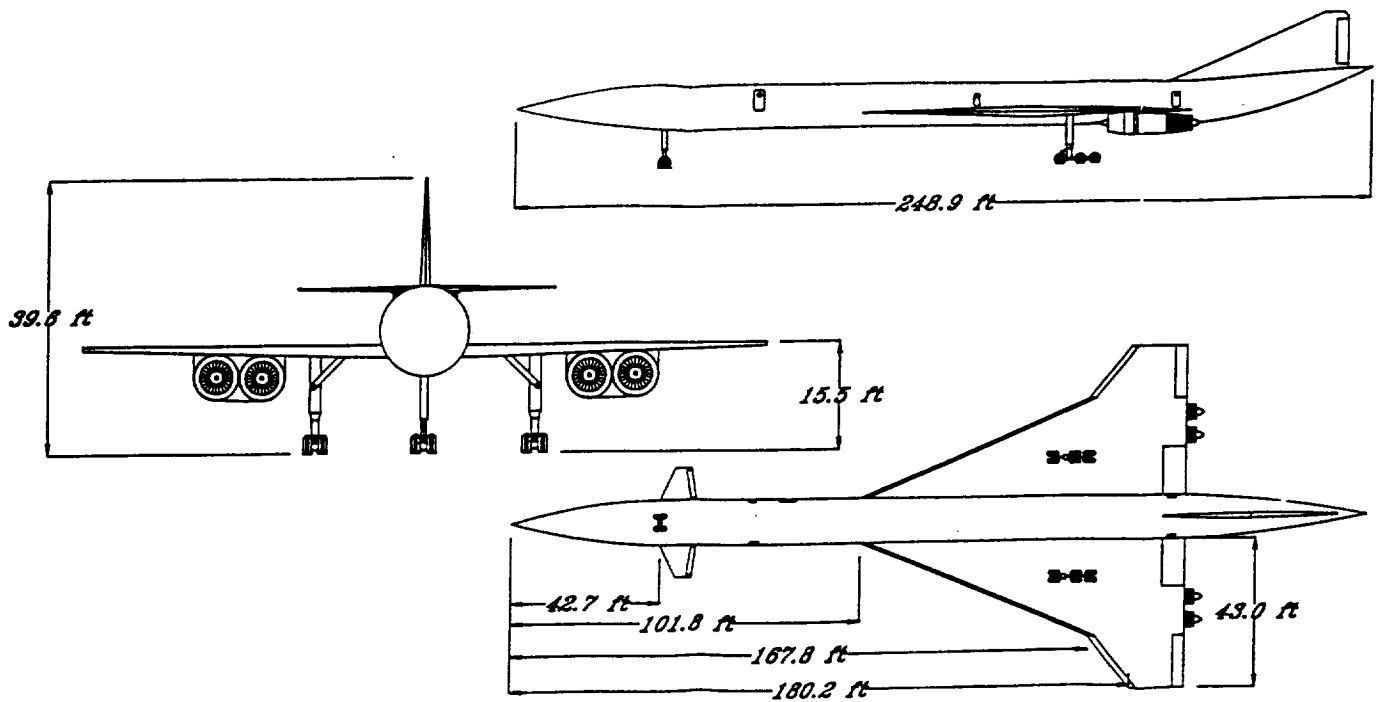


Fig. 10 Three-view of Phoenix

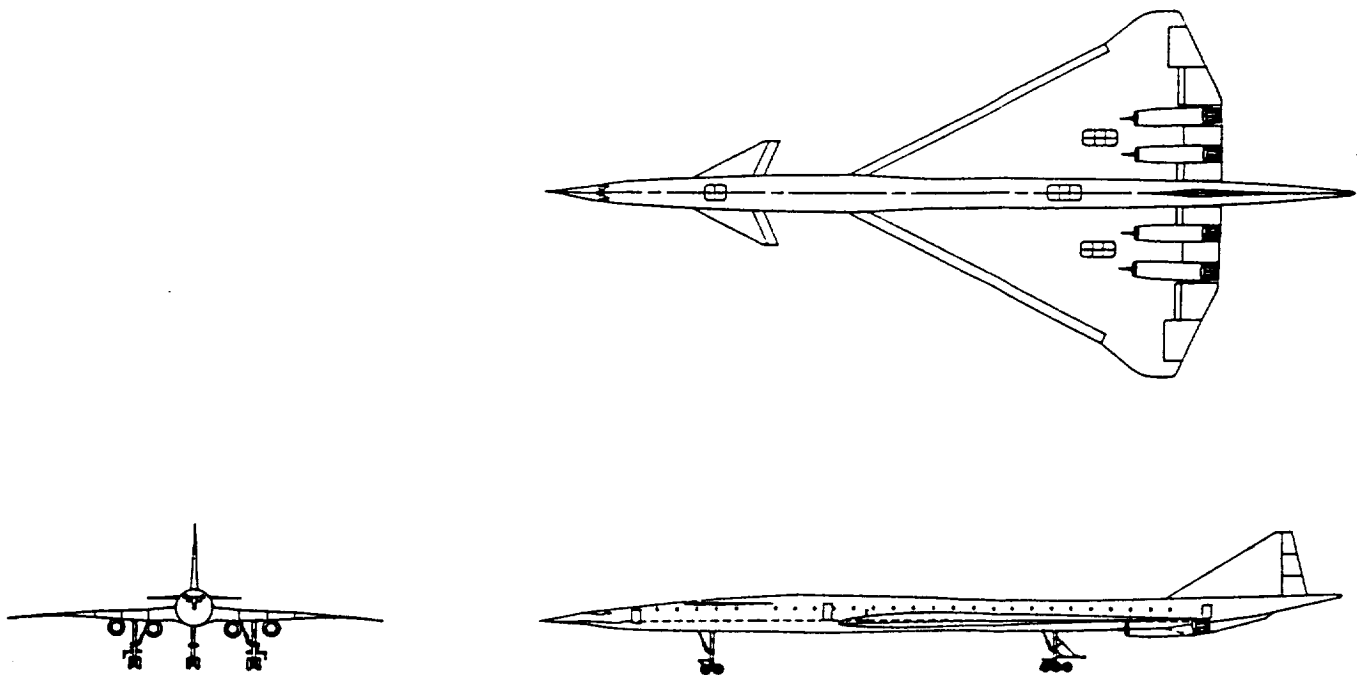


Fig. 11 Three-view of MM-122

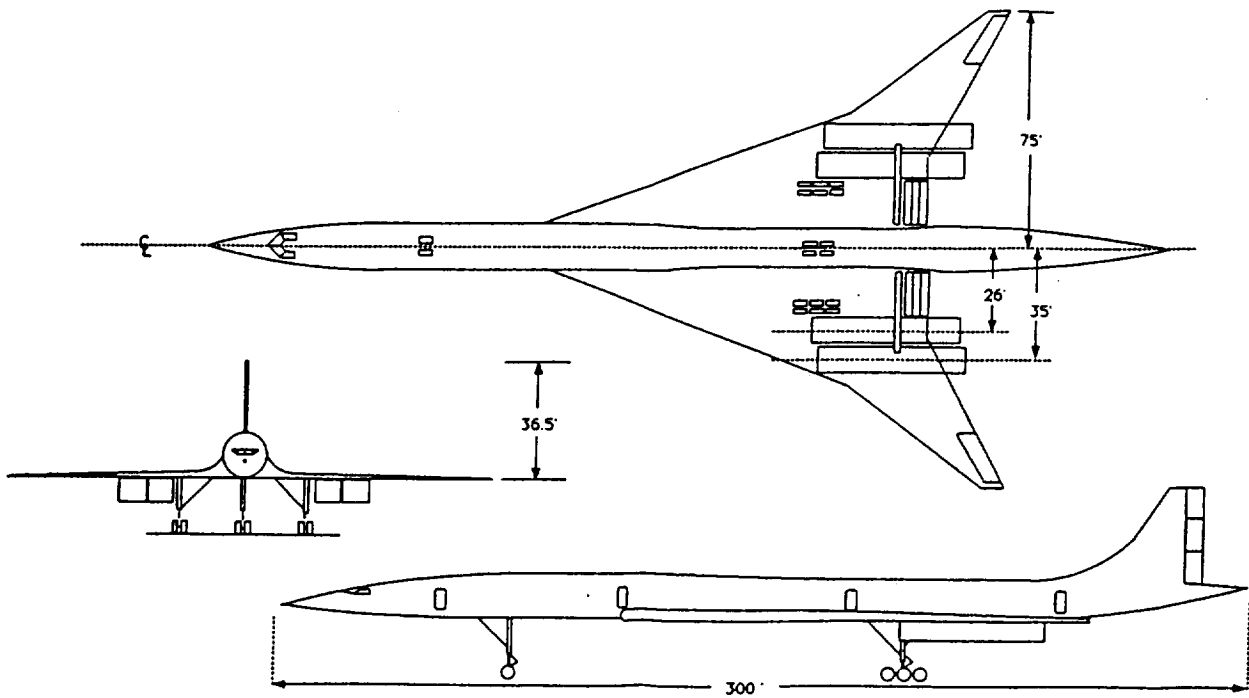


Fig. 12 Three-view of the Trojan

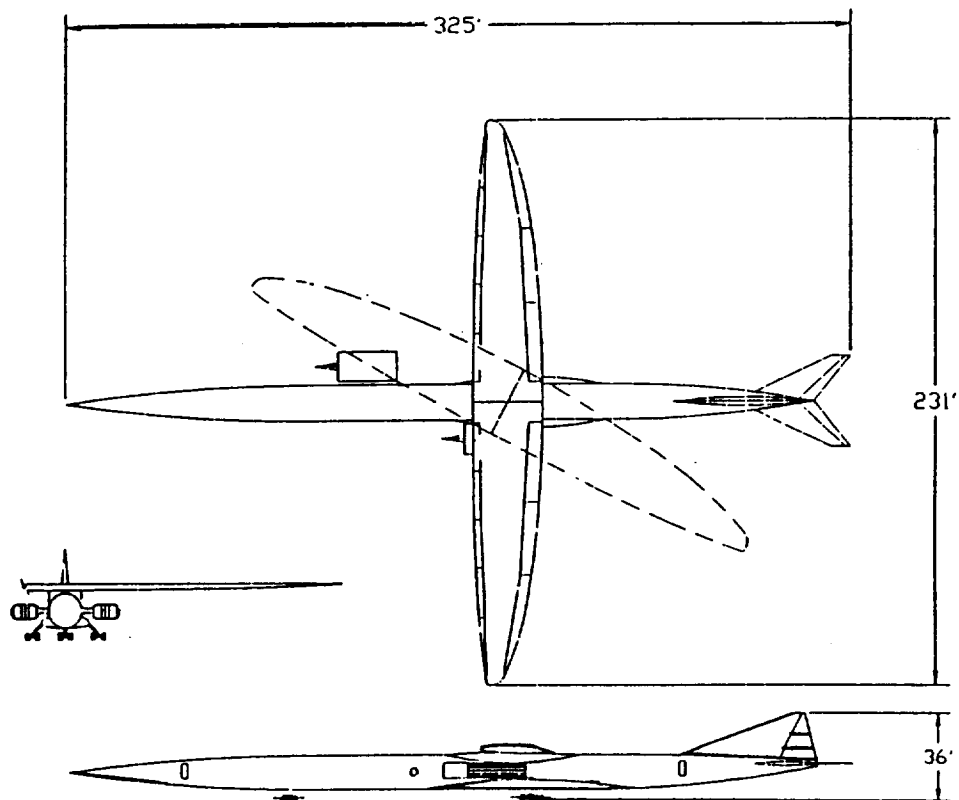


Fig. 13 Three-view of the RTJ-303

design strives to be a realistic solution to the supersonic transport problem.

### **MM-122**

The MM-122 is the answer to the international market desire for a state of the art, long range, high speed civil transport. It will carry 250 passengers a distance of 5,200 nm at over twice the speed of sound. The MM-122 (Figure 11) is designed to incorporate the latest technologies in the areas of control systems, propulsions, aerodynamics and materials.

The MM-122 will accomplish these goals using the following design parameters. First, a double delta wing planform with highly swept canards and an appropriately area-ruled fuselage will be incorporated to accomplish desired aerodynamic characteristics. Propulsion will be provided by four low bypass variable cycle turbofan engines. A quad-redundant fly-by-wire flight control system will be incorporated to provide appropriate static stability and Level I handling qualities. Finally, the latest in conventional metallic and modern composite materials will be used to provide desired weight and performance characteristics.

The MM-122, priced competitively at \$249 million, incorporates the latest in technology and cost minimization techniques to provide a viable solution to this future market potential.

### **The Trojan**

As the name suggests, the Trojan is a very safe and reliable supersonic aircraft (Figure 12). This high speed civil transport aircraft carries 250 passengers over 5,200 nm at a Mach of 2.0. Trojan incorporates unique features such as windowless cabin, low arrow-wing configuration, and no horizontal stabilizer. To be competitive, the Trojan has a unit price of \$200 million.

### **RTJ-303**

In recent years, designs for high speed civil transports have been studied for their feasibility in the commercial market. The oblique, variable sweep wing supersonic

transport configuration (Figure 13) was first proposed by Dr. R. T. Jones, former chief scientist of the NASA Ames Research Facility, who spent most of his life studying oblique aerodynamics. Studies of the oblique wing concept have shown substantially improved transonic performance at Mach numbers up to 1.4 and the elimination of sonic booms (audible at ground level) in flight at Mach numbers as high as Mach 1.2. Also predicted is an increase in low-speed performance, as well as the potential for increased range and/or reduced takeoff weight for a given payload. Further, a reduction of airport and takeoff noise to well within current standards is expected. Data for this rather unique type of configuration is limited, but enough research has been done to demonstrate some of the clear advantages of this type of aircraft. Although no supersonic flight test data has been obtained to date, supersonic wind-tunnel data has been obtained by NASA for Mach numbers up to 1.4 with wing sweep angles up to 60 degrees. Subsonic flight tests have been conducted by NASA using a remotely piloted aircraft and a low-cost piloted vehicle known as the AD-1.

The final payload of 300 passengers was a compromise between length restrictions on the aircraft weighted against the desire to remain competitive in the market with the maximum number of passengers carried for each flight. The range of 4,700 nm was decided upon to include Los Angeles to Tokyo in the city pairs to the Pacific Rim. Three hundred nautical miles are given in addition to this range to account for reserves and a flight to an alternate airport. This resulted in an aircraft sized for a range of 5,000 nm.

### **The Edge**

As the intercontinental business and tourism volumes continue their rapid expansion, the need to reduce travel times becomes increasingly acute. The Edge Supersonic Transport Aircraft (Figure 14) is designed to meet this demand by the year 2015. With a maximum range of 5,750 nm, a payload of 294 passengers and a cruising speed of Mach 2.4, the Edge will cut current international flight durations in half, while maintaining competitive first class, business class, and economy class comfort levels. Moreover, this transport will render a minimal impact upon the environment, and will meet all Federal Aviation Administration Part 36, Stage III noise requirements.



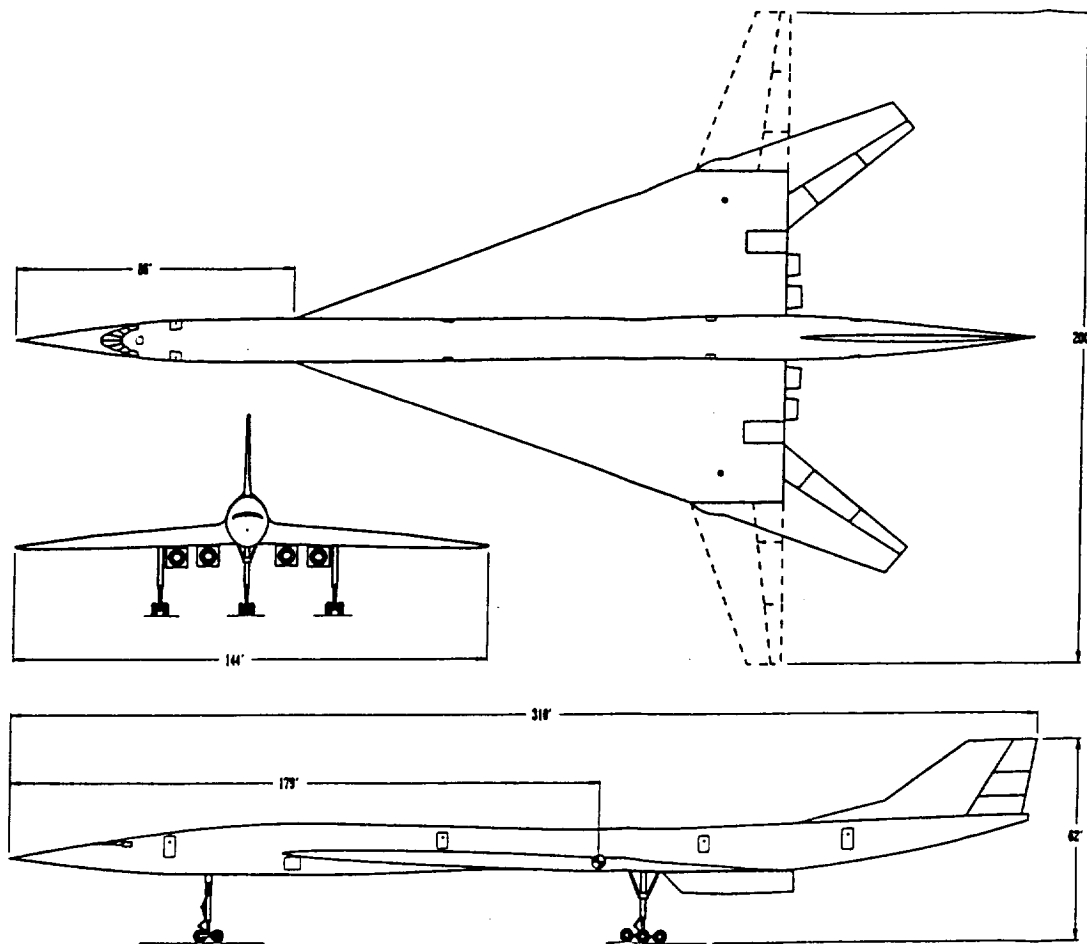


Fig. 14 Three-view of the Edge

The cornerstone of the Edge's superior flight performance is its aerodynamically efficient, dual-configuration design incorporating variable-geometry wingtips. This arrangement combines the benefits of a high aspect ratio wing at takeoff and low cruising speeds with the high performance of an arrow-wing in supersonic cruise. And while the structural weight concerns relating to swinging wingtips are substantial, the Edge looks to ever-advancing material technologies to further increase its viability.

Heeding well the lessons of the past, the Edge design holds economic feasibility as its primary focus. Therefore, in addition to its inherently superior aerodynamic performance, the Edge uses a lightweight, largely windowless configuration, relying on a synthetic vision system for outside viewing by both pilot and passengers. Additionally, a fly-by-light flight control system is incorporated to address aircraft supersonic cruise instability.

The Edge will be produced at an estimated volume of 400 aircraft and will be offered to airlines in 2015 at \$167 million per transport (1992 dollars).

### Conclusions

The nine aircraft design teams at Cal Poly, San Luis Obispo have examined a wide variety of solutions to the High Speed Civil Transport problem. These solutions vary from conservative, realistic approaches, such as double delta wing planforms and the use of conventional materials, to more exotic designs, such as variable planform geometry, application of advanced materials, the selection of canards, and even an oblique wing design. Both Class I and Class II preliminary design analysis were performed on all nine resulting aircraft.

Cal Poly has shown, in these analyses, that a second generation High Speed Civil Transport is technically, environmentally, and economically viable. This viability is strongly dependent on continued advances in the following key areas: improved thrust-specific fuel consumption coupled with a decrease in nitrous oxide emissions, aerodynamic tailoring through increased use of analysis tools such as computational fluid dynamics (CFD) and the use of more advanced materials capable of meeting high strength, high temperatures, and lowered

structural weight requirements. With these advancements on the horizon, the time has come for the second age of supersonic travel - the High Speed Civil Transports.

### References

1. Fitzsimmons, R.D. and Roensch, R.L. "Advanced Supersonic Transport," Douglas Aircraft Company, MDC Corp., 1975.
2. Mizuno, H. and Hagiwara, S. (Tokyo: Japan Aircraft Development Corporation, 1991), Hanai, T. and Takami, H. (Nagoya: Mitsubishi Heavy Industries, Ltd., 1991), AIAA-91-3104: Feasibility Study on the Second Generation SST. Baltimore, AIAA Aircraft Design Systems and Operations Meeting, 1991.
3. Boeing Commercial Airplanes, NASA CR-4234, High Speed Civil Transport Study. Seattle: BCA New Airplane Development, 1989.
4. Blackall, T.E. Concorde: The Story, the Facts and Figures. Foulis & Co.: Oxford, England.
5. McLean, F.E. NASA SP-472, "Supersonic Cruise Technology," NASA Scientific and Technical Information Branch, Washington, D.C., 1985.

**SUPERCRUISER ARROW HS - 8**

**California State Polytechnic University, Pomona  
Aerospace Engineering Department  
Pomona, California**

**Professor Paul Lord**

**Edward Kao, Teaching Assistant**

**Joey B. Abobo, Todd A. Collins, Leong Ma, Adnan Murad, Hitesh Naran, Thuan P. Nguyen,**

**Timothy I. Nuon, Dimitri D. Thomas**

**Abstract**

Technology in aeronautics has advanced dramatically since the last design of a production High Speed Civil Transport (HSCT) aircraft. Newly projected requirements call for a new High Speed Civil Transport aircraft with a range of approximately 5500 nm. and at least 275 passenger capacity. The aircraft must be affordable and marketable. The new HSCT must be able to sustain long-duration flights and to absorb the abuse of daily operation. The new aircraft must be safe and simple to fly and require a minimum amount of maintenance. This aircraft must meet FAA certification criteria of FAR Part 25 and environmental constraints. Several design configurations were examined and two designs were selected for further investigation. The first design employs the delta planform wings and conventional empennage layout. The other design uses a swing wing layout and conventional empennage. Other engineering challenges, including materials and propulsion are also discussed. At a cruise flight speed between Mach 2.2 and Mach 3.0, no current generation of materials can endure the thermal loading of supersonic flight and satisfy the stringent weight requirements. A new generation of lightweight composite materials must be developed. A new class of engines must also be developed for the HSCT. With the enforcement of stage 3 noise restrictions, these new engines must be able to propel the aircraft and satisfy the noise limit. The engine with the most promise is the variable cycle engine. At low subsonic speeds the engine operates like a turbofan engine, providing the most efficient performance. At higher speeds the variable cycle engine operates as a turbojet power plant. The two large engine manufacturers, General Electric and Pratt & Whitney in

the United States, are combining forces to make the variable cycle engine a reality.

**Introduction**

The Concorde, a supersonic passenger transport resulting from the joint efforts of the British Aircraft Corporation and the French Aerospatiale, flew for the first time on March 2, 1969. It was a monumental technical achievement; however, economically it proved to be a tremendous failure.

The obstacles facing the High Speed Civil Transport (HSCT) are mainly technical, economical and environmental. Because of the sonic boom generated by supersonic flight, the HSCT is banned from overland flight. Other environmental restrictions include the Federal Aviation Administration's requirement of low nitric oxide emissions and new lower noise level requirements. With these restrictions the building of an aircraft that meets these requirements will impose a major technical challenge. With the overland supersonic flying restriction, the HSCT market is thus limited. This reduced market threatens to make the HSCT an economically unfeasible aircraft.

The challenge to produce an environmentally and economically acceptable HSCT is the subject of the senior design project study of a team of undergraduate aerospace engineering students at California State Polytechnic University, Pomona.

## **Requirements**

The request for proposal (RFP) supplied to California State Polytechnic University, Pomona, included requirements proposed by the Association of European Airlines (AEA). The objective is the design of a High Speed Civil Transport aircraft for entry into the marketplace by year 2015.

### **Design Mission**

1. Incorporate payload of 275 passengers (minimum) with baggage.
2. Cruise to a point 6500 nm from takeoff.
3. Land with sufficient reserves.

### **Performance**

1. Determine best cruise Mach number.
2. Do not exceed 1.25g rate of climb to assure passenger comfort.
3. Satisfy second stage climb requirements performance.
4. Take off and land from 10,000 ft runway with 50 ft obstacle.

### **Environmental**

1. Meet any regulatory requirement for emissions at time of service.
2. Reduce the effect of the sonic boom.

### **Propulsion**

The engines should be designed to be operated with standard jet fuel.

### **Supportability**

To remain profitable, an airline must be able to utilize its aircraft around the clock throughout its useful life. Since corrosion, wear, and aging degrade an airplane, the aircraft must be easily inspectable. If a problem with a critical part is discovered, the part must be available to the mechanic and easily installed. The main structure should be designed and tested for a fatigue life of not less than 75,000 flight hours and 25,000 cycles.

## **Certification**

The aircraft must meet standards, rules, and regulations in FAR Part 25.

The aircraft is intended to be used in long range flights so it must be safe, simple to fly, and require minimal maintenance. Furthermore, this aircraft should require minimal personnel conversion training in both operation and maintenance. In addition, this aircraft must be able to be certified and fit in with the current designs in both the air traffic system and in the ground support system. A safety factor of 1.5 must be incorporated into the design.

## **Vehicle Development**

### **Concepts**

The first consideration was the type of fuselage needed in order to meet the RFP requirements. With this in mind, four fuselages were considered: cylindrical, twin fuselage, blended wing/body, and oblique flying wing. A comparison of the practicability of these configurations in the marketplace was considered along with market acceptability. The second consideration was the type of particular wing configuration that would optimize the HSCT performance in subsonic, transonic, and supersonic regimes. Four wing configurations have been considered the most practical for a HSCT aircraft. These four wing configurations are: fixed swept, variable sweep, double delta/cranked arrow, and oblique wings. These four wing designs have been experimentally tested in the realm of supersonic cruise flight and have been proposed as viable design features for our HSCT program.

### **Fuselage Configurations**

The first fuselage configuration to be considered is the conventional cylindrical fuselage. This configuration is a streamlined tube shaped for supersonic flight. Another configuration considered is the twin fuselage. The twin fuselage configuration offers more capacity and internal layout flexibility than the conventional single fuselage layout. The third fuselage configuration to be considered is the blended wing/body configuration. This particular configuration integrates both the fuselage and wing

configurations into one composite body to offer better aerodynamics.

The final fuselage configuration to be considered is the oblique flying wing. This configuration is the most radical of all the fuselages considered. The oblique flying wing does not have the same interior fuselage attributes as the cylindrical fuselage configuration. The only noticeable difference between the two fuselage designs is that there is basically no fuselage, by definition, present in the oblique flying wing. Unlike the other fuselages at subsonic speeds, the oblique flying wing would be capable of maintaining aerodynamic efficiency while accelerating from subsonic to supersonic speeds.

### Wing Configurations

The first wing configuration design considered was the fixed swept wing. Even though this wing configuration provides sufficient performance at supersonic speeds, its performance is poor when flying at subsonic and transonic speeds. In order to improve the poor aerodynamic performance of the fixed swept wing in subsonic flight, a variable sweep wing configuration has been proposed. This configuration has similar supersonic performance to the fixed swept wing, and good subsonic performance with the wings extended outward. However, the variable swept wing adds a weight penalty.

The third wing configuration to be considered for the HSCT program was the double delta/cranked arrow wing configuration. The double delta/cranked arrow wing shows the most potential. The arrow wing helps smooth out the area distribution of the HSCT, thus reducing the sonic boom overpressure. This configuration takes advantage of the physical and aerodynamic characteristics of the fixed swept and variable sweep wing design configurations.

The final wing design to be considered was the variable sweep oblique wing. This configuration has been shown to be quite efficient at low and supersonic speeds. Aerodynamic, aeroelastic, structural, and flight control studies have indicated that this variable sweep oblique wing concept leads to a more fuel efficient and quieter aircraft than those designed for the same HSCT requirements.

### Initial Configurations

An investigation was made into the possibility of supersonic flight over land. The sonic boom overpressure would have to be lowered such that the aircraft could maintain supersonic flight over land and populated areas. However, the acceptable overpressure level was difficult to attain. A mixed flight profile consisting of supersonic and subsonic phases was developed as an alternative to achieve overland flight. This criterion required that the aircraft have a good performance in both the subsonic and supersonic flight regimes.

Out of the initial vehicle concepts researched and reviewed, the following was concluded: The four fuselage configurations (cylindrical, twin fuselage, blended wing/body, and oblique flying wing) were studied and compared with each other. The missile (cylindrical) fuselage was the most economical in terms of passenger, payload, and production considerations. The twin fuselage and oblique flying wing configurations, on the other hand, exemplify distinctive ideas based on theory. The blended wing/body configurations represent a unique step into the integration of the fuselage and wing components into one composite body. This design is worth investigating for future possibilities, since it conforms to the passenger capacity of the missile fuselage and exploits the aerodynamic characteristics of an entire lifting surface. However, it has been ruled out due to its greater manufacturing cost.

From the four wing configurations (fixed, variable sweep, double delta/cranked arrow, and oblique wings) the fixed swept has poor subsonic performance. The variable sweep wing configuration adds unwanted structural and weight problems. In order to compensate for the above mentioned problems, the double delta/arrow wing configuration provides both good subsonic performance and less complicated structure. A unique wing configuration is the oblique wing, which was studied by the Boeing Commercial Airplane Company. However, with its radical looking configuration, getting public acceptance of the oblique wing will be difficult. From the comparison between the various wing configurations proposed, the double delta/arrow wing appears to be the design best suited for supersonic transportation. Two designs will be investigated further, the swing wing and the double delta/arrow wing, in order to determine the best design.

### Variable Geometry Wing

The first configuration selected for detail study is the variable geometry wing. Figure 1 shows the evolution of the variable geometry wing as it survived the initial design phase. The most beneficial characteristic of the swing wing was the aerodynamic compromise between the supersonic and subsonic flight regimes. With the wing swept back, the configuration maximizes its supersonic cruise performance. When the wings are fully extended, the configuration's subsonic performance resembles that of a subsonic aircraft.

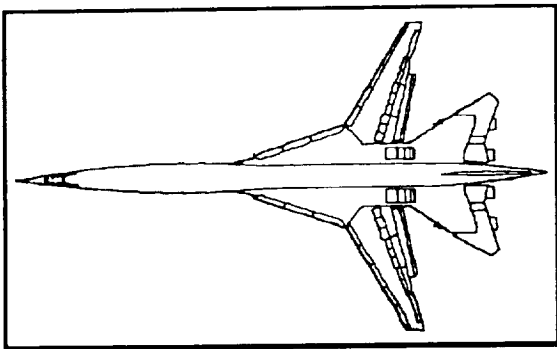


Fig. 1 Variable swept wing design

In the supersonic flight regime, the swing wing could reduce its aspect ratio to 2.17 with the wings fully swept. In this configuration, the aircraft would have less wave drag, thus reducing the required fuel load for the mission. With the exception of its variable geometry system, the swing wing would have structural similarities to those of the current subsonic aircraft. Even though the variable sweep wing appears to be the ideal wing configuration of choice, it is unfortunately not immune to the disadvantages. Due to the complexity of the mechanisms constituting the variable sweep wing, this variable sweep feature poses structural design and weight penalties. The variable sweep wing configuration for the HSCT was abandoned after the first quarter of detailed study.

### Double Delta/Cranked Arrow Wing

The evolution of the double delta configuration as it survived the first iteration of the design process is shown in Figure 2. Like the swing wing, the double delta configuration offered good subsonic and supersonic

characteristics. This optimum balance between the two flight regimes is achieved by the breaking of the wing into two regions. One region falls within the supersonic Mach cone and the second region is outside the Mach cone. The region outside the Mach cone allows for better subsonic performance, since it has less sweep. The inverse is true for the inboard portion of the wing. In addition to the favorable aerodynamic qualities of the double delta configuration, the wing is capable of carrying a large fuel capacity. Thus the double delta was chosen as the final wing configuration to be used in the second iteration phase.

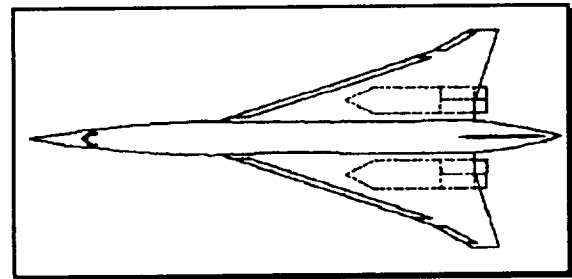


Fig. 2 Double delta/cranked arrow design

### Constraint Diagram

Constraint diagrams were optimized for aircraft flight profile and aircraft flight requirements, with the additional limitations set by the environmental restrictions. The following flight requirements were considered for the Supercruiser design.

- Range: 6,500 nm
- Rate of climb: 89 ft/s
- Takeoff Distance: 10,000 ft
- Landing Distance: 10,000 ft
- Cruise Speed: Mach 3.0

The Mach 3.0 cruise speed was chosen for the first design iteration, between the Mach 2 and 5 range. A sensitivity study for the cruise speed was conducted concurrently. The study showed that the cruise speed should be reduced to around 2.6. Unfortunately, due to time constraint, a second design iteration was not completed.

The constraint diagram is shown in Figure 3. The Supercruiser's design will fall within the area that satisfy the RFP requirements and associated constraints. The figure shows that the optimum aircraft designs falls between wing loading of 23 and 110 pounds per square foot, and thrust to weight ratio between 0.4 and 1.4. The initial design point was selected with 0.3 thrust to weight ratio and a wing loading of 104 lb/ft<sup>2</sup>.

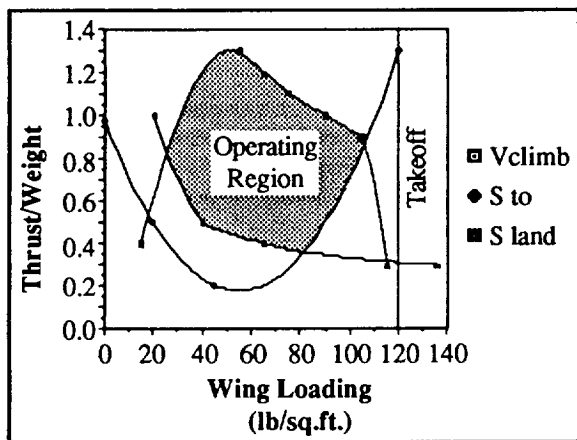


Figure 3. Supercruiser Constraint Diagram

## Aerodynamics

### Wing Design

Before any wing can be designed, appropriate airfoils must be selected. Compromise between structural integrity and aerodynamic effectiveness is required for a supersonic airfoil. The airfoil selected for the Supercruiser is a modified NACA 65-006. The maximum thickness is moved to be 3 percent of the chord. The wing planform chosen for the Supercruiser is a double delta, which is shown in Figure 4. The wing span of 130 feet and a total planform area of 10,000 ft<sup>2</sup> was selected for the Supercruiser. The aspect ratio and the inner and outer wing taper ratios are 1.69, 0.28, and 0.25, respectively. The inboard leading edge of the wing is swept back 72 degrees so that the wing is contained within the Mach 3 Mach cone. A rounded leading edge airfoil was selected for the inboard portion of the wing. The outboard leading edge is swept back 61 degrees. This portion of

the wing will experience supersonic flow normal to the leading edge.

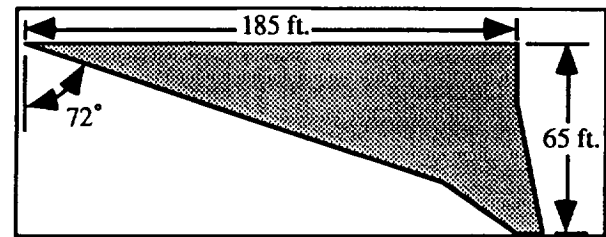


Fig. 4 Supercruiser wing semi-planform

### High Lift Devices

In order for the Supercruiser to have superior takeoff and landing performances, high lift devices such as trailing edge flaps and leading edge flaps were considered. The Arrow HS - 8 configuration has been fitted with full-span leading edge flaps to improve the takeoff performance of the aircraft. These leading edge flaps provide adequate control for pitch acceleration at the designated rotation speed to achieve the required liftoff speed.

### Trailing Edge Flaps

The design of trailing edge flaps depends on the following parameters:

- Airfoil used: 65A003
- Airfoil Lift Curve Slope: 0.106/deg
- Airfoil zero lift angle of attack: -2.6 deg
- (C<sub>L</sub>)max: 1.6

The behavior of the airfoil section as a function of flap deflection is shown in Table 1.

Table 1  
Behavior of airfoil section as a function of flap deflection

| Deflection (deg) | Zero lift (deg) | Stall (deg) | $C_L$ max |
|------------------|-----------------|-------------|-----------|
| 10               | -7.01           | -0.5        | 0.69      |
| 15               | -9.89           | -0.8        | 0.96      |
| 20               | -11.22          | -1.0        | 1.08      |
| 25               | -11.92          | -1.4        | 1.17      |
| 30               | -13.26          | -1.8        | 1.21      |
| 35               | -13.75          | -2.4        | 1.26      |
| 40               | -15.43          | -3.0        | 1.32      |
| 45               | -16.73          | -3.7        | 1.38      |
| 50               | -17.19          | -4.2        | 1.38      |
| 55               | -18.13          | -5.0        | 1.39      |
| 60               | -18.94          | -5.8        | 1.39      |

Once the airfoil behavior was determined, the wing behavior was then calculated. The  $(C_L)_{\max}$  of the wing was determined to be 1.13 and the stall angle of attack was found to be 28 degrees. These two parameters were shown to vary with flap deflection. Table 2 shows the variation of  $C_{D0}$  with trailing edge flap deflection.

Table 2  
Behavior of the wing as a function of flap deflection

| Flap deflection (deg) | $C_L$ max | $C_{D0}$ |
|-----------------------|-----------|----------|
| 10                    | 0.198     | 0.006562 |
| 15                    | 0.2755    | 0.009843 |
| 20                    | 0.310     | 0.019687 |
| 25                    | 0.3358    | 0.022968 |
| 30                    | 0.3473    | 0.026775 |
| 35                    | 0.3317    | 0.038062 |
| 40                    | 0.3789    | 0.04725  |
| 45                    | 0.3961    | 0.0525   |
| 50                    | 0.3961    | 0.063    |
| 55                    | 0.399     | 0.070875 |
| 60                    | 0.399     | 0.078225 |

Trailing edge flaps do not prevent flow separation; in fact, they aggravate flow separation slightly due to the increase in upwash at the leading edge due to increased circulation. Trailing edge flaps become less effective as

the wing sweep is increased. Trailing edge flaps are very effective on wings that are swept up to 35 degrees.

### Leading Edge Flaps

With the facilities currently being utilized, only experimental and statistical data were used to predict the change in  $(C_L)_{\max}$  for a wing with leading edge devices. The computed values for the change in  $(C_L)_{\max}$  due to leading edge flap deflection are shown in Table 3.

As noted earlier, the trailing edge flaps are not as effective with increasing sweep angle. The leading edge flaps are able to achieve the desired  $(C_L)_{\max}$  at landing and takeoff. Therefore, limiting the complexity of the wing while still maintaining adequate lift and control of the Supercruiser, the trailing edge flaps were dropped from the final design configuration.

Table 3  
Change in  $(C_L)_{\max}$  due to leading edge flap deflection

| Deflection (Deg) | $C_L$ max |
|------------------|-----------|
| 10               | 0.4329    |
| 15               | 0.6023    |
| 20               | 0.6778    |
| 25               | 0.7338    |
| 30               | 0.7593    |
| 35               | 0.7908    |
| 40               | 0.8284    |
| 45               | 0.8660    |
| 50               | 0.8660    |
| 55               | 0.8724    |
| 60               | 0.8724    |

### Vertical Tail Design

Two vertical tail concepts were considered for the Supercruiser's lateral directional control. The two concepts are an all-movable vertical tail and a conventional vertical tail/rudder combination. Control about the lateral directional axis is sensitive to changes in Mach number, dynamic pressure, and load factor. This sensitivity is due to strong nonlinearities in key stability derivatives and considerable reductions of control effectiveness caused by structural flexibility.



Utilizing stability computer simulation, the Supercruiser's stability behavior was analyzed for the all-movable vertical tail and the conventional vertical tail. Dynamically, the vertical tail with rudder was preferred because higher overall flying quality was achieved. However, the magnitude of the lateral force generated on the tail is proportional to flight speed and it was calculated to be 13,700 lb at Mach 3.0. This force, which is acting only on the rudder area, could twist the tail structure to a point at which it would fail and no longer function properly. Therefore, it was determined that the Supercruiser would utilize the all-movable vertical tail as its vertical stabilizer.

### Fuselage Design

One of the primary drivers in the fuselage design was its ability to accommodate the 275+ passengers including the associated baggage. With this requirement in mind, a baseline payload of 300 passengers including baggage was considered. The length of the fuselage and its maximum diameter was determined according to its ability to accommodate 300 passengers including baggage, flight deck, and required facilities and systems to properly maintain the aircraft. Those parameters resulted in a fuselage length of 318 ft and a maximum diameter of 17.1 ft.

Utilizing area ruling and wave-drag computer simulation, the fuselage's diameter was varied according to longitudinal location. This was done in order to optimize its performance in the supersonic flight regime. Figure 5 shows the final configuration of the fuselage.

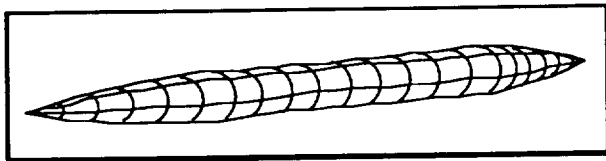


Fig. 5 Supercruiser's final fuselage shape

In order to determine the fuselage's impact on the overall performance of the aircraft, the fuselage drag

coefficient was evaluated at three different stages. The three stages are as follows:

- Subsonic drag coefficient
- Transonic drag coefficient
- Supersonic drag coefficient

### Subsonic Fuselage Drag Coefficient

In calculating the drag coefficient due to lift, the angle of attack was assumed to be 6 degrees. The value of the coefficient was predicted to be 0.0026 at Mach 0.3 and an altitude of 20,000 feet.

### Transonic Fuselage Drag coefficient

The transonic drag coefficient was determined to be 0.0027, at a Mach number of 1.1, altitude of 30,000 feet.

### Supersonic Fuselage Drag Coefficient

For the supersonic drag coefficient, the angle of attack was assumed to be 1 degree. The value of the supersonic drag coefficient was calculated to be 0.0015 at Mach 3.0 and an altitude of 60,000 feet.

The drag coefficients of the fuselage evaluated at three different Mach regimes are comparable to or less than those of current supersonic aircraft. The lowest drag is achieved at the supersonic cruise phase, since the aircraft is optimized for cruise. This indicates that our chosen fuselage configuration is aerodynamically acceptable.

## Propulsion System

### Engine Candidates

In order for the Supercruiser to achieve the optimum cruise number specified in the RFP (ultimately determined to be Mach 3.0) and to be environmentally acceptable, its engines must provide a considerable amount of thrust with low specific fuel consumption and low emissions. In this section, an evaluation of engine candidates will be conducted.

## **Turbojet**

At Mach numbers above 2.5, the afterburning turbojet becomes significantly efficient due to the pressure rise linked with diffusion in the inlet. This raises the nozzle pressure ratio to a higher value. However, the turbojet suffers in the subsonic region and does not meet the current noise and emission limits.

## **Turbofan**

The turbofan engine has better propulsive efficiency than the turbojet engine. The high values of static thrust ratio at low bypass ratios show the usefulness of the turbofan engine for takeoff, which is one of its main advantages.

## **Future Engine Designs**

Research has indicated that there are three different engine concepts which seem very promising for future utilization. These three engines concepts are a result of research done by General Electric and Pratt & Whitney. The engine concepts are listed below.

- GE 21/F14, augmented variable-cycle engine
- GE 21/FLA1, two-stream exhaust, nonaugmented high-flow fan variable-cycle engine
- GE 21/FLA, three-stream exhaust, nonaugmented high-flow fan variable-cycle engine
- P&W STF947 augmented variable-stream control engine, with chute suppressor and with a high-flow mixer/ejector nozzle
- P&W STJ950 single spool nonaugmented turbine bypass engine with a convergent-divergent ejector nozzle with suppressor

Two important parameters in engine performance evaluations are cruise overall efficiency and takeoff thrust-to-weight ratio. Another important engine performance parameter is specific fuel consumption during climb, which accounts for approximately 25 percent of the total block fuel. Takeoff thrust-to-weight ratio is important because engine thrust requirements are generally sized by takeoff field length.

After much analysis it was determined that there is no engine concept that exists at this point which will adequately satisfy all HSCT propulsion system requirements. There is a tradeoff between noise-level and range. However, with the further research and development of the variable cycle engine, a satisfactory candidate should appear around year 2010.

## **Engine Inlet System**

For sustained supersonic cruise (cruise at Mach numbers greater than approximately 1.4 for prolonged operation), there are basically two types of inlets. These inlets are the conical inlet (also referred to as the axisymmetric or conical spike inlet) and the two-dimensional ramp inlet. The conical spike inlet is known to have better pressure recovery than the two-dimensional inlet, the difference in pressure recovery being approximately 1.5% for well designed inlets. The conical spike inlet also tends to be lighter than the two-dimensional inlet. While the conical spike inlet offers better pressure recovery and weight savings, the two-dimensional inlet offers more simplicity in the variable geometry systems. From a reliability and maintainability point of view, the two-dimensional system was selected for the Supercruiser.

## **Inlet**

A mixed compression inlet was chosen for the Supercruiser. The external compression is to be achieved by a double wedge variable geometry ramp splitter system. The splitter translates horizontally to insure that shock wave impinges on the cowl lip. The total range of travel for the splitter system from Mach 1.5 to Mach 3.0 would be 8.5 ft.

The maximum mass flow rate of a rubber engine sized by compressor diameter to meet the demand of an HSCT aircraft was calculated. The mass flow rate was determined to be 607 lb/sec per engine. Thus the total mass flow rate for the two-engine pod inlet system is 1215 lb/sec. The total cross-sectional capture area for the two-engine inlet was determined to be 95.82 ft. From this value, the inlet height and width were determined to be 6 ft and 15.97 ft, respectively. The total inlet length was calculated to be 55.37 ft. For this design, the total pressure recovery was determined to be 76% at Mach 3.0.

## Future Design Considerations

The inlet design is an important part of the conceptual design of the aircraft. It was for this reason that the time was taken to develop an inlet design for a rubber engine since no current engine has been selected for the aircraft. Once the actual engine is selected, the optimum ramp angles can be determined for all the stages of flight. With the addition of a boundary layer removal system and system optimization, the pressure recovery would rise to between 80% and 87% at Mach 3.0.

## Structural Analysis

To reduce the weight of the Supercruiser, a sandwich construction panel method is utilized instead of the conventional skin-stringer stiffening design. Sandwich construction offers higher strength-to-weight ratios, better stability and load carrying capacity, increased fatigue life, and higher sonic fatigue resistance. Sandwich construction structures have the potential of reducing the structural weight by 12% to 25%.

Advanced composite materials are utilized to further reduce the weight of the aircraft. With composite materials, the best material properties are utilized for maximum material load-carrying efficiency. In selecting materials to construct an HSCT, many important factors must be taken into account in order to select the "best" material. Factors that must be considered are yield and ultimate strength, stiffness, density, temperature limit, fatigue properties, crack resistance, fracture toughness, corrosion, creep, cost, and producibility.

Since the Supercruiser will operate above Mach 2.0, the skin of the aircraft will incur temperatures ranging from -50° F to 600° F. Therefore, the chosen material must be able to withstand extreme temperature variances. Furthermore, the chosen materials must also have high strength-to-weight, and stiffness-to-weight ratios in order to keep the aircraft weight as low as possible so that fuel consumption is kept at a minimum. In addition, these materials must be able to maintain their integrity so that the transport will require minimum maintenance and repair through its 15 to 20 year life span.

After comparing various types of materials, it is determined that composite materials are best suited for

the Supercruiser. The specific strength and stiffness of composites are about 3 to 5 times greater than aluminum. An all-composite aircraft has the potential of reducing empty weight by 25 to 30 percent in comparison to an all-aluminum aircraft. Note that thermal expansion for composites is about 5 to 10 times less than that of titanium. This would greatly reduce the thermal expansion problem that high speed aircraft encounter while in flight.

The Supercruiser will use high temperature, unidirectional fiber polymeric, and metal matrix composites. The fiber will be graphite and the matrix materials will be thermoplastic, thermoset, and aluminum. In selecting composite materials, some additional aspects that must be considered are moisture absorption, impact resistance, thermal stability, and thermal expansion. Currently, there are composites that can operate in the temperature regime of the Supercruiser. Graphite/polymide and aluminum metal matrix composites can operate in environments exceeding 600° F, but they do not have enough thermal stability to meet the required life cycle of the aircraft. In addition to thermal stability, impact resistance is another property that must be improved. More research is required for a better understanding of these materials. For the Supercruiser, the feasibility of using composites will depend on their development in the next 10 to 15 years.

## Thermal Management

At Mach 3.0, aerodynamic heating is a problem that requires investigation. The temperature on the skin can reach as high as 600° F. Therefore, the Supercruiser must be properly insulated in order to maintain a comfortable cabin temperature as well as keeping the fuel below its boiling point.

Criteria for insulation sizing included insulation weight and thickness and heat flux into the cabin and fuel. The fuselage shell consists of a graphite-polymide/ aluminum honeycomb core panel, a layer of insulation, an air gap, and the cabin lining. The wing shell construction is exactly the same as the fuselage except that the insulating material is attached to the fuel tank instead of the skin panel.

It is noted that active cooling will be required for the engine inlet and nozzle, wing leading edge, and nose tip.

## Wing Structure

For the Supercruiser, the face sheets of the sandwich skin panel consist of 18 plies of graphite polyimide with the fibers oriented in the  $[0, -45, +45, 90]$  deg directions. The laminate is stacked up symmetrically to prevent tension and twisting coupling. Aluminum is used for the honeycomb core. The cell size ranges from 1/8 to 1/4 inch. Smaller cell sizes are required for bolt connection areas.

A finite element (FE) analysis was conducted on I-DEAS for structural sizing. The finite element model of the Supercruiser's wing represents the skin panel, spars and ribs. It consists of 208 nodes and 672 elements. In the FE model, the 18-ply laminate was modeled as a 7-ply laminate and the honeycomb core was modeled as an orthotropic laminate. The face sheets and the honeycomb were combined into one element. Quadrilateral and triangular thin shell elements were used to model the wing skin panels and spar and rib webs. Beam elements were used to model the flange.

The total force on the wing for a 3g lift load is 960,000 lb. For the double delta wing configuration, the first 20 feet of the wing span from the root will carry 50% of the total load, while the next 20 feet and the last 20 feet of the span will carry 32% and 17% of the total load, respectively. A thermal loading applied to the wing was also modeled.

For the wing, the maximum tip deflection for 3g loading is 8.15 feet. Furthermore, Tsai-Wu failure criterion was used to check for laminate failure. All the laminates were well below the maximum failure index, and the strain energy was located at the center of the wing. For structural optimization, thicker spars will be required in this region. However, the thickness of the spars and ribs everywhere else on the wing can be reduced to minimize the weight.

## Fuselage Structure

The fuselage of the Supercruiser uses the sandwich construction concept described in the Wing Structure section. The stiff skin panel greatly reduces the size of the ring frame and longerons, while in the case of the wing, the bending load was carried by the skin panel.

The fuselage structural elements are primarily designed based on the loading conditions defined below.

**Dynamic heating.** At the nose tip of the Supercruiser, it is expected that the skin temperature at a cruise condition of Mach 3.0 could reach 600° F. Representative temperatures and temperature gradients at certain fuselage stations are obtained from experimental data of the NASA supersonic aircraft model 969-512B.

**Fuselage concentrated loads.** The calculated static load of the nose landing gear is 82,751 lb acting at fuselage station 99 ft from the nose tip. Reaction loads at the wing root due to load factor of  $n=3$  are the primary loads considered in the design of the wing box.

**Pressurization.** Pressurization of the fuselage was analyzed using the pressure gradient between the inner and the outer wall of the fuselage. Assuming standard atmospheric conditions, the value was calculated to be 2022 lb/ft<sup>2</sup>.

## Fuselage Structural Elements

The fuselage structure is divided into forward, mid, and aft sections. The three sections have very similar semi-monocoque structures. However, for each section, specific design criteria drew special attention.

**Fuselage forward section structure.** The forward section structure covered fuselage sections (FS) from zero to 99 ft. The sandwich shell construction is the primary structural design concept. The supporting frames are joined using mechanical fastening and bonding. The nose tip skin should be made of Ti-alloy whose temperature limit is high enough to withstand the dynamic heating problems incurred at Mach 3.0.

**Fuselage midsection structure.** The primary structure of this section is the wing box construction. A design concept of the wing box is based on the typical design of most modern transport aircraft in which main frames of the fuselage are bolted to the main spars of the wing box. Both spar moment and shear connections are spliced into the fuselage forward and aft bulkheads. The bulkheads and wing spars are rigidly connected together as one

integral unit. This concept is chosen primarily because of its wide usage and high reliability.

**Fuselage aft section structure.** The main concern of the construction of this section is the mechanism that supports and rotates the vertical tail. The two main spars of the vertical tail structure are connected to the aft fuselage bulkheads by means of a system of gears driven by a hydraulic system.

### **Tail Structure**

Sandwich construction is also applied to the tail structure. The required thickness of the sandwich panel is approximately 1.0 inch in order to provide stiffness and prevent fluttering. Two spars and three ribs are used to help support the skin.

The tail leading edge could reach temperatures near 4790 F. Therefore, it is suggested that Ti-alloy be used in the leading edge section.

### **Landing Gear**

The Supercruiser will employ a tricycle landing gear configuration. The location of the gears with respect to the center of gravity (CG) location indicates that the overturn angle is 66 deg, which satisfies the requirement outlined by FAA regulations. Calculation of the rotation angle yielded the value of 16 deg, thus guaranteeing that the tail section has sufficient clearance during takeoff.

Both the nose and main gear use oleo shock absorbers which have the highest energy absorbing efficiency of all absorbers presently available. The nose gear is operated by a hydraulic system which retracts the landing gear system forward and mechanically releases with free-fall in an emergency condition. The twin wheel nose gear could withstand a maximum static load of 86,000 lb. The main gears are also hydraulically operated to retract forward into the wheelwells located in the wing structure. The two six-wheel bogie main gear could carry a maximum static load of 732,000 lb.

### **Stability and Control**

The Supercruiser's supersonic cruise stability is surprisingly well-behaved. Cruise stability is achieved

without the use of flaps, ailerons, or a horizontal tail. Instead, cruise stability is achieved by the management of the aircraft's CG. The aircraft's CG management gives it natural stability without the use of a stability augmentation system (SAS). Although complete stability was not achieved in all realms of lateral motion, management of the CG allowed for a less complex stability enhancement system. During takeoff and landing the Supercruiser demonstrated level 2 flying qualities; thus a stability augmentation system is employed during takeoff and landing, as well as an ILS system.

### **Fuselage Interior Layout**

#### **Passenger Seating Arrangements**

The main driver for the passenger seating arrangement was that the Supercruiser was to be capable of accommodating 300 passengers including baggage, eight flight attendants, and a flight crew of two. With these parameters in mind, the maximum diameter of the fuselage was calculated to be 17.1 ft. The diameter of the fuselage at specific points along its length was dictated by area ruling and a wave-drag computer simulation program. This was necessary in order to reduce supersonic drag.

Due to marketability demands, the seating arrangement was designed by considering a tri-class arrangement. The three class seating arrangement is as follows: 7, 36, 57 percent for first, business, and economy classes, respectively. The first class section is positioned in the forward zone of the fuselage, the business class section is positioned in the mid-zone, and the economy class section is in the aft portion of the fuselage. A 20-inch minimum aisle width and 84-inch aisle height accommodate passenger space requirements. Seat widths are 47-inch double-seat assembly for first class, 40-inch double-seat assembly for business class, and 39-inch double-seat assembly and 55.5-inch triple-seat assembly for economy class. The first, business, and economy classes have a four-across, six-across, and seven-across seating arrangement, respectively. The comfort levels for the passengers are implemented at a level comparable with the standards of current subsonic carriers.

### **Capacity and Payload Accommodations**

The Supercruiser's cargo/baggage holds are designed in order to accommodate the passengers' baggage and secondary items such as freight and mail. The overhead stowage bins, which are located along both sides of the entire cabin, are capable of holding 1.8 cubic feet per passenger, while lower cargo bays, located underneath the cabin floor, are proportionally sized for multi-shelf containers. Thus, the belly capacity per passenger seat is set around 8 cubic ft. and the baggage weight per passenger is averaged around 45 lb.

In order not to incur additional costs, the Supercruiser will utilize standard containers and pallets currently being used by other airline carriers.

### **Interior Facilities**

The interior facilities provide contemporary service for 300 passengers based on a maximum flight duration of four hours. Each class has its own galley, lavatories, closets, and cabin attendant stations. The cabin attendants are adjacent to each exit door.

Interior facilities such as service areas and lavatories are positioned with the maximum interior flexibility in mind. Each class section has its own service area and other interior facilities that are equal to those standards set by long-haul subsonic carriers. Furthermore, flight entertainment is provided by separate view-screens located in each class section and music control units located on each seat. For the protection of passengers from lethal doses of ozone and radiation, a climitization system is installed to deliver maximum climatic comfort comparable to subsonic carriers.

### **Doors, Emergency Exits, and Windows**

Since all doors, emergency exits, and windows are potential sources for leaks, noise, drag, and excess weight, they are designed to maximize passenger comfort and meet those emergency requirements dictated by the FAA. The number and the particular size of doors and emergency exits required in the HSCT type aircraft are defined in FAR 23 and 25 parts 807-813. The number and types of required exits for the Supercruiser was dependent upon the number of passengers carried.

Since all doors and emergency exits must meet the "unobstructed access" criteria, the designers used Type I, II, and III access doors to fulfill this requirement. There are a total of 6 access doors: two passenger Type I doors, two emergency Type II doors, and two emergency Type III doors. Service access doors are located mainly on the starboard side of the aircraft to ease the ground support operation.

Each emergency exit and the two passenger doors are equipped with an Emergency Escape Chute Deployment System. This system is composed of evacuation slides that are deployed in case of an emergency. The following are the characteristics of such a system.

- Inflatable slides automatically deploy upon opening of each exit.
- Stored gas inflates slides.
- Escape system disarms when door is opened from outside airplane.
- Slides usable in all landing gear conditions.

Note that standard life rafts would be stowed in overhead stowage bins located near each emergency exit and passenger door.

The passenger windows on the Supercruiser are shaped like circles that are spaced according to the fuselage's frames and not necessarily spaced according to passenger seat location. This particular shape of the window is utilized in order to avoid unnecessary stress concentrations and large pressure differentials that will be encountered while flying supersonically. The windows are located so that there is no discomfort to the average passenger when viewing through them.

### **Marketability**

#### **Potential Markets**

In order to produce a viable HSCT, the market demand must be sufficient to sustain a fleet of approximately 500 aircraft. A preliminary analysis determined that the Supercruiser could acquire a significant portion of the growing long-range Atlantic and

Pacific Rim markets. Present statistical data projects that the worldwide demand for long-range air travel will almost double by the year 2000, with a growth potential of 53% in the Pacific Basin and 27% in the North Atlantic region. Figure 6 shows the international traffic distribution based on the year 2000 with a traffic distribution of 200,000 passengers per day. This figure shows that the greatest market demand is located in both the Atlantic Rim and Pacific Rim regions.

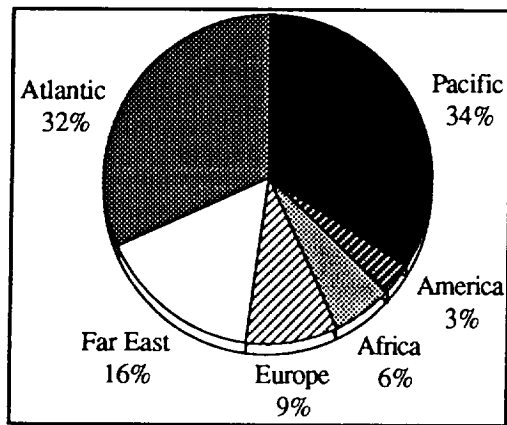


Fig. 6 International traffic breakdown by year 2000

The Supercruiser's potential as a viable long-range carrier is dependent not only on the market demand but also on its performance characteristics such as speed, design range, and total number of passengers carried. For this airplane configuration, the speed is fixed at Mach 3.0 and the range was determined to be below 4000 nm. Even though the range falls short of the expected 5500 nm, the effectiveness of the Supercruiser to capture a proportional amount of revenue passenger miles (RPM) depends upon the market in which it operates. The revenue potential for the Pacific and Atlantic Rim markets are as follows: first class projected 6% of total revenue, business 45%, and economy 49%. Therefore, by concentrating on the revenue potential, the Supercruiser can be a viable addition to the current long-range carriers operating in these markets.

### Airport Compatibility

Operations from conventional airports require that the Supercruiser must meet anticipated weight and field-length constraints as well as operate in conjunction with subsonic carriers during approach to avoid system degradation. Since the Supercruiser weighs less than 800,000 lb and takes off within 12,000 ft, it can be accommodated by selected high-demand airports such as Los Angeles Airport (LAX) and Tokyo Airport (NRT). The high speed of travel and the high altitude of the Supercruiser don't require special equipment on part of the Air Traffic Control (ATC) services. Since the Supercruiser will be outfitted with enhanced avionics systems, it will easily integrate into the ATC environment.

Because the Supercruiser is considerably larger than subsonic carriers such as the 747-400 (length of 231.8 ft), some modifications to the runway fillets may be necessary in order to maintain an acceptable runway-edge safety margin while maneuvering on the ground from runway-to-taxiway and taxiway-to-taxiway intersections with the cockpit over the centerline.

Gate parking in front of a terminal can be achieved with the Supercruiser positioned at an angle. Because of the Supercruiser's length and door sill height, minor adjustments might have to be made in order to connect the passenger entrance umbilical to the passenger doors.

Supercruiser servicing operations will be tasked to minimize 'turn-around' time as much as possible. Typical services such as loading and unloading of passengers and cargo and refueling and reoiling are pertinent tasks that must be performed in a minimal amount of time.

### Cost Analysis

For the Supercruiser to become marketable and meet the demands of future air travel, it must be cost effective within its life cycle. Utilizing a cost analysis computer simulation program, the Supercruiser was determined to be unprofitable with its range less than 3183 nm. Three primary costs were determined: Research, Development, Test and Evaluation cost (RDTE); manufacturing and acquisition cost (MACQ); and operating cost (OPS). The life cycle cost is being considered over a 16-year period. Note that an estimated cost for a prototype program

consisting of two airplanes cost roughly \$423 million 1992 United States dollars (USD)

In order to accurately surmise the cost evaluation of the Supercruiser, it was compared with three potential competing aircraft: the 747-400, the MD-12, and the A340-300. These three aircraft represent the primary competition that the Supercruiser will face in the 21st century. Figure 7 shows the cost comparison with the competitive aircraft. Note that the Supercruiser does cost more in development and manufacturing; however, as more units are sold the cost becomes considerably less. It was determined that the operating cost of the Supercruiser and its LCC is three times less than the competing aircraft.

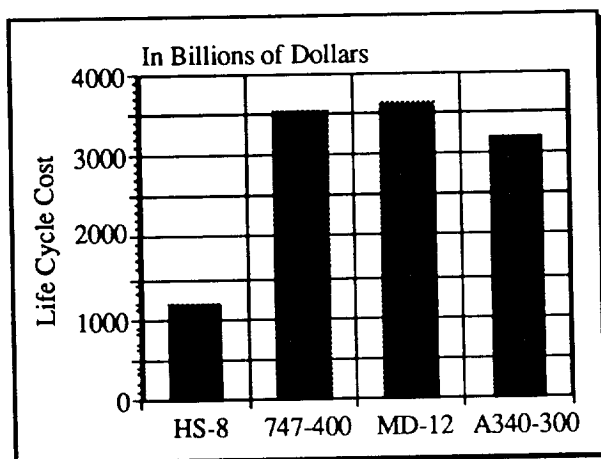


Fig. 7 Life cycle cost comparisons

In a competitive market such as the airline industry, one of the primary drivers for market capture is the airfare charged to passengers. In order for the Supercruiser to be competitive, its airfare must be comparable to those of the competing subsonic carriers. For ranges greater than 5000 nm, coach fares are set between \$600 and \$800 1992 USD. These fares were determined from current airlines such as United, Northwest, and American. To be competitive, the Supercruiser must charge a coach fare rate between \$650 and \$950 1992 USD. This coach fare is based on a range greater than 5500 nm, 80% of available seats filled, and a profit range between 10% and 62%. The 80% of available seats filled is acceptable in current subsonic carriers. In addition, the profit range mentioned above is

considered acceptable for continuing operations. Utilizing the same methods to determine the primary costs, it was determined that the Supercruiser meets the above criteria for the coach fare charged to passengers. Therefore, if a range of 5000 nm was achieved, the Supercruiser will be a profitable carrier and a competitive opponent of the subsonic carriers.

## Environmental Impact

### Sonic Boom

The environmental disturbance of the sonic boom is well known by those individuals who live near certain military facilities. As a result of the annoyance of this disturbance, a possibility of supersonic flight over land exists. Many tests have been conducted which aimed at determining the maximum levels of overpressure (measure of sonic boom intensity) which could be produced by supersonic aircraft which would be acceptable to the public and the environment. The results of such studies have varied. Depending on the author of the study, the range of acceptable overpressures is from as low as no increase in overpressure to a maximum increase of 0.5 to 1.0 psf. Today, the absolute best levels of overpressure that can be achieved are about 1.5 psf. As a result, it is not expected that the HSCT will be allowed to travel over land supersonically in the near future.

## Recommendations for the Future

Technology changes in leaps and bounds. The future poses increased possibility for the impossible to become possible. Limitations become viable and economical alternatives. Currently, aircraft engine technology has not progressed far enough where we can meet the range requirement of 5,500 nm. Furthermore, the engine's fuel consumption is much too high, thus reducing the range of the Supercruiser. In order for the Supercruiser to meet the RFP range of 5500 nm, a more fuel-efficient engine needs to be conceived. This aircraft is expected to be introduced in the year 2020, and it is assumed that an engine fulfilling noise and emissions requirements, as well as the necessary fuel consumption and thrust rating, would have been conceived and introduced into the mass market.



### References

1. Anderson, John P. Jr. Introduction to Flight, McGraw-Hill: New York, 1989.
2. Boeing Commercial Airplane Company. New Airplane Development; High Speed Civil Transport Study, NASA CR-4233, September 1989.
3. Boeing Commercial Airplane Company. New Airplane Development; High Speed Civil Transport Study, NASA CR-4234, September 1990.
4. Boeing Commercial Airplane. Oblique Wing Transonic Transport Configuration Development, NASA CR-151928, January 1987.
5. Domack, Christopher S. Concept Development of a Mach 4 High-Speed Civil Transport, NASA TM-4223, 1990.
6. Douglas Aircraft Company. New Commercial Programs; Study of High Speed Civil Transports, NASA CR-4235, December 1989.
7. Douglas Aircraft Company. New Commercial Programs; Study of High Speed Civil Transports, NASA CR-4236, August 1990.
8. Nelms, Walter P. Application of Oblique-Wing Technology - An Overview, AIAA-76-943, September 1976.
9. HSCT Concept Development Group, Douglas Aircraft Company. High Speed Civil Transport Studies, NASA CR-4375, May 1991.
10. McCormick, Barnes W. Aerodynamics and Flight Mechanics, John Wiley and Sons: New York, 1979.
11. McLean, F. Edward. Supersonic Cruise Technology, NASA SP-472, 1985.
12. Raymer, Daniel P. Aircraft Design: A Conceptual Approach, AIAA: Washington D.C., 1989.
13. Roskam, Jan. Airplane Design Series Vol 1 - 8, Roskam Aviation and Engineering Corporation: Kansas, 1989.
14. Shevell, Richard S. Fundamentals of Flight, Prentice Hall: New Jersey, 1989.
15. Schartz, R.T. and Rosato, D.V. Composite Engineering Laminates.
16. Sweetman, Bill et. al. The Great Book of Modern Airplanes, Portland House: New York, 1987.
17. Turner, M.J. and Grande, D.L. Study of Advanced Composite Structural Design Concepts for an Arrow Wing Supersonic Configuration, NASA CR-2825, April 1978.
18. United States Federal Government. Code of Federal Regulations, Title 14, Aeronautics and Space, Parts 1 to 59, 1991.
19. Wood, Richard M. Supersonic Aerodynamics of Delta Wings, NASA TP-2771, 1988.

**PROJECT ARES III**

**California State University, Northridge  
Mechanical Engineering Department  
Northridge, California**

**Professors Dan Raymer, Phyllis Russell, and Tim Fox  
Doug Meyers, Teaching Assistant**

**Steven Lovric, Robert Grabow, Manfred Epp, Warren Wynn Jr., Zoltan Mako, Gunther Linzner, Dante DeLeo,  
Chris Parker, Chris Kelley, Leeor Gorstein, Yaron Shani, Enrique Chavez, and Yakem Habtemariam**

**Abstract**

The mission of Project Ares is to design and fabricate an Earth prototype, autonomous flying rover capable of flying on the Martian surface. The project was awarded to California State University, Northridge (CSUN) in 1989 where an in-depth paper study was completed. The second year's group, Project Ares II, designed and fabricated a full-scale flight demonstration aircraft. Project Ares III, the third and final group, is responsible for propulsion system design and installation, controls and instrumentation, and high altitude testing.

The propulsion system consists of a motor and its power supply, geartrain, and propeller. The motor is a four-brush DC motor powered by a 50-V NiCd battery supply. A pulley and belt arrangement is used for the geartrain and includes light weight, low temperature materials. The propeller is constructed from composite materials which ensures high strength and light weight, and is specifically developed to provide thrust at extremely high altitudes.

The aircraft is controlled with a ground-based radio control system and an autopilot which will activate in the event that the control signal is lost. A transponder is used to maintain radar contact for ground tracking purposes. The aircraft possesses a small, onboard computer for collecting and storing flight data. To safeguard the possibility of computer failure, all flight data is transmitted to a ground station via a telemetry system.

An initial, unpowered, low-level test flight was completed in August of 1991. Testing of systems integration in the second low-level test flight resulted in loss of elevator control which caused considerable

damage on landing. Complete failure analysis and repairs are scheduled for September of 1992.

**Introduction**

An ultra-high altitude, battery-powered, remote controlled aircraft has been developed to collect low Reynolds number performance data for the wing airfoil and propeller efficiency. The aircraft is designed to fly at an altitude of 104,000 feet and at a speed of Mach 0.2. The aircraft configuration is similar to that of a powered glider with a low power to weight ratio and an aspect ratio of 10. The aircraft has a wing span of 32 feet and a length of 20 feet while weighing only 62 pounds. It is constructed of carbon graphite, kevlar, mylar, styrofoam, and Nomex honeycomb.

The aircraft is controlled with a ground-based radio control system equipped with autopilot. The autopilot will engage if contact is lost between the ground station and the aircraft. If contact is not established after a predetermined time period, the self-destruct mechanism will engage, thus separating the wing from the fuselage. The aircraft is equipped with a transponder which assists in radar contact to assist the pilot in maneuvering.

Although originally designed to incorporate solar cells to power the motor, we were unable to obtain the cells that met our weight and power requirements due to their overwhelming cost. Nickel-cadmium (NiCd) batteries were selected to power the 1.4 horsepower DC motor. The motor is connected to an 11:1 gear reduction employing low weight, low temperature materials. The propeller is constructed from a composite of carbon and

foam, and was specifically designed to provide thrust in a low Reynolds number environment.

The aircraft is equipped with a microprocessor possessing low power mode capability, analog to digital conversion, digital input/output, expandable data storage, and PC-compatible programming. The microprocessor is the heart of the data acquisition system which collects data such as motor rpm and power consumption, air temperature, propeller thrust, air speed, altitude, and the pressure distribution over the wing.

The testing will consist of a series of low-level test flights to test guidance and control and to calibrate data measurement equipment, as well as a high altitude test flight to measure low Reynolds number airfoil data and propeller performance. The aircraft is deployed to an altitude of 110,000 feet via a weather balloon with the nose positioned downward and then released. After a gradual pullout, the aircraft will then proceed to collect low Reynolds number data for the duration of the level flight.

### **Background**

CSUN'S Mechanical Engineering department has a unique design program for the senior level student. The course is designed to imitate a "real world" engineering atmosphere. The students form an organization which is administered by several levels of student management. Faculty advisors are available for technical and administrative support. The program enables the student to experience the design process and actually build hardware. Many student projects have been used in nationwide competitions.

NASA/USRA funded CSUN'S Mechanical Engineering Department through the Advanced Design Program for a 3-year aircraft design project. The objective of the project was to design and build a prototype Mars aircraft to investigate Martian lower atmosphere and geological features as a prelude to a manned mission to Mars.

Last year's design team designed and fabricated such an aircraft and successfully completed an unpowered, tow-assisted test flight in August of 1991. This year's team is responsible for the design and installation of the

propulsion system and controls and instrumentation. The low-level systems integration test flight of May 1992 ended when elevator control was lost due to engine interference with the control signal. The aircraft was heavily damaged on landing. This is an initial estimation of the failure, and more failure analysis is scheduled for the near future. Aircraft repair is also scheduled for the immediate future.

### **Vehicle Group**

The Vehicle Group for Project Ares II has a different task than the traditional design and production of an aircraft. Project Ares III has inherited the aircraft the Project Ares II produced. As such, the Vehicle Group for Project Ares III was concerned mainly with preparing the airplane for flight. The majority of effort was directed toward repairing the fuselage, wing and tail. Other important tasks of the Vehicle Group were maintaining the weight and balance of the aircraft for stability, ensuring fail-safe considerations in the event of loss of radio contact, and coordinating with Propulsion and Controls & Instrumentation Groups for the installation of their various subsystems.

Although generalized discussions of the construction of the aircraft will be made, the reader should be familiar with the final report of Project Ares II. No attempt is made here to cover in detail the design considerations that went into fabrication of the aircraft. However, important aspects of the aircraft design will be reiterated whenever necessary, such as in discussion of stability and control.

### **Repairs-General**

The aircraft has sustained some damage during the test flight that Project Ares II performed, as well as ground handling by both Ares II and Ares III teams. Additionally, installation of sensor packages in the wing and tail required stripping the mylar covering off the aircraft and recovering it.

### **Fuselage Repairs**

In the case of the fuselage, the largest consideration was that the two halves were joined properly. There were four general types of repairs made on the fuselage: re-gluing the two halves together; patching areas where the

halves did not meet; repairing areas where there was a length mismatch between the halves; and repairing one area of the tail that was cracked. Additionally, the paint and excess glue were removed from the fuselage in an effort to reduce weight.

### **Wing Repairs**

The two innermost ribs, adjacent to the fuselage, were broken on the wing during assembly of the airplane. Replacement ribs have been fabricated and epoxied to the wing. These ribs have been laminated to the outside of the existing ribs to provide clearance between the wing and the fuselage. There were also some ribs that had fractured where lightning holes had been made. Graphite/Nomex sandwich doubles were epoxied to the broken areas. Additionally, the wing mylar was removed and re-applied in certain areas. This was necessary due to rips in the mylar and some areas that the Controls & Instrumentation Group needed to access to install various sensors inside the wing. The last step was to re-tension the mylar from last year that had not been replaced.

### **Tail Repairs**

The tail mylar was replaced, again due to tears and to provide access to the tail for sensor mounting. This required removal of the elevator and the rudder and re-hinging of the surfaces. The hinges were full-length, made with wide mylar tape.

### **Stability**

The neutral point of the airplane was calculated using the airfoil and fuselage data provided by the Project Ares II. The neutral point was determined to be 80 inches from the back of the spinner. This placed the neutral point at approximately 50% of chord. For 15% static margin, the required center of gravity was at 74 inches from the back of the spinner. The center of gravity was found by:

$$(X_{np} - X_{cg}) / C = \% \text{stability}$$

where  $X_{np}$  and  $X_{cg}$  are the distances from the datum (the back of the spinner) to the neutral point and center of gravity, respectively, and  $C$  is the mean aerodynamic chord of the wing. Weighing of the aircraft was delayed until just prior to the test flight.

### **Safety Considerations**

A self-destruct mechanism is required for termination of the flight in case control of the aircraft is lost. This is accomplished by separating the wing from the fuselage at the wing attach point. The wing is held in place by two plates epoxied on the wing box. These plates fit between two plates in the fuselage that are held secure by two pins. The plates on the wing were cut in half, and two tubes were epoxied and riveted on both halves of each plate. Smaller tubes were epoxied inside the tubes on the upper plates to maintain alignment of the wing, and the two halves are held together by a connecting rod. In the event of loss of uplink signal, a 15-minute countdown timer would be started. At the end of 15 minutes explosive line-cutters would be activated, severing the rods, and allowing the wing to separate from the fuselage.

### **Test Flight**

After all systems were installed, the wing and fuselage/tail assembly were weighed. The wing weighed 20.5 pounds and the fuselage and tail assembly weighed 50 pounds. This includes the weight of the landing gear (approximately 12 pounds) that will not be used on the high altitude flight. Once the aircraft was weighed and assembled for the test flight, a fairing was made between the wing and fuselage to reduce the interference drag. Then the aircraft was balanced, and the center of gravity was found to be too far aft. The aircraft was ballasted with weights to reach the proper center of gravity location.

### **Propulsion**

The propulsion system was developed with the goal of providing the required thrust for level flight during which the data collection would take place. The propulsion system was divided into four separate tasks: power source, motor, geartrain, and propeller.

The plane was originally designed to incorporate solar cells as its power source for the propulsion system for both the Earth prototype and the actual future Mars explorer. However, the solar arrays that met power and weight criteria for this aircraft far exceeded our budget. This introduced a new twist into the scope of the propulsion system: 100% battery powered flight. The

two main criteria for battery selection were energy density, weight, discharge rate, and costs. The batteries selected were to provide power to sustain the aircraft in level flight for a duration of two minutes. The batteries considered were: carbon-zinc, zinc-mercury, lithium, alkaline, and nickel-cadium.

Our final selection was the NiCd batteries. Their weight is 1.7 oz per cell, which was heavier than some of the others considered, but they provided the maximum current discharge of 30 amps. This far exceeded any of its competitors. Forty-eight cells would be required for the motor selected by last year's group at a total weight of nearly 5 pounds.

The motor selected by last years group is a four-brush DC motor built by Astroflight Inc. Performance tests yielded an output torque of 0.6 ft-lbs at approximately 12,000 rpm. The motor required 50 volts and 30 amps which are provided by our battery selection. Motor selection was based on power available, weight and size of the unit, type of motor, and costs. An initial range for horsepower requirements was made based on historical data ranging from fractional to 10 hp motor and backed up by the initial estimates of power required.

The geartrain was necessary because it was determined that the propeller being designed would operate much more efficiently at a lower rpm than the motor provided. The design considerations for the geartrain were light weight, maximum efficiency, and reliability. The expected life cycle was to be under 200,000 revolutions. A prominent concern dealt with the effects of the low operating temperature of approximately -70° Fahrenheit. The materials selected were required to maintain their strength and possible ductility for the duration of the flight.

The transmission methods considered were toothed Delrin gears, a chain and sprocket system, and toothed belt and pulley arrangement. The toothed belt and pulley arrangement were chosen because the others were much more sensitive to misalignments, displayed a higher weight, and operated at a lower efficiency. To ensure that the belts would not fracture due to the low temperatures, low temperature rubber belts reinforced with Kevlar strands were purchased. These belts maintained their ductility and strength even at these low temperatures. Self-aligning "swivel" bearings were designed and

fabricated to combat the potential problem of shaft misalignment. The shafts used were hollow, anodized, 2024 aluminum.

The propeller provided the greatest challenge for the propulsion group. The propeller would have to be light in weight, possess high strength, as well as provide thrust in a low Reynolds number environment. Blade element theory was used to obtain the following calculated values that would meet the thrust requirements:

Radius: 3.9 feet  
average chord: 0.45 feet  
rotation angle @ hub: 85 degrees  
rotation angle @ tip: 28 degrees  
aspect ratio: 9

Construction was begun with the fabrication of a single blade plug that was used to construct a mold from which the actual propeller could be formed using composite material and foam.

### Avionics

The role of the Avionics group was to design, test, and fabricate the flight control system, data acquisition sensors, and data recording subsystems for the Ares III Project aircraft.

In the design of the Flight Control System, two modes of controlling the aircraft were chosen. One is manual control via a modified radio-control model aircraft hardware.

This system is a Futaba 1024 Pulse Code Modulator which allows control of both elevator and rudder deflection as well as motor control. The Futaba output signal is only 1 watt and 50 MHz and must be amplified to reach the aircraft at high altitudes. This is accomplished by a 10 gain RF amplifier which boosts the control signal to a maximum allowable by the FCC of 1 watt. The signal is then transmitted through a high gain, multi-element, directional Yagi antenna to the aircraft. The control signal is received via a unidirectional trailing antenna and delivered to a receiver. The receiver directs control of the control surfaces' servos and motor. In the event that the control signal is lost, the second mode of control, the autopilot, would assume control. The autopilot, manufactured by BTA Systems Inc., would lock the

control surfaces into a predetermined position causing the aircraft to slowly spiral to ground level. The autopilot will unlock control in the event that the control is regained. The aircraft will also carry a miniature radio transponder to aid in tracking with radar.

## FLIGHT CONTROL SYSTEM

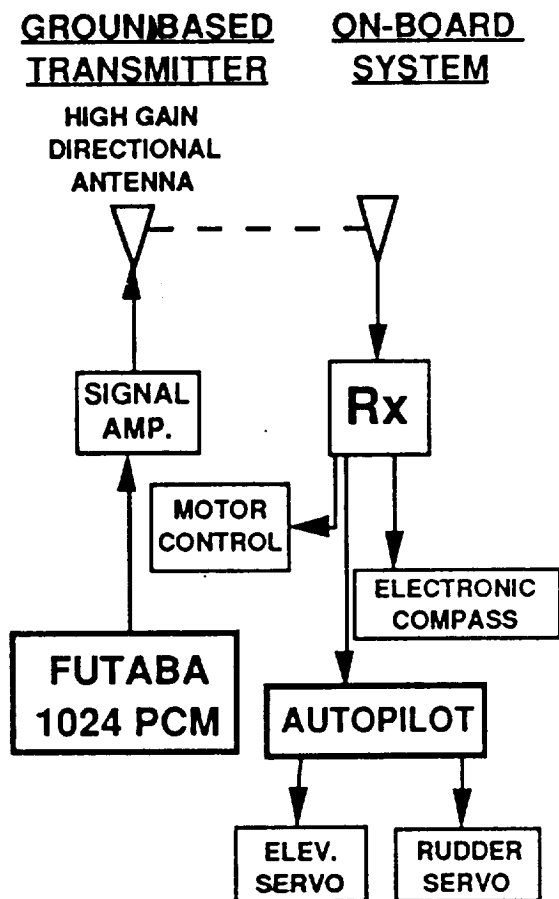


Fig. 1 Flight control system

The ultimate goal of our high altitude testing program will be to collect data to evaluate the performance of our design. This includes both vehicle flight performance as well as performance of various aircraft subsystems. For the evaluation of the vehicle flight characteristics, measurements of airspeed, altitude, inside air temperature, and outside air temperature will be taken. For the propulsion system, sensors will measure motor power, propeller thrust, and motor RPM. Additionally,

differential pressure ports located in the wing will record pressure distribution along the chord-wise location on the wing. This data will be used to provide essential data to validate computational fluid dynamic modeling for low Reynolds number flights.

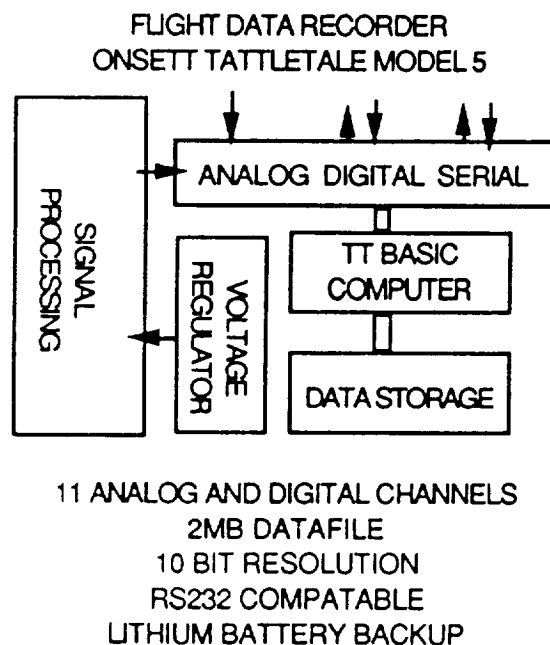


Fig. 2 Flight data recorder

This information will be stored for later retrieval by the Flight Data Recorder. The Flight Data Recorder (FDR), manufactured by Onset, Inc., uses the latest in large scale integration (LSI) and surface mount chip technology to pack essentially a complete microcomputer onto a board a few inches square. The FDR will also provide sensor signal conditioning and supply regulated reference voltages. Also, as a fail-safe in the event of flight failure, a telemetry or "downlink" was installed for data acquisition. The telemetry operation is essentially the same as the Flight Control system except that the signal is encoded in a serial format for eight analog and digital data channels. While providing a back-up system for data acquisition, the telemetry also is beneficial in that it allows for real-time data acquisition.

Because of the extreme temperatures encountered at flight altitude, the instrumentation package will be installed in an insulated, temperature-controlled avionics

bay. The flight data recorder will be able to monitor and regulate the payload bay temperature with the aid of a small film resistance heater to a temperature above 0 degrees Celsius.

Power for the onboard avionics will be provided by NiCd batteries. A battery system consisting of 24 cells delivering 28 volts at 1200 mah will supply all avionics. The FDR will be independently powered with an additional battery backup in the event of main power loss. The complete controls and avionics package will have an installed weight of less than six pounds.

### **Test Flight**

The Test Flight group dealt with two main areas of flight testing of the Ares aircraft: low level testing and high altitude test flights. Low level test flights have been carried out with the aircraft. The high altitude flight has been planned and found feasible, but due to complexity and cost, it has not been carried out.

#### **Low Altitude Flight Testing**

Low altitude flight testing has been carried out at El Mirage dry lake bed in California. The aircraft was towed by car to an altitude of several hundred feet. The cable was then released and the aircraft glided to a safe landing. Flight control was achieved with the use of the regular radio control Futaba unit. The pilot controlled the aircraft from a car while being driven behind and below the aircraft. Test flights were performed in the summer of 1991 and 1992. The 1991 summer flight was carried out with no avionics and proved the plane was stable and air worthy. The 1992 flight was carried out with full avionics to test system integration.

#### **High Altitude Flight Testing**

In order to test the Ares aircraft in a Martian-like environment, the aircraft would have needed to be towed to an altitude of 104,000 feet. At that altitude, the air density closely resembles the Martian atmosphere. The only safe way to deliver the aircraft to high altitude is via a helium balloon system. The plane would be hung from the balloon with a special release mechanism and launched nose down upon reaching altitude. After a short level test flight with full system information being

recorded, the aircraft would glide to a landing site under control from the ground station. The pilot can glide the plane to the landing site with the aid of radar until eye contact is established.

The helium balloon system needed to deliver the aircraft to altitude was found to be very complex and costly. It was decided that the group would use the services of professionals since building and testing a balloon system of this type is a several year project in itself. Two organizations have been contacted, the National Scientific Balloon Facility in Palestine, Texas, and the Department of Atmospheric Science at the University of Wyoming. Both organizations have been involved in the project and, depending on the location and date of the flight, one would be chosen to perform the balloon ride to 110,000 feet and launch the aircraft.

Finding a test area for the high altitude test flight has also been a major task. After much discussion, the Federal Aviation Administration has refused to allow a flight in unrestricted, uninhabited airspace mainly due to the concern that the aircraft could wander into occupied airspace or crash in an inhabited area. Due to that restriction, the test flight has to be carried out within a restricted area big enough and high enough for the entire flight to be conducted inside the area. Several of these areas exist in the United States; most of them are controlled by various branches of the military. These areas were investigated, and it was determined that the cost of the radar facilities is substantial. Also, the safety review and damage assessment process required is complex and time consuming. At this time, negotiations are underway with Edwards Air Force Base in California and Hill Air Force Base in Utah to try to find ways to incorporate the cost of the test range services within the limited budget available to Project Ares III.

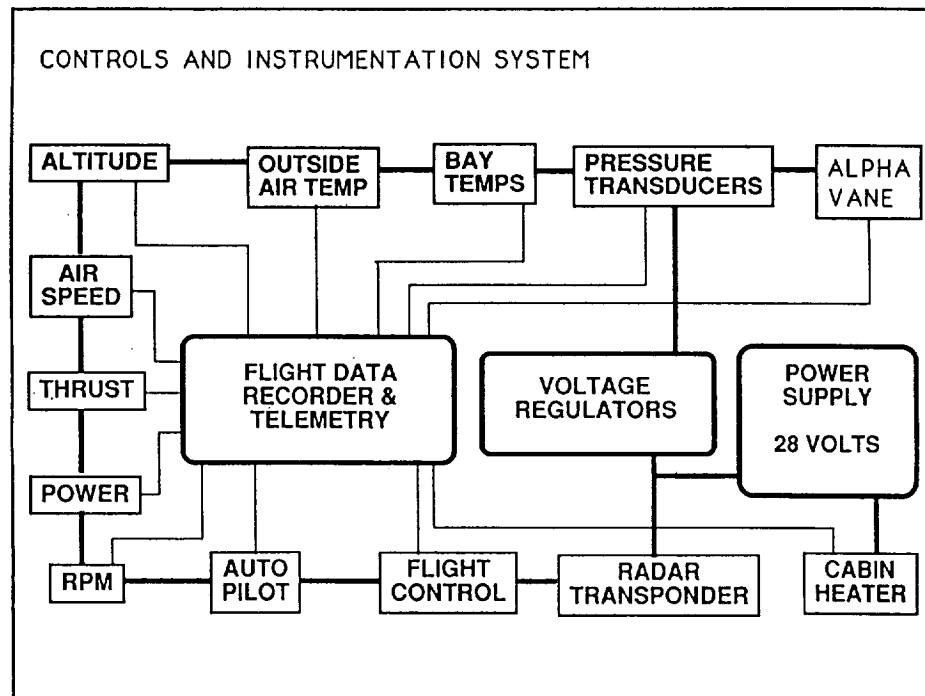


Fig. 3 Controls and instrumentation system

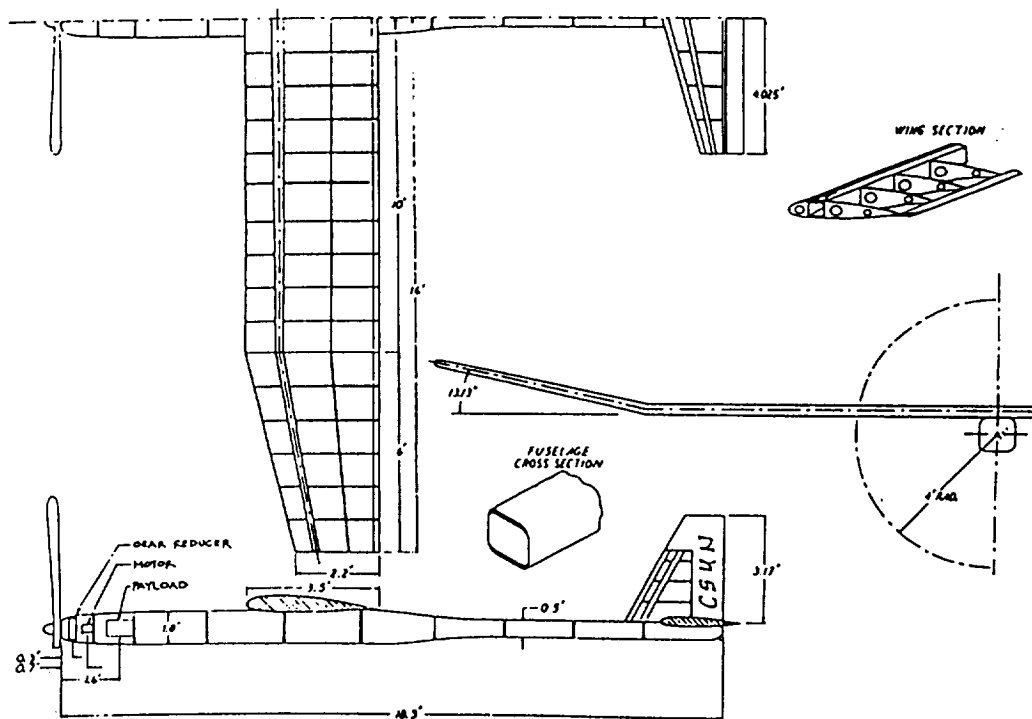


Fig. 4 Side view of Project Ares III



**TESSERACT SUPERSONIC BUSINESS TRANSPORT**

**Case Western Reserve University  
Mechanical and Aerospace Engineering  
Cleveland, Ohio**

**Professor Eli Reshotko  
Gary Garbinski, Teaching Assistant**

**James Fellenstein, Team Manager; Mary Botting; Joan Hooper; Michael Ryan; Peter Struk;  
Ben Taggart; Maggie Taillon; Gary Warzynski**

**Abstract**

This year, the senior level Aerospace Design class at Case Western Reserve University developed a conceptual design of a supersonic business transport. Due to the growing trade between Asia and the United States, a transpacific range has been chosen for the aircraft. A Mach number of 2.2 was chosen, too, because it provides reasonable block times and allows the use of a large range of materials without a need for active cooling. A payload of 2,500 lbs. has been assumed corresponding to a complement of nine passengers and crew, plus some light cargo. With these general requirements set, the class was broken down into three groups. The aerodynamics of the aircraft were the responsibility of the first group. The second developed the propulsion system. The efforts of both the aerodynamics and propulsion groups were monitored and reviewed for weight considerations and structural feasibility by the third group. Integration of the design required considerable interaction between the groups in the final stages. The fuselage length of the final conceptual design was 107.0 ft, while the diameter of the fuselage was 7.6 ft. The delta wing design consisted of an aspect ratio of 1.9 with a wing span of 47.75 ft and mid-chord length of 61.0 ft. A SNECMA MCV 99 variable-cycle engine design was chosen for this aircraft.

**Introduction**

The Aerospace Design class was given the task of developing a conceptual design of a supersonic business transport. The initial specifications for the design were developed by the class and are listed in Table 1.

Table 1 Design Specifications

| Range                     | Transpacific |
|---------------------------|--------------|
| Mach Number               | 2.2          |
| Passenger & Crew Capacity | 9            |
| Total Payload             | 2,500 lbs    |

With these guidelines, the class was broken down into three groups. Each of the three groups was placed in charge of one of the following design areas:

- aerodynamics,
- propulsion, and
- structures.

The iterative process of aircraft design began with an initial sizing of the aircraft. For the specifications listed above, a takeoff gross weight of 107,000 lbs. was estimated. Also, a fuselage length of 107.0 ft and a diameter of 7.6 ft were determined in the initial study. After the initial sizing was completed, each of the three groups began a detailed analysis of their respective design areas. During the design process, constant communication between the groups was required to keep the project on line. Included in this report is an overview of all the work completed by May 14, 1992, by each of the three groups.

**Analysis****Aerodynamics**

During the initial conceptual sizing of the proposed supersonic business jet, similar designs indicated that the jet would have approximately a maximum lift to drag ratio (L/D max) of 8. Historical trends indicated that the most

efficient cruise for jet aircraft occurs at velocities higher than those that would generate a maximum lift to drag ratio. This higher velocity is at a L/D of 86.6% of maximum.<sup>1</sup> In our case, cruise L/D would be roughly 7.

A design cruise lift coefficient ( $CL_{cruise}$ ) was now determined from initial mission requirements and basic flight mechanics. For an aircraft with a takeoff gross weight (TOGW) of 107,000 lbs. and a cruising Mach number (M) of 2.2, a reasonable  $CL_{cruise}$  needed to be selected. A target range for the cruising CL from 0.12 to 0.13 was selected based on similar designs. After some iteration, a design lift coefficient of 0.128 was determined. This cruising CL was designed for a wing reference area of roughly 1200 square feet and an initial cruising altitude of 55,000 feet.

Maintaining a constant lift coefficient during the cruising portion of the mission while accounting for a constantly changing weight (fuel consumption) can be accomplished by increasing the altitude of the aircraft periodically as the fuel supply is diminished. Alternately, velocity can be altered (reduced) to accomplish the same effect, but obviously this method is not practical.

Table 2 Altitude vs Fuel and  $CL_{Cruise}$

| $CL_{Cruise}$ | Fuel Remaining (%)<br>(weight) | Altitude<br>(ft) |
|---------------|--------------------------------|------------------|
| 0.128         | 88                             | 55,000           |
| 0.128         | 53                             | 60,000           |
| 0.128         | 25                             | 65,000           |

From the above analysis, a change in cruising altitude of roughly 10,000 feet would be required to maintain a constant lift coefficient. Such a flight profile (Figure 1) might have restrictions due to flight regulations of maintaining constant altitude during all or portions of the mission.

Although, at present, such altitudes are not as populated as some lower flight levels, such considerations must be mentioned in the early design stage. Implications of this may result in the aircraft not flying at its design lift coefficient during the entire cruise.

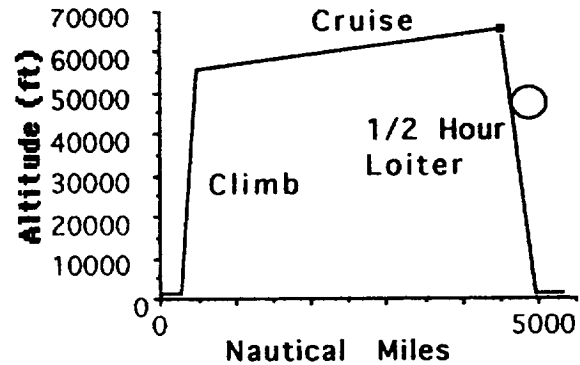


Fig. 1 Tesseract's Mission Profile

Before the analysis could proceed any further, a wing planform needed to be selected. Several wing planform designs with subsonic or supersonic leading edges were investigated. Forward swept and eccentric wings were considered (primarily for novelty), but were unfortunately discarded due to a lack of literature and supporting data available. A delta configuration with subsonic leading edges was chosen primarily because theories for wing performance of deltas existed and were readily available.

A subsonic leading edge was desired to minimize the supersonic wave drag. To guarantee this, the leading edge sweep back angle must lie within the Mach cone. Based upon a free stream cruise Mach number of 2.2 and a normal to the leading edge Mach number of 0.8, the sweep back angle was calculated to be  $68.7^\circ$ . This lies within the Mach cone of  $63.0^\circ$ .

Based on the previous discussion, and to minimize induced drag (to be discussed hereafter), an aspect ratio of 1.9 was desired. Based on the pure delta configuration, an aspect ratio of 1.56 was calculated. This aspect ratio needed to be increased without changing the reference area of the wing. The main motivation for this was to minimize the induced drag, which is inversely proportional to the aspect ratio. To accomplish this a triangular section was removed from the trailing edge of the wing.

There are theories available to predict the performance of delta wings. One such theory developed by Brown<sup>3</sup> for the lift curve slope (a) is as follows:

$$a = 2 \Pi^2 \tan e / (\Pi + \lambda b d a)$$

Lambda is a function of the ratio of one-half the apex angle tangent ( $\tan \epsilon$ ) to that of the tangent of the Mach angle. For the particular configuration shown, lambda is equal to 1.25, which, in turn, gives a lift curve slope of 1.76.

Airfoil selection is difficult due to the unavailability of recent airfoil developments. An airfoil must be selected to meet the above mentioned parameters. Based on historical trends for this type of aircraft, a thickness ratio ( $t/c$ ) between 0.07 and 0.09 is predicted. This range excludes the use of present day supercritical airfoils, because they tend towards higher thickness ratios (roughly 0.15).

The next step in aerodynamic considerations was the calculation of the total drag on the aircraft during cruise. To determine the parasite drag coefficient, the component buildup method as prescribed in Raymer<sup>1</sup> was followed. This method considered each portion of the aircraft separately. The value of the overall coefficient was then found by summing the drag of the individual components. Each component's skin friction drag was determined using flat plate approximations. These values for Mach 2.2 are summarized in Table 3.

Table 3 Drag Summary during Cruise

| Parasite Drag Coefficient |       |
|---------------------------|-------|
| Skin friction drag        | .0051 |
| Wave drag                 | .0068 |
| Miscellaneous             | .0005 |
| Total $C_{D,0}$           | .0124 |
| Induced Drag              |       |
| Induced drag $C_{D,i}$    | .0058 |
| Total Drag Coefficient    |       |
| Parasite drag             | .0124 |
| Induced drag              | .0058 |
| Total $C_D$               | .0182 |

In lieu of the effects of lights, antennae, and other manufacturing defects, along with other unaccountable factors, an exact coefficient cannot be determined. A correction factor of 10 percent can be added to the skin friction drag of the aircraft as prescribed by Raymer.<sup>1</sup>

The wave drag of the aircraft was determined using an approximation method described in Raymer.<sup>1</sup> This method is valid only for a cross-sectional area distribution of the aircraft similar to a Sears-Haack distribution (Figure 2).

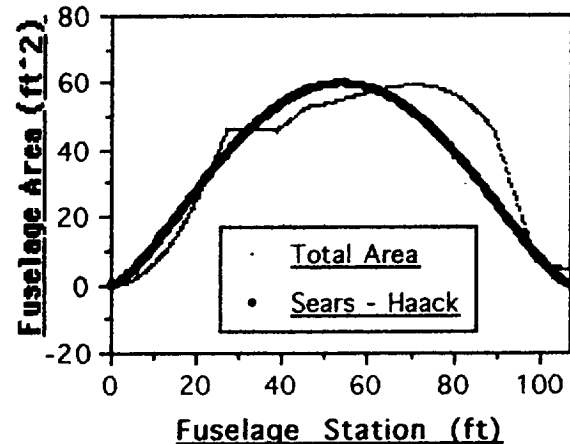


Fig. 2 Area Distribution

Aimed at minimizing wave drag, the aircraft was designed as close as possible to this ideal distribution. For the aircraft, the wave drag coefficient corrected for Mach number and non-ideal area distribution is 0.0068. The values for the induced drag at supersonic speeds were calculated using a theory developed by Brown<sup>3</sup> similar to that used for determining the lift curve slope. This method produces an induced drag value of 0.0058 for the aircraft.

Drag calculations for the subsonic and transonic regimes were calculated for various altitudes using software developed by Kern<sup>4</sup> International entitled *Basic Aircraft Performance Analysis*. This program calculated parasite drag for Mach numbers ranging from 0.0 to 1.0. These values were predicted by simply smoothing the curve generated from the data above. While this may seem a crude approximation, such a technique will suffice for the preliminary design.

Longitudinal static stability of most conventional aircraft requires the use of a horizontal stabilizer or simply a horizontal tail. For an aircraft with a delta wing configuration, an actual horizontal tail separate from the wing is not always present. Rather, the horizontal tail surface is part of the delta wing configuration.

Several difficulties, however, arise from not employing a horizontal tail separate from the wing. To maintain longitudinal static stability, the tail of the aircraft may need to produce a force in the direction of gravity to balance the moments of the aircraft about the center of gravity. This will require a portion of the wing to generate negative lift. This then requires the portion of the wing generating positive lift to balance the negative lift, as well as to support the weight of the aircraft to maintain level flight.

Analysis of the static stability for the aircraft showed that a horizontal stabilizer was essentially unnecessary for the cruising speed of Mach 2.2. However, for flight at speeds lower than our cruising speed, the aircraft becomes inherently unstable. This is primarily due to the large shift in the aerodynamic center of the aircraft. The analysis for low speed static stability needs to be evaluated, and an appropriate control system needs to be incorporated. For the present, a tail has been added to the design in anticipation of its use in maintaining low speed static stability.

For this design, the pertinent stability figures are listed in Table 4.

Table 4 Stability Analysis

|  |                      |
|--|----------------------|
| Location of the center of gravity as a fraction of root chord (Empty Weight) | 0.70                 |
| Location of the aerodynamic center as a fraction of root chord at M=2.2      | 0.77                 |
| Moment coefficient of the wing body about the aerodynamic center at M=2.2    | 0.00                 |
| Tail Area  | 50 ft <sup>2</sup>   |
| Distance of tail aerodynamic center to the center of gravity                 | 30 ft                |
| Wing Reference Area  | 1200 ft <sup>2</sup> |
| Mean aerodynamic chord of the delta wing                                     | 33.6 ft              |
| Tail Volume Coefficient  | .037                 |
| Static Margin at M=2.2   | .09                  |

The aerodynamic center of the delta wing was determined using a graphical method prescribed in Raymer.<sup>1</sup> This method allows us to determine the

location of the aerodynamic center of the wing as a fraction of the root chord.

To maintain longitudinal static stability, the aircraft's center of gravity throughout the flight must remain in front of the neutral point. This distance as a fraction of the chord is known as the static margin and should not go less than 5 percent during any portion of flight. If the static margin falls below 5 percent, the forces required to maintain balance may become too large. However, if the static margin exceeds 15 percent the aircraft becomes "sluggish." This essentially means that the restoring forces resulting from changes in angle of attack are small, resulting in slow response time.

### Propulsion

The propulsion system consists of two variable cycle engines mounted under the wings toward the rear of the aircraft. The system is designed for a flight cruise speed of Mach 2.2. The fuel-to-air ratio for this system was assumed to be 1/35. The thrust required at Mach 2.2 is 7180 lbf. The mass flow rate of air at cruise is 79.45 lbm/s. The fuel mass flow rate at cruise is 2.27 lbm/s. The propulsion system is designed to handle the one-engine-out FAA requirement.

The propulsion system was divided into three sections: the inlet, the turbomachinery, and the exhaust. Both inlet and exhaust air flows were modeled as adiabatic and compressible. A two-dimensional square inlet controls the velocity and pressure of the air into the engine core. Engine mounting is less complex for a rectangular inlet than for a circular one. The different mass flows associated with the range of flying conditions are accommodated by the use of a variable area ramp. A circular exhaust nozzle controls the velocity leaving the engine. The exhaust nozzle, like the inlet ramp, is variable to allow for the necessary exit velocities required at various flying conditions. Two convergent nozzles are employed when flying at subsonic speeds. Supersonic speeds require the use of a convergent-divergent nozzle.

A SNECMA MCV 99 variable-cycle engine design was chosen for this aircraft. This variable-cycle engine has four operating modes: take-off, climb, subsonic cruise, and supersonic cruise. The climb operating mode is also used for transonic acceleration. This cycle's use of

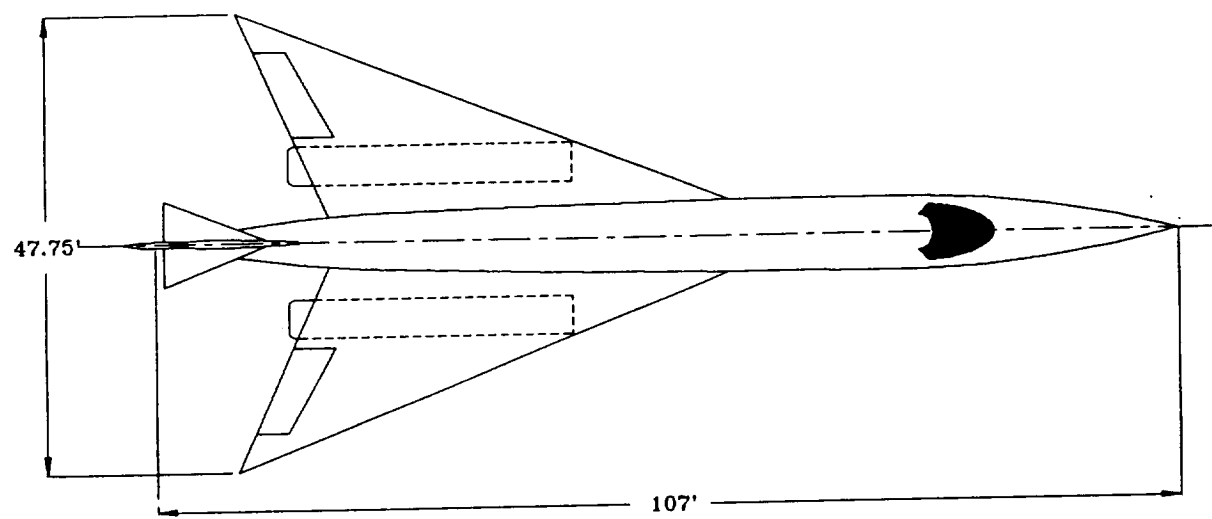


Fig. 3 Top view of Tesseract

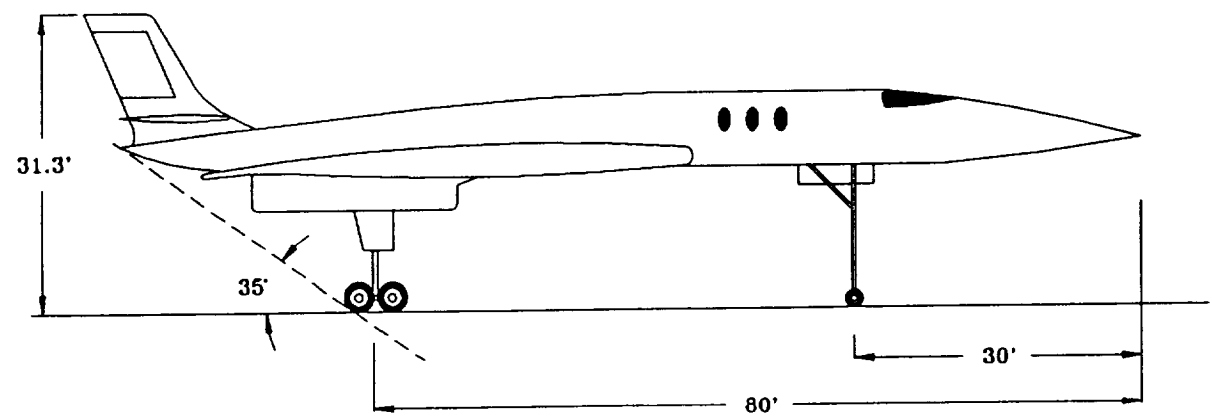


Fig. 4 Side view of Tesseract

premixing before combustion, staged burning, rich burn/quick quench/lean burn combustor, and a variable area geometry reduces pollutant emissions into the atmosphere by 50 percent when compared to other current cycle emissions.<sup>6</sup>

### Inlet Design

The purpose of the inlet is to bring free stream air to the required velocity of Mach 0.5 at the entrance to the compressor with a minimum total pressure loss. Since the aircraft will spend the majority of its flying time at cruise conditions of Mach 2.2 and an altitude of 55,000 feet, the inlet was designed for these conditions. A variable ramp will accommodate the adjustments needed for the other stages of flight. A square inlet with a width of 3.66 feet and a capture area of 13.4 square feet was designed. Two oblique shocks and a normal shock slow the free stream air flow to Mach 0.5 at the compressor entrance. As suggested by Connors and Meyers,<sup>5</sup> the ramp deflection angles are 9.9 and 10 degrees, respectively.

To achieve a minimum total pressure loss at supersonic flight conditions, internal contraction was used to swallow the normal shock. The pressure recovery with internal contraction, allowing for some losses, is 0.91. The concept behind using internal contraction as opposed to other types of supersonic inlets is the variation in pressure recovery. By increasing the throat area, the normal shock is swallowed further back allowing a higher percentage of pressure recovery. The design method for internal contraction began with the evaluation of pressure, area, and temperature ratios of the two oblique shocks and the normal shock. The second step involves swallowing the shock by increasing the area of the throat. This is referred to as internal contraction. Area ratios with respect to throat area for isentropic flow were found for the Mach number before the normal shock ( $M_x$ ) and for the Mach number after the normal shock ( $M_y$ ). These area ratios were then divided to determine the internal contraction area ratio. The area ratio at Mach 0.5 at the face of the compressor and the isentropic area ratio for  $M_y$  were used to calculate the ratio of the compressor face area to the throat area.

The boundary layer is susceptible to separation during supersonic cruise. Separation occurs from the development of a severe pressure gradient. In order to prevent separation, a channel-type boundary layer

diverter system on the ramp removes most of the boundary layer before the shocks. In this removal system, the boundary-layer air is caught between a splitter plate and the fuselage. This caught air is then removed from the channel by diverting ramps angled at approximately 30 degrees.

There are blow-in doors near the fan that only feed into the fan. Therefore, these doors only need to be opened from takeoff to high transonic flight conditions when the fan is in use.

Following the throat, a diffuser with a length of two ft diffuses the flow from approximately Mach 0.72 after the normal shock to Mach 0.5 at the compressor entrance. A variable inlet ramp adjusts for the varying flight conditions from takeoff through transonic and to cruise at Mach 2.2. For takeoff conditions the ramp is retracted to lead the air directly to the compressor inlet without a contraction. This position allows greater airflow into the engine to achieve the necessary greater thrust level.

Inlet drag is approximated from the inlet drag trends plot for a two-dimensional inlet. This plot was compiled from typical data previously collected.<sup>1</sup> Inlet drag for different modes of flight for this design was estimated high due to the generality of the sources (Table 5). The maximum drag occurs at approximately Mach 1.3.

Table 5 Inlet Drag Estimates

| Mach Number | D/q/A | D (lbs) |
|-------------|-------|---------|
| 2.20        | 0.10  | 911     |
| 1.30        | 0.23  | 1723    |
| 0.95        | 0.18  | 713     |
| 0.10        | 0.02  | 3.8     |

D = Drag q = Dynamic Pressure A = Capture Area

### Exhaust

The exhaust nozzle provides back pressure control for the engine and an acceleration device converting gas potential energy into kinetic energy. The throat area is the controlling factor. Since the pressure loss is less for a circular shape, a circular nozzle was chosen instead of a rectangular shape. The circular nozzle assembly also

weighs less and is less complex compared to a two-dimensional nozzle.<sup>1</sup>

A variable-area exhaust nozzle is utilized to accommodate the varying flight conditions. Two convergent nozzles are utilized during subsonic flight, one for the fan and one for the core. A convergent-divergent nozzle is used during supersonic flight. During supersonic cruise at Mach 2.2, the nozzle increases the velocity of the mass flow from approximately Mach 0.5 to Mach 2.8. Since the ratio of specific heat decreases through the engine cycle, an average of exit areas calculated with different specific heat ratios (1.3-1.4) was used. The calculated exit area was 26.9 square feet with a throat area of 6.8 square feet.

Exhaust nozzle analysis involves the use of two-dimensionless coefficients, the discharge coefficient and the velocity coefficient. The discharge coefficient represents the difference between ideal mass flow and actual mass flow. The velocity coefficient represents the frictional losses in the boundary layer of the nozzle. The angle geometry of the nozzle was determined from these coefficients. The primary half angle is 10 degrees, and the secondary half angle is 15 degrees.

### **Turbomachinery**

Selection of the engine to power the aircraft was constrained by the need to have good fuel efficiency at several flight speeds and altitudes while keeping noise low on takeoff. Single cycle engines (plain turbojets and turbofans) were considered, but found lacking in one or more areas. High exhaust velocity allows turbojets to give

engine-out takeoff for this aircraft required only approximately 20,000 lb of thrust per engine at sea level. This is considerably less than the engine size needed for cruise. The MCV 99 engine has a thrust of 49,455 lb, and was scaled down for use in this design using a modified "rubber engine" process presented by Raymer.<sup>1</sup> The resulting engine dimensions are in Table 6.

good supersonic performance, but they are too noisy for civilian use. Turbofans have a lower exhaust velocity and are, therefore, quieter, but their supersonic performance is poor. As a result, a dual-cycle engine that combines the advantages of both turbojet and turbofan was chosen. The design is basically a scaled-down SNECMA MCV99 dual-cycle engine. At cruise, this gas turbine acts like a normal turbojet, but at lower speeds a fan mounted around the narrow core section is started to give greater efficiency by reducing the exhaust velocity (and, therefore, noise as well). This concentrically mounted fan is driven by its own combustor and turbine-fed by bleed air from the core engine. Cruise efficiency is improved over a turbofan engine because the low-velocity fan, which does not give much thrust at supersonic speeds, is shut down when it is not needed. This engine is also fuel-efficient because it does not require an afterburner in any part of its operational envelope.

Originally three engines were to be used for safety in case of engine failure. However, it was decided to use two engines to reduce weight and to eliminate some of the problems involved in mounting an engine to the centerline of the aircraft, such as boundary layer removal, foreign object damage, and accessibility.

Selection of engine thrust was constrained by the cruise condition. At 55,000 ft in level flight each engine had to deliver 7,180 lb of thrust. A sea level static thrust of 25,000 lb was then fixed representing an 8.1% improvement over a sample engine's altitude performance.<sup>1</sup> Analysis of Federal Airworthiness Regulations found that the most demanding part of a one-

Table 6 Engine Dimensions

|                     |         |
|---------------------|---------|
| Length              | 12 ft   |
| Compressor Diameter | 3.41 ft |
| Fan Shroud Diameter | 4.13 ft |
| Fan Hub Diameter    | 2.21 ft |

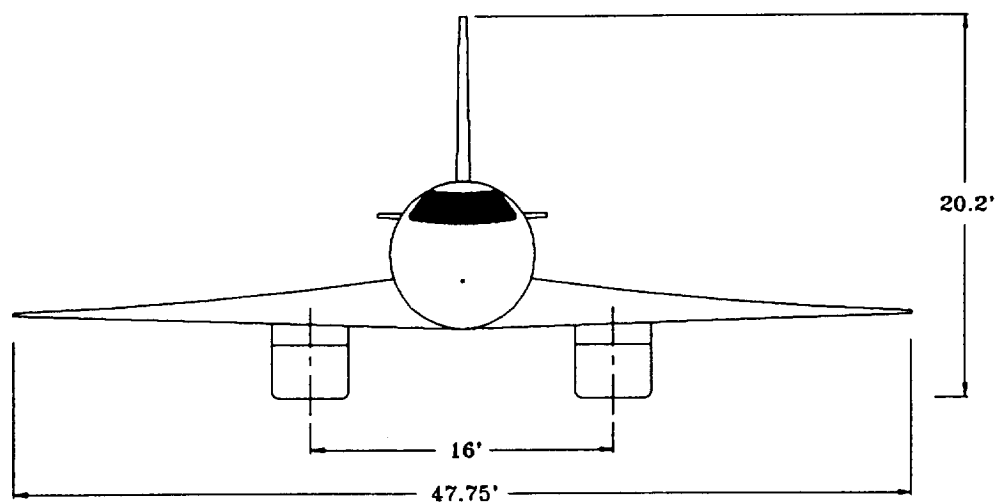


Fig. 5 Front view of Tesseract

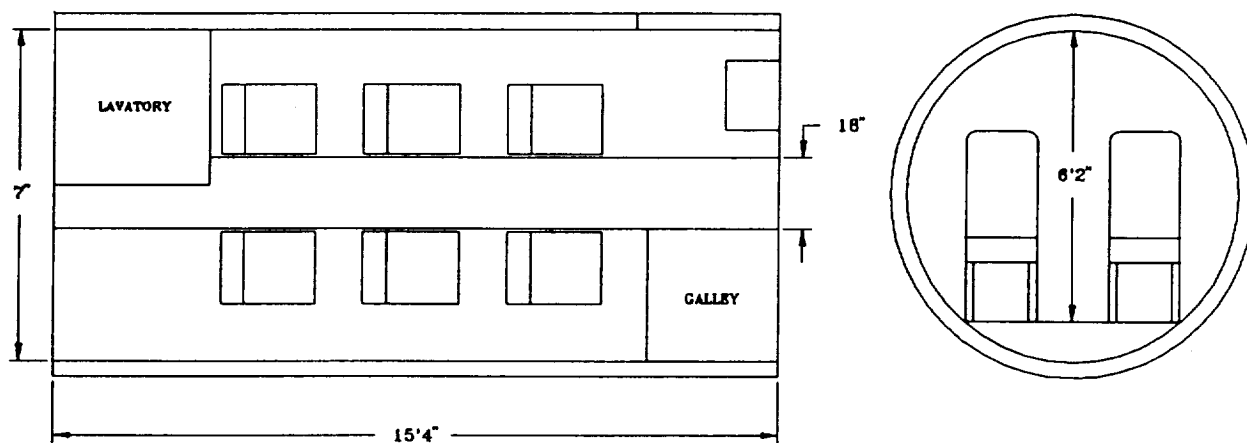


Fig. 6 Cabin layout



Table 7 SNECMA Engine Characteristics

|                     | Takeoff (sea level) | M=2.2 Cruise | M=1.3 Climb | M=0.95 Cruise |
|---------------------|---------------------|--------------|-------------|---------------|
| SFC (lbf/lbm/hr)    | 0.638               | 1.138        | 1.000       | 0.873         |
| Pressure Ratio      | 19.2                | 17           | 18.8        | 19            |
| Bypass Ratio        | 1.0                 | 0            | 1.04        | 0.994         |
| Fan Pressure Ratio  | 2.5                 | n/a          | 2.46        | 2.48          |
| Bleed Ratio for Fan | 0.45                | 0            | 0.36        | 0.34          |

The hub ratio for the fan was found to be 0.535, greater than the 0.5 minimum given by SNECMA as necessary for the compressor.<sup>6</sup> The weight of the engine was set at 5,000 lb, based on a historical thrust-to-weight ratio of five for recent supersonic engines.<sup>7,8,9</sup> Blow-in doors are needed to provide correct airflow when the fan is operating, and these have been designed as doors that open out 0.65 ft. on either side of the engine nacelle to give an additional 6.41 square feet of capture area for the fan. These doors close and the fan shuts down as high supersonic speeds are reached.

The figures given for this engine by SNECMA are shown in Table 7. It is assumed that these figures can be held constant even for a lower thrust engine.

At cruise condition, a common air/fuel ratio of 35/1 was assumed to give an air mass flowrate of 79.45 lbm/s. The fuel flowrate at the same condition is 2.27 lbm/s, and the exit velocity is 4237 ft/s.

Thermodynamic analysis<sup>10</sup> of the engine gives an ideal Brayton cycle thermal efficiency of 55.49% at cruise. For a maximum constant turbine inlet temperature of 3060 R<sup>6</sup> and assuming an 85% efficient compressor and a 90% efficient turbine, the actual thermal efficiency goes down to 45.9%.

A rich burn/quick quench/lean burn combustor has been chosen as a promising solution<sup>6,11</sup> to avoid creating large amounts of the pollutant nitrogen oxide. NO<sub>x</sub> is produced in the largest amounts when combustion is at stoichiometric ratios. To avoid this, the first stage of the combustor is run at over-stoichiometric levels of fuel. This rich mixture is then mixed with air quickly, and the combustion continued at less than stoichiometric levels. The ratios that cause NO<sub>x</sub> production are then avoided completely during the combustion process.

## Structure

The structural design team was responsible for the following tasks: 1) estimating an initial takeoff gross weight (TOGW) and the initial sizing of the aircraft; 2) the final weight estimation; 3) landing gear; and 4) a finite element analysis of the aircraft.

### Initial TOGW and Sizing

The initial TOGW of the aircraft was determined by a statistical comparison of current aircraft designs based on the following specifications listed in Table 8.

Table 8 Design Specifications

|                           |           |
|---------------------------|-----------|
| Range                     | 5,000 nm  |
| Passengers and crew       | 9         |
| Passenger and crew weight | 1,800 lbs |
| Payload weight            | 700 lbs   |

In the initial study, the effects of varying the range, crew and passenger size, cruise altitude, specific fuel consumption, lift to drag ratio, and the weight equation constants (either jet transport or jet fighter) were examined with respect to the TOGW. The estimated TOGW varied from 103,000 lbs to 117,000 lbs in this study, so a target weight of 107,000 lbs. was set.

Next, the fuselage length was found from the estimated TOGW and a statistical relationship based on current aircraft designs.<sup>1</sup> Using this method, a fuselage length of 107.0 ft was calculated. With the length set, the diameter of the fuselage was determined to be 7 ft 8 in based on a supersonic fineness ratio of 14.<sup>1</sup> The fineness ratio is the ratio between fuselage length and diameter, which

minimizes wave drag. The inner diameter of the fuselage was set to 7 ft after allowing for a 4-in fuselage thickness.

With the initial sizing complete, a cabin layout was generated using the values for economy and high density passenger compartments presented by Raymer.<sup>1</sup> The total passenger cabin length is 15 ft 4 in. A recessed floor was used to allow for a 6-ft-2-in-high aisle 18 in wide. The passenger compartment seats six people; a jump seat is available for the flight attendant. Three seats with a width of 18 inches and a seat pitch of 36 inches were placed on each side of the aisle. The headroom was 5 ft 10 in. The cabin also included a 40 sq in lavatory and a small galley.

### Final Weight Estimation

After the initial analysis from both the aerodynamics and propulsion groups was completed, it was decided that a more accurate weight estimate for the aircraft was required. Five different weight approximation methods<sup>1,12</sup> were tested on the Concorde to determine their accuracy for supersonic aircraft. The Concorde was chosen for the comparison because it has a comparable speed of Mach 2.2, but is almost twice the size of our initial TOGW estimate. In each case, a discrepancy of 10% or more was found between the estimated empty weight and the actual Concorde empty weight. To compensate for the large errors in using any of the methods individually, a combination of the weight estimation equations that best approximated the individual components of the aircraft was calculated. The difference between the estimated empty weight and the actual empty weight using the combined method was 3.7%. Applying this technique to our design and using the 3.7% difference as a correction factor, we estimated the empty weight of Tesseract to be 42,878 lbs. Based on a composite utilization by weight of 55%<sup>12</sup> the final empty weight of the design was estimated at 37,778 lbs. With the weight of each of the individual components of the aircraft known, the empty weight center of gravity was calculated to be 73.1 ft from the nose.

### Landing Gear

The main landing gear is located 80 ft from the nose of the aircraft and is 16 ft off the centerline of the fuselage. It will be positioned on the wing next to the engines. It will fold in towards the fuselage and most likely will need

a pod to house part of the gear that does not fit in the wing. The total length of the main landing gear is 20 ft, preventing the tail of the airplane from dragging on the ground during takeoff. The main gear was designed using an estimate of the forward center of gravity (CG), aft CG, and aerodynamic center. The values used were 76 ft, 80 ft, and 86 ft, respectively, from the nose of the airplane. An oleo shock-strut is used for all the gear. The main landing gear is comprised of two struts with each strut having two sets of tires for a total of eight tires. Diameter of the tires is 37 in; width, 12 in. The maximum static load on each main gear strut was calculated to be 48,600 lbs.

The nose gear is located 30 feet from the nose of the airplane. It is located on the fuselage and will fold forward into the fuselage to allow the gear to free-fall down in case of a failure in the extension system. The nose gear will be slightly longer than the main gear. It will also have an oleo shock-strut and two tires, with a diameter of 22 in and width of 8 in. The maximum static load calculated for the nose gear was 17,500 lbs., which is 18% of the maximum static load for the main gear. This percentage is higher than the suggested 14% or less. The minimum static nose gear load is 9,700 lbs and the maximum braking load is 12,000 lbs. All the landing gear calculations are based on information presented by Raymer<sup>1</sup> and Currey.<sup>14</sup>

### Finite Element Analysis

A finite element analysis was completed on the fuselage and wing using the software "GIFTS."<sup>13</sup> The cabin section, the fuselage wing root section, and the internal wing structure were modeled during the analysis. Aluminum alloy 2014-T6 was used for all of the structural members used in the analysis. Due to the fact that this analysis coincided with the aerodynamic and propulsion studies, the initial numbers used in the finite element analysis do not reflect the most recent changes in the design.

The cabin section was idealized with 96 nodes and 160 elements. The bulkhead and stringers were idealized as hollow square cross-sections that were evenly spaced in a circular configuration. The maximum bending moment the airplane would experience and the shear load were calculated using a maximum load factor of 2.5. The internal cabin pressure was assumed to be small

compared to the force of the bending moment and was therefore ignored.

Stress due to pressure exerted on the cabin was calculated be 8,500 psi. A value of 31,000 psi was obtained for the total stress of the airplane at lift-off based on the maximum moment and shear stresses. Therefore, 40,000 psi should be the total stress that the plane would have to withstand.

The second test section, where the wing attaches to the fuselage, was modeled in a more simplistic manner. It had eight booms in a hexagonal shape with "I" beams as internal support. Furthermore, "I" beams were used to represent the wing. The maximum bending moment and shear forces were also applied to this section.

The finite element analysis of the wing was completed by modeling the spars as "I" beams. The "I" beams varied in size from the largest at the root (2'-0") to the smallest at the outermost rib (0'-6"). The ribs were idealized as 3/16" flat plates that also ranged in height through the structure. Over 150 elements were used for the interior of the wing to improve the accuracy of the results.

The design specifications shown in Table 9 were used in the analysis.

Table 9 Finite Element Design Specifications

|                     |          |
|---------------------|----------|
| Wing Loading        | 100 psf  |
| Aspect Ratio        | 1.7      |
| Wing Span           | 47.31 ft |
| Center Line Chord   | 57.73 ft |
| Maximum Load Factor | 2.5      |

GIFTS showed the maximum deflection for the interior of the wing to be six inches. At the root, the maximum normal stress for the spars ranged from  $1.24 \times 10^6$  psf to  $1.61 \times 10^6$  psf. The wing also showed warping at the outer trailing edge with the distributed  $100 \text{ lb/ft}^2$  load.

The skin of the wing was also examined for our wing configuration, but was not included in the report because the software used would not allow the marriage of the internal structure and the skin to be joined in one complete structure. This inability of the software resulted

in the skin analysis to be inconclusive in the overall design of the wing.

## Conclusion

The initial iteration of the Tesseract Supersonic Business Transport was a success. However, to complete the conceptual design of this aircraft a final iteration of the data is required to mesh the simultaneous work of the three design groups. For example, the initial takeoff gross weight estimates may have been too high. Initially, the weight of the aircraft structure was estimated between 40% to 50% of the takeoff gross weight. During the final weight estimation, based on a composite utilization by weight of 55%, the aircraft structural weight was estimated at 35% of the takeoff gross weight. Furthermore, the specific fuel consumption for the SNECMA MCV 99 variable-cycle engine was lower than the 1.3 lbf/16m/hr expected, resulting in further reduction of the required takeoff gross weight for the aircraft. Also, the aerodynamic analysis for low speed static stability needs to be evaluated and an appropriate control system needs to be employed. Even though the conceptual design of this aircraft was not completed to incorporate the latest changes of each of the design groups, this project has developed the basis for a future supersonic business transport design.

## Acknowledgments

- Professor R. Quinn and the Spring, 1992 EMAE 376 Class
- Mr. Art Glassman of NASA Lewis
- NASA/USRA

This summary report was prepared by James Fellenstein and Peter Struk.

## References

1. Raymer, D.P. Aircraft Design: A Conceptual Approach, American Institute of Aeronautics and Astronautics: Washington, D.C., 1989.
2. McCormick, B.P. Aerodynamics, Aeronautics, & Flight Mechanics, John Wiley & Sons: New York, 1979.

3. Brown, C.E. Theoretical Lift and Drag of Thin Triangular Wings at Supersonic Speeds, NACA Report 839, 1946.
4. Kern International, Basic Aircraft Performance Analysis (Program).
5. Connors and Meyers (NACA Report of Supersonic Flow Charts).
6. Habrard, A. The Variable Cycle Engine-A Solution To the Economical and Environmental Challenge of the Future Supersonic Transport.
7. "International Gas Turbine Engines," Aviation Week and Space Technology, March 18, 1991, pp. 136-138.
8. "Gas Turbine Engines," Aviation Week and Space Technology, March 18, 1991, pp. 133-135.
9. "Multinational Gas Turbine Engines," Aviation Week and Space Technology, March 18, 1991, p. 139.
10. Cengel, Y and Boles, M. Thermodynamics, An Engineering Approach, McGraw-Hill: New York, 1989.
11. Bahr, D.W. "Supersonic/Hypersonic Propulsion Systems Exhaust Emission Characteristics and Abatement Technology."
12. Nicolai, L.M. Fundamentals of Aircraft Design, Mets, Inc.: San Jose, 1984.
13. CASA, Gifts (Program) University of Arizona, 1979.
14. Currey, N.S. Landing Gear Design Handbook, Lockheed-Georgia Company: Marietta, Georgia, 1982.

## A REVOLUTIONARY APPROACH TO COMPOSITE CONSTRUCTION AND FLIGHT MANAGEMENT SYSTEMS FOR SMALL, GENERAL AVIATION AIRPLANES

University of Kansas  
Department of Aerospace Engineering  
Lawrence, Kansas

Professor Jan Roskam  
Ed Wenninger, Teaching Assistant

### Abstract

The design studies for two composite general aviation airplanes are presented. The main consideration for both of the designs was to avoid the typical "metal replacement" philosophy that has hindered the widespread use of composites in general aviation aircraft. The first design is for a low wing aircraft based on the Smith Aircraft Corporation GT-3 Global Trainer. The second aircraft is a composite version of the Cessna 152. The project was conducted as a graduate level design class under the auspices of the KU/NASA/USRA Advanced Design Program in aeronautics. This paper will present the results obtained from the Fall semester of 1991 and the Spring semester of 1992.

### Nomenclature

|      |   |
|------|---|
| CRT  | Cathode Ray Tube                        |
| GPS  | Global Positioning System               |
| HUD  | Heads Up Display                        |
| KU   | University of Kansas                    |
| LCD  | Liquid Crystal Display                  |
| RTM  | Resin Transfer Molding                  |
| USRA | Universities Space Research Association |

### Introduction

For the 1991-1992 academic year, the Advanced Design Program at the University of Kansas concentrated on two main subjects. The first is in the area of composite construction. The second is in the area of improving flight management and control systems.

Most existing composite aircraft structures have been designed by using the "metal-replacement" philosophy.

As a result, many mechanical fasteners are required, which drive up the weight and cost while also introducing delamination problems. Sad examples of the "state-of-the-art" are: Beech Starship I, Boeing-Bell V-22, McDD AV-8B, and the Boeing A-6 re-wing program, all of which outweigh aluminum equivalents.

The project for the Advanced Design Program at the University of Kansas will be to develop methods in which conventional mechanical fasteners (bolts, rivets, screws, etc.) can be eliminated in the construction of all-composite aircraft. These techniques will then be applied to two different aircraft. The two aircraft chosen were the Smith Aircraft Corporation GT-3 Global Trainer and the Cessna 152. These two aircraft were chosen because information was readily available to the design teams, and they represent what can be considered to be typical configurations for low and high wing aircraft. The class produced scaled production drawings and models that show how the manufacturing process will work.

The second area of study was in the area of flight management and flight control systems. This subject was investigated only during the Fall 1991 semester. Most existing general aviation airplanes use mechanical flight controls. The handling qualities of these airplanes are often compromised by the friction and hinge moment feedback associated with such flight controls. In addition, many of these airplanes have undesirable Dutch roll and spiral mode characteristics. This increases pilot workload in conditions of turbulence and poor visibility. To remedy these problems, a de-coupled flight control system was investigated. Such a system has been shown to be very easy to fly. The results of the study included functional diagrams and drawings describing such a system. In addition, a complete list of component weights, geometries, power consumption, and cost data was generated.

Another problem with existing general aviation airplanes is that pilots are required to be familiar with all navigation systems on board as well as with all FAA rules with regard to air traffic control. This has made the current pilot environment extremely user-unfriendly. To relieve these problems, a very user-friendly flight management system was developed. This system should be able to allow a low-time pilot to fly safely in the air traffic control system without the need for extensive training. This type of system was investigated in the 1990 academic year at the University of Kansas, and this study was a continuation of that work.

### Advanced Flight Management/Control Systems

The purpose of this section is to present the main results from the advanced flight management and control study. This study was conducted only during the Fall 1991 semester.

### Advanced Flight Control System

The Advanced Primary Flight Control System (APFCS) is a decoupled flight control system. Decoupled flight controls force the response of the airplane to be a function of only one input variable. This system is very different from conventional flight control systems which often require some combination of two or more pilot inputs to achieve a constant response. For example, to climb at a constant rate requires that the pilot pull back on the stick (or wheel) and add thrust through the throttle. To perform a steady level turn requires that the pilot pull the stick to the side to bank the airplane, pull back on the stick to maintain altitude, and add thrust through the throttle to maintain a constant airspeed. The purpose of the decoupled flight control system is to reduce pilot workload by eliminating the coupling of control inputs necessary to produce steady-state responses from the airplane. The three motion variables that are controlled by the pilot through the APFCS are:

- vertical speed
- airspeed
- heading rate

The APFCS couples the appropriate direct control signals and performs iterations until the response of the airplane matches the signal input given by the pilot. This

system has proven easy to fly and is a promising solution to increasing safety in general aviation.

The system described above requires the use of a fly-by-wire flight control system. Two main considerations of such a system are the actuation method and the computer hardware that are required.

### Actuation Method

For system redundancy and to allow for smaller, less powerful (and presumably less expensive) actuators, multiple servo tabs are used for each control surface. The selected values are as follows:

- Aileron 6
- Elevator 6
- Rudder 4

The forces for each actuator were calculated and an extensive search was made to find a suitable actuator. The Nash DL 1020 linear actuator was chosen. For parts commonality, the same actuator is used for all control surfaces. The installation of the actuator into an aileron is shown in Figure 1. The installation of the actuator is similar for the other control surfaces.<sup>1</sup>

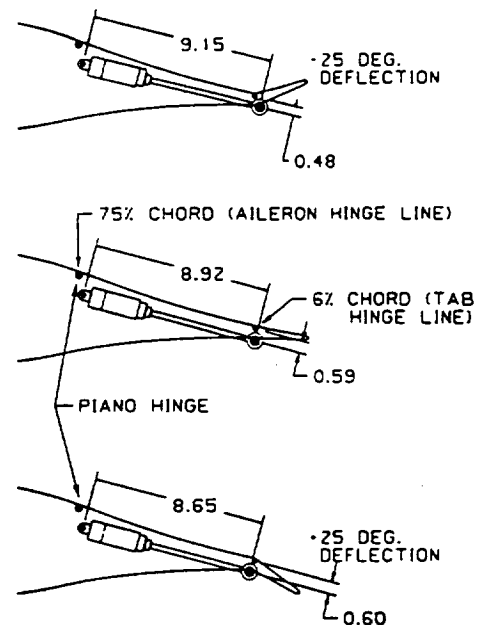


Fig. 1 Installation of aileron actuators

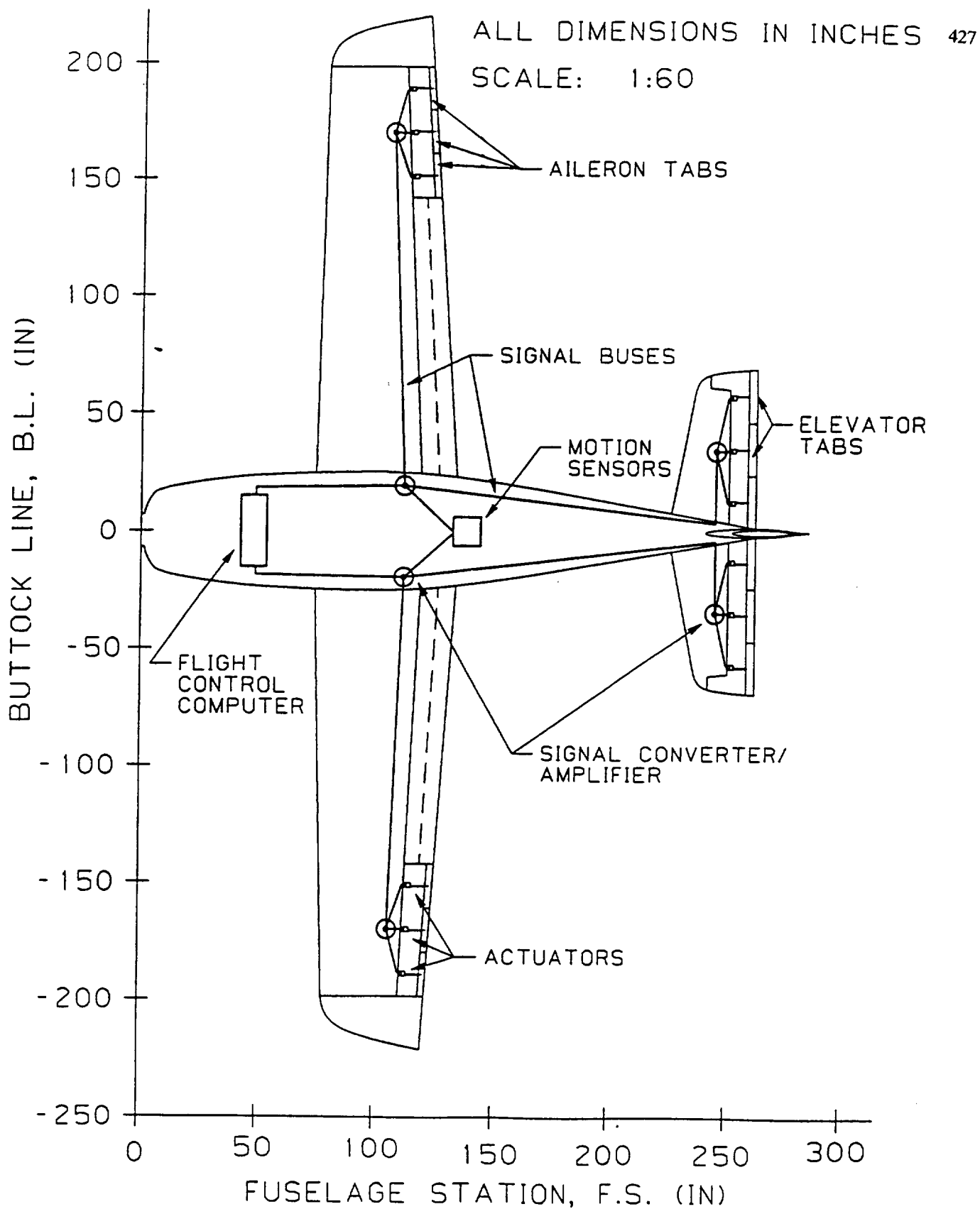


Fig. 2 Flight control system general layout (top view)

The other required equipment and the associated costs are given in Table 1. The installation of these systems is shown in Figure 2.

Table 1 Total system costs for the APFCS

| Component           | Cost (US \$ 1991) |
|---------------------|-------------------|
| Actuators           | \$ 3,200          |
| Rate transducers    | 18,255            |
| Vertical gyroscopes | 15,540            |
| Computers           | 30,000            |
| Batteries           | 316               |
| Total               | \$ 67,311         |

### Advanced Flight Management System

The main objective of the flight management study was to determine the feasibility of a very user-friendly system developed at the University of Kansas during the 1990-91 academic year.<sup>2</sup> The system is designed to allow an inexperienced pilot to fly anywhere in virtually any weather. To do this requires Category II landing minimums. It was determined that GPS with Selective

Availability turned off would give sufficient accuracy for Category II landings.

To effectively inform the pilot, it was decided to use a Heads Up Display (HUD). This will allow the pilot to continually look outside the aircraft instead of having to monitor instruments inside the cockpit. This will give the pilot greater time to see and avoid other aircraft, thus increasing safety. An LCD HUD with a display size of 24 x 6 inches was chosen because it is lighter and requires less power than a conventional CRT HUD.

To insure a safe airplane, designers conducted a failure analysis to determine the minimum number of components required for redundancy. An acceptable failure rate was assumed to be 1 in  $10^6$  flight hours for non-flight-critical systems and 1 in  $10^9$  for flight-critical systems. The failure analysis was conducted for two different scenarios. The first was called the not-too-distant future system and the other was a more technologically demanding system. The main difference between the two systems is that the not-too-distant future system uses existing components and the futuristic system uses much more integration. The listing of the required components for the not-too-distant future system is given in Table 2.

Table 2 Required components for the advanced flight management system

| Component                           | Weight (lbs) | Power (watts) | Volume (in <sup>3</sup> ) | Retail price (91 \$ US) | Number needed for redundancy |
|-------------------------------------|--------------|---------------|---------------------------|-------------------------|------------------------------|
| Nav. computer/<br>memory/ data base | 8.5          | 103.6         | 272                       | 23,572                  | 3                            |
| MFD                                 | 7.7          |               | 335                       | 22,500                  |                              |
| TCAS II                             | 40.5         | 206           | 1558                      | 127,533                 | 2                            |
| Airdata computer                    | 2.74         | 4.2           | 192                       | 6465                    | 3                            |
| Flight computer                     | 23.1         | 83.0          | 962                       | 30,000                  | 3                            |
| HUD                                 | 24.0         | 200           | 1200                      | 16,000                  |                              |
| GPS                                 | 1.6          | 5.0           | 49                        | 2,610                   | 3                            |
| FCI                                 | 5.0          |               | 88                        | 14,905                  |                              |
| TAS indicator                       | 0.94         |               | 40                        | 120                     | 2                            |
| Altimeter                           | 1.1          |               | 41                        | 220                     | 2                            |
| Totals including<br>backups         | 228.0        | 1,199         | 9,245                     | 496,752                 |                              |



From Table 2 it can be seen that this system requires a large amount of power, volume, weight, and cost. Considering the nature of the airplane (a light general aviation trainer), such a system is not feasible using existing technology. A reduction of the weight and cost by 50% was determined to be the upper bound of the advantage that can be obtained by using the futuristic system. This results in a system that will weigh on the order of 100 pounds and cost in the neighborhood of \$250,000, still too expensive for a light trainer. However, such a system could be used in larger aircraft such as corporate or commercial transports.

### Composite Structure Design

The purpose of this section is to present the results of the composite construction and manufacturing study. This study was conducted during both the Fall and Spring semesters. The main objective of the Fall semester was to find ways in which all mechanical fasteners could be eliminated from the structure. For a representative aircraft, the Smith Aircraft Corporation GT-3 Global Trainer was used. The main objective of the Spring semester was to try to incorporate these ideas into a design, and to compare the resulting structure with an aluminum design. The airplane chosen for the Spring semester was the Cessna 152.

### Composite Manufacturing Technique

The importance of concurrent engineering has been increasingly evident in recent years. This is even more the case with composite structures. If the designer does not consider manufacturing from the start, it is quite possible that the resulting product will be both overweight and over cost. For this reason, an extensive search of the various manufacturing methods available was made. The method that seemed to have the most promise was Resin Transfer Molding or RTM, a process in which dry fibers are placed in a double-sided mold. The resin is injected into the dry fiber at a constant rate so that all of the fibers are exposed to the resin. The process is shown schematically in Figure 3.

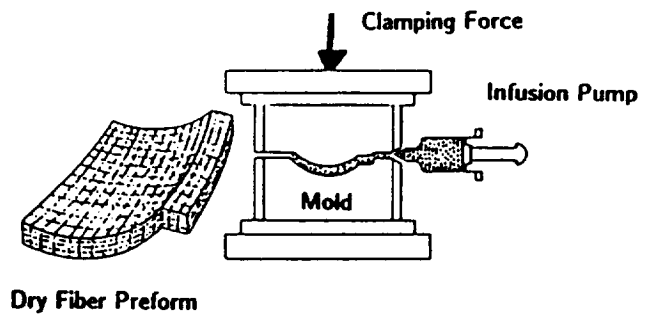


Fig. 3 Fundamentals of Resin Transfer Molding

The main advantage of RTM is that the resulting part has a controlled surface on all or most surfaces. This will significantly reduce the amount of refitting required when all of the components of the airplane are joined together. Another advantage is that the materials are cheaper than conventional pre-preg materials. This is because the resin is injected into the fibers by the partmaker instead of by the company selling the service to the manufacturer. No freezers are required to store the materials, and the part is in near net shape after being released from the mold, further reducing costs.

The main disadvantage of this process is that twice the usual number of molds is required. This would make the process difficult for a start-up company to use due to the large initial capital investment. Finally, the technology is not yet perfected. Despite these disadvantages, it was felt that the advantages far outweigh the disadvantages and that in a few years the technology will be ideal for making composite parts.

### Wing

The GT-3 wing is designed to emphasize the elimination of mechanical fasteners. At the locations of mechanical fasteners, the composite needs to be built up because an interruption of the composite fibers weakens its structural integrity. This buildup around the fasteners increases the weight of the composite, which is unacceptable. Another design driver in the wing design is ease of removal and replacement for the purposes of repairability and maintainability. The wing designs were conceptualized with these factors in mind:

- slide-on wing
- key-way joint
- conventional pin joint

The slide-on wing concept will be used for the GT-3 trainer. The slide-on wing consists of a "stub" type fixture extending from the fuselage. The stub is integral to the fuselage/carry-through structure. The stub is designed to act as an inner layer of skin attached to the inboard portion of the wing. However, the wing will be assembled and then slid on this stub and attached with adhesive. This adhesive bond will then act as an interlaminar bond allowing the stub to act as a layer of skin. The stub will extend to buttock line 68 to allow for attachment of the fixed landing gear to the stub structure. The stub will be shaped as the outer skin of the inboard wing to allow for a tight fit as the wing is slid over the stub. In the chordwise direction, the stub will extend aft to approximately 0.70 chord where it will be rounded to an oval-type shape (Figure 4).

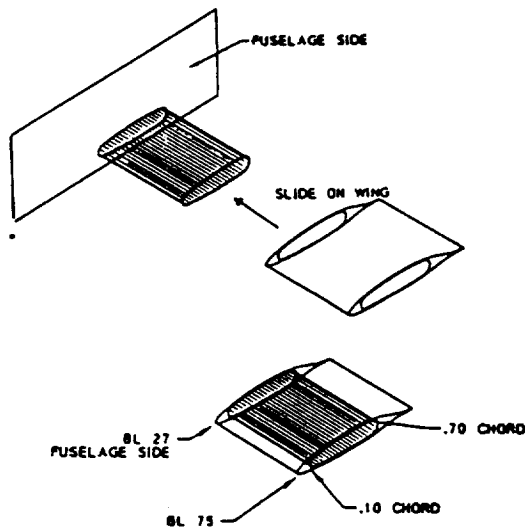


Fig. 4 Slide-on wing concept

The advantages of using the slide-on stub joint to attach the wing include:

- ease of assembly
- joint/structure synergism
- landing gear mounting synergism

- repairability

The assembly of the wing onto the stub consists primarily of sliding the wing on, attaching the landing gear, and applying the adhesive to hold the wing on. The stub will not be symmetrical; thus, there should not be any problems with mounting the wing upside down. The actual application of the adhesive is to be investigated further. Synergism is achieved when the stub is used both for mounting the wing and for wing strength. The stub is an integral part of the structure of the inboard portion of the wing. The landing gear mounting presents another advantage to using the stub. Because the stub extends to the landing gear attachment, the stub can be used synergistically as part of the landing gear attachment. Some of the actual structural strength required for the landing gear attachment and the inboard portion of it already exist in the stub.

Some of the disadvantages of using the slide-on stub joint include:

- difficulty of wing removal
- tolerances

Adhesives must be used to attach the wing because of the assumption that the stub will act as part of the wing skin. Thus the bond between the wing and the stub must be viewed as an interlaminar bond. This also assumes that the tolerances between the stub and the wing skin are very small (a similar metal joint requires approximately 0.0006-0.0012 inches).<sup>6</sup> This exact tolerance could present an accuracy problem during manufacturing.

Another concept that was developed was called the key-way joint. This joint allows the wing to slide on parallel to the x-direction of the aircraft. This concept is shown in Figure 5.

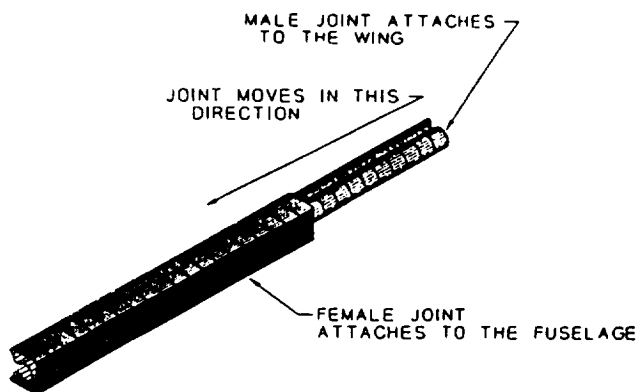


Fig. 5 Key-way joint concept

The advantage to this joint is that it is not required to take as much load as the slide-on wing does. This is because all of the bending loads are taken out by the unique shape of the joint. Some adhesive will still be required to prevent the wing from sliding off. The main disadvantages are its very complex shape and, like the slide-on wing, the extremely narrow tolerances required to prevent any movement. A model was built using fiberglass and epoxy resin to gain further insight into the merits of the joint. During the course of many assemblies and disassemblies, the joint became worn and became more and more loose-fitting. Clearly this would not be allowable for an actual installation, so a remedy to this problem must be found.

The final wing-to-body joint that was investigated was a conventional pin joint. While the pin violated the principle of no mechanical fasteners, it was required for the composite wing design for the Cessna 152. This is because the 152 uses a strutted high wing. By using a strut, Cessna was able to eliminate the bending moments at the root, and thus very little carry-through structure was required. To ensure that the bending moment remained zero, it was necessary to use a conventional pin joint. The configurations are shown in Figure 6.

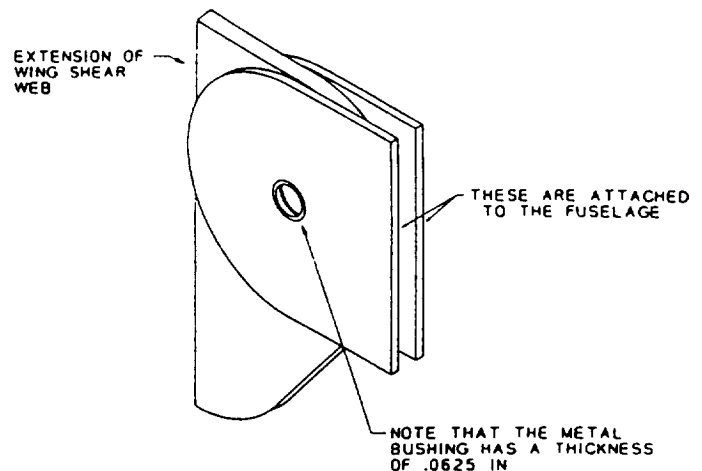


Fig. 6 Configuration of the pin joint

**Structural Layout for the GT-3 Wing.** A primary design goal of this design is to eliminate the use of mechanical fasteners. To accomplish this goal, the decision was made to develop a design that would distribute the loads and stresses more evenly throughout the wing as opposed to channeling each load into a specific structural member. The ultimate manifestation of this concept is the monocoque wing. The pure monocoque wing, with no internal ribs, spars, or stiffeners, represents a limiting structure which designers can approach in an attempt to obtain thin, hollow wings with low fabrication and assembly costs. Since the skin is the only structural element, all loads on the wing will be distributed throughout the skin. This concept is not feasible using conventional metal fabrication because of the high weight that would be required to provide the necessary structural stiffness. Even using high-modulus graphite composites, the concept is impractical. For virtually any material, ribs are required to hold the aerodynamic contour of the wing and to prevent the wing from flattening out, which would result in structural instability. A rib is also required to distribute the landing gear loads into the skin. Spanwise stiffeners are desirable to reduce the panel width of the skin in compression, thus raising the buckling strength of the skin.

The structural item that can be eliminated is the spar. The web of a spar concentrates the shear created by the wing lift into a few finite points along the chord of the wing. The spars can be eliminated along with the concentrated loads associated with them, allowing the leading and trailing edges of the wing to serve a structural function.

**Structural Layout for the 152 Wing.** Due to the configuration of the Cessna 152, a no-spar wing as previously discussed is not possible. This is due to the large cutout required for the doors. There simply is not enough room to distribute the loads. For this reason the composite wing for the 152 uses conventional shear webs placed at the same locations as the standard 152. These shear webs channel the forces into bulkheads in the fuselage on both sides of the door. The composite wing differs from the conventional wing in that the upper skin between the shear webs acts as the spar cap. Figure 7 is an exploded view of the wing showing the shear webs and the required ribs.

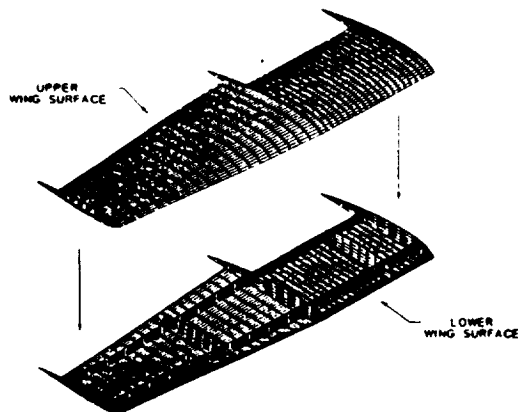


Fig. 7 Exploded view of composite 152 wing

## Fuselage

The purpose of this section is to present the concept chosen for construction of the fuselage of the Smith GT-3 Global Trainer and the composite 152.

Several fuselage construction concepts were investigated before deciding on a construction technique:

- one-piece construction-wing and body
- one-piece fuselage
- two-piece fuselage
  - front/back
  - side/side
  - top/bottom

A top/bottom concept was chosen for the construction of the GT-3 and the composite 152 fuselage. It has several advantages over the other ideas. A manufacturer can lay up the bottom half of the airplane at room temperature or in an autoclave and then install most or all of the systems without having to crawl inside the fuselage. The idea is to put the bottom half on "sawhorses" and have excellent access all around the fuselage, saving equipment installation man-hours. The top half can be set over the entire assembly to see if all the systems and equipment fit inside. Then, the top can be lifted off and installation can continue, or the two halves can be bonded together. The two-piece fuselage will have pieces that will be easier to manufacture and work with than a one-piece fuselage.

A complex curve or a stair-step may be required for the joint along the aft end of the fuselage, which could increase the complexity of the manufacturing process.

Current examples of the top/bottom construction include:

- Smith GT-3 Trainer
- Wheeler Express
- Fitzgerald Cozair

Wheeler actually purchased and built a Glasair before they designed the Express and decided against the left and right half concept. An additional benefit of this concept is that small, non-load bearing structures could be taped in to run the flight controls. Figure 8 shows how the top/bottom construction technique is implemented on the composite 152.

C-6.

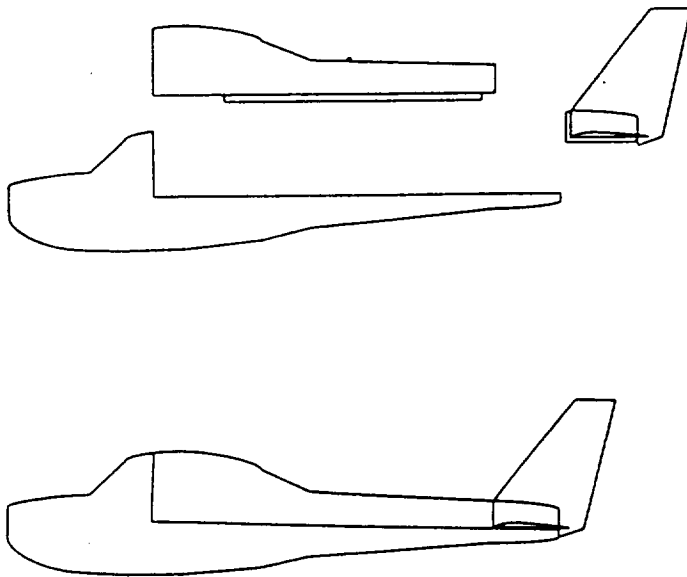


Fig. 8 Demonstration of top/bottom construction

The empennage could be designed so that it fits inside grooves in the bottom half of the fuselage. Then, the top half could fit over a section of the empennage, "locking" it in place. This is also shown in Figure 8.

The components of the wing-body joint are the wing joint and the fuselage carry-through structure. The wing-body joint attaches the wing to the fuselage and also transfers the lifting loads from the wing to the fuselage structure.

The design criteria for the wing-body joint follow:

- even distribution of loads
- no mechanical fasteners
- secure attachment of wing to fuselage
- repairability and replaceability

**Joint Concepts.** Several joint concepts were developed during the preliminary design phase of this task. The three most promising concepts were the stub slide-on joint, key-way joint, and one-piece wing.

An attachment mechanism must be determined for each of these joint types. Residual clips and adhesives are

some of the attachment mechanisms available. A residual clip joint is one in which one piece must "snap" into place. That part can be removed by collapsing the joint with a special tool.

Hot-melt adhesive is suggested as the attachment mechanism for the stub slide-on type joint. The wing is attached to the fuselage by sliding it onto a stub that is part of the fuselage. By using an adhesive that melts at a temperature below the cure temperature of the wing and fuselage, but above the maximum operating temperature of the airplane, the wing can be removed without damaging other airplane components. The stub is itself the carry-through structure.

**Carry-through Structure.** The design of the carry-through structure uncovered several problems with the design of the Smith GT-3. Currently, the Smith GT-3 uses two spars to carry the wing loads. The leading spar is located at 0.45 chord, and the trailing spar is located at 0.70 chord. The leading spar carries most of the load, and the trailing spar simply acts as a mount for the trailing edge devices. The wing leading spar runs through the cockpit directly below and behind the pilot's back. In the case of a crash which broke the spar, the spar would drive up through the back of the seat, severely damaging the pilot's spine. With the loads concentrated on one spar, the likelihood of the spar's breaking is increased. This design was considered unacceptable.

Since the pilot seat location and the aerodynamic shape of the airplane were not items which the group was allowed to alter, the carry-through structure must be located behind 0.45 chord. Since the structure will still be located behind and beneath the pilot's back, the design driver for the carry-through structure was crashworthiness. The two main methods used to achieve this objective are:

- distribution of the loads
- controlled failure design

By distributing the loads over a larger area, the likelihood of the structure's breaking is diminished. Additionally, the carry-through structure was designed so that, in the case of a crash, the wing would fail before the carry-through structure. Since the structure is designed in this manner, the fracture location is moved away from the pilot and passengers.

The maximum loading placed on the carry-through structure occur in the one-wheel landing cased. The loads are:

|         |                |
|---------|----------------|
| bending | 834,000 in-lbs |
| shear   | 22,400 lb      |
| torsion | 113,000 in-lbs |

**Conceptual Design.** A tube-type design was chosen for the carry-through structure. Use of a box or tube carry-through structure rather than a two-spar structure was shown to save weight while maintaining the required load-carrying capability. Additionally, the tube structure lends itself more easily to the use of the stub slide-on joint and the no-spar wing concepts.

The actual shape of the structure will follow the internal contour of the wing airfoil shape. The structure will be rounded at the leading and trailing edges. The shape will be approximately an ellipse. Once the structure penetrates the fuselage skin, the leading edge will curve back from the leading edge to 0.45 chord to fit around the pilot seats. This cutout significantly reduces the torsional strength of the structure, but has little effect on the shear or bending strengths. To recover some of the torsional strength lost, stiffeners will be added along the 0.45 chord location in the carry-through structure. Additional stiffeners will be added for support of the wing structure, the fuel tanks and the control runs. In addition to the stiffeners, the fuselage structure will add torsional stiffness to the carry-through structure.

By over-designing the strength of the structure and adding stiffeners to further improve the strength, the designers have chosen not to take full advantage of the weight savings possible over a conventionally designed tube structure. However, the pilot's safety in the event of a crash is greatly improved.

### Empennage

Though the empennage was discussed previously, the details of its attachment will be discussed in this section. The empennage is clamped in place by both the upper and lower fuselage skins and by two bulkheads located where the front and rear spars of the horizontal tail intersect the fuselage. At these points a clamped joint is used. The clamps used for this joint do not require holes

drilled in the composite. Thus, the full strength of the composite can be expected. A cross-section of this joint is shown in Figure 9.

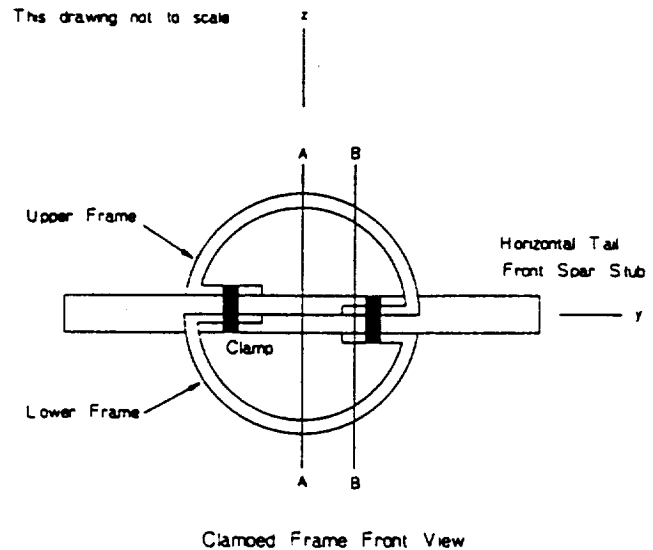


Fig. 9 Clamped joint concept

### Landing Gear

Composite landing gears have been used for many years in general aviation aircraft, so design of the gear legs is not all that difficult. However, one of the main problems with landing gear design is finding a way which will introduce the fairly large point loads into the structure. For composite design, distributed loads are much easier to accommodate. One possible solution to this problem is the concept shown in Figure 10.

In this concept, the cross at the top of the landing gear strut is designed to take out all the landing gear loads. This also would eliminate the need for a drag brace, reducing drag.

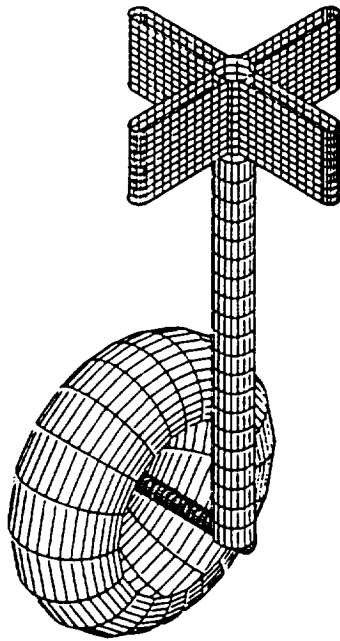


Fig. 10 Landing gear attachment concept

### Engine Mount

The engine mount for the composite 152 also posed the problem of how to introduce a point load into a composite structure. A "bathtub" type fitting was developed (Figure 11) at five different locations around the firewall. The engine mount uses the same metal structure that the standard 152 uses.

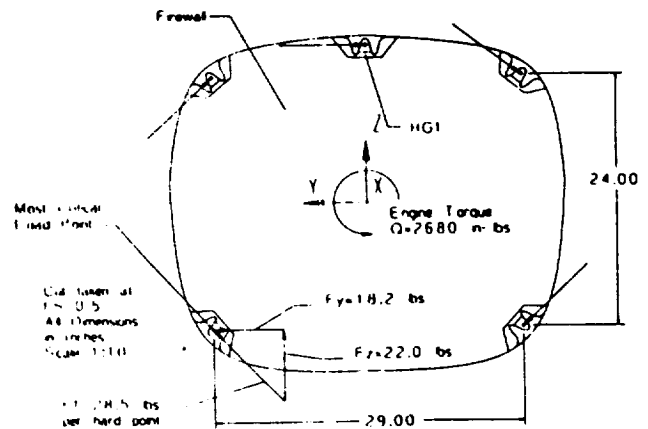


Fig. 11 Engine mount concept

### Conclusions

By using novel techniques of composite construction, designers may avoid the problem of bolts and screws in composite structures. Table 3 makes a comparison of the structural weights for a composite and a conventional aluminum 152.

Table 3 Comparison of composite and conventional structural weights

| Component    | Composite | Aluminum |
|--------------|-----------|----------|
| Wing         | 206       | 216      |
| Fuselage     | 138       | 231      |
| Empennage    | 28        | 31       |
| Landing Gear | 80        | 96       |

Table 3 shows that the differences in weight, with the exception of the fuselage, are generally not significant. This indicates that, considering the assumptions required for preliminary design of the composite aircraft, there is no significant advantage from a weight standpoint to either material.

### References

1. Jones and Winger. Advanced Primary Flight Control System for the Smith Aircraft Corporation GT-3.

Lawrence, Kansas: The University of Kansas, December 1991.

2. Clatterbuck, Newton, and Widup. Advanced Flight Management System Study for the Smith Aircraft Corporation GT-3. Lawrence, Kansas: The University of Kansas, December 1991.
3. Hoffman, Rodkey, and Roper. Advanced Guidance and Display Study for the APT. Lawrence, Kansas: The University of Kansas, Fall 1990.
4. Krause, Miller, Mouch, Schmitz, and Houdeshell. Wing Design and Manufacturing Study for the Smith Aircraft GT-3. Lawrence, Kansas: The University of Kansas, December 1991.
5. Krause and Wenninger. Composite Wing Design for the Cessna 152. Lawrence, Kansas: The University of Kansas, April 1992.
6. Hixson, Thacker, and Ellrott. Fuselage Design for the Smith Aircraft GT-3. Lawrence, Kansas: The University of Kansas, December 1991.
7. Thacker, M. Composite Fuselage Design for the Cessna 152. Lawrence, Kansas: The University of Kansas, April 1992.
8. Jones, V. Composite Empennage Design for the Cessna 152. Lawrence, Kansas: The University of Kansas, April 1992.
9. Schmitz, K. Landing Gear Study for the Composite Version of the Cessna 152. Lawrence, Kansas: The University of Kansas, March 1992.
10. Headrick, J. Engine Attachment Design for a Composite Version of the Cessna 152. Lawrence, Kansas: The University of Kansas, March 1992.
11. Headrick and Schmitz. Manufacturing and Assembly for the Redesign of a Metal Cessna 152. Lawrence, Kansas: The University of Kansas, April 1992.



**DESIGN STUDY TO SIMULATE THE DEVELOPMENT  
OF A COMMERCIAL FREIGHT TRANSPORTATION SYSTEM**

**University of Notre Dame  
Department of Aerospace and Mechanical Engineering  
Notre Dame, Indiana**

**Dr. Stephen M. Batill  
Kevin Costello and Jim Pinkelman, Teaching Assistants**

**Abstract**

The Notre Dame Aerospace Engineering senior class was divided into six design teams for the purpose of this study. A request for proposals (RFP) asking for the design of a remotely piloted vehicle (RPV) was given to the class, and each design team was responsible for designing, developing, producing, and presenting an RPV concept. The RFP called for the design of commercial freight transport RPV. The RFP provided a description of a fictitious world called 'Aeroworld'. Aeroworld's characteristics were scaled to provide the same types of challenges for RPV design that the real world market provides for the design of commercial aircraft. Fuel efficiency, range and payload capabilities, production and maintenance costs, and profitability are a few of the challenges that were addressed in this course. Each design team completed their project over the course of a semester by designing and flight testing a prototype, freight-carrying remotely piloted vehicle.

**Introduction**

The undergraduate Aerospace Engineering design project is presented to the senior class as a single semester course. The focus of this class is the "design process." The design process is the sequence of steps which an engineering group follows from the initiation of a project through to its completion. In this course it involves the definition of the mission, the determination of goals, the development of concepts, the selection and technical analysis of a concept, prototype production, and testing of the finished product. In the students' previous engineering courses, class projects typically focused on the solution of specific technical problems with little effort spent on the design process. The senior design class was created to augment the emphasis on engineering analysis by introducing the students to the design process.

The purpose of the design class is twofold. First, it serves as a capstone Aerospace Engineering course where the students have the opportunity to apply all of their knowledge from previous courses to a single, integrated project. Secondly, the class serves to bridge the gap between typical engineering coursework and engineering practice. This twofold purpose is fulfilled by structuring the course around the process of design, rather than the solution of an intricate technical problem.

The project for the 1992 design course was the development of a remotely piloted vehicle (RPV) to fulfill a commercial cargo carrying role. A model world called "Aeroworld" was created with its economic, geographic, and demographic characteristics tailored to provide similar design challenges for small remotely piloted vehicles that the real world provides for actual commercial cargo transport aircraft. The simple technologies involved in the design and construction of electric-powered RPVs allowed students with limited knowledge to experience the entire design process despite the time and resource limitations of a one semester undergraduate course. Using RPVs and the "Aeroworld" model allowed the students to address their design project from the very beginning of the design process all the way through to the production and flight testing of the actual product.

The following are some of the specific goals of the course:

- Introduce the student to system design methodology and, in particular, aircraft design.
- Illustrate the interactive interface between each of the technologies that influence the performance of a system.
- Provide an opportunity to integrate each of the independent technical disciplines at a level where the students understand the technology and can effectively use the appropriate tools.

- Develop an understanding of the planning, coordination, and communication necessary in a team project.
- Expose the students to numerous phases of the system development process, from problem definition to system operation.
- Provide the opportunity to experience the process of transitioning ideas to an actual product.

The course meets each of these goals by leading the students through a team-oriented, mission-directed, aircraft design project. The following section is the request for proposals which provided the students with a detailed description for the course project.

### **Request for Proposals - (RFP)**

The mission and project requirements, as well as the Aeroworld model, were defined for the students in the request for proposals. This request placed some additional requirements and constraints on the basic mission specifications. In order to keep the project as open-ended as possible, the design teams were notified that certain aspects of the mission were open for modification, given sufficient justification for these changes.

### **Air Transport System Design**

The successful development of an air transportation system depends upon a sound understanding of the market and efficient development of an aircraft system which can operate effectively in that market. Since a particular aircraft cannot satisfy every possible user need, it must be evaluated on how well it meets its own design objectives.

In order to be considered as a reasonable aircraft system for a commercial venture, it must be able to operate at a profit which requires compromises between technology and economics. The objective of this project will be to gain some insight into the problems and trade-offs involved in the design of a commercial transport system. This project will simulate numerous aspects of the overall systems design process so that you will be exposed to many of the conflicting requirements encountered in a systems design. In order to do so in the

limited time allowed for this single course, a "hypothetical world" has been developed and you will be provided with information on geography, demographics, and economic factors. The project is formulated in such a fashion that you will be asked to design a basic aircraft configuration which will have the greatest impact on a particular market. The project will not only allow you to perform a systems design study, but will provide an opportunity to identify those factors which have the most significant influence on the system design and design process. Formulating the project in this manner will also allow you the opportunity to fabricate the prototype for your aircraft and develop the experience of transitioning ideas to "hardware" and then validate the hardware with prototype flight testing.

An aircraft which is simply the fastest or "looks neat" will not be considered a marketable product. Economic feasibility and, in particular, compliance with the group's design objectives will provide the primary means for evaluating the system design of that group.

### **Opportunity**

The project goal will be to design a commercial transport which will provide the greatest potential return on investment. Maximizing the profit that your airplane will make for an "overnight" package delivery network can be accomplished by minimizing the cost per "package." G-Dome Enterprises has conducted an extensive market survey for an airborne package delivery service and is now in the market for an aircraft which will allow them to operate at a maximum profit. AE441, INC. has agreed to work with them to establish a delivery system. This includes a market analysis, the establishment of a distribution concept and the development of a number of aircraft concepts to help meet this market need. This will be done by careful consideration and balancing of the variables such as the payload, range, fuel efficiency, production costs, as well as maintenance, operation and disposal costs. Appropriate data for each is included later in the project description.

The "world" market in which the airline will operate is shown in Figure 1. The service may operate in any number of markets provided that they use only one airplane design and any potential derivatives (your company does not have the engineering manpower to

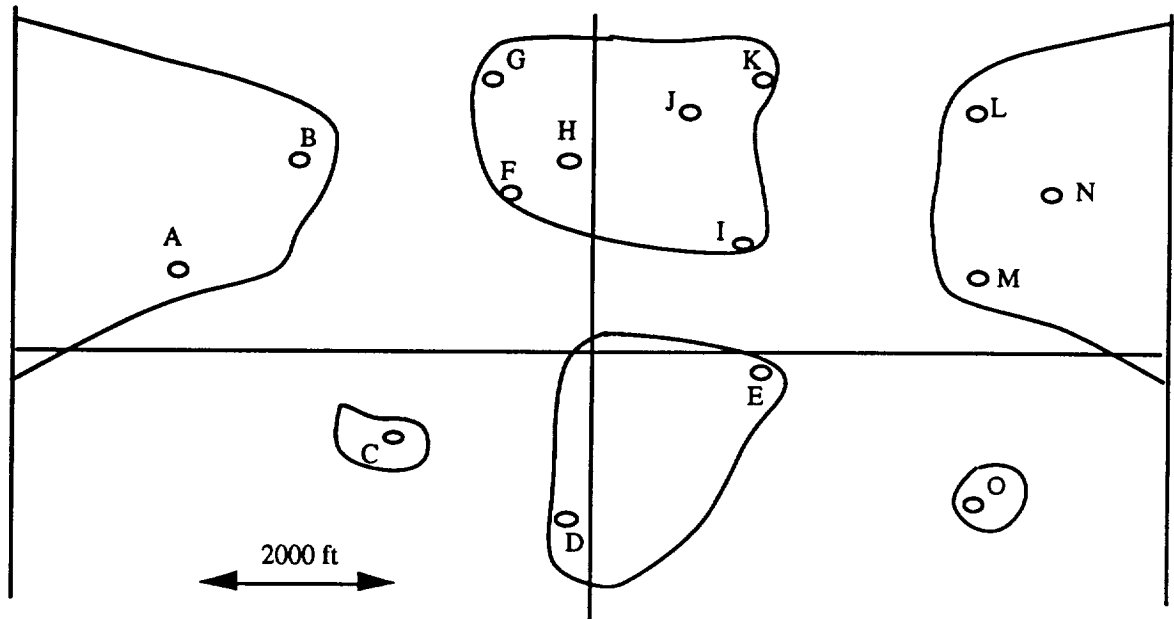


Fig. 1 Geography of "Aeroworld"

develop two different designs). Consider derivative aircraft as a possible cost-effective way of expanding the market.

### Requirements

1. Develop a proposal for an aircraft and any appropriate derivative aircraft which will maximize the return on investment gained by the airline through careful consideration and balance of the payload/volume, the distance traveled, the fuel burned, and the production cost of each plane. The greatest measure of merit will be associated with obtaining the highest possible return on investment. You will be expected to determine the freight cost for all markets in which you intend to compete. The proposal should not only detail the design of the aircraft but must identify the most critical technical and economic factors associated with the design.

2. Develop a flying prototype for the system defined above. The prototype must be capable of demonstrating

the flight worthiness of the basic vehicle and flight control system and be capable of verifying the feasibility and profitability of the proposed airplane. The aerodynamic performance of the prototype will be evaluated using a "stick-fixed" catapult launch of the aircraft carrying a specialized instrument package and where the range of the aircraft under specified launch conditions will be the primary measure of aerodynamic efficiency. Flightworthiness and handling qualities of the prototype will be demonstrated by flying a closed figure "8" course within a highly constrained envelope.

### Basic Information for "Aeroworld"

The following information is to be used to define special technical and economic factors for this project. Some information is specific, other information provides ranges which are projected to exist during the development of this airplane.

1. Payload: There are two standard parcel packing

containers, a 2"cube and a 4"cube. Remember these are cargo, therefore items like access and ease in loading are important. Since various types of cargo can be considered, cargo weight/volume requirements are also important. Cargo weights can vary from 0.01 to 0.04 oz/cubic inch.

2. Range: distance traveled in feet.
3. Fuel: battery charge measured in milli-amp hours.
4. Production cost =  $400 \times (\text{total cost of prototype in dollars}) \$ + 1000 \times (\text{prototype construction man-hours}) \$$ .
5. Operation costs =  $(\text{number of servos in the aircraft}) \times \text{flight time in minutes}$  - this is a cost per flight.
6. Maintenance costs = \$50 per man-minute for a complete "battery" exchange - this is a cost per flight.
7. Fuel costs = \$5.00 to \$20.00 per milli-amp hour.
8. Regulations will not allow your plane to produce excessive "noise" from sonic-booms; consider the speed of sound in this "world" to be 30 ft/s.
9. The typical runway length at the city airports is 75 ft, this length is scaled by a runway factor in certain cities.
10. Time scale: "Aeroworld day" is 30 minutes.
11. Propulsion systems: The design, and derivatives, should use one or a number of electric propulsion systems from a family of motors currently available.
12. Handling qualities: To be able to perform a sustained, level 60' radius turn.
13. Loiter capabilities: The aircraft must be able to fly to the closest alternate airport and maintain a loiter for one minute.
14. Aircraft Life: Is based upon a scaled fatigue life of the materials used in Aeroworld.

### **Special Considerations for the Technology Demonstrator**

The prototype system will be an RPV and shall satisfy the following:

1. All basic operation will be line-of-sight with a fixed ground-based pilot, although automatic control or other systems can be considered.
2. The aircraft must be able to take off from the ground and land on the ground under its own power.
3. The prototype flight tests for the Technology Demonstrator will be conducted on a closed course in the Loftus Center. The altitude must not exceed 25' at any point on the course.
4. Catapult launch tests will be conducted in the Loftus Center. Details on the catapult and instrument package will be provided.
5. The complete aircraft must be able to be disassembled for transportation and storage and must fit within a storage container no larger than 2' x 2' x 5'.
6. Safety considerations for systems operations are critical. A complete safety assessment for the system is required.
7. The Technology Demonstrator will be a full-sized prototype of the actual design and must be used to validate the most critical range/payload condition for the aircraft.
8. Take-off must be accomplished within the take-off region of 75 ft.
9. A complete record of prototype production cost (materials and manhours) is required.
10. The radio control system and the instrumentation package must be removable, and a complete system installation should be able to be accomplished in 30 min.
11. System control for the flight demonstrator will be a Futaba 6FG radio system with up to 4 S28 servos or a system of comparable weight and size.

12. Each group must comply with all FAA and FCC regulations for operation of remotely piloted vehicles and others imposed by the course instructor.

### Student Response to RFP

Each of the six student design teams responded to the RFP by defining mission priorities for their design within the framework provided by the RFP. The groups established Design Requirements and Objectives (DR&O) for their RPVs according to the mission priorities that they set for themselves. The DR&Os consisted of target performance goals such as payload and range requirements as well as configurational data dealing with the RPV's manufacturing and operating requirements. With these goals established, the members in each group created specific RPV concepts to satisfy the mission. From these individual concepts, each group selected one for their team concept. The team concept was developed throughout the course up to the actual construction and flight testing of a prototype. The following section describes the six group concepts.

### Concept Descriptions

The following summaries provide an overview of each of the six team concepts. These summaries describe the final concept and address specific technical merits and limitations of each group's RPV. It is interesting to note that each of the six groups created different designs although they were all given the same request for proposals.

The following are edited versions of the final proposal executive summaries. Further technical detail on each proposal is available upon request.

#### S.T.o.R.M.

The members of Team Asylum have proposed a helicopter design concept, called the S.T.o.R.M., in order to meet the market demands for an aircraft to perform overnight package delivery services in Aeroworld. Many critical design areas needed to be investigated as part of the helicopter concept's selection.

One of the most significant design factors was the weight of the aircraft. This determined the selection of the propulsion system necessary to get the S.T.o.R.M. off the ground, and maintain flight once airborne. After an analysis of helicopter flight principles, it became apparent that if the S.T.o.R.M. could be provided with the necessary power to hover, it would also be able to sustain forward flight at a cruise velocity of 25 ft/sec. This is due to the fact that a helicopter requires more power to hover than to maintain forward flight. Using the provided data bases along with researched weight estimates, the S.T.o.R.M. was determined to weigh within the range of 4.77 lbs and 7.33 lbs, depending upon the weight of the payload being transported. In an attempt to fulfill the mission requirement mandating delivery of the .04 oz/cu in cargo, a propulsion system which enabled the S.T.o.R.M. to carry 2.56 lbs of cargo within a 1024 cu in payload bay would be required. An Astro 25 motor was selected because of its ability to deliver the necessary power required, while minimizing the battery-package and motor weights.

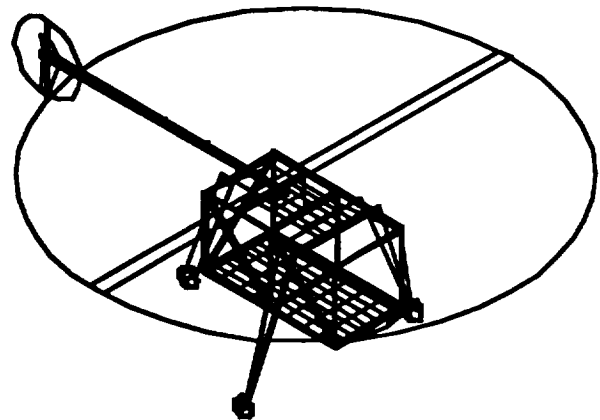


Fig. 2 The S.T.o.R.M.

Another significant factor closely related with the motor selection was the choice of the main rotor. Since the main rotor is the primary source of lift for the helicopter, its proper selection became increasingly important. The rotor diameter needed to be large enough to provide the necessary lift within the bounds of the power available limits of the Astro 25 motor, yet not be so large that it would suffer severe drooping at the rotor tips or be in

danger of clipping the tail rotor during rotation. A main rotor diameter of 50 inches was chosen in order to best fulfill these constraints.

Upon first analysis, a helicopter concept provides many advantages for the required mission. The S.T.o.R.M.'s ability to eliminate takeoff distance, landing distance, and loiter time constraints due to its vertical takeoff and landing capabilities was viewed as a major advantage in time and fuel savings. The S.T.o.R.M.'s ability to fly at slow speeds and thus stay under the Aeroworld sound barrier of 30 ft/sec was also a desirable design aspect. Also, the S.T.o.R.M.'s maneuverability would enable it to avoid obstacles better than a conventional airplane design.

However, some disadvantages for this concept exist as well. The excessive weight of S.T.o.R.M.'s design along with the tremendous power requirements necessary for its flight hinder the helicopter's range and endurance capabilities. Thus, it became necessary to decrease the market that could be served. Instead of servicing all of Aeroworld, only the central continent could be serviced for the concept to remain economically feasible. The cost associated with the technological complexity of the S.T.o.R.M.'s development became a hindrance. Although the smaller market (the central continent) would provide an estimated 48% profit based on the original investment, it seems that the helicopter concept falls somewhat short of the objective to fulfill all of the mission requirements. However, the evaluation of a radical vehicle system was bold, exciting, and innovative and should provide future design studies with the valuable information necessary to successfully complete other missions.

The final design characteristics of the S.T.o.R.M. incorporated an Astro 25 motor, powered by 14 Panasonic 140SCRC batteries, thus allowing the helicopter to fly at a cruise velocity of 25 ft/sec. With a payload volume of 1024 cubic inches and a full payload of 2.56 lbs., the S.T.o.R.M. would require 255 watts of power to hover and 237 watts of power to fly at cruise velocity. The lift for the aircraft is provided by a Clark-Y 50-inch diameter main rotor, which in turn is stabilized by an 8-inch diameter, symmetric tail rotor. An overall length of 31 inches, a height of 16 inches, a fuselage width of 8.25 inches, and a landing gear base width of 20 inches round out the critical dimensions for the S.T.o.R.M., thus making it compact enough to fit in the 2' x 2' x 5' storage container area. The helicopter has an empty weight of

4.77 lbs and a full-cargo weight of 7.33 lbs, with a maximum range capability of 5875 feet. The S.T.o.R.M., despite its technological complexities, was an invaluable source of new technical information.

## Jeff

Jeff is a remotely piloted vehicle concept developed to fulfill the mission proposed by G-Dome Enterprises: to build a cost efficient aircraft to service Aeroworld with overnight cargo delivery. The design of Jeff was most significantly influenced by the need to minimize costs. This objective was pursued by building fewer large planes as opposed to many small planes. Thus, by building an aircraft with a large payload capacity, G-Dome Enterprises will be able to minimize the high costs and the large number of cycles that are associated with a large fleet. Another factor which had a significant influence on our design was the constraint that the RPV fit into a 2' x 2' x 5' storage container. This constraint meant that Jeff's wing span would be limited to 10 feet unless we wanted to build foldable wings. To avoid this and to provide enough lifting surface to suit our needs a canard configuration was chosen.

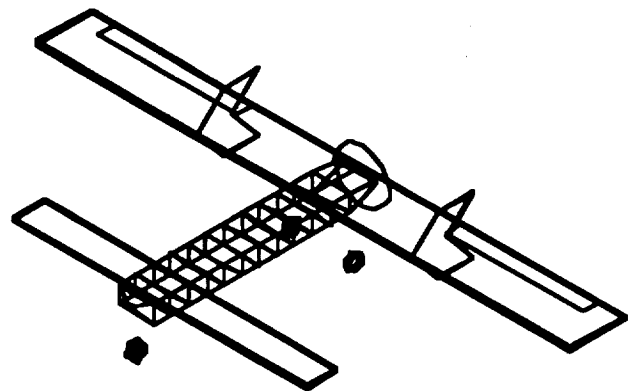


Fig. 3 Jeff

Because of the canard configuration, stability of the aircraft became a main design concern. To achieve acceptable static margins, the interior of the aircraft was carefully configured and wing and canard carefully sized and placed. The aircraft achieves good static margins (10-20%) at full payload and also at a decreased payload with the addition of ballast. Control surfaces were sized

accordingly. Ground control is achieved with a movable nose wheel, and elevons on the main wing provide pitch and roll control.

Economically, the aircraft is very cost efficient. A fleet of 19 aircraft is sufficient to service our target market--the upper hemisphere of Aeroworld. The lower hemisphere of Aeroworld was left out because it was thought that the long distances between cities in this hemisphere outweighed the benefits of the limited cargo that existed in this market. At \$287,000 per plane, fleet life cost is \$33,800,000. This figure translates to a unit volume cost of \$3.72/in<sup>3</sup> of cargo. Thus G-Dome Enterprises can charge a competitive price of approximately \$4/in<sup>3</sup> and maintain a profit of \$12,261,388 per year.

Some areas of concern still remain. Static stability, although achieved, was a difficult issue. The stability depends largely on payload weight and payload distribution within the fuselage because the center of gravity of the plane when empty differs greatly from that when full. Also, propeller ground clearance may be a concern as the plane rotates on takeoff. Finally, because the aircraft is so large and because the airfoil chosen has a sharp trailing edge, the manufacturing process was somewhat time-consuming and difficult.

The aircraft was designed to fly at a maximum altitude of 25 ft and at low speeds (less than 30 ft/sec). To carry large amounts of payload, Jeff consists primarily of a 1408 in<sup>3</sup> fuselage (44" x 8" x 4"). A rear-mounted pusher propeller was chosen. The FX63-137B airfoil was selected for both the wing and canard because of its high lift characteristics and moderate thickness. Both lifting surfaces are rectangular, with aspect ratios of 10. Sized to provide static stability as well as lift, the wing planform area is 10.0 ft<sup>2</sup>; canard planform area is 3.0 ft<sup>2</sup>. Each of the two vertical stabilizers have an area of 0.75 ft<sup>2</sup> and is mounted above and below the wing 3 ft inboard from the wing tips.

The aircraft is constructed mainly of balsa, with spruce wing and canard spars and a monokote covering. It was designed to support a maximum payload weight of 35 oz (total aircraft weight of 108 oz) and withstand a maximum load factor of 2.5. Tricycle landing gear support the plane up to a load factor of 4.0 during landing, and ensure propeller clearance during takeoff rotation.

The propulsion system consists of an Astro 15 motor, which was chosen because it can provide the power required for our large aircraft to take off and fly at a cruise velocity of 28 ft/sec. Twelve 1.2 volt batteries are required to power the system and to ensure takeoff in a distance of 60 ft, a maximum range of 9770 ft, and a maximum endurance of 11.50 minutes.

Despite the technical challenges, Jeff provides the Aeroworld market with a large cargo carrying capacity which will ensure that all cargo can be delivered to its target cities efficiently overnight. It provides G-Dome Enterprises with a low-cost small fleet of aircraft that will operate at a profit over the life span of the structure, and it can fully accomplish the specified mission.

### Hermes CX-7

The Hermes CX-7 has been designed to service the overnight parcel package delivery needs of the cities of Aeroworld as determined in the G-Dome Enterprises market survey. The design optimization centers on the prime goal of servicing the needs of these cities as efficiently and profitably as possible. The greatest factors which affect the design of an aircraft for the mission outlined in the RFP are cost, construction feasibility, and effectiveness of the design. Other influencing factors are given by the constraints of the market, including a maximum take-off and landing distance of 60 feet, storage capability in a container of size 5' x 3' x 2', cargo packages of 2 and 4 in cubes, and ability to turn with a radius no larger than 60 feet. Safety considerations, such as flying at or below Mach one (30 ft/sec), controllability, and maintainability must also be designed into the aircraft. Another influential factor is the efficiency of the aircraft as a system involving optimizations and tradeoffs of such factors as weight, lifting surface sizing, structural redundancy, and material costs.

The design market will consist of all Aeroworld cities except C, D, E, and O due to low demand in these cities and their excessive distances from the northern cities. A routing system was designed to service the needs of the target cities overnight using a fleet of 22 planes. The routing system is based on two main hubs at cities F and K. Each aircraft will make two round-trips on one leg of the route. To minimize cost, the route structure is designed such that it uses as few aircraft as possible, and

these aircraft cover the shortest distance possible each night.

The constraint which sized the engine and propeller was take-off performance. The Hermes CX-7 employs the Astro 15 engine and the TopFlight 12x6 propeller. This engine/propeller combination provides the necessary power needed for take-off in less than 60 feet, while minimizing the fuel burned during cruise. The Astro 15 was the engine that weighed the least of those which provided sufficient power for take-off. The TopFlight 12x6 was the smallest diameter propeller which fulfilled the necessary take-off distance requirement. The TopFlight version of this propeller was chosen because it exhibits the best efficiency of the brands available. The aircraft will be powered by 12 Panasonic 600 milli-amp hour batteries having voltage capacity of 1.2 volts each. These provide sufficient power for both takeoff and cruise conditions to meet the restrictions on take-off distance and on range needed.

The wing section will be constructed from the NACA 6412 airfoil. This airfoil section was chosen because it provides the desired lift capability while also minimizing the difficulty in construction because of its simple structure. The wing has an area of 8 square feet and an aspect ratio of 12. There is no sweep or taper on the wings because this will greatly simplify construction. The wings will be mounted as two plug-in sections, low on the fuselage at a dihedral of 6 degrees and an angle of incidence of 1 degree. The wing will have three spars and will be built primarily from spruce, bass, balsa, and monokote.

The fuselage will have a rectangular cross-section of area 4.6 in x 6.9 in and a length of 54 in. It is constructed of spruce and balsa wood and includes a cargo space 4 in x 4 in x 40 in. The aircraft was laid out such that the center of gravity is located 24 in from the front of the fuselage regardless of whether the aircraft is empty or full of cargo.

The Hermes CX-7 is designed to be controlled with rudder and elevator deflections. There are no ailerons. This minimizes the number of servos needed to control the aircraft. Turning is achieved through the use of the rudder and dihedral effects. The horizontal and vertical surfaces of the tail both consist of flat plates for simplicity. The elevator area is 30% of the horizontal tail and the

rudder area is 50% of the vertical tail. The c.g. travel is constrained by static and dynamic stability considerations and is limited to 10% forward and 5% aft of the design c.g. position (24 inches from the front of the fuselage).

The Hermes CX-7 will meet and surpass the performance requirement of the mission and market. The take-off distance is 32 feet, and the landing distance is 47 feet, well below the constraint of 60 feet. The design range is 10,655 feet, and endurance is 355 seconds. The maximum range is also 10,655 feet; maximum endurance is 356 seconds. The aircraft can execute a 48-foot radius turn, which is less than the 60-foot restriction, at a 30-degree bank angle.

The Hermes CX-7 will cost an estimated \$390,000 (in Aeroworld dollars). The recommended charge is \$10.50 per cubic inch for an average delivery distance. This will enable G-Dome Enterprises to break even in less than half of the life of the aircraft.

#### **Arrow 227**

The Arrow 227 is a commercial transport designed for use in an overnight package delivery network. The major goal of the concept was to provide the delivery service with the greatest potential return on investment.

The first step in the design process was to conduct a detailed mission evaluation followed by a thorough market analysis. The market analysis of Aeroworld led to the implementation of a hub system of delivery with the hub located at city K. The analysis also revealed that service to cities C, D, and O should be excluded due to small runways and a negative profit margin due to excessive fuel costs. In order to execute this delivery plan, the Arrow 227 will be required to fly intercontinental flights with a minimum range of 9720 feet and a minimum endurance of 6 minutes. The flight route suggested by the producers of the Arrow 227 requires a fleet of 16 aircraft. The fleet services twelve cities in Aeroworld, and each craft carries a maximum volume load of 1000 in<sup>3</sup> to each city. This proposed service also requires the Arrow 227 to take off within a distance of 60 feet due to restrictions at Aeroworld's city B airport. Finally, the RFP also required a minimum turn radius of 60 ft and a packaging constraint of 5' x 2' x 2'.



The design objectives of the Arrow 227 were based on three parameters: production cost, payload weight, and aerodynamic efficiency. Low production cost helps to reduce initial investment. Increased payload weight allows for a decrease in flight cycles and, therefore, less fuel consumption than an aircraft carrying less payload weight and requiring more flight cycles. In addition, fewer flight cycles will allow a fleet to last longer. Finally, increased aerodynamic efficiency in the form of high L/D will decrease fuel consumption.

The aerodynamics of the design were driven mainly by the desire for the minimization of drag and production cost. The wing planform was designed to minimize induced drag through the use of an aspect ratio equal to 10.5. A rectangular configuration was implemented to reduce production cost. The GO-508 airfoil was selected on the basis that it enabled cruise at the minimum point of the airfoil drag curve, and its simple shape helped to reduce production cost. Drag minimization was also apparent in the component drag breakdown. The fuselage and landing gear were designed to minimize their contribution to total parasite drag of the aircraft.

The design of the propulsion system was driven by three main objectives: 60-ft take-off distance, minimal weight, and minimal current draw. The Astro 15 engine was chosen because it provided enough power to allow the aircraft to take off under 60 feet. The Zinger 10-6 was chosen as the propeller because it performed close to its maximum efficiency at cruise, and it provided enough thrust to take off within 60 feet. Twelve 1.2 volt, 900 milliamp-hour batteries were used to provide enough power for the engine during takeoff and enough endurance for cruise.

The Arrow 227 is stabilized by employing a horizontal tail, a vertical tail, and dihedral. A conventional wing/tail configuration was chosen for the Arrow 227 so the stability of the aircraft would be less sensitive to the center of gravity shift that occurs in cargo transport aircraft. The wing location and the center of gravity location of the loaded aircraft were positioned so that no trim drag occurred at the cruise conditions. Such placement maximized the aerodynamic efficiency. Longitudinal and lateral control are achieved through the use of an elevator and a rudder. Ailerons were not employed since they would introduce additional cost and weight. Instead, lateral control was obtained by coupling

the yaw and roll axis by using a high wing with 8 degrees of dihedral.

Because the structure of the aircraft is the major weight component, it must be light in order to meet our weight objective. With this in mind, the fuselage was designed as an all-balsa wood, truss structure with all unnecessary support beams eliminated. The Arrow 227 is a cargo plane flying at low velocities. Since it is not expected to fly high g-maneuvers, the limit load factor is only 1.5. This allowed the wing and fuselage to be designed as light as possible, resulting in a structural weight fraction of less than 30%.

The strengths of the Arrow 227 are:

- large payload volume
- low weight
- large payload fraction
- simple design.

The aircraft design was based on a 1000 in<sup>3</sup> cargo hold. The desire for a maximum cargo hold was to decrease the number of flights and increase profit for G-Dome Enterprises. The 1000 in<sup>3</sup> cargo hold can carry maximum capacity at an average package weight of .032 ounce per in<sup>3</sup>. The total aircraft weight of 6.0 lbs loaded was due to material selection, lightweight design of the fuselage and wing, and careful construction. By excluding control surfaces on the wing and implementing dihedral, added weight due to hinges and control rods was eliminated.

The weaknesses of the Arrow 227 are:

- inability to service all of Aeroworld
- low take-off thrust from small propeller.

The aircraft was designed to have a maximum full weight of 6.0 lbs carrying 1000 in<sup>3</sup> of cargo. However, this payload volume and projected range and endurance do not allow all of Aeroworld to be serviced. The cargo volume carried to and from each of the three cities eliminated from service was not sufficient to provide a profit for G-Dome Enterprises, and these cities do not have sufficient runway lengths to accommodate the Arrow 227.

The Zinger 10-6 was chosen as the propeller for the Arrow 227. The propeller was designed to provide enough thrust at take-off, but there were two factors that led to uncertainty in these findings. The first was the high

friction coefficient, 0.15, of the flight test range, which would increase the take-off thrust requirement. The second was the size of the fuselage. The fuselage cross section was 7.5 x 4.0 in. Considering the diameter of the propeller was only 10 inches, the effect of fuselage interference on the propeller was uncertain.

### Exodus Prime Mover

The Exodus Prime Mover (Figure 4) is an overnight package delivery aircraft designed to serve the Northern Hemisphere of Aeroworld. The preliminary design goals originated from the desire to produce a large profit. The two main driving forces throughout the design process were, first, to reduce the construction man-hours by simplifying the aircraft design, thereby decreasing the total production cost of the aircraft. The second influential factor affecting the design was minimizing the fuel cost during cruise. The lowest fuel consumption occurs at a cruise velocity of 30 ft/s. Overall, it was necessary to balance the economic benefits with the performance characteristics in order to create a profitable

product that meets all specified requirements and objectives.

The SPICA airfoil section and a rectangular planform were selected to reduce construction hours necessary to produce the wing. Its flat bottom and lift characteristics provide a balance between aircraft performance and construction simplicity. The wing area of 9.62 square feet ensured the necessary lift both during cruise and takeoff. In addition, cruise conditions occur at maximum lift to drag ratio.

The Astro 15 electric motor and the ZingerJ 11-5 propeller comprise the propulsion system of the Prime Mover. The propeller selection was based upon the take-off distance requirement of 60 feet; the ZingerJ 11-5 provided the highest efficiency while still meeting this requirement. Twelve batteries of 1.2 volts and 1000 mah each were selected to power the system. The battery pack provides the voltage needed for take-off and the capacity required for the flight time of the aircraft.

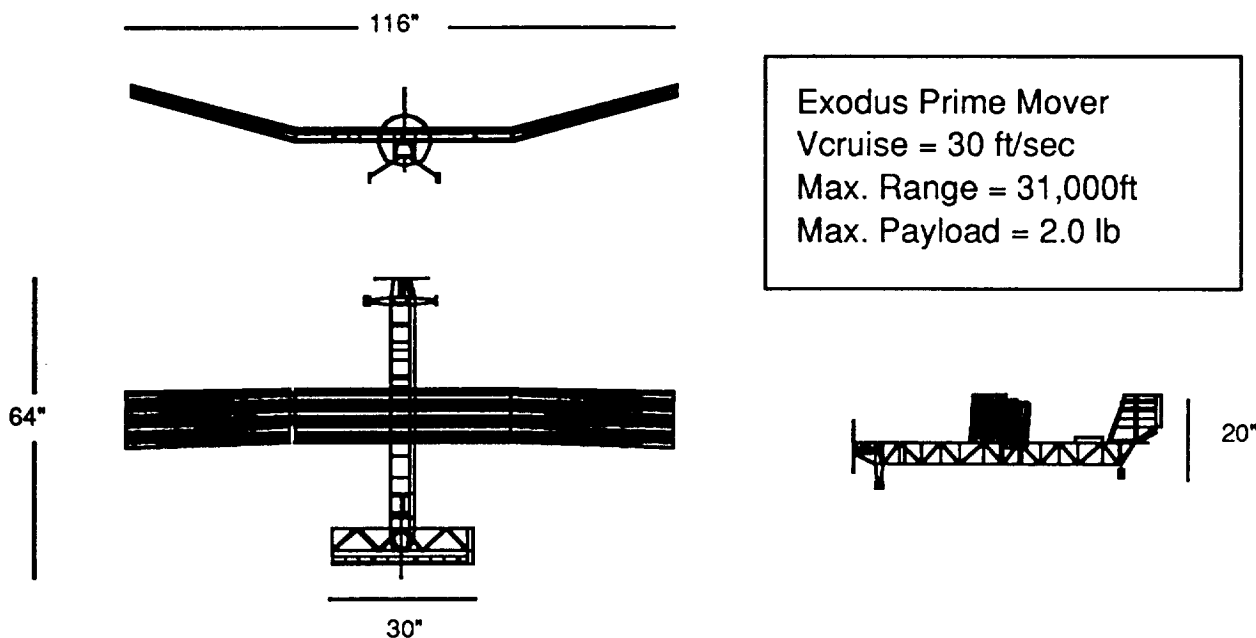


Fig. 4 Exodus Prime Mover

Directional and longitudinal control have been achieved through the use of a rudder and an elevator. A polyhedral concept has also been adopted for roll control. The polyhedral was chosen over the dihedral to decrease the amount of structure needed to withstand the bending moment at the root of the wing.

The Prime Mover is capable of guaranteeing overnight delivery for the entire Northern Hemisphere due to the proposed fleet size of 42 airplanes and the high range and endurance capabilities. The design objectives required the aircraft to meet a 8600 foot range minimum. The final design has displayed a cruise range of 24,000 feet, enabling the aircraft to complete its nightly schedule without the need to refuel. This reduces the operating costs of the aircraft. The maximum range and endurance of the fully loaded aircraft is 31,000 feet and 13.5 minutes, respectively. The take-off distance at maximum take-off weight is 59 feet.

The Prime Mover has a rectangular frontal area of 4.6 inches by 4.4 inches and a fuselage length just under 5.0 feet to provide 800 cubic inches of cargo space. The fuselage, wing, and empennage were designed to withstand a landing load factor of 4.0, a cruise load factor of 2.5, and a catapult launch load factor of 2.0.

The wing and the empennage will be removable in order to fit the disassembled aircraft within a 2 ft x 2 ft x 5 ft box. Although this design increases the complexity of the structure, it enables the use of a modular construction technique. Each component of the aircraft may be built separately and assembled at a later time. This construction method will decrease the construction man-hours.

As a result of the previously mentioned design characteristics, Exodus confidently presents the Prime Mover, an aircraft created to harmonize technical and economic considerations. The total production cost is estimated at \$376,000. Based upon the production, operating, maintenance, and fuel costs Exodus recommends the price per cubic inch for intracontinental and overseas shipping be \$8.74 and \$11.01, respectively, in order to break even on the original investment.

## Reliant

In formulating the Reliant design, the driving philosophy was not just to fulfill the mission requirements, but to do so in a creative manner. This explains the unconventional aircraft design, named the F-92 Reliant. Although unconventional, and perhaps more expensive to produce, the design has distinct advantages which could only be attained through such a creative design.

Major components of the F-92 Reliant include:

- unobstructed cargo bay, 1024 in<sup>3</sup> capability
- loading ramp
- dual wing configuration
- polyhedral wing configuration

These design components combined to create an aircraft that would most effectively meet the goals of cargo transportation in Aeroworld at minimum cost.

The unobstructed cargo bay and rear loading ramp allow for ease of cargo loading and unloading. These concepts were born at the initiation of the design; the rest of the aircraft developed around the fuselage cargo bay. It is not surprising that the aircraft design started here, since the main purpose of the Reliant is to transport cargo.

The volume cargo capacity of 1024 in<sup>3</sup> was established as the desired capacity based on an extensive market survey of Aeroworld. This large volume allows for a reduced number of flights required per day, yet still avoids flights with large amounts of unused cargo space. This component of the design is based on the reasoning that reducing the number of flights reduces fuel costs and also increases aircraft longevity.

The large horizontal tail and elevator allow for a large range of center of gravity locations; this allows for flexibility in cargo loading. This feature, in combination with the open cargo bay, reduces time and costs associated with cargo balancing and planning.

To effectively utilize the large volume capacity, the Reliant also must be capable of the large weight associated with the volume. To ensure that the Reliant is capable of carrying cargo and its own structural weight, a large lifting surface was designed for the aircraft. It was determined that for a single wing, the necessary 13 ft<sup>2</sup> of

wing area would be very difficult to build. The dual wing configuration permits 13 ft<sup>2</sup> of lifting surface while avoiding the structural complication and weight penalties of a single large wing. The placement of the wings with respect to each other maximizes aerodynamic performance without violating stability and control requirements.

The polyhedral design of the upper wing, combined with

a large rudder, allows for roll control of the Reliant without ailerons. This decision was based on the assumption that fixed polyhedral joints are less complex to incorporate into the plane than control-dependent ailerons, especially when considering that the wing must be segmented anyway because of packaging constraints. Furthermore, the polyhedral option, unlike ailerons, avoids the extra costs of an additional servo.

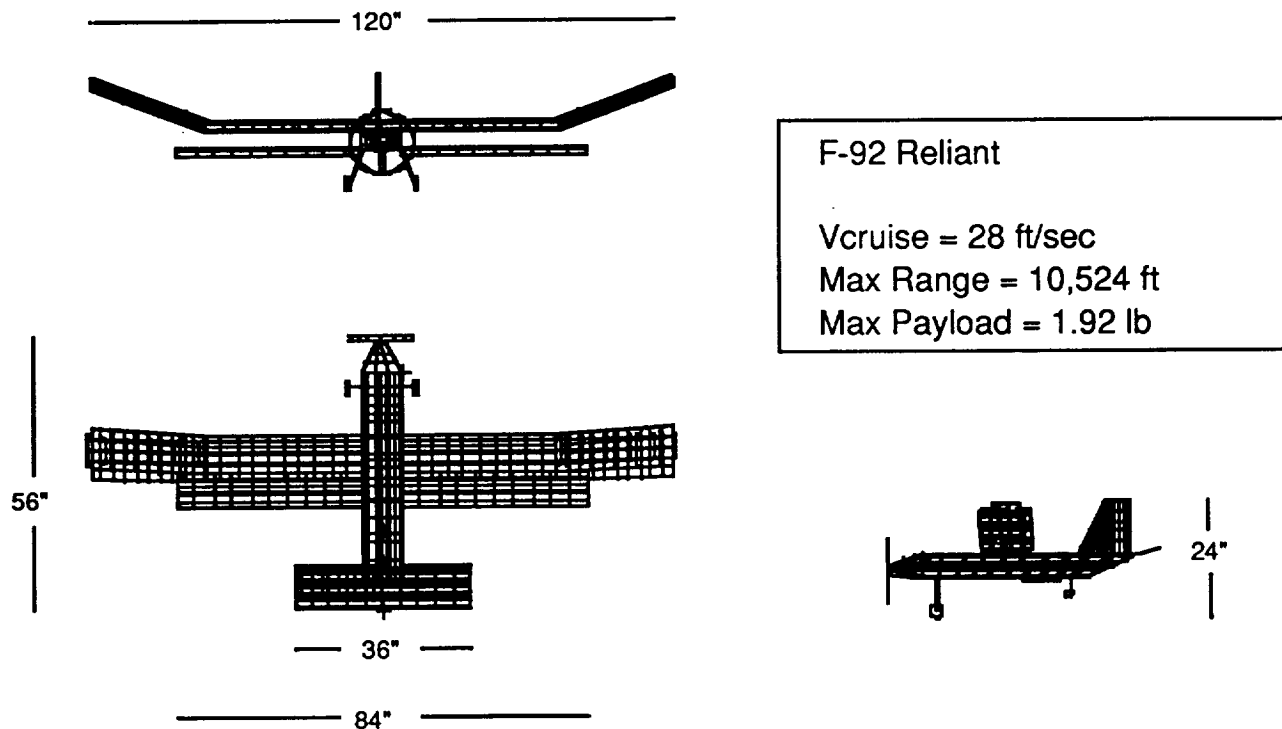


Fig. 5 Reliant

Thus, the unique design of the Reliant grew from the most basic goal of providing a highly cost-effective, reliable means of cargo transportation. On this foundation, with the help of a team of seven engineers, the Reliant evolved to its present configuration. General information about the Reliant is presented below.

The empty weight of the aircraft is 5.5 lbs and the maximum take-off weight is 7.5 lbs. The range of the aircraft with full cargo load is 8100 feet. The propulsion system includes a Cobalt-15 motor, a 13-inch propeller, and 12 Panasonic 1.2-volt high discharge rate batteries

with 900 milliamp-hour capacity. Avionics include a receiver, a speed controller, a servo and pushrod to control the elevator, and a servo and pushrod to control the rudder and tail wheel. The landing gear consists of two forward gear and a tail dragger.

### Design Issues

The following sections address the major technical areas in electric powered RPV design and construction. Weights, structures, propulsion, aerodynamics, stability

and control, economics, and production are all covered. A final paragraph will then describe the concept technology demonstrators and their flight validation.

### Weights

Overall weight is a critical issue in the design of any aircraft type because of the adverse effects upon range and performance from excess aircraft weight. RPV design is no different. The students were primarily concerned with minimizing the structural weight of their RPVs while maximizing their payload weight capacity. Figure 6 shows the weight breakdown for the Arrow 227 design. Note the large percentage devoted to payload.

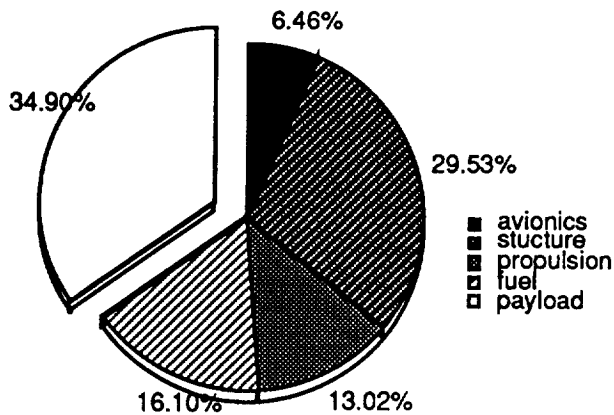


Fig. 6 Subsystem weight breakdown

Analysis of a rather large data base of old RPV designs provided the student design teams with some preliminary weight estimates, but accurate preliminary weight prediction was difficult because of the significant dependence of overall weight upon manufacturing techniques.

### Structures

The primary concern of the students in this area was to create the lightest possible structure that could handle the maximum flight loads that the RPV would encounter. A finite element structural optimization program called

SWIFTOS, written by Richard Swift, was a particularly useful tool employed by the student groups for the structural design of their wings. Truss structures were typically used for the RPV fuselage designs, with a three-dimensional finite element truss program used for the primary analysis. The limited manufacturing expertise of the students along with the construction time limitations posed serious barriers for the use of more advanced structures such as circular fuselage sections and tapered wings. Another factor in the structural design was the amount of labor hours necessary to fabricate the RPV. High labor hours increased the production cost which adversely affected the economic profitability of the RPV in the Aeroworld market.

### Propulsion

Electric propulsion systems were required for the RPV designs primarily because of safety considerations. Electric propulsion provides some unique challenges in RPV design as opposed to gas propulsion due to its significantly lower thrust to weight ratio. Determination of the proper propulsion system combination of batteries, an electric motor, and a propeller proved to be critical in the success of each RPV. Figure 7 is a schematic diagram of the propulsion system arrangement used in the Hermes CX-7.

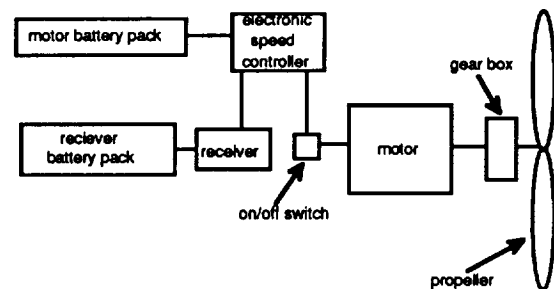


Fig. 7 Schematic of basic propulsion system

Take-off power requirements exceeded the low speed, steady cruise requirements as the primary driver in

propeller selection; whereas current draw at steady cruise proved to be the primary factor in battery selection. Various computer-based methods were available to provide performance predictions for the electric motors. Propeller analysis was primarily done with a computer program based upon simple blade element theory. Accurate performance predictions for the propellers operating in this low Reynolds number regime proved difficult and the flight validation indicated that some of the propeller selections could have been improved. All of the RPVs except the helicopter used the Astro-15 motor. The helicopter group used a special Astro-05 helicopter motor for their prototype RPV as a substitute for the Astro-25 in their design. None of the other student groups deemed the extra power of the Astro-25 and its corresponding weight increase to be necessary, nor did they believe that the weight benefit of the lighter Astro-05 would overcome the handicap of that motor's significantly lower power.

### Aerodynamics

Induced drag and the low Reynolds number flight regime, along with the Aeroworld constraints of airport gate size and a 30 ft/s "speed of sound" limitation were some of the primary drivers in the aerodynamic design of the RPV wings. The desire for high aspect ratio wing designs to reduce induced drag conflicted with the Aeroworld gate limitations on wing span.

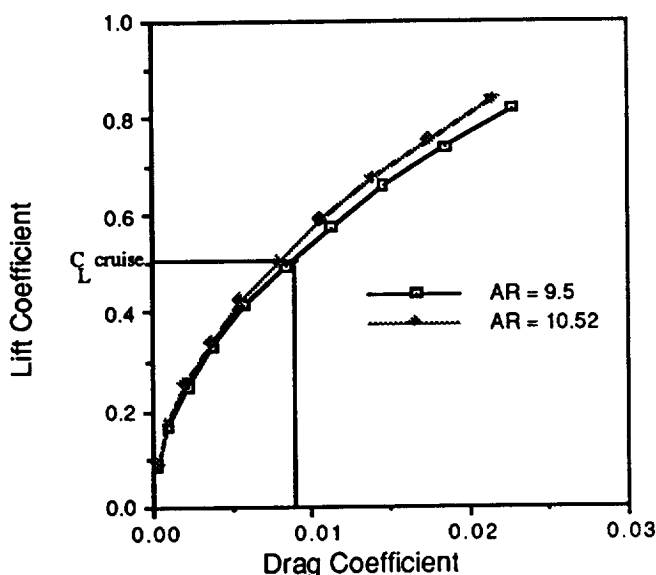


Fig. 8 Induced drag dependence on aspect ratio

Figure 8 illustrates the drag reduction benefits of higher aspect ratio wings. A number of groups opted for folding wing tips as a compromise.

The low Reynolds number flight regime, typically  $10^5$  to  $1.5 \times 10^5$ , made drag prediction difficult. The use of low Reynolds number airfoil sections was typical. Certain advanced aerodynamic characteristics such as taper, twist, or complex airfoil geometries were often eliminated from the wing designs due to anticipated fabrication problems. The "Mach number" limit did not carry a "penalty" and was primarily invoked only for safety considerations associated with the indoor flight tests. Most groups attempted to achieve cruise near  $L/D_{max}$ . Typical cruise speeds ranged between 25 ft/s and 30 ft/s. Although the high induced drag and low Reynolds number flight regime imposed by the "Mach number" limit made this difficult, most groups had at least some degree of success with their efforts.

### Stability and Control

Most groups concentrated their efforts in this area at providing adequate static pitch stability and the necessary roll control to perform the closed course, indoor maneuvers. Static stability was of particular concern to this year's students since their payload, the cargo cubes, had both variable weight and volume. Particular attention was given to center of gravity travel under a variety of loaded, unloaded, and partially loaded payload configurations. The added complexity of the pitching stability problem in the canard design proved to make that RPV difficult to manage in flight testing.

Control of the RPVs was usually accomplished with two channels, elevator, and rudder. This eliminated the extra weight and complexity of the additional controls for ailerons. Turning was accomplished using the combination of rudder and wing dihedral. One RPV, the canard configuration, had a single control surface which alternately performed aileron and elevator functions. Flight success was limited as that RPV did crash a few times during flight testing due to marginal pitching stability and control. Previous RPV designs had demonstrated the feasibility of the two-channel control concepts and other than issues related to control surface sizing and actuator sensitivity and installation, few

significant problems were encountered.

### Economics

The overall goal of each design team, regardless of the particular market they wished to address or the type of RPV they designed, was to make a profit based upon the Aeroworld economy. Most groups decided that fuel costs and production costs were the primary economic drivers, with maintenance costs and other operational costs being less critical. The most prominent economic trade-offs occurred when the groups decided the extra production cost of more advanced aerodynamic designs, such as circular fuselage sections and tapered wings, would offset any reduction in fuel costs due to the reduced drag. Hence most groups chose to quickly build the most aerodynamically efficient rectangular wings and truss fuselages that they could, rather than spend extra production time and money on more advanced designs.

Although the Aeroworld economy may not exactly reflect the real world economy with regard to the relative scale of its economic drivers, it did fulfill its primary purpose which was to make the students include economic constraints as well as technical constraints in their designs.

### Production

Since each group has limited manufacturing experience and only two weeks to construct the technology demonstrator, the design is largely influenced by ease of construction. Airfoil complexity, wing taper, fuselage cross-section, type and placement of the control systems, and internal structural arrangement are all influenced by the manufacturing requirement. The tools and materials available to the students make it more difficult to incorporate new technologies, such as metal structures and circular fuselages. Complex airfoil shapes coupled with inexperienced wing builders have been the cause of many problems with some RPVs in testing because slight inaccuracies in the construction of airfoils can cause large differences in aerodynamic performance. A few unwanted degrees of twist in either side of an RPV wing can cause a large asymmetry in lift.

The requirement to produce a product in a finite time,

with a limited budget, is probably the most important design driver. Every decision appears to be influenced by this factor.

### Technology Demonstrators

Each design team constructed their prototype RPVs during the last three weeks of the project. All groups except the helicopter group were provided with a remote control radio system and an Astro-15 engine. The helicopter group was provided with a specialized helicopter engine, gear set, and transfer case, as well as tail and main rotors. All construction took place in the Hessert Aerospace Design Lab, where simple construction equipment was available for student use. After a construction period of approximately two weeks, a series of taxi tests was performed to test the propulsion and control systems and to check the RPVs for basic flight worthiness. All but one of the RPVs experienced problems, especially in the areas of CG placement, control surface sensitivity, asymmetric lift distribution, and propulsion system battery performance. As expected, those designs which were the most conventional had the most success in initial flight tests.

On Friday, May 1, 1992, the flight demonstrations were held in the Loftus indoor sports arena. Three of the six aircraft and the helicopter successfully performed take-off and sustained, controlled flight. The three successful RPVs were the conventional designs: Hermes CX-7, Arrow 227, and Exodus Prime Mover. The other two aircraft, the canard and biplane configurations, Jeff and Reliant, attained flight, but could not be kept under control for a sustained period of time. The canard's primary flight difficulty was caused by the combination of marginal pitching stability, oversensitive elevator control and thrust coupling to pitch control. The biplane suffered from an asymmetric lift distribution which was the result of construction difficulties with the wings. Considering the lack of experience of the builders and the time constraints placed on the teams, this flight demonstration was considered a great success, and showed the students the difference between a conceptual success and success in the real world.

### **Conclusions**

The students entered the course with the knowledge required to complete the mission. The learning process involved the ability to incorporate that knowledge into a single integrated design. They were involved with the design process all the way from the mission definition to the prototype flight testing. Each student encountered many real world problems including working with a team of peers on a single aircraft design. The construction process allowed the students the experience of transforming a design concept from paper into a flightworthy aircraft.

The attempt to simulate numerous issues related to a commercial cargo transportation system design through the use of an RPV system and the Aeroworld economic and demographic model was largely successful.

### **Acknowledgments**

This project was supported by NASA/USRA Advanced Aeronautics Design Program. Technical assistance and guidance was provided by the Boeing Company under the coordination of Mr. Cal Watson. Thanks also to Boeing's Mr. Ben Almojuela for his participation in the preliminary design review. The course was presented by Dr. Stephen M. Batill and graduate teaching assistants Jim Pinkelman, Ken Cheung, Nat Georges, and Kevin Costello. Finally, thanks to Mr. Joseph Mergen, Mr. Tony DeRoza, Mr. Kane Kinyon, Mr. Joel Preston, and Mr. Mike Swadener for their technical assistance and advice throughout the semester.



## THE DESIGN OF FOUR HYPERSONIC RECONNAISSANCE AIRCRAFT

The Ohio State University  
Department of Aeronautical and Astronautical Engineering  
Columbus, Ohio

Professor G.M. Gregorek  
D.T. Detwiler, Teaching Assistant

### Abstract

Four different hypersonic reconnaissance aircraft were designed by separate student teams. These aircraft were designed to provide the U.S. with a system to acquire aerial tactical reconnaissance when satellite reconnaissance proved unobtainable or ineffective. The design requirements given for this project stated that these aircraft must carry a 7500 lb, 250 cu ft payload of electronic and photographic intelligence gathering equipment over a target area at speeds between Mach 4-7 and at altitudes above 80,000 ft. Two of the aircraft were required to be manned by a crew of two and have a range of 12,000 nmi. One of these was to use airborne refueling to complete its mission while the other was not to use any refueling. The other two aircraft were required to be unmanned with a range of 6,000 nmi. One of these was to take off from a naval vessel while the other was to be launched from another aircraft. This paper provides the final details of all four aircraft designs along with an overview of the design process.

### Introduction

The Ohio State University (OSU) Advanced Design Program (ADP) continues the tradition of hypersonic vehicle design with this year's project. Past projects for this program at OSU range from high speed cruise vehicles, including commercial 250-passenger transports and executive 10-passenger aircraft, to accelerating type vehicles, such as a Mach 10 scramjet test bed and a two stage to orbit vehicle. This year's project, a hypersonic reconnaissance aircraft, presents its own set of unique design challenges.

The majority of U.S. reconnaissance and surveillance intelligence is obtained by satellites. These spy satellites are sometimes unable to obtain vital intelligence due to

orbital restrictions or weather conditions. This gap in U.S. reconnaissance capabilities was filled in the past by the Lockheed SR-71 reconnaissance aircraft until its retirement in January, 1991. A replacement for this exceptional aircraft is needed. The four aircraft presented in this paper are intended for this purpose.

### Project Requirements

The design requirements set for the four aircraft were intended to represent current U.S. reconnaissance needs. These needs include a real time response coupled with a near-global range. This combination requires cruising at hypersonic speeds between Mach 4-7. The upper limit of Mach 7 was imposed because of thermal and structural constraints determined from current literature. These aircraft will be required to complete their mission over hostile territory. The high cruising speed and a cruising altitude above 80,000 ft are advantageous for survivability. There has been a serious debate over the necessity of a crew for this type of aircraft. Therefore, two of the aircraft were required to be manned while the other two were unmanned to provide a comparison. The diverse nature of these types of missions make several different operational capabilities attractive. Four possible mission scenarios were created, two with ranges of 12,000 nmi for the manned aircraft, and the other two with ranges of 6,000 nmi for the unmanned aircraft (Figures 1 and 2)

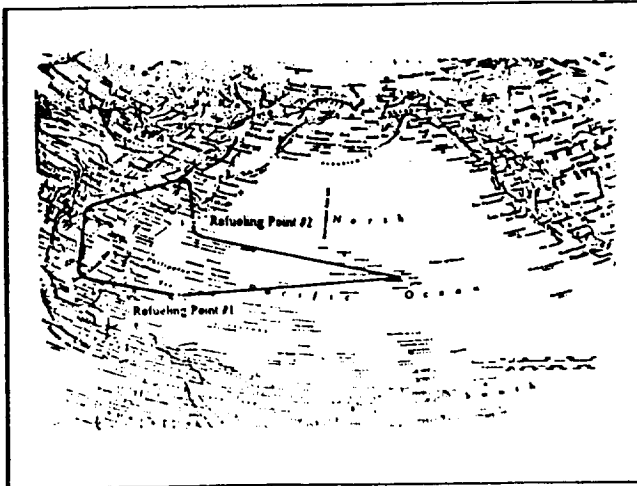


Fig. 1 12,000 nmi reconnaissance mission

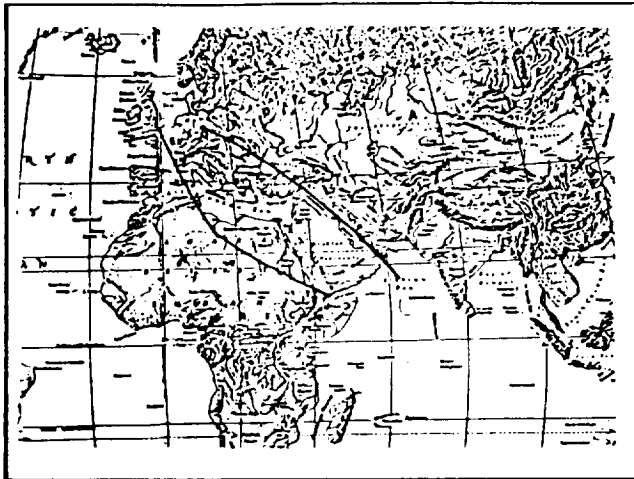


Fig. 2 6,000 nmi reconnaissance mission

The possibility of airborne refueling was studied by requiring one of the manned aircraft to use airborne refueling, while the other was required to complete the same mission without it. The tanker aircraft that provided the refueling for the above case was designed by engineering students from Ecole Polytechnique Feminine (EPF) in Paris, France. The possibilities of sea launch from a naval vessel and air launch from another aircraft were examined for the two unmanned vehicles. The general design requirements for all four aircraft and the mission specific requirements for each aircraft follow in Tables 1 and 2.

Table 1 General Design Requirements

|                     |                       |
|---------------------|-----------------------|
| Cruise speed        | Mach 4-7              |
| Propulsion          | Airbreathing (cruise) |
| Payload weight      | 7500 lbs              |
| Payload volume      | 250 cu ft             |
| TO/Landing distance | 10,000 ft             |

Table 2 Design Team Requirements

| Group      | Mission            | Range (nm) | Crew     |
|------------|--------------------|------------|----------|
| GRAY I     | Airborne refueling | 12,000     | 2        |
| GRAY II    | No refueling       | 12,000     | 2        |
| SCARLET I  | Air launched       | 6,000      | Unmanned |
| SCARLET II | Sea launched       | 6,000      | Unmanned |

### Design Program Outline

The ADP at OSU consists of three separate classes over the entire academic year. These include a one credit hour seminar during Autumn Quarter, a four credit hour Aerospace Vehicle Design Course during Winter Quarter, and an Advanced Vehicle Design Course during Spring Quarter.

The first course offers the students the opportunity to hear seminars from design engineers in the industry and government. These professionals speak about the design process and some specific problems created by operating in a hypersonic speed regime. The students were also asked to do a conceptual design of a primary trainer aircraft for this course. This allowed the students to familiarize themselves with the aspects of aircraft design. Roskam's first *Aircraft Design* book<sup>1</sup> was used for this project.

The students were divided into four separate design teams at the beginning of Winter Quarter. These teams consisted of a team leader and members specializing in one or more disciplines, such as aerodynamics, propulsion systems, etc. Since there is a separate structural design course offered at OSU, no structural design was required

for this project. The four groups were given the project requirements, which they incorporated into their own design goals. Trade studies were conducted by the groups dealing with different aerodynamic configurations and propulsion systems. The results of these studies and estimates of dimensions and weights were used to create a conceptual design and to do initial trajectory analysis.

The design cycle was continued during Spring Quarter by employing an iteration process. The groups attempted to optimize their trajectories and thereby minimize their weights. The details of each design, such as stability and control, thermal protection systems, and component weight analysis, were included. The groups were expected to give oral presentations on their progress on a regular basis and to turn in a final paper at the end of each quarter.

### Aircraft Designs

The four design groups were designated GRAY I and GRAY II for the two manned aircraft and SCARLET I and SCARLET II for the two unmanned aircraft. Each group operated independently and in a spirit of friendly competition with the others. The Teaching Associate functioned as a project manager to make sure that all the groups stayed on track.

The GRAY I aircraft (Figure 3) is a 207 ft-long conventional double delta wing-body configuration. It cruises at a speed of Mach 5 and an altitude above 80,000 ft for most of its 12,000 nmi range. However, this aircraft does descend to an altitude of 40,000 ft and decelerates to a speed of Mach 0.8 for two airborne refueling maneuvers to complete its mission. This wing-body configuration was selected for its balance of low speed and high speed capabilities and its volumetric efficiency. The aircraft is powered by three integrated turbo-ramjets that burn liquid hydrogen fuel. This integrated engine system allows the aircraft to operate at a wide range of speeds while reducing the weight produced by two separate engines. The single fuel, liquid hydrogen, was selected to simplify refueling systems while allowing the aircraft to reach Mach 5. The GRAY I aircraft has a takeoff weight of 281,000 lbs and operates from a standard runway.

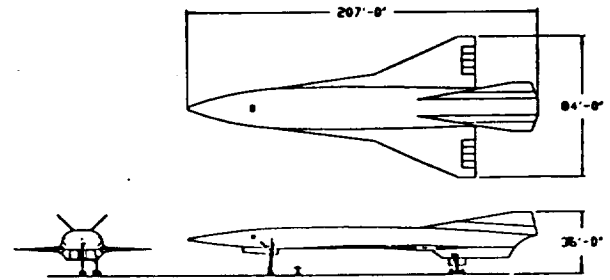


Fig. 3 GRAY I (3-view)

The GRAY II aircraft (Figure 4) is a 188-ft long waverider configuration. It cruises at Mach 4 and 80,000 ft. This aircraft was required to complete its mission range of 12,000 nmi without refueling. Therefore, the GRAY II group optimized their aircraft for hypersonic cruise conditions. A waverider vehicle was chosen for this purpose. The aircraft is powered by six augmented turbojet engines that burn liquid hydrogen fuel. The weight of the fuel was determined to be the critical design variable for this aircraft. This engine system was chosen to minimize specific fuel consumption. The liquid hydrogen fuel was selected for its high energy per unit mass content. The GRAY II aircraft has a takeoff weight of 558,000 lbs and operates from a standard runway.

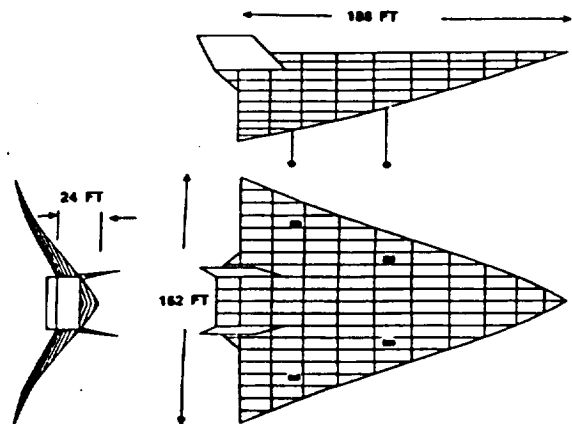


Fig. 4 GRAY II (3-view)

The SCARLET I aircraft (Figure 5) is a 61-ft long, lifting body configuration. It cruises at Mach 5 and 80,000 ft. This aircraft was designed to be launched from another aircraft traveling at Mach .8 and 35,000 ft. The capabilities of possible launch aircraft imposed serious size and weight constraints for this group. A lifting-body configuration was chosen for its volumetric efficiency. The aircraft is powered by four over/under rocket-ramjet engines. The liquid oxygen-hydrogen burning rockets power the vehicle during ascent, while the methane burning ramjets are used during cruise. The rockets were selected for the quick ascent to minimize engine weight. Methane was used to power the ramjets because it provided the necessary SFC while meeting the size and weight constraints. The SCARLET I aircraft has a launch weight of 130,000 lbs and lands unpowered on a standard runway.

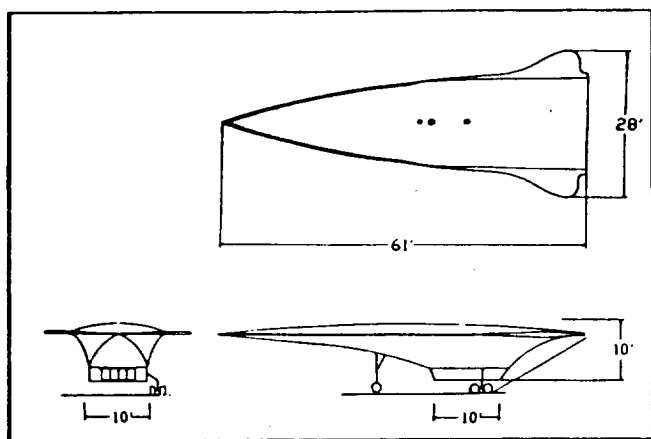


Fig. 5 SCARLET I (3-view)

The SCARLET II aircraft (Figure 6) is a 79.5-ft long waverider configuration. It cruises at MACH 4 and 80,000 ft. This aircraft was designed to operate from a Naval aircraft carrier. The constraints imposed on carrier-based aircraft include a maximum length of 80 ft, a maximum wing span of 52 ft, and a maximum weight of 100,000 lbs. A waverider configuration was selected because it provided optimal cruising characteristics while meeting all of the constraints. The aircraft is powered by two augmented turbofan engines burning JP-X. The turbofan was chosen for its superior performance at takeoff speed and to minimize engine system weight. The JP-X fuel was selected to meet volume constraints imposed by the waverider configuration and

environmental requirements for storage aboard an aircraft carrier. The SCARLET II aircraft has a takeoff weight of 100,000 lbs and operates from a naval aircraft carrier. The carrier's catapult is used for an assisted takeoff.

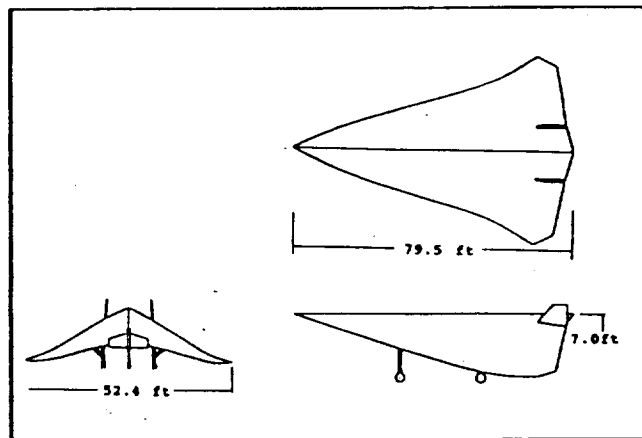


Fig. 6 SCARLET II (3-view)

### Design Methods

The hypersonic reconnaissance aircraft is a cruise vehicle. Therefore, it is advantageous to optimize for a set cruise condition. However, the various constraints placed on the four aircraft by their respective missions often conflict with this optimization. This leads to a series of compromises to reach the desired design goals. The following sections provide details of the various technical disciplines incorporated into the design process.

### Propulsion

The focus in designing a propulsion system is to select engine and fuel types that satisfy the mission requirements while minimizing the overall weight of the aircraft. This requires initial trade studies that compare the various possibilities. Figure 7 shows the mass and volumetric energy density comparison for various fuels for airbreathing engines. Liquid hydrogen possesses the highest mass energy density, but its low volumetric density produces serious volume requirements. The JP fuel has a much lower mass energy density and therefore a greater relative weight, but its high volumetric density provides greater volumetric efficiency. The methane fuel is a balance between the two others. Cryogenic fuels such as

liquid hydrogen and corrosive fuels such as methane have several operational problems which must be answered before use. The JP fuel has a maximum speed capability of Mach 4.

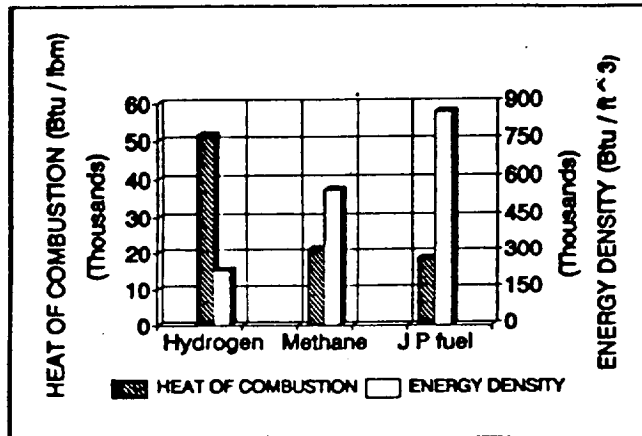


Fig. 7 Comparison of fuels

A single, multiple, or hybrid engine system must be selected to produce the required thrust over the entire flight envelope. Figure 8 shows several engine types. A cruising speed of Mach 4-7 for this type of vehicle requires a turbojet or ramjet engine. The turbojet has an operational speed limitation of Mach 4. A rocket engine is also a possibility, but its low specific impulse makes it very inefficient for long cruise applications. These aircraft are required to operate over a wide range of Mach numbers during the takeoff/landing and ascent/descent phases of the mission. Those aircraft equipped with ramjets for cruise must have multiple or hybrid systems for lower speeds.

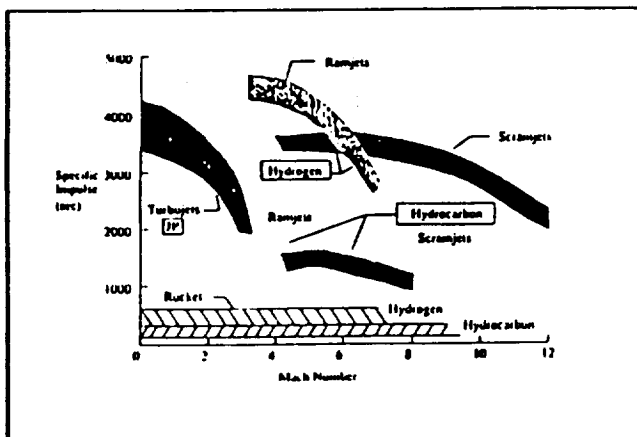


Fig. 8 Propulsion alternatives

The maximum net thrust produced by each group's propulsion system at specified Mach numbers and altitudes was obtained (Figure 9). This was done in part by scaling performance data provided by General Electric on several turbojet, turbofan, and ramjet concepts. The flexible ramjet/scramjet engine simulation program, RAMSCRAM, provided by NASA Lewis Research Center was also used to generate engine performance data.<sup>2</sup> All engine data assumes mil-spec inlet and nozzle efficiencies.

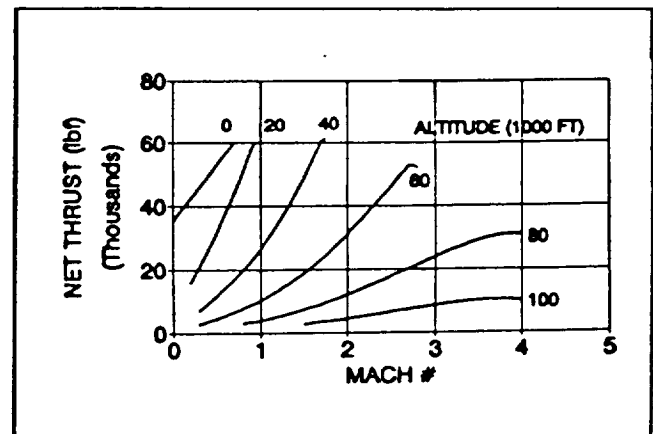


Fig. 9 Engine performance

This engine data was incorporated into the trajectory analysis as thrust available. The results of the trajectory analysis were then used to scale the number and size of the engines according to the critical design point.

### Aerodynamics

The aerodynamic analysis of the vehicles was conducted using a variety of methods. Those methods outlined in Nicolai's book, *Fundamentals of Aircraft Design*,<sup>3</sup> and Raymer's book, *Aircraft Design: A Conceptual Approach*,<sup>4</sup> were primarily used along with shock expansion theory and Newtonian methods. The two waverider configurations were approximated by equivalent flat plate delta-wings.

These waverider configurations were created using the MAXWARP program developed at the University of Maryland.<sup>5</sup> The waverider is optimized for a given Mach number and altitude. This makes it ideal for a cruise

vehicle.

The hypersonic aerodynamic characteristics for the lifting-body configuration were obtained using the computer panel code called APAS developed by NASA Langley Research Center.<sup>6</sup> The body geometry was broken down into several meshed surfaces. The code then analyzed them using the tangent cone, tangent wedge, and Dahlem Buck theories.

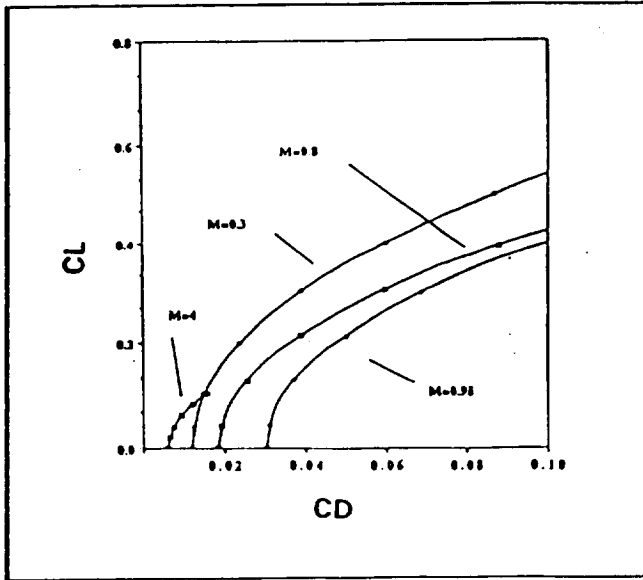


Fig. 10 Drag polar

All of the aerodynamic characteristics were used to generate drag polars for each aircraft (Figure 10). These drag polars were in turn used to produce lift-to-drag ratios for the trajectory analysis (Figures 11 and 12).

Wind tunnel models were constructed for the wing-body and lifting-body configurations. These models were tested in the OSU Low Speed Wind Tunnel. Figure 13 shows the suspension of the wing-body model from the test mount. This arrangement was used to produce experimental lift-to-drag ratios. This experimental data was used for correlation with the analytical results.

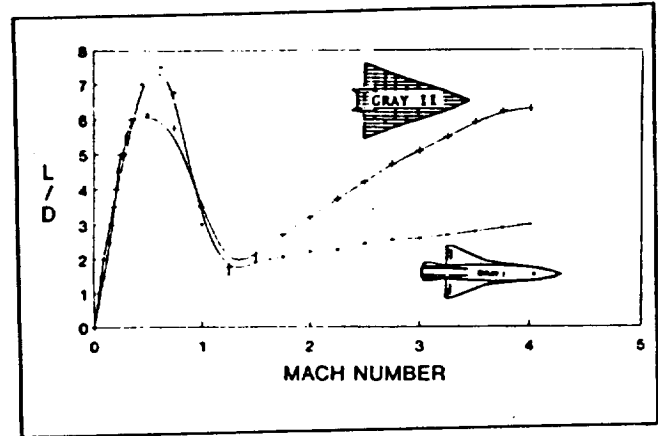


Fig. 11  $L/D$  vs. Mach number

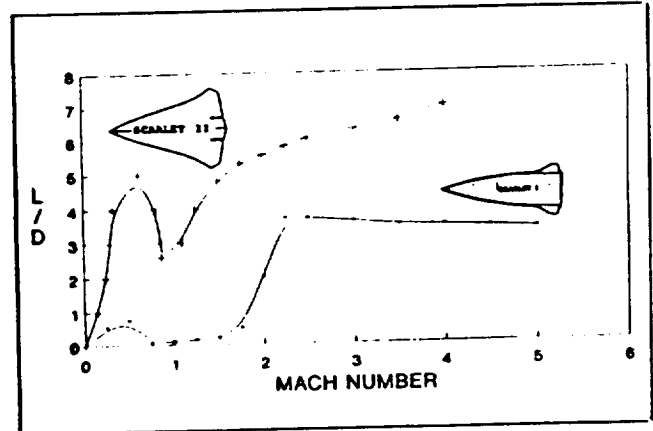


Fig. 12  $L/D$  vs. Mach number

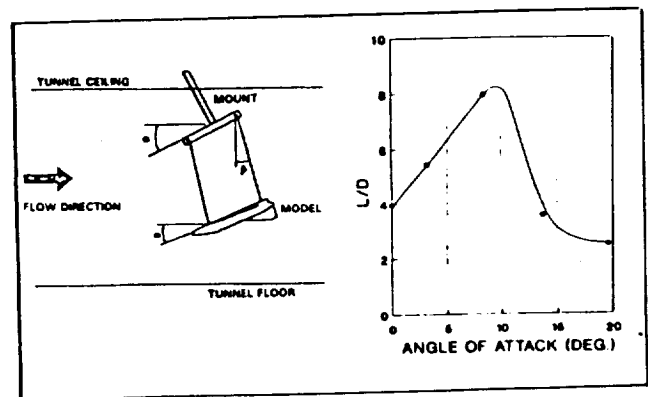


Fig. 13 Wind tunnel testing

## Weight

The component weight analysis for the aircraft was obtained using the WAATS<sup>7</sup> and HASA<sup>8</sup> computer programs provided by the NASA Lewis Research Center. These programs used aerodynamic geometry and propulsion parameters as inputs. The weights calculated in this fashion were used in the trajectory analysis. As the design iteration process continued, these inputs were updated to recalculate the weights.

A component weight breakdown for each aircraft is shown in Figure 14. The fuel weight comprises over fifty percent of the total weight for all the aircraft. This is expected for a cruise vehicle. The two GRAY aircraft are much heavier than the two SCARLET aircraft. This is mostly due to the greater range (12,000 nmi) of the GRAY aircraft. The use of airborne refueling produces a lighter weight of 281,000 lbs for the GRAY I aircraft compared to 558,000 lbs for the GRAY II aircraft. The air-launched SCARLET I and the sea-launched SCARLET II aircraft have almost identical weights of 130,000 lbs and 100,000 lbs respectively.

## Trajectory

The trajectory analysis is the core of the aircraft design process. The propulsion, aerodynamic, and weight data are used as inputs to determine the aircraft's ability to meet the mission requirements. If these requirements are not met, then the previous propulsion, aerodynamic, and weight data must be updated and the cycle repeated until a viable design is produced. Once an aircraft that satisfies all requirements has been obtained, optimization procedures are used to produce the best possible design according to determined design goals.

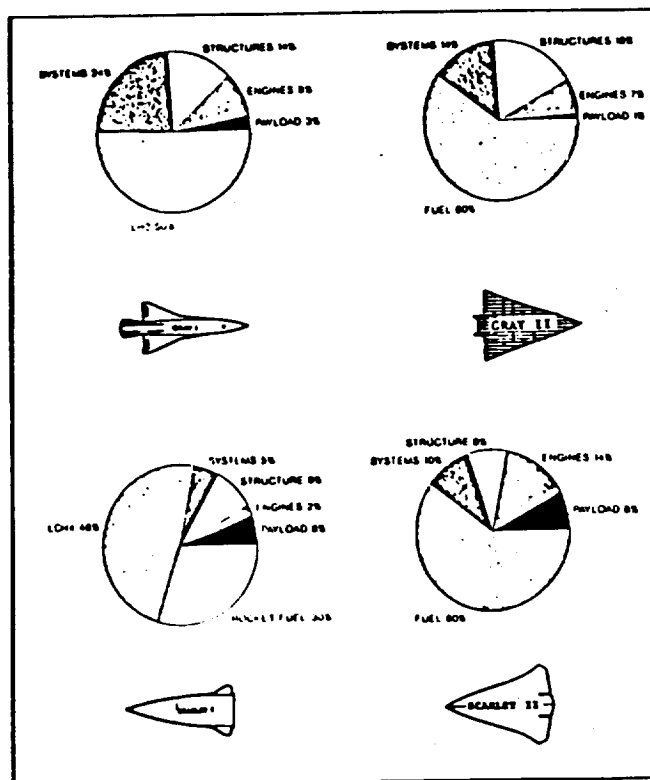


Fig. 14 Total weight breakdown

All four hypersonic reconnaissance aircraft follow very similar mission profiles. After takeoff or launch, the aircraft climb and accelerate toward Mach 1. The aircraft must punch through the transonic region. They then continue to accelerate and climb at a constant dynamic pressure up to cruise altitude and speed. After cruising the required mission range the aircraft descend, possibly at the maximum lift-to-drag ratio, until landing. Figure 15 shows the mission acceleration profile for the GRAY II aircraft. In this case the aircraft executes a constant specific energy dive to pass through the transonic region. This allowed the team to reduce the size of their aircraft's engines and thereby reduce the overall weight of their aircraft.

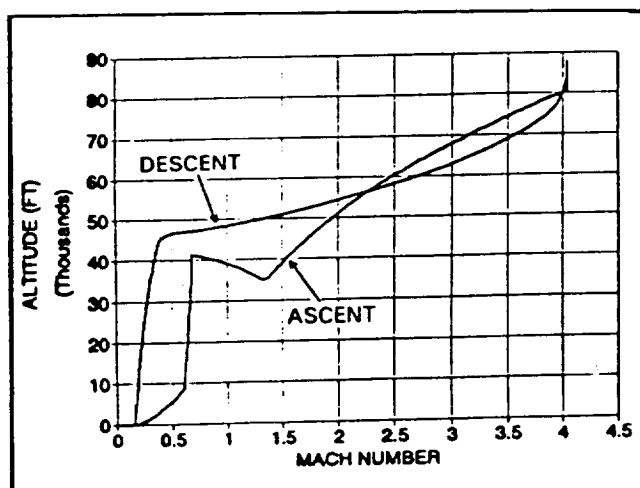


Fig. 15 Mission acceleration

A viable aircraft design is one for which the thrust available is greater than the thrust required throughout the mission trajectory. The thrust available is the maximum net thrust produced by the engines at determined flight path altitudes and mach numbers. The thrust required is the minimum thrust to allow the aircraft to climb and accelerate through a determined flight path. Figure 16 shows curves of thrust available and thrust required versus Mach number for the GRAY I aircraft. If the thrust available curve fell below the thrust required curve at any point then the design parameters would be changed and another analysis conducted. The closest point between the two curves is the critical design point. The aircraft's engine system is sized for this region.

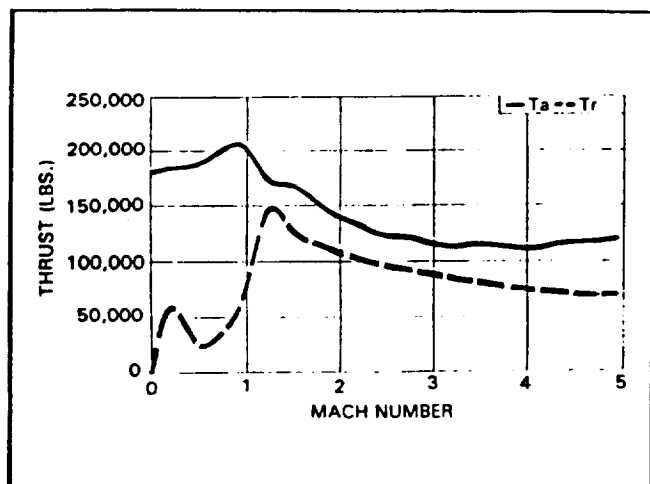


Fig. 16 Thrust available and required vs. Mach number

The GRAY I team chose to optimize further their ascent trajectory. This was accomplished using energy-state methods. The curves shown in Figure 17 are specific fuel consumption contours. Specific fuel consumption is defined as the change in specific energy with respect to the change in fuel weight.<sup>4</sup> These contours are plotted along with constant total energy curves not shown in the figure. The points where the two sets of curves become tangent mark the minimum fuel-to-climb trajectory. This minimum fuel-to-climb flight path is followed until it intersects the constant dynamic pressure flight path. Since the weight of fuel was found to have a significant effect on the total weight of the aircraft, this trajectory minimized the total weight.

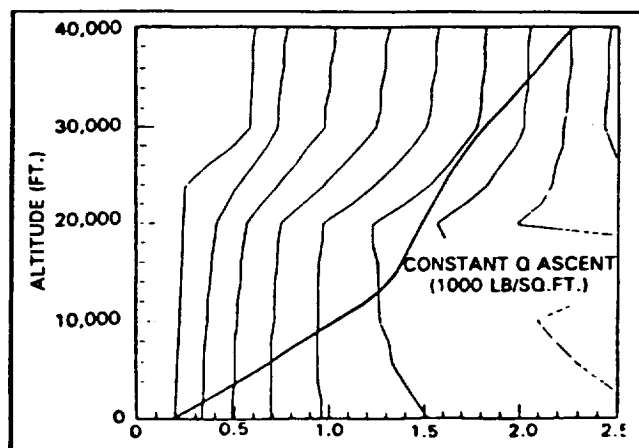


Fig. 17 Minimum fuel-to-climb rate

### Conclusion

Four conceptual designs of hypersonic reconnaissance aircraft have been completed by independent student design teams. These aircraft were designed to provide the U.S. with a flexible and reliable system to collect intelligence data around the globe within hours. This type of aircraft is seen as a next generation replacement of the Lockheed SR-71.

Table 3 compares the four different aircraft designs. There is a large difference in total weights of the two manned and the two unmanned aircraft. This is due to the difference between their respective ranges. The addition of two crew members and a cockpit is only a very small fraction of the total weight. The real differences between the two cases are operational and economic



factors that still need to be examined.

The capability of airborne refueling contributed to an aircraft with a total weight of approximately fifty percent less than one without it. The problems of airborne cryogenic refueling were studied by the French design team from EPF.

There are still questions to be answered and details to be added to these conceptual designs. But, this project has achieved its goal. The students have discovered the cooperation and compromise necessary to conduct multidisciplinary design in a team effort.

### References

1. Roskam, J. Airplane Design, University of Kansas, 1986.
2. Burkhardt, L. and Franciscus L. "RAMSCRAM - A Flexible Ramjet/Scramjet Engine Simulation Program." Technical Manual, 1990.
3. Nicolai, L.M. Fundamentals of Aircraft Design, San Jose, CA: METS, Inc., 1974.
4. Raymer, Daniel P. Aircraft Design: A Conceptual Approach, AIAA, 1989.
5. Corda, S. "Viscous Optimized Hypersonic Waveriders Designed from Flows over Cones and Minimum Drag Bodies," University of Maryland, 1988.
6. NASA Langley Research Center. APAS Computer Software, 1991.
7. Glatt, C.R. "WAATS - A Computer Program for Weights Analysis of Advanced Transportation," CR-2420, 1974.
8. Harloff, G.J. and Berkowitz, B.M. "HASA - Hypersonic Aerospace Sizing Analysis for the Preliminary Design of Aerospace Vehicles." CR-182226, 1988.

Table 3 Aircraft specifications

|                       | GRAY I                        | GRAY II               | SCARLET I                    | SCARLET II            |
|-----------------------|-------------------------------|-----------------------|------------------------------|-----------------------|
| Configuration         | Wing-body                     | Waverider             | Lifting body                 | Waverider             |
| Planform area (sq ft) | 3,000                         | 13,475                | 854                          | 2,300                 |
| Cruise speed (kts)    | Mach 5.0                      | Mach 4.0              | Mach 5.0                     | Mach 4.0              |
| Cruise altitude (ft)  | 92,000                        | 80,000                | 80,000                       | 80,000                |
| Mission time (hrs)    | 3.0                           | 5.5                   | 2.1                          | 3.0                   |
| Total weight (lbs)    | 281,000                       | 558,000               | 130,000                      | 100,000               |
| Engines               | 3 integrated turbojet/ramjets | 6 augmented turbojets | 4 rocket/ramjets             | 2 augmented turbofans |
| Fuel                  | LH <sub>2</sub>               | LH <sub>2</sub>       | LO/LH <sub>2</sub> + methane | JP-X                  |

## DESIGN OF A REFUELING TANKER DELIVERING LIQUID HYDROGEN

Ecole Polytechnique F  minine  
Paris, France

Professor Daniel Lourme  
Caroline Barnier, Sabine Faure, Marie-H  l  ne Pompei, and Karine Pruniaux

### Abstract

A refueling tanker that could deliver 155,000 lb of liquid hydrogen to a hypersonic tanker in 15 min was designed. A flying boom system was chosen to fit strict delivery criteria. Tank design and material specification were also addressed. To assure the flow required, it was important to cancel the pressure drop phenomenon. Geometry, aerodynamics, weight considerations, propulsion, stability, and performance for the tanker were also considered. Finally, the cost of developing three prototypes was estimated.

### Introduction

Ecole Polytechnique F  minine designed a refueling tanker to deliver liquid hydrogen to a hypersonic aircraft designed by a team from the Ohio State University.

The aircraft had to comply with the following requirements:

|  |   |
|--|---|
| Refueling altitude                           | 40,000 ft   |
| Refueling Mach number                        | $M = 0.8$   |
| Fuel transferred                             | 155,000 lbs of liquid hydrogen (LH <sub>2</sub> ) |
| Range to rendezvous                          | 2000 Nm   |
| Total range                                  | 4500 Nm   |
| Time spent refueling                         | 15 min  |
| Maximum take-off and landing runway distance | 14,674 ft   |

In order to choose an appropriate aircraft to carry out such a mission, it was important to know the characteristics of the LH<sub>2</sub> tanks. Once the dimensions (particularly the weight and the length) were known, we were then able to design the aircraft. It is for this reason that the first part of this paper deals with the refueling system and the liquid hydrogen tanks, whereas the second

part presents the characteristics of the aircraft (geometry, weight estimation, aerodynamics, performance, mission).

### The Refueling System

There are two principal types of refueling systems:

- The probe and drogue system consists of a long flexible tube ending in a mesh covered cone. This system enables simultaneous refueling of up to three aircraft at the same time, but the flow rate is rather low.
- The flying boom system consists of a telescopic extension that is guided into the receiving aircraft's refueling receptacle. This system allows a higher flow in the boom.

As our aircraft has to deliver 155,000 lb of fuel in 15 minutes and since the density of the LH<sub>2</sub> is 4.42 lb/ft<sup>3</sup>, we chose to use a flying boom.

### Calculation of the pressure drop

Once the refueling system was chosen, we had to evaluate the pressure drop in the system in order to find the pressure of the LH<sub>2</sub> tanks.

Our calculation was based on the comparison with the KC-10's pressure drop:

$$\Delta P = 2.84 \text{ bars}$$

### LH<sub>2</sub> tanks

Table 1 gives the dimensions of the three tanks.

Table 1 Tank dimensions

|               | Diameter | Length   | Volume                 |
|---------------|----------|----------|------------------------|
| Tank 1        | 11.48 ft | 49.21 ft | 5,085 ft <sup>3</sup>  |
| Tanks 2 and 3 | 19.68 ft | 49.87 ft | 15,183 ft <sup>3</sup> |

The shapes of the tanks are depicted in Figure 1.

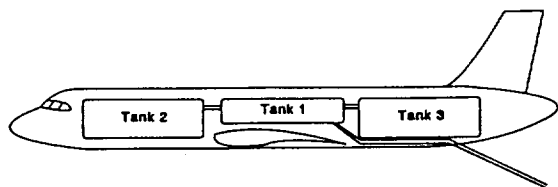


Fig. 1 Refueling tanks

The tanks were made of Al 2219; because of the temperature of the LH<sub>2</sub> (20° K), they were insulated with polyurethane foam. Tank weights are shown in Table 2.

Table 2 Tank weights

|               | LH <sub>2</sub> (lb) | Al 2219 (lb) | Insulation (lb) |
|---------------|----------------------|--------------|-----------------|
| Tank 1        | 22,480               | 4,011        | 2,292           |
| Tanks 2 and 3 | 67,000               | 11,990       | 2,369           |

To assure the flow required, it was important to cancel the pressure drop phenomenon. The tanks were insulated so that the pressure inside them would rise naturally from 1 bar (initial pressure of the LH<sub>2</sub> when filling the tanks) to 1.5 bar (pressure needed in the tanks of the refueled aircraft). We injected gaseous hydrogen to assure the rise from 1.5 bars to 4 bars (1.5 + 3 bars of pressure drop). In order to obtain this gaseous hydrogen, a small quantity of LH<sub>2</sub> was heated before going through a compressor.

## Main Aircraft Characteristics

### Geometry

A three-view of the aircraft is depicted in Figure 2. The main dimensions of the aircraft include 1) a wing area of 7,750 sq ft, 2) wing span of 268.47 ft, 3) length of 252.95 ft, and 4) fuselage width and height of 22.96 ft.

### Aerodynamics

The aerodynamic coefficient was calculated and plotted in Figure 3, which shows drag vs lift.

### Weight estimation

Weight estimation utilized a method from Aerospatiale. The weight estimates shown in Table 3 include an assumption that the structural weight would be reduced about 5 per cent in the next ten years.

Table 3 Aircraft weight estimation

|                                     |            |
|-------------------------------------|------------|
| Glider                              | 352,888 lb |
| Propulsion                          | 62,924 lb  |
| All mission accommodations          | 18,424 lb  |
| Accommodations according to mission | 54,023 lb  |
| Crew                                | 750 lb     |
| Fuel                                | 405,116 lb |
| Variable payload                    | 155,000 lb |
| MTOW                                | 848,765 lb |
| EW                                  | 448,655 lb |

### Propulsion

Our aircraft has four engines, each with a nominal thrust of 57,000 lbs. Three engines are suitable: 1) Pratt & Whitney PW 4000, 2) Rolls Royce RB 2111, or 3) General Electric CF6-80 C2.

### Stability

The stability of an aircraft depends on the position of the center of gravity compared to the aerodynamic center. To insure stability, the center of gravity should be in front

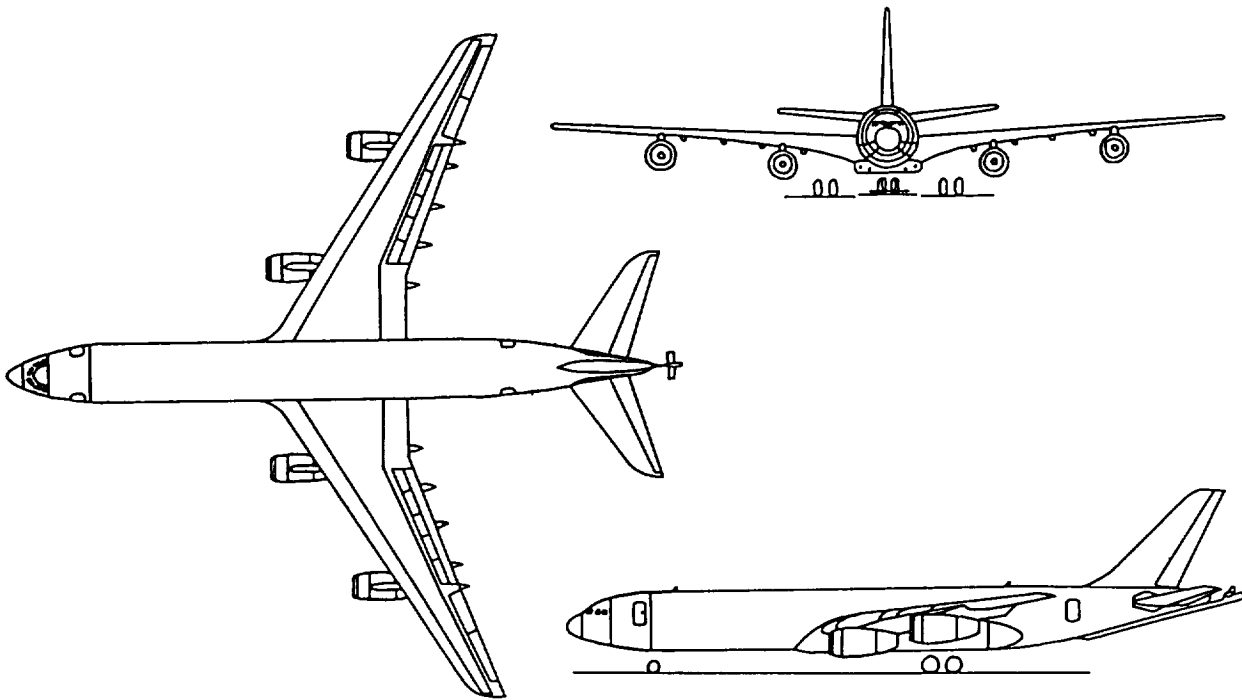


Fig. 2 Three-view of the refueling tanker

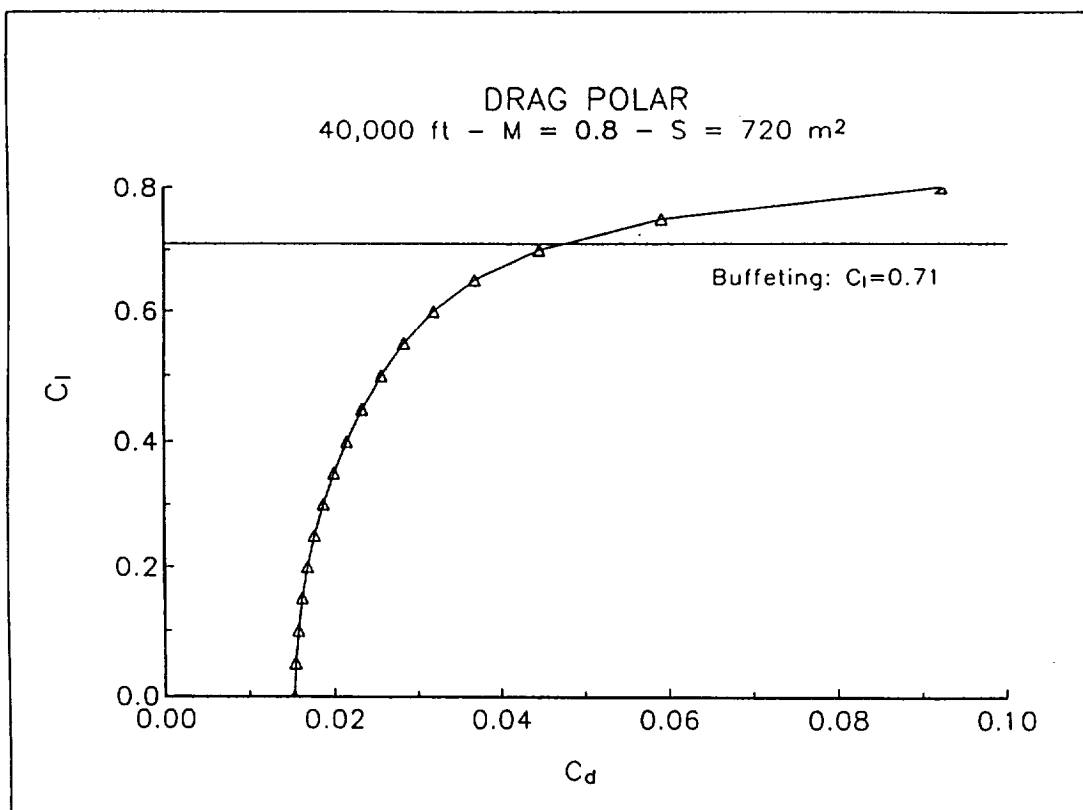


Fig. 3 Calculation of the drag polar

of the aerodynamic center by 10%. The aerodynamic center was calculated to be at 134.77 ft using a method from Aerospatiale. The center of gravity of the aircraft was estimated based on component weights and locations; the c.g. was calculated to be 130.77 ft from the nose of the aircraft.

This puts the relative position of the center of gravity from the aerodynamic center at 10.51%. In order to obtain this value, the wings of the aircraft must be placed at 55% of the length of the cabin.

### Aircraft Performance

The refueling aircraft must travel a distance of 2000 Nm at an altitude of 40,000 ft and a cruise Mach number of 0.8 to deliver 155,000 lbs of liquid hydrogen to a hypersonic aircraft in less than 15 minutes. These strict performance requirements are presented in Figure 4.

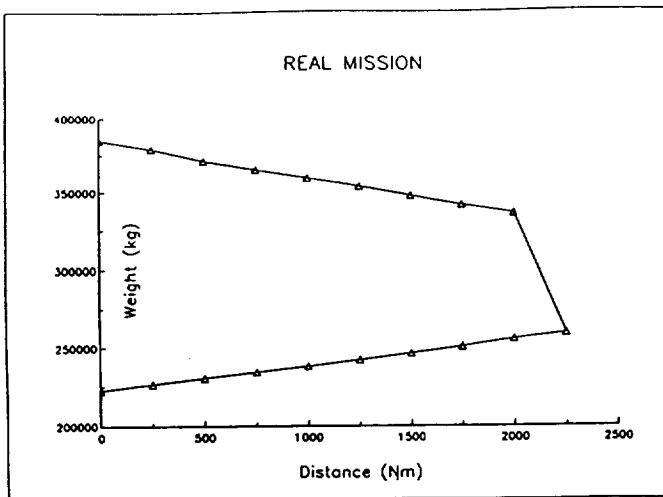


Fig. 4 Real mission profile

### Conclusion

The optimal aircraft designed by the EPF team has the following characteristics:

|           |            |
|-----------|------------|
| Wing area | 7750 sq ft |
| Wing span | 268.47 ft  |
| MTOW      | 848,765 lb |
| Payload   | 155,000 lb |

|                |           |
|----------------|-----------|
| Nominal thrust | 57,000 lb |
| Mach           | 0.8       |
| Ceiling        | 40,000 ft |

Compared to existing civil aircraft, our tanker has a wing area 1.5 times that of the Boeing 747. This factor of 1.5 is due to the requirement of reaching 40,000 ft after having flown 2000 Nm.

We could have chosen to design two smaller aircraft to do the refueling simultaneously, but the tendency in the aircraft world is to design larger aircraft with bigger payloads. Further, we can imagine that in a few years refueling aircraft may become supersonic or even hypersonic. We estimate that it would cost \$38 billion to develop three prototypes of our aircraft.

## THE DESIGN OF A LONG-RANGE MEGATRANSPORT AIRCRAFT

Purdue University  
School of Aeronautics and Astronautics  
West Lafayette, Indiana

Professor Terrence A. Weisshaar  
Carl L. Allen, Graduate Teaching Assistant

### Abstract

Aircraft manufacturers are examining the market and feasibility of long-range passenger aircraft carrying more than 600 passengers. These aircraft would carry travelers at reduced cost and, at the same time, reduce congestion around major airports. The design of a large, long-range transport involves broad issues such as: the integration of airport terminal facilities; passenger loading and unloading; trade-offs between aircraft size and the cost to reconfigure these existing facilities; and, defeating the "square-cube" law. Thirteen Purdue design teams generated RFP's that defined passenger capability and range, based upon team perception of market needs and infrastructure constraints. Turbofan engines were designed by each group to power these aircraft. This paper will review the design problem and the variety of solutions developed.

### Introduction

During 1991 the operating losses of major airlines exceeded the total profits earned since the introduction of jet transportation in the 1950's. Despite this disaster and the worldwide economic recession, the demand for air travel is predicted to resume its growth within the next few years. This growth will be accelerated as the world becomes more economically and politically dependent.

The number of airline revenue passenger miles (RPM) is predicted to more than double by the year 2010. Boeing predicts that the number of available seat miles (ASM) will increase by more than 180 percent to meet air travel demands in the year 2010.<sup>1</sup>

The increased air travel demand will be an opportunity for airlines to increase revenues and an opportunity for airframe manufacturers to sell airplanes. On the other hand, increased traffic may also place a burden on airports around the world, many of which are at or near traffic saturation levels.

To take advantage of increased traffic, while recognizing airport congestion difficulties, airlines are considering new airplanes with more than 150% the capacity of the Boeing 747-400. Predictions for the number of new large transports needed by 2010 range as high as 550 units.<sup>2</sup>

The new large capacity airliners have been referred to as "super-jumbos," "megatransports," or "megajets." We will use the term "megatransport" because it conjures up visions of large size and weights. The term "mega" refers to the projected take-off gross weight (TOGW) of these aircraft, a number expected to exceed 1,000,000 lbs.

The megatransport efficiency will place them in competition with existing Boeing 747 designs, the proposed MD-12 and possible new SST's being proposed for long-range use. Although both competitors have smaller seating capacities, the SST is faster and as productive, while the subsonic 747 models are proven items.

This paper reviews the design challenge, its objectives and its constraints, and summarizes some of the solutions developed by student design teams. It begins with a discussion of the market needs and the economic risks involved in such a project. It then summarizes some of the different approaches taken to solve the problem and the difficulties faced by the design teams. Finally, some "lessons learned" are discussed at the end of the paper.

### Design Problem - Markets, Needs, and Constraints

Design addresses a customer need and proposes a solution. The consideration of need requires an answer to the question "Where are the markets for large capacity, megatransport airliners?" The answer to this question will determine the minimum range of the new aircraft.

#### Markets

First of all, domestic markets were considered, but these markets concentrate on frequent service and have nowhere near the number of passengers per flight to justify a large capacity aircraft. If a plane with large capacity is operated at low passenger load factors, then economic disaster for the airline is certain.

Overseas markets with high demand but only a few flights a day appear to have the most potential for generating revenue. The fastest growing markets for North America appear to be in the Pacific Rim region. The economic growth there indicates that this trend will continue.

Table 1 shows a prediction of the ASM categories by routes for U.S., European, and Asian airlines.<sup>1</sup>

Table 1 Percentage of total available seat miles by airlines to and from three regions (1991 value / 2010 forecast)

| Travel to/by  | US Airlines | European  | Asian     |
|---------------|-------------|-----------|-----------|
| North America | 61% / 56%   | 32% / 26% | 28% / 28% |
| Europe        | 21% / 20%   | 40% / 36% | 17% / 28% |
| Asia-Pacific  | 12% / 20%   | 12% / 27% | 47% / 41% |

The design teams found that most attractive city pairs could be serviced with an aircraft whose range was 7000 nautical miles (New York/Hong Kong). The fuel fraction (ratio of fuel weight to take-off gross weight) for long flights is very large, even if the aerodynamic efficiency is high and the engine thrust specific fuel consumption (TSFC) is low.

Airlines are known to favor buying aircraft with range equal to the B-747. On the other hand, the design teams felt that extreme range was an expensive objective. As a result they focused on high passenger loads at the expense of extreme range. Even then, the aircraft TOGW is in the 1,000,000 lb weight class compared to the B-747 aircraft with 850,000 lbs at take-off.

#### Special problems - technology and terminals

The long-range markets with high passenger demand are currently served by B-747, DC-10 and MD-11 aircraft. Boeing 747 class airplanes are very large. They are not only the competition for the megatransport, but they are the standard for designing terminal facilities and runways. Further increased size might require modifications to runway thicknesses and widths, taxiways and terminal facilities. The primary considerations are:

- landing gear design to prevent damage to the concrete runways and provide capability to fit on runways

- airport gates and runways built to accommodate wingspans less than 220-240 feet constrain the span of the megatransport wings

- logistics of quickly loading or unloading as many as 700 passengers. This includes terminals and emergency conditions.

Changes in the existing infrastructure would be costly and something the airlines cannot afford. If one accepts the infrastructure as a constraint, the design of a megatransport aircraft requires consideration of design drivers not normally considered in conventional aircraft design.

In addition, this design effort requires careful use of the database generated for smaller aircraft.

The large size of a transport with passenger capability exceeding the B-747 also places demands on technology, including structures, manufacturing, landing gear, and passenger configuration.<sup>3</sup>

#### Unique megatransport design issues

There are other design issues related to the size of this aircraft. These issues provide a challenge and may be summarized as follows:

**Defeating the "Square-Cube Law"** The so-called Square-Cube Law states that, for similar structures of different scale, the load (assumed to be proportional to weight) increases as the cube of linear dimensions, while the cross-sectional areas that resist the load increase as the square of the linear dimension. As a result, the stress increases as the linear dimension. For instance, doubling size doubles the weight.<sup>4</sup>

This law says that if structural loads depend upon vehicle weight, then the load increases with the volume (cube of the scale dimension) of the object while the load carrying area increases as the square of the scale dimension. As a result, the stress increases with the scale of the object.

If we simply double the size of an object, then the stresses double. Eventually there is a physical limit to size for which no material can be found. The square-cube law has been held in check by finding new materials, increasing the wing loading of aircraft and reducing the density of airplanes. In addition, the weight of some items on an aircraft are not functions of scale.

#### Fuselage design (People packaging)

Containment of passengers on a large transport requires less wetted area per unit volume. Safety and comfort require consideration of single and multiple deck configurations. Fuselage design is challenging because of aircraft maximum length constraints imposed by terminal facilities and the requirements for aerodynamic efficiency of the fuselage shape.

The passenger "packaging requirement" motivated team consideration of unconventional fuselage designs such as elliptical cross sections, double deck fuselages, and even dual fuselages.

**Wing design** The use of existing terminal facilities will impose wingspan constraints. This constraint was addressed by using folding wing tips and multiple lifting surfaces, including tandem wings, canard configurations and three surface configurations.



The reader will note that the terminal and infrastructure requirements were treated as constraints. It would be interesting to understand the penalty that these constraints place on the design. However, except for examining the effect of wing span on weight and efficiency, little was done by any of the teams to address this issue.

**Extrapolating empirical relations generated on the basis of smaller aircraft** The database for preliminary design consists of design data from smaller aircraft. Careful use must be made of these formulas.

### Engines

Large transports must have efficient propulsion units. Although newer aircraft such as the Boeing 777 are powered by twin engines, the large TOGW of the megatransport requires more than two engines. All teams chose to use four engines for power. These engines were turbofans with relatively high bypass ratios so that they could meet noise constraints and have TSFC's of about 0.5 at cruise.

The team design TOGW for the aircraft designs range from just slightly below 1 million pounds to about 1.2 million pounds. The propulsion requirements for the size airplane being considered are not met by an "off-the-shelf" engine. The engines used on the Purdue designs were designed to meet the requirements of their airplane. The cycle analysis programs ONX and OFFX, developed by Mattingly and Heiser,<sup>5</sup> were used for engine design and performance predictions.

Large engines create design problems over and above the usual problems of finding an efficient design cycle. The large intakes require severe restrictions on ground clearance. This leaves the designer with a choice of lengthening the landing gear, adopting a high wing design or mounting the engines on top of the wing.

To achieve the typical take-off thrust to TOGW values of 0.30, four engines generating over 80,000 pounds of thrust each are required. Since the FAR 36 noise requirements do not account for growth above 900,000 pounds, the noise requirements for the engines will be much more restrictive than those in force now.

### Inherent advantages of the megatransport

In addition to being more efficient economically, the dimensions and size of the megatransport allow for:

- more efficient use of high strength materials in the structure and more dramatic weight savings if advanced composite materials are used
- increases in aerodynamic efficiency due to the large Reynolds number at which the aircraft operates.

### Cost estimation

To meet the world air traffic needs while remaining economical, the megatransport must have low operating expenses compared to existing aircraft such as the B-747 aircraft. These operating expenses translate into cost per block hour of operation and direct operating costs (DOC) given in terms of cost per available seat mile. The requirement of low DOC for a long-range transport will dictate a design that is efficient in long-range markets as well as for multiple medium range hops.

The estimation of direct operating costs requires an estimate of airplane cost and fuel requirements. The production costs to build the aircraft were estimated using the DAPCA IV model discussed by Raymer.<sup>6</sup> This model estimates cost on the basis of empty weight, production quantity, maximum airspeed, and engine and avionics cost. The production quantity and schedule were set by the teams based on what the market would support, the profit margin, and the estimated cost of capital.

The price of the aircraft was calculated using a cash flow analysis. This calculation considers production cost, quantity and schedule, and the cost of raising capital (interest on borrowed money) to initiate the program. The cost of capital is very important to the success or failure of a commercial venture.

Direct operating costs (DOC) were estimated using a model suggested by the Association of European Airlines. These costs were calculated, using a computer model supplied by Professor J.W. Drake,<sup>7</sup> as cost per block hour, where the total block time is the time required to travel from gate to gate. The input to this model includes mission data such as block time, fuel requirements, cost data for labor rates, fuel prices, engine prices, aircraft purchase price, maximum weight, stage length, payload, and number of crew members.

### Design resources and Organization

Teams were composed of from 5 to 6 members, each with a primary responsibility. There were 5 such teams during the Fall semester and 8 teams the Spring Semester. To address this design problem in the few weeks allotted to each team was a challenge.

The design course at Purdue is one semester long. This allows about ten weeks of group effort to produce a preliminary design after all the basic areas of effort are reviewed. In addition to the emphasis on technical effort, the requirements for communication in terms of writing quality and oral presentations are stressed.

During the two semesters of the academic year, the classes were presented with resources to accomplish their

tasks. Resources consist of reports, papers and data obtained from the summer intern during June-August 1991. In addition, guest lecturers are invited to Purdue to share their expertise.

This year we were very fortunate to host Mr. Bud Nelson of Nelson Associates in Washington and Mr. John Roncz of Gemini Technologies. In addition, Mr. Robert Matson of the USAir Maintenance Facility in Pittsburgh lectured the class on the importance of maintainability in design.

The Thiokol Corporation developed a one-day short course in technical writing and sent Mr. Alan Hanline to lecture to the Fall semester class. Thiokol also sponsored a technical writing award for the Fall and Spring semester design teams.

### Design Summaries

With a knowledge of the market and the effects of aircraft weight and fuel requirements on the success of various designs, the 13 Purdue design teams were free to establish their own requirements for passengers and range. On the basis of market studies and their interpretation of available data, the teams chose to design airplanes capable of carrying 650-750 passengers over ranges of 5800-7000 nautical miles.

Describing each of the 13 team designs individually and in detail is beyond the scope and purpose of this paper. Instead, a few representative aircraft have been selected for examination and highlighted in the discussion to follow.

### Design descriptions

Five of the designs generated during the two semesters will be described. Each of these designs represents a different path taken by students. The design teams produced design solutions that fell into two broad categories. These were referred to simply as "747-ish" and "different."

During the class discussions, a high premium was placed on identifying several possible solutions. Having done this, the teams were encouraged to be practical and tough in their assessment of design possibilities. They were also encouraged to take chances. Some did; some didn't.

An excellent example of the 747-like design is the Hastings 1066, shown in Figure 1. This aircraft was designed to take-off from Denver and cruise for 6830 nmi with 740 passengers at Mach 0.87.

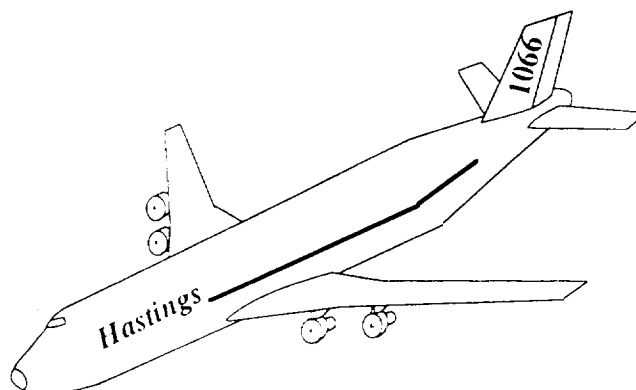


Fig. 1 Hastings 1066

An example of a different design is the WB-670, shown in Figure 2. The WB-670 airplane is a dual fuselage configuration designed to fly 6500 nautical miles with 670 passengers. The cruise Mach number is 0.87.

The dual fuselage design was chosen for two reasons. First, by using two simpler (perhaps existing) fuselages the designers believed that production costs could be reduced. Second, with the current design of airport gates, it would be more efficient to load two smaller fuselages than one large, double deck fuselage. These advantages are realized at the expense of increased wetted area and concerns for aircraft evacuation in emergencies.

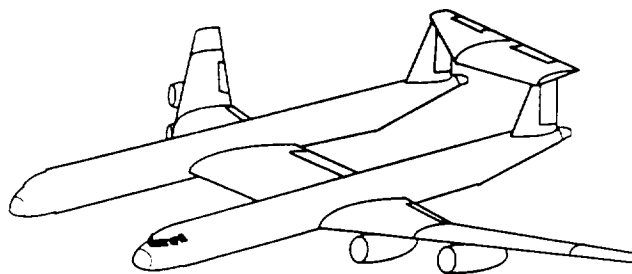


Fig. 2 WB-670 aircraft

The Twin 600, shown in Figure 3, was another different design. This design was generated during the Fall semester and attempted to address the issue of wingspan

constraints. The Twin-600 airplane is a tandem wing configuration designed to fly 6700 nautical miles with 600 passengers at a cruise Mach number of 0.87.

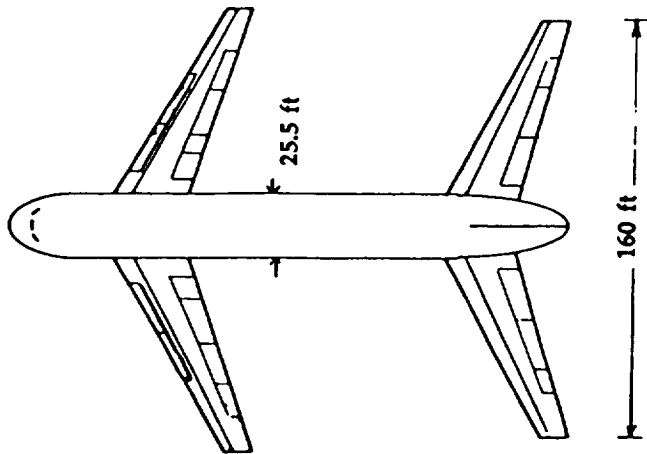


Fig. 3 The Twin 600

The tandem wing design was chosen to provide a wingspan to fit into existing airport gates without the use of folding wing tips. Folding wing tips are optional on the new Boeing 777, but no customer has selected that option. The interference between the two wings was a concern to the team, but the schedule of the class did not permit an extensive examination of this issue.

The advantages of the tandem wing go beyond airport compatibility. Since the wings are smaller, they can be manufactured using proven methods. The root bending moments will be smaller, allowing a lighter wing root structure. Derivatives of this airplane are possible by inserting fuselage plugs *between* the wings.

The JM-90P took up where the Twin 600 left off. This design, shown in Figure 4, attempted to use the interference between the two lifting surfaces rather than to eliminate it. The JM-90P aircraft is a three-surface configuration designed to fly 7000 nautical miles with 608 passengers at a cruise Mach number of 0.87.

The engines on the JM-90P are mounted over the wing to reduce the ground noise levels. Noise regulations are severe at many airports in the US and Europe. The limits set by FAR 36 Stage 3 do not acknowledge weight increases above 900,000 pounds.

The JM-90P design was done during the Spring semester and reflects the influence of Mr. John Roncz on the class. Mr. Roncz, the designer of the Voyager airfoils, urged the class to consider three-surface airfoil solu-

tions to the problem. The DAC-701, shown in Figure 5, was a very successful effort to use interference between the canard and the main lifting surface.

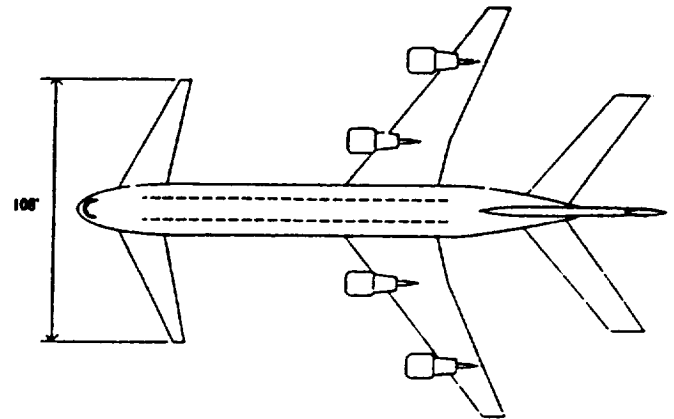


Fig. 4 JM-90P

The JM-90P uses leading edge suction laminar flow control devices in addition to the use of supercritical airfoils. This is expected to increase the drag divergence Mach number and therefore allow less sweep angle. The structural weight savings in the wing is expected to be greater than the increased weight of the laminar flow control devices (including a leading edge bug shield to prevent contamination during take off and landing).

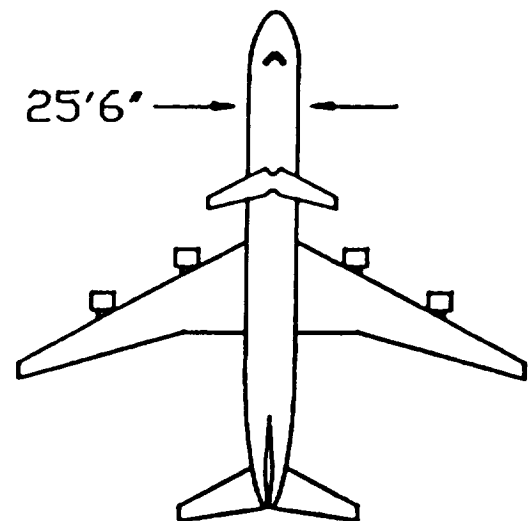


Fig. 5 DAC-701

The DAC-701 airplane, shown in Figure 5, is a three-surface configuration designed to fly 7000 nautical miles, carrying 701 passengers. The cruise Mach number was chosen to be 0.85. The "high-wing" design of the canard was chosen to create wing/canard interference to provide an increased effective wingspan. This increase occurs because the biplane effect will reduce the induced drag on the main wing.

Finally, the LiNK-92, shown in Figure 6, represents an example of a single deck fuselage design and a three-surface design. The high wing design of the Link-92 creates a problem with the carry through wing box, but is nonetheless noteworthy.

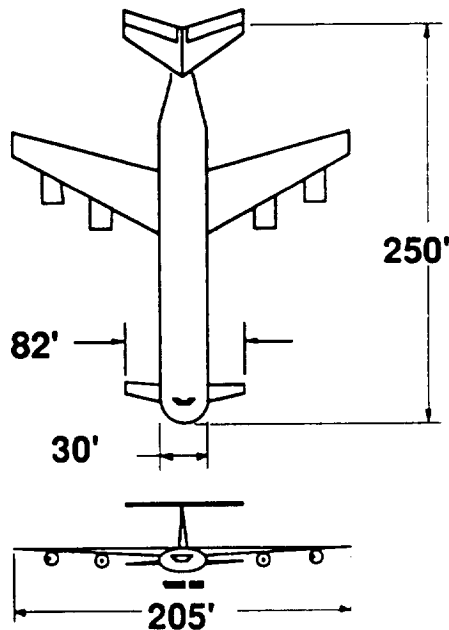


Fig. 6 LiNK-92

The 747-200, 300 and 400 models represent the largest passenger aircraft flying today. The Purdue designs appear to lie very close to this curve fit data. The weights used for the graph in Figure 7 were generated from component weight estimates that reflect design details such as wing geometry.

The fact that the second semester designs lie below the curvefit line in Figure 7 probably reflects a special emphasis placed on composite material use and three-surface design. No one design used advanced composites extensively, but they all took special care to use composites more extensively than used at the present time.

Figure 7 shows operating empty weight plotted against TOGW, plotted in a log-log format. The straight line represents the curve fit for the data base chosen for this study. This data base includes medium range aircraft with large carrying capacity and long range transports such as the Boeing 747-400. Existing aircraft are shown as circles on this graph. Note that not all aircraft used for the curve-fit are shown. The aircraft TOGW are very near 1,000,000 lbs, as predicted in early studies. Note also that these designs do not have exactly the same mission. Lower TOGW is usually indicative of shorter ranges and lower passenger capacities.

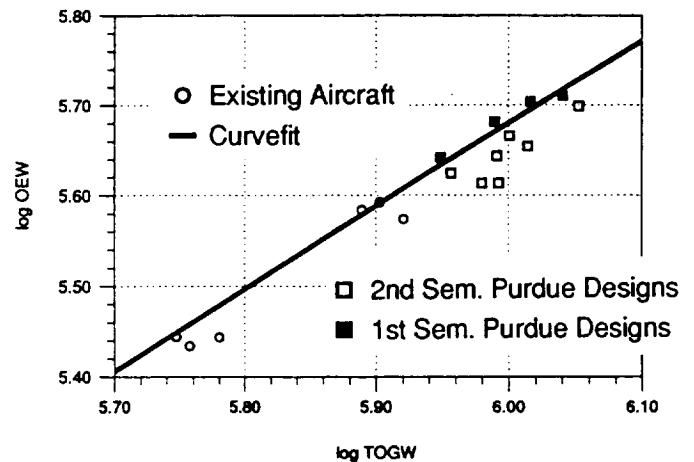


Fig. 7 OEW vs. TOGW - comparison of database and Purdue designs

Range, payload and TOGW data for these representative configurations are presented in Table 2.

Table 2 Range, Payload and TOGW

| Aircraft | range<br>(nmi) | passengers | TOGW<br>(lbs) |
|----------|----------------|------------|---------------|
| JM-90P   | 7000           | 608        | 1033200       |
| LiNK-92  | 6000           | 700        | 904900        |
| DAC-701  | 7000           | 701        | 1128700       |
| WB-670   | 6500           | 670        | 976200        |
| Twin 600 | 6200           | 600        | 977300        |

An indication of size and efficiency of each of these aircraft is provided by the data in Table 3. This table shows operating empty weight (OEW), wing span and direct operating cost per available seat mile, calculated on the basis of the ranges shown in Table 2.

Table 3 Design OEW, wing span, DOC

| Aircraft | OEW<br>(lbs) | wing span<br>(ft) | DOC<br>cents/ASM |
|----------|--------------|-------------------|------------------|
| JM-90P   | 451200       | 197               | 2.96             |
| LiNK-92  | 420800       | 205               | 2.77             |
| DAC-701  | 499800       | 260               | 3.05             |
| WB-670   | 480500       | 250               | 3.30             |
| Twin 600 | 531200       | 175               | 2.77             |

### Fuselage design

The heart of the design of a transport aircraft, as far as the passenger is concerned, is the fuselage. The aerodynamic efficiency, in terms of minimizing drag, requires a slender fuselage. On the other hand, the fuselage cannot be too long so that it cannot fit in terminal areas or move unobstructed on taxiways.

One design considered by several groups was a flying wing. While aerodynamically efficient, the flying wing seats passengers in very wide rows. This makes it difficult to evacuate the aircraft in an emergency. It also makes it awkward to service the cabin in flight.

Fuselage designs finally centered on two configurations. These were the double deck configuration, such as shown in Figure 8, and the single deck configuration shown in Figure 9. In the case of the double deck, the sections considered were either circular or modified ellipses. The circular section is easy to manufacture and resists pressurization more efficiently, while the elliptical section uses material more efficiently.

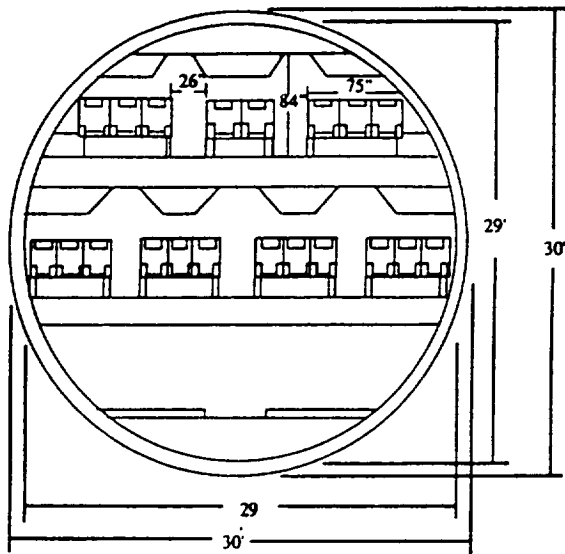


Fig. 8 Double deck fuselage design (Hastings 1066)

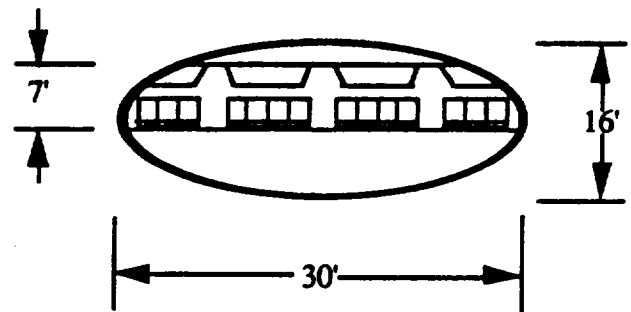


Fig. 9 Single deck fuselage design - (LiNK-92)

In both cases, cargo storage is a criteria, as is the ability to provide a carry-through structure. With so many passengers on board, internal traffic patterns must be considered. Also, the requirements placed on a cargo hold to carry so much baggage are severe. The megatransport then has very little volume for other revenue-producing cargo.

The issue of safety during evacuations is a concern when using the double deck configuration. The exits are high off the ground and require long chutes that weigh more than standard chutes. The issue of evacuation and creative solutions to this problem need to be addressed in the future.

### Engine design

Engine design is an integral part of the senior design course at Purdue. Each group was required to design an engine around a baseline engine provided to them. Design included the design of the engine cycle and included specifying the turbine inlet temperature, compressor pressure ratio, and engine bypass ratio.

Engine design efforts were supported by the ONX and OFFX analysis programs mentioned earlier. The TSFC at cruise altitudes ranged from a low of 0.495 to a high of 0.540. Bypass ratios between 8 and 10 were common.

The design groups used the take-off requirements from Denver on a hot day as their most severe take-off condition. This off-design condition for the engine created a conflict with the desire to cruise efficiently. As a result, the engines generated far more thrust than necessary to take off.

An example of the size of the engine designed for this aircraft is given in Figure 10. This engine, the JG-1996-83K turbofan, was designed by Jason Gries. It is a two-shaft high bypass ratio turbofan with separate converging exhaust ducts. The single stage fan and a 3-stage low

pressure compressor are driven by the same 4-stage low pressure turbine.

This engine can generate 83,500 lbs of thrust at sea level and has a TSFC of 0.554 at cruise. The engine used a turbine inlet temperature of 3100 deg. Rankine at sea level and 2900 deg. Rankine at cruise. The bypass ratio is 8.5.

The weight of this engine is estimated to be 12,150 lbs. This includes the engine core, the nacelle, plumbing and thrust reversers. The total length of the engine is seen to be 14.4 feet with an engine diameter of 10.9 feet. This engine diameter and the fact that the engine is suspended from the wing required a landing gear length of 15 feet for the aircraft to which this engine was attached.

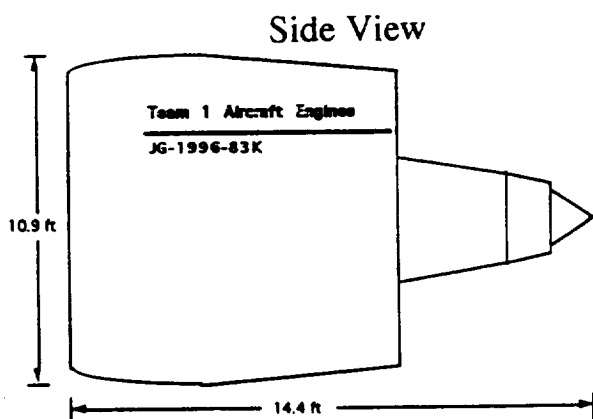


Fig. 10 JG-1996-83K Megatransport engine

## Aerodynamics

For the operator and the passenger, the fuselage is the heart of the airplane. However, for the engineer, it is the wing that makes or breaks the design. The wing design is affected by considerations of performance, such as landing, take-off and cruise. On the other hand, the wing design must take into consideration added weight and the ability to house fuel and landing gear as well as to carry engines.

Most of the team designs used wing loadings near 150 lbs per square ft. This wing loading allows the aircraft to operate efficiently at cruise; however, at landing and take-off leading edge and trailing edge devices must be used to operate at the airfields specified in the RFP's.

The primary trade-offs for wing design are airfoil thickness-to-chord ratio, wing sweep and aspect ratio. In addition, taper ratio is also a consideration.

Wing placement on the fuselage is a consideration also. In the vertical plane of the design, the wing may be placed high on the fuselage, in the middle of the fuselage or low on the fuselage. There are advantages and disadvantages to all of these choices.

The megatransport designs generated by the teams used a variety of wing mounting positions. The high wing position was popular because the engines could be mounted under the wings and still have ground clearance with relatively short gear. In some cases, the low wing position was combined with engines mounted over the wings to take care of ground clearance.

The main problem with high mounted wings is that the engines are mounted in line with the passenger cabin, creating the possibility of noise transmission into the cabin. The teams choosing the high wing did not regard this as a serious problem.

All teams used supercritical airfoils. The cruise Mach numbers were all in the range of 0.87. The designer of the DAC-701 wing, Mark Manglesdorf, used the Roncz TFB-3 airfoil, shown in Figure 11. This airfoil has a drag divergence Mach number about  $M = 0.77$ . It is 13% thick at the 50% chord position. At the design point of  $M=0.75$  this supercritical airfoil is predicted to have about one-third more usable lift coefficient with about one-third less pitching moment, compared to a typical NASA supercritical airfoil.



Fig. 11 Roncz TFB-3 airfoil cross-section

To operate efficiently at the design cruise speed, the wing must trade thickness and sweep. Increasing wing thickness reduces wing weight while it reduces the drag divergence Mach number. On the other hand, increasing the wing sweep will increase the drag divergence Mach number, but will increase the weight. In addition, increasing the wing sweep, all other parameters held fixed, will help the wing fit into gate areas.

Figure 12 shows the Hastings 1066 wing planform. This wing design is mounted low on the aircraft fuselage and has wing mounted engines.

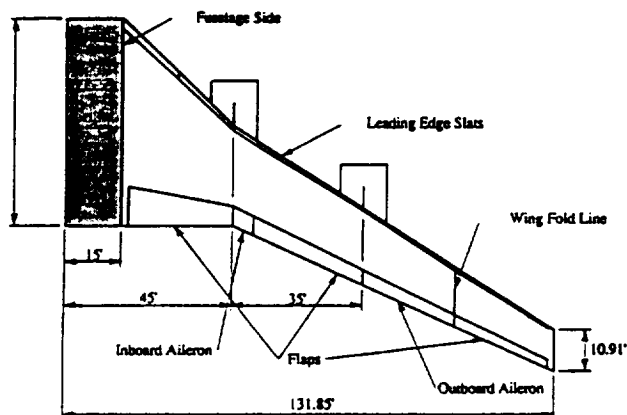


Fig. 12 Hastings 1066 wing planform

This wing has a planform reference area of 7320 sq ft and operates at a cruise lift coefficient of about 0.55. (This compares with the DAC-701 design wing lift coefficient at cruise of 0.49.) The mean thickness to chord ratio of this wing is 0.11, with the wing root being 13%, the thickness at the kink 11%, and the thickness at the tip being 8%.

### Cost and price data

Because the School of Aeronautics and Astronautics has an Air Transportation program, the issues of price and cost of aircraft and the cost of operations are emphasized. Cost of production and cost of operation are fed back to the RFP to make sure that what is being asked for is realistic.

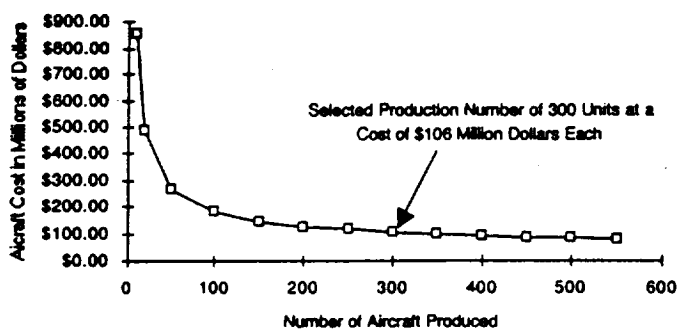


Fig. 13 Aircraft unit cost vs. number produced (JM-90P)

The team member responsible for economic success of the project must choose a price for the aircraft based upon the number of aircraft he/she sees as a market. If the number of aircraft produced is large, then the cost per aircraft and the price per aircraft will be low. Figure 13

shows the relationship of cost per aircraft to the number produced, generated using the DAPCA IV model suggested by Raymer.<sup>6</sup>

As noted previously, the market for this type of airplane is estimated to be about 550 units by 2010. On the other hand, a company cannot be expected to capture the entire market. Design teams estimated as few as 200 units and as many as 400 units that they could sell. As a result, the prices of the aircraft varied from \$144 million to \$179 million. This compares with a price of about \$130-\$140 million for the B-747.

Spreadsheet software has been developed, with the assistance of Professor J.W. Drake, to estimate DOC and to use a cash flow analysis to compute the price of the aircraft.<sup>7</sup> This cost estimation requires a knowledge of basic operational characteristics of the aircraft.

An example of the cash flow analysis used to estimate the price of an airplane is shown below in Figure 14. This figure plots the money invested in the production program as a function of time. During this time, costs are being incurred for engineering and production, but sales of aircraft are only beginning. As a result, the cash flow is out of the company (negative) and a "cash bucket" results.

The price of the aircraft is also sensitive to market conditions. The so-called "cost of capital" or interest rate has a strong effect on the price of the aircraft. Figure 15 shows the effect of this cost of capital on break-even price.

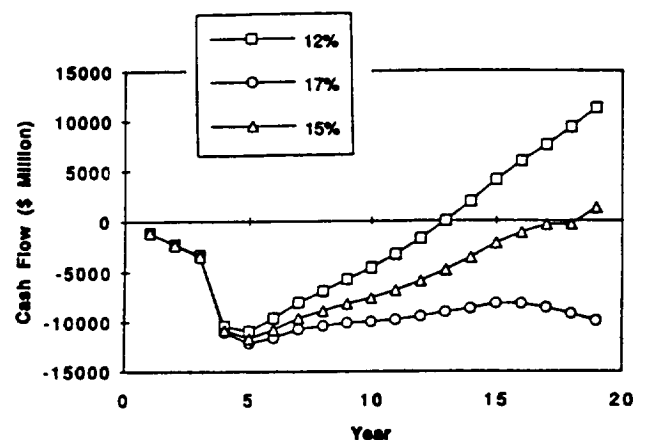


Fig. 14 Cash flow for an aircraft program, plotted against year from program start, at 3 different costs of capital (DAC-701)

The DAC-701 serves as an example of the determination of aircraft price. The selling price for the DAC-701 is \$166 million based on 15% cost of capital. Their program assumed a 19-year production run. The average production cost per aircraft was determined to be \$103.15 million based on a production run of 400 aircraft. The break-even price for their program is \$163.5 million dollars.

### Conclusion

Two Purdue design classes considered the engineering and economic tasks of designing a megatransport aircraft. Market considerations drove the designs to over 600 passengers and ranges greater than 6000 nautical miles.

Due to the emphasis placed upon the use of existing airport facilities, many airplanes were of unconventional design. The use of supercritical airfoils and composite materials was considered as methods of reducing weight. The result was decreased acquisition cost and operating costs.

The megatransport design task requires more careful study of infrastructure/aircraft cost trades. For instance, the decreased operating costs and acquisition costs of the aircraft when wing span and landing gear footprint are allowed to grow should be traded against the cost to reconfigure airports.

As aircraft grow in size, the effect of the square-cube law on the structure absolutely demands a fresh look at advanced, integrated configurations. Most teams accomplished this task, but to differing degrees. The issue of interfering three surface airfoils is the most challenging and has the largest potential for payoff.

In addition, reduced weight from advanced technology, even though risky from a maintenance standpoint, requires a look at concepts such as fly-by-wire and more composite materials in the primary structure.

### Acknowledgments

The opinions expressed in this paper are solely those of the authors and the students involved in this project. In addition, the authors recognize the individual and group efforts of the 73 students who participated in the project. Finally, we wish to acknowledge the support of NASA and USRA for funding provided as part of the Advanced Design Program.

Special thanks to the following teams:  
Fall 1991

Hastings 1066 - Arnold, Boddy, Lee, Muller, O'Keefe, Thomas.

WB-670 - Chlystun, Lighthill, Rose, Stokman, Weissmuller.

Twin-600 - Moore, Pardieck, Sandys, Scheitlin, Vaughn.

Spring 1992

LiNK-92 - Mencone, Myers, Struckel, Weltzer, Winkleman.

JM-90P - Gruber, Minniti, Nebuda, Spangler, Wilson.

TLS-5880 - Alcenius, Courtney, Greenwald, Halgren, Heinemann, Peters.

DAC-701 - Frotton, Jankowski, Manglesdorf, Pongracic, Queiser.

### References

1. "1992 Current Market Outlook - World Market Demand and Airplane Supply Requirements," Boeing Commercial Airplane Group, Seattle, Washington, February 1992.
2. "Outlook for Commercial Aircraft 1991-2010," Douglas Aircraft Company, Market Assessment, Long Beach, California, January 1992.
3. Cleveland, F.A., "Size Effects in Conventional Aircraft Design," Journal of Aircraft, Vol. 7, No. 6, Nov.-Dec. 1970.
4. Keith-Lucas, D. "Defeating the Square-Cube Law," Flight International, Vol. 94, No. 3106, Sept. 1968, pp.440-442.
5. Mattingly, J.D., Heiser, W.H., and Daley, D.H., Aircraft Engine Design, American Institute of Aeronautics and Astronautics, Washington, D.C., 1987.
6. Raymer, D.P., Aircraft Design: A Conceptual Approach, American Institute of Aeronautics and Astronautics, Washington, D.C., 1989.
7. Drake, J.W., Course Notes: AAE 210 - Introduction to Air Transportation, School of Aeronautics and Astronautics, Purdue University, West Lafayette, Indiana, 1990.



# SOLAR POWERED MULTIPURPOSE REMOTELY POWERED AIRCRAFT

Worcester Polytechnic Institute  
Mechanical Engineering Department  
Worcester, Massachusetts

Dr. A. N. Alexandrou, Dr. W. W. Durgin, Dr. R. F. Cohn, Dr. D. J. Olinger  
Charlotte K. Cody, Teaching Assistant  
Agnes Chan, Kwok-Hung Cheung, Kristin Conley, Paul M. Crivelli, Christian T. Javorski,  
Nancy P. Torrey, Michael L. Traver

## Abstract

Increase in energy demands coupled with rapid depletion of natural energy resources have deemed solar energy as an attractive alternative source of power. The focus of this work was to design and construct a solar powered, remotely piloted vehicle to demonstrate the feasibility of solar energy as an effective, alternate source of power. The final design included minimizing the power requirements and maximizing the strength-to-weight and lift-to-drag ratios. Given the design constraints, *Surya* (the code-name given to the aircraft), is a lightweight aircraft primarily built using composite materials and capable of achieving level flight powered entirely by solar energy.

## Introduction

### Mission Requirements

As civilization enters the 21st century, considerations for alternative energy sources are becoming necessary. Natural energy sources such as coal, oil, and fossil fuels are quickly depleting. In addition, they are harmful to the environment. Their use has caused a substantial increase in air pollution, and they have thus been major contributors to the greenhouse effect. Although nuclear energy is immediately available, high operational risks and environmental issues have made it a questionable option. Solar energy is not only pollution-free, but it is also available in abundance. Proper utilization of the sun's energy can result in an inexpensive and effective power source. One of the main objectives of this project was to demonstrate the effectiveness and feasibility of using solar energy to power an airborne vehicle. The final

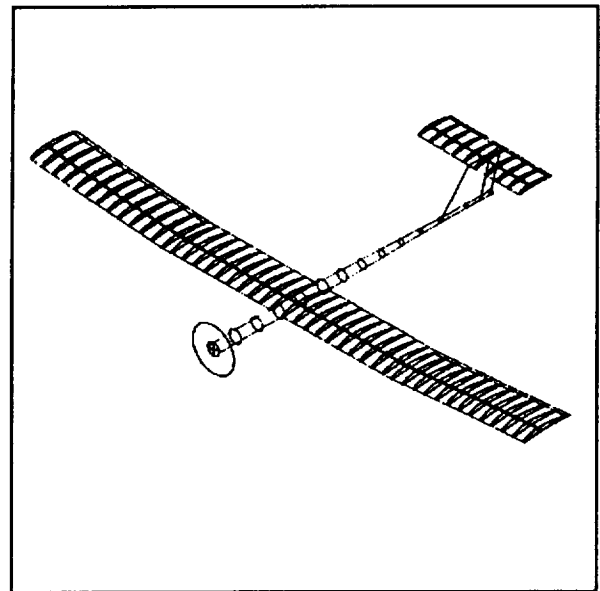


Fig. 1 *Surya* Isometric View

Table 1 General Data

|                     |                    |                           |
|---------------------|--------------------|---------------------------|
| Weight              | $W_{\text{gross}}$ | 40 N                      |
| Wing Area           | $S$                | 1.48 m <sup>2</sup>       |
| Wing Loading        | $W$                | 27.03<br>N/m <sup>2</sup> |
| Aspect Ratio        | AR                 | 8.25                      |
| Wingspan            | $b$                | 3.5 m                     |
| Cruise Altitude     | $h$                | 50 m                      |
| Cruise Velocity     | $V$                | 7 m/s                     |
| Design Lift Coeff   | $C_L$              | 0.83                      |
| Design Lift-to-Drag | $L/D$              | 15.75                     |
| Cruise Power Req'd  | $P$                | 15.9 W                    |
| Design Load Factor  | $n$                | 7                         |

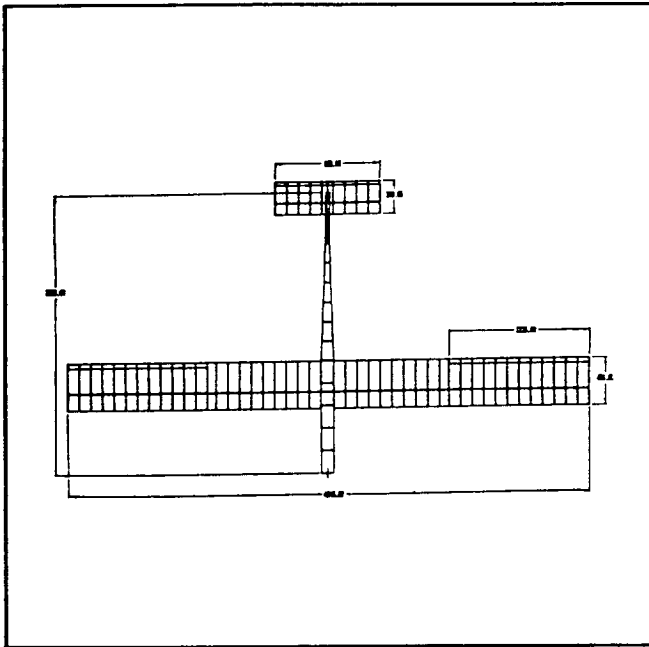


Fig. 2 *Surya* Top View

configuration of the solar plane was optimized for minimum level flight power.

#### Aircraft Configuration

The proposed vehicle is shown in Figures 1 and 2. General data and design parameters are summarized in Table 1.

The wing has a span of 4.5 m, a chord length of 42.4 cm, an aspect ratio of 10.61, and is positioned at a geometric attack angle of 4 degrees. A lift coefficient of 0.8274 is generated by the wing during level flight. The tail is oriented at an angle of attack of 0 degrees and its lift coefficient is 0.4053. The tail efficiency is assumed to be 0.85.<sup>1</sup> The overall configuration has a total lift coefficient of 0.8816, a total drag coefficient of 0.0451, yielding a L/D ratio of 19.548.

The wing design includes a dihedral of 2.5 degrees. The vertical stabilizer has an effective area of 900 cm<sup>2</sup>, the rear half being the rudder. Situated 1.6 meters behind the aerodynamic center of the wing, the horizontal stabilizer spans one meter and is composed of a NACA 6409 airfoil with a 30 cm chord. The rear quarter of this chord is a hinged flap which serves as the elevator. The ailerons are

located on the modular wing sections, occupying the aft 12% of the chord and spanning the entire length. To ensure pitch stability and optimum lift for the plane as a whole, the center of gravity is maintained a tenth of the wing's chord behind its aerodynamic center. The location of the electronics harness in the nose of the fuselage is adjustable and can be moved either forward or backward to insure the center of gravity is positioned to maintain static stability.

A total of 120 solar cells are contained within the wing of *Surya*. This number was determined through required power estimations. Conservative estimates predicted about 100 watts for the array output at any given time during flight. Although this number is rather high, the actual amount of power delivered to the motor and propeller was much less. On an open circuit, the cells developed a potential of 5.8 volts while producing approximately 19 amps of current when short circuited. As load is applied to the array, these values drop to 4.7 volts and between 12 and 14 amps. To produce the required power, 12 arrays containing 10 cells were constructed. The five volt potential is the result of the 10 cells wired in series with each individual cell producing 0.5 volts. The 12 amp current is generated by wiring the 12 sub-arrays in parallel at 1 amp each.

The solar array is split into three rows per wing section. The leading edge row is placed underneath the skin to preserve the integrity of the front part of the airfoil, where it is most crucial. The trailing rows adhere directly to the skin on the outside of the wing to increase power production. The first row sits at an angle of 12° with respect to the chord, while the back rows sit at an angle of 6°. As a result, optimum power is produced by the array during level flight with the plane flying directly away from the sun.

*Surya's* total coefficient of lift was estimated at 0.88, and both the tail and the wing act as lifting surfaces. With a weight of 52 N and an estimated parasitic drag coefficient at 0.148, the plane is expected to have a minimum flight speed of 7.1 m/s and a minimum required power to achieve this speed of 18.8 Watts.

The climb capability of the plane is strictly determined by the amount of excess power available. *Surya's* climb rates vary depending on the output of power from the

solar cells at that time interval, and the position of the plane relative to the sun.

Banking and turning are basic maneuvers at which the plane must remain in level flight. Since the flight velocity of the solar plane is low, the banking angles are small. With small banking angles between 3 and 4 degrees, the turn radii necessary are 89 and 67 m respectively. Hence, the proposed spiral climb scheme for the 50 m altitude climb can be accomplished in about five minutes within a 200 m length field.

Table 2 Wing Component Masses

| Wing                    | Mass (g) | % Wing |
|-------------------------|----------|--------|
| Carbon Composite Spars  | 478.0    | 15.9   |
| Ribs                    | 132.0    | 4.4    |
| Leading Edge            | 116.0    | 3.8    |
| Trailing Edge           | 58.0     | 1.9    |
| Ailerons                | 99.0     | 3.3    |
| Spar Webs               | 44.8     | 1.5    |
| Skin (Mylar)            | 254.4    | 8.4    |
| Wing Tips               | 36.1     | 1.2    |
| Solar Cells             | 1142.0   | 37.9   |
| Servos                  | 43.0     | 1.4    |
| Wiring                  | 148.0    | 4.9    |
| Reinforced Rib          | 158.0    | 5.3    |
| Modular Tube Connection | 107.0    | 3.6    |
| Landing Gear            | 58.0     | 1.9    |
| Miscellaneous           | 139.0    | 4.6    |
| Total                   | 3013.4   | 100    |

### Design and Analysis

#### Aircraft Sizing and Weight Estimation

Preliminary component sizing was dictated by set parameters such as the chosen airfoil, the size of the solar cells, and the desired lift-to-drag ratio. The optimization of the design included the minimization of the power requirements and the maximization of the strength-to-weight and lift-to-drag ratios. The resulting configuration has a wing span of 4.5 m, a tail span of 1 m, and a fuselage

length of 2.5 m. Due to the large span, the wing was constructed in modular sections for storage purposes. Tables 2 through 4 break down the masses of individual elements of the plane showing their percent contribution to each section of the aircraft.

Table 3 Fuselage Component Masses

| Fuselage               | Mass (g) | % Fuse |
|------------------------|----------|--------|
| Carbon Composite Frame | 900.0    | 48.9   |
| Servo                  | 21.5     | 1.2    |
| Wiring                 | 98.3     | 5.3    |
| Motor                  | 245.7    | 13.3   |
| Nose Cone              | 56.8     | 3.1    |
| Propeller              | 42.9     | 2.3    |
| Receiver Battery       | 101.1    | 5.5    |
| Receiver               | 44.0     | 2.4    |
| On/Off Switch          | 63.3     | 3.4    |
| Emergency Batteries    | 238.0    | 12.9   |
| Miscellaneous          | 32.0     | 1.7    |
| Total                  | 1843.5   | 100    |

#### Aerodynamic Design and Analysis

The wing has a rectangular platform with a wing span of 4.5 m and a chordlength of 0.424 m. The aspect ratio of the wing is 10.61 and the geometrical angle of attack is  $4^\circ$ . The wing generates a lift coefficient,  $C_L$ , of 0.8274 at level flight conditions. The tail has a rectangular platform, a tail span of 1 m, and a chordlength of 0.3 m. The resulting aspect ratio of the tail is 3.333. At level flight conditions, the geometrical angle of attack of the tail is  $0^\circ$  and the  $C_L$  is 0.4053. The tail efficiency was assumed to be 0.85.<sup>1</sup> With this configuration, the aircraft has a total lift coefficient of 0.8816 and a total drag coefficient of 0.0451. As a result, the total lift to drag ratio is equal to 19.548.

The chord Reynolds number is relatively low since a solar aircraft has a fairly slow cruise velocity. Theoretically, viscous effects dominate the flow at low Reynolds numbers, thus resulting in flow separation and a laminar separation bubble. However, at Reynolds number of 200,000 or higher, a turbulent boundary layer develops and gives more resistance to flow separation

during the pressure recovery. For this reason, it was decided to operate the plane at a Reynolds number based on the chord of about 200,000. In addition, the effects of compressibility are neglected in the entire aerodynamic analysis, since the Mach number during level flight is much less than 0.3.

The NACA 6409 was chosen as the airfoil section for the wing and the tail. It has a 9% maximum thickness and a 6% maximum chamber at a distance of 40% of the chord from the leading edge. Figure 3 shows the experimental lift and drag characteristic of the NACA 6409 airfoil at the Reynolds number of 200,100.<sup>2</sup> The sectional lift curve slope of the airfoil is about 5.17 per radian between an angle of attack of -0.87 and 7.32 degrees. At an angle of attack of 9.32 degrees, the sectional lift coefficient reaches a maximum value of 1.342. Meanwhile, the sectional drag coefficient varies parabolically and has a minimum drag coefficient of 0.0112 at an angle of attack of 1.20 degrees. The lift to drag ratio of the airfoil is calculated and summarized in Figure 4. As shown in the figure, the airfoil provides a constant high lift to drag ratio between the angles of attack of 2 and 8 degrees and therefore allows for a wide range of favorable operating conditions.

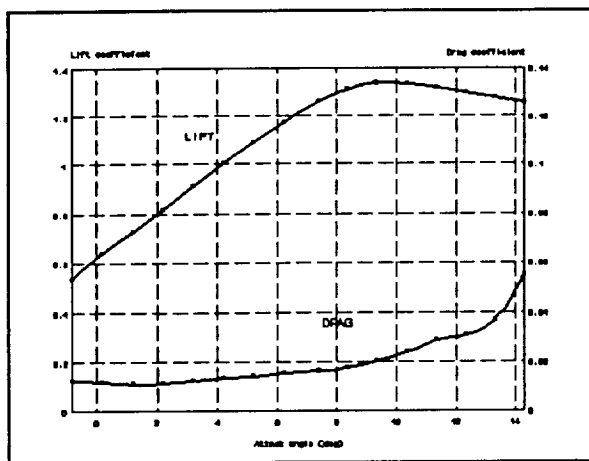


Fig. 3 Sectional Lift and Drag Coefficients

In order to increase the power generated by the solar propulsion system, cells are placed on the surface of the wing. Since the solar cells are flat and not flexible, the shape of the airfoil is slightly changed. As a result, the sectional characteristics of the airfoil are affected. By

using the vortex panel method,<sup>3</sup> the inviscid pressure distribution of the original NACA 6409 was calculated as shown in Figure 5. In the figure, it is clearly shown that the majority of the lift is generated in the front 40% of the airfoil. Therefore, in order to minimize the aerodynamic effects due to the solar cells placement, the cells were placed behind a distance of 40% of the chord from the leading edge (see Figure 6). The inviscid pressure distribution of the airfoil which has the solar cells on the back is shown in Figure 7. At an angle of attack of 4°, the difference between the inviscid lift coefficients of the original airfoil and the one which has solar cells on the back is only about 0.25%.

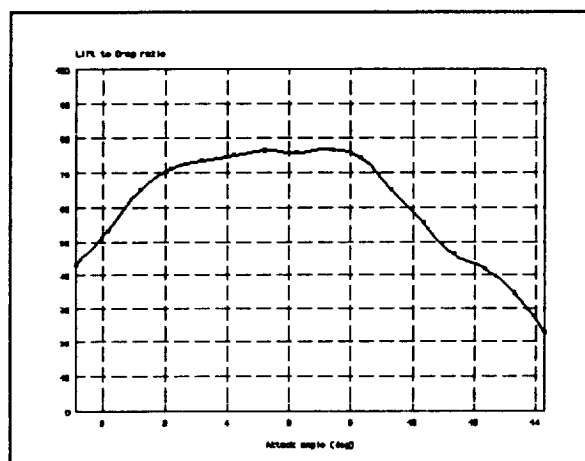


Fig. 4 Sectional Lift-to-Drag Ratio

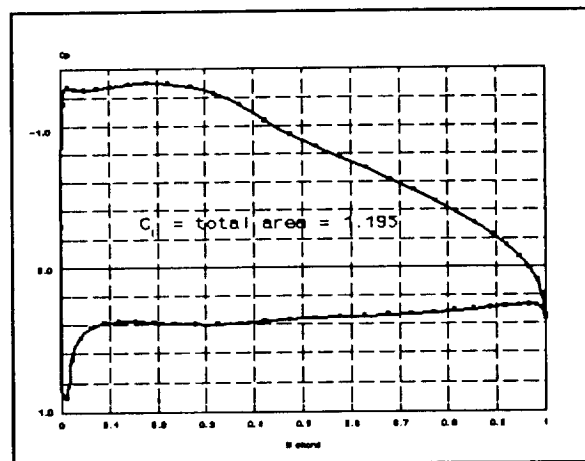


Fig. 5 Inviscid Pressure Distribution

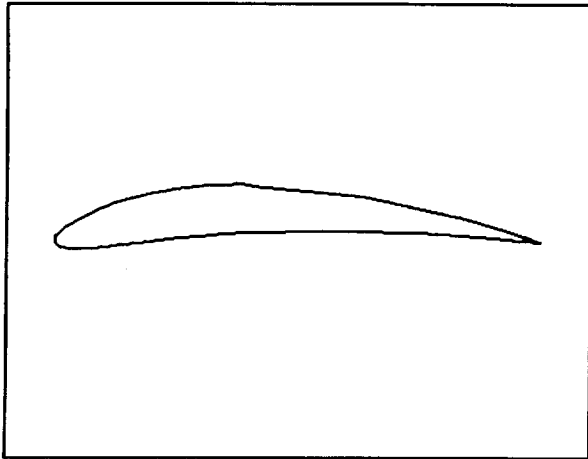


Fig. 6 Modified NACA 6409 with Flattened Back

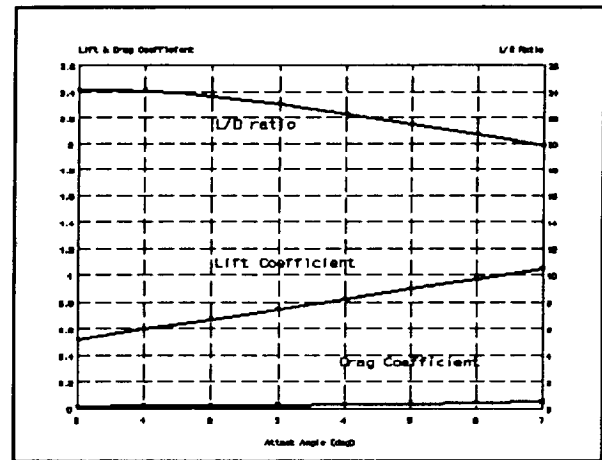


Fig. 8 Lift and Drag Characteristics of the Finite Wing

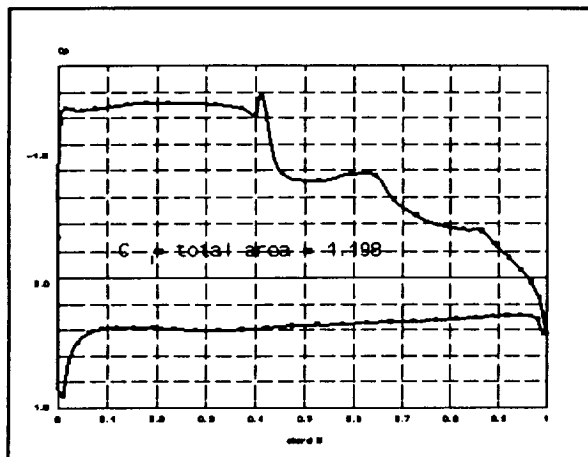
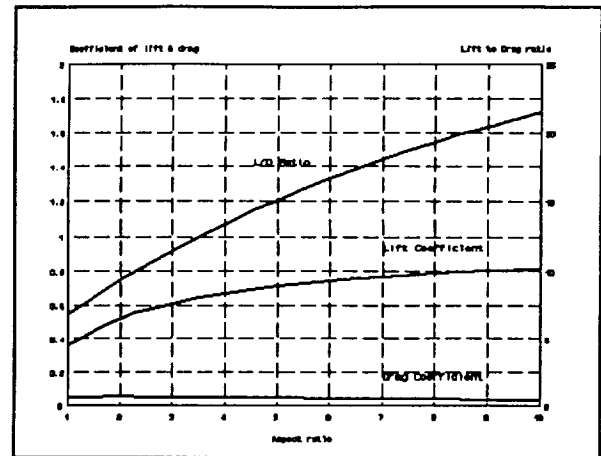
Fig. 7 Inviscid Pressure Distribution  
for Modified NACA 6409

Fig. 9 Effects of the Aspect Ratio on Lift and Drag

Assuming the flow does not separate before the first 40% of the chord, the aerodynamic characteristics of the modified airfoil are apparently similar to the original NACA 6409. Therefore, the experimental data of the NACA 6409 airfoil are assumed to be valid for the design.

Using the Glauert Method and the modified flat plate theory,<sup>1</sup> the finite lift and drag coefficients of the wing and tail are determined. Figure 8 shows the finite lift and drag characteristic of the wing at different attack angles. In addition, the aspect ratio effects or the L/D ratio are

investigated. With a higher aspect ratio, the wing behaves closer to the predicted performance of the airfoil section. As a result, the wing generates more lift and experiences less induced drag. Figure 9 shows clearly that the lift to drag ratio increases while the aspect ratio of the wing increases.

The power required for level flight at different velocities is summarized in Figure 10. As the figure shows, the optimum level flight speed is 6.388 m/s and the corresponding attack angle is 6.77 degrees. At this

condition, the power required for level flight is equal to 18.682 Watts. Due to safety considerations, it was decided to operate at an attack angle of  $4^\circ$ , with the corresponding cruising speed is 7.104 m/s. The required power is 18.839 Watts, which is 0.84% higher than the power required at the optimum condition.

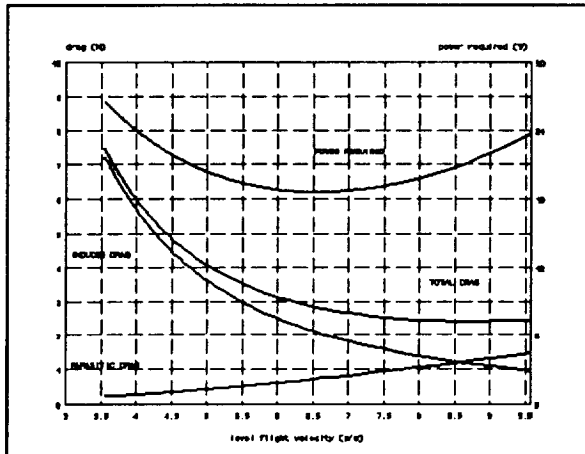


Fig. 10 Power Required vs Flight Velocity

### Structural Design and Analysis

The main supporting structure of the wing is a rigid tube running the length of the span, effectively acting as a wing spar. The outer diameter of the tube was limited by the thickness of the airfoil. The thickness of the tube was determined by a simplified stress analysis of the loads applied to the spar.

A simplified half wing loading model was developed to estimate the maximum stress on the wing spar (see Figure 11). The carbon spar was to assume all of the loads due to the lift generated. The wing was modeled as a cantilevered beam with a distributed load, and a moment load applied at the free end. The lift of 48.3 Newtons was represented by a distributed load of 10.73 N/m acting along the full span. This load produces an effective moment of 5.36 N-m located at the connection point, shown at the free end of the beam. These calculations were adjusted to account for the potential gust load the wing may endure. With a gust load factor of 3, the loads were increased to a distributed load of 32.19 N/m and an effective moment of 16.09 N-m.

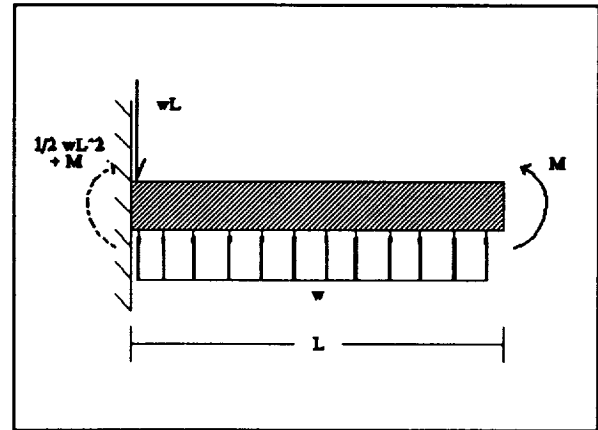


Fig. 11 Wing Loading Model

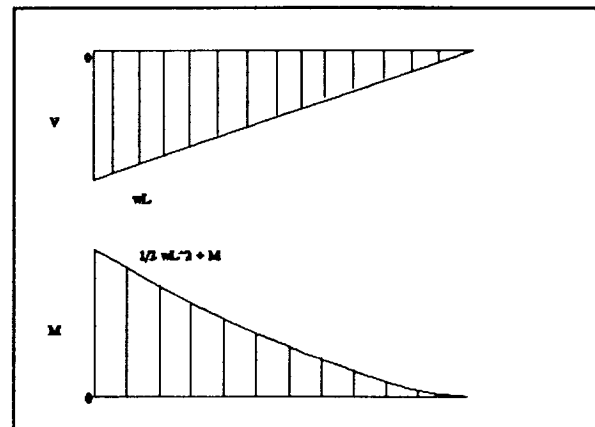


Fig. 12 Shear and Moment Diagrams

The shear and moment distributions of the wing are illustrated in Figure 12. The locations of maximum shear and maximum bending moment were determined from these diagrams, 40.24 N and 41.24 N-m respectively. The maximum normal stress resulting from expected loads and the material properties of carbon fiber were considered; shear stress was determined to be negligible in comparison. Carbon composite spars were constructed and tested to obtain accurate material properties. Considering the maximum expected load and a safety factor of 1.2, the maximum allowable stress for the spar

was calculated and determined to be  $2.75\text{E}+8 \text{ N/m}^2$ . The minimum required spar thickness was iteratively determined. A wing spar having an outer diameter of 20.1 mm, 0.53 mm thickness (3 layers of fabric), and capable of withstanding a maximum load of  $3.303\text{E}+8 \text{ N/m}^2$  was constructed. The tail was modeled and analyzed similarly to that of the wing, differing only by the absence of a moment at the free end. The lift on the tail was calculated to be 3.7 Newtons and a distributed load of  $3.7 \text{ N/m}$  was modeled. The resulting tail spar dimensions are an outer diameter of 1.38 cm and a thickness of 0.53 mm. The sizing of the fuselage was dependent on the placement of the tail and the area required to house the electronics and was determined to be 2.5 meters. The anterior portion of the fuselage is 10.5 cm in diameter, which was determined by an estimation of the size of the electronic components. This diameter gradually decreased with length in order to minimize weight. The posterior segment has a diameter of 3 cm. This value was determined to be the minimum within the margin of safety. The required thickness of the fuselage wall for this design was 0.36 mm (2 fabric layers).

### Material Selection

The material selection process played a key role in the design. Since the limited power available from the solar cells mandated weight minimization, effective material selection was crucial in the design process. While the weight of the structure needed to be minimized, a high strength material was desired to withstand the applied loads. This dictated the use of composite materials because they exhibit a high strength to weight ratio.

Many composite fabrics were tested including carbon, kevlar, and fiberglass. Carbon was selected due to its high strength-to-weight ratio and inherent rigidity. Consequently, the wing spar, tail spar, and fuselage were constructed using this material. Furthermore, a number of different spar configurations were tested to determine the material constraints at different loads. These tests led to the selection of a hollow circular cross-section. Sample hollow rod configurations were tested to determine the thickness of the tube required to withstand the expected stress.

The vertical stabilizer which supports the tail spar was constructed using a foam structure that was reinforced with carbon composite fabric on both sides. The carbon

composite provided the strength needed to support the tail, and foam was used as a spacer.

Since the wing spar was modular, a connecting support was used to form the dihedral angle in the wing and withstand the load applied at the connection. The modular connection supports utilized a foam and carbon composite combination much like that of the vertical stabilizer with foam sandwiched between two layers of carbon composite fabric. Foam was used as a spacer in the vertical stabilizer and modular connection supports because of its low density, making it the most lightweight material used in the plane. The carbon composite fiber and foam combination proved to be ideal when used on components that were designed to withstand pure bending loads. Foam was used to construct components without structural applied loads, such as the solar cell braces, nose cone, and wing tips.

Balsa wood was utilized for many components that sustained small loads and required a precise shape. Since balsa is the lightest of all wood and very easily shaped it was favored over foam. Balsa wood was used for components such as the ribs, the leading and trailing edges, the ailerons, the elevator, and the horizontal stabilizer. The ailerons and the horizontal stabilizer utilized balsa wood in a truss structure designed as an extension of the airfoil.

Heat shrinking mylar was used for vehicle's skin. It was necessary to use a material with a high transmissivity on the top of the wing allowing the sunlight to reach the solar cells underneath the skin, but at the same time the material had to be strong enough to sustain the shape of the airfoil it formed. Another concern about the material of the skin was a desired resistance to tear as deformation of the wing was experienced. Mylar becomes rigid after being heat shrunk over a surface but it remains adequately flexible enough to deform.

### Propulsion System Design and Integration

The modified remote control radio system and the necessary hardware for controlling deflecting surfaces and switches via servo-motor, shown in Figure 13, is the essence of the controls and interface scheme.

The Astro Cobalt 05 electric, geared motor and a two-bladed, folding propeller with a diameter of 33 cm and

pitch of 16.5 cm manufactured by Aero-Haute were chosen for their combined efficiency. A combined contour plot of electrical input power, shaft torque, shaft RPM, and motor efficiency versus voltage and current is shown in Figure 14. Several motor-propeller combinations were tested in the WPI wind tunnel under conditions similar to those in flight. Figure 15 illustrates the results of the tests performed for the chosen motor-propeller combination.

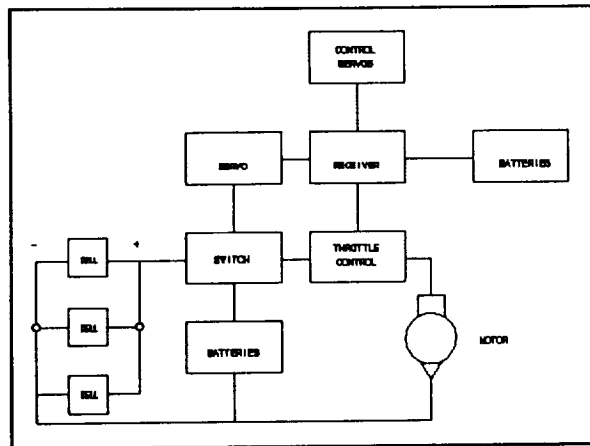


Fig. 13 Controls Layout

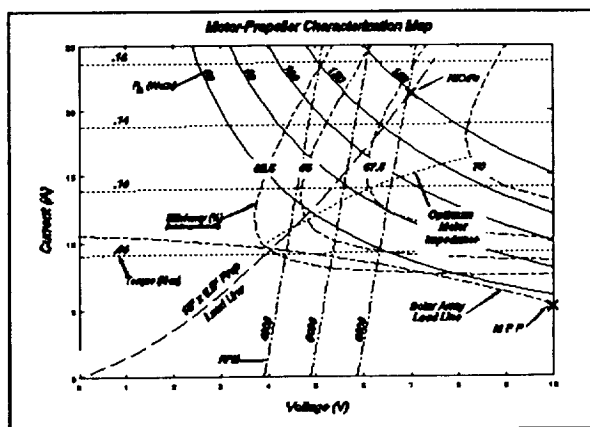


Fig. 14 Combined Contour Plot for Design Motor-Propeller

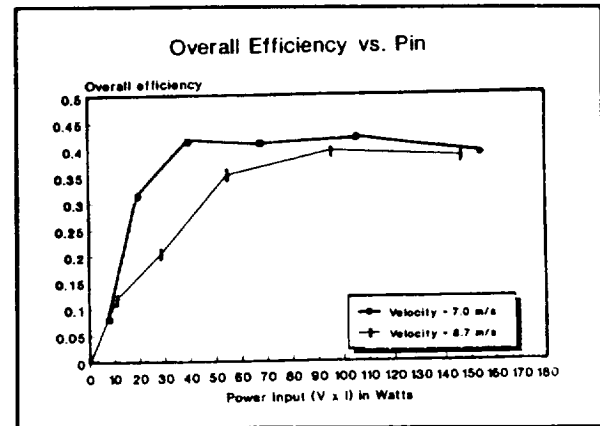


Fig. 15 Efficiency vs Power Input for Design Motor-Propeller

As a safety feature, there is a NiCad battery pack installed in the fuselage of the plane. At full power the batteries produce eight to nine volts and upwards of 20 amps. The use of these batteries is limited as their lifespan is not more than five or six minutes. A manual switch shifts the power source from the cells to the batteries. The batteries can be slowly recharged up to five volts during glides if the motor is turned off. A diode connected between the cells and the batteries prevents the batteries from charging the array.

The control surfaces are operated by remote control through the use of the servos. A very small current needed to run each servo is controlled by its own channel frequency. Both ailerons are wired into the same channel to act in opposite directions. The rudder and the horizontal stabilizer are wired separately and receive their own channels. All servos are wired to the receiver box where they pick up the signals for operation. The receiver itself needs a small battery pack to operate. These are four rechargeable 1.2 volt cells. There are enough channels available on the receiver not only to handle the control surfaces, but also the throttle and the main power switch.

The power requirements for level flight are met through the utilization of silicon solar cells. The level flight speed of 7.1 m/s and the weight of 52 Newtons dictate a



minimum power requirement of 18.8 Watts. The solar array implemented on the plane produces approximately 108 Watts for the test flight date (April 11, 1992). This power production is calculated with the plane flying away from the sun thus exposing the greatest cell area to the sun's rays. The power produced for the plane flying toward the sun is approximately 98 Watts. These values do not include the power losses suffered in the motor/propeller transmission, since even an optimized power train reduces the power by more than half.

A number of parameters control the amount of power produced as well as the construction of the array. The weight of the cells is considerable and compose a large portion of the overall weight of the plane. Therefore, the cells must produce more power to the overall thrust than they contribute to weight. The photovoltaic cells are rated at an efficiency of 12.5%, determined at ideal conditions in a laboratory. The actual efficiency is lower due to design conditions. Substantial power loss occurs due to impedance matching and resistance of the wiring. The wing geometry allows only a limited number of possible array configurations and limits the number of possible voltage- current options.

A basic solar cell (Figure 16) consists of two layers of Silicon glass. The top layer is doped with Phosphorous to produce an excess of electrons while the bottom layer is doped with Aluminum to produce an abundance of electron holes. As photons strike the surface of the cell, they knock loose the excess electrons in the SiP bond. The net effect is the creation of free conduction electrons and positively charged holes which generate an electric potential between the top and bottom layers. Basic inefficiencies in this process are reflection and recombination of the photons striking the cell. Also, some photons do not possess the energy to knock loose the electrons thus rendering some of the incident light ineffective. Other photons possess too much energy and waste the excess when striking the electrons.<sup>4</sup>

The amount of solar power reaching the cells on a given day relies on many geometric and atmospheric variables. Obviously, a clear sunny day is better than an overcast day, yet summer months are not necessarily better than winter. Air pollution and building reflection contribute to the decrease in power availability. However, the position of the sun relative to the cells is the dominating factor.

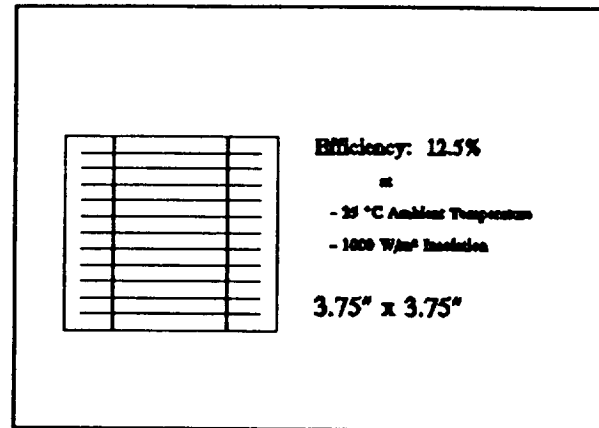


Fig. 16 Mobil Solar Silicon Photovoltaic Cell

The power received is not the available energy, since the cells can only convert around 12.5% to electric power. This electric power is eventually transformed into thrust through the motor and propeller configuration. Therefore, the cells must produce enough power to overcome the losses induced by the power train to sustain level flight. Assuming that the power train will convert only about 20 to 30%, this target and the estimated power produced dictate the initial number of cells to be installed upon the plane. With 18.8 Watts needed to fly the plane and the wing geometry in mind, the number of cells to be placed upon the wings is 120.

A random sampling of solar cells was taken to the roof of Salisbury Laboratories on the 18th of November 1991, and tested for their open circuit voltage and short circuit current. On that day, the individual cells produced approximately 0.5 Volts and, depending upon the orientation, 0.6 - 1.1 Amps. A similar test was performed on February 6, 1992. This test used a ten cell array; the characteristic I-V curve and maximum power point for the array were determined (see Figures 17 and 18). The clear mylar skin array reduces the amount of current produced, thus affecting the power available. For this reason, as many cells as possible were placed on the outside of the wing to maximize power production. Each array on the plane must have an equal number of cells, avoiding losses due to internal circuits.

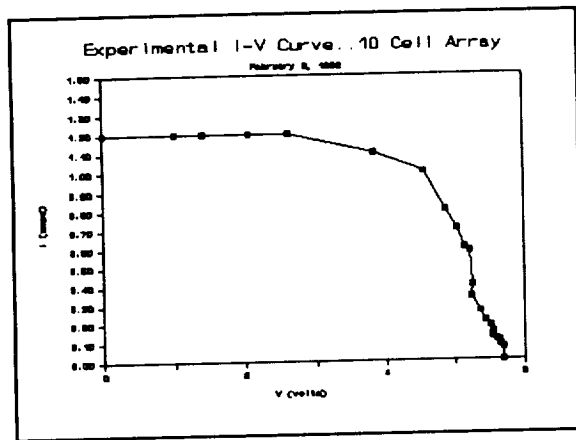


Fig. 17 Experimentally Determined I-V Curve

The array was configured to accommodate the desired wing geometry and the predicted load. The chord of the wing allows for the placement of three rows of cells along the entire span. In order to maintain the desired aerodynamic characteristics of the aircraft the first row on the leading edge is placed underneath the wing skin. The second and third rows are placed on the outside of the wing on the rear of the airfoil. The arrays should be angled to receive the greatest amount of sunlight at any given time. On a stationary platform the array would be angled at about  $45^\circ$  to the horizontal. Since the plane is constantly moving in the horizontal and vertical planes, the best inclination is to place the array close to the horizontal. The front cells are inside facing forward and placed as close to horizontal as the wing geometry will allow at an angle of  $12^\circ$  to the chordline. The rear cells are subject to geometric constraints as well and are placed directly onto the flatback airfoil at angles of approximately  $6^\circ$  to the chordline.

The constructed array consists of twelve sub-arrays of ten cells placed on both the main and modular sections of the wing and integrated into the propulsion system. All twelve are connected in parallel to generate an anticipated 5 Volts and 12 Amps.

#### Construction Process

The wing and tail supporting spars and the tapered fuselage were uniquely constructed using a woven carbon

fabric and West System epoxy to create durable, lightweight components. A piece of ordinary PVC wrapped in mylar, to prevent any adhesion to the resultant carbon tube, served as a mold for the spars. The fuselage mold was constructed using PVC tubing of the desired diameters with a tapered section made of foam connecting them. Wrapping the carbon fabric about the molds and applying epoxy generated components with desirable strength-to-weight characteristics. A microlyte filler was applied to the finished carbon structure to smooth out the imperfections and reduce the drag on this member. The main wing was connected to the fuselage by drilling a hole through the fuselage and passing the wing tube through the center of the body. The connection was reinforced using carbon fiber sleeves. Subsequent tasks included gluing the ribs to the wing spar, applying the mylar, and wiring all of the electrical components and solar cells.

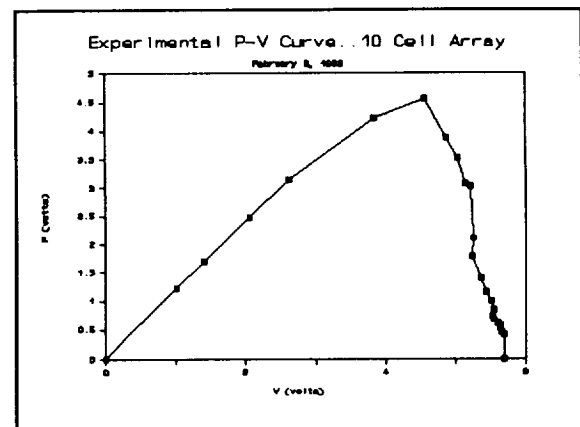


Fig. 18 Experimentally Determined P-V Curve

The solar cell array was connected entirely by hand. Each of the 120 cells donated by Mobil Solar arrived naked. Two metal ribbon leads were soldered to one side of every cell. This was accomplished with a small soldering iron and 60/40 lead/tin solder. Once completed, ten unit arrays were assembled by soldering the leads of one cell to the back of another in a long chain. Integrating the cells of the wing created a slight problem. The front row could be easily placed upon small styrofoam shelves underneath the coating of plastic, but the back rows needed some way to adhere directly to

the covering. Fortunately, a roll of double-sided adhesive was donated by Flexcon Corporation. This adhesive was applied in two half-inch strips to the backside upon which the array rested. To prevent disintegration of this bond and the cells, a small strip of plastic ran along the leading edge of the array and joined the wing approximately 1.5 inches in front of the cells. This prevented the airstream from finding its way underneath the cells and ripping them off.

### Stability

Longitudinal and lateral stability was evaluated by classical analysis methods and a study of historical trends.<sup>5</sup> The horizontal tail and the location of the center of gravity were sized to provide static longitudinal stability.<sup>1</sup> The effects of expected gust induced loads in the longitudinal direction, pitch, results in a rate of change of the pitching moment with the total airplane lift ( $dC_M/dC_L$ ) of  $-0.310$ , rendering static stability to the configuration.

Historical trends were studied,<sup>5</sup> and a total dihedral angle of  $2.5^\circ$  was determined to ensure sufficient roll stability, while not hindering the collection of solar power. A compound dihedral angle was chosen. The dihedral angle begins at the modular wing connections. The modular wing sections are positioned at an angle of  $5^\circ$ , insuring a total dihedral angle of  $2.5^\circ$ . The vertical tail and dihedral were sized to provide lateral stability. The vertical tail has a Vertical Tail Volume Coefficient of approximately  $0.02$ , typical for a sailplane. The tail has an area of  $900 \text{ cm}^2$ , and furnishes directional stability.

The necessary control surface sizes for the plane were determined using a combination of historical trends for similar aircraft<sup>5</sup> and recommendations taken from model aircraft publications. Approximately half of the vertical stabilizer surface area was removed and replaced by a rudder. The rear quarter of the horizontal stabilizer's chord is occupied by an elevator spanning the entire length (1 m) of this component. These control surfaces are actuated by Futaba electronic servos housed within the horizontal stabilizer. Due to the solar cell placement, the chord of the ailerons was limited. To conform to the limited width, the ailerons span the entire length of the modular wing sections. The servos that control them are located directly in front of the ailerons, adjacent to the modular wing connections.

### Performance and Mode of Operation

Solar propulsion is very appealing on the basis that it is harmless to the environment and cost efficient. The performance of a vehicle, however, is very confined to the weather, time of day, location, season, and efficiency of its solar power system. The available solar cells for this aircraft configuration were not the most efficient or light weight, yet did allow for excess power for take-off and climb. A computer code was developed to predict the performance of the aircraft in level flight.

The aircraft is designed to climb in a circular flight path to an altitude of 50 m in approximately 5 minutes, as shown in Figure 19. This mission requires 5.5 complete revolutions about a 200 m field. The climb rate is a function of the angle of incidence between the sun and the solar cell array; the aircraft climbs at a rate of  $0.06 \text{ m/s}$  away from the sun and  $0.02 \text{ m/s}$  towards the sun.

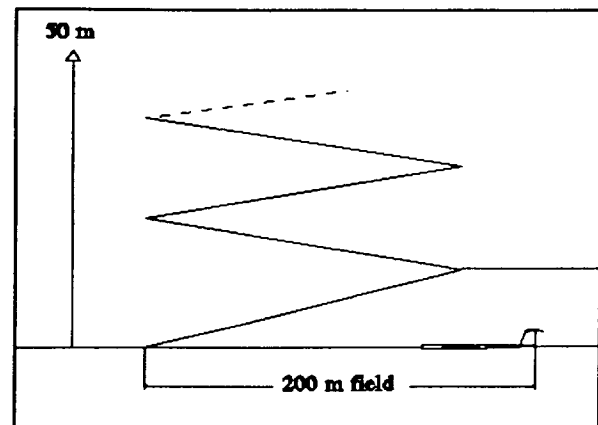


Fig. 19 Proposed Climb Scheme

At the design altitude,  $18.8 \text{ W}$  is required from the propulsion system to maintain flight at  $7.1 \text{ m/s}$ . A sustained figure eight flight pattern will be achieved with an angle of attack of  $4^\circ$ , banking angle between  $3^\circ$  and  $4^\circ$ , and a turning radius varying from  $67 \text{ m}$  to  $89 \text{ m}$ .

## Results and Recommendations

### Flight Testing

*Surya* underwent four flight tests between February and April of 1992. These tests proved not only to be valuable tools in the final design modifications but also as evidence of the sturdiness of the carbon composite structure. Due to the fragility of the solar cells, the first three test flights were completed before the cells were mounted. However, weights were used in place of the solar cells to estimate the behavior of the plane. The first flight test was without propulsion to verify that the location of the center of gravity was the same as that calculated theoretically. In this test, a slight wing twist was detected by the pilot, as well as a shift of the center of gravity from the desired location.

An overcorrected wing twist as well as another shift in the center of gravity persisted in the first powered flight test. The wing twist, now in the opposing direction, was again detected by the pilot. After adjustments were made to correct this by repositioning the modular wing sections, the plane proved to be responsive to controls and relatively easy to maneuver. The second powered flight test utilized the propeller's full power, and the need to optimize the propulsion system with a more efficient motor and propeller became evident. Again, the plane responded well to controls and flew for a short amount of time before landing quietly on simple yet effective landing skids.

In the fourth test flight, proxy cell weights were replaced by the actual solar cells. The wing twist was corrected as attested by the pilot. However, the new electronic components installed for the wiring of the cells shifted the center of gravity once again. This center of gravity shift and the presence of wind gusts caused the climb performance to be sluggish.

### Recommendations

Many engineering difficulties were incurred during the design and construction of the solar plane, *Surya*. After the plane construction was completed, there appeared to be many components and processes which could be further optimized through more research, development, and testing. Of course many of these revelations were not obvious to the project team before the construction

began. The performance of *Surya* depends upon the following criteria: overall efficiency of the propulsion system, structural design, material selection, stability, aerodynamic analysis, and the overall weight of the plane.

The efficiency of the propulsion system is determined by its individual components including the solar cells, wiring, motor, propeller and the electronic configurations. It is obvious that the propulsion system is limited by the 12.5% efficient solar cells, but the system could be further optimized through improved matching of the motor and propeller. A more efficient motor along with a more powerful propeller would further optimize the propulsion system. To aid in the conservation of the weight budget, lighter wire could be used in the solar cell configuration.

Difficulties in maintaining the stability of the plane were experienced during flight testing. The center of gravity was not easily maintained at one tenth of the chord length. The majority of the stability problems could be eliminated by changing the propulsion configuration to include a pusher propeller. This configuration would enable the center of gravity to be kept ahead of the main wing and additional cells to be placed on the horizontal stabilizer. In addition to improved stability, the pusher propeller configuration would allow additional solar cells and power acquired from the cells.

Though *Surya* is structurally sound, the weight of the plane could greatly be reduced in most of the structural components. The handmade carbon composite fuselage and the wing and tail spars could be constructed more exactly to fully optimize the weight. The diameter of the fuselage could be reduced to conserve the weight of the plane. This dimension was originally dictated by a linkage used in the electronics. This linkage was later redesigned so that the fuselage diameter could be reduced. Many processes requiring the application of glue were done using epoxy, which tended to be heavier than standard superglue. Using the glue more sparingly would aid in the minimization of the weight of the plane.

The large size of the plane required that the wing sections of *Surya* be modular. The modular connections of the wing were constructed using a foam and carbon composite combination. These connections could be further optimized to conserve weight and possibly increase stability.

The control surfaces of the plane were increased in size to account for the increase in the size of the entire plane. After completion the plane seemed to be harder to control than had been anticipated. Enlarging the size of the control surfaces would aid in the overall performance of the plane.

The recommendations mentioned above indicate areas in which the design team felt limited. Most of these recommendations occurred at the completion of construction and were realized through experience. Further research and development in these areas are encouraged since the possibilities for various design configurations of this type of aircraft are numerous.

### Environmental Impact

Society is faced with various self-induced environmental problems. Implementation of solar energy as a replacement of traditional energy resources provides an economical solution. The design and construction of this solar powered aircraft attempts to contribute to this cause and encourage future research into alternative energy resources.

### Acknowledgments

The assistance and technical support of the NASA contacts, Mobil Solar, Aerospace Composites, faculty, staff, students, and many other interested aircraft modelling enthusiasts were numerous and very greatly appreciated. Special thanks to Art Glassman, our NASA/USRA mentor and the advising professors, Prof. William W. Durgin, Prof. Andreas N. Alexandrou, Prof. Ralph F. Cohn, Prof David J. Olinger, Prof. Edward Clarke, and Kurt Heinzmann for their faithful guidance. The educating assistance on aircraft design vital to the required mission provided by Adam Szymkiewicz and Arthur Lavallee has been invaluable. Also thanks to the many helpful staff from WPI especially Todd Billings, Bob Taylor, and Roger Steele for sharing their expertise and equipment.

### References

1. Shevell, R.S. Fundamentals of Flight, Prentice Hall, Englewood Cliffs NJ, 1989.
2. Selig et. al. Soartech 8: Airfoils at Low Speeds. H.A.
3. Kuethe, A. and Chow, C. Foundations of Aerodynamics, 4th Ed. John-Wiley and Sons: New York, 1986.
4. Hu, C. and White. R.M. Solar Cells From Basic to Advanced Systems. McGraw Hill: New York, 1983.
5. Raymer, D. Aircraft Design: A Conceptual Approach. AIAA, Inc.: Washington, DC, 1989.

